

Konferenzbeiträge / Atti / Proceedings

Building Simulation Applications BSA 2015

2nd IBPSA-Italy conference
Bozen-Bolzano, 4th–6th February 2015

Edited by
Marco Baratieri, Vincenzo Corrado,
Andrea Gasparella, Francesco Patuzzi

bu,press

bozen
bolzano
university
press

unibz
—
Freie Universität Bozen
Libera Università di Bolzano
—
Università Lìdia de Bulsan

Konferenzbeiträge / Atti / Proceedings

Building Simulation Applications BSA 2015

2nd IBPSA-Italy conference
Bozen-Bolzano, 4th–6th February 2015

Edited by
Marco Baratieri, Vincenzo Corrado,
Andrea Gasparella, Francesco Patuzzi

bu,press

bozen
bolzano
university
press

Scientific committee

Ian Beausoleil-Morrison, Carleton University, Canada
Jan Hensen, Technische Universiteit Eindhoven, The Netherlands
Ardeshir Mahdavi, Technische Universität Wien, Austria
Athanasios Tzempelikos, Purdue University, USA
Natale Arcuri, Università della Calabria, Italy
Paolo Baggio, Università degli Studi di Trento, Italy
Vincenzo Corrado, Politecnico di Torino, Italy
Andrea Gasparella, Free University of Bozen-Bolzano, Italy
Livio Mazzarella, Politecnico di Milano, Italy

Organizing committee

Paolo Baggio, Università degli Studi di Trento, Italy
Marco Baratieri, Free University of Bozen-Bolzano, Italy
Francesca Cappelletti, IUAV University of Venice, Italy
Alfonso Capozzoli, Politecnico di Torino, Italy
Vincenzo Corrado, Politecnico di Torino, Italy
Enrico Fabrizio, Politecnico di Torino, Italy
Andrea Gasparella, Free University of Bozen-Bolzano, Italy
Norbert Klammsteiner, Energytech Ltd., Bozen-Bolzano, Italy
Marco Noro – Università degli Studi di Padova
Fabian Ochs, Universität Innsbruck, Austria
Francesco Patuzzi, Free University of Bozen-Bolzano, Italy
Paola Penna, Free University of Bozen-Bolzano, Italy
Giovanni Pernigotto, Università degli Studi di Padova, Italy
Alessandro Prada, Free University of Bozen-Bolzano, Italy
Piercarlo Romagnoni, IUAV Università di Venezia, IBPSA, Italy

Other reviewers and chairmen

Anna Atzeri, Free University of Bozen-Bolzano, Italy
Adolfo Palombo, Università degli Studi di Napoli, Italy
Fabio Sicurella, Professional Engineer, Catania, Italy
Francesco Asdrubali, Università degli Studi di Perugia, Italy
Luigi Marletta, University of Catania, Italy
Marco Manzan, University of Trieste, Italy
Laura Bellia, Università degli Studi di Napoli, Italy
Jerome Kämpf, École Polytechnique Fédérale de Lausanne, Switzerland
Ulrich Pont, Technische Universität Wien, Austria



This work—excluding the cover and the quotations—is licensed under the Creative Commons Attribution-ShareAlike 4.0 International License.

Cover design: DOC.bz

© 2015 by Bozen-Bolzano University Press

Free University of Bozen-Bolzano

All rights reserved

1st edition

www.unibz.it/universitypress

ISSN 2531-6702

ISBN 978-88-6046-074-5

Preface

In recent years, Building Simulation has been confirmed as the technique based on computer calculation to estimate either the energy or the non-energy performance of buildings, building components and systems, considering in particular its detailed variability in time.

In the past, most of the efforts were put into improving the detail and increasing the reliability of the results and the capability of describing the behavior of the building more realistically. In this respect, validation has been one of the major concerns of the building simulation tool. The main aim of simulation was to understand better the behavior of some specific processes, their interaction and the behavior of the building. Modelling was particularly useful to compensate for missing experimental data and to overcome the impossibility of obtaining enough experimental data or any data at all, due to the complexity of the investigated system, the slow dynamic or long period of time. Starting from very specific aspects or components, BS has progressively included, typically with a modular approach, the whole building or even the urban scale.

In recent years, building simulation has increasingly taken advantage of the tremendous growth in the availability of computational capacity, thanks to new processors, parallel calculation, cloud computing, etc., and has opened new perspectives and uses. The enhancement of the level of detail, the extension of the size and application range of the domain of investigation and the increase in the level of accuracy and generality of the results have all been established as mainstream focal points. In parallel, the diffusion of calculation capacity has awoken the interest of practitioners and professionals in new practical applications.

These trends also characterized the second IBPSA-Italy conference, which took place for the second time at the Free University of Bozen/Bolzano from 4 to 6 February 2015. Almost 100 attendees, 198 authors, 67 presentations, and 4 keynote speakers confirmed not only the interest in building simulation, but also the relevance and coherence of the above

focuses. In particular, four sections were devoted to the detailed modelling of phenomena and components (advanced modelling, solar radiation, energy systems and envelope modelling), three to the integrated and non-energy performance analysis (lighting and user behavior), three to the optimization techniques for high performance buildings and retrofit, and two to the development and validation of new tools.

The participation of authors and delegates from 15 countries, together with the keynote speakers Ardeshir Mahdavi (Vienna University of Technology), Ian Beausoleil-Morrison (Carleton University), Jan Hensen (Eindhoven University of Technology) and Athanasios Tzempelikos (Purdue University), offered the opportunity to discuss issues with an international audience as well as to compare and to enhance the quality of the national research.

The presentation of the first IBPSA Italy Awards for PhD Student Papers demonstrated the commitment towards the growth of a new generation of young researchers who will be able to sustain and diffuse the best use of BS.

The presentation of the first IBPSA Italy Awards for Simulation Assisted Design to distinguished practitioners using building simulation in their business confirmed how seriously the IBPSA takes practical applications of BS.

The presence of the local Engineers and Architects Orders, of the AICARR (the Italian Association of Air conditioning, Heating and Refrigeration), ANDIL (the Italian Association of Clay Brick and Roof Tile Producers) and ASSOVETRO (the Italian Association of Glass and Glazing Systems Producers), together with the institutional support of the Autonomous Province of South Tyrol and of the CasaClima Agency, allows us to be even more confident that the journey undertaken has been, and will continue to be, a great success.

Andrea Gasparella, Free University of Bozen-Bolzano

Table of Contents

Preface.....	V
Common fallacies in representation of occupants in building performance simulation <i>Ardeshir Mahdavi</i>	1
The importance of software's and weather file's choice in dynamic daylight simulations <i>Laura Bellia, Alessia Pedace, Francesca Fragiasso</i>	9
Outdoor Comfort: the ENVI-BUG tool to evaluate PMV values point by point <i>Kristian Fabbri, Antonello Di Nunzio, Ernesto Antonini, Andrea Boeri</i>	17
Aspects of uncertainty in representation of occupants' diversity in building performance simulation <i>Ardeshir Mahdavi, Farhang Tahmasebi</i>	23
Prediction of vertical irradiance on building surfaces: an empirical comparison of two models <i>Ehsan Vazifeh, Matthias Schuss, Ardeshir Mahdavi</i>	27
Improving energy efficiency through the optimization of buildings' operational regime: simulation based case studies <i>Farhang Tahmasebi, Mahnameh Taheri, Matthias Schuss, Ardeshir Mahdavi</i>	33
Performance evaluation towards improved BiPV-Systems – Simulation of BiPV-systems installed on existing building facades using TRNSYS <i>Sascha Lindig, David Moser, Stefano Avesani, Roberto Lollini</i>	41
Appraising the effects of window opening behaviour in an office building in different climates <i>Sara Torabi Moghadam, Federica Soncini, Valentina Fabi, Stefano P. Corgnati</i>	51
Prediction of the Sound Insulation of Double Leaf Facades with Openings for Natural Ventilation <i>Egzon Bajraktari, Josef Lechleitner, Ardeshir Mahdavi</i>	59
Influence of varying mix proportions on thermal performance of soil-cement blocks <i>Balaji N.C, Praseeda K. I., Monto Mani, Venkatarama Reddy B. V.</i>	67
Achieving High-Performance Building Design in the Tropics through Modelling and Simulation: A case study in Singapore <i>Bharath Seshadri, Zhou Jian, Vincent Partenay, Priya Pawar, Adrian Lamano</i>	75
Modelling, testing and optimization of a MVHR combined with a small-scale speed controlled exhaust air heat pump <i>Fabian Ochs, Dietmar Siegele, Georgios Dermentzis, Wolfgang Feist</i>	83
BIM and interoperability for energy simulations <i>Bernardino Chiaia, Sanaz Davardoust, Anna Osello, Niccolò Aste, Manlio Mazzon</i>	93
Urban heat island in Padua, Italy: simulation analysis and mitigation strategies <i>Luca Battistella, Marco Noro</i>	99
Multi-zone buildings thermo-hygrometric analysis: a novel dynamic simulation code based on adaptive control <i>Annamaria Buonomano, Umberto Montanaro, Adolfo Palombo, Stefania Santini</i>	109
Energy simulation in early stage building design: simplified models and impact on results <i>Marco Picco, Marco Marengo</i>	119
The Solar Response Factor for the dynamic response of buildings to solar heat gains <i>Gianpiero Evola, Luigi Marletta</i>	127
Comparison of energy simulations for a residential unit: a rapid method for an integrated decision tool <i>Alberto Beltrami, Marco Picco, Marco Marengo</i>	137
Thermal modelling of complex fenestration systems – Comparison of a BSDF-based model with simplified approaches <i>Hauer Martin, Geisler-Moroder David, Hiller Marion</i>	147

A new climate-based daylight metric for hot climates <i>Islam Ayman Mashaly, Yussra Mohamed Rashed, Muhammad Adel, Khaled Nassar</i>	155
The effect of vegetation on daylight availability <i>Islam Ayman Mashaly, Yussra Mohamed Rashed, Muhammad Adel, Khaled Nassar</i>	163
Solar assisted ground source heat pump performance assessment for residential energy supply in southern European climates <i>Natale Arcuri, Francesco Reda, Pasquale Loiacono, Domenico Mazzeo</i>	171
Energy consumption of buildings and occupant behavior. An investigation in Mediterranean climatic conditions <i>Piero Bevilacqua, Cristina Carpino, Dafni Mora, Marilena De Simone</i>	181
Energy retrofit and conservation of built heritage using multi-objective optimization: demonstration on a medieval building <i>Francesca Roberti, Ulrich Filippi Oberegger, Elena Lucchi, Andrea Gasparella</i>	189
Energy performances of a passive house for Mediterranean climate: a case study <i>Cristina Carpino, Piero Bevilacqua, Roberto Bruno, Natale Arcuri</i>	199
Building simulation based optimization through design of experiments <i>Jay Dhariwal, Rangan Banerjee</i>	207
A verification of CitySim results using the BESTEST and monitored consumption values <i>Walter Emmanuel, Kämpf Jérôme</i>	215
Integrated design and dynamic simulation for a new zero energy building <i>Dama Alessandro, Angelotti Adriana, Penso Davide</i>	223
A parametric approach to design a wooden climatic responsive village in Atacama Desert (Chile) <i>Francesco Leccese, Alessandro Mattoccia, Michele Rocca, Rodrigo Rubio, Giacomo Salvadori</i>	231
Energy Saving Exploiting Light Availability: A New Method to Evaluate Daylight Contribution <i>Claudio Campanile, Francesco Leccese, Michele Rocca, Giacomo Salvadori</i>	239
Estimation of the water flow rate and energy consumption of a central heating system in an office building using system identification <i>Daniele Antonucci, Federico Noris, Ulrich Filippi Oberegger, Andrea Gasparella</i>	247
Comparison between hourly simulation and bin-method for the seasonal performance evaluation of electric air-source heat pumps for heating <i>Claudia Naldi, Matteo Dongellini, Gian Luca Morini, Enzo Zanchini</i>	255
Cost optimal and net zero energy office buildings solutions using small scale biomass-based cogeneration technologies <i>Ayman Mohamed, Ala Hasan, Kai Sirén</i>	263
Integrated performance simulation of an innovative net zero energy modular building <i>Francesco Fantauzzi, Paolo Belardi, Francesco Asdrubali, Samuele Schiavoni, Sara Sambuco</i>	273
Study of the energy performance of a retrofitting office <i>Paolo Valdiserri</i>	281
Coupling dynamic energy and daylighting simulations for complex fenestration systems <i>Giuseppe De Michele, Ulrich Filippi Oberegger, Luca Baglivo</i>	289
Simulation experiences for the thermal performance improvement of naturally ventilated classroom in the tropics of Costa Rica <i>Emily Vargas Soto, Gerardo Saelzer Fuica</i>	297
A new computational model: G.E.A.R. Graphical Expert Analytical Relations <i>Martino Marini, Roberto Baccoli, Costantino Carlo Mastino, Valerio Da Pos, Zoltán Tóth</i>	305
A new simulation tool for the evaluation of energy performances of green roofs <i>Domenico Mazzeo, Piero Bevilacqua, Marilena De Simone, Natale Arcuri</i>	313
A holistic method for energy renovation of buildings: focus on users' involvement <i>Giulia Degan, Carsten Rode, Daniele Vettorato, Marco Castagna</i>	323
The role of user behavior modeling on the energy performance simulations <i>Marco Aldegheri, Alessandro Prada, Paolo Baggio, Michela Chiogna</i>	331

Application of Building Simulation to support ISO 50001 Energy Management: Case study of Fiumicino Airport <i>Luis M. Blanes, Andrea Costa, Marcus M. Keane</i>	339
Dynamic simulation and on-site monitoring of a combined solar and pellet system in a low energy house <i>Elisa Carlon, Alessandro Prada, Markus Schwarz, Christoph Schmidl, Marco Baratieri, Andrea Gasparella, Walter Haslinger</i>	347
A parametric design-based methodology to visualize building performance at the neighborhood scale <i>Giuseppe Peronato, Emilie Nault, Francesca Cappelletti, Fabio Peron, Marilyne Andersen</i>	351
Exploring the occupancy behaviour and perception in an office building <i>Livia Seres, Ulrich J. Pont, Matthias Schuss, Ardeshir Mahdavi</i>	359
Window shades: selecting optical properties for visual comfort <i>Ying-Chieh Chan, Athanasios Tzempelikos</i>	367
ProCasaClima 2013: CasaClima building simulation software <i>Matteo Rondoni, Ulrich Santa, Ulrich Klammsteiner, Martina Demattio, Mariadonata Bancher, Alexander Told, Thomas Zelger</i>	377
Graphic and parametric tools for preliminary design stage of natural ventilation systems <i>Margherita Ferrucci, Maurizio Brocato, Fabio Peron, Francesca Cappelletti</i>	383
Advancement in the development of an Open Source Object Oriented BPSt: development methodology <i>Livio Mazzarella, Martina Pasini</i>	391
A methodology to integrate advanced lighting and thermal analyses for building energy simulation <i>Silvia Cammarano, Anna Pellegrino, Valerio R. M. Lo Verso, Chiara Aghemo</i>	399
BIM-generated data models for EnergyPlus: A comparison of gbXML and IFC Formats <i>Ira Ivanova, Kristina Kiesel, Ardeshir Mahdavi</i>	407
Passive solutions for the optimization of the indoor environmental quality: a case study <i>Fabio Sicurella, Perla Colamesta</i>	415
Modelling of domestic fine particles indoor exposure, its main sources and potential mitigation measures: the case of Beijing <i>Sandra Stefanović, Žarko Stevanović</i>	423
Application of aerogel-based plaster towards thermal retrofit of historical facades: A computational assessment <i>Olga Proskurnina, Ulrich J. Pont, Mirosława Kornicki, Ardeshir Mahdavi</i>	431
Long-term and spatial evaluation of the integrated performance of a window-shade system in an open space office located in Rome <i>Anna Maria Atzeri, Francesca Cappelletti, Athanasios Tzempelikos, Andrea Gasparella</i>	439
Energy cost and discount rate influence on the optimal packages of energy efficiency measures <i>Vincenzo Corrado, Ilaria Ballarini, Ilenia Ottati, Simona Paduos</i>	447
Energy building retrofitting of a multifamily house: a case study <i>Chiara Dipasquale, Roberto, Diego Bertesina, Alessandro Bellini</i>	455
The use of biomass in the building renovation: a cost-optimal perspective analysis <i>Enrico De Angelis, Giorgio Pansa, Martina Cereda</i>	463
Passive cooling strategies in the refurbishment of Mediterranean buildings: simulation analysis of thermal mass and natural ventilation combination <i>Filippo Calcerano, Carlotta Cecchini</i>	473
Daylighting optimization for informal settlements in Cairo, Egypt <i>Ayman Wagdy, Ahmed Abdelghany, Mohamed Amer Hegazy</i>	483
CFD vs. lumped models applied to HAM: a comparison between HAM-Tools and Comsol <i>Amos Ronzino, Vincenzo Corrado, Maximilian Neusser, Thomas Bednar</i>	491
Optimizing Window size of South Facades in Tehran City and the Environmental Impacts <i>Fazel Khayatian, Seyed Amin Tabatabaei Fard, Maryam Meshkin Kiya</i>	499
Analysis of energy efficiency measures on envelope and control systems: case study for an existing building <i>Giovanni Semprini, Alessandro Gober, Francesca Zandi</i>	507

Robustness of multi-objective optimization of building refurbishment to solar radiation model <i>Alessandro Prada, Giovanni Pernigotto, Francesca Cappelletti, Andrea Gasparella</i>	517
The impact of thermal comfort in multi-objective optimization of buildings refurbishment <i>Paola Penna, Alessandro Prada, Francesca Cappelletti, Andrea Gasparella</i>	527
A multi-objective optimization analysis on high-performance buildings connected to district heating-CHP system <i>Dario Prando, Alessandro Prada, Fabian Ochs, Andrea Gasparella, Marco Baratieri</i>	537
Experimental characterization of the dynamic thermal properties of opaque elements under dynamic periodic solicitation <i>Giovanni Pernigotto, Alessandro Prada, Francesco Patuzzi, Marco Baratieri, Andrea Gasparella</i>	547
Re-thinking of energy consumption classification by the patterns of occupant behaviour: a conceptual framework <i>Gülsu Ulukavak Harputlugil, Timuçin Harputlugil</i>	557

Common fallacies in representation of occupants in building performance simulation

Ardeshir Mahdavi – Department of Building Physics and Building Ecology, Vienna University of Technology, Austria – bpi@tuwien.ac.at

Abstract

This keynote address offers a number of critical observations with regard to the representation of occupants' presence and behaviour in building performance simulation applications, tools, and processes. The objective is to contribute to a more reflective attitude and to further productive discussions of the subject in the relevant research community

1. Introduction

In this keynote presentation, I would like to briefly address a number of critical issues with regard to the representation of occupants' presence and behaviour in building performance simulation models.

As the use of the first person singular pronoun in this presentation implies, I do not intend to provide here a strictly technical treatment of the subject (i.e., one that follows the typical structure of a scientific contribution with obligatory parts such as hypothesis, research design, experiments, analysis, conclusion, references, etc.). Rather, the impetus behind this talk comes mainly from personal experiences in the course of various professional interactions with colleagues and students, as well as in my role as reviewer of various topically related conference and journal papers. In the course of these interactions and activities, I have observed a number of explicitly stated and tacitly implied opinions, beliefs, and attitudes, which I consider to be at least partially fallacious or misguided. In order to avoid the impression of bias or *ad hominem* criticism, I have abstained from pinpointing specific papers, individuals, or software implementations. The intention is to discuss the logical consistency and

empirical validity of ideas and models and not personal proclivities.

It is perhaps appropriate to state upfront my two main reasons to raise these issues. Firstly, I suspect that certain fallacies have led – and are still leading to – misguided tendencies in representation of building occupants in performance simulation and may thus impede sound progress in this area. Secondly, I hope to contribute to a healthy and enlightening debate, which – thorough thoughtful consideration of the pertinent arguments – could deepen the level of discourse and research quality in the field.

A number of my comments may appear to be self-evident – particularly to scientists not directly from the field. These include, specifically, references to some of basic principles of logical discourse and scientific research. However, past experiences lead me to the conclusion that perhaps occasionally even the obvious needs to be stated.

2. Background

Let us consider the thermal performance of buildings and related simulation procedures, models, and tools. To conduct performance simulation, typically four sets of model assumptions are required, i.e., representations of the building fabric (i), its systems (ii), internal (occupancy-driven) processes (iii), and external (climatic) boundary conditions (iv). These representations and associated specific data sets are then supplied to the simulation application's algorithmic core (mathematical formulation of the pertinent physical processes). It can be cogently argued that the quality of performance simulation, i.e., its fidelity and reliability in representation of

reality, depends on both the soundness of the algorithmic core and the accuracy of the aforementioned model input assumptions.

I shall not discuss here the validity considerations of simulation tools' algorithms for the representation of the physical (e.g., heat transfer) processes. Rather, I shall focus on the representational matters pertaining to building occupants. The thermal performance of buildings is not only affected by the people's presence as a source of (sensible and latent) heat (the so-called passive effect), but is also influenced by their actions, including use of water, operation of appliances, and manipulation of building control devices for heating, cooling, ventilation, and lighting (the so-called active effect).

There has been arguably significant progress made in the last decades concerning methods and practices for specification of building geometry, material properties, and external (weather) conditions. Yet modelling practices pertaining to people's presence and behaviour in buildings are still in need of substantial improvement. Only relatively recently the detailed consideration of the effects of people's presence and their actions on buildings' performance has become a key topic in simulation research and application. There is still a lack of well-established and widely shared methods and standards for representing people in the building simulation practice.

It seems to me that the ongoing research efforts to develop more detailed and more robust building occupants' presence and (control) action models suffer in part from both conceptual fallacies and methodical shortcomings.

In the remainder of the present treatment, I would like to offer some related random thoughts and observations, meant as a constructive contribution toward a deeper and more systematic approach toward incorporation of occupancy-related representations in building performance simulation. To improve readability and simplify formulations, I shall henceforth refer to models of occupants' presence and (control-oriented) behaviour in buildings as occupancy-related models.

3. Some random observations

3.1 Occupancy and energy use

The motivation and background section of many recent contributions regarding occupancy-related models mention the following: Data on energy use of similar buildings (e.g. row house units of similar size and orientation located in the same site) often display a remarkable variance. The authors then infer from this observation that given the similarity of all the other factors, occupancy-related circumstances must be responsible for the variance. There is not a fundamental problem with such a conjecture per se. In such situations, the variation in the patterns of presence and behaviour of buildings' occupants may indeed explain – at least as a key contributing factor – the bulk of the variation in energy use data. But the assertion is often followed by the claim that more detailed and more sophisticated occupancy-related models would have facilitated more accurate energy use predictions. Therein lies a potential misunderstanding.

The actual energy use of a building is the result of a large number of influencing factors subject to various levels of uncertainty and unpredictability. More detailed and realistic representations of occupancy-related processes in buildings and their statistical fluctuations can shed much useful light on statistical variance of energy use patterns. However, I see no reason to suggest that they would necessarily result in accurate long-term energy use predictions of individual buildings. Strictly speaking, the energy use of a specific building cannot be predicted beyond a rather short time horizon: Alone the chaotic nature of weather patterns makes long-term building energy performance predictions infeasible, notwithstanding the quality of the building, systems, and occupancy-related models.

3.2 The so-called deterministic simulation

Recently, one reads and hears a criticism of conventional performance simulation as being "deterministic". The idea appears to be as follows: Conventionally, a fixed set of input variable values

are fed into the simulation and a fixed set of indicator values are obtained as output. This makes simulation deterministic and a misrepresentation of the inherently uncertain reality. But in this seemingly straightforward assertion lies another potential fallacy.

Let us explore this matter more closely. Most algorithmic representations of the physical phenomena in building performance simulation (expressed, typically, in terms of differential equations) are indeed deterministic in nature. For that matter, even the second-order partial differential equations of Quantum Mechanics (which is popularly perceived as non-deterministic) are as such deterministic. For instance, the Schrödinger equation describes the deterministic evolution of the "wave function" of a particle. Of course, even the exact knowledge of the wave function does not remove the uncertainty of a specific measurement on the wave function. Going back to the nether regions of building-related heat transfer, we can argue that the non-deterministic nature of the model input variables does not make the computational core of a simulation model (the partial differential heat transfer equations) non-deterministic. You can of course generate a statistical variance in the output of a deterministic model, if you subject the model to a variance (statistical fluctuations) in input variables. And doing such a thing may be quite expedient (it is called sensitivity analysis). But the recent use of the determinism parlance, which – in the philosophy of science – has all kinds of specific connotations (as associated with, for example, Pierre-Simon Laplace), is fairly irrelevant (if not misleading), when unreflectively applied to building performance simulation discourse.

I do not think that the simulation experts, who have been regularly computing certain fixed numbers for the values of various building performance indicators for a given fixed set of input variables have been ignorant to the fact that all engineering computation is subject to uncertainty. Probably, they were also not thinking that people really do "deterministically" enter and leave buildings or simultaneously open and close windows like a pack of robots that follow strictly some script according to diversity profiles found in

various codes and guidelines.

Now, it may or may not be a proper procedure to compare the simulation-based (fixed) value of a performance indicator (say, annual area-specific heating demand of a building) with a respective (likewise) code-based threshold value. But it is important to understand the logic and purpose of such comparisons. In many instances, they are geared toward benchmarking (comparison of calculated and mandated values of certain performance indicators) and not about making specific predictions pertaining to the performance of a building during a specific period of time.

3.3 Variance in, variance out

Assuming you have confidence in your simulation model's fidelity in representing physical (i.e., heat transfer) processes, you still need to worry about the uncertainty of input assumptions and how they may affect your simulation results. As mentioned earlier, sensitivity analysis is one tool that can provide you with a sense of your model's behaviour in the face of the variance of model input assumptions. It is thus entirely reasonable to explore the implications of occupancy-related uncertainties for the outcome of thermal simulation runs. Rather than using just standard diversity profiles, you could use a variety of methods and approaches to "randomise" occupancy-related input data. So where is the fallacy here? None, or not one yet.

The problem starts, when the source of assumed variance (spread of an input variable's values) is not empirically substantiated. Probabilistically induced variations in simulation results via fluctuations of input data can be argued to be informative to the extent that empirical basis of such fluctuations is trustworthy or representative. It seems fallacious to me, to argue that by the virtue of introducing some kind of stochastic variations in simulation input assumptions (irrespective of their grounding in reality), more trustworthy or reliable building performance predictions can be made. There is one thing to explore the behaviour of a model via systematic input-output mapping based on generic (or arbitrary) statistical distributions, but entirely

another thing to claim such exercise augments predictive capacity with regard to the performance of specific buildings under specific circumstances. We can avoid such misconceptions in part via general reflections on the complexity of human behavior, especially in socially relevant contexts. More specifically, we must assiduously uphold the proper scientific requirements pertaining to model development and evaluation. These include, amongst others, careful collection and preparation of representative observational data, clean separation of underlying data sets for *a*) model generation and *b*) model evaluation, and candid declaration of model limitations as well as proper description of the model application scope.

With regard to models' reliability and predictive performance, ultimately, double-blind studies (where the empirical data collection, the model development, and the comparison of measurements and predictions are done by separate agents) or round-robin tests would be most convincing. I think we can and should do a better job in this area.

3.4 About use cases

3.4.1 Occupancy-related model options and simulation application scenarios

Let us further explore the relevance of the use cases of building performance simulation with regard to occupancy-related models deployed. It seems to me that neither the choice of the occupancy-related models, nor the choice of the criteria for gauging their reliability is independent of the simulation's use case. Focusing on thermal building performance simulation, we can think, right off the bat, of multiple application scenarios:

- Simulation studies can target components of a building (say, for thermal bridge analyses), parts of a building (for example, simulation of a typical floor of a high-rise building), whole buildings, or even groups of buildings (district or urban simulation).
- We can distinguish application scenarios in view of the deployment phase of simulation (e.g., preliminary design support, detailed design support, systems design support, building/system operation support).

- We can distinguish application scenarios in view of the spatial (e.g., single-zone versus multi-zone) and temporal resolution (e.g., 15 minute intervals versus hourly simulations).
- Application scenarios could be also distinguished in terms of the ultimate use of the computed parameter (generating an energy certificate, benchmarking a design proposal with regard to applicable standardised performance criteria, comparison of alternative designs at a certain stage of the building design process, design and sizing of buildings' mechanical equipment, real-time use of recurrent dynamic simulations in a predictive building systems control routine).

The above cursory list provides an impression of the considerable diversity of simulation-based building performance assessment scenarios. It seems to me that the dependency of occupancy-related model selection (and the associated evaluation criteria) on the type and nature of the specific simulation use case at hand is insufficiently understood.

To explore this point more thoroughly, consider the case of the applicability of two different representational approaches of occupancy-related processes. Let us call them "non-probabilistic" (NP) and "probabilistic" (PR). The NP approach is typically expressed in terms of code-based diversity profiles, which – as I mentioned before – are sometimes (or one could say notoriously) referred to as deterministic. The PR approach aims at representational formalizations, which are intended to capture the arguably stochastic nature of actual occupancy-related processes. Independent of the question of the predictive performance of PR methods, are they to be exclusively applied in all simulation-based performance queries? Let us consider, in the following two sections, a few exemplary instances.

3.4.2 Code compliance and benchmarking

What kind of occupancy-related simulation input assumptions would make sense, when simulation is used to provide values for a number of aggregate performance indicators (such as buildings' annual heating and cooling loads) that

are declared, for example, in energy certificate documents? Note that such aggregate indicators are typically meant to benchmark a specific building design brief against applicable codes, standards, and guidelines. Naturally, this is done under "standardized" conditions pertaining to external climate (typically represented in terms of a standard weather file), but what about occupancy? The use of a PR model would generate, per definition, more or less different occupancy-related input data for each simulation run, resulting in correspondingly different simulation results. This could represent a problem not only for code-based compliance checking, but also for the performance analyses of design alternatives, when the aim is to compare multiple (alternative) designs irrespective of variance in contextual boundary conditions (weather) and occupancy. Presumably, one can argue that the repeated simulation runs (with incorporated PR models) would ultimately converge to stable values for aggregate performance indicators. But the question is if this use scenario and the kind of time, effort, and (often non-existent) background occupancy information it requires can actually generate any convincing added (procedural or predictive) value.

3.4.3 Spatial and temporal distribution of thermal loads and capacities

Consider now a different use case. We know that variance in occupancy-related patterns over time and location can be quite significant. Such variance can be critically important, for example, when we would like to gauge the dynamics of thermal loads in various zones of a building and deduce the correspondingly required capacities of building's thermal control systems. Toward capturing the temporal and zonal variations of thermal loads toward design, sizing, and configuration of indoor climate control systems, we would surely benefit from the deployment of appropriate PR methods. It seems to me that in this instance, using rigid NP models of user presence and behavior that ignore associated stochastic fluctuations (and the resulting uncertainties) would be rather problematic. While dealing with the requirement of providing sufficient heating and cooling capacity to different zones of a building in an efficient manner, the

variability of required thermal loads needs to be systematically explored. This cannot be based on spatially and temporally averaged occupancy assumptions.

3.4.4 Design versus control

As I mentioned before, the nature of the applied occupancy-related models are often claimed to determine the reliability of building performance predictions. But what does such an assertion really mean, and how can we validate it? As I mentioned before, it would be rather incoherent to expect that simulation use cases in the design phase would lead to the specific long-term predictions of a specific building's energy use. Consequently, to evaluate the occupancy model deployed (whatever kind it may be), it would be not appropriate to conduct a kind of interval for interval comparison of "predicted" and actual values of performance indicators. Rather, in such a case, the long-term comparison of modelled and actual general patterns (overall statistical resemblance) of occupants' presence and behavior appears to be more appropriate.

Imagine, on the other hand, that an occupancy-related model is intended to be deployed in the context of a predictive building systems control scenario. Thereby, one is on the lookout for a model that provides, for relatively short time horizons (let us say 24 or 48 hours) the most reliable predictions of occupancy-related events in a specific building. In such a case, the aforementioned interval by interval comparison of predicted and actual events appears to be entirely coherent

3.4.5 Reflections

I do not imply that the above – rather brief – discussion of simulation deployment scenarios and the corresponding choice of proper occupancy-related representational methods is either exhaustive or definitive. Nonetheless, it does seem to suggest that different approaches to representation of occupancy-related processes in building performance simulation may be appropriate given different application scenarios and different types of queries. If consideration of the implications of variance in input assumptions is evidently critical

to a specific performance inquiry, then properly developed and calibrated probabilistic models of occupancy presence and control actions would be necessary. On the other hand, when the objective of a simulation-based inquiry is to benchmark design proposals against applicable codes and standards or to parametrically compare design alternatives, consideration of random variations of boundary conditions and internal processes in simulation runs may be less critical – or, the intended objective of analysis could be achieved via means (such as the old-fashioned "factors of safety") that do not necessarily require the run-time execution of PR occupancy-related algorithms.

An analogous observation applies to the question of occupancy-related model evaluation. It seems to me that not only the choice of the model, but also the evaluation of how good it performs, requires the consideration of the use case and the nature of the simulation-supported queries. The way I see it, optimization of building designs does not require from a PR model to deliver faultless short-term predictions of actual occupancy processes. I suppose in this case the role of the PR model is to test – for more or less longer observational periods – the robustness of the projected design performance in the face of occupancy-related uncertainties. On the other hand, given an application scenario involving simulation-assisted predictive building systems control, the short-term predictive performance of the occupancy-related model is of critical importance. The choice of model evaluation criteria does need to consider the specifics of the simulation application case.

The sketchy discussion above obviously represents only a preliminary treatment of this matter. I suggest we need much more work and thinking toward a clear picture of the interdependence of simulation model usage and respective representations of occupancy-related phenomena.

4. Conclusion

To conclude:

- There are all kinds of good and important reasons to work toward better and more sophisticated methods of representing

people's presence and behaviour in building performance simulation applications. So the question is not if we need more advanced models. The question is how we get there.

- Simulation studies can support the understanding of a buildings' behaviour (its performance) given a number of assumptions. Treatment of the uncertainties associated with these assumptions – e.g., via uncertainty and sensitivity analyses – can be both useful and illuminating, but does not necessarily translate in provision of accurate "prediction" of the real future buildings' performance over the long run. Moreover, mapping the variance of input assumptions to the variance of simulation output is only then truly useful, when the variance of the former is empirically grounded.
- Whatever the underlying logic of an occupancy-related model (probabilistic or non-probabilistic), its reliability depends on the underlying observational data and the care with which such data has been collected and processed. Moreover, the application of a model to those kinds of cases that have not been statistically present in the model's underlying observational basis (i.e., other building types, construction, and system types, other locations and climates, other user populations, etc.) cannot be expected to yield reliable results.
- The choice of the modelling approaches and techniques, as well as the choice of model evaluation criteria are not independent of the intended purposes (application scenarios) of the building performance simulation studies. To identify one specific modelling technique and to suggest it to be applied to all stages, resolution levels, and queries in the building delivery process is reminiscent of the proverbial hammer looking everywhere for nails.

5. Acknowledgement

The present keynote address was triggered by (and greatly benefited from) multiple discussions with

many colleagues around the world, who deal with building performance simulation. Specifically, meetings and conversations in the framework of the IEA Annex 66 provided me with the opportunity to exchange thoughts and arguments regarding the benefits and challenges of various occupancy-related modelling ideas and approaches from multiple vantage points. Needless to say, the responsibility for all the stated positions and opinions lies with me. Related (and earlier) discussions of some of my views on the subjects could be also found, amongst other publications, in the small selection of the references listed below.

References

- Mahdavi, A. and F. Tahmasebi. 2015. "Predicting people's presence in buildings: An empirically based model performance analysis." *Energy and Building* 86 (2015) 349 – 355.
- Mahdavi, A. 2011. "The Human Dimension of Building Performance Simulation" (keynote). In *Proceedings of the 12th Conference of The International Building Performance Simulation Association*", edited by V. Soebarto et al. K16 - K33. ISBN: 978-0-646-56510-1.
- Mahdavi, A. 2011: "People in building performance simulation." In *Building Performance Simulation for Design and Operation*, edited by J. Hensen, R. Lamberts, 56–83. Spon Press, Taylor & Francis. ISBN: 9780415474146.

The importance of software's and weather file's choice in dynamic daylight simulations

**Laura Bellia – Department of Industrial Engineering, University of Naples Federico II –
laura.bellia@unina.it**

**Alessia Pedace – Department of Energy, Information Engineering and Mathematical Models, University
of Palermo; Department of Industrial Engineering, University of Naples Federico II –
alessia.pedace@unipa.it**

**Francesca Fragliasso – Department of Industrial Engineering, University of Naples Federico II –
francesca.fragliasso@unina.it**

Abstract

The prediction of daylight availability in indoor environments is nowadays an extremely relevant topic in the design practice for many reasons: it affects the design of the electric lighting system and therefore the calculation of the related energy consumption; it also has an impact on evaluation of comfort. Dynamic daylight simulations are a helpful tool to predict daylight availability in indoor environments and consequently to evaluate the possible reduction in energy consumptions. However, there are different software packages that perform dynamic daylight simulations and they use different engines and calculation methods which may be a source of differences in the results. Moreover this type of analysis requires a weather data file of the building's location to be performed. Since there are many of them available, which are developed from historical sets of weather measurements using different methods, the use of one or another can affect the simulations' results. Therefore in this paper an example of the impact on dynamic daylight simulations' results of different weather data files (IWEC, Meteonorm, TRY and Satel-Light) and different software (Daysim and 3ds Max Design®) will be reported.

1. Introduction

The reduction of energy consumption is an extremely important topic in the field of building design. Lighting design is also involved in the pursuit of this goal since, by maximizing the use of daylight (while avoiding overheating and glare), the use of electric light is reduced as well as the heating and cooling loads.

Software simulations are an extremely helpful tool to evaluate the energy consumption of different design options but daylight simulations present a series of problems.

The first problem concerns the approach to daylight simulations: static or dynamic. The static approach is based on the calculation of the daylight factor (DF) (Waldram, 1950; Moon & Spencer, 1942) and it has been criticized over the years.

The dynamic approach is based on dynamic daylight simulations and dynamic daylight metrics: Daylight Autonomy (DA) (Reinhart & Walkenhorst, 2001), Continuous Daylight Autonomy (DAcon) (Rogers, 2006), Useful Daylight Illuminances (UDI) (Nabil & Mardaljevic, 2005 and 2006). This approach allows us to better analyze daylight availability (Mardaljevic et al., 2009). Moreover the use of these metrics is recommended by some new laws and green building rating systems. In particular the IESNA introduced the use of Spatial Daylight Autonomy (sDA) and Annual Sunlight Exposure (ASE) (IES LM-83-12, 2013), and the USGBC set them as

evaluation parameters in the LEED protocol (USGBC, 2014).

There are different software packages that allow us to perform dynamic daylight simulations and they use different engines and calculation methods. Therefore the use of one software or another may affect the results.

Moreover calculation software needs a weather data file referring to the environment's location to perform the simulation. For a given location, different files may be available and final results obviously depend on the weather data used as input. The effects of the use of different weather data files referred to the same location on daylight simulation results have not been widely studied (Iversen et al., 2013).

Given these principles, the goal of this paper is on one hand to investigate differences in simulation results provided by different software and, on the other hand, to compare final results obtained by using the same software but different weather data file.

The simulations were carried out modelling a simple environment with a south-facing window and located in Rome (Italy). The comparison between software was carried out using Daysim and 3ds Max Design®. The choice of the latter software was made because, contrary to Daysim, it has not been widely studied and so far only one research project on it has been carried out (Reinhart & Breton, 2009). For these simulations IWEC data file was used.

For the analysis of differences in simulation results obtained with different weather files, the simulations were performed using only Daysim software and four different weather files: IWEC, Meteonorm, Satel-Light and TRY.

2. Simulations

2.1 Method

The geometric characteristics of the room and the analysis grid (3m x 3m) can be seen in Figure 1.

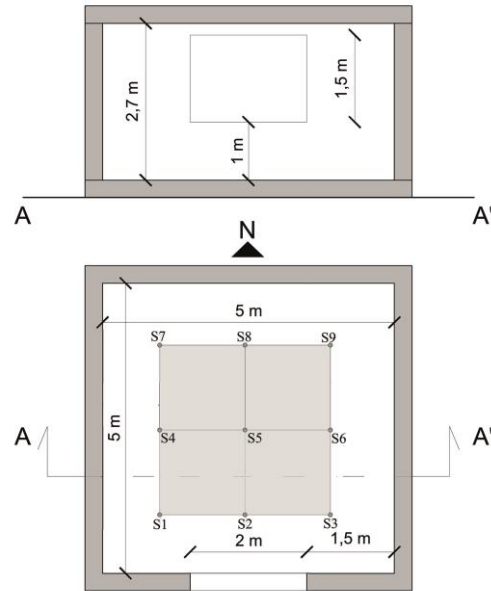


Fig. 1 – Model's measured plan and section

The room has only a south-oriented window with a double pane glazing (4-16-4 mm), characterized by a visual transmission equal to 82%.

The reflectances of the internal surfaces in the modelled environment are the following: walls 65%; floor 30%; ceiling 80%. A ground plane (45 x 45 m) was also modelled with a 20% reflectance.

300 lux is the target illuminance considered on the workplane (EN 12464-1 Light and Lighting of work places - Part I: Indoor work places, 2011). Annual daylight simulations were carried out considering an occupancy schedule that goes from Monday to Friday from 8:00 to 16:00 without breaks; Daylight Saving Time goes from April 1st to October 31st.

2.2 Software information

Daysim is one of the most widespread and studied software for dynamic daylight simulations and, like the majority of this type of software, it is based on the Radiance simulation engine. The simulation parameters are seen in Table 1.

Table 1 – Daysim simulation parameters

Parameter	Value
Ambient bounces	7
Ambient divisions	1500
Ambient super samples	100
Ambient resolution	300
Ambient accuracy	0.05
Limit reflection	6
Specular threshold	0.1500
Specular jitter	1.0000
Limit weight	0.004000
Direct jitter	0.0000
Direct sampling	0.200
Direct relays	2
Direct pretest density	512

3ds Max Design® is not based on Radiance but on the Exposure® technology and, starting from its 2009 release, it includes the possibility of performing static and dynamic daylight simulations. The simulation parameters referred to 3ds Max Design® can be seen in Table 2.

Table 2 – 3ds Max Design® simulation parameters

Render Rollout	Dialog Section	Parameter
Rendering Algorithms	Scanline	Off
Rendering Algorithms	Raytracing	On Max Trace Depth, Reflections, Refractions : 10
Shadows & Displacement	Shadows	On Mode: Simple
Final Gather	Advanced	Noise Filtering: None Max Depth, Reflections, Refractions: 10 Use Falloff (Limit Ray Distance): Off
Final Gather	FG Point Interpolation	Use Radius Interpolation Method: Off
Caustics & Global Illumination	Caustics	Off
Caustics & Global Illumination	Global Illumination	Off

2.3 Weather data files information

To carry out this study, four weather data files were selected: IWEC, Meteororm, TRY and Satel-Light. Generally, weather data files represent a typical year, which includes 8760 hourly data that provide typical meteorological characteristics of a given location. These hourly data are deduced from historical sets of annual weather measurements (at least 20 years) using different statistical calculation processes. This is the case of IWEC, Meteororm and TRY weather data files. IWEC files are freely available online (U.S. Department of Energy, Energy Efficiency & Renewable Energy) and were developed by ASHRAE (ASHRAE, 2001); these weather data files

are built selecting the most representative months from up to 18 years of data using a statistical method.

Meteonorm weather files can be bought online (Meteonorm) and are generated from data obtained by meteorological stations using a stochastic model to build a typical year.

The European Test Reference Years were developed under contract of the Commission of the European Communities in Brussels. A TRY file is built from a true sequence of 12 months of measured weather data (CEC, 1985) using a statistical method named "Belgian".

A separate discussion has to be had for Satel-Light. This database was funded by the European Union to generate a European solar radiation database based on data measured by Meteosat satellites. At the present time it only includes the years from 1996 to 2000, so it is not possible to derive a typical year.

Nonetheless comparing the results obtained using Satel-Light with those achieved using the other weather files can give interesting insights about if and how a typical year differs from a real one. Therefore to perform this study the year 1998 was chosen from the Satel-Light database to build a weather file to use as input in the simulation software, for the other weather data files (IWEC, TRY and Meteonorm) the available files for Rome were used.

3. Discussion and results analysis

Both the comparison between the results obtained from the different weather data files and that obtained with the two software packages were carried out referring only to sensors S2, S5 and S8 (see Figure 1). Moreover in some of the graphs reported in this section, the following abbreviations will be used: I for IWEC file, M for Meteonorm, T for TRY, S for Satel-Light, 3ds for 3ds Max Design® and D for Daysim, $E_{glob-3ds}$ and E_{glob-D} for global illuminances referred respectively to 3ds Max Design® and Daysim, $E_{dir-3ds}$ and E_{dir-D} for direct illuminances referred respectively to 3ds Max Design® and Daysim.

3.1 Software comparison

The analysis of the results obtained using the two software was carried out by comparing them in terms of global and direct components of daylight (since the diffuse component can be obtained as a difference of these two) and dynamic daylight metrics (UDI).

Figure 2 shows cumulative frequency for which the percentage ratio $|E_{glob-3ds} - E_{glob-D}| / E_{glob-3ds}$ is lesser or equal to certain values on the x axis.

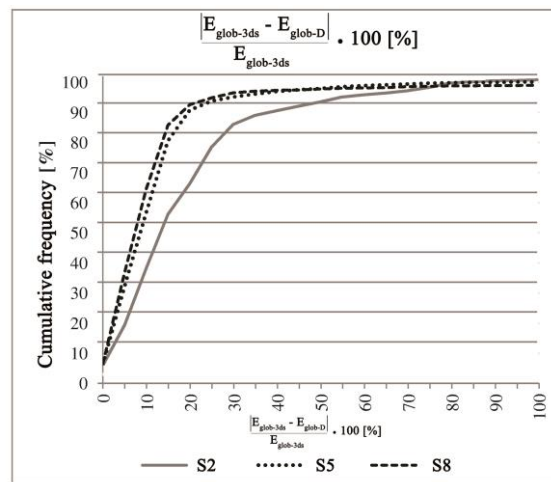


Fig. 2 – $|E_{glob-3ds} - E_{glob-D}| / E_{glob-3ds} \cdot 100$ calculated for each sensor

It can be observed that S5's and S8's trends are quite similar whereas S2's trend differs. For S5 and S8m, differences are lower than 20% for 90% of the year whereas for S2 only for 60% of the year. This may depend on a different calculation of the direct component of daylight since S2 is the sensor closest to the window and therefore the contribution of direct daylight is more significant.

Figure 3 shows the annual frequencies for which only Daysim, only 3ds Max Design® or both softwares calculate the presence of the direct component of daylight.

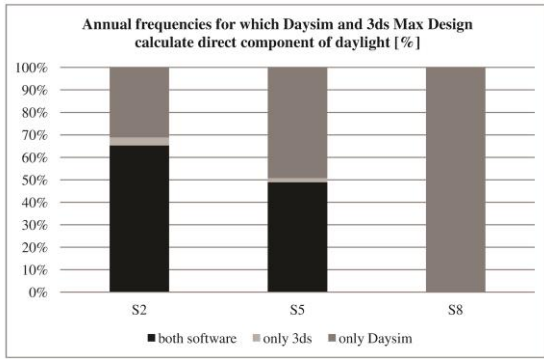


Fig. 3 – Annual frequencies for which Daysim and 3ds Max Design calculate direct component of daylight

It is interesting to highlight that the percentage of the year during which only 3ds Max Design calculates the presence of the direct component of daylight is small and for S8 is even equal to zero and only Daysim calculates the presence of the direct component of daylight.

For S2 during the greater part of the year both softwares predict the presence of direct daylight whereas for S5 only Daysim calculates it for the majority of times. To further analyze differences in direct daylight calculation, Figure 4 was developed. It shows the cumulative frequencies for which the percentage ratio $|E_{dir-3ds} - E_{dir-D}| / E_{dir-3ds}$ is less or equal to the values on the x axis. These cumulative frequencies were calculated considering only the hours during which both softwares calculate the presence of the direct component of daylight. For this reason in the graphs there are only the curves related to S2 and S5 since, as was demonstrated in Figure 3, for S8 only Daysim calculates the presence of direct daylight.

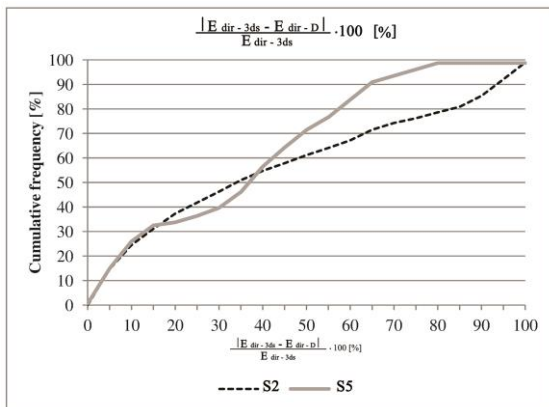


Fig. 4 – $|E_{dir-3ds} - E_{dir-D}| / E_{dir-3ds} \cdot 100$ calculated for each sensor

The trends related to the two sensors vary considerably and if a percentage difference equal to 30% is taken as a reference, the corresponding cumulative frequency is about 38% for S5 and about 48% for S2.

Figure 5 shows UDI values calculated for each sensor and software. As for the weather file comparison, it was decided to divide UDI in four steps.

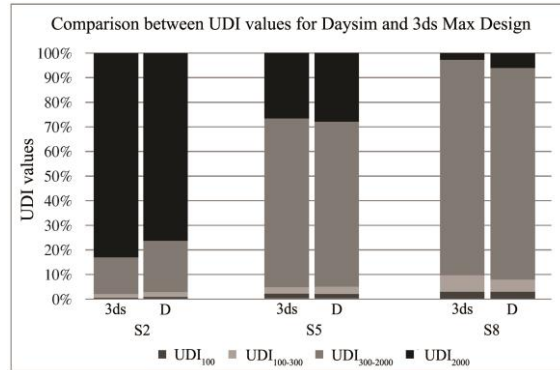


Fig. 5 – UDI values calculated with each software

It is interesting to notice that the greatest differences between the two softwares can be found between UDI₂₀₀₀ values.

For S2 (the sensor closest to the window) 3ds Max Design® calculates values higher than Daysim ones whereas for S8 (the sensor farthest from the window) the opposite is true. However, in all the cases the differences are quite limited.

3.2 Weather data files comparison

The comparison between the results obtained with the different data files was carried out by analyzing global and diffuse irradiances, Annual and Monthly Light Exposures and UDI.

Figure 6 and 7 show, for each weather data file, cumulative frequency curves referred to global and diffuse irradiances.

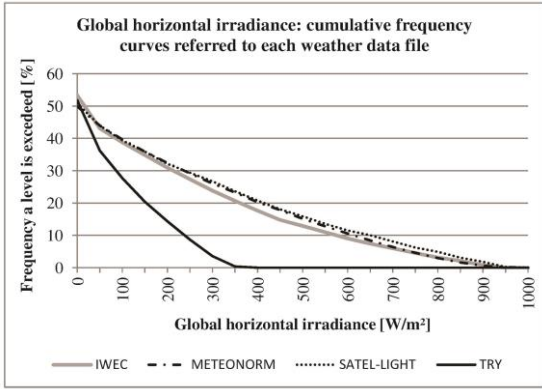


Fig. 6 – Cumulative frequency curves for global horizontal irradiance

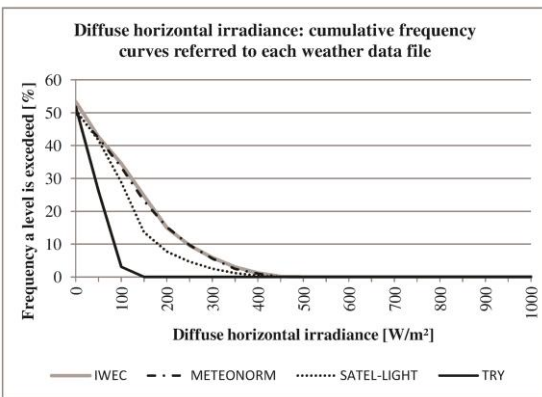


Fig. 7 – Cumulative frequency curves for diffuse horizontal irradiance

What is interesting to notice is that TRY weather files always show values considerably lower than those referred to the other files. IWEC and Meteornorm show almost coincident diffuse irradiance's trends whereas for global irradiance there is more difference. However, it has to be pointed out that IWEC, Meteornorm and Satel-Light have really close trends.

Figure 8 shows Annual Light Exposures calculated for each weather file and sensor.

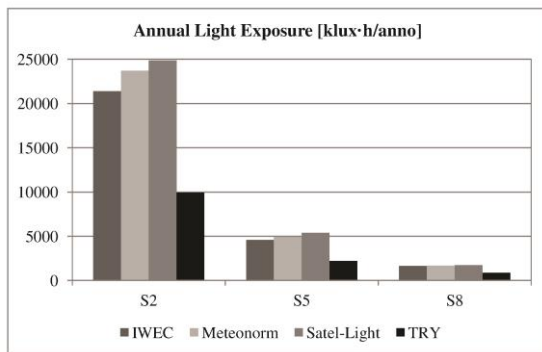


Fig. 8 – Annual Light Exposures for each weather file and sensor

Again, it can be noted that TRY values are remarkably lower than those related to the other weather files. It is also interesting to highlight that Annual Light Exposures calculated for Meteornorm and Satel-Light are almost coincident for all the sensors while IWEC's values are always a little lower.

Figures 9a,b,c show Monthly Light Exposures calculated for each sensor and weather data file.

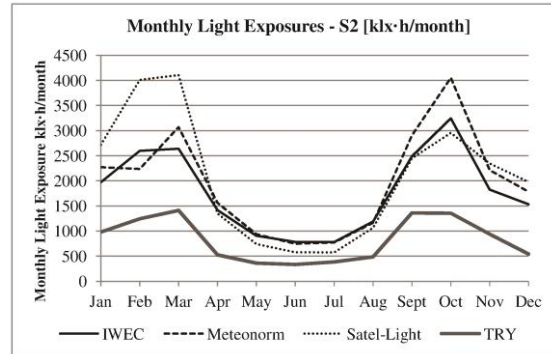


Fig. 9a – Monthly Light Exposure for S2

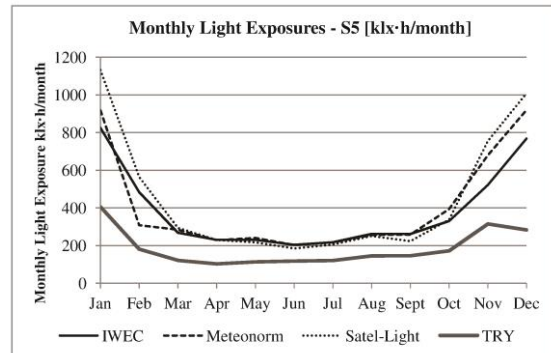


Fig. 9b – Monthly Light Exposure for S5

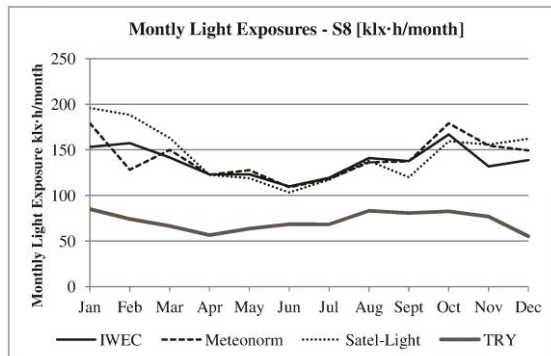


Fig. 9c – Monthly Light Exposure for S8

It is interesting to observe that the trends remain similar for the sensors farthest from the window and that only the order of magnitude varies.

In more detail, TRY again shows the lowest values and IWEC, Meteonorm and Satel-Light ones are very close from March to September. During the other months, differences increase and reach their maximum values in December and January.

Figure 10 shows the comparison between UDI values calculated for each sensor and weather data file. UDI were divided in four steps: $E < 100$, $100 < E < 300$, $300 < E < 2000$, $E > 2000$. This choice was made in order to perform a more detailed analysis of daylight variation inside the room.

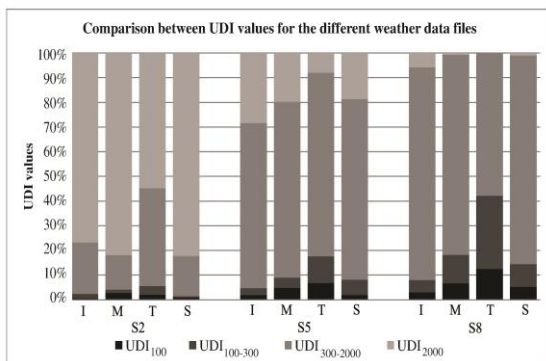


Fig. 10 – UDI values calculated with the different weather data files

One of the most evident findings is that the use of TRY determines results that are very different from those obtained with the other weather data files. In more detail, the greatest differences are observed for $UDI_{100-300}$ for which TRY always calculates values considerably higher than those related to the other weather data files.

With regard to IWEC, Meteonorm and Satel-Light weather files, differences are more limited. It is interesting to notice that Meteonorm always determines UDI_{100} values slightly higher than IWEC and Satel-Light ones; moreover, Meteonorm and Satel-Light determine almost coincident $UDI_{300-2000}$ values.

4. Conclusion

From the results reported in the previous sections, it can be stated that for the examined case the use of IWEC, Meteonorm and Satel-Light weather files determines results with small differences. The

same conclusion does not apply to TRY weather file, which always shows results considerably lower than those obtained using the other weather files.

The analysis of differences in simulation results obtained with Daysim and 3ds Max Design® highlighted that these differences vary much depending on a sensor's position.

In more detail, the greatest differences are found for the sensors located in positions where the contribution of direct daylight is more significant. Indeed, it was found that generally Daysim calculates the presence of the direct component of daylight for a greater number of hours compared to 3ds Max Design®.

However, it is important to highlight that when analyzing UDI values, differences are reduced both in the case of software and weather data file comparison.

Differences in results can affect both the prevision of energy savings due to daylight and the evaluation of visual discomfort, consequently a progression of this research project would be beneficial

Further investigation into the two topics should include the analysis of other locations, exposures and weather data files as well as comparisons between the results obtained from the simulations and field measurements.

References

- ASHRAE. 2001. *International Weather for Energy Calculations (IWEC Weather Files) Users Manual and CD-ROM*. Atlanta: ASHRAE.
- CEC. 1985. *Test Reference Year TRY Weather Data Sets for Computer Simulations of Solar Energy Systems and Energy Consumption in Buildings*. Commission of the European Communities, Directorate General XII for Science, Research and Development.
- EN 12464-1 Light and Lighting - Lighting of work places - Part I: Indoor work places. 2011.
- IES LM-83-12 "Approved Method: IES Spatial Daylight Autonomy (sDA) and Annual Sunlight Exposure (ASE)", 2013.
- Iversen A, Svendsen S. and Nielsen T. 2013. "The effect of different weather data sets and their

- resolution on climate-based daylight modelling". *Lighting Research & Technology*, no. 45, p. 305–316.
- Mardaljevic J., Heschong L. and Lee E. 2009. "Daylight metrics and energy savings," *Lighting Research Technology*, no. 41, p. 261–283.
- Meteonorm. Accessed November 8, 2014, <http://meteonorm.com/>.
- Moon P., Spencer D. 1942. "Illumination form a non-uniform sky". *Illuminating Engineering Society*, no. 37, pp. 707-726.
- Nabil A., Mardaljevic J. 2005. "Useful Daylight Illuminance: A New Paradigm to Access Daylight in Buildings". *Lighting Research & Technology*, n. 37(1), pp. 41-59.
- Nabil A., Mardaljevic J. 2006. "Useful Daylight Illuminances: A Replacement for Daylight Factors". *Energy and Buildings*, n. 38(7), pp. 905-913.
- Reinhart C., Walkenhorst O. 2001. "Dynamic RADIANCE-based Daylight Simulations for a full-scale Test Office with outer Venetian Blinds". *Energy & Buildings*, no. 33(7), pp. 683-697.
- Reinhart C. R., Breton P.-F. 2009. "Experimental Validation of Autodesk® 3ds Max® Design 2009 and Daysim 3.0." *LEUKOS: The Journal of the Illuminating Engineering Society of North America* (6), 7-35.
- Rogers Z. 2006. "Daylighting Metric Development Using Daylight Autonomy Calculations In the Sensor Placement Optimization Tool". Accessed November 7, 2014, <http://www.archenergy.com/SPOT/download.html>.
- Satel-Light, the European database of Daylight and Solar Radiation. Accessed November 8, 2014, <http://www.satel-light.com/core.htm>
- U.S. Department of Energy, Energy Efficiency & Renewable Energy. Accessed November 10, 2014, http://apps1.eere.energy.gov/buildings/energyplus/weatherdata_about.cfm.
- USGBC (2014). LEED Reference Guide for Building Design and Construction (v4). US Green Building Council. Accessed November 13, 2014, <http://www.usgbc.org/resources/leed-reference-guide-building-design-and-construction>.
- Waldram P. 1950. "A Measuring Diagram for Daylight Illumination". London: B T Batsford Ltd.

Outdoor Comfort: the ENVI-BUG tool to evaluate PMV values point by point

Kristian Fabbri – Department of Architecture – University of Bologna (Italy)

Antonello Di Nunzio – School of Architecture – University of Bologna (Italy)

Ernesto Antonini – Department of Architecture – University of Bologna (Italy)

Andrea Boeri – Department of Architecture – University of Bologna (Italy)

Abstract

Studies on Outdoor Comfort in urban open spaces adopt several tools and software to simulate a microclimate model, energy performance and the fluid-dynamics of winds. The output data, therefore, of these software solutions, e.g. temperature, wind velocity, relative humidity, should be the input data to evaluate the comfort indexes. In the present paper, we describe ENVI-BUG, an ENVI-met algorithmic app developed by Grasshopper, that uses the LadyBug method to rapidly calculate the distribution of local PMV.

1. Introduction

The Building Simulation Application research fields include three points of view:

- a) a study from an energetic point of view e.g. the energy needed by building envelopes, or only envelope systems, HVAC components, building control, etc.;
- b) the study of the effect of human behaviour and user behaviour on building energy consumption; also included in this field are the laws and regulations for the effectiveness on energy policies for the building and real estate sectors;
- c) the study of the effect of buildings on human comfort, thermal comfort, Indoor Air Quality, Indoor Environmental Quality, Lighting, Acoustic, etc.

Therefore, in Building Simulation another kind of comfort and building effect on human comfort could be considered: outdoor comfort simulation.

Outdoor Comfort is a specific field of study and is

combined with the Urban Heat Island (UHI) phenomenon; in other words, if the outdoor temperature increases, the UHI increases. Therefore, energy consumption by HVAC in cooling mode increases, because people prefer to stay inside buildings rather than in outdoor open spaces. Following this point of view, a greater understanding of outdoor comfort could increase the use of outdoor open spaces.

Outdoor comfort depends on the Built Environment, on the relationship between materials and energy use, on Global Climate change and local micro-climate: Temperature, Solar Radiation, Wind distribution, Wind Speed, Absolute and Relative Humidity.

The relationship between energy and climate in the urban building environment and the factors that influence the Urban Heat Island are described in several studies, some of these summarised by M. Santamouris (Santamouris, 2011), G.M. Stavrakakis et al. (Stavrakakis, 2012) and in RUROS by CRES (CRES 2014).

The main common software solutions to model outdoor comfort, also described in Dessì V. (Dessì, 2008) and UHI-CE Project, are:

- ENVI-met, is a three-dimensional microclimate model designed to simulate the surface-plant-air interactions in an urban environment with a typical resolution of 0.5 to 10 m in space and 10 sec in time. Typical areas of application are Urban Climatology, Architecture, Building Design or Environmental Planning, etc. ENVI-met is a prognostic

model based on the fundamental laws of fluid dynamics and thermo- dynamics;

- RayMan is a freely available radiation and human bioclimate model. The model simulates the short and long-wave radiation flux densities from the three-dimensional surroundings in simple and complex environments, described in Matzarakis et.al. (Matzarakis, 2007);
- SkyHelios (Tzu-Ping Lin, 2012) is a tool for applied climatology, calculating the continuous sky view factor and sunshine duration in high spatial and temporal resolution for each point in a complex area.

All the software above requires expert users - it is not simple to use – therefore not useful during the design-process.

2. Goal of paper

In this paper, we describe a tool to support designers in order to evaluate Outdoor Thermal Comfort, by PMV index, in 3-D. The new tool, called ENVI-BUG, is used to model outdoor comfort and combines ENVI-met and LadyBug input data.

3. Methodology and software solutions

The methodology developed concerns a contemporary use of three kinds of software:

- ENVI-met, to obtain microclimate data distribution in outdoor spaces;
- LadyBug. Rhinoceros and Grasshopper to develop ENVI-met data in 3-D and to input data by human body to evaluate a PMV index;
- ENVI-BUG to see 3-D results.

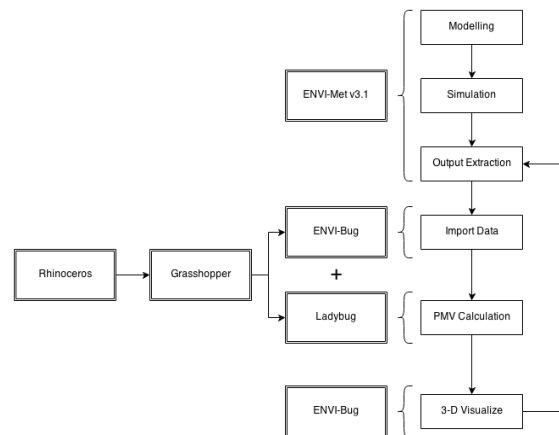


Fig. 1 – ENVI-BUG flow chart

3.1 ENVI-Met and LadyBug

ENVI-met software is a freeware to analyse the outdoor microclimate around a single building, an open space or a neighbourhood. It is possible to visualize ENVI-met results with the Leonardo application. The result is a 2D coloured planimetry or section, in which each colour corresponds to a range value.

LadyBug software is an open source environmental plugin for Grasshopper3D that helps architects and engineers create an environmentally conscious architectural design. LadyBug imports standard EnergyPlus Weather files (.EPW) into Grasshopper and provides a variety of 3D interactive graphics to support the decision-making process during the initial stages of design. LadyBug was developed by Mostapha Sadeghipour Roudsari. (Sadeghipour Roudsari, 2013),

3.2 ENVI-BUG

ENVI-BUG Software is a generative algorithm (or plugin) that combines ENVI-met, Rhinoceros, Grasshopper and LadyBug.

The aim of ENVI-BUG is to obtain 3-D output results of ENVI-met and to simulate a punctual distribution of PMV, in 3D space, with several human body and clothes data.

In order to use ENVI-met and ENV-bug, we need to arrange (Figure 4):

- the “file folder” (called OUT_ENVIMET_CSV) where we will save all input data file. In order to allow the plugin to make a complete file directory, the file must be a test (*.csv) file;
- the Rhinoceros file (*.3dm), of the case study, because Grasshopper can only run after Rhinoceros has started. The ENVI-BUG files are in *.3dm in order to:
 - o save any 3-D geometry, tree or graphics changed;
 - o insert a “model-man” to represent punctual PMV;
- the Grasshopper file (*.gh) with ENVI-BUG plugin.

To start ENVI-BUG, we must to drag “ENVI-BUG.gh” into the Grasshopper Canvas.

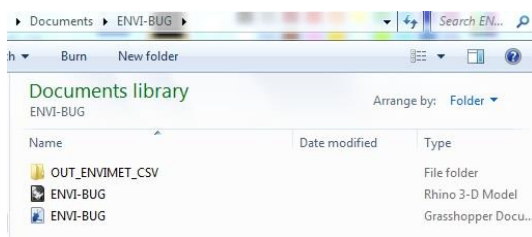


Fig. 2 – File folder for ENVI-BUG

4. Modelling results

ENVI-Met v3.1 includes 4 output modules: Configuration Editor, ENVIEddi, LEONARDO 3.75 and “Xtract tool”. The “Xtract tool” is to export output data.

The ENVI-BUG permits two kinds of simulation for the PMV index:

- a) Plan-space distribution - in this case we need to set ENVI-met “Xtract tool” with the human body at a height of 1.6 m. Then we need to export file data into the *.csv file.
- b) Urban Canyon (section) simulation - in this case we need to set an ENVI-met section, then use “Xtract tool” to export file data into the *.csv file.

The above extraction will be done for each variable: air-temperature, wind speed, mean

radiant temperature, Relative Humidity. The Open space (building, place, train, people etc.) must be simulated in 3-D with Rhinoceros.

When we start ENVI-BUG, it instantly reads the *.csv data in the OUT_ENVIMET_CSV folder and subsequently converts data into point grid values. Then the above grid is visualized in Rhino Viewport and each grid node has a PMV number (Figure 3).



Fig. 3 – The 3-Dimension visualization of PMV vectors (z)

5. Case-study and results

An example of ENVI-BUG application is discussed in the following paragraphs.

The case study is a Social Housing District called “Pilastro” located in Bologna (44.511°N, 11.397°E).

The scenarios are:

- a) the Actual Condition of things of Urban Canyon, the Height/Width ratio is 1, the track road and car parks are in asphalt; the vertical building surface has several textures and colours (red, grey and white);
- b) the Designed/Simulated Condition, concerns the horizontal surface of Urban Canyon, especially if we simulate:
 - a new road (one way) instead of a car-park;
 - a substitution of the current road with grass.



Fig. 4 – Case Study portion of “Pilastro District”

5.1 Results of PMV indexes in Horizontal Distribution

The Analysis of Actual Condition (a) reports a homogeneous zone of maximum discomfort in the central area. The main discomfort is when human body activity is just 1 met (sitting).

Figures 5.a, 5.b show the results of PMV distribution in Actual Condition within the space of urban canyon, for human body activities: Sitting (a), Standing (b)

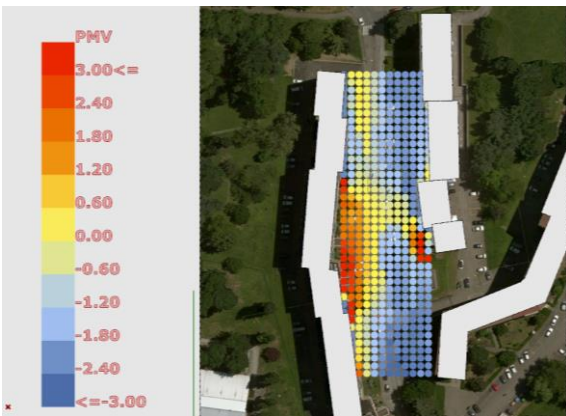


Fig. 5.a – Actual Condition of PMV Distribution – Metabolic Activity: Sitting (1 met)

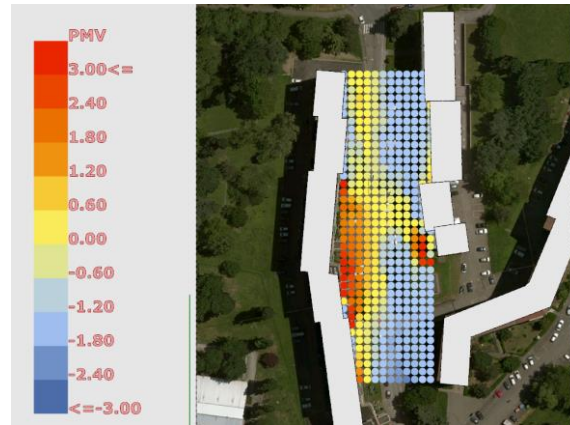


Fig. 5.b – Actual Condition of PMV Distribution – Metabolic Activity: Standing (1.2 met)

The results of (b) Designed/Simulated Condition show a decrease of the discomfort area.

Figures 6.a, 6.b show results of PMV distribution for human body activities: Sitting (a), Standing (b), Walking 2mph (c)

As shown in the case of Walking, the discomfort area is larger than the Sitting or Standing activities, depending only on metabolism (met). In spite of this, Figure 14.c of the Simulated Condition shows a lower discomfort compared with the Actual Condition.

In the case of Sitting, the comfort condition, before and after simulation, shows a decrease in the discomfort-area.

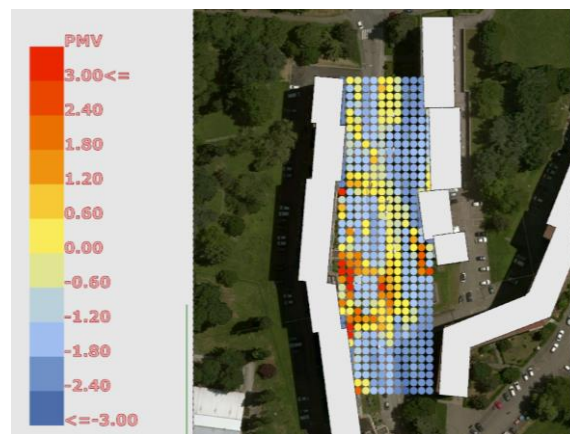


Fig. 6.b – Design Condition of PMV Distribution – Metabolic Activity: Standing (1.2 met)

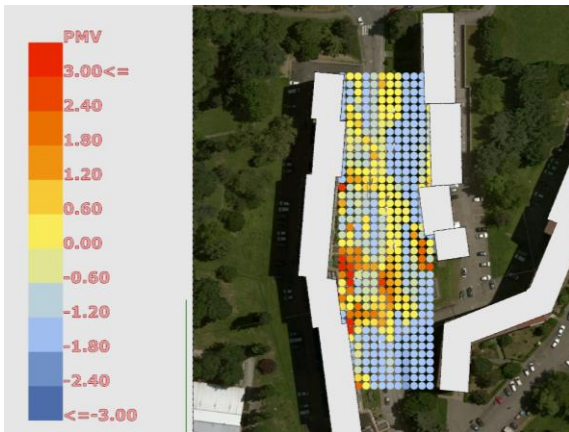


Fig. 6.b – Design Condition of PMV Distribution – Metabolic Activity: Standing (1.2 met)

6. Conclusions

The present outdoor comfort simulation tools – like ENVI-met – show some lack of usefulness and interface with the users.

This study describes a new tool to improve ENVI-met use, in order to simulate several input data and to show the spatial distribution of PMV.

In order to make and to assess design choices, it is better to have a good graphic visualization of the results.

References

- CRES. 2004. RUROS - Rediscovering the Urban Realm and Open Spaces. CRES (Centre for Renewable Energy Sources) Buildings Department, 2004, ISBN: 960-86907-2-2, <http://alpha.cres.gr/ruros>
- Dessi, V. 2008. Use of simplified tools to evaluate thermal comfort in urban spaces in the teaching experience. In 25th Conference on Passive and Low Energy Architecture (PLEA) Dublin, 22 and 24 October 2008
- ENVI-met <http://envi-met.com/>
- Matzarakis Andreas, Rutz Frank, Mayer Helmut. 2007. Modelling radiation fluxes in simple and complex environments—application of the RayMan model, International Journal of Biometeorology. (51) 323–334, DOI 10.1007/s00484-006-0061-8
- Santamouris, M. 2011. Energy and climate in the urban built environment, Routledge, First

edition 2001 James & James (Science publisher), ISBN 978-1-873936-90-0

Sadeghipour Roudsari Mostapha, Smith Adrian, 2013, LADYBUG: a parametric environmental plugin for Grasshopper to help designers create and environmentally conscious design, Proceedings of BS2013 13th Conference of International Building Performance Simulation Association, Chambèry, France, August 26-28, pg.3128-3135

Stavarakakis G.M., Tzanakic E., Genetzaki V.I., Anagnostakis G., Galetakis G., Grigorakis E. 2012. A computational methodology for effective bioclimatic-design applications in the urban environment. Sustainable Cities and Society 4. (2012) 41– 57

Tzu-Ping Lin, Kang-Ting Tsai Ruey-Lung Hwang, Andreas Matzarakis. 2012. Quantification of the effect of thermal indices and sky view factor on park attendance, Landscape and Urban Planning Volume 107, Issue 2, August 2012, Pages 137–146

UHI Project aims at developing mitigation and risk prevention and management strategies concerning the urban heat island (UHI) phenomenon. <http://eu-uhi.eu/>

Aspects of uncertainty in representation of occupants' diversity in building performance simulation

Ardeshir Mahdavi – Department of Building Physics and building Ecology, Vienna University of Technology – amahdavi@tuwien.ac.at

Farhang Tahmasebi – Department of Building Physics and building Ecology, Vienna University of Technology – farhang.tahmasebi@tuwien.ac.at

Abstract

Recently, increased efforts have been invested to enhance the sophistication of occupancy modelling approaches in building performance simulation. However, the effectiveness of such approaches depends on the robustness of the underlying empirical information. Thereby, an important question pertains to the existence and level of inter-individual differences in occupancy patterns. In the present contribution, we use a repository of monitored occupancy data in an office building to address this problem empirically. The results of the study facilitate a discussion of the diversity in observed occupancy profiles and the implications for relevant occupancy models in building performance simulation.

1. Introduction

Given the impact of occupants on building performance, modelling occupants' presence and behaviour is one of the critical topics in the studies pertaining to building performance simulation (Mahdavi 2011). Specifically, numerous libraries of typical occupancy profiles (see, for example, ASHRAE 2013, Davis et al. 2010, Duarte et al. 2013) and a number of probabilistic and non-probabilistic models (e.g., Reinhart 2001, Page et al. 2008, Richardson et al. 2008, Mahdavi et al. 2015) have been proposed to represent the complex nature of occupancy patterns in building performance simulation tools. In this context, one important open question concerns the differences between building occupants with regard to their patterns of presence. Independent of the characteristics of the proposed and applied occupancy models, the diversity of occupants and its implications must be addressed, lest systematic

representation of occupancy processes in building performance simulation would not be warranted.

While extensive and comprehensive occupancy information is rarely available for model development purposes, systematic statistical analyses of existing data can improve the state of art in consideration of occupancy diversity in respective modelling efforts. Knowledge of the diversity among the occupants and corresponding models could also help to bring about a proper balance between simulation accuracy and computational costs by selecting the optimum sample size and targeting for the suitable complexity level in occupancy-related models.

Given this background, the present study focuses on the extent of uncertainty related to occupancy related events in office buildings (e.g., arrivals, short-term absences, departures). Specifically, observational occupancy data are used to explore if and to which extent event-related uncertainties may be influenced by the diversity of individual occupancy patterns. Toward this end, occupancy-related data obtained from a university campus office area were subjected to statistical analysis. The office area is equipped with a monitoring infrastructure and accommodates a number of staff in administrative and academic positions. Long-term high-resolution monitored occupancy data from a number of workspaces in this office area was obtained.

2. Methodology

For the purpose of the present study, we use data obtained from an office area in a university

building in Vienna, Austria. This office area is equipped with a monitoring infrastructure to continuously collect data on indoor environmental conditions, state of devices (luminaires, radiators, windows and doors), and occupancy (presence). Specifically, we present and discuss here data regarding the presence of eight occupants who work in this area. The occupants include both academic and administrative staff, and both faculty members and graduate students. The area layout includes a single-occupancy closed office, two single-occupancy semi-closed offices, and an open plan office area.

The occupancy data have been obtained via wireless ceiling-mounted sensors (motion detectors). The internal microprocessors of the sensors are activated within a time interval of 1.6 minutes to detect movements. The resulting data log entails a sequence of time-stamped occupied to vacant (values of 0) or vacant to occupied (values of 1) events. To facilitate data analysis, the event-based data streams were processed to generate 15-minute interval data. This procedure derives the duration of occupancy states (occupied / vacant) from the stored events and returns the dominant occupancy state of each interval. Occupancy periods before 8:00 and after 19:45 were not included in the study to exclude, amongst other things, the presence of janitorial staff at the offices. Occupancy data for a 35-month period (April 2011 to February 2014) were used to conduct the current study.

Data was analysed via basic means of visualisation and descriptive statistics. The results are expressed in terms of the following indicators:

- First arrival time (FA)
- Last departure time (LD)
- Occupancy duration (OD)
- Number of transitions (NT)

The first arrival time (FA) and last departure time (LD) are derived by detecting the first and last occupied 15-min intervals in a day. The occupancy duration (OD) is calculated by counting the number of occupied intervals in a day. Number of transitions (NT) represents the number of daily occupied-to-vacant transitions.

Note that, given the very small number of occupants, the present analysis is merely of exploratory nature. The idea is to obtain a first impression of the critical issues and examine the structure of the research conducted as a starting framework for future – more detailed and more comprehensive – studies.

3. Results

Table 1 summarizes the eight occupants' presence monitoring results in terms of six basic statistics, namely mean, standard deviation, coefficient of variation (CV), median, mode, and interquartile range for the four indicators (FA, LD, OD, and NT). Despite the small number of occupants, the values of the four indicators for all occupants were displayed in terms of box plots. Figures 1 and 2 provide two instances of such box plots (for FA and NT).

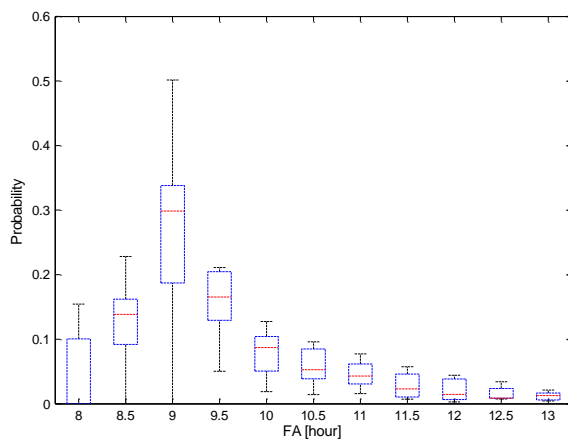


Fig 1 – First arrival time boxplot

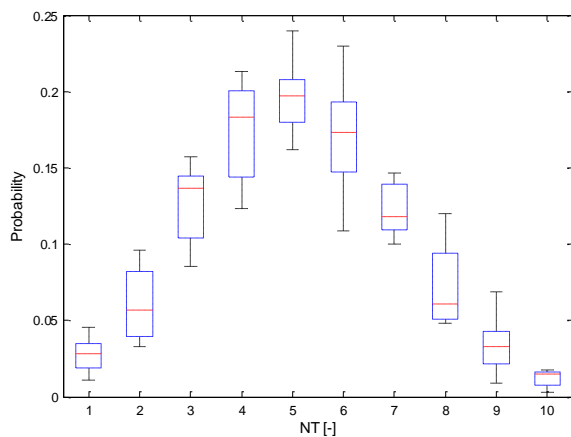


Fig. 2 – Number of transitions boxplot

Table 1 – Summary of the statistical analysis results

Indicators	Statistical measures	Occupants							
		P1	P2	P3	P4	P5	P6	P7	P8
FA	<i>mean</i>	11.1	8.7	9.7	9.8	9.6	10.0	10.0	9.4
	<i>median</i>	10.75	8.25	9.25	9.50	9.25	9.50	9.63	9.25
	<i>standard deviation</i>	1.2	1.1	1.2	1.3	1.4	1.4	1.4	0.8
	<i>mode</i>	10.8	8.3	8.8	9.3	9.3	9.3	9.0	9.3
	<i>CV</i>	0.11	0.13	0.13	0.13	0.15	0.14	0.14	0.08
	<i>IQR</i>	0.75	0.75	1.00	1.00	1.00	1.50	1.75	0.50
LD	<i>mean</i>	18.0	16.7	18.2	18.0	17.7	17.6	18.3	16.2
	<i>median</i>	18.25	17.00	18.50	18.50	18.25	17.75	18.50	16.50
	<i>standard deviation</i>	1.4	0.9	1.6	1.7	1.8	1.7	1.2	1.2
	<i>mode</i>	18.8	17.3	20.0	19.3	19.0	17.8	18.8	17.3
	<i>CV</i>	0.08	0.05	0.09	0.09	0.10	0.09	0.07	0.07
	<i>IQR</i>	1.88	0.75	2.00	2.00	2.25	2.00	1.25	1.25
OD	<i>mean</i>	3.3	4.4	4.0	3.9	3.7	3.4	3.9	3.2
	<i>median</i>	3.25	4.50	4.00	3.75	3.75	3.25	3.75	3.25
	<i>standard deviation</i>	1.3	1.4	1.4	1.5	1.4	1.3	1.2	1.0
	<i>mode</i>	3.0	4.8	4.3	3.3	3.8	3.3	3.5	2.5
	<i>CV</i>	0.40	0.31	0.36	0.37	0.37	0.39	0.31	0.31
	<i>IQR</i>	2.00	1.75	2.00	2.00	1.75	1.75	1.75	1.50
NT	<i>mean</i>	4.7	5.4	5.6	4.9	5.0	4.8	5.6	4.9
	<i>median</i>	5.00	5.50	6.00	5.00	5.00	5.00	6.00	5.00
	<i>standard deviation</i>	1.9	1.9	2.2	2.1	2.1	2.0	1.9	1.7
	<i>mode</i>	4.0	6.0	5.0	5.0	6.0	4.0	6.0	5.0
	<i>CV</i>	0.40	0.34	0.40	0.43	0.41	0.42	0.34	0.34
	<i>IQR</i>	3.00	3.00	3.00	3.00	2.00	3.00	3.00	2.00

4. Discussion and conclusion

The monitoring results and the associated statistics support a number of observations:

- Some indicators (OD, NT) appear to display a normal (symmetrical) distribution pattern, whereas others (FA, LD) are non-symmetric. Specifically, as one could expect, FA is left skewed (most arrivals before noon) and LD is right skewed (most departures after noon).
- The skewedness of FA and LD is not well represented in the statistical mean, but the

position of median (and mode) with regard to mean provides pertinent information. For instance, in case of FA, all median and mode values are smaller than mean, whereas in case of LD, median and mode values are consistently larger than mean. This observation is also consistent with the relative magnitude of the interquartile range and the mean values. The former values are smaller in the FA case whereas they are larger in the LD case.

- The values of the standard deviation and CV suggest a larger spread of data in case of the OD and NT as compared to FA and LD.
- When thinking about the level of the diversity amongst the occupants, the following impression emerges: In those cases, where the inter-individual differences appear to be large, the absolute magnitude of variance is rather small (FA, LD). On the other hand, in those cases where the absolute magnitude of variance is larger (OD, NT), the inter-individual differences are relatively small. This observation, if confirmed by future studies (involving larger sets of occupants in a multitude of buildings), could imply that the inter-individual differences amongst occupants' presence patterns do not necessarily represent a major statistically relevant concern.
- The indicator NT shows remarkable consistency across multiple occupants (as expressed in the values of almost all statistics considered). Again, one could cautiously suggest that this indicator might display – to a certain degree – values that are fairly consistent across multiple occupants

5. Acknowledgement

The research presented in this paper benefited from the authors' participation in the ongoing efforts of the IEA-EBC Annex 66 (Definition and Simulation of Occupant Behaviour in Buildings) and the associated discussions.

References

- ASHRAE, 2013. ASHRAE 90.1-2013 Appendix G. Building Performance Rating Method, ASHRAE.
- Davis, J.A., Nutter, D.W., 2010. Occupancy diversity factors for common university building types, *Energy and Buildings* 42 (2010) 1543–1551.
- Duarte, C., Wymelenberg, K.V.D., Rieger, C., 2013. Revealing occupancy patterns in an office building through the use of occupancy sensor data, *Energy and Buildings* 67 (2013) 587–595.
- Mahdavi, A., 2011. People in building performance simulation, in J. Hensen, R. Lamberts (Eds.), *Building Performance Simulation for Design and Operation*, Taylor & Francis, New York, ISBN: 9780415474146, pp. 56-83.
- Mahdavi, A., Tahmasebi F., 2015. Predicting people's presence in buildings: An empirically based model performance analysis, *Energy and Buildings* 86 (2015), pp. 349–355.
- Page, J., Robinson, D., Morel, N., Scartezzini, J. L., 2008. A generalized stochastic model for the simulation of occupant presence, *Energy and Buildings* 40 (2008), pp. 83–98.
- Reinhart, C.F., 2001. Daylight availability and manual lighting control in office buildings simulation studies and analysis of measurements, Ph.D. thesis, Technical University of Karlsruhe, Germany.
- Richardson I., Thomson, M., Infield, D., 2008. A high-resolution domestic building occupancy model for energy demand simulations, *Energy and Buildings* 40 (2008), pp. 1560–1566.

Prediction of vertical irradiance on building surfaces: an empirical comparison of two models

Ehsan Vazifeh – Vienna University of Technology, Austria – ehsan.mahmoudzadehvazifeh@tuwien.ac.at

Matthias Schuss – Vienna University of Technology, Austria – matthias.schuss@tuwien.ac.at

Ardeshir Mahdavi – Vienna University of Technology, Austria – bpi@tuwien.ac.at

Abstract

Computational assessment of buildings' thermal and visual performance as well as the estimation of building-integrated solar-thermal and photovoltaic collectors require detailed boundary condition information regarding sky conditions. Advanced building performance simulation tools for energy and daylight modelling typically rely on high-resolution sky models that provide radiance and luminance values of discrete sky patches. Perez et al. (1993) and CIE (1996) represent instances of such models, incorporated, for instance, in the RADIANCE lighting simulation application. The performance of such models needs to be examined against measured data in various locations. In this paper, we used the RADIANCE application to compute irradiance values on vertical surfaces facing four cardinal for a location in Vienna, Austria. Thereby, both Perez et al. and CIE models were deployed. The simulated vertical irradiance values were compared with corresponding measurement results. The statistical appraisal of the comparison points to limits in the predictive accuracy of both models. The results are discussed to address potential contributing factors and future research needs.

1. Introduction

Deployment of performance simulation in building design and control phase is believed to have the potential to enhance the buildings' performance in their life cycle. This requires reliable input data for simulation models. Specifically, obtaining high-resolution solar radiation data can represent a challenge. Consequently, a number of models have been developed to compute radiance/luminance data for arbitrary patches of the sky dome

(Nakamura et al. 1985, Perez et al. 1991, Brunger and Hooper 1993, Igawa et al. 1997, Kittler et al. 1997, Kittler et al 1998, Darula and Kittler 2002, Mahdavi and Dervishi 2013). Among these models, two (CIE 1996 and Perez et al. 1993) are well-known and applied in RADIANCE application (Ward 1994). This paper reports on the comparison of simulated vertical irradiance values (obtained using the above mentioned sky models incorporated in the RADIANCE application) with corresponding measurements (April to November 2014) for the location Vienna, Austria (48N11'54", 16E22'10").

2. Methods

2.1 Models

Combining physical principles and a large set of experimental data, Perez et al. 1993 introduced a model to predict the sky luminance for discrete sky patches. Basically, the model contains two variables and five coefficients (See equation 1). The variables are zenith angle of the considered sky point and angular distance between the sky point and the sun disk. The coefficients resulted from least square fitting of the data and can be obtained from a table.

$$L_r = \left[1 + a e^{\frac{b}{\cos z}} \right] \times \left[1 + c e^{d\xi} + e \cos^2 \xi \right] \quad (1)$$

Here, ξ is the angular distance between the sky element and the sun disk, z is the zenith angle of considered sky element and a , b , c , d , and e are the mentioned coefficients. In order to select from the

table the values of the five coefficients, two variables, namely, sky brightness (Δ) and sky clearness (ϵ) must be calculated (See equation 2, 3).

$$\epsilon = \frac{\left[\frac{I_{h,dif} + I_{n,dir}}{I_{h,dif}} + 1.041z_s^3 \right]}{1 + 1.041z_s^3} \quad (2)$$

$$\Delta = \frac{m_{air} \times I_{h,dif}}{I_{n,ext}} \quad (3)$$

Here, $I_{h,dif}$ is horizontal diffuse irradiance, $I_{n,dir}$ normal direct irradiance, z_s solar zenith angle, m_{air} optical air mass, and $I_{n,ext}$ is the extraterrestrial normal irradiance. $I_{n,dir}$ is generated based on the Perez et al. global to direct conversion model (1991).

To deploy the currently implemented version of the CIE model in RADIANCE, we made use of the option to assign specific values to the tool's pertinent parameter in accordance with the relevant sky category. Toward this end, we considered the following four categories: clear, intermediate without sun, intermediate with sun, and overcast. In order to map our weather station data into these four categories, we used a simple assignment rule based on the magnitude of the direct normal and diffuse horizontal irradiance components (see table 1).

Table 1 – Categorization of CIE skies in the model

$I_{n,dir}$	$I_{h,dif}$	Column 3
≥ 120	< 130	Clear sky
≥ 120	≥ 130	Intermediate sky without sun
< 120	< 100	Overcast sky
< 120	≥ 100	Intermediate sky with sun

2.2 Data

Department of Building Physics and Building Ecology at Vienna University of Technology is equipped with high-resolution microclimatic monitoring station. This station is located at the roof top of the main building of the university, which is situated in the Vienna city centre. To assess the performance of the models in capturing the sky radiance distribution, we used measured irradiance data incident on the aforementioned four vertical surfaces. Moreover, measured horizontal global (or direct normal) and diffuse irradiance data was used as input for CIE and Perez et al. models to generate the sky radiance distributions. In the present contribution, we focus on the 15-minute interval data collected in the period between April and November 2014.

2.3 Comparison

The RADIANCE lighting simulation program (Ward 1994) was used. Perez et al. 1993 and CIE 1996 sky models are embedded in the RADIANCE program in terms of Gendaylit (Ward 2014a) and Gensky (Ward 2014b) routines. Simulation results (vertical irradiance values) using these two models were compared with corresponding measurement results. Toward this end, a number of statistical measures were used, namely, root mean square error (RMSE), r-square (R^2), relative error (RE), coefficient of variation of RMSE (CV_{RMSE}), and cumulative distribution function.

3. Results

Figure 1 entails the fisheye false colour images of the sky hemisphere based on both sky models and HDR camera for partly cloudy and clear sky instances. The images are taken in 5-minute intervals using a LMK 98-3 luminance camera equipped with neutral density filter. In the presence of the clear sky instance, Perez et al. model (Gendaylit) appears to be more realistic than CIE (Gensky). However, in the presence of the cloudy sky instance, none of the models appear to generate a faithful representation of reality. This circumstance could be attributed to the complexity

of the radiance distribution under cloudy conditions.

To compare the calculated vertical irradiance values with the measured one, the aforementioned statistics were derived (Table 2). Figure 2 shows the cumulative distribution function and histogram based on relative errors (RE) in percentages for the four cardinal directions plus the horizontal plane. The Perez et al. model displays a slightly better performance. Model errors are largest for the north orientation (almost half of results based on the Perez et al. model display a relative error larger than 20%) and smallest for the south orientation (some 80% of the results based on the Perez et al. model show errors less than 20%). With regard to the horizontal irradiance, both models perform quite satisfactorily. However, this was expected, given the fact that measured irradiance data is already fed to the RADIANCE as input information. The respective small errors may be due to the adopted approach to categorization of skies (Table 1).

Table 2 – Statistical measures of models based on measurements for different directions

	Direction	RMSE	CV _{RMSE}	R ²
Perez CIE	North	30.6	31.7	0.567
		34.3	35	0.495
Perez CIE	East	97.23	33.3	0.924
		99.1	32.4	0.926
Perez CIE	South	32.9	12.9	0.981
		35.1	13.8	0.981
Perez CIE	West	60.1	22.4	0.965
		61.4	21.8	0.963
Perez CIE	Horizontal	16.1	3.6	0.999
		15.8	3.6	0.999

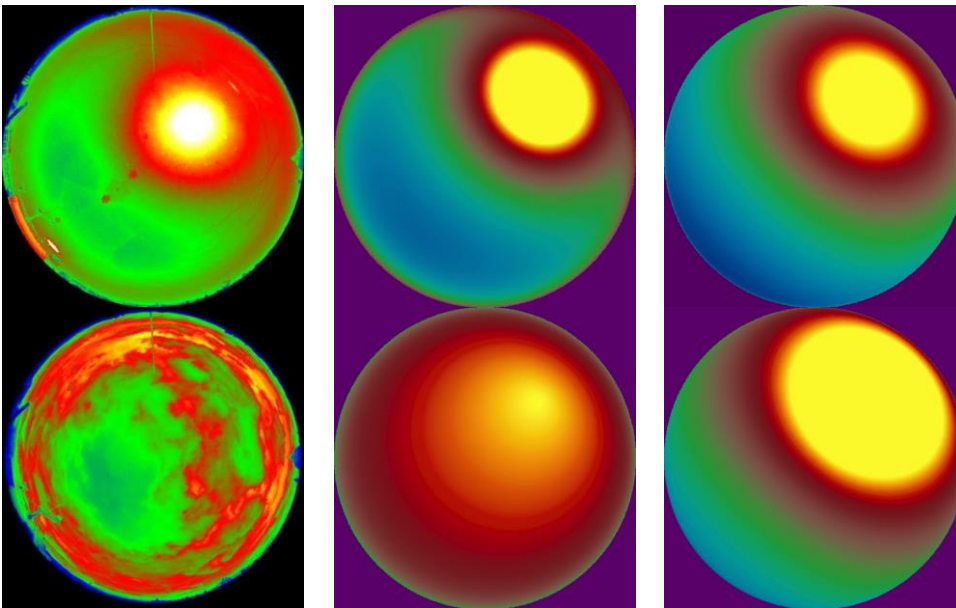


Fig. 1 – From left to right (HDR fisheye image, Gendaylit false color, Gensky false color), upper row: clear sky (4 July 2014 10:45 am local time), lower row: cloudy sky (10 July 2014 10:45 am local time)

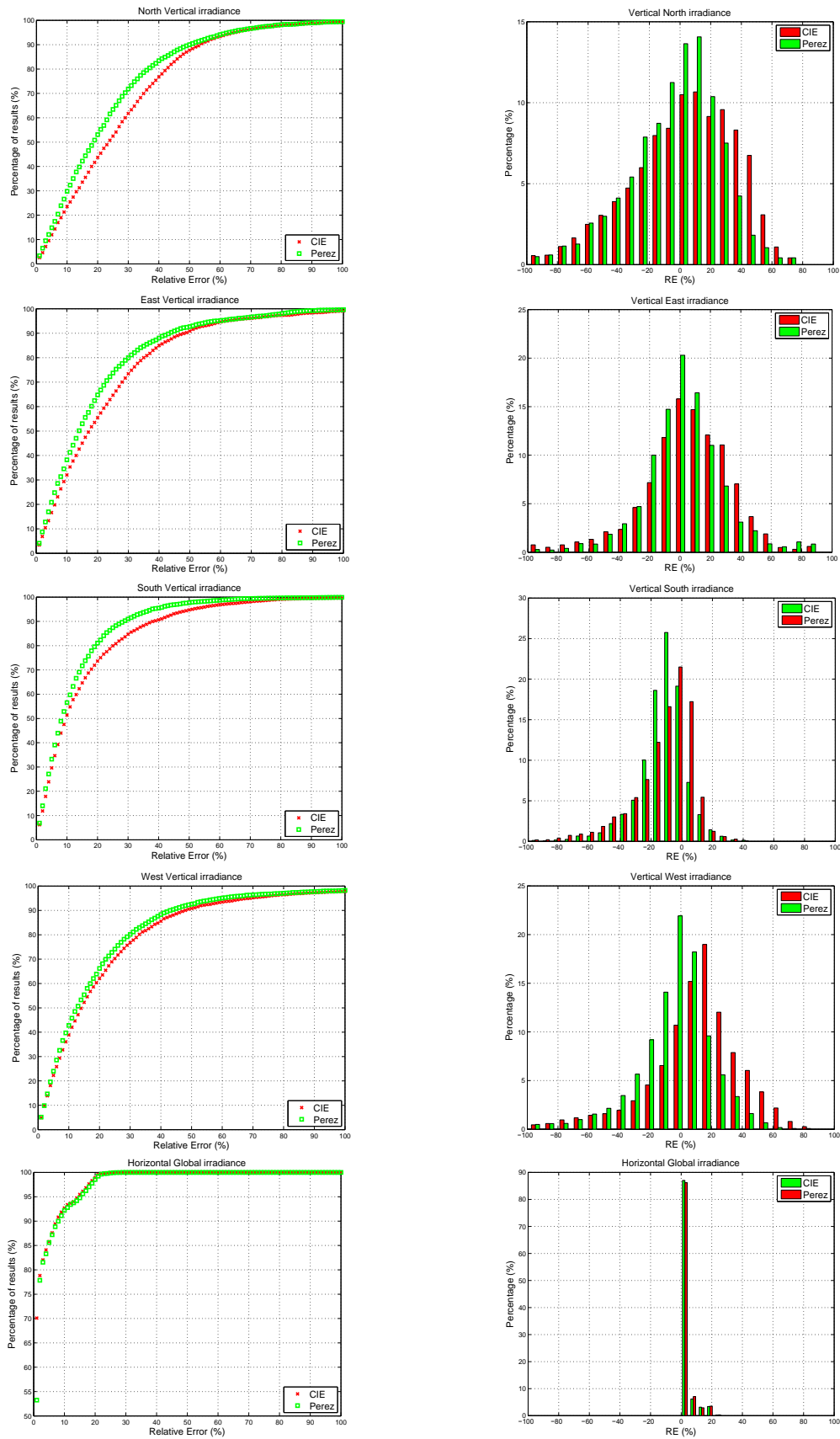


Fig. 2 – Comparison of CIE (Gensky) and Perez et al. (Gendaylit) sky models for vertical surfaces facing the four cardinal directions in terms of cumulative distribution functions (left) and distributions (right) of relative errors (location: Vienna, Austria)

4. Conclusion

Irradiance on four vertical surfaces was estimated using the RADIANCE application. Thereby, two embedded sky models (Perez et al., CIE) were deployed. The comparison of the computational results with corresponding measurements conducted in Vienna, suggests these sky models would have to be improved – or calibrated – to reproduce the measured data with sufficient accuracy. Future research will address a multi-location model comparison. Moreover, a more recent CIE sky model (Darula and Kittler 2002) involving the categorisation of sky conditions into 15 types will be considered for evaluation.

5. Acknowledgement

The research presented in this paper was supported in part with a fund from the Seventh EU Framework Program-ICT "CAMPUS 21" (Project-Nr: 285729). Additional support is provided within the framework of the "Innovative Projekte" research funding program of the Vienna University of Technology. Mr. Josef Lechleitner supported the authors with regard to the retrieval and pre-processing of the microclimatic monitoring station data.

6. Nomenclature

Symbols

Δ	sky brightness defined by Perez et al.(-)
ϵ	sky clearness defined by Perez et al.(-)
$I_{h,dif}$	horizontal diffuse irradiance (W/m ²)
$I_{n,dir}$	normal direct irradiance (W/m ²)
$I_{n,ext}$	normal extraterrestrial irradiance (W/m ²)
L_r	Relative luminance (Perez et al.)
m_{air}	Optical air mass (-)
ξ	angular distance between the sky element and the sun disk (degrees)

z	zenith angle of considered sky element (degrees)
z_s	zenith angle of the Sun (degrees)

References

- Brunger, AP. and Hooper, FC. 1993. "Anisotropic sky radiance model based on narrow field of view measurements of shortwave radiance." *Solar Energy*, Vol. 51 (1), pp: 53–64.
- CIE. 1996. "Spatial distribution of daylight." CIE Standard Overcast Sky and Clear Sky. CIE S 003/E-1996.
- Darula, S. and Kittler, R. 2002. "CIE general sky standard defining luminance distributions." *eSim 2002*, Montreal, Canada.
- Igawa, N., Nakamura, H., Matsuzawa, T., Koga, Y., Goto, K., and Kojo, S. 1997. "Sky luminance distribution between two CIE standard skies." *Proc. Lux Pacifica*, E7-E18.
- Kittler, R. Perez, R., and Darula, S. 1997. "A new generation of sky standards." In: proceedings of the Lux Europa 1997, pp: 359-373
- Kittler R., Perez R., and Darula S. 1998. "A set of standard skies characterizing daylight conditions for computer and energy conscious design." US SK 92 052 Final Report, ICA SAS Bratislava, Polygrafia Bratislava.
- Mahdavi, A. and Dervishi, S. 2013. "A simple all-weather sky radiance model." *IBPSA, Chambery*. 916-921.
- Nakamura, H., Oki, M., and Hayashi, Y. 1985. "Luminance distribution of intermediate sky." *J. Light and Vis. Envir.*, 9, 1, 6-13.
- Perez, R., Ineichen, P., Maxwell, E., Seals, R., and Zelenka, A. 1991. "Dynamic global-to-direct irradiance conversion models." *ISES Solar World Congress*, Denver USA, pages 951-956.
- Perez, R. Seals, R. Michalsky, J., and Steward, R. 1993. "All-weather model for sky luminance distribution-preliminary configuration and validation." *Solar energy*, Vol: 50 (3), pp: 235-245
- Ward, G.J. 1994. "The radiance lighting simulation and rendering system." In Proceedings of the

21st annual conference on Computer graphics and interactive techniques, pages 459–472. ACM Press.

Ward, G.J. 2014a. http://radsite.lbl.gov/radiance/man_html/gendaylit.1.html (Accessed November 2014)

Ward, G.J. 2014b. http://radsite.lbl.gov/radiance/man_html/gensky.1.html (Accessed November 2014.)

Improving energy efficiency through the optimization of buildings' operational regime: simulation based case studies

Farhang Tahmasebi – farhang.tahmasebi@tuwien.ac.at

Mahnameh Taheri – mahnameh.taheri@tuwien.ac.at

Matthias Schuss – matthias.schuss@tuwien.ac.at

Ardeshir Mahdavi – amahdavi@tuwien.ac.at

Department of Building Physics and Building Ecology, Vienna University of Technology

Abstract

The ongoing EU-funded project RESSEEPE explores, in addition to the hardware-centric solutions, the potential for the enhancement of energy efficiency in public edification through the optimization of buildings' operational regime. For the purpose of this contribution, we report on the simulation-based studies on three public buildings across Europe within the framework of the RESSEEPE project: A secondary School in Skellefteå, Sweden, a hospital in Terrassa, Spain, and a university building in Coventry, UK. The case studies provide a basis for the formulation of a general modelling and analysis process for the implementation of advanced control scenarios, as well as an evaluation of the extent to which these measures can contribute to enhancing the building performance in different European climates.

1. Introduction

Energy efficiency measures in the domain of existing buildings may be broadly classified as either hardware-centric or software-centric. While the former measures target building hardware (e.g., thermal quality of the building envelope, efficiency of environmental control equipment), the latter focus on building operation processes (Schuss et al. 2013). Given this background, the ongoing EU-funded project RESSEEPE (RESSEEPE, 2014) explores, in addition to the hardware-centric solutions, the potential for the enhancement of energy efficiency in public edification through the optimization of buildings' operational regime. Specifically, one of the project's objectives is to compare the energy and indoor-environmental performance of a number of existing facilities

before and after real or virtual implementation of control improvement measures. The suggested control scenarios focus on predictive building systems control and passive environmental strategies. For the purpose of this contribution, we report on the simulation-based studies on three public buildings across Europe within the framework of the RESSEEPE project: A secondary School in Skellefteå, Sweden (Balderskolan), a hospital in Terrassa, Spain, and a university building in Coventry, UK (George Eliot building). The case studies provide a basis for the formulation of a general modelling and analysis process for the implementation of advanced control scenarios, as well as an evaluation of the extent to which these measures can contribute in enhancing the building performance in different European climates.

2. Approach

2.1 Small-scale energy models

In order to evaluate the effectiveness of advanced control scenarios with the aid of dynamic performance simulation, a number of demo buildings' small-scale thermal performance models have been built in the well-known building performance simulation tool EnergyPlus (EnergyPlus 8.1.0, 2014). In the case of the George Eliot building, the model includes a large classroom, four small classrooms/offices and the corridor between these rooms. The Balderskolan model consists of a number of classrooms located on the ground floor. In the Terrassa hospital model four typical north-facing and south-facing patient

rooms were modelled. Figures 1 to 3 illustrate the geometry of the small-scale EnergyPlus models (visualized by OpenStudio plugin for SketchUp) for demo buildings in three RESSEEPE demo sites. The building models were generated based on the best information available and a number of assumptions. The small-scale energy models enabled us to perform faster parametric simulations to evaluate the effectiveness of the retrofit measures with different configurations. It is also worthwhile to mention that the small-scale energy models have a relatively generic nature. That is, even though they have been derived from specific buildings, they can serve to evaluate the effectiveness of measures in the same type of rooms (with similar functions) in similar weather conditions.

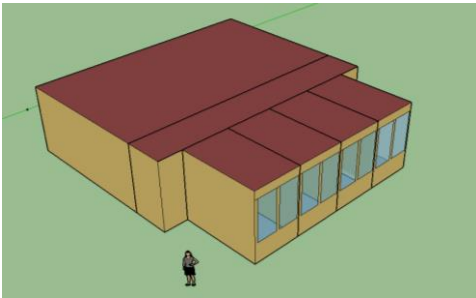


Fig. 1 – EnergyPlus model geometry for George Eliot building

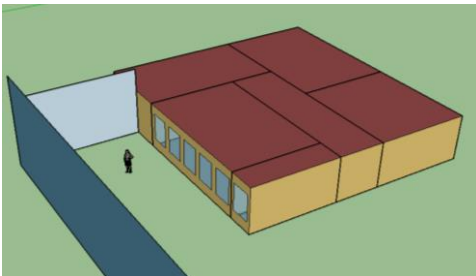


Fig. 2 – EnergyPlus model geometry for Balderskolan

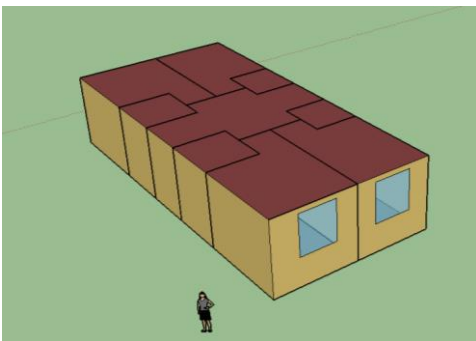


Fig. 3 – EnergyPlus model geometries for Terrassa hospital

2.2 Typical year historic weather data

To perform dynamic simulation studies on potential retrofit measures, we obtained hourly weather data from the closest possible weather stations to the demo sites, namely Coventry airport, Skellefteå airport, and Sabadell (as an interpolated city). The Meteonorm 7.1 software tool (Meteonorm, 2014) was used to provide the data and generate typical year weather data files for the simulation tool. To generate the typical year weather data, temperature data from the period 2000 – 2009 and radiation data from 1991 – 2010 were used.

2.3 Dynamic simulation-based studies

2.3.1 Baseline model

Table 1 summarizes the baseline HVAC system operational assumptions. Note that, in case of Skellefteå demo building, it has been assumed that the HVAC system does not operate during the summer holidays (i.e. June to mid-August).

Table 2 summarizes the baseline assumptions in small-scale demo building energy models with regard to infiltration, mechanical ventilation and ventilation heat recovery.

2.3.2 Conventional HVAC system time scheduling and set points optimization

To evaluate the impact of adjusting heating and cooling set-points (and where applicable the system scheduling) on building heating and cooling

Table 1 – Assumptions with regard to HVAC set-points and availability schedule

Demo building	Coventry	Barcelona	Skellefteå
Heating set-point	21	21	21
Cooling set-point	24	24	24
Heating availability schedule	Weekdays: 5:00 to 22:00 Weekends:	Always on	Weekdays: 5:00 to 17:00 Weekends: off
Cooling availability schedule	Nominal working hours	Always on	Nominal working hours

Table 2 – Modelling assumptions pertaining to infiltration, mechanical ventilation & heat recovery

Demo building	Coventry	Barcelona	Skellefteå
Infiltration rate [h ⁻¹]	0.55	0.2	0.2
Mechanical ventilation availability	No	Yes	Yes
Mechanical outdoor air flow rate per zone [m ³ /s]	-	0.02	0.30
Mechanical ventilation availability schedule	-	Occupied hours	Occupied hours
Ventilation heat recovery availability	-	No	Yes
Sensible heat recovery effectiveness	-	-	0.80

demands, we conducted parametric simulations using each demo building energy model. The parametric study involved simulating all demo building models with heating set-points of 18 to 24°C and cooling set-points of 21 to 27°C (with steps of 0.5).

In the case of the Coventry and Skellefteå demo buildings, which do not operate constantly, we also considered the impact of setting back the thermostat during the early morning preheating phase.

2.3.3 Predictive HVAC systems time scheduling and set points optimization

Integrating short-term weather forecast data and occupancy predictions in the building or zone controller provides opportunities to maintain thermal comfort conditions more efficiently, i.e. with less heating and cooling loads on the secondary and primary systems. More specifically, weather forecast and predicted occupancy data allow the controller to detect those days of the year that despite having relatively cool temperatures in the morning, the building/zone is expected to be overheated at midday due to high solar gain, high outdoor temperatures, high internal gains or a combination of these factors. In such a situation, the early morning preheating (or the whole heating

when applicable) can be deactivated without compromising thermal comfort. Such a predictive control does not only reduce/remove the morning heating demand, but also reduces the afternoon cooling load, as a smaller amount of heating energy should be removed from the building.

To evaluate the effectiveness of this strategy, we exposed the demo building energy models to specific outdoor environment conditions obtained from local historic data, which offer the above-mentioned possibility.

2.3.4 Passive cooling with day-time ventilation

One of the strategies considered to be implemented in demo buildings is the use of ventilation to reduce the building cooling load. Introducing outdoor air to the building can be accomplished via manually or automatically operable windows or via the HVAC system, which is known as free cooling or outdoor air economizer.

In a simulation-based evaluation of this strategy, in order to avoid overcooling, a minimum indoor temperature was set to activate natural ventilation (or free cooling). Clearly, this can only be applied in automated implementations. Table 3 summarizes the assumptions with regard to daytime ventilation strategy for different demo building models.

2.3.5 Passive night-time ventilation using weather forecast

Predictive nighttime ventilation involves ventilating the building during the night if predicted performance of the building shows cooling

Table 3 – Modelling assumptions in daytime natural ventilation

Demo buildings	Coventry	Barcelona	Skellefteå
Air change rate [h ⁻¹]	4	4	4
Minimum indoor temperature	23.0	23.0	23.0
Availability schedule	Occupied hours	8:00 to 16:00	Occupied hours

demand on the following day. Due to the lack of real-time indoor environment and weather forecast

data at this stage in RESSEEPE, to evaluate the potential of this strategy, we replicated this predictive strategy as follows: The night-time ventilation is applied to the building energy models if the following day’s temperature exceeds 18°C for at least four hours. In the case of the Terrassa demo building, which is operating constantly, we also set a minimum outdoor temperature for ventilation to prevent an increase in heating loads caused by the cold outdoor air entering the zones.

2.3.6 Automated shading

To numerically analyze the effectiveness of automatically controlled shading devices, we applied a low-reflectance medium-transmittance shade (see Table 4) inside and outside of the models’ windows, controlled based on the amount of radiation on the windows (150 W/m² as baseline shading operation threshold and variable set-points in parametric simulations). To see the impact of utilizing a shading device on both thermal and lighting electricity demands, we used EnergyPlus daylighting simulation module. Toward this end, one or two daylight control points (depending on the zone area) were placed in each zone. We set 500 [lux] as the desired lighting level on these control points. The overhead lights dim continuously and linearly from (maximum electric power, maximum light output) to (minimum electric power, minimum light output) as the daylight illuminance increases. The lights switch off completely when the minimum dimming point is reached.

Table 4 – Assumed properties for the modelled shade

Shade properties	Value
Solar Transmittance [-]	0.4
Solar Reflectance [-]	0.2
Visible Transmittance [-]	0.4
Visible Reflectance [-]	0.2
Infrared Emissivity [-]	0.9
Infrared Transmittance [-]	0.0
Thickness [m]	0.005
Conductivity [W/m.K]	0.1

3. Results and discussions

This section presents the results of the conducted simulation studies to evaluate the effectiveness of the proposed technologies in reducing the building heating and cooling demands.

The parametric study to evaluate the impact of adjusting heating and cooling set-points involved simulating all demo building models with heating set-points of 18 to 24°C and cooling set-points of 21 to 27°C. Figure 4 shows the results of parametric simulation for the Coventry demo building. Even though the impact of this technology can be considered as “common sense”, the quantitative results could encourage more sensitivity to the operating indoor temperature in demo buildings.

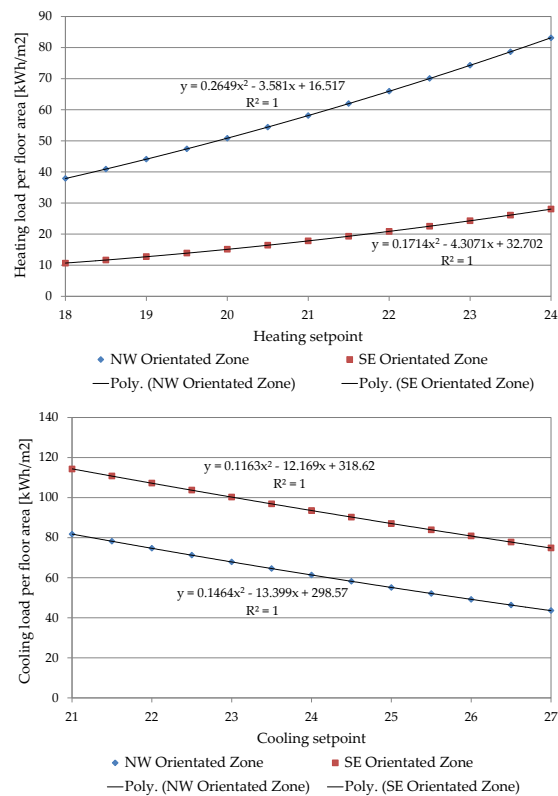


Fig. 4 – Heating (up) and cooling (down) load per floor area with different set-points, Coventry demo building

Table 5 and Table 6 show the results of setback temperature parametric simulations for Coventry and Skellefteå demo buildings. From the tables, even with a setback temperature of 16°C during early morning hours, heating demand can be reduced noticeably, especially in the classrooms with high heat gains during the day.

Table 5 – Coventry demo building heating load with different setback configurations

Models	Setback temperature	Heating load [kWh/m ²]	
		SE	NW
Baseline	-	17.8	58.1
Thermostat setback 3 hours before occupancy	14	8.7	47.0
	15	9.3	47.7
	16	10.1	48.7

Table 6 – Skellefteå demo building heating load with different setback configurations

Models	Setback temperature	Heating load [kWh/m ²]	
		North	South
Baseline	-	42.2	34.1
Thermostat setback 3 hours before occupancy	14	33.0	25.7
	15	33.7	26.3
	16	34.5	27.2

The results of time scheduling and set points optimization simulations show that in both the Coventry and Skellefteå demo buildings, predictive HVAC scheduling and set-point optimization can contribute to reduce heating and cooling demands. Figure 5 compares the simulated indoor temperature of the Coventry demo building, with baseline conventional control and the predictive scheduling strategy on a spring day. From the figure, it can be seen that, without compromising thermal comfort during working hours (indoor temperature above 18°C), implementation of predictive control reduces both heating and cooling loads, as it sets back the thermostat or deactivates the heating system in the early morning hours, which lowers the midday indoor temperatures and the associated cooling demand. It should be noted that, due to the continuous operation of HVAC system in hospital buildings, this technology is not applicable in the Barcelona demo building.

Table 7 to Table 9 show the results of heating and cooling loads obtained from baseline and daytime ventilated models for the Coventry, Barcelona and Skellefteå demo buildings. The results clearly show

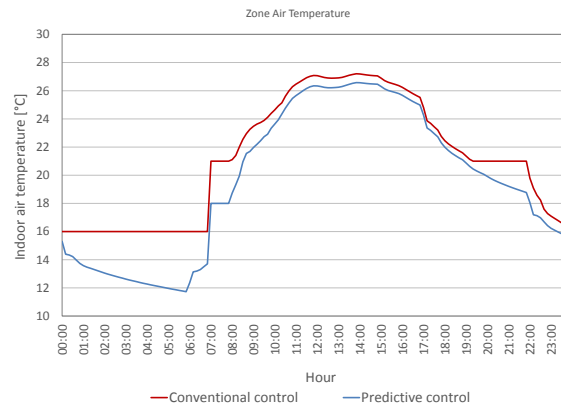


Fig. 5 – Simulated hourly indoor air temperature on a spring day with conventional and predictive control, Coventry demo building

the effectiveness of this technology in RESSEEPE demo buildings. From the tables it can be seen that, with controlled daytime ventilation (here based on minimum indoor temperature), it is possible to largely reduce the cooling demands in all demo sites without any noticeable increase in heating loads.

Table 7 – Coventry demo building heating & cooling demands with & without daytime ventilation

Models	SE zones		NW zones	
	Heating demand [kWh/m ²]	Cooling demand [kWh/m ²]	Heating demand [kWh/m ²]	Cooling demand [kWh/m ²]
Baseline	17.8	93.5	58.1	61.3
Daytime ventilation	19.4	39.4	58.7	34.4

Table 8– Barcelona demo building heating & cooling demands with & without daytime ventilation

Models	North zones		South zones	
	Heating demand [kWh/m ²]	Cooling demand [kWh/m ²]	Heating demand [kWh/m ²]	Cooling demand [kWh/m ²]
Baseline	60.3	75.4	21.9	95.3
Daytime ventilation	60.4	69.1	22.0	83.9

Table 9 – Skellefteå demo building heating & cooling demands with & without daytime ventilation

Models	North zones		South zones	
	Heating demand [kWh/m ²]	Cooling demand [kWh/m ²]	Heating demand [kWh/m ²]	Cooling demand [kWh/m ²]
Baseline	42.2	5.7	34.1	12.3
Daytime ventilation	42.5	2.6	34.7	6.4

Table 12, the parametric simulation results show that the night-time cooling strategy can contribute to a reduction in cooling load up to 10% in the Coventry and Sweden demo buildings and more than 15% in the Barcelona demo building. However, it may also lead to a smaller increase in heating demand, which can be avoided by setting a minimum outdoor temperature for ventilating the building (as modelled here for Barcelona demo building).

Table 10 – Coventry demo building heating & cooling demands with & without night time ventilation

Scenarios	ACH	SE zones		NW zones	
		Heating demand [kWh/m ²]	Cooling demand [kWh/m ²]	Heating demand [kWh/m ²]	Cooling demand [kWh/m ²]
Base	-	17.8	93.5	58.1	61.3
1	4	18.6	90.6	58.9	57.8
2	6	18.8	90.1	59.2	56.9
3	8	19.0	89.7	59.4	56.3
4	10	19.1	89.4	59.6	55.8

Table 11 – Barcelona demo building heating & cooling demands with & without night time ventilation

Scenarios	Min outdoor temperature	SE zones		NW zones	
		Heating demand [kWh/m ²]	Cooling demand [kWh/m ²]	Heating demand [kWh/m ²]	Cooling demand [kWh/m ²]
Base	-	60.3	75.4	21.9	95.3
1	-	64.6	62.7	25.8	81.7
2	16	60.4	64.1	21.9	83.4
3	17	60.3	65.2	21.9	84.7
4	18	60.3	66.7	21.9	86.4

Table 12 – Skellefteå demo building heating & cooling demands with & without night time ventilation

Scenarios	ACH	SE zones		NW zones	
		Heating demand [kWh/m ²]	Cooling demand [kWh/m ²]	Heating demand [kWh/m ²]	Cooling demand [kWh/m ²]
Base	-	42.2	5.7	34.1	12.3
1	4	43.0	4.9	34.6	10.9
2	6	43.5	4.8	35.1	10.7
3	8	44.0	4.7	35.5	10.5
4	10	44.4	4.7	36.0	10.4

With regard to the automated control of the shades, first, we controlled the shading devices with a set-point of 150 W/m² for the amount of radiation on the windows. The simulation results (Table 13 to Table 15) suggest that in the Coventry and Barcelona demo buildings an exterior shade can largely decrease the cooling demand without any noticeable increase in heating and electricity demands. In the case of the Skellefteå demo building, only an exterior shade in the south zone can be beneficial to some extent. However, considering climatic conditions and the adjacent buildings (see Figure 2), adding automated shading devices does not seem to be a promising measure for this building.

We also simulated the variations in building energy demands with different thresholds of incident solar radiation on windows. The results suggested that a set-point of 150 W/m² incident solar radiation can be seen as an optimum threshold to activate the shading device for all demo buildings. Figure 6 shows the variations in the Coventry demo building’s energy demands with different activation set-points for shading devices.

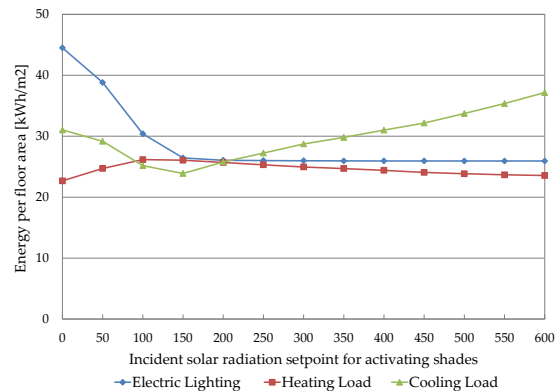


Fig. 6 – Variations in heating, cooling & electric lighting demand with different set-points to activate the shades, Coventry demo building, SE zone (up), NW zone (down).

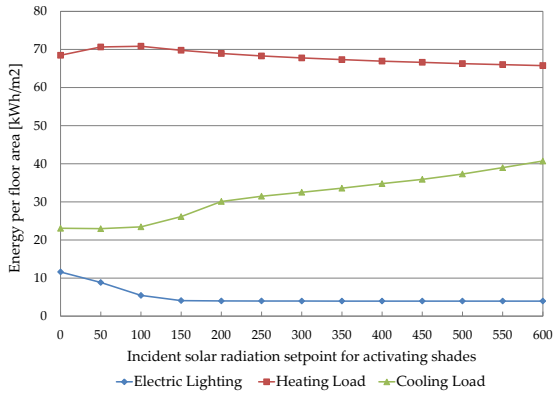


Table 13 – Coventry demo building heating, cooling & lighting electricity demands with shades (Activation set-point of 150 W/m²)

Scenarios	SE zones			NW zones		
	Heating demand [kWh/m ²]	Cooling demand [kWh/m ²]	Lighting demand [kWh/m ²]	Heating demand [kWh/m ²]	Cooling demand [kWh/m ²]	Lighting demand [kWh/m ²]
Baseline	23.2	48.1	25.9	65.4	45.3	4.0
Interior shade	24.2	42.3	26.5	67.6	43.1	4.1
Exterior shade	26.1	23.9	26.4	69.8	26.1	4.1

Table 14 – Barcelona demo building heating, cooling & lighting electricity demands with shades (Activation set-point of 150 W/m²)

Scenarios	North zones			South zones		
	Heating demand [kWh/m ²]	Cooling demand [kWh/m ²]	Lighting demand [kWh/m ²]	Heating demand [kWh/m ²]	Cooling demand [kWh/m ²]	Lighting demand [kWh/m ²]
Baseline	51.3	61.5	9.0	14.8	103.8	6.4
Interior shade	53.7	60.6	11.1	22.1	93.0	7.8
Exterior shade	54.3	56.4	11.0	32.8	71.0	7.5

Table 15 – Skellefteå demo building heating, cooling & lighting electricity demands with shades (Activation set-point of 150 W/m²)

Scenarios	North zones			South zones		
	Heating demand [kWh/m ²]	Cooling demand [kWh/m ²]	Lighting demand [kWh/m ²]	Heating demand [kWh/m ²]	Cooling demand [kWh/m ²]	Lighting demand [kWh/m ²]
Baseline	42.7	3.7	9.2	34.5	9.0	8.6
Interior shade	42.8	3.6	9.3	35.0	8.4	8.9
Exterior shade	43.0	3.4	9.3	36.5	5.4	8.8

4. Conclusion

This paper reports on the simulation-based studies on the effectiveness of advanced control strategies in three public buildings across Europe within the framework of the RESSEEPE project: A secondary

School in Skellefteå, Sweden, a hospital in Terrassa, Spain, and a university building in Coventry, UK.

5. Acknowledgement

The presented research is supported by funds from the "Retrofitting Solutions and Services for the enhancement of Energy Efficiency in Public Edification" project (RESSEEPE, Project number: 609377) under the EU's 7th Framework Programme.

References

- EnergyPlus 8.1.0, U.S. Department of Energy,
<http://apps1.eere.energy.gov/buildings/energyplus/>.
- Meteonorm 7.1, Meteotest,
<http://meteonorm.com/en/>.
- RESSEEPE. Retrofitting Solutions and Services for the enhancement of Energy Efficiency in Public Edification. <http://www.resseepe-project.eu>.
- Schuss, M., Tahmasebi, F., Vazifeh, E.M., Mahdavi, A. 2013. Toward Improving Energy Efficiency of Existing Buildings via Monitoring-Supported Predictive Systems Control, CLIMA 2013 - 11th REHVA World Congress and the 8th International Conference on Indoor Air Quality, Ventilation and Energy Conservation in Buildings, Prague, Czech Republic.

Performance evaluation towards improved BiPV-Systems – Simulation of BiPV-systems installed on existing building facades using TRNSYS

Sascha Lindig – EURAC – sascha_lindig@gmx.de
David Moser – EURAC – david.moser@eurac.edu
Stefano Avesani – EURAC – stefano.avesani@eurac.edu
Roberto Lollini – EURAC – roberto.lollini@eurac.edu

Abstract

The main focus of this work was the simulation and optimization of a BiPV-façade-system configuration through the development of simulations using the "TRNSYS" software. First, several limitations and constraints within the TRNSYS framework needed to be solved to develop a reliable simulation environment. Various parameters were detected which influence the temperature distribution over a BiPV-system and thus the PV-efficiency. Several configurations were selected and optimized in order to maximize the energy yield of the system by varying the air gap between the building structure and the external pane of the BiPV-installation. Furthermore, the impact on the building behavior was examined. The achieved results showed the positive contribution of the integration of PV in a façade system to the building energy balance.

1. Introduction

1.1 Building integrated PV

Building integrated photovoltaic (BiPV) systems are conventional building applied photovoltaic systems with additional functions. PV-modules, which are integrated in or on a building envelope, replace parts of the building construction components and need to fulfill partly their properties. Often PV-modules are applied or integrated on buildings without taking into account influences of the temperature effect on the PV-production, the heating and cooling exchange

with the building, and ultimately the indoor comfort.

Further to electricity production, possible benefits of BiPV-systems can be achieved by taking into account the thermal behavior of the system and the impact on the building itself (Sinpasis et al., 2012). The temperature distribution between the building where the PV-array is applied and the system has a significant effect on the overall performance of the system and the indoor conditions (Gan, 2009). The distribution of the temperature depends on different parameters. These parameters need to be clarified and investigated in order to improve the temperature distribution within the air gap between the building envelope and the installed PV-array. The temperature in the channel rises together with the height of the system. This temperature gradient directly influences the PV-cell temperature and thus also the overall efficiency of the installed system.

The first aim of this work was to specify the parameters that affect the PV-efficiency. Two different target buildings (one residential and one office) were investigated and thus two simulation set-ups with PV-system - with a certain size installed on the façade of the target buildings – were created. Additionally, the height of the PV-array was investigated. Since the PV-array is installed along the façade of the building envelope, the module angle is 90° and the azimuth angle was fixed to 0° (south oriented). Several simulations within the TRNSYS simulation environment were carried out while varying the air gap size (range 1-200 mm). Every simulation covered one year with a one-hour resolution and the chosen location was Bolzano. Based on the results, optimal air gap sizes

between the system and the buildings were investigated by evaluating the energy yield and thus the annual power output of the system.

1.2 Effect of temperature on PV-performance

The temperature dependency of solar cells is one of the most critical points while installing a photovoltaic system. Depending on the used photovoltaic technology, the power output decreases up to 0.6%/K of increased cell temperature (Kamalanathan et al., 2002). However, not just the direct energy conversion is negatively influenced by higher temperature working conditions. In fact, the degradation rate increases significantly. Already in the FSA project, which was funded by the U.S. Government and carried out in the mid-eighties with the purpose of the investigation of the applicability of terrestrial photovoltaic systems, it was mentioned that the degradation rate of PV-modules doubles for an increase of 10 K in temperature (Smokler et al., 1986). Many factors besides the ambient temperature affect the operating temperature, such as the radiation intensity or the airflow behind the PV-application.

Every PV-module has a specific temperature coefficient γ , which is given by the manufacturer. The coefficient mainly depends on the chosen photovoltaic material. The higher this value is, the higher is the temperature dependency of the respective system. Crystalline silicon (c-Si) solar cells are highly dependent on the temperature. Temperature coefficients of around -0.45%/K are usual. This value expresses that if the cell temperature rises by 1 K the power output decreases under constant irradiation by 0.45 percent. Amorphous silicon cells in turn are less affected by temperature what can be seen in lower coefficients of about -0.13%/K. The temperature coefficient of modules made out of copper-indium-(gallium)-selenide is with roughly -0.36%/K slightly lower than the one of c-Si (Virtuani et al., 2010). These three kinds of modules are the most commonly used systems. Crystalline silicon modules were considered in this work as they represent the highest share on the market.

2. BiPV-simulation

Based on the temperature dependent behavior of photovoltaic systems, it is possible to carry out simulations with which a specific installation might be evaluated as well as optimized. A simulation environment which suits this purpose is TRNSYS (Klein, 2012). It is a FORTRAN-based simulation software and consists of subroutines, called "Types". Each type represents a specific system with several inputs, outputs and parameters. To create a simulation, different types need to be chosen and linked together in a logical way.

One of such a type is the multi-zone building type 56. It is used to simulate a specified target building. In order to create a proper TRNSYS simulation of a BiPV-installation, multiple steps are required.

First, the defined target building, divided in an appropriate number of thermal zones, needs to be modelled within Google SketchUp with help of a TRNSYS-3D-plugin. Each thermal zone can be considered independently from each other and it is possible to specify the zones later on in an appropriate level of detail. While modelling the building in SketchUp, the outside boundary condition of each wall has to be set. These conditions are outdoor, ground, zone and other side coefficients. The outdoor condition relates to walls which are facing the outer world, the ground condition needs to be chosen if the wall is the floor of the basement and walls between thermal zones are set as zone. Other side coefficients are inputs that will be defined later.

By starting a new "3D Building project" the SketchUp model will be integrated into the TRNSYS Simulation Studio. The desired location, in our case Bolzano, needs to be set and the weather characteristics are automatically linked to the building type. The building itself has to be specified in TRNBuild, an add-on of TRNSYS, which can be accessed through type 56. The wall and window constructions will be defined as well as ventilation and infiltration values, temperature set points and additional gains for each thermal zone. Desired inputs and outputs might be chosen as well. Additionally, the connection to the

building integrated photovoltaic system has to be prepared.

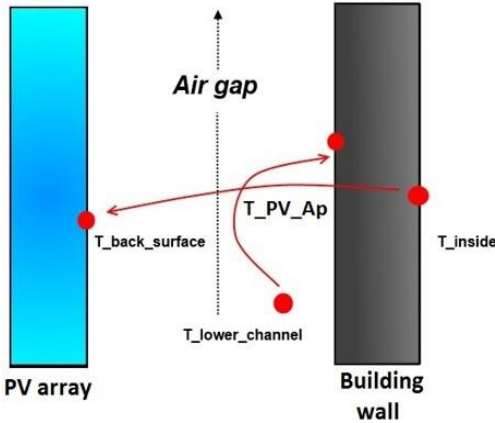


Fig. 1 – Connection between BiPV-type & building wall

The heart of the simulation is the BiPV-type 567. It has to be coupled to the multi-zone building type 56 within the TRNSYS Simulation Studio. The connection is illustrated in Fig. 1.

One TRNSYS BiPV-type 567 needs to be used for each façade of each floor of the building which is covered by the PV-array in order to provide a well-connected BiPV-system along the whole building. If an installed PV-system is located in more than one position per floor, more BiPV-types need to be included. One floor corresponds to one thermal zone within TRNBuild.

In Fig. 1 it is visible that the connection between the building envelope and the PV-array is realized by a two-sided temperature transfer. This transfer provides the heat exchange between the BiPV-modules and the building. The inside surface temperature of the relevant wall is given to the BiPV-type as an input called the “back surface temperature”. The category of the corresponding wall was set to “other side coefficients”, which means that the wall requires a temperature value as an input. This temperature is provided by the output “lower channel temperature” of type 567. It is the temperature in the air gap between the PV-array and the building. The multi-zone building model calculates the temperature of the inside surface of the corresponding wall depending on this input. This value is then sent back again to type 567, and it re-calculates the temperature of the lower air channel. The exchange repeats until convergence is reached (Bradley et al., 2004).

Further types need to be included to design the

final simulation such as output-types, calculators and conversion routines.

Furthermore, the photovoltaic type 194 is used to simulate a specific free-standing photovoltaic module to consider its properties and its temperature behavior. The resulting efficiency of this PV-type under the prevailing conditions is used in the following equation:

(1)

$$\eta_{BiPV} = \eta_{PV} * (1 - \gamma_{PV} * (T_{BiPV} - T_{PV}))$$

Here, the efficiency of the BiPV-type is calculated. The temperature coefficient γ of the given PV-system is multiplied by the temperature difference between the well-ventilated free-standing PV-module and the BiPV-installation. Due to higher operating temperature conditions, the product reduces η_{PV} and results in the BiPV-efficiency, which is given as an input into type 567. That allows us to include the effect of higher temperatures due to a non-optimal ventilation of the system while installing it along a building façade.

Furthermore, with help of equation 2, the airflow within the air gap between the building envelope and the PV-system is considered:

$$\dot{m}_{vent} = \rho_{air} * (\dot{V}_{wind} + \dot{V}_{thermal}) = \rho_{air} * (C_v * A_{in} * U_{\infty} + C_D * A_{in} * \sqrt{2g * \Delta H_{NPL} * \frac{T_{cav} - T_{amb}}{T_{cav}}}) \quad (\text{if } T > T_{amb}) \quad (2)$$

The incoming air mass flow from natural forces is calculated by the product of the air density ρ_{air}

and the volumetric flow rate of air ventilating in and out of the cavity from wind and buoyancy-driven flows. C_v and C_D are fixed coefficients, g is the standard gravity, the wind velocity U_{∞} and the

ambient temperature T_{amb} are outputs given from the weather data and T_{cav} is the temperature in the air channel. If T_{amb} is higher than T_{cav} these values are exchanged with one another in equation 2. A_{in} is the opening of the airflow and it changes with the size of the air gap and the width of the PV-system. ΔH_{NPL} is the height from the midpoint of the lower opening to the neutral pressure level, in case of a vertical symmetric air gap it is the half

length of the air channel and thus of the PV-system (Griffith, 2006).

In order to create an airflow along the whole cavity the flow rate and the air temperature in the air gap of one type 567 is always given as an input to the next one which is located above.

The modelled buildings are a multi-family house and an open space office building. Both consist of five floors (88 m² each apartment and 140 m² the open office) with a height of 2.7 m each (see Fig. 2). The U-values for the external wall and window are 0.81 and 2.83 W/(m²K) and 0.42 and 1.43 W/(m²K) for the residential and office building, respectively.

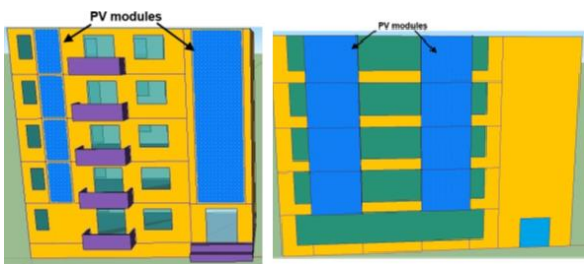


Fig. 2 – SketchUp models of simulated buildings (residential building on the left and office building on the right)

The residential building is designed for four people per apartment, the office building for 16 people per office. The PV-system is installed along the façade wall of the residential building. In the case of the office building, it also covers a part of the glazing and it has the double width compared to the installation in front of the apartment envelope of the residential building. Here lies an important achievement of this work. The positioning of the PV-systems in front of the windows is not yet implemented within TRNSYS. Because of that, the explained process of the connection of the types 567 and the building needs to be expanded. For each BiPV-type an extra thermal zone has to be modelled in TRNSYS. An example is shown in Fig. 3.

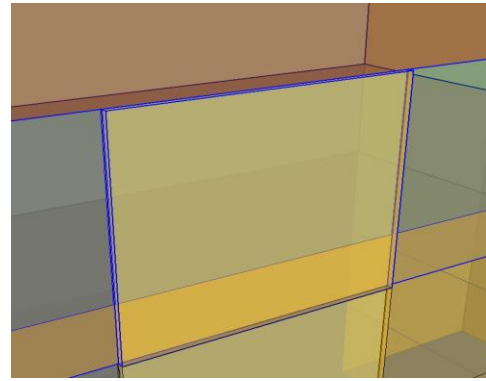


Fig. 3 – Extra thermal zone SketchUp

The area of the additional thermal zone, which is placed partly in front of a window and partly in front of an opaque part of the building envelope, is equal to the size of the PV-array. The depth of the zone corresponds to the depth of the air gap. The adjacent wall of the zone that faces the building consists of an adjacent window. The category of the wall, which represents the BiPV-array, is “other side coefficients”. This wall needs to be connected to the BiPV-type 567 as explained before. The other four walls are set as virtual surfaces, which means that they are practically nonexistent in the simulations and not visible in TRNBuild.

3. Results and Discussion

Simulations on two different target buildings to simulate BiPV-systems were performed using TRNSYS. This was done to investigate the buildings, which are used for different purposes, especially in relation to the needs of the occupants and the building structure. Apart from the actual electricity generation of the BiPV-system, the heating demand (provided by an ideal heating system with infinite power) of the buildings was compared with and without installed PV-modules. The same was additionally done in case of the office building for the cooling demand based on electrical cooling.

The BiPV-type 567 has optical parameters which lower the final power output of the system and thus the performance ratio (PR) and the energy yield. The energy yield gives information about the system behavior depending on the amount of absorbed irradiation and the prevailing cell

temperature. It is the relation between the power output and the installed capacity and given in kWh/kWp. The PR, however, describes the temperature dependency of a system since it includes the incoming radiation of the sun. It is given in percentage and is an indication of how well an installed system works.

Within this study the default optical parameter values of type 567, given by TRNSYS, were used (transmittance-absorptance $\tau\alpha = 0.85$, IAM constant = 0.1). They overestimate the losses and thereby underestimate the power generation of the PV-array. These parameters do not affect the efficiency output of type 567. For that reason, the results of the efficiency and the generated power show similar trends but the absolute values do not match.

Generally, expected trends were seen. Time periods with higher insolation in module level lead to a higher amount of generated power. Higher working temperatures of the observed system due to high ambient temperatures decrease the performance, expressed in the performance ratio. This can be also seen while investigating larger PV-systems. Because of the higher installed capacity, the annual power output increases. In turn, the PV-temperature increases and thus decreases the PR. There are mainly two reasons for the mentioned effects.

First, the higher amount of irradiation heats a larger system to a greater extent. Second, the chimney effect within the air gap based on wind driven and thermal buoyancy causes a temperature gradient ascending with the height of the system. The higher the system is, the greater is the temperature at the top of it and thus the maximum operating temperature of longer systems. Nevertheless, a PV-array should not be too small in size. An appropriate installed capacity is important.

The investigated photovoltaic material is crystalline silicon. Based on the high temperature coefficient of the selected material the performance of the system is strongly affected by high temperatures. The performance of the system is dropping under non-optimal installation conditions. The advantage of this technology is the

higher installed capacity per m^2 compared to thin film systems.

While considering a selected system that shall be installed on a façade, the air gap between the array and the building determines optimal working conditions of the PV-array. The closer the system is installed along the building the more significant is the temperature gradient within the air gap. This can be seen in Fig. 4.

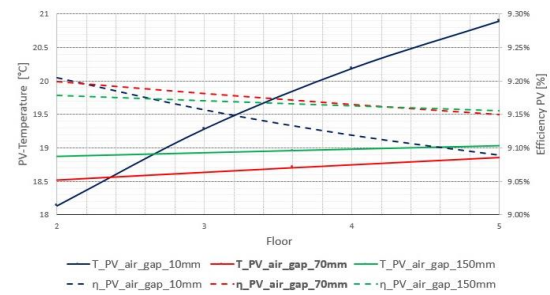


Fig. 4 – Res. Building – Aver. T & η -distribution along the air gap. Values are averaged over the year excluding nights.

The annual averaged values of the temperature and the corresponding efficiency distributions for three different air gap sizes are plotted against an ascending building height. The investigated building is in this case the residential one. The distribution of an air gap size of 70 mm is plotted under which the system performance is at an optimum while the BiPV-system is installed on the residential building. Additionally, the temperature in air gaps with sizes of 10 mm and 150 mm are shown. The solid lines represent the operating PV-temperature, the dotted one the PV-efficiency. It can be seen that the temperature propagation depends strongly on the size of the air gap. The smaller the air gap, the steeper the temperature curve becomes. Although the temperature is lower at the lower part of the PV-system which is installed close to the building, it becomes higher at the top, compared to a bigger air gap size. If just the lowest part of the PV-system is considered, the efficiency of it is higher for systems which are installed in the smallest possible distance to the façade. However, over the whole array the non-optimal temperature distribution results in a performance drop along the PV-system. Considering the highest part of the system, a large air gap has a beneficial effect on the efficiency. The

optimum for the whole array lies between the investigated extremes.

Similar observations were made while investigating the office building. Optimal conditions have been reached under an air gap size of 100 mm. The higher value for the optimized air gap in comparison to the residential building is due to different installation conditions since the system is located partly in front of a glazed part of the building envelope and also on the width of the system. The optimization of the energy yield is shown in Fig. 5. The 3D-plot illustrates the dependence of the energy yield on the PV-system length and the air gap size.

It is visible that the energy yield decreases in a certain frame with an increasing length of the PV-system. An optimum in terms of the air gap size is reached between 40 and 100 mm depending on the array size (e.g. 40 mm for an array size of 2.7 m, 100 mm for an array size of 10.8 m). The larger the opening becomes, the less the energy yield is affected by the array length.

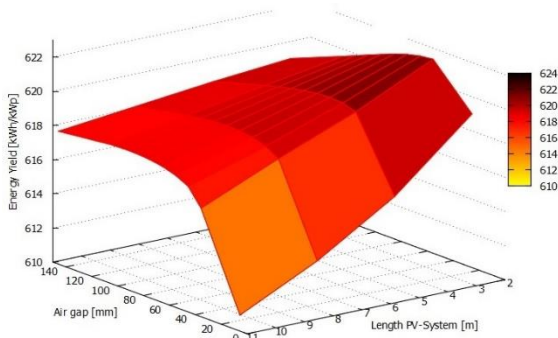


Fig. 5 – Office Building - Energy Yield Dependence

The temperature rise within smaller air gaps as well as larger PV-systems is higher. For the size of a given PV-array a suitable air gap needs to be found. This arrangement determines the created flow rate within the gap and thus the distribution of the cell temperature.

It was shown that the PV-temperature increases with a decreasing air gap. This is due to the smaller flow rate in the air channel. Warm air rises with low speed and heats up the upper part of the system. The wind speed in the gap rises together with the size of it. A higher wind speed in the channel cools the air itself and lowers the buoyancy driven chimney effect. This results in a

decreasing temperature gradient, visible in the comparison of the PV-temperature gradient in Fig. 6. Here, the temperature distribution from the bottom to the top of a PV-system, which is installed in distances of 100 mm as well as 1 mm to the envelope of the office building, is shown at an irradiation of 900 W/m² and an ambient temperature of -3 °C.

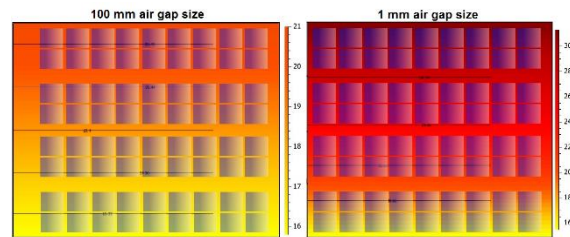


Fig. 6 – T-gradient depending on the air gap size – 900 W/m²

At the lowest part of the system, the PV-temperature and therefore the efficiency difference is relatively small in comparison. It rises with an increasing system height. The gradient increases with a decreasing air gap. The observed temperature rise of more than 15 °C in case of an air gap of 1 mm leads to the discussed efficiency drop and a decreasing power generation from the bottom to the top of the PV-array. The working temperature in case of the 100 mm wide air gap increases just about 5 °C.

While investigating a PV-array which is installed on a consisting building façade, not just the performance of the system but also the impact on the building is an important issue. The environmental influence on building parts which are covered by PV-modules changes. For example, the amount of incoming sunlight or the air flow along the surface is affected. These changes have an impact on the amount of energy needed to ensure a desired room climate.

In case of the observed residential building, this amount is equal to the heating demand. The heating demand is the amount of supplied energy that is used to provide a specified minimal room temperature. The office building is additionally cooled. It is assumed that these demands are provided by electrical energy. If no PV-system is installed the residential building requires 60.38 kWh/m² per year and the office building 14.55 kWh/m² for heating and 38.8 kWh/m² for

cooling needs. These values serve as a reference. Fig. 7 shows, in how far these amounts change while installing the BiPV-system along 10.8 m respectively 4 floors.



Fig. 7 – Energy Demand Buildings

The stated values are relative. Additionally the absolute differences between the reference cases and the buildings including installed photovoltaic systems are given. The plotted values refer to the adjusted air gap size, under which the energy yield of the PV-system reached a maximum. It is visible that the heating demand of the residential building can benefit from an installed BiPV-system. The amount of supplied energy is lower compared to the reference case. Furthermore, the variation of the air gap has just a small effect on the building behavior. BiPV-systems applied along a building façade affect the covered wall in different ways.

Less irradiation hits the building envelope. Because of that, less heat, produced mainly by shortwave radiation of the sun, is transferred to the façade. The applied system acts as kind of a protection layer in terms of low ambient temperatures. The chimney effect within the air gap creates an airflow along the building. These effects lead to the observed savings.

In contrast to the residential building, the heating demand increases while installing a PV-system along the envelope of the office building. At the same time, the cooling demand decreases to a greater extent. The increasing heating demand is mainly due to the large photovoltaic installation. The wide PV-system creates a strong airflow in the channel between the modules and the building. This cools the outer wall of the building. Since the PV-system is partially installed in front of

windows, the cooling effect has even a greater impact on the interior.

Another issue is the reduced solar gain. The panels absorb or reflect a substantial part of the insolation. The absorbed part is then converted into heat or into electrical energy. The portion that is converted into heat will be again submitted to the outside world. Due to the shading, less solar energy is transmitted into the building interior. More than 50% of the office window area is covered with photovoltaic panels. In turn, the transmitted solar gain is roughly halved. The thermal energy, which is lost by shadowing must be compensated by electrically supplied heat. On the other hand, the previous observations are also the reason for the savings in cooling energy. The BiPV-system acts like a shading system, avoiding solar gain to reach the building façade and the indoor environment. Additionally, the created air stream is cooling the building interior. During warm months in summer, the building has to be cooled to a lesser extent.

Table 16 – Overview of annual Energy Balance

	Res. Building Heating	Of. Building Heat. & Cool.
Energy Demand without BiPV	60.38 kWh/m ²	53.34 kWh/m ²
Energy Demand with BiPV	58.36 kWh/m ²	45.78 kWh/m ²
Difference: Reference – BiPV	2.02 kWh/m ²	7.56 kWh/m ²
Energy Generation	3,762 kWh	4,983 kWh
PV-system efficiency	9.17%	9.17%
Energy Demand Savings	10.57 kWh/m² 17.51%	14.67 kWh/m² 27.51%

Table 16 summarizes the discussed results. The annual values of the energy demand with and without an installed BiPV-system and their differences are given as well as the maximum achievable energy output, the system efficiency and the possible energy savings.

It is visible that both investigated building types benefit from the installation of a PV-system in matters of the energy balance. In addition, a part of the needed energy can be saved if the generated energy is used directly in the building. The amount

of savings depend on the installed capacity. For the considered cases, the savings are between 17% and almost 28%. The higher value in the case of the office building is due to the large number of possible savings in terms of the cooling demand and the higher installed capacity of PV. It can be seen that the efficiencies of the systems, using similar PV-modules, are similar under optimized conditions. As indicated above, the resulting amount of the annual energy output is reduced by TRNSYS provided parameter.

4. Conclusion

Within TRNSYS, a BiPV-installation on the opaque as well as the glazed envelope of buildings was simulated. It was demonstrated, that the simulation is not straightforward and has to be adapted in order to receive meaningful results. While developing the simulations some mistakes and ambiguities were clarified and solved.

In future simulations, a closer investigation of the power reducing parameters of the BiPV-type 567 has to be carried out.

Nevertheless, a certain understanding of the behavior of an installed PV-system on the façade of a building was gained. It was simulated that various parameters affect the performance of a BiPV-system. In the selection of a suitable PV-array, the cell temperature behavior and the nominal power of the PV-modules should be taken into account. Furthermore, it is important to pay attention on the dimensions of the array and the distance between the PV-system and the building envelope to ensure a beneficial temperature distribution within the air channel. The results proved the importance of proper simulations of BiPV-systems. A better knowledge and a deeper understanding of the dependency of the parameters and adjustments of building integrated photovoltaic systems to each other are necessary to optimize the build-up and to ensure the best working conditions of the PV-array. The aim of future simulations will be an improvement of the result accuracy as well as an increase of the level of the simulation-detail.

5. Acknowledgement

The authors would like to thank the fund FESR/EFRE/ERDF Provincia Autonoma di Bolzano/South Tyrol for the financial contribution through the project 5-1a-232 “Flexi-BIPV”.

6. Nomenclature

A_{in}	Opening area of the air flow [m ²]
BiPV	Building integrated photovoltaic
C_D	Opening discharge coefficient
C_V	Effectiveness of openings
c-Si	Crystalline silicon
g	Standard gravity [9.81 m/s ²]
\dot{m}_{air}	Air mass flow [kg/h]
PR	Performance ratio
T	Temperature [°C]
U_∞	Wind velocity [m/s]
\dot{V}	Volumetric flow rate [m ³ /s]
ΔH_{NPL}	Height from midpoint of lower opening to neutral pressure level [m]
η_{PV}	Efficiency photovoltaic-system [%]
γ	PV-temperature coefficient [%/K]
ρ_{air}	Air density [kg/m ³]

References

- Bradley, Thornton. “TYPE 567: Glazed building-integrated photovoltaic system (interacts with type 56).” In *TESS Libraries version 2.0 General Descriptions*, Wisconsin
- Gan, G.. 2009. “Effect of air gap on the performance of BiPV” *Solar Energy* 83.8: 1253-1273. doi:10.1016/j.solener. 2009.02.008
- Griffith, B.. 2006. “A Model for naturally ventilated cavities on the exteriors of opaque building thermal envelopes.” *Conference Paper SimBuild 2006*: doi:NREL/CP-550-39829
- Kamalanathan, H., and M. D. Bazilian. 2012. “Thermographic analysis of a building integrated photovoltaic system.” *Renewable Energy* 26.3: 449-461. doi:10.1016/S0960-1481(01)00142-2

- Klein, S. A.. 2012. "TRNSYS 17, A Transient Simulation Program." *Solar Energy Laboratory, University of Wisconsin-Madison*
- Sinapsis, K., M. van den Donker. 2012. „State of the art in BiPV – Technical report.“ In *SEAC BIPV Report 2013*, Eindhoven
- Smokler, M.I., and R. G. Ross. 1986. "Flat-plate solar array project." *Engineering sciences and reliability* 6: doi:19870011218
- Virtuani, A., D. Pavanello, and G. Friesen. 2010. "Overview of temperature coefficients of different thin film photovoltaic technologies." *Conference Paper 25th EU-PVSEC*: doi:10.4229/25thEUPVSEC2010-4AV.3.83

Appraising the effects of window opening behaviour in an office building in different climates

Sara Torabi Moghadam – Energy Department, Polytechnic of Turin, Italy – sara.torabi@polito.it

Federica Soncini – Energy Department, Polytechnic of Turin, Italy – federica.soncini@studenti.polito.it

Valentina Fabi – Energy Department, Polytechnic of Turin, Italy – valentina.fabi@polito.it

Stefano P. Corgnati – Energy Department, Polytechnic of Turin, Italy – stefano.corgnati@polito.it

Abstract

There is extensive pressure on sustainable buildings to deliver energy efficiency, but in practice, designs often fail to achieve the expected level of in-use energy consumption. One of the main factors behind this discrepancy between designed and real total energy use in buildings is the window opening behaviour. Towards nearly zero energy building (NZEB), building performance simulation is being increasingly deployed beyond the building design phase.

With the aim to investigate how the climate affects the probabilistic model of window behaviour, the case study is simulated in different locations, i.e. Continental (Turin) and Mediterranean (Athens). Moreover, each simulated model refers to three comfort category heating and cooling set point conditions (Category I, II, III) as defined in Standard EN 15251:2006. Comparing the results, the influence of window behaviour on energy consumption in different climates generates energetically different outcomes. The present study highlights the importance of users' interaction with window control systems in order to design sustainable and energy-efficient office buildings in a more realistic way.

1. Introduction

Energy reduction in the built environment is an essential issue; particularly, an improved building design during the early design phase is instrumental in the efforts of reducing energy (Clarke, 2001). Therefore, it is required to understand the factors that influence the energy consumption in a building.

Measured real energy use of buildings demonstrates large differences from predicted ones, even between buildings with the same

functions but located in different climates.

Following the literature, human behaviour can be considered one of the key driving factors in changes in energy consumption; especially it has been shown to have a large impact on heating, cooling, ventilation demand and lighting (Page, 2008). Accordingly, several stochastic models have been expanded to model occupant presence and interaction with the building system. Based on measurements in office rooms without mechanical ventilation, a Markov chain model for actions on windows, with the outside temperature as a driving variable, was propounded by Fritsch et al. (1990). Reinhart et al. (2004) defined occupant presence in lighting software by employing a simplified stochastic model divided into sub-models based on users' arrival and departure. Wang et al. (2005) applied Poisson distributions with the aim to generate daily occupancy profile in a single-occupied office. Mahdavi et al. (2008) inquired the possibilities of identifying general patterns of user control behaviour as a function of indoor and outdoor environmental parameters such as illuminance and irradiance.

Since energy building simulation tools are used to estimate the future performance of the building, dissimilar input parameters may introduce uncertainties. Besides, it is assumed that user behaviour is one of the most important input parameters influencing the results of building energy simulations. Accordingly, it is fundamental deploying a model that considers the randomness of human behaviour through a probabilistic approach with the purpose of predicting the actual energy demand of the building. However, it is difficult to completely identify the influences of

occupant behaviour and activities through simulation owing to users' behaviour diversity and complexity; while most current simulation tools can only imitate behaviour patterns in a strict way, occupants' behaviour is the result of a continuous combination of several factors crossing different disciplines (Fabi et al., 2013) and therefore is still an object of investigation.

Rijal et al. (2007), Haldi and Robinson (2009), Herkel et al. (2008), Yun and Steemers (2008) have been pioneering a method to represent occupant interaction with buildings using stochastic models which later can be used to create window control strategies. The general trend has been to infer the probability of the window state as a function of indoor and outdoor temperature, while other studies have investigated the probability of opening a window (change from one state to another) as a function of indoor temperature (Yun and Steemers, 2008, Yun et al., 2008).

Actually, two important parameters influencing energy consumption in buildings are indoor temperature and air change rate, which are directly linked to the occupant's usage of the window. According to studies conducted by Raja et al. (2001), windows had the biggest effect on indoor climate of all available controls. Consequently, it is crucial to take window opening behaviour into consideration.

In office buildings, fully automatic controlled solutions are becoming progressively more common since they can simultaneously enhance individual comfort and use a reduced amount of energy. However, these systems frequently offer limited user autonomy, since user satisfaction and freedom are strongly connected. Moreover, the ability to control their own indoor environment contributes significantly to their satisfaction and general perception of the indoor climate (Wagner et al., 2007).

With these premises, the current paper investigated how different occupant-related models, assuming a behavioural pattern of window-opening, can affect the energy use of an office building. Precisely, a dynamic numeric simulation application was deployed to compare a model based on a fixed schedule with probabilistic models, at first in a Continental (Torabi Moghadam

et al., 2014) and then in Mediterranean weather, in order to analyse the discrepancy between predicted and simulated energy performance in different climates.

2. Simulating Window Behaviour

2.1 Case study

An office building with fifteen cellular office spaces was selected as a case study to evaluate the influence of window operation on thermal simulation results. The floor plan of the basic building model was designed in the framework of the Developing Architectural Education in Response to Climate Change program (DARC program, Polito).

The case study building consists of 5 floors (see Figure 1): each of them has a surface area of about 1400 m². As regards the orientation of the building, the two main façades are oriented south-west and north-east. The floor-to-floor height is 3.5 m; hence the building's total height is 19.3 m.

For more exhaustive energy or load calculations in each office room, a more detailed zoning is required. Therefore, each office cell is modelled as a single zone (see Figure 2).

The modelling assumptions for the building use are listed in Table 1. Simulations were carried out for 3 different categories pertaining to the heating and cooling set points of the building's control systems as relevant to the office spaces. These categories are defined in Standard EN 15251:2006 and included in Table 2.



Fig. 1 – 3D model of the office building and modeled zones

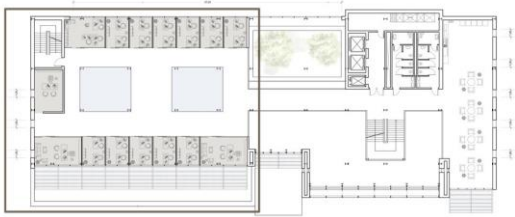


Fig. 2 – Building standard floor plan

Table 1 – Modelling assumptions for building use

Modelling assumptions	Offices
Installed lighting power	10 W/m ²
Occupancy	8:00–18:00
Air change rate ⁽³⁾	1 h ⁻¹
Equipment (occupied period) / (unoccupied period)	15 W/m ² / 5% of total emitted heat

Table 2 – Standard EN 15251:2006. Recommended temperature ranges for the internal temperatures in office buildings.

Type of building	Cat	Operative temperatures [°C]		ACH [h ⁻¹]
		Min. for heating (~1,0 clo)	Max. for cooling (~0,5 clo)	
Office rooms	I	21	25.5	1
	II	20	26	
	III	19	27	

2.2 Methodology

The main purpose of the research was to understand the influence of the climate on probabilistic windows' opening and closing behaviour by performing simulations in two different climate zones (Turin and Athens), taking 2012 as a typical meteorological year (TMY).

Since many office buildings are provided with a hybrid ventilation system, in the current study, in the probabilistic scenario, every office room was equipped with a combination of mechanical ventilation and operable windows. Furthermore, two dissimilar window controls were compared in order to highlight differences in window behaviour impact on the energy consumption discrepancy, during the design phase.

First, the windows were scheduled to be constantly closed and fresh air is supplied exclusively via the mechanical ventilation system (1h⁻¹); this kind of

control is called “*deterministic*” by the authors. Secondly, the windows were simulated to be opened in accordance with the stochastic model of Haldi and Robinson (2009) implemented in the simulation tool used in the current study (IDA ICE, 4.21.); authors defined this control type on windows as “*probabilistic*”. Afterward, the case study is simulated in different locations, i.e. Continental (Turin) and Mediterranean (Athens), using the relative weather data, with the aim to investigate how the different climates affect the office building's energy performance.

For each thermal zone, in every selected climate - Turin and Athens - the algorithm describing users' interactions with windows was implemented in the dynamic simulation tool. Simulations were run 30 times for three comfort categories (see table 2) setting all fixed inputs and one occupant, to understand the impact of the windows' behaviour on the investigated performance indicators.

Since most window openings can be associated with the arrival of an occupant in the office, the probabilities of opening and closing windows were separately estimated in three different sub-models representing the situations of occupants' arrival, departure and during their presence (Herkel et al., 2008). This dynamic method can account for the real adaptive processes of occupants by performing for each of those sub-models a logistic regression which takes into account the most relevant environmental parameters (indoor and outdoor temperature, prior absence duration and rainfall).

In the following research an experimental approach into subsequent scenarios has been developed which was based on two steps, where two window controls were defined: firstly the study has treated office energy performance as automatically performed in the design stage of energy dynamic simulation software; secondly, the model that assumes a probabilistic interaction between users and window opening and closing has been built.

The work focuses on the relationship of window opening behaviour, and the model describing the use of shading system is not applied to the reference building.

Table 3 – Regression coefficients of the probability functions of the window submodels. Previous absence, occurrence of rain and next absence are binary variables.

	Physical driving variables							
	T_{in} [°C]	T_{out} [°C]	Previous absence [-]	Rain [-]	Ongoing presence [min]	$T_{out,daily}$ mean [°C]	Next absence [-]	
Sub models	a	b T_{in}	b T_{out}	b _{abs_pr}	b _{rain}	b _{Tpres}	b _{Tout,dm}	b _{abs_next}
Opening at arrival	-13.7	0.308	0.0395	1.826	-0.43	0	0	0
Closing at arrival	3.95	-0.286	-0.05	0	0	0	0	0
Intermediate opening	-11.78	0,263	0.0394	0	-0.336	-0.0009	0	0
Intermediate closing	-4.14	0.026	-0.0625	0	0	0	0	0
Opening at departure	-8.72	0	0	0	0	0	0.1352	0.85
Closing at departure	-8.68	0.222	-0.0936	0	0	0	0	1.534

3. Discussion and results

The subsequent graphs (Figures 4, 5 and 6) provide a summary of simulated air change rate, heating loads and cooling loads for the above mentioned two scenarios (“deterministic” and “probabilistic”). Moreover, table 4 describes the variation of the results by the fluctuating categories of comfort.

Especially, each performance indicator is presented comparing the Turin and Athens climates in order to corroborate the impact of different climates on energy consumption and window opening and to investigate for each control, as well as each simulation set, what influence the climate would have on the fluctuation of the result, due to the changes in behaviour of the window. The investigations were carried out with the main goal of identifying the influence of climate on the alteration in results between the deterministic and probabilistic approach to the building energy simulation.

Great variations in energy consumption emerged from the data elaboration, switching from a deterministic to a probabilistic approach to

window opening (Figure 4, 5 and 6), for both the climate zones. Actually, using a deterministic approach, the windows are always supposed to be closed according to the fixed schedule, while the stochastic model calculates the probability of a window being opened or closed without been driven by physical thresholds.

In particular, in a hybrid ventilated building the energy use increases because of more frequent occupant-window interactions. In other words, if the opportunity to open the window is given, occupants tend to open it more often than expected; accordingly the average values coming from the simulation sets are higher than the hygienic mechanical ventilation of the deterministic model, for both climate zones (i.e. maximum variation in Turin: 230%; maximum variation in Athens: 440%).

Figure 4 shows the change on air change rate moving the simulation to different climates. The warmer climate presents a higher frequency of window opening of 69.5% compared to the colder

climate. Specifically, as it can be seen in Table 4, in Turin the probabilistic model provides air change rate predictions closer to the ones coming from the standard model (i.e. maximum $ACH_{CatIII_{Turin}} = 4.81 \text{ h}^{-1}$ in summer season), while in Athens the gap between results is more significant (i.e. maximum $ACH_{CatII_{Athens}} = 6.99 \text{ h}^{-1}$, during the summer, instead of 1 h^{-1} of the hygienic mechanical ventilation). Note that the ACH is calculated by dividing the volumetric flow rate of air with the space volume of the rooms.

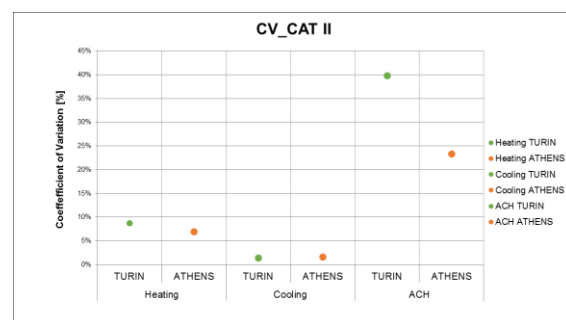
As a result, in models using a probabilistic algorithm for the window opening, the higher energy use for heating is in Turin with a discrepancy of 87.8% with respect to Athens (Figure 5). Conversely, the higher energy use for cooling is in Athens with a gap of 57.6% compared to Turin (Figure 6).

The variation of the results is a consequence of the influence of the climate on this probabilistic model. Specifically, the effect of climate on mean values of heating and cooling energy consumption and air change rate are different in the two climate conditions. Simulated models in Athens always show the maximum cooling energy use and air change rate and the lowest heating energy consumption; while in Turin they have the highest energy use for heating in all scenarios and the lowest air change rate and cooling energy consumption.

Once the influence of probabilistic control on energy demand is evaluated, the fluctuation of results within the same set of simulation is analyzed for the entire building using the Coefficient of Variation (CV). In probability theory and statistics, this indicator is a normalized

measure of dispersion of a probability distribution or frequency distribution and it is defined as the ratio of the standard deviation to the mean. Therefore we used it to quantify the sensitivity of the performance indicator respect to changes in simulations. However, it can be seen that the two climate zones have similar values of CV, with the only exception of the air change rate in which Turin is about 40%, while Athens amounts to 25% (Figure 3).

Fig. 3 – CV values for annual heating load, cooling load and air change rate (Scenario II)



Once this analysis of the results is completed, it seems appropriate to ask whether users behave exactly the same way within a building. What if active or passive users will be simulated in Athens and Turin? An interesting development in the current research could be to investigate the influence of different types of users on the predicted energy consumption, in different climate zones.

Table 4 – Fluctuation of the results in the air change rate, heating load and cooling load calculations between different comfort categories

		Comparison between categories: deterministic VS probabilistic Approach					
		CAT I_TURIN	CAT II_TURIN	CAT III_TURIN	CAT I_ATHENS	CAT II_ATHENS	CAT III_ATHENS
Air Change Rate [h ⁻¹]	Scenario I_deterministic	1.00	1.00	1.00	1.00	1.00	1.00
	Scenario II_probabilistic	3.25	3.18	3.31	5.38	5.39	5.37
Heating Loads [kWh/m ²]	Scenario I_deterministic	45.65	43.82	42.31	13.75	12.74	12.00
	Scenario II_probabilistic	75.44	70.75	68.64	42.81	37.67	33.84
Cooling Loads [kWh/m ²]	Scenario I_deterministic	16.58	16.01	14.99	31.71	30.91	29.40
	Scenario II_probabilistic	14.81	13.75	11.91	34.41	32.46	28.92

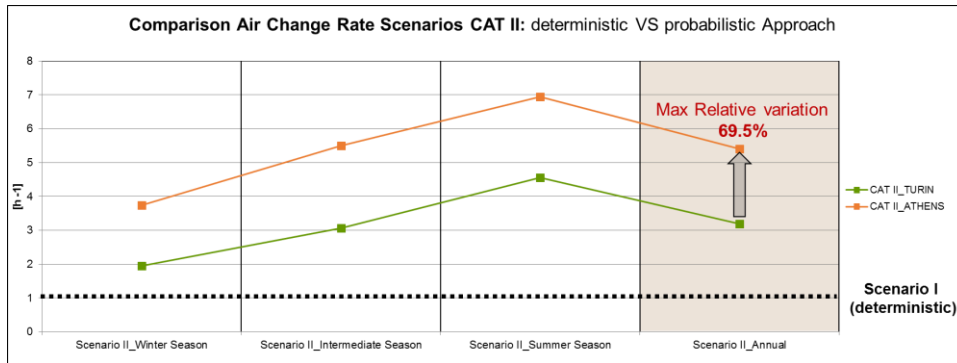


Fig. 4 – Comparison Air change rate scenarios of Cat II

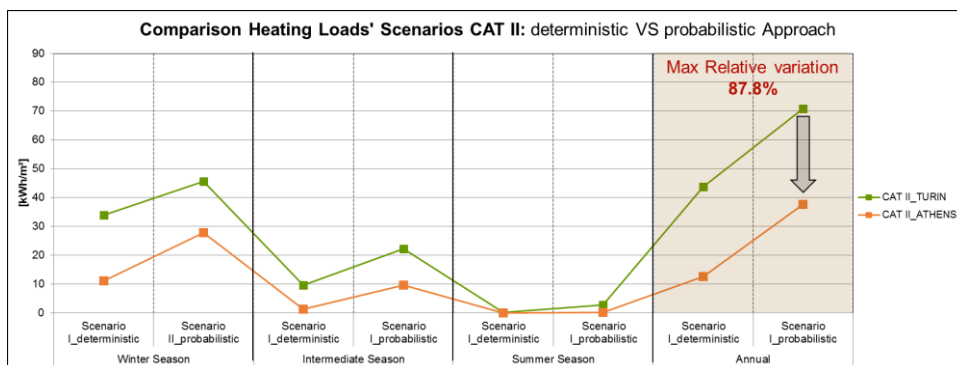


Fig. 5 – Comparison heating loads' scenarios of Cat II

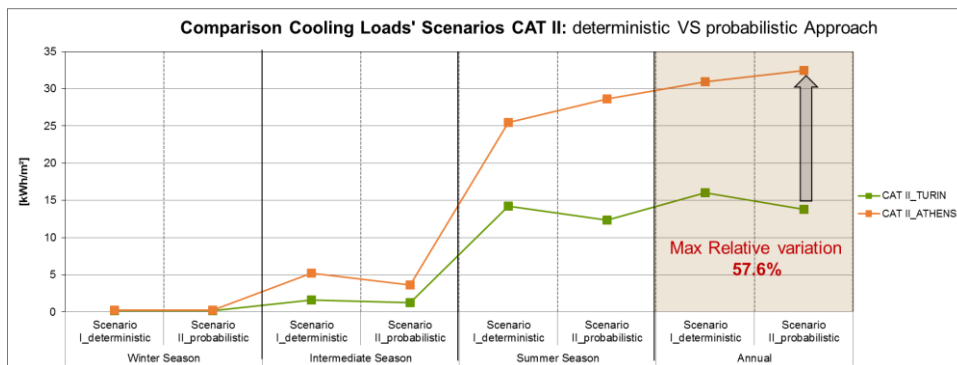


Fig. 6 – Comparison cooling loads' scenarios of Cat II

4. Conclusion

This paper aimed at highlighting the gap between two approaches of simulation, deterministic (with occupants' schedules fixed and always repeatable) and probabilistic (defined by a stochastic schedule of the building occupants). The huge gap often resulting between the predicted and the actual heating and cooling demands relies on the actions that building occupants perform in the indoor environment. The two approaches to simulate the occupants' activities, in an office building are simulated in different climates, through the

implementation of a behavioural model taken from the literature, in a building energy dynamic simulation tool. Using a stochastic model, the use of the window is not predictable with certainty, but it is linked to the behaviour of the occupants. Accordingly, results show different energy outcomes between different control systems, in different climate locations.

In both climate locations, in winter the heating system has to compensate for the higher heat loss due to a more frequent interaction with windows leading to an increase of heating delivered energy. This discrepancy is particularly more pronounced

in Athens (e.g. from 12.74 to 37.67, that is + 196%), where the users, because of the warmer climate, tend to open the windows more frequently than in Turin (e.g. from 43.82 to 70.75, that is + 61%).

Conversely, in summer, the probabilistic model seems to have a lesser but positive influence, but only in the Continental climate of Turin since operations on windows seem to support the system to cool down the building reducing the expected cooling consumption (e.g. from 16.01 kWh/m² to 13.75 kWh/m², with a decrease of 14%, see table 4). The same notion was not valid for Athens (e.g. from 30.91 kWh/m² to 32.46 kWh/m², with an increase of 5%, see table 4), probably because of the high temperatures of the Mediterranean weather. As a matter of fact, in warmer climates naturally ventilated buildings tend to become overheated during summer periods and consequently users tend to open windows more frequently. This interaction necessarily leads to an increase in ventilation losses and hence cooling delivered energy.

Based on that, there is a difference in heating and cooling loads of fixed control versus manual, and it is necessary to clarify this discrepancy with further more detailed studies. Further research will identify different types of users (active and passive), analysing how they affect the predicted energy consumption in office buildings.

References

- Clarke, J.A. 2001. *Energy Simulation in Building Design*, Second Edition, Butterworth-Heinemann, Oxford.
- Fabi, V. 2013. "Influence of Occupant's Behavior on Indoor Environmental Quality and energy Consumption", doctoral dissertation.
- Fritsch, R., Kohler, A., Nygård-Ferguson, M., Scartezzini, J.L. 1990. "A Stochastic Model of User Behavior Regarding Ventilation." In *Building and Environment* 25, 173-81.
- Haldi, F., Robinson, D. 2009. "Interactions with Window Openings by Office Occupants." In *Building and Environment* 44, 2378-2395.
- Herkel, S., Knapp, U., Pfafferott, J. 2008. "Toward a Model of User Behavior Regarding the Manual Control of Windows in Office Buildings." In *Building and Environment* 43, 588-600.
- Humphreys, M.A., Nicol, J.F. 1998. "Understanding the Adaptive Approach to Thermal Comfort." In *ASHRAE Transactions* 104, 991-1004.
- Mahdavi, A., Mohammadi, A., Kabir, E., Lambeva, L. 2008. "Occupants' Operation of Lighting and Shading Systems in Office Buildings." In *Journal of Building Performance Simulation* 1, 57-65.
- Page, J., Robinson, D., Morel, N., Scartezzini, J.L. 2008. "A Generalized Stochastic Model For The Simulation Of Occupant Presence." In *Energy and Building* 40, 83-98.
- Raja, I.A., Nicol, J.F., McCartney, K.J., Humphreys, M.A. 2001. "Thermal Comfort: Use of Controls in Naturally Ventilated Buildings." In *Energy and Buildings* 33, 235-244.
- Reinhart, C.F. 2004. "Lightswitch-2002: A Model for Manual and Automated Control of Electric Lighting and Blinds." In *Solar Energy* 77, 15-28.
- Rijal, H.B., Tuohy, P., Humphreys, M.A., Nicol, J.F., Samuel, A., Clarke, J. 2007. "Using Results from Field Surveys to Predict the Effect of Opening Windows on Thermal Comfort and Energy Use in Buildings." In *Energy and Buildings* 39, 823-836.
- Wagner, A., Gossauer, E., Moosmann, C., Gropp, Th., Leonhart, R. 2007. "Thermal Comfort at Workplace Occupant Satisfaction – Results of Field Studies in German Low Energy Office Buildings." In *Energy and Buildings* 39, 758-769.
- Wang, W., Zmeureanu, R., Rivard, H. 2005. "Applying Multi-Objective Genetic Algorithms in Green Building Design Optimization." In *Building and Environment* 40, 1512-25.
- Yun, G.Y., Steemers, K. 2008. "Time-Dependent Occupant Behaviour Models of Window Control in Summer." In *Building and Environment* 43, 1471-1482.
- Yun, G.Y., Steemers, K., Baker, N. 2008. "Natural Ventilation in Practice: Linking Façade Design, Thermal Performance, Occupant Perception and Control." In *Building Research & Information* 36, 608-624.

Prediction of the Sound Insulation of Double Leaf Facades with Openings for Natural Ventilation

Egzon Bajraktari – University of Prishtina, Prishtina, Kosovo – egzon.bajraktari@uni-pr.edu

Josef Lechleitner – Vienna University of Technology, Vienna, Austria – bpi@tuwien.ac.at

Ardeshir Mahdavi – Vienna University of Technology, Vienna, Austria – bpi@tuwien.ac.at

Abstract

This paper explores the reliability of acoustical simulation for the prediction of the sound insulation of double leaf facades with openings for natural ventilation. The subject of the study is an experimental modular double-leaf wall with multiple opening possibilities. Different elements can be opened in both (i.e., internal and external) layers, so that multiple opening configurations can be studied both empirically and computationally. The actual acoustical performance of the wall was captured through parametric laboratory measurements. The respective configurations were then modelled using a state-of-the-art room acoustics simulation program. Thereby, alternative representations of the double leaf facade were considered. In one representation, the facade layers were explicitly modelled in terms of two separate entities with the facade cavity as an interstitial space. In other representations, the sound transmission through the wall and the acoustical coupling between openings on the two layers were modelled as separate processes. The initial acoustical model was calibrated by comparing the measured and the simulated reverberation times in the laboratory's two chambers. Specifically, the calibration involved the adjustment of the absorption properties of surfaces of the laboratory chambers so that an improved match between the measured and simulated reverberation times could be achieved. Computer simulation and laboratory measurement results pertaining to the sound insulation of the experimental wall were compared for multiple opening configurations. The results illustrate the potential as well as the considerable limitations of acoustical performance simulation toward prediction of the sound insulation of double-leaf wall systems. Likely reasons for this circumstance as well as potential improvements are discussed.

1. Introduction

Computer simulation techniques have increased the potential for the evaluation of buildings' acoustical performance (Svensson 2008). Computer simulations in room acoustics have been widely studied in the last 50 years (Vorländer 2013). A number of commercial acoustic simulation tools have been developed and are already in use, most of them following principles of classical geometric acoustics. Their reliability and usability in room acoustics is tested and discussed (Vorländer 1995, Bork 2000, 2005, Mahdavi 2011). Some acoustical simulation applications have advanced their algorithms for calculating sound transmission through partition elements (Rindel and Christensen 2008).

Following up on a previous report (Bajraktari et al. 2014), this contribution explores the reliability of acoustical simulation for predicting the sound insulation of double leaf facades (DLF) with openings for natural ventilation.

2. Approach

The Department of Building Physics and Building Ecology at the Vienna University of Technology has conducted studies for developing a double leaf façade that allows natural ventilation while providing sufficient sound insulation (Mahdavi et al. 2012, 2013). Thus, a modular flexible instance of a double leaf facade is installed in our laboratory (Fig. 1 and 2) placed in the opening between two adjacent reverberant chambers. The source room and receiving room of the laboratory have a floor surface of 30.4 m² and 30.6 m² respectively and a

height of 6.8 m. The experimental DLF (dimensions 3.1 x 3.1 m) consists of two layers (0.43 m apart from each other) of acoustically reflective chip-board panels tightly mounted on aluminium bars. In a grid structure of 5 x 5, each layer has 25 dismountable chip-board square panels (dimension 0.50 x 0.50 m).



Fig. 1 – View of the experimental double-wall with the frame structure for the installation of flexible (individually removable) modular components.

1	2	3	4	5
6	7	8	9	10
11	12	13	14	15
16	17	18	19	20
21	22	23	24	25

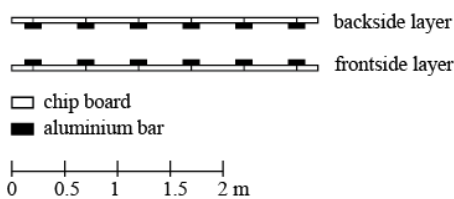


Fig. 2 – Schematic illustration of the double-layered modular experimental wall.

This flexible construction allows us to parametrically modify a number of relevant variables that affect the sound insulation of double leaf facades. Namely, opening area (we can open and close one or more panels in each layer), distance between openings (openings on both layers can be arranged so as to face each other, or

to be shifted – see Figure 3), and cavity sound absorption (we can increase the cavity's mean absorption by adding absorption panels in the cavity space between two layers). Sound insulation properties of a comprehensive sequence of DLF configurations were captured via systematic laboratory measurements (Mahdavi et al. 2012, 2013). These configurations are summarized in Table 1.

For simulation, the modelling of the geometry of both acoustic laboratory chambers and the experimental DLF in between was done via SketchUp 8.0 (TNL 2012). This geometry was modelled in a relatively simple fashion (see Figure 4), as adding further details to geometry did not have a noteworthy impact on the simulation results (see also Bork 2005, Siltanen et al. 2008).

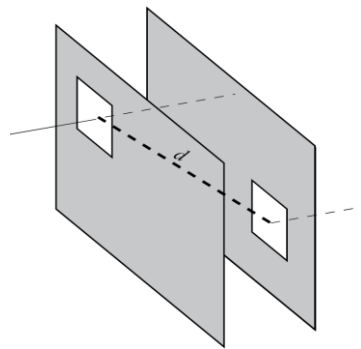


Fig. 3 – Illustration of distance between open elements (d).

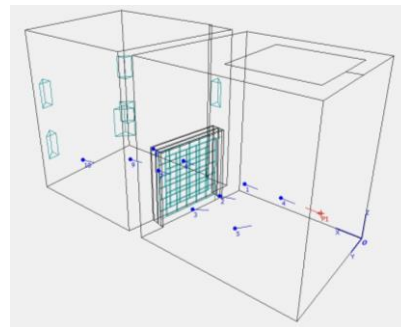


Fig. 4 – Screenshot of the simulation model.

The respective configurations were then modelled and simulated using Odeon 12.0 (Odeon 2013). Odeon combines image source method and ray-tracing for calculating room acoustic parameters (Christensen and Koutsouris 2013).

Alternative representations of the double leaf facade were considered for simulation (Fig 5). In

representation A, the facade layers were explicitly modelled in terms of two separate entities with the facade cavity as an interstitial space. In representations B and C, the sound transmission through the wall and the acoustical coupling

between openings on the two layers were modelled as separate processes. The latter is approximated with tubes connecting respective openings in the first and second layer.

Table 17 – Measured and simulated configurations of DLF (see Figure 2 for the numeric code of the elements). Note that the elements' distance (d) denotes the spatial distance between the centre points of the open elements (Fig. 3).

Configurations simulated in alternative models			Code of the open elements in the front layer	Number of added absorption panels	Code of the open elements in the back layer	Number of added absorption panels	Distance d (m)
A	B	C					
1	1	1	none	none	none	none	
2			none	none	all	none	
3			7	none	all	none	
4			1	none	1	none	0.43
5			1	none	7	none	0.83
6			1	none	13	none	1.48
7			1	none	19	none	2.16
8			1	none	25	none	2.86
9	9	9	6, 16	none	6, 16	none	0.43
10			6, 16	none	7, 17	none	0.66
11	11	11	6, 16	none	8, 18	none	1.09
12			6, 16	none	9, 19	none	1.56
13	13	13	6, 16	none	10, 20	none	2.05
14			1, 6, 11, 16, 21	none	1, 6, 11, 16, 21	none	0.43
15			1, 6, 11, 16, 21	none	3, 8, 14, 18, 23	none	1.09
16			1, 6, 11, 16, 21	none	5, 10, 15, 20, 25	none	2.05
17	17	17	6, 16	ten panels	6, 16	none	0.43
18	18	18	6, 16	ten panels	8, 18	none	1.09
19	19	19	6, 16	ten panels	10, 20	none	2.05
20			1, 6, 11, 16, 21	ten panels	1, 6, 11, 16, 21	none	0.43
21			1, 6, 11, 16, 21	ten panels	3, 8, 14, 18, 23	none	1.09
22			1, 6, 11, 16, 21	ten panels	5, 10, 15, 20, 25	none	2.05
23	23	23	6, 16	ten panels	6, 16	ten panels	0.43
24	24	24	6, 16	ten panels	8, 18	ten panels	1.09
25	25	25	6, 16	ten panels	10, 20	ten panels	2.05
26			1, 6, 11, 16, 21	ten panels	1, 6, 11, 16, 21	ten panels	0.43
27			1, 6, 11, 16, 21	ten panels	3, 8, 14, 18, 23	ten panels	1.09
28			1, 6, 11, 16, 21	ten panels	5, 10, 15, 20, 25	ten panels	2.05

The difference between B and C models is based on the tubes' length. In B, the length of the tubes is determined by the actual distance between openings in the experimental wall (see Table 2). After comparing the error in weighted sound reduction index of B simulations to the actual length of the tubes, in model C the tube length is adjusted accordingly to reduce the error.

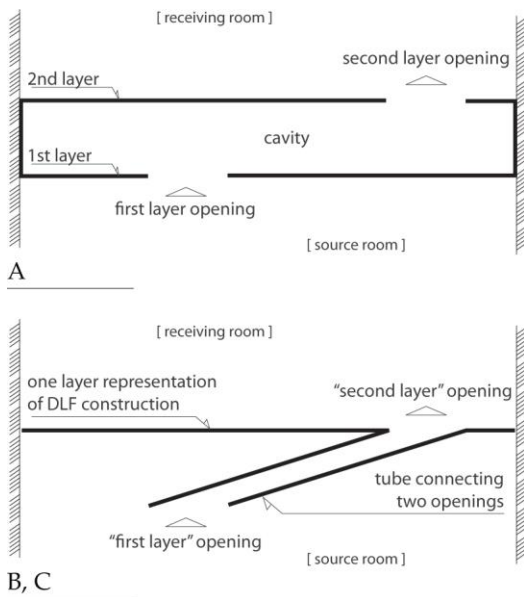


Fig. 5 – Alternative representations of the DLF A model (above) and B and C models (below).

The initial acoustical model was calibrated through an iterative process (Tugrul et al. 2012). Thereby, absorption coefficients of certain surface materials (namely the laboratory chambers' envelopes) were adjusted to achieve a better match between the measured and the simulated reverberation times in the laboratory's two chambers.

Materials and their absorption coefficients were chosen from the existing library, related literature sources, and when available, from producer specifications. In models B and C, the estimated mean absorption coefficient of the DLF cavity is assigned to the tube surfaces.

As to the simulation settings, "Precision" setting was used, as well as transition order 2, number of late rays 32000, impulse response length 5000 [ms]. The calculation of sound transmission from one space to another in Odeon is handled so that a certain fraction of sound "particles" are let through the transmitting "wall" and the rest are reflected

back, whereas energy is adjusted by multiplying in both cases with respective factors (Rindel and Christensen 2008). Sound reduction index in third-octave bands for the transmitting "wall" must be given, and in this case, it is taken from the laboratory measurement results.

The aforementioned configurations (Table 1) were computed using the calibrated simulation model – in total 28 configurations were simulated in model A, and 10 of them were also simulated using models B and C. Subsequently, the simulation results were compared with measurement results. Thereby, measured and simulated reverberation times as well as frequency-dependent and weight sound reduction indices were compared.

3. Results

3.1 Reverberation time (T)

In general, for all the models (A, B, and C), a good agreement between simulated and measured reverberation time values was achieved (Figure 6). The errors (particularly in the low-frequency range) may be due, in part, to the fact that the simulation neglects the complex vibrational behaviour of the double layer structure (Bajraktari et al. 2014). Hence, simulation delivers the same values for configurations 1 and 2 (taking into account simply the surface absorption properties), whereas measurements reflect the behaviour of the entire complex structure (in this case of the DLF) (Figure 7).

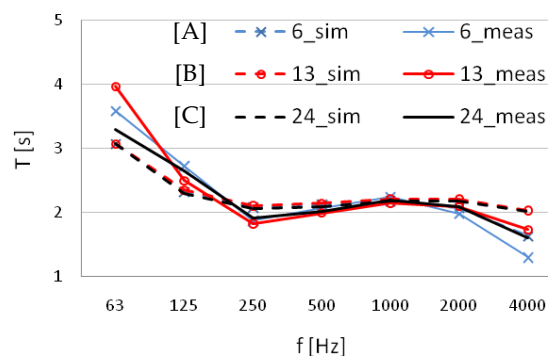


Fig. 6 – Comparison of simulated vs. measured reverberation time (T) in configurations no. 6 (model A), 13 (model B), and 24 (model C) (See Table 1 for the configuration properties).

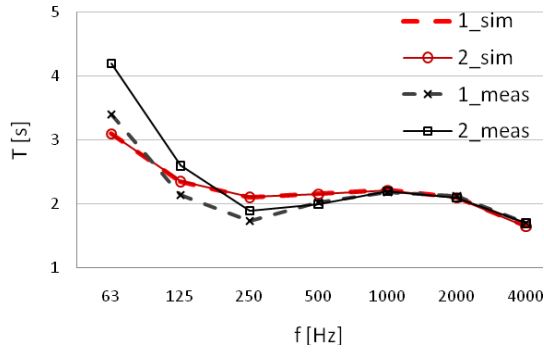


Fig. 7 – Comparison of simulated (_sim) vs. measured (_meas) reverberation time results of configurations no. 1 (both layers closed – double leaf facade) and 2 (one layer closed – single leaf facade).

3.2 Sound reduction index (R)

Figure 8 shows both measured and simulated (model A) sound reduction indices for a number of configurations. Simulation results show large errors especially in low frequencies (125, 250 Hz). At higher cavity sound absorption and with displaced openings the errors tend to become smaller (Figure 8b). The simulation using model B shows a similar performance (Figure 9). The simulation using model C (which is developed after adjusting the length of the tubes in order to compensate for the error found in B simulation results) shows that the alternative modelling of DLF with open elements allows for simple adjustments and leads to better simulation results.

Table 2 shows the overall accuracy of simulation results (for all the models A, B, and C) in terms of R^2 and RMSE, regarding simulated frequency-dependent sound reduction index (R).

Table 18 – Overall performance of the simulation models regarding sound reduction index (comparison only for the 10 configurations modelled with all models A, B, C)

	A	A	B	C
	28 config.	10 config.		
R^2	0.79	0.807	0.751	0.807
RMSE	4.3	5.0	5.5	4.5

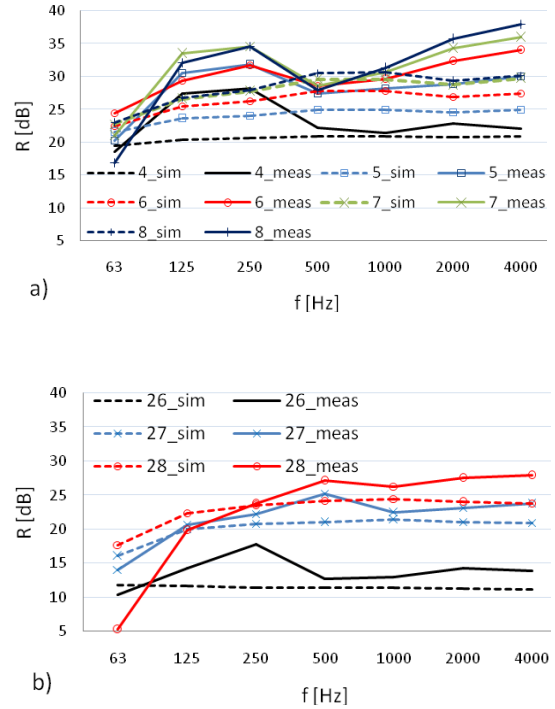


Fig. 8 – Comparison of simulated (_sim, dotted lines) vs. measured (_meas, continuous lines) sound reduction index (R) for two groups of configurations (model A): a) configurations 4-8; b) configurations 26-28 (see Table 1 for configuration specifications).

3.3 Weighted sound reduction index (R_w)

Using simulation results and following the standard procedure (ISO 2013), weighted sound reduction index (R_w) was calculated for each of the simulated DLF configurations. Table 3 shows the overall accuracy of the simulation models (in terms of R^2 and RMSE) with regard to simulation-based weighted sound reduction index values ($R_{w,sim}$).

Table 19 – Overall performance of the simulation models regarding weighted sound reduction index (comparison only for the 10 configurations modelled with all models A, B, C).

	A	A	B	C
	28 config.	10 config.		
R^2	0.963	0.974	0.897	0.945
RMSE	2.5	3.4	3.9	2.5

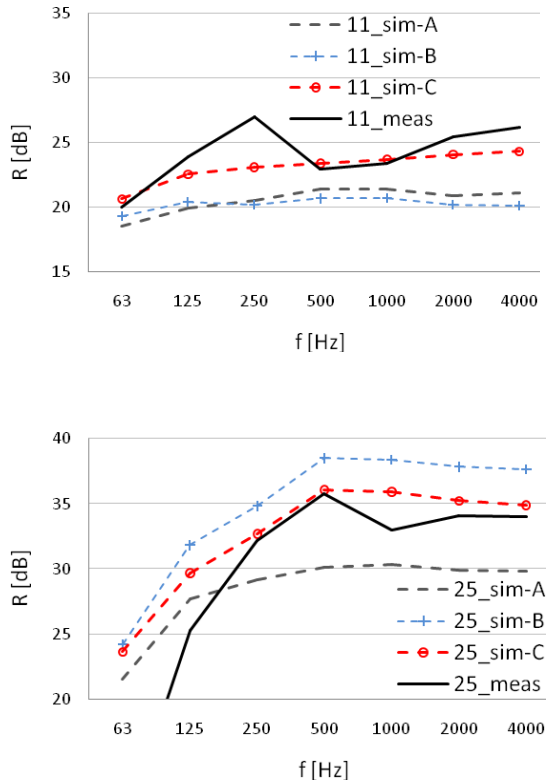


Fig. 9 – Comparison of simulated (model A, B and C) vs. measured sound reduction index (R) for configuration 11 (above) and 25 (below) (see Table 1 for configuration specifications).

4. Discussion

From the comparison results, we can conclude that the simulation results do not reproduce the frequency-dependency visible in the measurement results (Bajraktari et al. 2014). A potential explanation for this circumstance may stem from the fact that the deployed simulation tool currently does not model the complex wave phenomena inside the DLF cavity (Bork 2005, Vorländer 2013). Alternative representations of DLF did not compensate for the simulation tool's limitation, but allowed for simple and intuitive adjustments that led to improved simulation results.

5. Conclusion

The comparison results suggest that currently the acoustical performance of the double leaf facade cannot be accurately predicted using a room acoustics simulation application, even though the

simulation model was calibrated using measured values of reverberation time (Bajraktari et al. 2014). Specifically, the frequency dependency of the measured sound insulation of the DLF could not be accurately reproduced via simulation. A contributing factor to this circumstance may lie in the simulation algorithm's disregard of complex wave phenomena in the cavity space between the two layers of the DLF. On the other hand, a better predictive performance could be achieved while computing the weighted sound reduction index values. In this case, a RMSE of 2.5 was achieved. It is expected that ongoing efforts in advanced room acoustics simulation including wave phenomena (Savioja 2010, Kowalczyk and van Walstijn 2011, Borrel-Jensen 2012) could improve the overall performance of simulation tools, leading also to better future results concerning DLF analysis.

References

- Bajraktari E, Lechleitner J, Mahdavi A. 2014. Measurement and Simulation of the Sound Insulation of Double-leaf Facades with Openings for Natural Ventilation. Proceedings of the 2nd ICAUD International Conference in Architecture and Urban Design. Epoka University, Tirana, Albania, 08-10 May 2014. Paper No. 139, 8p.
- Bork I. 2000. A comparison of room simulation software – The 2nd round robin on room acoustical computer simulation. *Acustica united with acta acustica* 86 (2000) 943–956.
- Bork I. 2005. Report on the 3rd Round Robin on Room Acoustical Computer Simulation – Part II: Calculations. *Acta Acustica united with Acustica*, Vol. 91, 753-763
- Borrel-Jensen N. 2012. Real-time auralisation of the lower frequency sound field using numerical methods on the GPU. Master thesis, RWTH Aachen University, and University of Copenhagen.
- Christensen C L, Koutsouris G. 2013. ODEON Room Acoustics Software, Version 12 – User Manual. 2nd Edition. Odeon A/S, 2013, Lyngby, Denmark.
- ISO. 2013. ISO 717-1, Acoustics – Rating of sound

- insulation in buildings and of building elements. Part 1: Airborne sound insulation
- Kowalczyk K, van Walstijn M. 2011. Room acoustics simulation using 3D compact explicit FDTD schemes. *IEEE Trans. Audio, Speech, Lang. Process.* 19(3), 34 (2011).
- Mahdavi A. 2011. "Room acoustics performance prediction" in: "Building Performance Simulation for Design and Operation", J. Hensen, R. Lamberts (Ed.); Taylor & Francis, New York, 2011, ISBN: 9780415474146, S. 218 - 234.
- Mahdavi A, Çakir O, Pröglhöf C, Lechleitner J. 2012. Sound insulation of a double-leaf wall system with openings for natural ventilation. *Proceedings of the 5th International Building Physics Conference (IBPC), Kyoto, Japan.* pp: 1115-1118.
- Mahdavi A, Bajraktari E, Hintermayer M, Lechleitner J. 2013. Sound Insulation of Double Facades with Operable Windows: an Empirical Inquiry. "CLIMA 2013 - 11th REHVA World Congress and the 8th International Conference on Indoor Air Quality, Ventilation and Energy Conservation in Buildings", K. Kabele, M. Urban, K. Suchý, M. Lain (Ed.); Society of Environmental Engineering (STP), 1/1/1 (2013), Paper-Nr. 275, 8 S.
- Odeon. 2013. Odeon 12.0 Combined. Odeon A/S, Denmark. (www.odeon.dk, accessed 12.02.2014)
- Rindel J. H., Christensen C. L. 2008. Modelling airborne sound transmission between coupled rooms. *Joint Baltic-Nordic Acoustics Meeting 2008*
- Savioja L. 2010. Real-time 3D finite-difference time-domain simulation of mid-frequency room acoustics. In *Proceedings of the 13th International Conference on Digital Audio Effects, DAFx Graz, Austria (2010)*, p. 43.
- Siltanen S, Lokki T, Savioja L, Christensen C L. 2008. Geometry Reduction in Room Acoustics Modeling. *Acta Acustica united with Acustica*, Vol. 94 (2008)
- Svensson P. 2008. The Early History of Ray Tracing in Room Acoustics. Reprint from "Reflections on sound In honour of Professor Emeritus Asbjørn Krokstad", Edited by Peter Svensson, Trondheim, June 2008. ISBN 978-82-995422-3-4
- TNL. 2012. SketchUp Version 8.0. Trimble Navigation Ltd. (www.sketchup.com, accessed 03.12.2013)
- Tugrul A, Lechleitner J, Schuß M, Mahdavi A. 2012. Exploring the role of simulation in room acoustical retrofit of office spaces: a case study. *Fourth German-Austrian IBPSA Conference BauSIM 2012*
- Vorländer M. 1995. International round robin on room acoustical computer simulations. *15th International Congress on Acoustics, Trondheim, Norway 26-30 June 1995.*
- Vorländer M. 2013. Computer simulations in room acoustics: Concepts and uncertainties. *J. Acoust. Soc. Am.*, Vol. 133, No. 3, March 2013

Influence of varying mix proportions on thermal performance of soil-cement blocks

Balaji N.C, Senior Research Fellow, Centre for Sustainable Technologies, Indian Institute of Science, balajinallaval@gmail.com

Praseeda K. I, Assistant Professor, Department of Civil Engineering, Federal Institute of Science and Technology, Ernakulam, Kerala, ki.praseeda@gmail.com

Monto Mani, Associate professor, Centre for Sustainable Technologies, Indian Institute of Science, monto@astra.iisc.ernet.in

Venkatarama Reddy B. V, Professor, Centre for Sustainable Technologies and Department of Civil Engineering, Indian Institute of Science, venkat@civil.iisc.ernet.in

Abstract

Soil-cement blocks generally comprise graded soil, cement and sand to varying proportions to achieve desired structural performance and durability. In their actual integration as part of a building masonry element (envelope), the thermal performance of these blocks determines the climate-responsiveness of the building. However, little study has been done in discerning the influence of varying mix-proportion on the thermal performance of these blocks. The current study examines the role of physio-chemical properties, determined by the varying mix-proportions, on the thermal performance of soil-cement blocks. The paper discerns the influence of the clay content, cement content and dry density on the thermal conductivity of the soil-cement blocks. For this study, soil-cement blocks casted with locally available materials been adopted. Preliminary results revealed that as the clay content increases from 10.5 to 31.6% the thermal conductivity value increases. Further, with an increase in cement content from 5 to 16% the thermal conductivity values also increases.

The thermal conductivity tests conducted using QTM-500 thermal conductivity testing instrument. Further investigation included the influence of soil-cement blocks' thermal properties on dynamic building thermal performance such as time lag and decrement factor. The results of the study are expected to support design of climate-responsive building envelopes for various climatic conditions.

1. Introduction

The physio-chemical properties of soils can be altered or modified by adding stabilizers (admixtures) such as cement and lime, a process termed as soil-stabilization. Cement stabilized soils are used in the constructions of roads, pavements, slope protections, canal linings, etc. They are also used for preparing high-density soil-cement blocks for load-bearing masonry structures. A block-making machine used to compact soil into high-density blocks.

Earlier studies on the soil-cement blocks give broad guidelines to select suitable soils for making blocks and the range of strength and water absorption values for blocks. Most soil-cement blocks' properties (mechanical and durability), production techniques, density, soil-sand mix, soil-cement mix designs (% of clay content, soil, sand cement contents) etc. is very well established. Mechanical properties such as compressive, flexural and direct tensile strength and moisture content of soil-cement blocks are most commonly studied properties of soil-cement blocks. More information on such properties of soil-cement blocks can be found in the studies of Venkatarama Reddy (1995, 2006 and 2007).

There are barely any studies specifically dealing with thermal properties of soil-cement blocks. There is a need for understanding and also for a methodology for such studies. Thermal properties of building materials include thermal conductivity,

diffusivity, emissivity and specific heat, and for practical purposes they are generally determined through their thermal conductivity and specific heat. Hence, the present paper focuses on understanding thermal properties such as thermal conductivity and specific heat capacity of soil-cement blocks having different cement content, densities and clay content, while still retaining structural performance and durability.

2. Experimental Programme

2.1 Materials used for soil-cement blocks

A locally available natural red loamy soil has been used for block making. The soil having a composition of sand (48%), silt (28.6%) and clay (23.4%) is used. The natural soil is reconstituted by blending with river sand in the ratios so that the resulting soil-sand mixture comprises varying clay, silt and sand fractions. Thus, 3 completely different soils (varying clay content) were generated without altering the characteristics of clay mineral;

Ordinary Portland cement conforming to IS 8112 - 1989 is used for the casting of blocks as a binder material.

2.2 Soil-cement block making procedure

Soil-cement blocks are manufactured by using natural soil and the reconstituted soil-sand mixture to obtain 8 different types of blocks with different percentages of cement contents, dry density and clay content. The block density controlled during the manufacturing process (for each set of blocks). Soil-cement blocks of the size 230 x 100 x 75 mm are used in this study. Three varying dry densities of the soil-cement blocks were adopted for this study. A total of 48 blocks consisting of 6 blocks in each category were manufactured. Thus, there are 3 different clay fractions in combination with 4 cement contents and 3 different densities; further the details are given in Table 1. The thermal conductivity and specific heat capacity values of the soil-cement blocks are experimentally determined.

Table 1 – Details of Soil-cement blocks proportion, density, specific heat capacity, and thermal conductivity values

SI No.	Material ID	Clay content in %	Cement content in %	Dry density in kg/m ³	Specific heat capacity in J/kg K	Thermal conductivity in W/ (m K) *(SD, CoV)
1	SCB 1	31.6	8	1700	1096.4	1.065 (0.029, 2.710)
2	SCB 2	10.5	8	1700	1016.7	1.008 (0.042, 4.139)
3	SCB 3	16	5	1700	1028.4	0.842 (0.026, 3.069)
4	SCB 4	16	12	1700	1053.1	1.076 (0.065, 6.072)
5	SCB 5	16	16	1700	938.3	1.097 (0.073, 6.658)
6	SCB 6	16	8	1700	1065.3	1.066 (0.056, 5.277)
7	SCB 7	16	8	1800	1065.3	1.201 (0.033, 2.751)
8	SCB 8	16	8	1900	1065.3	1.303 (0.051, 4.250)

SCB = Soil-cement block, and *within parenthesis is standard deviation (SD) and coefficient of variation (CoV) of thermal conductivity values

3. Testing Procedure

3.1 Thermal Conductivity

Thermal conductivity (λ) is a property of a material that determines how much heat conducted through it for a given temperature gradient. As per IS 3792-1978, thermal conductivity can be defined as “The

quantity of heat in the ‘steady state’ conditions flowing in unit time through a unit area of a slab of uniform material of infinite extent and of unit thickness, when unit difference of temperature is established between its face”.

3.2 Measurement of Thermal Conductivity

Methods for measuring thermal conductivity can be classified into two broad categories: steady-state methods and transient-state heat transfer methods. The line heat source method / hot wire method is the most widely used transient-state method for measuring thermal conductivity of materials. In this study, the instrument used is QTM-500 which measures thermal conductivity based on the transient hot wire method.

3.3 Thermal conductivity test

The quick thermal conductivity meter QTM-500 instrument from Kyoto Electronics Manufacturing Company Ltd, used to measure thermal conductivity values.

In actual conditions, the hygroscopic property of a building masonry element also influences its thermal performance. This is not within the scope of the current study. However, to maintain consistence in the hygroscopic test conditions amongst the samples tested, all the specimens were conditioned (for ~72 hours) and tested at 25°C temperature and relative humidity in the range of 50% to 60%.

4. Results and Discussions

4.1 Thermal Conductivity of Soil-cement blocks

Thermal conductivity of soil-cement blocks with different cement contents, dry densities and clay contents examined. It is a function of material (mineral) composites. The details of the soil-cement blocks tested for thermal conductivity value given in Table 1.

Figure 1 shows the variation in thermal conductivity with the varying clay content, cement content, and dry density of the soil-cement block. The analysis and results discussed in the following sections.

4.1.1 Thermal conductivity with varying clay content of the soil-cement block

The investigation by Reddy and Latha (2013) shows the influence of clay fraction in the soil mixture and void ratio on the characteristics of cement stabilised soil compacts. In this study, the thermal conductivity of soil-cement blocks lies in the range of 1.008 W/ (m K) to 1.065 W/ (m K) for the different clay content of 10.5% to 31.6%. With the increase in the clay content from 10.5 to 16% and 16 to 31.6%, there is an increase of 5.8% and 0% of the thermal conductivities respectively. The overall increase in the thermal conductivity values for clay contents of 10.5 to 31.6% is 5.8% (Figure 1). It can be seen that over a certain percentage of clay content the thermal conductivity value becomes constant.

As the size of clay particles are less than 0.002mm, it acts as a filler material and forms a fine pore structure in material. The effect of increasing clay content on soil-cement blocks decreases their porosity while increases the thermal conductivity, thereby making soil-cement blocks more solid in nature. As the solidity of the block increases, total pore volume reduces, thereby increasing thermal conductivity.

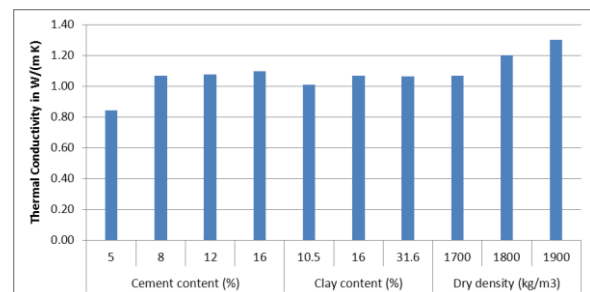


Fig. 1 – The variation in thermal conductivity with clay content, cement content, and dry density of the soil-cement block

4.1.2 Thermal conductivity with varying cement content of the soil-cement block

Bhattacharjee has obtained thermal conductivity values for dry soil-cement blocks for varying cement contents of 4% 6%, 8% and 10%, the thermal conductivity value ranges from 0.437 to 0.670, 0.490 to 0.572, 0.565 to 0.630 and 0.570 to 0.670 respectively.

Adam and Jones (1995) studied thermal conductivity of stabilised soil blocks for the oven

dry samples is in range of 0.25 – 0.55 W/ (m K). Studies by Akinmusuru (1995), on thermal conductivity values of the lateritic soil-cement bricks show the addition of cement decreases the thermal conductivity value for plain brick. Bahar et.al, (2004) studied the electrical conductivity of compacted cement-stabilised soil in order to assess thermal conductivity of the material. The result shows that conductivity decreases slightly with the increase of cement content and sand content. As the cement content of the block increases, the total pore volume reduced and tends to increase heat flow through the block by increasing thermal conductivity. Increasing cement content of the soil-cement block increases the quantity of hydrated products, which helps to reduce the pore volume by developing hydration products (Generally, C_2S , C_3S , C_3A and C_4AF are the main components formed during the hydration of the cement) into the pores of the blocks. Venkatarama Reddy and Ajay Gupta (2006) showed that the pore size of the blocks varies with the cement content, and pore size decreases with an increase in cement content. Blocks having lower cement content show larger size pores compared to blocks with higher cement content that has a large number of smaller pores. Rübner and Hoffmann (2006) studied the variation of total pore volume (one of the pore parameters) under different bulk densities of the same standard brick materials. They found that the denser the materials, the smaller the total pore volume, thereby resulting in the conductive heat transfer being more dominant in comparison with other modes of heat transfer.

The thermal conductivity of soil-cement blocks lies in the range of 0.842 W/ (m K) to 1.097 W/ (m K) for the cement content variation of 5% to 16%. The thermal conductivity of the blocks depends on the cement content and it increases with an increase in cement content (Figure 1). Cement content of the block predominately reduces the internal pore volume as the cement content increases. With the increase in the cement content from 5 to 8%, 8 to 12% and 12 to 16%, there is an increase of 26.60%, 0.94% and 1.93% of the thermal conductivities respectively. The overall increase in the thermal conductivity values from 5 to 16% is 30.28%

4.1.3 Thermal conductivity with varying density of the soil-cement block

Generally, thermal conductivity of the material increases as the density increases from literature (Max Jakob, 1959). Khedari et.al, (2005) casted soil-cement blocks having a composition ratio of 1:1:6 (cement: sand: soil) by volume and obtained thermal conductivity value of 1.4823 W/ (m K); bulk density is 1913.17 ± 27.65 kg/m³, and tested according to the JIS R 2618 standard. Balaji (2012) studies the thermal conductivity of soil-cement blocks having a composition of 1:7:7 (cement: sand: soil) by weight. The thermal conductivity test done as per ASTM C 1113-99 and conductivity value of 1.231 W/ (m K) obtained having a block density 1800 kg/m³. Adam and Jones studied the effect of a stabilizer on density and obtained an exponential relationship with dry density and thermal conductivity for the stabilized soil building blocks. They suggested the need for research to correlate between thermal conductivity and soil type, and to determine the effect of density on thermal conductivity of the soil-cement blocks by varying the density. Balaji (2014) showed that the pore parameter (such as total pore volume) entirely depends on the particle packing. In building materials, this pore parameter depends on the density of the materials.

As the density of the block increases, the percentage of total pore volume decreases and thermal conductivity increases proportionally. The thermal conductivity of soil-cement blocks lies in the range of 1.066 W/ (m K) to 1.303 W/ (m K) for the dry densities variation of 1700 to 1900 kg/m³. Generally, density of material is taken as an indicator of the thermal conductivity (Koenigsberger et. al., 1975), as the denser the material, the higher the thermal conductivity values (Figure 1). Density of the block depends on how the particles of the materials packed with minimal voids/pores. With the increase in the density from 1700 to 1800 kg/m³ and 1800 to 1900 kg/m³, there is an increase of 12.7% and 8.5% of the thermal conductivities respectively. The overall increase in the thermal conductivity values from 1700 to 1900 kg/m³ is 22.2%, is almost 1.22 times of 1700 kg/m³ block thermal conductivity value. As an increase in density by 100 kg/m³, the thermal

conductivity value increases approximately by 1/8th times. The thermal conductivity value varies as the density of the material increases. For this study, a total number of 51 test results considered for obtaining a regression equation, which has a coefficient of determination of 0.987. Experimentally determined thermal conductivity values of soil-cement blocks under varying dry density were used to obtain equation (1). The equation (1) is applicable for the soil-cement blocks having 8% cement content, 16% clay content and for 1700 to 1900 kg/m³ densities.

$$\lambda = 0.1945 \exp\left(\frac{1.0044 \text{ Density}}{1000}\right) \quad (1)$$

Where,

Density in kg/m³

Thermal conductivity (λ) in W/ (m K)

The equation (1) cannot be a generalized thermal conductivity value based only on density. Other than density, several other parameters influence the block thermal conductivity, such as porosity, mineralogical composition, cement content, clay content, degree of saturation, temperature and others. The density is one of the indicative properties which can be used to derive thermal conductivity of the soil-cement blocks.

5. Envelope Studies

The design of the building materials for a required thermal performance is crucial (Richard Hyde, 2000), which depends on the constituent material and microstructure (Balaji et.al. 2013). In the current section, an attempt being made to understand the influence of soil-cement blocks with varying mix proportion and densities through dynamic thermal properties such as time lag and decrement factor. These properties been computed as per UNI EN ISO 13786 – 2008.

5.1 Studies on time lag and decrement factor

The thermal characteristic of the building wall envelope depends on the individual material configuration and its thermal properties. The heat flow through the material is a combined influence of the heat storage capacity and thermal resistance characteristics of the wall elements, which consequently regulates the indoor temperature conditions. The building envelope configuration and its thermal properties such as heat capacity and thermal diffusivity affect the time lag and decrement factor (Koray Ulgen, 2002; Vijayalakshmi, 2006). These can be obtained based on the materials' thermo-physical properties (Asan, 1998). Time lag (Φ) is the time difference between the temperature maximum at the outside and inside when subjected to periodic conditions of heat flow (IS 3792-1978), and a decrement factor is the ratio of the maximum outside and inside surface temperature amplitudes (Koenigsberger, 1973). Asan and Sancaktar (1998) found thermo-physical properties of the envelope material and the type of material (Asan, 2006) has a profound effect on the time lag and decrement factor, and computed time lag and decrement factor for different building materials. Jeanjean et.al (2013) also shows the time lag will increase by lowering thermal conductivity or by increasing its Specific heat capacity. Asan (2006) in another study shows different building materials results in different time lags and decrement factors. Like that, each mix-proportion block behaves differently and has different thermo-physical properties.

In this section, dynamic thermal properties such as time lag and decrement factor calculated for different soil-cement blocks and obtained values shown in Table 2. Further, the same has been plotted in figure 2, 3 and 4 shows the variation in time lag and decrement factor with respect to varying clay content, cement content and dry density of the soil-cement blocks

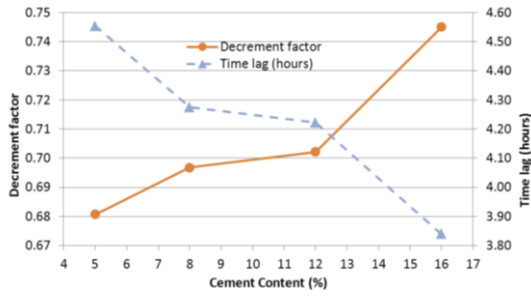


Fig. 2 – Variation of Time lag and Decrement factor on the varying cement content of the soil-cement block

Figure 2 shows the time lag and decrement factor variation on varying cement content. There will be decrease in time lag values as the cement content of block increases, and similarly, the decrement factor value also increasing as the cement content increases.

The time lag and decrement factor depends on the thermal properties of the materials. From figure 1, it can be seen that an increase in cement content increases the thermal conductivity value. These conductivity values directly affect the time lag, and the decrement factor, which also depends on the specific heat capacity of the material. As the cement content increases, the heat capacity of the materials also increases. This shows that the increase in the heat capacity of material directly influences the inside surface temperature of the material, by storing the sufficient amount of heat energy in the material. To obtain a better time lag and decrement factor by using soil-cement block material, it can be recommended that 5 to 12% cement content is suitable.

Table 2 – Calculated dynamic thermal properties of the soil-cement blocks

Material ID	Density in kg/m ³	Specific heat capacity in J/kg K	Thermal conductivity in W/ (m K)	Thermal Mass in kJ/K m ²	Decrement factor	Time lag in hours
SCB 1	1700	1096.4	1.065	1863.9	0.69	4.37
SCB 2	1700	1016.7	1.008	1728.4	0.71	4.21
SCB 3	1700	1028.4	0.842	1748.3	0.68	4.55
SCB 4	1700	1053.1	1.076	1790.3	0.70	4.22
SCB 5	1700	938.3	1.097	1595.1	0.75	3.84
SCB 6	1700	1065.3	1.066	1811.0	0.70	4.27
SCB 7	1800	1065.3	1.201	1917.5	0.74	3.84
SCB 8	1900	1065.3	1.303	2024.1	0.73	3.93

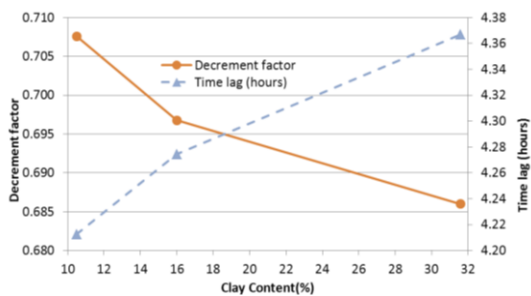


Fig. 3 – Variation of Time lag and Decrement factor on the varying clay content of the soil-cement block

Figure 3 shows the time lag and decrement factor variation on varying clay content. There will be increase in time lag value as the clay content of the block increases, and similarly, decrement factor value also decrease as the clay content increases. The effect of varying clay content of blocks has a negligible variation on time lag and decrement factor.

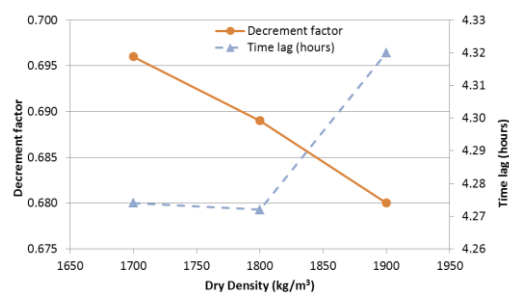


Fig. 4 – Variation of Time lag and Decrement factor on the varying dry density of the soil-cement blocks

Figure 4 shows the time lag and decrement factor variation on varying dry density. In general, an increase in density of the material reduces the decrement factor and increases the time lag. For this study, the blocks' mixed proportion used are the same for all the three type of density blocks, and same specific heat capacity value. The time lag value is almost the same for 1700 and 1800 kg/m³

density material, but for 1900 kg/m³ density the value is a little higher than previous values. The decrement factor value gradually falls as the density of the materials increases. The variation in time lag and decrement factor values is not showing any significance in this study. Use of 1800kg/m³ density soil-cement blocks is more preferable in construction, because casting 1900kg/m³ density blocks through static compaction is impractical; up to 1800kg/m³ density blocks can be casted efficiently. The reason is that human (animate) energy required to cast higher (1900 kg/m³) density soil-cement blocks will be high compare to other lower (1700 & 1800 Kg/m³) density blocks.

6. Summary and Conclusions

Thermal conductivity of soil-cement blocks with different cement contents, dry densities and clay contents examined. The general details of the soil-cement blocks tested for thermal conductivity value given in Table 1.

The thermal conductivity of soil-cement blocks for different clay contents of 10.5% to 31.6% for blocks having 1700 kg/m³ dry density and 8% cement content increases from 1.008 to 1.065 W/ (m K). The overall increase in the thermal conductivity values for clay contents of 10.5 to 31.6% clay content is 5.8%. The percentage of clay content in blocks increases by the decreasing porosity of the block, thereby making blocks more solid in nature. The blocks' conductivity will gradually increases by increasing the clay content.

An increase in the cement content of blocks increases thermal conductivity values from 0.842 to 1.097 W/ (m K) by 30.28% increase. This is due to an increase in hydration products into pores of the blocks, which reduce porosity and conducts more heat through blocks.

Generally, thermal conductivity of material increases by increasing density. Soil-cement blocks under different dry densities (1700 to 1900 kg/m³) show increasing thermal conductivity value from 1.066 to 1.303 W/ (m K). For every 100 kg/m³ increase in density of soil-cement blocks, the

thermal conductivity value increases approximately by 12.5%. Density of the block depends on the particles packing of the materials: the higher the density, the lower the porosity of the block. However, the lower the material porosity, the higher the thermal conductivity value will be.

The thermal conductivity of the soil-cement blocks found to influence by the density, cement content and clay contents. The mix-proportion of the blocks directly regulates the heat storing capacity and thermal resistance characteristics of blocks. The study on time lag and decrement factor shows that the thermal properties of the materials play an important role in regulating these factors. Soil-cement blocks having 16% clay content, 1700 kg/m³ to 1800 kg/m³ density and 5% to 12% cement content may be recommended to obtain better results.

Acknowledgement

Participation at the BSA 2015 conference held at the Free University of Bozen–Bolzano, Italy was financially supported by the Indian Institute of Science (IISc) under GARP International conference funds.

References

- Adam, E A, and P J Jones. 1995. "Thermophysical Properties of Stabilised Soil Building Blocks." *Building and Environment* 30 (2).
- Akinmusuru, J. O. 1995. "Thermal Conductivity of Earth Blocks." *Journal of Materials in Civil Engineering* 6 (3): 341–51.
- Asan, H, and Y S Sancaktar. 1998. "Effects of Wall's Thermophysical Properties on Time Lag and Decrement Factor." *Energy and Buildings* 28 (2): 159–66.
- Asan, H. 1998. "Effects of Wall's Insulation Thickness and Position on Time Lag and Decrement Factor." *Energy & Buildings* 28: 299–305.
- Asan, H. 2006. "Numerical Computation of Time Lags and Decrement Factors for Different Building Materials." *Building and Environment* 41 (5): 615–20.
- ASTM C1113-99. "Standard Test Method for Thermal Conductivity of Refractories by Hot Wire (Platinum Resistance Thermometer Technique)." West Conshohocken, PA.
- Bahar, R., M. Benazzoug, and S. Kenai. 2004. "Performance of Compacted Cement-Stabilised

- Soil." *Cement and Concrete Composites* 26 (7): 811–20.
- Balaji, N.C. 2012. "Personal Communication." Bangalore.
- Balaji, N.C., Monto Mani, and Venkatarama Reddy, B.V. 2014. "Discerning Heat Transfer in Building Materials." *Energy Procedia* 54 (0): 654–68.
- Balaji, N.C., Monto Mani, and Venkatarama Reddy, B.V. 2013. "Thermal Performance of the Building Walls." In *Building Simulation Application 2013, 1st IBPSA Italy Conference*, edited by Marco Baratieri, Vincenzo Corrado, Andrea Gasparella and Francesco Patuzzi, 151–60. Bozen-Bolzano: Bozen-Bolzano University Press.
- Bhattacharjee, B. 1990. "A Study on the Influence of Void and Moisture Contents of Some Building Materials on Their Thermal Transport Properties and Implications on Thermal Performance of Building Envelope." Indian Institute of Technology, Delhi.
- Hyde, R. 2000. *Climate Responsive Design: A Study of Buildings in Moderate and Hot Humid Climates*. E & FN Spon.
- IS 3792 – 1978. "Guide for Heat Insulation of Non-Industrial Buildings." India: Bureau of Indian Standards.
- IS 8112 – 1989. "Specification for 43 Grade Ordinary Portland Cement." India: Bureau of Indian Standards.
- Jeanjean, Anaïs, Régis Olives, and Xavier Py. 2013. "Selection Criteria of Thermal Mass Materials for Low-Energy Building Construction Applied to Conventional and Alternative Materials." *Energy and Buildings* 63 (August). Elsevier B.V.: 36–48.
- Khedari, Joseph, Pornnapa Watsanasathaporn, and Jongjit Hirunlabh. 2005. "Development of Fibre-Based Soil-cement Block with Low Thermal Conductivity." *Cement and Concrete Composites* 27 (1): 111–16.
- Koenigsberger, O H, and T G. 1975. *Manual of Tropical Housing and Building*. Orient Longman Private Limited.
- Kyoto Electronics. "Quick Thermal Conductivity Meter, QTM-500, Operation Manual." Kyoto, Japan: Kyoto Electronics Manufacturing Co., Ltd.
- Max Jakob. 1959. *Heat Transfer, Vol -1*. 7th Edition. New York: John Wiley and Sons, Inc.,.
- Rübner, Katrin, and Dirk Hoffmann. 2006. "Characterization of Mineral Building Materials by Mercury-Intrusion Porosimetry." *Particle & Particle Systems Characterization* 23 (1). WILEY-VCH Verlag: 20–28.
- Ulgen, Koray. 2002. "Experimental and Theoretical Investigation of Effects of Wall's Thermophysical Properties on Time Lag and Decrement Factor." *Energy and Buildings* 34 (3): 273–78. doi:10.1016/s0378-7788(01)00087-1.
- UNI EN ISO 13786 - 2008. "Thermal Performance of Building Components – Dynamic Thermal Characteristics – Calculation Methods." Italian Standards.
- Venkatarama Reddy, B. V., and Jagadish K. S. 1995. "Influence of Soil Composition on the Strength and Durability of Soil-Cement Blocks." *The Indian Concrete Journal* 69 (9): 517–24.
- Venkatarama Reddy, B. V., and A Gupta. 2006. "Strength and Elastic Properties of Stabilized Mud Block Masonry Using Cement-Soil Mortars." *Journal of Materials in Civil Engineering* 18 (3). American Society of Civil Engineers: 472–76.
- Venkatarama Reddy, B. V., and M. S. Latha. 2013. "Influence of Soil Grading on the Characteristics of Cement Stabilised Soil Compacts." *Materials and Structures* 47 (10): 1633–45. doi:10.1617/s11527-013-0142-1.
- Venkatarama Reddy, B. V., Richardson Lal, and K S Nanjunda Rao. 2007. "Optimum Soil Grading for the Soil-Cement Blocks." *Journal of Materials in Civil Engineering* 19 (2): 139–48.
- Vijayalakshmi M.M. Natarajan E. and Shanmugasundaram V. 2006. "Thermal Behaviour of Building Wall Elements." *International Journal of Applied Sciences* 6 (15). ANSINET publishing: 3128–33.

Achieving High-Performance Building Design in the Tropics through Modelling and Simulation: A case study in Singapore

Bharath Seshadri - Nanyang Technological University - s.bharath@ntu.edu.sg

Zhou Jian - Nanyang Technological University – zhoujian@ntu.edu.sg

Vincent Partenay - Nanyang Technological University – vpartenay@ntu.edu.sg

Priya Pawar - Nanyang Technological University – priya.pawar@ntu.edu.sg

Adrian Lamano - Nanyang Technological University – adrianlamano@ntu.edu.sg

Abstract

As part of a Scientific Planning and Support (SPS) initiative for designing buildings, a team of researchers from the Energy Research Institute @ Nanyang Technological University (ERI@N) in Singapore helped design a high performance building using extensive benchmarking, modelling and simulation studies. The building is designed to perform well beyond Singapore’s highest energy efficiency standard – The Green Mark Platinum rating.

Designing high performance buildings in the tropics poses a unique set of challenges. Typical to the region, all non-residential buildings require robust air-conditioning and ventilation systems to fulfil high cooling demands (which typically comprises close to 50% of the building’s total energy demand). The SPS team organized a Design Charrette to address problems such as (i) efficient cooling solutions, (ii) developing tropic-specific standards and schedules, (iii) separating latent and sensible cooling loads, (iv) increasing indoor thermal comfort, (v) passive air-distribution, (vi) centralized water cooling, (vii) intelligent chiller sizing and optimization, (viii) maximizing of natural ventilation and (ix) maximizing of natural lighting.

This paper presents the modelling and simulation results which were used to design energy efficient solutions specific to the problems faced in the tropics, as mentioned above.

1. Introduction

The building project – The North Spine Academic Building (NSAB) is a 25,000m² multi-tenanted, laboratory intensive academic building located at the Nanyang Technological University in Singapore. In line with the vision to meet high

performance standards, the building owners fittingly chose to use the SPS team from ERI@N [Seshadri et al, 2013] to design and plan the building (Figure 1).

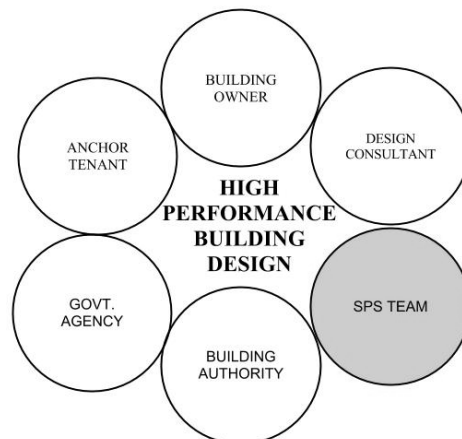


Fig. 1 – The Building Design Working Group [Seshadri et al., 2013]

The following points are a summary of the proposed approach to achieve the greenest building concept that will surpass Singapore’s Building and Construction Authority (BCA) Green Mark (GM) v4.1 Platinum standard [BCA, 2013]. Further elaboration of the below mentioned points are in the following sections.

- (i) Establish Key Performance Indicators (KPIs) for the building that targets BCA’s Green Mark v4.1 Platinum standard and beyond
- (ii) Passive Technology Recommendations : Building Orientation and Façade; Air-tightness of Building Envelope; Building Envelope material characteristics; and Day-lighting and Shading analysis

- (iii) Active Technology Recommendations: Innovative cooling and ventilation; Building information management and Intelligent building controls; Building integrated power generation
- (iv) Modelling and Simulation: Investigating design assumptions (weather data, internal loads and operational schedules); Building energy simulation for predicting energy performance using OpenStudio (OS) and EnergyPlus (E+); Air-Conditioning and Mechanical Ventilation (ACMV) simulation using TRNSYS; Airflow simulation for natural ventilation using ANSYS FLUENT; and Day lighting and shading simulation by using Ecotect Analysis and Radiance

2. Overall Building Design Performance

Compared to the BCA GreenMark established baseline standard (also referred to as building compliance), the NSAB design aims to make a 40% improvement in energy performance, 10% higher than the highest performance rating GM Platinum. Figure 2 shows a tentative (yet to be verified) proposed building performance of the different sub-systems.

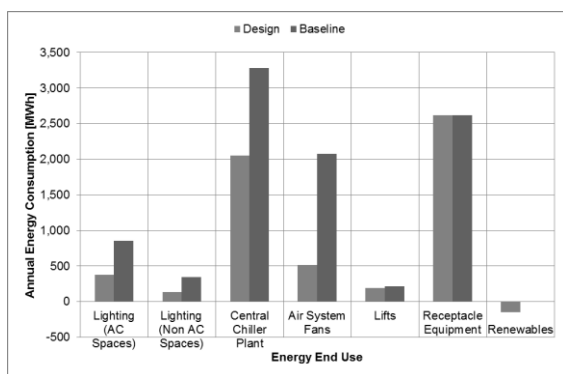


Fig. 2 – Predicted annual Energy Consumption (MWh) categorized into end-use according to design and baseline parameters

The notable improvements made to the baseline (code compliant) design were:

- (i) Lowering average annual environmental heat gain from 50 W/m² to 17 W/m² by minimizing East-West facade gains, using double-glazed windows, high reflective paints, vertical greenery and appropriate shading.
- (ii) Using a high-efficiency medium-temperature central chiller plant, energy-recovery de-humidification units and fan-less (passive) air distribution in rooms
- (iii) Maximizing daylight, using energy efficient LED and task lighting

3. Benchmarking Input Data

3.1 Metering Equipment Loads

To accurately model the heat gains inside building spaces, it was necessary to meter the tenants' existing spaces: which included equipment, lighting and operational schedules of the tenants [Leung et al., 2012]. Hence, the design team avoided risking incorrect ACMV equipment sizing by not making assumptions regarding internal heat load calculations.

Figure 3 and Figure 4 represent a plug-load metering study, done on weekdays and weekends respectively, conducted by the authors over a 1 month period.

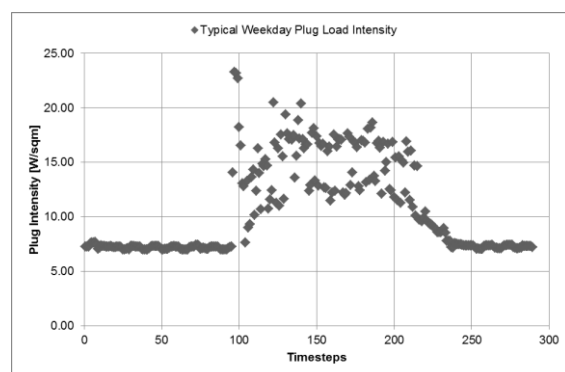


Fig. 3 – Metered weekday plug load intensity data for research office space during 01 to 31 Oct 2014 (Mon - Fri)

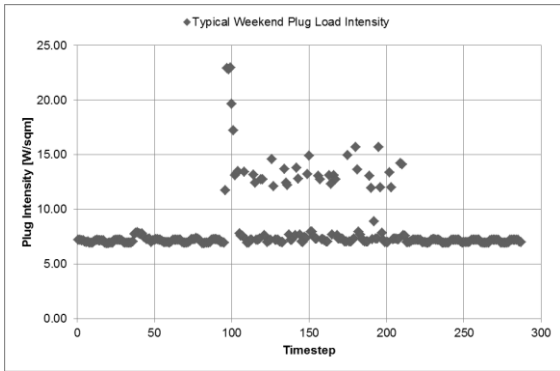


Fig. 4 – Metered weekend plug load intensity data for research office space during 01 to 31 Oct 2014 (Sat-Sun)

The above figures show that for research specific office spaces, the peak (0800 – 2000 hrs) equipment load was not significantly different from design assumptions [BCA, 2013]. But, the off-peak (2000-0800 hrs) plug load was higher than conventional office spaces. Upon further investigation, it was found that usage of high-performance processors (which could be accessed remotely) during off-peak hours was the reason for this unusually high load.

3.2 Laboratory Fume-hoods

Another example of accurately modelling equipment according to the operational performance was the laboratory fumehoods exercise. Laboratory fumehoods are responsible for high ventilation rates in labs and as such have to be controlled according to demand [Mathew, et al., 2007]. It was decided to quantify an occupancy sensor-control for fumehood-intensive laboratories. During the exercise, fumehood occupancy sensors, which were to be modelled for fumehood-intensive labs at NSAB, were installed at a test lab. The power consumption of the fumehood was measured for 1 month with the occupancy sensor and without. The results of the study, summarized in Figure 5, showed ~28.5% savings, marginally lower than 30% claimed by the equipment supplier based on previous case studies [White and Wu, 2014].

For modelling purposes, a 28.5% ‘control-factor’ was taken into account based on the exercise.

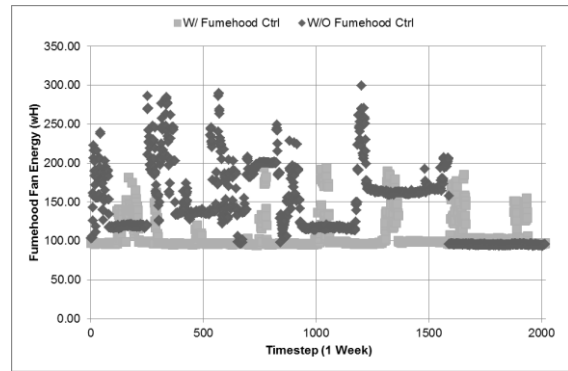


Fig. 5 – Laboratory Fumehood Operation with and without Occupancy Controls

4. ACMV Modelling

4.1 Central Chiller Plant

Instead of an exclusive chiller plant to supply chilled water to NSAB, it was decided to procure a central chiller plant to supply chilled water to NSAB and 2 of its surrounding buildings – the North Spine Learning Hub (NSLH) and Block N4. The SPS team was tasked to simulate the building loads and calculate the hourly annual cooling load demand of the 3 buildings.

Preliminary calculations showed that a total of 5 chillers were needed – Two 275 RT (Refrigerant Tons) Units (Unit 1, 2) for off-peak hours (2000 – 0800 hrs.) and Three 550 RT Units (Unit 3, 4, 5) for peak hours (0800 – 2000 hrs.). A simulation schematic is shown in Figure 6.

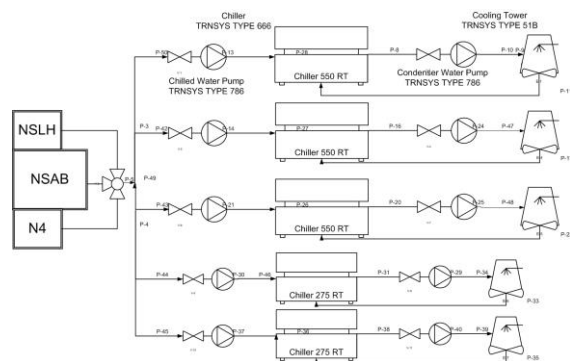


Fig. 6 – System modelling schematic for Central Chiller Plant

Annual cooling simulations from NSAB and NSLH, and metered data from Block N4, suggested that the chiller plant had to be sized to provide a maximum cooling demand of 2100 RT, as shown in Figure 7.

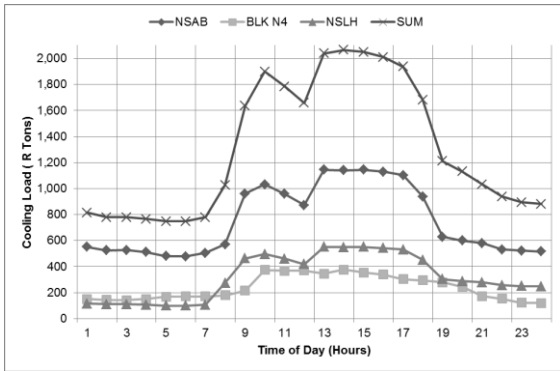


Fig. 7 – Annual maximum hourly cooling loads for the Central Chiller plant

4.2 Chiller Selection and Control Optimization

Even before the modelling exercise for the chiller plant was done, the modelling team offered their recommendations on best-efficiency chiller types based on their simulated performances for the total cooling loads.

Once the performance of the chillers, pumps and cooling towers were established, the modelling team set forth various control and optimization scenarios to maximize the frequency of best efficiency ‘sweet-spots’. The two control methodologies [Wei, et al., 2014] which achieved the highest rated annual chiller plant performances were (i) schedule controlled operation and (ii) iterative control optimization.

The (i) schedule controlled operation method chooses when to switch ON and OFF Units 1-5. The schedule is based on maximum, minimum and average time-dependent cooling load demands. The individual, overall plant efficiency (global efficiency) and the operational frequency of the individual units are shown in Figure 8.

The (ii) iterative control operation method, an ideal-case operation, represents the best-possible chiller plant operation and the most difficult to achieve. The control operation tries to run each of the operating chillers at their individual best-efficiency ‘sweet-spot’ at all times. The individual, overall plant efficiency (global efficiency) and the operational frequency of the individual units are shown in Figure 9.

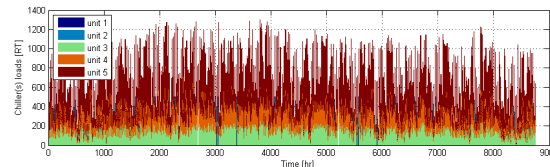
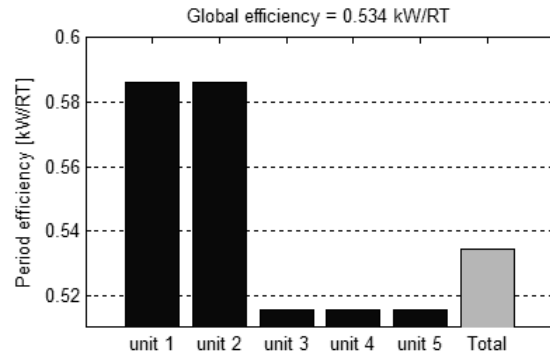


Fig. 8 – Annual Performance of the Chiller Plant using (i) schedule controlled operation: Individual unit performance (top) and frequency (below)

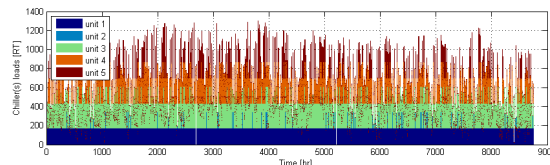
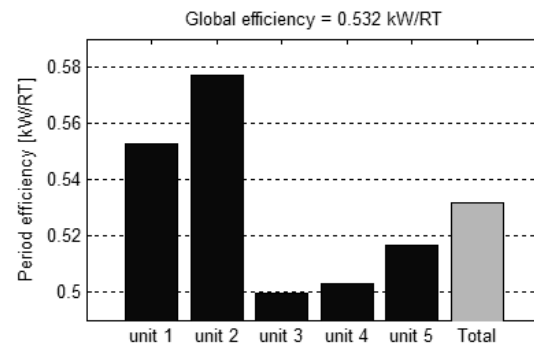


Fig. 9 – Annual Performance of the Chiller Plant using (ii) iterative control operation: Individual unit performance (top) and frequency (below)

It was concluded that the scheduled chiller plant control operation was sufficiently close to the ideal iterative control operation (differing by 0.002 kW/RT) and was chosen to operate the chiller plant.

4.3 Energy Recovery Units for Dedicated Outdoor Air System

Moisture control in the tropics is the biggest obstacle to achieving air-conditioning energy efficiency [Dong et al., 2005]. As is the case in most tropical locations, Singapore’s daily relative

humidity ranges from 65% to 95% [Dong et al., 2005]. As such, fresh air is cooled to low temperatures to control moisture before being supplied to the building spaces. This often results in over-cooling and thermal discomfort among occupants.

The above mentioned problems are magnified if spaces require high fresh air demands. Laboratory spaces require upwards of 6 L/s/sqm [Mathew, et al., 2007] of fresh air, as compared to 0.56 L/s/sqm [BCA, 2013] for conventional office spaces, which would make lab spaces even more susceptible to the above mentioned problems.

Hence, NSAB being a laboratory intensive building, it was decided to employ an energy-recovery mechanism to pre-cool the outdoor air, before the primary cooling stage, and re-heat the air-stream, after the primary cooling stage, using the incoming outdoor air to achieve optimal supply air conditions. This unit was designer to be a Dedicated Outdoor Air System (DOAS), with remaining zone sensible cooling demands met by Fan-Coil Units. A schematic of this Dehumidification Unit (DHU) is shown in Figure 10.

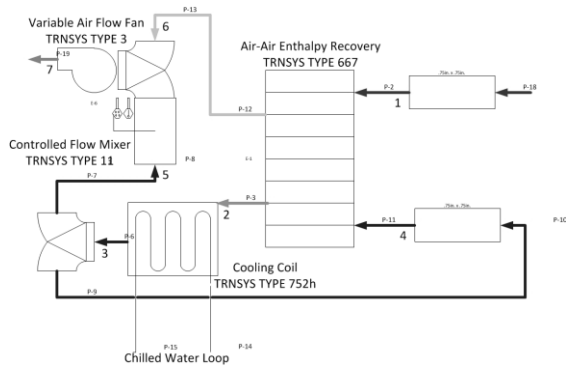


Fig. 10 – System modelling schematic for Dehumidification and Cooling using an air-air energy recovery unit (DHU)

A damper control was installed to maintain the supply air set-points by controlling the mixing of re-heated and non-reheated air. As shown in Figure 11 and Figure 12, the supply air conditions of 22°C and 55% RH fluctuate by <0.2°C and < 2.5% respectively, which is acceptable.

The cooling demand of the fresh air was simulated using a conventional AHU and the above mentioned DHU using energy recovery mechanism. It was found that the DHU energy

performance was 13% better than conventional AHUs.

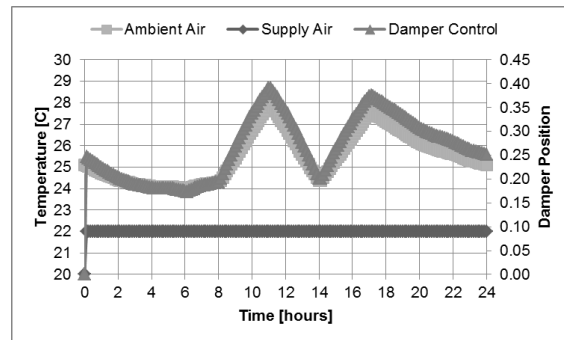


Fig. 11 – The DHU Damper control which maintains setpoint humidity of the conditioned Supply Air

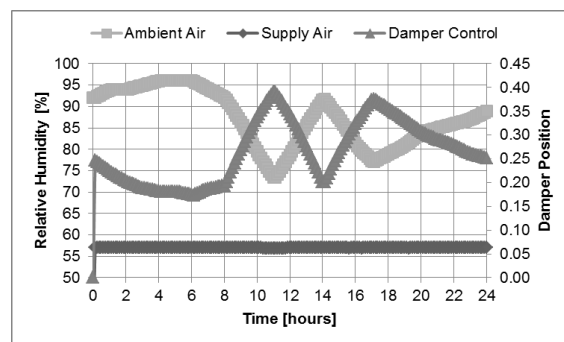


Fig. 12 – The DHU Damper control which maintains setpoint humidity of the conditioned Supply Air

5. Daylighting Simulations

5.1 Outdoor Areas

Daylighting for outdoor areas was done, using Ecotect Analysis and Radiance to establish the natural light levels and comfort in common spaces such as staircases, corridors and the plaza. Using results derived from daylight simulations the lighting engineers were able to identify areas which are expected to receive lower natural light levels (< 150 lux), and were able to make informed decisions on the locations of photo-sensors to activate electric lighting.

It was found that, despite being surrounded on all sides by buildings of equal height, only fully enclosed corridors were in danger of having low natural light levels and had to have photo sensors installed. Other common areas had good natural light levels between 0700hrs and 1800hrs every day. These areas only needed timer switches to switch electric lights on after 1800hrs and before 0700hrs.

Figure 13 and Figure 14 are examples of Radiance outdoor area simulations.

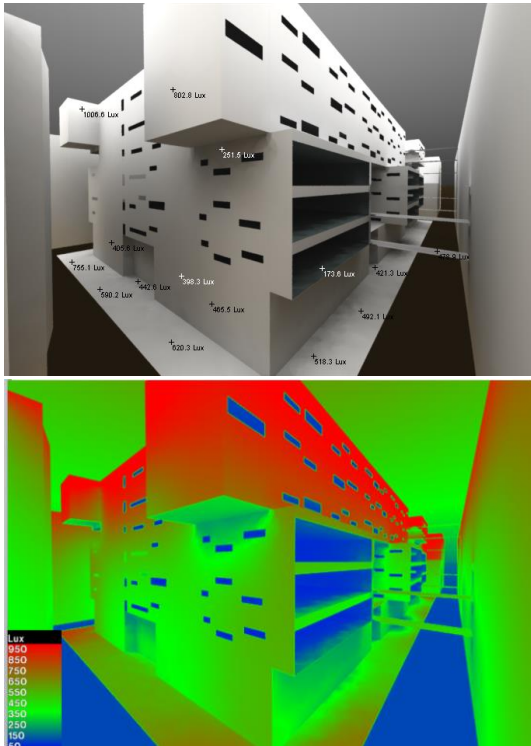


Fig. 13 – Outdoor Daylighting levels (Overcast) using Radiance

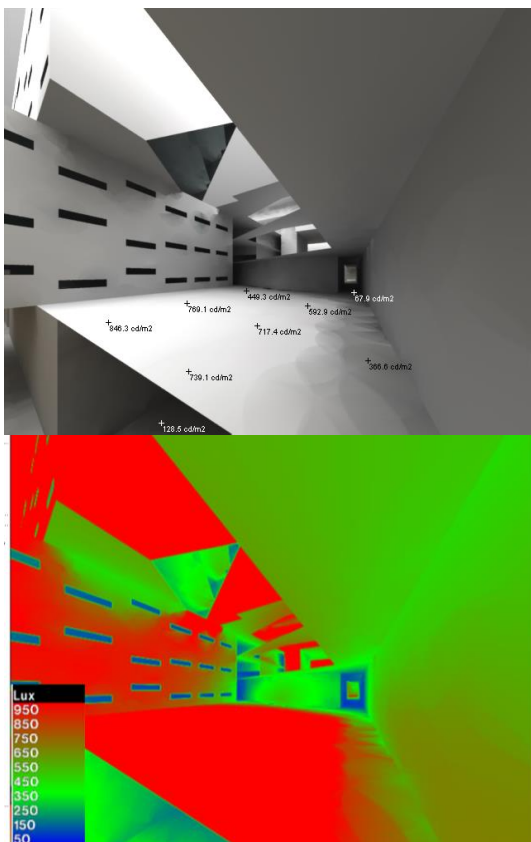


Fig. 14 – Outdoor Daylighting levels (Overcast) using Radiance

5.2 Indoor Areas

Daylighting for outdoor areas was done using Ecotect Analysis and Radiance, to establish the natural light levels and comfort in indoor air-conditioned spaces. Using results derived from daylight simulations the lighting engineers were able to measure daylight perimeters receiving good natural light levels (>500 lux) to install light sensors which could de-activate electric lighting [SPRING Singapore, 2006].

It was found that the daylight penetration in the indoor spaces was minimal due to the surrounding buildings that deflected direct solar radiation. Typical to tropical architecture, the East-West facades featured very little window area, and hence the daylight penetration was negligible (Figure 15). However, the North-South façade which featured higher window-wall ratio had better natural light levels, especially rooms with shop-front type of windows (Figure 16). Although limited, these rooms were able to receive 2.5 – 3m daylight penetration from the window.

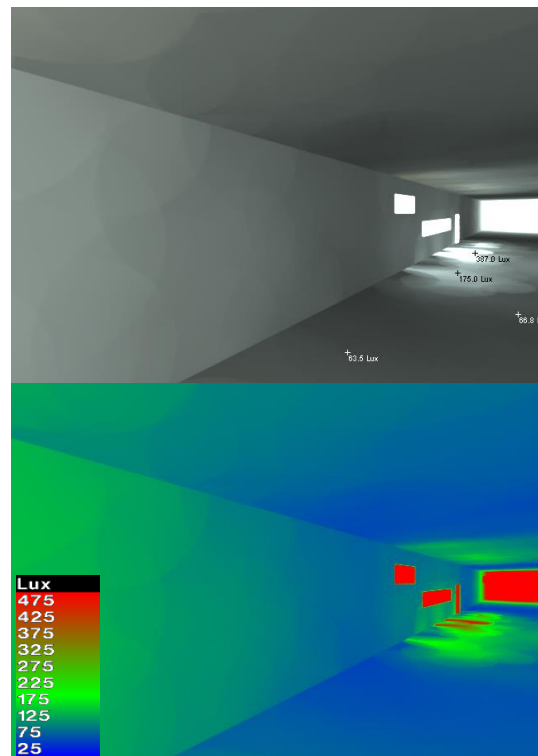


Fig. 15 – Indoor Daylighting levels (Overcast) to measure Daylight perimeter using Radiance for a Level 2 Space

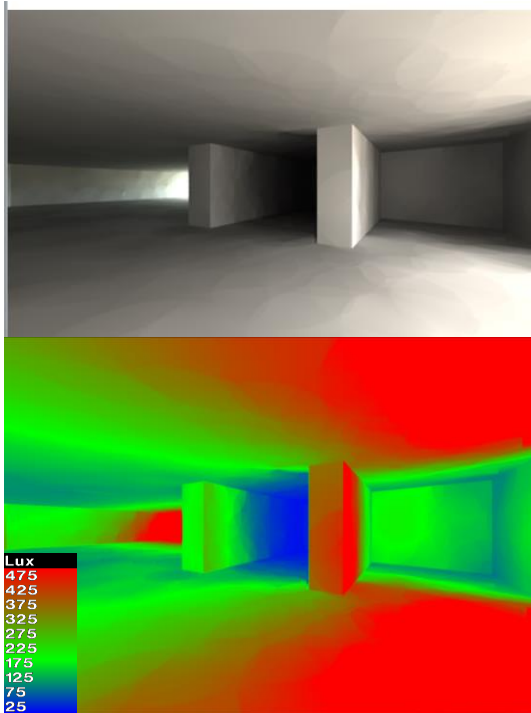


Fig. 16 – Indoor Daylighting levels (Overcast) to measure Daylight perimeter using Radiance for a Level 2 Space

5.3 Daylight Maximization Devices

It was concluded through previously described daylighting simulations that the surrounding building structures prevented deep penetration of sunlight into indoor spaces. Hence, the implementation of skylights and light shelves, popular daylight maximization devices, was considered. The SPS team measured the effect of these devices using another round of simulation exercises.

5.3.1. Solar Light Tubes

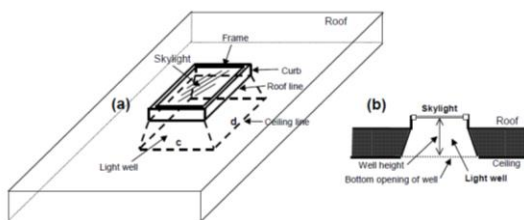


Fig. 17 – Roof-mounted sky lights [EnergyPlus, 2010]

Light tubes are light transmitting fenestration forming all, or a portion of, the roof of a building's space for daylighting purposes (Figure 17). A 2x2m grey glass panel, (0.65 Visible Light Transmittance)

was used to model the light tube. A snapshot of the results is shown in Figure 18.

It was concluded that the light tube could increase the ambient lighting level inside the office space by 120 lux during a sunny day, as shown in Figure 18, but was also capable of causing excessive glare during 1200-1400 hrs. Owing to potential for glare and due to space constraints on the roof due to air-conditioning equipment, the light tubes were not employed.

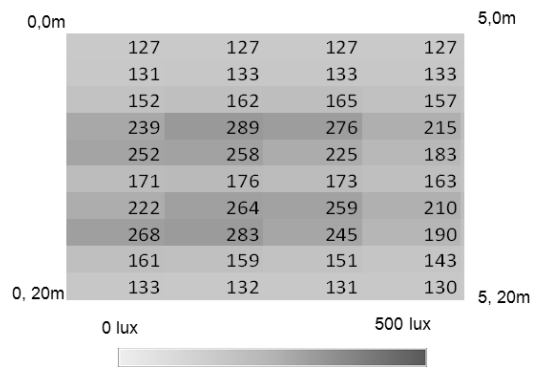


Fig. 18 – Increase in lighting levels due to sky lights at an office space on the highest level at 0900hrs on Dec 21st

5.3.2. Light Shelves

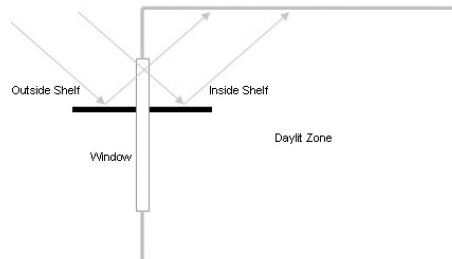


Fig. 19 – Daylight Re-direction louvers or Light Shelves [EnergyPlus, 2010]

Light Shelves re-direct daylight to the back of the room, hence distributing the amount of daylight that falls on the window plane to the indoor space (Figure 19). These devices are expected to extend the daylight perimeter and reduce electrical lighting consumption [Guglielmetti et al., 2011].

It was concluded that the daylight re-direction louvers were able to redistribute the daylight from the daylight perimeter zone to the back of the room, providing a comfortable ambient light for the entire space and increasing the average lighting level in the room by 20-80 lux depending on the

Modelling, testing and optimization of a MVHR combined with a small-scale speed controlled exhaust air heat pump

Fabian Ochs – University of Innsbruck, Austria – Fabian.Ochs@uibk.ac.at

Dietmar Siegele – University of Innsbruck, Austria – Dietmar.Siegele@uibk.ac.at

Georgios Dermentzis – University of Innsbruck, Austria – Georgios.Dermentzis@uibk.ac.at

Wolfgang Feist – University of Innsbruck, Austria; PHI, Germany – Wolfgang.Feist@googlemail.com

Abstract

A micro-heat pump in combination with a mechanical ventilation with heat recovery (MVHR) unit is developed and integrated in the façade in the framework of the iNSPiRe project. The heat pump uses the exhaust air of the MVHR unit as a source and provides heat to the supply air of the ventilation system. Thus, one compact unit can be used for combined ventilation and heating (and/or cooling). Fresh outdoor air flows into the MVHR unit, where it is heated with a heat recovery efficiency of up to 90%. It is then further heated by the micro-heat pump up to a maximum of 52 °C in order to supply space heating (reverse operation for cooling possible in future versions). A simulation study has been performed to investigate the energy performance of the micro-heat pump. A detailed physical model of the μ HP is developed within the Matlab simulation environment and validated against measurements of two functional models in so-called PASSYS test cells. The performance of the system is investigated for different renovation standards (EnerPHit with 25 kWh/(m²·a) and PH with 15 kWh/(m²·a)) at 7 different climatic conditions.

1. Introduction

The majority of existing building stock in Europe and worldwide is poor energy performance buildings and renovation plays a major role in achieving climate protection and energy independence. Deep renovation solutions in combination with integrated HVAC systems are developed within the framework of the iNSPiRe European project. In this work the development, testing and modelling of a façade integrated micro-heat pump (μ HP) in combination with mechanical ventilation with heat recovery (MVHR) is

presented. Different functional models are developed in the framework of the iNSPiRe EU-project and are measured in PASSYS test cells (Passive Solar Systems and Component Testing) at the laboratory of Innsbruck University and will be later monitored in a demo building in Ludwigsburg, Germany. It is an example of social housing built in the 1970s, which contains 4 flats on 4 storeys. During the renovation process, a prefabricated timber frame façade will be fitted onto the building. The reliability and durability of the unit will be tested and the components and the system including control will be optimized.

2. Motivation and Concept

The main objective of the development of a façade integrated micro-heat pump (μ HP) is a cost-effective mechanical ventilation system with heat recovery (MVHR) in combination with a vapour compression cycle for heating/cooling (μ HP) for the application in very energy efficient buildings with a specific heating load in the range of 10 W/m². The exhaust air of the MVHR is the source of the micro-heat pump with a heating power of approx. 1 kW, which heats the supply air to max. 52 °C. A pre-heater (defroster) and backup heater for peak load coverage are required. For comfort reasons, an additional bathroom radiator is recommended.

The prefabricated unit is designed as a compact system for façade integration and thus minimal space use. With this compact mechanical ventilation heating (and cooling) system, cold ducts inside the thermal envelope can be avoided.

As the whole solution will be prefabricated, the construction and installation time can be kept as short as possible. A minimal installation effort is desirable for economic reasons. With the micro-heat pump, renovations with minimum intervention are enabled (minimum invasive renovation). A simplified hydraulic concept is shown in Figure 1.

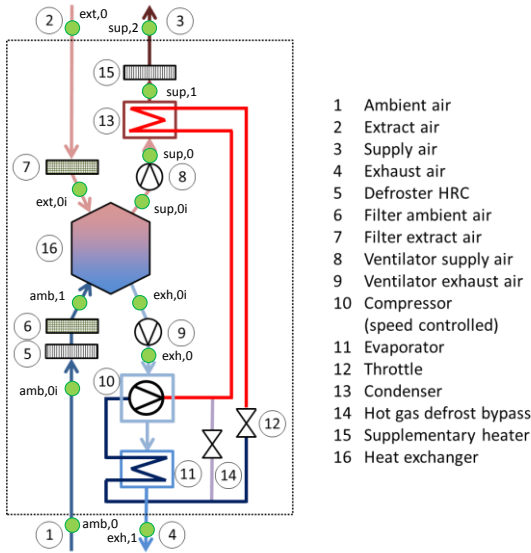


Fig. 1 – Hydraulic scheme of the micro-heat pump

The ambient air (1) will be heated with the defroster (5) if the ambient temperature drops below -3 °C (optionally -5 °C). The filter for the ambient air (6) is situated in front of the heat exchanger (16). The ventilator for the supply air (8) is situated after the heat exchanger. The supply air will be heated in the condenser (13) of the micro-heat pump. If the temperature of the supply air after the condenser is too low to cover the heat load, a supplementary heater (15) will heat the supply air (3) up to 52 °C. The extracted air (2) of the room is filtered (7) before the heat exchanger. After the heat exchanger, the ventilator for the exhaust air (9) is situated. The compressor of the heat pump is situated in the air flow of the exhaust air in front of the evaporator (11). This is changed to the ambient air in the most recent version. The expansion valve (12) reduces the pressure between condenser and evaporator. Hot gas defrost (14) is necessary in case of ice formation in the evaporator.

3. Thermodynamic Analysis

The MVHR, the vapour cycle and the air heating/cooling are modelled in steady state with Matlab using the CoolProp functions [CoolProp2014] to derive the thermodynamic states of the refrigerant and of the air.

3.1 MVHR

The enthalpy balance (eq. 1) of the heat exchanger (excluding the ventilators) includes thermal losses to the ambient and gains from the room, respectively:

$$H_{ext} - \min(H_{exh,0,i}; H_{exh,0,i,s}) = H_{sup,0,i} - H_{amb,1} - \dot{Q}_{loss,MVHR} \quad (1)$$

The effective heat transfer capability UA_{eff} can be calculated based on the effectiveness of the MVHR η_{PHI} acc. to the definition of Passive House Institute (PHI)

$$\eta_{PHI} = \frac{(\vartheta_{ext} - \vartheta_{exh,0}) + \frac{P_{el,vent}}{\dot{m} \cdot c_p}}{(\vartheta_{ext} - \vartheta_{amb,1})} \quad (2)$$

which is measured for conditions that exclude the occurrence of condensate. The effectiveness is published for many products, see Feist (2014). The effective heat transfer capability is assumed to be constant for all operation conditions (as there is always laminar flow) except for the case when condensation occurs, see Siegele (2014). The actual heat transferred from the warm to the cold stream depends on the flow rate as well as on the ambient and extract air conditions (temperature and rel. humidity) and can then be calculated by

$$\dot{Q}_{MVHR} = UA_{eff} \cdot \Delta\vartheta_{log} \quad (3)$$

with the logarithmic temperature difference

$$\Delta\vartheta_{log} = \frac{(\vartheta_{ext,1} - \vartheta_{sup,0,i}) - (\vartheta_{exh,0,i} - \vartheta_{amb,1,i})}{\ln\left(\frac{(\vartheta_{ext,1} - \vartheta_{sup,0,i})}{(\vartheta_{exh,0,i} - \vartheta_{amb,1,i})}\right)} \quad (4)$$

Here, the power of the ventilators $P_{el,vent}$ has to be considered:

$$\vartheta_{sup,0,i} = \vartheta_{sup,0} - \frac{P_{el,vent}}{2 \cdot \dot{m} \cdot c_p} \quad (5)$$

$$\vartheta_{exh,0,i} = \vartheta_{exh,0} - \frac{P_{el,vent}}{2 \cdot \dot{m} \cdot c_p} \quad (6)$$

where the index i is used for the temperatures inside the MVHR (i.e. before each ventilator). Note that the condensation is accounted for with the effective heat transfer capability (which is a

function of the extract air humidity ratio and the ambient temperature) and therefore the approach must be considered as non-physical. For a physical approach, a discrete MVHR model has also been developed and used for comparison. The discrete model is significantly more time consuming.

For the performance of the MVHR the pre-heater power

$$\dot{Q}_{preheater} = \dot{m}_a \cdot (h_{amb,1} - h_{amb,0}) \quad (7)$$

has to be considered. The COP of the MVHR can then be calculated as follows

$$COP_{MVHR} = \frac{\dot{Q}_{preheater} + \dot{Q}_{MVHR}}{\dot{Q}_{preheater} + P_{divert}} \quad (8)$$

3.2 Vapor Cycle

A simplified physical vapour cycle model for the HP is used to perform a sensitivity analysis and to optimize the components. Pressure losses in and between the components are disregarded with the exception of the pressure loss in the condenser which is considered by a given pressure difference Δp_{cond} . Subcooling and superheating are considered in a simplified way with given temperature differences ΔT_{sub} and ΔT_{super} , respectively (Fig. 2).

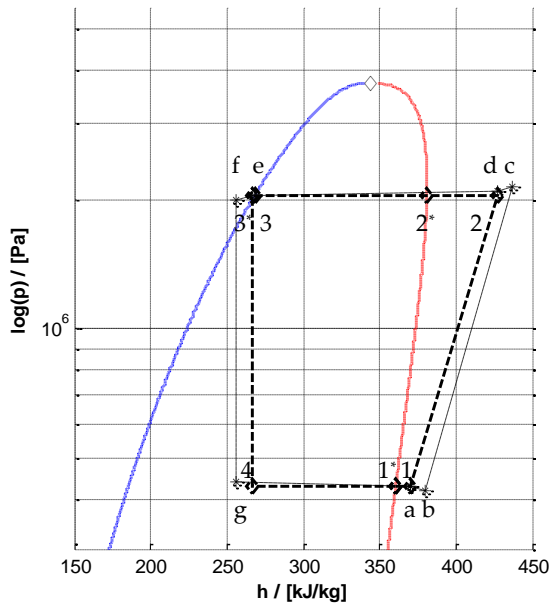


Fig. 2 – Pressure vs. enthalpy diagram of the heat pump cycle, Heat Pump Cycle (thin dashed line): a) evaporator outlet, b) compressor inlet, c) compressor outlet, d) condenser inlet, e) condenser outlet, f) expansion valve inlet, g) evaporator inlet Simplified heat pump cycle (thick dashed line): 1) superheated vapor, 2) condenser inlet, 2*) saturated vapor at p_{cond} , 3*) boiling liquid at p_{cond} , 3) sub-cooled vapor, 4) evaporator inlet, 1*) saturated vapor at p_{evap}

The evaporator is divided in three sections (film evaporation, evaporation and superheating) with varying shares of the total evaporator area A_{evap} , which is 4 m² in the functional model. The heat transfer coefficients are assumed to be constant in each section. Correspondingly, the condenser is divided in de-super-heating, condensation and sub-cooling sections, again with varying shares of the total condenser area A_{cond} and constant (i.e. given) heat transfer coefficients. The section areas of evaporator and condenser are determined iteratively.

The mass flow of the refrigerant

$$\dot{m}_{ref} = D \frac{N_{min}}{60 \text{ s/min}} \cdot \rho_{suc} \cdot \eta_{vol} \quad (9)$$

is a function of the displacement which is here $D = 6.2 \text{ cm}^3$ (Embraco, hermetic reciprocating compressor, speed controlled) and of the volumetric efficiency which is approximated by the following equation

$$\eta_{vol} = 1 - V_c \cdot \left(\tau^{\frac{\kappa}{\kappa-1}} - 1 \right) \quad (10)$$

Here, V_c is the clearance volume fraction, which is a function of the compression ratio and the compressor speed and has to be determined from compressor data. For sake of simplicity instead of the polytropic exponent n , the isentropic exponent

$$\kappa = \frac{c_p}{c_v} \quad (11)$$

is used. The compression ratio

$$\tau = \frac{p_{dis}}{p_{suc}} \quad (12)$$

is a function of the compressor discharge p_{dis} and suction p_{suc} pressure and determines the isentropic efficiency, which can be approximated by a polynomial or implemented by means of a 2D-lookup table.

The electrical efficiency of the inverter depends on the speed of the compressor and can be approximated with the following polynomial

$$\eta_{el,inv} = (-1.09 \cdot 10^{-7} \cdot (N/RPM)^2 + 0.0009 \cdot (N/RPM) - 1.034) \% \quad (13)$$

Finally, the performance of the heat pump

$$COP_{HP} = \frac{\dot{Q}_{cond}}{P_{compressor}} \quad (14)$$

and the system performance can be calculated

$$COP_{sys} = \frac{\dot{Q}_{preheater} + \dot{Q}_{MVHR} + \dot{Q}_{cond} + \dot{Q}_{postheater}}{\dot{Q}_{preheater} + P_{divert} + P_{d,HP} + \dot{Q}_{postheater}} \quad (15)$$

Here, the electric consumption of the heat pump is

$$P_{el,HP} = \frac{P_{el,comp}}{\eta_{HP}} \quad (16)$$

The post-heater power is included

$$\dot{Q}_{postheater} = \dot{m}_a \cdot (h_{sup,2} - h_{sup,1}) \quad (17)$$

For the post-heater either a given temperature e.g. $\theta_{sup,2} = 52 \text{ }^\circ\text{C}$ is assumed or alternatively the power of the post-heater is calculated given a constant required total heating power which is

$$\dot{Q}_{tot} = \dot{m}_a \cdot (h_{sup,2} - h_{amb,0}) \quad (18)$$

4. Simulation Results and Sensitivity Study

4.1 Reference Case

The performance of the micro heat pump is a function of the following boundary conditions:

- Speed of the compressor (rounds per minute, rpm) (high influence)
- Volume flow (high influence)
- Ambient temperature (small influence)
- Room temperature (small influence)
- Room humidity (very small influence)

The resulting temperature vs. humidity ratio diagram is shown in Fig. 3.

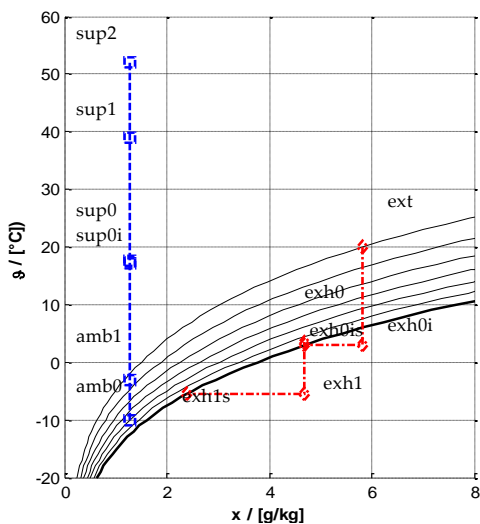


Fig. 3 – Temperature vs. humidity ratio diagram

Taking a flow rate of $90 \text{ m}^3/\text{h}$ and maximum compressor speed (4500 rpm) as an example, for

the boundary conditions of $-10 \text{ }^\circ\text{C}$ and $-5 \text{ }^\circ\text{C}$ ambient temperature and $20 \text{ }^\circ\text{C}$ extract air temperature with a relative humidity of 35% and the parameters mentioned in table 2 below the following results are obtained:

Table 1 – Performance of the μHP

Parameter	-10 $^\circ\text{C}$	-5 $^\circ\text{C}$
COP _{sys} w\ post-heat. to 52 $^\circ\text{C}$	1.93	2.15
COP _{sys} = 2.56 w\ o post-heat.	2.07	2.31
COP _{HP}	1.54	1.53
\dot{Q}_{tot} / [W]	1594.2	1448.5
$\dot{Q}_{pre-heating}$ / [W]	179.9	51.3
\dot{Q}_{cond} / [W]	766.3	763.6
\dot{Q}_{MVHR} / [W]	539.9	548.5
$\dot{Q}_{post-heating}$ / [W]	108.1	85.0
\dot{m}_{MVHR} / [g/h]	50.2	56.0
$\dot{m}_{condensat}$ / [g/h]	194.8	192.3

The pre-heater is assumed to work ideally, here (pre-heating to $-3 \text{ }^\circ\text{C}$). Due to the cyclically required deicing of the evaporator the system COP decreases from 2.31 to 1.88 at $-5 \text{ }^\circ\text{C}$. The deicing control offers potential for optimization.

The parameters used for the simulation correspond to the design of the first functional model (see section 5) and are summarized in table 2. An improved version is currently being measured in the lab and better performance can be expected. The aim is a heat pump COP of at least 2, see also section system simulation, below.

Table 2 – Parameter of the MVHR and μHP , see Siegele (2014)

Parameter	Symbol	Value (range)	Unit
Volume flow rate	V	90 (60 ... 150)	m^3/h
Specific ventilation power	$p_{el,vent}$	0.4	Wh/m^3
Heat recovery efficiency (PHI definition)	η_{PHI}	0.85	-
Heat losses of MVHR	$Q_{loss,MVHR}$	0	W
Compressor displacement	D	6.2	cm^3
Clearance	V_c	0.0375	-
Volume fraction			
Compressor frequency	N_{min}	2000 (1000 ...	rpm

Refrigerant	-	4000)	-
		R290	
		(R134a)	
Heat loss compressor	$Q_{loss,comp}$	0	W
Electrical efficiency of compressor	η_{comp}	0.85	-
Area of evaporator	A_{evap}	4	m^2
Heat transfer coefficient of evaporator	U_{film}	20	$W/(m^2 K)$
	U_{evap}	6	
	U_{super}	6	
Area of condenser	A_{evap}	3	m^2
Heat transfer coefficient of condenser	$U_{desuper}$	10	$W/(m^2 K)$
	U_{cond}	3	
	U_{sub}	3	
Superheating	ΔT_{super}	5	K
Subcooling	ΔT_{sub}	1	K

4.2 Sensitivity Analysis

The ambient conditions have no significant influence on the COP of the heat pump (if a constant i.e. given compressor speed is assumed). However, they have significant influence on the defrosting (i.e. pre-heating), backup (i.e. post-heating) and the deicing demand and thus on the system COP. The compressor frequency (i.e. compressor power) and the volume flow influence the COP and COP_{sys} most, see Fig. 4 for the sensitivity of various parameters.

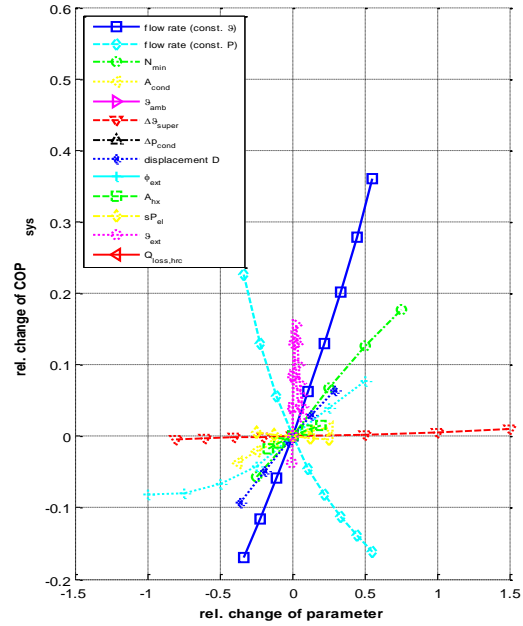
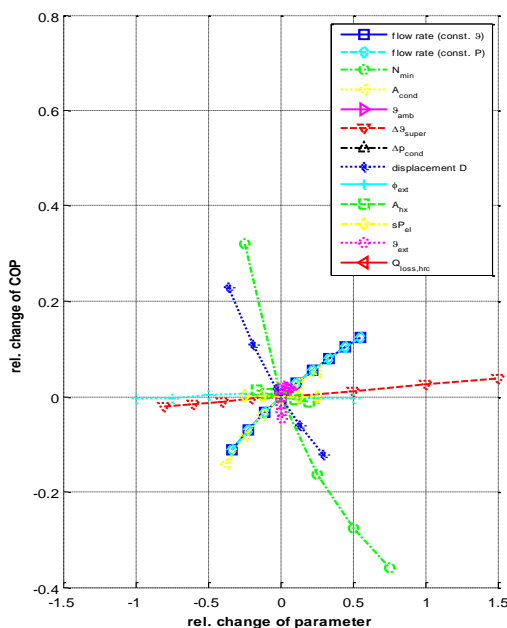


Fig. 4 – Relative change of COP and of system COP vs. relative change of various parameters

5. Functional Model, Measurements and Validation System simulations

5.1 Performance measurements

Different functional models of façades with an integrated mechanical ventilation system with heat recovery are developed in the framework of the iNSPiRe EU-project and are measured in PASSYS test cells (Passive Solar Systems and Component Testing) at the laboratory of Innsbruck University.

The investigation of constructional and building physics aspects was in the focus of the development of the first functional model of a façade with integrated MVHR. Furthermore, practical aspects such as accessibility (maintenance, repair, filter change) have been addressed. A second functional model - the micro-heat pump in combination with MVHR unit - is developed and integrated in a timber frame façade and tested in the second PASSYS test cell. The second functional model is primarily designed to measure the performance of the MVHR unit and of the micro-heat pump and to validate the simulation model. It was therefore built in a façade without a window. The second functional model was optimized based on experimental and simulation results and is currently being tested.

A third functional model will be installed in the acoustic test rig for sound measurements.

Figure 5 shows both functional models installed in COP_{sys} the PASSSYS test cells at UIBK.



Fig. 5 – PASSSYS test cell at UIBK with installed functional models, left cell: 1st functional model (MVHR next to window), right cell: 2nd functional model (μ HP and MVHR) – photo: UIBK

To achieve better agreement between simulation and measurement instead of a constant UA-value, a calibrated function is used. The effective UA-value is decreasing for higher relative humidity due to condensation inside the heat exchanger. For boundary conditions without condensate, the effective UA-value can be assumed to be constant. The effective UA-value drops to 50% in case of high amounts of condensate; see Siegele (2014) for details.

5.2 Validation of the Simulation Model

The measured and simulated coefficient of performance of the system is displayed in Fig. 6 as a function of the ambient temperature with the speed of the compressor as parameter. The simulation model slightly overestimates the COP_{sys} for lower ambient temperatures and underestimates in case of higher ambient temperatures. Overall, relatively good agreement can be achieved; see Siegele (2014) for more details.

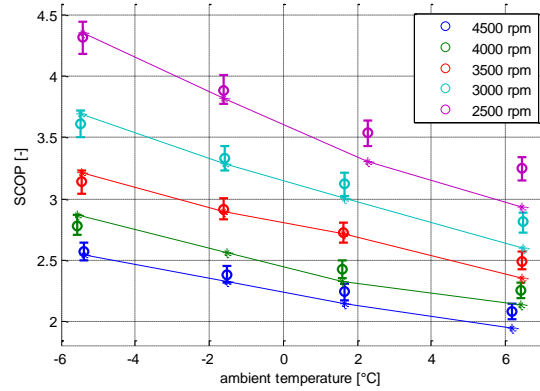


Fig. 6 – Simulated and measured system COP as a function of the ambient temperature with the compressor speed as parameter

The COP of the μ HP is, with values below 2, relatively poor. An improved version has been developed (a compressor with higher capacity situated in the supply air before the condenser, refrigerant R134a, condenser area 4 m²) with the aim to obtain a heat pump COP higher than 2 and system COP of at least 3 for 4500 rpm. Measurements are ongoing.

6. System Simulation

The validated physical model is used to generate a performance map of an improved μ HP for system simulations. The heating with the μ HP of a single family house with two levels of heating demand (15 kWh/(m² a) and 25 kWh/(m² a) is simulated in seven European climates (see Dermentzis et al. 2014 for a detailed description). Here, detailed results for the location Stuttgart (Meteonorm) are presented.

6.1 Building Model

The building considered in this study is a semi-detached single-family house, with a tempered floor area of 78 m². It is defined within the iNSPiRe project [iNSPiRe, 2014] as a typical European single-family house construction. The actual building is located in London, UK, and consists of two floors and an unheated attic, with an insulated ceiling between the top floor and the attic [Gustafsson, et al., 2014]. The ventilation rate is taken to be 0.4 h⁻¹ and the infiltration rate 0.1 h⁻¹. Two renovation levels (i.e. U-values of roof, floor,

walls and windows) are defined: EnerPHit (EN) and Passive House standard (PH).

In MATLAB Simulink the complex building model of the Carnot Blockset is used. In this study, only space heating is investigated. Total energy consumption includes heat pump compressor, backup heater, defroster of heat recovery and ventilator fans. Thus, all energy consumed is electricity.

6.2 Influence of the size of the heat pump power and of the control strategy on the performance

A set of dynamic simulations is performed to investigate the influence of the controller. At a first step, sensitivity analysis is performed assuming constant compressor frequency. The on/off controller with hysteresis is used. The different RPM correspond to different heating capacity of the micro-heat pump as shown in Table 3.

Additionally, dynamic simulations are performed using a PI controller parameterized for the frequency-controlled compressor with a range of 2000 to 4500 rpm. In Fig. 7 the total electrical consumption is presented. The results show an improvement of system performance by using a PI controller. The benefit of a PI controller compared to the on/off controller with maximum frequency (4500 RPM) is about 13% for EnerPHit and 20% for PH standard, but only 2 to 3% in case of the optimal dimensioned speed. The main advantage of the speed-controlled compressor might be that the possibilities of an improperly dimensioned heat pump with regard to the building load is reduced.

Table 3 – Heating capacity of micro-heat pump

RPM	P_{hp} / [W]	COP
2000	384	3.84
2500	453	3.33
3000	520	2.96
3500	584	2.68
4000	646	2.40
4500	710	2.11

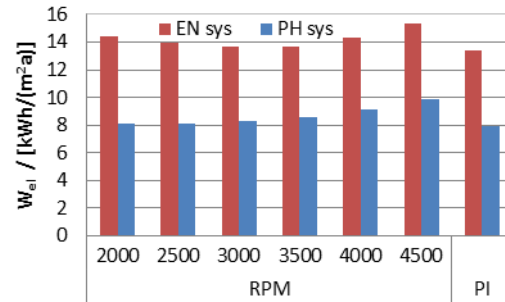


Fig. 7 – Total electrical consumption using PI or on/off controller.

Fig. 8 shows the load duration curve of the building heating load and the load covered by the micro-heat pump. Results are presented for two control strategies: PI controller (continuous line) and on/off controller with constant compressor speed (dotted line) - the optimum speed is chosen (see Fig. 7).

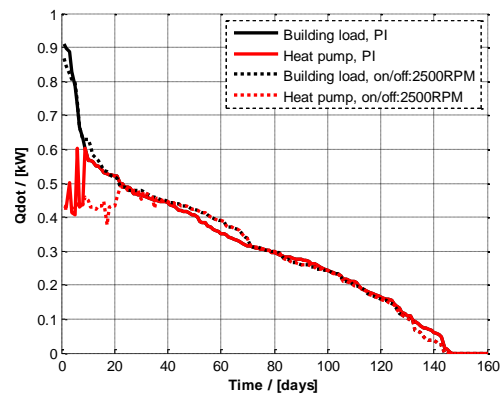


Fig. 8 – Load duration curves of the building and load covered by the micro-heat pump using PI controller and on/off controller (@ 2500 RPM) with the building in PH standard; daily average values

Also with a PI controller, the backup heater is needed for the peak loads. In the case of the on/off controller, the share of the backup heater increases significantly.

7. Outlook & Conclusion

The aim of this work is the development of a μ HP with a MVHR and to establish a cost-effective and reasonably efficient system for ventilation, heating and optional cooling for very efficient buildings such as Passive Houses or buildings renovated to EnerPHit standard. Functional models have been built and are tested in PASSYS test cells. Measurement results are used to validate a new

simplified physical MVHR and heat pump model. The physical model delivers results with relatively good accuracy. The model can be used to assist optimizations and further developments. Simulation is used to show that the performance of the heat pump can be further improved. This is part of ongoing and future developments. Furthermore, the results delivered by the physical model can be used as input for system simulations. Results of simulation studies show that the concept of the μ HP is feasible. The micro-heat pump will be monitored in a demo building in Ludwigsburg. The μ HP represents a cost-effective compact heating system for buildings with very high-energy performance (new buildings as well as for deep renovations) which - integrated in a prefabricated façade - can be applied with minimum space use and reduced construction and installation effort and time.

8. Acknowledgement

These results are part of the research and simulation work of the iNSPiRe European project funded under the 7th Framework Program (Proposal number: 314461, title: Development of Systematic Packages for Deep Energy Renovation of Residential and Tertiary Buildings including Envelope and Systems, duration: 01.10.2012 - 30.09.2016).

9. Nomenclature

Symbols

A	area (m ²)
c_p, c_v	specific heat capacity (J/(kg K))
COP	coefficient of performance
D	displacement (m ³)
H	enthalpy (J)
h	efficiency (-)
κ	isentropic exponent (-)
m	mass flow (kg/s)
N	revolutions (rpm)
n	polytropic exponent (-)
p	pressure (Pa)

P	power (W)
ρ	density (kg/m ³)
ϑ	temperature (°C)
sP	specific power (Wh/m ³)
T	temperature (K)
τ	compression ratio (-)
U	overall heat transfer coefficient
V	Volume (m ³)

Subscripts/Superscripts

a	air (dry air)
amb	ambient
C	Clearance
comp	compressor
cond	condenser
dis	discharge
el	electric
eff	effective
exh	exhaust
ext	extract
evap	evaporator
HP	heat pump
i	inside/internal
inv	inverter
min	minute
MVHR	mech. vent. with heat recovery
ref	refrigerant
s	saturation
suc	suction
sub	sub-cool
super	super-heat
sup	supply
sys	system
tot	total
vent	ventilation
vol	volumetric

References

- CoolProp2014 <http://coolprop.sourceforge.net>, 2014
- Feist, W. (editor), EnerPHit Planerhandbuch - Altbauten mit Passivhaus Komponenten fit für die Zukunft machen. Autoren: Zeno Bastian, Wolfgang Feist 2012.
- Feist W., passiv.de Database of Certified Passive House Components; Building Services; 2014
- Gustafsson M., Dermentzis G., Myhren J.A., Bales C., Ochs F., Holmberg S., Feist W., Energy

performance comparison of three innovative HVAC systems for renovation through dynamic simulation – 2014

Hafner, Bernd. 2012. CARNOT 5.2 Manual. 2012.

The Mathworks, Inc. 2012. Matlab R2012a Help.

iNSPiRe, Proposal number: 314461, title: Development of Systematic Packages for Deep Energy Renovation of Residential and Tertiary Buildings including Envelope and Systems, WP 2, Deliverable 2.1 Report, 2014.

Ochs F., Dermentzis G., Siegele D., Konz A., Feist W., Use of Building Simulation Tools for Renovation Strategies - a renovation case study. Energy Forum, Bressanone 2013.

Ochs F., Dermentzis G., Siegele D., Konz A., Feist W., Façade integrated active components in timber-constructions for renovation - a case study. NSB 2014

Ochs F., Dermentzis G., Siegele D., Feist W., Feasibility of a micro-heat pump - Energy performance simulation, Energy Forum, Bressanone 2014.

Passive House requirements [Online]. - 9 4 2014. -

Passive House Institute (a). PHPP – The energy balance and passive house planning tool. Retrieved 4 9, 2014, from http://passiv.de/en/04_phpp/04_phpp.htm

Siegele D., Measurement and Simulation of the Performance of a Façade-integrated MVHR with Micro Heat Pump, Master Thesis, University of Innsbruck, 2014.

BIM and interoperability for energy simulations

Bernardino Chiaia – Politecnico di Torino – DISEG – bernardino.chiaia@polito.it

Sanaz Davardoust – Politecnico di Torino – DISEG – sanaz.davardoust@polito.it

Anna Osello – Politecnico di Torino – DISEG – anna.osello@polito.it

Niccolò Aste – Politecnico di Milano – D.A.B.C. – niccolo.aste@polimi.it

Manlio Mazzon – Politecnico di Milano – D.A.B.C – manlio.mazzon@polimi.it

Abstract

Energy efficiency issues are being integrated into Building Information Modeling (BIM) quickly by the InnovANCE Italian research project which provides the creation of the first Italian open-source construction "unified database", shared by all stakeholders: public and private clients, construction companies, professionals and manufacturers.

The aim of this research is to define a methodology by which to obtain data flows and information exchanges, with as small as possible data losses, from architectural software (as Revit Architecture) and energy analysis software, mainly those based on transient-state.

The transient-state tool analyzed for this study was the EnergyPlus simulation engine, which represents the state of the art tool in building energy simulation.

As the process of exchanging data from Revit to EnergyPlus is not direct, "Space Boundary Tool" (SBT) middle-ware was used as an "interoperable bridge" with good results passing through the Industry Foundation Classes (IFC) format, analysing problems and possible solutions. Up to now, SBT is used for three different purposes:

- (i) To apply needed geometric transformations in order to transform an architectural model into a two-dimensional surfaces model;
- (ii) To assign thermal boundary conditions to model surfaces and adding materials thermal properties;
- (iii) To get an .idf file that can be processed by EnergyPlus simulation engine.

The correct data exchange obtained makes the energy optimization process easier, mostly if applied in preliminary design phases (when energy analysis can be more effective in driving to the "zero energy building" goal), by avoiding building a new energy model for each architectural design variation.

1. Introduction

Energy efficiency issues need to be integrated in the building design process, mostly in the preliminary phase, to reach the zero energy goals. A way to make this operation easier is to provide a unique design base on which both architectural and energy experts can share their analysis and modification proposals. Providing a shared design base is one of the BIM aims. To actually ensure high-energy performances, transient-state simulation engines, like EnergyPlus (Crawley et al., 2001), should be used, but the complexity and particularity of models and data requested by these engines often make it hard to directly match with a BIM model.

The InnovANCE Italian research project was focused also on these items. It provided a web-based unified construction database shared by all stakeholders: public and private clients, construction companies, professionals and manufacturers. Some of the provided features of this web database, built together with SAP - Systems, Applications and Products in data processing, allow designers to download and upload information on materials, components, building spaces and projects, and their corresponding BIM objects with all needed properties already applied.

Therefore, starting from this data collector system, a workflow was developed in this study to build BIM models and perform transient state energy simulations on them during the design phase. The information transferring process between different tools belongs to the so-called interoperability issue, which was investigated in this study, by using the

“Industry Foundation Classes” (IFC) standard.

The BIM software used to perform these analyses was Revit Architecture, on which the “Add-In Innovance” was developed together with One Team software house to link the BIM model together with the InnoVANCE web database. EnergyPlus was the simulation engine on which energy evaluations were run.

2. Description of the experimental procedure of the InnoVANCE web database

In order to test the interoperability process, a simplified model was built, according to the BESTEST ASHRAE 140 reference. Therefore, the testing model was a single parallelepiped formed cell whose internal dimensions were 6.00 m x 8.00 m and 2.70 m height. Its longest side was oriented parallel to the East-West direction. On the south-facing façade two transparent components were considered, centered on the same, of dimensions 3.00 x 2.00 m.

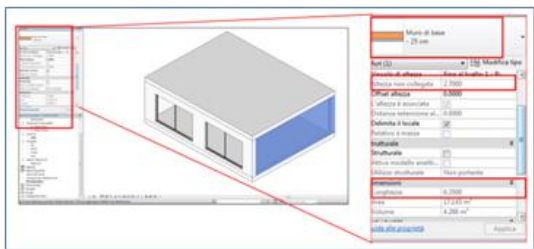


Fig. 1 – BIM model view of the test cell.

On the InnoVANCE web database the layers of the wall are looked up in the database of "element in opera" and, if they already exist, will be used in the "BOM creation"-Bill Of Material creation- of the parent material. In the case in which there is a layer that does not satisfy the requirements as requested, it will be necessary to create a new layer with the desired characteristics. This procedure can be done in two distinct ways: creating from scratch a new code which will be assigned to each of the seven characteristics - Function, Typology, Geometry, Heat resistance, Physic-chemical properties and Thickness - or by creating a copy of an existing code (which automatically assigns a new code to

the new copy layer) and then modifying one or more existing characteristics. This procedure guarantees an excellent applicability on the part of experts.

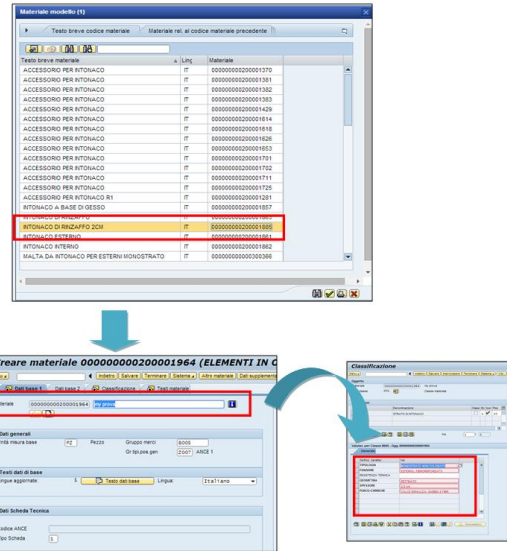


Fig. 2 – Possibility to rename the material and change each feature keeping other data.

3. Coding association in a parametric environment: description of the procedures

The association of a code in a parametric environment is necessary to identify each object in a unique way in the web database. This was done in Revit by using the InnoVANCE Add-In, which generates a two-way connection with the SAP programming code. In order to associate the BIM object, this has to be created before the object. Subsequently, in the Add-In box of InnoVANCE, clicking on ASSOCIATES, the "update objects – InnoVANCE materials research" dialog box is opened in which, under the heading "ANCE CODE" the code corresponding to the parent material to be associated to BIM object is inserted. In the "propriety of type" it is possible to find the characteristics assigned in the encoder for code generation. In the enclosed propriety under the heading "Other" the following fields are present: Thickness, Thermal transmittance, Physic-chemical properties, Function, geometry, Type, Ance code, extended text Ance material, Ance material.

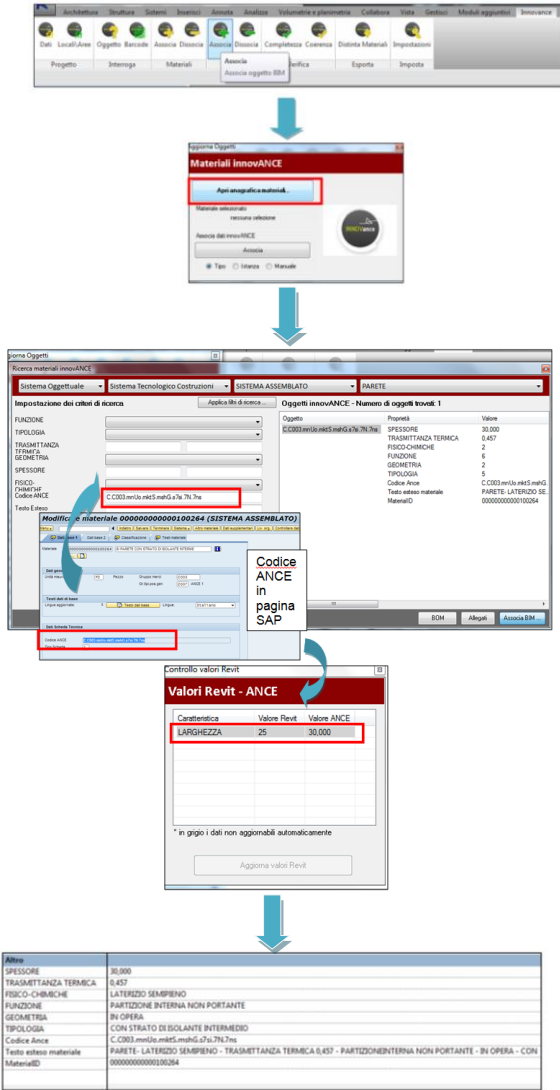


Fig. 3 – Association of a code to BIM object and visualization of characteristics in a parametric environment.

4. Information's transfer checking from a BIM model to the .ifc file format by Revit

Once the code association of BIM objects to the Revit model was complete, the exportation in .ifc format was performed. Among the options that can be set in the procedure to generate .ifc files, users can also map BIM objects with the corresponding IFC classes, to ensure a conversion that corresponds to the standard of the format. In particular, some text files are already available with these pre-compiled maps and they can be loaded in order to automate this operation.

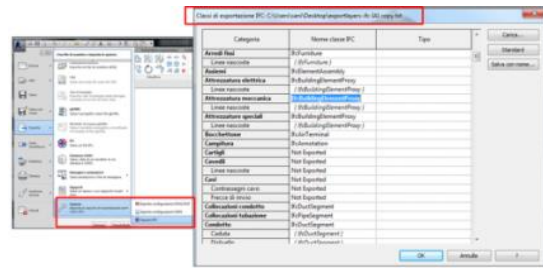


Fig. 4 – Mapping of BIM objects with the corresponding class according to the IFC standard.

The exportation was performed using the "IFC-EXPORTER" Plug-in from inside the Revit Architecture, by the settings of the version "IFC 2x3 Concept Design BIM 2010".

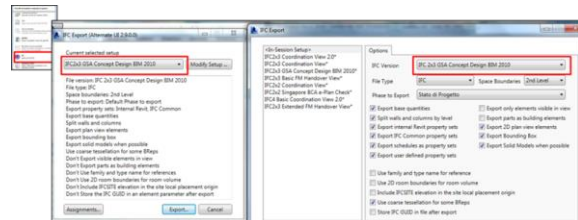


Fig. 5 – Parameters settings for .ifc file generation.

After that, the generated .ifc file is verified in Solibri Model Checker. In particular, as can be seen in the following figure, the geometric dimensions defined in the BIM model and those exported in the .ifc file, relatively to the highlighted wall in Fig. 6, (in other words these parameters as "height", "length" and "width"), appears to be exported successfully.

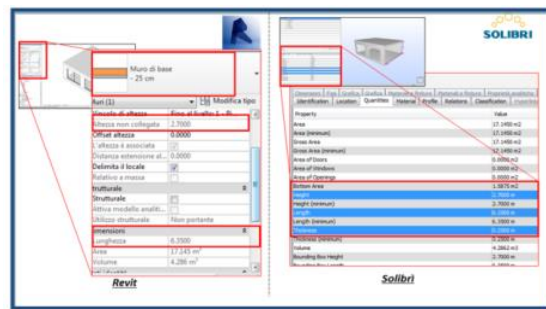


Fig. 6 – Comparison between the geometric dimensions of a defined wall in the BIM model and the ones which were written in the exported .ifc file.

Analyzing the thermal properties of the components of the envelope, it can be noticed that the thickness and the total value of the thermal transmittance of the same were exported as well as

the names and the thicknesses of the individual materials. It is not possible for the thermo-physical characteristics of each material layer (especially thermal conductivity, density, specific heat and absorption coefficients) to be exported as these represent the necessary information about the construction of a thermal model to be evaluated in dynamic state.

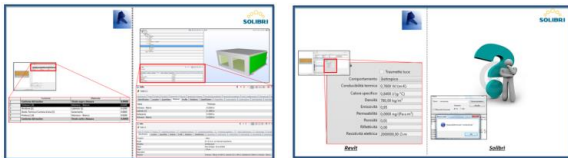


Fig. 7 – Non-response in the .ifc file about the thermo-physical properties of each material defined in the BIM model.

5. From .ifc to .idf file

EnergyPlus simulation engine, like many engines, can manage only its own text-file format (.idf). Therefore, even if the .ifc format is going to be the most acknowledged international standard for interoperability, the .ifc model exported by Revit should be converted into an .idf file to run a simulation on it by using EnergyPlus. In addition, as already highlighted in the previous section, in the .ifc exporting process, many thermal properties are not written. So, since the interoperability process between BIM models and .idf thermal models (by passing through .ifc standard) is not direct (Bazjanac at al., 2013), Space Boundary Tool middle-ware was used to add missing information and fixing geometry (Bazjanac, 2010). This intermediate software allows the user to convert an .ifc file to an .idf file by adding boundary conditions to thermal surfaces, fixing some geometries, and writing material thermal properties by referencing to a “library” .idf file. To automatically create this support file from the Revit model, an additional routine was developed together with One Team software house, to be added to the Addin Innovance tool. This routine can write an .idf file by copying material thermal properties used in the BIM model with the correct EnergyPlus syntax, simply by clicking on a toolbar button.

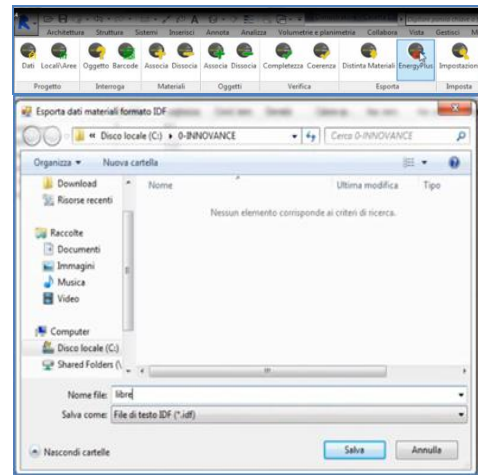


Fig. 8 – .idf library generator button in Addin InnovANCE

Then, the exported .ifc file can be processed by the Space Boundary Tool, together with the .idf library file, to obtain a first stage of the thermal model.

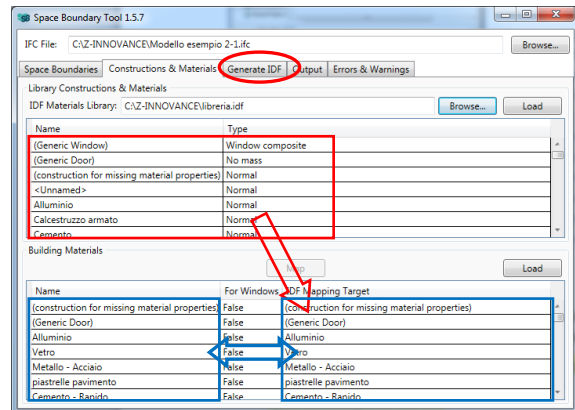


Fig. 9 – Materials thermal property assignment and .idf model generation in Space Boundary Tool.

The obtained thermal model contains information about building geometry and envelope thermal properties. User behaviour should also be added. This can be done directly by the EnergyPlus idf editor or by other EnergyPlus-based interfaces such as OpenStudio or DesignBuilder, simply by opening the .idf file. After that, the model will be ready for a first simulation to obtain energy demands.

To obtain building energy consumptions, also a mechanical system should be modelled. However, to do this, a very good knowledge of EnergyPlus is needed. Further, once the .idf model is available, many other aspects can be investigated, such as thermal comfort, by adding more EnergyPlus objects by an expert user.

6. Conclusion

Nowadays, it is not possible that simply by clicking on a button, a BIM model is correctly converted into a transient-state energy model and a reliable result on the building energy performance will be provided. This is mainly due to the different aims of BIM and energy models, whose approximations and rules are significantly different. Consequently, a fine checking by an expert user must always be done, to ensure the final result is accurate.

Many processes can be automated and the construction of a thermal model will be faster than starting from a blank sheet. Improving the level of automation, as this study has tried to do, will make the integration of energy evaluation in building design more affordable for design teams.

References

- Bazjanac, Vladimir, "Space Boundary Requirements For Modeling Of Building Geometry For Energy And Other Performance Simulation." In *Proceedings of the CIB W78 2010: 27th International Conference*. Cairo, Egypt.
- Bazjanac, V., J.T. O'Donnell, T. Maile, C. Rose, N. Mrazović, E. Morrissey, C. Regnier and K. Parrish. 2013. "Transforming BIM To BEM: Generation Of Building Geometry For The NASA Ames Sustainability Base BIM."
- Crawley, D. B., L. K. Lawrie, F. C. Winkelmann, and C. O. Pedersen. 2001. "EnergyPlus: A New-Generation Building Energy Simulation Program." *Proceedings of Forum 2001: Solar Energy: The Power to Choose*.
- ANSI/ASHRAE Standard 140-2011 – "Standard Method of Test for the Evaluation of Building Energy Analysis Computer Programs", 2011.
- Buildingsmart Official Website 2014. Accessed July 2014. <http://www.buildingsmart-tech.org>.
- LNBL Simulation Research Group 2014. "Space Boundary Tool". Accessed July 2014. <https://simulationresearch.lbl.gov/projects/space-boundary-tool>
- OpenStudio Official Website 2014. "OpenStudio". Accessed July 2014. <https://www.openstudio.net/>
- DesignBuilder Official Website 2014. "DesignBuilder". Accessed July 2014. <http://www.designbuilder.co.uk/>

Urban heat island in Padua, Italy: simulation analysis and mitigation strategies

Luca Battistella – Department of Management and Engineering – University of Padua, Italy – luca.battistella.2@studenti.unipd.it

Marco Noro – Department of Management and Engineering – University of Padua, Italy – marco.noro@unipd.it

Abstract

The Urban Heat Island effect has been widely studied in large cities around the world, more rarely in medium-size ones. The paper reports on the study of the UHI phenomenon in Padua, a medium-size city in the northeast of Italy, one of the most industrialized and developed parts of the country.

Experimental measurements were carried out during summer 2012, recording the main thermo-hygrometric variables by mobile surveys along an exact path crossing different zones of the city area (urban, sub-urban and rural). Some measurements in situ in characteristic sites of the city area (like the city centre, high and low density populated residential zones, industrial zone, rural zone) were carried out in order to evaluate thermal comfort indexes. The analysis of the data highlights the presence of the UHI effect with different magnitudes depending on the function of the zone of the city. In the city centre, a historical zone, the effect was up to 7 °C.

The ENVI-met simulation model was used in order to quantify possible increases in thermal comfort as a consequence of some mitigation strategies. In particular, a very famous square of the city (Prato della Valle) was analysed: it can be considered representative of the phenomenon because of the size and so the very different characteristics from the UHI effect point of view. Two scenarios were analysed besides the actual one (“AsIs” scenario): “Green ground” (halving the asphalt surface and doubling the green and plants surface) and “Cool Pavements” (increasing the albedo of impervious horizontal surfaces).

The simulation results are presented both in terms of UHI intensity (difference in air dry-bulb temperature between Prato della Valle and a reference rural site) and in terms of mean radiant temperature and thermal comfort sensation. The results are presented both in spatial and temporal terms for a typical summer day. The “Green ground” scenario allows up to a 1.4 °C and 3 °C decrease in air temperature, respectively during the night and the day. The same items for the “Cool Pavements” scenario are, respectively, 1.8 and 4 °C.

1. Introduction

As is well known, the Urban Heat Island phenomenon (UHI) is the systematic higher air temperature of an urban environment with respect to a rural one. This results from many causes that interact with one another, according to the particular situation of each city (Lazzarin, 2011). Briefly, the main factors are the following:

- the structure of urban canyons that affect the shortwave radiation heat exchange capacity of the urban surfaces towards the sky;
- the typically low albedo of the urban surfaces that increase the heat absorbed by buildings, pavements, roads and roofs;
- the anthropogenic heat produced by heat engines of the motorcars and chillers condensation heat;
- the greenhouse effect that is amplified by the higher pollutant concentration in the urban atmosphere;

- the shortage of green areas that increases the heat exchange with air and decreases the evaporative cooling effect due to the lack of evapotranspiration of trees and grass.

The literature on the UHI effect is very rich; for the sake of brevity refer to the authors' previous work (Noro et al., 2014a) to find some references. UHI has been studied worldwide (Athens, London, Berlin, Vancouver, Montreal, New York, Tokyo, Hong Kong for example) since the sixties (Santamouris, 2007). In Italy, only a few studies are available for some major cities like Bologna (Zauli Sajani et al., 2008), Milan (Bacci and Maugeri, 1992), Florence (Petralli et al., 2006) (Petralli et al., 2009) (Petralli et al., 2011) and Rome (Fabrizi et al., 2010). Very few data are available concerning the existence of the urban heat island phenomenon in medium-size cities, the most widespread in Italy (Modena (Bonafè, 2006) and Trento (Lora et al., 2006) (Giovannini et al., 2011) for example), and none in the Veneto Region in the northeast of Italy. The University of Padua has been studying the Padua city's UHI effect since 2010. In previous works the authors have described the results of the 2010, 2011 and 2012 measurement campaigns done by the research group of the Department of Environmental Agronomy and Crop Productions and by the authors themselves (University of Padua) (Busato et al., 2014) (Noro et al., 2014a). In other previous studies, the authors described the activities on the simulation of UHI in characteristic sites of the fabric of the city of Padua developed within the framework of the European Project "UHI"¹ (Noro and Lazzarin, 2014) (Noro et al., 2014b).

In this paper, the use of the ENVI-met simulation model allowed to investigate the effects of possible mitigation strategies in one of the most characteristic sites of the city, Prato della Valle.

2. UHI Mitigation Strategies by Simulations

2.1 Methods

In order to accurately simulate the physics of the atmospheric boundary layer of an urban area, the

modeling software should meet the following requirements (Huttner, 2012) (Xiaoshan et al., 2012):

- the grid size of the model area should be small enough to resolve buildings, i.e. grid size ≤ 10 m;
- the model should implement the energy balance of surfaces of all types;
- the simulation of the physical and physiological properties of plants should be included;
- the calculation of the atmospheric processes should be prognostic and transient.

The three-dimensional microclimate model ENVI-met (www.envi-met.com) (Bruse and Fleer, 1998) is one of the few microscale models that fulfill all of the above-mentioned criteria. It is freeware and runs on a standard x86 personal computer with a Microsoft Windows operating system. In this work, the authors conducted simulations using the ENVI-met model (rel. 3.5) in order to quantify the effects of selected mitigation actions in one of the most characteristic areas of Padua, Prato della Valle.

ENVI-met is a three-dimensional microclimate model designed to simulate the surface-plant-air interactions in the urban environment with a typical resolution of 0.5 to 10 m in space and 10 s in time. The model area is described in Figure 1. The main area is a 111x88x35 grid (in a x,y,z tridimensional reference system), with a 5x5x3 m grid dimension. An appropriate number of nesting grids (five) was set in order to minimize boundary effects. Seven specific points of interest were identified in the zone to characterize the dry-bulb air temperature (AT), the mean radiant temperature (MRT) and the predicted mean vote (PMV) at 1.80 m above ground during 24 hours, from 6am to 6pm (Table 1). Because the simulations were very time-consuming, they lasted 72 hours; only the last 24 hours were considered for the results because they were the least influenced by the initial and boundary conditions. The daily mean air temperature of the day before the start simulation was used as the initial air temperature at 6am of the first day. Simulations used the default values of ENVI-met except for the ones reported in Table 2.

¹ "UHI - Development and application of mitigation and adaptation strategies and measures for counteracting the global Urban Heat Islands phenomenon" (3CE292P3).

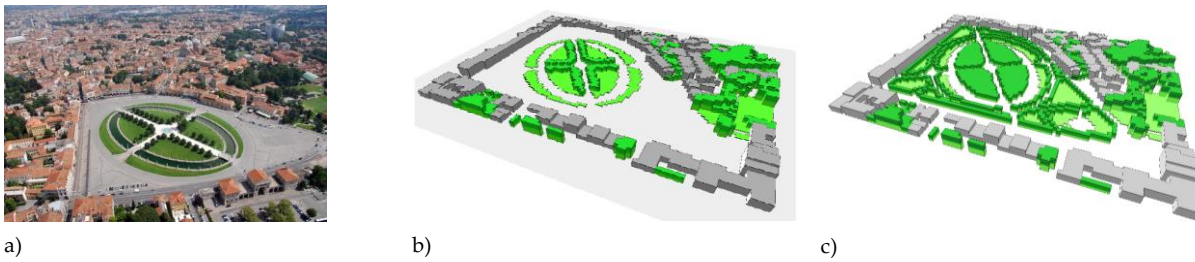


Figure 1 – The area (a) and the model area in ENVI-met used for the simulations of the “AsIs” scenario (b) and the “Green ground” scenario (c)

Table 1 – Description of the seven characteristic points in the two simulated scenarios

	Position	Scenario “AsIs”	Scenario “Green ground”
	1	Asphalt – far from buildings	Green – far from water
	2	Asphalt – near to buildings	Asphalt – near to buildings
	3	Gravel – near to water	Gravel – near to water
	4	Gravel – far from water	Gravel – far from water
	5	Green – far from water	Green – Trees
	6	Green – near to water	Green – Trees
	7	Green – Trees	Green – Trees

Table 2 – Configuration values in ENVI-met

Simulation tool: ENVI-met 3.5 Start Simulation at Day (DD.MM.YYYY): 27.07.2012 (Summer) Start Simulation at Time (HH:MM:SS) = 06:00:00 Total Simulation Time in Hours = 72.00 Save Model State each ? min = 60 Wind Speed at 10 m ab. ground [m s^{-1}] = 2 Wind Direction (0:N.. 90:E.. 180:S.. 270:W..) = 45 Roughness Length z_0 at Reference Point = 0.2 Initial Temperature Atmosphere [K] = 299.1 K Specific Humidity at 2500 m [$\text{g}_{\text{water}}/\text{kg}_{\text{air}}$] = 7 Relative Humidity at 2 m [%] = 76	Building properties Inside Temperature [K] = 298 Heat Transmission Walls [$\text{W m}^{-2} \text{K}^{-1}$] = 1 Heat Transmission Roofs [$\text{W m}^{-2} \text{K}^{-1}$] = 2 Albedo Walls = 0.2 Albedo Roofs = 0.3 Emissivity of all the surfaces = 0.9 People velocity [m s^{-1}] = 0.3 Metabolic rate [W m^{-2}] = 116 Clothing insulation [clo] = 0.5
---	---

It is worth stressing that while other indexes (like PET and SET*) were specifically defined to assess outdoor thermal comfort (Matzarakis et al., 2007) (Matzarakis et al., 2010) (Mayer, 1993) (Gagge et al., 1986) (Höppe, 1999) (Mayer and Höppe, 1987), the use of PMV is not universally recognized. In addition, the ISO 7730 standard focused on the use of PMV only as the indoor thermal comfort index. Nevertheless, some authors applied the use of PMV to outdoor environments (Matzarakis et al., 2007) (Matzarakis et al., 2010), (Berkovic et al., 2012) (Honjo, 2009) (Jendritzky and Nubler, 1981) (Jendritzky, 1993) (Thorsson et al., 2004). ENVI-met uses the Klima-Micheal-Model (KMM) that adds complex energy balance equations referred to outdoor to the classic Fanger’s model (Jendritzky

and Nübler, 1981) (Honjo, 2009).

To measure the UHII, a set of simulations were performed in the rural zone just outside Padua (Via Roma in Legnaro) as well, in order to calculate a temperature profile for the reference zone. Two scenarios were supposed besides the actual one (“AsIs” scenario):

- “Green ground”: increasing the pervious surfaces of the area from 23% to 43% by planting trees, 10 m height, within and around the ellipse, and converting a large part of the impervious zone - e.g. asphalt car park surface - to a pervious zone by planting grass. The circle street was left in order not to modify the traffic (Figure 1). The main effects were: Sky View Factor (SVF) decreased for the presence

of trees along the streets; impervious surface fraction decreased (and pervious surface fraction increased) because the green area increased; the albedo slightly increased; other thermo-physical properties of the surfaces/materials remained more or less the same. The impact on UHII reduction was the air cooling mainly due to the evapotranspiration effect of the green surfaces.

- b) “Cool pavements”: substituting all the traditional asphalt (albedo 0.2) and concrete (albedo 0.4) of roads and pavements with “cool materials”, that is materials with higher albedo (0.5) and also high emissivity in the infrared radiation. The main effect was a significant increase in the albedo while other properties remained the same. The impact on UHII reduction was mainly due to the minor air heating caused by the lower urban surfaces’ temperature; the limitation in the solar radiation absorption and the high emissivity of this kind of surfaces were the main causes.

It is worth highlighting that in case b) ENVImet has some limitations; in fact it is not possible to simulate:

- pervious asphalts or green/asphalt mixed surfaces (the only pervious surface that can be modelled is the soil beneath the green and pavements);
- surfaces with phase change materials, able to limit the temperature thanks to the melting process of the micro-encapsulated nanomaterials inside;
- asphalts/concretes with light pigments, able to reflect most part of the visible radiation;
- different emissivity values for different range of wavelength (that is ENVImet considers all the surfaces as greys).

For all these reasons the “Cool pavements” scenario was simulated only by the increased albedo of asphalt and concrete surfaces.

2.2 Results and Discussion

Results, in terms of AT, UHII with respect to Via Roma (rural zone), MRT and PMV (at 1.80 m above ground), are summarized in Table 3 and Table 4 for

the seven points (the most significant of Table 1 as representative of the area) respectively for a typical daytime and night time hour. Summarizing, the main results are:

- In terms of AT, differences between the different points on the square are never greater than 1.5 °C. This is in line with other studies (Iziomon Moses et al., 1999) (Bruse et al., 2009). Experimental studies show that the green surfaces absorb almost a quarter of the solar radiation allowing a lower outside adduction heat exchange with respect to traditional impervious surfaces (even lower with wet green); the evapotranspiration effect allows a further heat exchange (higher with wet green) so that green surfaces’ temperature is normally lower than impervious ones, even lower the wetter the green is (Lazzarin et al., 2005). ENVImet does not allow us to force the ground humidity, i.e. simulating watering of green surfaces; considering that, as previously stated, simulations lasted 72 hours but only the last 24 hours were considered for the results, the green surfaces were substantially dry, thus limiting their performances.
- UHI intensity assumes high values in the AsIs scenario: the highest temperatures (8-9 °C) was noticed after the sunset (8pm) and till the first sunrise (4am).
- a quite similar value (7.7 °C) for the UHII during the day was noticed only for point 2, which is a point on the asphalt near the buildings (characterized by low SVF and impervious surface); for the other points the maximum daytime UHI intensity was always lower or equal to 7 °C.
- AT in Pos. 3 (gravel near to water) is probably overestimated, as ENVImet is not able to simulate moving water systems like rivers and fountains (Bruse and Fleer, 1998) so there is no evaporative cooling effect. This affects both AT and PMV (Bisson, 2010).
- MRT in the AsIs scenario is almost the same in the different points at 3pm, except for the ones shadowed by trees (Pos. 2 and 7); such very large differences in MRT are consistent with other studies (Iziomon Moses et al., 1999) (Mayer, 1993) (Bruse et al., 2008). A main

consequence is the very great values of PMV (greater than 6 in the most exposed positions) indicating a sensation of great heat and so of great discomfort. However, as reported in literature (Bruse and Flerer, 1998) (Bruse, 2005) (Candidi et al., 2006) (Honjo, 2009) (Thorsson et al., 2004) (Baker et al., 2001) values of PMV over the scale -4/+4 are not significant, indicating a great discomfort sensation.

- The “Green ground” UHI mitigation strategy allowed around a 1°C decrease in UHI maximum night time intensity (but till 2 °C decrease in day time intensity). The greatest advantage from the mitigation action was recorded on the asphalt (points 1 and 2, but

greater on point 2 with lower SVF). Note that, while Pos. 1 passes from asphalt to green surface, Pos. 2 remains the same: increasing the green has an effect on reducing AT both directly (Pos. 1, reduction of 0.8 and 1.5 °C respectively at 3am and 3pm) and indirectly (Pos. 2, reduction respectively of 1 and 2.3 °C). This affects the PMV reducing its values, also considering the decrease in MRT in positions where trees were planted (Pos. 1 and 5). It could be concluded that even small but near green areas have a positive effect on reducing AT and so UHI, as proved also by (Candidi et al., 2006) (Jauregui, 1990) (Abu et al., 1998) (Gaj et al., 1998) (Cubasch et al., 2012).

Table 3 – Data obtained by ENVI-met simulations for the three scenarios on July, 29th, 3pm

		Pos.1	Pos.2	Pos.3	Pos.4	Pos.5	Pos.6	Pos.7
AsIs	AT (°C)	36.1	36.9	35.8	36.0	36.2	35.7	35.4
	UHII (°C)	6.9	7.7	6.6	6.9	7.0	6.5	6.2
	MRT (°C)	80.2	40.9	70.9	70.9	81.3	65.0	36.8
	PMV	6.7	3.6	5.9	6.1	6.8	5.3	3.1
Green ground	AT (°C)	34.6	34.6	34.4	34.6	34.1	34.1	34.2
	UHII (°C)	5.4	5.5	5.3	5.5	5.0	5.0	5.0
	MRT (°C)	70.2	39.7	70.5	70.9	35.3	65.4	35.5
	PMV	5.7	3.2	5.7	5.8	2.8	5.2	2.8
Cool Pavements	AT (°C)	32.3	33.0	32.2	32.6	32.5	32.2	31.9
	UHII (°C)	3.1	3.8	3.1	3.4	3.4	3.0	2.7
	MRT (°C)	85.3	35.6	68.1	68.2	77.7	62.2	32.4
	PMV	6.0	2.6	5.0	5.0	5.6	4.5	2.2

Table 4 – Data obtained by ENVI-met simulations for the three scenarios on July, 30th, 3am

		Pos.1	Pos.2	Pos.3	Pos.4	Pos.5	Pos.6	Pos.7
AsIs	AT (°C)	29.1	29.3	28.8	29.0	28.8	28.7	28.6
	UHII (°C)	8.4	8.6	8.1	8.4	8.1	8.1	8.1
	MRT (°C)	23.0	22.5	18.5	18.4	19.6	17.5	18.8
	PMV	1.1	1.1	0.8	0.8	0.8	0.7	0.8
Green ground	AT (°C)	28.3	28.3	28.2	28.2	27.8	27.9	28.1
	UHII (°C)	7.6	7.6	7.5	7.6	7.1	7.3	7.4
	MRT (°C)	18.3	21.9	12.7	19.3	18.0	18.3	18.1
	PMV	0.7	0.9	0.7	0.7	0.6	0.6	0.6
Cool Pavements	AT (°C)	27.4	27.6	27.2	27.4	27.2	27.2	27.1
	UHII (°C)	6.7	6.9	6.5	6.7	6.5	6.5	6.4
	MRT (°C)	20.7	20.2	16.8	16.9	17.5	15.9	16.8
	PMV	0.6	0.7	0.4	0.4	0.4	0.3	0.4

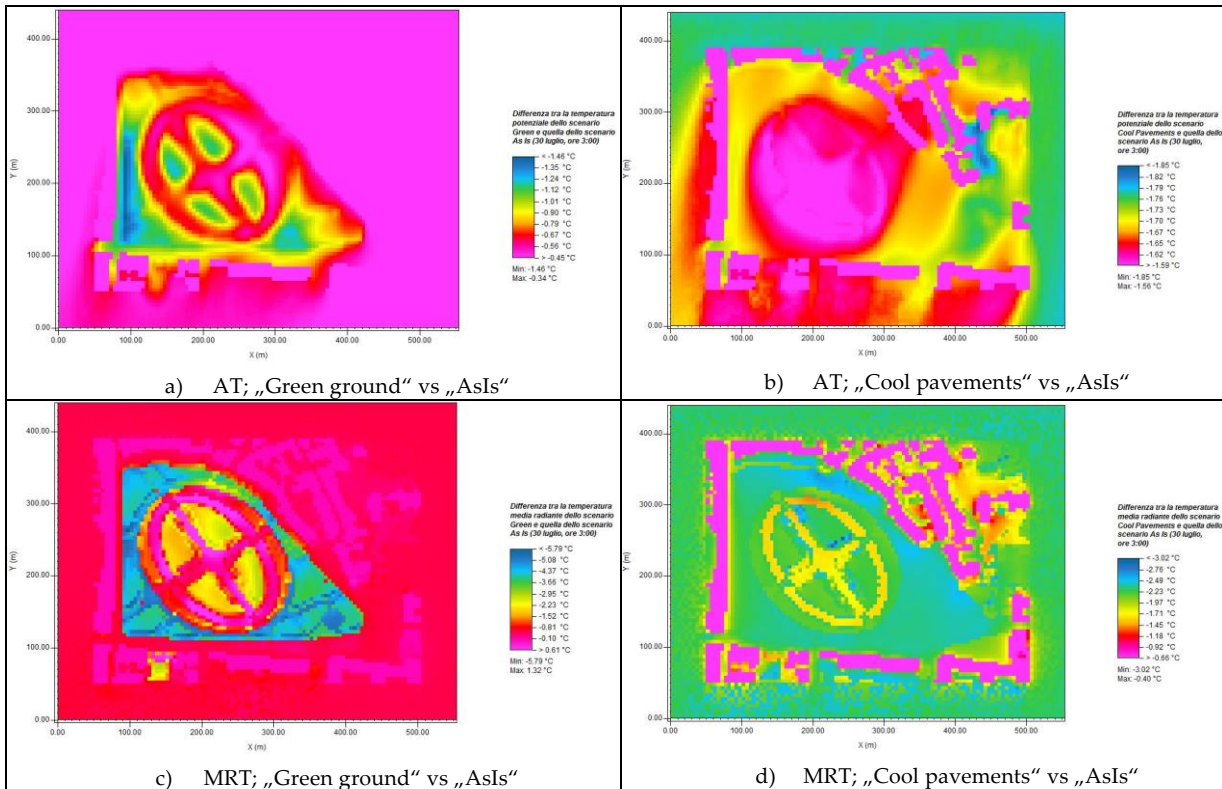


Fig. 2 – Air temperature (a – b) and mean radiant temperature (c – d) at 1.80 m above the ground at 3am on 30th July: comparison between „Green ground“ and „AsIs“ scenarios (a – c) and between „Cool pavements“ and „AsIs“ scenarios (b – d))

- It is important to note that the positive effect of the “Green ground” mitigation action is mainly due to the shadowing effect of trees (during daytime); this could be detrimental during night time if the foliage were too dense because of the reduced SVF, also considering the already cited limit of the model to simulate green watering.
- The “Cool pavements” UHI mitigation strategy allowed around a 1.5-2 °C decrease in UHI at 3am and till 3-4 °C at 3pm. This positive effect is mainly due to the increased albedo of asphalt and the connected reduced surface temperature (for example in Pos. 1 at 3pm the asphalt temperature decreases from 51.9 °C to 42.6 °C). Such results are in line with other studies: (Akbari et al. 2001) found that increasing albedo by 0.25 allows a surface temperature decrease of 10 °C; in other cases, introducing cool materials with albedo between 0.4 and 0.85 brings the surface temperature to decrease by 7.5-15 °C and AT to decrease by 4 °C (daytime) and 2 °C (night

time) (Berdahl and Bretz, 1997) (Livada et al., 2006). Also considering the MRT, the “Cool pavements” mitigation action is positive, allowing a greater decrease with respect to the “AsIs” and “Green ground” scenarios. Only in Pos. 1, which is in the asphalt far from buildings, does MRT increase with cool materials, due to the greater reflected radiation during the day. This mitigation action allows to decrease the PMV inside the comfort range (-0.5/+0.5) during the night for most positions.

- Comparing the distribution of the differences between the two mitigation actions and the “AsIs” scenario for both AT and MRT at 3am (Fig. 2): the “Cool pavements” scenario allows a slightly greater and more uniform reduction on AT with respect to the “Green ground”, while referring to MRT the latter seems to perform better than the former.

3. Conclusions

The experimental analyses highlighted the presence of a not negligible UHI effect also in medium-size cities like Padua of up to 6-7°C, resulting in a thermal stress for people living in urban environments. The UHI phenomenon was very intense in the old town, where streets are characterized by highH/W ratio, small SVF and no presence of pervious surfaces. However, in residential areas, the UHI intensity was lower on average with a decreasing trend going from more densely populated streets to less densely populated ones.

In order to test different possible mitigation actions, the particular case of Prato della Valle was studied by the ENVI-met model. Introducing new green areas instead of impervious ones allows a decrease in AT till 2 °C and in MRT until some ten degrees. Even more interesting results can be reached using cool materials, even if the model presents some limits in modelling these kind of surfaces. The study highlights that possible advantages in mitigating UHI effect are possible installing small green areas and introducing new materials when maintenance operations of the pavements are foreseen.

4. Nomenclature

Symbols

AT	air temperature	°C
MRT	mean radiant temperature	°C
PET	physiological equivalent temperature	°C
PMV	predicted mean vote	
SET*	new standard effective temperature	°C
SVF	sky view factor	
UHI	urban heat island	
UHII	urban heat island intensity	°C

References

- Abu, E.M., T. Asaeda, V.T. Ca. 1998. "Reduction in air conditioning energy caused by a nearby park". *Journal of Energy and Buildings* 29: 83-92.
- Akbari, H., M. Pomerantz, H. Taha. 2001. "Cool surfaces and shade trees to reduce energy use and improve air quality in urban areas". *Solar Energy* 70 (3): 295-310.
- Bacci, P., M. Maugeri. 1992. "The urban heat island of Milan". *Il Nuovo Cimento C* 15(4): 417-424. doi:10.1007/BF02511742.
- Baker, N., M. Nikolopoulou, K. Steemers. 2001. "Thermal comfort in outdoor urban spaces: understanding the human parameter". *Solar Energy* 70(3): 227-235.
- Berdahl, P., S. E. Bretz. 1997. "Preliminary survey of the solar reflectance of cool roofing materials". *Energy and Buildings* 25: 149-158.
- Berkovic, S., A. Yezioro, A. Bitan. 2012. "Study of thermal comfort in courtyards in a hot arid climate". *Solar Energy* 86: 1173-1186.
- Bisson, M. A.Y. 2009/2010. "Simulazione del microclima urbano di Milano mediante il software ENVI-met: studio degli effetti dell'inserimento di aree verdi sulla sollecitazione termica degli edifici" ("Simulation of the urban microclimate of Milan by ENVI-met model: study of green areas in buildings performance", in Italian). Master's Degree Thesis. Supervisor Prof. Luca Pietro Gattoni. Politecnico di Milano.
- Blazejczyk, K., Y. Epstein., G. Jendritzky, H. Staiger, B. Tinz. 2012. "Comparison of UTCI to selected thermal indices". *International Journal of Biometeorology* 56: 515-535. doi:10.1007/s00484-011-0453-2.
- Bonafè, G. (edited by) (ARPA Emilia-Romagna). 2006. "Microclima urbano: impatto dell'urbanizzazione sulle condizioni climatiche locali e fattori di mitigazione" ("Urban microclimate: urbanization impact on the local climatic conditions and mitigation factors", in Italian).
- Bruse, M., H. Fler. 1998. "Simulating surface-plant air interactions inside urban environments with a three dimensional numerical model". *Environmental Modelling and Software* 13: 373-384.
- Bruse, M. 2005. "Assessing urban microclimate from the user's perspective - Multi-Agent systems as a new tool in urban biometeorology". *Annalen der Meteorologie* 41: 137-140.

- Bruse, M., P. Dostal, S. Huttner. 2008. "Using ENVI-met to simulate the impact of global warming on the microclimate in central European cities". *Berichte des Meteorologischen Instituts der Albert-Ludwigs-Universität Freiburg* Nr. 18. Helmut Mayer e Andreas Matzarakis (eds.). 5th Japanese-German Meeting on Urban Climatology. 307-312.
- Bruse, M., P. Dostal, S. Huttner, A. Katzschner. 2009. "Strategies For Mitigating Thermal Heat Stress In Central European Cities: The Project Klimes", *The seventh International Conference on Urban Climate*. 29 June - 3 July 2009. Yokohama. Japan.
- Busato, F., R. Lazzarin, M. Noro. 2014. "Three years of study of the Urban Heat Island in Padua: Experimental results". *Sustainable Cities and Society* 10: 251-258. doi:10.1016/j.scs.2013.05.001.
- Candidi, P., G. Galli, A. Vallati. 2006. "Studio dell'influenza di diversi materiali di rivestimento sul microclima di aree urbane in piccola scala" ("Study of the influence of different covering materials on microclimate of urban areas", in Italian). 61° National Congress ATI - Perugia.
- Cubasch, U., I. Langer, S. Sodoudi. 2012. "Using the ENVI-MET program to simulate the micro climate in new Town HASHTGERD". *The International Conference on Computing, Networking and Digital Technologies (ICCNDT2012) - Bahrain*, 61-64.
- Fabrizi, R., S. Bonafoni, R. Biondi. 2010. "Satellite and Ground-Based Sensors for the Urban Heat Island. Analysis in the City of Rome". *Remote Sens* 2: 1400-1415. doi:10.3390/rs2051400.
- Gagge, A. P., A. P. Fobelets, L. G. Berglund. 1986. "A standard predictive index of human response to the thermal environment". *ASHRAE Trans* 92: 709-731.
- Gaj, E., F. Gomez, A. Reing. 1998. "Vegetation and climatic changes in a city". *Ecological Engineering* 10: 355-360.
- Giovannini, L., D. Zardi, M. De Franceschi. 2011. "Analysis of the Urban Thermal Fingerprint of the City of Trento in the Alps". *Journal of Applied Meteorology and Climatology* 50: 1145-1162.
- Honjo, T. 2009. "Thermal comfort in outdoor environment". *Global Environmental Research* 13: 43-47.
- Höppe, P. 1999. "The physiological equivalent temperature-a universal index for the biometeorological assessment of the thermal environment". *International Journal of Biometeorology* 43: 71-75.
- Huttner, S. 2012. "Further development and application of the 3D microclimate simulation ENVI-met". Ph.D. Thesis, Johannes Gutenberg-Universität Mainz, Germany.
- Iziomon Moses, G., A. Matzarakis, H. Mayer. 1999. "Applications of a universal thermal index: physiological equivalent temperature". *International Journal of Climatology* 43: 76-84.
- Jauregui, E. 1990. "Influence of a large urban park on temperature and convective precipitation in a tropical city". *Journal of Energy and Buildings* 15-16: 457-463.
- Jendritzky, G., W. Nubler. 1981. "A model analysing the urban thermal environment in physiologically significant terms". *Meteorology and Atmospheric Physics* 29: 313-326.
- Jendritzky, G. 1993. "The atmospheric environment—an introduction". *Experientia* 49(9): 733-740. doi:10.1007/BF01923541.
- Lazzarin, R., F. Castellotti, F. Busato. 2005. "Experimental measurements and numerical modelling of a green roof". *Energy and Buildings* 37:1260-1267. doi:10.1016/j.enbuild.2005.02.001.
- Lazzarin, R. 2011. "Le isole di calore nelle aree urbane" ("Urban heat islands", in Italian). *Casa&Clima* 34: 34-40.
- Livada, I., M. Santamouris, A. Synnefa. 2006. "A study of the thermal performance of reflective coatings for the urban environment". *Solar Energy* 80: 968-981.
- Lora, C., M. De Franceschi, M. Sitta, D. Zardi. 2006. "Determinazione dell'effetto "isola di calore urbana" in una città alpina mediante l'utilizzo di reti di sensori a basso costo" ("Determination of the "urban heat Island" effect in an Alpine city by using low cost sensors", in Italian).

- Proceedings of XXXth Conference on hydraulic and hydraulic constructions-IDRARome. Italy.
- Matzarakis, A., F. Rutz, H. Mayer. 2007. "Modelling radiation fluxes in simple and complex environments - application of the RayMan model". *International Journal of Biometeorology* 51: 323-334.
- Matzarakis, A., F. Rutz, H. Mayer. 2010. "Modelling Radiation fluxes in simple and complex environments - Basics of the RayMan model". *International Journal of Biometeorology* 54: 131-139.
- Mayer, H., P. Höppe. 1987. "Thermal comfort of man in different urban environments". *Theor Appl Climatol* 38: 43-49.
- Mayer, H. 1993. "Urban bioclimatology". *Experientia* 49: 957-963.
- Noro, M., R. Lazzarin, F. Busato. Pre-published online January, 13, 2014a. "Urban heat island in Padua, Italy: experimental and theoretical analysis". *Indoor and Built Environment* doi: 10.1177/1420326X13517404.
- Noro, M., F. Busato, R. Lazzarin. 2014b. "UHI effect in the city of Padua: simulations and mitigation strategies using the RayMan and ENVI-met model". *Geographia Polonica* 87(4): 517-530. doi: 10.7163/GPol.2014.35.
- Noro, M., R. Lazzarin. 2014. "Theoretical and experimental analysis of the UHI effect in a medium size city of Italy". *Proceedings "3th International Conference on Countermeasures to Urban Heat Island"*. Venice, paper ref. 143, 1012-1023, ISBN 978-88-906958-2-7.
- Petralli, M., L. Massetti, S. Orlandini. 2009. "Air temperature distribution in an urban park: differences between open-field and below a canopy". *The seventh International Conference on Urban Climate*, Yokohama, Japan.
- Petralli, M., L. Massetti, S. Orlandini. 2011. "Five years of thermal intra-urban monitoring in Florence (Italy) and application of climatological indices". *Theor Appl Climatol* 104: 349-356. doi:10.1007/s00704-010-0349-9.
- Petralli, M., A. Prokopp, M. Morabito, G. Bartolini, T. Torrigiani, S. Orlandini. 2006. "Ruolo delle aree verdi nella mitigazione dell'isola di calore urbana: uno studio nella città di Firenze" ("The role of green areas in UHI mitigation: a study in the city of Florence", in Italian). *Rivista Italiana di Agrometeorologia* 1: 51-58.
- Santamouris, M. 2007. *Advances in Building Energy Research: v1*. Earthscan Ltd. ISBN-13: 978-1844073894.
- Thorsson, S., M. Lindqvist, S. Lindqvist. 2004. "Thermal bioclimatic conditions and patterns of behaviour in an urban park in Göteborg, Sweden". *International Journal of Biometeorology* 48: 149-156.
- Xiaoshan, Y., L. Zhao, M. Bruse, Q. Meng. 2012. "An integrated simulation method for building energy performance assessment in urban environments". *Energy and Buildings* 54: 243-251.
- Zauli Sajani, S., S. Tibaldi, F. Scotto, P. Lauriola. 2008. "Bioclimatic characterisation of an urban area: a case study in Bologna (Italy)". *International Journal of Biometeorology* 52: 779-785. doi:10.1007/s00484-008-0171-6.

Multi-zone buildings thermo-hygrometric analysis: a novel dynamic simulation code based on adaptive control

Annamaria Buonomano – Department of Industrial Engineering, University of Naples Federico II, Italy – annamaria.buonomano@unina.it

Umberto Montanaro – Department of Industrial Engineering, University of Naples Federico II, Italy – umberto.montanaro@unina.it

Adolfo Palombo – Department of Industrial Engineering, University of Naples Federico II, Italy – adolfo.palombo@unina.it

Stefania Santini – Department of Electrical Engineering and Information Technology, University of Naples Federico II, Italy – stefania.santini@unina.it

Abstract

This paper presents a novel dynamic simulation model for the analysis of multi-zone buildings' thermal response and the assessment of building energy performance and indoor comfort. In this new release of the code, called DETECt 2.3, two important innovations are implemented. They regard the simulation model of multi-zone buildings, consisting of thermal zones totally enclosed in others, and the design of a novel temperature-humidity control algorithm. The developed innovative control strategy is based on a reference adaptive control scheme for the online adaptation of the control gains, with the aim of overcoming the well-known problems of classical fixed gain control algorithms. This feature will be a key tool for the next generation of building performance simulation codes (also toward NZEB analyses). Both the innovations embedded in the code can be exploited to simulate special indoor environments of hospitals / laboratories, rooms or museum halls. With the aim of showing the features and the potentialities of the simulation code coupled with the new control scheme, a suitable case study related to an expo indoor space of a museum building, including a display case with an accurate climate control, was developed. Details about heating and cooling demands and loads are provided. Good tracking performance for both the temperature and humidity control are obtained through the presented control scheme.

1. Introduction

A crucial challenge for the next generation of buildings is the capability to overcome the trade-off between low energy demands and high thermal and hygrometric comfort levels. The growing attention to these issues has led the research interest toward the use of building management strategies with the aim of improving both building energy efficiency and occupants' comfort. In this regard, Building Energy Performance Simulation (BEPS) tools play a key role. In the last years, recent advances in the numerical analysis based on computational methods, as well as computer calculation power, provided significant opportunities for developing and/or improving a new generation of BEPS codes. Here, particular attention was paid to: i) investigating new building envelope technologies and innovative HVAC systems, often supported by renewable energies; ii) implementing advanced control algorithms and systems (Shaikh P. H. et al. 2014).

The presented paper focuses on this specific framework. In particular, the article describes the new features included in DETECt 2.3, which updates a previous release (DETEct 2.2 (Buonomano A. and Palombo A. 2014)) validated by means of the BESTEST procedure. Specifically, DETECt 2.3 enables the simulation of multi-thermal zones (in particular of zones totally enclosed in others). Furthermore, it implements advanced thermo-hygrometric control actions able

to automatically adapt to the variations of the simulated system and its surrounding environment. The code, purposely developed by the authors for research aims, is conceived as a reliable thermo-hygrometric calculation tool for building energy design and performance analysis. DETECt allows one to dynamically calculate heating and cooling demands of multi-zone buildings and to assess the benefits of different and advanced building envelope techniques (PCM, BIPV, BIPV/T, sunspace, etc.). Thus, designs of high-performance buildings can be obtained. It is worth noting that often several research topics cannot be analysed by commercial BEPS codes (e.g. recent prototypal technologies, non-standard operating conditions, particular system scheduling, etc.). Such inconvenience can be exceeded by developing in-house codes such as DETECt. Here, updating and modifications of the included models can be carried out by authors for all the occurring research needs.

The aim of this paper is to show the effectiveness of the code in predicting the behaviour of building thermal zones with rigid thermo-hygrometric constraints. Such a goal is achieved by exploiting the features of the adaptive control scheme embedded into in DETECt 2.3, based on a new optimal model reference scheme (named LQ-EMRAC, Linear Quadratic Extended Model Reference Adaptive Control). The major advantage of this control technique is the control of the thermo-hygrometric variables for indoor spaces in uncertain conditions, without requiring an *a priori* knowledge of the building dynamics. To this aim, different from standard fixed gains techniques such as, for example, the PI approach implemented in the previous DETECt 2.2 release, the implemented control algorithm is able on-line to automatically vary its gains values to contract abrupt and unknown changes in the building behaviour and/or its features and external conditions. The idea behind this approach is to achieve great control flexibility and robustness in order to guarantee, at the same time, optimality with respect to a certain cost function subject to some constraints. The LQ-EMRAC approach extends and fuses the classical Model Reference Adaptive Control (MRAC) scheme that has been

proved to be effective in controlling uncertain plants (Di Bernardo M. et al. 2008), with an LQ algorithm, typical in the optimal control theory.

A suitable case study is here developed in order to show the effectiveness of the adopted approach. In particular, it refers to an indoor hall of a museum building with an included glass display case. Here, an accurate climate control (rigid constraints of temperature and humidity of the case indoor air) is required. As is well known, such an occurrence is mandatory in case of particular exhibited items contained in museum glass cases (e.g. archival artifacts, paper-based objects, etc.). Here, preservation techniques must be emphasized in order to avoid any irreversible damage. The case study building is located in the Mediterranean weather zone of Naples, southern Italy. To the best of the authors' knowledge, this is the first attempt in literature to model in BEPS codes: i) control by means of advanced schemes (able to guarantee rigorous constraints of temperatures and humidity, simultaneously); ii) thermal zones totally included into others.

2. Thermodynamic model

In this paper, a suitable resistive-capacitive (RC) thermal network simulation model (assuming 1D transient heat transfer) for the thermo hygrometric analysis of two thermal zones (one optionally completely enclosed in the other one) is described. It is embedded in the new release of DETECt (Buonomano A. and Palombo A. 2014). Through such a model, the assessment of the dynamics of temperatures and humidity, as well as of heating and cooling loads and demands, can be carried out. A sketch of the modelled RC thermal network is shown in Fig. 3. The calculation procedure concerns the heat flows between: i) the outdoor environment and the main modelled thermal zone (zone 1 in Fig. 3); ii) the zone 1 and the related included thermal zone 2 (Fig. 3). The following model simplifications are considered: i) the indoor air of each thermal zone is uniform and modelled as a single indoor air temperature node; ii) the building envelope of zone 1 is subdivided into M multi-layer elements (adopting a high order RC thermal network); iii) the

construction envelope of zone 2 is lumped in a single node; iv) each m -th multi-layer building element of zone 1 is subdivided in N sub-layers (of different thicknesses), where thermal masses and conductivities are uniformly discretised; v) $N+2$ capacitive and surface nodes are accounted for each m -th envelope component of zone 1, while 1 node is referred to its indoor air; vi) 2 nodes are modelled for zone 2, each one for the lumped envelope and the indoor air.

For zone 1, in each τ -th time step and for each n -th capacitive node ($j = 1, \dots, N$) of the m -th element ($m = 1, \dots, M$), the differential equation describing the energy rate of change of each temperature node of the building envelope is:

$$C_{m,n} \frac{dT_{m,n}}{dt} = \sum_{j=n-1}^{n+1} \frac{T_{m,j} - T_{m,n}}{R_{m,j}^{eq}} \quad (1)$$

where C and T are the thermal capacitance and temperature of the node, respectively. $R_{m,j}^{eq}$ is the sum of the halves sub-layers thermal resistances $R_{m,j}^{cond}$ (that links the n -th node to their neighbours, Fig. 3). For non-capacitive outer ($n = 0$) and inner ($n = N+1$) surface boundary nodes, the algebraic equation describing the heat transfer is:

$$\sum_{j=n-1}^{n+1} \frac{T_{m,j} - T_{m,n}}{R_{m,j}^{cv}} + \dot{Q}_{m,n} = 0 \quad (2)$$

$R_{m,j}^{cv}$ is either a convective (external $R_{m,0}^{conv}$ or internal $R_{m,N+1}^{conv}$) or a conductive resistance ($R_{m,n}^{cond}$), depending on the side layer of the considered node (Fig. 3). $R_{m,0}^{conv}$ and $R_{m,N+1}^{conv}$ connect non capacitive nodes to those related to the outdoor air temperature (T_{out}) and to the indoor air one ($T_{in,1}$), respectively. In case of floor elements, T_{out} and $R_{m,j}^{cv}$ are replaced with the ground temperature (T_{gr}) and an equivalent thermal conductive resistance (R_{gr}^k). The modelled forcing function $\dot{Q}_{m,n}$ includes the incident solar and the long-wave radiation exchange acting on outer and inner surfaces of zone 1 (Buonomano A. and Palombo A. 2014).

A simplified approach is adopted for zone 2. Here, the differential equation describing the energy rate of change of the temperature node of the zone 2 envelope ($T_{w,2}$) is calculated as:

$$C_{w,2} \frac{dT_{w,2}}{dt} = \sum_{j=1}^2 \frac{T_{in,j} - T_{w,2}}{R_j^{glob}} \quad (3)$$

where $C_{w,2}$ is the envelope lumped thermal capacitance, whose indoor air temperature is $T_{in,2}$; R_j^{glob} is a global thermal resistance that takes into account all the heat transfer effects. For zone 1, R_1^{glob} is calculated by adding the half sub-layer conductive thermal resistance of the zone 2 envelope node to the equivalent convective and radiative thermal resistance (modelled by a combined linearized convective-radiative thermal resistance). A simplified approach is considered for zone 2. Here, the radiative exchange only takes into account the long-wave fraction vs. the zone 1. Thus, for zone 2, the equivalent global thermal resistance (R_2^{glob}) includes combined conduction and convection phenomena only.

The differential equations on the thermal network nodes related to the indoor air of zone 1 and zone 2 must be solved simultaneously with the system of eqs. (1), (2) and (3). The sensible energy rate of change of zone 1 and zone 2 indoor air masses (at $T_{in,1}$ and $T_{in,2}$, respectively) can be calculated as:

$$C_{in,1} \frac{dT_{in,1}}{dt} = \sum_{m=1}^M \frac{T_{m,N} - T_{in,1}}{R_{m,N}^{conv}} + \frac{T_{w,2} - T_{in,1}}{R_1^{glob}} + \frac{(T_{out} - T_{in,1})}{R_v} + \frac{(T_{in,2} - T_{in,1})}{R_{v,zns}} + \dot{Q}_{g,1} \pm \dot{Q}_{AC,1} \quad (4)$$

$$C_{in,2} \frac{dT_{in,2}}{dt} = \frac{T_{w,2} - T_{in,2}}{R_2^{glob}} + \frac{(T_{in,1} - T_{in,2})}{R_{v,zns}} + \dot{Q}_{g,2} \pm \dot{Q}_{AC,2} \quad (5)$$

where the thermal resistances R_v and $R_{v,zns}$ describe the air ventilation and infiltration thermal loads: R_v links the indoor air node of zone 1 to the external one (outdoor air at T_{out}), $R_{v,zns}$ links the indoor air node of zone 2 to the one related to zone 1.

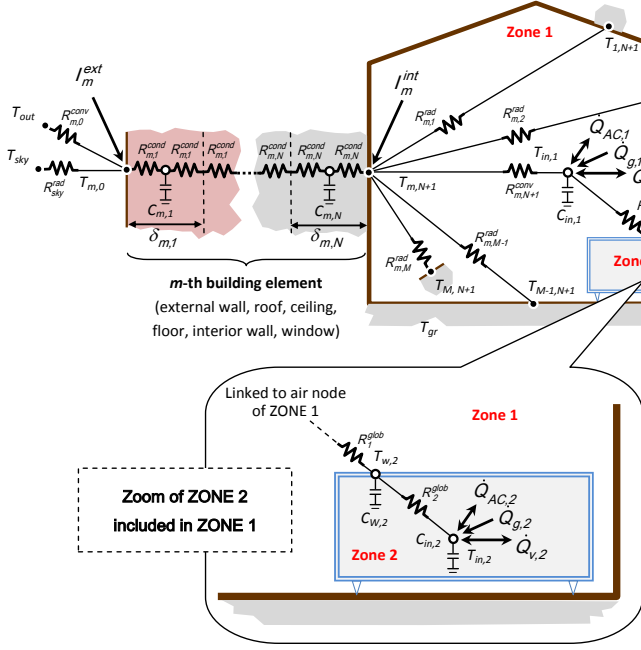


Fig. 3 – Sketch of the RC thermal network

Except for the thermal load due to the solar radiation transmitted through the windows and incident on the indoor surfaces, included in $\dot{Q}_{m,n}$, (I_m^{int} , Fig. 3), all the remaining sensible heat gains are considered as convective lumped heat source terms, networked to the indoor air nodes only. They include: i) the thermal zone internal gains due to occupants, lights and equipment, $\dot{Q}_{g,1}$ and $\dot{Q}_{g,2}$; ii) the sensible heat to be supplied to (or removed from) the building space by an ideal HVAC system, aiming at maintaining the indoor air at the desired set point temperature, $\dot{Q}_{AC,1}$ and $\dot{Q}_{AC,2}$. Therefore, the whole system including zone 1 and zone 2 is modelled through a thermal network of $(M \times N) + 5$ nodes. The differential and algebraic equations describing the system thermal behaviour are: (1), (2), (3), (4) and (5).

The assessment of the latent energy to be added to (or subtracted from) both the thermal zones 1 and 2 (for maintaining the selected relative humidity set-point of the indoor air) is carried out by adopting a decoupled approach (Ghiaus C. 2014). For each indoor space the moisture balance is calculated by neglecting the moisture exchange between the air node and the surrounding building surfaces. In each τ -th simulation time step and for each thermal zone ($z = 1, 2$), the adopted moisture balance is:

$$\Omega_{in,z} \frac{d\omega_{in,z}}{dt} = \dot{m}_{v,z} (\omega_{out^*,z} - \omega_{in,z}) + \dot{m}_{wg,z} \pm \frac{\dot{Q}_{AC,z}^{lat}}{\Delta h_{vs}} \quad (6)$$

where Ω_{in} is the indoor dry air mass; \dot{m}_v is the air ventilation mass flow rate; \dot{m}_{wg} is the inlet water vapour mass flow rate to the thermal zone (due to occupants); ω_{out^*} and ω_{in} are the external and indoor air specific humidity, respectively (note that the external air specific humidity is referred to: i) outdoor air for zone 1; ii) zone 1 air for zone 2); h_{vs} is the water latent evaporation heat at 0°C.

2.1 Reduced order model

For control aims, a linear simplified model was derived. Such a model stems from the above presented high order one (of $(M \times N) + 2$ nodes (eqs. (1) and (2)) related to zone 1) which has been simplified into a linear and second-order model, exploited for the reference model design, where: i) the thermal capacity of the whole building envelope of zone 1 is lumped in a single node; ii) the input signals acting on the thermal network nodes are: T_{out} , I^{ext} , T_{gr} and $\dot{Q}_{g,1}$; iii) an equivalent thermal resistance of the building envelope for internal and external surfaces is adopted; iv) weighted average thermal properties are assumed. Thus, eqs. (1) and (2) become:

$$C_{w,1} \frac{dT_{w,1}}{dt} = \frac{T_{out} - T_{w,1}}{R_{ext}^{eq}} + \frac{I^{ext} h_{out}^{eq}}{R_{ext}^{eq}} + \frac{T_{in,1} - T_{w,1}}{R_{int}^{eq}} + \frac{T_{gr} - T_{w,1}}{R_{gr}^{eq}} \quad (7)$$

As a consequence, equation (4) becomes:

$$C_{in,1} \frac{dT_{in,1}}{dt} = \frac{T_{w,1} - T_{in,1}}{R_{int}^{eq}} + \frac{T_{w,2} - T_{in,1}}{R_{int}^{glob}} + \frac{(T_{out} - T_{in,1})}{R_v} + \frac{(T_{in,2} - T_{in,1})}{R_{v,2ns}} + \dot{Q}_{g,1} \pm \dot{Q}_{AC,1} \quad (8)$$

As an example, for the sensible load calculation, the following vectors and matrices are considered: i) temperatures vector of the lumped envelope and indoor air thermal capacitances of both the zones, $x_0 = [T_{w,1} \ T_{in,1} \ T_{w,2} \ T_{in,2}]$; ii) vector of sensible heat to be supplied or removed from the building space, $u = [\dot{Q}_{AC,1} \ 0 \ \dot{Q}_{AC,2}]$; iii) the tuple (A_0, B_0, C_0) of dynamic matrix A_0 , input and the output vectors B_0 and C_0 (e.g. $B_0 = [0 \ C_{in,1}^{-1} \ 0 \ C_{in,2}^{-1}]^T$ and $C_0 = [0 \ 1 \ 0 \ 1]$ for the sensible load calculation), see Section 3.

3. The enhanced optimal LQ-MRAC algorithm

In order to control the thermo-hygrometric behaviour, a new control scheme that enhances the classical Model Reference Adaptive Control (MRAC) strategy proposed by Landau (Landau I. D. (1979)) is adopted. The novel control algorithm (named Liner-Quadratic Enhanced Model Reference Adaptive Control, LQ-EMRAC) includes additional control actions to improve the closed-loop performance with respect to those provided by the more classical MRAC approach. Furthermore, it embeds as a reference model a rough plant model controlled via an LQ strategy (Anderson B.D.O. and Moore J.B. 1971). This implies that closed-loop dynamics, optimal with respect to a given performance index, are imposed to the plant under investigation via the adaptive action. More precisely, the reference model is a rough estimation of plant dynamics:

$$\dot{x}_0 = A_0 x_0 + B_0 u, \quad y = C_0 x_0 \quad (9)$$

(where $x_0 \in \mathfrak{R}^n$ is the plant state, $u, y \in \mathfrak{R}$ are the control input and the system output, respectively, $A_0 \in \mathfrak{R}^{n \times n}$ is the dynamic matrix, and $B_0 \in \mathfrak{R}^n$, $C_0 \in \mathfrak{R}^{1 \times n}$ are the input and the output matrices, respectively, with n being the state space dimension) driven by a full state optimal feedback control action as:

$$u_{opt} = K^{opt} x_0 + K_R^{opt} r \quad (10)$$

being $K^{opt} \in \mathfrak{R}^{1 \times n}$, $K_R^{opt} \in \mathfrak{R}$ some fixed control parameters. From Optimal Control theory, it follows that the control signal in (10) minimizes a quadratic functional of the form:

$$J = \int_{t_0}^{+\infty} \left[(y(t) - r)^T Q (y(t) - r) + u^T(t) R u(t) \right] dt \quad (11)$$

(where $r \in \mathfrak{R}$ is the set-point to impose to the plant output, t_0 is the initial time instant, $Q \in \mathfrak{R}$ and $R \in \mathfrak{R}$ are some positive matrices). As a result, the closed-loop optimal dynamics to be imposed to the plant are the solutions, x_m , of the following optimally-controlled time-invariant system:

$$\dot{x}_m = A_m x_m + B_m r \quad (12)$$

being $A_m = A_0 + B_0 K^{opt}$ and $B_m = B_0 K_R^{opt}$. Details on the control algorithm and the control gains adaptation mechanism can be found in the following Appendix.

4. Case study and design of the LQ-EMRAC algorithm

The presented case study refers to a museum indoor space in which two thermal zones are modelled. In particular, the first zone refers to a museum hall while the second one (totally included in the first zone) to a glass display case with an accurate climate control (rigid constraints of temperature and humidity of the case indoor air) necessary to preserve collected exhibits such as: paints, woods, papers and leathers (which require suitable conditions of indoor air temperature and relative humidity, simultaneously). The sketch of the two-zone building is shown in Fig. 3. The simulation, carried out by DETECT 2.3, refers to the weather zone of Naples (southern Italy), by using a Meteororm hourly data file.

For zone 1, a typical Italian building envelope is taken into account, with length, width and height equal to 20, 10 and 3.5 m, respectively. The building's longitudinal axis is east-west oriented and a south-facing windows (4-6-4 air filled double-glazed system) of 32 m² is taken into account. The thickness of the building's walls and floor/ceiling are 25 and 30 cm, respectively. Their stratigraphy is designed by concrete bricks ($\lambda = 0.51$ W/mK, $\rho = 1400$ kg/m³, $c = 1000$ J/kgK) and thermal insulation ($\lambda = 0.04$ W/mK, $\rho = 15.0$ kg/m³, $c = 1400$ J/kgK). Note that each building element is subdivided in 10 sub layers of equal thickness. The direct solar radiation transferred through the windows to the inside zone is assumed to be absorbed by the floor with an absorption factor of 0.3. The absorption and emission factors of interior surfaces are assumed to be equal to 0.15 and 0.9, respectively. For such a zone, a ventilation rate equal to 1 Vol/h and a crowding index of 0.12 person/m² are taken into account. A cubic shaped zone 2 with a 1 m length side is considered. In particular, a glass envelope of 3 cm thickness, with an occurring air infiltration of 2 l/h is modelled.

The simulation starts on 0:00 of January 1st and ends at 24:00 of December 31st. The heating/cooling system of the thermal zone 1 is switched on from 07:00 to 18:00, from November 1st to March 31st (heating mode) and from June 1st to September 30th (cooling mode). The heating and cooling set points

indoor air temperature are set at 19 and 25°C, respectively. The relative humidity of the zone 1 indoor air is controlled at 50%. The heating/cooling system of the thermal zone 2 is switched on 24/7 to accurately conserve the case exhibited items. Here, the indoor air temperature and relative humidity are controlled throughout the year at 20°C and 65%, respectively.

The LQ-EMRAC has been implemented to control the air temperature and humidity, simultaneously, of both the modelled thermal zones. In particular, following a decentralized control approach (each control variable is used to impose the dynamic behaviour of only one variable to be controlled, see Pedro A. and Sala A. (2004)), four different and independent adaptive controllers are synthesized. In order to design the LQ-EMRAC control, the simplified models (see Section 2.1) were adopted as nominal models to be optimized via the LQ approach, by setting to zero the disturbance acting on the plant dynamics. Note that the choice of these simplified models reduces the complexity of the control design, without jeopardizing the closed-loop performance. Note that the optimality and robustness of the closed-loop control is guaranteed by the adaptive actions, whose gains evolve to compensate any parameter mismatch and/or presence of unmodelled dynamics (see Appendix), and to assure the minimization of a quadratic cost function, for indoor air temperature and humidity tracking errors and sensible and latent loads. Thus, the minimization of heating and cooling demands can be also achieved. In so doing, different from classical fixed gains algorithms like PI (implemented in the previous DETECT release), the proposed approach allows one to impose, on the system under control, a dynamic behaviour that can also be optimal from the energy demand point of view. The weight matrices (Q and R , which define the cost function in eq. (11)) were set in order to impose: i) a settling time of 50 minutes for zone 1 and 10 minutes for zone 2; ii) absence of overshoots for any step variation of the reference signal. The choice of the relaxation time of zone 1 is done according to (Ghiaus C. and Hazyuk I. 2010), with the aim to ensure a smooth daily transition during the transient operation toward the regime set-point (control system is switched on from 7:00 to 18:00).

Contrarily, a faster transient requirement is imposed on the settling time of zone 2 because of its rigorous thermo hygrometric requirements. Finally, the reference input signals (r in Section 3) depends on the selected temperature and humidity set points. Note that the humidity control is obtained through the input reference set point of indoor air specific humidity (ω_{sp}), in order to achieve the selected relative humidity set-point (ϕ_{sp}).

5. Results and discussion

In the following, the results related to the effectiveness assessment of the novel DETECT control approach, in imposing reference indoor air temperature and humidity dynamics, are shown. The analysis refers to both the investigated thermal zones 1 and 2. As mentioned above, temperature and humidity are controlled daily from 07:00 to 18:00 in zone 1 and 24/7 in zone 2 (for preservation purposes of the exhibited items). Fig. 4 shows the dynamic trend of zone 1 indoor air temperature, for two sample winter days (January 13th and 14th, i.e. the 13th and 14th days of the year) and for two sample summer days (July 25th and 26th, i.e. the 206th and 207th days of the year). Here, a satisfactory performance of the developed closed-loop control scheme can be observed (coincident reference and obtained temperature profiles). Note that the set point temperature shifts from 19°C (for the winter season) to 25°C (for the cooling season). In Fig. 5 the time history of the indoor air temperature during the transient HVAC system regime (settling time from 07:00 to 08:30) is shown for January 13th. Also here the obtained temperature profile overlaps the desired reference one.

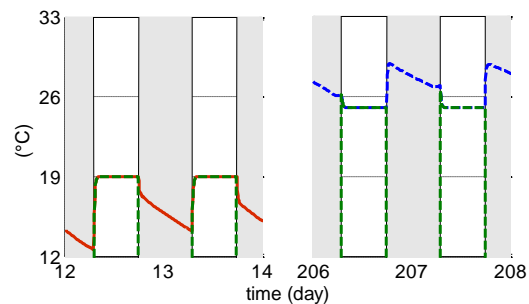


Fig. 4 – Zone 1 - Controlled indoor air temperature (red solid line for January 13th and 14th and blue dashed line for July 25th and 26th) and reference temperatures (green dashed line).

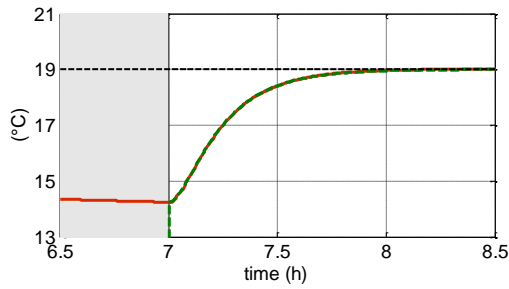


Fig. 5 – Switched on HVAC system in zone 1 in January 13th - Time history of the indoor air temperature (red solid line), reference temperature (green dashed line), set point temperature (black dashed line).

Fig. 6 shows the dynamic trend of zone 1 indoor air humidity for July 25th and 26th (Fig. 6a) and the latent load (dehumidification) resulting from the control action (Fig. 6b).

Here, the specific humidity set point is 10 g/kg, corresponding to a relative humidity of 50%. As in Fig. 5, Fig. 6c shows the time history of the indoor air humidity during the settling time, for July 26th. Note that the obtained humidity profiles overlap the desired reference ones.

In Fig. 7, the sensible thermal load ($\dot{Q}_{AC,I}$), calculated according to the temperature control of Fig. 4, is reported. A similar behaviour is obtained for $\dot{Q}_{AC,I}^{lat}$ (not shown for sake of brevity).

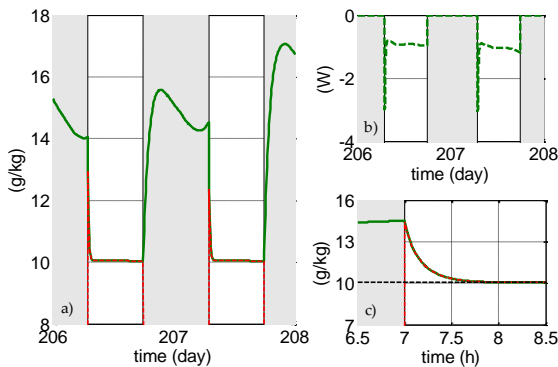


Fig. 6 – Zone 1: a) controlled indoor air humidity (green solid line), b) latent thermal load (green dashed line), c) humidity time history during the settling time (green solid line) - Reference humidity (red dashed line).

In all these figures, the grey shaded regions refer to unoccupied hours, during which the HVAC system is switched off and free floating thermo-hygrometric conditions and null control actions occur.

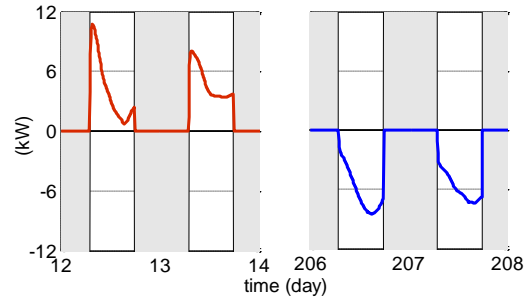


Fig. 7 – Time history of zone 1 sensible thermal load (red line heating mode - January 13th and 14th, blue line for cooling mode - July 25th and 26th) - $\dot{Q}_{AC,I}$.

With the help of these simulation results, some conclusions can be highlighted, such as: i) temperature and humidity set points (control aim) are always satisfactorily achieved for any initial indoor air temperature and humidity and every disturbance; ii) typical exponential behaviours of asymptotically stable liner-time-invariant systems (with unit gain, real eigenvalues and a settling time of about one hour) occur for both the temperature and humidity controls during the transient HVAC regimes; iii) smooth dynamic trends of the controlled variables and corresponding heating and cooling demands (control actions) are obtained. It is noteworthy to remark that a good tracking performance of the closed-loop controls is achieved. Very low root mean squared errors are obtained (0.024°C and $1.21 \cdot 10^{-7}$ g/kg for the air temperature and humidity control, respectively).

In Fig. 8, for zone 2 (where a continuous control of both the temperature and humidity is required), the obtained regulation error for the indoor air temperature is shown (from April 29th to May 2nd). Such control error is bounded within 0.01°C, despite the significant oscillation of the yearly indoor air temperature of zone 1 (which range from the minimum winter temperature of 12°C and the maximum summer one of 30°C).

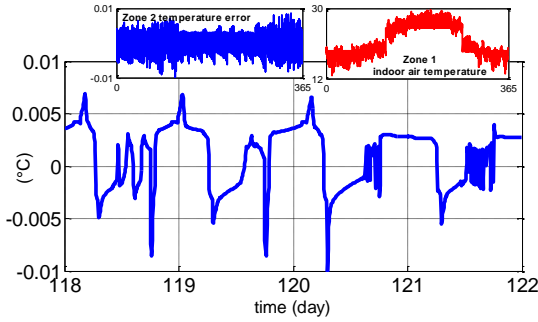


Fig. 8 – Regulation temperature error within zone 2 and indoor air temperature of zone 1 (up-right corner).

Correspondingly, the humidity control error vs. the selected set point in zone 2 is lower than 10^{-8} for the entire simulated year, despite a significant zone 1 humidity variation (from 4- to 15-g/kg), as clearly depicted in Fig. 9.

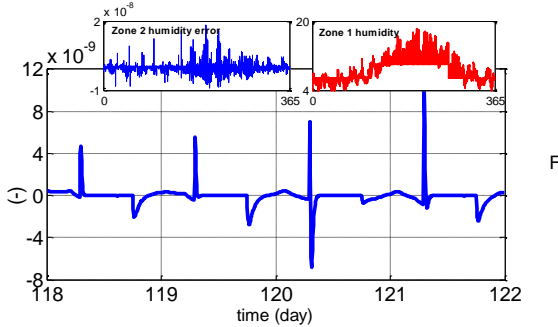


Fig. 9 – Regulation humidity error within zone 2 and indoor air humidity of zone 1 (up-right corner).

Obviously, bounded control actions are the result of bounded control gains, as clearly shown in Fig. 10. Here, as an example, the dynamic trend of the sensible thermal load of zone 2 ($\dot{Q}_{AC,2}$), resulting from the control of the indoor air temperature from April 29th to May 2nd (see also Fig. 8) is reported. As expected, the zone 2 thermal loads are much smaller than those in zone 1. Note that, in Fig. 10, heating and cooling loads (as well as humidification and dehumidification demands) are detected, because of the continuous thermo-hygrometric control (i.e. no grey shaded regions occur in figure).

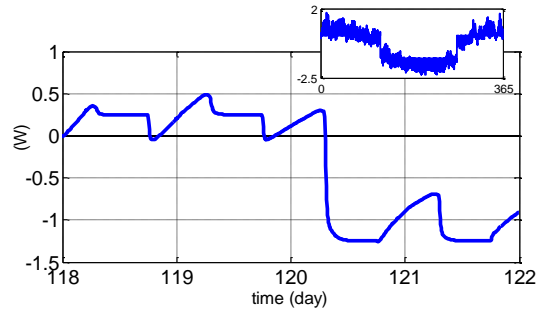


Fig. 10 – Time history of zone 2 sensible thermal load - $\dot{Q}_{AC,2}$.

Finally, in Fig. 11 for both the investigated thermal zones, the calculated heating and cooling (sensible and latent) yearly unitary demands, are shown. Here, it can be observed that the cooling demands are remarkably higher than the heating ones (according to the high internal gains assumed for zone 1 and to the simulated weather conditions). In addition, it is worth noting that for zone 2 the humidification and dehumidification demands vs. the sensible ones are proportionally higher than those occurring in zone 1.

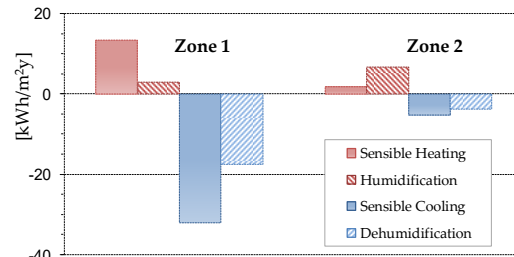


Fig. 11 – Heating and cooling sensible and latent demands.

This result is due to the continuous humidity control of zone 2 and to the considered indoor air temperature and relative humidity set points ($T_{in,2} = 20^{\circ}\text{C}$, $\phi_{sp} = 65\%$). Notice that, during the heating and cooling periods selected for the thermal zone 1, the humidification and dehumidification requirements of zone 2 are about 78 and 89% of the related yearly calculated demands, respectively.

6. Conclusion

In this paper, new features of the in-house developed computer code (called DETECT 2.3) for the building dynamic energy performance simulation are presented. The code, developed for

research purposes, enables the authors to model and analyse new prototypal technologies, non-standard operating conditions, particular system scheduling, etc., which cannot be deal with (or simultaneously taken into account) through commercial BEPS codes. From this point of view, another advantage of DETECT is the possibility to update and modify all the included models for each occurring research need. With the help of the presented code release, multi-zone buildings, consisting of thermal zones totally enclosed into others, can be modelled. In addition, all the simulated zones can be governed by rigid assigned thermo-hygrometric constraints.

This is accomplished through an innovative adaptive control strategy (called LQ-EMRAC). Here, the online adaptation of the control gains is achieved in order to assure the minimization of a quadratic cost function, which weights both the temperature / humidity tracking error and the sensible / latent energy demand. The control algorithm was designed on a simplified fourth order model. Then, it was tested and applied on the original and detailed DETECT one, based on more than 70 differential equations.

In this paper, the effectiveness of the proposed novel building simulation tool was verified through a suitable case study in which two thermal zones of a museum building are modelled. Here, a glass display case with a rigid temperature / humidity micro-climate control (for preserving aims) is enclosed in a large indoor space. Simulation results show very good tracking performance of air temperature and humidity, simultaneously, in both the simulated thermal zones. Bounded control gains and heating and cooling loads (during the transient regime) are obtained. Results also confirm the robustness of the developed control approach for unmodelled dynamics.

Appendix

The LQ-EMRAC control action is:

$$u(t) = u_{MRAC}(t) + u_I(t) + u_E(t) \quad (13)$$

with $u_{MRAC}(t) = K(t)x(t) + K_R(t)r(t)$, $u_I(t) = K_E(t)\text{sgn}(y_e(t))$,

$u_I(t) = K_I(t)x_I(t)$ and $x_I(t) = \int_{t_0}^t x_e(\tau)d\tau$. The time-varying control gains (adaptive gains) are computed as:

$$\begin{aligned} K(t) &= \int_{t_0}^t y_e(\tau)x^T(\tau)\Gamma_\alpha d\tau + y_e(t)x^T(t)\Gamma_\beta \\ K_R(t) &= \int_{t_0}^t y_e(\tau)r(\tau)\Psi_\alpha d\tau + y_e(t)r(t)\Psi_\beta \\ K_I(t) &= \int_{t_0}^t y_e(\tau)x_I^T(\tau)\Omega_\alpha d\tau + y_e(t)x_I^T(t)\Omega_\beta \\ K_E(t) &= \gamma \int_{t_0}^t |y_e| d\tau \end{aligned} \quad (14)$$

where $\Gamma_\alpha, \Gamma_\beta, \Omega_\alpha, \Omega_\beta \in \Lambda_n$, with Λ_n being the subspace of diagonal matrices in $\mathfrak{R}^{n \times n}$ and $\Psi_\alpha, \Psi_\beta, \gamma \in \mathfrak{R}$ are some adaptive weights with the same sign of K_R^{opt} assumed to be known (Ioannou P. and Fidan B. 2006). The output error y_e is computed as $y_e(t) = C_e x_e(t)$, being $x_e(t) = x_m(t) - x(t)$ and $C_e = B_m^T P$ with P solution of the Lyapunov equation (Anderson B.D.O. and Moore J.B. (1971), $PA_m + A_m^T P = -M, M > 0$).

Nomenclature

Symbols

C	thermal capacitance (J/K)
h	convective heat transfer coeff. (W/m^2K)
h_{vs}	water latent evaporation heat (J/g)
I	irradiance (W/m^2)
\dot{m}	flow rate (g/s)
\dot{Q}	thermal load (W)
R	thermal resistance (K/W)
T	temperature (K)
t	time (s)
ω	air specific humidity (g/g)
Ω	dry air mass (g)

Subscripts/Superscripts

AC	referred to the HVAC system
cond	conduction
conv	convection
eq	equivalent
ext	external
g	internal gain
glob	global
gr	ground
in	indoor air
int	internal
lat	latent
out	outdoor air

v ventilation
 w enclosed zone envelope
 wg water vapour

References

- Anderson B.D.O. and Moore J.B. (1971). *Linear Optimal Control*, Englewood Cliff NJ, Prentice Hall.
- Buonomano A. and Palombo A. (2014). "Building energy performance analysis by an in-house developed dynamic simulation code: An investigation for different case studies." *Applied Energy* 113(0): 788-807.
- Di Bernardo M. et al. (2008). "Novel hybrid MRAC-LQ control schemes: synthesis, analysis and applications." *International Journal of Control* 81(6): 940-961.
- Ghiaus C. (2014). "Linear algebra solution to psychometric analysis of air-conditioning systems." *Energy* 74(0): 555-566.
- Ghiaus C. and Hazyuk I. (2010). "Calculation of optimal thermal load of intermittently heated buildings." *Energy and Buildings* 42(8): 1248-1258.
- Ioannou P. and Fidan B. (2006). *Adaptive Control Tutorial: Advances in Design and Control*, SIAM.
- Landau I. D. (1979). *Adaptive Control, the model reference approach*, Springer-Verlag.
- Pedro A. and Sala A. (2004). *Multivariable Control Systems: An Engineering Approach*, Springer.
- Shaikh P. H. et al. (2014). "A review on optimized control systems for building energy and comfort management of smart sustainable buildings." *Renewable and Sustainable Energy Reviews* 34(0): 409-429.

Energy simulation in early stage building design: simplified models and impact on results

Marco Picco – Dept. of Engineering, University of Bergamo, Italy – marco.picco@unibg.it

Marco Marengo – School of Computing, Engineering and Mathematics, University of Brighton, UK – m.marengo@brighton.ac.uk

Abstract

The paper stems from the benefits of the application of energy analysis in the early-stage building design combined with the difficulties that prevent this integration due to the complexity of the needed simulations. The most common solution to overcome this obstacle is to simplify the building energy model, but not enough attention is paid to understand or predict the consequences of this action. The paper focuses on discussing the difference in results evaluated comparing the simulation of a detailed building model, based on all information available on the building during operation, and a simplified one, suitable for the application in early stage design. This result is achieved by defining a methodology, which consists in developing a simplification protocol and applying it to a suitable number of case studies starting from a detailed model and ending in the simplified one after the application of said protocol. The protocol is based on the use of EnergyPlus software both to develop a detailed model of the building, under various system hypothesis, and the simplified models. Three different case studies, featuring large non-residential buildings each with specific peculiarities, are discussed in this paper and simulated under three different system hypotheses each, resulting in nine different simplified models. Simulations are performed for the duration of a solar year, the differences registered between a fully simplified model and the corresponding detailed models are discussed both in term of total energy needs and peak loads, both for heating and cooling. Lastly, based on the results of the case studies, the possibility of integrating the presented simplification protocol into a simplified simulation tool is evaluated, discussing the possible advantages said tool would bring to the integration of energy simulation in early stage building design.

1. Introduction

The building energy problem concerns all the advanced countries in different ways, not only in terms of air pollution or emissions but also with regard to the preservation of energy sources and the rational use of energy itself. According to reports from the U.S. Department of Energy, buildings are responsible for a large portion of total yearly energy consumptions and greenhouse gas emissions, ranging from 40% to 50% (Chen, 2009), and Europe shows similar results (Economidou, 2011). As a result, various national and supranational initiatives and regulations, and various programs are flourishing in the private sector, such as LEED, CASBEE and others; defining standards and parameters to evaluate the level of sustainability of buildings and reduce their energy use, both voluntary and mandatory.

The framework, knowledge, materials and systems to achieve high levels of energy efficiency in buildings and strongly reduce energy consumption are readily available and can make a positive impact, but they need to be properly implemented from design to construction and operation of buildings. A possible solution to incorporate all these elements in the building sector is the implementation of the “Integrated Building Design” approach, or more in general an Integrated Design Process (IDP), shifting design decisions upstream in the project’s process, when the occasion to influence positive outcomes is maximised and the cost of changes minimised (Aziz, 2011). In this context, the use of building energy simulation could provide invaluable help to the IDP, providing information otherwise unavailable. Building performance simulations can

help to reduce emission of greenhouse gasses and to provide substantial improvements in fuel consumption and comfort levels, by treating buildings and their thermal systems as complete optimized entities, and not as the sum of a number of separately designed and optimized sub-systems or components (Hensen, 2004).

Many existing energy simulation tools for buildings are very sophisticated and promise a high level of accuracy. Popular tools such as EnergyPlus and DOE-2 are quite effective at simulating final building designs and are typically used for demonstrating compliance with performance standards such as LEED. However, despite the proliferation of many building energy analysis tools in the last ten years, architects and designers are still finding difficult to use even basic tools (Punjabi et al., 2005).

Although a building energy simulation is a useful tool for predicting performance and comparing design options, most of the energy simulations occur too late in the design process. In the traditional design process, the energy engineer carries out simulations, if at all, as a tool for equipment sizing and code compliance only after the architect has completed the architectural design. Part of the problem is that existing simulation tools are not practical for the design process; however, experiences with real buildings have shown that low-energy design is not intuitive and that simulation should therefore be an integral part of the design process (Hayter S.J., et al. 2001; Torcellini P.A., et al. 1999).

Needs related to the design process can be easily identified in time and accuracy. Accuracy is an essential prerequisite to every analysis used to support decision-making in every field. But accurate energy analysis requires time, up to several weeks in more complex cases, and the more accurate the analysis must be, the more time it will require. This is in contrast with the necessity to minimize the time requirements of the analysis so that it can be compatible with IDP times, but to do so simplifications of the building model and simulation tool are needed, with the drawback of a loss in accuracy. It is therefore essential to devote some research effort in trying to quantify the effects of simplifications applied in simulation

practice to evaluate, if and when those assumptions can be considered acceptable, and eventually to identify possible solutions to minimize the differences obtained between detailed and simplified models of the same building. A simplified building model still delivering useful results could drastically decrease the amount of information required to perform a simulation and the time requirements to implement the model itself. In addition to this, if the simplified model allows it, the implementation of such a model in a simplified building generation tool able to generate the model from a limited number of numerical inputs and database selections could greatly help in the integration of building simulation during IDP and early stage design. This paper discuss the application of such a simplified model to various case studies compared against a detailed modelling in term of accuracy of the results.

2. Methodology

To evaluate the impact of simplifications on simulation results in building model descriptions both a detailed model and a simplified model of each analysed building are implemented. Results of the two simulations are compared in terms of total energy needs and peak loads for both heating and cooling season; for this study peak loads are represented by the maximum heating/cooling load encountered during the whole year simulation. For the purpose of this paper, a detailed model is defined as a complete and exhaustive building model able to adequately represent the real behaviour of the building, implemented with full knowledge of the building itself and its use, such as a model developed during building operation. The simplified model is instead obtained through the application of a simplification protocol previously developed by the authors and discussed in other publications (Picco et al., 2014). For each model, simulations are performed in EnergyPlus software for the duration of a solar year, and the differences registered between each pair of models, detailed and simplified, are then calculated and reported.

2.1 Simplification Protocol

To obtain the simplified models a simplification protocol is applied.

The simplification protocol itself is defined as a series of consecutive simplification steps starting from a detailed model and culminating in a simplified model with the objective of evaluating the impact of simplifications on simulation results.

The simplification protocol is defined in eight consecutive steps concerning the model description including, primarily, all the most common simplifications used during the practical application of dynamic energy simulation. Later steps perform heavier and less commonly implemented simplifications.

The result of the application of the protocol is an extremely simplified model of the building representative of a simulation model deployable during early design stages based only on information, at least in some form, already available at each design stage and easily obtainable. Due to the lack of complexity, the model also requires a limited amount of time to be implemented, compatible with time requirements during the first stages of design. Also, due to how it is defined, the simplified model can be easily integrated into a simplified interface able to automatically generate the model starting from a limited number of numerical input and database selections. For the purpose of this paper, we will focus on this final simplified model and compare it with the detailed model before the application of the protocol. The simplification protocol in all of its steps and its application to the building description model is further detailed in a previous paper published by the authors (Picco et al., 2014).

2.2 Case studies

Three case studies are presented in this paper to evaluate the accuracy of results of the simplified models in comparison with detailed ones. For the purpose of this work, all case studies are chosen from large non-residential buildings, considered the ones that could benefit the most from early integration of energy simulation in the design process and the most difficult to do energy simulations on, especially during early stage

design, due to the lack of information needed. Starting from this restriction, the single case studies are chosen with varying energy performances and occupational behaviours, to evaluate if those aspects have an effect on the impact of simplifications.

An office building, identified hereinafter as CS1, represents the first case study analysed; the structure was originally built in 1954 and fully renovated in 2007. During the renovations two storeys were added to the existing three and major improvements to the energy efficiency of the building were added, resulting in a highly insulated structure with a 35 cm EPS shell (thermal transmittance of 0.08 W/(m²K) for external walls) and 3-pane type windows (thermal transmittance of 0.781 W/(m²K) and SHGC of 0.466), achieving Klimahaus Gold certification for passive buildings. The structure is characterized by a uniform distribution in terms of internal loads typical of an office building with high occupancy levels during the day. Usage and HVAC parameters are similar for the various zones both on the single floor plan and for the elevation of the building, ventilation rates are controlled by a mechanical ventilation system that ensures appropriate air changes during occupancy. The shape of the building is also sufficiently uniform in terms of the floor plan switching from floor to floor.

The second case study is a private clinic, identified hereinafter as CS2, built in 1933 and further expanded in various steps between 1930 and 1970. Due to the age of the building and the nature of the expansions, the structure is characterized by a low level of energy efficiency, with a complete absence of insulation layers in the walls (e.g. thermal transmittance of 1.3-2.1 W/(m²K) for external walls) and low thermal resistance windows (thermal transmittance of 1.96-5.89 W/(m²K) and SHGC of 0.691-0.861).

Being a hospital clinic, the building is characterized by a relatively uniform usage and internal gains for the single floors. However, differences in those properties becomes relevant for the elevation of the building, alternating between floors dedicated to bedrooms, to examination rooms or surgery rooms. Time distribution of internal loads also differ, with examination rooms active during the day while

bedrooms are active for the whole 24h. Ventilation is natural for the majority of the building and important infiltration rates are present due to the scarce air tightness of the envelope. HVAC parameters are constant for the entire building with the exception of surgery rooms positioned on the fifth floor. The same floor also constitutes a variation in the otherwise uniform shape of the floor plans.

The third and last case study is a recently built Bingo hall with complementary functions like betting and slot machine rooms, identified hereinafter as CS3. The structure was built in 2010, and therefore complies with current regulations in Italy, granting an adequate level of insulation (e.g. thermal transmittance of 0.363 W/(m²K) for external walls, thermal transmittance of 1.828 W/(m²K) and SHGC of 0.775 for windows) and thermal efficiency. The building has one conditioned floor, with only technical spaces on the second floor and an indoor parking lot underground, but presents a strong lack of uniformity in term of internal loads and HVAC parameters, especially in terms of ventilation air volumes, moving from room to room of the conditioned floor. Internal loads are high, especially due to equipment loads and mainly focused during the night, when the building is fully operating.

For each of those case studies a detailed simulation model has been produced in EnergyPlus based on available design documentation, field surveys and monitored data creating a detailed model characterized by the real usage, internal loads and HVAC parameters of the building during operation. Each model was then associated to three different HVAC system representations to evaluate the impact of simulation results based on the system hypothesis.

The three system hypotheses are summarized as:

- An “Ideal loads” air system, which represents the simplest system possible and operates by ideally adding or removing thermal energy from the air balance of the zones;
- a “Unitary” system in which each single zone is provided with a separate conditioning system comprised of an AHU with direct

expansion electric cooling coil and gas heating coil;

- a more detailed system based on the real HVAC system of the building, defining a variable air volume (VAV) system for CS1 and a “Fan-coil” air system, in which conditioning is achieved with recirculating fan-coil units powered by natural gas boilers and electrical chiller for CS2 and CS3.

This adds up to a total of nine pairs of detailed and simplified models, results of which are discussed in this paper. To successfully compare the results obtained by the various simplification steps to the ones of the corresponding detailed models, a number of relevant parameters of comparison are identified.

Simulations are performed for the duration of a full solar year based on climate year Bolzano 160200 (IGDG) for CS1 and Bergamo-Orio al Serio 160760 (IGDG) for CS2 and CS3, depending on their actual location. All weather data comes from the Italian Climatic data collection “Gianni De Giorgio”.

3. Results

Based on the results of the detailed and simplified simulations for each pair of models, the difference between the results of the two is calculated. Table 1 shows the percentage differences in results for total energy needs for both heating and cooling loads.

Table 1 – Total energy needs differences for various case studies

		Total Diff. [%]	
		Heating	Cooling
CS1	Ideal	-2.2	12.9
	Unitary	-12.8	-5.1
	VAV	-15.6	-14.6
CS2	Ideal	-2.1	-1.0
	Unitary	11.0	-8.6
	Fancoil	10.0	-1.8
CS3	Ideal	-7.6	-7.9
	Unitary	-10.4	-16.2
	Fancoil	-15.3	-5.4

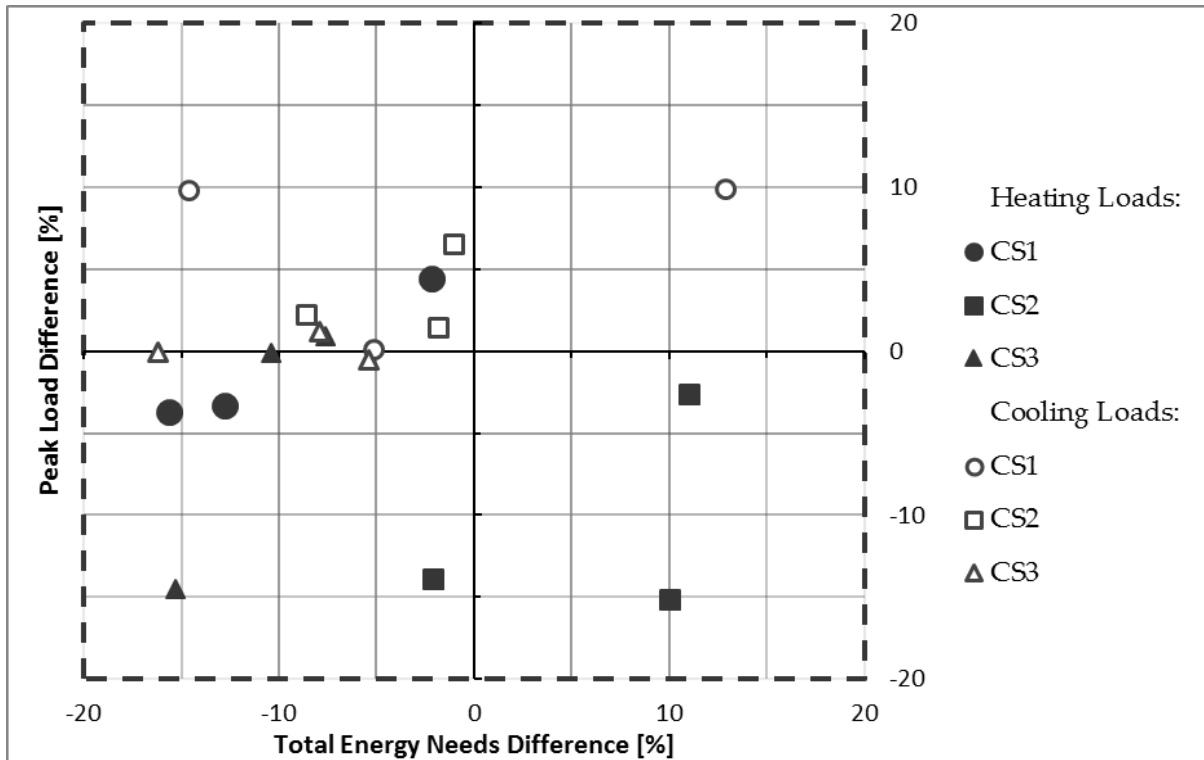


Fig. 1 – Comparison results for all the case studies highlighted based on Case study

Differences vary significantly from one case study to the other and from one system hypothesis to the next, ranging from absolute values of 2.1% up to 15.6% for heating energy needs and from 1.0% to 16.2% for cooling energy needs. In addition, in terms of total energy needs, on average, both heating and cooling needs tend to be underestimated by the simplified models compared to the detailed ones.

Table 2 – Peak load differences for various case studies

		Peak load diff. [%]	
		Heating	Cooling
CS1	Ideal	4.4	9.9
	Unitary	-3.3	0.1
	VAV	-3.7	9.8
CS2	Ideal	-13.9	6.5
	Unitary	-2.6	2.2
	Fancoil	-15.1	1.4
CS3	Ideal	0.9	1.2
	Unitary	-0.1	-0.1
	Fancoil	-14.5	-0.5

This behaviour can be motivated with the ability of the detailed models to detect extreme conditions in selected thermal zones while the simplified model ignores them due to the limited number of modelled zones and associated internal gains.

Table 2 shows the results in terms of peak loads for both heating and cooling seasons. Compared to differences in total energy needs, peak loads seem to show fewer differences from detailed to simplified models, ranging from 0.1% up to 4.4% for the majority of cases and only reaching 9.9% for cooling power in CS1 and 15.1% for Heating power of CS2.

In addition, CS3 shows a difference in peak loads of 14.5% for the fan-coil model. Another interesting, although qualitative, consideration that can be extrapolated from those results is how the simplified models tend to underestimate the heating Peak Power requirement of the buildings while overestimating the cooling Peak loads, with some exceptions.

Results of the comparison applied to all the case studies are also summarized in Figure 1 for more visibility, showing the percentage differences in terms of total energy needs for the simulation on

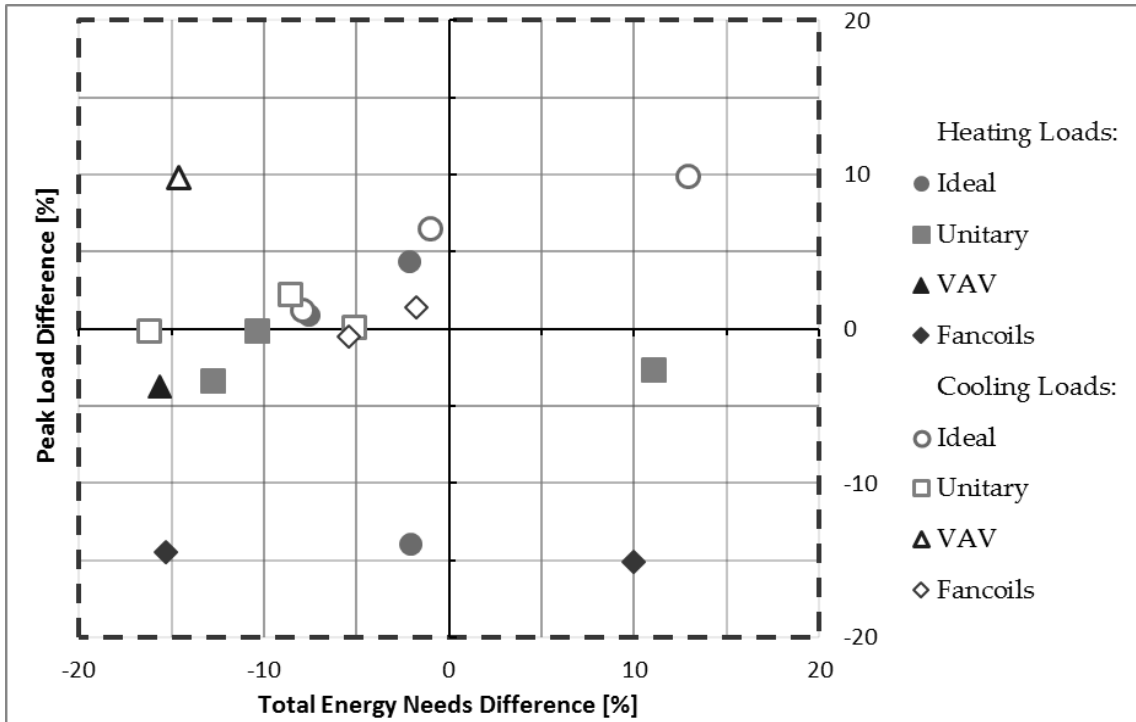


Fig. 2 – Comparison results for all the case studies highlighted based on system hypothesis

the x-axis of the chart and percentage differences in terms of peak loads in the y-axis. Results are visible in terms of heating or cooling loads depending on the filling of the indicator while its shape references the case study as shown in the attached chart. As there is no available threshold, in literature or legislation, to determine if the results of the simplified model are acceptable, through the experience in the field of building design and energy simulation a practical margin of 20% is identified as a reference and considered an acceptable margin of difference between the results of a simplified and detailed model.

As shown in the chart, results of the implementation of the simplified model on all the analysed case studies fall within the aforementioned margin of acceptability both in terms of total energy needs and Peak loads for heating and cooling needs. Results also show how differences in total energy needs are more scattered on the chart while differences in Peak loads are mainly centred in the range from -5% to +5%, showing smaller differences.

For the case studies analysed, there seems to be no major variability in total difference results as a function of the analysed building. Ideal loads

system and Unitary system hypothesis are applied to all case studies while Variable air Volume is only implemented in CS1 and fan-coil system is applied to case studies 2 and 3. Figure 2 shows the same results identified in terms of system hypothesis as detailed in the attached chart. From the Figure, it is possible to notice how, in term of total energy needs, the ideal loads system hypothesis seems to be the one showing fewer differences between simplified and detailed models.

In terms of peak load estimation, the Unitary system hypothesis seems to give the best results with all cases inside the $\pm 5\%$ margin. Complex systems such as VAV and fan-coil system hypothesis, featuring modelled plant and air loops linked to distribution terminals in the zones, seem to show more varying results but always inside the 20% margin of tolerance.

4. Conclusions

Of the total energy consumption, a significant portion is consumed by buildings, and the problem is more relevant due to their particularly long

lifetime and continued use. Efficient design is critical to reduce those consumptions, even more during its first stages, as poor design decisions can greatly impact the performance of the building and are typically difficult or impossible to rectify. Dynamic energy simulation could significantly increase efficiency in design, especially during early design phases. However, the complexity of simulations models and required detail hinder this integration. To overcome this obstacle, simulation models must adapt to the design process. The results presented in this paper give a new insight into the use of simplified building models and their impact on results.

As expected, different buildings perform differently under various simplifications; nonetheless, general conclusions can be drawn.

In terms of total differences between detailed model and fully simplified model, all the case studies here analysed results in differences never above 16.2% for total energy needs and 14.5% for peak loads. Due to the lack and uncertainty in information provided during early design phases, differences within the practical margin of 20% between the simplified simulation and the detailed model can still be considered acceptable by the authors, meaning those models can still produce useful information to fuel the design process.

The modelling and simulation time of the simplified models are of the order of a few hours, significantly lower compared to detailed models, but enough to allow the integration of building energy simulation in early stage design.

In addition, the simplified model is defined in such a way as to be easily implemented into a model generator tool, able to automatically generate the building model starting from a limited number of numerical inputs and database selections, at the moment 33 inputs are required to define the simplified model, further reducing required time.

Nonetheless, the use of a simplified building model can produce misleading results if used when one or more of the simplifications involved is not acceptable. It is therefore essential for the operator to correctly understand the model and critically evaluate the single instances to determine if the simplified model is suitable for the analysed building.

In addition, the application of the simplified model to a simplified simulation tool would partly result in a black box. In addition, it is possible that the relation of single inputs to the simplified model is not clear, depending on the operator, therefore in this hypothesis, an exhaustive description of the single inputs, also with examples, becomes essential to avoid interpretation errors.

Even so, considering these critical issues together with the results shown in this paper, the authors believe that the use of the simplified model at the beginning of building design can be useful to the design process, at least for non-residential buildings. Furthermore, the application of simplified models during early stage design lessens some of the issues, as, due to lack of information needed, a detailed model would suffer from the same simplifications and hypotheses.

References

- Aziz, Z., 2011. Integrated Design and Delivery Systems, Lecture Notes. Orbee learning package. Open Resources in Built Environment Education
- Chen, A. 2009. Working Toward the Very Low Energy Consumption Building of the Future. Retrieved from Lawrence Berkeley National Laboratory website
- Economidou, M. 2011. Europe's buildings under the microscope. A country by country review of the energy performance of buildings. Published in October 2011 by Buildings Performance Institute Europe (BPIE). ISBN: 9789491143014
- Hayter, S.J., Torcellini, P.A., Hayter, R.B., Judkoff, R. 2001. The Energy Design Process for Designing and Constructing High-Performance Buildings. Clima 2000/Napoli 2001 World Congress - Napoli (I), 15-18 September 2001
- Hensen, J. 2004. Towards more effective use of building performance simulation in design. 7th International Conference on Design & Decision Support Systems in Architecture and Urban Planning, Eindhoven, July 2-5, 2004
- Picco, M., Lollini, R., Marengo, M. 2014. Towards energy performance evaluation in early stage building design: A simplification methodology for commercial building models. Energy and

Buildings, Volume 76, June 2014, Pages 497-505
Punjabi, S., Miranda, V. 2005. Development of an integrated building design information interface, Building Simulation 2005 Ninth International IBPSA Conference, Montréal, Canada, August 15-18, 2005

Torcellini, P.A., Hayter, S.J., Judkoff, R. 1999. Low-Energy Building Design - The Process and a Case Study. ASHRAE Transactions, V 105, Part 2, pp. 802-810. Atlanta, GA: American Society of Heating Refrigerating and Air-Conditioning Engineers.

The Solar Response Factor for the dynamic response of buildings to solar heat gains

Gianpiero Evola – Department of Industrial Engineering, University of Catania – gevola@unict.it

Luigi Marletta – Department of Industrial Engineering, University of Catania – luigi.marletta@dii.unict.it

Abstract

The contribution of the solar heat gains to the cooling load is usually calculated through accurate procedures implemented in several simulation programs. Some simplified methods, such as the ASHRAE method, are also available for hand calculations, but they are based on tabular data that apply only to specific conditions.

This paper discusses a newly introduced parameter for the evaluation of the cooling load due to the solar radiation incident on the glazed surface of a building. This is the Solar Response Factor (SRF): it is a complex number, and can be rigorously defined and calculated as a combination of the thermal and the optical properties of walls and glazing.

In particular, the usefulness of the SRF is twofold. First, it allows us to classify the response of the enclosure to the solar radiation by means of a couple of parameters (amplitude and phase), which makes it easy to perform comparisons amongst different envelope solutions. Then, it allows for an easy analytical estimation of the cooling load in dynamic conditions, starting from the decomposition of the cyclic solar gains in a series of sinusoidal functions.

The paper discusses how the Solar Response Factor depends on the main thermo-physical and geometrical properties of the opaque and the glazed envelope. Moreover, an example is discussed to show how the use of the SRF allows us to evaluate the effectiveness of a series of solutions to limit the cooling load. The outcomes of this analysis provide very useful information for a conscious design of buildings, oriented to the limitation of the cooling load and the overheating of indoor spaces.

1. Introduction

In many buildings, the solar heat gains through the glazed envelope are a major portion of the total cooling load. However, it is not easy to estimate

accurately these contributions, as they are transient in nature and due to thermal storage effects induced in the building mass.

Nowadays, several computer programs for the calculation of the cooling load are available. Most of them are based on the Heat Balance method (HB), which solves the problem rigorously, i.e. by calculating a conductive, convective, and radiative heat balance for each room surface, as well as a convective heat balance for the room air. As an example, the HB method is the basis of the BLAST (BLAST, 1991), the TARP (Walton, 1983) and the DOE-2 (York et al., 1980) energy analysis programs, implemented in several commercial software. However, the use of these programs implies a certain computational effort, as they require complex and very detailed input data concerning the building and the local weather conditions. This might be a problem for most designers, who tend to prefer a more straightforward and easy approach for the calculation of the cooling load.

Another approach for the cooling load calculation is the use of conduction transfer functions, as in the Transfer Function Method (TFM) (Mitalas, 1968). In this case, the time-varying response of the building, i.e. the cooling load, is related to the driving element, i.e. the weather data, through a series of transfer coefficients depending on the properties of the building envelope. Due to its user-friendliness, the TFM is a widely used computer-aided load calculation method in the air conditioning industry.

An approach similar to TFM is proposed in the Radiant Time Series method (RTS) (Spitler et al., 1997), which relies on a series of 24 response factors to compute conductive heat gains, and on a second series of 24 terms (the radiant time series)

to convert instantaneous radiant heat gains to cooling loads.

The research has also led to the definition of even simpler methods, to be used for manual calculation of the cooling load. In particular, in 1965 the *thermal storage factors* were defined – in the context of the Carrier method – as the ratio of the rate of instantaneous cooling load to the rate of solar heat gain (Carrier, 1965). The thermal storage factors have to be determined through appropriate tables depending on both the weight per unit floor area of the opaque components and the running time. Therefore, their use requires interpolation among tabular data; they are also rather rough, as they do not take into account the actual sequence of the wall layers, and they lack any theoretical basis, as they result from numerical simulations.

Similarly, the cooling load temperature difference (CLTD)/solar cooling load (SCL)/cooling load factor (CLF) method was more recently formulated (ASHRAE, 2009). Here, the space sensible cooling load from solar heat gains transmitted through the glazing can be calculated through a series of *solar cooling load factors* (SCL). ASHRAE has developed SCL values to be used for typical buildings in North America with weather data associated to July 21st at a latitude of 40°N. The accuracy of this approach is questionable for locations that are not placed at 40°N; in any case, up to now this cooling load calculation method has been widely used by HVAC designers.

In this paper, a substantially different approach is proposed. This approach is developed in the framework of the Admittance Procedure, a methodology built up in the early '70s, where the dynamic heat transfer through the opaque walls is assessed by means of the so-called *dynamic thermal properties* (Davies, 1973), (Millbank et al., 1974), (Loudon, 1970). In this context, a new parameter called the Solar Response Factor (SRF) has been recently introduced by the authors (Evola et al., 2013). The SRF is a complex number, quantified in terms of amplitude and phase; it is calculated as a combination of the thermal and the optical properties of walls and glazing. The use of the SRF allows managing analytically the calculation of the cooling load due to solar heat gains under steady-periodic conditions.

The reliability of this approach is successfully proven by comparison with a series of simulations carried out with EnergyPlus. Then, the paper discusses how the Solar Response Factor depends on the main thermo-physical and geometrical properties of the envelope. Finally, an example is presented to show how the use of the SRF allows us to evaluate the effectiveness of a series of solutions to limit the cooling load.

2. The Solar Response Factor

2.1 Definition and formulation

The rigorous calculation of the cooling load due to solar heat gains through the glazing is quite complex, as it involves several phenomena. Indeed, the solar radiation penetrating the glazing is firstly absorbed by the inner surface of the opaque envelope components. Then, the absorbed heat is partially transferred towards the indoor environment, due to the surface overheating: only the convective part of such thermal transfer contributes to the cooling load of the indoor space. Furthermore, in order to assess the cooling load, one must not forget the radiant energy absorbed by the glass itself and transferred by its inner surface to the indoor environment: this last component raises its importance as the glazed area increases.

All of these mechanisms are rigorously taken into account in the formulation of the *Solar Response Factor* SRF. This is defined as the overall convective heat flux released to the indoor air by all the inner surfaces of the envelope (walls plus glazing) per unit cyclic solar irradiance acting on the outer glazed surface. In formulae:

$$\text{SRF} = \frac{\sum_w (\tilde{q}_{w,c} \cdot A_w) + \sum_g (\tilde{q}_{g,c} \cdot A_g)}{\sum_g (\tilde{I}_g \cdot A_g)} \quad (1)$$

It is important to remember that the formulation of the SRF is based on the concept of Surface Factor. According to the definition provided by (Millbank et al., 1974), this parameter quantifies the heat flux released by a wall to the environmental point per unit radiant heat gain collected on its inner surface, when the air temperatures on both sides of the wall

are held constant and equal, see Eq. (2). As discussed in (Evola and Marletta, 2013), the surface factor can be calculated through Eq. (3), where Y is the thermal admittance of the wall.

$$F = \frac{\tilde{q}_i}{\tilde{q}_{\text{abs}} \Big|_{\tilde{\theta}_i = \tilde{\theta}_0 = 0}} = \frac{\tilde{q}_i}{\alpha \cdot \tilde{\phi}} \quad (2)$$

$$F = 1 - Y \cdot R_{\text{si}} \quad (3)$$

Starting from these definitions, it is possible to derive an operational formulation for the SRF. The demonstration has already been presented in (Evola et al., 2013), and is here omitted. Eq. (4) reports this formulation in the case of an enclosure with only one window.

$$\text{SRF} = \frac{\sum_w (\alpha_{w,\text{sw}} \cdot F_w \cdot A_w \cdot h_{c,w} \cdot R_{\text{si},w})}{\left[(1 - \rho_{g,\text{sw}}) \cdot f + (1 - f) \cdot \bar{\alpha}_{w,\text{sw}} \right] \cdot A_{\text{tot}}} \cdot \tau_g + 0.53 (g_s - \tau_g) \cdot \frac{\sum_w (F_w \cdot A_w \cdot h_{c,w} \cdot R_{\text{si},w})}{A_{\text{tot}}} + 0.47 (g_s - \tau_g) \quad (4)$$

In Eq. (4), f is a non-dimensional parameter, which measures the fraction of glazed surface to the overall surface of the enclosed space ($f = A_w / A_{\text{tot}}$). According to Eq. (4), the SRF depends on the optical properties of the envelope (α_w , Q_g , τ_g), as well as on the composition of the walls, which affects the calculation of the surface factors F_w .

Since the SRF depends on the Surface Factor, it results to be a complex number, characterized by an amplitude $|\text{SRF}|$ and a phase ϕ_{SRF} .

2.2 Calculation of the cooling load

According to its definition, the usefulness of the SRF lies in the possibility of predicting the cooling load of a building due to solar heat gains, analytically and in the time domain.

To this aim, it is important to remember that any periodic function can be decomposed, by means of the Fourier analysis, in a series of sinusoidal functions, called *harmonics*, whose frequency is a multiple of the first harmonic, called *fundamental*.

Hence, the first step is the application of the Fourier analysis to the solar irradiance $I_g(t)$, in order to determine its mean value I_{gm} and the harmonic components, up to the order NH needed for a sufficient precision. The period of the n -th harmonics is $P_n = P/n$, where $P = 24$ h.

The second step is the calculation of the Solar Response Factor for the enclosure, see Eq. (4). This operation has to be repeated for each harmonic component: in this case, the surface factors F_n have to be calculated with reference to the period P_n . It is also necessary to determine the stationary Solar Response Factor (SRF_s): it is a real number obtainable through the same relations as those used for SRF, but using the thermal transmittance U in place of the thermal admittance Y .

Finally, the time profile of the cooling load due to solar heat gains can be assessed through Eq. (5), where the harmonic components of the response are summed up to the order NH .

$$Q_c(t) = A_g \cdot \left[\text{SRF}_s \cdot I_{gm} + \sum_{n=1}^{NH} |\text{SRF}_n| \cdot \tilde{I}_{gn} \cos \left(\frac{2\pi t}{P_n} + \phi_{\text{SRFn}} \right) \right] \quad (5)$$

The reliability of this approach is verified in the following section, based on the comparison with the results obtained through accurate and well-established methods.

3. Validation of the proposed approach

In order to verify the reliability of the formulation proposed in Section 2 to calculate the cooling load due to solar radiation, a preliminary validation is performed. This is based on the comparison between the results of Eq. (5) and those obtained with accurate simulations on EnergyPlus for a simple test room, whose size is $5 \times 5 \times 3$ m³. As far as the envelope of the test room is concerned, four different building typologies are considered:

- *Case A*: heavy masonry walls (stone walls);
- *Case B.1*: double-leaf cavity walls with the insulation placed in the air gap;
- *Case B.2*: double-leaf cavity walls with the insulation placed on the inner side of the wall;
- *Case C*: single leaf lightweight clay walls.

The details concerning the composition of walls, floors and ceilings are reported in the Appendix, where the values of the corresponding surface factors F are also provided. In the calculation, two walls are considered as external walls, whereas the others look like internal walls. In any case, all opaque surfaces have the same short-wave absorptance ($\alpha_{\text{sw}} = 0.3$).

Furthermore, the room is equipped with a window, whose size is $A_g = 5.5 \text{ m}^2$, which corresponds to $f = 0.05$. The window has double glazing filled with air ($U_g = 2.9 \text{ W m}^{-2} \text{ K}^{-1}$). In the calculation of SRF, no obstruction or shadings are considered.

For each type of envelope, four different simulations are carried out, to investigate all the possible exposures of the glazing. The optical properties of the double glazing, used in the calculation of the SRF, are reported in Table 1. They are determined through UNI EN 410:2011, and taking into account the average angle of incidence for each orientation. The weather data are those available on EnergyPlus for Catania (southern Italy).

Furthermore, it should be remembered that no forcing condition other than the solar radiation incident on the glazing must be taken into account in this context, according to the definition framework of both the *surface factor* F and the *solar response factor* SRF. For this reason, in the simulations with EnergyPlus a constant air temperature was imposed in the test room ($\theta_i = 26^\circ\text{C}$), and all the envelope elements were considered adjacent to other rooms with the same temperature.

Finally, Table 2 shows the values retained for h_c and R_{si} . As already discussed in a previous work by the authors (Evola and Marletta, 2013), these values are different from those usually adopted by international standards. This position derives from the specific definition framework of SRF, which implies a certain homogenization of the inner surface temperatures. Consequently, a lower rate of surface-to-air convective and reciprocal radiant heat transfer is expected if compared to an “ordinary” situation.

Table 1 – Average optical properties of the glazing

Glazing type	South	East/West	North	
τ_g	Single	0.647	0.748	0.719
	Double	0.472	0.588	0.588
	Double reflective	0.243	0.305	0.290
g_s	Single	0.674	0.774	0.744
	Double	0.547	0.663	0.633
	Double reflective	0.363	0.425	0.410

Table 2 – Values retained for h_c and R_{si}

	Ceiling	Floor	Walls
h_c [$\text{W}\cdot\text{m}^{-2}\cdot\text{K}^{-1}$]	1.0	1.2	1.4
R_{si} [$\text{m}^2\cdot\text{K}\cdot\text{W}^{-1}$]	0.9	0.75	0.65

Table 3 – Amplitude and phase of SRF for the test room (double glazing, $\alpha_{sw} = 0.3$, $f = 0.05$)

		South	East/West	North
SRF	Case A	0.080	0.091	0.088
	Case B.1	0.140	0.165	0.158
	Case B.2	0.174	0.207	0.198
	Case C	0.146	0.173	0.166
ϕ_{SRF}	Case A	1.82	1.97	1.94
	Case B.1	1.99	2.08	2.03
	Case B.2	1.60	1.67	1.65
	Case C	1.80	1.88	1.86

The amplitude |SRF| and the phase ϕ_{SRF} for the test room, calculated through Eq. (4) for all the exposures and all the envelope typologies, are shown in Table 3. Here, it is possible to observe that massive walls (Case A) imply lower amplitude |SRF| than in the other cases, thanks to their high inertia. Hence, a lower cooling load is expected. The difference between the building solutions is less pronounced when looking at ϕ_{SRF} , which is always close to 2 h. Furthermore, placing the insulation layer close to the indoor environment (case B.2) determines the worst performance, with the highest values of |SRF| for all the exposures.

As far as the comparison between the proposed methodology and the results obtained with EnergyPlus is concerned, the outcomes are shown in Fig. 1. The comparison is based both on the peak cooling load (Fig. 1a) and the daily energy demand (Fig. 1b), i.e. the time integral of the cooling load over a daily period. In order to calculate the cooling load, $NH = 6$ has been set in Eq. (5); the introduction of further harmonics would not modify the result.

The discrepancy on both parameters never exceeds 10%, and actually rarely exceeds 5%. The outcome of the validation is very satisfactory, given that quite a large window area is considered ($A_g = 5.5 \text{ m}^2$): even better results were obtained in the case of an enclosure with smaller windows.

Another interesting result is shown in Fig. 2. Here, one can observe that $NH = 3$ is sufficient to produce a reliable profile of the cooling load. Indeed, the highest discrepancy between $NH = 3$ and $NH = 6$ is around 2% on the peak cooling load. Similar results are obtained for other envelope solutions.

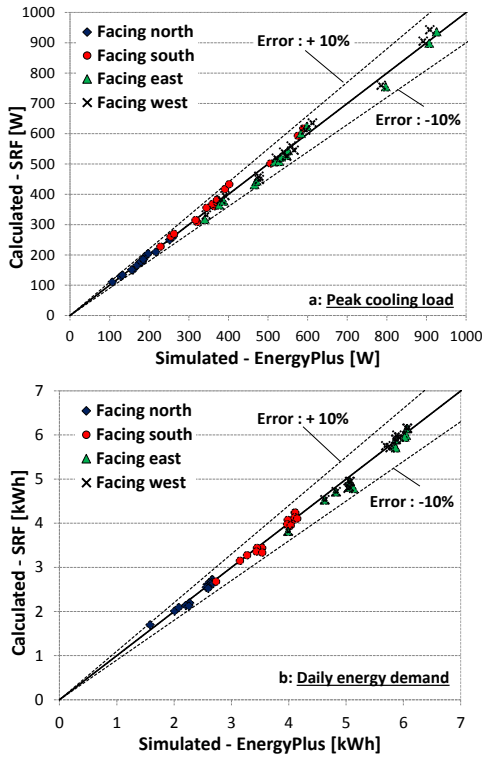


Fig. 1 – Discrepancy between calculated and reference results

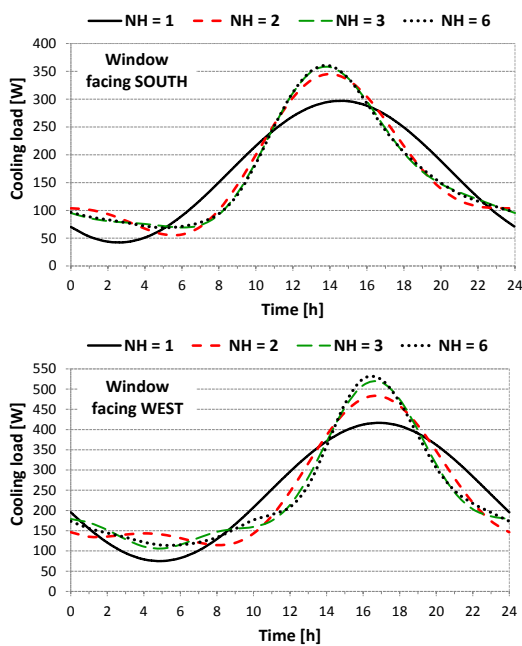


Fig. 2 – Summation of the harmonics in Eq. 5 (case B.1)

4. Parametric analysis

In this section, the paper discusses how the SRF depends on the glazing type, the size of glazed surface – described through the non-dimensional parameter f – and the solar absorptance α of the inner surfaces. Here, three different glazing solutions are considered, i.e. single glazing, double glazing and double glazing with a reflective outer pane; the average optical properties for all typologies are those listed in Table 1.

The amplitude $|SRF|$ and the phase ϕ_{SRF} of the Solar Response Factor, calculated through Eq. (4) for several combinations of these parameters, are reported in Fig. 3. The calculation is extended to all the envelope solutions and the window exposures.

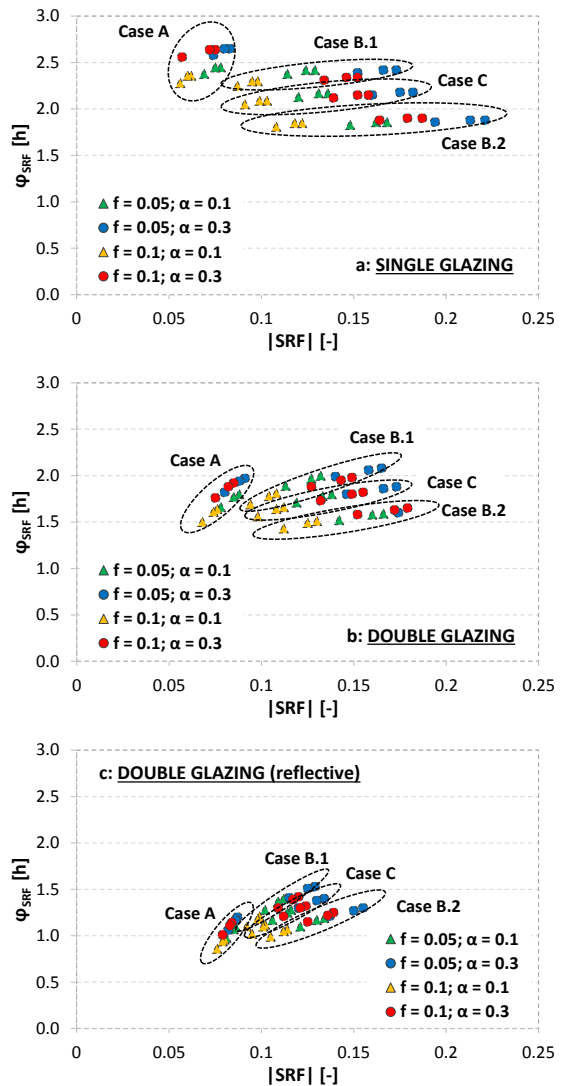


Fig. 3 – The Solar Response Factor of the sample room for different glazing types and size

As is possible to observe, the use of a reflective glazing tends to reduce the differences between the envelope solutions, since the solar gains are significantly cut by the glazing itself. Hence, the thermal inertia of the opaque envelope has a lower importance. A reflective glazing yields lower $|SRF|$ than common double glazing. However, the phase is also lower, due to the higher rate of solar irradiance absorbed by the glazing, and then transferred by convection to the indoors.

5. Useful application of the SRF

The SRF can also be conveniently used to perform comparisons between different strategies for the reduction of the cooling load.

As an example, let us consider the test room described in Section 3. Starting from the configuration already introduced (double glazing, $\alpha = 0.3$, $f = 0.05$), which is identified as the “base case” in the following, several potential strategies are suggested to reduce the cooling load, namely:

- Outer reflective pane on the window;
- Low absorptance of the inner surface ($\alpha = 0.2$);
- Installation of an insulating layer (40 mm of polystyrene) either on the inner or on the outer side of the external wall.

Hence, for each proposed intervention, the SRF of the room is calculated through Eq. (4), and the daily profile of the cooling load is determined by means of Eq. (5). This analysis is applied to Case A and Case C, with reference to a window due south. The results are shown in Fig. 4. Here, we can observe that the application of an insulation layer on the outer wall is not a good idea. In particular, placing the insulation on the inner side significantly increases the peak cooling load, especially in Case A, where the detrimental effect on the thermal inertia of the wall is more pronounced. In case C, placing the insulation on the outer side has no effect on the cooling load.

On the other hand, the use of a lighter inner plaster ($\alpha = 0.2$) has a positive effect, as expected. However, the reduction of the peak cooling load due to this intervention is not significant. The best solution consists in the use of a reflective pane on the outer side of the window.

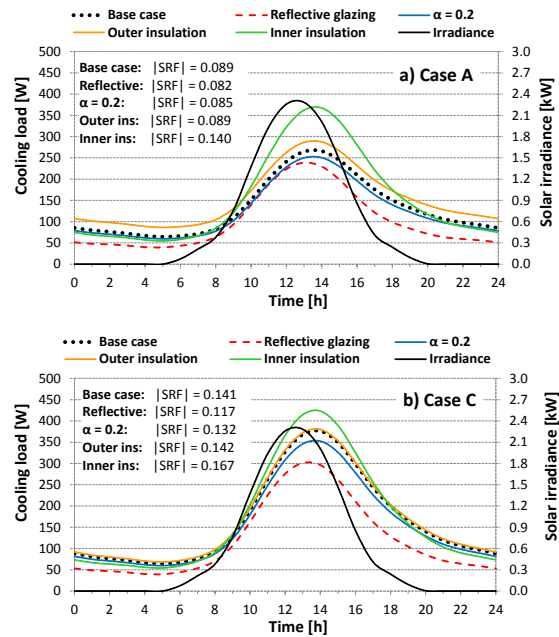


Fig. 4 – Cooling load of the test rom for different configurations.

In any case, the same conclusions about the effectiveness of such strategies could be foreseen from the values of $|SRF|$ reported in the graphs of Fig. 4. Indeed, the higher $|SRF|$, the higher the resulting peak cooling load.

6. Conclusion

The Solar Response Factor proves to be very useful to assess the energy performance of buildings.

The main quality of the SRF is that it represents a transfer function of the whole enclosure in relation to solar excitations, in the form of a single complex number. Its formulation is derived analytically, and involves all the thermo-physical properties of the envelope.

The SRF can be used to make comparisons between different building solutions in the design stage, or to classify existing buildings in relation to their capacity to attenuate the effects of solar radiation, without the need of complex dynamic simulations.

If compared to the Solar Cooling Load factor (SCL) defined by Ashrae, the SRF shows solid theoretical bases and is more general and rigorous.

For all these reasons, the use of the SRF can be recommended to professionals and researchers as a very useful tool to evaluate the response of buildings to solar heat gains.

7. Nomenclature

Symbols

A	area (m ²)
f	fraction of glazed surface (-)
F	surface factor (-)
g _s	glass g-value (-)
h	heat transfer coefficient (W m ⁻² K ⁻¹)
I	solar irradiance (W m ⁻²)
n	order of the harmonic (-)
NH	total number of harmonics (-)
P	time period (h)
q	density of heat flux (W m ⁻²)
Q _c	cooling load (W)
R	thermal resistance (m ² K W ⁻¹)
SRF	solar response factor (-)
U	thermal transmittance (W m ⁻² K ⁻¹)
Y	thermal admittance (W m ⁻² K ⁻¹)

Greek letters

α	absorptance (-)
ρ	reflectance (-)
τ	transmittance (-)
φ	time shift (h)
φ	radiant heat flux (W m ⁻²)

Subscripts/Superscripts

abs	absorbed
c	convective
g	glazing
h	harmonic
i	indoor
o	outdoor
si	inner surface
sw	short-wave
w	wall

References

ASHRAE, American Society of Heating, Refrigerating and Air Conditioning Engineers. 2009. "Chapter 18: Nonresidential cooling and heating load calculations". In *ASHRAE Handbook of Fundamentals*, edited by ASHRAE.

BLAST Support Office. 1991. *BLAST user reference*.

Urbana Champaign: University of Illinois.

Carrier Air Conditioning Co. 1965. *Handbook of Air Conditioning System Design (1st ed.)*. New York: McGraw-Hill.

CIBSE. 2006. *Environmental Design CIBSE Guide A*. London: The Yale Press Ltd.

Davies M. G. 1994. "The thermal response of an enclosure to periodic excitation: the CIBSE approach". *Building and Environment* 29 (2): 217-235. doi:10.1016/0360-1323(94)90072-8.

EN 410:2011. "Glass in building – Determination of luminous and solar characteristics of glazing".

Evola G., Marletta L. 2013. "A dynamic parameter to describe the thermal response of buildings to radiant heat gains". *Energy and Buildings* 65: 448-457. doi:10.106/j.enbuild.2013.06.026.

Evola G., Marletta L., Sicurella F. 2013. "A dynamic parameter for dealing with solar gains in buildings". In *Proceedings of Building Simulation 2013*, edited by Etienne Wurtz, 161-168.

ISO 13792:2012. "Thermal performance of buildings – Calculation of internal temperatures of a room in summer without mechanical cooling – Simplified methods".

Loudon A. G. 1970. "Summertime temperatures in buildings without air conditioning". *Journal of the Institution of Heating and Ventilation Engineers* 37: 280-292.

Millbank N. O., Harrington-Lynn J. 1974. "Thermal response and the admittance procedure". *Building Service Engineering* 42: 38-51.

Mitalas G. P. 1968. "Calculation of transient heat flows through walls and roofs" in *ASHRAE Transactions* 74 (2): 182-188.

Spitler J. D., Fisher D. E., Pedersen C. O. 1997. "The radiant time series cooling load calculation procedure" in *ASHRAE Transactions* 103 (2): 503-515.

Walton G. 1983. *Thermal Analysis Research Program reference manual*. National Bureau of Standards.

York D. A., Tucker E. F., Cappiello C. C. 1980. *DOE-2 engineers manual (Version 2.1A)*. Lawrence Berkeley Laboratory and Los Alamos National Laboratory.

External wall: Case A

Material	s [m]	F [-]	ϕ_F [h]	U [W/m ² K]
Inner plaster	0.01			
Lava stones	0.60	0.086	2.3	1.90
Outer plaster	0.01			

External wall: Case B.1

Material	s [m]	F [-]	ϕ_F [h]	U [W/m ² K]
Inner plaster	0.01			
Hollow clay bricks	0.08			
Air cavity	0.03	0.318	3.5	0.35
Polystyrene	0.05			
Hollow clay bricks	0.25			
Outer plaster	0.01			

External wall: Case B.2

Material	s [m]	F [-]	ϕ_F [h]	U [W/m ² K]
Inner plaster	0.01			
Polystyrene	0.05			
Hollow clay bricks	0.08	0.644	1.6	0.35
Air cavity	0.03			
Hollow clay bricks	0.25			
Outer plaster	0.01			

External wall: Case C

Material	s [m]	F [-]	ϕ_F [h]	U [W/m ² K]
Inner plaster	0.01			
Light bricks	0.38	0.364	2.5	0.35
Outer plaster	0.01			

Internal partitions: Case A

Material	s [m]	F [-]	ϕ_F [h]	U [W/m ² K]
Inner plaster	0.01			
Lava stones	0.40	0.084	2.2	1.66
Outer plaster	0.01			

Internal partitions: Case B + Case C

Material	s [m]	F [-]	ϕ_F [h]	U [W/m ² K]
Inner plaster	0.01			
Hollow clay bricks	0.08	0.305	2.3	0.89
Outer plaster	0.01			

Floor: Case A

Material	s [m]	F [-]	ϕ_F [h]	U [W/m ² K]
Concrete tiles	0.01			
Lean concrete	0.06			
Pumice/gypsum	0.12	0.150	3.8	0.75
Inner plaster	0.01			

Table 8 – Floor: Case B + Case C

Material	s [m]	F [-]	ϕ_F [h]	U [W/m ² K]
Concrete tiles	0.01			
Lightweight screed	0.05			
Concrete-slabs flooring	0.20	0.260	2.2	0.92
Inner plaster	0.01			

Ceiling: Case A

Material	s [m]	F [-]	ϕ_F [h]	U [W/m ² K]
Inner plaster	0.01			
Pumice/gypsum	0.12			
Lean concrete	0.06	0.296	2.8	0.30
Concrete tiles	0.01			

Ceiling: Case B + Case C

Material	s [m]	F [-]	ϕ_F [h]	U [W/m ² K]
Inner plaster	0.01			
Concrete-slabs flooring	0.20			
Polystyrene	0.05	0.112	2.6	0.11
Lightweight screed	0.05			
Concrete tiles	0.01			

Comparison of energy simulations for a residential unit: a rapid method for an integrated decision tool

Alberto Beltrami – Dept. of Engineering and Applied Science, University of Bergamo, Italy – alberto.beltrami@unibg.it

Marco Picco – Dept. of Engineering and Applied Science, University of Bergamo, Italy – marco.picco@unibg.it

Marco Marengo – University of Brighton, School of Computing, Engineering and Mathematics, UK – m.marengo@brighton.ac.uk

Abstract

This work defines a methodology aimed at the creation of a simplified energy model able to simulate a residential building with a reasonable workload. The simulation results should have a sufficient accuracy at any stage of a building design, by exploiting the benefits of a modular approach with increasing detail rendition. The idea is to verify the accuracy of the simulations comparing different methodologies, from stationary simulations, using a Italian software called TERMUS, to more sophisticated, even if standard, dynamic simulations, using TRNSYS. Such comparisons have already been carried out in the past in different papers, but a thorough analysis of the envelope-plant system using progressive simplification steps has not yet been done, especially for a residential test case in an on-going retrofit process. The results indicate that with the proper simplification steps, shown in the analysis, the accuracy in terms of energy needs and power curves is very high (the difference with the most complete analysis is always below 12% for all the output parameters) with a workload of a few hours for the preparation of the model and the simulations. The fact of having considered a case in northern Italy does not limit the universality of the procedure, which may be applied for a very large number of built environments in residential areas.

1. Introduction

The daily operation of commercial and residential buildings comprises roughly one-third of the world's primary energy consumption. Because buildings typically operate for many years, there is great potential for reducing global energy needs

through improved building design (Urban et al., 2006).

Computer modelling and simulation are powerful technologies for addressing interacting architectural, mechanical, and civil engineering issues in buildings. Building Performance Simulations (BPS) can help to reduce emissions of greenhouse gases and to provide substantial improvements in fuel consumption and comfort levels, by treating buildings and their thermal systems as optimized entities, and not as the sum of a number of separately designed and optimized sub-systems or components (Hensen, 2004).

Experience with real buildings has shown that low-energy design is not intuitive and that simulations should therefore be an integral part of the design process (Torcellini et al., 1999; Hayter et al. 2001).

In fact, for energy saving components, an intuitive selection appears to have additional drawbacks: for example the efficiency of these components cannot be studied in isolation. They are dependent on building characteristics whereas interaction between components can have a substantial effect on the efficiency of each individual component. The impact of climate conditions and occupant behaviour adds to the complexity and makes it almost impossible to predict performance without use of computational tools (De Wilde et al., 2001).

However, architects and designers are still finding it difficult to use even basic tools (Punjabi et al., 2005). Findings confirm that most BPS tools are not compatible with architects' working methods and needs (Attia et al., 2009; Gratia et al., 2002).

Needs related to the design process can be easily

identified as time and accuracy. Accuracy is an essential prerequisite for every analysis used for decision-making and becomes significantly more relevant during the design process of buildings, where decisions taken can concern a large amount of energy and can affect the building for a large number of years. Accurate energy analysis requires time but this is in contrast with the necessity to minimize the time requirements to make it compatible with design times. A way to reduce time requirements could be the introduction of default values and databases for inputs, with the possible risk of reducing the model detail level and degree of freedom, themselves influencing the accuracy or relevance of the final result (Picco et al., 2013).

Considering the whole building-plant system, results from a stationary simulation are compared with different dynamic simulations characterized by gradually increasing simplifications both in terms of building envelope and plant. A very detailed model is simulated in order to define the reference case, in terms of building energy loads, power curves and the efficiency of all the subsystems belonging to the heating system. Differences between the detailed and the simplified models are analysed to determine the quality of the results of the latter.

2. Building Description

The case study under exam is a standard residential unit in a building built in 1989, situated in Bergamo, Italy. The use of such a test case was chosen due to the large number of residential buildings with such construction characteristics in the area of northern Italy. In future years, a great part of the energy retrofit will be carried out on such kinds of units and there is an important interest in offering low cost, but still accurate, dynamic simulations of such situations.

The building consists of three floors, the basement for the garage and winery, and the ground and first floors, each intended for residential purposes. In particular, as opposed to one on the first floor, the apartment on the ground floor is not currently

used and needs a renovation in order to make it habitable.

Retrofit design and simulations focus just on this portion of the building, characterized by an usable floor area of 86.25 m², a total net volume of 232.88 m³, 7 heated spaces/rooms and a central unheated stairwell necessary to connect the basement to the ground floor apartment (Figure 1).

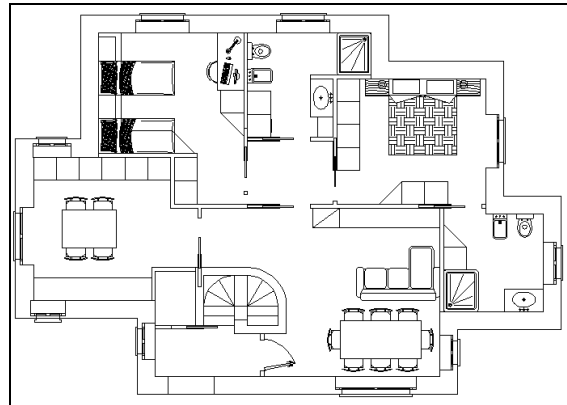


Figure 1 – Design of the interior layout of the apartment

Currently the building envelope, except the ceiling adjacent to the upper apartment, is only composed of the structural part made of reinforced concrete, and the renovation design provides to isolate the internal surface of 311 m² through wall and window stratigraphy, able to ensure both high energy performances and the access to the tax benefits expected for this kind of building work.

In particular, as provided by retrofit design, the opaque vertical surfaces will have a transmittance equal to 0.262 W/m²K, while the floor adjacent to the basement will have a transmittance of 0.285 W/m²K and for the 14.88 m² of transparent dispersants a global average transmittance of 1.5 W/m²K is set for the simulations. The HVAC plant is expected to meet only the winter thermal load through a heating system composed of 7 aluminum radiators (one for each room) powered by a 5 kW condensing natural gas boiler.

A climate control for the supply temperature of the heating plant is provided, together with an internal regulation composed of thermostatic valves able to reduce or increase the flow rate of the heat transfer fluid to the radiators. The isolated distribution network piping will be placed inside the heated

environments in order to reduce losses to a minimum value.

3. Stationary simulation

Once the key features of the building-plant system have been defined, a first stationary simulation was carried out using TERMUS software (produced by ACCA software S.p.a., M. Cianciulli road - 83048 Montella (AV), Italy - more information at www.acca.it).

The TERMUS model consists of a single thermal zone divided into 7 rooms and of all other heated areas (first floor apartment) and unheated spaces (basement, stairwell and the boiler room) necessary to determine, with monthly time-steps, the average temperatures of all the surfaces (Figure 2).

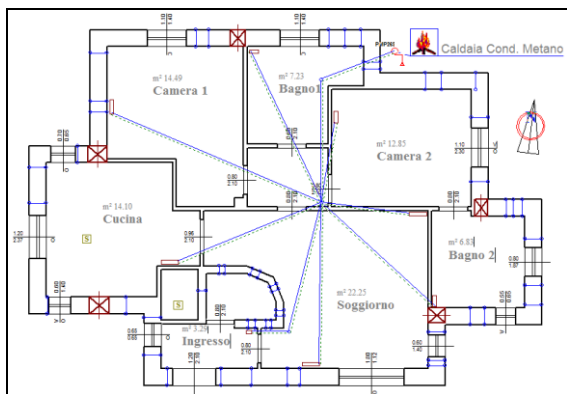


Figure 2 – TERMUS simulation model and heating plant design

The wall stratigraphy of the model consists of 22 different types identified with 15 different materials. A basic time schedule for the heating system has been defined as input and the following quantities have been estimated:

- Losses related to thermal bridges;
- Geometric shadowing objects and obstruction due to the building and its urban context;
- Standard values for infiltration and internal contributions (values recommended by current legislation);
- Standard values of efficiency for the emission, regulation, distribution and generation subsystems (even for these, the software considers values recommended by current legislation);

The software generates as main output results the

following parameters:

- Maximum thermal power required from each room in the design conditions (kW);
- Monthly thermal energy demand of the whole zone simulated (kWh);
- Monthly Primary energy demand of the entire simulated zone (kWh);

Then, based on the first output described, it proceeds to the heating plant design, sizing the components and verifying their operation in the maximum load condition (Figure 2).

The software does not consider the possible presence of a storage tank and does not take into account the recovery of the potential distribution losses.

4. Dynamic Simulations

As a second step, a complete dynamic energy simulation of the entire building-plant system was performed through the TRNSYS software. This complete model was subjected to a series of simplifications both for the building envelope and for the plant, in order to determine deviations and therefore quality of the results of the simplified models.

4.1 Detailed model

In terms of building envelope, as seen for the stationary simulation, the model consists of seven homogenous thermal zones, fully describing all conditioned rooms, underground non-conditioned space, and all accessory non-conditioned volumes like the stairwell, boiler room and attic.

Through the specific Trnsys3D tool, the three-dimensional modeling of the entire building was created, as well as all relevant shadowing objects comprising all the adjacent building structures and the specific solar obstructions (Figure 3).

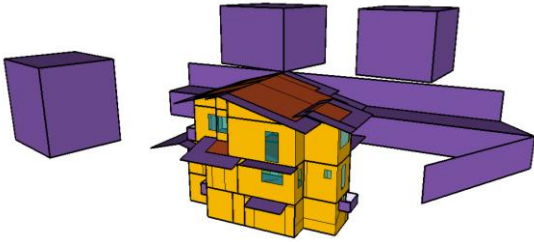


Figure 3 – Complete model for building envelope (Trnsys3D)

To characterize the various zones, each one defined in terms of materials and stratigraphy of walls and windows, thermal bridges, internal gains, temperature set-points and time heating schedule, the same data of the previous stationary simulation were used, adding all parameters not considered by this kind of design, as the heat capacity of the materials or external and boundary conditions with hourly rather than monthly time-step.

This characterization was achieved by TRNBuild tool, the Trnsys software tool specifically dedicated to the characterization of the building envelope.

Finally, in order to simulate the dynamic operation of the HVAC plant of the apartment, the integration of all subsystems was carried out, starting from the emission until the generation sub-system. This step led to the creation of a dynamic and integrated building-plant model consisting in total of 81 components (Type), all connected according to an input – output logic.

In fact, in Trnsys software each Type can be considered as a “black box”, which processes input data as a function of defined algorithms, starting from user-defined parameters, and produces output data. The task of each Type is to solve simple problems, and their interconnection allows the user to solve the complex problem that is being analyzed.

In the case study shown here, each Type corresponds to a single component of the entire building-plant system. In particular, the model created for the heating plant is synthetically structured as follows:

- Generation + storage sub-systems: natural gas boiler whose operation is governed on the basis of the temperatures measured inside the buffer tank placed downstream;
- Distribution sub-system: three-way diverter and mixing valves able to ensure at each moment the correct flow temperature regulated depending on

the outdoor temperature (climate control), variable speed pump, distribution piping from the storage tank to the supply/return manifold and from the latter to radiators;

- Emission subsystem: aluminum radiators;
- Regulation subsystem: individual room PI type able of acting on the flow of heat transfer fluid to the single radiator, with feedback constituted by the actual ambient temperature recorded.

The characterization of all TRNSYS Types used for the plant components has been made from data resulting from the stationary plant design made previously, with the difference that the model created allows us to check the actual operation of the entire and dynamic building-plant system at any variation of all possible internal and external conditions, taking into account each instant the interaction of all the components.

This model represents the highest degree of simulative details with a high number of outputs made available at each time-step (up to about 700 outputs), from the operating temperatures in all components to the unsteady heat balance regulating each component, the cumulative efficiencies of the various sub-systems installations, and the indicator of the overall quality of the designed system.

4.2 Building envelope simplification

As previously mentioned, the complete dynamic model has been subjected to simplifications, in order to test the quality or accuracy of the results of the simplified models, also in relation to the lower work-load required for the latter, during the building retrofit design.

For the building envelope, a simplified protocol already tested by Picco et al. (2013) was adopted, divided into the following steps:

- Step 1 - Simplified construction: reducing the number of constructions to only 7 archetypes reflecting the average transmittance of each type of dispersant surface considered for the whole building (no simplification provided for thermal bridges);
- Step 2 - Removal of external obstructions: Elimination of all the external shading elements modeled;

- Step 3 - Zone lumping: the apartment is reduced to a single thermal zone with constant parameters and internal gains representing mean values of the zones previously considered;
- Step 4 - Simplified transparent surfaces: Modeling only one window for each cardinal direction that considers all of the windows present in that direction;
- Step 5 - Squaring Zone: The "squaring" of the areas of the zones is meant to define a zone as an element composed of only six surfaces making up a box. In order to allow such simplification for the present case the main information to maintain as close as possible to the full model are the dispersant surfaces.

The output of this simplification protocol for the apartment analyzed is reported in Figure 4 and it is called simplification A.

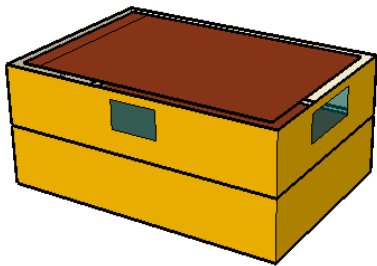


Figure 4 – Simplification protocol (A): Simplified 3D model

4.3 Heating plant simplifications

About the plant, two different macro simplifications were adopted (called B and C):

1) Heat regulation with external energy input (B): This simplification involves the replacement in the detailed model of the component related to the simulation of the building behaviour with one or more Types (depending on the number of zones simulated) constituted by external data files that gives, at each time-step, the ideal thermal useful energy demand of each zone considered.

These data files represent the new external input of the environmental control sub-system, no longer based on the internal temperature of the zones simulated, assumed equal to the set point temperature as a boundary condition for the radiators.

Data files of the ideal energy demand were obtained, as shown later, from previous simulations regarding only the building envelope.

2) Resizing in a single zone (C): the reduction of all zones simulated to a single zone is necessarily accompanied by a new sizing of the plant, in particular of the emission and distribution subsystems:

- The seven radiators considered before were replaced by a single radiator, sized according to the total power requirements of the new single zone;
- The diameter of the distribution network piping from the supply/return manifold to the radiator was increased reaching the dimensions of the piping from the storage tank to the outlet/return manifold, in order to ensure the transport of the proper hot water flux, while the piping length was assumed, both for supply and the return, equal to the outer perimeter of the zone.

5. Case studies and comparison parameters

Thanks to the stationary case, the complete dynamic simulations done for the entire building-plant system, and its simplifications (A), (B), (C), 8 different annual simulations were identified and carried out, summarized in the following table:

Table 1 – Case studies (with * is indicated the most complete and detailed simulation)

CASES		ENVELOPE		
		TERMUS	TRNSYS	
		DETAILED MODE	DETAILED MODE	DETAILED MODE - (A)
HVAC	IDEAL LOADS	1	2	3
	DETAILED MODE	4	5*	/
	DETAILED MODE - (B)	/	6	/
	DETAILED MODE - (C)	/	/	7
	DETAILED M. - (B) - (C)	/	/	8

In particular, the articulation of the simulations is the following:

- Case study 1: a complete stationary energy simulation of the building, through TERMUS software (time-step 1 month), i.e. a stationary simulation only for the building envelope, or, in other words, the determination of ideal loads through a stationary model (ideal loads means that

all the thermal efficiencies of the heating plant subsystems are set equal to one);

- Case study 2: a complete dynamic energy simulation of the building system, through TRNSYS software (time-step 1 hour), i.e. a detailed model only for the building envelope, without the integration of all the subsystems of the heating plant (determination of the ideal loads through a complete dynamic model);

- Case study 3: dynamic energy simulation of the simplified building system through TRNSYS software (time-step 1 hour), i.e. Case study 2 + building envelope simplification (A);

These first three simulations, only related to the building envelope have been considered to determine the comparison of the following three parameters:

- P_{max} (kW) = Maximum ideal thermal power required by the apartment during the heating season;

- Q_h (kWh) = annual ideal thermal energy demand of the whole apartment;

- (P_h, t) = Thermal power curves describing, in addition to the two previous parameters, the distribution of the ideal power required during the entire year of the simulation, as shown in the example in Figure 5 (pay attention that this curve cannot be obtained for Case study 1).

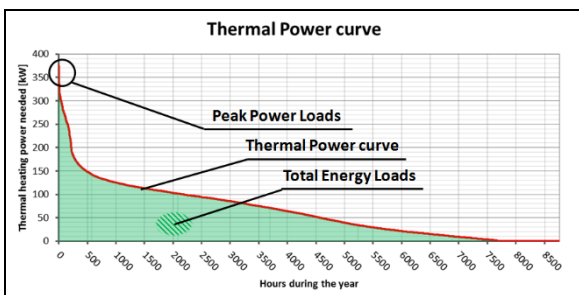


Figure 5 – Example of thermal power curve

Furthermore:

- Case study 4: stationary energy simulation of the entire building-plant system, through TERMUS software (time-step 1 month) = Case study 1 + application of standard efficiency values for all the subsystems of the heating plant;

- Case study 5: dynamic energy simulation of the entire building-plant system, through TRNSYS

software (time-step 5 min) = the most complete detailed model.

It should be noted that this is the case study taken as a reference for comparison with the results of all the other cases analyzed, constituting the highest degree of detailed simulation for both the building envelope and the heating plant.

- Case study 6: dynamic energy simulation of the entire building-plant system + Regulation with external energy input, through TRNSYS software (time-step 5 min) = Case study 5 with simplification (B);

- Case study 7: dynamic energy simulation of the entire building-plant system + building envelope simplification + Sizing for single zone, through TRNSYS software (time-step 5 min) = Case study 5 with simplification (A) and (C);

- Case study 8: dynamic energy simulation of the entire building-plant system + building envelope simplification + Sizing for single zone + Regulation with external energy input, through TRNSYS software (time-step 5 min) = Case study 5 with simplification (A), (C) and (B);

Due to the high number of available outputs, the comparison has been restricted to the output parameters and curves able to describe the annual operation:

- P_{max} (kW) = Maximum useful thermal power required during the heating season, equal to the maximum power introduced by the emission subsystem and by the recovered distribution losses (it has been assumed a recovery rate of 100% of the losses of the distribution subsystem)

- (P_h, t) (kW) = Thermal power curves of the apartment, referring in this case to the annual trend of the useful thermal power introduced in the apartment described in the previous point;

- E_{Ph} (kWh) = annual primary energy heating demand;

- η_x = annual average efficiencies of all subsystems of the heating plant and annual average overall performance of the heating plant;

For the last five simulations the annual ideal thermal energy demand Q_h is obviously equal to the one resulting from the simulations carried out only for the building envelope (cases 1,2,3, see value of Q_h reported in Table 2).

6. Final results

The results of the 8 simulations carried out in absolute values and percentage differences compared to the reference Case study 5 (highest degree of detailed simulation for both the building envelope and the heating plant), are summarized in the following tables and graphs. The workload required to perform each case has been added, in order to evaluate not only the accuracy of the results, but also a rough estimation the time required to obtain them.

Workload, estimated from repeated attempts, has been defined as the time (days) spent to carry out each simulation, considering that all the data needed to characterize the various zones are already available. For dynamic simulations, the time required for the input-output connections of TRNSYS Types has not been considered. In fact, the detailed model has a general scheme and may be applied for a very large number of residential buildings, only changing the components' input data.

Table 2 – Results – absolute values

COMPARISON RESULTS – ABSOLUTE VALUES									
Symbol	U.m.	CASE 1	CASE 2	CASE 3	CASE 4	CASE 5	CASE 6	CASE 7	CASE 8
Timestep	h	744.00	1.00	1.00	744.00	0.08	0.08	0.08	0.08
Ph_max	kW	4.67	7.17	6.25	4.67	9.75	5.04	9.30	6.51
Qh	kWh	8151.25	8243.14	7738.65	8151.25	8243.14	8243.14	7738.65	7738.65
EPh	kWh	8151.25	8243.14	7738.65	9265.67	10049.22	9403.37	9561.60	8863.54
$\eta_e \cdot \eta_{rg}$	/	1.00	1.00	1.00	0.94	0.90	1.00	0.90	0.99
η_d	/	1.00	1.00	1.00	0.96	1.01	1.00	1.00	1.01
η_s	/	1.00	1.00	1.00	1.00	0.91	0.90	0.90	0.90
η_{gn}	/	1.00	1.00	1.00	0.97	0.97	0.97	0.97	0.97
η_g	/	1.00	1.00	1.00	0.88	0.82	0.88	0.81	0.87
Workload	days	2.5	3.5	1	3	6	5.5	3.5	3

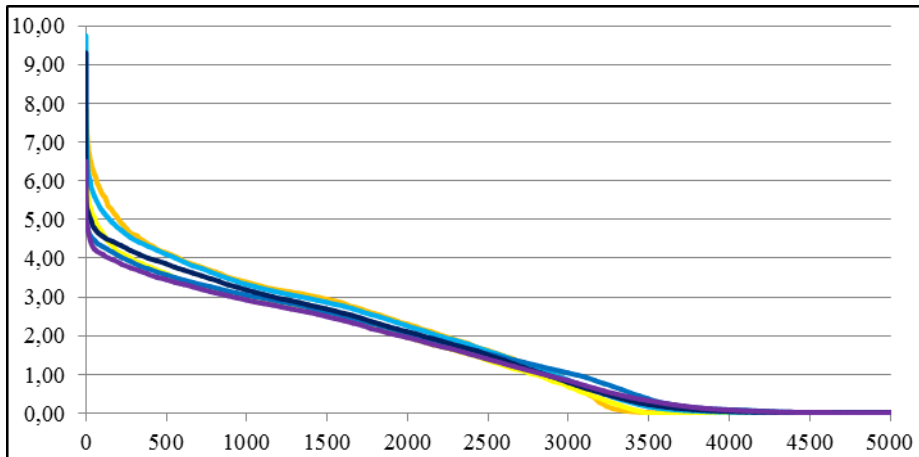


Figure 7 – Results - thermal power curves

Table 3 – Results – Percentage deviations

COMPARISON RESULTS - % DEVIATIONS COMPARED TO CASE 5									
Symbol	U.m.	CASE 1	CASE 2	CASE 3	CASE 4	CASE 5	CASE 6	CASE 7	CASE 8
Ph_max	kW	48%	74%	64%	48%	100%	52%	95%	67%
Qh	kWh	99%	100%	94%	99%	100%	100%	94%	94%
EPh	kWh	/	/	/	92%	100%	94%	95%	88%
$\eta_e \cdot \eta_{rg}$	/	/	/	/	105%	100%	111%	100%	110%
η_d	/	/	/	/	95%	100%	99%	99%	100%
η_s	/	/	/	/	110%	100%	99%	99%	98%
η_{gn}	/	/	/	/	100%	100%	100%	100%	100%
η_g	/	/	/	/	107%	100%	107%	99%	106%
Workload	days	42%	58%	17%	50%	100%	92%	58%	50%

It can be stated that:

- The value of the maximum useful thermal power Ph_{max} , introduced in the building to ensure the temperature set point, has a fairly high variation, with peak values higher for cases 5 and 7, i.e. for dynamic simulations where the feedback of the regulation subsystem is constituted by the interior temperature of the simulated zones. However, observing the thermal power curves, it is possible to note that such peak values are required for a number of hours per year absolutely negligible, while the curves indicate the presence of a peak around the mean power of 5.5 kW, however higher to that returned by the first stationary simulation, equal to 4.67 kW.
- Thermal power curves (Ph , t) have a very similar trend. In the central part of the curves, there are constant differences between cases 2-3, 5-7 and 6-8, due to the simplification (A), which underestimates the useful energy requirements of the building envelope. There are small opposite deviations in the intervals near the maximum and minimum power in particular for the cases 5-6 and 7-8, where the simplifications adopted for the plant become more important, going to affect in particular the operation of the emission and regulation subsystems (simplification B), which are stressed for low and high thermal powers;
- The value of the annual ideal thermal energy demand (Q_h) has a maximum variation of 6%. In particular, by adopting for both the detailed stationary and the dynamic simulations the same characterization of zones (notice that thermal bridges on a small building play a very important role and in both simulations are estimated with stationary algorithm), the values of Q_h for these simulations are very close. The simplification (A) determines an acceptable underestimation equal to 6%, equal to the difference of the areas under the thermal power curves of the cases 2 and 3.
- The energy efficiencies of the distribution (η_d), storage (η_s) and generation (η_g) sub-systems, for all the dynamic simulations concerning the whole building-plant system (cases 5,6,7,8), are almost constant. They assume quite different values in the stationary simulation (case 4), which does not take into account the possible recovered distribution losses and the storage subsystem.

In particular the efficiency of the distribution network piping for dynamic simulations assumes high values, due to the total recovery of distribution losses and the partial thermal recovery of the energy consumed by the distribution pump.

- Both in the stationary simulation (case 4) and in the dynamic simulations 6 and 8, in which the controller feedback is an external energy data file reporting the ideal heating requirements of the simulated zones, the emission and regulation efficiency ($\eta_e^* \eta_{rg}$) is overestimated compared to cases 5 and 7, where the feedback is more realistically represented by the internal ambient temperature.

As expected, the simplification procedure (B) has a stronger effect on regulation, bringing the plant to provide almost perfectly the ideal energy requirements of the building.

- Finally, the primary energy demand of the building E_{Ph} has a fairly limited variability, with an underestimation of up to 12% for case 8, i.e. for the dynamic simulation characterized by the highest degree of simplification. Even the stationary simulation underestimates the E_{Ph} value compared to the case 5.

- About the workload, it is possible to note how, compared to a maximum loss of accuracy of 12% of the most simplified case 8, the time required to perform a simplified dynamic simulation of the entire building-plant system is reduced to one half, and becomes equal to the time required to perform a complete stationary simulation (Case 4). However, the latter is not able to ensure benefits that only a dynamic simulation is able to guarantee, such as the full control of the integrated operation of all the heating plant components at any variation of internal and external conditions.

7. Conclusions

The present analysis shows the great potential of dynamic energy simulations during any stage of the integrated design of the entire building-plant system.

The main results are:

- Stationary and dynamic simulations may lead to close global results;

- Results for individual components and subsystems may differ because of the more accurate algorithms and assumptions used during the development of dynamic simulations
- The dynamic simulations are able to provide a number of output far greater than those given by a stationary approach and therefore allow a more precise evaluation of the instationary power loads.
- A simplified dynamic approach provides a complete energy simulation with a very high accuracy and a workload equal or even less than the time necessary to perform a complete stationary simulation.

Finally, it can be stated that rapid but still accurate and integrated dynamic simulations, like the ones shown in this paper, have the potential to be the perfect answer to the growing demand, both in terms of quality and low engineering costs, in the residential retrofit design.

Acknowledgements

The authors thank the graduating students S. Rondi and A. Beretta, for their work and input on this project.

References

- Attia, S., et al., 2009. Architect friendly: a comparison of ten different building performance simulation tools. Building simulation 2009, Eleventh International IBPSA Conference Glasgow, Scotland July 27-30, 2009.
- De Wilde, P., G. Augenbroe, M. van der Voorden, J. Brouwer, and H. Kaan 2001: 'The need for computational support in energy efficient projects in the Netherlands'.
- Gratia, E., De Herde, A. 2002. A simple design tool for the thermal study of an office building. *Energy and Buildings*, 34: p. 279-289.
- Hayter, S.J., Torcellini, P.A., Hayter, R.B., Judkoff, R. 2001. The Energy Design Process for Designing and Constructing High-Performance Buildings. *Clima 2000/Napoli 2001 World Congress - Napoli (I)*, 15-18 September 2001.
- Hensen, J. 2004. Towards more effective use of building performance simulation in design. 7th International Conference on Design & Decision Support Systems in Architecture and Urban Planning, Eindhoven, 2-5 July 2004.
- Picco, M., Lollini, R., Marengo, M., 2014. Towards energy performance evaluation in early stage building design: A simplification methodology for commercial building models. *Energy and Buildings*, Volume 76, June 2014, Pages 497-505.
- Punjabi, S., Miranda, V. 2005. Development of an integrated building design information interface. in IBPSA. *Building Simulation 2005*, Ninth International IBPSA Conference, Montréal, Canada, August 15-18, 2005.
- Torcellini, P.A., Hayter, S.J., Judkoff, R. 1999. Low-Energy Building Design - The Process and a Case Study. *ASHRAE Transactions*, V 105, Part 2, pp. 802-810. Atlanta, GA: American Society of Heating Refrigerating and Air-Conditioning Engineers.
- Urban, B., Glicksman, L. 2006. The MIT Design Advisor - A fast, simple tool for energy efficient building design. *Simbuild 2006 Second National IBPSA-USA Conference* Cambridge, MA August 2-4, 2006.

Thermal modelling of complex fenestration systems – Comparison of a BSDF-based model with simplified approaches

Hauer Martin – University of Innsbruck – martin.hauer@uibk.ac.at

Geisler-Moroder David – Bartenbach GmbH – david.geisler-moroder@bartenbach.com

Hiller Marion – Transsolar Stuttgart – hiller@transsolar.com

Abstract

In this paper the theoretical concept of modelling complex fenestration systems is shown firstly by the development of two simplified modelling approaches and secondly by a newly developed model in TRNSYS17 based on BSDF-data and the ISO15099 standard.

Final results of a comparison between the more detailed BSDF model and the simplified models based on the bi-directional SHGC will be worked out and described. By simulating two different blind systems incorporated in the façade of a standard office room (Fig. 1), the capabilities and restrictions of the simplified approaches in modelling conventional, diffuse shading blinds and daylight deflecting, specular blinds are shown.

Depending on the external boundary conditions and pre-defined settings to be done for the simplified model approaches by parameter studies, the results show satisfying correlations between all models for static and dynamic boundary conditions.

1. Introduction

The use of complex fenestration systems (CFS) offers a high potential in energy savings compared to the state of the art shading systems mainly installed in the commercial building stock. Especially for office buildings, light-redirecting systems allow an improvement of both, visual and thermal comfort (Fig. 1). Former research work showed a significant potential in reduction of artificial lighting due to higher workplace luminance by daylighting (Hauer et al. 2011). Furthermore a reduced solar gain in summer season through transparent facades and energy efficient shading control leads in a significant reduction of the cooling energy demand.

To account for these requirements in the building design, a detailed numerical method for a coupled thermal and lighting simulation of complex façade with integrated daylight deflecting (specular) systems in TRNSYS and RADIANCE is worked out on the national research project lightSIMheat, funded by the Austrian Research Agency (FFG).

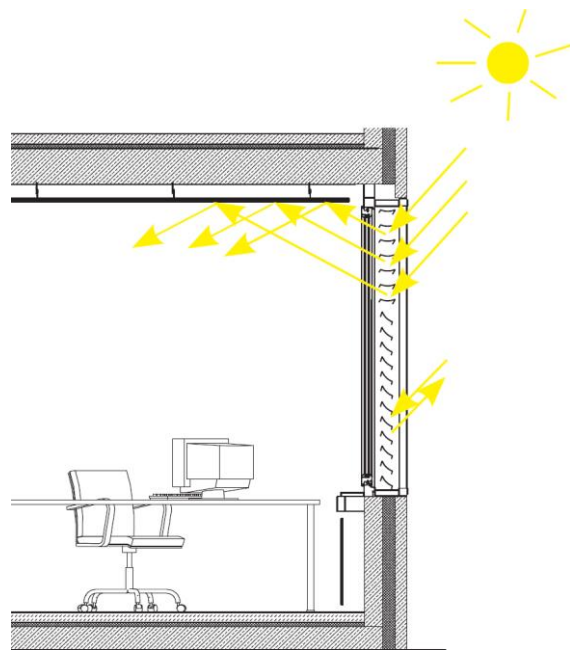


Fig. 1 – Light redirecting facade system

For the thermal evaluation of such a complex façade, simplified approaches based on a two-dimensional solar heat gain coefficient are worked out.

Originally intended as a first possibility to implement complex glazing systems in TRNSYS, ongoing developments in the field of thermal modelling of CFS are based on the use of bi-directional-scattering distribution functions (BSDFs).

Although simulation models for CFS based on BSDF-data enables high accuracy in modeling purposes, an extensive amount of input data as well as a high level in specific user expertise for the time-consuming data pre-processing is necessary. Besides them, detailed product specification of every single component of the system (glazing, blind...) is necessary for the overall setup.

In contrast to the BSDF-model, the idea behind the simplified approaches is to use the angular dependent g-value instead of the comprehensive BSDF dataset to characterize the thermal properties of the CFS.

In this paper, a comparison of these simplified modeling approaches with the more detailed BSDF-model is presented. Besides a conventional façade system with an outside raffstore, further investigations are made for a specular (daylight deflecting) blind system. Optical BSDF data are generated by external ray-tracing and used in WINDOW7 to set up an overall system including the glazing.

2. Modelling of CFS

Compared to conventional glazing systems, CFS including a shading layer (venetian blinds, screens or woven shades) shows a bidirectional scattering of the radiation striking the shading layer.

Due to the high flexibility of the system, the setup of CFS and the interconnection of the occurring physical phenomena, (e.g. radiative heat exchange, natural or forcing convection, conduction) and the modelling of optical and thermal properties of such a system is very complex. Furthermore, blind surface properties (diffuse reflective or specular reflection) as well as their geometry (planar, curved, or multi-curved) extend the variations in modelling purposes.

In former releases of TRNSYS Type56 (Multizone-building model) the amount of shaded solar fraction was treated as blocked sun radiation by a flexible shading factor (Fc-factor). Internal radiation exchanges between glazing and blinds and between blinds themselves were possible to

model by fixed values to describe the radiative interaction approximately.

As these processes are dynamically and strongly affected by the real system setting, the calculation procedure was extended to calculate the absorbed solar radiation in the different layers describing the energy demand and comfort situation in the room behind in more detail. By developing simplified approaches, first investigations were undertaken in an improved modelling of glazing systems incorporating venetian blinds. At the same time decreasing the high efforts of modelling and detailed product data for simulation input, major simplifications were realized.

2.1 Simplified approaches

For glazing systems without shading devices a solar heat gain coefficient (SHGC) one-dimensional dependent from the incident beam radiation is sufficient for exact calculations (standard window model in TRNSYS). However, for an accurate modelling of complex glazing system including blinds, the SHGC has to be defined in a bi-directional dependency of the incoming solar radiation by the azimuth- θ and zenith angle γ .

By this fact and based on the standard window model in TRNSYS, two methods were implemented to improve the thermal modelling of complex fenestration systems:

- g- model
- Abs- model

Both methods calculate out of pre-calculated datasets with values for transmission, absorption and SHGC, depending on the solar azimuth and zenith angle separately, for beam and diffuse radiation the solar energy passing the CFS. The calculations for the diffuse radiation part is additionally divided into sky- and ground diffuse radiation. Different slat angles as well as changes of the blind position during the simulation can be taken into consideration.

The calculation of the passing energy is executed "externally" from the building model and further linked as input into the multizone-building model (Type 56) in TRNSYS. The calculations are done for each time step and split up into both the physical

parts of the SHGC - transmission and secondary heat flux (Fig. 2).

The former is treated as fully radiative internal gain and is directly connected to the zone air node. The second is treated as wall gain representing the thermal radiation part of the passing energy and is in exchange by longwave radiation and convection with the zone air node. For a correct representation of the thermal losses/wins (u-value) within the zone model, the internal window model in Type56 has to be defined corresponding to the system glazing, but in a fully shaded situation ($F_c = 1$).

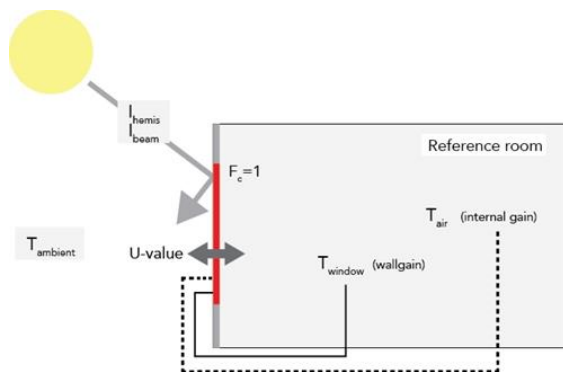


Fig. 2 – Integration of the simplified approach via internal gain and wall gain in the multizone-building (Type56)

In the *g-model* the solar radiation through the transparent façade area is calculated – like the naming - by the pre-calculated overall SHGC (or *g-value*). The separation into transmission and secondary heat flux (internal gain / wall gain) is done by a constant ratio between transmission and secondary heat flux over the yearly trend. The factor has to be defined for each system separately in advance and varies slightly with glazing type and tilt angle of the blind.

The *Abs-model* allows the implementation of absorption- (angle dependent) and emission coefficients for glass panes and blinds (fixed). This enables a more accurate modelling of the longwave radiation exchange in between the layers. Both models do not include detailed effects of IR-transparency, longwave radiation in slat cavities by view-factors and detailed convective behaviour between and around the blind layer.

2.2 BSDF-model

For a detailed modelling of CFS within dynamic thermal simulation tools, the latest research models based on bi-directional scattering distribution functions (BSDF) are available (Hiller und Schöttl 2014).

The modelling method is separated into shortwave radiation modelling by the pre-calculated BSDF data and the longwave radiation modelling according to algorithms defined in the ISO15099 standard as the current most comprehensive modelling standard for blind systems (Norm ISO 15099:2003).

Based on the established concept of a layer-by-layer calculation for glazing systems, the ISO15099 standard is an enhancement of this method to be also adaptable for CFS (Fig. 3). It specifies detailed calculation procedures determining the optical and thermal properties of shading layer by a discretized blind model as well as the convective behavior by a comprehensive pressure drop model.

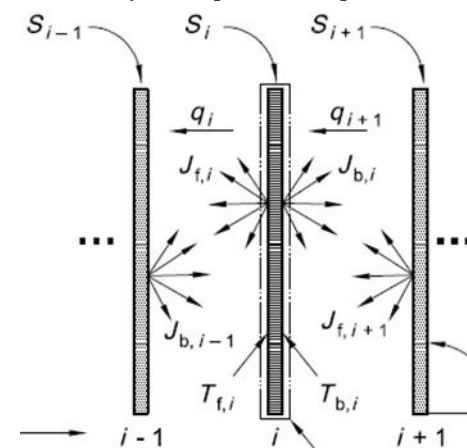


Fig. 3 – Layer-by-layer modelling according to ISO15099

Both transmitted solar radiation depending on geometry and optical surface properties as well as the thermal driven radiosity balance depending on solar-thermal properties are calculated in detail by the view-factor method and determine the overall energy transmittance of the CFS. Therefore as a main contrast to the simplified *g-model*, the BSDF model calculated the SHGC instead of using it as a pre-calculated input, while the *Abs-model* is positioned in between both concerning modelling accuracy. The BSDF model in TRNSYS implies the detailed thermal model according to Fig. 3. The

calculation of the optical properties is fully adapted by the integration of external BSDF data. This method was introduced by (Klems 1994) and describes a flexible method to calculate the bi-directional solar transmission of a CFS by simple matrix multiplications. In discretizing the hemisphere at the front and the back side of the CFS-layer into 145 areas (Klems-patches), a detailed specification of the optical properties of each layer depending on azimuth and zenith angle is possible. The resulting data matrix contains in its standard resolution 145 outgoing values in overall transmission and reflection of the CFS for each of the 145 incoming values on the CFS. This dataset is defined as BSDF and covers the optical blind modelling for the full hemisphere at the front and back of the complex glazing (Fig. 4).

$$\tau = \frac{I_{out}(\theta_{out}, \gamma_{out})}{I_{in}(\theta_{in}, \gamma_{in})} \quad (1)$$

Furthermore, the new implemented BSDF model in TRNSYS has a modular structure, which allows, in combination with the well-established software tool WINDOW7 from LBNL, a flexible implementation of different glazing systems including blinds. For all different slat angle positions needed in the simulation, a separate BSDF dataset has to be pre-generated. Also changing system properties (blind geometry, optical surface properties...) used in one simulation needs to be provided by separate BSDF datasets.

In previous research work, static validations of the new BSDF model with WINDOW7 as well as quasi-dynamic validations with the implemented BSDF model of EnergyPlus8.0 by comparative simulations under varying system parameters were presented.

The new BSDF model shows excellent accordance with WINDOW7 results under static conditions. The model comparison with EnergyPlus8.0 shows slight deviations, which mainly result from general modelling differences between TRNSYS and EnergyPlus as well as existing limits in EnergyPlus for setting steady boundary conditions.

Detailed analyses and results of the undergone

model validations are described in published work by (Hiller und Schöttl 2014) and (Hauer et al. 2014).

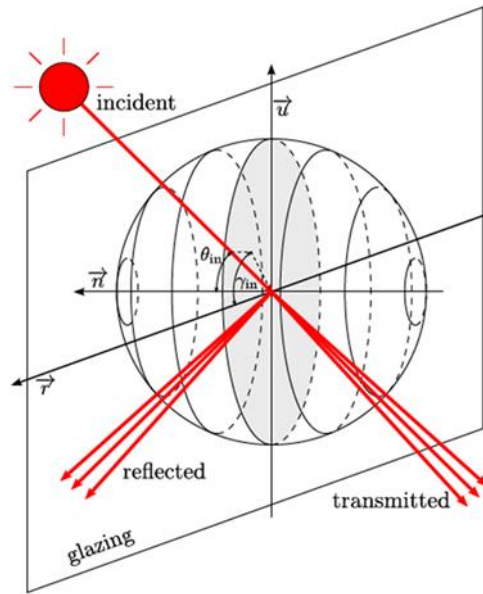


Fig. 4 – Optical modelling with BSDF data

3. Simulation setup and variants

3.1 Reference room

For the comparison of the simplified approaches against the detailed BSDF model, two blind systems are investigated. For the simulations of an exemplary office, a reference room with standard interior design and geometrical dimensions according to Fig. 5 is defined.

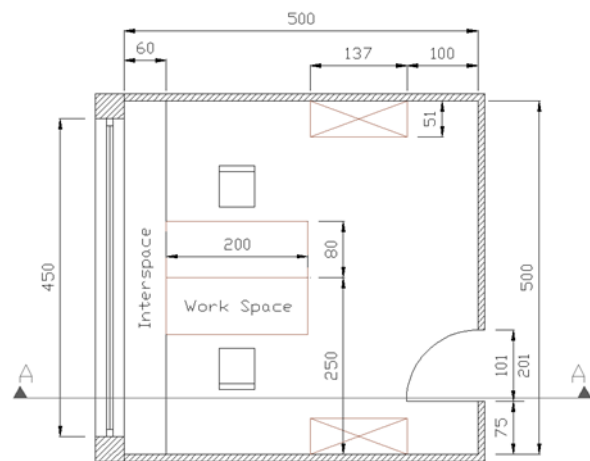


Fig. 5 – Dimensions of the double-office reference room

All walls are modelled as boundary walls except the external south façade including the window.

The façade consists of a parapet for technical equipment and a large window area, which offers all opportunities for an advanced daylighting system.

Table 5 – Boundary definition for the reference room

Definitions – Reference room	
Climate	Graz, Austria
U-value wall	0,15 W/m ² K
U-value window	0,8 W/m ² K
Window surface	9m ² (w: 4,5m / h: 2m)

Profiles for internal gains, operating hours, heating/cooling and air change rate are defined according to SIA 2024 standard.

3.2 Systems

The comparative simulations are undertaken for a conventional (diffuse) outside raffstore (Fig. 6) and an in-between specular (re-directing) blind system “Alar Lamella” (Fig. 7).

WINDOW7 as a well-established software tool, developed and regularly updated by the LBNL, and is used for the input data pre-processing for the BSDF model according to the layer specifications in Table 6 and Table 7. The product data for the glazing and the gas layers are imported from the included database (IGDB). The shading layers are BSDF datasets, generated with the RADIANCE program genBSDF (Geisler-Moroder 2011).

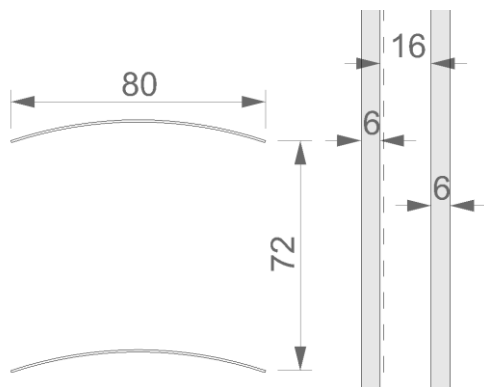


Fig. 6 – Geometrical definition [mm] - external raffstore „RAF“

Table 6: layer definition - external raffstore

ID	external raffstore (Raf)	[mm]
	BSDF (Raffstore – 45deg)	56.5
1	Gas 1 (Air)	43.5
7111	Glazing 1 (ip_ip16E.ipe)	6.0
2	Gas 2 (Argon, 100%)	16.0
7199	Glazing 2 (ip_fl_6.ipe)	6.0

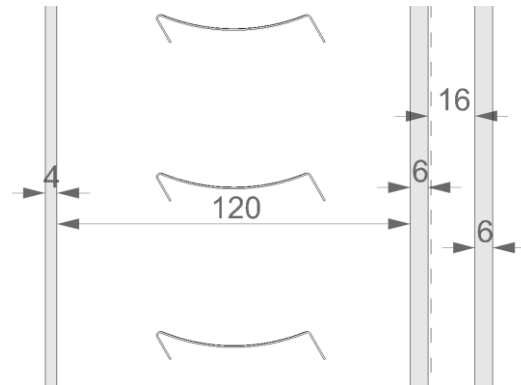


Fig. 7 – Geometrical definition [mm] spec. in-between blind „Alar“

Table 7: layer definition - specular in-between blind

ID	Alar Lamella (Alar)	[mm]
7197	Glazing 1 (if_fl_4.ipe)	4.0
1	Gas 1 (Air)	33.5
	BSDF (Alar_SUN – 45deg)	53.0
2	Gas 2 (Air, 100%)	33.5
7111	Glazing 2 (ip_ip16E.ipe)	6.0
	Gas 3 (Argon 100%)	16.0
7199	Glazing 2 (ip_fl_6.ipe)	6.0

The input data for the simplified approaches are provided as pre-calculated datasets separately for the beam- and diffuse components of:

- Solar transmission (overall system)
- Bi-directional SHGC (overall system)
- Absorption coefficients (for each layer)

The matrix for the beam components implies values in 5°-intervals for the azimuth range (0-360°) and the zenith range (0-90°) of the whole hemisphere, which ends up in a 73x19 matrix for each component and slat angle. The data set for the diffuse components consists of three separate values for the sky, hemisphere and ground part for each slat position.

The main difference between the BSDF model and the simplified approaches is therefore defined in

the different dataset structure and the method of different modelling as mentioned in 2.1.

3.3 Simulation variants and boundaries

3.4 Static simulation

In a first step, stationary calculations are realized by simulating the reference room (3.1) as full adiabatic with a sun-exposed window including the blind system with a slat angle of 45°. Internal gains are neglected for the static case and quasi-static case.

Table 8 – Conditions for static simulation

Boundaries – static simulation	
T _{amb} /T _{sky} /T _{grd}	20°C
I _{sol}	783 W/m ²
AI	Var.1: 0° / Var.2: 45°
Heating/ Cooling	20°C

Due to this fixed simulation conditions the resulting SHGC can be calculated by the cooling load and the incident radiation on the window:

$$SHGC = \frac{Q_{Cool}}{I_{window} * Area} \quad (1)$$

3.5 Quasi-static simulation

For the quasi-static calculations, the reference room is again modelled fully adiabatic with constant outside boundary temperatures according Table 8. The incident radiation and sun angle are dynamic and read in from the climate data (Location: Graz). The simulation was now undertaken for both systems with all models in a yearly term. The modelling accuracy is shown by the resulting cooling load for three different slat positions. Furthermore resulting room temperatures as well as glazing temperatures are analyzed as graphs based on hourly values. A week in February (01. – 07.) representing winter conditions and a period in July (01. – 07.) representing summer conditions were used as examples.

3.6 Dynamic simulation

In a final stage the simplified approaches were compared with the BSDF model under fully dynamic conditions in the simulation. The simulations are done for both systems again over a year including all definitions concerning reference room and the internal loads from 3.1.

4. Results

4.1 Static results

The results for both systems and both incident radiation scenarios are shown in Table 9 / Table 10. The results are presented as absolute values for each model and the relative deviation in relation to the BSDF model results, as this is assumed to be the most accurate one.

In general, the results for the external raffstore have a better accordance with the BSDF model for the perpendicular radiation. For the tilted radiation the absolute values decreases, which leads to higher relative deviations although the absolute values are still in the range.

Table 9 – Stationary results of SHGC for the external raffstore

SHGC (I _{sol} = 783W/m ² , γ _s = 90°, θ _s = 0°, AI = 0°)				
Slat angle		0°	45°	75°
BSDF		0.482	0.168	0.021
G	abs. value	0.421	0.121	0.013
	rel. dev.	13%	28%	41%
ABS	abs. value	0.429	0.124	0.014
	rel. dev.	11%	26%	36%
SHGC (I _{sol} = 783W/m ² , γ _s = 45°, θ _s = 0°, AI = 45°)				
BSDF		0.161	0.043	0.015
G	abs. value	0.085	0.021	0.008
	rel. dev.	47%	51%	47%
ABS	abs. value	0.088	0.023	0.009
	rel. dev.	45%	48%	41%

Table 10 – Stationary results of SHGC for the Alar Lamella

SHGC ($I_{sol} = 783W/m^2$, $\gamma_s = 90^\circ$, $\theta_s = 0^\circ$, $AI = 0^\circ$)				
Slat angle		0°	45°	60°
BSDF		0.477	0.431	0.179
G	abs. value	0.336	0.301	0.129
	rel. dev.	29%	30%	28%
ABS	abs. value	0.340	0.318	0.135
	rel. dev.	29%	26%	24%
SHGC ($I_{sol} = 783W/m^2$, $\gamma_s = 45^\circ$, $\theta_s = 0^\circ$, $AI = 45^\circ$)				
BSDF		0.441	0.062	0.051
G	abs. value	0.330	0.051	0.046
	rel. dev.	25%	17%	9%
ABS	abs. value	0.353	0.051	0.047
	rel. dev.	20%	17%	8%

4.2 Quasi-static results

The quasi-static results show a very good agreement for the external raffstore. In the case of the specular Alar Lamella, the difference between the BSDF model and the simplified approaches increases with lower slat angles (Table 11). This can be caused by a lack in detail modelling for the simplified models as mentioned in 2.1.

Table 11 – quasi-static results for the cooling load of both systems

Slat angle	0°	45°	75°
Raffstore	[kWh/m ²]	[kWh/m ²]	[kWh/m ²]
BSDF	29.99	10.45	3.00
G	27.57	9.34	3.25
ABS	28.01	9.44	2.67
Alar	[kWh/m ²]	[kWh/m ²]	[kWh/m ²]
BSDF	35.97	20.85	12.07
G	24.47	17.68	8.59
ABS	26.66	17.94	8.73

The following graphs show the hourly trend for the resulting room temperature (TAIR) in Fig. 8 and inner glazing temperature (TIGL) in Fig. 9.

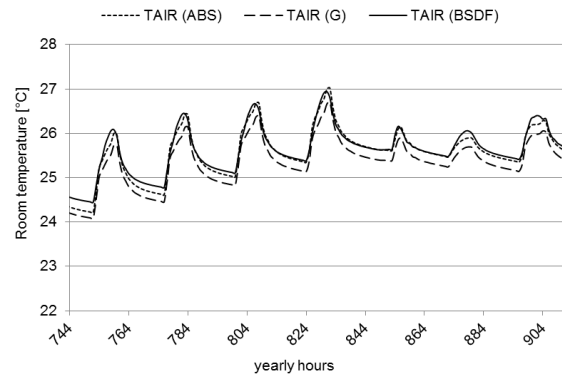


Fig. 8 – Room temperature (Raffstore) - winter condition

The room temperature shows a very good agreement of the Abs-model with the BSDF model in the winter period. In the summer period there is an almost perfect correlation between all approaches for this certain period.

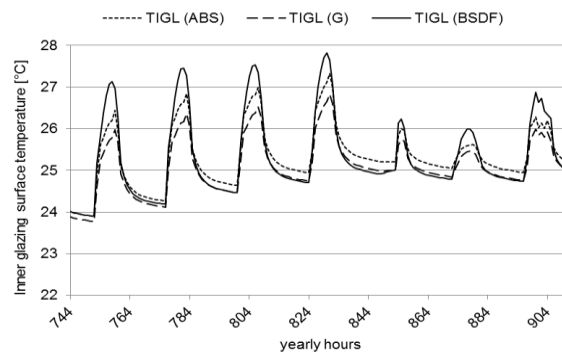


Fig. 9 – Inner glazing temperature (Raffstore) - winter condition

As in case of the simplified methods, the wall gain (secondary heat flux) is calculated externally and not directly within the window model like in the BSDF-model, the results show a high sensibility on linking the wall gain whether inside or outside the glazing. In the case of the external raffstore, the highest result correlations with the BSDF model are reached by linking the wall gain on the outer pane. In the case of the Alar Lamella, which is positioned in-between the glazing, the wall gain is partly linked on the inner and outer pane surface to get best result correlation.

4.3 Dynamic results

In Table 12 the dynamic results for the yearly heating and cooling load for the reference room with both systems and all three models are listed.

For all situations the simplified models show a good correlation – in direct comparison to the BSDF-model the results are slightly higher for both systems.

Table 12: Results for dynamic simulation

Raffstore	Q_{HEAT} [kWh/m ² a]	Q_{COOL} [kWh/m ² a]
BSDF	12.07	4.45
G	16.41	7.02
ABS	17.32	6.11
Alar Lamella		
BSDF	8.87	6.51
G	11.18	10.90
ABS	10.11	13.09

5. Conclusion

In this paper comparative simulations between the complex BSDF-model and two simplified approaches based on a bi-directional SHGC are presented.

The simplified approaches and the BSDF method are based on the same modelling concept by separating beam and diffuse radiation as well for the individual optical and thermal modelling. Nevertheless, a clearly reduced effort in detailed modelling, especially of the blind layer compared to the complex model in the ISO15099, can be seen. Shortcomings in detailed physical modeling are compensated by empirical validation and individual correction factors depending on the modelled system. Further investigations into these aspects by validations with measured data will be done.

As a conclusion, the simplified methods show, compared to the comprehensive BSDF data, an efficient and flexible modeling of CFS with less complex input data necessary. At the same time, the simplifications and assumptions undertaken fit specific systems settings. This fact leads to necessary pre-studies in order to fit the model to the individual system, which is rather more work compared to the flexible BSDF concept.

6. Nomenclature

SHGC	Solar heat gain coefficient (-)
Q_{Cool}	Cooling load (kWh)
I_{Window}	Radiation on Window (m)
Area	Window area (m ²)
I_{sol}	Solar radiation (W/m ² K)
γ_s	Solar zenith angle (deg.)
θ_s	Solar azimuth angle (deg.)
AI	Angle of Incidence

References

- Norm ISO 15099:2003: Thermal performance of windows, doors and shading devices - Detailed calculations.
- Geisler-Moroder, David (2011): Integrated thermal and light simulations for complex daylight systems using TRNSYS and RADIANCE. In: *10th Intl. RADIANCE Workshop*.
- Hauer, Martin; Hiller, Marion; Kofler, Christian; Streicher, Wolfgang (2014): Comparative thermal simulation of conventional and daylight deflecting systems with BSDF-based models in TRNSYS and EnergyPlus. In: *EuroSun Conferene Proceedings*.
- Hauer, Martin; Neyer, Daniel; Geisler-Moroder, David; Knoflach, Christian; Streicher, Wolfgang; Pohl, Wilfried (2011): Combined thermal and light simulation method for daylight utilization. In: *ISES Solar World Congress*.
- Hiller, Marion; Schöttl, Peter (2014): Modellierung komplexer Verglasungssysteme in TRNSYS. In: *BauSIM Conference*.
- Klems, J. H. (1994): A new method for predicting the solar heat gain of complex fenestration systems. I. Overview and Derivation of the matrix layer calculation. In: *ASHRAE Transactions* (100).

A new climate-based daylight metric for hot climates

Islam Ayman Mashaly – Research Assistant, Department of Construction and Architectural Engineering, American University in Cairo – islam.akm@hotmail.com

Yussra Mohamed Rashed – Research Assistant, Department of Construction and Architectural Engineering, American University in Cairo – yussra.mer@hotmail.com

Muhammad Adel – Researcher, Housing Building National Research Center (HBNRC) – muhmd.adel@yahoo.ca

Khaled Nassar – Associate Professor, Department of Construction and Architectural Engineering, American University in Cairo – knassar@aucegypt.edu

Abstract

Daylight performance metrics are moving away from the traditional daylight factor and average illuminance to more climatic-based metrics such as Daylight Autonomy (DA) and Useful Daylight Index (UDI). These metrics offer a better measure of the daylight performance throughout the year and incorporate the varying weather conditions and as such are dubbed climatic-based metrics. However, in hot climates where the ratio of direct to diffuse is highest, achieving these metrics may result in over-heating the spaces. Achieving acceptable climatic-based metrics for the space may result in unacceptable heat gains. The Daylight Autonomy and the Useful Daylight Index do not account for the total amount of lux-hours achieved throughout the year. The solution thus far has been to run coupled-energy and daylight simulations in order to assess the effect of achieving certain climatic-based metrics on the heat gain and thermal performance of the space. In this paper a new metric is proposed that takes into account the total amount of lux-hours achieved throughout the year and the irradiation for different time steps into a single measure. Details about the measure and sample test cases are presented.

1. Introduction

In order to assess the daylighting performance of a particular design climatic (often called dynamic), daylighting measures are used. These measures relate to the degree to which a particular level of required illumination is achieved throughout the year. Since there is a direct relationship between the total number of lux-hours and thermal heat

gains, it may be of importance to develop a metric that rewards achieving the required illuminance levels throughout the year while minimizing the total amount of lux-hours that are achieved in times of the year where cooling may be required for example. This means that the weather conditions at the times in which the designer daylight metrics were computed need to be taken into consideration. An accurate indication of the weather conditions at different times is cooling and heating degree days. It is therefore desirable to increase the number of lux-hours when the heating degree days are highest and minimize the lux-hours values during hot times when the cooling degree days are highest, simultaneously while increasing metrics such as the DA and the UDI.

Our aim here is to develop a new measure that takes into account the thermal aspects associated with daylighting. Daylighting and solar thermal gains are often positively correlated. In particular, if a specific design achieves acceptable scores for the climatic-based daylighting measures, then it may be often the case that this can be on the account of exceedingly high thermal gains. A number of previous studies have considered the interrelation between daylight performance and thermal performance such as R. Sullivan et al. (1992) and C.A. Johnson et al. (1999) and more recently Ochoa et al. (2012), Tsikaloudak, et al. (2012), Aldawoud (2013), Lee and Tavit (2007) Inoue et al. (2008), Athienitis and Tzempelikos (2002).

Without any particular design treatments, as more daylight is achieved the thermal loads would

increase. To examine this, a chart was created to assume the relation between daylight and thermal load, as shown in figure 1. In figure 1, the theoretical values for the irradiation and the number of lux-hours achieved throughout a year for a standard room is plotted. By increasing the window size, the lux-hours increase as well as the amount of direct and diffuse solar gains of the space. The amount of lux-hour increase is one measure of daylighting performance but as several researchers have noted before is not a very valid or accurate one. Hence the need for the climatic-based or dynamic based measures. It is expected that there is a direct relationship between the thermal gain and the daylighting performance for a particular design. The thermal gains could be measured in many terms, one of the most direct measures is, for instance, the cumulative hourly direct irradiation, but on the other hand we may make use of the several climatic-based measures. The relationship may assume a linear or exponential form and with a typical range of values depending on the actual design parameters, i.e. there may be some designs that allow for the same daylight performance but with a varied degree of thermal gains. This happens in cases where complex fenestrations systems for example can be used or when specific shading devices or glazing treatments are utilized. In the absence of complex window designs or treatments, it is expected that this range is minimal.

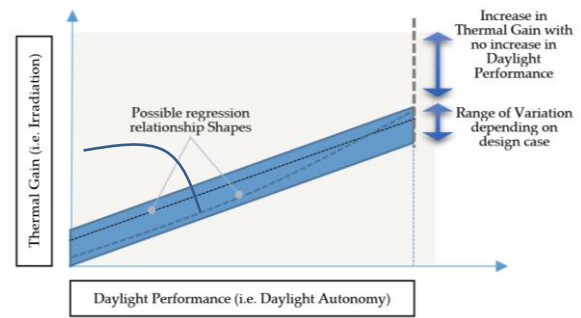


Fig. 1 – An assumed relationship between daylight performance and thermal performance

This trend continues until the maximum value for the daylight measure can be achieved after which no possible improvements in the daylight performance can be achieved. The remaining design cases after this point all increase the amount of thermal gains with no or even worsening values for the daylight performance measures. Some climatic-based or dynamic based measures may result in worse values after a certain point and others may reach their maximum value and hold. Those measures that penalize for over lighting for example would start to drop while others that do not will hold at maximum values. This specific trend is explored in this paper and will be described in the next sections. The remainder of this paper is organized as follows; we first start with a description of the experimental set up and then go to discuss the simulation parameters and methodology. This is followed by a presentation of our proposed measure and a review of the simulation results. Finally conclusions and recommendations for future research are presented.

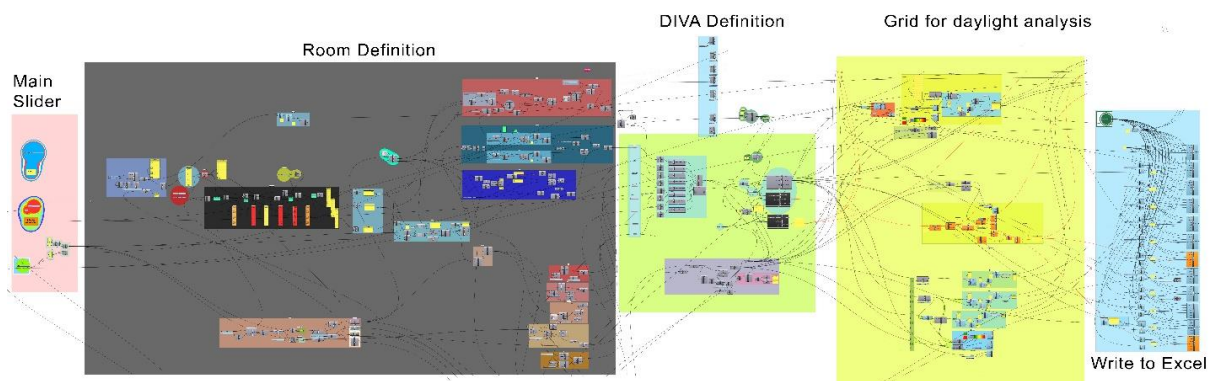


Fig. 2 – The developed Grasshopper definition

2. Considered layout and configurations

In order to be able to study the interrelation between daylighting performance and thermal performance and explore the theoretical relationship proposed above, a parametric model using Grasshopper for Rhino was developed. The model is shown in figure 2 and is divided into five main parts. The first portion of the definition is used to control the various parameters used in the simulation. The second part of the model is used to modify the window to wall ratio of the typical room used. The standard room used is based on the one developed in Wagdy (2013). In this part of the model the window to wall ratio is varied in a

systematic method as described in Wagdy (2013), so that the various design parameters are varied systematically to increase the increments of the window to wall ratio. Firstly, the height is changed to the maximum value, then the width and finally the sill height are increased at certain increments to maintain unit step increases in the WWR. This is shown in more detail in figure 3. The developed grasshopper model then makes use of the Diva interface to send the simulation to RADIANCE for a full analysis and results generation, which makes up the third part of the grasshopper definition. In the fourth part the grid and sensor values are calculated and finally in the last part the results are exported to excel.

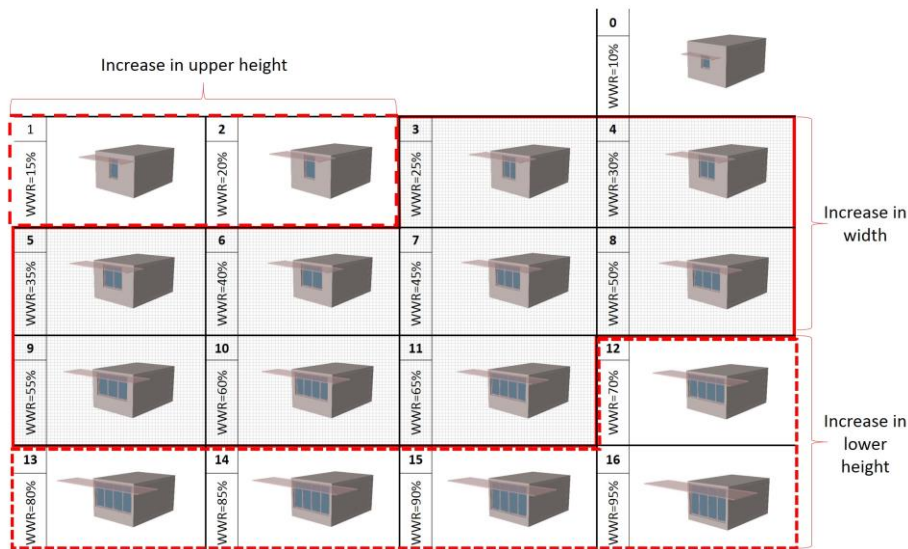


Fig. 3 – Variation of the Window to Wall Ratio in our model

It is important to note that a shading device is used so that a constant shading angle is kept constant throughout our simulations as shown in figure 4. The two extreme cases of south and east facades are considered here, since they would tend to more clearly demonstrate the relationship between daylight and thermal performance.

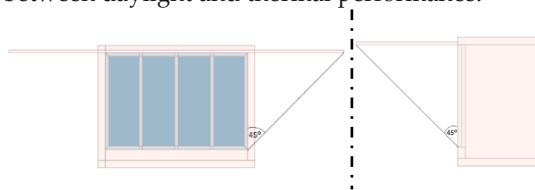


Fig. 4 – Shading Geometry, this shading angle is constant for all cases

Simulations are carried out and in total 17 cases are considered as can be seen in figure 3. For each case, the solar irradiation is calculated at each of the room's sensor points. In addition, for each case considered, the Daylight Autonomy (DA) was calculated. Daylight Autonomy (DA) is one of a number of daylight metrics that consider the annual performance of a particular design. DA basically represented as a percentage of annual daytime hours that a given point in a space is above a specified illumination level (Reinhart and Walkenhorst, 2001). The measure was originally proposed by the Association Suisse des Electriciens in 1989 and was later developed by

Christoph Reinhart between 2001 and 2004 (Reinhart et al, 2006). Daylight Autonomy considers the specific geographic location for a particular space and hence uses the actual weather information on an annual basis. In addition, since it represents the times that artificial lighting may not be needed, it is strongly related to electric lighting energy savings if the user defined a specific threshold that would be based upon electric lighting criteria. The designer is usually free to set a specific limit above which Daylight Autonomy is calculated. In our simulations we used a typical value for Daylight Autonomy

threshold of 300 lux (DA300). The Daylight Autonomy percentage calculation represents how much of the floor area achieved 50% or more daylight autonomy in DIVA analysis.

$$\text{Room sDA \%} = \frac{(\text{No. of nodes})_{\text{sDA} \geq 300}}{\text{Total No. of Nodes}} \quad (1)$$

Table 1 shows the different parameters used in running the simulation. The RADIANCE parameters are shown in terms of the number of ambient bounces and ambient divisions as well as other parameters. In addition, the different parameters used for the typical space are shown.

Table 1 – The room and simulation parameters used for all simulation cases

Room Dimensions	Length=6m, Width=4m, Height=3m	
Simulation Parameters	ab (ambient bounces)	6
	ad (ambient divisions)	1000
	as (ambient supersamples)	20
	ar (ambient resolution)	300
	aa (ambient accuracy)	0.1
	Assigned Materials	Walls
	Floor	Generic Floor [Reflectance=20%]
	Ceiling	Generic Ceiling [Reflectance=80%]
	Window Frame	Metal Diffuse
	Window Glazing	Double Pane, Clear [Transmittance=80%]
	Shading	Outside Façade [Reflectance=35%]
	Ground	Outside Ground [Reflectance=20%]

3. Results and discussion

Coupled thermal and daylight simulations were first carried out for the 17 cases of different WWR to increase the solar irradiation and the lux-hours coming into the room. Figures 5 and 6 shows the annual cumulative irradiation at each sensor point for all the 17 cases versus the average Daylight Autonomy values at those same sensor points. This is shown for the south and east facades separately. The graphical percent values represent the percentage of the floor area that exceeds 300 lux for at least 50% of the time. The results follow the assumed shape discussed in figure 1. Note that there may be different sensor points, where higher irradiation values are realized, while achieving the same DA performance. This is due to the fact that points on the inside of the space in one of the cases for example may have the same daylight

performance as another sensor point further out in another case. It is also interesting to note that the variation in the east is more profound, i.e. that for the east façade points such as the ones we noted in different cases will result in wider variations in thermal irradiation with the same values for DA performance. This means that the gap in the assumed figure 1 is wider for the east façade compared to the south one. This is expected since the east façade will have a varying amount of direct radiation due to the movement of the sun compared to the southern façade that may have more uniform solar radiation falling on it.

In order to study the results further, figures 7 and 8 show the solar irradiation versus the DA for the south and east facing orientation for the 17 test cases. The results shown in these figures are basically the aggregated values of each of the sensor points for each case. The average

cumulative annual irradiation for all the sensor points for each case is presented with the average DA performance for the sensor points in each case. As such there are 17 data points in each graph, one for the south facing façade and another for the east facing façades. Again the same trend expected as in figure 1 above holds for the aggregated values of the test cases. In fact, one may be able to add a clear regression line between the solar irradiation as the dependant variable and the DA as the independent variable for both the south and each facades. For the east façade the linear regression equation is:

$$y = 0.3247x + 5.1363 \quad (2)$$

where x is the DA and y is the expected average cumulative annual irradiation for all the sensor points. We are therefore able to predict what the maximum value for the average cumulative annual irradiation would be from this equation. In this case for example, if we plug in a value of one for x to try to find the maximum value for the average cumulative annual irradiation, we would obtain about 38 kWh for every meter squared. Although this is evident from the chart in our case, it may not be for other cases where it is more expensive to conduct a full simulation analysis for every possible design case. In our simple example, we were able to do so because our only varying parameter was the

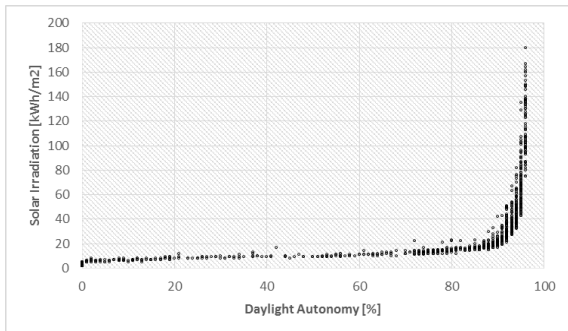


Fig. 5 – The solar irradiation versus the DA for the south facing orientation at different sensor points for all 17 cases

window to wall ratio. However, in more complex examples that may not be the case and therefore one will be able to simulate only a small subset of the design parameter values and then plot these values to come up with a similar regression equation.

It is important to note, however, that the degree of confidence limits of this regression equation will vary. For example for the east facing façade, the R² value was 0.996. While the equation for the south facing façade was

$$y = 0.2348x + 2.7396 \quad (3)$$

The R² value for the south facing façade was 0.9841, which is slightly lower than that of the east façade. Therefore, as noted, the regression equations will vary with firstly the degree of sophistication of the design parameters considered and secondly with the orientation of the façade. In any case a new proposed measure for the combined performance may be expressed as

$$\text{Proposed Measure} = \frac{\text{Max}\{1, DA\}}{\text{Irradiation}} \quad (4)$$

This measure would reward higher daylight performance in terms of Daylight availability up to a maximum value of 100% while penalize higher irradiation values gained. Such cases on the inflection point of the curves in figures 7 and 8 would be considered superior and would achieve higher scores in our proposed measure compared to cases which increase the irradiation without increasing the DA values. Table 2 shows details of some of the extreme cases.

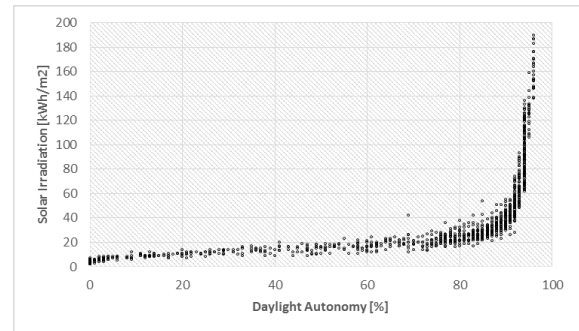


Fig. 6 – The solar irradiation versus the DA for the east facing orientation at different sensor points for all 17 cases

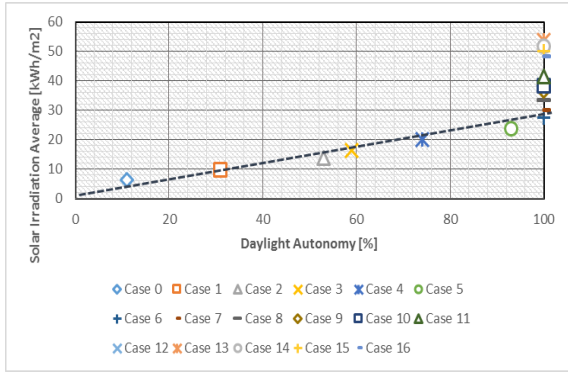


Fig. 7 – The solar irradiation versus the DA for the south facing orientation for the 17 test cases

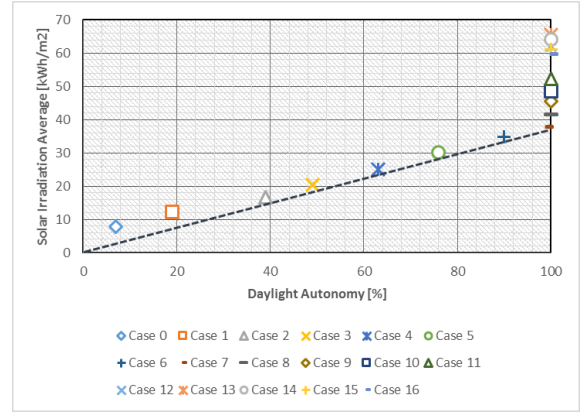
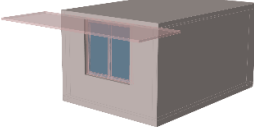
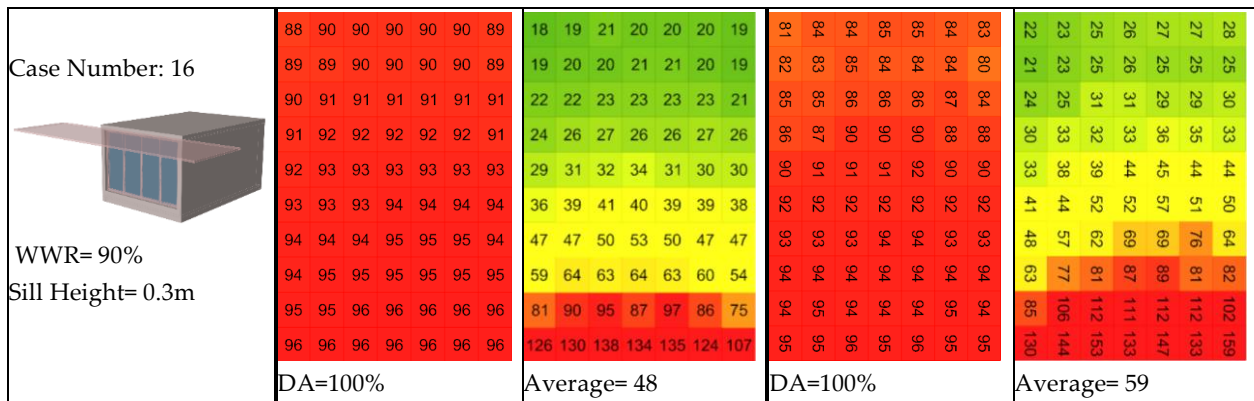


Fig. 8 – The solar irradiation versus the DA for the east facing orientation for the 17 test cases

Table 2 – The sensor points data for some extreme cases

Case Description	South		East	
	Daylight Autonomy	Solar Irradiation	Daylight Autonomy	Solar Irradiation
Case Number: 0  WWR= 10% Sill Height= 1.0m	0 0 0 0 0 0 0 0 0 6 0 0 0 0 0 1 11 9 7 10 3 4 19 38 52 26 18 5 12 32 66 78 75 30 9 2 42 85 92 91 21 2 0 0 47 82 30 0 0	2 2 2 2 2 2 2 3 2 3 3 2 2 2 3 3 3 3 3 3 3 3 4 4 4 4 3 3 4 4 5 4 5 4 4 5 6 6 6 7 5 5 6 7 10 10 9 8 7 8 9 13 14 12 8 7 7 17 23 31 23 12 6 2 4 11 16 10 5 2	0 0 0 0 1 1 0 0 0 0 0 0 0 0 0 0 2 0 0 0 0 0 1 0 0 0 0 0 2 1 0 0 0 0 6 3 0 3 3 12 15 5 1 8 20 31 31 9 0 17 41 55 49 33 0 0 69 88 69 36 0 0 17 33 0 0	2 3 3 3 3 4 3 2 3 3 4 4 3 3 4 4 5 6 3 3 4 5 6 8 3 3 4 5 6 8 4 4 6 8 14 3 3 4 5 7 12 4 3 4 5 7 16 3 3 4 5 7 20 4 4 6 7 7 23 5 5 5 7 7 26 4 4 4 7 7 28
	DA=11%	Average= 6	DA=7%	Average= 8
Case Number: 5  WWR= 35% Sill Height= 1.0m	37 41 53 52 49 47 31 39 55 64 58 66 58 38 66 68 73 74 75 71 56 77 81 82 82 81 76 73 81 89 90 89 90 87 88 88 91 91 91 91 91 90 91 92 93 93 93 93 92 91 93 94 94 94 94 93 91 93 95 95 95 94 93 79 88 92 92 92 89 80	9 10 9 10 10 9 9 9 9 10 10 10 9 9 10 11 13 13 12 11 10 12 14 16 14 14 14 13 17 18 18 18 18 17 15 20 20 24 24 24 22 19 25 29 34 34 33 25 24 35 43 47 51 47 37 32 42 63 73 84 69 49 32 16 23 35 38 38 21 15	26 29 30 37 40 33 29 28 37 38 47 45 39 36 41 50 54 57 51 54 47 55 65 75 67 68 69 60 67 77 78 82 76 78 76 80 84 86 87 85 80 80 85 89 90 91 88 86 86 87 92 93 94 93 88 87 82 92 94 94 94 87 87 58 75 87 88 86 61 61	12 13 14 13 15 14 13 13 13 16 18 15 12 15 13 16 18 19 22 23 23 14 17 19 21 22 23 28 14 17 19 21 22 31 31 14 17 19 21 22 31 44 14 17 19 21 22 31 46 14 17 19 21 22 31 46
	DA=93%	Average= 24	DA=76%	Average= 30
Case Number: 6  WWR= 40% Sill Height= 1.0m	55 61 65 66 61 63 56 62 67 70 72 74 73 58 75 77 74 78 77 78 75 80 85 88 88 87 86 78 88 88 91 91 91 90 88 91 92 92 92 92 92 91 91 93 93 94 94 93 93 92 93 94 94 95 94 94 92 94 95 95 95 94 94 85 90 92 92 92 91 86	11 11 11 12 11 11 10 11 10 12 13 12 11 11 13 12 14 14 14 14 13 15 17 15 18 17 17 15 18 19 21 23 22 20 19 23 25 26 28 27 25 22 30 31 35 36 37 33 27 37 48 56 58 49 44 37 49 70 87 90 81 62 35 20 29 41 49 36 28 18	37 47 60 53 49 50 45 47 51 58 60 54 52 47 58 63 65 60 69 61 61 75 74 77 70 77 75 72 76 84 86 77 84 82 80 85 88 89 85 90 88 86 89 91 92 89 92 91 86 91 92 94 94 94 91 89 89 83 88 88 88 89 89 70 83 88 88 88 88 72	12 13 14 14 16 16 15 13 13 16 18 15 12 15 13 16 18 19 22 23 23 14 17 19 21 22 31 31 14 17 19 21 22 31 44 14 17 19 21 22 31 46 14 17 19 21 22 31 46
	DA=100%	Average= 28	DA=90%	Average= 35



4. Conclusions

Daylighting and solar thermal gains are often positively correlated. In particular, if a specific design achieves acceptable scores for the climatic-based daylighting measures, then it may be often the case that this can be on the account of exceedingly high thermal gains. In this paper a new metric is proposed that takes into account the total number of lux-hours achieved throughout the year and the distribution of these lux-hours with the cooling and heating degree days for different time steps. There remains more work to be done. The proposed metric is limited to conventional fenestration and would not apply to complex fenestration systems where no correlation is expected between energy gains and lighting performance such spectrum selective fenestration systems. Large solar irradiation values mean extensive thermal gain loads which is an undesirable effect in hot zones most of the year. However, higher values are beneficial whenever the temperature drops below comfort levels. Therefore, it may still be wise to develop a performance index that can be calculated on seasonal basis, with the solar irradiation increase being favourable during winter only.

References

Wagdy, A. New parametric workflow based on validated daylighting simulation. Proceedings of the Building Simulation Conference, Cairo, Egypt; 2013.

Reinhart, C. F., Mardaljevic, J., & Rogers, Z. (2006). Dynamic Daylight Performance Metrics for Sustainable Building Design. *Leukos*, 3(1), 7-31.

Reinhart, C. F., & Walkenhorst, O. (2001). Validation of dynamic RADIANCE-based daylight simulations for a test office with external blinds. *Energy and Buildings*, 33(7), 683-697.

Carlos E. Ochoa, Myriam B.C. Aries, Evert J. van Loenen, Jan L.M. Hensen, Considerations on design optimization criteria for window providing low energy consumption and high visual comfort, *Appl Energy*, 95 (2012), pp. 238-245

K. Tsikaloudaki, K. Laskos, Th. Theodosiou, D. Bikas, Assessing cooling energy performance of windows for office building in the Mediterranean zone, *Energy Build*, 49 (2012), pp. 192-199

Abdelsalam Aldawoud, Conventional fixed shading devices in comparison to an electrochromic glazing system in hot, dry climate, *Energy Build*, 59 (2013), pp. 104-110

E.S. Lee, A. Tavit, Energy and visual comfort performance of electrochromic windows with overhangs, *Build Environ*, 42 (2007), pp. 2439-2449

Takashi Inoue, Masayuki Ichinose, Naoyoshi Ichikawa, Thermotropic glass with active dimming control for solar shading and daylighting, *Energy Build*, 40 (2008), pp. 385-393

- A.K. Athienitis, A. Tzempelikos, A methodology for simulation of daylight room illuminance distribution and light dimming for a room with a controlled shading device, *Sol Energy*, 72 (2002), pp. 271–281
- R. Sullivan, E.S. Lee, S. Selkowitz, A method of optimizing solar control and daylighting performance in commercial office building, *Proc ASHRAE Conf Therm Perform Exterior Envelops Build* (1992), pp. 313–319
- C.A. Johnson, R.W. Besant, G.J. Schoenau, Economic preferred window orientation and optimum fenestration design of a non-daylit and daylit large office building for different climate conditions and different billing structures, *ASHRAE Trans*, 96 (1990), pp. 23–33

The effect of vegetation on daylight availability

Islam Ayman Mashaly – Research Assistant, Department of Construction and Architectural Engineering, American University in Cairo – islam.akm@hotmail.com

Yusra Mohamed Rashed – Research Assistant, Department of Construction and Architectural Engineering, American University in Cairo – yusra.mer@hotmail.com

Muhammad Adel – Researcher, Housing Building National Research Center (HBNRC) – muhmd.adel@yahoo.ca

Khaled Nassar – Associate Professor, Department of Construction and Architectural Engineering, American University in Cairo – knassar@aucegypt.edu

Abstract

Simulating daylight in building spaces is becoming an increasingly important task to achieve sustainable and healthy building designs. However, accurate modeling of daylight necessitates the inclusion of environmental conditions as well as accurately modeling the buildings' surroundings, including obstructions. Obstructions in the form of vegetation such as trees and shrubs can significantly impact the daylight performance. This paper presents a parametric study of the effect of vegetation on the daylight performance of the building spaces. RADIANCE is used to simulate the effect of the vegetation obstructions on the daylighting. A routine is developed to parametrically create vegetation and outputs geometric descriptions that in the rad format, so that they can be easily incorporated into the RADIANCE scene description file. The developed routine allows for parametric variations of the tree shapes and configuration so that these values can be studied. A standard office space is used and the daylight performance is assessed using a daylight climate-based metrics namely daylight availability. The results demonstrate the importance of taking vegetation obstructions into account when modeling daylight performance.

1. Introduction

The effect of vegetation outside windows has not received enough attention in the literature on daylighting. Vegetation outside windows, similar to other obstructions, can significantly affect the lighting conditions inside any space. One can spend a significant amount of time designing and modeling windows and fenestrations to achieve a specific lighting performance inside a space only to find that unplanned vegetation outside the window has affected the simulated performance. This is true with many of the outside obstructions that need to be considered when modeling and simulating lighting conditions. However, with the case of vegetation, it may be easier to model and therefore predict the effect on lighting. The correct positioning of vegetation can also improve the daylighting performance of specific designs through shading, which decreases the amount of glare and maintains desirable illumination levels inside.

Given that vegetation can affect the lighting conditions in a space, a number of questions now need to be answered, firstly, how vegetation affects lighting conditions inside the space. A number of realistic and extreme case scenarios can be considered to answer this question. Secondly, how does the plant type affect the lighting conditions? Thirdly, what is the increased computational time taken to model the vegetation and when is it warranted to model and simulated it? Fourthly,

what are the best ways to account for vegetation in a simulation, i.e. what is the best way to model the vegetation (in terms of detail, reflectivity, shape, etc...) and what is the best way to simulate the effect of vegetation?

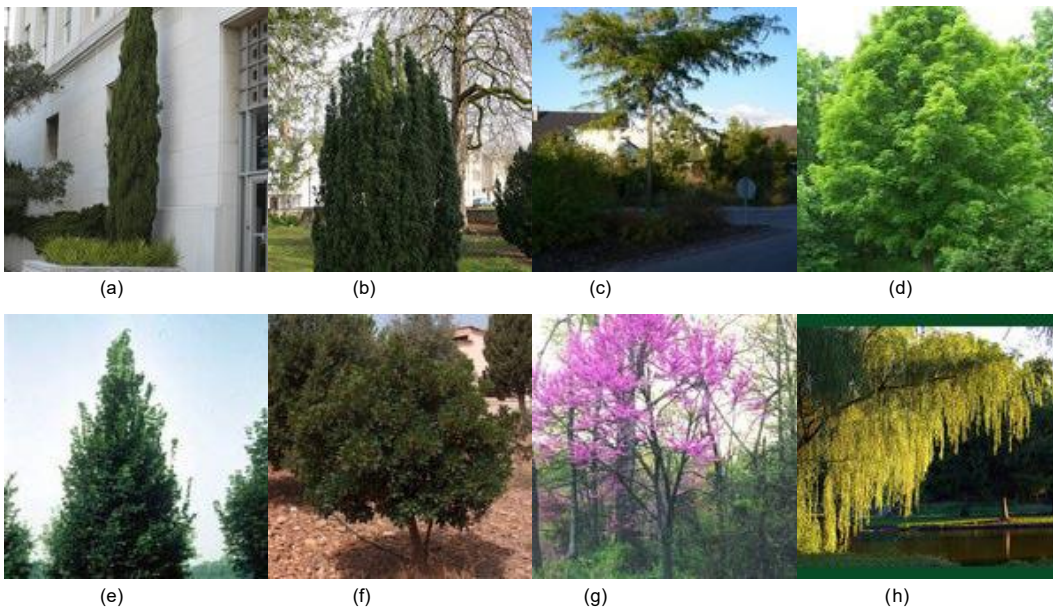
The main objective of this paper is to study the effect of vegetation on daylight performance in building spaces. In particular it may be possible to positively influence the daylight performance inside the space by correct position of vegetation outside the window. We therefore, briefly, explore the effect of trees' location, configuration and shape parameters on the daylighting performance inside a space through a parametric study. We also develop a systematic parametric simulation model that determines the effect of the tree location, spacing, and corresponding window configuration in order to maximize the daylight performance of a typical building space.

This paper is organized as follows; in the next section we present the parameters of the trees used in the study as well as the variables considered. In the following section we discuss the other parameters studied and details about the

simulation. Then, we present some of the results and analysis and this is followed by conclusions and recommendations for future research.

2. Considered tree types and parameters

Our study will only focus on trees rather than other types of vegetation such as shrubs or grass. Grass or shrubs outside a window, for example, can also have an effect on the lighting inside a room. In fact, in this paper we will only study two of the most common tree shapes namely, column and round trees. Trees come in several basic shape and configurations. Once recent classification (Nystad, 2010) included Spherical, Hemispherical, Cylindrical, Tapered cylindrical, Flame, Inverse conical and Tend flame tree shapes. Another classification is shown in figure 1. We will study round and column tree shapes and their impact on daylighting.



(a) Columnar Tree Shape, (b) Fastigate Tree Shape, (c) Irregular Tree Shape, (d) Oval Tree Shape, (e) Pyramidal Tree Shape, (f) Round Tree Shape, (g) Vase Tree Shape, (h) Weeping Tree Shape

Fig. 1 – Basic Tree Shapes (adapted from <http://treesandshrubs.about.com/od/treeshrubbasics/ig/Tree-Shape/>)

We are primarily interested in creating a parametric model of a tree that changes its shape seamlessly from round to column shaped.

Parametric trees are ones which are geometrically modeled using specific shape parameters and which are used in generating single body

polygonal models of those trees that account for natural rules of growth. Parametric trees can be generated by a variety of techniques as discussed in de Reffye, et al 1988, Felkel et al, 2002, Felkel et al, 2002b, Honda, 1971, Prusinkiewicz and Lindenmayer, 1990 and Weber and Penn, 1995. Nystad, 2010 developed an algorithm that considers the number of branch levels to be produced, the shape exponent in da Vinci's equation, a parameter to describe the upward growth tendency, and the base tree scale. Also considered in this research were various leaf parameters.

In this research however, we opt to develop our own algorithm for generating parametric trees for simplicity and due to the need for robust calculations during simulation routines. We only seek to present a preliminary exploration of the effect of tree shape on daylighting and find indications on the best tree shape (column or round) and leaf density as well as the positioning and spacing. Therefore the algorithm developed here accounts for three main parameters namely, width, height and leaf density. Inherit in our algorithm is the leaf and trunk reflectivity values. The algorithm for generating a tree is developed in Grasshopper for Rhino and is based on generating an ellipsoid which is then sliced into different

sections. Points are then randomly generated on the perimeter of those slices at various intervals and leaves are created at those points. The shape of the underlying ellipsoid and the number and location of slices and points is also parameterized. For the leaves, shapes and density are also controllable. A leaf-shaped surface is generated from 2 spline curves at a certain scale. The leaves are assigned to the points on the tree. The scale is divided into two discrete scale steps so that the scale of the leaves does not vary significantly on the same tree. Each leaf is assigned a random scale from 1.0 to 2.0 and another set from 2.0 to 3.0 the size of a base leaf size. This allows modeling trees with randomly generated sizes at two scale steps that may represent different kinds of trees or two different seasons (broad leaf trees for example versus evergreens). We are therefore able to vary the shape of the tree easily by varying the height and width of the underlying ellipsoid as well as varying the leaf density. The leaf density is a variable calculated using the following equation:

$$\text{Density} = \frac{\text{Total Area of Leaves}}{\text{Volume of Tree Boundary}} \quad (3)$$

A parametric analysis can be easily conducted now taking into consideration the location of the trees outside the window as will be described next.

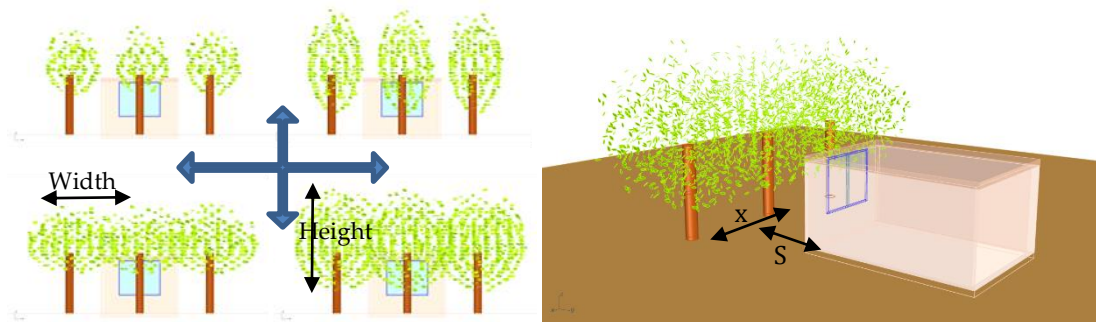


Fig. 2 – The two different shapes of trees considered and their parameters

Table 1 – The range of the parameters considered

Simulation Parameters	ab (ambient bounces)	6	
	ad (ambient divisions)	1000	
	as (ambient supersamples)	20	
	ar (ambient resolution)	300	
	aa (ambient accuracy)	0.1	
Assigned Materials	Walls	Generic Wall [Reflectance=50%]	Interior
	Floor	Generic Floor [Reflectance=20%]	Floor
	Ceiling	Generic Ceiling [Reflectance=80%]	Ceiling
	Window Frame	Metal Diffuse	
	Window Glazing	Double Pane, Clear [Transmittance=80%]	
	Ground	Outside Ground [Reflectance=20%]	Ground

3. Considered layout and configurations

In order to run the parametric analysis, a typical room design was considered representing a standard office. The room dimensions were 6 meters in length, 4 meters in width and with a height of 3 meters. The other room specifications are shown in table 1. The window for the space is facing south. The spacing (s), distance between the trees (x) shown in figure 1, the width, height and density of the tree can now be parametrically varied to study the effect on the overall lighting performance of any particular design. In order to run the daylighting analysis, Diva for Rhino was used and these parameters were varied. The RADAINCE specifications and simulation parameters are also shown in table 1.

Table 2 – The range of the parameters considered

Variable	Range
Width	4, 6
Height	3, 5
Scale	z, 2z*
x	2, 3, 4
S	3, 4

* Where z is the leaf size.

Table 2 shows the ranges of the parameters that were considered. The values were varied and each step was considered for evaluation. We had a total of 48 different cases resulting from 2 values for width, 2 values for height, 2 values for leaf size (which is translated to density according to the number of leaves; which increases according to the width and height of the tree), 3 values for spacing between trees and 2 values for distance between the trees and room ($2 \times 2 \times 2 \times 3 \times 2 = 48$). However, these 48 cases were divided by the scale parameter into two different sets of 24 cases each. This was done to insure that a reasonable scaling for the tree leaves was used. These two sets of 24 cases each were then run through RADIANCE and appropriate daylighting performance measures were calculated as discussed next.

4. Results and discussion

Daylight Availability (DA) was one of a number of daylight metrics that consider the annual performance of a particular design (as opposed to instantaneous measures such as daylight factor), now commonly referred to as 'dynamic daylight metrics'. DA is defined as 'the percentage of the occupied hours of the year when a minimum illuminance threshold is met by daylight alone' (Reinhart C F & Walkenhorst O, 2001)." Daylight availability is meant to amalgamate Daylight Autonomy and Useful Daylight Index information into a single figure.

In calculating the DA, any number which is 'negative' represents 'over-lit' nodes (for example a DA value of -5% of occupied hours with 10-times the threshold illumination value). Any number between 49-100 percent represents 'day-lit' nodes (i.e. >48% of occupied hours with threshold

illumination values). Similarly, any numbers 0-48 represents 'partially-lit' nodes (i.e. 0-48% of occupied hours with threshold illumination values). Table 3 summarizes this information. Therefore the Daylit, Partially Daylit or Overlit percentage for the space would be equal to:

$$DA_{\text{or Partial or Overlit}} = \frac{\text{Number of Nodes in Range}}{\text{Total Number of Nodes}} \quad (2)$$

The DA values in terms of Daylit percentage, and partially Day lit and overlit are calculated for the two different values of scale (leaf density) and are shown in figures 3 and 4. The values shown are for the entire space, they summarize the data for each

case. Each case has 3 values; Daylit, Partially Daylit and Overlit. In order to determine what would be the best of these design options, we need to rank them according to a single criterion.

Table 3 – The levels of Daylight Autonomy Used

Indices	Range
Daylit	50% to 100%
Partially Daylit	0% to 50%
Overlit	< 0%

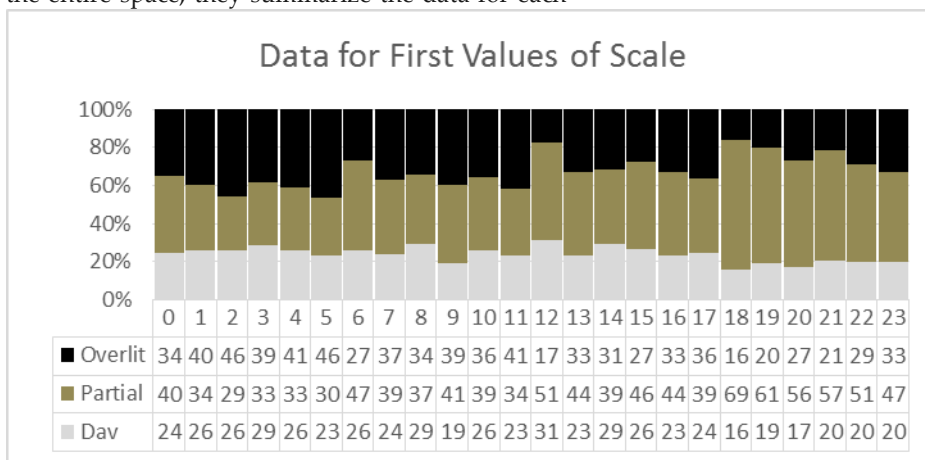


Fig. 3 – The Daylight Availability Values for the first set of scale values (z)

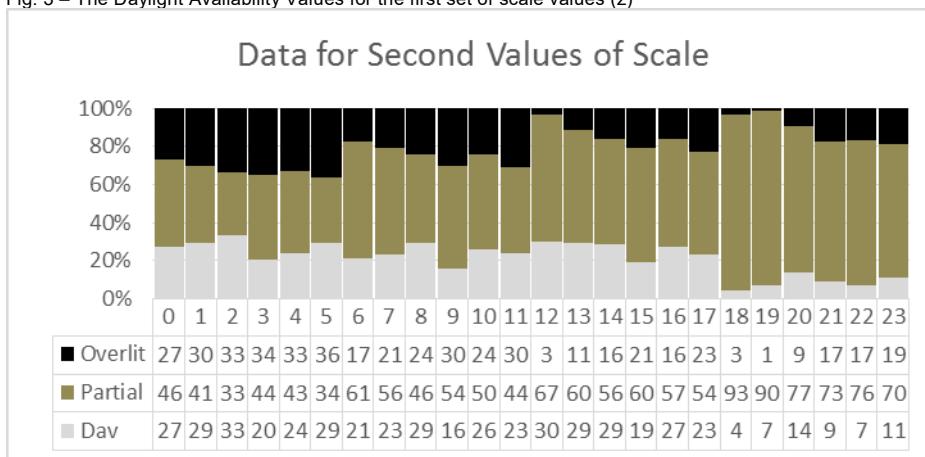


Fig. 4 – The Daylight Availability Values for the second set of scale values (2z)

Therefore, we used a measure that combines the three values of percentage over lit, partial Overlit and Day lit into one single measure. This measure may be more representative for ranking the design cases in terms of their daylight availability performance. Since we want to maximize the Daylit percentage and minimize the Overlit, we can divide the Daylit percentage by the Over lit percentage. This ensures that the bigger the difference, the higher is our factor since a higher nominator and a lower denominator increases the overall factor.

$$\text{Measure 1} = \frac{\text{Daylit}}{1 + \text{Overlit}} \quad (3)$$

Although this measure does not explicitly include the partially lit values, the percentage of the space that is partially lit is already inherit in this measure since the Daylit + the Overlit + the Partially Daylit must equal one. Therefore the bigger the difference between the Daylit and Overlit value, the higher the partially lit values. Another measure which takes the three values was also used and in this measure we penalize the high Overlit and Partially Daylit values and we reward the high daylight availability values by using the following formula:

$$\text{Measure 2} = \frac{\text{Daylit}}{\text{Overlit} \cdot \text{Partially lit}} \quad (4)$$

Both of these measures were calculated for the 24 cases and the results were plotted in figure 5. In figure 6, we present a comparison of some of the results from the most extreme cases in the data set.

The grid values for daylight availability and the corresponding design scenarios are presented. It is evident from this data that for a simple design such as the one shown, circular trees are more favorable than column shaped trees. Also, it seems higher leaf density is favorable. This is probably due to the south-facing window. We simulated the best and worst cases with 6 ambient bounces for more reliable data and results and found improvement in the overall readings. Although we only simulated 3 conditions, which are the best case (12), the worst (5) and one in the middle (2) all for 2 ambient bounces, they have managed to maintain the same ranking within the 3 simulations.

Due to the time factor, we have managed to produce quick results with 2 ab, since they take far less time (10 mins each) while using 6 ab would take around 1 and 2 hours each. The results with 2 and 6 ambient bounces are shown in figure 7, while table 4 shows the data for some of the extreme cases.

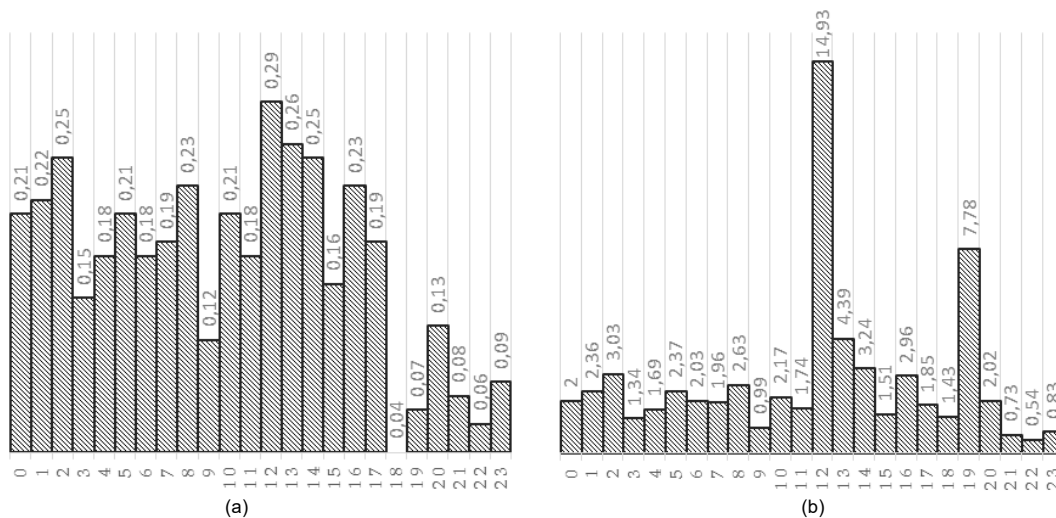


Fig. 5 – A comparison based on the two combined measure (a) measure 1 and (b) measure 2

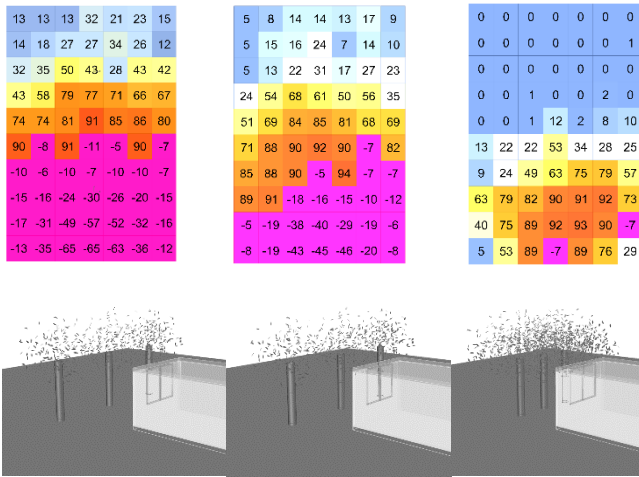


Fig. 6 – Comparison between cases 2, 5 and 12 showing the DA Values for the standard room grid under three different cases of design

Table 4 – The data for some extreme cases

Case 2		Case 5		Case 12	
Number of Bounces		Number of Bounces		Number of Bounces	
2	6	2	6	2	6
S_R_2	S_R_2	S_R_5	S_R_5	S_R_12	S_R_12
2	2	5	5	12	12
WWR	WWR	WWR	WWR	WWR	WWR
40%	40%	40%	40%	40%	40%
Half Width		Half Width		Half Width	
2	2	2	2	3	3
No. of Leaves	No. of Leaves	No. of Leaves	No. of Leaves	No. of Leaves	No. of Leaves
645	645	645	645	1662	1662
Density	Density	Density	Density	Density	Density
0.695063	0.695063	0.359112	0.359112	0.787968	0.787968
Half Height		Half Height		Half Height	
1.5	1.5	1.5	1.5	1.5	1.5
X [tree-tree]	X [tree-tree]	X [tree-tree]	X [tree-tree]	X [tree-tree]	X [tree-tree]
4	4	4	4	2	2
S [tree-room]	S [tree-room]	S [tree-room]	S [tree-room]	S [tree-room]	S [tree-room]
3	3	4	4	3	3
DAv	DAv	DAv	DAv	DAv	DAv
33	64	23	51	30	59
partial DA	partial DA	partial DA	partial DA	partial DA	partial DA
33	1	30	0	67	39
Overlit	Overlit	Overlit	Overlit	Overlit	Overlit
33	34	46	49	3	3

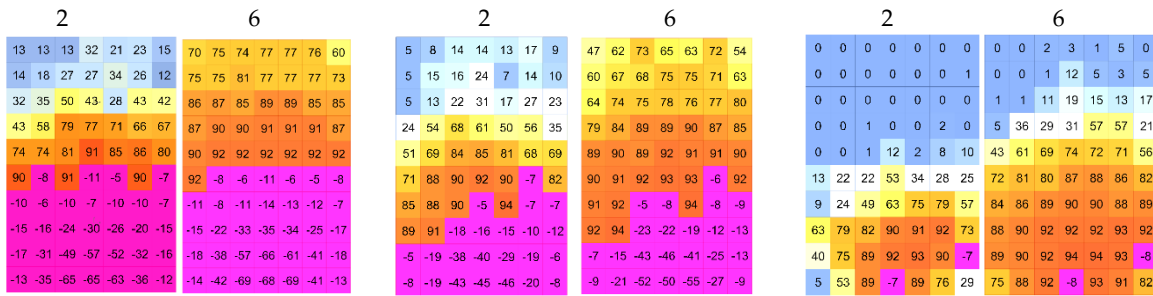


Fig. 7 – The results with 2 and 6 ambient bounces

5. Conclusions

Tree parameters studied were reflectivity of tree leaves, density of leaves and tree size. A parametric study was conducted using a fixed tree type and variable parameters, which include tree dimensions, leaf density, spacing and distance from window. It demonstrates that vegetation can affect the lighting conditions in a space to a significant degree. For a simple rectangular south-facing window, round trees are more favourable with a higher tree density and a relatively close spacing with a relatively small distance from the window. It is possible to determine a relatively good solution in reasonable simulation time, by considering a basic tree model such as the one described in this paper. Future recommendations include studying more tree types and various other design parameters as well as better parametric tree models account for other tree morphological aspects.

References

Jørgen Nystad, *Parametric Generation of Polygonal Tree Models for Rendering on Tessellation-Enabled Hardware*, Master of Science in Computer Science, Norwegian University of Science and Technology, Department of Computer and Information Science, 2010

Phillippe de Reffye, Claude Edelin, Jean Françon, Marc Jaeger, and Claude Puech. *Plant models faithful to botanical structure and development*. In SIGGRAPH '88: Proceedings of the 15th annual conference on Computer graphics and interactive techniques, pages 151–158, New York, NY, USA, 1988. ACM.

Petr Felkel, Anton L. Fuhrmann, Armin Kanitsar, and Rainer Wegenkittl, *Surface reconstruction of the branching vessels for augmented reality aided surgery*, 2002.

Petr Felkel, Armin Kanitsar, Anton L. Fuhrmann, and Rainer Wegenkittl, *Surface models of tube trees*. In *Computer Graphics International*, pages 70–77, 2002.

Hisao Honda. *Description of the form of trees by the parameters of the tree-like body: Effects of the branching angle and the branch length on the shape of the tree-like body*. *Journal of Theoretical Biology*, 31(2):331 – 338, 1971.

P. Prusinkiewicz and Aristid Lindenmayer. *The Algorithmic Beauty of Plants*. Springer-Verlag New York, Inc., New York, NY, USA, 1990.

Jason Weber and Joseph Penn. *Creation and rendering of realistic trees*. In SIGGRAPH '95: Proceedings of the 22nd annual conference on Computer graphics and interactive techniques, pages 119–128, New York, NY, USA, 1995. ACM.

Wagdy, A. *New parametric workflow based on validated daylighting simulation*. Proceedings of Building Sim. Conference, Cairo, Egypt; 2013.

Reinhart, C. F., Mardaljevic, J., & Rogers, Z. (2006). *Dynamic Daylight Performance Metrics for Sustainable Building Design*. *Leukos*, 3(1), 7–31.

Reinhart, C. F., & Walkenhorst, O. (2001). *Validation of dynamic RADIANCE-based daylight simulations for a test office with external blinds*. *Energy and Buildings*, 33(7), 683–697.

Solar assisted ground source heat pump performance assessment for residential energy supply in southern European climates

Natale Arcuri – Department of Mechanical, Energy and Management Engineering (DIMEG), University of Calabria P. Bucci 46/C, 87036, Rende (CS), Italy – natale.arcuri@unical.it

Francesco Reda – Technical Research Centre of Finland VTT, PO Box 1000, FI-02044 VTT, Finland – francesco.reda@vtt.fi

Pasquale Loiacono – Department of Mechanical, Energy and Management Engineering (DIMEG), University of Calabria P. Bucci 46/C, 87036, Rende (CS), Italy – pasquale-loiacono@hotmail.it

Domenico Mazzeo – Department of Mechanical, Energy and Management Engineering (DIMEG), University of Calabria P. Bucci 46/C, 87036, Rende (CS), Italy – domenico.mazzeo@unical.it

Abstract

The awareness about environmental problems due to fossil fuel consumption is increasing widely; therefore, efforts are being made to develop energy efficient and environmentally friendly systems by utilisation of non-polluting renewable energy sources. Ground source heat pumps (GSHPs) belong to this category. Many variations of geothermal system typologies exist, with different configurations suitable in different situations and most locations around the world. One emergent configuration is the solar assisted GSHP (SAGSHP). The paper focuses on different control strategies of a solar assisted ground source heat pump (SAGSHP) for different Italian locations. Dynamic simulation approach has been used through TRNSYS software. The impact of the considered strategies on the seasonal performance factor has been evaluated. Results have shown that the strategy strongly affects the system consumption; therefore, it needs to be chosen appropriately in the design phase. Furthermore, when solar energy is driven into the ground, the temperature difference between solar collectors and the ground, which has to be a positive value to charge the ground, plays a fundamental role. In particular, solar thermal energy injected into the ground decreases to zero moving from a humid sub-tropical (Cfa) to a dry-summer subtropical (Csa) climate. Therefore, a compromise between the operation of the circulation pumps used for supplying free cooling energy and for driving solar thermal energy into the ground has to be found for each climate.

1. Introduction

The 2010/31/EU Directive of the European Parliament and the Council of 19 May 2010 have set, as a priority under the “20-20-20” objectives, the reduction of the energy consumption of the building sector, which represents 40% of the European Union’s (EU) total energy consumption [1]. Solar thermal systems are key technologies to achieve this goal, indeed they are spreading in the European countries [2]. They receive particular interest from southern European countries, in particular from Italy and Spain, which have high solar heat generation targets accordingly to their National Renewable Energy Action Plans [3]. Indeed, in Italy, which has been considered in this study, solar thermal technology is mandatory in new and in renovated buildings [4]. Three different climates have been taken into account: humid subtropical climate (Cfa, in accordance with the Köppen climate classification [5]), Mediterranean climate with mild, humid winters and hot, dry summers and hot-summer (Csa) Mediterranean climate (Csa). They refer respectively to the cities of Milan, Rome and Palermo and they can be considered representative of many southern European locations. Solar thermal energy can be used also unconventionally. In fact with regard to ground source heat pump (GSHP), solar thermal collectors can also supply heat directly to the ground, increasing the temperature of the evaporator in the GSHP, in addition to providing building heating energy. Since one machine is able

to provide heating and cooling building energies, they could play a significant role in reducing CO₂ emissions [6]. The GSHP systems have been investigated by many scientists for many applications, from residential to public buildings, affirming that they effectively make use of renewable energy stored in the ground to supply building thermal energy in a new and clean form [7-13]. They are particularly indicated for low environmental impact projects around the globe. Indeed, heat pumps utilize significantly less energy than alternative heating systems in various climatic contexts, from cold to mild temperate conditions [7, 8, 10, 12- 16]. One promising configuration is the solar assisted GSHP (SAGSHP) [17]. In such systems, the solar collectors may supply heat directly to the domestic hot water systems, the building heat distribution systems, increasing the temperature of the evaporators in the heat pumps, recharging the boreholes or combinations of all [18]. The effective use of these systems might play a leading role in the world in the foreseeable future [19]. Moreover, a free ground cooling (FGC) loop can be implemented easily in the same machine, using the ground as a thermal cooling source; therefore, the building space cooling (SC) requirements can be satisfied only consuming a small amount of electricity if the thermal condition of the ground are suitable [20]. Many scientists [16-29] have investigated the design, the modelling and the testing of SAGSHP solutions. The efficiency of SAGSHPs can be further increased, thus supplementary research on solar thermal system operation strategy and control is needed [18]. The aim of this research is to assess the long-term performance of a SAGSHP in southern European climates for residential thermal energy supply; therefore, results refer to the 21st year of analysis. In particular, the final energy consumption and the seasonal performance factor (SPF) have been evaluated. A FGC system for supplying the building cooling requirement, as the good practice suggests, and a PV system, as the Italian law imposes [4], have been considered. The study is performed with a simulation approach due to the complexity of the proposed system, as suggested by C. Montagud [23]. In addition, TRNSYS v.17® [30] has been used in accordance to

many scientists [25, 29]. The first part of the paper concentrates on the building and heating/cooling system configurations. The second part regards the results of the considered systems, while the last the conclusions.

2. Case study

2.1 Building

The analysed building is a four-storey building (Figure 1) consisting of two flats of about 110 m² per floor. The pitched roof has a tilted angle of 20°. General information about the building can be seen in Table 1. Internal and external superficial thermal resistances have been assumed accordingly to UNI EN ISO 6946 [31], while the infiltration rate and the envelope thermal properties for the considered localities respectively refer to the standard UNI 11300 – Part 1 [32] and Italian Presidential Decree of April, 2009 N°59 [33].

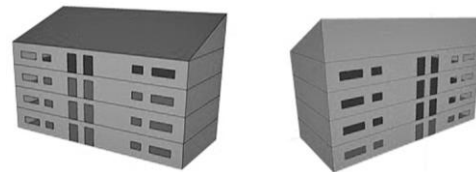


Fig. 1 – Building front and back views

Table 1 – Thermal features of the building envelope elements: external wall, roof and window and main data of the building

Building thermal data [33]				
	U Value [W/m²K]			g factor
	Milan	Rome	Palermo	
External Wall	0,3	0,4	0,45	-
Roof	0,3	0,35	0,4	-
Window	2,2	2,2	2,2	0,701
Building general data				
Location	Milan, Latitude 47° 27' N and longitude and 9° 10' E Rome, Latitude 41° 54' N and longitude and 12° 27' E Palermo, Latitude 38° 7' N and longitude and 13° 22' E			
Floor surface	880 m ² -two flats of about 110 m ² per each floor(4-strorey building)			
Internal - external superficial thermal resistances	0,2 - 0,05 m ² K/W [39]			

Mechanical exhaust air ventilation rate	0,3 ACH [40]
Cooling - heating set point temperatures	26°C - 21°C
DHW set point	45 °C
Heating supply inlet temperature	40 °C
Cooling supply inlet temperature	17 °C
Water network temperature	7 °C
Storage tank set point	55 °C

The DHW hourly profile shown in Figure 2 has been implemented [34] into the building thermal model. The building model has been built in TRNBuild [35], which is a TRNSYS subroutine able to generate the thermal loads profile of a building.

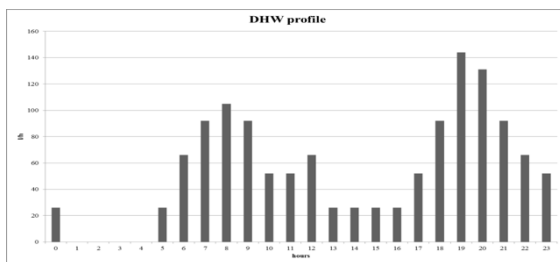


Fig. 2 – DHW hourly profile [34]

The design features of the solar thermal system, including the storage tank are shown in Table 2. An auxiliary system, consisting of a gas boiler, of 11 kW has been connected to the hot tank (Figure 3); it works if heating building energy is requested and temperature of the storage tank is below 55 °C.

Table 2 – Solar thermal system design

Rotex V26P, Flat plate collector [37]	
Net surface (one panel)	2,6 m ²
Number of panels connected in series – number of rows	6 – 3 (Milan, 46,8 m ²) 6 – 0 (Rome, 15,6 m ²) 4 – 0 (Palermo, 15,6 m ²)
ECO COMBI 2 VC Cordivari [38]	
Capacity	1500 l (Milan) – 600 (Rome, Palermo)

2.2 Borehole heat exchanger (BHE)

BHE plays a key role in GSHP systems as a thermal source for the heat pump and the FGC loop. Usually for a single-family dwelling one BHE is enough. Therefore, since the considered building is a multi-family house, a specific procedure has been used in order to design the nominal borehole field in case of absence of solar thermal system [39]. It has to be pointed out that the designed borehole field parameters are similar to each city. Precisely, the results achieved for Milan and Palermo were almost the same in terms of borehole configuration features. However, with regard to Rome, the borehole configuration slightly differs from Palermo. Therefore, the authors preferred to consider the same configuration for all the cities for the sake of comparison and so the biggest BHE nominal configuration calculated with the aforementioned methodology has been considered. Table 3 shows the main BHE and soil characteristics and the undisturbed temperature has been assumed as the yearly average external air temperature of each location. BHE thermal behaviour has been simulated utilizing Type 557 available in the TESS library of TRNSYS [40].

Table 3 – Main BHE and soil characteristics

BHE, single U tube system	
Pipe Outer radius	0,025 m
Pipe Inner radius	0,020 m
Centre to centre half distance	0,0265 m
Pipe thermal conductivity	0,42 W/mK
Distance between boreholes	5 m
Number of BHE	5
Depth	100 m
Soil	
Conductivity	2 W/mK
Storage heat capacity	2400 kJ/m ³ K
Undisturbed temperature	13,72 °C (Milan) 15,54 °C (Rome) 18,60 °C (Palermo)

2.3 Heat pump

The considered heat pump refers to the SI 10MR model manufactured by Dimplex® [41]. The heat pump supplies heating load networks by means of the storage tank, while cooling loads have been

directly supplied. Therefore, storage tanks supply both DHW and heating loads.

3. System configurations

Three system configurations have been evaluated. Particularly, the first configuration is a conventional GSHP without a solar thermal system and with a FGC loop, which has been taken as a reference. The second one is a SAGSHP with solar thermal system used only conventionally, for the building’s heating energy supply. The latter is a SAGSHP, where solar thermal energy can be used conventionally or unconventionally. In particular, the solar thermal energy is used principally to supply building heating energy and its surplus is driven into the BHE accordingly to the implemented controlling temperature difference between solar collectors and BHE. A schematic representation of the SAGSPH is shown in Figure 3. PV panels feed the battery pack by means of the inverter, which extracts electricity from the batteries to supply the heating and cooling system or it drives the PV produced electricity to the grid, in case of full battery. The system carrier fluid is a mixture of water and glycol, it has a specific heat capacity of 3,795 kJ/(kgK) [42]. The circulation pumps work only when the heat pump run [24].

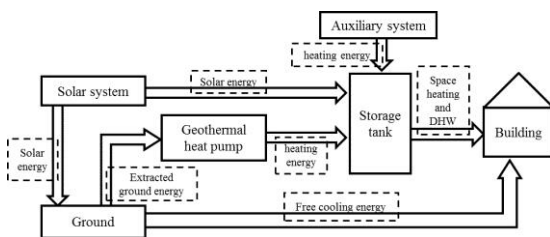


Fig. 3 – SAGSHP simplified scheme. Generic diagram

3.1 GSHP

Four main connections can be identified within Figure 3:

1. Ground – Geothermal heat pump;
2. Ground – Building (FGC);
3. Geothermal heat pump – Storage tank;
4. Storage tank – Building.

In particular, GSHP configuration does not include the solar thermal system but is connected to the hot

tank and to the BHE and directly to the heating and cooling building loads loop.

3.2 SAGSHP_C

SAGSHP_C configuration consists of the aforementioned connections and it also includes the connection between the solar thermal system and the storage tank (Figure 3). Precisely, the solar circulation pump drives the carrier fluid through the solar thermal fluid driven collectors and the hot tank when a temperature difference between the bottom part of the hot tank and the solar thermal collector outlet is higher than 4 °C.

3.3 SAGSHP_U

SAGSHP configuration adds the connection between the solar thermal system and the ground to the SAGSHP_C configuration (Figure 3). Control strategy between solar thermal field, BHE and hot tank is hierarchical. The solar circulation pump draws the carrier fluid through solar collectors when the solar collector outlet temperature is higher than the BHE outlet temperature and the hot tank does not require solar energy. The strategy used in this configuration maximises the use of solar heat. Indeed, it is used primarily for DHW and SH supply through the storage tank and secondarily for charging the ground. In particular, when the storage tank does not require solar heat and a specific temperature difference between ground and solar thermal field occurs solar heat is driven into the ground (Figure 3). Furthermore, many temperature differences between solar thermal field and BHE have been evaluated; only the best cases have been reported in the result session as regard Milan.

4. Result

Table 4 – Cases summary

Simulation case	Concept	Free ground cooling	Solar heat injected to ground
Case1, ref.	GSHP	X	
Case 2	SAGSHP_C	X	
Case 3	SAGSHP_U	X	X

Results regard the cases listed in Table 4 and they refer to the last year of the simulation period (21 years). Table 4 lists the simulation cases giving a brief description of their main features, especially how and if solar thermal energy is used. Simulations were carried out for three different Italian locations with BHE depths of 100 m Results in terms of SPF, SF and FGC fraction indexes have been calculated. They are stated respectively as:

$$SPF = Q_{u}/E_{tot} = (Q_{SH}+Q_{SC}+Q_{DHW}+Q_{FGC})/(E_{P1}+E_{P2}+E_{P3}+E_{P4}+E_{GSHP}+E_{aux}) \quad (1)$$

$$SF = Q_{sol}/Q_{SH} = Q_{sol}/(Q_{SH}+Q_{DHW}) \quad (2)$$

$$FGC = Q_{FGC}/Q_{SC} \quad (3)$$

Moreover, the final energy balance:

$$Final \ energy \ balance = E_{tot}-PV_{consumed} \quad (4)$$

The results refer to the building energy needs showed in Table 5.

Table 5 – Building cooling - heating loads and DHW energy.

Building thermal loads [kWh]			
	Milan	Rome	Palermo
Q _{SH}	29529	12157	2866
Q _{SC}	8250	11725	18074
Q _{DHW}	18366	18366	18366

Clearly, the building loads are heating dominated in Milan, balanced in Rome and cooling dominated in Palermo (Table 5). Firstly the ground injected and extracted energy, the solar fraction (SF) and the free ground cooling (FGC) fraction have been analysed for all the considered solutions and, then, the final energy consumption and balance.

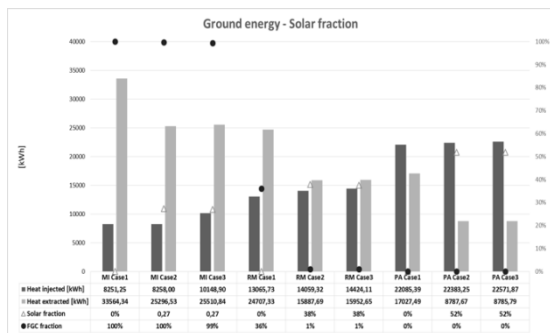


Fig. 4 – Annual ground extracted - injected energy and solar fraction of Case 1, Case 2 and Case 3 solutions for Milan, Rome and Palermo

4.1 Ground energy balance and solar fraction

SAHGSP configurations strongly impact on the extracted and injected ground energy (Figure 4). The link between SF and injected/extracted ground energy is evident. Indeed, Case 2 systems have a solar fraction which is slightly higher than Case 3 systems. It is worth noticing that this happens because the controlling temperature difference between solar collectors and BHE of Case 3 systems have been optimized. In fact, the lower this temperature difference is, the lower the SF of Case 3 systems. Obviously, Case 2 and Case 3 systems show a ground extracted energy less than Case 1 systems, since in the first solutions solar thermal energy is also used to supply building heating energy. Due to the higher ground temperature of the dry-summer subtropical (Csa) climate (Rome and Palermo), the free ground cooling is difficult to attain during the summer. Only for the Case 1 solution in Rome is the FGC fraction around 40%. In such a case, the FGC is possible because of the high extracted ground energy. However, in a humid sub-tropical (Cfa) climate, a suitable method to cover the building cooling demand is the FGC. Indeed, the FGC fractions for all the solution are almost 100% (Figure 4). With regard to Milan and the Case 3 solution, it is extremely important to find a good balance between solar conventional and unconventional operations to have also a high FGC fraction and, therefore, to maximize the energy saving. The controlling temperature difference between solar collectors and BHE is again crucial in this case and the optimum controlling temperature difference, set to 29 °C in Milan, allows us to achieve high SF and FGC fraction.

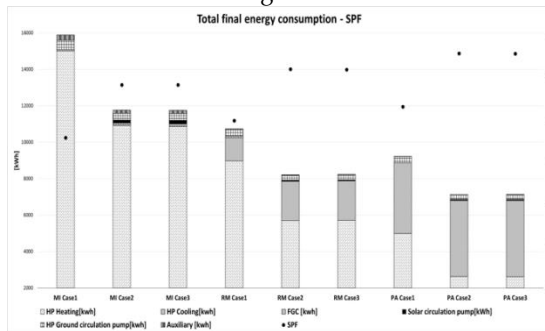


Fig. 5 – Total final energy consumption and SPF of the analysed cases for the considered localities

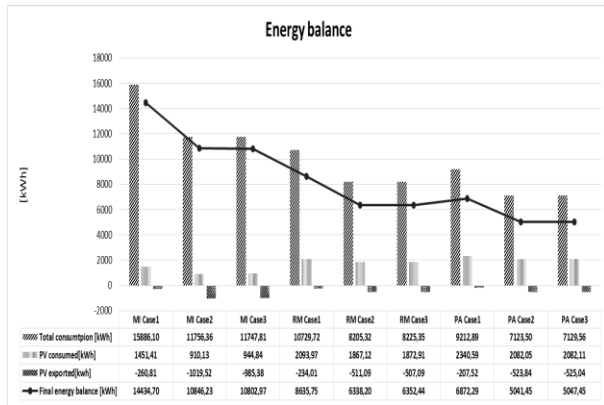


Fig. 6 – Annual final energy consumption, PV consumed and exported energy and energy balance of the considered cases.

On the other hand, the use of low controlling temperature difference values causes a lower FGC fraction, since more solar thermal energy is driven into the ground. As far as Rome and Palermo are concerned, the controlling temperature difference of Case 3 systems has been set respectively to 54 °C. This confirms that using solar thermal energy to load the ground is not appropriate as stated in section 2.2. The performances of Case 3 systems are almost the same as the related Case 2 system, since almost the whole solar thermal energy is used for supplying building heating energy.

4.2 Final energy consumption and balance

Obviously, the Case 1 solutions (Figure 5) have the highest final energy consumption in all the considered localities. Consequently, the SPF of Case 1 systems are the lowest. The Case 3 solution is effective in Milan, while it is not in Rome and in Palermo. In fact, the final energy consumption of Case 3 systems is slightly higher than the related Case 2 system in Rome and Palermo (Figure 5), because of the high controlling temperature difference between the solar thermal collectors and the BHE (see the section 5.2 for more detail). However, with regard to Milan, the Case 2 system has a similar final energy consumption to the Case 3 system. GSHP are able to reach high value of SPF in both Csa and Cfa climates. Indeed, Case 1 systems show a SPF value of 3.53, 3.94 and 4.27 respectively for Milan (Cfa), Rome (Csa with mild, humid winters and hot, dry summers) and Palermo (Csa with hot summer). It is worth noticing that the

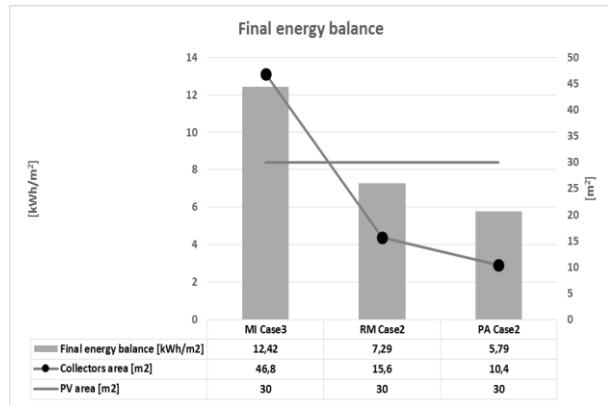


Fig. 7 – Final energy balance referred to m2 of floor area. The best solution for Milano, Rome and Palermo.

performances of the GSPHG are higher than that of an air-to-water heat pump used in a building with the same thermal features, which shows an annual SPF of 2.78, 3.47 and 3.6 respectively for Milan, Rome and Palermo [43]. The use of the solar thermal system leads the system to higher SPF. The SFPS of the best solutions are 4.78 for Milan (Case 3), 5.14 for Rome (Case 2) and 5.52 for Palermo (Case2). With regard to the same locality, Case 3 and Case 2 systems have very close SPF. The use of a PV system has been considered to assess the final energy balance. Indeed, figure 6 shows the final energy consumption, the PV consumed, through the battery pack, and exported energy and the final energy balance, calculated as stated in (4), of the best cases of each location. As expected, going from Milan to Palermo, the produced PV energy increases. With regard to Case 1 solutions, the battery pack allows it to consume almost all the PV produced energy, reducing the energy fed into the electricity national grid. However, with regard to the SAGSHP systems (Case 2 and Case 3), the PV exported energy is less in Csa locations (Rome and Palermo) than in the Cfa. This is due to the matching of the cooling load and the PV production. The authors have also carried out simulations without the battery pack, finding that the PV exported energy is much higher than a system with battery pack. Solar energy plays a fundamental role in the SAGSHP systems. It leads to low energy consumption especially in localities reached by a lot of solar irradiance like Rome and Palermo; where the use of a PV and a small solar thermal systems create high energy savings (figure 7).

5. Conclusion

Serious environmental problems due to fossil fuel consumption are an increasing world issue. Today, efforts are being made to develop energy-efficient and environmentally friendly systems by utilising non-polluting renewable energy sources. Solar technologies play a fundamental role in achieving these goals, especially in southern European countries, such as Italy, which has been considered in this study. In particular, three different climates have been taken into account: humid subtropical climate (Cfa, in accordance with the Köppen climate classification), Mediterranean climate with mild, humid winters and hot, dry summers and hot-summer (Csa) Mediterranean climate (Csa). They refer respectively to the cities of Milan, Rome and Palermo. A promising technology is the solar assisted GSHP (SAGSHP). In such systems, the solar collectors may supply building heating energy directly, conventional operation, or loading the ground, unconventional operation.

The aim of this research is to assess the long-term performance of a SAGSHP in southern European climates for residential thermal energy supply. In particular, the final energy consumption and the seasonal performance factor (SPF) have been evaluated. Moreover, a free ground cooling (FGC) system for supplying building cooling requirement, as good practice suggests, and a PV system, as the Italian law imposes, have been considered. Furthermore, a PV system with batteries has been considered, since their usage allows higher self-consumption rates of the PV produced energy. The analysed systems configurations are listed in Table 4. It has to be mentioned that solar thermal energy has to be used only conventionally in semi-arid climates (Rome and Palermo). Results show that in Milan almost the whole building cooling demand is satisfied by the FGC, while in the other cities it has not been used. Only in Rome does the FGC fraction assume 40% for the Case 1 system and very small values during the transitional months for the Case 2 system. The lowest energy consumption is achieved by the Case 3 solution in Milan and by the Case 2 solution in both Rome and Palermo. Moreover, with regard to the Case 3 solution in

Milan, it is extremely important to find a good balance between solar conventional and unconventional operations to have high FGC fraction and SF. Indeed, the optimum controlling temperature difference has been set to 29 °C. On the other hand, the use of low controlling temperature difference values causes a lower FGC fraction, since more solar thermal energy is driven into the ground. GSHPs are able to reach higher values of SPF in both Csa and Cfa climates than an air-to-water heat pump. As expected, going from Milan to Palermo, the produced PV energy increases. With regard to Case 1 solutions, the battery pack allows it to consume almost all the PV produced energy, reducing the energy fed into the electricity national grid. However, with regard to the SAGSHP systems (Case 2 and Case 3), the PV exported energy is less in Csa locations (Rome and Palermo) than in the Cfa one. This is due to the matching of the cooling load and the PV production. Finally, the use of SAGSHP with PV system show a final energy balance (4), of 12.42 kWh/m², 7.29 kWh/m² and 5.79 kWh/m² respectively for Milan, Rome and Palermo.

6. Nomenclature

Symbols

E_{aux} [kWh]	auxiliary heater consumption
E_{GSHP} [kWh]	GSHP energy consumption
E_{P1} [kWh]	solar circulation pump energy consumption
E_{P2} [kWh]	solar boost pump energy consumption
E_{P3} [kWh]	GSHP - BHE circulation pump energy consumption
E_{P4} [kWh]	FGC - BHE pump energy consumption
E_{TOT} [kWh]	total energy consumption
EER	energy efficiency ratio [-]
FGC	free ground cooling
GSHP	ground source heat pump
PER	primary energy ratio [-]
Q_{DHW} [kWh]	DHW supplied energy
$Q_{heating}$ [kWh]	heating supplied energy
Q_{sc} [kWh]	space cooling supplied energy

Q_{SH} [kWh]	space heating supplied energy
Q_{sol} [kWh]	solar hot tank supplied energy
Q_u [kWh]	useful supplied energy
Q_{FGC} [kWh]	FGC supplied energy
SAGSHP	solar assisted ground source HP
SAGSHP_C	ground source HP with solar thermal system used only for building heating energy (conventional operation)
SAGSHP_U	ground source HP with solar thermal system used for building heating energy and for loading the ground (unconventional).

7. References

- [1] Directive 2010/31/EU of the European Parliament and of the council of 19 May 2010 on the energy performance of buildings.
- [2] Solar Thermal Markets in Europe. 2013. European Solar Thermal Industry Federation (ESTIF). <http://www.estif.org>;
- [3] European Solar Thermal Industry Federation. 2014. Brussels–Belgium. <http://www.estif.org/>;
- [4] Italian Ministry of Economic Development. 2011. Dlgs 3 marzo 2011, n. 28. Attuazione della direttiva 2009/28/CE sulla promozione dell'uso dell'energia da fonti rinnovabili, recante modifica e successiva abrogazione delle direttive 2001/77/CE e 2003/30/CE.
- [5] Wikipedia. Köppen climate classification. Accessed 2014, http://en.wikipedia.org/wiki/K%C3%B6ppen_climate_classification;
- [6] Abdeen Mustafa Omer. 2008. "Ground-source heat pumps systems and applications." *Renewable and Sustainable Energy Reviews* 12 (2): 344-371.
- [7] Erhan Pulat, Salih Coskun, Kursat Unlu, Nurettin Yamankaradeniz. 2009. "Experimental study of horizontal ground source heat pump performance for mild climate in Turkey." *Energy* 34 (9): 1284-1295.
- [8] Kadir Bakirci. 2010. "Evaluation of the performance of a ground-source heat-pump system with series GHE (ground heat exchanger) in the cold climate region." *Energy* 35 (7):3088-3096.
- [9] Christopher J. Wood, Hao Liu, Saffa B. Riffat. 2010. "An investigation of the heat pump performance and ground temperature of a piled foundation heat exchanger system for a residential building." *Energy* 35 (12): 4932-4940.
- [10] X. Yu, R.Z. Wang, X.Q. Zhai. 2011. "Year round experimental study on a constant temperature and humidity air-conditioning system driven by ground source heat pump". *Energy* 36 (2): 1309-1318.
- [11] Wei Yang. 2013. "Experimental performance analysis of a direct-expansion ground source heat pump in Xiangtan, China". *Energy* 59: 334-339.
- [12] Kadir Bakirci, Derya Colak. 2012. "Effect of a superheating and sub-cooling heat exchanger to the performance of a ground source heat pump system." *Energy* 44 (1): 996-1004.
- [13] Kojo Atta Aikins, Jong Min Choi. 2012. "Current status of the performance of GSHP (ground source heat pump) units in the Republic of Korea." *Energy* 47 (1): 77-82.
- [14] Stuart J. Self, Bale V. Reddy, Marc A. Rosen. 2013. "Geothermal heat pump systems: Status review and comparison with other heating options." *Applied Energy* 101: 341-348.
- [15] Omer Ozyurt, Dundar Arif Ekinci. 2011. "Experimental study of vertical ground-source heat pump performance evaluation for cold climate in Turkey." *Applied Energy* 88 (4): 1257-1265.
- [16] Onder Ozgener. 2010. "Use of solar assisted geothermal heat pump and small wind turbine systems for heating agricultural and residential buildings." *Energy* 35 (1): 262-268.
- [17] Yuehong Bi, Tingwei Guo, Liang Zhang. 2004. "Solar and ground source heat-pump system." *Applied Energy* 78 (2): 231-245.
- [18] X.Q. Zhai, M. Qu, X. Yu, Y. Yang, R.Z. Wang. 2011. "A review for the applications and integrated approaches of ground-coupled heat pump systems." *Renewable and Sustainable Energy Reviews* 15 (6): 3133-3140.
- [19] Onder Ozgener, Arif Hepbasli. 2007. "A review on the energy and exergy analysis of

- solar assisted heat pump systems." *Renewable and Sustainable Energy Reviews* 11 (3): 482-496.
- [20] Xiao Wang, Maoyu Zheng, Wenyong Zhang, Shu Zhang, Tao Yang. 2010. "Experimental study of a solar-assisted ground-coupled heat pump system with solar seasonal thermal storage in severe cold areas." *Energy and Buildings* 42 (11): 2104-2110.
- [21] R. Yumrutaş, M. Ünsal. 2000. "Analysis of solar aided heat pump systems with seasonal thermal energy storage in surface tanks." *Energy* 25 (12): 1231-1243.
- [22] Chen Xi, Yang Hongxing, Lu Lin, Wang Jinggang, Liu Wei. 2011. "Experimental studies on a ground coupled heat pump with solar thermal collectors for space heating." *Energy* 36(8): 5292-5300.
- [23] Carla Montagud, José Miguel Corberán, Félix Ruiz-Calvo. 2013. "Experimental and modeling analysis of a ground source heat pump system." *Applied Energy* 109: 328-336.
- [24] V. Trillat-Berdal, B. Souyri, G. Fraisse. 2006. "Experimental study of a ground-coupled heat pump combined with thermal solar collectors." *Energy and Buildings* 38 (12): 1477-1484.
- [25] Enyu Wang, Alan S. Fung, Chengying Qi, Wey H. Leong. 2012. "Performance prediction of a hybrid solar ground-source heat pump system." *Energy and Buildings* 47: 600-611.
- [26] Huajun Wang, Chengying Qi. 2008. "Performance study of underground thermal storage in a solar-ground coupled heat pump system for residential buildings." *Energy and Buildings* 40 (7): 1278-1286.
- [27] Xi Chen, Hongxing Yang. 2012. "Performance analysis of a proposed solar assisted ground coupled heat pump system." *Applied Energy* 97: 888-896.
- [28] Renato M. Lazzarin. 2012. "Dual source heat pump systems: Operation and performance." *Energy and Buildings* 52: 77-85.
- [29] Francesco Reda, Ari Laitinen. 2015 "Different strategies for long term performance of SAGSHP to match residential energy requirements in a cold climate." *Energy and Buildings* 86: 557-572
- [30] S.A. Klein, et al. 2009-2012. TRNSYS—A Transient Systems Simulation Program, Version 17.1, Solar Energy Laboratory, University of Wisconsin-Madison
- [31] Norma UNI EN ISO 6946, Resistenza termica e trasmittanza termica. Metodo di calcolo, 2007. UNI — Ente Nazionale di Unificazione, Milano;
- [32] UNI 11300 – Parte 1: "Determinazione del fabbisogno di energia termica dell'edificio per la climatizzazione estiva ed invernale", (2008). UNI — Ente Nazionale di Unificazione, Milano;
- [33] DPR 59/09. Decree of the Italian President n°. 59 issued on 2 June 2009;
- [34] Lazzarin R. 1981. Sistemi solari attivi – Manuale di calcolo, Franco Muzzio & C. editore, Padova
- [35] TRNSYS 17. 2012. TRNbuild and multi-zone building modelling. TRNSYS 17 Manual Vol. 5
- [36] Meteonorm. METEOTEST. Bern, Switzerland. <http://meteonorm.com/products/meteonorm/database/>;
- [37] Daikin Europe N.V. Oostende, Belgium. <http://it.rotex-heating.com/professionisti/documentazione-tecnica/attuale/solaris.html>;
- [38] Cordivari srl. Morro D'Oro (TE), Italy. <http://www.cordivari.it/>;
- [39] Philippe M., Bernier M., Marchio D. 2010. "Sizing Calculation Spreadsheet Vertical Geothermal Borefields." *Ashrae Journal* 52(7): 20-28;
- [40] TESS, TRNSYS17, Thermal Energy System Specialist, LLC. <http://www.trnsys.com/tess-libraries/>;
- [41] Glen Dimplex Deutschland GmbH, Kulmbach, GERMANY. <http://www.dimplex.de>;
- [42] David Banks. 2012. Introduction to Thermo-geology: Ground source heating and cooling. John Wiley & Sons Ltd, Oxford;
- [43] Francesco Madonna, Francesca Bazzocchi. 2013. "Annual performances of reversible air-to-water heat pumps in small residential buildings." *Energy and Buildings* 65: 299-309.

Energy consumption of buildings and occupant behavior. An investigation in Mediterranean climatic conditions

**Piero Bevilacqua - Department of Mechanical, Energy and Management Engineering (DIMEG),
University of Calabria, Italy - piero.bevilacqua@unical.it**

**Cristina Carpino - Department of Mechanical, Energy and Management Engineering (DIMEG), University
of Calabria, Italy - cristina.carpino@unical.it**

**Dafni Mora - Department of Mechanical, Energy and Management Engineering (DIMEG), University of
Calabria, Italy - dafni.mora@unical.it**

**Marilena De Simone- Department of Mechanical, Energy and Management Engineering (DIMEG),
University of Calabria, Italy - marilena.desimone@unical.it**

Abstract

The article illustrates the results of a study regarding occupancy profiles and energy needs of residential buildings located in a Mediterranean climate (southern Italy). Different parameters are collected by using surveys: data from bills, characteristics of buildings, family composition and practices, heating, cooling and DHW systems, control strategies. The data processing is used in order to identify occupancy scenarios and representative case studies. The influence of the occupancy profiles on thermal performances of selected buildings is investigated by energy simulations comparing thermal losses and gains obtained by means of the application of Standard procedures contained in UNI/TS 11300-1 and real patterns. Heating energy needs and comfort parameters are studied considering the variables influenced by occupant behavior: set point temperature, ventilation, lighting, appliances and shading systems.

1. Introduction

An integrated building design process needs the analysis of the interactions of all building components and external factors on the energy demand: location, building envelope, heating, ventilation, air conditioning, lighting systems, appliances. In particular, it is difficult to predict the energy consumption patterns in residential buildings, considering that they depend on the cost

of energy, gender, age, employment, family size, socio-cultural belonging, etc (Steemers and Yun, 2009). The effect of occupant behavior on building energy consumption was examined by many researchers. The results come to a consensus that the occupant behavior has a large influence on the indoor environment and energy demands. Studies in the USA and the Netherlands have determined that building characteristics explain only from 40 to 54% of variation in energy use (Guerra-Santin, 2010). Investigations conducted in China reveal that socio-economic and behavior variables are able to explain 28.8% of the variation in heating and cooling energy consumption (Chen et al., 2013).

The control of indoor conditions, such as ventilation and air temperature, has a strong effect on the interaction between the household and the dwelling. In fact, buildings usually do not perform as predicted, even when very sophisticated energy simulation methods are used. For this reason accurate use profiles should be introduced in energy calculations and simulation programs to deliver more accurate energy performances (Motuziene and Vilutiene, 2013). This means that use profiles of HVAC systems, domestic hot water systems and electricity have to be known. Hetus (Harmonised European Time Use Survey) provides statistical data of people's use of time in different European countries. The data analysis shows that there are differences in time spent for different activities depending on culture. In addition, there is the

dependency on the climate zone. For example, in the southern part of Europe, people spend more time eating and for leisure purposes compared to the north. In different countries, inhabitants behave differently and this aspect has to be taken into account when predicting the building energy demand by means of simulation tools. In (de Meester et al., 2013) the influence of family size, control of the heating system and management of the heated area on the heating loads of a standard dwelling in Belgium is investigated. Simulations of the building with different insulation levels showed that the impact of internal gains (occupant's lifestyle) on energy consumption is more significant for the case with better thermal insulation. In (Deurinck et al., 2012) the effect of building retrofit taking into account different occupancy patterns is analyzed and the gap between predicted and actually achieved energy saving is correlated to the indoor temperature take back.

The aim of this article is to investigate the influence of building occupancy on the prediction of energy needs and comfort conditions of residential buildings in Mediterranean climate conditions. The study is carried out by using data collected by surveys and energy simulation of representative case studies. The data processing is used to identify reference construction types, family compositions and occupancy profiles. The influence of occupant behavior on energy performances is investigated by simulations using DesignBuilder, which is an interface of simulation engine EnergyPlus (DesignBuilder, 2014).

2. Data collection

The study focuses on residential buildings and the sources of information are questionnaires, energy bills and statistical data. The collection activity started in 2012, the participants were the families of engineering students at the University of Calabria. The investigated area is the Calabria region located in southern Italy with a population of about 2 million. In total, 111 households were interviewed, obtaining 98 available ones, with a response rate of 88%. The survey consists of 63 questions divided in six groups of parameters:

general information, energy consumptions, conditioning and DHW, appliances, occupant behaviors and renewable energy systems. With the aim of determining the characteristics of the building stock and occupancy profiles, the paper presents a partial elaboration of the entire available data, in particular of:

- 1) parameters describing physical characteristics of dwellings;
- 2) climatic conditions;
- 3) family information;
- 5) heating system;
- 6) daily routine about the use of heating system, windows, lighting, shutters, sunshades.

In order to know if the data set is representative of the population, it was compared with data provided by the National Institute of statistics (Istat, 2014). The average age of the respondents was 36.9 years in accordance with the average age of population of 42.9 years. The gender distribution in the data set was 46.3% males and 53.7% females, in good accordance with the regional repartition, 48.7% males and 51.3% females. 53.8% of responses stated a family income of lower than 30,000 euro, and the average regional value is €23,995. The average annual household electricity consumption is 2,509 kWh for the Calabria region comparable with 2,733 kWh of the data set.

3. Data presentation and analysis

The data regarding general information of the sample are reported in table 1.

The mean floor area of dwellings is 140.8 m² and the majority of respondents, 55.9%, live in an apartment, 24.3% in a detached house and 7.2% in a semi-detached house.

28.8% of buildings were built before 1980 and 44.1% before 1990. With relation to the structures, 78.4% of the buildings are made of reinforced concrete and 6.3% in stone. This last typology is traditional in the considered region. Mainly windows are classified as having double-glazing with 69.4% of responses, whereas 28.6% of buildings present single glass. Considering the national classification in climatic zones, 9.5% of the cases correspond to the climate zone B, 33.3%,

46.4% and 10.7% to the climate zones C, D and E respectively.

38% of annual income is less than €30,000, 30% between €30,000 and €70,000, 30% of people did not answer, probably related to the privacy of personal information. The mean number of family members is 3.71 and, in terms of age, 53.4% of people are younger than 30 years. Table 2 shows the results regarding heating and thermal comfort.

The type of heating generation system mostly used is a wall-mounted gas boiler: 57.6%; a fire place follows with 14.4% of the responses. In relation to the fuel, 72.5% of buildings use methane, 8.8% LPG and 11.3% biomass.

Generally, occupants are satisfied with the thermal sensation.

Table 1 – General information: building characteristics, climatic conditions, family composition. N number of cases.

Variable		Responses	N	Percentage [%]
Building	Type	1. Single house	27	24.3
		2. Apartment	62	55.9
		3. Double house	8	7.2
		4. Other	1	0.9
		5. Don't answer	13	11.7
	Year of construction	1. Before 1980	32	28.8
		2. 1980 - 1990	17	15.3
		3. After 1990	49	44.1
		4. Don't know	0	0
		5. Don't answer	13	11.7
	Floor area (m ²)	1. Less than 69	9	8.1
		2. 70-100	22	19.8
		3. 101-149	36	32.4
		4. More than 150	31	27.9
		5. Don't answer	13	11.7
Structure	1. Reinforced concrete	87	78.4	
	2. Stone	7	6.3	
	3. Wood	0	0	
	4. Other	4	3.6	
	5. Don't answer	13	11.7	
Type of windows	1. Double glass	68	69.4	
	2. Single glass	28	28.6	
	3. Other	2	2.0	
	4. Don't know	0	0	
	5. Don't answer	0	0	
Climate	Climate zone / Heating degree day	1. A (less than 600)	0	0
		2. B (601-900)	8	9.5
		3. C (901-1400)	28	33.3
		4. D (1401-2100)	39	46.4
		5. E (2101-3000)	9	10.7
		6. F (more than 3000)	0	0
Family information	Age (years)	1. Less than 30	194	53.4
		2. 30-50	33	9.1
		3. 50-65 years	120	33.1
		4. More than 65	4	1.1
		5. Don't answer	12	3.3
	Gender	1. Female	182	53.7
		2. Male	157	46.3
	Total annual income (€)	1. Less than 30000	42	37.8
		2. 30000-70000	33	29.7
		3. 70000-100000	2	1.8
4. More than 100000		1	0.9	
5. Don't answer		33	29.7	

In table 3 and 4 information about occupant behavior in relation to the use of lighting and windows opening, external shutters and sunshades is shown.

Data reveal that 27% of houses have energy saving lamps, 52.3% partially use energy saving lamps.

Occupants switch lamps on when it is too dark in both the living room and bedroom and open windows at a fixed time in the morning.

The majority of buildings have external shutters used following different methods: 26.1% always open and 13.5% open at a fixed time in the living room, 18% always open and 15.3% always closed or open at a fixed time in bedrooms.

Table 2 – Heating system and thermal comfort conditions. N number of cases.

Variable		Survey responses	N	Percentage [%]
Heating	Generation system	1. Air source heat pump	3	2.5
		2. Electricity	10	8.5
		3. Wall-mounted gas boiler	68	57.6
		4. Fireplace	17	14.4
		5. Pellet	1	0.8
		6. Other	6	5.1
		7. No answer	13	11.0
	Fuel	1. Methane	58	72.5
		2. LPG	7	8.8
		3. Diesel	1	1.3
		4. Biomass	9	11.3
		5. other	1	1.3
		6. No answer	4	5
	Thermal sensation	1. Very satisfied	22	19.8
		2. It doesn't matter	12	10.8
3. Satisfied		42	37.8	
4. Not satisfied		17	15.3	
5. No answer		18	16.2	

Sunshades are not used diffusely and they are adopted both in summer and winter.

Table 3 – Daily routine of occupants, lighting and windows opening. N number of cases.

Variables		Survey responses	N	Percentage [%]
Lighting	Type of lighting	1. All are energy saving	30	27.0
		2. Some are energy saving	58	52.3
		3. No energy saving lamps	8	7.2
		4. No answer	15	13.5
	Switch lamp - Living room	1. Always switch on as long as entering the room	9	8.1
		2. When too dark	82	73.9
		3. Other	4	3.6
		4. No answer	16	14.4
	Switch lamp - Bedroom	1. Always switch on as long as entering the room	8	7.2
		2. When too dark	82	73.9
3. Other		5	4.5	
4. No answer		16	14.4	
Windows	Opening - Living room	1. Always open	18	16.2
		2. Always closed	7	6.3
		3. Open at fixed time	31	27.9
		4. Other	35	31.5
		5. No answer	20	18.0
	Time of the day it is open - Living room	1. Morning	16	69.6
		2. Afternoon	4	17.4
		3. All day	3	13.0
	Opening - Bedroom	1. Always open	11	9.9
		2. Always closed	2	1.8
		3. Open at fixed time	41	36.9
		4. Other	36	32.4
		5. No answer	21	18.9
	Time of the day it is open - Bedroom	1. Morning	27	84.4
		2. Afternoon	2	6.3
3. All day		3	9.4	

4. Occupancy profiles and cases study

The data processing evidences the characteristics of the analyzed building stock in terms of building types, climatic conditions, family composition and heating system.

In addition, representative occupants’ behaviors in managing windows and lighting are shown. In order to investigate the importance of the use of real occupancy profiles in determining energy needs by simulation, two cases study were chosen according to the results of data analysis. For both cases, dynamic calculations of heating energy need are carried out considering input data provided by the Standard UNI/TS 11300-1, with reference to the most common situation in which occupant behavior is not available, and introducing as input real modalities about occupancy, ventilation, appliances, lighting, windows components. This last analysis is possible when an accurate investigation is used. In particular, a single-family house and an apartment were analyzed. The study was carried out by comparing the results obtained adopting the Standard procedure and those based on real occupancy profiles achieved by interview.

Table 4 – Daily routine of occupants, shutters and sunshades use. N number of cases.

Variables		Survey responses	N	Percentage [%]
Shutters	Have shutters	1. Yes	69	62.2
		2. No	24	21.6
		3. No answer	18	16.2
	Opening – Living Room	1. Always open	29	26.1
		2. Always closed	12	10.8
		3. Open at fixed time	15	13.5
		4. Other	13	11.7
		5. Don't have	24	21.6
		6. No answer	18	16.2
Opening – Bedroom	1. Always open	20	18.0	
	2. Always closed	17	15.3	
	3. Open at fixed time	17	15.3	
	4. Other	12	10.8	
	5. Don't have	24	21.6	
	6. No answer	21	18.9	
Sunshades	Have sunshades	1. Yes	23	28.8
		2. No	40	50.0
		3. No answer	17	21.3
	Position related to the glazed system	1. External	19	23.8
		2. Interpane	1	1.3
		3. Internal	3	3.8
		4. Don't have	40	50.0
		5. No answer	17	21.6
	Type	1. Awning	4	5.0
		2. Venetian blind	4	5.0
		3. Brise-soleil	0	0
		4. Screen	2	2.5
		5. Shutter	12	15.0
		6. Pleated curtain	1	1.3
		7. Don't have	40	50.0
8. No answer		17	21.3	
Seasonal use	1. Only during the summer	3	3.8	
	2. Only during the winter	0	0	
	3. In winter and summer	20	25.0	
	4. Don't have	40	50.0	
	5. No answer	17	21.3	

4.1 Description of dwellings

The considered houses are situated in the climate zone C, the heating period is from 15 November to 31 March.

The climate file used for dynamic simulations was created from the data reported in the Standard UNI 10349 for the city of Cosenza (UNI 10349, 1994).

The single-family household is represented in figure 1. It was built in 1978, the external walls are in masonry without thermal insulation and the thermal transmittance is equal to 1 W/m²K.

The building consists of two floors with a net area of 134 m².

Transparent surfaces have single glazing, the frames are made of wood. The family is composed of three people and inhabited zones are located on the first floor.



Fig.1 – Single family house.

The house has seven rooms, see fig. 2, five of which are heated (living room, two bedrooms, bathroom and utility room); in the kitchen and hallway there is no control of the internal conditions.

The generator system is a wood-burning boiler fireplace and the internal air temperature is controlled by a thermostat.

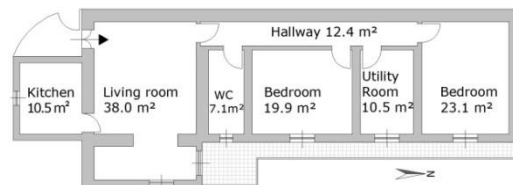


Fig. 2 – Map of the single family house.

The second case study is an apartment of 80 m², built in 2008 in reinforced concrete (see fig. 3).



Fig. 3 – Apartment in condominium.

The insulated walls have thermal transmittance of 0.6 W/m²K, windows assemble double glazing and frame with thermal break. The apartment is located

on the second floor and there is one inhabitant, the heated zones are shown in fig. 4. The heating system is autonomous with a zone thermostat and gas boiler.

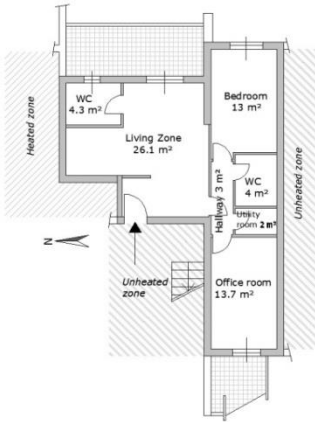


Fig. 4 – Map of the apartment.

4.2 Calculation of heating energy needs according to UNI/TS 11300-1

The heating requirement is calculated according to the type of evaluation A2 Standard (AssetRating), which allows to determine conventional energy needs, useful for comparing buildings in their actual use (UNI/TS 11300-1, 2014).

This method assumes the operation of the heating system in continuous regime and a fixed set point temperature of 20 °C. The internal heat loads are obtained by the sum of sensible contribution, calculated in relation of the floor area or equal to 450 W/m² for dwellings with floor area greater than 120 m², and latent contribution evaluated using the relation:

$$Q_{wv,int} = \frac{h_{wv} \times (G_{wv,oc} + G_{wv,A}) \times t}{3600} \quad (1)$$

where h_{wv} is the specific enthalpy of water vapor, conventionally set equal to 2544 J/gr; ($G_{wv,oc} + G_{wv,A}$) is the flow rate of water vapor due to the presence of people and equipment, mediated on time, set equal to 250 gr/h for dwellings. The total value of internal loads amounts to 4.7 W/m² for the single house and 8.1W/m² for the apartment. In DesignBuilder the “Lumped” mode was used according to which all internal gains including occupancy, equipment miscellaneous, catering process and lighting are grouped into a single value. Regarding ventilation, the Standard assumes a constant air change that includes both the effect of infiltrations, due to air

permeability of the envelope, and external flow rate provided for environmental comfort.

The air flow rate $q_{ve,k,mn}$ is calculated according to the procedure of the "Ventilation flow in reference conditions", using the equation:

$$q_{ve,k,mn} = q_{ve,0,k} \times f_{ve,t,k} \quad (2)$$

where $q_{ve,0,k}$ is the minimum amount of outdoor air, in m³/s; $f_{ve,t,k}$ is a correction factor representing the fraction of time in which the k-th air flow takes place and which considers the use profile and infiltrations that occur even when the ventilation is not operating. Its value is set at 0.60 for both the cases of study, $q_{ve,0,k}$ is evaluated using the relation:

$$q_{ve,0,k} = n \times V / 3600 \quad (3)$$

where n is the air change for hour and V is the net volume of the thermal zone, including kitchens, bathrooms, hallways and utility rooms. The flow rate obtained is equal to 0.3 ach.

In DesignBuilder the “Scheduled Natural Ventilation” mode with the outside air definition method “By zone” was adopted, which allows us to set the air changes per hour.

Table 5 summarizes the terms of the energy balance influenced by occupant behaviors and the heating energy need obtained by simulation.

In particular, thermal losses through glazed surfaces, the heat lost by natural ventilation, solar and internal gains are considered in order to quantify in a detailed way the effects of user profiles.

Table 5 – Standard procedure application. Seasonal energy contributions and heating need.

	Glazing [kWh/m ²]	Natural Ventilation [kWh/m ²]	Solar gains [kWh/m ²]	Internal loads [kWh/m ²]	Heating [kWh/m ²]
Single house	-13.4	-9.2	10.3	14.2	48.4
Apartment	-8.0	-9.7	7.0	26.6	16.5

For the single house, the thermal losses through the windows represent the main negative contribution, solar gains and internal loads are comparable. The heating energy need is 48.4 kWh/m².

For the apartment, the evaluated energy performance is 16.5 kWh/m² and is influenced in a large amount by the internal loads that are about triple if compared with the other energy inputs.

4.3 Heating energy needs according to the actual use of dwellings

In the single house, the heating system is switched on from 8:00 to 23:00 during the day and the set point temperature is 20°C.

Internal gains of occupants, equipment and lighting were defined by schedules in order to specify use time-profiles in each zone.

The presence of occupants was detailed considering the sensible and latent thermal loads related to the specific activity (AICARR, 2005). Table 6 shows the occupancy profiles set in Design Builder.

Knowing the electrical power of each appliance, the corresponding thermal power and the hourly usage, the thermal power per unit area was calculated. Table 7 shows the equipment schedule. Also for the lighting, operating schedules were created and its thermal input was calculated taking into account that 75% of the electric power is converted into thermal power (see table 8).

Table 6 – Occupancy profile for the single-family house.

Room	Hours	Occupants	Occupant density [person/m²]	Thermal load [W/person]
Kitchen	3	3	0.28	132
	1	2	0.19	
	2	1	0.09	
	18	0	0	
Living room	2	3	0.08	116
	1	2	0.05	
	21	0	0	
Bathroom	3	1	0.14	132
	21	0	0	
Bedroom	18	1	0.05	97
	6	0	0	
Bedroom	8	2	0.09	97
	1	1	0.04	
	15	0	0	

Table 7 – Equipment schedule for the single-family house.

Room	Appliance	Electric power [W]	Thermal Power [W]	Days of operation per week	Hours of operation per day	Average hourly power [W/m²h]
Kitchen	Refrigerator	180	90	7	24	8.5
	Freezer	110	55	7	24	5.2
Living room	Tv	87	78	7	4	0.34
Bathroom	Washing machine	800	160	1	1	0.94
	Boiler	1200	240	1	1	1.42
Bedroom	Pc	65	58	7	8	0.97
Utility room	Iron	800	400	1	0.3	0.45

Table 8 – Lighting schedule for the single-family house.

Room	Usage per day [h]	Electric power [W]	Thermal power [W/m²]
kitchen	1	36	2.6
Living room	0	92	1.8
Bathroom	2	44	4.7
Bedroom	1	27	0.9
Utility room	1	18	1.3

Air changes were treated by adopting the “Calculated Natural Ventilation” mode that allows us to determine the airflow between internal and external environment, according to the building orientation and wind exposure, envelope air permeability and windows openings.

Generally, windows are opened every morning from 8:00 to 9:00 and one hour after midday. External shutters operate during the night in order to reduce heat losses.

A similar approach was used in order to create using profiles for the apartment.

Tables 9–11 summarize occupancy, equipment and lighting schedules.

Table 9 – Occupancy profile for the apartment.

Room	Hours	Occupants	Occupant density [person/m²]	Thermal load [W/person]
Living zone	5	1	0.04	116
Bathroom 1	2	1	0.25	132
Bedroom	9.5	1	0.08	97
Utility room	0.5	1	0.50	116
Office room	0.5	1	0.07	116
Hallway	0.5	1	0.33	116
Bathroom 2	0	1	0.00	0

Table 10 – Equipment schedule for the apartment.

Room	Appliance	Electric power [W]	Thermal Power [W]	Days of operation per week	Hours of operation per day	Average hourly power [W/m²h]
Living zone	Microwave	1200	600	7	0.5	0.48
	Refrigerator	180	90	7	24	3.44
	TV	150	135	7	2	0.43
	DVD	40	36	1	2	0.02
	Iron	800	400	1	1	0.09
Bathroom 1	Hairdryer	2000	1900	2	0.5	1.41
Utility room	Washing machine	1850	370	1	3	3.30
Office room	PC	55	49.5	2	2	0.04

Table 11 – Lighting schedule for the apartment.

Room	Usage per day [h]	Electric power [W]	Thermal power [W/m²]
Living zone	4	142,5	5.45
Bathroom 1	2	18,75	4.69
Bedroom	1	60	4.62
Utility room	0,5	52,5	26.25
Office room	0,5	60	4.37
Hallway	0,5	30	10.00

The heating system operates from 18:00 to 23:00 and the indoor air temperature is set to 22°C.

Windows are opened in the living room and bedroom for one hour in the morning, sunshades

are activated in the bedroom and office room all day. In table 12, the results obtained by energy simulation of both the cases study are summarized. The use of real occupancy profiles for the single house determines a substantial increase in the energy need, equal to 61%, with respect to the value obtained by application of the Standard calculation. Fundamentally, this result is a consequence of the considerable increment of the thermal losses by natural ventilation.

In fact, the adoption of real scenarios in windows opening increases the air changes from 0.3 ach to 1.28 ach.

Table 12 – Real occupancy profile application. Seasonal energy contributions and heating need.

	Glazing [kWh/m ²]	Natural Ventilation [kWh/m ²]	Solar gains [kWh/m ²]	Internal loads [kWh/m ²]		
				Lighting	Equipment	Occupancy
Single house	-11.4	-46.3	10.3	0.8	5.9	6.8
Apartment	-6.2	-8.0	5.7	1.5	6.2	3.1
Heating [kWh/m ²]						
Single house	77.8					
Apartment	20.9					

The application of actual schedules regarding shutter use and internal loads determines moderate changes in comparison to the results provided by the Standard.

The heat losses through the windows record a reduction of 15%, for internal loads the reduction is 5%. Occupancy contributes for 50% to the internal gains.

For the apartment, the heating energy need is subjected to an increase of 27% due to a significant reduction of internal loads equal to 60%.

In this dwelling, equipment contributes for the most part to internal gains. The usage of sunshades determines a reduction of 23% in heat losses and of 19% in solar gains through the glazed surfaces.

Air changes increase from 0.3 ach to 0.33 ach, but thermal losses by ventilation report a reduction as window opening takes place when the heating system is switched off.

Occupant behavior influences both energy needs and the quality of indoor environments.

In tables 13 and 14 the thermal comfort conditions for the single house and the apartment respectively are shown.

Discomfort time represent the percentage of time when both the humidity ratio and operative temperature do not respect the ASHRAE 55 comfort criteria.

Furthermore, discomfort time percentage calculated with respect to the occupation time is marked for each room.

Table 13 – Single house, predicted mean vote (PMV) and discomfort hours for the occupied periods.

Zone	PMV	Discomfort (h)	Discomfort time (%)
Bedroom	-1.76	2210.3	90
Bathroom	-0.31	343.7	84
Double room	-1.92	1141.1	93
Kitchen	-0.91	715.9	88
Living Room	-0.90	387.6	95

Table 14 – Apartment, predicted mean vote (PMV) and discomfort hours for the occupied periods.

Zone	PMV	Discomfort (h)	Discomfort time (%)
Bathroom 1	-0.69	137.5	51
Hall way	-1.10	30.8	45
Bedroom	-2.64	1009	78
Utility room	-1.07	30.0	44
Office room	-1.11	35.0	51
Living Room	-1.47	369.7	54

For the single house, 90% of the time spent in the bedroom is characterized by discomfort conditions and thermal sensations of cool, in the apartment the hours of discomfort are 78% of the total. For both the cases of study, the comfort analysis reveals a thermal sensation of slightly cool in the majority of the heated zones.

5. Conclusions

Data collected by surveys were processed in order to identify the main characteristics of residential buildings located in southern Italy. Two representative cases study were selected and the influence of occupancy profiles on energy simulation results was analyzed.

In particular heating energy needs have been obtained by DesignBuilder using the calculation

procedure of the UNI/TS 11300-1 Standard regarding occupancy and ventilation and by application of real use profiles summarized in schedules.

The results of the energy simulation show the importance of occupancy contribution on the final thermal performance of dwellings.

For the single-family house, window opening has the most important role and determines an increase of 61% in energy demand when real profiles are applied.

The application of the standard procedure for the apartment causes the overestimation of internal loads and the energy need increases of 27% in actual usage conditions.

In addition, internal comfort quality is related to daily routine of inhabitants. For both the cases under study, thermal sensations of slightly cool are reported in the heated zones.

References

- AICARR, Miniguida (2005). Servizi Grafici Editoriali, Padova
- Chen, J., Wang, X., & Steemers, K. (2013). A statistical analysis of a residential energy consumption survey study in Hangzhou, China. *Energy and Buildings*, 66, 193–202. doi:10.1016/j.enbuild.2013.07.045
- De Meester, T., Marique, A.-F., De Herde, A., & Reiter, S. (2013). Impacts of occupant behaviours on residential heating consumption for detached houses in a temperate climate in the northern part of Europe. *Energy and Buildings*, 57, 313–323. doi:10.1016/j.enbuild.2012.11.005
- DesignBuilder Software Ltd. (2014). DesignBuilder Tutorials. <http://www.designbuilder.co.uk/>
- Deurinck, M., Saelens, D., & Roels, S. (2012). Assessment of the physical part of the temperature takeback for residential retrofits. *Energy and Buildings*, 52, 112–121. doi:10.1016/j.enbuild.2012.05.024
- Guerra-Santin, O. (2010). Actual energy consumption in dwellings -The effect of energy performance regulations and occupant behaviour. IOS Press, Amsterdam.
- Hetus (Harmonised European Time Use Survey). <https://www.h2.scb.se/tus/tus/Default.htm>
- Istat - Istituto nazionale di statistica. (2014). I.Stat. Italy. Retrieved September 10, 2014, from <http://www.istat.it/it/>
- Motuziene, V., & Vilutiene, T. (2013). Modelling the Effect of the Domestic Occupancy Profiles on Predicted Energy Demand of the Energy Efficient House. In 11th International Conference on Modern building materials, structures and techniques, MBMST (Vol. 57, pp. 798–807). Elsevier B.V. doi:10.1016/j.proeng.2013.04.101
- Steemers, K., & Yun, G. Y. (2009). Household energy consumption: a study of the role of occupants. *Building Research & Information*, 37(5-6), 625–637. doi:10.1080/09613210903186661
- UNI 10349 (1994), Heating and cooling of buildings. Climatic data. Italy.
- UNITS 11300-1 (2014), Energy performance of buildings. Part 1: Determination of the thermal energy demand of the building for air conditioning in summer and winter. Italy.

Energy retrofit and conservation of built heritage using multi-objective optimization: demonstration on a medieval building

Francesca Roberti – EURAC research - Free University of Bolzano/Bozen – francesca.roberti@eurac.edu

Ulrich Filippi Oberegger – EURAC research – ulrich.filippi@eurac.edu

Elena Lucchi – EURAC research – elena.lucchi@eurac.edu

Andrea Gasparella – Free University of Bolzano/Bozen – andrea.gasparella@unibz.it

Abstract

Energy retrofit of historic buildings is a complex activity, which requires a multidisciplinary approach. Interventions should limit energy consumption, consider users' comfort and preserve cultural and aesthetic values. While the impacts of interventions on energy performance and comfort can be quantified in advance using simulation software, conservation aspects are less tangible. In this paper, we propose a method to identify retrofit strategies that are optimal from an energy, comfort and conservation point of view. The first step is to choose a set of interventions and conservation aspects to consider. This requires a multidisciplinary team of experts. Next, quantitative metrics for assessing energy performance, comfort and conservation are defined. Through a multi-objective optimization, the combinations of interventions that yield the best tradeoffs among these objectives are found. We demonstrate the method on a calibrated EnergyPlus model of the "Waaghaus" (weigh house), a medieval building in Bolzano located in the north of Italy. The aim is to transform this currently vacant building into a cultural center. We considered the following interventions: external and internal envelope insulation with varying materials and thicknesses, airtightness improvements, replacement of windows and summer ventilation availability. Conservation aspects taken into account were visual, physical and spatial impact of the interventions on the building's heritage significance. We selected the hourly sum of all sensible and latent ideal loads for heating and cooling over a year as energy performance metric. All internal loads were modelled according to the planned future use of the building. We assigned a score to each intervention equal to the number of conservation aspects met. The yearly average of the absolute values of the predicted mean vote was used as a proxy for comfort. We performed the multi-objective optimization with the C code NSGA-II,

which implements a genetic algorithm based on non-dominated sorting. As a result, we obtained solutions with an absolute mean PMV of 0.5, an annual ideal load for heating and cooling of 20 kWh/m² and a good level of conservation.

1. Introduction

The European building sector has a consistent number of historic buildings that can significantly affect the urban settlement. A substantial share of the European stock is older than 50 years with many buildings in use today that are hundreds of years old (European Commission, 2006). The potential for saving energy and reducing CO₂ emissions in existing buildings is high. For this reason, the European Commission has decided to develop a specific legislative framework in order to cut CO₂ emissions (Directives 2002/91/CE and 2010/31/UE), to increase the share of renewable sources (Directive 2009/28/CE) and to enhance the energy performance of existing buildings (Directive 2012/27/UE) by 2020. Many of these measures also affect the cultural heritage buildings that consume lots of energy (Mazzarella, 2014, De Santoli, 2014). Improving the energy efficiency and comfort in historic buildings, while simultaneously preserving and promoting the value and the historical character, is viable only by balancing the requirements of cultural protection, indoor comfort and energy efficiency. Only in this way is it possible to minimize the aesthetic, physical and visual impact of the energy efficiency measures on the conservation aspects (European Projects

3ENCULT, EFFESUS, Sechurba, New4Old, Co2oBricks).

This work presents a method for optimizing retrofit solutions for historic buildings in order to improve their energy performance and internal comfort, and to preserve their cultural value.

For this purpose we developed a methodology based on the following steps:

- selection of a general set of energy retrofit for historic buildings, considering conservation aspects, energy performance and comfort;
- evaluation of the conservation impact on each retrofit measure;
- quantification of energy consumption and comfort using a dynamic simulation model;
- definition of the combinations of interventions that yield the best tradeoffs between these objectives, through a multi-objective optimization.

This method has been applied to the “*Waaghaus*” (German for “weigh house”), a medieval building located in the historic center of Bolzano, a city in the north of Italy. It represents a typical historic Tyrolean building, 4 with floors and basement in stone and a wooden roof. It is one of the case studies of the FP7 European project 3ENCULT (Efficient Energy for EU Cultural Heritage). This allowed us to conduct a series of diagnostic and energy modelling activities in order to acquire a deeper knowledge of the energy performance of the building. In particular, a calibrated EnergyPlus model has been realized to quantify the energy consumptions in detail with the objective to define the most appropriate interventions. With this model, a multi-objective optimization has been carried out using the genetic algorithm NSGA-II in order to identify the optimal solutions as regards energy consumption, compatibility with conservation and comfort.

2. Methodology

2.1 The case study

The “*Waaghaus*” was built at the end of the twelfth century and formed part of the first nucleus of the city centre. Until 1780, the building accommodated

the *Fronwaage*, an officially calibrated public set of scales. Afterwards it was used for commercial and residential purposes. By the 1990s, the house was no longer in use.

The “*Waaghaus*” has all floors and the cellar built in masonry composed of natural stone with lime mortar joints. Exterior walls have a thickness of about 60 to 80 cm. Except for the basement, the stonework on both sides of the walls is mostly covered with historic lime plaster, and in parts with wall paintings and frescoes that should be preserved. Most of the original windows were replaced by box-type windows in the 1950s/60s ($U_g=5.8 \text{ W/m}^2\text{K}$; $U_w=2.7 \text{ W/m}^2\text{K}$) that are now heavily damaged and dirty. The building has a saddle roof with wooden rafters and casing, a roofing cardboard (bitumen) on the wooden casing, and above it a tile cladding. In its current state, it is partially insulated with 8 cm of mineral wool between the rafters covered with gypsum plasterboard.



Fig. 1 The Waaghaus in Bolzano (© Florian Berger/EURAC)

2.2 Selection of the retrofit interventions

The retrofit solutions considered are commonly used for historic buildings to balance conservation aspects, comfort, and energy performance (Changeworks, 2008; English Heritage, 2008; SPAB, 2014). We focused mainly on passive solutions for the building envelope. The interventions encompass: airtightness improvements, exterior walls insulation, whole window or pane replacement, roof insulation, and the installation of a mechanical cooling system. We did not consider floor and ceiling insulation due to the technical difficulties in applying it to vaults and decorated

ceilings. For the exterior walls and the roof, we considered both exterior and interior insulation applied either to all surfaces or only to surfaces without any historic significance (surfaces without frescos or visible parts of historic value).

For the external insulation, we chose between permeable (rock wool $\lambda=0.038$ W/mK; expanded cork $\lambda=0.043$ W/mK) and impermeable (calcium silicate $\lambda=0.076$ W/mK) materials, with thicknesses from 10 to 20 cm. For the interior insulation, we chose between natural (rock wool $\lambda=0.038$ W/mK; expanded cork $\lambda=0.043$ W/mK) and artificial materials (aerogel $\lambda=0.013$ W/mK; capillary active insulation $\lambda=0.031$ W/mK; calcium silicate $\lambda=0.076$ W/mK), with thicknesses from 3 to 10 cm (1 cm of aerogel). To improve the performance of the roof, we considered 20 cm of rock wool or cork insulation on the outside and 10 cm of one of the above mentioned insulation materials on the inside. Two interventions were considered for the windows: pane replacements with low-e glass ($U_g=2.126$; $\tau_v=0.81$; $g=0.79$) and full window replacements with triple-glazed units ($U_g=0.57$; $\tau_v=0.68$; $g=0.56$). Both interventions were accompanied by airtightness improvements of the whole building (0.3 modelled air changes per hour). In addition, we optimized the natural ventilation air change rates and the minimum temperature difference between the inside and the outside for which natural ventilation was active, in order to investigate if comfort could be reached also without a mechanical cooling system. The air change rates ranged from 0.5 to 10 h⁻¹ and the temperature differences from 1 to 5 K.

2.3 Quantifying the impact of each intervention on conservation aspects

A number of studies deal with the conciliation of energy and conservation related aspects in historic building retrofits. In the EFFESUS Project (Eriksson, Hermann, Hrabovszky-horváth, & Rodwell, 2014) the intervention impact on conservation has been divided into visual, physical and spatial impact.

“Visual impact” (V) refers to the alteration of the aesthetic appearance of the building; “physical impact” (P) refers to the conservation of the original materials, and “spatial impact” (S) refers to the retention of the original shapes and dimensions. The impact of the most common energy retrofit measures on each envelope component (exterior wall, interior wall, roof, etc.) was analyzed from a conservation point of view. The Austrian Bundesdenkmalamt (Bundesdenkmalamt, 2011) presented the visual and physical impact of many types of energy retrofit, coupled with qualitative indications for energy efficiency. The Italian ENEA (Borani, Giambruno, & Garzulino, 2011) also presented indications for physical and spatial impact on conservation, energy savings, costs and durability of the retrofit interventions. All these works can be thought of as qualitative guidelines for the energy refurbishment of historic buildings. Finally, a study conducted by the Technische Universität Dresden - TUD (Grunewald, Will, & Pohl, 2010) presented more quantitative results on the compatibility of energy saving measures with conservation. Table III summarizes the most important aspects taken into account by these works.

	Conservation			Energy	Economy		Durability
	Visual	Physical	Spatial	Consumptions	Energy savings	Intervention costs	
EFFESUS	x	x	x				
BUNDESDE MALAMT	x	x		x			
ENEA		x	x	x		x	x
TUD	x	x		x	x		

Table III Results from a literature review on the impact of energy retrofit measures on the conservation of historic buildings

We decided to start from the EFFESUS approach ((Eriksson, Hermann, Hrabovszky-horváth, & Rodwell, 2014), analyzing the visual, physical and spatial impact of different energy retrofit measures on the conservation of each building component and distinguishing between exterior (roof, exterior and interior surfaces of the exterior wall, windows) and interior (ceilings, internal walls) components.

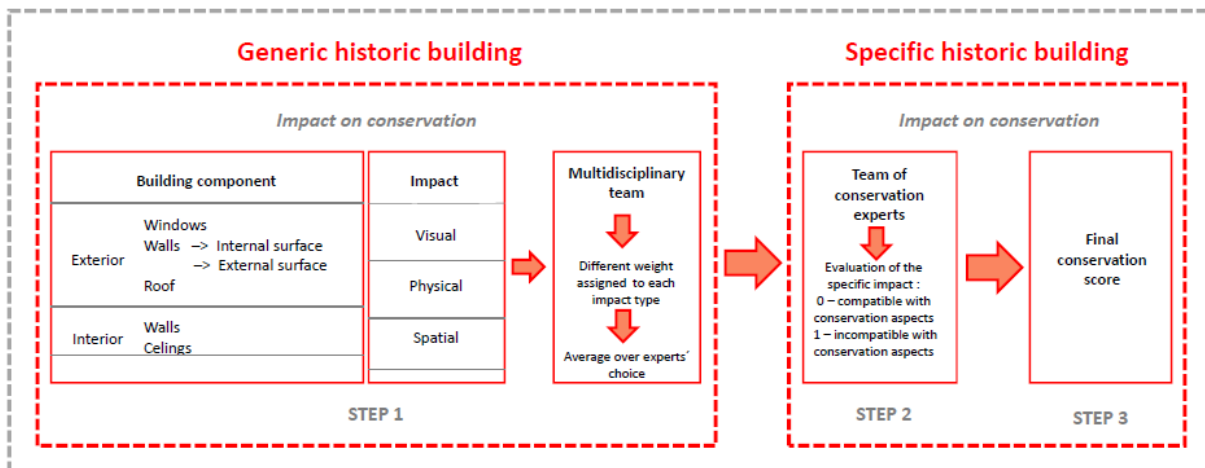


Fig. 2 – Steps to define the impact of retrofit measures on conservation

Three steps were performed to assign a conservation score to each type of impact and each type of retrofit. As a first step, a multidisciplinary team of technicians and conservation experts assigned different weights to each impact type (V, P, S) and for each considered building component. We then calculated the average of the experts' choices to take them into account in equal measure. The results of this first step are independent from the specific case study and can be applied to historic buildings in general.

As a second step, a team of conservation experts evaluated for each type of impact and each considered building component whether a retrofit intervention was compatible with conservation or not. The evaluation could thus be 0 (incompatible) or 1 (compatible). In this phase the specific characteristics of the case study (in our case the "Waaghaus") are taken into account.

The final conservation score for each retrofit intervention was calculated as the sum of the zeros and ones obtained in the second step. This means that each type of impact and building component was given equal importance. The highest conservation score (no retrofit) was 24, the lowest (all interventions) was 8. The overall methodology is sketched in Fig. 2.

2.4 Quantification of energy consumption and comfort

In order to estimate the hourly ideal heating and cooling load and the comfort, we modelled the

Waaghaus in EnergyPlus 7.2 dividing the building into 29 thermal zones. To obtain reliable results, the model was calibrated to indoor air temperatures monitored in representative zones.

In accordance with the plan to transform the building into a museum after the refurbishment, we considered all thermal zones as occupied and therefore air-conditioned except for the basement and the wings on the top floor. We modelled the internal gains as per ASHRAE Fundamentals (ASHRAE, 2009): 145 W/person (75 sensible heat; 70 latent heat), 14 m² occupied space per person (own estimation); 11.84 W/m² for lighting (57% radiant sensible heat); no other equipment; all gains active from 10:00 until 18:00. The heating system was set up with unlimited power and the cooling system as well in case the retrofit measures included the installation of a mechanical cooling system.

Setpoint and setback in winter (from 15 October to 15 April) were 20 and 16°C, respectively. The setpoint in summer (from 15 June to 15 September) was 26°C.

Overheating was prevented with an external shading system that was activated if the solar horizontal radiation exceeded 400 W/m². The outdoor conditions were taken from the Typical Meteorological Year (TMY) file for Bolzano available on the Meeonorm website (<http://meeonorm.com>).

2.5 Multi-objective optimization

Multi-objective optimization of energy models with the purpose to find optimal tradeoffs between

energy savings and costs is quite in use (Chantrelle et al., 2011; Hamdy, Hasan, & Siren, 2011; Murray, Walsh, Kelliher, & O'Sullivan, 2014). In this work, we propose to consider within this framework also the compatibility with conservation.

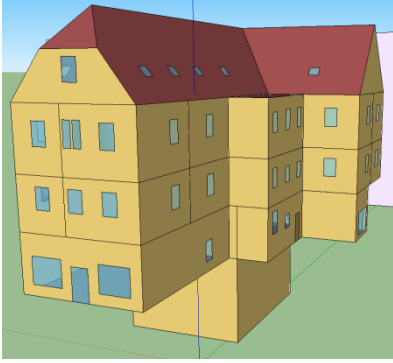


Fig. 3 – Geometry model of the *Waaghaus*

To perform an optimization simultaneously taking into account energy performance, comfort and conservation, we used the NSGA-II algorithm (Deb, Member, Pratap, Agarwal, & Meyarivan, 2002). NSGA-II is a genetic algorithm that performs a non-dominated sorting of the retrofit solutions, keeping those with the highest rank in the pool. To avoid crowding, optimal solutions which are distant from other optimal solutions are preferred. Within the pool, tournament selection, crossover and mutation operations are performed. Further, *elitism* is used to prevent the loss of optimal solutions once they have been found.

We minimized (maximized in case of the conservation score) the following objective functions:

- total annual sensible and latent ideal heating and cooling load;
- comfort, expressed as mean absolute Predicted Mean Vote (PMV) during the occupation hours, averaged over all thermal zones weighted by zone volume;
- conservation score, computed as explained in Section 2.3.

We simulated 20 generations of an evolving set consisting of 300 retrofit solutions.

3. Results and discussion

3.1 Check on the number of generations

In order to check that the number of simulated generations was necessary and sufficient, we plotted the non-dominated retrofit solution sets up to the 10th and 15th generation (Figs. 4 and 5). Fig. 6 shows the final non-dominated solutions.

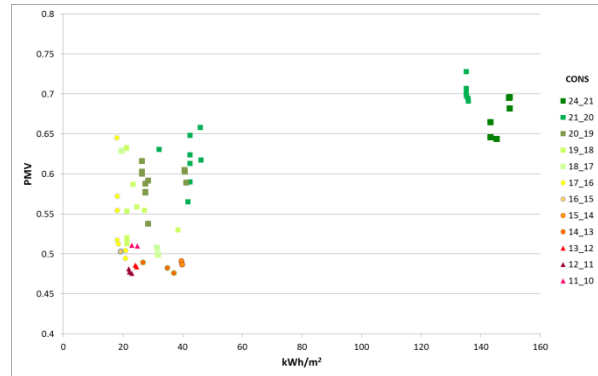


Fig. 4 – Non-dominated retrofit solutions up to the 10th generation

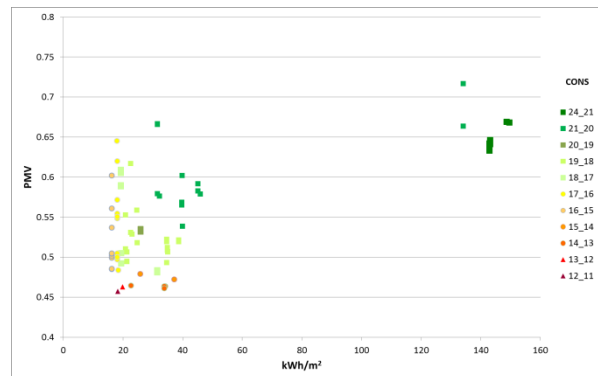


Fig. 5 – Non-dominated retrofit solutions up to the 15th generation

One expects that the number of dominated solutions is higher in the first generations and gets progressively lower thereafter. A solution is said to be dominated by another solution if the latter is better with respect to all objective functions than the former. Further, solutions should gradually move towards the theoretical Pareto front (which is the theoretical surface composed of all globally optimal solutions) and spread on it. Finally, solution sets should change less and less over time except for sporadic and random wiggling motions induced by the mutation operator. Judging from Figs. 4 to 6, the 20th generation seems to us a reasonable milestone in reaching these objectives, although one could arguably obtain improvements by simulating more generations.

3.2 Discussion on the optimal retrofit solutions

81 optimal (non-dominated) retrofit solutions were identified (Fig. 6). As all these solutions are optimal, an improvement of one performance target (energy, comfort, or conservation) is always associated with a deterioration of another performance target. Nevertheless, there can be better or worse solutions, in the sense that a slight deterioration of one target could lead to big improvements in other targets.

The retrofit solutions decompose into two clusters. The cluster on the right in Fig. 6 contains all the retrofit solutions without any intervention related to the airtightness or the windows. Whole window or pane replacements were always associated with comprehensive airtightness improvements at building level, which explains why there is such a big difference in ideal load and comfort between the two clusters.

No airtightness or fenestration provisions. The annual ideal heating and cooling load for retrofit solutions without any intervention on the airtightness or the windows is high (between 130 and 150 kWh/m²) and the discomfort as well (mean absolute PMV above 0.63), especially because of the high infiltration rate caused by the numerous cracks in the external wall and damaged windows, but the conservation score is of course excellent.

Airtightness provisions and replacement of windowpanes. Solutions where only the windowpanes were replaced are located on the left cluster, with ideal loads between 19 and 46 kWh/m², mean absolute PMVs ranging from 0.46 to 0.68, and conservation scores between 13 and 21. If insulation was applied only to surfaces without any historic value, ideal loads and mean absolute PMV were at least 40 kWh/m² and 0.52, respectively. These targets and a conservation score of 20 were reached by insulating the parts of the façade and the roof without any historic value from the outside with 20 cm expanded cork. Practically the same performance was obtained with rock wool. This is not surprising as both materials have comparable thermal properties and a lower thermal conductivity than calcium silicate. Insulating both the façade and the roof from the

inside with 3 cm of capillary active material or rock wool increased the ideal load by 5 kWh/m² compared to insulating from the outside. The lowest mean absolute PMV was 0.58. A higher comfort could be attributed to some extent to an increase in the natural ventilation rate, which varied between 2 and 10 h⁻¹. The minimum temperature difference between the inside and the outside for which natural ventilation was active ranged between 1.0 and 2.6 K.

Airtightness provisions and replacement of windows. Focusing only on retrofits where surfaces with historic value were preserved, little could be gained in terms of energy savings and comfort by replacing the whole windows instead of the windowpanes. This indicates that other factors such as infiltration play a major role. Further, the glass to wall ratio of the building is only 10%.

Façade insulation. We concentrate on retrofit solutions in which airtightness provisions were taken and all surfaces with historic value were preserved. Both external and internal insulation solutions were identified.

Façade insulation from the outside. In case of external insulation, total ideal load, mean absolute PMV and conservation score varied between 37 and 40 kWh/m², 0.52 and 0.64, and 19 and 20, respectively. A façade insulation with 10 or 20 cm rock wool applied from the outside was the preferred choice. The roof could be insulated from the outside or from the inside with rock wool or expanded cork. Mechanical cooling was switched off in all cases. Instead, cooling was provided by natural ventilation. The lower mean absolute PMVs were obtained with air change rates varying between 7 and 10 h⁻¹.

Façade insulation from the inside. Retrofits performed with 3 cm rock wool or the capillary active insulation were fairly competitive with the external insulation solutions insofar as ideal loads of 45 kWh/m² along with mean absolute PMVs of 0.58 could be reached. The conservation score was 21.

Insulation of surfaces with historic value. In order to understand what could be gained in terms of load reduction or comfort increase, we considered also retrofit solutions in which all surfaces were insulated, independent of their historic value. In case of the Waaghaus, surfaces with historic value

take up about 25% of the total available façade surface for insulation. We would like to stress that these retrofits are unacceptable, as they would definitely spoil the heritage value of the building. A solution with low ideal load and mean absolute PMV (16 kWh/m² and 0.49, respectively) was given by insulating façade and roof from the outside with 20 cm rock wool. In addition, windows were replaced. Although during the heating season the ideal heating system was switched on during opening hours, visitors of the museum were cold

(PMV lower than -0.5) approximately 40% of the time because of the low radiant temperature in the morning. This issue can be resolved by switching the heating system on a couple of hours before the museum opens. Outside the heating season, in case mechanical cooling was switched off, visitors were hot (PMV higher than 0.5) only about 20% of the time thanks to the high natural ventilation rate (9 h⁻¹). The conservation score of this solution was 16. Good tradeoffs for all the three performance targets are highlighted in Fig.6 (black circle).

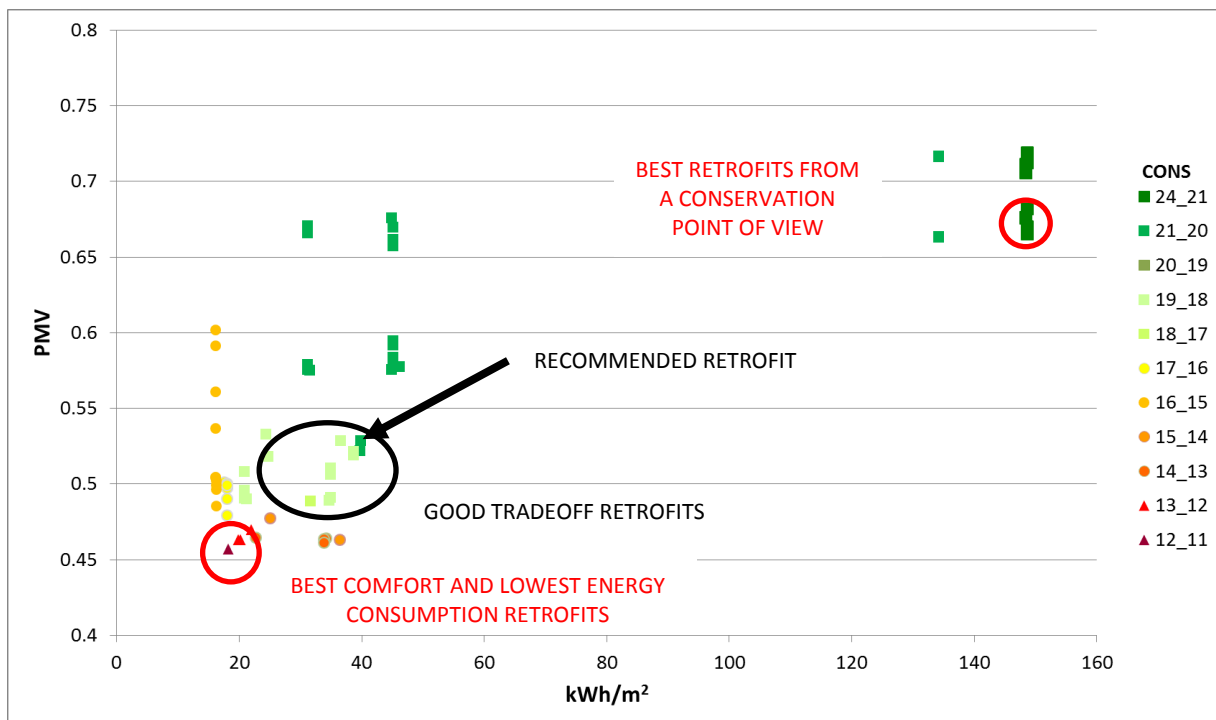


Fig. 6 – Optimal retrofit solutions up to the 20th generation

4. Conclusion

In this paper, we have presented a methodology aimed at identifying retrofits for historic buildings which are optimal in terms of three performance targets: potential energy savings, comfort, and conservation. An important step has been to assign a conservation score to each intervention, based on the opinion of technicians and conservation experts. The best trade-off retrofit solutions have been computed performing a multi-objective optimization. We have discussed different interventions and have quantified their impact on the performance targets.

Within the limitations of this study, we recommend a retrofit with an annual ideal heating and cooling load of 40 kWh/m², a mean absolute PMV of 0.52 and a conservation score of 20 out of a maximum of 24 (cf. Fig. 6). In this solution, the façade and the roof are insulated from the outside with 20 cm rock wool and 20 cm expanded cork, respectively. To reduce infiltration and further enhance the thermal performance of the façade, the building is made airtight and the windowpanes are replaced. Finally, no mechanical cooling system is provided. Instead, natural ventilation is maximized in terms of duration and air changes per hour.

Acknowledgement

“3ENCULT - Efficient Energy for EU Cultural Heritage” is receiving co-funding from the EC’s Seventh Framework Programme (FP7/2007-2013) under grant agreement n° 260162.

References

ASHRAE, (2009), *ASHRAE Handbook Fundamentals*, ASHRAE, Atlanta.

Borioni M., Giamburino M. & Garzulino A., (2011), *Studio, sviluppo e definizione di schede tecniche di intervento per l’efficienza energetica negli edifici di pregio*, ENEA, Roma.

Bundesdenkmalamt, (2011), *Richtlinie: Energieeffizienz am Baudenkmal*, Bundesdenkmalamt Hofburg, Wien.

Changeworks, (2008), *Energy Heritage. A Guide to Improving Energy Efficiency in Traditional and Historic Buildings*, Changeworks, Edinburgh.

Deb K., Member A., Pratap A., Agarwal S. & Meyarivan T., (2002), *A Fast and Elitist Multiobjective Genetic Algorithm*, in *Ieee Transactions On Evolutionary Computation*, VOL.6, NO.2, pp. 182–197.

de Santoli L., (2015), Guidelines on energy efficiency of cultural heritage, in *Energy and Buildings*, n. 86, pp.534–540, <http://dx.doi.org/10.1016/j.enbuild.2014.10.050>.

English Heritage, (2008), *Energy Conservation in Traditional Buildings*, English Heritage, London.

Eriksson P., Hermann C., Hrabovszky-Horváth S. & Rodwell D. (2014). *EFFESUS methodology for assessing the impacts of energy-related retrofit measures on heritage significance*, in Kalliopi F. & Cassar M., *The Historic Environment: Policy & Practice: Energy Efficiency and Heritage Values in Historic Buildings*, pp. 132–139.

European Commission, (2006), *Libro verde: una strategia europea per un’energia sostenibile, competitiva e sicura*, European Commission, Bruxelles.

Grunewald J., Will T. & Pohl M. (2010). *Pilotstudie zum Modellprojekt des Sächsischen Staatsministeriums des Innern: Energetische Sanierung von Baudenkmalen*.

Hermann C. & Rodwell D., (2014), *Heritage Significance Assessments to Evaluate Retrofit Impacts*, in IoA workshop "Retrofit in practice: What next?", Newcastle University, Newcastle.

Livio Mazzarella L., (2014), Energy retrofit of historic and existing buildings. The legislative and regulatory point of view, in *Energy and Buildings*, <http://dx.doi.org/10.1016/j.enbuild.2014.10>.

SPAB (2014), *Energy Efficiency in Old Buildings, The Society for the Protection of Ancient Buildings*, London.

Online resources

3ENCULT Energy Efficiency for EU cultural heritage, EU FP7 project. Accessed November 2014. <http://www.3encult.eu>

EFFESUS Energy Efficiency for EU Historic Districts’ Sustainability, EU FP7 project. Accessed November 2014. <http://www. effesus.eu>

SECHURBA Sustainable Energy Communities in Historic Urban Areas, IEE project. Accessed November 2014. <http://www.sechurba.eu>

New4Old ,New energy for old buildings , IEE project. Accessed November 2014.
<http://www.new4old.eu>.

Co2ol Bricks, Climate Change, Cultural Heritage & Energy Efficient Monuments, Baltic Sea Region Programme. Accessed November 2014.
<http://www.co2olbricks.eu>.

Legislative framework

DIRETTIVA 2002/91/CE DEL PARLAMENTO EUROPEO E DEL CONSIGLIO del 16 dicembre 2002 sul rendimento energetico nell'edilizia.

DIRETTIVA 2010/31/UE DEL PARLAMENTO EUROPEO E DEL CONSIGLIO del 19 maggio 2010 sulla prestazione energetica nell'edilizia (rifusione).

DIRETTIVA 2009/28/CE DEL PARLAMENTO EUROPEO E DEL CONSIGLIO del 23 aprile 2009 sulla promozione dell'uso dell'energia da fonti rinnovabili, recante modifica e successiva abrogazione delle direttive 2001/77/CE e 2003/30/CE.

DIRETTIVA 2012/27/UE DEL PARLAMENTO EUROPEO E DEL CONSIGLIO del 25 ottobre 2012 sull'efficienza energetica, che modifica le direttive 2009/125/CE e 2010/30/UE e abroga le direttive 2004/8/CE e 2006/32/CE.

Energy performances of a passive house for Mediterranean climate: a case study

Cristina Carpino – DIMEG, University of Calabria, Italy – cristina.carpino@unical.it

Piero Bevilacqua – DIMEG, University of Calabria, Italy – piero.bevilacqua@unical.it

Roberto Bruno, Ph.D. – DIMEG, University of Calabria, Italy – roberto.bruno@unical.it

Natale Arcuri – DIMEG, University of Calabria, Italy – natale.arcuri@unical.it

Abstract

An energetic analysis of an office building located in southern Italy and properly designed to have energy consumption almost zero, has been carried out by means of the Design Builder simulation software. The choices of opaque surfaces, glazed surfaces and appropriate external shading devices have been made to reconcile the different and conflicting needs of the investigated building. Several simulations of different opaque surfaces have allowed the choice of adequate materials for the dispersing walls, to reduce thermal losses and attenuate summer thermal waves. Glazed surfaces have been conveniently selected, to exploit their optical properties both in winter and in summer. Finally, an appropriate sizing of unmovable external shading devices has allowed the optimization of winter solar gain and the reduction of summer solar load. These choices have demonstrated that, in Mediterranean climate conditions, the design process of the building envelope follows a completely different approach compared to the method typically used for the realization of passive houses conceived for continental climates. With reference to the primary energy requirements, simulation results have been used to design a proper generation system coupled with active solar systems in order to obtain a NZEB building.

1. Introduction

The passive house can be defined as a set of technical sizing criteria, focused on the construction of a building in which the energy

consumptions are almost “zero” (Gonzalo and Vallentin, 2014). The passive house concept has been developed in the last twenty years, in order to find a solution to the increase in building energy consumptions, by means of the exploitation of particular heating and cooling plants coupled to appropriate building envelopes (Jacobson, 2014). In the Mediterranean region, the energy consumption is high in office buildings, where the summer energy requirements are usually greater than the winter energy requirement (Ferrante, 2012). Moreover, these requirements are continuously increasing due to design criteria that do not take in account the geographic context (Mlakar and Strankar, 2013). Nowadays, with reference to the first prototype built in 1990 (Van Huffelen, 1992), the passive house system has notably improved, offering evident advantages compared to traditional houses. However, designers do not take sufficiently in account that the climate characteristics of the geographical area, where the first model has been built and optimized, are typical of central Europe. Consequently, the realization of the successive passive houses are characterized by building envelopes sized mainly to provide a good behaviour for severe winter weather conditions. This local and geographical aspect results in the development of sizing procedures that considers large south-facing windows and high insulation thickness in the dispersing opaque walls.

These procedures, however, are not an ideal solution in the Mediterranean areas, where the climate conditions are markedly different from those of continental Europe. Moreover, an excessive exposure to solar radiation usually

results in an overheating of the indoor environment, also in the heating period, with a correspondent worsening of the thermal comfort. Consequently, the controversies relative to the exploitation of the standard passive houses procedures in the Mediterranean region are still much debated (Ferrante and Cascella, 2011). Nevertheless, the key concept of passive house remains valid also in Mediterranean areas and so the development of new construction techniques for new building systems, which keep the indoor air temperature comfortable both in summer and in winter, with a minimal contribution of the air conditioning plants, is requested.

In this paper, the results provided by the dynamic simulation code Design Builder have been used to evaluate the most suitable construction procedures of passive houses in Mediterranean climate conditions. With reference to an office building, a parametric study of the properties of walls and transparent surfaces and of unmovable shading systems has been carried out. Heating energy requirements are calculated supposing a 24-hour plant operation, according to the Italian regulations (DPR 59/09, 2009; DL 102/2014, 2014; EN ISO 13790, 2008).

This study has allowed the most appropriate choice of the main components, the criteria for choosing transparent surfaces and type and size of the correspondent shading systems. Finally, the energy labelling of the investigated building has been carried out, considering a generation system of the air-conditioned plant coupled with active solar systems.

2. The reference building

The investigated building is shown in Fig. 1; it consists of an air-conditioned ground floor, with rooms having a net height of 2.7 m, and a correspondent gross volume of 291 m³. Large glazed surfaces are located on the south-facing wall, while the west façade is equipped with more limited transparent surfaces. The space under the pitched roof, oriented toward south with 10° tilt to allow a suitable installation of active solar systems, is not conditioned. The lightweight roof is made of

two metallic frames to interpose a compact high density insulation layer (polyurethane, $\lambda=0.032$ W/mK), with a global heat loss coefficient (U_{roof}) of 0.265 W/m²K and a periodic thermal transmittance Y_{TE} of 0.12 W/m² K. The inner volume is conditioned by means of a suspended radiant ceiling system, with an active surface made of plasterboard and insulated by a polyurethane layer, with pipes located in parallel. The ground floor is insulated by 6 cm of polystyrene with a bottom layer made of 50 cm of gravel to limit the water rise by capillarity. The correspondent heat loss coefficient (U_{floor}) is 0.360 W/m²K.

The building investigated is located in Cosenza (southern Italy, latitude of 39.3°N) characterized by climatic conditions which consist in warm winters and hot summers. The main weather parameters are listed in Tab. 1 at monthly average daily level.

Nowadays, in accordance with the accepted standards, the investigated building can be considered passive if an energy performance index of the air conditioned volume, equal to 5.55 kWh/m³, evaluated with reference to the thermal energy requirements, is reached both in winter and in summer (Wienke, 2002).



Fig. 1 – The investigated building

3. Opaque surface simulation

Four different typologies of opaque dispersing walls have been considered.

- Traditional wall with hollow bricks, representative of a typical constructive solution diffused in the Mediterranean area: the masonry envelope is made of solid or perforated brick,

depending on the structural function of the wall. The thermal insulation is located on the external side to attenuate thermal bridges, therefore the thermal mass is concentrated towards the inside. Figure 2 shows the stratigraphy of the brick wall used in the simulation. Tables 2 and 3 summarize the main layer thermal properties and the wall thermal performance indexes. In particular, in Tab. 3 the values of overall loss coefficient U , surface mass SM , thermal periodic transmittance Y_{IE} , phase shift PS and attenuation factor AF of the thermal wave are reported. The overall loss thermal coefficient has been calculated considering external and internal surface resistances respectively equal to $0.04 \text{ m}^2\text{K/W}$ and $0.13 \text{ m}^2\text{K/W}$. The surface mass was calculated without considering the thickness of internal and external plaster layers, in accordance to the Italian normative (Italian Decree DPR 59/09, 2009). The dynamic parameters have been determined in accordance to the standard EN ISO 13786 (EN ISO 13786, 2008).

Table 4 – Cosenza: monthly average daily values for outdoor air temperature (T_{oa}), total solar radiation incident on a south vertical surface (SR_{90}) ad on a 10° tilted surface (SR_{10})

Months	T_{oa} [°C]	SR_{90} [MJ/m ²]	SR_{10} [MJ/m ²]
Jan	8.1	12.5	9.5
Feb	8.8	15.4	13.8
Mar	11.3	15.7	19.1
Apr	14.4	12.6	22.7
May	18.1	10.5	25.8
Jun	23.1	9.8	29.2
Jul	26.0	10.3	28.7
Aug	25.8	12.7	26.7
Sep	22.7	15.4	28.5
Oct	17.8	14.9	14.7
Nov	13.4	15.2	11.5
Dec	9.4	13.8	9.8

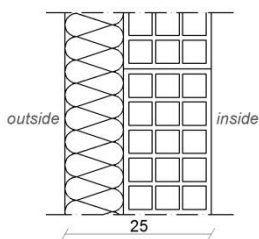


Fig. 2 – Section of hollow bricks wall with external insulation layer

Table 5 – Thermal properties of the wall layers

Material	Thickness [m]	Thermal resistance [m ² K/W]	Density [kg/m ³]	Heat capacity [J/kgK]
Polyurethane	0.10	3.125	40	1400
Brick	0.15	0.333	1800	840

Table 6 – Thermal performance indexes of the considered wall

U_{wall} [W/m ² K]	SM [kg/m ²]	Y_{IE} [W/m ² K]	PS [h]	AF [-]
0.275	274	0.064	8.57	0.234

- Wall made of precast materials, built by assembling concrete panels, with an internal insulation layer, usually employed for fast and standardized installations (Fig. 3).

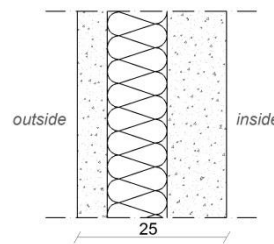


Fig. 3 – Section of wall with precast concrete panels

Table 4 – Thermal properties of the wall layers

Material	Thickness [m]	Thermal resistance [m ² K/W]	Density [kg/m ³]	Heat capacity [J/kgK]
Concrete	0.05	0.033	2800	1000
Polyurethane	0.10	3.125	40	1400
Concrete	0.10	0.066	2800	1000

Table 5 – Thermal performance indexes of the considered wall

U_{wall} [W/m ² K]	SM [kg/m ²]	Y_{IE} [W/m ² K]	PS [h]	AF [-]
0.294	424	0.082	8.41	0.277

- Wall made of *Gasbeton* blocks, with better thermal insulation properties than traditional bricks, equipped with an additional insulation layer on the external side to attenuate the effects of thermal bridges.

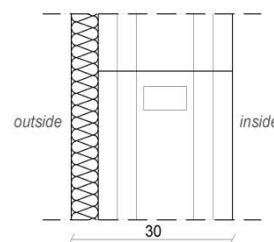


Fig. 4 – Section of wall made of *Gasbeton* blocks

Table 6 – Thermal properties of the wall layers

Material	Thickness [m]	Thermal resistance [m ² K/W]	Density [kg/m ³]	Heat capacity [J/kgK]
Polyurethane	0.05	1.563	40	1400
Gasbeton	0.25	2.174	400	1000

Table 7 – Thermal performance indexes of the considered wall

U_{wall} [W/m ² K]	SM [kg/m ²]	Y_{IE} [W/m ² K]	PS [h]	AF [-]
0.256	102	0.050	10.82	0.194

• On site dry assembled wall, equipped with two wood panels containing a massive sand layer, to combine requirements of demountability, reversibility, reusability and energy savings, allowing the reuse of involved materials. A self-supporting frame is used to fix the panels, whereas the thermal insulation is located on the external side, so that the sand layer can play the function of heat storage system.

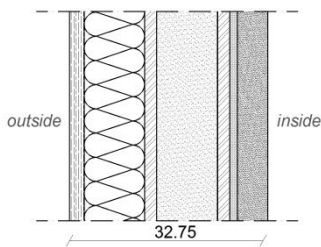


Fig. 5 – Section of the investigated massive drywall

Table 8 – Thermal properties of the wall layers

Material	Thickness [m]	Thermal resistance [m ² K/W]	Density [kg/m ³]	Heat capacity [J/kgK]
Wood coating	0.024	0.185	500	1600
Polyurethane	0.10	3.125	40	1400
OSB panel	0.02	0.154	650	1030
Sand layer	0.10	0.167	1700	910
Aluminium foil	0.001	0.000	2800	896
OSB panel	0.02	0.154	650	1030
Plasterboard	0.0125	0.042	900	1000
Plaster	0.05	0.063	1600	1000

Table 9 – Thermal performance indexes of the considered wall

U _{wall} [W/m ² K]	SM [kg/m ²]	Y _{IE} [W/m ² K]	PS [h]	AF [-]
0.246	226	0.037	11.00	0.149

A first building simulation campaign has been addressed by using the base slab, the roof and the geometrical characteristics of the building envelope described in the prior section. Moreover, glazed system with double clear glass (U_{WIN}=2.8 W/m²K, g=0.75) and the absence of external shading devices have been initially imposed. Using alternatively the investigated vertical wall, the energy performance index evaluated in function of the thermal energy requirement has been determined. The results of Fig. 6 show that all the investigated walls allow the respect of the winter limit value (5.55 kWh/m³). In particular, the dry assembled wall presents performances slightly better than the other solutions. With reference to the summer performances, the choice of the vertical wall is not sufficient to decrease substantially the energy requirements. In addition, the dry assembled wall

presents performances slightly better than the other investigated walls, and the achievement of the best dynamic parameters suggest the choice of this wall. Moreover, it does not lead to a worsening of the winter indexes and it presents the advantage to be more sustainable than the other walls.

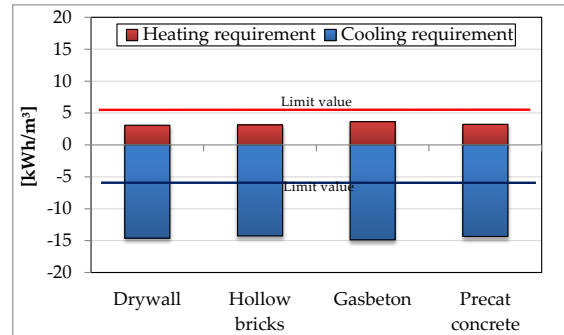


Fig. 6 – Building energy consumption in function of the different opaque walls

4. Windows and external shading devices

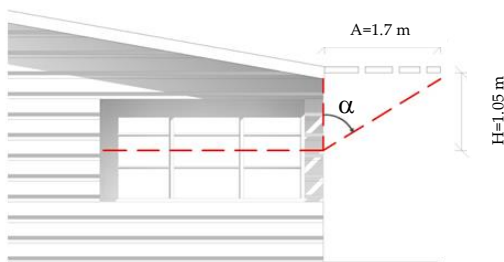
To respect the summer performance index, it is extremely important to reduce the solar load, therefore the employment of appropriate strategies in the design process have to be assumed. Appropriate technical solutions have to maximize the solar gain in winter and, at the same time, have to limit the entering solar radiation in summer. The investigated building presents 22 m² south-facing glazed surface, 4.5 m² transparent on the west façade and 7 m² toward north. To improve the thermal energy requirements, the employed glazed surfaces are different in function of the exposure. In fact, to ensure appropriate natural illumination conditions and to limit the thermal losses, the north exposure is equipped with windows mounting triple glass, while south exposure presents double pane windows with a high solar gain coefficient to exploit solar radiation during winter. Finally, to reduce the risk of indoor overheating during the afternoon in winter and in summer, the west-facing room is equipped with a double pane window but with a low solar gain coefficient. The overall heat loss coefficient and the solar gain coefficient of the simulated windows are listed in Tab. 10; all the investigated glazed systems are equipped with air-gap containing argon.

Table 10 – Type of windows and properties

Exposition	Type	U_{WIN} [W/m ² K]	g [-]
South	4-12-4	1.61	0.71
North	4-12-4-12-4	0.89	0.71
West	4-12-4	2.53	0.11

A proper positioning and sizing of external unmovable overhangs and sunbreakers, and the employment of mobile internal shading devices, can help the rational use of the solar gains. Therefore, the reference building has been investigated by analyzing three different shading systems in order to identify the more efficient solution in relation to the orientation. The efficiency of the shading devices was evaluated by quantifying the variation of energy requirements for heating and cooling. For each exposure, the investigated shading systems are:

- Horizontal overhangs, sized to reduce solar load in summer, without providing excessive limitation of solar gains in winter. In function of the solar data listed in Tab. 1, the optimal are reported in Fig. 7, obtaining a correspondent yearly average shading factor value of 0.61.
- External sunbreakers, with horizontal louvres width of 10 cm, pitch of 10 cm and 45° tilted.
- Internal light-colored venetian blinds, with horizontal slats width of 2.5 cm and spaced 5 cm from the glass surface.



α	H[m]	A [m]	F [-]
60°	1.05	1.70	0.61

Fig. 7 – Overhang sizing for the South exposure obtained by simulation results

Assuming an envelope made of dry assembled walls, fig. 8 shows for the south exposure the energy requirements hypothesizing the separated employment of the considered shading devices. Contrary to the case of the opaque vertical walls, the type of shading system produces a more evident variation of the results. All the shading

devices provide a considerable reduction of cooling energy requirement, but at the same time an inevitable slight increase in winter due to the reduction of solar gains. Therefore, in Mediterranean areas the choice of appropriate glazed surfaces and shading systems appears more important than opaque surfaces.

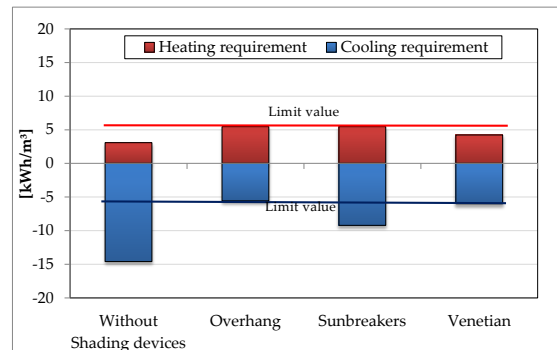


Fig. 8 – Energy performance indexes assuming different types of shading devices on the building south façade

The worst results have been obtained for external sunbreakers devices, as they produce the lowest decrement of cooling demand. In winter, all the shading systems provide a worsening of the heating demand. Nevertheless, the winter performances are respected, but the sunbreakers systems do not allow for the achievement of the summer limit value. On the other hand, horizontal overhangs and internal venetian blinds represent a good compromise for both conditioning seasons. Considering that horizontal overhangs ensure important energy savings and they do not create visual barriers on the glass surfaces, which is completely unobstructed, they seem the best solution for windowed surfaces with a south exposure. Successively, fixing overhangs on the south façade, the same analysis has been carried out for the west orientation, observing that external sunbreakers are the more appropriate devices. In fact, Fig. 9 shows that these systems allow the achievement of appropriate annual energy performance indexes, for both heating and cooling. The contemporary employment of the identified shading systems allow the respect of both seasonal limits. Therefore, with reference to the heating and cooling period, the investigated building can be labeled as passive only if the envelope is made of dry assembled vertical walls and, overall, it is equipped with overhangs on the south exposure

and sunbreakers on the west façade. The employment of hollow bricks or a precast concrete wall, however, does not allow for the respect of the winter limit, due to the excessive worsening of the solar gains through the windowed surfaces. For the detected building envelope, the annual values of the performance indexes for heating and cooling are shown in Tab. 11.

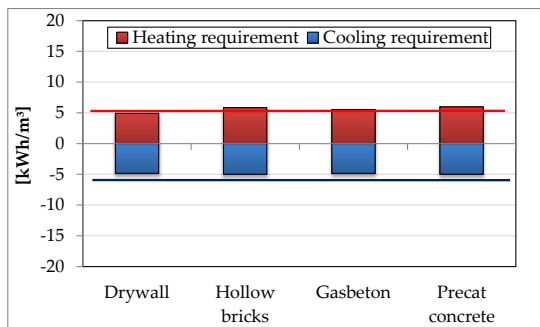


Fig. 9 – Energy performance indexes assuming overhangs on South façade and sunbreakers on West exposure, in function of the vertical wall type

Table 11 – Winter and summer energy performances indexes obtained for the better building configuration

Heating Demand	Cooling Demand
5.15 kWh/m³	-4.91 kWh/m³

5. Renewable sources

To reduce the energy supply from fossil sources, an air-conditioned plant that exploits renewable energy is requested. Therefore, active solar systems have been employed to reduce the exploitation of fossil sources. Since the building has been designed with a suitable pitched roof for solar device installation, the generation system is made of an air-water electric heat pump that interacts with:

- Solar thermal collectors;
- Single effect absorption chiller;
- Photovoltaic modules.

Solar thermal collectors are employed to cover the limited DHW requirement, part of the heating requirement by direct supply of radiant ceilings and, for the cooling period, the generator requirement of the absorption chiller. For an office building, the annual domestic hot water requirement is determined according to Italian standard (UNI 11300-2, 2014); and in the specific case, an annual value of 825.1 MJ has been

obtained. The annual thermal energy required from the absorption chiller generator was determined by dividing the cooling requirement for an average seasonal value of the COP of 0.6. The heating requirements are those determined in function of the configuration detected for the envelope. Tab. 12 lists the monthly values of the thermal energy requirements concerning the production of domestic hot water (Q_{DHW}), heating (Q_h), absorption chiller generator (Q_{cool}) and global requirement (Q_{tot}). By using the solar radiation data of Tab. 1, supposing the use of heat pipes technology, a limited collection surface of 5 m² has been obtained, with a correspondent average annual thermal efficiency of 71.8%. The employment of such collectors allows the achievement of an average annual solar fraction equal to 87 %.

Table 12 – Monthly energy requirements for heating, cooling and domestic hot water production, with solar fraction F.

Month	Q_{DHW} [MJ]	Q_h [MJ]	Q_{cool} [MJ]	Q_{tot} [MJ]	F [%]
January	70.1	1693.3	0	1873.7	44.9
February	63.3	1279.0	0	1426.3	79.2
March	70.1	993.4	0	1130.1	100.0
April	67.8	321.9	0	414.1	100.0
May	70.1	0	616.2	729.2	100.0
June	67.8	0	1659.7	1835.7	100.0
July	70.1	0	2331.0	2551.4	100.0
August	70.1	0	2266.0	2482.3	89.1
September	67.8	0	1313.2	1467.4	100.0
October	70.1	0	410.4	510.5	100.0
November	67.8	267.2	0	356.0	100.0
December	70.1	1225.1	0	1376.2	64.1
Yearly	825.1	5780.0	8596.5	16153.0	87.0%

The electric heat pump acts as an auxiliary system both in winter and in summer, absorbing part of the electric load provided by the PV field. It has been sized considering the full coverage of other electric loads such as the office equipment and artificial lightning, and by hypothesizing the employment of polycrystalline modules technology, with nominal efficiency of 15.2 % and peak power of 250 W per module. In function of the data of Tab. 1, a photovoltaic modules surface of 60 m² has been determined (about 10 kW_p). Tab. 13 reports the monthly values concerning the global electric energy requirement, the electric energy provided by the PV field and the electric energy absorbed from the external grid.

electric energy from the external grid. In this case, the primary energy for the building heating is represented by the fossil sources involved in the production of the electric energy absorbed from the grid. Considering a national electric system efficiency value of 0.45 (AEEG, Italian Authority for Electric Energy and Gas), a global performance index of 3.47 kWh/m³ per year has been obtained, allowing to label the reference building as A⁺.

7. Conclusions

An energetic analysis of an office building located in southern Italy properly designed to achieve energy consumption almost zero, has been carried out by the Design Builder simulation software. According to the results of different simulations, an appropriate choice of opaque surfaces, glazed surface and external shading devices has been made to meet the climatic conditions of Mediterranean areas. A well-insulated envelope, equipped with large glazed surface toward South, is performing in winter but produce high summer energy requirements, therefore the typology of opaque vertical walls is not sufficient to consider the building passive during the whole year. Regarding the thermal wave delivered through the opaque wall, high values of the attenuation factor and phase shift are achievable by dry assembled walls. To reduce the cooling energy requirements, glazed systems equipped with suitable shading devices, in function to the wall exposition, have to be selected. In the presence of high solar gains, great values of the solar gain coefficient are recommended. To limit solar gains during summer, the simulation results have shown that overhangs with appropriate size south facing, and sunbreakers for East/West exposures appear appropriate. The shading systems produce an inevitable worsening of the winter performances, but the winter limit is still respected. For the detected envelope, the employment of small surfaces of active solar systems, linked to a heat pump generation system, is satisfactory in order to design a ZEB building.

References

- Gonzalo, R., Vallentin R., 2014. "Passive House Design", *Green Books edition*
- Jacobson R., 2013, "Performance of 8 Cold-Climate Envelopes for Passive Houses", *Master Thesis*
- Ferrante A., 2012, "Zero- and low-energy housing for the Mediterranean climate", *Advances in Building Energy Research*, Vol. 6, N. 1, pp. 81-118
- Mlakar J., Strankar J., 2013, "Temperature and humidity profiles in passive-house building blocks", *Building and Environment*, N. 60, pp.185-193
- Van Huffelen C., 1992, "Passive houses: energy efficient homes", *Ed. Braun*
- Ferrante A., Cascella M.T., 2011, "Zero energy balance and zero on-site CO₂ emission housing development in the Mediterranean climate", *Energy and Building*, N°43, pp.2002-2010
- DL 102/2014 Attuazione della direttiva 2012/27/UE sull'efficienza energetica, che modifica le direttive 2009/125/CE e 2010/30/UE e abroga le direttive 2004/8/CE e 2006/32/CE
- EN ISO 13790, 2008, Energy performance of buildings – Calculation of energy use for space heating and cooling
- Wienke U., 2002, "L'edificio passivo. Standard, requisiti, esempi", *ALINEA edition*
- DPR 59/09, 2009, Regolamento di attuazione dell'articolo 4, comma 1, lettere a) e b), del decreto legislativo 19 agosto 2005, n. 192, concernente attuazione della direttiva 2002/91/CE sul rendimento energetico in edilizia.
- EN ISO 13786, 2008, Thermal performances of building components: dynamic thermal characteristics
- UNI 11300-2, 2014, Determinazione del fabbisogno di energia primaria e dei rendimenti per la climatizzazione invernale e per la produzione di acqua calda sanitaria
- Italian Authority for Electric Energy and Gas. www.autorita-energia.it

Building simulation based optimization through design of experiments

Jay Dhariwal – Dept of Energy Sc and Engg, IIT Bombay, Mumbai, India – jaydhariwal@gmail.com

Rangan Banerjee – Dept of Energy Sc and Engg, IIT Bombay, Mumbai, India – rangan@iitb.ac.in

Abstract

Building thermal simulation based parametric methods are computationally intensive for optimizing the building design. This work uses experimental design techniques, i.e. fractional factorial design and response surface methodology, for sensitivity analysis and surrogate modeling respectively. These techniques find the solution in a reasonable time. Their application for building design optimization has not been found in the literature before.

Fractional factorial design has been used to identify the significant design variables. These variables are used to form a correlation for annual cooling load prediction, using response surface methodology. These methods are illustrated using two cases to minimize the life cycle cost of a single-storeyed, air-conditioned, solar powered, detached home, with 64 sq. m. floor area, for the warm and humid Mumbai climate.

For this climate, window solar heat gain coefficient, window to wall ratio, overhang depth and roof reflective coatings turn out to be the most important among the design variables used for this case study. The created response surface models show an error of less than 5% for more than 99% of the test data, which is comparable to other such models. Strategies are suggested to bring the error for the entire search space to less than 10%.

Life cycle cost minimization using the model for case 2 does 12 million iterations as opposed to 250 iterations using a parametric EnergyPlus simulation run at the same time. The solution is better and the design achieved is also different. The optimum design has a cooling load of 55 kWh m⁻² yr⁻¹, while it varies from 46 to 118 kWh m⁻² yr⁻¹.

This work adds an intuitive method for building design and opens up possibilities for optimization.

1. Introduction

Detailed thermal simulation programs like EnergyPlus, TRNSYS, etc. are needed to accurately estimate the cooling and heating loads in buildings. These programs can take from a few seconds to hours to find the building performance for each run. To find the optimal building designs for desired objective functions like minimum lifecycle cost (LCC), minimum discomfort hours, etc., simulation based parametric methods may not be viable as they are computationally intensive. The time taken may be in the order of years, for iterating over 15 design variables having 3 levels each, assuming 7 seconds per simulation run. A typical building design could easily have more than 30 design variables. Techniques like sensitivity analysis and optimization methods, coupled with simulation programs, are used to reduce the computational run time, while maintaining the accuracy of results.

1.1 Literature review

Sensitivity analysis (SA) can be used to find the design variables, having the most impact on the response variable, like the cooling load. Local SA involves changing one factor at a time over the base case. It is easy to use but does not consider the interactions between the variables. Global SA spans the entire input space and is preferred. Variance based methods give the most reliable results for global SA, as per the review paper by (Tian, 2013).

After eliminating the unimportant variables using SA, optimization methods can be used to find the optimal building design. Nguyen et al. (2014) and Machairas et al. (2014) provide a review of the building design optimization methods used. Genetic algorithm based direct search methods are

most popular (Machairas et al., 2014). Nguyen et al. (2014) suggest that improvements in surrogate or meta-models hold a lot of promise, however, there have only been limited studies using these models for building design.

Surrogate models (SMs) overcome the high run time limitation of simulation based optimization methods by creating an approximate model or a correlation, using a limited simulation run for predicting simulation outputs. Machine learning models like support vector machines and artificial neural networks have been mostly used to develop surrogate or meta-models (Machairas et al., 2014). Once the SMs are created and validated, they can be used parametrically or coupled with other optimization algorithms to optimize the design.

Nguyen et al. (2014) suggest that the performance of the optimization methods may be different for cold and warm climates.

1.2 Problem definition

This paper proposes fractional factorial design (Montgomery, 2007) for global SA, not used for building design before. This statistical method gives very reliable results, like other variance based global SA methods, but overcomes their limitation of high computational time by using only a fraction of parametric simulation runs to identify the most significant variables, while also analysing the key interactions between them. This technique can easily analyse 50 or more design variables in a short time. Gong et al. (2012) have used a factorial design technique called orthogonal method, for local SA only, to improve upon the base case.

Response surface methodology (Montgomery, 2007) has been used to create a surrogate model for cooling load prediction. Although response surface models (RSM) are the most popular surrogate models in general (Wikipedia, 2014), they have not been used for building design before. RSM is very intuitive to use and builds on fractional factorial design used for SA, to form a model for the significant variables, for further optimization. Using statistical methods like RSM can help avoid learning artificial intelligence techniques like artificial neural network or support vector

machines, which require expert knowledge and have been the main reason for the limited use of SMs for building design so far (Machairas et al., 2014). Some commonly used RSM designs are Box-Behnken design and central composite designs (Montgomery, 2007).

The surrogate models developed in this paper are also tested to assess their accuracy and strategies are proposed for the regions with high error.

In addition, there is a dearth of studies on the application of building design optimization for warmer Indian climates. Hence, these methods are presented in an optimization framework to minimize LCC for an air-conditioned, single zone, solar powered, detached home, with a floor area of 64 m², based in the warm and humid Mumbai climate. It is inspired by the Indian team's house "h-naught" from Solar Decathlon Europe 2014 (SDE, 2014).

2. Methodology

Figure 1 explains the flowchart of the methodology used to optimize the building design. Other methodology related key points are addressed in this section. The simulation model for the base case is built in EnergyPlus. The design variables are estimated for their ranges, thermal properties and cost data. Local and global SA, surrogate modelling and optimization algorithm are applied as per the framework.

For global SA, the runs for the fractional factorial design are limited to 512 to achieve a target of finishing the simulations within an hour, with each simulation in EnergyPlus taking 7 seconds, on average, for the present case study. To create the fractional factorial design, Box-Behnken RSM design and ANOVA, Design-Expert software (Stat Ease, 2014) has been used. For running simulations in a batch mode, VBA programming language is used. If the simulated test cases for SM show an error of greater than 10%, then the region of high error should be identified and another SM should be fit for this region to reduce the error. For optimization, the best 5 solutions should be used to choose the most robust design among them.

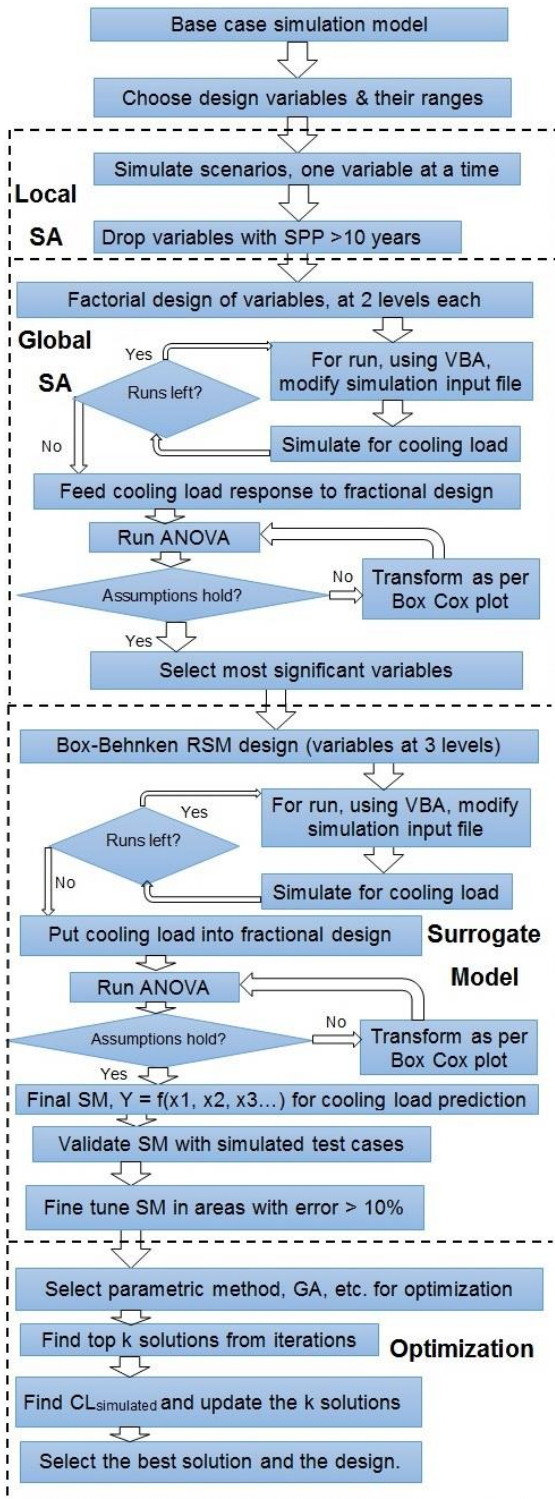


Fig. 1 – Flowchart for optimization methodology

3. Case study input data

The methodology is illustrated considering two cases for the Figure 2 building in Mumbai. The structural material for the base case is taken as concrete (Ramesh et al., 2012) for it to be

representative of Indian buildings.

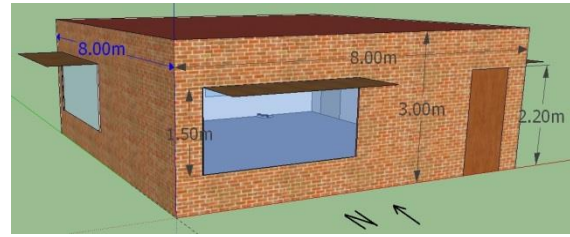


Fig. 2 – Detached home in Mumbai

Table 1 shows the important input parameters for the simulation. AC schedule was arrived at, from the survey of the load profile of the homes of middle class households of Gujarat, India (Garg et al., 2010). Other internal gains include the use of cooking gas, fridge and lighting.

Table 1 – Important input parameter assumptions

Input parameter	Data assumptions
Occupants	6 (for a middle class family)
Occupancy schedule	4 people on weekdays from 8 am to 6 pm; 6 people during rest of the time.
AC set points	T_{opt} : 22°C to 27°C (Manu et al., 2014)
AC schedule	April to June: 9 pm to 5 am, 2 pm to 4 pm for, July to October: 2 pm to 4 pm (Garg et al., 2010)
Infiltration rate	0.4 air changes per hour
Internal mass	40 m ² (partitions), 20 m ² (furniture)

Table 2 shows the 16 design variables along with their ranges to be used for the simulation runs. Insulation, thermal mass and PCM thickness have 3 variables each for wall, roof and floor. The WWR lower limit was fixed as per the requirements for LEED IEQ credit 8.1 (IGBC, 2011) using day-lighting simulation in EnergyPlus. Day-lighting controls in the simulation maintain the lighting levels in the house to greater than 100 lux. Curtains are used only when the solar radiation is greater than 500 W/m² to avoid the glare from the direct solar radiation. Glasswool is used for thermal insulation, having a density of 48 kg/m³ (Twiga,

2014) and water is used for thermal mass. The base case run yields a cooling load of 100 kWh m⁻² yr⁻¹.

Table 2 – Design variables and their range

Design Variable	Range
WWR	15% to 40% (IGBC, 2011)
Window U value	1 to 6
Window SHGC	0.2 to 0.8
Overhang depth	0 to 1 m (BIS, 2005)
Fin depth	0 to 0.5 m
Curtains SHGC	0.2 to 1.0
Cool roof ρ	0.25 to 0.85 (SSEF, 2014)
Insulation t	0-0.1 m (Wall), 0-0.2 m (Roof, Floor)
Thermal mass t	0-0.1 m (Wall), 0-0.2 m (Roof, Floor)
PCM t	0-0.1 m (Wall), 0-0.2 m (Roof, Floor)

4. Application of optimization method

Each step in the optimization method is applied as per Figure 1 for two cases, case 1 and case 2. The difference between the two cases is in the number of design variables. Case 1 has the 16 design variables, as per Table 2. For case 2, the design variables, namely, WWR, window U-value, overhang-depth, fin-depth and window SHGC have been made different for each façade. For example, WWR would be treated as four design variables, namely, WWR for north, east, west and south facades, respectively. This would result in a total of 31 design variables. Case 1 is easier to understand, whereas case 2 shows how SM could be used for designs with many design variables.

4.1 Local sensitivity analysis

As per the local sensitivity analysis and payback analysis of the costly items, shown in Table 3, it is seen that PCM would not be cost effective as its SPP is far greater than 10 years, as per scenarios run over the base case to find its cooling load reduction benefit, with utility rates of € 0.13 per

kWh. So, it is eliminated at this step. This leaves 13 design variables for case 1 and 28 design variables for case 2.

Table 3 – Cost analysis for variables (1 € = 75 Indian rupees)

Variable	Cost (in €)	SPP
PCM	6000	100 years
Low solar gain windows	660	10 years
Cool roof	800	8 years
Glasswool insulation	260	4 years

4.2 Global sensitivity analysis

For case 1, with the range of 13 design variables as per Table 2, the fractional factorial design chosen is resolution VI 2¹³⁻⁴ design with a single replicate. This design can estimate the main effects and two factor interactions. It was created in Design-Expert software (Stat Ease, 2014). 512 simulation runs based on this design were automated using VBA, calling EnergyPlus batch file for each simulation and took a time of 55 minutes on an Intel® Core™ i7-2670QM processor. The cooling load varied from 43 to 143 kWh m⁻² yr⁻¹, with a mean of 81 kWh m⁻² yr⁻¹.

For case 2, for the 28 design variables, the factorial design has a resolution V. 408 simulation runs based on this design took a time of 45 minutes. The cooling load varied from 45 to 138 kWh m⁻² yr⁻¹, with a mean of 83 kWh m⁻² yr⁻¹.

The normal probability plot of residuals is well behaved for both the cases, suggesting that the normality assumptions hold.

Figure 3 shows that case 1 and case 2 have the same significant variables selected, albeit with different contribution levels. Window SHGC, WWR, cool roof ρ , overhangs and the interactions involving them explain more than 85% of the total variance in the model for both the cases. The most significant positive interaction is between the cool roof ρ and the roof insulation, which suggests that when the cool roof ρ is high, then the roof insulation has little effect. Figure 4 shows the breakup of facade-wise contribution for case 2. The west and east facade contribution for SHGC is

higher than the north and south facade as the direct radiation is able to enter at a lower altitude angle for these facades.

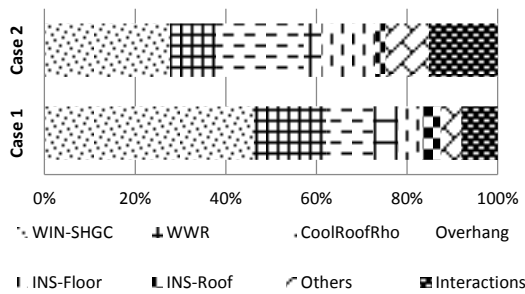


Fig. 3 – Percent contribution of design variables to cooling load

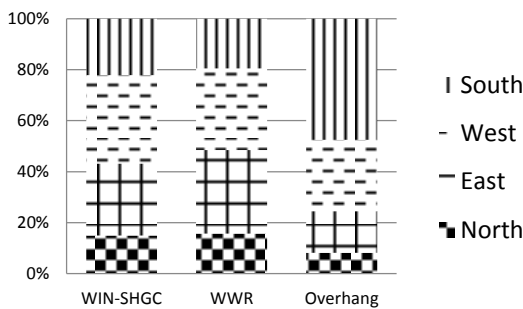


Fig. 4 – Breakup of variables for the façade wise contribution

The thermal mass, wall insulation and window U-value variables do not have a major effect as the temperature in Mumbai is fairly constant throughout the year. Curtains can be useful to avoid solar radiation but they also lead to blocking of daylight and views so they are only used to avoid harsh direct radiation, which happens only for a little time, when the AC is used. The variables, which are left out, are set at base case values in the simulation model. In most cases, it would mean removing these variables from further analysis. For example, thermal mass is removed but window is set at U-value of 6 W/m²-K.

To create the surrogate model, the floor and the roof insulation are left out. The presence of floor insulation has a negative effect on the cooling load and it does not have any interaction with any other variables to be concerned about. For the roof, cool roof material is better suited than the roof insulation as per Figure 3. Thus, for case 1, four design variables, namely, cool roof ρ, window SHGC, overhang depth and WWR, and for case 2, the same variables for all four facades would be

used to form the surrogate model, making it a total of 13 design variables.

4.3 Surrogate Model

4.3.1 SM for Case 1

Using RSM, a second order polynomial is fit to the 4 design variables to obtain the surrogate model, using the range from Table 2. Box-Behnken design is created in Design-Expert software using 3 levels for each factor, taking the lower and upper limit and the middle value of the range. For example, for the overhang depth, levels correspond to 0 m, 0.5 m and 1 m. The design leads to 29 simulation runs, which takes less than 3 minutes of computational time.

The fitted model has an adjusted R-squared of 0.99. The variables A, B, C and D have been defined in the nomenclature section.

$$\text{AnnualCoolingLoad} = 63.6 - 3.5A + 64.8B - 43.8C + 0.8D - 17.0 AB - 11.7 AC - 0.3 AD + 11.8 BC + 0.8 BD + 0.5 CD + 11.5 A^2 - 44.5 B^2 - 11.4 C^2 \quad (1)$$

4.3.2 SM for Case 2

Like in section 4.3.1, a second order polynomial is fit for cooling load as the response, using RSM. Box-Behnken design leads to 220 simulation runs. The Box-Cox plot in Design-Expert software recommends a power transform to meet the normality assumptions for the residuals, as shown for the cooling load on the LHS of equation (2). The fitted model on the RHS of equation (2) has linear, quadratic and interaction terms between the variables for all façades. The fitted model achieves an adjusted R-squared of 0.99.

$$\text{AnnualCoolingLoad}^{2.1} = f(\text{overhang depth, window SHGC, WWR, cool roof } \rho) \quad (2)$$

4.3.3 Validation of SM

Table 4 shows the testing datasets created for the two cases. For case 1, the variables are varied parametrically. For example, WWR is varied from 15% to 40% in steps of 5%. For case 2, since the variables are large, so 4 fractional designs, with 512 runs each, have been created, to test for the entire range of variable values. WWR, window SHGC, overhang for all four facades and cool roof ρ would be varied at 0 & 100%, 10 & 90%, 25 & 75% and 40

& 60% of the range for the 4 fractional designs respectively. For example, WWR (%) for all facades would be 15 & 40, 17.5 & 37.5, 21.25 & 33.75, 25 & 30 respectively for the four fractional designs with 512 runs each. Table 4 shows a case 2 design. Total test cases for case 1 and case 2 are 2058 and $512 \times 4 = 2048$ respectively. The error statistic MAPE for the difference between the simulated vs. SM predicted cooling load is less than 1% for both cases. The data point with minimum error for case 1 and case 2 are -12% and -36% respectively. The maximum error is less than 5% for each case. The areas with high error need to be analysed further.

Table 4 – Range of variables for testing

Variable	Case 1	Case 2 (design 1)
WWR (in %)	15-40 step 5	15, 40
Window SHGC	0.2-0.8 step 0.1	0.2, 0.8
Overhang (in m)	0-1 step 0.17	0, 1
Cool roof ρ	0.25-.85 step 0.1	0.25, 0.85

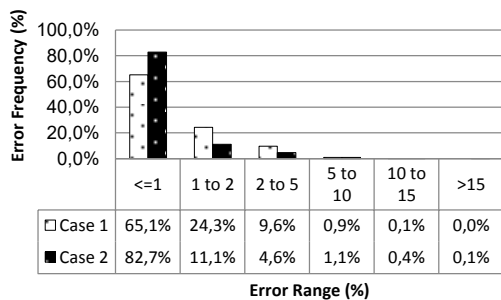


Fig. 5 – Error frequency for the surrogate model prediction

Figure 5 shows that about 98% of the test data have errors of less than 5%. These results are promising and validate the effectiveness of the surrogate model. However, for case 2, 0.5% of the test cases have errors higher than 10% and ways need to be found to reduce this error as well to make the SM valuable for the entire search space.

The analysis of high error points shown using Figure 6 suggests that the error has a tendency to increase on the negative side, with the reduction in the simulated cooling load, resulting in the underprediction of cooling load. This problem is fixed by using a reduced variable SM, having the same form as case 1, for the region of case 2 with

CL less than $60 \text{ kWh m}^{-2} \text{ yr}^{-1}$ (as shown in Figure 6 with a vertical dotted line). This region accounts for 3.5 % of the total search space. The only difference between the reduced model and the case 1 model is the range for cool roof reflectivity, which is 0.65 to 0.85 for the reduced model. This strategy brings the error for all test data for case 2 to less than 10% but the detailed design ability of case 2 would be lost for this region.

To avoid compromising on the detail that case 2 offers, while keeping the error low, the optimization algorithm in the next section is made to search the space with CL less than $60 \text{ kWh m}^{-2} \text{ yr}^{-1}$, for both the reduced case 1 model with less error and case 2 model with higher detail. The best 5 solutions are found from both the models and the optimum among them is chosen.

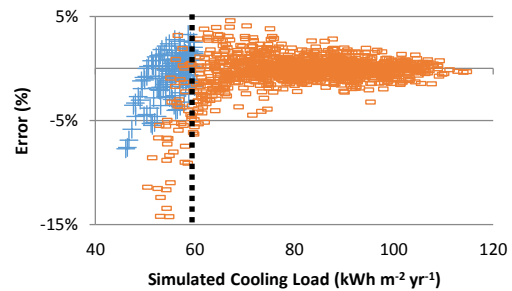


Fig. 6 – Error reduction for Case 2 ('o') with reduced model ('+')

4.4 Optimization for LCC

Using the surrogate model, LCC is optimized parametrically. As per the cost functions given in Table 5 and discount factor of 10%, the results for the minimum LCC design in constant euros are given in Table 6. The base case cost includes the construction cost of the house and the cost of the solar thermal hot water system. The life of the building components is given in Table 5.

As per Table 6, parametric EnergyPlus run method, case P is able to search 256 combinations of input parameters only as compared to 12 million iterations for case 2 in the same time. If the iterations for case 2 were done parametrically, it would have taken 2.7 years. In this case, SM is able to search 50000 times more solution space than parametric methods. This is where the real power of SM based methods lies.

Table 5 – Cost functions for design variables

Material	Cost function (in €)
Base cost of house	13.3 per sq. ft. (50 years life)
Solar PV	1066.7 per kWp (25 years life)
AC	400 per TR of capacity (10 years life)
Windows	$10000/75 \times (0.6 - 1.35B + 0.85B^2) \times WWR$
Overhangs	12 per m ²
Cool roof ρ	$(12\rho/0.85)$ per m ²

Table 6 – Comparing results for optimized building design

	Case P	Case 1	Case 2
Method used	Parametric	SM	SM
Total iterations	256	0.3 mn	12 mn
Time taken (hrs)	0.5	0.05	0.5
LCC _{optimum} (in €)	13973	13824	13757
Overhang depth	0.7 m	0.9 m	0, 1, 1, 1 m*
Window SHGC	0.6	0.375	0.2, 0.6, 0.6, 0.6*
WWR	15%	15%	15, 15, 15, 15%*
Cool roof ρ	0.65	0.85	0.85
CL for this design	69.3	51.8	55.1

*for N, E, W, S facades respectively

For case 2, since the cooling load for the minimum LCC lies in high error region as per Figure 6, so both the case 2 and reduced models were run in this region but the case 2 model gave a better solution in this instance. The minimum LCC for case 2 is 1.6% less than case P. The design is also different for all variables except WWR.

4.5 Applicability

For this paper, all variables chosen were continuous variables but this framework can be used for discrete variables in the same manner. In this case, for SM, for each combination of discrete variable values, there will be a separate equation. SM was used for cooling load prediction only as

heating is not required for the Mumbai climate but the methodology could be easily extended for cold climates as well.

SMs can be used as a correlation for mass housing projects for a given climate by architects or other building industry professionals, who do not have a background in building simulation.

5. Conclusion and next steps

A building simulation assisted optimization methodology has been presented for a single storeyed house in Mumbai. Fractional factorial design was used to find the significant variables for cooling load prediction. A correlation for cooling load prediction was fit for these variables and was used to optimize the life cycle cost. The entire process was completed in a couple of hours.

The surrogate model used to find the correlation was found to be thousands of times faster than the parametric method. The test data also showed that the prediction error could be kept to be less than 10% for the entire search space. This correlation, when used for optimization, also found a better solution with a different building design.

The case study revealed that for the Mumbai climate, window solar heat gain, window to wall ratio, roof reflective coatings and overhang depth are the most important design variables.

This work adds an intuitive optimization method into the building design kit. This approach opens up a lot of possibilities for building design optimization and could be used for the prediction of any simulation output. This method can also be extended to consider the effect of uncertainty in parameters like infiltration rate, occupancy schedule, etc. on building design.

6. Nomenclature

Symbols

ρ	reflectance
A, B, C,	overhang depth to window height,
D	window SHGC, cool roof ρ , WWR
AC	air conditioning
CL	cooling load (in kWh m ⁻² yr ⁻¹)
hrs	hours
INS, WIN	insulation, windows
k, U	thermal conductivity, overall heat transfer coefficient (in W m ⁻² K ⁻¹)
kWp	kilo-watt peak
LCC	life cycle cost
LHS, RHS	left hand side, right hand side
m	metre
mn	million
MAPE	mean absolute percentage error
min, max	minimum, maximum
N, E, W, S	north, east, west, south
PCM	phase change material
PV	photo-voltaic
RSM	response surface methodology
SA	sensitivity analysis
SHGC	solar heat gain coefficient
SM	surrogate model
SPP	simple payback period
sq. ft.	square feet
t	thickness
T _{opt}	operative temperature (Celsius)
VBA	Visual Basic for Applications
WWR	window to wall ratio

Subscripts/Superscripts

opt	operative temperature
-----	-----------------------

References

- BIS. 2005. *National Building Code of India 2005*. New Delhi: Bureau of Indian Standards.
- Garg A., Maheshwari J., Upadhyay J. 2010. *Load Research for Commercial and Residential Establishments in Gujarat*. ECO-III-1024
- Gong X., Akashi Y., Sumiyoshi D. 2012. "Optimization of passive design measures for residential buildings in different Chinese areas" *Building and Environment* 58: 46-57
- IGBC. 2011. *Green Building Rating System*. LEED 2011 for India.
- Machairas V., Tsangrassoulis A., Axarli K. 2014. "Algorithms for optimization of building design: A review" *Renewable and Sustainable Energy Reviews* 31: 101-112
- Manu S., Shukla Y., Rawal R. 2014. *India Model for Adaptive (Thermal) Comfort*. Accessed Nov 15, 2014. www.cept.ac.in/carbse
- Montgomery D.C. 2007. *Design and Analysis of Experiments*. New Delhi: Wiley India Edition.
- Nguyen A., Reiter S., Rigo P. 2014. "A review on simulation-based optimization methods applied to building performance analysis" *Applied Energy* 113: 1043-1058
- Ramesh T., Prakash R., Shukla K.K. 2012. "Life cycle energy analysis of a residential building with different envelopes and climates in Indian context" *Applied Energy* 89: 193-202
- SDE. 2014. "Home page" Accessed Nov 15, 2014. <http://www.solardecathlon2014.fr/en/>
- Stat-Ease, Inc., MN, USA. 2014. *Design-Expert® software, version 9*. www.statease.com
- Tian Wei. 2013. "A review of sensitivity analysis methods in building energy analysis" *Renewable and Sustainable Energy Reviews* 20: 411-19.
- Twiga. 2014. "Twiga Insul" Accessed Nov 15, 2014. <http://www.twigafiber.com/twigainsul.php>
- Wikipedia. 2014. "Surrogate Model" Accessed Nov 15, 2014. en.wikipedia.org/wiki/Surrogate_model
- SSEF. 2014. "Cool Roofs for Cool Delhi" Accessed Nov 17, 2014. <http://shaktifoundation.in/initiative/cool-roofs-for-cool-delhi/>

A verification of CitySim results using the BESTEST and monitored consumption values

Walter Emmanuel – kaemco LLC, La Riaz 6, 1426 Corcelles-Concise, Switzerland – ew@kaemco.ch

Kämpf Jérôme – LESO-PB / EPFL, Station 18, 1015 Lausanne, Switzerland – jerome.kaempf@epfl.ch

Abstract

This paper presents a verification of CitySim, a large-scale building energy simulation tool based on a simplified thermal model. First, the main assumptions behind the simplified model are presented. Then, CitySim is compared to other detailed simulation tools on case studies defined in the Building Energy Simulation Test (BESTEST) validation procedure. Finally, the predictions of CitySim regarding the annual heating load are compared with the monitored consumption of a building located on the campus of the Swiss Federal Institute of Technology Lausanne (EPFL). Regarding the BESTEST, CitySim gives annual heating and cooling results together with peak heating and cooling loads that are within the acceptable range defined by reference simulation tools except for the annual heating load of case 960 and the peak cooling of case 610 but the differences are rather small (less than 1%). Regarding the EPFL campus building, CitySim gives an annual heating consumption within a 5% range of the monitored consumption of two reference years. The paper concludes that despite its simplified thermal model, CitySim results remain consistent with more detailed programs and the monitored heating consumption of an office building. These results reinforce the confidence in the tool to predict annual and peak load energy needs for conditioning buildings.

1. Introduction

According to UN and IEA forecasts (UN, 2011) and (IEA, 2008), the urbanized population is expected to grow tremendously in the future and likewise their fossil fuel energy consumption. To moderate this non-renewable energy consumption in urban areas, shelters must be planned, designed and refurbished in an efficient way.

With this aim in mind, CitySim (Kämpf, 2009), a large-scale dynamic building energy simulation tool, was developed at the Swiss Federal Institute of Technology Lausanne (EPFL). The tool includes an important aspect in the field of many building simulations: the building interactions (shadowing, light inter-reflections and infrared exchanges). Furthermore, CitySim is based on simplified modelling assumptions to establish a trade-off between input data needs, output precision requirements and computing time. These simplifications may be the cause of possible over or underestimations in the program outputs. The objective of this paper is to make sure that CitySim gives reasonable results despite the simplifications. According to (Judkoff, 1988), a complete validation methodology for building energy simulation programs is composed of three main pillars: the analytical verification, the comparative testing approach and the experimental verification.

The first pillar consists of comparing the program with a known analytical solution, which was already applied on CitySim in its initial developments (Kämpf, 2009).

This paper addresses the two other approaches: CitySim is confronted with more detailed simulations tools within the frame of the Building Energy Simulation Test (BESTEST) method (Judkoff and al., 1995) and its accuracy is verified experimentally by a comparison with monitored data for an EPFL campus building.

2. CitySim building model

This paragraph briefly illustrates the characteristics of the simplified thermal model used within

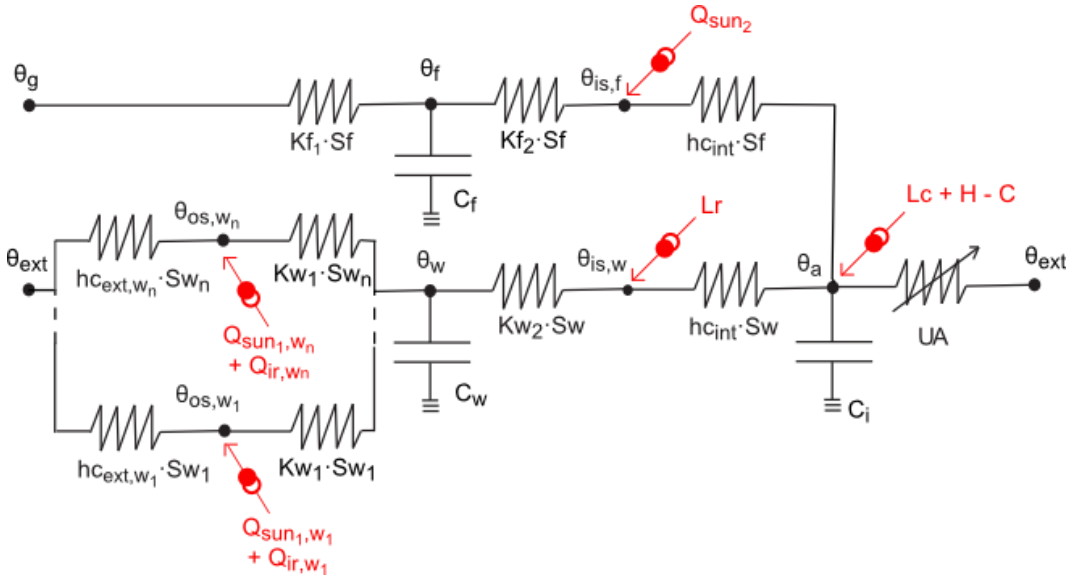


Fig. 12 – The four node thermal model as an equivalent electric circuit not showing the roof node for simplification (roof node similar to wall node)

CitySim. The building envelope is composed of three surface types: the floors, walls and roofs, each of which is considered to have a homogeneous temperature. A building thermal zone can therefore be represented by a four node model (see Fig. 12), in which the light materials of a room (air and furniture) are represented by a node of temperature θ_a (°C) and capacitance C_i (J/K). This node is connected to the exterior air temperature θ_{ext} (°C) through a conductance representing the windows and the air infiltration/ventilation UA (W/K). Furthermore, the node θ_a receives the convective internal gains Lc (W) and the heating H (W) and cooling C (W) loads.

The floor is represented by a node of temperature θ_f (°C) and capacitance C_f (J/K). The total floor surface S_f (m²) is taken into account to compute the conductances to the interior surface temperature $\theta_{is,f}$ (°C) and the ground temperature θ_g (°C) through the specific conductances: Kf_1 and Kf_2 (W/(m²·K)). The internal surface convection coefficient hc_{int} (W/m²·K) is considered to be the same for all kind of surfaces and equal to 3 W/(m²·K) (CIBSE guide). Kf_1 and Kf_2 are calculated using eq. 1 and 2 for a floor of l different layers each of which being represented by a capacitance C_j (J/K) and a conductance K_j (W/(m²·K) where $j = 1..l$ (Lorentz et al., 1982).

$$Kf_1 = \frac{\sum_{j=1}^l C_j}{\sum_{j=1}^l C_j \cdot \left(-\frac{1}{2} \frac{1}{K_j} + \sum_{i=1}^j \frac{1}{K_i} \right)} \quad (1)$$

$$Kf_2 = \left(\sum_{j=1}^l \frac{1}{K_j} - \frac{1}{Kf_1} \right)^{-1} \quad (2)$$

The transmitted light flux through the glazed surfaces Q_{sun2} (W) is considered to reach the floor internal surface node.

The walls and roofs consisting of m and n surfaces are defined in a similar way to the floors, except that each different wall and roof surface has its own outside surface temperature node respectively θ_{os,w_i} and θ_{os,r_j} with $i=1..m$ and $j=1..n$ and a distinct area (respectively Sw_i and Sr_j with $i=1..m$ and $j=1..n$). Finally, the exterior wall and roof surface convection coefficients hc_{ext,w_i} and hc_{ext,r_j} (W/(m²·K)) depend on the wind speed and direction impinging on each wall ($i=1..m$) and roof ($j=1..n$) surfaces. Temperature computations are influenced by radiant and convective exchanges through source terms in the energy balance of the thermal nodes: θ_{os,w_i} and θ_{os,r_j} (°C) depends on the absorbed incident light flux (Q_{sun1,w_i} and Q_{sun1,r_j} in watts) and on the infrared energy flux exchange (Q_{ir,w_i} and Q_{ir,r_j} in watts).

3. Methodology

3.1 Comparative testing approach: BESTEST procedure application

The Building Energy Simulation Test (BESTEST) is a series of test suites developed by the US National Renewable Energy Laboratory, the International Energy Agency and the US Department of Energy. The approach is to compare a candidate program with a set of reference programs that represent the state-of-the-art of building simulation on a series of simulation benchmark test cases. The aim is to identify major errors in the software package.

In this paper, the ability of CitySim to correctly simulate the building envelope is investigated using the IEA BESTEST suite (Judkoff and al., 1995). In this suite, the reference kernel is composed of ESP (UK), BLAST 3.0 Level 215 (USA), DOE2.1E-W54 (USA), SERIRES/SUNCODE (USA), SERIRES-1.2 (USA), S3PAS (Spain), TRNSYS (USA) and TASE (Finland).

The base case (600) is a rectangular single room building whose main characteristics are presented in Table 1 and illustrated in Fig. 13. The base case is declined in subcases (610 to 960) with different subsequent changes in the building mass, the windows orientation and shadings summarized in Table 2.

The comparison is carried out on the annual heating and cooling loads and the annual peak heating and cooling loads considering an ideal heating and cooling control system. The comparison is done in sequence, case-by-case, for each output categories. The distribution of the reference programs results defines a validity range in which CitySim results should fall to pass the test.

The main assumptions that were made for the simulation of the test cases are as follow:

- The climate file available in the online resources of the BESTEST does not include the diffuse horizontal irradiance that is required for CitySim simulations. This value is therefore recalculated using the sun altitude and position given by CitySim. Values for the cloud cover fraction, the relative humidity and the precipitations are extracted from Meteonorm for the Denver location.

- The floor insulation thickness is very large in the BESTEST to reduce the heat flux to the ground. For CitySim simulations, the density and specific heat capacity of this insulation materials is chosen to be 1 kg/m^3 and $100 \text{ J/(kg}\cdot\text{K)}$ respectively similarly to the assumptions taken during ESP-r validation (ESP-r, 2015).

- In the definition of the BESTEST, 3.5% of transmitted solar gains is lost through the windows (reflected back outside of the room). The glazing g-value is therefore decreased by 3.5% to represent this effect.

- The Air Change per Hour (ACH) is corrected to take into account the variation of air density with altitude.

- Other diagnostic cases (195 to 440 and 800 to 810) defined in the IEA BESTEST suite that consider the variation of the shortwave reflectance and long-wave emissivity coefficients, internal heat gains, air change per hour and windows U-values were executed but are not presented in this paper.

- Tests including advanced control strategies for ventilation (650 and 950) and temperature set-points setback (640, 940) are not modelled with CitySim as the tool was not aiming at addressing control strategies. The ground coupling case (990) is also not carried out as it is irrelevant for CitySim simulations.

Table 7 – BESTEST base case building description

Dimensions	L = 8m, P = 6m, h = 2.7m
Envelope	U _{wall} = 0.514 W/(m ² ·K) U _{roof} = 0.318 W/(m ² ·K) U _{floor} = 0.039 W/(m ² ·K)
Air renewal	0.5 h ⁻¹
Internal gains	200 W (60% radiation, 40% convection)
External short-wave absorbance	0.6 [-]
External long-wave emissivity	0.9 [-]
Windows	U _{windows} = 3 W/(m ² ·K) g-value = 0.72129 [-]
System	Ideal air heating and cooling
Setpoint	T _{min} = 20°C, T _{max} = 27°C

Table 8 – BESTEST cases definition

Case	Description
600	Base case, Lightweight envelope, 2 windows of 6 m ² of the south façade
610	Case 600 with 1 m overhang on the south
620	Case 600 windows on east and west
630	Case 620 with 1m fins and overhangs
900	Case 600 with heavy inertia envelope
910	Case 610 with heavy inertia envelope
920	Case 620 with heavy inertia envelope
930	Case 630 with heavy inertia envelope
960	Multizone case (unheated sun-zone on the south side)

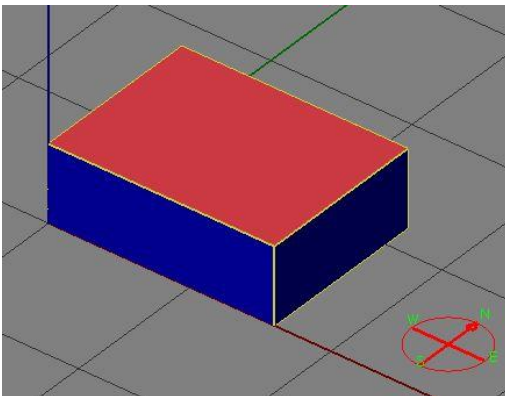


Fig. 13 - BESTEST base case geometry in CitySim Designer

Considering the above-mentioned assumptions, CitySim results are compared within the frame of the BESTEST procedure.

3.2 Experimental verification: Simulation of an EPFL campus building

The predictions of CitySim are compared with the monitored consumption of the LE building located on the EPFL campus. The LE building was built in 1977 for the School of Architecture, Civil and Environmental Engineering and is composed of two main entities: the south zone is considered as an office space and the north zone as a store house (see Fig. 3).

The 3D digital model of the building geometry is based on the work of Carneiro (2011). The weather file is obtained from the Meteonorm software (Meteonorm, 2014) for Ecublens city in which the building is located. The typical meteorological year taken into account is an average of temperatures

over the years 2000 to 2009, and an average of the radiation (direct solar and diffuse) over the years 1991 à 2010. The construction materials were defined by Morel (2004) and from the building plans available at the Real Estate and Infrastructure Department of the school (DII). Associated thermal conductivity, density and specific heat are extracted from LESOSAI material database (Material-db, 2014). The internal heat gains and the air renewal rates are determined using the characteristics of an office and storehouse as defined in the SIA norm (SIA, 2006). The setpoint definition is taken from a previous study on the EPFL campus (Helms, 2009). The glazing ratios of the different facades are estimated using pictures of the building such as Fig. 15. The different building characteristics are summarized in Table 3.

Table 9 – LE building description

Envelope	$U_{wall} = 0.207 \text{ W}/(\text{m}^2\cdot\text{K})$ $U_{roof} = 0.174 \text{ W}/(\text{m}^2\cdot\text{K})$ $U_{floor} = 0.526 \text{ W}/(\text{m}^2\cdot\text{K})$
Air Change per Hour	$ACH_{offices} = 0.3 \text{ h}^{-1}$ $ACH_{storehouse} = 0.14 \text{ h}^{-1}$
Occupants and equipment maximal density (associated schedules in documentation)	Office $Q_{occ} = 14 \text{ m}^2/\text{pers}$ $Q_{equ} = 7 \text{ W}/\text{m}^2$ Storehouse $Q_{occ} = 40 \text{ m}^2/\text{pers}$ $Q_{equ} = 0 \text{ W}/\text{m}^2$
SW abs, LW em	0.8 [-], 0.93 [-]
Windows	$U_{windows} = 1.4 \text{ W}/(\text{m}^2\cdot\text{K})$ $g\text{-value} = 0.7 [-]$
Setpoint	$T_{min} = 21.5^\circ\text{C}$

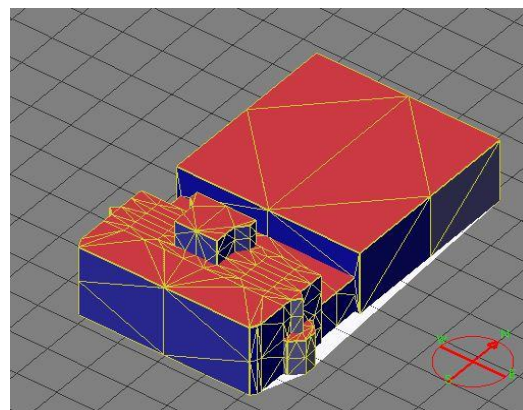


Fig. 14 – LE building in CitySim Designer



Fig. 15 – Picture of the LE South façade (credits: CHABOD Louis, 21.10.2012)

4. Results and discussion

4.1 Comparative testing approach

The results of the BESTEST are presented in Fig. 16. On the considered cases, CitySim outputs are consistent with those of more detailed programs. The results for the annual heating are rather concentrated around the lower limit of the validity range. Those results are close to the ones of ESP which is not a surprise as CitySim was initially compared to ESP-r in its early developments (Kämpf, 2006). Results for peak heating are close to the middle of the validity range in all cases.

CitySim outputs for the annual cooling are close to the high limit of the range, in particular for cases 900 to 930 that have a heavyweight envelope. The peak cooling is rather on the low end of the range in all cases. Exception cases, peak cooling (610) and

annual heating load (960) are outside the range by approximatively 0.14% and 0.53%, but these errors are rather small.

The application of the BESTEST methodology on CitySim revealed that hypothesis concerning the windows are critical. In particular, it showed the necessity to vary the glazing g-value according to the solar angle of incidence. In cases with shadings (610, 630, 910, 930), considering the exact window shape and position rather than just a glazing to wall ratio permitted us to improve the results significantly.

Concerning the envelope, the tests showed that the thermal inertia of the floor and roof have a major effect on the inside air temperature regulation.

Considering those results, CitySim can be considered as validated by the BESTEST protocol and therefore comparable to more detailed programs.

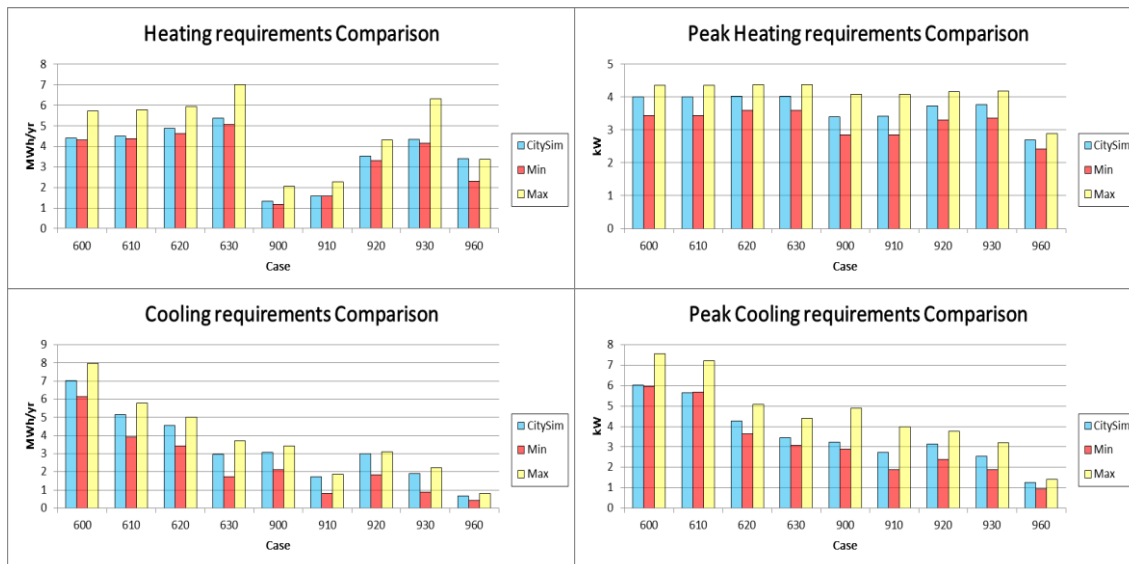


Fig. 16 - BESTEST results for the annual heating and cooling loads and the peak heating and cooling requirements

4.2 Experimental verification

Table 10 summaries the results of monitoring of the annual heating consumption and simulation for the LE building of the EPFL. The heating demand in 2013 is 0.6% lower than the predicted consumption. In 2012, the gap increases to 5.1%. In both cases, CitySim result is over the monitored consumption.

Table 10 – Heating consumption prediction and monitored values

CitySim result	152 651 kWh
Heating 2012	145 237 kWh (-5.1%)
Heating 2013	151 693 kWh (-0.6%)
Average consumption (2012-2013)	148 465 kWh (-2.8%)

This result illustrates that CitySim results are consistent with reality. However, one may question consistency of the hypothesis on which the model is based. Indeed, the weather file obtained from Meteonorm is an average of several different years. There is no guarantee that these climatic data correspond to the actual climate in 2012 and 2013. Differences in temperature or irradiation could alter significantly the heating consumption. The SIA norm represents a standard in Switzerland but might not well represent the occupation schedule of a campus building. Indeed, the scheduled presence of internal gains due to occupants and equipment does not include particular period such as weekends or holidays.

Furthermore, the effects of occupants' stochastic behaviour such as windows opening are not taken into consideration. This effect can be significant in middle season periods. Finally, the air tightness of the envelope (through wall cracks and window joints) decreases after years of operation.

Moreover, the definition of a 21.5°C inside temperature set-point, which is a volumetric average between heated and unheated zones, may not be constant throughout the year as occupants have individual choices of temperature set-points in the different office rooms.

The effect of the separating walls' thermal mass is neglected in the CitySim model, which is not a bad approximation as the separating walls are lightweight structures.

Considering the above-mentioned assumptions, the LE building was quickly modelled using CitySim with a limited number of parameters. The obtained results were shown to be consistent with monitoring. However, only the annual heating consumption of the LE building could be compared, limiting the scope of this experimental validation. This was due to the fact that the building is located in a cold dominated climate and is not equipped with air conditioning system. Furthermore, the monitoring of the building was not available on an hourly basis, making the comparison with peak heating requirements impossible.

5. Conclusion

In this paper, the results of a large-scale building energy simulation tool called CitySim, which uses a simplified building model to reduce data input requirements and computing time, are verified using two distinct methodologies.

First, the tool is shown to produce results comparable to those of more detailed programs by applying the BESTEST comparative testing approach. Only a couple of errors arose on the simulation of the peak cooling demand (610) and the heating load (960). However, those differences only diverge from the expected result by less than 1%. CitySim can therefore be considered as validated by this BESTEST procedure.

Then, the accuracy of the tool is verified experimentally by comparing the program outputs with the monitoring of the annual heating consumption of an EPFL campus building. The difference in results is around 5% with broad hypothesis.

CitySim therefore proved to be a reliable tool for quickly determining the heating and cooling needs of buildings for design and retrofit stages. Therefore, this program could have a role to play in mitigating the foreseen energy consumption increase in the urban context due to the growth of urbanized population.

6. Acknowledgement

Many thanks to kaemco LLC for providing help, funding and technical support for the CitySim software. Thanks to the DII department of EPFL for providing the necessary documentation and data.

7. Nomenclature

ACH	Air Change per Hour
C	Cooling power
C_f	Capacitance of the floor
C_i	Capacitance of the inside air
C_j	Capacitance of layer j
C_w	Capacitance of the wall
g-value	Solar energy transmittance of glass

h	BESTEST Building height
H	Heating power
$h_{c_{int}}$	Internal convection exchange coefficient
$h_{c_{ext,w_i}}$	External convection exchange coefficient of roof surface j
$h_{c_{ext,w_i}}$	External convection exchange coefficient of wall surface n
K_{f1}	Specific floor conductance to the exterior of the thermal zone
K_{f2}	Specific floor conductance to the interior of the thermal zone
K_j	Specific conductance of layer j
K_{w1}	Specific wall conductance to the exterior of the thermal zone
K_{w2}	Specific wall conductance to the interior of the thermal zone
L	BESTEST base case length
L_c	Convective internal gains
L_r	Radiative internal gains
P	BESTEST base case width
Q_{ir,r_j}	Longwave light flux exchange on roof surface j
Q_{ir,w_n}	Longwave light flux exchange on wall surface n
Q_{sun1,r_j}	Absorbed incident light flux on roof surface j
Q_{sun1,w_n}	Absorbed incident light flux on wall surface n
Q_{sun2}	Light flux transmitted to the interior
Q_{occ}	Occupants density
Q_{equ}	Equipment density
S_f	Total surface of the floor
S_{r_j}	Area of roof surface j
S_{w_n}	Area of wall surface n
S_w	Total surface of the wall
θ_a	Inside air temperature
θ_{ext}	External air temperature
θ_f	Temperature of the floor
θ_g	Temperature of the ground
$\theta_{is,f}$	Floor inside surface temperature
$\theta_{is,w}$	Wall inside surface temperature
θ_{os,r_j}	Outdoor temperature of roof surface j
θ_{os,r_n}	Outdoor temperature of wall surface n
θ_w	Wall temperature
UA	Window and infiltration/ventilation conductances
U_{floor}	Thermal conductivity of the floor
U_{roof}	Thermal conductivity of the roof
U_{wall}	Thermal conductivity of the wall

References

- Carneiro, C. 2011. *Extraction of Urban Environmental Quality Indicators using LiDAR-Based Digital Surface Models*. Ph.D. Thesis. Swiss Federal Institute of Technology. Switzerland
- DII. 2008. *Bilan des énergies du site de l'EPFL à Ecublens 2007*. Swiss Federal Institute of Technology. Switzerland.
- ESP-r, 2015, Accessed January 15 <https://espr.svn.cvsdude.com/esp-r/>
- Helms, T. 2009. *Energy System Analysis of a University Campus: Energy consumption and efficiency measures for the Ecole Polytechnique Federal Lausanne (EPFL)*. Swiss Federal Institute of Technology. Switzerland
- IEA 2008. *World Energy Outlook 2008*. International Energy Agency
- Judkoff, R. 1988. "Validation of Building Energy Analysis Simulation Programs at the Solar Energy Research Institute." *Energy and Buildings* 10: 221-239. doi: 10.1016/0378-7788(88)90008-4.
- Judkoff, R. Neymark, J. 1995. *International Energy Agency building energy simulation test (BESTEST) and diagnostic method*. Golden: National Renewable Energy Laboratory. United States
- Kämpf, J. Robinson, D. 2006. "A simplified thermal model to support analysis of urban resource flows." *Energy and Buildings* 38: 445-453. doi: 10.1016/j.enbuild.2006.09.002.
- Kämpf, J. 2009. *On the modelling of Urban Energy Fluxes*. Ph.D. Thesis. Swiss Federal Institute of Technology. Switzerland
- Lorenz, F. Masy, G. 1982. *Méthode d'évaluation de l'économie d'énergie apportée par l'intermittance de chauffage dans les bâtiments. Traitement par différences finies d'un modèle à deux constantes de temps*. Technical report, Building physics Laboratory, Liège University.
- Material-db, 2014. Accessed September 19 <http://www.materialsdb.org/>
- Meteonorm, 2014. Accessed November 25 <http://meteonorm.com/>
- Morel, N. 2004. *Description of the LESO Building*. Swiss Federal Institute of Technology. Switzerland.
- SIA. 2006. *Condition d'utilisation standard pour l'énergie et les installations du bâtiment*. Swiss society of engineers and architects. Switzerland.
- UN. 2011. *World Urbanization Prospects: The 2011 Revision*. United Nations, Department of Economic and Social Affairs, Population Division. United States

Integrated design and dynamic simulation for a new zero energy building

Dama Alessandro – Politecnico di Milano, Dipartimento di Energia – alessandro.dama@polimi.it

Angelotti Adriana – Politecnico di Milano, Dipartimento di Energia – adriana.angelotti@polimi.it

Penso Davide – Politecnico di Milano, Dipartimento di Energia – davide.penso@mail.polimi.it

Abstract

The European Directive 2010/31/EU on the energy performance of buildings introduces the nearly zero-energy requirement, by 2020 and 2018 for new buildings in general and for public buildings respectively. This challenging target requires a complete assessment and optimization of the integration of efficient systems and renewable energy technologies in the building design. Dynamic energy simulation represents an essential tool in this regard.

In this context, we present an integrated approach applied to the design of a new university building in Milan, in northern Italy. This case study consists of a four-storey building dedicated to offices, laboratories and classrooms.

The building envelope design was formerly optimized, adopting passive strategies, like thermal insulation, solar control, daylighting and night natural ventilation, to reduce heating, cooling and lighting needs.

In order to meet the net zero energy requirement, locally available renewable energy sources and energy efficient systems have to be taken into account. Therefore in this case dynamic energy simulations in EnergyPlus are used to compare different heating and cooling plants options. A reference plant consists of a condensing boiler and a chiller coupled to a cooling tower, and an alternative system is based on a Ground Source Heat Pump coupled to a vertical ground heat exchanger. A VAV distribution system is assumed. Finally, PV devices are integrated in the building roof.

The simulation allows to choose the most efficient plant and to assess the overall strategy. Finally, the net zero energy target is tested and critically related to the different uses available in the building and to the climatic context.

1. Introduction

According to the European Directive 2010/31/EU on the energy performance of buildings, by 2020 all new buildings should comply with the nearly zero-energy standard. This deadline was recently put forward to the end of 2015 by the Regional Council of Lombardy, northern Italy.

The design of a Zero Energy Building (ZEB) cannot be separated from the climatic context. On the envelope design side, the ZEB concept can follow the principles of the passive and low energy building, taking advantage of the natural sinks and of the climatic drivers. On the energy supply and production design side, including RES, the ZEB concept has to take into account locally available energy technologies and sources. Therefore, ZEB examples in different European countries are needed to demonstrate the feasibility of the EPBD target.

Regarding southern Europe, some authors addressed the issue of residential ZEBs in the Mediterranean climate either analysing examples (Ferrante and Cascella, 2011; Evola et al. 2014, Cellura et al. 2014) or providing general frameworks (Oliveira et al. 2013). Yet the feasibility of the ZEB target for tertiary buildings, where internal loads and ventilation requirements can be important, still lacks in demonstration.

This paper presents the EdZEN project, namely the design of a Zero Energy multi-function university building for the Politecnico of Milan. The present study follows previous studies by the authors (Grecchi et al., 2012, Dama et al., 2014) facing the EdZen envelope design, and addresses the supply and production systems design.

2. Methodology

The Net Zero Energy target is chosen, namely providing through building integrated renewables the primary energy required for climatisation and lighting on a yearly basis.

The methodology is based on the following steps:

- firstly a low energy demand for heating, cooling and lighting is achieved, by means of a careful envelope design, adopting passive strategies and daylighting (Dama et al., 2014; Grecchi et al., 2012);
- secondly the HVAC systems are optimised in order to achieve high energy efficiency;
- finally RES technologies on site are adopted to provide the necessary energy.

As already mentioned, the present paper focuses on the second and third steps.

The analysis was performed by means of dynamic energy simulations carried out in EnergyPlus. In Section 3 the main characteristics of the EdZen building and its simulation model are presented. In Section 4 the two HVAC systems configuration analysed are introduced as well as the EnergyPlus models adopted for the main components. In Section 5 the results of the annual simulations are reported and discussed. Finally, in Section 6 some conclusions are provided.

3. The EdZEN building

The preliminary design of the EdZEN consists of a four-storey building dedicated to offices, laboratories and classrooms.

Offices are located on the first, second and third floor. Laboratories cover the underground area and the first and second floors of the west wing, a large classroom is located at the ground level in the east wing. The building entrance, the two wings and the south strip are connected by a central Atrium, which is not conditioned. Two views of the building rendering are shown in Fig. 1 and 2. The building is more thoroughly described in (Grecchi et al. 2012).

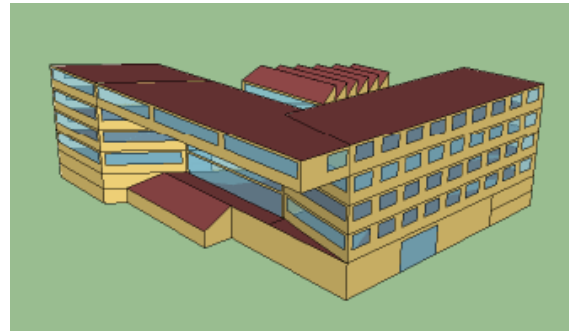


Fig. 1 – EdZEN South/East view

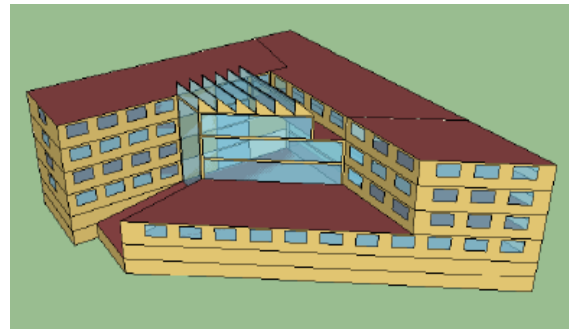


Fig. 2 – EdZEN North/West view

The building envelope components are characterised by a high level of thermal insulation and air tightness. The transparent portions are protected by external shading devices to prevent unwanted solar gains and glare effects.

A set of passive strategies for the office zones was evaluated and optimized in (Dama et al., 2014); in this work, some of those strategies are extended to the classroom and to the laboratories as can be seen in Table 1. In the office zones the lighting system uses highly efficient sources (LED) with continuous dimmer controlled by daylighting sensors.

The building was modelled in EnergyPlus (v. 8.1). 25 thermal zones were identified and simulated: 14 office zones, 3 laboratories, 1 classroom, 6 service areas (corridors, stairs and technical rooms) and 1 atrium.

Focusing on offices, classroom and laboratories internal loads due to occupancy, equipment and lighting as well as minimum outdoor ventilation rates are shown in Table 2. The minimum outdoor ventilation rates have been set according to EN 15251.

Table 1 – Passive strategies adopted in each consumer

Strategies	Offices	Classroom	Labs
Solar Control	x	X	x
Natural Night Ventilation	x		
Daylighting	x	x	
LED	x		

Table 2 – Design internal loads and ventilation rates

	Offices	Classroom	Labs
Floor area (m ²)	1133	379	1705
People (m ² /p)	10	2	20
ACH (1/h)	1.68	5.04	2.94
Equip. (W/m ²)	10		10
Lights (W/m ²)	6	12	12

4. HVAC systems

Two HVAC systems configurations were studied, differing only in the heating/cooling plants. An air distribution system was adopted for all the cases, including 5 Air Handling Units (AHU) with enthalpy recovery and Variable Air Volume (VAV) distributions, dedicated to the following groups of thermal zones:

- offices on the east wing,
- offices on the west and south wings,
- classroom,
- laboratories at ground and first floor,
- laboratories underground level.

The two configurations are:

1. Base: a Condensing Boiler (CB) for heating and a water-to-water Chiller (C) coupled with a Cooling Tower (CT) for cooling (Fig. 3);
2. Advanced: a vertical Ground Heat

Exchanger (GHE) coupled to a Water-to-Water Heat Pump (HP) for winter heating and to the water-to-water Chiller (C) for summer cooling. In this case a ground Free Cooling (FC) option was also investigated (Fig. 4).

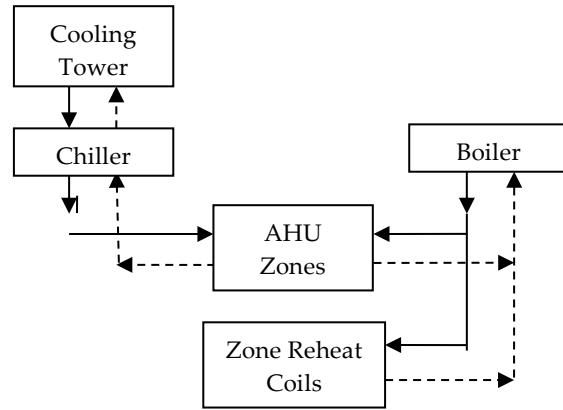


Fig. 3 – Base configuration

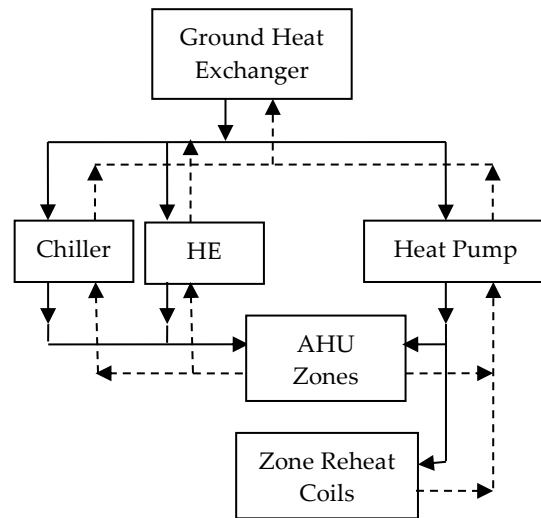


Fig. 4 – Advanced configuration

The AHU and the VAV distribution are illustrated in Fig. 5. Each AHU incorporates an enthalpy recovery system (*Heat Exchanger: AirToAir: SensibleAndLatent*) with a sensible and latent effectiveness at 100% and 75% flow rate equal to 85% and 80% respectively.

The Heat Recovery control of the classroom differs from the one employed in the other zones, which is only based on temperature differences. For the classroom, in both system configurations, the option for Indoor High Humidity (IHH) control

was employed: if zone relative humidity is over 60% and the outdoor humidity ratio is below the indoor humidity ratio, then the outdoor mass flow rate increases and the heat recovery is bypassed. This option had shown significant savings in controlling high latent loads.

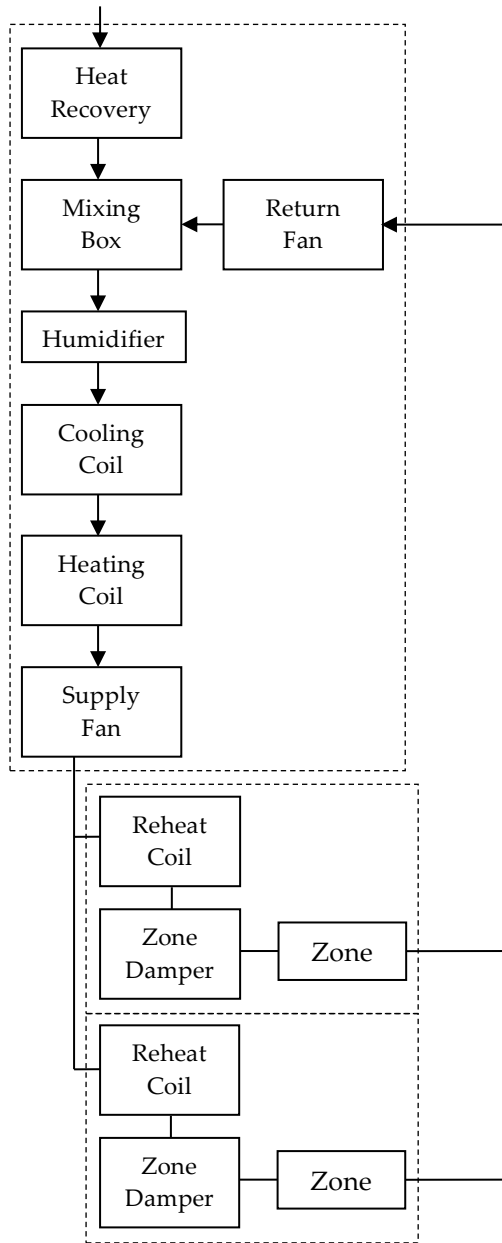


Fig. 5 – AHU and VAV

For the Gas Condensing Boiler simulation Boiler: Hot Water model in EnergyPlus was adopted. The inputs required are the boiler nominal capacity, the thermal efficiency and some performance curves. The boiler nominal capacity is 180 kW with

efficiency equal to 98.4% for a water return temperature equal to 60°C. At every time step the effective thermal efficiency is calculated according to a biquadratic efficiency curve with Part Load Ratio and return temperature as independent variables.

The EnergyPlus model *Chiller: Electric EIR* was adopted for simulating the water-to-water Chiller. In this case the required inputs are the nominal cooling capacity and EER (cooling rate output to electric power input ratio) and three performance curves, allowing us to model the Chiller behavior as a function of the temperatures at the evaporator outlet and at the condenser inlet and of the Part Load Ratio. For the case study, with evaporator outlet temperature at 7°C and condenser inlet temperature at 30°C, the nominal full load capacity was 197 kW and the EER was 4.6.

A parametric model was used also for the Heat Pump, namely the *Heat Pump: Water to Water: Equation: Fit Heating*. The nominal heating capacity at 45°C condenser outlet temperature was 209 kW with a COP = 4.1 (heating rate output to electric power input ratio).

The Cooling Tower adopted in the condenser loop of the Chiller in the Base configuration is modeled as a counterflow heat exchanger with a single-speed fan by means of the *Cooling Tower: SingleSpeed* model.

The Ground Heat Exchanger was modeled by means of the *GroundHeatExchanger: Vertical model*, based on both long-term (Eskilson, 1987) and short-term (Yavuzturk and Spitler, 1999) response factors named g-functions. The borehole field was made up of a rectangular configuration of 5 x 10 U-pipes, with a distance equal to 7 m and a depth of 100 m. The ground thermal conductivity was assumed to be 2.4 W/(m.K), a typical value for a saturated sandy aquifer, and the undisturbed ground temperature was set at 14°C.

The Free Cooling option was implemented by introducing a *HeatExchanger: WaterToWater*, allowing us to couple directly the Ground Heat Exchanger loop with the supply loop and thus bypassing the Chiller. Free Cooling is active from October to May, whenever the GHE outlet temperature lies in the range between 14 and 16 °C. Such temperature levels are suitable for removing

only sensible cooling loads. Therefore, since latent cooling load is very high and permanent in the Classroom, the Free Cooling Loop was coupled only to the AHU serving offices and laboratories.

Considering the very modest local wind velocities (the yearly average velocity is 0.9 m/s), the only renewable energy locally available is solar energy. Therefore, after choosing the most efficient HVAC configuration between the Base and the Advanced, a yearly energy balance for the three destinations, namely offices, classrooms and laboratories, was performed. Then we assumed that PV panels with a nominal efficiency equal to 17% could be placed on the EdZEn roof with a South orientation and a tilt angle equal to 30°. The PV yearly electricity generation was then calculated and compared with the energy needs of the different destinations.

The simulations were carried out with a timestep of 15 minutes for one year, with the climatic data of Milano (Linate Airport).

The comfort set points were chosen according to standard EN 15251. In category II ($-0.5 < PMV < +0.5$), the following set points were adopted:

- Winter condition, operative temperature higher than 20°C and air relative humidity higher than 25% ;
- Summer condition, operative temperature lower than 26°C and air relative humidity lower than 60%.

5. Results and discussion

In Table 3 we show the annual specific (sensible and latent) thermal energy need for heating (ETH) and for cooling (ETC), and the annual specific electrical energy need (LENI) for lighting, for each area. The thermal power was computed from the heat exchanged on the coils, as the enthalpy difference between the air inlet on the cooling coil and the air outlet on the reheat coil.

The results in Table 4 confirm that thermal and artificial lighting demand in office zones are considerably low: this assessment was formerly given in (Dama et al., 2014) as a result of the adoption of the passive strategies listed in Table 1. The classroom is characterised by a high

occupancy level (see Table 2) which turns out in a very high specific demand for cooling and dehumidification. The energy demand in laboratories is dominated by the electric lighting, which is due to the fact that a large area is located underground.

Table 3 – Annual specific thermal energy and lighting needs

kWh/m ²	Offices	Classroom	Labs
ETH	7.4	0.0	0.9
ETC	19.5	97.1	25.7
LENI	5.5	13.6	38.2

Table 4 reports the comparison between the Base and the Advanced plant configuration in terms of annual specific primary energy consumption for heating and humidification (EPH) and for cooling and dehumidification (EPC), for each destination. Figures 6, 7 and 8 show the incidence of the use of each component.

Table 4 – Annual specific thermal energy for Base (1) and Advanced (2) configurations

kWh/m ²	Offices	Classroom	Labs
EPH-1	9.5	0	5.9
EPH-2	5.9	0	5.5
Relative difference	-38%		-7%
EPC-1	14.9	147.9	27.5
EPC-2	11.9	109.5	23.5
Relative difference	-20%	-26%	-14%

The primary energy used by boiler, chiller and heat pump was split among the destinations with the same proportion of the power exchanged on the water loops serving the corresponding AHU and reheat coils. Primary energy conversion factors assumed are 2.5 for electricity and 1.1 for gas.

Table 4 shows that the advanced solution produces

a significant energy saving for the office heating. The saving potential in the laboratory heating is much lower since in this case the fan operation has a larger impact on the energy used (see Figure 8).

A considerable saving potential can be seen for cooling in all the destinations. In this comparison only a modest contribution comes from the increase of the chiller efficiency condensed with the ground water loop. Actually the major saving contribution comes from eliminating the evaporative tower and its consumption.

The comparison between the seasonal generator efficiencies is reported in Table 5.

Table 5 – Systems seasonal efficiencies in the two configurations

Base configuration		Advanced configuration	
Boiler efficiency	Chiller EER 1	Heat pump COP	Chiller EER 2
1.09	5.24	3.99	5.47

Figure 9 shows the dynamic profile of the Chiller EER together with the inlet water temperatures in the condenser and the Partial Load Ratio (PLR). In the considered week, the return temperature of the ground heat exchanger is 4-5 degrees below the return of the evaporative tower, resulting in an efficiency increase in the same order of magnitude of the difference in the seasonal values.

Figure 10 shows an example of free cooling operation: the GHE outlet temperature, directly sent to the Heat Exchanger, ranges between 14°C and 16°C as expected. The outlet and inlet air temperatures at the cooling coil of the offices on the south/west wing highlight when Free Cooling is exploited in those zones. On a seasonal basis the adoption of the Free Cooling strategy in the Advanced configuration results in an additional primary energy saving for cooling equal to 5% and 4% in the for offices and laboratories respectively.

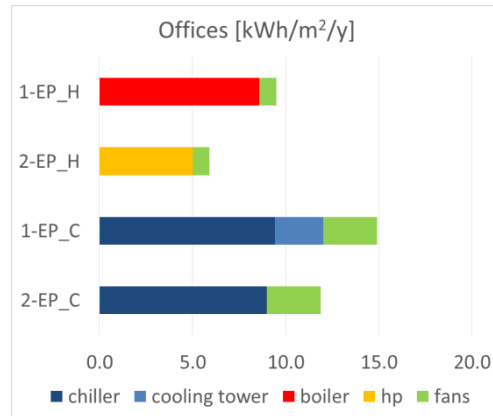


Fig. 6 – Offices: specific primary energy for cooling and for heating in the Base (1) and Advanced (2) configurations

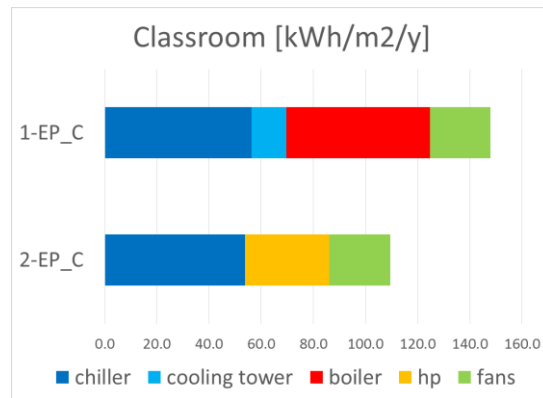


Fig. 7 – Classroom: specific primary energy for cooling and for heating in the Base (1) and Advanced (2) configurations

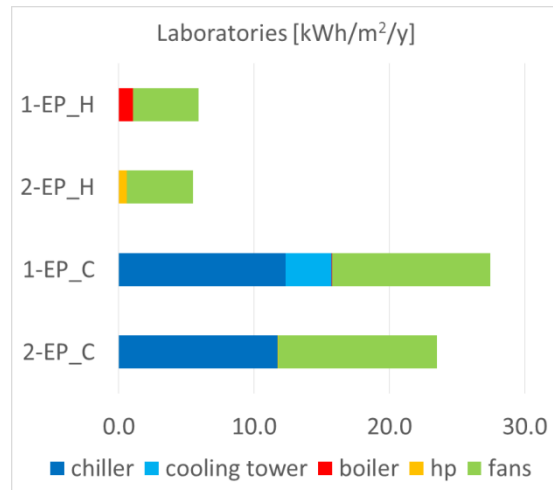


Fig. 8 – Laboratories: specific primary energy for cooling and for heating in the Base (1) and Advanced (2) configurations

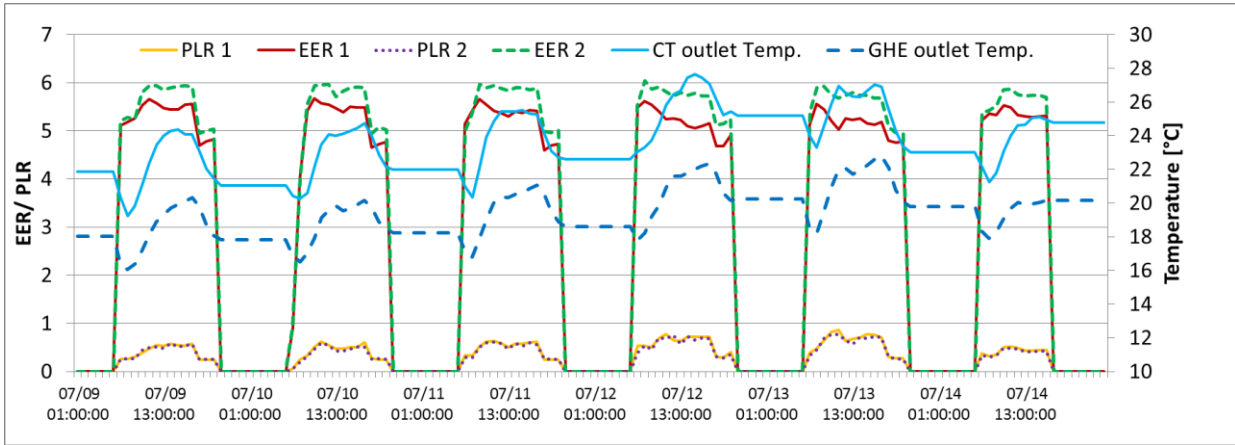


Fig. 9 – Chiller behavior in a typical summer week: EER and water temperature at condenser inlet, Base (1) and Advanced (2) configuration

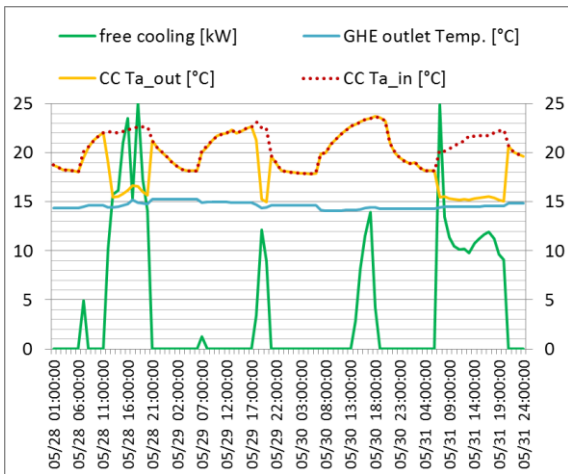


Fig. 10 – Free cooling operation in a typical summer week

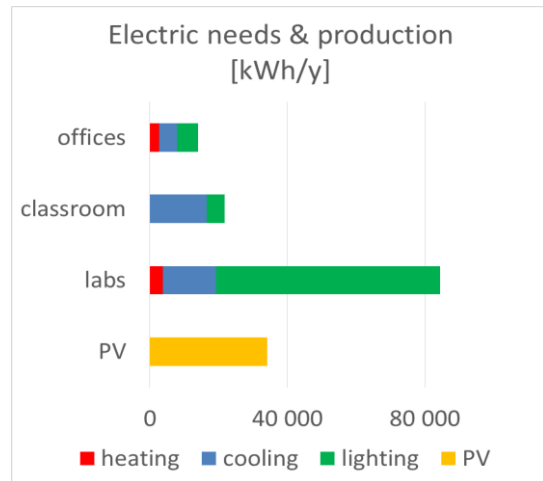


Fig. 11 – Electrical needs and PV production on a yearly basis

In Figure 11, the annual electricity need for the three destinations is shown, together with the PV plant production. It can be noticed that, limited to offices and classroom, the Zero Energy target is almost achieved: about 95% of the energy need can be covered by the PV production on site. This outcome suggests the importance of reducing the lighting need in the laboratories, by introducing high efficiency sources (LED) and by designing proper light-shelves to convey daylighting at the underground level.

On the supply side, the possibility to adopt PV systems in the façade, integrated into the present shading systems, should be investigated.

6. Conclusions

A comparison between two HVAC plants configurations for the EdZen building has been carried out allowing to quantify the benefits of the advanced one, which exploits the potential of the heat exchange with the ground. The building's electricity need has been broken down into the different space typologies, namely offices, classrooms and laboratories, and compared with a preliminary hypothesis for a PV production on site. Among the investigated destinations, the classroom presents the highest specific energy need, due to the high occupancy level and the consequent high ventilation rates and latent loads. It was found that exploiting the heat exchange with the ground (Advanced configuration) results in 38% and 7% heating primary energy saving in the

offices and in the laboratories respectively, and in a cooling primary energy saving ranging between 14% and 27% depending on the destination. Free cooling can provide an additional 4-5% saving. In this regard, as a future development, the possibility to adopt a mixed (air and water) distribution system will be investigated, with the aim to separate sensible and latent loads control and to better exploit Free Cooling for the sensible one.

Limited to offices and classrooms, the Zero Energy target is nearly achieved: about 95% of the energy need can be covered by the PV production on site. In this regard, adopting energy saving strategies related to lighting is crucial for achieving the zero energy goal in non-residential buildings, as the interventions adopted in the offices and in the classrooms demonstrate. Therefore, such strategies will be designed and implemented in the laboratories as well.

As a further development, on the supply side, the possibility to adopt PV systems in the façade, integrated into the present shading systems, should be investigated.

7. Nomenclature

Symbols

ACH	Air Changes per Hour
AHU	Air Handling Unit
C	Chiller
CB	Condensing Boiler
COP	Coefficient Of Performance
CT	Cooling Tower
EER	Energy Efficiency Ratio
ETH	Annual specific thermal energy for heating and humidification [kwh/m ²]
ETC	Annual specific thermal energy for cooling and dehumidification
EPH	Annual specific primary energy for heating and humidification
EPC	Annual specific primary energy for cooling and dehumidification
LENI	Lighting Energy Numeric Indicator
GHE	Ground Heat Exchanger
HVAC	Heating Ventilation Air Conditioning

PV	Photovoltaic
RES	Renewables
VAV	Variable Air Volume

References

- Cellura, M., Guarino, F., Longo F., Mistretta, M. 2014. „Energy life-cycle approach in Net zero energy buildings balance: Operation and embodied energy of an Italian case study“. *Energy and Buildings* 72: 371-381.
- Dama, A., De Lena, E., Maserà, G., Pagliano, L., Ruta, M., Zangheri, P., 2014. „Design and passive strategies optimization towards zero energy target: the case study of an experimental office building in Milan“. *Proceedings of BSO14 Building Simulation and Optimization*, London, UK, 23-24 June 2014.
- Eskilson, P. 1987. *Thermal Analysis of Heat Extraction Boreholes*. Ph.D. Thesis, Department of Mathematical Physics, University of Lund, Lund, Sweden.
- Evola, G., Margani, G., Marletta, L. 2014. „Cost-effective design solutions for low-rise residential Net ZEBs in Mediterranean climate“. *Energy and Buildings* 68 (A): 7-18.
- Ferrante, A., Cascella, M.T. 2011. „Zero energy balance and zero on-site Co2 emission housing development in the mediterranean climate“. *Energy and Buildings* 43 (8): 2002-2010.
- Grecchi, M., Maserà, G., Ruta, M., Pagliano, L., Dama, A., Zangheri, P., 2012. „Experimental nearly zero-energy office building in Mediterranean climate“ in *The missing brick: towards a 21st-century Built Environment Industry*, Maggioli Editore, Italy.
- Oliveira Panão, M. J.N., Rebelo, M.P., Camelo, S.M.L. 2013. „How low should be the energy required by a nearly Zero-Energy Building? The load/generation energy balance of Mediterranean housing“. *Energy and Buildings* 61: 161-171.
- Yavuzturk, C., J.D. Spitler. 1999. „A Short Time Step Response Factor Model for Vertical Ground Loop Heat Exchangers“. *ASHRAE Transactions* 105(2):475-485.

A parametric approach to design a wooden climatic responsive village in Atacama Desert (Chile)

Francesco Leccese – University of Pisa, School of Engineering, Dept. of Energy Engineering, Systems, Territory and Constructions (DESTeC) – f.leccese@ing.unipi.it

Alessandro Mattoccia – University of Pisa, DESTeC – mattoccia.alessandro@gmail.com

Michele Rocca – University of Pisa – DESTeC – michele.rocca.au@gmail.com

Rodrigo Rubio – Institute for Advanced Architecture of Catalonia, IAAC (Barcelona, Spain) – rodrigo@iaac.net

Giacomo Salvadori – University of Pisa, DESTeC – giacomo.salvadori@ordineingegneripisa.it

Abstract

The typical architecture of countries in a hot arid climate is a valuable source of principles that today we call bioclimatic and sustainable. Ancient people knew very well how to avoid the harshness of the desert and their knowledge came from centuries of experience and attempts. Among these principles, we can remember the typical narrow winding alleys, the courtyard houses, the domes and the large thermal mass of the walls. It was decided to combine this knowledge with computer techniques to try to parameterize these aspects in order to optimize and make them as effective as possible, allowing us to add something to what had been handed down. The project was born from a practical need, creating new settlements in places far from civilization, but close to important human activities. The first aim of the project is to design self-sufficient houses, using the sustainable desert principles, and the second aim is to use the concept of folding architecture to build a village as soon as possible. From an energetic point of view, the patio has a crucial role to enhance the inner environment: producing shade, it supports natural ventilation. Starting from a “zero organism”, through generative algorithms made in *Rhino/Grasshopper*, this effect is optimized by maximizing the area of the shadow produced by the roof inside the patio, during the hottest hours. By classifying the various organisms obtained, through structural (i.e.: length, compressive stress) and energetic parameters (i.e.: radiation analysis, cooling loads), a ranking open to various solutions has come out.

1. Introduction

The research described in this paper explores the potential of using digital technologies in architecture, particularly for developing more

sustainable buildings. The argument is that technology, in general, and computation in particular, allows architecture to respond to geographical and individual requirements. The use of technology to develop responsive and customized buildings represents a change and an opportunity for a more ecological approach. A clear understanding of the main problems and site surrounding conditions, which influence building design, increases the possibility of adopting environmentally friendly strategies in the early stages of design, even before a building form exists. Meaningful data visualization can assist designers in making better design judgments. The proposed houses system uses digital tools to find a solution that could adapt to different locations and weather conditions. In particular, this project was born from a practical need (Mattoccia, 2014): creating new settlements in places far from civilization but at the same time close to important human activities, as a mining activity in Atacama Desert could be. The first aim of the project is to design Self-Sufficient Houses, able to create a comfortable environment in this extreme climate, using the desert sustainable principles (see Sec.1.3). At first, we solved the problem to build the village as quickly as possible using the concept of Folding Architecture (see Sec. 2.1). Then, to reproduce the traditional urban fabric of a desert city, characterized by a natural growing, we used the idea of Cellular Automata (see Sec. 2.2). All these concepts converge in Desert Architecture as shown in Fig. 1. The settlement is characterized by a folding base module that can be aggregated in an independent way. The research is based on the optimization and the design of this module.

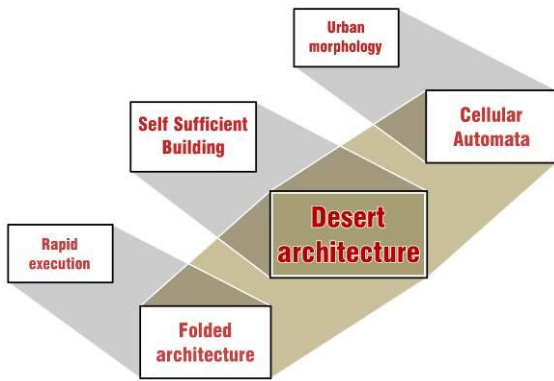


Fig. 1 – Desert Architecture: scheme of design aims.

1.1 Parametric Architecture

Coding in architectural design can be understood as representation of algorithmic processes that express architectural concepts or solve architectural problems, as generative tools for the shape design which follows well-defined criteria, such as sun, wind, environment or other considerations. To apply computational methods, first of all we have to translate the thought process into a computer program by a programming language. In a Textual Programming Language (TPL), the codes are linear sequences of characters, while, in a Visual Programming Language (VPL), the codes consist of iconic elements that can be interactively manipulated according to some spatial grammar. *Grasshopper*, a plug-in of *Rhinoceros*, is a VPL; it increases a large set of primitive components, mathematical functions and modifiers, allowing an effective reduction in the implementation effort and a significant advantage in working in visual scheme.

In a parametric model, the schema is the collection of relationships between functions and parameters, where the form is a function of the latter. The connections allow dataflow from primitive to primitive, until it reaches the end of the graph that creates geometric models.

While algorithms assist the examination of complex strategies, human reasoning still governs the selection of appropriate input parameters to take in consideration. Choices are born from human capacity, so the real advantage of a parametric approach is the rapidity with which it can carry out certain operations, such as optimization, which would have been impossible

to develop by hand. The role of the architect is crucial, both from a technical point of view, for instance by setting the range of the input, and for the design strategy, choosing the most effective one.

1.2 Climate

The climate of the Atacama Desert is characterized by wide daily thermal fluctuations, with a high temperature difference between night and day. In summer, daily temperatures range from under 14 °C to over 32 °C, and in winter from 0 °C to 22 °C, with an average temperature difference of 20 °C during the year. These conditions are accompanied by low daytime relative humidity, intense solar radiation (Fig. 2) and strong hot dusty winds, predominantly from the south-east. During the year, there is very little rainfall, which causes a very low vegetation cover and limited water supplies.

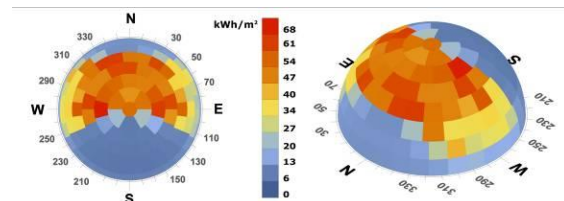


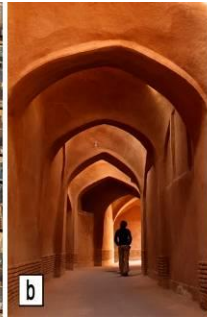
Fig. 2 – Solar radiation analysis: Sky Dome (*Grasshopper*, *Ladybug*).

1.3 Desert architecture

Nowadays to obtain a comfortable environment we consume a lot of energy to heat or cool buildings. In a more or less remote past, when energy was not so easily available, architects had to resort to other, often clever systems to provide maximum comfort to the indoor environment. Briefly, Desert Architectural principles of hot arid climate are the following (Maleki, 2011): Town planning, Courtyard house, Dome and Thermal inertia.

Town planning. An important strategy against the extreme climate is the agglomeration of the buildings, which limits the total surface exposed to solar radiation, reducing therefore also the heat absorption overall, and diminishing the penetration of dusty wind within the village. The urban form of a traditional city is highly centralized and inward looking, with a continuous

pattern of courtyard houses (Fig. 3a).



density (Fig. 3d).

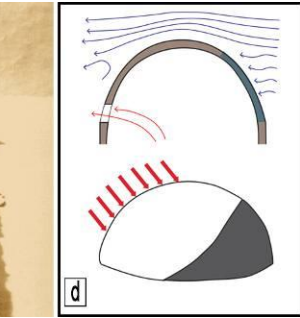
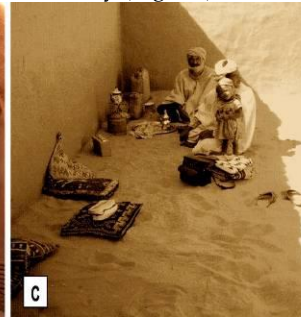


Fig. 3 – Desert Architecture: a) A typical desert pattern; b) Covered alleys; c) The shadow casts by a courtyard; d) The dome's advantages.

Each building is joined together by common walls and connected by a very diffuse network of narrow alleys (Fig. 3b) departing from the main road system. The directions of this pattern are conceived to avoid wind and to produce as much shade as possible.

Courtyard house. This shape is a microclimate modifier, which may improve thermal comfort conditions in the inner enclosed space. The building shades the courtyard (Fig. 3c) and the streets as well; this shading effect lowers the overall cooling load (Scudo, 1988). A well-designed courtyard house is cool during the day, when ambient temperature is high and warm at night when it is low. During the night, the cool air is stored until the mid-hours of the next day, and during the day the courtyard acts as an air shaft: cool air begins to rise and also leaks out of the surrounding rooms. It is a simple design strategy for bringing both air-movement and natural light into the entire house.

The dome. The roof is the most critical component of the whole building: it receives the greatest amount of solar radiation during the day, and emits the greatest quantity of heat by night radiation to the sky. The dome, compared with equivalent flat covers, ensures thermal performance considerably more effective. A dome has a greater area of assignment of heat by convection and transfers heat more efficiently than a flat roof. Furthermore, when the dome is exposed to not zenith sunlight, it always has a part in the shade and a part in the sunlight. This means that there should be a difference of temperature between the two parts and a corresponding movement of air, due to the difference in air

Thermal inertia. When outdoor conditions are very extreme, the system has to resist thermal gains, minimizing hot air infiltration, solar radiation and heat conduction. Thick walls of brick or stone have been traditionally used in construction of buildings. These walls perform the dual function of isolating the internal environment from outside and of storing the absorbed heat during the day. Thus, heat flow from outside to inside is delayed, while in the cooler hours the heat, stored in the walls, partially heats the indoor environment. The consequence is a leveling of the curve of the temperature changes inside the building.

2. Simulation

2.1 Tectonic system

The necessity of having a foldable structure arises from the need to build our houses as quickly as possible given the extreme climate in which our project takes place. One answer to this problem is given by *origami*. An origami form is constituted by patterns that are the repetition of similar geometric shapes, which will form a deployable surface: this means it is possible to fold this pattern to a compact-package state. We have chosen the famous "Miura pattern" (Fig. 4) to design the complete structure that arrives folded on site and that can easily be opened. This pattern can be obtained by a repetition of reverse folds in lines producing symmetric trapezoids that form a herringbone tessellation, in which, in each corner, we have 3 mountains and 1 valley or 1 mountain and 3 valleys. The folded pattern has a

characteristic *zigzag* corrugation that allows extending and retracting in both directions. As you can see in Fig. 4, we have chosen this pattern inspired by the use of the dome in the desert whose purpose is to always have a shady and a light area that allow convective motions within the building. The Miura pattern works in the same way, for each little module, red in Fig 4.

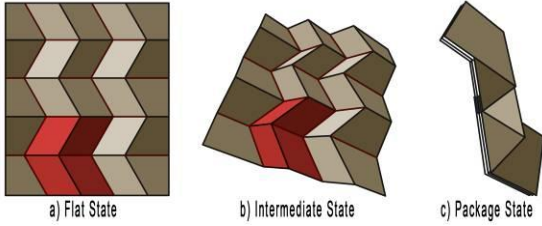


Fig. 4 – Miura Pattern, in red a single module: a) Flat State, b) Intermediate State, c) Compact-Package State.

For the optimization, we need something that can assume all possible shapes, not necessarily regular and symmetric, demanded by the environment. To generalize the Miura pattern, we used the relationships presented by Tachi (Tachi, 2009). A vertex (Fig. 5) with 4 fold lines, and thus with 4 sector angles θ_i ($i=0,1,2,3$), produces a one degree of freedom mechanism.

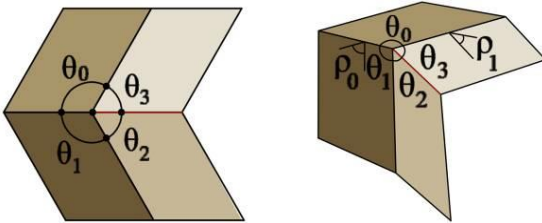


Fig. 5 – The relation between angles.

To obtain a flat-foldable and developable surface, these angles have to respond to the following conditions:

$$\sum_{i=0}^3 \theta_i = 2\pi \quad (1)$$

$$\sum_{i=0}^3 (-1)^i \theta_i = 0 \quad (2)$$

Thus the sector angles satisfy the equations:

$$\theta_0 = \pi - \theta_2 \quad (3)$$

$$\theta_1 = \pi - \theta_3 \quad (4)$$

The fold angles ρ_i and ρ_j incident to the vertex are related as follows (Tachi, 2009):

$$\tan\left(\frac{\rho_i}{2}\right) = \begin{cases} A_{i,j} \tan\left(\frac{\rho_j}{2}\right) & (i - j = 1 \text{ or } 3) \\ \pm \tan\left(\frac{\rho_j}{2}\right) & (i - j = 2) \end{cases} \quad (5)$$

where the latter represents that pairs of opposite fold lines having an equal absolute folding angles. $A_{i,j}$ is a coefficient between these two equivalent pairs determined by $\theta_0 \dots \theta_3$ for instance intrinsic measure in the crease pattern independent from the folding angles. If $|\rho_0| = |\rho_2| > |\rho_1| = |\rho_3|$, we obtained (Tachi 2009):

$$|A_{0,1}| = \sqrt{\frac{1 + \cos(\theta_0 - \theta_1)}{1 + \cos(\theta_0 + \theta_1)}} \quad (6)$$

Now we have something that can communicate with the genetic solver that will work on the angles θ_i and ρ_i (in) to obtain an optimized surface (out). Moreover, with this system, from a structural point of view, we can use the modern technology X-Lam, a panel made of different wood crossed fiber layers with excellent mechanical and thermo-hygro-metric properties (Buri and Weinand, 2010).

2.2 Cellular Automata

Desert agglomerations are villages that grow spontaneously and without a plan, imposed by the administration. Cellular Automata (CA) gives a very realistic prediction of urban structural evolution, and in particular, it is able to replicate the various fractal dimensionalities and self-organizing structures of a desert cities pattern.

A CA may be defined as a discrete Cell Space, with a set of possible Cell States and a set of Transition Rules that determine the state as a function of the states of all cells within a defined Cell-Space Neighborhood. Time is discrete and all cell states are updated simultaneously at each iteration (White, 1997). From an urban modelling point of view, we have a Cell Space of 3.5x3.5x3 meters for two storeys, using the typical Cell State of computer language, 0 and 1, to represent land use. In bi-dimensional CA, the most used neighborhoods are the Von Neumann (4-cell) and the Moore (8-cell). In one-dimensional CA (here used preliminarily) we studied left and right cells, so we have 256 possible patterns and the cell changes according to the state of its neighborhood in each level. All these

parameters are controlled inside *Rabbit*, a set of components within *Grasshopper*. Using this approach, we can choose the position of patios and loggias in our module, in order to obtain something more spontaneous. In Fig. 6 we show the four steps of how the cells grow and we added a set of random point in which the cells have a default state; but this solution is only one of many possibilities, making every module of the agglomeration unpredictable and different from the next.

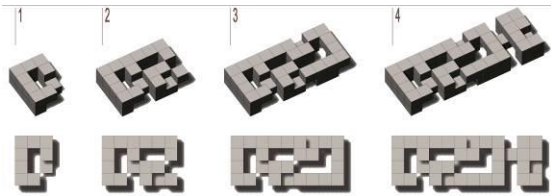


Fig. 6 – The steps of a Cellular Automata generation (*Grasshopper*, *Rabbit*).

2.3 Generative design algorithm

Now we can start to optimize our “zero organism” for 25 people of two storeys, which is obtained joining the concept of the *origami* and the Cellular Automata (Fig. 7).

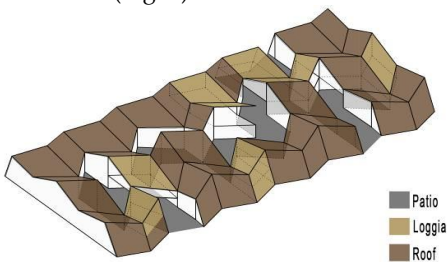


Fig. 7 – Zero organism.

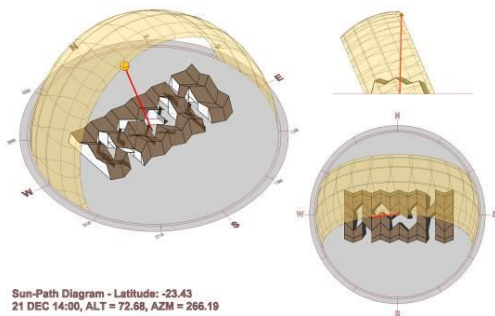


Fig. 8 – Solar path with the worth solar radiation (*Grasshopper-Ladybug*).

Among all the parameters we can optimize, we chose the ventilation. The patios are crucial for the working of internal ventilation, as mentioned in Sec. 1.3. They work with the wind, but in the desert

it is hot and dusty, or with a difference of pressure due to different temperatures between the shady and the light parts. Therefore, we decided to optimize the shadow that the roof casts inside the patios in order to have a large area where people can stay and to improve the ventilation during the day reducing the cooling load. Thus we need a specific solar radiation and we considered the worst one during the worst day of the worst month of the year: for the Atacama Desert it is 21 December at 2:00pm (Fig. 8). On this day, the sun is high, so the shade is very small and by optimizing this situation, we are sure to reach a comfortable condition throughout the day. To reach this aim, we selected three criteria (Caruso et al, 2013):

- maximize the shadow cast from the roof;
- minimize the difference between the patio's area and the shade area;
- minimize the ratio between the previous quantities.

To start, we picked an organism facing south and using the first criterion we saw the organism was inclined to open itself independently from the patio's shape. Therefore, we introduced the second criterion using the patio's area, but in this case the body tended to close regardless the shadows produced inside the patio. To balance both the effects we launched the third criteria. To set this process inside *Grasshopper*, we needed to fix the range of all the parameters, in order to get a structure that is possible to build and in which we have living spaces. Both for structural reasons concerning the resistance of the material and for the transportability of the folded structure, all the data ranges are set in order to have shorter lengths than eight meters. The algorithm can change the angles and the length of each panel with the constraint of obtaining a deployable roof at the end, so all the quantities are linked together with the relation explained in Sec. 2.1. To optimize the shape, we used *Galapagos*, which is a genetic and evolutionary solver. It applies the principles of evolution found in nature to the problem of finding an optimal solution. It starts by generating a population of random solutions, evaluating their fitness (objective function), and subsequently applying the basic genetic operators of reproduction, crossover and mutation.

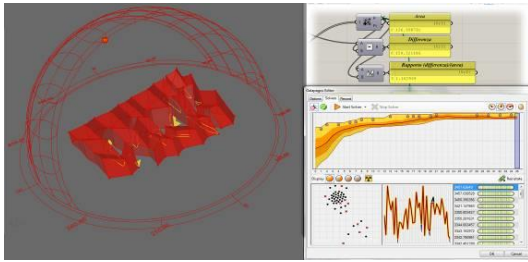


Fig. 9 – A screenshot of Galapagos during the optimization.

This generates a new population with higher average fitness than the previous one, which will in turn be evaluated as shown in Fig. 9.

Summarizing, the input of the algorithm comprises the angles and the length of the *origami*, the output is the shape of the module. The algorithm calculates the shade inside the patios using a specific solar radiation with *Ladybug* (Roudsari et al, 2013), a set of components for environmental analysis, and the genetic solver tries to reach the objective function modifying all the input parameters until the fitness is appropriate.

3. Results, a set of solution

After the simulation, a different population of surfaces was obtained, exactly 25 organisms, because we used different criteria and above all because the genetic solver is not a deterministic process. Each time we ran an optimization, we obtained a different result, with a different shape, even though only in the details, as shown in Fig. 10. This set of solutions is related to the orientation: if we had chosen a different orientation at the beginning, we would have obtained different solutions, one for each direction. After the optimization, we had different types of sections (Fig. 11), because the roof tried to rise as much as possible with various configurations to achieve the most efficient shape.

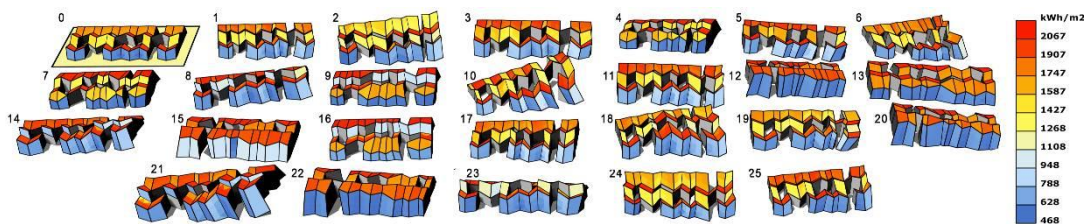


Fig. 10 – A set of solution, different 25 organisms with incident solar radiation values on the envelope (kWh/m²).

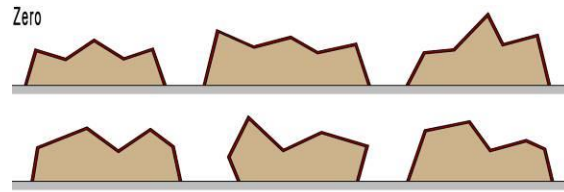


Fig. 11 – Typological sections of the organisms.

Before choosing the best organism, we analyzed the solar radiation of all the organisms in order to decide on the best strategy. We have classified all the elements relying on each criteria: from the best to the worst, we assigned a score based on the standings at each element and at the end we produced a ranking by adding the scores obtained by each organism. Among the criteria in addition to energetic principles (the shade), structural criterion was introduced (the maximum length of each panel) as shown in Table 1. With this ranking, we are open to different solutions depending on the design strategy. For instance, for a hot climate, by analyzing the solar radiation incident on any surface, we can choose the organism with the least amount for having less heat transmitted within the building. If we want to maximize the functioning of the solar panels (DHW productions or electricity generation), we can choose the shape with the best incident solar radiation. In our case, we chose the second strategy, in order to have a self-sufficient building, and the organism has obtained the highest score between solar and structural criteria. In Fig. 12 and in Table 1 we show how improved the shade produced by the roof is and how decreased the area's percentage exposed to direct solar radiation within the courtyards is.

3.1 The building

The plan of the building is completely free because the roof is self-supporting, so we could choose different solutions.

Table 1 – Energetic and structural ranking of the first twenty organisms.

Rank	area shadow (m ²)	%	area patio (m ²)	Difference (m ²)	%	Ratio	%	max length (m)	energy ratings	structural ratings	total ratings	total radiation (kWh/year)
Zero	60,00		167,6	107,6		1,79		5,00				1008417
1	71,5	19,2	116,4	44,9	-58,2	0,63	-64,9	7,50	75	19	94	1189514
2	83,7	39,5	142,2	58,4	-45,6	0,70	-61,0	6,75	65	28	93	1217178
3	80,1	33,5	138,2	58,2	-45,9	0,73	-59,5	7,42	62	22	84	1045507
4	66,1	10,2	112,4	46,2	-56,9	0,70	-60,9	7,85	67	10	77	773916
5	62,7	4,57	115,4	52,7	-51,0	0,84	-53,2	6,95	50	25	75	962300
6	65,1	8,63	107,3	42,1	-60,8	0,65	-63,9	8,45	69	3	72	1013998
7	64,9	8,30	115,2	50,2	-53,3	0,77	-56,9	7,53	56	16	72	1139801
8	67,4	12,4	121,9	54,4	-49,4	0,81	-55,0	7,60	56	14	70	974846
9	90,8	51,3	170,9	80,2	-25,5	0,88	-50,7	7,51	52	18	70	1197409
10	79,4	32,4	161,0	81,5	-24,2	1,03	-42,7	6,94	42	26	68	1023435
11	72,8	21,3	125,4	52,6	-51,1	0,72	-59,6	9,75	66	1	67	1305800
12	87,5	45,9	162,3	74,7	-30,5	0,85	-52,4	6,88	54	11	65	1314111
13	44,0	-26,6	90,6	46,6	-56,7	1,06	-40,9	6,97	37	24	61	922216
14	59,9	-0,12	117,2	57,3	-46,7	0,96	-46,7	7,49	38	20	58	944317
15	62,4	4,08	118,5	56,1	-47,8	0,90	-49,9	7,61	43	13	56	881543
16	60,1	0,10	136,4	76,3	-29,0	1,27	-29,1	7,48	26	21	47	1097412
17	65,1	8,42	136,4	71,3	-33,6	1,10	-38,8	7,88	35	9	44	982568
18	92,8	54,6	198,9	106,1	-1,38	1,14	-36,2	8,76	39	2	41	1097354
19	55,7	-7,13	120,8	65,1	-39,4	1,17	-34,8	7,54	26	15	41	823836
20	77,6	29,3	177,5	99,9	-7,10	1,29	-28,1	7,99	31	8	39	1260171

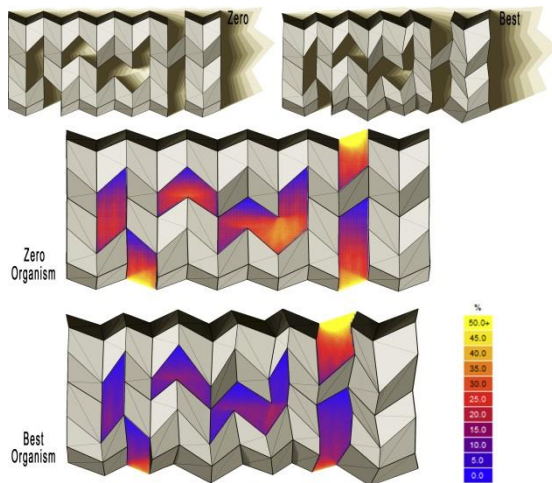


Fig. 12 – Zero and best organism, with the shadow and the percentage exposed (*Ecotect*).

For instance, we can accommodate eight families: we have two flats for two people, four flats for three people and two flats for four people.

The entrances are arranged inside the courtyards, thus a protected road system and a public space are created (Fig. 14a). The second element to be designed is the skin. All the package wall is prefabricated, the stratigraphy consists from inside to outside in (Fig. 15): a X-lam bearing layer of 12 cm, a vapor barrier, an insulating layer of mineral wool of 10 cm, a waterproofing layer and a wooden covering of 3 cm, obtaining 0,25 m thick wall, with a thermal transmittance of 0,25 W/m²K, a surface mass of 94 kg/m², an attenuation factor of 0,15 with a time lag of 12h 37'. We can notice the

ratio S/V (S is the external surface, V is the volume) of the zero and optimized building (best organism) is improved, going from 1,14 m⁻¹ to 0,93 m⁻¹.

With regard to the interior lighting, we have placed double skin glass facades all around the courtyards, avoiding the outside, to prevent direct solar radiation. Instead, for the cross ventilation, we have placed well protected openings on the outside skin (Fig. 14b). Now having determined the number of people and the characteristics of the skin, we can place the photovoltaic panels. Considering the appliances and the requirements for lighting, we need an average production of electricity equal to 24000 kWh per year, for all the families. We selected the roof panel with the best solar radiation for square meters; to produce the electricity demand stored in a battery, we need the first eighteen roof panels. To keep the logic of constructing our building in the shortest possible time, we took the amorphous silicon panels that allow a fast assembly and a freedom of forms to the detriment of a reduced efficiency equal to 6%.

4. Conclusions

In this paper an evolutionary algorithm is developed in *Grasshopper*, whose main feature is the automatic integration within the energy simulation. The program was employed to obtain a self-sufficient building starting to decrease the thermal loads due to solar radiation and maximizing natural ventilation. After the

optimization of the foldable module, we analyzed the building in *Ecotect*, choosing all the internal environment parameters (i.e. air temperature, relative humidity, air change rate).

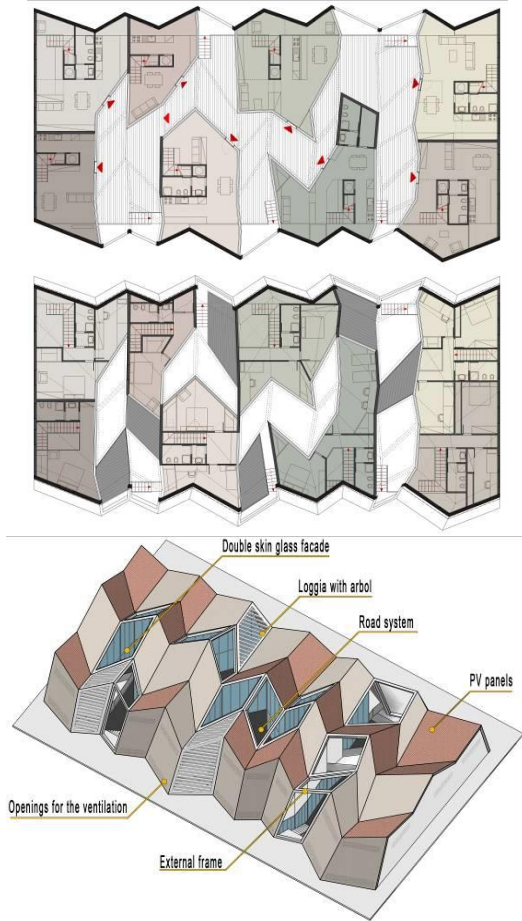


Fig. 14 – (up) Ground floor; (middle) First floor; (down) Axonometric view.

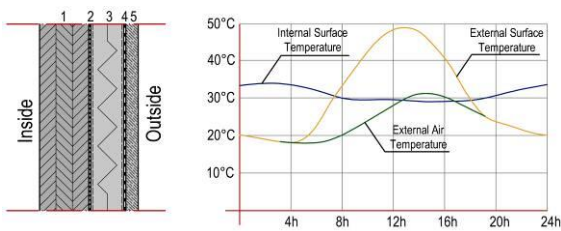


Fig. 15 – Skin stratigraphy (Layer 1: X-Lam, 2: vapor barrier, 3: thermal insulation, 4: waterproofing layer, 5: wooden covering).

Increasing the ratio between the shade and courtyard area of 65% (Table 1), the cooling load decreased by 38% (Table 2). Even though the building has not changed substantially in shape, the advantages are recognizable. The whole study is placed in a specific site and climate, but with the parametric approach, we can change the environmental initial parameters, maintaining the

same process, we can achieve the same purpose. The optimization can be a valuable instrument in the early design stages; it provides a high number of solutions to be presented to the decision makers for the ultimate choice.

Table 2 – Cooling load (kWh) during summer (*Ecotect*).

Month	Zero	Winner	%
Jan	3440	2919	15
Feb	3023	1930	36
Mar	2145	622	71
May	124	20	84
Nov	572	274	52
Dec	1340	837	38
Total	10647	6604	38

5. Acknowledgement

The results discussed in this paper have been obtained in part within the *European Lifelong Learning Programme (LLP)-Action Erasmus Student Mobility for Placement (SMP)*, co-funded by University of Pisa in the year 2014. The Authors would like to thank the staff members of DESTeC (Pisa, Italy) and IAAC (Barcelona, Spain).

References

- B. A. Maleki. 2011. "Traditional Sustainable Solutions in Iranian Desert". *Technical and Physical Problems of Engineering* (3): 84-91.
- G. Scudo. 1988. "Climatic Design in the Arab Courtyard House". *Environmental design: Journal of the Islamic environmental design center*, 82-91.
- T. Tachi. 2009. "Freeform Rigid-Foldable Structure using Bidirectionally Flat-Foldable Planar Quadrilateral Mesh". *Journal of the International Association for Shell and Spatial Structures* (3) 173-179.
- H. Buri, Y Weinand. 2010. "Origami - Folded Plate Structures". *Ph.D. Thesis, Université de Lausanne*.
- R. White. 1997. "Cities and Cellular Automata". *Discrete Dynamics in Nature and Society*, 111-125.
- M. Roudsari, M. Pak, A. Smith. 2013. "Ladybug: a Parametric Environmental Plug-in for Grasshopper to Help Designers to Create an Environmentally - Conscious Design". *13th Conference of International Building Performance Simulation Association*, 3128-3135.
- A. Mattoccia. 2014/2015. "Folded Wooden Responsive Architecture in hot arid climate in Atacama Desert". *Master Thesis in Building Engineer and Architecture, University of Pisa* (tutors: M.G. Bevilacqua, F. Leccese, R. Rubio).
- G. Caruso, F. Fantozzi, F. Leccese. 2013. "Optimal Theoretical Building Form to Minimize Direct Solar Radiation". *Solar Energy* (97): 128-137.

Energy Saving Exploiting Light Availability: A New Method to Evaluate Daylight Contribution

Claudio Campanile – University of Pisa, DESTeC – claudio.campanile1@gmail.com

Francesco Leccese – University of Pisa, School of Engineering, Dept. of Energy Engineering, Systems, Territory and Constructions (DESTeC) – f.leccese@ing.unipi.it

Michele Rocca – University of Pisa, DESTeC – michele.rocca.au@gmail.com

Giacomo Salvadori – University of Pisa, DESTeC – giacomo.salvadori@ordineingegneripisa.it

Abstract

Rhinoceros and *Grasshopper* have the extensibility which makes architects able to study forms, structures, acoustic behaviour, energy consumption, etc. as well as daylight availability: the most important aspect in this study. The software described has been useful to evaluate running costs including heating, cooling, electrical devices and lighting systems.

The software used includes *Ladybug* and *Honeybee*; they connect the *Radiance* and *Daysim* engines to *Grasshopper* and *Rhinoceros*.

The building analyzed in this study is a competition proposal for the New Town Hall in Remseck Am Neckar (Germany). The simulation started by designing the electric lighting system while the daylight availability was evaluated afterwards. The core study is the critical investigation of the daylight contribution necessary to satisfy the lighting demand.

Two simulations were run: the first one followed the European Regulation EN 15193, the second one was based on *Daysim*. If these methodologies gave two equivalent results for the north-exposed offices, on the other hand the south-exposed rooms obtained slightly different values. The idea consists in developing a third method to use opposed to the others described before, called the 'Octopus method' (OM) and based on *Octopus*, a multi-objective evolutionary algorithm integrated within *Grasshopper*. The new feature the OM introduces is the annual illuminance data computation being different from *Daysim*. The latter just makes a multiplication between the illuminance deficiency and the required comfort level. The OM considers the comfort level throughout the year simulating the real illuminance distribution within the ambient of study and the effect of electric light system installed.

1. Building Simulation: Nowadays

A critical approach is introduced to evaluate the lighting system consumption depending on the daylight availability – the most critical aspect about energy demand for office buildings (Tuoni et al., 2010; Leccese et al., 2012).

Originally, the matter of understanding and controlling the energy demand came from the need to check if the design proposed fulfills the requirements.

The more complex a project is, the more the desire to control it increases, due to the need to evaluate costs and benefits through simulation tools (Leccese et al., 2009; Angeli et al. 2005; Angeli et al. 2004; Lazzarotti et al. 2003).

Lately, software solutions have become more and more advanced to satisfy professionals' necessities as much as possible.

The authors looked for a software environment for having both a strong reliability and a smart user interface to focus on the physical behaviour.

2. The choice of the software environment

The choice was *Rhinoceros* (RH) and *Grasshopper* (GH). The software environment, thanks to its add-on architecture, allows us to pursue aspects more in depth than was possible until now. They have the extensibility that makes architects able to study daylight availability: the most important aspect in this study.

Since both RH and GH do not include any

environmental tools, but just geometry and data structure management engines, the *Ladybug* (LB) and *Honeybee* (HB) add-ons were added to the tool package.

For those who are not confident with this plug-in, a brief description follows.

LB and HB are a collection of user components developed in *Python* programming language within GH by Mostapha Sadeghipour Roudsari et al. at Thornton Tomasetti as Integration Applications Developer. The tool connects the *Radiance* and *Daysim* engines to *Grasshopper* and the *Rhinoceros* 3D-environment. The software described has been useful to evaluate running costs of the New Town Hall building including heating, cooling, electrical devices and lighting system which is deeply analyzed in this study.

The RH and GH interface is well known and generally user-friendly while the reliability has been checked through tests conducted on already-known conditions.

Once the tool-ecosystem is described, it is also necessary to talk about the environmental data source. The U.S. Department of Energy, thanks to their database based on *.epw files (*EnergyPlus weather* file format), was chosen thanks to its intrinsic interoperability and completeness. Consequently, input data were verified in comparison with the Italian Regulation Weather Data: the difference found was acceptable (Campanile, 2014).

In addition to this, it must be said that the reliability checking was done even for LB and HB *Radiance* implementation: a test model was processed both in *DIALux* and HB and then the results were compared (Campanile, 2014). The geometry is a simple room with one window and a test grid able to measure the illuminance level from a light source. Once again, difference was around 2%, which is more than acceptable.

The usage of GH and its add-ons led us to consider the overall software reliability. Since GH lets literally everyone able to make new open source *environmental plug-ins*, this has two effects. The first one, which is positive, is that researchers have either a flexible, free, powerful and diffused tool to deepen their studies. The other side of the coin is that sometimes these software extensions do not

follow a proper reliability check and might be fine for the purpose they was developed for, but not for other cases. As we expected from an add-on created by Thornton Tomasetti, the checking results have been excellent even if LB and HB are still a work in progress.

3. Case of study

The building tested is part of a competition proposal for the New Town Hall in Remseck Am Neckar (Stuttgart, Germany) designed by C. Campanile (Campanile, 2014) at MDU Architetti (Prato, Italy), see Figs. 1-3. The buildings are glaze-enveloped volumes which, on one hand are strongly naturally enlightened; on the other, they have been defined to create a strong linkage between external and internal spaces due to the high quality natural surrounding: the confluence of two rivers. This has been the result of the design research, conducted to be satisfactory in terms of the membrane's performance behaviour.

The analysis was run for the Town Hall Building for two reasons: firstly, this is the most complex building compared to the Library and the Civic Hall (Fig. 1). On the other hand, it is actually an office building: it is a much-diffused typology and mostly it is affected by high-energy consumption because of its electrical light system.

Before proceeding, it is useful to present the Town Hall Building (Fig. 4): a four-storey building with a courtyard closed with a transparent rooftop. The higher visitors go, the larger the internal void is: on the way up to the wedding room, two internal terraces host the public front offices. Around this space, the horizontal circulation is shaped through a timber stick membrane: they are for the horizontal circulation. Beyond them, office rooms are organized along the northern and southern facades.

3.1 Light Design

First of all, the simulation was conducted designing the electric lighting system, and daylight availability was evaluated afterwards.

Since the gross building area measures 6000 m², the lamp density is calculated on several test rooms

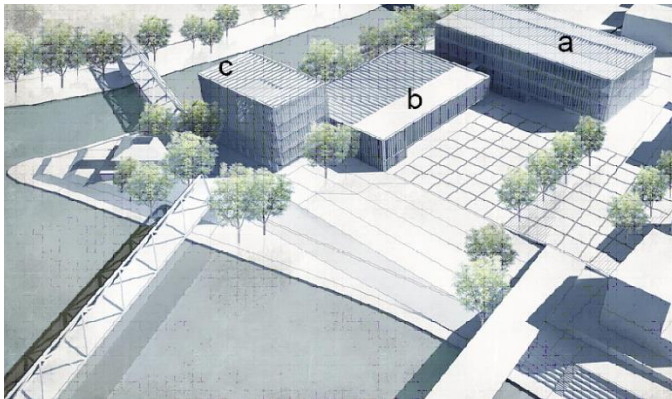


Fig. 1 – New Town Hall proposal: a) Town Hall, b) Civic Hall, c) Library.



Fig. 2 – New Town Hall proposal: plan of the first floor.



Fig. 3 – Rendering of the New Town Hall in Remseck am Neckar (Stuttgart, Germany): competition proposal.

and split between those exposed to the north and those exposed to the south.

The electric light system was designed studying four different test rooms: single (1P), double (2P), triple (3P) and open space office (S). Then, results were interpolated to devise a function able to match the power needed with their areas (Fig. 5). From this point forwards, we will consider the triple office (3P) as our test room for (Fig. 6). Illuminance and presence sensors have been added to the system. This feature allows the authors to consider the installed lights, which are sensitive to the illuminance levels. Therefore, the system is able to fix automatically the intensity (dimmer value) of

the lamps. It must be said that actual sensors are one per light line (Fig. 6), while in the GH definition they are on each point of the test grid (Paragraph 3.4). This has been affected because of the will to make the method flexible and helpful for other kinds of design.

3.2 Electrical Light and Daylight Interaction: An Actual Question

Evaluate daylight contribution means to study the illuminance level through a year and to figure out if the daylight is enough to satisfy the comfort level: if not, calculate the percentage of the electric light power usage.



Fig. 4 – Town Hall Building: perspective section.

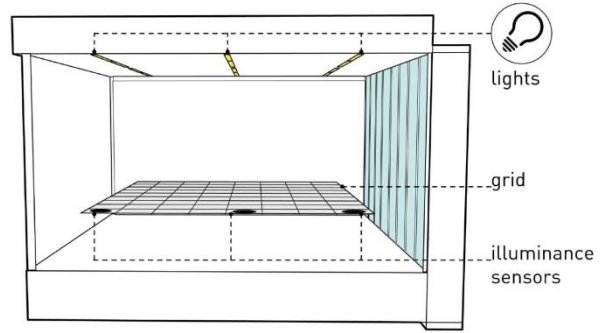


Fig 6 – 3P test room with the electric light system.

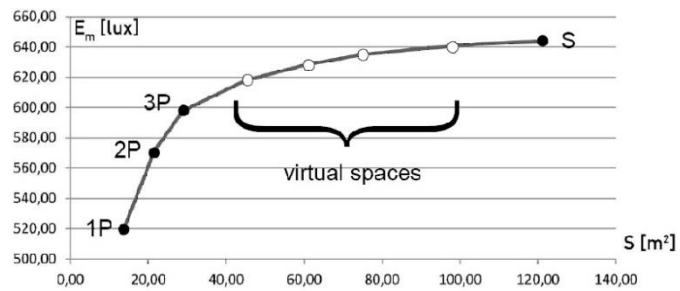
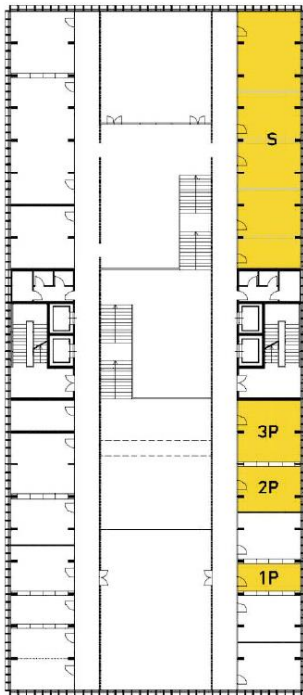


chart 1 - illuminance according to the office areas

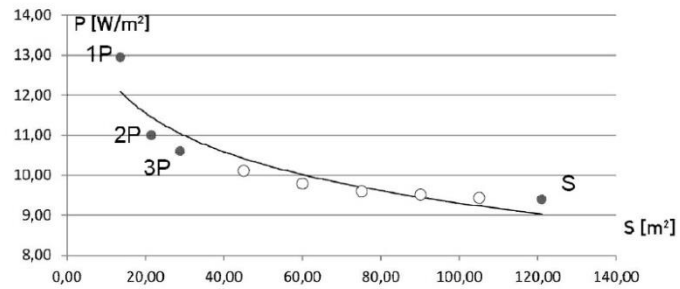


chart 2 - power requirement according to the office areas

Fig.5 – (left) Plan for the test rooms. In the charts (right) are represented the illuminance and the power requirement for the test rooms (1P: 1 person, 2P: 2 persons, 3P: 3 persons, S: open space). Virtual spaces has been returned from a double data interpolation.

This percentage is called dimmer value and it is between 0 (system turned off) and 1 (system at maximum power). Before introducing the OM, two simulations have been run using two already tested methods: the first one follows the European Regulation EN 15193 (EN 15193, 2007; Leccese et al. 2013; Bertozzi et al. 2012), the second is based on *Daysim*. The annual daylight dependence factor values are shown in Table 1. It is possible to say that (Reinhart, 2001; Daysim, 2014):

- 1) if these methodologies give two equivalent results for the North-exposed offices, on the other hand the South-exposed rooms get slightly different values;

- 2) they are both generic, the 1st one does not take into account both the physical situation of rooms and the electrical lights, the 2nd one just not the electrical light system which is just conceptualized. The goal of this study consists in developing a third method. The results of this third method can be useful compared with the results of the methods above.

Table 1 - Annual daylight dependence factor values.

	EN 15193	Daysim	Octopus
North	0.48	0.47	0.41
South	0.32	0.41	0.25

3.3 An Initial Daylight Evaluation

Since these two methods are commonly used for this purpose, we will skip the EN 15193 one and present briefly the second one because of its strong connection to the OM. *Daysim* is useful to calculate the Daylight Autonomy and has been integrated in HB. This properly means that, when an annual daylight study is run, it gives back the hourly illuminance level through the whole year. Even automatic systems and sensors are taken into account. In this case study two functions are considered as integrated in the system: illuminance sensors and automatic dynamic blinds. The second one useful for what concerns the comfort, but not influential for the OM. Once that *Daysim* returns the results about illuminance levels, an approximate system just makes a multiplication between the illuminance deficiency and the required comfort level. This is the way *Daysim* uses to "conceptualize" the electrical light system. From this point forward it is shown how to include the actual electrical light system into the evaluation through the OM. It must be said that its development is enough to use it not to substitute the other two methods, but to help users to understand the behavior.

3.4 The Octopus Method

The name 'Octopus Method' (OM) is due to the fact that it is based on *Octopus*, a multi-objective evolutionary algorithm integrated within *Grasshopper* (Octopus, 2014). The new feature the OM introduces is the annual illuminance data computation being different from *Daysim*. The latter just makes a multiplication between the illuminance deficiency and the required comfort level. The OM takes into account the comfort level throughout the year simulating the actual illuminance distribution within the ambient of study and the real electric light system installed.

(Step 1) The OM has been run inside a test room - once South-oriented, once North-oriented - already designed in RH and used for the *Daysim* method (Fig. 7). Since nothing changes talking about the method, only the South-oriented room is considered to show the OM, while both the results will be shown. The room test is intended in this

way: illuminance levels are measured on the desktop height where a grid has been created and it corresponds to zero (0 lx). Since this, illuminance graphs are drawn above. The grid definition has been tailored to its proper measure: $8 \times 9 = 72$ points. Basically one per half a meter.

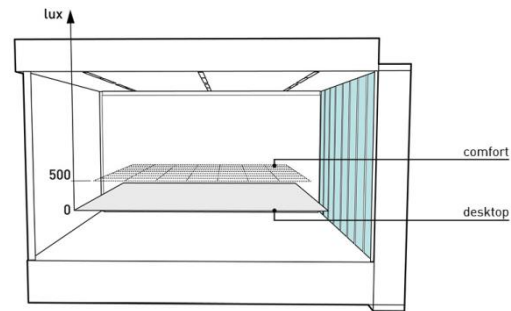


Fig. 7 – Test room: a typical office room (3P).

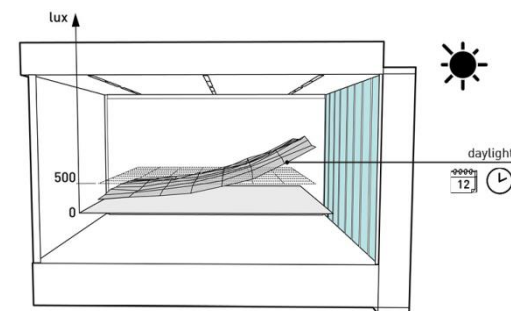


Fig. 8 – Sample 1: illuminance level at a random time.

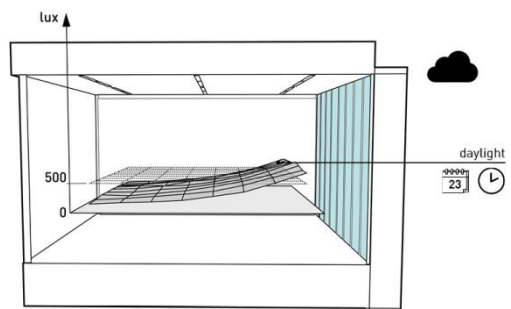


Fig. 9 – Sample 2: illuminance level at a random time.

(Step 2) *Daysim* data that comes from the annual analysis are collected into a database: it includes hourly illuminance level over the whole year. Since the grid has 72 points and the annual hours are 7860, the database is built of $72 \times 7860 = 630720$ values assembled in 7860 charts. A couple of examples are shown in Figs. 8-9.

(Step 3) A first data cleanup is made cutting out non-working hours because of no electric lights are turned on outside of the work schedule: Monday to

Friday (5 days per week), 8 am to 6 pm (10 hours per day). Holidays are not included: we will see later that this is not conclusive, and the reason is that the method is based on monthly average daylight availability. At the end of this step the data pattern is changed: only 50 out of 178 weekly hours are included in the calculation. Since one year is made of 52 weeks, the result is that in the whole year only 2600 hours (charts) out of 7680 are taken into account (and $2600 \times 72 = 187200$ point values).

Within the last step, the average monthly daylight availability (True Monthly Average, TMA) has been introduced: the method is based on the average since the goal is to calculate the energy consumption. From this point forward, the database is useless for the comfort level evaluation. Before going further, it is appropriate to show how the average is made up or, we could say, how we extrapolate 12 charts (one per month) from 2600. The TMA is calculated about the single value (grid point) in the chart, for that charts which are included in one month. We call it 'true', because actually, to go forward into the method, we need a Fake Monthly Average (FMA). It is so-called because it included all the 187200 point values, whereas it includes a condition: the values 'bigger than the comfort level' are considered 'at the comfort level' (500 lx). The reason of this is understandable through the following example: a grid-point, at a certain time, has the illuminance level at 200 lx. The same point, at another certain time, has the illuminance level at 800 lx. The average is $(200+800)/2=500$ lx, i.e. the comfort level. The average shows that no electrical light is required, while actually, it is. Since this thought, we can proceed as it follows.

(Step 4) Each point grid value bigger than the comfort level is equal to 500 lx. In Fig. 10 a cut chart is shown.

(Step 5) The FMA daylight availability is made from the cut charts (Fig. 11) for each month. Daylight availability data has been processed so far. The electric light effect is added from this point onwards: the overall system has illuminance sensors as introduced before (Step 4). The building considered is big enough for including automatic systems for environmental controls: it must be said

that the OM is available only for light systems that include this kind of amenities.

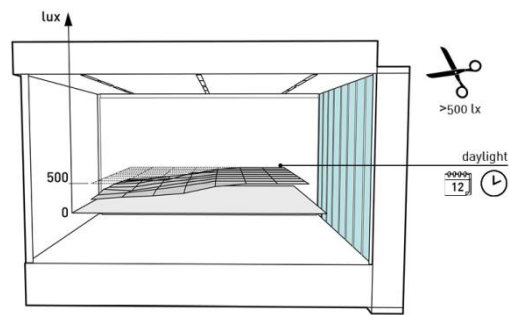


Fig.10 – Cut of bigger illuminance level values (>500 lx).

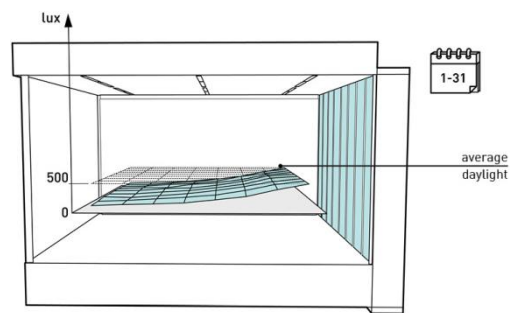


Fig.11 – Monthly average illuminance within working hours (8am-6pm, Mon-Fri).

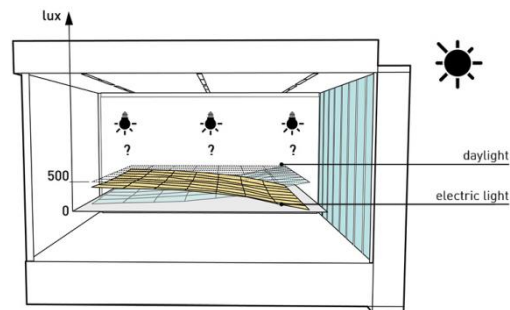


Fig.12 – Electrical light and daylight overlay for reaching the comfort.

(Step 6) In Fig. 12 we can see an example of the over layering effect of electric light (yellow chart) and daylight (blue chart): the latter is not enough to satisfy the comfort level, which is reached through the lamps usage. Therefore, the lamp graph shown represents the optimal dimmer setting to achieve the comfort level. As described at the Step 6, the ideal chart is known: on the other hand, lamp dimmers are not. Through OM it is possible to calculate the combination between electric light and daylight. In Fig. 12 is also clear

that the yellow chart can be affected by lower dimmer on the window side (right) and bigger values on the wall side (left).

Octopus is used to find it through "smart" iterations. Basically it makes several attempts (Figs. 13-15) trying to find that combination, which, if used, causes an illuminance, represented by the ideal chart. *Octopus* is able to "read" the output chart and "understand" if it fits the ideal one through a fitness parameter (called F1). Before running the process, it is useful to introduce an additional fitness parameter (called F2) which is able bring our GH definition closer to the effective physical situation: the illuminance uniformity, which is basically a ratio between the average illuminance level and the maximum value (both are taken from the TMA). The next steps are summarize as follows.

(Step 7) Setting of the *Octopus* reading definitions: the chart fitness F1 and the illuminance uniformity fitness F2.

(Step 8) Definition of the dimmer inputs: the multiplying factors are applied to the grid values and not to the light system. This is a means, which allows us to do the ray-tracing to compute the electric light one time instead of for each attempt.

(Step 9) *Octopus* is set to make 50 genes replicating 100 times. This is the minimum to consider the result acceptable.

(Step 10) In Fig. 16 the best solution found is shown. Since there are two fitness parameters, the choice is made considering F1 and F2 weight both at 50%. In Fig. 17 the chart represents the hundredth step i.e. the final one: the intersection between the bisector line and the Pareto Front point at the solution.

4. Conclusive remarks

The method described has been applied for each month in the overall year, which means for each FMA (Fig. 18). Steps 1 to 5 show how to build the database to extract the FMA and TMA. In other cases, of course, it can be done for different time steps or period, depending on the design needs.

In conclusion, the whole software environment allows designer to evaluate many aspects, included those which are within country regulations. The

case of study analyzed shown that Grasshopper reveals itself more convenient than conventional software solutions.

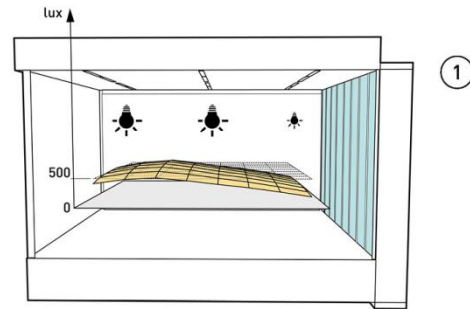


Fig.13 – Octopus: #1 attempt.

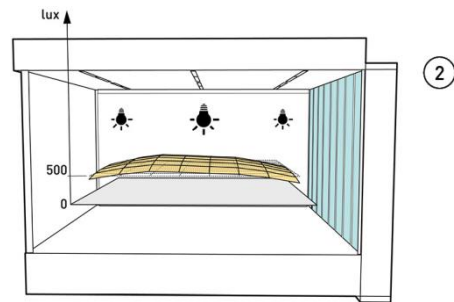


Fig.14 – Octopus: #2 attempt.

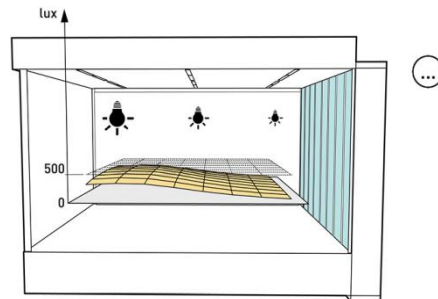


Fig.15 – Octopus try to come up a solution.

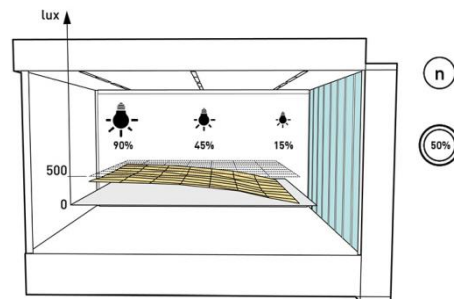


Fig.16 – A possible solution is got at the end of the process. The overall dimmer value is the average of the single ones.

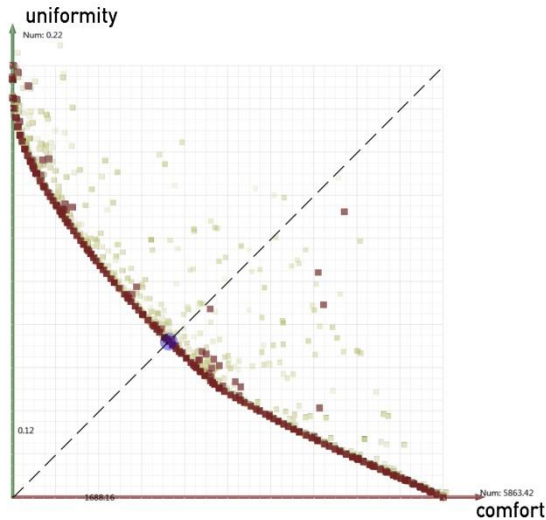


Fig.17 – Good solution (red) aggregated together from the Pareto Front. The best one (blue circle) is chosen due to its proximity to the bisector line.

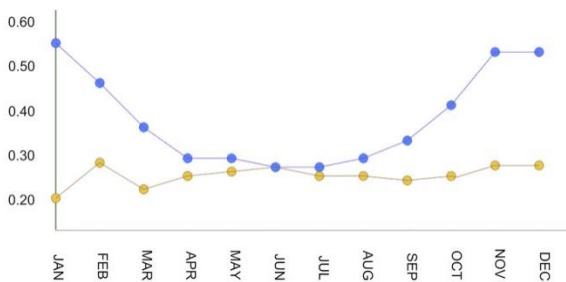


Fig.18 – Dimmer values returned through the OM: annual monthly results. The North-exposed test room (blue) shows a typical behavior because of the daylight availability. The South-exposed test room (yellow) shows a linear trend of the presence of the blinds. During the Daysim simulation, the blinds was down mostly from March to October, from 11 am to 3 pm.

The annual daylight dependance factor values are shown in Table 1. In the first column we can see Italian Regulations' results (according to EN 15193); in the second one, Daysim annual averages are shown (extracted from hourly dimmer level - properly processed). The OM returns a data, in the third column, which lead our choice through the EN 15193 results.

The big difference between the dimmer values for the South-exposed office is due to the fact that the direct daylight and the dynamic (automatic) blinds affects strongly the result. On the other hand, the North-exposed office room receive only diffused daylight: since it has not a direction, peculiarities do not affect the study case.

References

- C. Campanile. 2014/2015. "Design process for a new civic centre Remseck Am Neckar, Stuttgart". *Master Thesis in Building Engineer and Architecture, University of Pisa* (tutors: F. Leccese, V. Barberis).
- G. Tuoni, F. Fantozzi, F. Leccese, G. Salvadori. 2010. "The energy labeling of buildings based on winter heating, DHW production and lighting performance indicators". *CLIMA 2010 - 10th REHVA World Congress on Sustainable Energy Use in Buildings*, 1-8.
- F. Leccese, G. Salvadori, M. Casini, M Bertozzi. 2012. "Lighting of Indoor Work Places: Risk Assessment Procedure". *WIT Transactions on Information and Communication Technology* (44): 89-101.
- F. Leccese, G. Salvadori, G. Caruso, E. Batistini. 2009. "Daylighting and lighting energy demand analysis of the new town library of Piombino (Italy)". *CISBAT 2009 - International Scientific Conference on Renewables in a Changing Climate*, 249-254.
- B. Angeli, F. Leccese, G. Tuoni. 2005. "Daylighting illuminance analysis of a new university library using ADELIN". *LUX EUROPA 2005 - 10th European Lighting Conference on Lighting for humans*, 205-208.
- B. Angeli, F. Leccese, G. Tuoni. 2004. "Daylight simulations with advanced software tools: a case study of a university library in Pisa". *EUROSUN 2004 - 5th ISES Europe Solar Conference*, 463-472.
- F. Lazzarotti, F. Leccese., G. Tuoni. 2003. "Daylighting simulations in covered local markets with ADELIN software". *CISBAT 2003 - International Conference on Innovations in Building Envelopes and Environmental Systems*, 271-276.
- EN 15193. 2007. "Energy performance of buildings - Energy requirements for lighting".
- F. Leccese, G. Salvadori, G. Romei. 2013. "Indice di efficienza energetica dei sistemi di illuminazione dei luoghi di lavoro: il contributo della luce naturale". *neo-EÚBIOS* (45): 13-22.
- M. Bertozzi, M. Casini, F. Leccese, G. Salvadori. 2012. "Analisi fabbisogni energetici per illuminazione degli edifici: indice di efficienza energetica e prestazioni illuminotecniche". *neo-EÚBIOS* (41): 46-56.
- C. F. Reinhart. 2001. "Chapter 8 – Development of a Manual Lighting Control Model". *Daylight availability and Manual Lighting Control in Office Buildings – Simulation Studies and Analysis of Measurements*, 87-96.
- DAYSIM. 2014. "Lightswitch Model". (<http://daysim.ning.com/page/concept-lightswitch-model>).
- OCTOPUS. 2014. "Octopus Manual". (<http://www.food4rhino.com/project/octopus>).

Estimation of the water flow rate and energy consumption of a central heating system in an office building using system identification

Daniele Antonucci – Institute for Renewable Energy, EURAC research – Faculty of Science and Technology, Free University of Bolzano, daniele.antonucci@unibz.natec.it

Federico Noris – Institute for Renewable Energy, EURAC research – federico.noris@eurac.edu

Ulrich Filippi Oberegger – Institute for Renewable Energy, EURAC research – ulrich.filippi@eurac.edu

Andrea Gasparella – Free University of Bolzano – andrea.gasparella@unibz.it

Abstract

This study focuses on the application of system identification to estimate the flow rate and the heating consumption in a central heating system in an office building in San Michele all'Adige, Italy. The study was done within the European ICT PSP project Smart Build with the aim of reducing the energy consumption of existing public buildings through the application of ICT systems. The installed monitoring system, designed after an early energy auditing, foresaw the use of permanent temperature sensors coupled with a portable flow rate meter, to estimate thermal consumption. The flow rate varied with time depending on several factors therefore making it challenging to monitor it for only a short period. To overcome this obstacle, we monitored the flow rate for four workdays and one weekend to identify a mathematical model which could explain the real system behaviour. A statistical analysis was performed at first to assess the reliability of the monitored data. Subsequently, we focused on the identification of autoregressive models with exogenous inputs with a varying complexity and level of confidence. Different tests were performed on the hourly data to assess the reliability of the models. The best model was subsequently used to estimate the time-varying heating consumption for available monitoring periods with the aim to understand the impact of the ICT system as a function of the floor of the building and in order to show how system identification can reliably estimate the water flow rate in a central heating system and consequently be used to calculate the heating consumption. The calculated monthly average deviated from the bills by 20%, attributable to the heating consumption of the non-monitored ground floor.

1. Introduction

In the context of the EU project SmartBuild (<http://www.smartbuild.eu>), we wanted to calculate the heating consumption in a monitored old office building in San Michele all'Adige constructed in 1874 and renovated in 2000 (more building details are summarized in Tab.1). The projects aims to reach 30% of energy saving both in thermal and electrical consumption with the application of an ICT system. This latter has been installed in two of three building floors (1st and 2nd floor), but during the evaluation of the impact of ICT on energy consumption, a lack of flow rate data impeded the calculation of the heating consumption of each floor. This issue was overcome by monitoring the flow rate for a period of five days. These monitored data were then used to identify a series of Auto-Regressive with Exogenous Input (ARX) models capable of estimating the system behaviour. The ARX model structure has been found to be the simplest one to find analytical solutions with excellent performance and accurate descriptions of the physical model (Ljung, 1999). It is also widely applied in different research fields. For example, in (Ismail et al., 2011) an ARX model was identified to describe the partial input-output data of a heating process in a steam distillation essential oil extraction system. In (Yun., 2012) an ARX time and temperature indexed model was generated to predict the building thermal load.

In this paper, a method to identify the water flow rate of a heating system in order to estimate its heating consumption is shown. System identifica-

tion deals with the problem of describing a physical system with mathematical equations derived from measured data. In this context, the equations that describe the physical system are also referred to as “black box model”.

Important steps to identify a black box model are (Rabbani et al., 2013):

- Analysis of the monitored data;
- Selection of a family of models;
- Identification of a model that belongs to that family;
- Validation of the model.

Each of these stages have a high impact on the success of the identification process.

The identification of the models was done using both the R programming language and the System Identification Toolbox of Matlab in order to minimize the root mean square error between the measured and predicted values, analyse and evaluate the models.

The crucial step was the model validation. We carried out a series of tests in order to check that the identified models are suitable and to select the best one among them.

Tests included computing the coefficient of determination, autocorrelation of residuals, cross-correlation of residuals with input parameters, comparing the coefficient of determination over the training period with that over the validation period in order to detect overfitting.

Concerning the case study, the building has three main floors with offices and laboratories and an unheated underground floor used for laboratories and the thermal power station. After an energy audit, only the first and second floor (offices) were equipped with a monitoring system leaving the ground floor (laboratories) out of the analysis.

The heating and cooling facilities are:

- A district heating system with heat exchanger and heat tank, supplying hot water to the building;
- An external refrigeration plant and storage system to ensure the supply of cold water during the cooling season;
- 2 pipe fan-coils with manual temperature and fan control in all offices;
- radiators and ceiling fans in all laboratories;

- One Air Handling Unit (AHU) providing the labs with sensible and latent heat.

The thermal parameters measured were divided in three categories:

- Indoor Environmental Quality (IEQ) related parameters; indoor temperature, humidity, CO₂, occupancy and illuminance, measured in five offices (two on the first floor and three on the second floor);
- Climate parameters; outside temperature, global radiation, wind speed and humidity, from a weather station already installed on the building;
- Heating and cooling system parameters; water supply and return temperatures for first floor, second floor and bathrooms, water supply and return temperatures of the hot and cold AHU coils, temperature and humidity of the air supply duct.

The flow rate was monitored using a portable flow rate device (Type: Dynasonic® ultrasonic flow meter) during the period from 5/12/2013 to 10/12/2013.

Table 1 – Characteristics of the building

PARAMETER	QUANTITY	MEAS. UNIT.
Conditioned Volume	3825	m ³
Surface of each floor	425	m ²
Number of floor	3 conditioned floors + 1 underground floor not conditioned	
Intended use	Laboratory/Office	
Type of wall	Normal brick without insulation	

2. Simulation

2.1 Data set

The monitored data are summarized in Table 2.

Table 2 – INPUT/OUTPUT used for model estimation

NAME	SYMBOL	MEAS. UNIT.	Uncert.	INPUT/ OUTPUT
Flow_rate 1Floor	FR_1F	m ³ /h	±2 %	OUTPUT
Flow_rate 2Floor	FR_2F	m ³ /h	±2 %	OUTPUT/ INPUT
T_supply 1Floor	Tsupp_1F	°C	±0.3 °C	INPUT
T_return 1Floor	Tret_1F	°C	±0.3 °C	INPUT
T_supply 2Floor	Tsupp_2F	°C	±0.3 °C	INPUT
T_return 2Floor	Tret_2F	°C	±0.3 °C	INPUT
T_supply Bath	Tsupp_B	°C	±0.3 °C	INPUT
T_return Bath	Tret_B	°C	±0.3 °C	INPUT
External T	T_ext	°C	.*	INPUT
Global radiation	GR	W/m ²	.*	INPUT
Average Occup_BUI	Occ_BUI	[-]	-	INPUT
Average Temp_BUI	T_BUI	°C	±0.3 °C	INPUT

* Measurements taken by the weather station situated at "Fondazione Edmund Mach"

2.2 Reliability of the measured data

As a first step, the quality of the data measured by the sensors was assessed. Each physical quantity has a true value that is not observable. During the measurement of a physical quantity, it is common that errors occur. These can be of two types:

- Systematic errors, such as device accuracy, device construction defects and wrong sensor usage;

- Random errors due to uncontrollable factors, such as device precision, and variation of internal and external environmental conditions.

As ARX models are based on the assumption that the behaviour of a physical system varies about a stationary (not changing with time) working point, the first step is to verify the stationarity of the time series (Andrews, 2013). Indeed, a stationary time series is a series of successive measurements for which mean and variance are constant over time and the auto-correlation function depends on the lag alone. Therefore, by stationarizing the time series one is able to obtain meaningful sample statistics such as mean, variance, auto-correlation, and cross-correlation with other variables. Such statistics are useful as descriptors of future behaviour only if the series is stationary.

To assess the stationarity of the flow rate time series, the Augmented Dickey-Fuller (ADF) t-statistic test was carried out.

This test uses the following regression model:

$$y'_t = \theta y_{t-1} + \beta_1 y'_{t-1} + \beta_2 y'_{t-2} + \dots + \beta_k y'_{t-k} \quad (1)$$

Where:

y'_t : is the differenced series ($y'_t = y_t - y_{t-1}$)

k : is the maximum lag

If the null hypothesis $H_0: \theta = 0$ of the ADF test is rejected, the data is stationary and does not need to be differenced.

Table 3 shows the ADF test for flow rates of the 1st and 2nd floor:

Table 3 – Augmented Dickey-Fuller (ADF) test for FI_rate1f and FI_rate2f

Data	ADF test	Lag order	p-value
FI_rate1f	-4.2143	4	0.01
FI_rate2f	-4.0124	4	0.01

According to the t-statistic, the p-value is lower than the selected significance level of 5 % for both variables. The two time series can therefore be considered stationary and do not need to be differenced.

The mean can then be subtract from the data:

$$Z = x - \mu \quad (2)$$

Where x is the samples variable and μ is the mean. Indeed, for steady state data it is reasonable to assume that the mean corresponds to a physical equilibrium and the aim to build linear models is to describe deviations from this equilibrium, which are responses to excitations of the physical system (Ljung, 1999).

2.3 Methodology

The flow rates were measured every hour for five days, for a total of 120 samples. The data were subsequently divided in two parts. The first part was used for the model calibration and the second one for the validation. We varied the amount of data used for calibration. The best models were obtained using 70% of the data for calibration and the remaining 30% for validation (Mourad et al., 2005).

The estimation of the ARX model was done through the application of a MATLAB script that tries out and evaluates different input combinations and polynomial orders. The best model among all identified models was then chosen as follows. For each model, we computed three performance indicators: i) the coefficient of determination over the calibration period R_{cal}^2 , ii) the coefficient of determination over the validation period R_{val}^2 , and iii) the absolute difference between the two coefficients of determination $\Delta R^2 = |R_{val}^2 - R_{cal}^2|$. In addition, all residuals autocorrelation values up to lag 20 had to be inside the 95% confidence interval. Next, we considered only those models as valid that satisfied the following inequalities:

- $R_{val}^2 > 0.7$;
- $\Delta R^2 < 0.1$.

At the end, the achieved list was sorted by descending R_{val}^2 .

The first three models in the list were investigated further as follows:

- Computation of the autocorrelation to lag 20. If all values were inside the 95%-confidence interval, we could assume randomness;
- Visual inspection of a scatter plot of residuals against fitted values. The points should be randomly distributed around

the zero line and form a horizontal band, showing that variances of the residuals are equal and that there are no outliers;

- Computation of the cross-correlations between residuals and inputs, to see if a specific input generates a pattern in the residuals;
- Visual inspection of the distribution of the residuals with a QQ-plot and a histogram;
- Multicollinearity analysis through Besley collinearity diagnostics.

2.4 Results and discussion

The first model identified is the flow rate of the second floor (FR_2F). The output of this model is subsequently used to identify the flow rate model of the first floor (FR_1F). This choice was made because the two circuits are directly connected to the same collector and because the flow rate profile of the first floor follows the profile of the second floor.

The inputs used are shown in Table 4.

Table 4 – Second floor model inputs

Model	Inputs
Mod_1.2F	Tsupp_2F; Tret_2F; Tret_B; T_ext; T_BUI;
Mod_2.2F	Tsupp_2F; Tret_2F; Tret_B; T_ext; T_BUI; Occ_BUI
Mod_3.2F	Tsupp_2F; Tret_B; T_ext; T_BUI;

The performance indicators for the best three models are shown in Table 4.

Table 5 – Coefficients of determination of 2nd floor flow rate models

Model	R_{cal}^2	$R_{Adj.cal}^2$	R_{val}^2	$R_{Adj.val}^2$	ΔR^2
Mod_1.2F	0.903	0.898	0.855	0.847	0.048
Mod_2.2F	0.904	0.898	0.847	0.839	0.057
Mod_3.2F	0.916	0.911	0.847	0.838	0.057

The low values of ΔR^2 in Table 5 show that models do not overfit the data. Indeed, the coefficients of determination and validation are very similar, and the model can predict in the best way the data as shown in Fig. 12.

The first model in Table 5 has the best $R^2_{Adj, val}$ and ΔR^2 . However, the other two models have values very close to the first one. Therefore, the best model is chosen depending on the residual analysis.

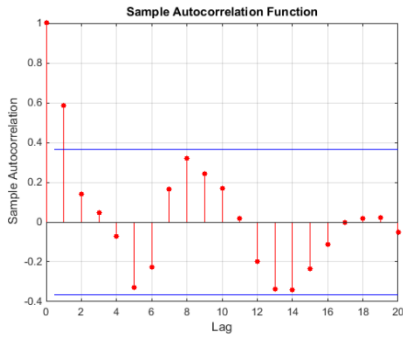


Fig. 1 – ACF Mod_2.2F

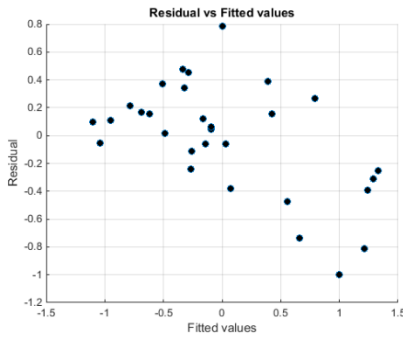


Fig. 2 – Residuals vs fitted values Mod_2.2F

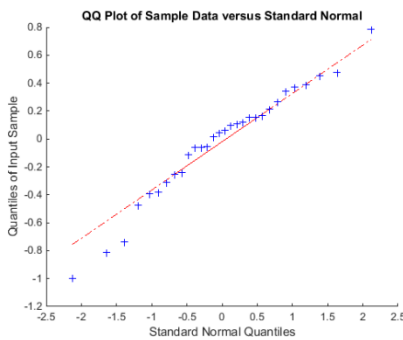


Fig. 3 – QQ plot residuals Mod_2.2F

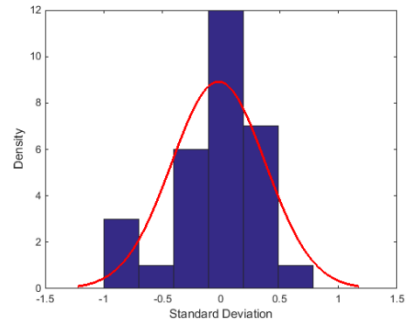


Fig. 4 – Normal distribution residuals of Mod_2.2F

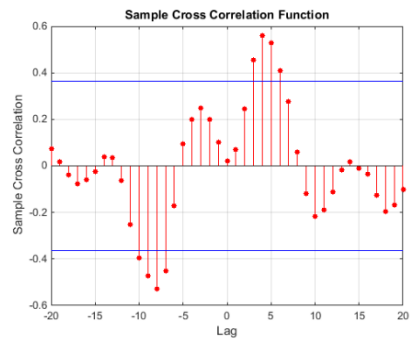


Fig. 5 – CRF Residuals vs Occ_BUI for Mod_2.2F

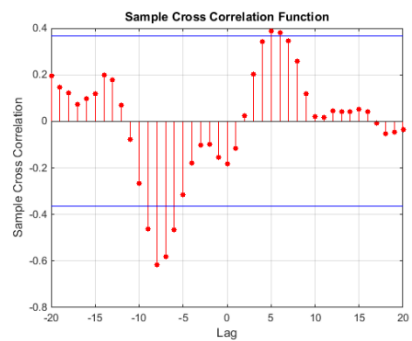


Fig. 6 – Residuals vs T_BUI for Mod_2.2F

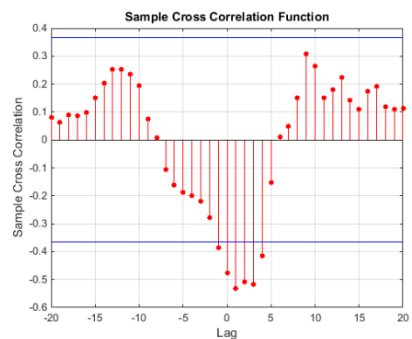


Fig. 7 – Residuals vs Tret_B for Mod_2.2F

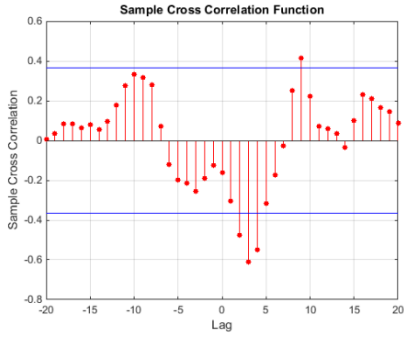


Fig. 8 – Residuals vs Tret_2F for Mod_2.2F

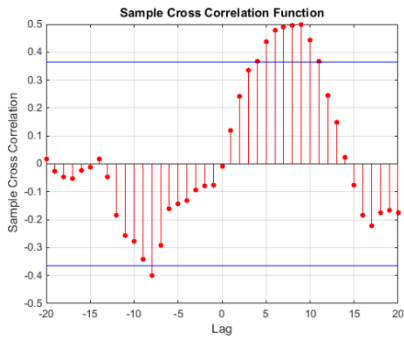


Fig. 9 – Residuals vs T_ext for Mod_2.2F

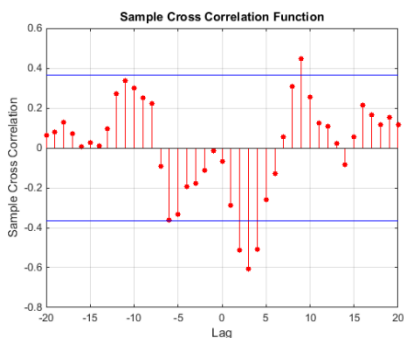


Fig. 10– Residuals vs Tsupp_2F for Mod_2.2F

Table 6 – Belsley multicollinearity test

CI	S- value	Tsupp_2F	Tret_2F	Tret_B	T_ext	T_BUI	Occ_BUI
1	1.956	0.004	0.002	0.015	0.000	0.012	0.008
2	1.130	0.001	0.000	0.024	0.349	0.049	0.002
3	0.707	0.002	0.000	0.255	0.437	0.162	0.012
4	0.486	0.106	0.010	0.569	0.064	0.201	0.002
5	0.371	0.054	0.000	0.018	0.003	0.561	0.600
13	0.146	0.833	0.887	0.117	0.146	0.015	0.374

The multicollinearity test shows that, although the variance decomposition proportions are high in the last line of Table 6 for Tsupp_2F and Tret_2F, the S-value is never below 0.1 and the Condition Indices (CI) are low. Indeed, the latter have a significance only if higher than 30, as specified in Belsley et al., 1980.

Based on the residual analysis results, the model that best represents the flow rates of the 2nd floor is Mod_2.2F. The estimated model equation is:

$$\begin{aligned}
 FR2F(t) &- 0.718 FR2F(t-1) + 0.1643 FR2F(t-2) - 0.06596 FR2F(t-3) + 0.1032 FR2F(t-4) - \\
 &0.1105 FR2F(t-5) + 0.06817 FR2F(t-6) + 0.007497 FR2F(t-7) = -67.98 Tsupp2F(t) - \\
 &13.73 Tsupp2F(t-1) + 83.56 Tret2F(t) - 30.42 Tret2F(t-1) + 3.5820 TretB(t) - \\
 &9.6160 TretB(t-1) - 67.98 Text(t) - 13.73 Text(t-1) - 23.14 TBUI(t) - \\
 &11.1200 TBUI(t-1) + 99.98 OccBUI(t) - 28.59 OccBUI(t-1) \quad (3)
 \end{aligned}$$

Table 7 – Distribution of model inputs

Quantile	Tsupp_2F	Tret_2F	Tret_B	T_ext	T_BUI	Occ_BUI
Min	23.15	24.31	16.01	1.40	17.20	0.00
25%	27.27	28.55	18.55	5.65	18.21	0.00
Median	47.52	39.31	37.33	8.00	19.30	0.00
75%	63.54	57.54	57.14	9.10	20.09	0.20
Max	69.41	63.38	61.96	12.50	21.22	0.78

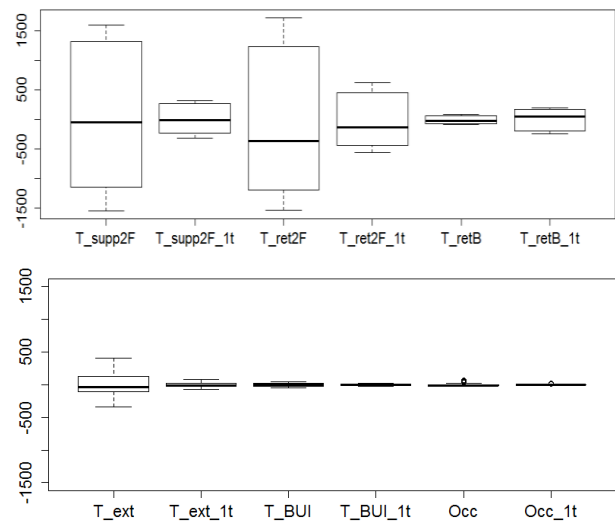


Fig. 11 – Impact of each input term in model equation (3)

The boxplot (Fig. 11) shows that the most important parameters influencing the flow rate are the supply and return temperature of the 2nd floor, the return temperature of the bathrooms and the external temperature. This assertion is confirmed by the fact that the system is controlled by an external temperature probe. The model calibration and validation plots are shown hereafter.

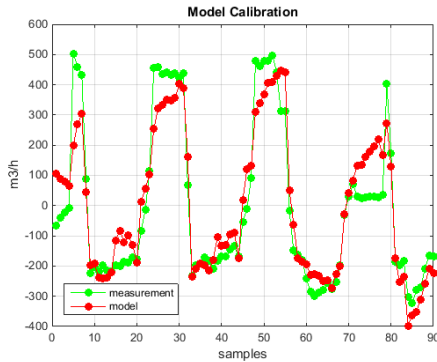


Fig. 42 – Calibration of Mod_2.2F

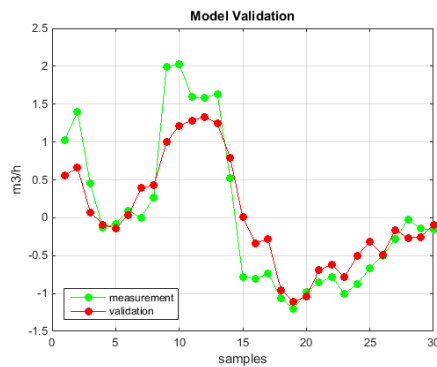


Fig. 53 – Validation of MOD_2.2F

An analogous process was carried out to identify a model for the first floor, with similar results.

Table 8 – 1st floor model inputs

Model	Inputs
Mod_1.1F	Tret_B; GR; FR_2F;
Mod_2.1F	Tret_B; FR_2F;
Mod_3.1F	Tret_2F; Tret_B; GR; FR_2F;

Table 9 – Determination coefficients of first floor model

Model	R_{cal}^2	$R_{Adj.cal}^2$	R_{val}^2	$R_{Adj.va}^2$	ΔR^2
Mod_1.1F	0.981	0.980	0.989	0.989	-0.008
Mod_2.1F	0.980	0.979	0.988	0.988	-0.008
Mod_3.1F	0.982	0.981	0.988	0.987	-0.005

Based on the results of Table 8 and on the residuals analysis, the best model chosen to evaluate the flow rate for the 1st floor is Mod_2.1F. Its model equation is:

$$FR1F(t) - 0.1492 FR1F(t - 1) + 0.0084 FR1F(t - 2) - 0.0503 FR1F(t - 3) + 0.0595 FR1F(t - 4) - 0.0387 FR1F(t - 5) - 0.0245 FR1F(t - 6) - 0.04106 FR1F(t - 7) = 33.6900 FR2F(t) + 0.8957 TretB(t) \quad (4)$$

The following figures show the model calibration and validation for the FR_1F.

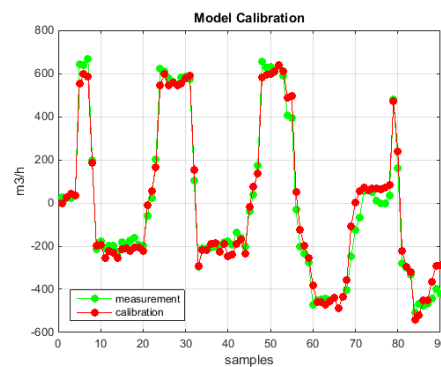


Fig. 14 – Calibration of Mod_2.1F

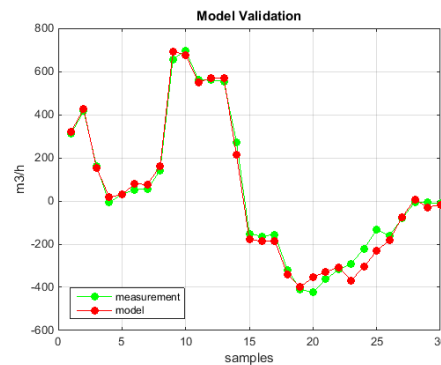


Fig. 65 – Validation of Mod_2.1F

The estimated models for both flow rates were used to find the heating consumption of the San Michele building for February, March, April, October and December 2013 (“heating season” in Table 9). In the other months, it was not possible to use the model due to a modification of the system setting. In November, billing data is not available. Table 9 shows the comparison between the utility meter (normalized by the area of all 3 floors: 1425 m²) and the modelling values (normalized by the area of the 1st and the 2nd floor: 950 m²).

Table 11 – Real and model values of building heating consumption

Season	Real value [kWh/m ²]	Modelling value [kWh/m ²]
Heating season	77.02	85.32
Average	15.40	17.06

The estimated average heating consumption differs from the real consumption by less than 10%. This value is influenced also by the fact that the ground floor was not monitored, therefore reducing the prediction accuracy. Additionally, due to the presence of only few offices on the ground floor it is expected to have a small heating requirement compared with the first and second floor.

3. Conclusion

We showed how system identification can help to estimate the water flow rates in a central heating system (and the relationship with influencing variables) and subsequently the heating consumption. We defined and demonstrated a methodology aimed at identifying the best model among the many generated. The results show that the identified model reliably estimates the measured heating consumption. However, there is room for improvement. An error model could increase the quality/fitness of the model and reduce the cross correlation of residuals with inputs.

References

[1] ICT PSP Smart-Build project <http://www.smartbuild.eu/> 10/11/2014

[2] L. Ljung, 1999. "System identification: Theory for the User, 2nd ed. New Jersey: Prentice Hall PTR

[3] N. Ismail, M.H.F. Rahiman, M. N. Taib. 2011. "Investigation of ARX Model on Partial Input-Output Data in Heating Process" IEEE Control System Graduate Research Colloquium 978-1-4577-0339

[4] K. Yun, R. Luck, P.J. Mago, H. Cho .2012. "Building hourly thermal load prediction using an indexed ARX model" Energy and

Buildings 54(2012):225-233.

[5] M.J.Rabbani, K.Hussain, A. jhan, A. Ali. 2013. "Model Identification and Validation for a Heating System using MATLAB system Identification Toolbox " ICSICCST:Material Science and Engineering 51 (2013). doi :10.1088/1757-899X/ 51/1/012022

[6] B.H.Andrews, M.D. Dean, R.Swain, C.Cole. 2013. "Buildng ARIMA and ARIMAX Models for predicting Long-term Disability Benefit Application Rates in the Public/Private Sectors". Society of Actuaries Health Section

[7] R.Nau, Fuqua School of Business Duke University, "stationarity and differencing" <http://people.duke.edu/~rnau/411diff.htm> 10/11/2014

[8] OTexts, online open access textbooks, "stationarity and differencing" <https://www.otexts.org/fpp/8/1> 10/11/2014

[9] M. Mourad, J.Bertrand, L.Krajewski, G. Chebbo. 2005. "Calibration and validation of multiple regression models for stormwater quality prediction: data partitioning, effect of dataset size and characteristics". Water Science & Technology 52(2005): 45

[10] D. A. Belsley, K. Edwin, E.W.Roy 1980. "Regression Diagnostics: Identifying Influential Data and Sources of Collinearity". New York: John Wiley and Sons.

Comparison between hourly simulation and bin-method for the seasonal performance evaluation of electric air-source heat pumps for heating

Claudia Naldi – DIN, Alma Mater Studiorum Università di Bologna – claudia.naldi2@unibo.it

Matteo Dongellini – DIN, Alma Mater Studiorum Università di Bologna – matteo.dongellini@unibo.it

Gian Luca Morini – DIN, Alma Mater Studiorum Università di Bologna – gianluca.morini3@unibo.it

Enzo Zanchini – DIN, Alma Mater Studiorum Università di Bologna – enzo.zanchini@unibo.it

Abstract

Air-source heat pumps in heating mode are characterized by performances strongly dependent on the value of the outdoor air temperature. The Italian standard UNI/TS 11300-4 indicates, for the evaluation of a heat pump seasonal efficiency, a method based on the local bin distribution of the external air temperature. The aim of this paper is to test the bin-method proposed by UNI/TS 11300-4 by comparing the results obtained through this method with the results deduced by using a more accurate dynamic simulation of the system. The heat pump Seasonal Coefficient Of Performance (*SCOP*) is calculated by means of a dynamic simulation code, written in MATLAB, in which hourly climate data distributions defined by CTI for different Italian towns are introduced as input data together with the thermal characteristics of the building. The thermal winter behaviour of the building is introduced in the models by using the Building Energy Signature. In the paper the values of the seasonal indexes *SCOP_{on}* and *SCOP_{net}* obtained by means of the bin-method and the dynamic hourly simulation, both for mono-compressor and inverter-driven heat pumps, in the service of several buildings placed in different Italian climates, are evaluated and compared to each other. Different buildings and different climate data are used in order to highlight the main conditions which are responsible for the difference between the predictions obtained with the bin-method and the results obtained by using the dynamic hourly simulation. The results presented in this paper show that the predictions of the bin-method tend to be in agreement with the results of the dynamic simulations based on the Test Reference Year only in particular conditions. The observed discrepancies in terms of *SCOP* between these two approaches can reach 23%, varying with the climate data and with the type of heat pump considered.

1. Introduction

The diffusion of air-source heat pumps in heating systems and for domestic hot water production has recently increased since these devices use athermal energy, which the Directive 2009/28/EC (European Parliament, 2009) recognizes as renewable energy. Moreover, thanks to their relative cheapness and to the air availability, air-source heat pumps are often used in energy retrofit of buildings to replace conventional heat generators. The performance of an air-source heat pump depends on building loads and on the outdoor air temperature, which is variable during the heating season; therefore, the evaluation of the heat pump seasonal efficiency should be performed through a dynamic simulation of the system. As an alternative, the Italian standard UNI/TS 11300-4 (UNI, 2012) suggests the use of the bin-method to obtain the Seasonal Coefficient Of Performance (*SCOP*) of an air-source heat pump.

The evaluation of a heat pump seasonal efficiency has been analysed in several recent studies (Kinab et al., 2010; Francisco et al., 2004; Sarbu et al., 2014 and Madonna et al., 2013). The present Authors have recently developed a mathematical model able to evaluate, through the bin-method, the *SCOP* of electric air-to-water heat pumps integrated by electric heaters (Dongellini et al., 2014) as well as a MATLAB code for the hourly simulation of air-to-water heat pump systems working in heating mode (Naldi et al., 2014).

In this paper the model based on the bin-method (Dongellini et al., 2014) is used together with the model based on the dynamic simulation (Naldi et

al., 2014) in order to compare the values of the Seasonal Coefficient Of Performance of different heat pump typologies, building thermal demands and climates. The analysis has been conducted by considering both on-off and inverter-driven mono-compressor air-source heat pumps, integrated by electric heaters as back-up system, in the service of buildings placed in different Italian climates.

The results obtained in this work highlight that the bin-method and the hourly dynamic simulation of a heating plant based on an air-source heat pump give comparable results in terms of seasonal performance coefficients; the larger relative difference in terms of $SCOP$ is observed for high values of the bivalent temperature in cold climates.

2. Simulation

2.1 Dynamic simulation

The hourly simulation of the heat pump heating system is carried out through the MATLAB code described in (Naldi et al., 2014). The main input parameters of the model are: the hourly values of the outdoor air temperature during the heating season, the hourly values of the thermal power required by the building, the heat pump and thermal storage volume technical data.

In the present study the hourly climate data defined in the Test Reference Year by CTI for three Italian towns (Naples, Bologna and Milan) are used.

If the heat pump has an on-off mono-compressor system, the heat pump technical data in input are: the Temperature Operative Limit (TOL), the values of the heat pump power and Coefficient Of Performance (COP) at the temperature of the hot water produced by the heat pump and for different values of the outdoor air temperature (T_{ext}). COP is the parameter which quantifies an electric heat pump efficiency and it is defined as the ratio between the thermal power delivered and the corresponding electric power needed by the heat pump.

If the heat pump is provided with an inverter compressor, the power and COP input data are

given in correspondence of different inverter frequencies.

The code evaluates for each hour of the heating season several parameters, including: the maximum power available from the heat pump, the energy supplied by the heat pump and, if needed, by the back-up system (electric heaters), the mean temperature of the water in the thermal storage, the electric energy used by the heat pump and by the back-up system.

The code then evaluates the values assumed by the $SCOP_{net}$ and $SCOP_{on}$ defined by UNI EN 14825 (UNI, 2013) as follows:

$$SCOP_{net} = \frac{Q_{HP}}{E_{HP,us}} \quad (1)$$

$$SCOP_{on} = \frac{Q_b}{E_{HP,us} + E_{BK}} \quad (2)$$

where Q_{HP} is the total thermal energy delivered by the heat pump during the heating season, $E_{HP,us}$ is the electric energy used by the heat pump, Q_b is the total thermal energy required by the building, and E_{BK} is the electric energy used by the back-up system.

2.2 Bin-method

The Italian standard UNI/TS 11300-4 utilizes the bin-method for the evaluation of an air-source heat pump seasonal performance. A bin is the number of hours, during a certain period of time, in which the external air has a temperature within a fixed interval, which is 1 K wide and centred on an integer value of temperature. The standard UNI/TS 11300-4 evaluates the bin trend of an Italian location by assuming a normal distribution of the outdoor air temperature, obtainable starting from the local values of outdoor design temperature (T_{des}), monthly average external air temperature and daily global solar radiation on horizontal plane. The bin distribution for the heating season in Milan (45.28 °N, 9.11 °E), Bologna (44.29 °N, 11.20 °E) and Naples (40.50 °N, 14.15 °E) has been evaluated as indicated by the Italian standard, considering the heating season from October 15th to April 15th for Milan and Bologna and from November 15th to March 31st for Naples. The obtained bin profiles are shown in Fig. 1-3 (blue colour), together with the bin trends derived from

the hourly values of the outdoor air temperature according to the Test Reference Year (TRY) defined by CTI (red colour) for the same locations.

It is evident from Figures 1-3 that the bins calculated by using the CTI's TRY and those evaluated by the method proposed by UNI/TS 11300-4 are different.

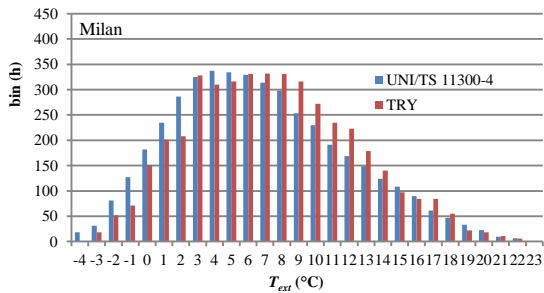


Fig. 1 – Bin profiles for Milan

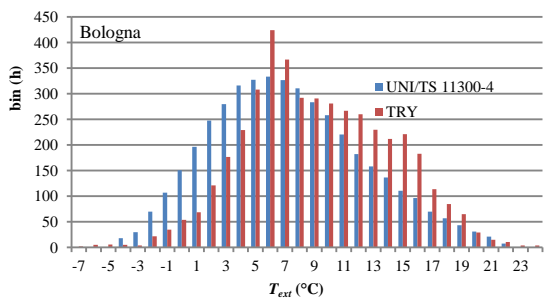


Fig. 2 – Bin profiles for Bologna

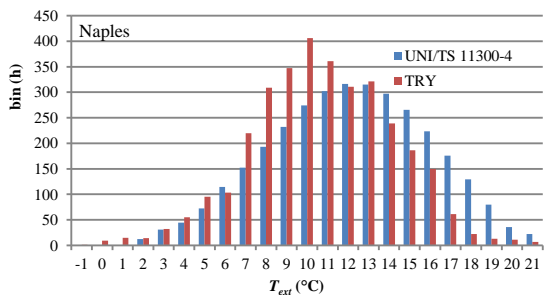


Fig. 3 – Bin profiles for Naples

For instance, the bin profiles evaluated according to UNI/TS 11300-4 are characterized by an average temperature of 6.8 °C in Milan, 7.3 °C in Bologna and 12.1 °C in Naples, versus the values of 7.4 °C (Milan), 9.2 °C (Bologna) and 10.7 °C (Naples) obtained by using the CTI's TRY.

2.3 Building Energy Signature

The thermal energy required by the building in correspondence of each bin is evaluated, as UNI/TS 11300-4 suggests, by means of the Building Energy Signature (*BES*), which is the straight line giving the power required by the building as a function of the external air temperature (i.e. red dashed line in Fig. 4).

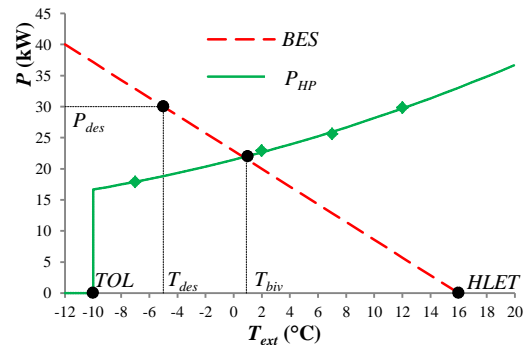


Fig. 4 – Building Energy Signature and heat pump power as function of the external air temperature

In order to consider different building loads and their effect on heat pumps' seasonal performances, several *BES* lines are here considered, by fixing the value of the external temperature where the building heating demand becomes zero (*HLET*: Heating Limit External Temperature) and by varying the value of the building design load (P_{des}) in correspondence of the outdoor design temperature (T_{des}). Indeed, once two points in the temperature-power diagram are known (e.g. (0, *HLET*) and (T_{des} , P_{des})), a *BES* straight line is univocally identified.

In order to compare the results obtained from the bin-method with those derived from the dynamic simulation, the hourly values of the energy required by the building in the dynamic simulation are calculated, in each case studied, by means of the same *BES* line as that used in the simulation with the bin-method.

2.4 Heat pump technical data

Both in the dynamic simulation and in the bin-method, the thermal power delivered by the heat pump, P_{HP} , is obtained by interpolation of the technical data given by the heat pump

manufacturer, for fixed temperatures of the outdoor air and of the hot water produced.

The green solid line in Fig. 4 is an example of the characteristic curve of an electric air-source on-off mono-compressor heat pump (ON-OFF HP), plotted as a function of the external air temperature, for a fixed temperature of the hot water produced. The heat pump characteristic curve is stopped in correspondence of the TOL .

The intersection between the Building Energy Signature and the heat pump characteristic curve is called the balance point, and the corresponding external air temperature is called the bivalent temperature (T_{biv}). In correspondence of T_{biv} the heat pump thermal power matches the thermal load of the building; when the external air temperature becomes lower than T_{biv} the heat pump is not able to completely satisfy the building heating demand, so that the back-up system must be activated; if T_{ext} is higher than T_{biv} , on the contrary, the heat pump power exceeds the building request, and the ON-OFF HP has to start on-off cycles, with efficiency losses.

For an Inverter-Driven Heat Pump (IDHP), the heat pump capacity P_{HP} is a function not only of the outdoor air and hot water temperatures, but also of the inverter frequency; T_{biv} is defined as the intersection between the BES line and the heat pump capacity at full load, namely at the maximum inverter frequency.

If the outdoor air temperature is higher than T_{biv} , an IDHP can reduce its working frequency in order to follow the building load (partial load condition), until the minimum frequency is reached. IDHPs must activate the on-off cycles only if the building load is lower than the heat pump capacity at the minimum inverter frequency, so that the on-off cycles are strongly delayed.

The characteristic curve of the COP of the heat pump at declared capacity is obtained from the manufacturer data, as described in (Naldi et al., 2014) and in (Dongellini et al., 2014).

Fig. 5 shows the characteristic curves at full load of the ON-OFF HP and the IDHP used for the simulations presented in this work, obtained by interpolation of the manufacturer data in correspondence of a temperature of the hot water equal to 35 °C (i.e. for radiant panels heating

systems). In the same graph the corresponding curves of the electric power $P_{HP,us}$ used at declared capacity by the heat pumps are also plotted. $P_{HP,us}$ is obtained as the ratio between P_{HP} and the COP at declared capacity. From Fig. 5 it can be noticed that the selected heat pumps are characterized by similar values of the power delivered at full load with the same outdoor temperature conditions.

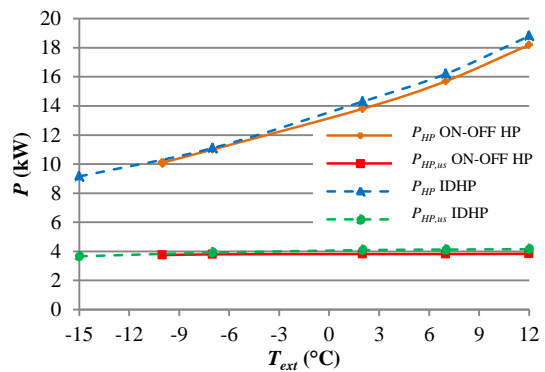


Fig. 5 – Thermal power delivered and electric power used by the heat pumps at full load

Table 1 shows the IDHP power and COP data given by the manufacturer for several inverter frequencies and external air temperatures (for a fixed hot water temperature equal to 35°C).

Table 1 – IDHP power (in kW) and (COP) at declared capacity, for different inverter frequencies and external temperatures

T_{ext} (°C)	Frequency (Hz)				
	85	69	53	36	20
-15	9.15 (2.50)	7.43 (2.57)	5.71 (2.56)	3.94 (2.42)	2.17 (1.98)
-7	11.10 (2.84)	9.06 (2.94)	7.00 (2.95)	4.86 (2.81)	2.67 (2.32)
2	14.30 (3.50)	11.60 (3.61)	8.93 (3.64)	6.28 (3.54)	3.42 (2.91)
7	16.20 (3.93)	13.20 (4.08)	10.30 (4.16)	7.23 (4.06)	3.94 (3.36)
12	18.80 (4.53)	15.30 (4.73)	11.90 (4.85)	8.38 (4.73)	4.60 (3.95)

By comparing the data shown in Table 1, it is evident that, while the values of P_{HP} obviously decrease with the reduction of the inverter frequency, the values of the COP become higher until a frequency around half the maximum is reached, after which they decrease.

3. Results and discussion

The mathematical models described in (Naldi et al., 2014) and in (Dongellini et al., 2014) have been applied to evaluate the seasonal performances of different heat pumps in Milan, Bologna and Naples. The reported main seasonal coefficients of performance of the heat pump, ($SCOP_{net}$, $SCOP_{on}$) are calculated by fixing $HLET$ equal to 16°C and varying the design load of the building for a fixed temperature of the hot water produced (35°C).

First of all, the coherence of the bin-method with the dynamic simulation has been tested. Starting from the CTI's TRY for Milan, a comparison has been made in terms of $SCOP$ by using the dynamic simulation and the bin-method in which the bins have been calculated by using the same TRY data used in the dynamic simulation. The data in Fig. 6 show the $SCOP$ obtained with the ON-OFF HP and IDHP for several buildings in Milan. As can be seen in Fig. 6, the achieved results in terms of $SCOP_{on}$ and $SCOP_{net}$ with the two different approaches are in agreement with each other; the maximum discrepancy recorded is about 9% on $SCOP_{on}$ of the ON-OFF HP in the service of a building with a value of T_{biv} equal to 6.6°C (rightmost point on the red and blue curves, Fig. 6a). This means that the bin-method is able to give an accurate prediction of the seasonal performance coefficients of the heating plant in good agreement with the more accurate results available after the dynamic simulation of the system, if the two methods use the same climatic data as input.

The results reported in Fig. 7-9 show the difference, in terms of the main seasonal performance coefficients ($SCOP_{net}$, $SCOP_{on}$), obtained by following the bin-method proposed by UNI/TS 11300-4 and the dynamic simulation based on the CTI's TRY for buildings located in Milan, Bologna and Naples, respectively. It is evident, since these

approaches are based on climatic data not exactly coincident, as can be seen in Fig. 1-3, that the difference in $SCOP$ values is larger than that in Fig. 6. More in detail, the two approaches tend to show larger differences in terms of $SCOP_{on}$ in correspondence of large bivalent temperatures, i.e. with under-sized heat pumps with respect to the building thermal demand. Indeed, the differences in terms of $SCOP_{on}$ are mainly related to the back-up activation which, under similar conditions, is relevant at larger values of T_{biv} . At low values of T_{biv} the influence on the $SCOP$ values of the climatic differences is combined with the effect due to the increase of the compressor on-off cycles, caused by the heat pump over-sizing with respect to the building thermal load. The effect of the on-off cycles is obviously stronger with the ON-OFF HP with respect to the IDHP, where the modulation capacity of the compressor delays the starting of on-off cycles.

The on-off condition determines a degradation of a heat pump performance quantified by multiplying the COP value at declared capacity by the COP correction factor, f_c , defined as:

$$f_c = \frac{CR}{1 - C_c + C_c CR} \quad (3)$$

where CR is the heat pump capacity ratio and C_c is the degradation coefficient, set by the standards equal to 0.9 in absence of more specific manufacturer indications.

As is evident from the results shown in Fig. 7, since the bin distributions derived from the TRY of Milan and UNI/TS 11300-4 method are very similar (the average temperature from TRY is 0.6 °C higher than the UNI/TS 11300-4 value (see Fig. 1)), the values of $SCOP$ obtained with the two methods tend to be very close to each other.

In Bologna (see Fig. 8) higher $SCOP$ are obtained with the dynamic simulation with respect to the results obtained with the bin-method, since CTI's TRY data present an average temperature 1.9 °C larger with respect to the bin distribution calculated through UNI/TS 11300-4. It is evident by comparing Fig. 7 and Fig. 8 that in Bologna the differences in terms of $SCOP_{on}$ obtained by using the dynamic simulation and the bin-method are larger with respect to the differences obtained in Milan. In addition, for a fixed value of the bivalent

temperature, the difference in terms of $SCOP_{on}$ is larger for the ON-OFF HP than for the IDHP. The difference in terms of $SCOP_{net}$ is very limited both for Milan and Bologna. In Fig. 9 the same evaluation has been made for Naples. In this case the dynamic simulation and the bin-method give very similar results in terms of $SCOP_{on}$ and $SCOP_{net}$ both for ON-OFF HP and IDHP. When the bivalent temperature is reduced (over-sized heat pump) the

$SCOP$ increase due to the hotter climate is reduced by the increase of the number of on-off cycles and the seasonal performance coefficients tends to become equal by using the dynamic simulation (hotter outdoor temperature, larger number of on-off cycles) and the bin-method based on UNI/TS 11300-4 distribution (colder outdoor temperature, lower number of on-off cycles).

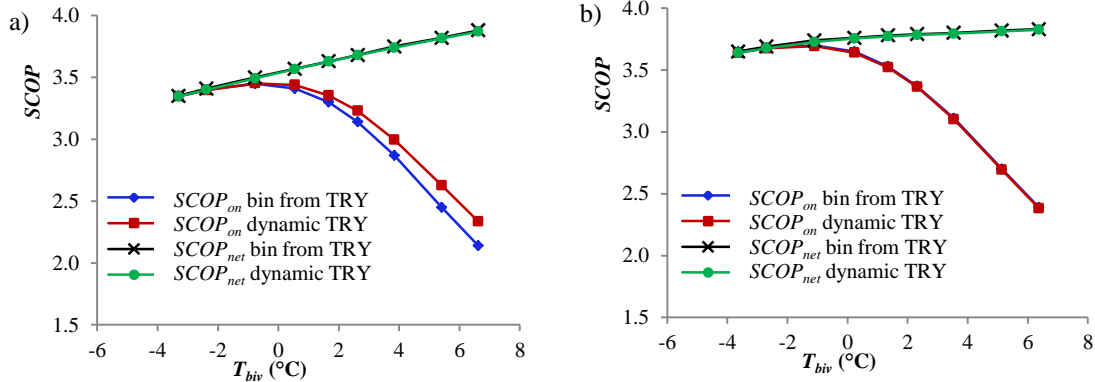


Fig. 6 – $SCOP$ as function of T_{biv} from the dynamic and bin simulations, ON-OFF HP (a) and IDHP (b), Milan

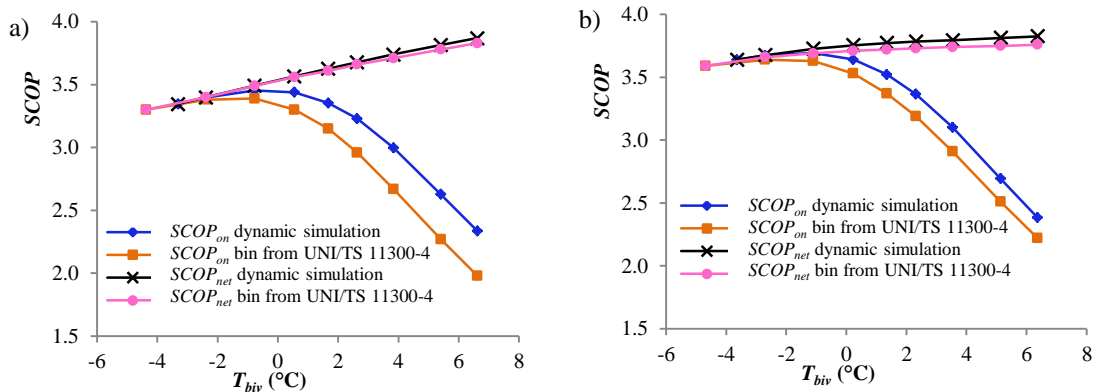


Fig. 7 – $SCOP$ as function of T_{biv} from the dynamic simulation and bin simulation from UNI/TS 11300-4, ON-OFF HP (a) and IDHP (b), Milan

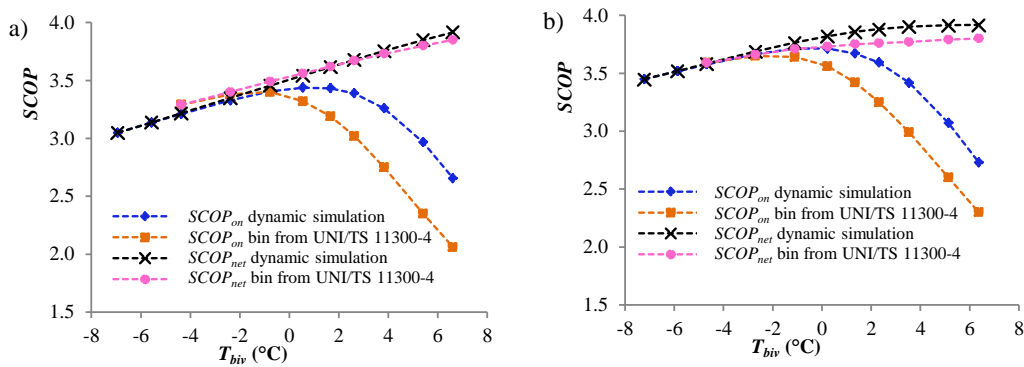


Fig. 8 – $SCOP$ as function of T_{biv} from the dynamic simulation and bin simulation from UNI/TS 11300-4, ON-OFF HP (a) and IDHP (b), Bologna

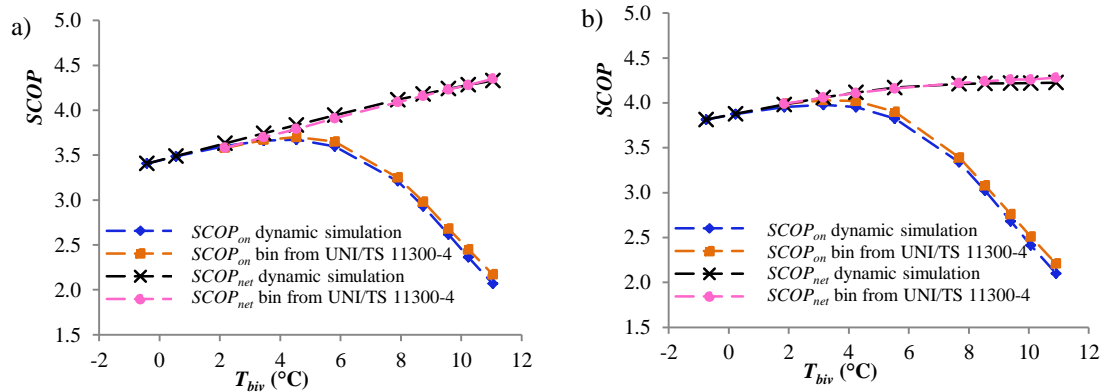


Fig. 9 – SCOP as function of T_{biv} from the dynamic simulation and bin simulation from UNI/TS 11300-4, ON-OFF HP (a) and IDHP (b), Naples

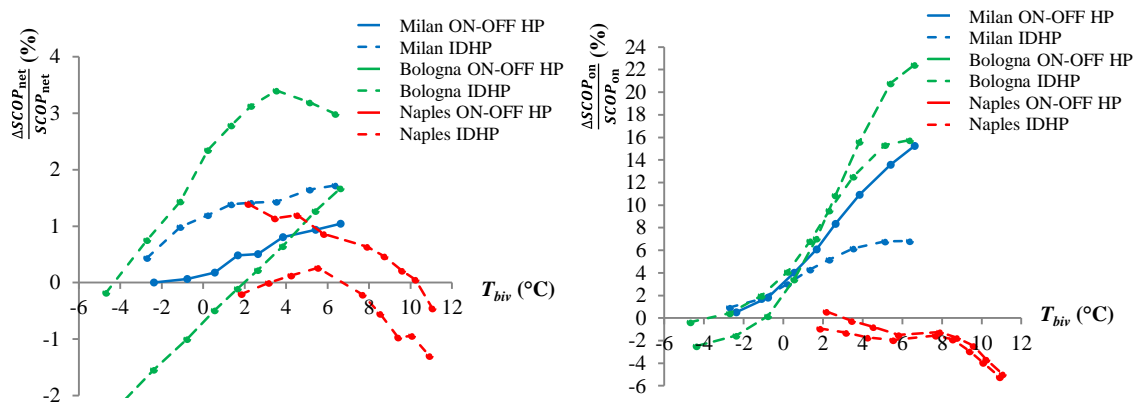


Fig. 10 – Relative differences on the seasonal indexes as functions of the bivalent temperature

Fig. 10 shows, as function of T_{biv} , the difference in terms of $SCOP$ obtained from the dynamic simulation and the bin-method. The choice of the calculation method influences especially the value of $SCOP_{on}$, whose relative difference reaches 22.4% (ON-OFF HP in Bologna with $T_{biv}=6.6$ °C), while the maximum relative difference on $SCOP_{net}$ is always very limited (i.e. 3.4% for IDHP in Bologna with $T_{biv}=3.5$ °C). These results highlight that the larger relative difference in terms of $SCOP_{on}$ is generally observed for the ON-OFF HP, with high values of the bivalent temperature.

4. Conclusions

In this paper a comparison between the results obtained by means of the bin-method proposed by UNI/TS 11300-4 and the dynamic hourly simulation of a heating system based on an air-source heat pump is shown in terms of seasonal

coefficients of performance ($SCOP$) in different Italian locations. The numerical results highlight that the bin-method is able to give numerical results in good agreement with the results obtained by means of a dynamic hourly simulation especially for low bivalent temperature values (over-sized heat pumps) both for ON-OFF HPs and IDHPs. However, for large values of the bivalent temperature (i.e. under-sized heat pumps with respect to the building thermal loads) the two methods give different results in terms of $SCOP$. More in detail, for typical Italian climate data, the maximum deviation between the predictions of these two methods in terms of $SCOP_{on}$ can reach 23% for ON-OFF HPs under-sized with respect to the building thermal loads. On the contrary, in terms of $SCOP_{net}$ the difference is always less than 4% both for under-sized and over-sized ON-OFF HPs and IDHPs.

5. Acknowledgement

This research was funded by the European Union's Seventh Framework Program, Theme EeB.NMP.2012-2, Project HERB (Holistic energy-efficient retrofitting of residential buildings), Grant agreement n°: 314283.

6. Nomenclature

Symbols

<i>BES</i>	Building Energy Signature
C_c	<i>COP</i> degradation coefficient
<i>COP</i>	Coefficient Of Performance
<i>CR</i>	heat pump capacity ratio
<i>E</i>	electric energy (kWh)
<i>HLET</i>	Heating Limit External Temperature (°C)
IDHP	Inverter-Driven Heat Pump
ON-OFF	ON-OFF Heat Pump
HP	
<i>P</i>	power (kW)
<i>Q</i>	thermal energy (kWh)
<i>SCOP</i>	Seasonal Coefficient Of Performance
<i>T</i>	temperature (°C)
<i>TOL</i>	Temperature Operative Limit (°C)
TRY	Test Reference Year
f_c	<i>COP</i> correction factor for on-off cycles

Subscripts

<i>BK</i>	of the back-up system
<i>HP</i>	of the heat pump
<i>b</i>	of the building
<i>biv</i>	bivalent
<i>des</i>	design
<i>ext</i>	of the external air
<i>net</i>	of the heat pump only
<i>on</i>	of the heat pump and back-up system
<i>us</i>	used

References

Dongellini, M., C. Naldi, and G. L. Morini. 2014. "Seasonal performance evaluation of electric air-to-water heat pump systems." In *Proceedings of the 13th International Conference on Sustainable Energy Technologies* Geneva, August 25-28.

E40123.

European Parliament. 2009. "Directive 2009/28/EC of The European Parliament and of the Council of 23 April 2009 on the promotion of the use of energy from renewable sources and amending and subsequently repealing Directives 2001/77/EC and 2003/30/EC." *Official Journal of the European Union* n. 52 of the 5 June 2009.

Francisco, P. W., B. Davis, D. Baylon, and L. Palmiter. 2004. "Heat pump system performance in northern climates." *ASHRAE Transactions* 110: 442-451.

Kinab, E., D. Marchio, P. Rivière, and A. Zoughaib. 2010. "Reversible heat pump model for seasonal performance optimization." *Energy and Buildings* 42: 2269-2280. doi:10.1016/j.enbuild.2010.07.007.

Madonna, F., and F. Bazzocchi. 2013. "Annual performances of reversible air-to-water heat pumps in small residential buildings." *Energy and Buildings* 65: 299-309. doi:10.1016/j.enbuild.2013.06.016.

Naldi, C., G. L. Morini, and E. Zanchini. 2014. "A method for the choice of the optimal balance-point temperature of air-to-water heat pumps for heating." *Sustainable Cities and Society* 12: 85-91. doi:10.1016/j.scs.2014.02.005.

Sarbu, I., D. Dan, and C. Sebarchievici. 2014. "Performances of heat pump systems as users of renewable energy for building heating/cooling." *WSEAS Transactions on Heat and Mass Transfer* 9: 51-62.

UNI. 2012. "Prestazioni energetiche degli edifici, Parte 4: Utilizzo di energie rinnovabili e di altri metodi di generazione per la climatizzazione invernale e per la produzione di acqua calda sanitaria." *Norma UNI/TS 11300-4*. Milano: Ente Italiano di unificazione.

UNI. 2013. "Condizionatori d'aria, refrigeratori di liquido e pompe di calore, con compressore elettrico, per il riscaldamento e il raffrescamento degli ambienti, Metodi di prova e valutazione a carico parziale e calcolo del rendimento stagionale." *Norma UNI EN 14825*. Milano: Ente Italiano di unificazione.

Cost optimal and net zero energy office buildings solutions using small scale biomass-based cogeneration technologies

Ayman Mohamed – Aalto University, Espoo, Finland – Ayman.mohamed@aalto.fi

Ala Hasan – VTT Technical Research Centre of Finland, Finland

Kai Sirén – Aalto University, Espoo, Finland

Abstract

In this study, four different small-scale biomass-based cogeneration heat and power (CHP) technologies along with three conventional energy generation systems serving an office building in Helsinki, Finland are investigated to find the local cost-optimal solutions for minimum energy performance for each as well as the global cost optimal solution. The Energy Performance of Building Directive (EPBD) comparative framework methodology is followed. All building combinations are simulated by IDA-ICE 4.5 software including building energy efficiency measures/packages; external wall insulation, window type, and envelope air-tightness, and building service system packages including ventilation system, and daylight control. The reference case is defined consisting of a reference building built in accordance with the current building code served by district heating and vapor compression cycle cooling system (DH-VCR). The results show that the pellet boiler with vapor compression refrigeration system (PB-VCR) has global cost-optimal solution. When the CHP capacities are sized to cover the peak thermal demands, the low power-to-heat (P/H) ratio CHP technologies have life cycle cost (LCC) less than the reference case, while the CHP technologies with high P/H have higher LCC. The reason for that is the high investment cost relating to higher associated electrical capacities as well as high operational energy costs due to lower thermal efficiency. However, optimizing the CHP capacity and installing an auxiliary pellet boiler means that all investigated CHP technologies have LCC less than the reference case. Furthermore, the net zero energy building (NZEB) solutions extended - by implementing photovoltaic system (PV) - for the cost-optimal solutions have lower LCC than those extended based minimum energy performance solutions.

1. Introduction

According to the Energy Performance of Building Directive 2010/31/EU, (EPBD) recast (Directive, 2010), all Member States (MS) shall ensure that minimum energy performance requirement achieving cost-optimal levels has to be set using a comparative methodology framework. The methodology framework was published as EU supplementary EBPB recast No 244/2012 (Supplementing-Directive, 2012). In the submitted Finnish report (Ministry-of-the-Environment, 2012), the cogeneration heat and power (CHP) was not investigated as an energy supply system. However, the CHP technologies have various energetic, economic, and environmental advantages over the separate production heat and power in large and district level (Salomón et al., 2011). In Finland, 115,882 GWh biomass fuel was consumed by the CHP plants in 2012 (Statistics-Finland, 2013). Moreover, biomass has the highest renewable energy source share (23% in 2011) which is considered a promising source alongside wind power to replace fossil fuels. This encourages the investigation of installing the small-scale biomass-based CHP systems as an energy generation system (EGS).

The objective of this study is to find the local cost-optimal solutions for four small-scale biomass-based CHP technologies along with three conventional systems as well as the global cost-optimal solution serving an office building in Helsinki, Finland. Furthermore, the cost-optimal and the minimum energy performance solutions are extended by installing a photovoltaic system (PV) to reach the NZEB balance. The aim of that is

to answer the question as to which solution has the lower NZEB life-cycle cost (LCC).

2. Methodology

2.1 Cost optimality calculation

The steps of cost-optimal framework methodology explained in (Supplementing-Directive, 2012) are followed. Step 1, the reference building is defined. It is a six-storey office building with a narrow shape (Fig. 1). The room height is 3.6 m. Each floor is 936 m² and the net heated floor area is 5615 m². The reference office building is built in compliance with the standards of the Finnish building codes (D3, 2012; D5, 2012). Its envelope properties, operation schedule, and set point temperatures are shown in Table 1. More detailed descriptions are presented in (Ministry-of-the-Environment, 2012). Step 2, the building energy efficiency measures (EEM) and all their combinations are identified and simulated using IDA-ICE 4.5 software. The simulation uses reference year weather data (Vantaa TRY2012) (Kalamees et al., 2012). The proposed EEM and packages are categorized into three groups; building structure measures, building service system packages (BSSP), and heating/cooling energy generation systems (EGS). The building structure packages are three wall insulation levels, four window types, and four air-tightness levels. Other EEMs related to the building structure such as roof /ground additional insulation, heavy thermal mass, optimal orientation, solar shading are not considered in this study, because they showed low energy-saving potential in a previous study (Flodberg et al., 2012). The BSSPs are three packages consisting of ventilation system and daylight control. All the suggested combinations of building structure measures and BSSPs ($3 \times 4 \times 4 \times 3 = 144$ building combinations) are simulated to get the heating, cooling, and electrical energy demands. The heating/cooling EGSs include three conventional systems, district heating and vapor compression refrigeration cooling system (DH-VCR), district heating and district cooling systems (DH-DC), pellet boiler and vapor compression refrigeration

cooling system (PB-VCR), and four biomass-based CHPs with VCR; organic Rankine cycle (ORC-VCR), internal combustion engine with gasifier (ICE-VCR), indirect fire gas turbine (IFGT-VCR), updraft gasifier with stirling engine (SE-VCR). Thereafter, in step 3, the delivered energies, the imported primary energy (PE), of 1008 cases (144×7) are calculated. The characteristics and costs of the building structure packages, BSSPs and EGSs are illustrated in Appendix A.

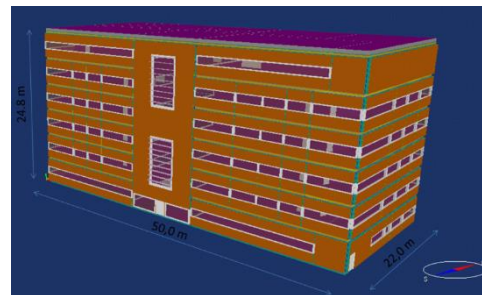


Fig. 1 – The 3D model of the simulated office building in IDA ICE.

Table 1 – Envelope properties, operation schedules, and set points of the reference office building (Ministry-of-the-Environment, 2012)

Property description	value
U-value of walls	0.17 Wm ⁻² K ⁻¹
U-value of roof	0.09 Wm ⁻² K ⁻¹
U-value of ground floor	0.16 Wm ⁻² K ⁻¹
U-value of windows	1.0 Wm ⁻² K ⁻¹
SHGC of Glazing factor	0.68 (-)
Overall window to wall ratio	27.2 %
Infiltration rate (air change/hour)	0.94 (50 Pa) h ⁻¹
Occupancy schedule	Weekdays 07:00–18:00 ^a
Lighting schedule and control	Weekdays 07:00–18:00 ^a
Appliances schedule and control	Weekdays 07:00–18:00 ^a
Ventilation schedules and control	Weekdays 06:00–19:00 ^a at other times 0.15 ls ⁻¹ m ⁻²
Winter set point temperature	21 °C
Summer set point temperature	25 °C
Heating system	Always On
Cooling system	Always On

^a All detailed profiles depend on the zone's utilization, for example, office, meeting rooms, etc.

The delivered energy is calculated by post-processing the annual energy demands taking into consideration the distributed and system efficiencies based on (D5, 2012). For the CHPs, it is assumed that the efficiencies are constant and equal to the nominal values obtained from different sources (Table A. 8, Appendix A). All CHPs are operated to track the thermal demands with ON/OFF operation using the dead band of a water storage system with a capacity of 3.0 cubic meters (Mohamed et al., 2014b).

The conventional systems are sized to cover the peak thermal demands. As a preliminary step, the CHPs are sized to cover the peak thermal demands as well. Thereafter, the CHP capacities are optimized.

Step 4, the imported PE is calculated for the cost-optimal calculations for the imported energies excluding any exported energy following the energy performance calculation method in the Finnish code (D3, 2012). The PE factors are given in Fig. 2. The life-cycle cost (LCC) calculation is the method used to assess the economic viability of the building performance (Supplementing-Directive, 2012). The LCC is the sum of the present value of the investment and discounted operational costs for the building and service systems, including those related to maintenance and replacement, including taxes, over a specified calculation period. In this study, the total incremental life-cycle cost (dLCC) is calculated and presented as a difference cost between each EGS cases and a reference case as given by Eq. (1).

$$dLCC = LCC - LCC_{ref} \quad (1)$$

The reference case consists of the reference building and DH-VCR as a heating/cooling EGS. In the urban area of the Helsinki region, 85% of the building stoke is served by the DH system (City-of-Helsinki, 2008), while the VCR system is the only system investigated with office building in (Ministry-of-the-Environment, 2012).

The LCC calculation follows a financial cost calculation concerning an individual owner perspective as given in ANNEX 1 of (Supplementing-Directive, 2012). The life-span for an office building is 20 years as recommended. The basic calculations are carried out using the 3% real discount rate. All building EEMs have life-spans

equal to the calculation period, therefore the residual value will equal zero for all EEMs and packages. No disposal cost for building elements and EEMs are taken into consideration. Fig. 2 shows the fuel and energy prices and their escalation rates. All energy prices include taxes and transportation costs. Under the current Finnish energy policy, the feed-in tariff of the exported electricity produced via new small scale biomass- and biogas-based CHP has a target price of €83.5 (MWh)⁻¹ (Energy-Authority, 2013).

Table 2 – Primary energy factors, fuel prices, and escalation rates

Energy carrier	Primary energy factor ^a kWh _{pe} (kWh) ⁻¹	Price ^b €(MWh) ⁻¹	escalation rate ^c %
Electricity	1.7	154.8	2.74%
DH	0.7	79.67	1.78%
DC	0.4	26.0	1.78%
Pellets	0.5	56.0	1.54%

^a PE factors based on Finnish code (D3, 2012).

^b All prices are annual average prices based on 2013 and obtained from (Statistics-Finland, 2013).

^c The escalation rate is calculated based on the energy price evolution for the last 10 years.

2.2 Net zero energy building calculation

The NZEB is defined as a building with greatly reduced energy demands through efficiency gains so that the balance of energy needs can be supplied with onsite or neighbouring renewable technologies (Torcellini et al., 2006). In this study, the NZEB building boundary is defined to include all EGSs as onsite supply options and the necessary space required to install any additional onsite or neighbouring renewable energy technology (Mohamed et al., 2014b). However, the imported fuel has to be taken into account in the NZEB balance. The typical operating energy uses are considered for the balance, including heating, ventilation, domestic hot water, lighting, HVAC equipment, and appliances. The import/export is the balancing type. Symmetrical primary energy factors are used for imported and exported electricity. Typically, the balance period is a year. The net PE is the metric balance. The NZEB balance is fulfilled when the net PE is equal or less than zero as shown by Eq. (2).

$$\text{net PE} = \sum \text{PE}_{\text{imp}} - \text{PE}_{\text{exp}} \quad (2)$$

where PE_{imp} is the sum of the annual imported primary energies, and PE_{exp} is the annual primary energy of the exported electricity.

According to the offer provided by a local energy distribution company (Fortum, 2013), the PV system is installed completely by this company and it purchases the surplus electricity. The installation price of the whole PV system is €427.60 m⁻² (including VAT) with a 20-year guarantee. The annual service fee is €46.70. In this study, the hourly electricity produced by the PV system is calculated by TRNSYS 17.1 software using the same reference year weather data. The orientation of the PV modules is selected to face south with a tilt angle of 45°. The calculated electricity production after the inverter of a one square meter of PV is 149.3 kWh y⁻¹. The hourly matching between the electrical demand and electricity produced via PV system is carried out using Matlab software. The exported price of the electricity produced via the PV system varies hourly depending on the spot market price. It is equal to the spot market price minus €2.40 (MWh)⁻¹ (margin fee) and €0.70 (MWh)⁻¹ (online service fee) (Fortum, 2013). The hourly and annual average spot market price of 2013 is obtained from Nord pool spot webpage (<http://www.nordpoolspot.com/>). The average price of €41.16 (MWh)⁻¹ is used.

3. Results and discussion

3.1 Energy demands

The simulated heating, cooling, electrical annual demands of the reference building and implementing separate building structure measures and building BSSP are shown in Fig. 2. The most efficient measures/packages among the packages are BSSP2 and BSSP3, where the ventilation control changed from constant air volume (CAV) to variable air volume (VAV), with saving potential of 24% for the space heating (SPH), 80% for ventilation heating, and 55% for ventilation cooling, while the space cooling (SPC) demand increases by 85%. The reason is related to

withdrawing the heat released by the internal heat and solar gains during the night in summer (unoccupied time) where the daytime is too long in the high latitude.

The total annual heating (including DHW, SPH and ventilation heating), cooling (including SPC and ventilation cooling), electrical (including lighting, appliances, and HVAC auxiliaries) demands of the 144 building combinations including the reference building are shown in Fig. 3. All building combinations are categorized into two group indicated by BSSP1 and both BSSP2 and BSSP3 with respect to the large saving potential in the SPH.

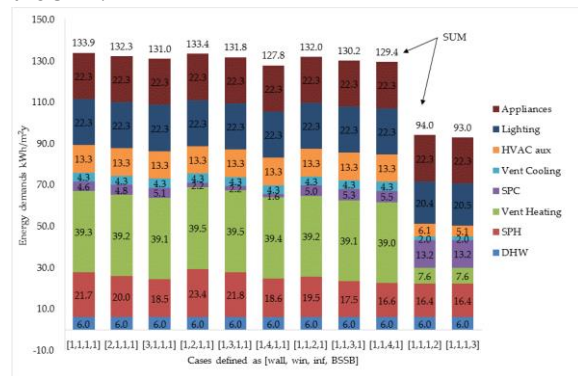


Fig. 2 – Annual energy demands of the reference building and those of implementing the EEM and the BSSP separately.

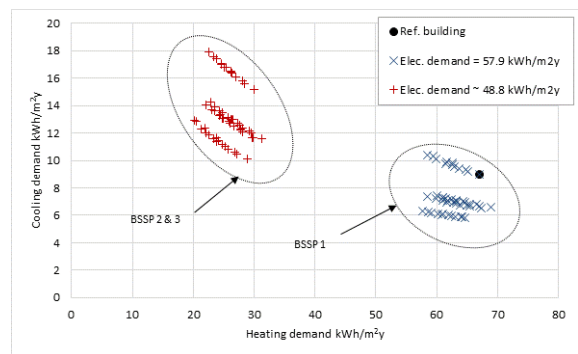


Fig. 3 – Heating, Cooling, and electrical demands of the 144 building combinations.

3.2 Cost optimality calculation

The reference case consisting of the reference building and DH-VCR has imported PE of 162.4 kWhm⁻²y⁻¹ and dLCC of €0 m⁻². The solution space has imported PE in range of 107.6 kWhm⁻²y⁻¹ and 177.0 kWhm⁻²y⁻¹, and the dLCC range of €-82.40 m⁻² and €306.00 m⁻². The cost optimal curves including all solutions that have either minimum dLCC or imported PE are shown in Fig. 4.

Table 3 – Local cost-optimal and minimum energy performance solutions and their building combinations for each EGS. The EGSs are in ascending order according to dLCC of the cost-optimal solutions.

Energy Generation System EGS	Local cost optimal solutions					Min energy performance solutions				
	dLCC €m ⁻²	PE _{imp} kWh m ⁻² y ⁻¹	PE _{exp} kWh m ⁻² y ⁻¹	EEM [wall, win, inf, BSSP]	PV area to reach NZEB m ²	dLCC €m ⁻²	PE _{imp} kWh m ⁻² y ⁻¹	PE _{exp} kWh m ⁻² y ⁻¹	EEM [wall, win, inf, BSSP]	PV area to reach NZEB m ²
PB-VCR	-82.4	117.1	0.0	[1,1,1,2]	2591	-61.5	107.6	0.0	[3,4,4,3]	2381
DH-VCR	-73.4	121.2	0.0	[1,1,1,2]	2683	-57.7	110.3	0.0	[3,4,4,3]	2442
ORC-VCR	-54.0	113.3	6.2	[2,2,4,2]	2369	-36.7	103.7	5.0	[3,4,4,3]	2295
SE-VCR	-53.8	112.2	7.5	[2,2,4,2]	2315	-36.5	107.7	6.0	[3,4,4,3]	2251
IFGT-VCR	-37.6	114.1	16.0	[2,2,4,2]	2173	-22.4	109.2	12.7	[3,4,4,3]	2418
DH-DC	-36.3	118.8	0.0	[2,2,1,2]	2629	-21.5	109.0	0.0	[3,4,4,3]	2133
ICE-VCR	-7.5	120.5	17.3	[2,2,4,2]	2285	1.4	113.4	12.8	[2,4,4,3]	2227

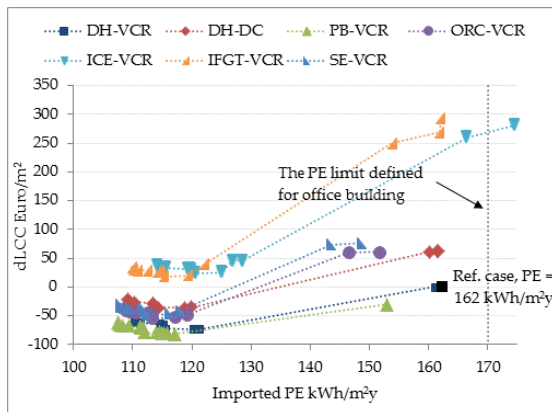


Fig. 4 – The cost optimal curve for all studied EGSs.

From Fig. 4, it can be concluded that biomass-based CHP technologies with a high power to heat ratio (P/H) (IFGT and ICE) have relatively high dLCC compared to those with low P/H. The reason for that is the high investment cost relating to higher associated electrical capacities as well as high operational energy costs due to lower thermal efficiency.

The PB-VCR has the global cost-optimal solution is with dLCC of €-82.40 m⁻² and imported PE of 117 kWhm⁻²y⁻¹ as given in Table 3.

The PB technology, which is a mature product, has relatively low investment and annual costs. The pellet fuel prices and its escalation rate are the lowest among all energy carriers (Table 2). Moreover, the VCR system has an advantage over the DC system because it has lower annual fees.

Based on the aforementioned results of cost optimality when the CHPs are sized depending on the peak thermal demand, the CHP capacities are re-sized to be a ratio of the thermal peak demand while the remaining demand can be covered by an auxiliary pellet boiler. The CHPs are operated to be a main heating EGS and it has the priority to run over the auxiliary PB boiler. The CHP capacities are optimized where the dLCC is reduced without any significant increase in the imported PE. The optimized small scale CHP capacity is constrained to be not less than the minimum defined capacity of small scale CHP of 30 kWe (Beith, 2011). The CHP range for all CHP technologies is given in (Table A. 8, Appendix A).

With optimized CHP capacities, the solution space has imported PE in range of 107.6 kWhm⁻²y⁻¹ and 161.7 kWhm⁻²y⁻¹, and the dLCC range of €-82.40 m⁻² and €71.80 m⁻². The cost optimal curves including all solutions which have either minimum dLCC or imported PE are shown in Fig. 5.

Table 3 shows the local cost-optimal and minimum energy performance solutions for all EGSs (after optimizing the CHP capacities).

Regarding the biomass-based CHP, both ORC and SE with low P/H have lowest dLCC and imported PE as well. This is basically due to accounting the imported energies while the exported electricity is excluded. Moreover, the onsite generated electricity has a low utilization ratio by the electrical demand ($\approx 34\%$ in case of cost-optimal solution of ORC-VCR). The low P/H yields to

reduce the imported fuel under the operational strategy of thermal tracking. The ICE-VCR system records the highest imported PE and dLCC, while it has the highest exported PE. Generally, the cost-optimal solutions of the investigated small scale biomass-based CHPs with optimal capacities have LCC less than the LCC of the reference case.

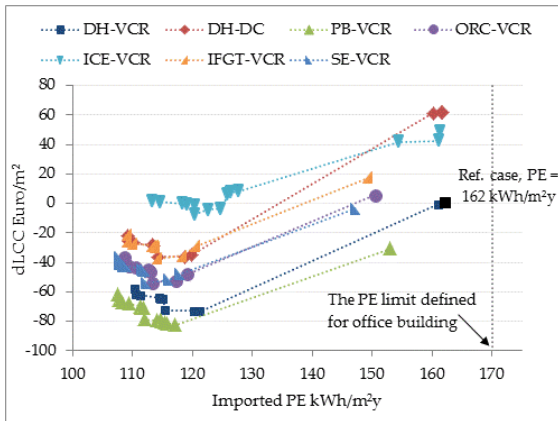


Fig. 5 – The cost optimal curve for all studied EGSs after optimizing the CHP capacities.

Regarding the building combinations of the cost-optimal solutions, the low investment and annual costs systems (PB-VCR and DH-VCR) have the most efficient package of BSSP2 with the same EEMs of the reference building without a need to invest more in other EEMs. Meanwhile, the biomass-based CHP with low thermal efficiency, need more investment in the building construction measures as wall 2, win 2, and inf 4 to reduce the thermal heating demand. The minimum energy performance solutions for all EGSs are the most efficient building EEMs and packages as shown in Table 3.

It must be emphasized that the results of this study do not take into account some issues relating to the EGS such as additional space required depending on the footprint, fuel procurement and storage, and the environmental impact of local emissions emitted from burning biomass onsite or in a dense area nearby.

3.3 Net zero energy building calculation

The NZEB calculations are carried out by extending the cost-optimal and minimum energy performance solutions by installing 200 m² as a module step as shown in Fig. 6. The PV area

required to fulfill the NZEB balance between the imported and exported PE are given in Table 3.

It can be noticed that the PV area ≤ 1000 m² has a small increase in the dLCC. The reason is mainly related to the high match between the PV electricity production and the electrical demand. The percentage of the onsite utilized electricity varies between 65% and 72% depending on the EGSs.

It can be concluded that the dLCC of the extended local cost-optimal solutions by a PV system are less than those of the extended minimum energy performance solutions. Therefore, the NZEB is achievable with economic viability with a slight increase in the dLCC by less than €20 m⁻² over the reference case when the cost-optimal solutions are extended by the PV system with PB-VCR, DH-VCR, ORC-VCR, SE-VCR as a EGSs. Of course, this conclusion helps the policy makers, building’s investors, contractors, as well as researchers to identify other barriers facing the NZEB implementation. As concluded in (Mohamed et al., 2014a) the low imported PE does not necessary indicate the high energy matching situation especially when different imported energies (i.e. fuels) are imported beside the electricity and thermal heat.

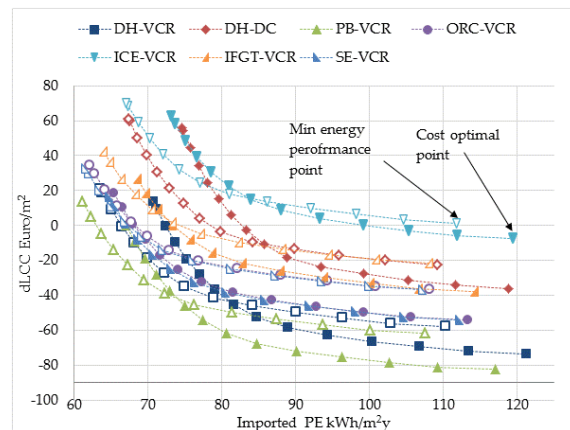


Fig. 6 – The dLCC of implementing PV system in 200 m² modules versus the imported PE for the local cost-optimal solutions (filled marker) and minimum energy performance solutions (unfilled marker) after optimizing the CHP capacities.

3.4 Sensitivity analysis

The sensitivity analysis is carried out with three other real discount rates for the cost-optimal solutions of optimized CHP capacities. Fig. 7

shows the imported PE and dLCC of the cost optimal solutions for the EGSs after optimizing the CHP with real discount rates of 1%, 6%, and 10% along with the based calculation of 3%. The EGSs are in ascending order according to the cost optimal solutions of the base calculation of 3%.

As shown in Fig. 7, the dLCC is calculated relatively to its reference case cost with the same real discount rate. The variation of the imported PE for each EGS with different real discount rates means a change in building combinations of the cost optimal solutions. The PB-VCR still has the minimum cost optimal solution among all EGSs, however, the difference between PB-VCR and DH-VCR reduces and becomes close to zero under the high real discount rate of 10%. The DH-VCR and DH-DC become more economical than the ORC-VCR and SE-VCR with a high real discount rate of 10%.

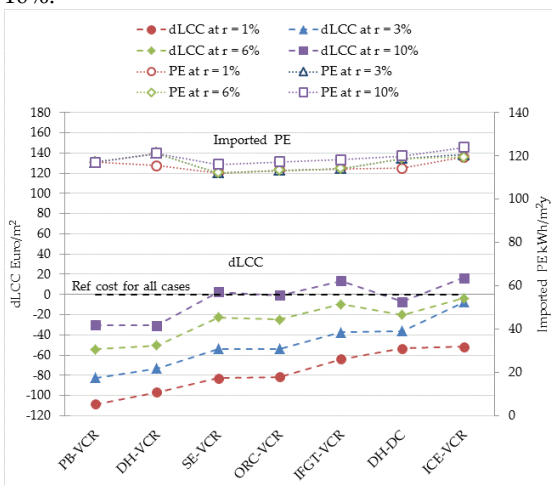


Fig. 7 – The local cost-optimal solutions versus imported PE consumption for each EGS at different real discount rates after optimizing the CHP capacities. The EGSs are in ascending order according to the local cost-optimal solutions of base calculation with 3% real discount rate.

4. Conclusion

This study followed the EBPD comparative framework methodology to find the local cost-optimal solutions of four biomass-based CHP technologies compared with three conventional heating and cooling systems serving an office building in Helsinki, Finland as well as the global cost-optimal solution. The building energy efficiency measures (EEM) combinations consisting

of building structure measures; external wall insulation, window type, and envelope airtightness, and building service system packages (BSSP) of ventilation system, and daylight control are involved. The reference case defined by the reference building built in accordance with the building codes currently in force served by a district heating and vapor compression refrigeration cooling system (DH-VCR). The results show that the pellet boiler (PB-VCR) has the global cost optimal solution. With the CHPs capacities covering the peak thermal demand, the low power-to-heat (P/H) ratio CHP technologies have a life cycle cost (LCC) less than the reference case, while the CHP technologies with high P/H have higher LCC. The reason for that is the high investment cost relating to higher associated electrical capacities as well as high operational energy costs due to lower thermal efficiency. The CHPs with optimal capacities and with auxiliary pellet boilers have cost-optimal solutions less than that of the reference case. Furthermore, the NZEB solutions extended based on the cost-optimal solutions for all EGSs have lower dLCC than those extended based minimum energy performance solutions.

5. Acknowledgement

The authors would like to acknowledge the Finnish Academy, Aalto University SAGA project, as well as Tekes RYM-Indoor Environment project for partly funding this research. The first author also would like to acknowledge K.V. Lindholms Stiftelse for the part support of this research.

6. Nomenclature

Symbols

BSSP	Building service system package
CAV	Constant air volume
CHP	Cogeneration heat and power
DC	District cooling
DH	District heating
dLCC	Incremental life-cycle cost (€/m ²)
EEM	Energy efficiency measure

EGS	Energy generation system
EPBD	Energy Performance of Building Directive
ICE	Internal combustion engine
IFGT	Indirect fire gas turbine
LCC	Life-cycle cost (€m ²)
NZEB	Net zero energy building
O&M	Operation and maintenance
ORC	Organic Rankine cycle
P/H	Power to heat ratio
PB	Pellet boiler
PE	Primary energy (kWh _{pe} m ⁻² y ⁻¹)
PV	Photovoltaic panels
Q	thermal capacity (kW)
SE	Stirling engine
SFP	Specific fan power (kWm ⁻³ s)
SHGC	Solar heat gain coefficient
SPC	Space cooling demand (kWhm ⁻² y ⁻¹)
SPH	Space heating demand (kWhm ⁻² y ⁻¹)
VAV	Variable air volume
VCR	Vapor compression refrigeration cooling system

Subscripts/Superscripts

c	cooling
exp	exported
h	heating
imp	imported
pe	primary energy
ref	reference

Appendix A

Building structure measures', building service system packages', and energy generation systems' characteristics and costs.

Table A. 1 – External wall insulation levels and its cost.

Wall insul.	Thickness m	U-values Wm ⁻² K ⁻¹	Investment cost €m ⁻³
Wall 1	0.24	0.17	64
Wall 2	0.35	0.12	
Wall 3	0.54	0.09	

Insulation material is mineral wool. (Isover, 2013)

Table A. 2 – Window types.

Window no	U-value Wm ⁻² K ⁻¹	T-value	SHGC	Cost €m ⁻²
Win 1 ^a	1.0	0.56	0.68	250 ^b
Win 2 ^a	1.0	0.34	0.46	258 ^b
Win 3 ^{a,b}	0.85	0.29	0.42	290 ^c
Win 4 ^a	0.7	0.2	0.3	350 ^b

^a In all windows, the blinds are between the outer panels.

^b The investment of win 1, 2, 4 are obtained from (Ministry-of-the-Environment, 2012) after subtracting the worker cost.

^c The investment of win 3 is obtained from (Hamdy et al., 2013)

Table A. 3 – Air-tightness levels.

Infiltration level	Specification n50 (h ⁻¹)	Additional labor cost (€m ⁻² of envelope)
Inf 1	1.0	0.0
Inf 2	0.74	4.15
Inf 3	0.49	8.3
Inf 4	0.37	9.6

Costs are taken from (Hamdy et al., 2011) and updated to 2013 ones by using 3.2 % escalation rate (Statistics-Finland, 2013).

Table A. 4 – System packages of ventilation system, daylight control, and building automation.

BSSP #	1	2	3
AHU #1			
Heat recovery effectiveness ^a	0.6	0.8	0.8
Maximum allowable exhaust air temperature	4.0	1.0	1.0
Ventilation control	CAV	VAV ^c	VAV ^c
Air flow rates of ls ⁻¹ m ⁻²	1.85	min 0.07 max 1.85	min 0.07 max 1.85
Specific fan power (SFP) kWm ⁻³ s	2	1.8	1.4
AHU #2			
Heat recovery effectiveness ^{a,b}	-	0.55	0.55
Maximum allowable exhaust air temperature	4.0	1.0	1.0
Air flow rate (constant flow), ls ⁻¹ m ⁻²	0.15	0.15	0.15
Ventilation control	CAV	CAV	CAV
Specific fan power (SFP) kWm ⁻³ s	2	1.8	1.4
Total ventilation system cost €m ⁻²	90	110	115
Daylight control (Yes/No)	No	Yes ^d	Yes ^d
Building automation cost €m ⁻²	10	15	15

^a Supply air heat recovery ratio

^b AHU #2 serves services zones, corridors, toilets, atrium, etc.

^c The ventilation control of VAV limits: minimum <600 ppm and up to > 900 ppm.

^d Daylight control limits: <500 lx illumination a fully enabled, >700 lx lighting off completely.

Table A. 5 – District heating and district cooling costs.

Sys.	Thermal capacity kW	Installation cost €	annual subscription costs €
DH ^a	61 > Q _h > 190	15500	22.7 Q _h + 2753.73
	191 > Q _h > 350	24800	22.7 Q _h + 2753.73
DC ^a	220 > Q _c > 315	372 Q _c	58.28 Q _c

^a costs are from (Fortum, 2013)

Q_h: thermal heating capacity

Q_c: thermal cooling capacity.

Table A. 6 – Pellet boiler costs.

Thermal heating capacity kW	Installation cost €	Annual operation and maintenance (O&M) €
Q _h < 20 ^a	5328	300
20 < Q _h < 30 ^a	6138	300
30 < Q _h < 60 ^a	10676	500
60 < Q _h < 80 ^a	11319	700
80 < Q _h < 200 ^b	85000	2100
200 < Q _h < 350 ^b	100000	2100
350 < Q _h < 600 ^b	130000	2100

^a costs of small pellet boiler capacities are from (Hemeltron, 2013)

^b costs of larger pellet boiler capacities are from (Janfire, 2013) annual average efficiency = 84 % based on Finnish code (D5, 2012)

Table A. 7 – Vapor refrigeration compression cooling system performance and cost.

System	Installation cost €	Annual O&M €
VCR	72020	620

annual average COP =3.0 based on (D5, 2012)

Table A. 8 – CHP technologies' characteristics and costs

Biomass-based CHP	η _e %	η _{th} %	η _{ov} %	P/H	Electric capacity range kWe
ORC	14	70	85	0.2	90–30 ^a 36–30 ^b
ICE	23	46	70	0.5	225–70 ^a 63–39 ^b
IFGT	28	56	84	0.5	225–70 ^a 45–38 ^b

SE	18	72	90	0.24	108–36 ^a 39–30 ^b
Biomass-based CHP	Inv. cost €kW _e ⁻¹	Variable O&M €(kW _{h_e)⁻¹}	Fixed O&M €(kW _{h_e)⁻¹y⁻¹}		
ORC	6696	0.0072	135		
ICE	5987	0.03	147		
IFGT	6800	0.024	131		
SE	7652	0.032	33		

^a The CHP capacity range covering the peak thermal demand.

^b The optimal sized CHP capacity range with auxiliary pellet boiler.

The biomass-based CHPs' references are (Wood and Rowley, 2011), (*Technology data for energy plants*, 2012), (Lukawski, 2010), and (Devlin, 2010).

References

- Beith, R., 2011. Small and Micro Combined Heat and Power (CHP) Systems: Advanced Design, Performance, Materials and Applications (Google eBook). Elsevier.
- City-of-Helsinki, 2008. State of the Environment in the City of Helsinki: Theme Report 1/2008. Helsinki.
- D3, 2012. Finland Code of building Regulation. Energy management in buildings, regulations and guidelines. Helsinki: Ministry of Environment. Ministry of Environment, Finland.
- D5, 2012. Finland Code of building Regulation. Calculation of power and energy needs for the heating of buildings, guidelines. Helsinki: Ministry of Environment. Ministry of Environment, Finland.
- Devlin, T.D., 2010. Commercial and Industrial CHP Technology Cost and Performance Data Analysis for EIA.
- Directive, 2010. Directive 2012/27/EU of the European Parliament and of the Council of 25 October 2012 on the energy efficiency. Official Journal of the European Union.
- Energy-Authority, 2013. Energy Authority, Renewable energy [WWW Document]. URL <http://www.energiavirasto.fi/en/web/energy-authority/renewable-energy> (accessed 7.30.13).
- Flodberg, K., Blomsterberg, Å., Dubois, M.-C., 2012. Low-energy office buildings using existing technology: simulations with low internal heat gains. *Int. J. Energy Environ. Eng.* 3, 19. doi:10.1186/2251-6832-3-19

- Fortum, 2013. Fortum Company [WWW Document]. URL <http://www.fortum.fi> (accessed 7.20.13).
- Hamdy, M., Hasan, A., Siren, K., 2011. Applying a multi-objective optimization approach for Design of low-emission cost-effective dwellings. *Build. Environ.* 46, 109–123. doi:10.1016/j.buildenv.2010.07.006
- Hamdy, M., Hasan, A., Siren, K., 2013. A multi-stage optimization method for cost-optimal and nearly-zero-energy building solutions in line with the EPBD-recast 2010. *Energy Build.* 56, 189–203. doi:10.1016/j.enbuild.2012.08.023
- Hemeltron, 2013. Hemeltron OÜ [WWW Document]. URL <http://www.lvi-viro.fi/>
- Isover, 2013. Saint-Gobain [WWW Document]. URL <http://www.isover.fi/> (accessed 7.30.13).
- Janfire, 2013. Janfire Company, direct contact.
- Kalamees, T., Jylhä, K., Tietäväinen, H., Jokisalo, J., Ilomets, S., Hyvönen, R., Saku, S., 2012. Development of weighting factors for climate variables for selecting the energy reference year according to the EN ISO 15927-4 standard. *Energy Build.* 47, 53–60. doi:10.1016/j.enbuild.2011.11.031
- Lukawski, M., 2010. Design and optimization of standardized organic Rankine cycle power plant for European conditions.
- Ministry-of-the-Environment, 2012. Minimum energy performance requirements for calculating cost-optimal levels-Finland. *Energiatohokkuutta koskevien vähimmäisvaatimusten kustannusoptimaalisten tasojen laskenta-SUOMI*.
- Mohamed, A., Cao, S., Hasan, A., Sirén, K., 2014a. Selection of micro-cogeneration for Net Zero Energy Buildings (NZEB) using weighted energy matching index. *Energy Build.* 80, 490–503. doi:10.1016/j.enbuild.2014.05.055
- Mohamed, A., Hasan, A., Sirén, K., 2014b. Fulfillment of net-zero energy building (NZEB) with four metrics in a single family house with different heating alternatives. *Appl. Energy* 114, 385–399. doi:10.1016/j.apenergy.2013.09.065
- Salomón, M., Savola, T., Martin, A., Fogelholm, C.-J., Fransson, T., 2011. Small-scale biomass CHP plants in Sweden and Finland. *Renew. Sustain. Energy Rev.* 15, 4451–4465. doi:10.1016/j.rser.2011.07.106
- Statistics-Finland, 2013. Statistics Finland [WWW Document]. URL <http://www.stat.fi/> (accessed 7.30.13).
- Supplementing-Directive, 2012. Guidelines accompanying Commission Delegated Regulation (EU) No 244/2012 of 16 January 2012 supplementing Directive 2010/31/EU of the European Parliament and of the Council on the energy performance of buildings by establishing a comparative methodology f. *Official Journal of the European Union, EU*.
- Technology data for energy plants, 2012. . Danish Energy Agency and Energinet.dk.
- Torcellini, P., Pless, S., Deru, M., Crawley, D., 2006. Zero Energy Buildings: A Critical Look at the Definition; Preprint. National Renewable Energy Laboratory (NREL), Golden, CO.
- Wood, S.R., Rowley, P.N., 2011. A techno-economic analysis of small-scale, biomass-fuelled combined heat and power for community housing. *Biomass and Bioenergy* 35, 3849–3858. doi:10.1016/j.biombioe.2011.04.040

Integrated performance simulation of an innovative net zero energy modular building

Francesco Fantauzzi – M.Sc. Student, University of Perugia – ffantauzzi@hotmail.it

Paolo Belardi – DICA, University of Perugia – paolo.belardi@unipg.it

Francesco Asdrubali – CIRIAF, University of Perugia – francesco.asdrubali@unipg.it

Samuele Schiavoni – CIRIAF, University of Perugia – schiavoni.unipg@ciriaf.it

Sara Sambuco – CIRIAF, University of Perugia – sambuco.unipg@ciriaf.it

Abstract

Currently the value and the appeal of a house are deeply influenced by its own energy performance and its comfort. As a consequence, several examples of net zero energy buildings have been realized worldwide in the last decade, using renewable energy sources for their moderate energy consumption. An architectural experiment of this kind of buildings is represented by shipping container houses that could be used not only in emergency situations but also as alternative guestrooms or also low-cost houses. The paper presents the results of software simulations carried out to evaluate the energy and lighting performance of three kinds of shipping container houses characterized by different floor areas and usage. The bigger one is a typical shipping container having a surface of about 14 m² and a height of 2.4 m; the others have the same height but smaller surfaces, respectively of about 7 and 5.6 m². The furniture was designed to be moved thanks to upper runners in order to use the same area for different domestic activities during the day. Each one of them was planned to be a net zero energy building obtaining energy from solar panels and clean water from rainfall. The lighting design was carried out using DIALux while energy performance was studied through Energy Plus. The first one allowed us to optimize the selection and the position of LED lighting systems in order to assure the recommended values of the Illuminance E. Moreover, some graphical renderings were realized in order to have a clear and simple evaluation of the visual performance of the internal spaces, also taking into account the contribution of daylighting. The characteristics of the lighting systems were used for the evaluation of the whole energy performance of the building. Energy Plus is the dynamic simulation software used to determine the energy demand of each container, taking into account the

heating and cooling facilities, the insulation properties of the building envelope, windows and doors included. The results of this theoretical study show that this solution is technically feasible, cheap and also comfortable not only for emergency housing.

Introduction

The global economic crisis has also affected the maritime freight in the EU-28. Eurostat shows that European ports in 2012 handled only 3,739 million tonnes of seaborne goods, respectively 0.8% and 6% below 2011 and 2008 data (Eurostat, 2014). Consequently, a large quantity of containers lies idle in port areas occupying spaces and causing disposal issues. The large availability, lightness and portability of these elements make their usage suitable for housing.

Several projects are currently focused on recycling these facilities as buildings; some examples are presented in (Container City, 2014) and in (Designboom, 2014). The challenges in using containers for residential purposes are to define the best thermo-insulation materials and to design the systems able to guarantee a comfortable indoor quality and wellbeing conditions. An example of a zero emission house made using containers was designed and monitored by Dumas (Dumas, 2014): in this case the indoor air conditioning is obtained using geothermal water. The scope of the present paper is to describe the thermal and lighting simulations performed to improve the indoor quality performance of temporary residential solutions realized using shipping containers. These

were designed to be net zero energy building (Sartori et al., 2012) considering the best available technologies and the advanced predictive control schemes (Kolokotsa et al., 2011).

2. Case study description

2.1 Shape and function

Standard ISO shipping containers are 2.44 x 2.59 x 6.10 m. Three case studies were analysed: XXS (equal to one third of the container, 5.6 m²), XS (half, 7.0 m²) and S (Fig. 1 and Fig. 2, a complete one, 14.0 m²). Since a small amount of surface is available, furniture configuration can be changed by users according to their needs. This particular type of furniture required a blind wall. Obviously, the connections with the water supply network and electricity grid are unmovable. Special rails are installed on the container's ceiling to permit the sliding of the furniture. Their small sizes allows their placement in urbanized areas so the cover materials are designed differently with the aim of integration between the containers and the context also considering sustainable materials (Asdrubali et al., 2012). The XXS and S solutions could be used respectively as short-term single guestrooms and emergency housing; for these reasons the research reported in the paper is focused on these two case studies.

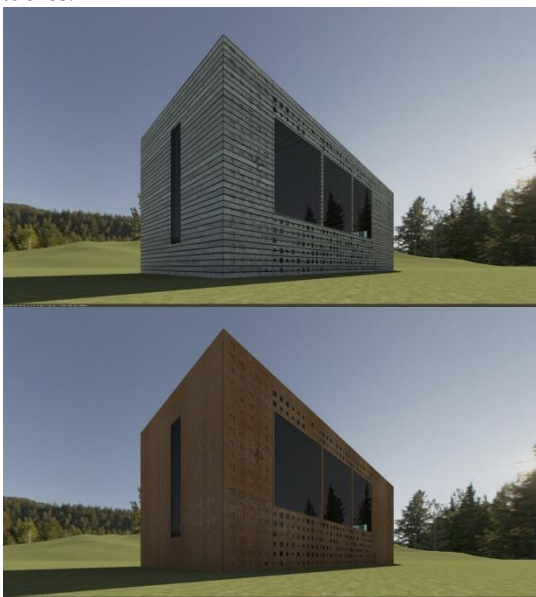


Fig. 1 – Render of an S case study. External view (wood and corten coverings)

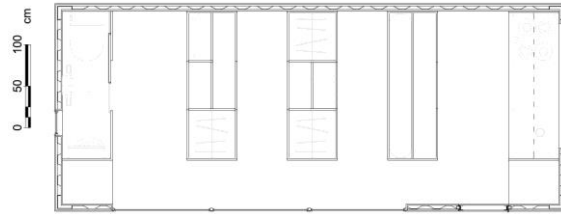


Fig. 2 – Planimetry of S case study

2.2 Energetic aspects

To provide low energy consumption values, the definition of the stratigraphy of the walls was conducted through the use of dynamic energy simulations. The walls, as well as the ceiling, are composed of an inner layer of Oriented Strand Board (OSB), two layers of polyurethane foam insulation separated by 1.8 cm of steel, a vacuum insulation panel and an outer covering panel. The floor is made of epoxy resin, steel, plywood, panel and vacuum insulation. The thickness of the layers was chosen after dynamic simulation to obtain the best configuration in terms of energy savings. The windows are double-glazed with argon, while the heating and cooling system is characterized by an air heat pump with split system. The installation of photovoltaic panels on the roofs was studied.

2.3 Lighting design

The lighting design for each case study was performed considering the change of the furniture arrangement during the 24h. Two configurations were analysed, *day* and *night*. In both cases, the position of the LED lamps should allow adequate Illuminance values on tables, floors and hobs also for poor daylighting contributions. LED lamps were chosen because even if their price is quite high, they are energy savers and do not emit heat. The LED lamps considered for the simulations are characterized by luminous flux of 1100 lumen, low energy consumptions (10 W, luminous efficacy 80.0 lm/W) and a colour temperature of 4200 K. Their optic allows a control of the luminance (UGR<19). The lamps are installed in recessed fixed luminaire, to avoid interferences with the sliding of the furniture. The optical characterization (in particular reflection and transmission coefficient) of floors, walls, ceilings, furniture, doors and windows was performed considering data from

scientific literature, certifications and spectrophotometric measurements (Asdrubali et al., 2009) (Baldinelli et al., 2014). Preliminary simulations were carried out to define the quantity of luminaires: five lamps are required for S and three for XXS case study; in each case study one lamp works only for bathroom lighting. These data were then used to perform energy simulations. Each case study has a blind wall; energy simulations were carried out to define the direction of exposure of this element.

3. Simulations

Energy and Lighting simulation were performed to characterize energy consumption and indoor comfort.

3.1 Energy simulations

3.1.1 Methods

In order to arrive as close as possible to developing “nearly zero energy buildings” defined in the European Directive 2010/31/UE, the energy simulations were performed using EnergyPlus [Energy plus website, 2014] and DesignBuilder [DesignBuilder website, 2014] not only to verify the energy consumption but also as design tools. EnergyPlus is a dynamic simulation software able to model the system of heating, cooling, ventilation and other energy flows. DesignBuilder is a graphical interface of EnergyPlus, which allows the user to implement the model of the building and assign the physical and thermal properties (size, materials, plants, thermal loads). Using the weather data of Perugia, the heating and cooling loads necessary to maintain thermal control setpoints (from 15th October to 15th April 20 °C and from 15th April to 15th October 26 °C), conditions throughout HVAC and the energy consumption of primary plant equipment were calculated.

Two steps of simulations were developed: the first to define the characteristic of the layers, of the glazed surfaces and the best orientation of the container and the second to verify the efficiency of the design phase. Calculations were carried out

considering the occupancy of 1 person per case study.

3.1.2 Results

The first step of simulations was carried out to define the stratigraphies and the building orientation.

Divided into six different layers characterized by a transmittance of 0.085 W/(m² K) for both the perimeter walls and the ceiling, the walls are composed of OSB (15 mm thick), polyurethane foam insulation (20 mm thick), steel (1.8 mm thick), foam polyurethane insulation (30 mm thick), vacuum insulation panel (50 mm thick), panel outer coating (if corian or corten: 12 mm thick, if wood: 30 mm thick). The thermal properties of vacuum insulation panels are: conductivity (0.007 W/(m² K)), specific heat (1000.0000 J/(kg K)) and density (180.00 kg / m³).

The stratigraphy of the floor is composed of epoxy resin (3 mm thick), steel (2 mm thick), plywood (30 mm thick), and vacuum insulation panel (50 mm thick), panel outer coating (if corian or corten: thickness 12 mm, if in wood: 30 mm thick). The floor has a transmittance of 0.099 W/(m² K) (Fig. 3).

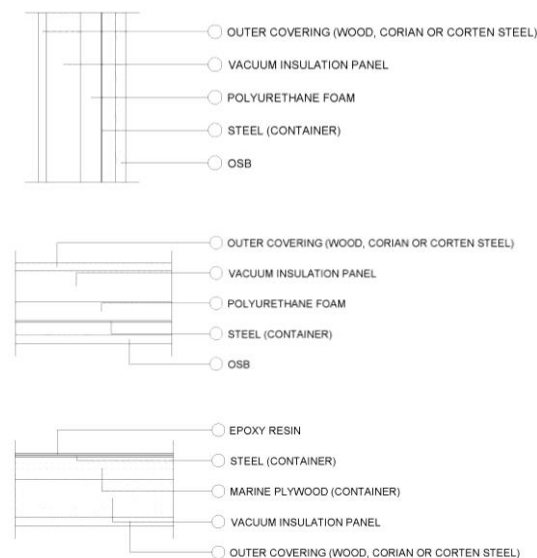


Fig. 3 – Coverage, wall and floor stratigraphies.

The chosen windows are double-glazed characterized by 6 mm thick inner and outer glass panes divided by a cavity of 13 mm filled with argon. The definition of glazed surfaces is associated to user needs, in particular to the

management of the internal space (Asdrubali et al., 2013).

The energy simulations performed probed that the blind wall should face south; this result was obtained analysing the difference between energy consumptions. Table 1 reports the energy production and consumption for the case study, considering respectively 7.2 m² and 4.3 m² of photovoltaic panels (Thin Film CdTe Module) on the S and XXS roofs. Total Energy Consumption is the sum of electricity consumption due to heat pump (air-conditioning and water heating) and to interior lighting. The buildings are supposed to be grid-connected, so that production in excess can be reversed into the grid which can be therefore used as storage.

Table 4 – Energy consumption and production for S and XXS case study.

Case Study	Total Consumption [kWh]	Specific Consumption [kWh/m ²]	Energy Prod. [kWh]
S	759	59.4	1188
XXS	391	70.8	713

After the definition of the geometry including windows, doors, stratigraphy, the definition of the plants and the definition of the thermal control setpoints, it was possible to include also the contribute of thermal loads of lighting carried out by the lighting simulations. Having designed the use of LED lights, the value of thermal loads is low and it was set to 1 W/m². Observing Fig. 4 and Fig. 5, it is possible to underline that the most important difference is the heating consumption while the difference of energy spent for cooling is less. Table 2 and Table 3 report respectively the total and specific electricity consumption for both case studies; the best configuration in terms of energy efficiency is the S container despite the XXS solution. The reason is related to the external surface area because the S/V ratio of XXS is higher than S/V ratio of S that limits deeply cooling energy consumptions. Table 4 shows a comparison in terms of water consumptions. Energy consumption due to home appliances was not considered in this stage of the study. The

connection to the natural gas network could be avoided since air-conditioning and water heating are performed using electricity.

Table 5 – Electricity consumption results obtained by EnergyPlus software of XXS and S case study. Total values.

	XXS Electricity [kWh]	S Electricity [kWh]
Heating	167.05	369.22
Cooling	111.70	115.81
Interior Lighting	20.09	45.44
Hot Water	92.10	228.83
Total	391	759

Table 6 - Electricity consumption results obtained by EnergyPlus software of XXS and S case study. Specific values.

	XXS Electricity [kWh/m ²]	S Electricity [kWh/m ²]
Heating	30.25	28.87
Cooling	20.24	9.06
Interior Lighting	3.64	3.55
Hot Water	16.68	17.90
Total	70.8	59.4

Table 7 – Water consumption results obtained by EnergyPlus software of XXS and S case study. Total and specific values.

XXS Total Water [m ³]	S Total Water [m ³]	XXS Specific Water [m ³ /m ²]	XXS Specific Water [m ³ /m ²]
1.44	3.58	0.26	0.26

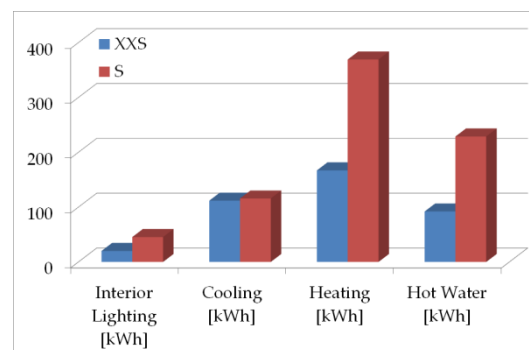


Fig. 4 - Comparison of electricity consumption results obtained by EnergyPlus software

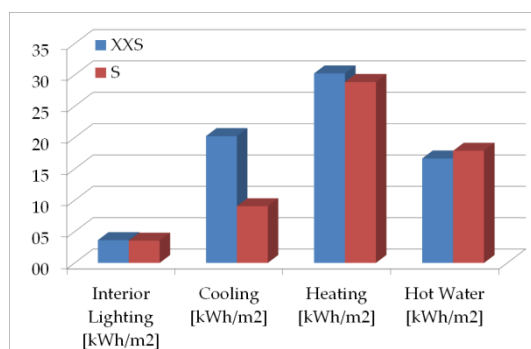


Fig. 5 - Comparison of specific electricity consumption results obtained by EnergyPlus software

3.2 Lighting simulations

3.2.1 Method

The simulations were performed using DIALux (DIALux website, 2014), a commercial software assessing artificial and natural lighting. 3D models of the S and XXS case study were realized including windows, doors and furniture. Grids of Illuminance calculations points were placed over tables (two for S and one for XXS case study), hobs and floors. Discomfort glares were evaluated. In each case study, the *day* and the *night* configurations were evaluated. In the latter case, daylighting was excluded. Glare was evaluated in compliance with the UGR method (UNI EN, 2011). The effects of daylighting were analysed assigning to the innovative modular buildings the geographical coordinates of Perugia (Italy), at the equinoxes and solstices and at the following periods: 2 hours after sunrise, noon, 2 hours before sunrise. The estimations of the daylighting contributions in the grids were calculated averaging the results of the 12 simulations (3 simulations for each one of the 4 days considered). Lighting simulations were performed to determine the optimal luminaires position that allows to obtain adequate Illuminance values and also to limit glare effects.

3.2.2 Results

The outcomes of the thermal simulations established that the solar panels, and consequently the blind walls, should face south. After defining the exposition, the daylighting simulations were carried out for both case studies. The calculation grids were placed over two tables

(respectively named S – table 1 and S – table 2) and the hub (S – hub) of the S case study and over the table (XXS – table) and hub (XXS – hub) of the XXS case study. In the present paper, only the results on tables are reported in detail (Table 5).

The results show that, in conditions of clear skies, Illuminance values are quite high for S – table 1 and XXS – table so windows should be provided with curtains. The Illuminance is low for S – table2 and consequently artificial light is needed. The values of the coefficient of uniformity U_0 , defined as the ratio between the minimum and the average value of the Illuminance in the calculation grid, can be considered compliant to the UNI EN 12464 requirements for areas characterized by writing and reading activities (0.6).

Table 5 – Illuminance values due to daylight in *day* configurations in the calculation grids placed on tables.

Calculation grids	Illuminance [lux]		Uniformity Coefficient U_0	
	Clear sky	Overcast sky	Clear sky	Overcast sky
S – table 1	1287	151	0.5	0.6
S – table 2	269	195	0.6	0.6
XXS - table	1093	373	0.6	0.4

Considering overcast sky conditions, Illuminance decreases dramatically under 500 lux on tables. Artificial lighting design assumes a decisive role to assure an adequate visual wellbeing in each configuration of the case studies.

Firstly, the LED luminaires described in section 2.3 were placed regularly: the line linking a luminaire with its closest luminaire is normal or parallel to the building walls. Artificial light simulations were then performed (without considering daylight) for both *day* and *night* configurations (Fig. 6). Table 86 reports the Illuminance and the coefficient of uniformity evaluated in the calculation grids considering the effect of artificial light due to the preliminary placement of luminaires in the *day* configuration of the two case studies. configuration of the two case studies.

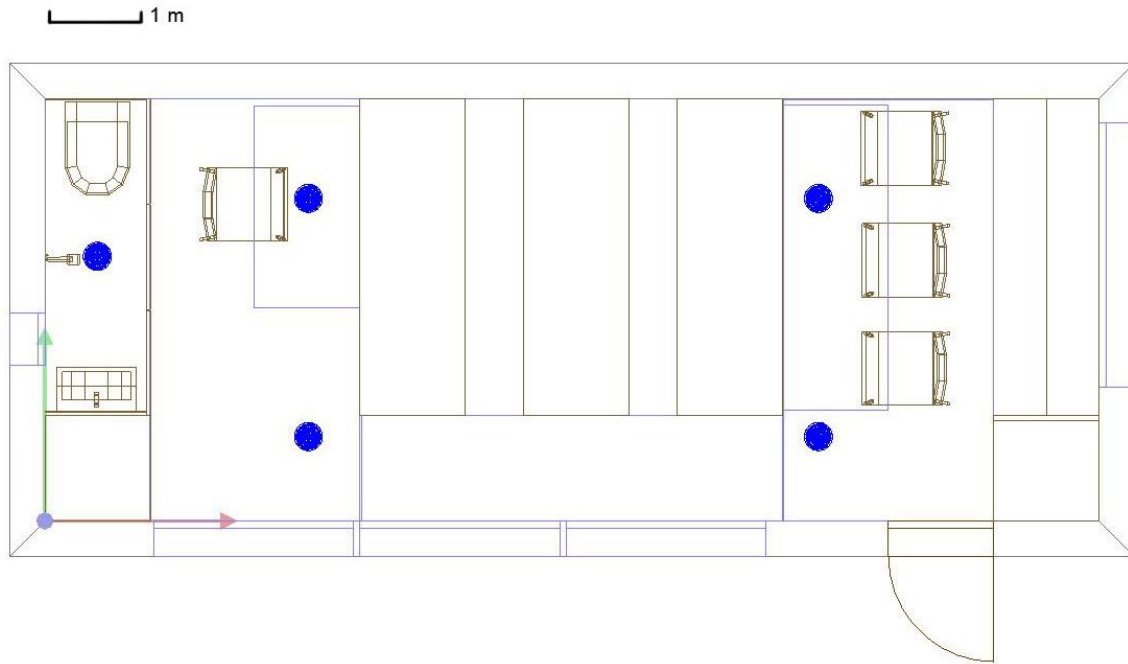


Fig. 6: Luminaires (in blue) for S case study. The pink bar is 1 m long.

Table 8 - Illuminance values due to artificial light in day configurations

Calculation grids	Illuminance [lux]	Uniformity Coefficient U_0
S – table 1	430	0.8
S – table 2	430	0.8
XXS – table	246	0.5

Concerning S – case study, the Illuminance values on tables are close to the 500 lux required by the UNI EN 12464 for areas characterized by writing and reading activities. These values can be considered adequate considering that the data in Table 8 do not consider daylight. For these reasons, the preliminary placement in the S – case study was considered the definitive one.

The low values observed on the table of XXS case study suggested changing the position of the luminaires. The average values of Illuminance, estimated on table and hob considering the optimised luminaires localisation (Fig. 7), can be seen in Table 7.

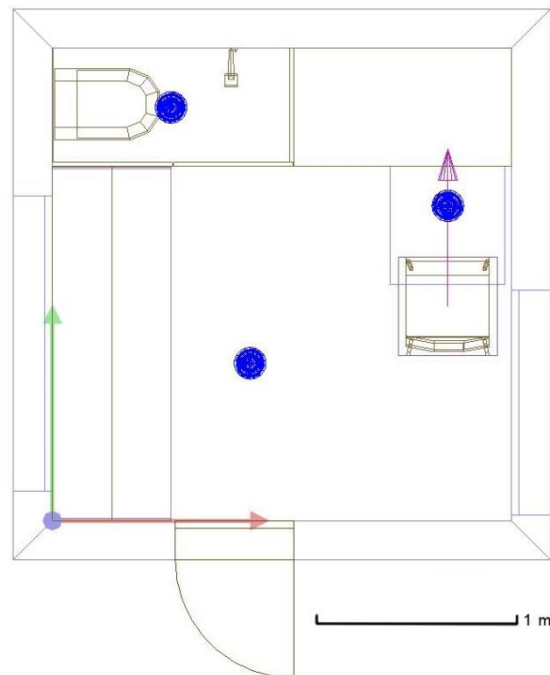


Fig. 7 - Luminaires (in blue) for XXS case study.

Concerning hobs, since they are placed in front of windows, the Illuminance values are always over the 500 lux, but also under the minimum value of U_0 recommended by UNI EN 12464 for kitchens (0.6).

Table 9 - Illuminance values due to artificial light in day configuration of XXS case study considering the optimised luminaire position.

Calculation grids	Illuminance [lux]	Uniformity Coefficient U_0
XXS – table	471	0.9
XXS - hub	160	0.3

This is due to the proximity of the hob to the window. The installation of curtains limits this effect, allowing a more diffusive distribution of daylight. The Illuminance values and the uniformity coefficient evaluated on floors due to daylight (day configuration) and to artificial light (night configuration) were respectively higher than the 100 lux and the 0.4 requested by the UNI EN 12464 for circulating areas and corridors. The positioning of the luminaires and the materials chosen for the furniture, walls, floors and ceilings allows us to maintain glare under the 20 UGR (Unified Glare Rating) in each case study for both *day* and *night* configurations. In 8 a lighting render is reported.



Fig. 8 - Render of XXS case study. Artificial light in day configuration

4. Conclusions and Discussion

The research analysed the energy and lighting performances of two examples of net zero energy modular buildings realized using recycled shipping containers. The first one, named XXS, was

designed as a short-term single guestroom; the second one, named S, as temporary accommodation for emergencies. The furniture is designed to be easily moved through special guides in accordance to users' needs. Firstly, preliminary lighting simulations were performed to define the kind and the number of lamps required in each case study. LED lamps were chosen because they are characterized by low energy consumption (the ones used in the study only require 10 W), an adequate luminous flux (1100 lumen) and a high colour temperature (4200 K). The preliminary evaluations established that 5 and 3 luminaires are needed respectively for S and XXS case study. Then these data were used for energy evaluations to set the values of thermal loads. The first step of energy simulations allowed us to define the building envelope (stratigraphy and windows) and the orientation: polyurethane foam, vacuum insulation panels and double glazed windows (6-13-6, filled with Argon) were chosen to optimise the energy performance. The energy simulations also demonstrate that the blind walls should face south.

The energy consumption estimated by EnergyPlus is 59.4 kWh/m² for S solution and 70.8 kWh/m² for XXS configuration. These results demonstrate that the containers are easy and cheap accommodation that provide optimized performances in terms of energy efficiency.

These data allowed us to perform lighting performance due to natural and artificial light on calculation grids placed over tables, hobs and floor. Two configurations of furniture were tested. The visual parameters tested are Illuminance, uniformity coefficient and glare. Several lighting simulations were carried out to define the most performing lamp positions. The lighting systems, the position of the windows and the optical characteristics of furniture, walls, ceilings and floor, ensure an adequate visual comfort.

The production of electricity thanks to PV panels is adequate to consider the building a net zero energy one (at central Italy latitudes).

Therefore, the theoretical, innovative building studied in the paper is not only an energy-saver but also a cheap and comfortable solution to be used not only for emergency housing but it is

possible to use them as temporary accommodation that can be placed in different areas and can be moved easily to different places.

References

- Asdrubali F., Baldinelli G. and Bianchi F. 2013. "Influence of cavities geometric and emissivity properties on the overall thermal performance of Aluminium frames for windows." *Energy and Buildings* 60: 298-309. doi: 10.1016/j.enbuild.2013.01.028.
- Asdrubali F. and Baldinelli G.. 2009. "Theoretical modelling and experimental evaluation of the optical properties of glazing systems with selective films." *Building Simulation* 2 (2): 75-84. doi: 10.1007/S12273-009-9112-5.
- Asdrubali F., Schiavoni S. and Horoshenkov K.. 2012. "A review of sustainable materials for acoustic applications." *Building Acoustics* 19 (4): 283-312. doi: 10.1260/1351-010X.19.4.283.
- Baldinelli G., Asdrubali F., Baldassarri C., Bianchi F., D'Alessandro F., Schiavoni S. and Basilicata C.. 2012. "Energy and environmental performance optimization of a wooden window: A holistic approach." *Energy and Buildings* 79: 114-131. doi: 10.1016/j.enbuild.2014.05.010.
- Container City website. 2014. Accessed November 28, <http://www.containercity.com/>
- Designboom. 2014. Accessed November 28 <http://www.designboom.com/architecture/top-10-shipping-container-structures-of-2013-12-2-2013/>.
- DesignBuilder website. 2014. Accessed November 28, <http://www.designbuilderusa.com/>.
- DIALux website. 2014. Accessed November 27 <http://www.dial.de/DIAL/en/dialux/archive/2012/april.html>.
- Directive 2010/31/EU of the European Parliament and of the council of 19 May 2010 on the energy performance of buildings.
- Dumas A., Trancossi M., Madonia M. and Coppola M.. 2014. "Zero Emission Temporary Habitation: A Passive Container House Acclimatized by Geothermal Water". *Journal of Solar Energy Engineering* 136 (4). doi: 10.1115/1.4027884
- EnergyPlus website. 2014. Accessed November 27 <http://apps1.eere.energy.gov/buildings/energyplus/>.
- Eurostat website. 2014. Accessed November 28 http://epp.eurostat.ec.europa.eu/statistics_explained/index.php/Freight_transport_statistics#Maritime_freight.
- Kolokotsa D., Rovas D., Kosmatopoulos E. and Kalaitzakis K.. 2011. "A roadmap towards intelligent net zero- and positive-energy buildings." *Solar Energy* 85: 3067-3084. doi:10.1016/j.solener.2010.09.001
- Sartori I., Napolitano A. and Voss K.. 2012. "Net zero energy buildings: A consistent definition framework", *Energy and Buildings* 48: 220-232. doi: 10.1016/j.enbuild.2012.01.032.
- UNI EN 12464-1:2011, Light and lighting - Lighting of work places - Part 1: Indoor work places.

Study of the energy performance of a retrofitting office

Paolo Valdiserri – CIRI Edilizia Costruzioni, Università di Bologna – paolo.valdiserri@unibo.it

Abstract

Building retrofitting is the most feasible and cost-effective method to improve building energy efficiency. To this aim, the building envelope should be equipped with new windows having low thermal transmission coefficients and/or with insulation material in the external partitions. This approach leads to considerable energy saving, but at the same time if the users do not properly ventilate the occupied spaces, it results in a worsening of indoor air quality.

The paper presents a comparative analysis of two different strategies to enhance the energy performance of an existing building. The first is to reduce the heat transfer by transmission (i.e. use of low-emissivity glass) and the second to decrease the heat transfer by ventilation (i.e. installation of a heat recovery). The study has been applied to an office block, located in the city of Bologna, Italy. Potential energy savings were calculated by dynamic simulation using Trnsys software. To this purpose, a reference office was selected and then the following cases were studied. The first one took into account the replacement of all the windows, the second one consisted in installing a total energy ventilation recovery system and the last one contemplated both the solutions. Finally, an evaluation of the simple payback time and the net present value was performed.

1. Introduction

Buildings consume around 40% of Europe's energy needs and account for 36% of EU CO₂ emissions. Member States of the European Union are required to implement energy efficiency measures for buildings under the Energy Performance of Building Directive. In order to reduce this consumption and pursue the goal imposed by the European Union, Italy issued several Legislative Decrees in particular no.192/2005, no.311/2006 and no.28/2011. The need to reduce energy consumption in buildings implies the use of

considerable thermal insulation, but at the same time, in the absence of a suitable ventilation system, it could result in a worsening of indoor air quality. A healthy life imposes a good indoor air quality especially where people spend a considerable amount of time, so adequate air exchanges should be guaranteed to reduce indoor pollution. Due to the increase of insulation and the decrease of the thermal transmission coefficients, ventilation constitutes a growing part of the heating demand; between 20–50% for new and retrofitted buildings, depending on the building's insulation, compactness, air change rate, indoor heat sources, indoor set points and outdoor climate. Heat recovery (HRV) from exhaust air in buildings is considered an important strategy to reduce the heat transfer by ventilation and generate consequent energy savings. The principle is to recover heat from the exhaust air and to transfer it to the supply air through a heat exchanger. Primary energy savings of HRV can be highly significant, depending on the type of heat supply system, the airtightness of buildings, and the use of electricity to operate the HRV system.

In Italy, like several other European countries, the existing dwellings constructed before the application of energy saving regulations, represent the majority of the edifices. Therefore, building renovation becomes a key strategy to reduce energy consumption and costs.

In the present work, simulations of an existing office building (where some energy saving methods were applied) were performed.

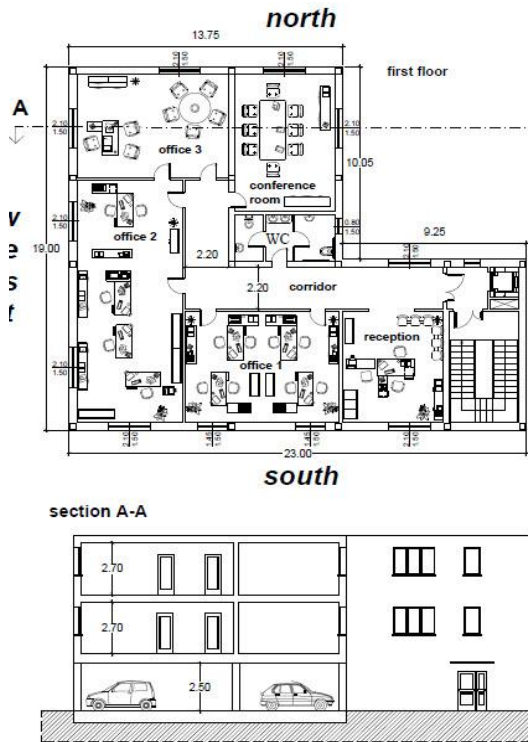


Figure 1 – Plant and section of the office block

The simulations were conducted using the Trnsys commercial code at the time step of 15 minutes. Trnsys is an extensible simulation environment for the transient simulation of energy systems including multizone buildings. It is used to validate new energy concepts, design and simulation of buildings and their equipment, including control strategies, occupant behaviour, and alternative energy systems (wind, solar, photovoltaic, hydrogen systems, etc.).

2. Description of the building under investigation

The numerical model has been applied to an office building, located in Bologna (Italy). The construction, shown in Figure 1, is a three-storey building having heated offices on the first and second floor and parking lots on the ground floor (not heated). The floor surface of the two offices is 534 m²; each floor is composed by one reception, three offices and a conference room. Table 1 illustrates the surface of each room and the acronyms used in the calculations.

Table 1 – surface of each room of the office and list of acronyms adopted in the simulations.

Room	Surface, [m ²]	Acronym
Reception	27.84	R1
Office 1	45.24	O1
Office 2	66.25	O2
Office 3	40.50	O3
Conference room	33.50	CR

Table 2 highlights the thermal characteristics of the building envelope (between the heated offices and the unheated spaces).

Table 2 - Values of thermal transmittance referred to the envelope elements.

Envelope element	Thermal transmittance U [W m ⁻² K ⁻¹]
Outside walls	0.51
First floor / Roof	0.44 / 0.46
Internal ceiling	1.57
Windows	2.85

The heating system is supposed to operate 14 hours a day from 5 a.m. to 7 p.m. from Monday to Friday. In this period, it is set to maintain the internal temperature of 20°C. The ventilation system is switched on from 7 a.m. to 7 p.m. every working day. In each floor, the fresh air enters the reception, the conference room and the three offices at the flow rate illustrated in Table 3 and extracted from the corridor. Whilst the ventilation is working, a humidification system operates to provide the relative humidity of 50% in the offices. During the night and at the weekend, the heating system is able to provide the temperature of 16°C without any humidity control and with the ventilation system switched off.

Table 3 also includes the occupancy and the personal computers (PCs) connected in each office

during working hours (7 a.m. to 7 p.m. – Monday to Friday).

Table 3 – Ventilation flow rate, number of people and computers during working hours (7 a.m. to 7 p.m. – Monday to Friday).

Room	Flow rate [m ³ h ⁻¹]	People and PCs
Reception	150	3 - 1
Office 1	244	4 - 4
Office 2	358	4 - 4
Office 3	219	1 - 1
Conference room	192	2 - 0

In the present study, the performance of the reference case (Case 0) and of other three cases of retrofitting (Case 1, 2 and 3) are simulated and calculated.

Trnsys simulations were conducted with a time step of 15 minutes. The weather data (such as external temperature, solar radiation etc.) are derived from the Meteororm database. The solar gains are calculated by the software Trnsys from the input of the Meteororm file.

All the cases under investigation refer to the period when the heating system is switched on (winter period) that is for Bologna from October 15 to April 15.

3. Description of the simulated cases

3.1 Case 0

This is the reference case and represents the “pre-retrofitting” condition, characterized by the features illustrated in the previous paragraph. All the windows have a thermal transmittance of 2.85 Wm²K⁻¹. The ventilation operates at the flow rate illustrated in table 3 with total external fresh air. The infiltration is set at the rate of 0.4 vol h⁻¹.

3.2 Case 1

Case 1 refers to the replacement of all the windows with new frames and low low-emissivity glass

having a thermal transmittance of 1.6 Wm²K⁻¹. The ventilation works at the same conditions as Case 0, but the infiltration is reduced to the rate of 0.2 vol h⁻¹.

3.3 Case 2

This is characterized by the introduction of a heat recovery ventilation system that can save energy from the ejected air, as depicted in Figure 2. The windows remain the same as Case 0.

The model employs a total energy recovery with an enthalpy wheel silica gel loaded, able to exchange both heat and humidity.

The sensible and latent effectiveness of the heat recovery system are defined as follows:

$$\varepsilon_S = \frac{T_S - T_O}{T_R - T_O} \quad \varepsilon_L = \frac{X_S - X_O}{X_R - X_O}$$

where:

T_S and X_S are respectively the temperature and the humidity ratio of the supply air.

T_O and X_O represent the temperature and the humidity ratio of the external air (outdoor air).

T_R and X_R are respectively the temperature and the humidity ratio of the extracted air (return air).

The heat recovery efficiency values adopted in the simulations derived from the Jeong and Mumma correlation. The authors developed effectiveness correlations as a function of inlet air temperature, relative humidity, and face velocity. In the simulation, the heat recovery is designed to work with a time variable effectiveness and a face velocity of 3 m s⁻¹. The ventilation system extracts air from the two corridors, with the flow rate of 1163 m³ h⁻¹ for each floor. The fresh air enters the two receptions, the two conference rooms and the six offices at the flow rate illustrated in Table 3. The air leaves the heat recovery at the temperature T_S and at the humidity ratio X_S which are a time dependent values.

The electric power needed for the heat recovery at the design condition is of 500 W.

Finally, it is important to highlight that 0.4 air changes per hour for infiltration are considered.

3.4 Case 3

Case 3 contemplates both the replacement of the windows (described in Case1) and the introduction of the total energy recovery (described in Case 2). This case considers a rate of 0.2 vol h⁻¹ for infiltration.

4. Simulation results

4.1 Case 0

The energy need for heating and humidification in the winter period is shown in Table 4:

Table 4 – Case 0: Energy need for heating and humidification

Energy need [kWh] for		
Month	Heating	Humidification
October	1395	78
November	6022	716
December	9668	1482
January	11330	2002
February	8003	1419
March	4419	997
April	669	42
TOTAL	41505	6736

The amount of energy need requested for ventilation and infiltration is equal to 14674 kWh and 9718 kWh, respectively. Given an energy efficiency of 85% for the heating and humidification system, the primary energy for heating and humidification is 48830 kWh and 7925 kWh, respectively.

4.2 Case 1

The energy need for heating and humidification in the winter period can be seen in Table 5.

Since the new windows are placed, the infiltration is reduced and the energy need for infiltration becomes 4933 kWh. Considering energy efficiency

of 85% for the heating and humidification system, the primary energy for heating and humidification is 40280 kWh and 6930 kWh respectively.

Table 5 – Case 1: Energy need for heating and humidification

Energy need [kWh] for		
Month	Heating	Humidification
October	1112	62
November	4966	619
December	7986	1301
January	9423	1767
February	6599	1245
March	3613	862
April	539	34
TOTAL	34238	5891

4.3 Case 2

Table 6 shows the energy need for heating and humidification in the winter period:

Table 6 – Case 2: Energy need for heating and humidification

Energy need [kWh] for		
Month	Heating	Humidification
October	813	17
November	4147	114
December	7007	265
January	8135	389
February	5734	258
March	2920	162
April	440	8
TOTAL	29196	1213

The energy need for ventilation is equal to 2185 kWh. Considering energy efficiency of 85% for the

heating and humidification system, the primary energy for heating and humidification is 34348 kWh and 1428 kWh respectively. In this case, the electric energy need for heat recovery accounts for an additional 786 kWh. Considering a conversion coefficient of 0.46, the primary energy for the ventilation recovery system is 1709 kWh.

4.4 Case 3

The energy need for heating and humidification in the winter period for case 3 is highlighted in Table 7:

Table 7 – Case 3: Energy need for heating and humidification

Month	Energy need [kWh] for	
	Heating	Humidification
October	542	10
November	3090	60
December	5324	137
January	6229	190
February	4330	133
March	2120	89
April	320	6
TOTAL	21954	626

Considering energy efficiency of 85% for the heating and humidification system, the primary energy for heating and humidification is 25828 kWh and 736 kWh respectively. The primary energy for the recovery system is 1709 kWh.

4.5 Comparison between the different solutions

Table 8 shows the primary energy demands for the different cases analysed. The primary energy include the energy for heating, humidification and the operation of the total recovery.

Table 8 – Primary energy for heating, humidification and recovery electricity for the four different cases.

Month	Primary energy [kWh]			
	Case 0	Case 1	Case 2	Case 3
October	1733	1382	1146	819
November	7926	6571	5300	3993
December	13118	10926	8829	6699
January	15684	13165	10329	7852
February	11084	9227	7310	5510
March	6372	5265	3914	2885
April	837	675	657	514
TOTAL	56754	47210	37485	28273

A mere comparison of the primary energy request among the simulated cases shows that case 3 (where the combination of window replacement and the total energy recovery introduction) is the most efficient. The primary energy saved in the different scenarios is:

- Scenario 1 (Case 1 versus Case 0): 9544 kWh;
- Scenario 2 (Case 2 versus Case 0): 19270 kWh;
- Scenario 3 (Case 3 versus Case 0): 28481 kWh;
- Scenario 4 (Case 3 versus Case 1): 18937 kWh.

The latter scenario was included to evaluate the advantages of the heat recovery installation following the windows replacement.

5. Economic issues

The two retrofitting solutions presented in this study aim at decreasing energy demand and improving energy performance of the office block. Nevertheless, the application of energy saving measures usually needs to be evaluated in relation to economic assessments.

Simple Payback Time (SPBT) and Net Present Value (NPV) are used as financial parameters for evaluating the economic feasibility of the different approach.

$$SPBT = \frac{I_0}{S} \quad NPV = -I_0 + \sum_{n=1}^{LS} \frac{S_n - C_n}{(1+r)^n}$$

where:

- I_0 is the initial investment cost of the project,
- S is the energy saving evaluated at year 0,
- S_n is the energy saving for year n ,
- C_n is the maintenance cost for year n ,
- n is the time period,
- LS is the lifespan,
- r is the cost of capital.

The economic analysis was carried out for the retrofitting cases in the four different scenarios and was based on the technical-economic situation in Italy in 2014.

The following data have been used for the evaluation:

- cost of the energy: natural gas: 0.10 €/kWh, electricity: 0.18 €/kWh,
- cost for replacement windows: 21 000 €,
- cost for installing the heat recovery system: 14 000 €.

The yearly cost for heating, humidification and electricity for heat recovery are reported below:

Case 0: €5,675

Case 1: €4,721

Case 2: €3,885

Case 3: €2,964

In Table 9 the initial investment, the energy saving obtained during the first year since the retrofitting, and the SPT are reported.

Table 9 – Initial investment, energy saving during the first year and Simple Payback Time for the four different scenarios.

	Sc. 1	Sc. 2	Sc. 3	Sc. 4
Investment (€)	21000	14000	35000	14000
Energy saving (€)	954	1790	2711	1757
SPBT (years)	22.0	7.8	12.9	8.0

NPV is calculated for each scenario considering different increments of the cost of energy (2%, 4% or 6%). In the present evaluation, we considered a lifespan of 30 years for windows, and of 15 years

for the heat recovery system.

According to the Italian regulation on energy saving, it is possible to claim a tax refund of 65% of the cost of the investment over 10 years. NPV was reported either without tax refund claim (i.e. NPV(0)) or considering a 65% tax refund over 10 years (i.e. NPV(65)).

NPV calculated for the different scenarios are reported in Tables 10-13.

Table 10 – Net Present Value calculated for Scenario 1 (Case 1 vs Case 0) at different increment of the cost of energy (i) considering or not the tax refund of 65% - lifespan 30 years.

Scenario 1	i = 2%	i = 4%	i =6%
NPV (0)	481	7620	17974
NPV (65)	11553	18691	29045

In the evaluation of NPV, the maintenance cost of the heat recovery system (1% per year, revaluated at 2% of inflation) was taken into account.

In the case of Scenario 2 (Table 11), the value of NPV was reported at two time points: i) 15 years (the lifespan of the recovery system), and ii) 30 years. In the case of the latter time points it is necessary to add the cost of the heat recovery replacement and extraordinary maintenance works on the entire system, for a total amount of €9,421 (to be paid 15 years after the retrofitting).

Table 11 – Net Present Value calculated for Scenario 2 (Case 2 vs Case 0) at different increment of the cost of energy (i) considering or not the tax refund of 65%, after 15 years and after 30 years.

Scenario 2	i = 2%	i = 4%	i =6%
NPV (0) – 15ys	7299	11081	15607
NPV (65) – 15ys	14680	18462	22988
NPV (0) – 30 ys	17985	31378	50806
NPV (65) – 30 ys	25366	38759	58187

In the case of Scenario 3 and 4 (Table 12-13) the evaluation of NPV was done only for time point 30 years, considering the replacement of the heat recovery and other extraordinary maintenance works after 15 years.

Table 12 – Net Present Value calculated for Scenario 3 (Case 3 vs Case 0) at different increment of the cost of energy (i) considering or not the tax refund of 65% - lifespan 30 years.

Scenario 3	i = 2%	i = 4%	i =6%
NPV (0)	17724	38008	67433
NPV (65)	36176	56460	85885

Table 13 – Net Present Value calculated for Scenario 4 (Case 4 vs Case 1) at different increment of the cost of energy (i) considering or not the tax refund of 65% - lifespan 30 years.

Scenario 4	i = 2%	i = 4%	i =6%
NPV (0)	17242	30388	49458
NPV (65)	24623	37769	56839

6. Discussion

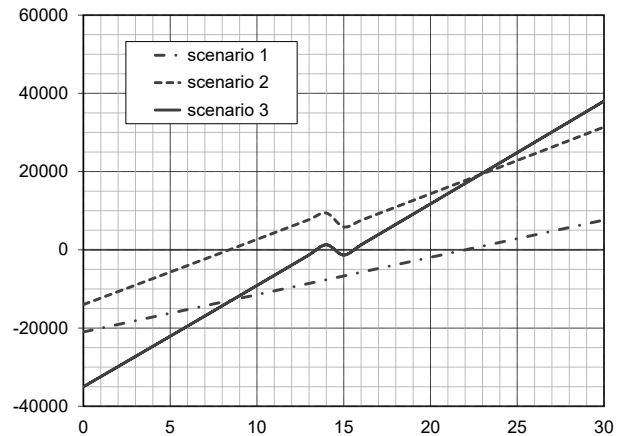
The conducted analysis highlighted that replacing windows (Scenario 1) does not produce a significant energy saving. Moreover, the SPBT is 22 years, a very long period of time compared to a 30-year lifespan. Conversely, the installation of a heat recovery system seems a valid alternative for saving energy, with an SPBT of 7.8 and 8 years, for Scenario 2 and Scenario 4 respectively. These observations are supported by the values of NPV shown in tables 10-13.

Fig. 3 and Fig. 4 represent the variation of Net Present Value during the 30 years for the different scenarios analysed with or without the tax refund. Here, NPV was calculated using an increment of the cost of energy of 4% per year. The curve of NPV for Scenario 4 was similar to the one of Scenario 2, and it not shown.

Figure 3 shows that the retrofitting solution with the highest NPV is the one which includes both windows replacement and the setting of a heat recovery system (Scenario 3). However, this solution is the one which requires a major investment. After 30 years, the difference of NPV between Scenario 3 and Scenario 2 is less than €7,000. For this reason it appears that the installation of the heat recovery system alone

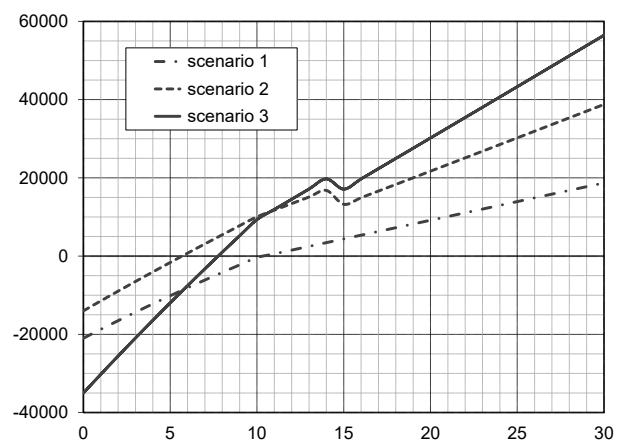
(Scenario 2) is better than the combination of the two investments (Scenario 3).

Figure 3 – Cash flows considering an increment of 4% in the cost of energy, without tax refund for Scenario 1, 2 and 3



The deflection of the curves of Scenario 2 and 3 at the end of year 14 is due the cost of the replacement of the heat recovery and extraordinary maintenance at year 15.

Figure 4 – Cash flows considering an increment of 4% in the cost of energy, and 65% of tax refund in 10 years for Scenario 1, 2 and 3



In Figure 4, the change of the slope at year ten is due to the end of the period of the tax refund. As shown previously without tax refund (Figure 3), also Figure 4 illustrates that the highest value of NPV is obtained with Scenario 3. In this case, at the end of the 10 years of tax refund the NPV values are roughly the same for Scenario 2 and Scenario 3. After 30 years the NPV difference between the two scenarios is about €17,700. For these two reasons, in the case of the tax refund, Scenario 3 is to be preferred.

7. Conclusion

In the present work, a dynamic simulation of an existing office building, located in Bologna, Italy was performed, where different energy saving variations were applied. Two different strategies to enhance the energy performance were used. The first consisted in reducing the heat transfer by transmission, the other implied the decrease of the heat transfer by ventilation.

Potential energy savings were calculated by transient simulation using Trnsys software and three hypothetic retrofitting cases were exploited. The first took into account the replacement of all the windows, the second consisted in installing a total energy ventilation recovery system and the last one contemplated both the solutions. Finally, an evaluation of the simple payback time and the net present value was performed.

From the conducted analysis, only changing the windows (Scenario 1) does not produce an interesting value of NPV, unless one could benefit from a tax refund.

Notably, the installation of a total energy recovery system resulted in sensible reduction of energy consumption and gave good values of NPV for all the three different analysed variation of the cost of energy. This is particularly relevant since the case studied was an office with high ventilation flow rate to guarantee a good air quality.

Clearly, when the cost of energy arises, individuals are driven to find energy-saving measures. Nevertheless, given the actual cost of energy, energy-saving measures in building renovation and subsequent maintenance, the key strategy to make the retrofitting on existing dwellings economically appealing is to introduce or maintain tax refunding.

8. Acknowledgement

The Author wish to thank the Italian Ministry of Education, University and Research for funding this study.

References

- Directive, 2002/91/EC of the European Parliament and of the Council of 16 December 2002 on the energy performance of buildings.
- Directive 2010/31/EU of the European Parliament and of the Council of 19 May 2010 on the energy performance of buildings.
- Dodoo A., L. Gustavssona L., Sathrea R., Primary energy implications of ventilation heat recovery in residential buildings, *Energy and Buildings*, vol. 43, pp. 1566–1572, 2011.
- European Commission, 2020 Vision: Saving energy, 2011, web accessed at <https://www.energy.eu/publications/saving-energy-2011.pdf>.
- Jeong J., Mumma S.A., Practical thermal performance correlations for molecular sieve and silica gel loaded enthalpy wheels, *Applied Thermal Engineering*, vol. 25, pp. 719-740, 2005.
- Legislative Decree n 192, August 19, 2005.
- Legislative Decree n 311, December 29, 2006.
- Legislative Decree n 28, March 3, 2011.
- Simonson C., Energy consumption and ventilation performance of naturally ventilated ecological house in a cold climate, *Energy and Buildings*, vol. 37, pp. 23–35, 2005.
- Solar Energy Laboratory, Manual of TRNSYS 17 – a TRaNsient SYstem Simulation program, Solar Energy Laboratory, University of Wisconsin-Madison, 2012. Reference List, Entry number 2. Reference style according to Chigaco Manual of Style. Paragraph style: Reference List Entry.
- UNI EN 308, Heat exchangers - Test procedures for establishing performance of air to air and flue gases heat recovery devices, 1998.

Coupling dynamic energy and daylighting simulations for complex fenestration systems

Giuseppe De Michele – Eurac Research – giuseppe.demichela@eurac.edu

Ulrich Filippi Oberegger – Eurac Research – ulrich.filippi@eurac.edu

Luca Baglivo – Eurac Research – luca.baglivo@eurac.edu

Abstract

A new tool for energy and daylighting analysis of complex fenestration systems (CFS) is presented. The tool couples the daylighting simulation engine Radiance with the dynamic building simulation engine TRNSYS and performs integrated simulations using the bidirectional scattering distribution function (BSDF) that characterizes the CFS. The use of the tool allows us to implement flexible shading controls based on thermal and daylighting comfort parameters. In order to demonstrate the tool functionality two different control strategies for a shading device, composed of movable venetian blinds, are compared and analyzed.

1. Introduction

The use of natural resources through innovative technologies is an excellent way to reach high energy savings and indoor comfort in a building. Daylight in particular influences the thermal and visual comfort, the well-being and health of the building's users, and the energy demand for artificial lighting, heating and cooling. In this work, we focus on the CFS technology (Complex Fenestration Systems). CFS are those systems that contain non-specular layers and whose optical properties present complex dependence on angle and wavelength. That dependence is described by the Bidirectional Scattering Distribution Function (BSDF) (F. E. Nicodemus, 1970; F. Nicodemus et al., 1977). The CFS include fritted and translucent glass and shading devices, such as venetian blinds, woven shades and perforated screens.

These systems provide a good management of

solar gains both in terms of energy saving and indoor comfort and are being increasingly used in sustainable design. Therefore, it is important to have a tool that is able to simulate these technologies reliably. In order to obtain accurate results about the thermal and optical response of the fenestration system, the tool has to include the BSDF data in the calculation method. Klems (J. H. Klems, 1994a; J H Klems, 1994b) developed a calculation method to evaluate the BSDF data, which can be generated using window modelling software (e.g. Window7 from LBNL) or simulation programs (e.g. TracePro or Radiance's "genBSDF"). The BSDF can be measured with a goniophotometer (Andersen et al., 2006).

Several tools on the market able to perform integrated energy and daylighting simulations already exist (e.g., DIVA, ESP-r, DesignBuilder, IES-VE), but all have certain limits: either they cannot be combined with TRNSYS or they do not offer the flexibility to decide at each time step during the simulation how to control the CFS.

OpenStudio integrates EnergyPlus for energy simulations and Radiance for daylighting simulations. The thermal model used to describe the CFS is based on BSDF data according to ISO 15099. On the other hand, the three-phase method (Saxena et al., 2010; Ward et al., 2011) algorithm provides climate-based daylighting simulation using the BSDF file. One limit is in the usage of BSDF data that are only contained in the *OpenStudio's* database. In addition, dynamic shading control is not supported, and lighting schedules for each window and shading state combination are pre-calculated and then passed to EnergyPlus for the thermal simulations.

"Mkschedule" (Molina et al., 2014) is a program

that provides integrated simulations for CFS using the Radiance's three-phase method (3PM) and EnergyPlus. The control algorithm is kept out of the main program and it can be defined through a "Lua" script. The control is flexible and can be based on weather file information or on the output of daylighting simulations. However, the tool does not allow us to apply a control based on thermal parameters.

Fener is a recent tool, developed at the Fraunhofer institute, that performs energy and daylighting simulations for advanced analysis of CFS in a single thermal zone (Bueno et al., 2014). The model uses the 3PM and the BSDF data to evaluate indoor illuminance measured by virtual sensors arranged on a sensors grid and solar irradiance absorbed by indoor surfaces. The solar gains are used to evaluate the heat balance of the building. *Fener* cannot perform multi-zone energy simulations.

"Artlight" is a tool that enables daylighting simulation for CFS in Trnsys. It was developed in the project "Light from Façade" promoted by "Haus der Zukunft" (Link01). The daylighting simulation was performed with the 3PM. The thermal simulations could be performed with Trnsys by choosing among three approaches (called "g-value", "fc model", and "abs") to evaluate the thermal behavior of the daylighting system (Geisler-Moroder et al., 2012). The control strategy could be done on thermal and daylighting parameters. The simulation tool has not been made available.

The present study, developed within the European EU/FP7 project CommONEnergy (Link02), presents a novel tool for the energy and daylighting simulation of CFS (De Michele, 2014). The tool is embedded in a TRNSYS "Type" (a functional block that can be used within the software environment) that calls Radiance's 3PM during the dynamic building simulation.

The tool allows us to share information among TRNSYS and Radiance at each time step. The control is done in TRNSYS in order to be able to choose at each time step the optimal configuration of the shading system. It also allows us to calculate the light dimming schedule within the TRNSYS environment. The control can be set on daylighting and thermal parameters, such as illuminance on

the work plane, total radiation on the façade, and internal air temperature, according to the designer's strategy.

To demonstrate the capabilities of the tool, we have compared two strategies for controlling venetian blinds with variable slat angle, with different objectives. The first control strategy aims to increase the energy saving (*Th-Control*), whereas the second one aims to improve the visual comfort (*DLT-Control*). In both cases, artificial lighting can be dimmed. The control strategies shown aim to demonstrate the capabilities and functionalities of the tool. Providing new optimal strategies is not an objective of this work

2. Method

2.1 Coupling thermal with daylighting simulation

Considering the state-of-the-art tools and their limitations, we have aimed at developing a simulation tool that can provide:

- Integrated dynamic energy and daylighting simulations for CFS using the BSDF data and the 3PM
- Dynamic shading optimization in terms of solar thermal gains and visual comfort at each time step
- Flexible user-defined control strategies

2.2 Trnsys

TRNSYS is an environment used to simulate the dynamic performance of building energy models. A main feature is its modular architecture. The several functional blocks provided by the software are called "Types", which can be compiled into DLLs (Dynamically Linked Libraries) for easy sharing and high computational speed. The Types can be linked together to model the interactions between the building components and systems. The linking of the Types is relatively user-friendly thanks to the graphical user interface. The Type dedicated to the thermal building simulations is the "Type56". Trnsys can embed also custom components developed with standard programming languages (C++ and Fortran).

At the state of art, TRNSYS cannot evaluate CFS in depth because it is not yet able to manage the BSDF data. Nevertheless, a new Type is under development that will take into account the BSDF according to ISO 15099 for detailed short wave radiation calculations (Hauer et al., 2014).

2.3 Radiance and the three-phase method

Radiance is a validated software already able to manage BSDF data in order to perform daylighting simulations of CFS. In particular, using the 3PM it is possible to perform dynamic daylighting simulations with a climate-based approach. The algorithm is based on the matrix equation $i=VTDs$, where i is the computed illuminance (or alternatively, irradiance), V is a view matrix that relates the sensors to the CFS, T is the transmission matrix that describes how radiation passes through the CFS and is defined through the BSDF file, D is the daylighting matrix that relates the outer surface of the window to the sky dome, and s is the sky vector that describes the sky condition using the Perez model (Perez et al., 1993; Perez et al., 1990).

2.4 Description of the novel TRNSYS Type_DLT

Taking advantage of the development framework offered by TRNSYS, we have developed a new TRNSYS functional block dedicated to daylighting simulations. The novel Type called "Type_DLT" (DayLighTing), written in the C++ programming language, performs the 3PM for dynamic, climate-based daylighting simulations of CFS.

The Type_DLT receives the following input from the weather file:

- Latitude and longitude
- Month, day of the month, hour of the day
- Direct normal illuminance
- Diffuse horizontal illuminance

In this way, it can identify the building location (and thus calculate the sun path) and the information for the climate-based analysis.

The following parameters are set in the Type's control panel:

- Thermal zone for which the shading system is controlled

- Shading state, determining which BSDF is used
- Number of windows associated with the same shading state

These parameters are necessary to identify the thermal zone where CFS are controlled, which CFS assigned to that zone are controlled, and which are the initial conditions for the simulation. A BSDF data file has to be provided for each shading state. In order to control a series of thermal zones independently, the Type can be added as functional block to the simulation model multiple times, with different parameters, inputs, and outputs.

The outputs of the Type are:

- Maximum (or average, minimum, etc.) illuminance value over the sensor grid
- Current shading state

The control algorithm, defined through a series of equations which can involve inputs and outputs of other Types, the Type56, and the Type DLT are interlinked. Loops between Types can be formed. By default, TRNSYS performs iterations within each time step until all parameters, inputs and outputs of every Type have converged.

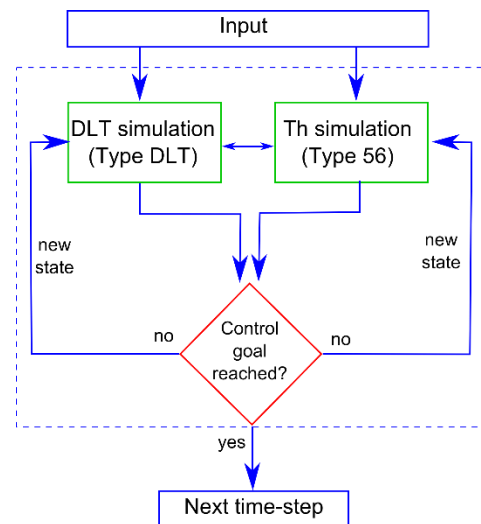


Fig. 8 – Flow chart of the iteration process between daylighting and thermal simulation within each time step

The control algorithm is not incorporated into the Type_DLT, but implemented through the "Equation" functional blocks that TRNSYS offers by default. This has the advantage that the Type_DLT does not need to be recompiled every

time the control strategy has changed and can thus be reused more easily by the user.

Fig. 8 shows the general workflow of the process. Both the daylighting (Type_DLT) and the thermal (Type56) simulations take their inputs. Then, the BSDF data and the Types' outputs are passed to a control "Equation" (a special functional block of TRNSYS in which an equation system can be defined) that modifies the shading states. By default, TRNSYS iterates until all Type outputs have reached convergence. Only then does it advance in time by performing the next time step.

2.5 Test model

A very simple but representative model has been chosen to show the capabilities of the Type_DLT. It consists of a single, box-shaped thermal zone, taken from a real project of a shopping mall located in Genoa, Italy (lat. 44.41°, long. 8.85°). The weather file used in the simulations has been taken from the Meteonorm database. The box dimensions are 50 m x 134 m x 7.4 m. It is located 4 m above ground level (Fig. 9).

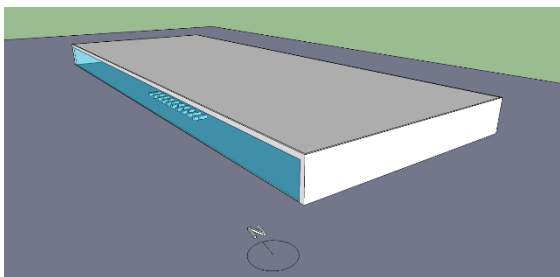


Fig. 9 – Geometry of the daylighting model

The surfaces facing north and south are modelled as adiabatic. The other surfaces are all connected with the outside. The west façade has a glazing area of 132 m x 6.3 m.

Two geometric models have been built, a simpler one for the thermal simulation and a more detailed one for the daylighting simulation. Both models have been drawn with Google SketchUp and exported to TRNSYS and Radiance respectively.

Eleven sensors have been located in a row in the working planes of the cash registers, 5 m from the façade, 0.8 m from the floor, and 1 m distant from each other (Fig. 10). The sensors disposition has

been chosen in order to guarantee the visual comfort on the workplace.

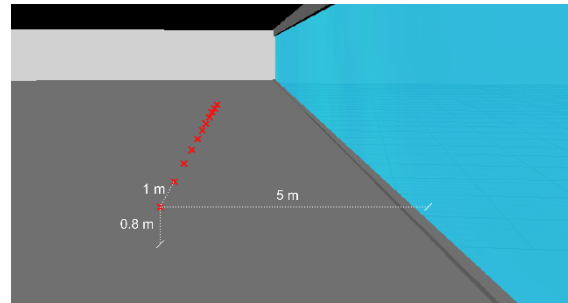


Fig. 10 – Grid of daylighting sensors

The surface reflectance factors used for the daylighting simulations can be seen in Table 10. Wall constructions are shown in Table 11.

Table 10 – Surface reflectance factors

Surface	Reflectance factor
Internal wall	0.5
Ceiling	0.8
Floor	0.2
External wall, ground	0.35

Table 11 – Wall constructions

Surface	Thickness [m]	U [W/m ² K]
Wall	0.3	0.367
Roof	0.59	0.207
Floor	0.36	0.353

The glazing consists of two panes (4-12-4) with low-e coating and argon filling. It has a U value of 1.36 W/m² K, a solar heat gain coefficient of 0.568 and a visible transmittance of 0.810.

The external shading system consists of venetian blinds which can be pulled up and down and whose slats can be tilted at angles ranging from zero (horizontal) to 60 degrees. The slats are 200 mm wide with a spacing of 180 mm and a rise of 20. The surface reflectance is 0.7.

2.5.1 Control strategies

We have tested and evaluated the Type_DLT's capabilities by comparing two different controls of the CFS (cf. Table 12). The first control aims at optimizing the energy saving (*Th-Control*), the

second at optimizing the visual comfort (*DLT-Control*).

Th-Control aims to increase the energy saving and thermal comfort by controlling the solar gains. In the cold season (15th of October – 15th of April) the trigger is the internal air temperature: if it is below 21°C, blinds are pulled up in order to maximize the solar gains. If the internal air temperature exceeds 23°C, blinds are pulled down. The latter condition has been added because people inside the shopping mall will probably be heavily dressed and in motion. During the warm season *Th-Control* closes the blinds whenever the incident solar radiation on the façade exceeds 55 W/m², in order to reduce the cooling load. The daylighting-based *DLT-Control* controls the daylight passing through the CFS by acting on the slat angle in such a way that the internal illuminance measured by the sensors (cf. Fig. 10) is always kept within the useful illuminance range as per LEED v.4 protocol (Link03).

Table 12 – Thresholds used to control the CFS

Season	Control	Threshold
Cold season	<i>Th-Control</i>	23°C (21°C)
Warm season	<i>Th-Control</i>	55 W/m ²
All year	<i>DLT-Control</i>	300 – 3000 lux

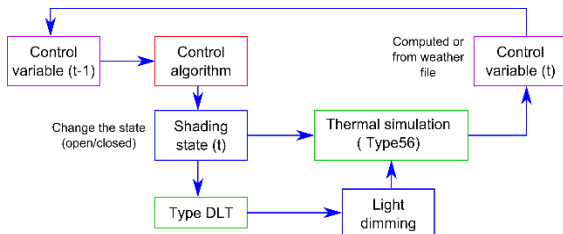


Fig. 11 – *Th-Control* algorithm

Th-Control gets the solar irradiance incident on the façade from the weather file (warm season) or the indoor air temperature from the Type56 (cold season). Then, it evaluates the shading state (blinds up or blinds down and closed, that is, with a slat angle of 60°) and passes it to Type_DLT and Type56 for the thermal and daylighting simulations (Fig. 11). The illuminance calculated by the Type_DLT is used to dim the artificial lighting. In the *DLT-Control* algorithm (Fig. 12), the control receives as input the illuminance from the Type_DLT and an initial shading state that

corresponds to the blinds pulled up. If the illuminance measured by the sensors is below 3000 lux, the initial shading state is kept. Otherwise, the blinds are pulled down with a horizontal slat angle. If the measured illuminance is still above 3000 lux, the slat angle is gradually changed from 0° to 60° in steps of 15° until the illuminance is below 3000 lux. In case daylighting provides less than 500 lux, artificial lighting is added to reach exactly this amount (as lights are dimmable). Otherwise, artificial lighting is switched off.

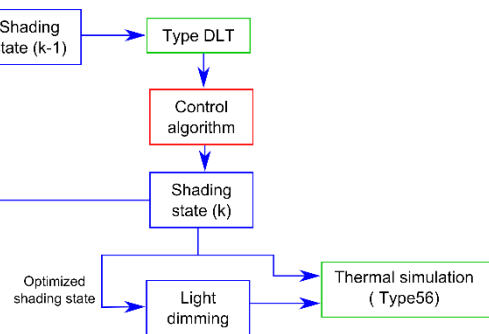


Fig. 12 – *DLT-Control* algorithm

Once the optimal shading state is found, the control passes the information to the Type56 for the thermal simulation.

Both the window and the shading device have been created with Window 6.3 from LBNL, as well as the BSDF data files for each shading state.

As this work is at an early stage, the thermal simulations have been conducted with a simplified approach using the Type56, not implementing BSDF-based calculations. The solar gains have been multiplied by a shading factor F_c calculated according to equation (1.1) from the Solar Heat Gain Coefficient (SHGC) computed in Window 6.3.

$$F_c = \frac{SHGC_{CLEARGLASS} - SHGC_{CFS}}{SHGC_{CLEARGLASS}} \quad (1.1)$$

2.5.2 Schedules and internal gains

The shopping mall is open from 8 am to 8 pm. Occupation during the day ranges from 50 to 1000 people. Setpoint and setback in the cold season are 17.5°C and 14°C, respectively. In the warm season, the setpoint is 24°C. Dehumidification takes place for relative humidities above 60% during opening

hours. The heating and cooling system has a maximum power of 120 kW and is turned on (off) one hour before (after) opening hours. The mass air change rates are 7.35 kg/m²h during opening hours and 3.00 otherwise, according to EN 10339. The internal gains are shown in Table 4. The lighting power is relative to 500 lux. For 85% of the floor surface, corresponding to the internal area of the shopping mall, artificial lighting provides 400 lux. In the remaining strip near the glazed façade (15% of the floor surface), artificial light is dimmed according to the amount of daylight in order to provide 500 lux on the working plane.

Table 13 – Internal gains

Typology	Gain	Unit
Persons	185	W/person
Artificial lighting	10.5	W/m ²
Fridges	-9.4	W/m ²

3. Results

First, we compare internal illuminances on the working plane and shading states (Fig. 15 and Fig. 16). As expected, the *DLT-Control* guarantees visual comfort all the year thanks to the broad range of shading states available. Glare and insufficient lighting are effectively avoided. The *Th-Control* optimizes the solar gains, in order to improve the energy saving and the thermal comfort, but without considering the glare problems during the cold season or the gains caused by the artificial lighting during the warm season in order to compensate for insufficient daylight.

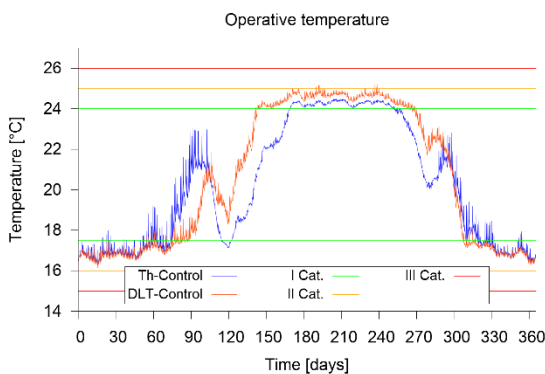


Fig. 13 – Hourly operative temperature. Both controls respect the design limits suggested by EN 15251. However, the *Th-Control* tends to stay closer to the first category, thus providing more comfort.

Observing the operative temperature (Fig. 13), thermal comfort is quite high for both controls. However, looking at the Percentage of Persons Dissatisfied (PPD) in Table 14, it can be seen that the *Th-Control* provides a more comfortable environment during opening hours except for category I, which is intended for sensitive environments, such as hospitals and nursing homes.

Table 14 – PPD values. Percentage of operative hours over the year in which the PPD complies with the categories reported in EN 15251.

Control	I cat.	II cat.	III cat.
	PPD < 6%	PPD < 10%	PPD < 15%
Th	44%	68%	90%
DLT	52%	57%	80%

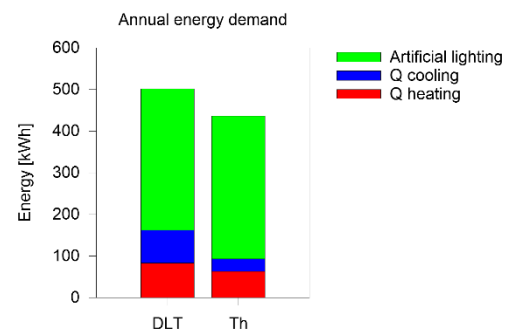
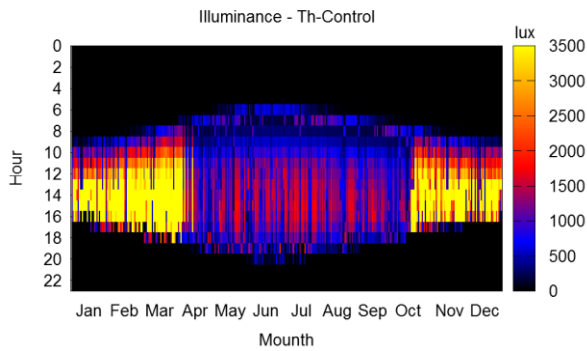


Fig. 14 – Annual energy required for heating, cooling and artificial lighting depending on the control. *Th-Control* requires substantially less energy for heating and cooling than *DLT-Control*.

The energy demand (Fig. 14) confirms our hypotheses regarding the control strategies. The *Th-Control* saves more energy in terms of heating and cooling. On the other hand, artificial lighting requires about 1% more energy, as blinds are pulled down during the warm season in order to reduce the cooling load. *Th-Control* provides energy savings for heating and cooling of about 70 MWh/year with respect to the *DLT-Control* that instead saves a small amount of electricity for artificial lighting equal to 2.25 MWh/year. The differences in terms of energy demand between *Th-Control* and *DLT-Control* are 24% for heating and 62% for cooling. Therefore, the major energy savings are obtained during the warm season. However, closing the blinds also if glare is not a problem significantly compromises the visual

comfort. On the other hand, keeping the blinds pulled up during the cold season causes serious



glare issues and reduces the energy demand by "only" 24%.

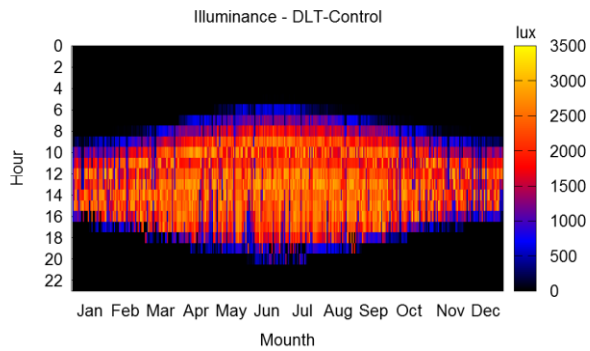


Fig. 15 – Maximum measured internal illuminance. Yellow areas indicate glare conditions. *DLT-Control* provides always a useful amount of daylight for the working activities. *Th-Control* tries to reduce the energy demand and to improve the thermal comfort by keeping the blinds pulled up during the cold season, thus enhancing the solar gains, and by keeping the blinds closed during the warm season in order to avoid an overheating of the zone. However, this strategy substantially deteriorates the visual comfort, especially during the cold season where glare is frequent.

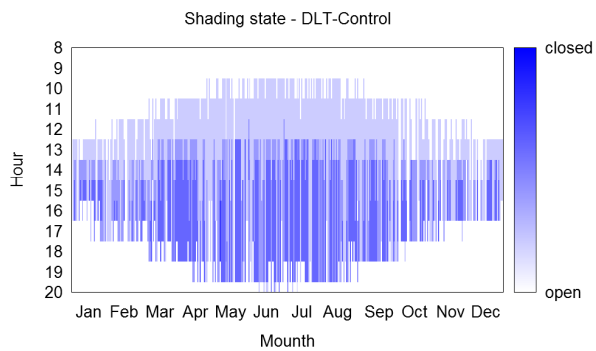
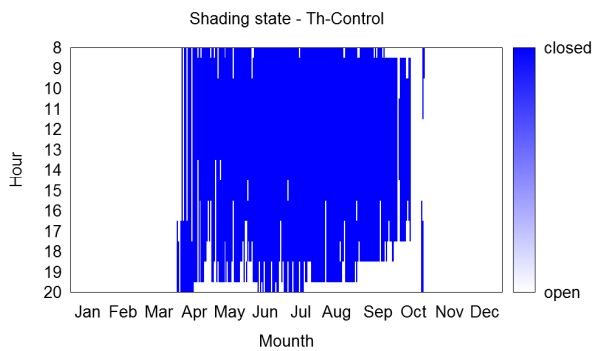


Fig. 16 – Hourly shading schedule. The several states available to the *DLT-Control* allow for a better control of the incident daylight, hence providing optimum illuminances in the range from 300 to 3000 lux.

4. Conclusion

We have presented a tool able to perform integrated energy and daylighting simulations of complex fenestration systems (CFS). The tool consists of a novel building block for TRNSYS called "Type_DLT". The Type_DLT uses the BSDF data characterizing the CFS to perform accurate daylighting calculations with Radiance's three-phase method. The method is involved from TRNSYS at each time step during the dynamic building simulation in order to compute illuminances on the working planes. The thermal simulation as well as the control of the CFS is performed in TRNSYS external to the Type_DLT, giving the user maximum flexibility regarding the control strategy, which can be based on both thermal and daylighting parameters.

We have demonstrated the capabilities of the tool

by implementing two different controls of a CFS. The thermal simulation is still simplified insofar as it excludes the BSDF. Instead, it is based on the shading factor. Nevertheless, the results are promising and proved to be consistent with the hypotheses made about the control algorithms.

5. Acknowledgments

The research leading to these results has received funding from Europe Community Seventh Framework Program (FP7/2007-2013) under grant agreement n_608678. The content of this document does not reflect the official opinion of the European Union. Responsibility for the information and views expressed in the document lies entirely with the authors.

References

- Andersen, Marilyne, and Jan de Boer. 2006. "Goniophotometry and Assessment of Bidirectional Photometric Properties of Complex Fenestration Systems." *Energy and Buildings* 38 (7): 836–48.
- Bueno, B, E Guidolin, J Wienold, and TE Kuhn. 2014. "A Radiance-Based Building Energy Model to Evaluate the Performance of Complex Fenestration Systems." https://www.ashrae.net/FileLibrary/docLib/Events/ASHRAE-IPBSA-USA/Presentations/14_Bueno.pdf.
- "CommONEnergy." 2014. Accessed November 29. <http://www.commonenergyproject.eu/>.
- De Michele, Giuseppe. 2014. "Coupling Energy and Daylighting Simulation for Complex Fenestration Systems." Trento University, Eurac Research.
- Geisler-Moroder, David, C Knoflach, W Pohl, M Hauer, D Neyer, and W Streicher. 2012. "Integrated Thermal and Light Simulations for Complex Daylight Systems Using TRNSYS and RADIANCE." *Radiance Workshop 2012*.
- Hauer, Martin, Marion Hiller, and Wolfgang Streicher. 2014. "Application of the New BSDF Window Model of Type 56 Preliminary Results Contents." *Trnsys Userday*.
- Klems, J H. 1994. "A New Method for Predicting the Solar Heat Gain of Complex Fenestration Systems - II. Detailed Description of the Matrix Layer Calculation." *ASHRAE Transactions* 100 (1). University of California: 1065–72. doi:citeulike-article-id:10521068.
- Klems, J. H. 1994. "A New Method for Predicting the Solar Heat Gain of Complex Fenestration Systems - I. Overview and Derivation of the Matrix Layer Calculation." *ASHRAE Transactions* 100 (1). ASHRAE: 1065–72.
- "LEED v.4 - Daylighting." 2014. <http://www.usgbc.org/credits/healthcare/v4-draft/eqc-0>.
- "LightFromFacade - Optimized Day- and Artificial Lighting by Facades." 2014. Accessed November 29. <http://www.hausderzukunft.at/results.html/id6014>.
- Molina, Germán, Sergio Vera, and Waldo Bustamante. 2014. "A Tool for Integrated Thermal and Lighting Analysis of Spaces with Controlled Complex Fenestration Systems and Artificial Lighting." *eSim*.
- Nicodemus, F E. 1970. "Reflectance Nomenclature and Directional Reflectance and Emissivity." *Applied Optics* 9 (6): 1474–75.
- Nicodemus, FE, JC Richmond, and JJ Hsia. 1977. "Geometrical Considerations and Nomenclature for Reflectance." *Science And Technology* 60 (October). National Bureau of Standards (US): 1–52. <http://graphics.stanford.edu/courses/cs448-05-winter/papers/nicodemus-brdf-nist.pdf>.
- Perez, R, Pierre Ineichen, R. Seals, J. Michalsky, and R. Stewart. 1990. "Modeling Daylight Availability and Irradiance Components from Direct and Global Irradiance." *Solar Energy* 44 (5): 271–89. <http://archive-ouverte.unige.ch/unige:17206>.
- Perez, R., R. Seals, and J. Michalsky. 1993. "All-Weather Model for Sky Luminance distribution—Preliminary Configuration and Validation." *Solar Energy* 50 (3): 235–45. doi:10.1016/0038-092X(93)90017-I.
- Saxena, Mudit, Greg Ward, Tymothy Perry, Lisa Hescong, and Randall Higa. 2010. "DYNAMIC RADIANCE - PREDICTING ANNUAL DAYLIGHTING WITH VARIABLE FENESTRATION OPTICS USING BSDF." *Fourth National Conference of IBPSA-USA*.
- Ward, G, R Mistrick, E S Lee, A McNeil, and Jacob C Jonsson. 2011. "Simulating the Daylight Performance of Complex Fenestration Systems Using Bidirectional Scattering Distribution Functions within Radiance." *Leukos* 7: 241–61.

Simulation experiences for the thermal performance improvement of naturally ventilated classroom in the tropics of Costa Rica

Emily Vargas Soto – University of Bío-Bío, Concepción, Chile – emily.vargas1301@alumnos.ubiobio.cl

Gerardo Saelzer Fuica – Department of Design and Theory in Architecture, University of Bío-Bío, Concepción, Chile – gsaelzer@ubiobio.cl

Abstract

In tropical developing countries, the considerations of energy efficiency and quality of school buildings are minimal, compromising the minimum internal comfort. This paper explores the effects on thermal comfort and energy generated by performing parametric variations on the typical configuration of naturally ventilated classrooms in tropical Costa Rica. Using dynamic simulations by the software Design Builder, weather data and surveys of comfort, classrooms with the same design pattern in three locations prone to overheating were analysed. Effects on energy demand and the operative temperature of the enclosure by varying bioclimatic parameters of passive cooling and solar control were reviewed.

The results indicate that certain configurations can optimize the performance of the typology of the cases studied, generating the possibility of applying these design parameters to new configurations of classrooms to be built in the area.

The impact of choosing appropriate design considerations and the use of simulation tools to verify building performance is demonstrated. In addition the combined potential of using passive cooling and solar control to achieve favourable thermal conditions for the user and to solve an energy demand improvement of school buildings was proved.

1. Introduction

In countries with tropical climates, where environmental conditions are hot and humid, a key challenge for the design and construction is proposed to balance the pulse asset utilization and air conditioning systems in order to have less impact on the economy, operating costs in the long

term, cultural conditions and resource efficiency. (Sosa Griffin and Siem 2004) The phenomenon of adaptive comfort, studied and defined by (de Dear and Brager 2001), and incorporated in ASHRAE 55 promotes the concept that people in naturally ventilated buildings (passive system) can feel comfortable in higher internal temperatures.

The buildings designed under the concept of natural ventilation have the potential to improve the work environments in relation to energy consumption and interior comfort compared with mechanically controlled systems. (Bordass et al. 2001; Givoni 2011; Rajapaksha and Hyde 2012)

The natural ventilation combined with other aspects related to architectural design and spatial configuration patterns can improve the internal airflow. (Prianto and Depecker 2003)

In addition, the user adaptation by exposure to a weather condition plays an important role in defining the spatial designs. An adequate knowledge of these aspects may potentiate the adjustments in the conditioning means, depending on the type of building, to reduce energy costs without limiting user comfort.

School buildings are the focus of this study. Authors like (Corgnati, Filippi, and Viazzo 2007; Liang, Lin, and Hwang 2012; Wargocki and Wyon 2007) have demonstrated the importance of the quality of the physical environment and environmental comfort (thermal comfort, ventilation, acoustics, lighting and air quality) is established for students. According to the above, the thermal comfort and ventilation are essential aspects to determine the quality of space, and the health of students that routinely remain in studio spaces for an extended period. (Hwang et al. 2009)

In the tropical region of Latin America, the development of educational infrastructure has gone through very similar processes of evolution and typology. The design of school buildings under the same pattern, spatial distribution and materials has been predominant and this has been repeated throughout the countries.

This use of the same typology has caused unsuitable internal conditions in the classrooms for every climatic zone. Moreover, many of these designs were imported. The use of foreign construction typologies that are not appropriate for the weather conditions, the cultural reality and the space requirements in the tropics compromise the thermal comfort. (Sosa Griffin and Siem 2004)

In Costa Rica, 43% of 4,071 existing schools have been designed using prefabricated industrial systems. For the next five years an increase of 3% of the infrastructure under a unique typology of construction with the same standards has already been planned. This led us to seek an improvement in the current typology to optimize its thermal and energy performance in different localities where new school buildings are going to be developed.

87% of schools are outside the metropolitan area. They are mostly divided among three central-coastal sectors with high rates of overheating in the dry season, with temperatures between 28°C and 36°C. It is possible to improve the thermal and energy behaviour of the current type of classroom if the influence of the shape, material and other micro-climatic variables in classroom performance is established.

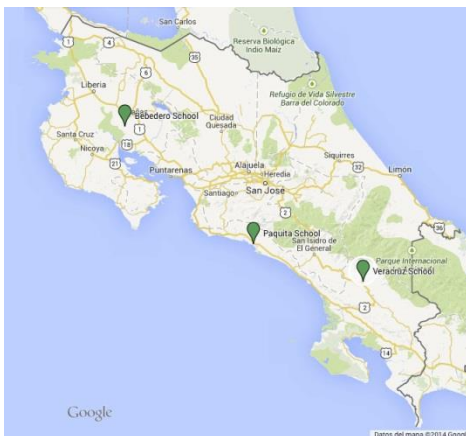


Fig. 1 – Location of schools utilized as case studies. Costa Rica map provided by Google Maps and modified by the author.

The aim of this study is to explore the effects on thermal comfort and energy performance generated by the change of architectural parameters (design) and configuration of typical classrooms in the Costa Rican tropics. Specifically, a review of the consequences is to be realized by applied passive cooling strategies (solar control, heat decrease and heat dissipate) and the possibility to improve the basic typology will be demonstrated.

2. Case studies: Bebedero, Paqueta and Buenos Aires Cities.

The case studies are found in the hot-humid tropical zone of Costa Rica, located between the area of the Tropic of Cancer and the Equator. The framework of microclimates is dominated by a non-seasonal climate with a rainy season from May to November and a dry season with little or no rain during the months of December to April.

Field studies were conducted for six (6) naturally ventilated classrooms, in three (3) different locations of Costa Rica's Pacific coast. The school buildings studied are located in Bebedero - Cañas (10°22'10.21 "N / 85°11'37.86" W and 12 m above sea level), Paqueta - Puntarenas (09° 27'40.57 "N / 84°10'50.81 "W and 10 m above sea level) and Veracruz - Buenos Aires (09°09'45.44"N / 84°19'26.35 "W and 385 m above sea level). Fig. 1 shows the location of each school on the map of Costa Rica.

The selected case studies based on existing constructions permit us to improve their performance through the use of thermal and energy simulation. Verification strategies can then be applied to new buildings to be constructed in areas with increased risk of overheating. These zones have ranges of average outdoor air temperatures between 25.4°C and 29.7°C, with a maximum of 34.4°C and a minimum of 19.1°C.

The elementary classrooms are occupied mainly by children between 9 and 13 years for academic activities. The average metabolic rate corresponds to 1.2 metabolic rate in accordance with the provisions of the ISO 7730: 1994 and ASHRAE 55: 2004. Within these spaces, operable windows on

opposite sides (cross ventilation) and ceiling fans are the main sources of natural ventilation, plus the teachers are given the freedom to operate the windows to change the indoor environment with respect to airflow rate.

2.1 Description of the classroom typology

The investigated classrooms use a unique model of classroom that was designed under the normative of the Compendium of Standards and Recommendations for the Construction of Buildings for Education with a series of minimum requirements. The rooms have internal dimensions of 50.50 m² of area and 2.50 / 2.70 m of height, built with a precast concrete system. Each one has a maximum occupancy of 34 students but the mean occupancy is 20 students. It is recommended to use the natural light from the north so that the orientation of the windows should respect this condition. The minimum size of the windows on facades is equivalent to a fifth of the floor surface; that corresponds to 10.1 m² of windows (single glazing), a 20% relative glazed / surface area; and are protected by external eaves. Fig. 2 shows the floor plan and the classroom configuration.

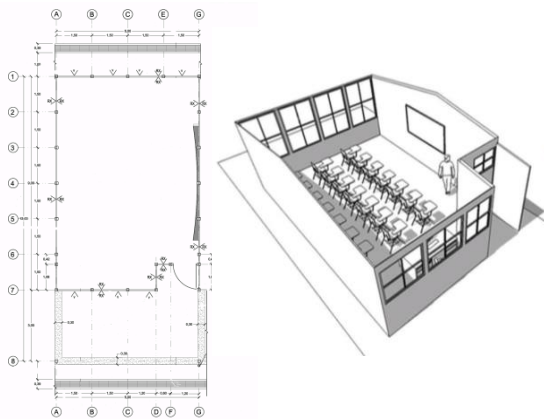


Fig. 2 – Floor plan and sketch 3D view of the classroom model. Source: Plans by DIEE- Ministry of Education- Costa Rica

2.2 Thermal conditions

During the dry season a survey was performed according to ISO 10551 - ISO 7730 and applied to 105 elementary students between 9 and 13 years of age. Furthermore, experimental measurements (dry bulb temperatures -interior and exterior-,

relative humidity, wet bulb temperatures, wind speed, CO₂) were carried out in order to evaluate the internal conditions and correlated to models of comfort. Results with respect to the Thermal Sensation Scale show that 67% of the students reported feeling comfortable or close to comfort (with scales between 1 and -1) with internal average temperatures near 30°C and relative humidity between 50 and 62%. The responses were obtained in a range of Tbs (dry bulb temperature) between 30.4°C and 33.1°C. 21.5% of students surveyed indicated feel neutral thermal condition (neither cold nor hot), with comfort index equal to 0. This confirms the statement by (Bravo and González 2001) in a study of the city of Maracaibo, Venezuela. They found that people who remain in environments subjected to free variation of temperature in unmanipulated environments acquire greater status adaptation and tolerance to high temperature and humidity. This is compared to people in other localities or people who are exposed to controlled conditions, especially in warm and tropical climates.

The results of the surveys and measurements were compared with simple adaptive models to find the perception of the user to overheating. In this case the formula adaptive comfort for buildings with passive operation (no mechanical systems) developed by (Humphreys, Nicol, and Raja 2007) was applied. (1)

$$T_c = 12.9 + (T_{avg} * 0.54) \tag{1}$$

Table 1 – Comparative table of comfort temperature ranges for the case of Bebedero City.

Case Bebedero -Dry Season					
	Dec	Jan	Feb	Mar	Apr
T ^o (1)				30,4°C	30,7°C
T ^o (2)	28,4°C	28,6°C	29,1°C	29,6°C	29,7°C
T ^o (3)	30,4°C	30,6°C	31,1°C	31,7°C	30,9°C
T ^o (4)	26,4°C	26,6°C	27,1°C	27,7°C	27,7°C

- (1) Comfort Temperature perceived for the students.
- (2) Comfort Temperature by simple adaptive model comfort
- (3) Upper Limit Comfort Zone by simple adaptive model.
- (4) Lower Limit Comfort Zone by simple adaptive model.

Table 1 shows an example of the data obtained for the Case of Bebedero with respect to the simple model of comfort for the dry season. Comfort temperature perceived by the user is within the limits established by the model, but closer to the upper limit. These data were taken into account in the simulation process to evaluate the comfort achieved through optimization processes. The lower limit of comfort is around 27°C in the three cities, which was set as the operating temperature to be reached in the simulations that use mechanical support by fans.

3. Definition of the simulation model

3.1 Parameters for simulation models of energy and comfort.

Dynamic simulations for a typical classroom model were realized using the software 'Design Builder' as an interface of 'Energy Plus' (version 8.0), and climate databases generated by 'Meteonorm 7.0'. The workflow of Design-Builder (Fig.3) starts with the selection of a location and the corresponding weather through a weather file (.EPW) followed by the creation of specific thermal building model geometry with the integrated CAD interface. Lists of definable parameters include internal loads (with occupancy patterns/activities), construction types, openings (windows and doors), lighting, and HVAC systems (if applied). Once the definition of all input parameters is complete, one can perform design day and/or annual simulations.

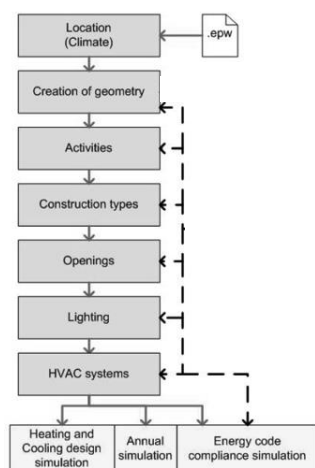


Fig. 3 – Definition of parameters in Design Builder. Source: (Rallapalli 2010) -edited by the author.

Two simulation models were performed. The first calculates the demand for cooling when setting a minimum operating temperature at the inner enclosure. The simulations are performed in order to evaluate the energy demand of ceiling fans in the actual configuration, and using technical solution proposals to improve the efficiency of the system.

The second model is free running (no mechanical constraints to achieve comfort), where the results show internal operating temperatures obtained with the variations realized in the pattern of simulation.

Calibration of the model with fixed parameters.

The simulation model is calibrated according to general design data classrooms defined in paragraph 2.1. These 'fixed parameters' are used for both the base case simulation (real current performance) and for optimization solutions raised in the calculation models of energy demand and comfort conditions.

The fixed parameters included internal loads, ventilation mode, and some physical characteristics.

- Internal loads (only during the occupation period) calculated according to ASHRAE: students with light study work 66 W; adults standing / walking 108 W; artificial lighting 300 lux classrooms – 11.25 W/m²; not considering the use of computers in the classroom; average occupational density of twenty (20) students per classroom and a teacher (0.39 persons/ m²).
- Occupation Period: Monday to Friday, from 8:00 to 12:00 and 13:00 to 17:00.
- Holiday periods: Half year, from 30 June to 11 July; and vacation season, from December 15 to February 10.
- Operating temperatures during the period of occupation: (This information was defined for the simulation model that calculates demand for cooling) 23°C minimum, 27°C average and 30°C maximum. In unoccupied periods, there is no limit temperature.
- Ventilation: simulations with 2 ac/h were performed on period occupation minimum. It was also considered to simulate the free additional ventilation by opening windows

when the temperature inside exceeds 23°C, from Monday to Friday between 8:00 and 17:00.

- Surfaces: the 3 schools studied have the same model classroom with a unique materiality. External walls in concrete tile (1% reinforced concrete steel) and a thickness of 0.038 m, with U-value of 5.36 W/m²-K. Roof of enamelled steel sheet of 0.44 mm thick with thermal insulation EPS (expanded polystyrene) of 5 mm thick. Over a frame of black iron metal of 15 cm, 1.5 mm thick with U-value of 3.773 W/m²-K. Ceiling suspended in plasterboard 1 cm thick with U-value of 2.229 W/m²-K. Floor compound by 10 cm thick slab with ceramic tile of 13 mm thick with U-value of 2.803 W/m²-K. Windows of two types: fixed window of 3 mm thick, aluminium frame and window blinds glass of 3 mm thick (opening percentage 95%) with aluminium frame. With a U-value of 5.894 W/m²-K.
- The exterior walls were considered adiabatic, except those with windows (to the outside and into the hall).

Variable parameters using in optimization solutions

Of the variable parameters, only those related to building orientation, ventilation rate and use /operation of windows to promote passive cooling strategies were considered for this study.

Variable parameters are based on design rules allowed for the type of building, according to paragraph 2.1 of this article, and intend to observe how it influences the change in ventilation management and use of the site on their performance. These are shown underlined in Table 2, which summarizes all possible combinations of variables for simulation.

Table 2 – Summary of simulations parameters

Parameters		Nº of variables
Orientation	<u>North, South, East, West,</u> <u>Northeast, Northwest,</u> <u>Southeast, Southwest</u>	8
Occupation (p/m ²)	<u>Average (20), Max (34)</u>	2
Glass Thickness	3 mm	1
Glazed Area / m ²	<u>20% Minimum, 30% Current</u>	2
Solar Control	Yes (Eaves)	1
Window Operating	<u>Only hours of lessons,</u> <u>Day and Night (Dry Season),</u> <u>All the year.</u>	3
% Of Operate Windows	<u>90% Open-10% closed;</u> <u>All Opened</u>	2
Envelope	Current material (wall, floor and roof)	1
	TOTAL	192 POSSIBILITIES

Note: Underlined parameters correspond to the options that were varied within the simulation settings.

According to the parameters used, 192 possible combinations (Table 2) were obtained per city. Probabilistic analysis was used to identify the possibilities with better performance. Of the 192 possibilities, twelve (12) cases simulated represent significant improvements. The study was bounded to five (5) solutions per city that demonstrated the highest reductions. The strategies aim to avoid thermal and solar gains and promote natural ventilation.

The five (5) different solutions were analyzed and compared with the current situation (base case):

- Case_1: The orientation of windows according to utilization of the wind direction is adjusted. The air changes set in 2 ac/h at the base are left free and the period of operation by keeping windows open stretches during the day and night in days of the dry season (the period of overheating)

- Case_2: Based on the case_1, the operation window for all operating days expands during the day and night.
- Case_3: Based on the case_1, window operation is extended to every day of the year without restriction.
- Case_4: Based on the case_3, the area of operating windows is expanded from 90% to 100%.
- Case_5: Based on the above improvement (case_4) the glazed area decreased from 30% to 20% of the classroom. This continues to maintain the required percentage of natural light and reduces heat gains generated by glazed surfaces.

Only the Case_5 proposes changes in the components of the envelope of the classroom. The other solutions demonstrate passive strategies to reduce heat gains and improve ventilation strategies.

The variables used in cases with a better performance are composed of two or more parameters simultaneously, demonstrating the need for a combination of strategies.

4. Simulation results

4.1 Energy performance

Different scenarios were simulated for each locality. The evaluation of the advantages achieved with regard to energy efficiency was performed for each proposal based of annual demand.

The simulation model was performed using mechanical ventilation and cooling by fans in the ceiling, supported with the use of natural ventilation. The highest energy savings occur in warm periods, especially between the months of December to April.

The combination of reduced heat gains for glazed area, a constant flow of ventilation and 100% operable windows (Case_5), shows the best performance. Fig.4 illustrated the results of the different cases for the Bebedero School and the decrease in the annual demand.

The individual parameter that influences mostly in energy saving corresponds to the amount of air

changes / infiltrations by 30.6%. The appropriate use and control of air changes, natural ventilation and orientation of windows led to a decrease in energy demand for the base cases of between 25% and 40%.

The second significant parameter (but on a smaller scale) is the orientation with 2.05%, predominantly with a better performance from the spaces oriented to the North.

The glass surface is a parameter with media influence but produces a higher incidence in cities with higher daily thermal oscillation; its impact is a 1.42% decrease in demand. Reducing average demand in the three (3) cases is between 30% and 40% annually. Table 3 shows the percentage of energy saving for the cities.

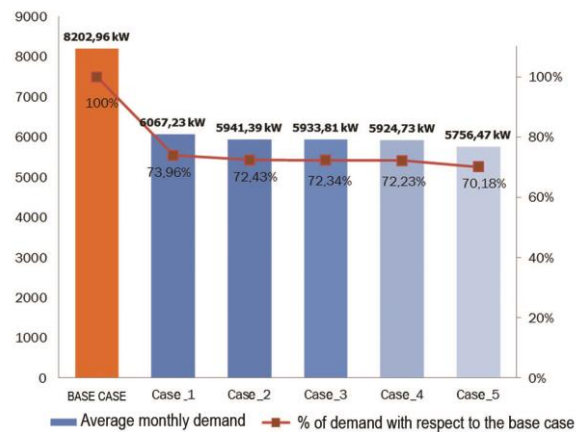


Fig. 3 – Decrease in annual demand by case. Analysis for the Bebedero School.

Table 3 – Energy saving (%) for solutions proposals respect to the annual demand of the base case.

Cities	Base Case AD	Energy Saving (%) Solutions				
		C_1	C_2	C_3	C_4	C_5
Bebedero	8202,96 kWh	27,57	27,66	27,65	27,77	29,82
Veracruz	3448,75 kWh	39,12	38,96	38,97	43,25	42,21
Paquita	6886,59 kWh	25,72	24,46	24,46	25,52	27,46

Note: The percentages in bold show the cases with better performance for each locality. C_1 (Case 1), C_2 (Case 2), C_3 (Case 3), C_4 (Case 4), C_5 (Case 5), AD (Annual Cooling Demand)

4.2 Comfort conditions

The current configuration of the classroom takes into account the use of ceiling fans. The ability to save on the use of the cooling system is demonstrated in the previous section. However, the design of classrooms should be improved from models without the use of mechanical systems.

Free running scenarios for the five (5) cases were simulated per city in order to achieve improvements in internal operating temperatures to implement variations in ventilation conditions and emplacement.

The overall results showed an improvement of between 6% and 27% in the internal operating temperature that are within the comfort zone according to the adaptive comfort model explained in section 2.2.

All operating temperatures calculated are among the upper and lower limit of the comfort zone indicated by the model, but closer to the lower area and the average of 27°C, which could be achieved with the support of a mechanical system.

Improvements include up to a decrease of 1°C in the operating temperature in the critical months.

Fig.4 shows the results of the base case operating temperatures and operating temperatures achieved for the Bebedero School.

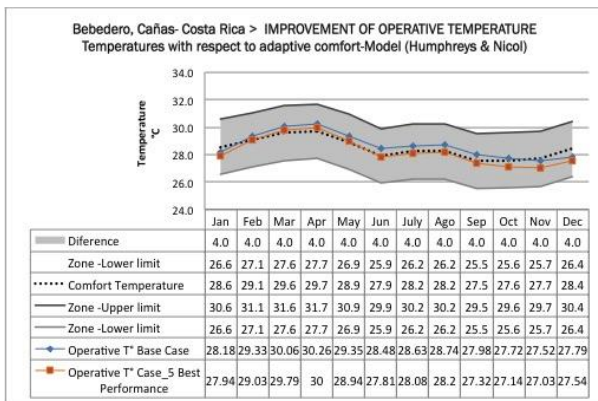


Fig. 4 – Improvement of operative temperature for the Bebedero case.

5. Conclusion

The thermal and energetic analysis of the three (3) case studies in the simulation tool allowed us to consider the performance of the current typology

in addition to achieving the factors that have a positive impact in terms of indoor comfort and energy efficiency (reduced cooling demand). through parametric comparison.

The simulations showed patterns known within the current architectural design of the classroom, such as the improved performance of the north facing classrooms and the effect of height and glazed in the thermal quality of the building area.

The possibility of enhancing air changes through natural ventilation and controlling the operation and heat gains proved to be key to slowing demand in refrigeration, for example with the use of mechanical ventilators or HVAC systems.

A cooling system with ceiling fans in one school (Bebedero) can reduce the annual consumption of 15,120 kWh to 10,584 kWh, a decrease of 30% in the annual cost of service. If we think of the 4,070 schools that exist in the country, this is a considerable number of savings in energy production and in the education budget, especially in rural areas where the budget is very limited.

The opportunity to use dynamic scenarios and validation with field studies allows us to define future parameters to use in the design to achieve an improvement in the actual performance of this type of buildings.

6. Acknowledgements

This work was developed within the Doctoral Program in Architecture and Urbanism at the University of the Bío-Bío, which facilitated the space and tools necessary for the development of this research. This study is part of the Doctoral Thesis: Optimization of Passive Cooling Systems for Improving Thermal School Classrooms in the Tropics. Gratitude to the University of Costa Rica, especially to the Office of International Affairs and the Laboratory of Tropical Architecture that have supported this work. Thanks also to the Ministry of Education of Costa Rica, Department of Infrastructure and Educational Equipment that allowed access to educational institutions and who provided important data for the development of this investigation.

7. Nomenclature

Symbols

T _c	Comfort temperature
T _{avg}	Average exterior temperature
W	Watts
kWh	Kilowatt hour
° C	Celsius Degrees
lux	Luxes
ac/h	Air changes per hour
T _{bs}	Dry Bulb Temperatures

References

- Bordass, Bill, Robert Cohen, Mark Standeven, and Adrian Leaman. 2001. "Assessing Building Performance in Use 3: Energy Performance of the Probe Buildings." *Building Research & Information* 29 (2) (March): 114–128. doi:10.1080/09613210010008036. <http://dx.doi.org/10.1080/09613210010008036>.
- Bravo, Gaudy, and Eduardo González. 2001. "Confort Térmico En El Trópico; Hacia Un Estandar En Viviendas Naturalmente Ventiladas." *Información Tecnológica (Chile)* 12 (5): 169–174.
- Corgnati, Stefano Paolo, Marco Filippi, and Sara Viazzo. 2007. "Perception of the Thermal Environment in High School and University Classrooms: Subjective Preferences and Thermal Comfort." *Building and Environment* 42 (2) (February): 951–959. doi:10.1016/j.buildenv.2005.10.027. <http://linkinghub.elsevier.com/retrieve/pii/S036013230500449X>.
- De Dear, Richard, and Gail S. Brager. 2001. "The Adaptive Model of Thermal Comfort and Energy Conservation in the Built Environment." *International Journal of Biometeorology* 45 (2) (July): 100–8. <http://www.ncbi.nlm.nih.gov/pubmed/11513046>.
- Givoni, Baruch. 2011. "Indoor Temperature Reduction by Passive Cooling Systems." *Solar Energy* 85 (8) (August): 1692–1726. doi:10.1016/j.solener.2009.10.003. <http://linkinghub.elsevier.com/retrieve/pii/S0038092X09002357>.

- Hwang, Ruey-Lung, Tzu-Ping Lin, Chen-Peng Chen, and Nai-Jung Kuo. 2009. "Investigating the Adaptive Model of Thermal Comfort for Naturally Ventilated School Buildings in Taiwan." *International Journal of Biometeorology* 53 (2) (March): 189–200. doi:10.1007/s00484-008-0203-2. <http://www.ncbi.nlm.nih.gov/pubmed/19132409>.
- Liang, Han-Hsi, Tzu-Ping Lin, and Ruey-Lung Hwang. 2012. "Linking Occupants' Thermal Perception and Building Thermal Performance in Naturally Ventilated School Buildings." *Applied Energy* 94 (June): 355–363. doi:10.1016/j.apenergy.2012.02.004. <http://linkinghub.elsevier.com/retrieve/pii/S0360261912000967>.
- Prianto, E, and P Depecker. 2003. "Optimization of Architectural Design Elements in Tropical Humid Region with Thermal Comfort Approach." *Energy and Buildings* 35 (3) (March): 273–280. doi:10.1016/S0378-7788(02)00089-0. <http://linkinghub.elsevier.com/retrieve/pii/S0378778802000890>.
- Rajapaksha, Upendra, and Richard Hyde. 2012. "Barriers to and Opportunities for Advanced Passive Cooling in Sub-Tropical Climates." *Architectural Science Review* 55 (1) (February): 49–60. doi:10.1080/00038628.2011.641730. <http://www.tandfonline.com/doi/abs/10.1080/00038628.2011.641730>.
- Rallapalli, Hs. 2010. "A Comparison of EnergyPlus and eQUEST Whole Building Energy Simulation Results for a Medium Sized Office Building." http://129.219.247.59/attachments/56303/content/Rallapalli_asu_0010N_10220.pdf.
- Sosa Griffin, María Eugenia, and Geovanni Siem. 2004. *Manual de Diseño Para Edificaciones Energicamente Eficientes En El Trópico*. Edited by IDEC. Primera Ed. Caracas.
- Wargocki, Pawel, and David P Wyon. 2007. "The Effects of Moderately Raised Classroom Temperatures and Classroom Ventilation Rate on the Performance of Schoolwork by Children." *HVAC&R Research* 13 (2): 193–220.

A new computational model: G.E.A.R. Graphical Expert Analytical Relations

Martino Marini – D.A.D.U. department University of Sassari – marini@uniss.it

Roberto Baccoli r – D.I.C.A.AR department University of Cagliari – rbaccoli@unica.it

Costantino Carlo Mastino – D.I.C.A.AR. department University of Cagliari – mastino@unica.it

Valerio Da Pos – Cadline Software srl ,Italy– valerio@cadlinesw.com

Zoltán Tóth Cadline Ltd Hungary– zoltan.toth@cadline.hu

Abstract

In recent years, there has been a gradual growth in the adoption of the new EU directives related to different topics in the field of construction. Consequently, professionals are forced to take care of different aspects in projects, which are related to limit performance requirements that the new buildings must ensure from the points of view of energy, acoustics, lighting and more in general of environmental and economic impacts. The present work deals with a new computational model (GEAR) dedicated to the multi-task simulation of buildings. GEAR is integrated with ARCHLine.XP (3D architectural cad) so that the several configurations encountered are more easily implemented.

1. Introduction

The European board has recently issued the EU directive “roadmap for moving to a competitive low carbon economy in 2050”[15,16] which lays down recommendations to achieve the reduction of greenhouse gas emissions under 80 per cent of the 1990 level by such a date. The directive gives a very important role to the efficiency enhancement in the building sector. Both new and upgraded buildings will have to achieve a higher energy performance but this has to be considered as just one of the design items for buildings even though energy and energy efficiency play an increasingly central role in the building industry. In this regard, the EN 15251 standard provides information for room design and for energy assessment of buildings, taking into account other performance

requirements that the new and upgraded buildings have to fulfil, for instance:

- interior air quality;
- thermal environment;
- lighting;
- acoustics.

Following on from that, buildings will need to state their performance from several different points of view, in order to be put on the market [2,3,4,5,6,7]. Procedures which enable us to rate together the different performance aspects are useful to gain an overall index.

Procedures for the indoor quality classification have been proposed taking into account different parameters i.e. comfort aspects [1]. Here the G.E.A.R. (Graphical Expert Analytical Relations) software is presented and discussed. It aims to evaluate the different building outputs by a unique procedure, taking advantage of interfacing with the Architectural 3D CAD modeller ARCHLine.XP. Details concerning the components of the model and its operation are provided.

2. Calculation method and software

The present calculation method is capable of managing the different physical aspects that the design of buildings involves at the same time. One of the basic requirements that the method fulfils, also as solicited by Cadline Software Ltd, consists in carrying out the calculations included in the procedures EN and ISO to which laws in force refer directly or make reference [8,9,10,11,12,13]. Another honoured requirement is the capacity of

interfacing and inter-operating with the three-dimensional models generated by the 3D Architectural CAD “ARCHLine.XP” by Cadline Ltd.

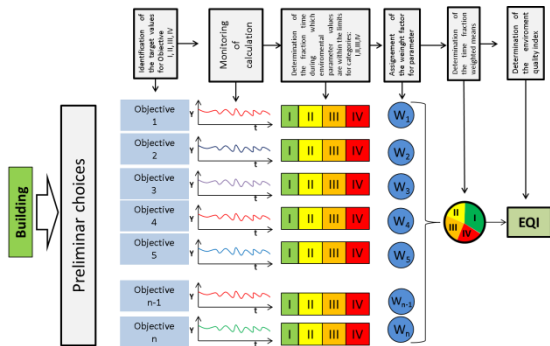


Fig. 1-Example of classification according to different goals [1]

The computational model has been developed within the environment Visual Studio by Microsoft, using C# and C++ as programming languages. Here below the main components of the GEAR model are shown (figure 2) and the user interface (figure 3) is sketched to remark its significance.

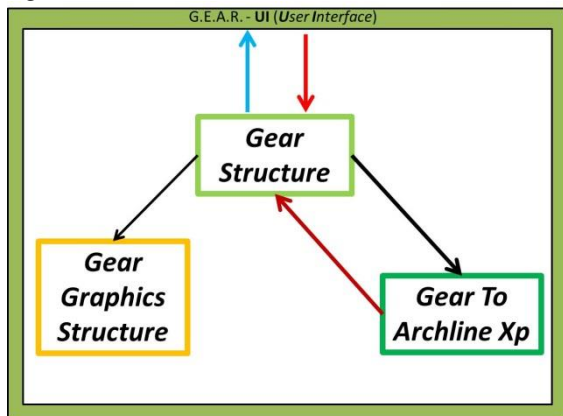


Fig. 2 – Main components of the computational model



Fig. 3 – Screen results and user interface for G.E.A.R.

In writing the code, the different menu items have been split and several projects have been

developed; their features have been linked by generating from each of them their own “dll library”. This option proved to be essential in the testing stage, in correcting the detected errors and in the algorithm optimization since each time we operated on a specific section of the code (component).

3. Structure and main components

The main components that form the model can be listed and analysed as follow:

- Gear Structure
- Gear to ARCHLine.XP
- Gear Graphics Structure

3.1 Gear Structure

The most demanding task concerned the component that organizes all the data that the computational model has to manage. GEAR Structure includes such a management system: the various functions developed and implemented are expounded in the following.

3.1.1 ClimateData

The “ClimateData” name space (such a term of information technology denotes “a group of classes”) includes all the classes and advanced methods to manage climatic data. It has been conceived with four classes (in figure 4 the UML diagram for these classes) which are named as follows:

ClimateData

The aim of this main class is to process the climatic data according to the selected calculation methodology. It enables the processing of e.g. the external monthly average temperature according to the location coordinates or the daily hourly average temperature profile calculated on a monthly basis. With this class, one can access the data loaded for each province and for the municipalities of each province; besides this, it enables the user to manage the data concerning the indoor conditions and to manage the constants database.

Constant (shared at design stage)

Inside this class, all constants used in calculations

are recalled. The same constants can be modified by the operator and made serial within the data flow or within the project backup.

InternalClimate

The class for the internal climate includes right inside the variables and the methods to obtain all the parameters the calculation needs. In detail, this class can be used to define the fixed (or calculated) climate for an entire zone or for a single room. All quantities which define the thermal, hygrometric and acoustic features of the inner environment as well as the daytime lighting, are included in such a class.

Province (provinces)

The object province checks on the list of municipalities of a specified province, but also all the data available for the province’s capital (for instance the climatic data included in UNI 10349 norm).

Common

This part of the structure manages all data concerning the specific municipality. It includes the various methods that enable us to modify default settings such as changing of temperature as a function of a.s.l. elevation; such a function can be started also by interacting with external applications, i.e. Google Earth, from which coordinates, orientation, etc... can be drawn.

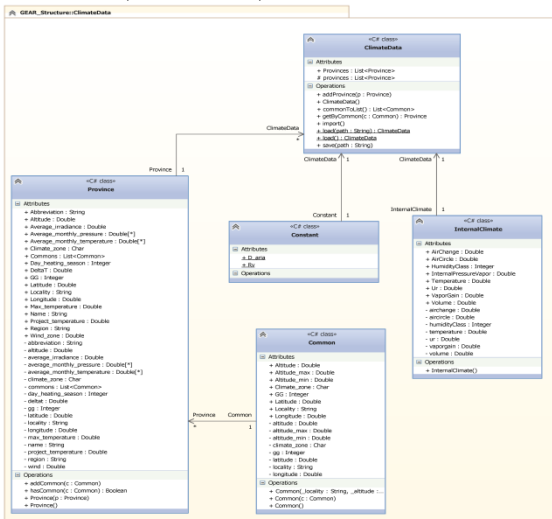


Fig. 4 – UML diagram for name space Climate Data

3.1.2 Gestore_Materiali (material manager)

The name space “Gestione Materiali” is devoted to single materials and architectural systems management. It stands for the heart of the

computational model, in some way, as all the name spaces and classes refer to it in order to carry out their various functions. This name has been conceived and developed taking into account the different physical and architectural properties that materials and architectures can possess. Such a manager is made up of five main classes and different codifications (formulas, reference month, type of material/layer). Classes have been arranged as follows:

Material

Such a class is about the different physical properties of materials. Variables such as vapor permeability, thermal conductivity and dynamic stiffness are defined within it. Moreover different methods are implemented which allow to set or give back values as heat transfer coefficients, for instance for a homogeneous insulating board, mass for a frontal unit area and thermal diffusivity. All these data are uploaded in order to manage the various features of materials or architectural systems.

Stratigraphy

The component stratigraphy can manage many compound materials. Namely, its purpose consists in managing the assembly of the different materials used to define the various building components both for interior partitioning and the exterior envelope. Various methods are implemented inside it, which allow the class to give back the different performance indices for the building component; if experimental values from laboratory tests are available, their input and setting is possible. For instance the following are given back or set:

- Thermal transmittance;
- Sound reduction index (curves for the frequency ranges 50-5KHz/ 100-3150Hz/ 100-5KHz);
- Permeance;
- thermal conductance;
- Reference sound reduction index
- Frontal mass
- Thermal capacity;
- Latent heat
- Cost;
- Areal heat capacities
- Periodic thermal transmittance

- Thermal admittances
- Periodic thermal conductances

Summarizing, the present component allows the user to set, calculate and manage all the physical/economic parameters that characterize the various building components.

Glaser

The class Glaser deals with the evaluation of vapor pressure trends inside construction elements. Computational procedures for vapor migration are mainly based on class EN 13788 which implements the norm with the same name.

Category stratigraphy

It manages a list of stratigraphic items that can be entered by different selection criteria. This class is very important for interactive research as it allows us to investigate all components included in the file archive and pick out just those which comply with the set up selection criteria.

Category material

It is similar to the previous class and manages the lists of specific materials (or architectural systems that can be assumed as “layers”, both homogeneous and not homogeneous). This class can also be accessed by interactive research procedures in order to select the most suitable materials for a given background, among those available.

Below can be seen the diagram of the name space called “Gestione Materiali”. The main links among the different components are drawn as well as associations, dependencies, aggregations among classes.

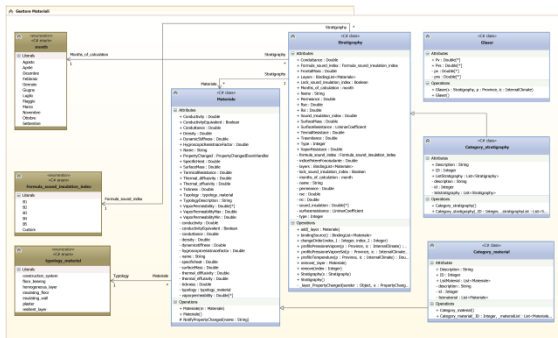


Fig. 5 – UML diagram for Gestione Materiali name space

3.1.3 Geometry

The framework of the name space called “Geometry” is shown in the following figure 6. In this section the adopted model deals with the

management of “geometries”(narrowly and broadly speaking); indeed it includes the different classes for the management of zones (for energy, acoustics and lighting applications) which in turn are formed by lists of Roombooks (rooms).

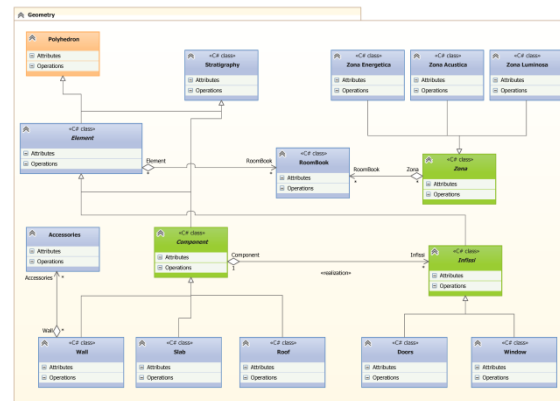


Fig. 6 – UML diagram for name space Geometry

As shown in the above UML diagram where the abstract classes are shown in green, the following main classes have been established.

Zona (Zone)

The abstract class “Zona” is needed to have a common basis for the three zone typologies that the model can manage. It recalls the properties that are included in the classes “Zona Luminosa”, “Zona acustica” e “Zona Energetica” (for lighting, acoustics, energy calculations). It is able to manage all the typical setting parameters, such as winter temperature of the internal zone, intended use for acoustic purposes or design day light factors, features of the plants on duty.

Component

This other abstract class manages all the methods and the basic variables of the different building components (walls, floors, roofs, windows and door fixtures). The calculation procedure included in the EN-ISO-Calcoli class is recalled inside such a class.

Roombook

This represents one of the most relevant classes of the model, and it is the class where the data about the single rooms that form the different zones are included, developed and given back. This class can manage several other lists of objects, such as lists of elements. It can belong to different zones like the acoustic and the energetic zones. Moreover, the

class includes a series of geometric data as areas, volumes, orientations and exposures of the different surfaces that define the room.

3.1.4 Space System

The name space system, for which the UML diagram is depicted in figure 7, includes classes, methods and databases to assess the yields of plants both from the energetic and from the acoustic points of view. Such a name space includes three main classes which in turn manage subclasses of plant subsets such as heat generation, distribution etc. In the following, the framework of the main classes which form the "System" name space can be seen.

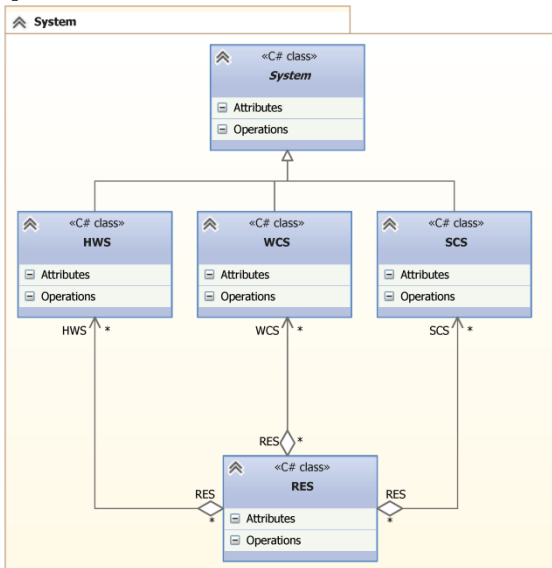


Fig. 7 – UML diagram UML for System name space

The main classes of the name space system implement the calculation methods for winter and summer air conditioning, production of household hot water etc. including plants exploiting renewable sources, following the main rules in force for building sector.

3.2 Gear To ARCHLine.XP

The dll library component Gear To ArchlineXp is the section of the model devoted to interfacing with the three-dimensional CAD Archline XP; it is one of the most innovative parts of the computational tool expounded here and deals with the geometry management. Interaction with CAD takes place through a dll library called ADE.dll. It has been assumed as a focus within the

computational model in order to be used properly. Hereinafter three excerpts of the code, written in the programming language C# that deal with: referencing the dll library ADE, transferring parameters to a dll library and generating the needed parameters to a given procedure (in the present case the conception of a stratigraphy)

1. Uploading of the dll library to get in touch with ArchlineXP
2. Feeding in of parameters to ArchlineXP
3. Generating the parameters to define stratigraphy

The example of sequence of instructions here shown illustrates how the transition to the class stratigraphy (str) is realized and how this is visited and then drawn in the ArchlineXP environment. By means of the three strings of instructions shown above, a bidirectional dialog with CAD and a management of all geometrical properties and of the zoning for them is possible.

3.3 Dynamic partialisation of surfaces

One of the most innovative features of the model which is managed by the component *GEAR to ArchlineXP*, it is named "dynamic partialization of geometries"; such a function enables the user to partialize in an interactive way the geometric data for the building elements according to the zoning of reference.

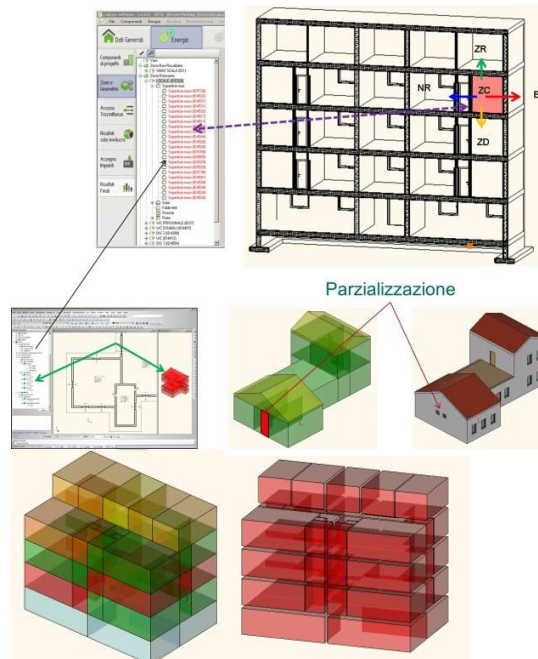


Fig. 8 - Example of partialization of surfaces

3.4 Gear Graphics Structure

The component Graphics Structure is committed to drawing in the guise of diagrams or sections (for instance the contour of the temperature trend inside a wall) all the results produced by the model. It is fully integrated and allows the user to implement several adjustments about results displaying. Here a figure (figure 9) with achievable results is shown.

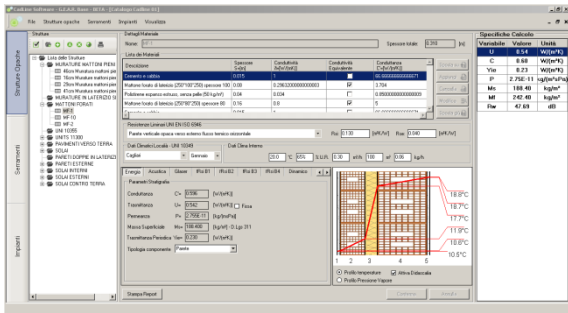


Fig. 9 – Screen displaying the calculation results

4. Application: example of zoning

The computational model constitutes a unified procedure for building design which deals with different sets of problems together. This result is obtained by logging on in a bidirectional way to the architectural cad Archline XP which forms the geometrical/graphical basis to enable the interactive operations of the model.

Among the features of the model the most innovative is called “dynamic partialization of surfaces”; it enables the user to divide the geometrical data of the building elements into parts in an interactive way as a function of the considered zoning.

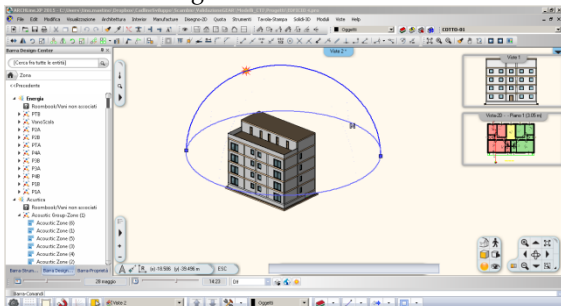


Fig. 10 – Model example

Hereinafter an application example, concerning the use of the model to implement the energy and

acoustic zoning and the input of the physical properties of building components, is referred to. The starting point is modeling the considered building by using the cad Archline Xp v.2015 (figure 10)

Then the subdivision into zones of the different rooms of the model is carried out in a graphical way (or after on GEAR tool) as a function of the physical problem examined (in the present example acoustics and energy are the matters).

After accomplishing the geometrical development with cad, the computational model GEAR is started including the geometrical modeling within it. In the following figures two screen shots concerning the energy and acoustic zoning are shown (figure 11 and figure 12)

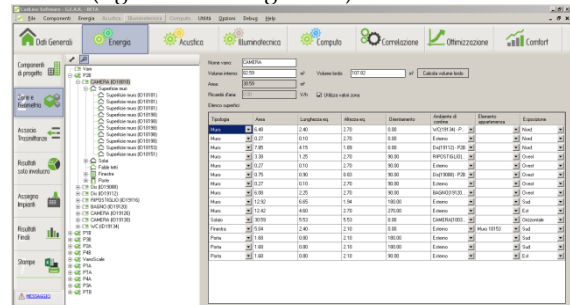


Fig. 11 – Energy zones

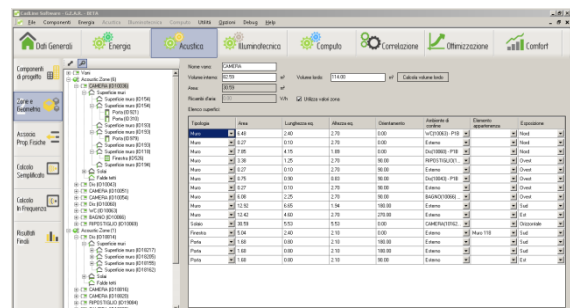


Fig. 12 – Acoustic zones

It is worthwhile noting that the above two zonings have been generated in the meantime by the same model keeping in such a way the uniqueness of rooms and constructive elements but analyzing them from different points of view.

For instance in the energy zoning, windows are grouped within the room while in the acoustic zoning windows belong to the wall where they are included. It is necessary to input all the physical properties into the correspondent elements in order to carry out the calculation for the present case. Such properties concern the set of problems

to be analyzed (GEAR takes into account just the properties defined for a single element; for instance if only the energy properties and not the acoustic one, are defined for a wall, GEAR will run just the energy calculations, pointing out the lacking acoustic data for some elements). Such an event can occur indiscriminately in the energy or in the acoustic sections as the constructive elements are unambiguous; Fig. 13 shows this, when the selected element receives in input its properties it is highlighted

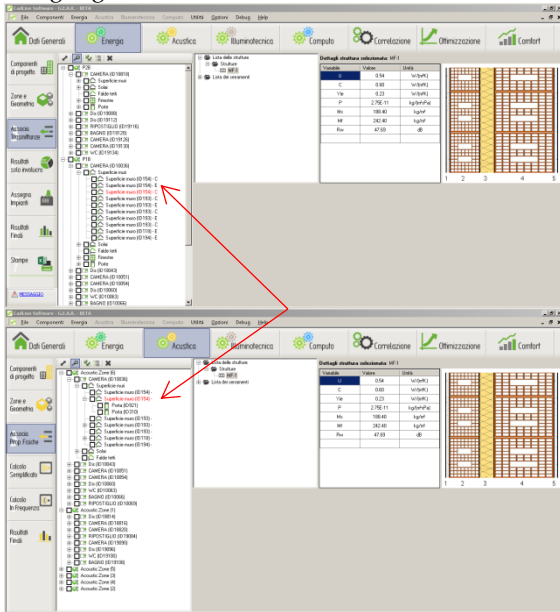


Fig. 13 – Assigning physical properties to the same element

When the input of the physical properties to the elements is carried out, further parameters that are specific of that kind of analysis can be defined (for instance thermal bridges for the energy section and connections between elements for the acoustic section). Finally, it will be possible to display the calculated predictions for the entire building or for the single room.



Fig. 14 – General results example of energy calculation

5. Conclusions

The unified handling of a set of physical problems can be seen as an innovative aspect of the developed model presented here that integrates effectively with the three dimensional architectural CAD. The model does not need any ad hoc three dimensional geometric modelling, but can make use of the same model developed for the architectural project. Furthermore, a cutting edge function is represented by the option of dynamic partialization of surfaces. Since calculations are based on a 3D model the dynamic partialization of surfaces enables the user to carry out a much larger number of simulations in the design stage to find out the best configuration for the studied case.

References

- [1] C. Marino, A. Nucara, M. Pietrafesa, Proposal of comfort classification indexes suitable for both single environments and whole buildings, 2012, Building and Environment, vol.57, pages 58-67.
- [2] A. Schlueter, F. Thesseling, Building information model based energy/exergy performance assessment in early design stages, Automation in Construction, vol.18, pages 153-163.
- [3] N. Fumo, P. Mago, R. Luck, Methodology to estimate building energy consumption using EnergyPlus Benchmark Models, 2010, Energy and Buildings, vol. 42, pages 2331-2337.
- [4] R.L. Hwang, S. Y. Shu, Building envelope regulations on thermal comfort in glass facade buildings and energy-saving potential for PMV-based comfort control, 2011, Building and Environment, vol.46, pages 824-834.
- [5] F. Nicol, M. Humphreys, Derivation of the adaptive equations for thermal comfort in free-running buildings in European standard EN15251, 2010, Building and Environment, vol. 45, pages 11-17.
- [6] M. Virtanen, J. Palmer (editors), Heating and Cooling with a Focus on Increased Energy Efficiency and Improved Comfort, ECBCS Annex 37, Low Exergy Systems for Heating and Cooling of Buildings, 2010.
- [7] D. Schmidt, ECBCS Annex 49 Low Exergy system for High-Performance Building and Communities, 2008.

- [8] EN 12354 - Building acoustics Estimation of acoustic performance of building from the performance of elements.
- [9] EN ISO 13790 - Energy performance of buildings Calculation of energy use for space heating and cooling
- [10] EN 13788 - Hygrothermal performance of building components and building elements Internal surface temperature to avoid critical surface humidity and interstitial condensation Calculation methods
- [11] EN ISO 6946 - Building components and building elements Thermal resistance and thermal transmittance. Calculation method
- [12] EN ISO 13786 - Thermal performance of building components Dynamic thermal characteristics. Calculation methods
- [13] EN ISO 7730 - Ergonomics of the thermal environment - Analytical determination and interpretation of thermal comfort using calculation of the PMV and PPD indices and local thermal comfort criteria (ISO 7730:2005)
- [14] EN 15251 - Indoor environmental input parameters for design and assessment of energy performance of buildings addressing indoor air quality, thermal environment, lighting and acoustics
- [15] COM/2011/112 Roadmap for moving to a competitive low-carbon economy in 2050 the March
- [16] COM/2011/885 Energy Roadmap 2050 the December

A new simulation tool for the evaluation of energy performances of green roofs

**Domenico Mazzeo – Department of Mechanical, Energy and Management Engineering (DIMEG)
University of Calabria, Italy- domenico.mazzeo@unical.it**

**Piero Bevilacqua – Department of Mechanical, Energy and Management Engineering (DIMEG)
University of Calabria, Italy – piero.bevilacqua@unical.it**

**Marilena De Simone – Department of Mechanical, Energy and Management Engineering (DIMEG)
University of Calabria, Italy – marilena.desimone@unical.it**

Natale Arcuri Department of Mechanical, Energy and Management Engineering (DIMEG) – University of Calabria, Italy – natale.arcuri@unical.it

Abstract

Among the different adoptable solutions for building envelopes, of particular interest is the green roof which allows us to obtain, at the same time, energy, economic and environmental benefits using solar energy as a source for its operation.

The aim of the proposed study is to evaluate the energy and economic savings achievable through the installation of an additional green roof stratigraphy on a variety of traditional roofs. The analysis was carried out with reference to the climatic conditions of the Calabria region (Italy), classified as Mediterranean.

Such assessment has been achieved by the use of a thermal model in dynamic regime formulated by the authors that allows us to determine the heat transfer in roofs with a green cover. The model is based on two energy balance equations for the vegetation and soil layer. The model has been implemented into the software tool ThermoGR that allows us to evaluate the thermal exchanges of a green roof with indoor and outdoor environments and the seasonal energy savings due to the presence of the green stratigraphy.

The reduction of the thermal load through the roof, due to the green roof, is used to perform an economic analysis based on the calculation of the cost of the energy saved per square meter of roof surface during the air-conditioning period both in summer and in winter. This analysis is used to identify the constructive typologies on which the application of the green roof is more advantageous.

1. Introduction

Greenhouse gas emissions are caused by human anthropogenic activities and to reverse the growing trend, it is important to mitigate the process in all sectors: residential, industrial and transportation.

The building sector is the largest consumer of energy, in which the main requirements are energy demand for space heating, cooling and domestic hot water production and electricity demand to illuminate and power household appliances (Masoso and Grobler, 2010). The continuous growth in energy demand for cooling and heating buildings makes the design and use of sustainable architectural solutions and plant systems for energy refurbishment of existing buildings necessary.

In this context, green roofs can be used to obtain, at the same time, energy, economic and environmental benefits. They are believed to mitigate the urban heat island effect, improve storm water management, filter fine particles, provide aesthetic and social benefits, reduce noise pollution, improve the durability of roofs, provide effective thermal insulation and reduce the cooling loads of buildings. Green roofs are often classified as intensive and extensive, according to the level of maintenance required and the depth of the growing media. The main elements of the stratigraphy are, from the top to the bottom: proper vegetation, lightweight growing media, filter layer, water storage and drainage layer and

root-barrier whose function is often provided by a waterproof layer.

Different physical phenomena are involved in the green roof energy balance that are not easy to model since they imply heat and mass transfers. Nevertheless, developers and architects need proper tools for assessing the likely amount of energy savings associated with diverse green roof options.

Several authors have proposed thermophysical models in the last few years, often based on energy balance equations. Each model supposes simplifying assumptions neglecting some factors and considering others in more detail.

Del Barrio (Del Barrio, 1998) proposed one of relevant initial models. She divided the green roof system into three main parts: canopy, soil and roof slab. A heat balance calculation was performed for each part in association with boundary conditions at the canopy-soil, soil-roof slab, and roof slab-indoor air interfaces.

Following another approach, Lazzarin et al. (Lazzarin et al., 2005) developed a numerical model. The green roof system has been investigated in dynamic state considering mono-dimensional analysis at the finite differences. The physical system is divided into different segments and nodes. The soil is described with three nodes, while one node describes the drainage layer, the waterproofing sheet and the structural concrete roof. The other elements are neglected for the limited thermal mass. The upper border is the ambient air and the lower one is the room underneath. In the energy and water model, fluxes take place. They depend on the evaporative flux and on the saturation or dryness condition of the soil: if a node reaches the saturation, the excess water drains down to the lower one, while if it becomes completely dry, it recalls the needed water from the same one.

Frankenstein and Koenig (Frankenstein and Koenig, 2004) developed the FASST (Fast All-Season Soil Strength) model. Two heat balances are considered, at the soil surface and at the foliage surface. The main influencing parameters that affect heat transfers for a green roof were considered: foliage height, leaf area index (LAI), fractional vegetation coverage, albedo, stomatal

resistance. The heat and mass transfers in the canopy were studied by considering the leaf as a solid body in which air circulates.

Following the study of Frankenstein and Koenig (Frankenstein and Koenig, 2004), Sailor (Sailor, 2008) developed a more accurate energy balance model. In particular, the energy budget is divided into the foliage layer and the ground surface. The model was linearized and the final set of equations are solved simultaneously to obtain the surface temperature of soil and foliage. According to Sailor (Sailor, 2008), moisture leaves the soil through runoff evaporation and evapotranspiration from vegetation surfaces. At each time step, the soil moisture state is updated based on the net inflow of moisture to the soil layer.

Tabares-Velasco and Srebric (Tabares-Velasco and Srebric, 2012) presented a quasi-steady state heat and mass transfer green roof model. It considers heat and mass transfer processes between the sky, plants and substrate. In particular, the formulation presents new equations to calculate substrate thermal conductivity, substrate resistance, and sets stomatal resistance functions to calculate plants transpiration.

On the basis of the work of Del Barrio (1998), Frankenstein and Koenig (2004) and Sailor (2008), Djedjig et al. (2012) reformulated the energy contributions of the energy balance equations and proposed a dynamic model. The thermal behavior of the green roof layers was coupled to the water balance in the substrate that was determined accounting evapotranspiration.

Finally, photosynthesis was included in the thermal balance by Feng et al. (2010).

The literature survey demonstrates the importance of thermal parameters of substrate and drainage layer, such as thermal conductivity and specific heat capacity, which in reality vary as a function of the moisture content. This last dependency is not always taken into account introducing in this way strong simplifications in the modelling.

In this study, energy and economic savings achievable through the installation of an additional green roof stratigraphy on traditional roofs are evaluated. The analysis is carried out with reference to climatic conditions of the Calabria region located in southern Italy. The climate is

Mediterranean, defined as subtype *Csa* according to the Köppen climate classification, characterized by hot and dry summers and wet winters. The choice of a lightweight extensive solution typically does not generate a problem of excessive structural load to be borne by the structural roof.

The evaluation is achieved by using a thermal model in dynamic regime formulated by the authors that allows us to determine the heat transfer in roofs with a green cover. The model is based on two energy balance equations, for the vegetation and soil, and takes into account the sensible and latent heat transfer, the effects associated with the heat capacity of the soil and the photosynthetic activity of plants. Furthermore, the model considers the variation of the substrate thermal properties with the water content.

The model has been implemented into the software tool ThermoGR that allows us to evaluate the heat transfers of a roof toward indoor and outdoor environment. These outputs can be used for the evaluation of building thermal loads through the building cover, in presence and absence of a green roof. The results of simulations, temperatures in the stratigraphy and thermal fluxes are used to assess seasonal energy savings due to the presence of the green cover depending on the roof type (construction, thermal insulation, etc.) and climatic conditions of the considered localities (solar radiation, air temperature, precipitation, etc.).

The assessment of the reduction of the thermal load through the roof cover, due to the green roof, is furthermore used to perform an economic analysis based on the calculation of the cost of saved energy during the air-conditioning period both in summer and in winter per square meter of roof. This analysis provides useful information about energy and economic benefits that can be obtained from each type of studied roof coverage allowing to identify the constructive typologies on which the application of the green roof is more advantageous.

2. The Thermophysical model

The thermophysical model developed by the authors is based on the relevant literature. For their

accuracy, the reference model for the formulation of radiative heat exchanges was (Ouldboukhitine et al., 2011), the model of Sailor (2008) was considered as a reference for the definition of sensible and latent heat exchanges. The model has been extended considering the FASST (Frankenstein and Koenig, 2004) for assessing the energy contribution associated with the precipitation, and the work proposed by Feng et al. 2010 (2010) regarding the energy contribution associated with photosynthesis and plant respiration.

The proposed model contains some novelties, or rather refinements, compared with the reference formulations. In particular, the contemporaneity of the following assumptions is considered:

- 1) the heat storage capacity of the growing media is introduced, through the calculation of the variation of its internal energy;
- 2) the thermal modelling of the drainage layer, partially filled with water is added;
- 3) the thermal conductivity and the specific heat of the substrate and of the drainage layer are expressed as a function of the water content;
- 4) the green roof is considered partially covered by vegetation, defining the fractional vegetative coverage σ_i ;
- 5) the heat flux associated with precipitations and photosynthesis is considered.

The green roof mathematical model is based on two instantaneous energy balance equations for the vegetated and soil layer, expressed as functions of the unknown variables temperature of foliage (T_f) and substrate surface temperature (T_g). The surface energy balance equation for the vegetation is given by:

$$R_{n,f} + H_f + L_f + P_f + P_{hf} = 0 \quad (1)$$

Where $R_{n,f}$ is the net radiative heat exchange, H_f is the sensible heat flux, L_f is the latent heat flux, P_f is the precipitation heat flux and P_{ph} is the heat flux associated with photosynthesis and plant respiration. The same formal equation is written for the soil surface:

$$R_{n,g} + H_g + L_g + P_g + C_g + \frac{\Delta U}{\Delta t} = 0 \quad (2)$$

Where $R_{n,g}$ is the net radiative heat exchange, H_g is the sensible heat flux, L_g is the latent heat flux, C_g is the conductive heat flux, P_g is the precipitation heat flux and ΔU is the variation of internal energy. In particular in the conductive term of the balance, C_g , the variability of the substrate thermal conductivity is expressed by the following relation (Sailor and Hagos, 2011):

$$\frac{K}{K_{dry}} = \frac{1.45 \exp(4.411S_r)}{[1 + 0.45 \exp(4.411S_r)]} \quad (3)$$

where K_{dry} is the thermal conductivity in dry condition and S_r is the degree of saturation. Furthermore, in the term ΔU the variability of the substrate heat capacity is introduced considering a linear interpolation between the dry C_{dry} and saturated condition C_{sat} :

$$C = C_{dry} + \frac{C_{sat} - C_{dry}}{\theta_{sat}} * S_r \quad (4)$$

In both energy balance equations, the unknown variables are the surface temperature of foliage (T_f) and the surface temperature of the substrate (T_g). The system of equations is linearized and solved in order to provide T_g and T_f as output. Once these temperatures are calculated, every energy contribution of the balances can be evaluated. The formulation has been successively completed by the thermal modelling of the layers underlying the substrate, interposed between the growing media and the internal environment, as shown in fig. 1.

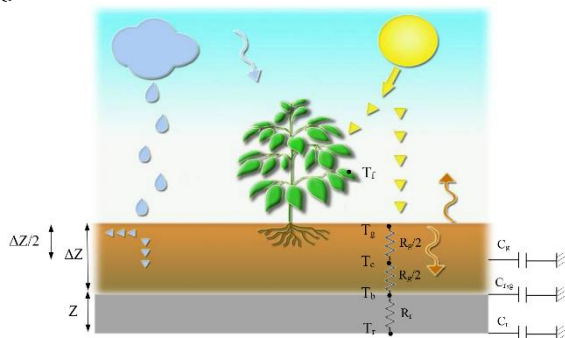


Fig. 1 – Schematic representation of the thermal variables considered in the energy balance

The drainage layer was modelled considering an equivalent thermal conductivity expressed in function of the thermal conductivity of air k_a , water

k_w , and drainage material k_p , weighted on the respective areas. In a similar way, an equivalent heat capacity was defined.

The finite difference method was implemented to solve the energy balance in every node between the growing media and the internal environment.

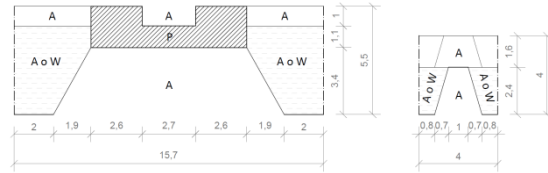


Fig. 2 – Schematic representation of the drainage layer for the thermal modelling. A: Air, W: Water, P: Material (Polystyrene)

Finally the resolution of the system of equations provide the node temperatures T_i , foliage temperature, T_g , surface ground temperature, T_c , temperature at the center of ground, T_b , ground-drainage interface temperature, T_r , drainage-structural roof interface temperature and the node temperature in the layers underlying the foliage-ground-drainage system.

3. The simulation tool ThermoGR

In order to create a user-friendly and useful tool, the mathematical model, written in C++ programming language, was implemented in a new software, named ThermoGR. Furthermore, the C++ subroutine can be coupled with common energy simulation software, some of which do not provide, at the moment, a library for the evaluation of the thermal performance of green roofs. For example, ThermoGR can interact with the Type 56 building model of Trnsys (TRNSYS 17, 2010).

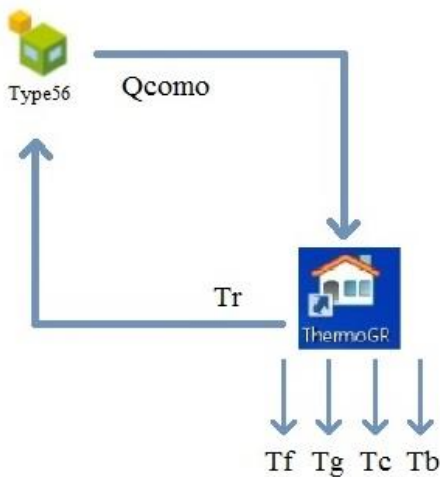


Fig. 3 – Flow Chart on which interaction TRNSYS-ThermoGR is based

In particular, Type 56 calculate the heat flux Q_{COMO} at the drainage-structural roof interface that constitute a data input for ThermoGR that evaluate the node temperature in the foliage-ground-drainage system (see fig. 3). At each time-step, the temperature T_r computed by the tool is then given to Type 56 until this cycle process reaches convergence, namely all thermal variables do not vary.

The ThermoGR is able to perform hourly dynamic simulations. The tool allows the setting of all the involved parameters through six windows for vegetation, substrate, drainage, structural roof and input and output data.

The software requires some input data: climatic conditions of the considered locality, type of structure, parameters defining the characteristics of the vegetated layers (leaf area index, SAI, fractional coverage of, height of plants, stomatal resistance, albedo, transpiration coefficient, evapotranspiration rate) and of the growing media (albedo, thermal conductivity, heat capacity) and simulation time period. This data can be entered manually in the software or by importing an external text file. The main outputs are temperatures of the different layers, energy contributions of the balance equations of soil and vegetation and heat flux through the entire roof. In the output windows, it is possible to visualize the data and export them into a *txt* or *xls* file. It is furthermore possible for the user to select a proper time range to show and export the simulation results.

4. Application of the simulation tool ThermoGR

Dynamic hourly simulations were carried out by ThermoGR. Simulations aim to evaluate the influence of the installation of a green roof stratigraphy on different types of roof in different localities by determining the entering and exiting heat fluxes from the internal environment. The considered extensive green roof is comprised of the following layers:

- vegetation;
 - substrate 8 cm;
 - drainage and storage layer in polystyrene 5.5 cm;
 - waterproof membrane;
- Four types of roof have been considered:
- 1 precast concrete and pre-stressed reinforced with polystyrene lightening elements;
 - 2 traditional roof with 16 cm hollow flooring blocks;
 - 3 traditional roof with 24 cm hollow flooring blocks;
 - 4 traditional roof with 16cm hollow flooring blocks and thermal insulation;



Fig. 4 – Examples of considered structural roofs. a) precast concrete and prestressed reinforced, b) traditional masonry

Three localities in the Calabria region were considered: Cosenza, Catanzaro and Reggio Calabria. According to the National regulations (DPR 412/93, 1993), the heating period for Cosenza and Catanzaro is from 15th November to 31st March, whereas for Reggio Calabria from 1st December to 31st March. For the summer season, a conventional cooling period from June to September was assumed. Temperatures for heating and cooling periods were set respectively to 20 °C and 26 °C.

4.1 Definition of green roof thermophysical parameters

The input data for vegetation and growing media were determined considering the experimental set-up of the University of Calabria. The main thermal properties of the substrate are: maximum water content 40%, dry density 1060 kg/m³, saturation density 1360 kg/m³, specific heat 1227 J/kg K in dry condition, specific heat 1388 J/kg K at saturation, average thermal conductivity equal to 0.27 W/m K. Regarding the vegetation, some in situ measurements carried out in August 2013, allowed us to obtain the following values: vegetation coverage $\sigma_f = 0.55$, leaf area index equal to 3, height of plants 12 cm.

4.2 Weather Data

Climatic data of the considered localities have been generated by the use of the software TRNSYS - (TRaNsient Systems Simulation – TRNSYS 17, 2010), using empirical methods and experimental available measurements.

Hourly data of total solar radiation on horizontal surface, humidity ratio and temperature were generated by Type 54a. Type 69b was used to calculate the sky temperature that is necessary to obtain the long-wave radiative exchange with the atmosphere. Type 33 was used for the calculation of wet bulb temperature. In the generation procedure, the hourly values are determined so that their associated statistic are approximately equal to the long-term statistics for the specified locality.

The hourly rainfall data were determined with a proper procedure. It can be observed that the probability of a rainfall event to occur is related to high relative humidity values and small differences between dry and wet bulb temperature of external air $\Delta T = T_{db} - T_{wet}$. The clearness index k was also considered to refine the selection of the hours in which a rainy event could occur. Particularly, hours with $k > 0.5$ were not taken into account. Concerning the night hours, cloudiness index N was used to assess when the precipitation phenomena happen; hours with $N < 5$ tenths sky cover were not taken into account. Table 1 shows the hours in which a rainy event can occur as a

function of temperature difference ranges considering different criteria: with no control (No cont), considering only the control on the clearness index (k) and both k and cloudiness index (N) control.

Table 1 – Number of hours in which rainfall occurs at variation of temperature interval ΔT . The values are determined by three different selection methods.

	0< ΔT <0.5	0< ΔT <1	0< ΔT <1.5	0< ΔT <2	0< ΔT <3	0< ΔT <4	0< ΔT <5
No cont	582	1242	1952	2730	4253	5434	6333
K	562	1129	1713	2309	3442	4254	4827
N	278	577	890	1191	1732	2074	2303

The ARPACAL (Center for Functional Comprehensive Regional Agency for Environmental Protection of Calabria) database provides the average yearly rainy days for Calabrian cities (ARPACAL). For Cosenza this number is 95, meaning 2,280 hours; therefore the results for the range $0 < \Delta T < 5$ were chosen considering both k and N control. The same procedure was applied for Catanzaro and Reggio Calabria. Considering monthly average precipitation values provided by ARPACAL, achieved in 96 years of observation, rain intensity has been linearly related to the cloudiness index N at each hour in which rainy event occurs.

5. Results

Table 2 shows the total ingoing and outgoing specific energy for the three considered localities for the four different types of roof, in summer and winter air-conditioning seasons. The total ingoing specific energy is calculated as the integral of the heat flux entering the indoor environment through the structural roof, whereas the outgoing specific energy is integral of the heat flux that leaves the environment through the same structural roof.

Table 2 – Results of winter and summer simulations

Roof Type	City	Summer air conditioning		Winter air conditioning	
		Ingoing energy [Wh/m ²]		Outgoing energy [Wh/m ²]	
		Without Green roof	With Green Roof	Without Green roof	With Green Roof
1	CS	6334.47	2424.58	9443.10	8047.43
	CZ	4233.69	1353.61	10156.21	8496.25
	RC	4427.19	1687.09	7339.14	5950.03
2	CS	9239.66	3367.88	19754.34	12440.28
	CZ	6017.96	1871.75	22196.47	13288.19
	RC	6320.34	2342.85	16174.87	9261.57
3	CS	8750.93	3239.61	17992.56	11904.52
	CZ	5602.43	1788.42	20095.71	12720.17
	RC	5911.76	2252.54	14625.46	8877.49
4	CS	4494.70	1786.70	5581.49	5397.82
	CZ	3071.28	1004.97	5885.29	5653.24
	RC	3192.77	1243.68	4237.90	3970.98

It appears the presence of a green roof is beneficial both in summer and in winter, reducing the energy loads if compared to the cases without green roofs. The maximum energy percentage reduction is found for the roof type 2 with values in summer and winter respectively of 64% and 37% in Cosenza, 69% and 40% in Catanzaro and 63% and 43% in Reggio Calabria with an absolute reduction of 5.9 kWh/m² in summer in Cosenza and 8.9 kWh/m² in winter in Catanzaro. In Catanzaro, due to the different climatic conditions, total ingoing specific energy is always lower than Cosenza in summer but the outgoing energy shows higher values in winter. In Reggio Calabria summer ingoing energy is similar to Catanzaro while in winter, it is the lowest of all the considered localities.

The evaluation of the energy saving achievable through the installation of the green roof is followed by an economic analysis to determine the convenience for the user. Usually the installation cost of a green roof varies between 30 €/m² and 70 €/m².

In summer, the presence of a green roof determines the reduction of the total specific ingoing energy to the conditioned environments. The reduction of the thermal load Q is calculated as the difference between the ingoing specific energy without the presence of the green roof (Q_{WGR}) and the value evaluated in presence of the green roof (Q_{GR}).

$$Q = Q^+_{WGR} - Q^+_{GR} \quad (5)$$

To determine the primary energy saving a COP equal to 3 was considered assuming the air conditioning plant is supplied by a heat pump. Considering the electricity energy cost C_{el} of 0.19 €/kWh the economic saving ES per square meter of roof is evaluable as:

$$ES \left[\frac{\text{€}}{\text{m}^2} \right] = E_{el} [kWh] * C_{el} \left[\frac{\text{€}}{kWh} \right] \quad (6)$$

where E_{el} is the electric energy consumed by the heat pump.

In winter the green roof reduces the outgoing specific energy, so that the reduction of the thermal load is calculated as:

$$Q = |Q^-_{WGR}| - |Q^-_{GR}| \quad (7)$$

In this case supposing the use of a natural gas boiler with an efficiency of 0.9, for the methane the lower calorific value of 35 MJ/m³ and a cost of 0.83 €/ m³, the achievable economic saving ES, in function of the fuel saving FS [m³/m²], per square meter of roof is calculated as:

$$ES \left[\frac{\text{€}}{\text{m}^2} \right] = FS \left[\frac{\text{m}^3}{\text{m}^2} \right] * c_{el} \left[\frac{\text{€}}{\text{m}^3} \right] \quad (8)$$

Results of the economic analysis are shown in table 3. The installation of a green roof provides always energy benefits and consequently economic savings.

Table 3 – Economic saving for the different roof solutions (S=Summer, W= Winter)

	Economic Saving [€/m ²]					
	COSENZA		CATANZARO		REGGIO CALABRIA	
	S	W	S	W	S	W
Roof 1	0.25	0.13	0.18	0.16	0.17	0.13
Roof 2	0.37	0.69	0.26	0.85	0.25	0.66
Roof 3	0.35	0.58	0.24	0.70	0.23	0.55
Roof 4	0.17	0.02	0.13	0.02	0.12	0.03

From an economic point of view, the effectiveness increases when the thermal performances of the structural roof decrease. In fact, the traditional roof with insulation, which performs the best from the thermal point of view, allows us to obtain the lowest results in term of economic savings from 17 €/cent/m² to 12 €/cent/m² in summer and from 2 €/cent/m² to 3 €/cent/m² in winter. The installation of the green cover on a roof with 16 cm hollow flooring block, characterized by lower thermal resistance, leads to economic savings ranging from 25 €/cent/m² to 37 €/cent/m² for electric costs in summer and from 66 €/cent/m² to 85 €/cent/m² for methane costs in winter. It is possible to conclude that in Mediterranean climatic conditions, such as those of the considered cities, the installation of the green roof allows for greater savings if the roof is poorly insulated.

6. Conclusions

An evaluation of energy and economic savings achievable through the installation of an additional green roof stratigraphy on traditional roofs was carried out. Three localities in Mediterranean climatic conditions have been considered.

The evaluation is achieved by the use of a thermal model in dynamic regime formulated by the authors. The model, based on the pertinent literature, contains some refinements given by the contemporary presence of different physical

phenomena. In order to predict the thermal behaviour of vegetated roofs, the mathematical model was written in C++ programming language. The C++ code was implemented in a new software, named ThemoGR that permits the user to calculate the outgoing and ingoing heat fluxes from and to the internal environments. The experimental set-up of University of Calabria has been considered to obtain vegetation and growing media parameters to be provided as input data in the simulation tool. The results of the energy simulations showed that for the three localities, the presence of a green roof is beneficial both in summer and in winter, reducing the thermal loads compared to the cases without green roofs.

The evaluation of the energy saving achievable through the installation of a green roof has been followed by an economic analysis to determine the economic savings achievable per square meter of installed green roof.

It is possible to conclude that in Mediterranean climatic conditions, such as those of the considered cities in Calabria region, the installation of the green roof allows for greater savings if the roof is poorly insulated. The maximum energy reduction was found for the roof type 2 with reduction in summer and winter respectively of 64% and 37% in Cosenza, 69% and 40% in Catanzaro and 63% and 43% in Reggio Calabria

Even though the economic saving evaluated with the simulation tool are not relevant in magnitude, especially if compared to the high installation costs, several other aspects can justify the choice of a green roof. First of all a proper national mechanism of financial support, identifying green roofs as a technology that provides energy savings, could help to spread this type of solution and at the same time reduce the installation costs allowing a quicker return of the investment. Finally, it has also to be considered that the expected lifetime of a vegetated roof is supposed to be more than twice as long as a traditional roof, because they are subject to lower thermal stress and that, added to the economic savings related to the lower energy consumption for the air-conditioning, lead to a smaller payback period.

References

- ARPACAL. Center for Functional Comprehensive Regional Agency for Environmental Protection of Calabria. www.arpacal.it
- Del Barrio EP. "Analysis of the green roofs cooling potential in buildings". *Energy and Buildings* 1998; 27:179-93.
- Djeding R., Ouldboukhitine S.E., Belarbi R., Bozonnet E., "Development and validation of a coupled heat and mass transfer model for green roofs". *International Communication in heat and mass transfer*. 2012:39.
- DPR 412/93, 1993, Regolamento recante norme per la progettazione, l'installazione, l'esercizio e la manutenzione degli impianti termici degli edifici ai fini del contenimento dei consumi di energia, in attuazione dell'art. 4, comma 4, della L. 9 gennaio 1991, n. 10.
- Feng C., Meng Q., Zhang Y. "Theoretical and experimental analysis of the energy balance of extensive green roofs". *Energy and Buildings* 2010; 42:959-65.
- Frankenstein S., Koenig G. "FASST vegetation models". *Technical Report TR-04-25*. Hanover, NH: US Army Engineer Research and Development Center, Cold Regions Research and Engineering Laboratory; 2004.
- Lazzarin R.M., Castellotti F., Busato F. "Experimental measurements and numerical modelling of a green roof". *Energy and Buildings* 37 2005; 1260-1267.
- Masoso O. T., Grobler L. J. "The dark side of occupants behaviour on building energy use". *Energy and Buildings* 2010; 42:173-7.
- Ouldboukhitine S.E., Belarbi R., Jaffal I., Trablesi A. "Assessment of a green roof thermal behavior: a coupled heat and mass transfer model". *Building and Environment*. 2011:49.
- Sailor DJ. "A green roof model for building energy simulation programs". *Energy and Buildings* 2008; 40:1466-78.
- Sailor D., Hagos M. "An updated and expanded set of thermal property data for green roof growing media". *Energy and Buildings* 2011, 43:2298-2303.
- Tabares-Velasco P.C., Srebric J. "A heat transfer model for assessment of plant based roofing systems in summer conditions". *Building and Environment* 2012; 49:310-323.
- TRNSYS 17 - A TRaNsient SYstem Simulation program - Volume 4. Mathematical Reference, 2010.
- VanWoert, N.D., D.B. Rowe, J.A. Andresen, C.L. Rugh, R.T. Fernandez, and L. Xiao. "Green Roof Stormwater Retention: Effects of Roof Surface, Slope, and Media Depth". *Journal of Environmental Quality*. 34:1036-1044, 2005
- DPR 412/93, 1993, Regolamento recante norme per la progettazione, l'installazione, l'esercizio e la manutenzione degli impianti termici degli edifici ai fini del contenimento dei consumi di energia, in attuazione dell'art. 4, comma 4, della L. 9 gennaio 1991, n. 10

A holistic method for energy renovation of buildings: focus on users' involvement

Giulia Degan – EURAC, European Academy of Bozen/Bolzano – giulia.degan@eurac.edu

Carsten Rode – DTU, Technical University of Denmark – car@byg.dtu.dk

Daniele Vettorato – EURAC, European Academy of Bozen/Bolzano – daniele.vettorato@eurac.edu

Marco Castagna – EURAC, European Academy of Bozen/Bolzano – marco.castagna@eurac.edu

Abstract

The energy renovation of existing building stock has been widely acknowledged as having a key role to tackle the 20-20-20 European targets (EuroACE, 2014). However, many open challenges characterize the effectiveness of building renovations, for instance, procedural methods that consider the interaction of multiple variables and their influence on a specific building are still inadequate. The aim of the paper is to investigate a holistic method (Eriksen et al., 2013) that, if used during the diagnostic pre-renovation phase, allows for the evaluation and planning of strategic renovations. To achieve the aim, the holistic method was applied on a multi-storey building for social housing that must be renovated. Thus, investigations about economic, architectural, technical, user and legislative aspects were carried out to create an overview of the building's features and needs. Thanks to the holistic diagnosis, the users' involvement and active participation was found to be a challenge. Therefore, TRNSYS simulation software was employed to specifically assess how much users can influence the success of the renovation project. Specifically, the first step was the creation of a baseline model for the existing building. The baseline model calibration was based on the current thermal performance, which was derived from data collected during the holistic method application. Afterwards, two borderline renovation scenarios were developed: on one hand, a model conforming to a pre-feasibility study that does not entail users' habits, and on the other a model that can be representative also of users' behaviour. The rationale behind is to quantify the impact of users in case they are not considered or they are not willing to be part of the project and, hence, they do not modify their habits accordingly.

Research results showed that the holistic method can contribute to optimizing the design that will be used in

the renovation as it effectively assesses the multiple effects of the variables and it incorporates the users' perspectives. Users are a crucial component to take into consideration from the beginning of a project. The paper represents other evidence of the importance of using building performance simulations (BPS) early in the design process to both assess the influence of users' habits on the energy consumption and become a system check for subsequent further design phases.

1. Introduction

The European Union (EU) has recognized the retrofit of existing building heritage as a priority since it represents one of the most cost-effective solutions to reduce global warming (EuroACE, 2014). Nevertheless, the available procedural tools are still inadequate (Ma et al., 2012). According to these authors, although there is a wide range of retrofit technologies available on the market, it remains a challenge to identify the most appropriate and cost-effective solution for a specific building because of the great number of variables that can widely change from building to building, e.g., climate, users' behavior, policy, financial limitations, services, maintenance, malfunctions. As a result, a discrepancy exists between the building's targeted energy performance and the real one. For the role of building users, a growing number of empirical studies has shown their crucial impact on the success of an energy retrofit. Tenants have an influence on the building's performance with their presence and activities (Hoes et al., 2009). They directly influence the energy demand when

operating windows, blinds and thermostats whereas they have an indirect effect on the energy consumption pattern due to the changes over time of occupancy schedules and usage patterns (Masoso and Grobler, 2010). However, Kashif A. et al. (Kashif et al., 2014) stressed that while great attention has been paid to the building's installations, the understanding of users' behavior has not been sufficiently investigated. Therefore, to optimize the outcome of a renovation, the design approach should integrate the influence of the building's technical aspects together with the users' behavior representation, giving them the same importance. This paper focused on testing the effectiveness of a holistic approach (Eriksen et al., 2013) that aims to provide a standardized evaluation of a building by investigating technical, economic, architectural and social aspects and by giving them the same importance. The application of such a method has allowed us to answer the following research questions:

1. How can a holistic approach contribute to optimizing the renovation of an existing residential building?
2. How does users' involvement influence the effectiveness of a renovation project?

2. Method

The two research questions were addressed by splitting the method in two parts: Part 1 regards the application of the holistic method to answer the first research question, while Part 2 answers the second research question through simulation modeling. The outcomes from Part 1 were used as input for Part 2.

2.1 Setting

The setting is the city of Bolzano, which is in the Autonomous Province of Bolzano (APB), in the north of Italy. According to UNI 10349 of the National Standard, the city's climate is continental. It belongs to zone E and it is characterized by 2791 Heating Degree Days (HDD). The subject of the research is a multi-storey building for social housing belonging to building stock from the

1970s. The targeted renovation's aim is the decrement in the energy needs for heating from the current average value of 100 kWh/m²/year to approximately 25-30 kWh/m²/year, the highest class of the regional rating system. Before the holistic method application, only data in Table 1 were available.

Table 1 – Building's available information pre-method application

Year built	1978
Shape	5 main bodies, block A'-B'-C'-D'-E'
Orientation	Orientation axis N-E/S-W. Blocks are differently orientated.
Stores number	8 stores for blocks A'-B'-C'-D' 7 stores for block E'
Area	Useful (walkable) area: 7.835,45 m ² ; Gross area: 9.402,54 m ² Business area= 0 m ²
Apartments	106
Preservation	Not rated as worthy of preservation

2.2 Danish holistic method overview

The holistic method elaborated by Eriksen et al. (Eriksen et al., 2013) has been taken as a starting point for Part 1. The method entails equivalent consideration of energetic, structural, economic, architectural and social aspects. The method was developed within the Danish context, it was applied to two case studies and it is still under finalization. Since its purpose is to provide a standardized and holistic evaluation of buildings to renovate during the prefeasibility study phase, its application on the Italian case study served to test the actual goal achievement. Fig. 1 depicts the method's structure: six constituent elements with the same importance led towards the determination of "focus points". Next to each element are listed the building's main aspects that were assessed. The investigations were carried out by means of available documentation, direct inspections, and by performing questionnaires and interviews with building users. Although the acquisition of data was an ongoing process, the arrows indicate the recommended way to progress. The analysis started with the *Master data collection* and *Economical investigation* to gather preliminary hints regarding both the building potential and the feasibility to perform holistic energy renovation.

Once verified the financial means, the *Architectural, Technical, Social* and *User investigations* were performed to obtain an overview of building defects to renovate. The coherent legislation was consulted across all previous elements to ensure the fulfillment of updated national laws requirements.

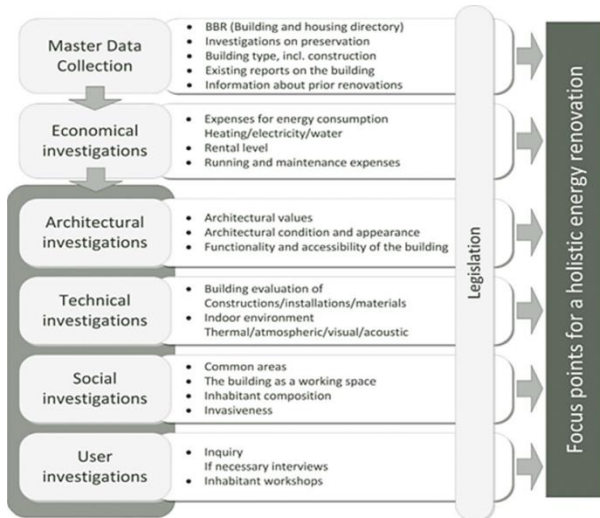


Fig. 1 – Holistic method structure (Eriksen et al., 2013)

2.3 Simulation modeling

Since the holistic method introduces the importance of building users, part 2 investigated their influence on the thermal energy performance once the building is renovated according to the given energy target.

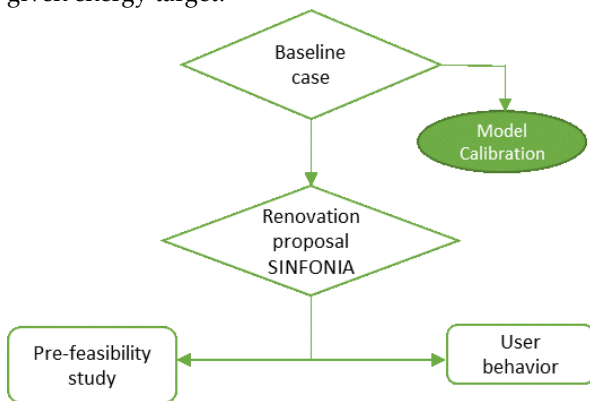


Fig. 2 – Simulation modeling structure

To achieve the goal, a baseline model was created based on the outcomes of the application of the holistic method. After the model creation and input definitions, the model was calibrated to obtain a simulation model's energy consumption for heating as close as possible to the real one, 118

kWh/m²year. This was accomplished by defining the only missing variable: the total air exchange rate, as further explained in 2.3.1.1.

Fig. 2 shows that the baseline-calibrated model was then renovated. Two proposals are presented: the first is explicitly inspired by the pre-feasibility study carried out by project designers; the second one shows one of the worst cases for post-renovation: unchanged users' behavior in terms of window opening compared to pre-retrofit situation.

2.3.1 Baseline case

The modeling framework incorporates a 3-D model of the multi-zone building, realized by means of the SketchUp building geometry design tool, into the TRNSYS 17 simulation model using the TRNSYS3d plug-in. The parameters assigned for the thermal performance evaluation of the existing building are:

Geometrical properties: found out in the *architectural investigations*, these were assumed according to available data and direct inspections, coherently with the UNI 11300 attachment B1.

Table 2 – Geometrical properties: baseline case

Element	Thickness [m]	U-value [W/m ² K]
Roof	0.25	1.70
External wall	0.30	0.90
Ground floor	0.36	0.79
Insulated divisions	0.41	0.70
Windows	Single glazed	4.00

Environmental properties: the building orientation was defined in SketchUp by orienting the geometrical model like the real building. The microclimate conditions, i.e. the incident solar radiation and the air temperature and relative humidity, were set up in TRNSYS Simulation Studio respectively by means of solar radiation processor and psychometric type 33. These data were collected from the meteorological radar in Bolzano, on an hourly basis for 2013.

Internal gains: according to results of questionnaires, most of the tenants are more than 60 years old and they occupy their own apartment for more than 18 hours per day. Therefore, it was

decided to define a constant internal gain equal to 4 W/m², according to UNI TS 11300 for residential buildings.

Natural ventilation - venting and infiltration: the building's total air exchange rate is the sum of window opening rate, which relies on users' habits, and of structural infiltration rate through the building envelope, which depends on its tightness. Given the complexity to properly define the infiltration rate at the initial stage, a constant value was initially assumed and later calibrated, as explained in Section 2.3.1.1.

Heating system: the building is connected to the district heating (DH) network that works from October 15th until April 15th. A schedule was created to diversify operation hours (6 a.m. – 10 p.m.) from switching off hours. When in operation, the temperature set point was assumed equal to 21 °C according to the questionnaire's results. Outside operating time, a set point temperature of 11°C was defined in order to avoid the heating system onset. Finally, the average efficiency of the system was assumed to be 87.5%, as the multiplication result of the efficiency coefficients of heat exchanger, distribution system and radiators, as indicated in UNI 11300.

2.3.1.1. Model calibration

Once having set up all inputs, the model was calibrated by defining the only missing variable: the total air exchange rate. The procedure consisted in a series of attempts with different values of total air exchange rate until the simulation results came very close to the real building energy consumption (equal to 118 kWh/m²/year for 2013, according to the DH provider datasheet). As mentioned in 2.3, the total value of air exchange rate can be split in two components, the window opening, which is the human induced component, and the structural infiltration component. Since the structural infiltration rate was assumed, through the calibration it was possible to settle the component influenced by users' habits: the window opening. The structural infiltration was set in TRNBuild after having assumed it according to (Paiola, 2014): with the Blower Door running and the house pressure at negative 50 Pa, a typical building of 70's can leak at the rate of 2-3 air changes per hour.

The value, which is usually expressed as $N_{50} = 2-3$, is the result of equation (1).

$$N_{50} = \frac{\text{average air flow rate of infiltration at 50 Pa}}{\text{Zone internal volume}} \quad (1)$$

From N_{50} it was possible to deduce the correspondent infiltration rate at normal pressure conditions, by means of the program Passive Haus Pojecterungs Paket (PHPP), approximate equal to 0,350 h⁻¹. The total air exchange rate during night hours (10 p.m – 7 a.m) was set equal to the infiltration rate because according to tenants' declarations, windows are open almost always during the day. While, during daytime the missing window opening rate was found through a series of simulations. Table 3 shows the results diversified between day and night.

Table 3 - Total air exchange rate: calibration results:

	Night	Day
Structural infiltration [h ⁻¹]	0.350	0.350
Windows opening [h ⁻¹]	0.049	0.391
Mechanical ventilation [h ⁻¹]	0.000	0.000
TOTAL AIR EXCHANGE RATE [h⁻¹]	0.399	0.741

Regarding the obtained window opening rates, they are to be considered just as time-averaged values calculated on a yearly basis, because the calibration process did not take into consideration any factor such as gender, age, perceptions of personal control, season, and weather conditions.

2.3.2 Renovation proposal

The calibrated baseline model was adjusted according to project targets. The shown renovation proposals include the following borderline cases:

1. Best case: Renovation conforming to the pre-feasibility study.
2. Worst case: renovation in case of unchanged user's habits (compared to current habits in terms of window opening).

2.3.1.2. Best case scenario

The renovation did not involve a change of environmental and heating system properties, nor of internal gains. Applied changes regarded the thickness of insulation, type of windows, as

pointed out in Table 4, and the implementation of a mechanical ventilation system.

Table 4 – Geometrical properties: best case scenario

Element	Thickness [m]	U-value [W/m ² K]
Roof	0.27	0.15
External wall	0,50	0.16
Ground floor	0.40	0.47
Insulated divisions	0.41	0.70
Windows	6/12/6/12/6 argon	0.70

In order to achieve the ambitiously targeted performance, it was necessary to adopt highly insulating materials so as to lower as much as possible the thermal transmittance of external elements (e.g., walls, windows, and horizontal divisions), thus incrementing the envelope's air tightness. As a direct consequence, the mechanical ventilation system was necessary in order to deliver the right amount of fresh air for indoor comfort conditions, whilst avoiding useless energy losses. The central ventilation plant was modeled as a heat recover ventilator (HRV) by inserting the type "Heat exchanger with constant effectiveness" in Simulation Studio interface and connecting it to the building type. The balanced air-to-air heat exchanger was sized in order to fulfill the UNI TS 11300 requirements. Thus, it provides a continuous value of 0.30 air changes per hour [ach] and it recovers some of the energy of the air passing through it when $T_{in} < 24^{\circ}\text{C}$ and $T_{out} < 12^{\circ}\text{C}$. To achieve the last condition, a control was created on the output air flow so as to let it passing through the HRV only in the case of favorable conditions. The annual recovery effectiveness of the mechanical system was assumed equal to 65% to take into account the conditions in which the system is expected to operate (Carbon trust, 2011). In addition, the renovated building was modeled with a new structural air infiltration rate that was approximated based on referential Blower Test n_{50} , which is 0.60 h⁻¹ for passive houses. As previously stated, PHPP software was useful to find the air exchange rate under standard pressure conditions, equivalent to 0,105 h⁻¹. Table 5 shows the total air exchange rate and the values per each entry.

Table 5 – Total air exchange rate: best-case scenario

	Night	Day
Structural infiltration [h ⁻¹]	0.105	0.105
Windows opening [h ⁻¹]	0.000	0.000
Mechanical ventilation [h ⁻¹]	0.300	0.300
TOTAL AIR EXCHANGE RATE [h⁻¹]	0.405	0.405

2.3.1.3. Worst case scenario

The worst-case scenario seeks to show a prospective negative impact of users' behaviour on the renovated building's energy performance. In particular, it was simulated the case in which users keep on opening their windows at the same rate that was found through the baseline model calibration, section 2.3.1.1. The rationale of this specific choice descends from the empirical factor according to which if occupants do not receive any information on the proper way to use mechanical ventilation, they will likely keep on acting as they do currently. Therefore, all input parameters of the best-case scenario were kept constant, except for the total air exchange rate. The simulation ran with a total air exchange rate equal to the sum of the value provided by the mechanical ventilation, the value depending on the structural infiltration and the value of windows opening found through model calibration, as shown in Table 6.

Table 6 – Total air exchange rate: worst-case scenario

	Night	Day
Structural infiltration [h ⁻¹]	0.105	0.105
Windows opening [h ⁻¹]	0.049	0.391
Mechanical ventilation [h ⁻¹]	0.300	0.300
TOTAL AIR EXCHANGE RATE [h⁻¹]	0.454	0.796

3. Results and Discussion analysis

To answer the first research question, the application of the holistic method allowed us to verify that it can effectively contribute to optimizing the renovation of existing residential buildings as it assesses the effects of multiple variables, it facilitates multi-professional and multi-disciplinary collaboration, and it incorporates the user perspective. Therefore, the holistic method was demonstrated to work

properly as a development tool also under different settings. In particular, it allowed us to identify the most important renovation focus points and it contributed to creating a broader perspective in the initial design stage that may be beneficial for further steps. When many stakeholders (consumers, policy makers, product manufactures, regulators, technology developers, investors, designers) use it, an extensive wider perspective can be created about a building to renovate. In particular, the method could avoid the misunderstanding about complete freedom of choice and experimentation that designers have had so far, and consequent repercussion on inhabitants that, on the contrary, have not had the possibility to express opinions based on their experience, culture, origin and needs (Civiero, 2012). However, some barriers limit the possible accomplishment of the holistic approach:

1. The widespread lack of information about both building parts and installations results in a prolonged time required to gather all information.
2. The multidisciplinary approach that can maximize the method's effect struggles to become established in the Italian public sphere as well as in academic research (Civiero, 2012).
3. The tenants' willingness to take an active role was found to be a challenge, which in itself reduces the potential benefits of the method.

In addition, the thesis has shown that the method has some deficiencies:

1. The method does not indicate the importance of using the building performance simulation (BPS) as a support to evaluate the multitude of parameters (Ratti et al., 2005). For instance, it lacks a real representation of users' behavior. It is restricted to the evaluation of users by means of questionnaires and interviews but it does not suggest putting into practice the acquired knowledge through modeling/simulation.
2. The Danish method considers the building as a self-confined entity, neglecting the importance of the interaction with the urban surroundings (NRDC, 2014), which would allow us to broaden the virtual boundaries of holistic method (Okeil, 2010). The resulting focus

points would change accordingly (Ratti et al., 2005; Xu et al., 2012) and they could be even as useful for the local surroundings (the neighborhood) contributing to finding solutions that, although conducted at the building level, have a positive influence on the surrounding urban area (Ferrante, Semprini, 2011).

To answer the second research question, in this study user involvement was found to be a challenge, which in itself reduces the potential benefits of the Holistic Method. However, when users were involved, it was possible to identify both hidden problems of the building and the effect of user behavior on performance of energy conservation measures. The results of the users and social investigations, and of the energy simulations, suggest that user involvement can influence the energy renovation of the building in two ways:

1. Users' opinions can help identify some "unspoken" problems correlated to their building that otherwise may be impossible to address, i.e. too many expenses for night garden lighting, or the malfunctioning of elevators that they often experience.
2. Users' behavior affects building energy performance, beyond efficiencies that can be gained through building renovation. In detail, training users can help to achieve larger energy savings.

From simulation results, the obtained energy needs for heating in the best case scenario corresponds to 16.03 kWh/m²year. The result is 30% lower than the expectations targeted for the project (25 kWh/m²year). Accordingly, the energy saved by renovating the building consistent with the pre-feasibility study corresponds to 102 kWh/m²year, thus obtaining a difference of 86.5%. The amount of saved CO₂ can be approximated to 354 tons (or 150 TEP), calculated using the National conversion factor of 0.44 tons of CO₂ (and 0.187 TEP) per MWh. Table 7 shows the prices of thermal energy (SEL, 2014), the thermal energy consumed and the relative annual expenses in both pre-renovation and post-renovation cases.

Table 7 - Annual heating costs: comparison

	Thermal energy price [€/kWh]	Thermal energy consumed [kWh]	Annual heating costs [€]
Baseline case	0.0651	930066.3	60547
Best case renovation	0.0651	146266.9	9521

From the listed values the annual economic saving in favor of tenants can be calculated, which comes to €51,000 per year.

However, in the worst-case scenario of unchanged users' behavior in terms of window opening, the building energy needs for heating is 291,700 kWh/year, which corresponds to 37.25 kWh/m²year. The result is 49% higher than the threshold needed to fulfill the project purposes, and the energy savings compared to the baseline case amount just to 81 kWh/m²year.

Fig. 3 depicts graphically the comparison in terms of annual energy needs for heating between the baseline model at the existing conditions (number 1) and the two renovated cases: best-case scenario (number 2) and worst one (number 3)

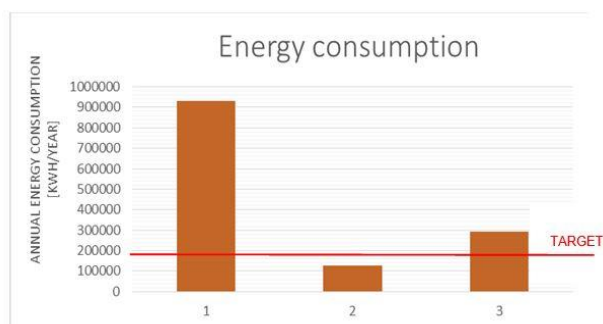


Fig. 3 – Energy needs for heating

4. Conclusion

In conclusion, the holistic method is a valid tool to start a holistic energy renovation, even though it could be further improved by also considering the urban context. The resulting outcome has been an extensive knowledge of building needs, problems and restrictions that, together, can form a solid baseline for further renovation stages. In particular, the main innovation of the method, i.e.,

the users' involvement, has been crucial to point out what their main habits and concerns can be (e.g., malfunctioning of the elevators), as well as their low level of knowledge about energy topics and low sense of ownership. On the other hand, the model design at the early stage of renovation project was an important part of preliminary documentation that, together with focus points, would become a system check for further design phases. The simulation energy modeling has been crucial to assess the building performance based on the investigations of the holistic method. The simulations showed that the building energy consumption can be reduced even more than the target if there is correct user behavior. They also allowed us to quantify the users' influence on the renovated building energy performance, showing that there exists a difference of 131% between the best and the worst scenarios. It was demonstrated, therefore, that the success of the renovation depends significantly on whether occupants accept the changes and modify their habits accordingly. To accomplish that, the suggestion is to take into consideration all highlighted issues, thus considering the building as a set of services at the users' disposal. In the case that interventions focus only on reducing the energy consumption, but do not contemplate elevators or garden lighting system, the refurbishment could be just partially successful because tenants will keep on complaining. In addition, if they do not take an active role in the renovation project and are not accurately informed about changes, they do not have the opportunity to know how to vary their own lifestyle and they can even lead to the project failure. Based on the results, it is possible to conclude that a recommended way to proceed regards not just a renovation of building parts but also a revision of occupants' habits.

5. Acknowledgement

The material of this paper was the subject of the master thesis entitled "Holistic method for energy retrofitting of buildings: application and analysis" written in collaboration between DTU – Technical University of Denmark and EURAC – European

academy of Bozen. The research was carried out in the framework of EU FP7 Smart cities and communities projects: SINFONIA.

References

- Carbon Trust, 2011. "Heat recovery: A guide to key systems and applications", Accessed November 4, 2014. http://www.carbontrust.com/media/31715/ctg057_heat_recovery.pdf
- Civiero P. 2012. "Approccio sostenibile al recupero dell'edilizia residenziale." *Hortus*. ISSN 2038-6095.
- Eriksen M. S., Rode C. 2013. "Method for Developing and Assessing Holistic Energy Renovation of Multi-storey Buildings." *In proc. Sustainable building, Munich, Germany, 2013*.
- EuroACE, 2014. "Renovate Europe - Energy Efficiency in Buildings." Accessed November 3, 2014. <http://www.euroace.org/LinkClick.aspx?fileticket=ecoJ1VICGzg%3D&tabid=40>
- Ferrante A., Semprini G. 2011. "Building energy retrofitting in urban areas". *In proc. International Conference on Green Buildings and Sustainable Cities, Bologna, Italy, 2011*.
- Hoes P., Hensen J.L.M., Loomans M.G., Vries B., Bourgeois D. 2009. "User behaviour in whole building simulation." *Energy and Buildings* Volume 41, Issue3: 295-302. doi:10.1016/j.enbuild.2008.09.008.
- Kashif A., Le X.H.B., Dugdale J., Ploix S., Bourgeois D. 2014. "Agent based framework to simulate inhabitants' behaviour in domestic settings for energy management." *In Proceedings of the 3rd International Conference on Agents and Artificial Intelligence, pages 190-199*
doi: 10.5220/0003150301900199
- Ma Z., Cooper P., Daly D., Ledo L. 2012. "Existing building retrofits: Methodology and state-of-the-art." *Energy and Buildings* Volume 55: 889-902, doi:10.1016/j.enbuild.2012.08.018
- Masoso, O.T., Grobler L.J. 2010. "The dark side of occupants' behaviour on building energy use." *Energy and Buildings* Volume 42, Issue 2: 173-177 doi:10.1016/j.enbuild.2009.08.009
- NRDC - Natural Resources Defense Council, 2014. "LEED for Neighborhood Development", Accessed October 6. <http://www.nrdc.org/cities/smartgrowth/leed.asp>
- Okeil A. 2010. "A holistic approach to energy efficient building forms." *Energy and Buildings* Volume 42, Issue 9: 1437-1444. doi:10.1016/j.enbuild.2010.03.013.
- Paiola L. 2014. "Blower door test". Accessed November 7. <http://www.ledenergy.it/pdf/121022-2313-Appuntamenti%20costruire%20qualit%C3%A0.pdf>
- Ratti C., Baker N., Steemers K. 2005. "Energy consumption and urban texture." *Energy and Buildings* Volume 37, issue 7: 762-776. doi:10.1016/j.enbuild.2004.10.010.
- SEL. 2014. "Tariffe Teleriscaldamento Bolzano - District heating tariffs Bolzano." Accessed July 11. <http://www.sel.bz.it/it/clienti/calore/teleriscaldamento-bolzano/tariffe.html>
- Xu X., Taylor J.E., Pisello A.L., Culligan P. 2012. "The impact of place-affiliation networks on energy conservation: A holistic model that integrates the influence of buildings, residents and the neighborhood context." *Energy and Buildings* 55 (2012): 637-646. <http://dx.doi.org/10.1016/j.enbuild.2012.09.013>

The role of user behavior modeling on the energy performance simulations

Marco Aldegheri – University of Trento – marco.aldegheri@hotmail.it

Alessandro Prada – Free University of Bozen/Bolzano – alessandro.prada@unibz.it

Paolo Baggio – University of Trento – paolo.baggio@unitn.it

Michela Chiogna – ITEA spa Trento – michela.chiogna@itea.tn.it

Abstract

Energy consumption strongly depends on the occupants' behavior for all types of buildings. However, the impact is greatly increased in high performance building, in which users can freely interact with the envelope system (opening windows and shading management) and with the HVAC control systems. The robustness of a design solution to suboptimal user's behaviors can thus become a distinguishing factor among different design alternatives.

One of the main issues regards the predictability of user choices and actions and its codification into a plausible simulating algorithm. Several strategies are presented in the literature, however energy modelers adopted to a large extent the schedule approach, to take into account users in energy simulations.

This paper describes two stochastic methods implemented in EnergyPlus to simulate the users' behaviors in managing opening surfaces and thermostat setpoint temperatures.

Using these methods, the impact of different user behavior on the energy performance of a multistory building is investigated. The aim of this work is to quantify the impact of users' behavior modeling on the results of dynamic energy simulations.

1. Introduction

After the coming into force of the European Directive EPBD on energy performance of building (European Commission, 2010), low energy consumption of buildings has become an important target to achieve and nearly zero energy buildings (nZEB) as well as comfort conditions are becoming essential requirements for the new generation buildings.

Nevertheless, sustainable and passive buildings, usually with a high level of thermal insulation, are subjected to a more active role of users' behavior (Hoes et al., 2009). Several studies in the literature compared energy consumption of identical buildings but subjected to different users. In these works, the ratio of the maximum over the minimum value is roughly in the range $1.2 \div 3$ (Fabi et al., 2012).

The role of users' behavior assumes significance especially in naturally vented buildings, where air change rates per hour (ACH) due to window opening by users can be up to 87% greater than the ACH measured during the non-occupied period (Iwashita and Akasaka, 1997).

Users' behavior has a particular significance for those constructions in which users can interact with the electric devices, shadings, lighting and HVAC system controls. In this way, occupants must be considered an integral and active part of the energy balance of a building, not limited to internal contributions due to their metabolic activity (Mahdavi, 2011). Scheduling occupancy is itself a source of uncertainty and its description could be dealt with non-probabilistic models rather than stochastic approaches (Mahdavi and Tahmasebi, 2015).

The base assumption in modeling occupancy interaction with the building is the adaptive comfort principle (Humphreys and Nicol, 1998). According to this approach, the occupant interacts with the HVAC and building envelope in order to restore the comfort conditions. Nonetheless, the parameters inducing users' interaction with the environment as well as the extent to which they

effectively manage their actions are not fully defined.

This study presents a comparison between two different models to take into account the users in building energy simulations.

The goal is to evaluate the stochastic distribution of results obtained from the user simulating approach and to compare it against the result provided by a scheduled approach, following the tailored rating simulation inputs according to the EN ISO 13790 standard (CEN, 2008). For this purpose, two user behavior models were implemented in EnergyPlus to simulate the users' behavior in managing opening surfaces and thermostat control setpoint. Additionally, the schedule approach proposed by the technical specification UNI/TS 11300 (UNI, 2008) was also adopted. The study focused on a new multistory residential building with a cross-laminated timber envelope (Xlam) built in Trento in 2013.

2. Models and simulations

2.1 Case of study

The construction (built in Trento - Italy in 2013) is a five-floor residential building composed of 14 residential units of various sizes.

The original structure is part of a residential complex composed of two twin dwellings.

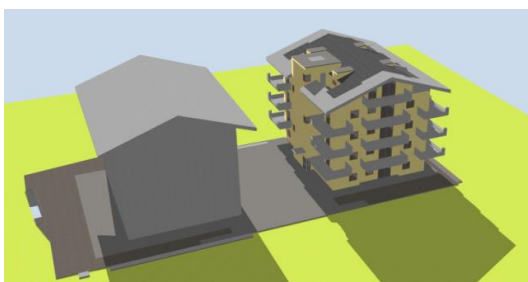


Fig. 1 – Model of the analyzed residential estate



Fig. 2 – Front view of the building (picture by ITEA s.p.a, 2014) and the geometric model used for numerical simulations

The southern building has a cross-laminated timber structure with a reinforced concrete stairwell and low emissivity windows. The northern building is identical except for a platform frame structure. The dwellings have a naturally ventilated wooden roof.

This study focused on the southern building, thus the north dwelling was modeled as an external obstruction. In the following table, the main parameters of the modeled envelope (transmittance and internal heat capacity) are reported.

Table 1 – Thermal transmittance (U value) and internal heat capacity (Cm) of the main envelope surfaces (* for Envelope walls the data refer to inner side; for Floors the data refers to the decking)

Surface type	U	Cm*
	Wm ² K ⁻¹	kJ m ² K ⁻¹
Envelope walls	Floor 0, 1	46.70
	Floor 2, 3, 4	27.50
	Floor 4, terrace side	51.28
Internal walls	Room-room	31.10
	Room-bathroom	34.70
	Room-common space	46.70
	Room-common space	46.70
	Flat-flat	36.50
	Semi-exposed	232.00
	Floors	Wood finishes semi-exposed
Ceramic finishes semi-exposed		188.48
Wood finishes internal		215.70
Ceramic finishes internal		232.98
Ceiling exposed terrace		13.75
Roof	Wooden naturally vented	81.07

The heating system is based on a centralized condensing boiler, with an outdoor reset control of the water supply temperature. The boiler produces the hot water that feeds the radiant floor systems. During the heating period, a mechanical ventilation system provides fresh air to the dwellings (with a lower threshold of 18°C for the supply air temperature). However, the occupants

can freely interact with the envelope by opening and closing the windows. The ambient temperature controllers are set to the constant value of 20°C during occupied time, with a setback temperature of 16°C. The infiltration and ventilation leakages have been modeled by means of the airflow network.

The building has been modeled with the dynamic simulation engine EnergyPlus 8.1 in which two calculation methods were implemented: a Standard Input Model (SIM) and a Stochastic Advanced Model (SAM). In the SIM approach the internal gains, the ventilation rates and the occupancy schedules are defined according to the standard EN ISO 13790 (CEN, 2008) and to the technical specification UNI/TS 11300 (UNI, 2008). The following tables summarize the scheduled internal lumped gains and heating radiant plant timesheet related to zone occupancy.

Table 2 – Internal gains profile in SIM model (CEN, 2008)

Days	Hours	Living Room plus kitchen	Other conditioned areas
		$(\varphi_{int,Oc} + \varphi_{int,A}) / A_f$	$(\varphi_{int,Oc} + \varphi_{int,A}) / A_f$
		W/m ²	W/m ²
Monday-Friday	07:00-17:00	8.0	1.0
	17:00-23:00	20.0	1.0
	23:00-07:00	2.0	6.0
	Average	9.0	2.67
Saturday-Sunday	07:00-17:00	8.0	2.0
	17:00-23:00	20.0	4.0
	23:00-07:00	2.0	6.0
	Average	9.0	3.83
Average		9.0	3.0

Table 3 – Hourly thermostat setting in SIM model

Days	Hours	Living Area	Sleeping Area
Monday-Sunday	07:00-17:00	Setpoint	Setback
	17:00-23:00	Setpoint	Setback
	23:00-07:00	Setback	Setpoint

In the SAM method, the user’s behavior was implemented through a stochastic algorithm while internal gains and schedules are defined with an occupant-tailored approach. The daily mean internal gain rate due to lighting system, electric devices and occupancy presence are equivalent in the two models.

2.2 Stochastic Advanced Model (SAM)

The SAM model simulates the user stochastic control of both the window opening and the adjustment of the thermostat setpoint temperature. The simulating process is obtained combining a series of sensors, programs and actuators organized to control independently each single zone and opening. These programs were implemented in EnergyPlus via the Energy Management System (EMS) module.

2.2.1 Windows Opening control algorithm

Humphreys’ stochastic control algorithm (Humphreys and Nicol, 1998) was modeled to simulate user managing of the windows. The control system manages the window open factor, which, in our model, can be set to 0 or 1 with the hypothesis of a fully closed/open window. The algorithm can be summarized in the following steps:

1) The daily mean values of outdoor running temperature (T_{rm}) were calculated according to the relation provided by the standard EN 15251 (CEN, 2007) and based on the previous 20 days as follow:

$$T_{rm} = (1-\alpha) \cdot \{\Theta_{ed-1} + \alpha \cdot \Theta_{ed-2} + \alpha^2 \cdot \Theta_{ed-3} + \dots\}$$
 (1)
 where Θ_{ed-1} is the daily mean outdoor air temperature of the "i-th" day before the current day of calculus and the constant parameter α assumes the suggested value of 0.8.

2) A comfort temperature has been derived from the previous step, according to the relations proposed by Rijal et al., 2007.

$$\text{if } T_{rm} > 10^\circ\text{C} : T_{comf} = 0.33 \cdot T_{rm} + 18.8^\circ\text{C}$$
 (2)

$$\text{if } T_{rm} \leq 10^\circ\text{C} : T_{comf} = 0.09 \cdot T_{rm} + 22.6^\circ\text{C}$$
 (3)

3) The comfort temperature has been used to define a 4 K wide comfort band, whose limits are defined increasing and decreasing the comfort

temperature by 2 K. In this way, it is possible to define for each timestep whether the zone operative temperature, T_{op} , belongs to the comfort range and, consequently, the users are in a comfort condition. Otherwise, if the zone operative temperature is outside the comfort zone, a discomfort condition of cold/heat arises.

4) When the zone operative temperature is outside the comfort band, a certain probability (p_w) to open (if $T_{op} > T_{comf} + 2$ K) or close (if $T_{op} < T_{comf} - 2$ K) the windows is calculated by the following empirical equation proposed by Rijal et al., 2007.

$$\text{logit}(p_w) = 0.171 \cdot T_{op} + 0.166 \cdot T_{out} - 6.4 \text{ K} \quad (4)$$

$$\text{logit}(p_w) = \ln [p_w / (1 - p_w)] \quad (5)$$

5) The probability, p_w , is compared with a pseudo random generated number between 0 and 1, $p_{w,lim}$, to define if a zone window is effectively opened or closed. If p_w is greater than $p_{w,lim}$, the T_{op} is greater than $T_{comf} + 2$ K and the window is closed, then its open factor is changed from the value of 0 to 1. If p_w is less than $p_{w,lim}$, the T_{op} is less than $T_{comf} - 2$ K and the window is open, then its open factor changes from the value of 1 to 0. In the other cases, the value of the open factor is not changed.

6) A minimum ventilation rate for sanitary purposes was set in addition to the Humphreys behavioral algorithm. In agreement with the hypothesis according to which the windows are open for 1% of the time, a rule that provides for the opening of the windows if they had been closed for the previous 8 hours was implemented. Once the window was open, its control falls within the provision of the Humphreys algorithm. Window control is performed only during the occupied hours and the value of the open factor during the unoccupied time is set to 0. Window control is performed with a frequency of 10 time steps per hour.

2.2.2 Temperature controller algorithm

The setpoint control algorithm, developed in this paper, is inspired by the Fanger comfort formulation. The user's control on the heating system is simulated with the possibility to increase or decrease the setpoint temperature by a pseudo

random numbers of degrees and in relation with defined conditions. The simulating system works under certain main hypothesis:

1) The setpoint modification is permitted between 6:00AM and 11:00PM (avoiding non-realistic temperature controller adjustments during night sleep-time) and only during the occupied period;

2) The increment (or decrement) of the temperature setpoint is kept for 1 hour from the moment of the setting (emulating the "party or saving mode" available for many temperature controllers);

3) The increment (or decrement) of the temperature setpoint is available no more than once every 2 hours.

The following points explain the main steps of the algorithm:

1) The metabolic rate and clothing level are evaluated at each timestep using some coefficients to emulate the different thermal perception:

1.1) a random variation of $\pm 10\%$ from the original value is adopted for the metabolic rate.

$$\text{Met}_{STO} = \text{Met}_{DET} \pm 10\% \quad (6)$$

1.2) the clothing level, Clo_{DET} , is randomly changed by a coefficient (m_{clo}) in the range $0.9 \div 1.5$, when a value of $\text{Clo}_{DET} = 1$ is adopted (wintertime), or $0.6 \div 1.9$, when a value of $\text{Clo}_{DET} = 0.5$ is adopted (summertime). These values are derived from the standard EN ISO 9920 (CEN, 2009) indications.

$$\text{Clo}_{STO} = m_{clo} \cdot \text{Clo}_{DET} \quad (7)$$

2) Since the setpoint adjustment is not a certain event, a probability of the event should be defined. The proposed algorithm assumes the value of percentage of dissatisfied users, PPD, as the probability of setpoint temperature change, P_t , for a defined thermal zone. The temperature controller adjustment is defined by comparing the value of this probability, P_t , with a random number, $P_{t,lim}$, generated by a pseudo random uniform distribution. If the action probability, P_t , is greater than the random generated value, $P_{t,lim}$, the change of the setpoint temperature is actually performed.

Otherwise, the setpoint temperature is not changed. The potential setpoint temperature change (the comparison between P_t and $P_{t,lim}$), is applied with an hourly timestep.

3) The sign of the PMV in each thermal zone is used to define the type of potential action on the temperature controller for a zone (temperature increase or decrease). A positive PMV indicates a perception of "warm", thus the temperature adjustment will be negative (a decrement). A negative PMV implies the increment of the setpoint temperature while the PMV equal to zero implies no variation. If the potential action on the temperature controller is actually performed ($P_t > P_{t,lim}$), the absolute value of the increment/decrement is chosen generating a random integer number between (1-3) K using a uniform distribution.

2.3 Standard Input Model (SIM)

The implemented Standard input model is based on standard input provided by the EN ISO 13790 (CEN, 2008) and by the technical specification UNI/TS 11300 (UNI, 2008). It includes scheduled profiles regarding occupancy, internal gains and ventilation rates (both infiltration and ventilation). The following table summarizes the main differences between the two calculation methods.

Table 4 – Natural ventilation and setpoint temperature in SAM and SIM

		SAM	SIM
Natural ventilation	From opening windows	Humphreys Algorithm	Scheduled 0.3 ACH
	Infiltration	Airflow Network	
Setpoint thermostat temperature		Stochastic Algorithm	Constant

2.4 Evaluation of Robustness

The effect of user behavior can be quantified by observing the standard deviation, σ , and the ratio of the maximum over the minimum value of annual energy consumption. In order to make a comparison between the robustness of different models, the use of a robustness index is proposed. The robustness index signals the sensitivity of the building energy performance with respect to

occupants' behavior. The robustness index is the reciprocal of the non-dimensional coefficient of variation for the stochastic data set:

$$i = \sigma^{-1} = \mu / \sigma \tag{8}$$

The numerical quantification of robustness is deeply related to the stochastic simulation model and the choice of a realistic simulation algorithm is of primary importance.

3. Results and Discussions

The hourly simulation was recursively run with different seed in the pseudo random generation in order to model different users' behaviors. The annual and monthly energy performance (EP) was computed for each of the 90 runs, starting from the hourly energy consumption of the heating and ventilation systems.

3.1 Annual energy consumption

The first result deals with the dispersion of the building annual EP caused by user behavior (Fig. 3). The interactions of the occupants with the thermostats and the windows opening induce a variability of the annual energy performance roughly equal to $\pm 1 \text{ kWh m}^{-2} \text{ y}^{-1}$ with respect to the mean value that means $\pm 950 \text{ kWh y}^{-1}$.

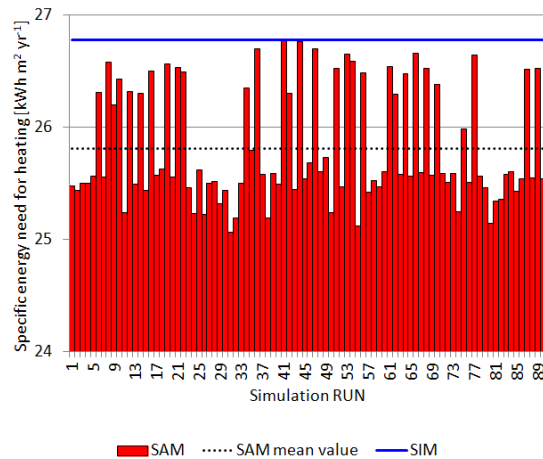


Fig. 3 – Distribution of annual EP of the building.

It should be stressed that this result has been obtained by considering independent user behaviors for each room of the building. This means that the variability of the EP takes into account the offsetting between virtuous and

negative behaviors. Hence, the results do not represent a quantification of the maximum variation of the EP and, consequently, it is not a quantification of the maximum risk of an incorrect assessment of the energy label of the building. The graph in Fig. 3 highlights the sensitivity of the building to user behavior. Table 5 summarizes the output data values for SIM and SAM.

Table 5 – Simulation results

SAM data values	
MAX Yearly EP	26.77 [kWh m ⁻² y ⁻¹]
MIN Yearly EP	25.06 [kWh m ⁻² y ⁻¹]
MAX/MIN Ration	1.07 [-]
μ Yearly mean value	25.81 [kWh m ⁻² y ⁻¹]
σ Standard deviation	0.508 [kWh m ⁻² y ⁻¹]
SIM data values	
Yearly EP	26.78 [kWh m ⁻² y ⁻¹]
Evaluation of robustness	
σ* = σ/μ	0.020 [-]
Robustness Index	50.826 [-]

The SIM and SAM models show similar results in terms of yearly energy consumption (the difference is roughly equal to 3.6%). The SAM model shows a lower energy consumption from 0.02% up to 6.41% if compared with the SIM model result. This result seems to indicate that the scheduled approach, according to the aforementioned technical standard, gives precautionary resultant energy consumption. Some conclusions on the sensitivity of the building can be drawn by analyzing the distribution of the results of the SAM model. The standard deviation, σ, assumes the value of 0.5 kWh m⁻² y⁻¹, and the ratio of the maximum over the minimum value is 1.07.

The robustness index for the analyzed building, according to (8), are reported in Table 5.

3.2 Monthly energy consumption

The analysis on the distribution of monthly energy needs gives information about the different sensitivity of the building to the user’s behavior. In order to compare the distributions of monthly EP, the deviation of each simulation run of the SAM is normalized in relation to the mean value.

The graph in figure 4 shows the distribution of the normalized EP deviation obtained in February. Notice that the EP deviation is distributed according to a Gaussian distribution. The graph also highlights as the deviations are in the range of ±2.5 % around the mean EP. The limited percentage variation is closely related to the external air temperature. The cold external air in winter months greatly decreases the number and duration of windows opening by users.

Besides, this result stresses the role of the insulated envelope and of the correct energy system design in increasing the indoor thermal comfort. Thus, the number of setpoint adjustments by users is limited in the hourly energy simulations due to the low number of dissatisfied ones.

The shape of the distribution of monthly EP deviations is different for intermediate and warmer months. For instance, Figure 5 shows the distributions obtained in March. Note that the variance increases from 0.57 in February to 1.92 in March.

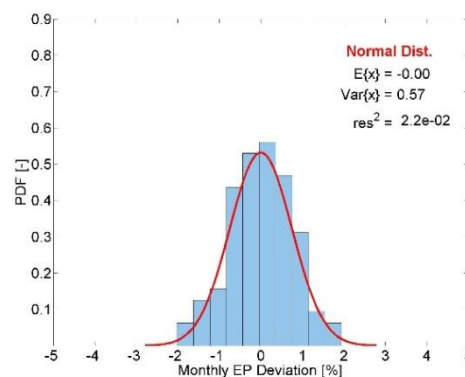


Fig. 4 – Distribution of February EP deviation caused by occupants

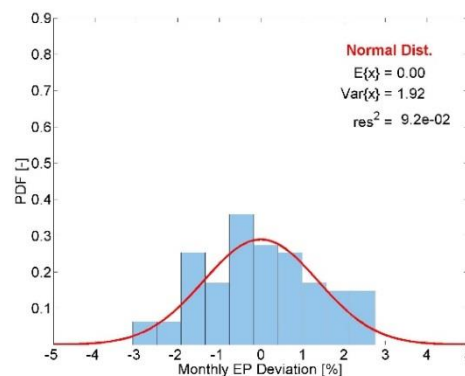


Fig. 5 – Distribution of March EP deviation caused by occupants

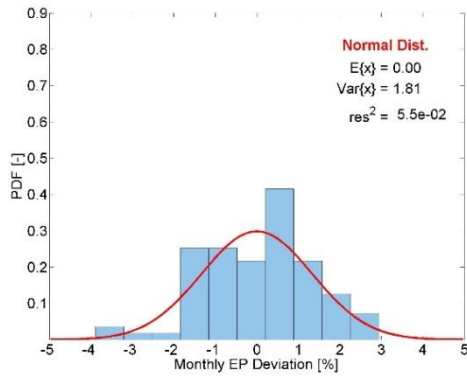


Fig. 6 – Distribution of April EP deviation caused by occupants

Therefore, the Gaussian distribution, which approximates the distribution of experimental data, demonstrates a greater dispersion of results around the mean value. In this case, the EP of the SAM runs are distributed around $\pm 3.7\%$ of the mean values. The distances increase up to $\pm 5\%$ at the beginning and ending of the heating season, i.e. in October and April.

These results highlight the greater impact on the EP variation of the window opening effect with respect to the setpoint adjustment. In fact, the data dispersion increases with a lower difference between internal and external temperatures. The behavior would be the opposite if the contribution due to the setpoint adjustment were larger than dispersions for ventilation.

The higher data dispersion in temperate months is linked to the intermittent operation of the energy systems that decrease the system efficiency. In fact, the manual window opening by occupants often induces the activation of the heating system. Probably, the use of a more sophisticated control of the setpoint temperature would ensure a greater sturdiness of the building in these months.

4. Conclusion

This study investigates the extent to which user behavior affects the predicted energy performance of a multistory building. For this purpose, a stochastic algorithm simulating the user's interaction with the temperature controller setpoint and the windows opening was implemented in

EnergyPlus through the Energy Management System sensors and rules.

For the test case, the average EP predicted by means of the stochastic method is about 3.6% lower than the EP obtained using scheduled ventilation rate and thermostats setpoints. The two methods therefore show a good agreement when the same daily average is used.

The randomness of user behaviors causes a variability of annual EP roughly equal to $\pm 1\%$ around the mean values. This limited variation is linked to the stochastic nature of the model. Virtuous user behaviors in some rooms or in some periods balance out the increase in energy demand caused by some negative effects from occupant behavior. In fact, the results show how the behavior of the occupants tends to affect much more the forecasts of consumption over limited periods of time, such as a monthly time base.

5. Acknowledgement

The authors want to thank ITEA s.p.a for the financial support and the fruitful collaboration in sharing data.

6. Nomenclature

Subscripts/Superscripts

clo	of clothing
DET	defined in a deterministic approach
i	current day of calculus
lim	Limit
STO	Stochastic
t	of thermostat management
w	of window management

Symbols

A	coefficient (-)
Clo _{DET}	clothing level (clo)
Clo _{STO}	clothing level (clo)
i	robustness index (-)
μ	mean value
m _{clo}	clothing coefficient (-)
Met _{DET}	metabolic rate (W)
Met _{STO}	metabolic rate (W)

PMV	predicted mean vote (-)
PPD	predicted percentage of dissatisfied (%)
p_t	probability of setpoint temperature change (%)
$p_{t,lim}$	limit probability of setpoint temperature change (%)
p_w	probability of open windows (%)
$p_{w,lim}$	limit probability of open windows (%)
σ	standard deviation
σ^*	coefficient of variation
T_{comf}	comfort temperature (°C)
T_{op}	operative temperature (°C)
T_{out}	site outdoor drybulb temperature (°C)
T_{rm}	daily running mean temperature (°C)
Θ_{ed}	site outdoor daily mean drybulb temperature (°C)

References

- CEN. 2007. "Indoor environmental input parameters for design and assessment of energy performance of buildings addressing indoor air quality, thermal environment, lighting and acoustics." *European Standard EN 15251:2007*.
- CEN. 2008. "Energy performance of buildings - Calculation of energy use for space heating and cooling." *European Standard EN ISO 13790:2008*.
- CEN. 2009. "Ergonomics of the thermal environment - Estimation of thermal insulation and water vapour resistance of a clothing ensemble" *European Standard EN ISO 9920:2009*.
- European Commission. 2010. "Directive 2010/31/EU of the European Parliament and of the Council of 19 May 2010 on the energy performance of buildings (recast)." *Official Journal of European Union* 153 (2010): 13–35.
- V. Fabi, R.V. Andersen, S. Corgnati, B.W. Olesen. 2012. "Occupants' window opening behaviour: A literature review of factors influencing occupant behaviour and models." *Building and Environment* 58 (2012): 188–198.
- P. Hoes, J.L.M. Hensen, M. Loomans, B. de Vries, D. Bourgeois. 2009. "User behavior in whole building simulation." *Energy and Buildings* 41 (2009): 295–302.
- M. Humphreys, J. Nicol. 1998. "Understanding the adaptive approach to thermal comfort." *ASHRAE Transactions* 104 (1) (1998): 991–1004.
- G. Iwashita, H. Akasaka. 1997. "The effects of human behavior on natural ventilation rate and indoor environment in summer - A field study in southern Japan." *Energy and Buildings* 25 (1997): 195–205.
- A. Mahdavi. 2011. "People in building performance simulation." In *Building Performance Simulation for Design and Operation*, edited by J. Hensen and R. Lambert, 56–83, Spon Press.
- A. Mahdavi, F. Tahmasebi. 2015. "Predicting people's presence in buildings: An empirically based model performance analysis." *Energy and Buildings* 86 (2015): 349–355.
- H.B. Rijal, P. Tuohy, M.A. Humphreys, J.F. Nicol, A. Samuel, J. Clarke. 2007. "Using results from field surveys to predict the effect of open windows on thermal comfort and energy use in buildings." *Energy and Buildings* 39 (2007): 823–836.
- UNI. 2008. "Energy performance of buildings – Part 1: Evaluation of energy need for space heating and cooling." *Italian Technical Specification UNI/TS 11300-1*.

Application of Building Simulation to support ISO 50001 Energy Management: Case study of Fiumicino Airport.

Luis M. Blanes – National University of Ireland Galway. Ryan Institute. – luis.blanes@nuigalway.ie

Andrea Costa – National University of Ireland Galway. Ryan Institute. – andrea.costa@nuigalway.ie

Marcus M. Keane – National University of Ireland Galway – Ryan Institute.- marcus.keane@nuigalway.ie

Abstract

In this paper we describe how simulation is used to support HVAC operational strategies within the context of the CASCADE project: a comprehensive platform that integrates Fault Detection and Diagnosis (FDD) techniques into an Energy Management System (EMS) that follows ISO-50001 guidelines. The CASCADE solution is conceived as an on-line application that combines a number of data intensive services using the internet as a data exchange medium. Among these services are an ontology-driven database, FDD engines, front-end visualization software and energy management tools. The project constantly monitors HVAC data and executes FDD routines that translate to specific actions rendered by the EMS software. The project is currently being implemented in two main EU airports: Rome Fiumicino (FCO) and Milan Malpensa (MXP). The ultimate intent of this research is to explore Whole Building Performance Simulation (WBPS) as a potential service to be integrated within the overall CASCADE solution. From a facility management perspective, models are commonly used as a test-bed to assess energy conservation measures before their implementation, to provide a fault free reference for recommissioning and a baseline for measurement and verification purposes. This theoretical perspective is confronted in this paper with the practical experience and lessons learned from one of the project's demonstrator buildings.

We describe the development of a WBPS model of the Terminal 1 of FCO airport. Large open space building types such as airport terminals pose some difficulties to be reflected as building models. Additionally the CASCADE data acquisition platform provides an uncommonly fine grained and highly detailed data set of the HVAC equipment representing a challenge to be used during the calibration process. The issues encountered

during the simulation and calibration stages are reported. Furthermore, old buildings such as airport terminals can actually suffer from substantial interventions that make them perform very differently from their design intent, as is the case in this demonstrator. In these circumstances, modelling strategies need to be reformulated to account for modifications and to reflect diverse operative conditions and major changeovers. In this sense, the model is also formulated as a tool to indicate a pathway for recommissioning of inefficient HVAC systems.

1. Introduction

Energy consumed in buildings represents between 20% and 40% of the total global energy consumption in developed countries. It is also estimated that HVAC equipment accounts for 50% of the energy consumption in buildings (Perez-Lombard et al., 2008). HVAC systems are among the more energy intensive users within buildings and also among the worst performers due to unnoticed faults, improper maintenance or wrong operational settings. HVAC inefficiencies are estimated to range between 20% and 30% (IEA, 2002). This scenario represents a huge opportunity for the implementation of Energy Conservation Measures (ECMs) where data monitoring, FDD and WBPS can play a major role. Significant effort is put in place regarding simulation to support design and analysis during the design phase of buildings. The operational efficiency and the commissioning aspects are still applications of building simulation that need to be further developed to facilitate its wider adoption.

2. Case Study: Rome Airport. (FCO)

The building modelled is Terminal 1 at Fiumicino Rome Airport (Latitude 41.8° North, Longitude 12.23° East). This building was first opened in 1961 and it is an open space concourse terminal of approximately 35,000 m² of floor area. An aerial view of this building is shown in Figure 1. The building geometry and construction model was developed using Design Builder® and is shown in Figure 2. This model was then exported to Energy+ (E+). Other tools like Simergy were also used to generate the HVAC models. Further model development, calibration and results were managed straightforward using E+ tools. Broadly speaking, the building is divided in two floors: (1) the ground floor is used for arrivals. Its internal height varies from 3.3 m to 4.55 m, and (2) the first floor which is the main concourse, dedicated to departures, with an average height of 14.5 m, therefore being an space with a huge air volume to be conditioned. These spaces are used for circulation and waiting areas, including ancillary spaces for offices, commerce and restaurants. Materials, thicknesses and thermal properties of the building envelope were estimated from design information and confirmed in site visits.

2.1 Thermal zoning

Airport terminals are conceived as big open spaces and represent a challenge when it comes to thermal zoning, as the open areas communicate between themselves and the same air is treated by several Air Handling Units (AHUs). This layout cannot be modelled in software tools such as E+ where the maximum HVAC Air Loops per thermal zone is only one and the loop models use HVAC air loop continuity as a main assumption. Subdivision of zones mirroring air distribution equipment is also difficult, as the real equipment is often the result of successive modifications or follows an uneven layout. A solution would be to subdivide the spaces following the AHUs layout and then estimate air exchange between zones. To apply this air exchange assumption we can use: (1) Air mixing statements, (2) Cross mixing statements, (3) Zone network, (4) Air network model with CONTAM, or more complex (5) CFD models.

Finally, the air exchange between zones was not modelled but air extraction in kitchens and toilet areas was considered. In further developments, some of these alternatives will be tested to quantify the model sensitivity to air exchange between zones.

2.2 Internal Loads

The criteria used in this model is to break down building zones according to AHU and aggregate the different loads (restoration, commercial, boarding desks, open spaces, etc.) in a global total for the zone served by the same AHU. Occupancy data was estimated based on two data sources: (1) past statistics and passengers forecast providing yearly and monthly figures (ENAC, 2011), (ENAC, 2013) and (2) daily profiles for significant days through the year using flight databases (Flightstats Inc., 2014). Flight occupancy was calculated using the Passenger Occupancy Rate (Load Factor) of 80.4 % (IATA, 2013). Occupancy times were estimated in 30' onwards for arrivals and 90' backwards for departures, similarly as described by Parker in the UK (Parker et al., 2011). Different profiles were used for weekdays and weekends, accounting also for significant bank holidays.



Fig. 1 – Aerial view of the FCO Terminal Airport

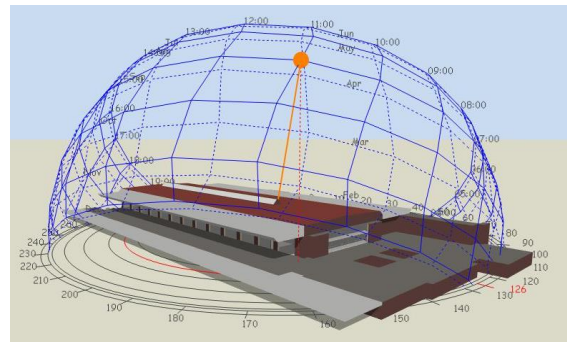


Fig. 2 – Model of the FCO Terminal Airport

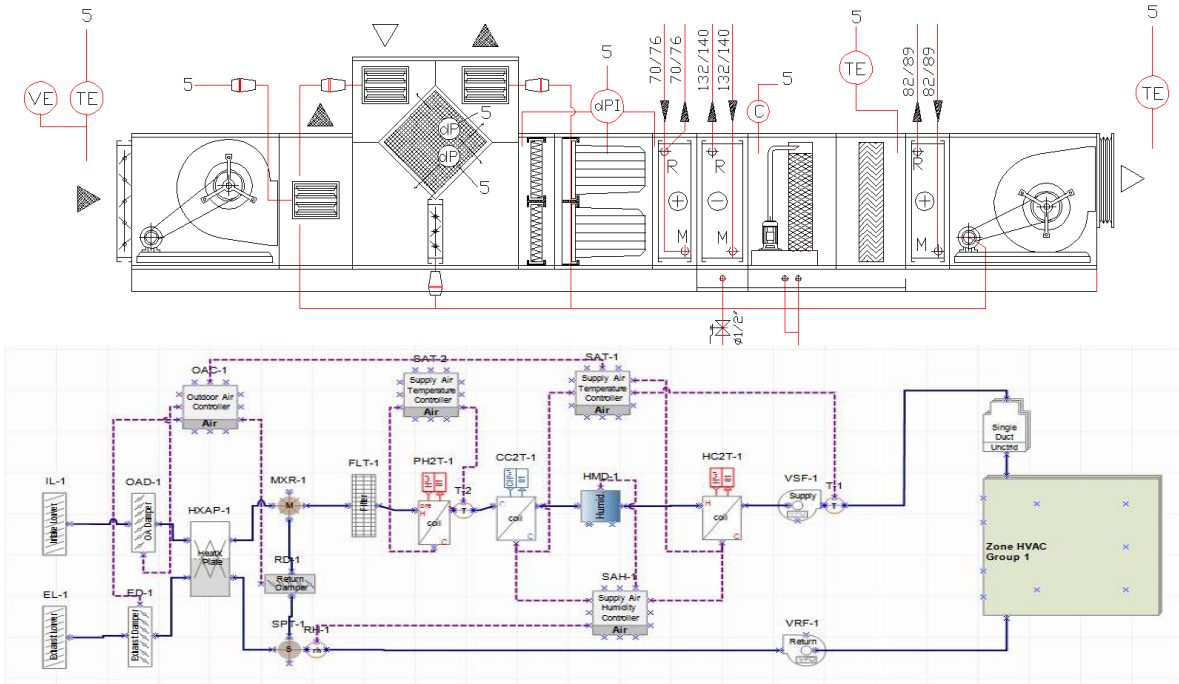


Fig. 3 – Actual (up) and modelled (down) schematic of the Air Handling Unit.

2.3 HVAC Model

The AHUs modelled are AHU No. 1, AHU No. 5, AHU No. 6 and AHU No. 11. These units are all serving thermal zones in the arrivals hall of the terminal at +1.00 m level (ground floor). Units show the following arrangement (see Figure 3): *Thermal Zone* → Exhaust Fan → Mixing Box → Filters → PreHeating Coil → Cooling Coil → Humidifier → Post Heating Coil → Supply Fan → *Thermal Zone*. The rest of the heating and cooling plant equipment has been idealized as district heating and cooling equipment. The AHUs are of Variable Air Volume with constant pressure setpoint.

2.4 HVAC Data analysis

HVAC data for calibration and analysis were retrieved using the CASCADE data acquisition platform. The data comprises more than 1060 data points along Terminal 1 systems, subsystems and components, among them: 11 AHUs, hydronic circuits, cooling towers and heat rejection groups. Data gathered included existing BMS sensed data and data gathered by additional sensors. Two AHUs were selected to install a high degree of instrumentation, these are AHU No. 1 and AHU No. 6. In these units, the additional sensors included water flow and temperature meters.

Analysis of the retrieved data was performed before the calibration process and resulted in a productive activity leading to the detection of a number of faults. These divergences are summarized in Table 1. The differences between design and actual values will be taken into account in the recommissioning described in Section 4. As it can be seen in Table 1, the supply fan (nominal power 75 kW) is actually functioning below its rated power at a 60 kW to 63 kW regime. While this could be reasonable, the return fan (nominal power 55 kW) is functioning at a considerable lower power rate of 13 kW to 14 kW. This difference may be due to faulty sensors, pressure anomalies or fan problems and needs further investigation. Figure 4 shows the fans' energy consumption revealing the difference between these two fans. The Pre-Heating Coil (PHC) was not in operation during the whole period and so there was no data available to consider. The Cooling Coil (CC) data revealed that although the water temperature differences were in the range of design intent (6 °C supply and 14 °C return), the power delivered was significantly (half) lower than the rated of 556 kW. This can be due to a low air flow or to an oversized coil.

Table 1 – AHU No. 1: Components Design and Actual parameters. (a) refers to actual data, (b)

means estimated and (c) that design or generic values have been considered as input.

AHU No. 1 Components	Variable (Units)	Design Value	Actual Value
Supply Fan	m ³ /h	55,000	N/A (c)
	Pa	1,200	N/A (c)
	kW	75	60 to 66 (a)
Mixing Box Exhaust	min m ³ /h	16,200	N/A (c)
	max m ³ /h	55,000	N/A (c)
Mixing Box Recirculated	min m ³ /h	0	N/A (c)
	max m ³ /h	38,800	N/A (c)
Mixing Box Fresh Air	min m ³ /h	26,000	N/A (c)
	max m ³ /h	64,800	N/A (c)
PHC	Power (kW)	216	N/A (c)
	Temp (°C)	80/70	N/A (c)
	W.Flow (l/s)	NA	N/A (c)
CC	Power (kW)	556	0 to 270 (a)
	Temp (°C)	6/14	6 to 10/ 10 to 20 (a)
	W.Flow (l/s)	NA	45 to 60 (a)
Humidifier	Pump (kW)	see footnote ¹	
HC	kW	255	0 to 150 (a)
	Temp (°C)	80/65	50 to 60/ 20 to 30 (a)
	W.Flow (l/s)	NA	0 to 10 (a)
Return Fan	m ³ /h	64,800	N/A (c)
	Pa	1,400	900(a)
	kW	55	13 to 14 (a)

The Heating Coil (HC) also operates at a lower energy rate than its nominal power of 255 kW, although as opposed to the Cooling Coil, the water temperature rate is quite different from the

intended design, which is also confirmed by the low water flow rate. This suggests a flow problem in that component. The supply and return temperatures are much lower than expected, and the difference between them is more than 40°C in some cases, which is very high in comparison with 15°C of the design specifications. This can be due to a very high flow rate and needs further investigation. Other differences cannot be precisely investigated requiring more profound e.g., air flow rates. Some other issues are very difficult to analyse as is the case of setpoints values and mixing box operation, due to control logics hidden by BMS internal operation. These differences between design parameters and actual parameters demonstrate that calibrating detailed white box WBPS models can be an arduous experience.

3. Calibration plan

The calibration process is based on previous work by Raftery (Raftery et al., 2012), and Mustafaraj (Mustafaraj et al., 2012). The calibration method used is performed by analysing and varying a set of input values iteratively to meet calibration criteria. Control version repository software and sub-hourly data gathered using the CASCADE platform were used. Input variation stands on confirmed information regarding the actual building that differs from usual default values. The information sources were: (1) design intent documents, (2) information obtained during site visits, and (3) fine grained data coming from the CASCADE platform that can be gathered at time steps as short as 5 minutes. The selection of the output variables for calibration supports the main intent of this model, which is to assist with the quantification of energy savings due to ECMs related to HVAC operation. Therefore, calibration focused on the targeted HVAC systems considering their main energy consumption variables, in this case: Supply and Return Fan Power Energy (kW); Preheating Coil Power Energy (kW); Cooling Coil Power Energy (kW); Heating Coil Power Energy (kW).

¹ The AHUs humidifier were disconnected thus disabled in the model

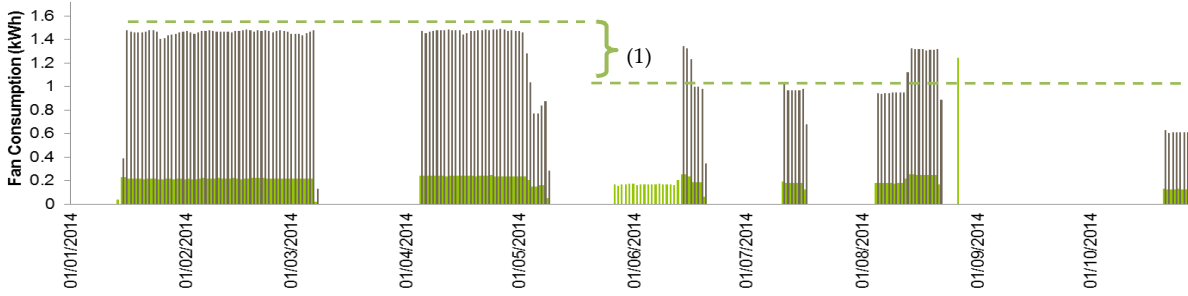


Fig. 4 – Actual AHU No. 1 Supply (Black) and return (Green) Fan Energy Daily Power Consumption for 2014. (1) Difference due to ECMs: Lower constant pressure setpoint and night setback.

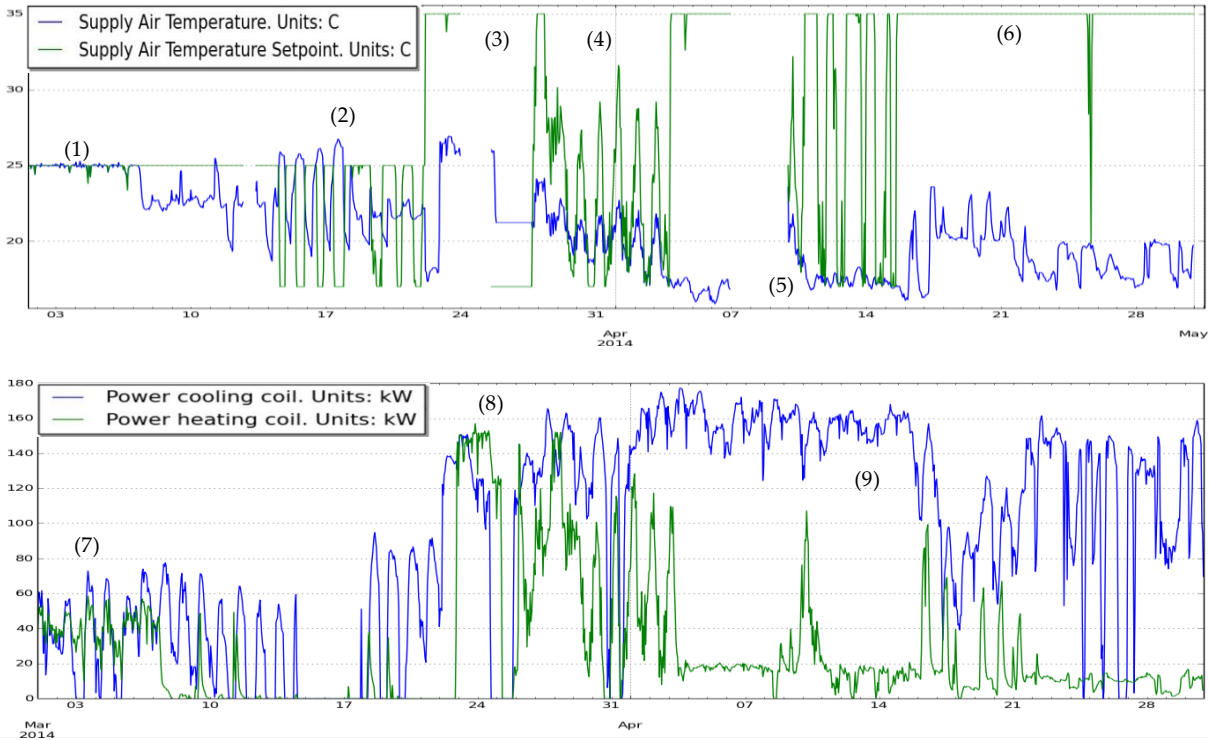


Fig. 5 – Up: Supply air temperature (blue) and setpoint (green). Down: HC (green) and CC (blue) power for March and April of 2014. (1) Shows an stable and tight control of supply air temperature. (2) Shows introduction of night setback. (3) Shows a setpoint of 35 °C that is not met. (4) In this period the setpoint varies and is not met. (5) Data gaps. (6) High setpoint value not met. (7) Simultaneous heating and cooling. (8) High spike on heating energy consumption linked with (3). (9) Shows apparently stable cooling coil in operation, residual heating energy consumption and no relationship with the setpoint for the same period.

The calibration of the fan electrical consumption was a relatively easy task due to the fans working at a constant regime. The adjustments were made to fan and fan motor efficiency parameters. For the calibration of the Heating and Cooling coils, as mentioned previously, data revealed a very different behaviour than nominal values. Different versions of the AHU using actual measured HC and CC (see Table 1) were tested but results were inconsistent with other variables such as water flow, water temperatures and setpoints. Finally, advice was given on how to solve these problems and nominal values were used for the ECMs study

that follows and savings were indicated in percentages from the baseline. Other issues such as the humidifier not working were reflected in the final model as it was easy to configure by setting an availability manager to constantly off. The development of white box WBPS models encompassing large quantities of parameters to adjust is a time consuming and sometimes unproductive activity. Regarding the period of calibration, a full 8760 hour data set is needed for an accurate calibration as defined by ASHRAE guideline 14 (ASHRAE 2002). It was difficult to carry out a thorough calibration procedure as

required by this guideline. The most remarkable issues detected were:

1. Numerous data gaps and incomplete 8760 h data set makes it difficult to comply with a whole year extent calibration;
2. Highly arbitrary air supply setpoint temperature. As can be seen in Figure 5, during the 2014 period, some periods show a tight control of the supply air temperature, others show very high temperatures (35 °C) and others a very unstable and probably a calculated varying setpoint. Some of the modifications are due to ad-hoc changes made by personnel;
3. Control sequences are not known. This means that the control sequences that coordinate heating and cooling coil valves can be difficult to simulate. Mixing box sequence is not known and this can result in unrealistic modelling assumptions;
4. A high difference between Supply and Return fan power consumption, which can be due to pressure or fan problems. This issue has to be confirmed further in order to recalibrate the simulation and use adequate inputs for the fans;
5. Differences between rated power and actual performance of CC and HC. This can be due to faults, e.g.: fouling, stuck valves, faulty sensors. These faults are difficult to be reproduced accurately in a simulation;
6. Simultaneous heating and cooling happening in November 2014;
7. Variable Air Volume (VAV) air loops working as Constant Air Volume (CAV).

As mentioned by Coakley (Coakley et al., 2014), calibrating WBPS models is an over-specified and undetermined problem. This statement is confirmed in this case study. A way of solving this problem would be to use component based inverse modelling or use BMS data as inputs. Nevertheless, advice was given on how to fix the

known problems with the units and the model was used as a stable baseline to explore known problems regarding HVAC operation and to assess the impact of different ECMs.

4. AHU Recommissioning pathway

In this section, we show the recommissioning pathway proposed for the AHU No.1 based on problems encountered during the modelling phase. This sequence is based on the calculated impact of the different faults simulated, being the first the one with the most impact. A finer analysis would consider a cross scenario of the ECMs proposed where the combined effect of the different ECMs can be assessed. At the current stage, only fan consumption is reported. Further analysis will include impact on heating and cooling coils. A summary of the ECMs simulated impact is shown in Figure 6 and the same figures have been translated on per cent of energy saving with respect to the baseline. The strategies are the following:

1. Baseline (CAV)
2. VAV operation
3. 2 + Supply Air Temperature optimization
4. 3 + Night Setback thermostat
5. 3 + Night Shutdown
6. 3 + CO₂-Outside Air Control

4.1 Constant Vs. Variable Air Volume

AHUs in FCO airport were originally designed to be of the Variable Air Volume (VAV) type. This variable flow is controlled by terminal VAV boxes at the duct ends and depends on local temperature control of the conditioned zones. The specific details of the VAV control strategy are not known. Data revealed that the fans were operating at constant electrical current (Amperes), electrical potential (Volts) and electrical power (Watts). The pressure at the ducts was also constant.

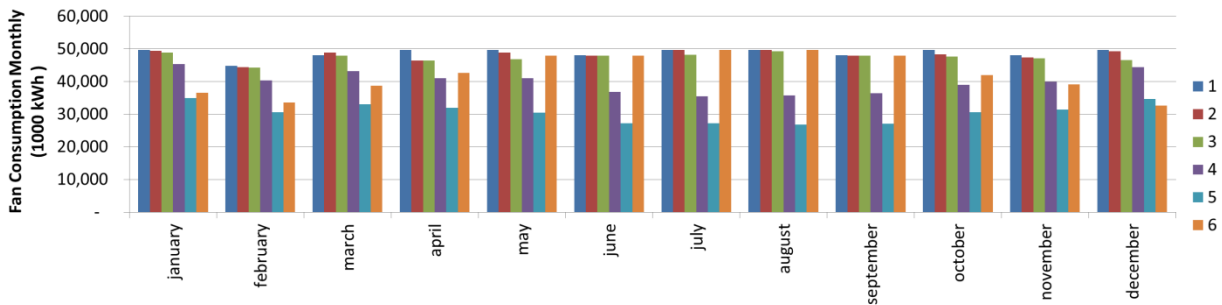


Fig. 6 – Monthly fan energy consumption for baseline (1) and the ECMs assessed

The conclusion was that the VAV boxes were not working. In order to assess the impact of bringing back the VAV boxes to a Variable Volume operation of the air loop, an initial run of the model was done and then the air flow was set to maintain 85% of the calculated airflow. This strategy (2) resulted on savings of 0% to 5% for fan consumption, and only for the months of April, May, October and November.

4.2 Unstable Supply Air Setpoint

Data in Figure 5 shows the air supply setpoint varying through the year. This setpoint is normally set by the operators. There is no information regarding criteria for setting up the setpoint. It can be seen that although the setpoint range has been set up in many different ways, it is very difficult for the system to meet the expected temperature. The strategy tested a wider supply air delivery threshold of 14°C for cooling and 29°C for heating. The baseline supply air setpoint has been set to a narrower range of 17°C for cooling and 22.5°C for heating, which is similar to the actual air supply temperature delivered. This strategy (3) was modelled on top of strategy 2 and demonstrated a saving of 4% to 7% on fan consumption. Again, this change was only effective for some months (April, May, July, October, November and December) and made no effect on others.

4.3 AHU working constantly

Data showed a constant operation of the AHUs 24 hours a day while the terminal real activity took place from 6.00 to 23.00 approximately, the remaining being the time in operation but with limited access; businesses are closed and there is a very reduced number of flights (normally only one

or two). Some strategies were tested to understand the potential for savings of a night setback. A further investigation will use optimization techniques to establish an optimum start-stop time in combination with a supply setpoint temperature. The model reveals it is of high value to convey the thermal lag effects of the building and the dynamic loads. The impact of this ECM can be clearly assessed in Figure 4, where the real implementation of this setback can be clearly seen from May 2014 resulting in a 33% reduction of fan energy consumption. Two scenarios have been simulated adding to strategy 3. The first one (4) implements a night setback temperature deadband of 14°C to 29°C of the conditioned zone from 23.00 to 05.00. This rendered a reduction of 10% to 30% on fan energy consumption and was more effective in summer than winter. The second scenario (5) implements a total shutdown of the fans for the same period at night, reflecting what has been implemented in the real building. This last strategy yielded a 30% to 45% reduction of fan energy consumption. Again, this strategy was more effective for the cooling season.

4.4 Outside Air Rate optimization

Design intent documents show that the AHUs were calculated to attend two requirements: (1) Air per person, and (2) Air per area. These are very different ways of establishing an optimal Outside Air renovation air. For (1) to be successful, a CO₂ sensor must be installed in the terminal and control sequence of the mixing box accordingly. The current Outside Control in the building is not known and controlled by the operator. In the actual simulation the baseline Outside Air is set to 1 ACH. The air renovation was set to meet 8

l/person, and a limit of 1000 ppm CO₂/m³. This strategy was revealed to be very successful in winter periods where AHU works at the minimum recirculated air (30%), although it is very sensitive to an unknown parameter as occupation and has to be used with caution.

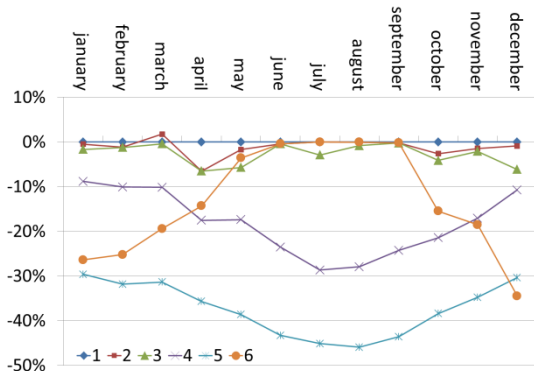


Fig. 7 – ECMs savings in percentage from the baseline.

5. Conclusions

In this research, a practical implementation of building simulation has been described. Whole Building Performance models can help final users to assess energy conservation measures before their implementation and this aspect of simulation is revealed by the ability of the model to simulate changes on operative conditions. Building models of large and open spaces represent a time intensive task. The model development and calibration process were revealed to be a useful way to discover problems of HVAC operation, despite calibration being difficult to achieve sometimes. The model was used to produce a sequenced recommissioning process. However, cross model configuration effects and cumulative effects need to be accounted for in potential variations of the savings estimates. The model developed demonstrates the usefulness of simulation in the implementation of the five ECMs selected: Variable air volume, Night Setback operation, optimized supply air temperature and CO₂ controlled Air Renovation. Simulation showed a substantial reduction in fan energy consumption of up to more than 40% in summer months. Further monitoring will verify the validity of the percentages estimated.

6. Acknowledgements

This research has been carried out within the project CASCADE. This project has received funding from the European Community's Seventh Framework Programme (FP7/2007-2013) under grant agreement No. 284920. Project website is available from <http://www.cascade-eu.org/cms/>

References

- ASHRAE. 2002. *ASHRAE Guideline 14-2002: Measurement of Energy and Demand Savings*. ISSN 1049-894X
- Coakley, D., Rafter, P., Keane M. 2014. "A review of methods to match building energy simulation models to measured data". *Renewable and Sustainable Energy Reviews*. 37. (123-141). doi: org/10.1016/j.rser.2014.05.007
- ENAC. 2011. Previsione dell'evoluzione del traffico nel sistema aeroportuale di Roma. [Online] Available from <http://www.enac.gov.it/Home/>
- ENAC. 2013. Dati di traffico 2013. [Online]. Available from <http://www.enac.gov.it/Home/Flighstats>
- Flighstats Inc. 2014. "Flightats API". Accessed 1 Dec. 2014. <http://www.flightstats.com>
- IATA. 2014. "Statistics.2014. Industry Facts" Accessed on 05 Nov 2014. http://www.iata.org/pressroom/facts_figures/fact_sheets/Documents/industry-facts.pdf
- IEA. 2002. Computer Aided Evaluation of HVAC System Performance.
- Mustafaraj, G., Marini, D., Costa, A., Keane, M.M. 2012. "Model Calibration for Building Energy Efficiency Simulation" *Applied Energy*. 130 (72-85). doi: org/10.1016/j.apenergy.2014.05.019
- Parker, J., Cropper, P., Shao, L. 2011. "Using Building Simulation to Evaluate Low Carbon Refurbishment Options for Airport Buildings". *In Proceedings of the BS 2011 conference. Sydney*.
- Perez-Lombard, J., Ortiz, J., Pout, C. 2008. "A review on buildings energy consumption information". *Energy and Buildings*, 40.(3)(2008), pp. 394-398.
- Raftery, P., Keane, M.M., O'Donnell, J. 2011. Calibrating Whole Building Energy Models: An Evidence-Based methodology. *Energy and Buildings* 2011 (43): 2356-2364.

Dynamic simulation and on-site monitoring of a combined solar and pellet system in a low energy house

Elisa Carlon – Bioenergy 2020+ GmbH / Free University of Bozen-Bolzano – elisa.carlon@natec.unibz.it

Alessandro Prada – Free University of Bozen-Bolzano – alessandro.prada@unibz.it

Markus Schwarz – Bioenergy 2020+ GmbH – markus.schwarz@bioenergy2020.eu

Christoph Schmidl – Bioenergy 2020+ GmbH – christoph.schmidl@bioenergy2020.eu

Marco Baratieri – Free University of Bozen-Bolzano – marco.baratieri@unibz.it

Andrea Gasparella – Free University of Bozen-Bolzano – andrea.gasparella@unibz.it

Walter Haslinger – Bioenergy 2020+ GmbH – walter.haslinger@bioenergy2020.eu

Abstract

This study focuses on the dynamic building simulation of a low energy house, situated in the region of Lower Austria. The pre-fabricated single family house has highly insulated lightweight walls and triple glazed windows. The house is heated by a 6 kW pellet boiler supplying hot water to a floor heating system. The boiler is also used for domestic hot water production, in combination with solar collectors, thus forming a combined solar-pellet system. The house was monitored in the frame of the BioMaxEff project (funded by FP 7), aiming at the demonstration of biomass boilers in real life conditions. Parameters describing the boiler operation as well as outdoor and indoor temperatures were monitored continuously for one year. The aim of this study is to develop a coupled simulation of the house and its heating and hot water supply systems has been set up in the TRNSYS simulation suite. System components have been simulated using both standard and non-standard TRNSYS Types. A new component was developed within this study to simulate the system's control unit. The comparison of monitoring data of the year 2013 and simulation results showed that the boiler operation in field conditions was accurately reproduced in the simulation environment.

1. Introduction

Nowadays pre-fabricated single-family houses are becoming increasingly popular in Austria, thanks to their high-energy performance. In Austria, houses having an annual heat demand below 50

kWh·m⁻² are certified as “Low Energy Houses” (Oberösterreich Energiesparverband, 2013).

The building under study is a pre-fabricated single-family house (Figure 1), whose envelope has highly insulated lightweight walls ($U_{\text{value}} 0.14 \text{ W}\cdot\text{m}^{-2}\cdot\text{K}^{-1}$) and triple glazed windows ($U_{\text{value}} 0.90 \text{ W}\cdot\text{m}^{-2}\cdot\text{K}^{-1}$). The house is heated by a 6 kW pellet boiler supplying hot water to a floor heating system. The boiler, manufactured by the Austrian company Windhager Zentralheizung Technik GmbH, is also used for domestic hot water (DHW) production, in combination with the solar collectors installed on the roof, thus forming a combined solar-pellet system, as shown in Figure 2. Additional details about the building and its heating and DHW supply system can be found in a previous paper (Carlon et al., 2014). Since November 2012, the house has been monitored in the frame of a FP7 project (BioMaxEff), aiming at the demonstration of biomass boilers under real life conditions.

The aim of this study is to supplement the monitoring activity with a coupled simulation of the house and its heating and DHW supply system, allowing to closely investigate the system's response to the heating and hot water demand. The main objective of the simulation was to accurately simulate the boiler operation in field conditions. The simulation has been conducted by means of the TRNSYS simulation suite. The main system components have been simulated using appropriate TRNSYS Types or developing new Types specifically designed for the devices installed in the house.



Fig. 1 – Monitored house

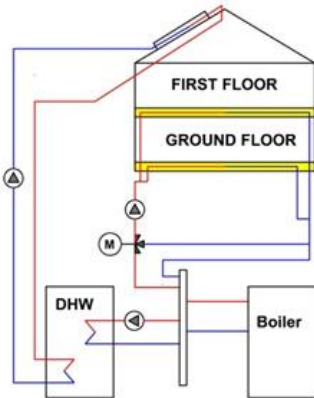


Fig. 2 – Scheme of the heating and DHW supply system

2. Method

2.1 On-Site Monitoring

The house has been monitored since November 2012. Parameters describing the boiler operation as well as outdoor and indoor temperatures provided a data set suitable to characterise the boiler’s performance in different seasons.

A heat meter installed at the boiler outlet measured the hot water production and an electricity meter measured the boiler’s electricity consumption. The weight measurement of a calibrated balance, placed under the pellet storage, was used to determine the pellet consumption. The outdoor temperature was measured by a NTC thermistor installed on the north wall of the house. Concerning the indoor environment, the temperature and relative humidity was measured in four different rooms using ASH 2200-1 wireless temperature and humidity sensors. Data were logged every 10 seconds by means of a PC-based data acquisition system connected to the boiler’s-internal data transmission system. Monitoring data of the year 2013 revealed that the house had an insufficient thermal comfort, as the indoor

temperature was very often below the set value chosen by the inhabitants (Carlón et al., 2014).

2.2 Dynamic simulation

A coupled simulation of the house and its heating and hot water supply systems have been set up in the TRNSYS simulation suite. The main system components have been simulated using both standard and non-standard TRNSYS Types. In particular, the pellet boiler has been simulated using the Type 869 boiler model (Haller et al., 2011) and the hot water storage tank using Type 534, available in the TRNSYS TESS library. In addition, a new component was developed within this study to simulate the heating system’s control unit. Table 1 reports the lists of the TRNSYS components used in this study.

Table 1 – TRNSYS components used in this study

System component	TRNSYS Type	Source
Building envelope, thermal zones, heat gains	Type 56	Standard TRNSYS Type
Pellet boiler	Type 869	Non standard TRNSYS Type (Haller et. al.)
DHW storage tank	Type 534	TRNSYS Type (TESS Library)
Floor heating system	Type 56 (Active layer)	Standard TRNSYS Type
Three way valve	Type 11-f	Standard TRNSYS Type
Pump - DHW circuit - boiler	Type 114	Standard TRNSYS Type
Pump - DHW circuit - solar	Type 114	Standard TRNSYS Type
Pump – Floor heating system	Type 114	Standard TRNSYS Type
DHW System control unit	Type 2b	Standard TRNSYS Type
Weather data processing	Type 99-2	Standard TRNSYS Type
Solar collectors	Type 1A	Standard TRNSYS Type
Valves – heating system	Type 11 a-f	Standard TRNSYS Types
Heating system control unit	Type 251	Developed in this study

2.2.1 Heating system control unit

The heating system of the house is controlled by a thermostat placed in the living room. Whenever the room temperature drops below the set value, the boiler is switched on and the water circulation through the floor heating system is started. The boiler continues operation until the room temperature is 2 K above the set value. Hot water leaving the boiler (at approximately 55 °C) is mixed with the cold water flow returning from the floor heating system (at approximately 25 °C). The position of a three-way valve is continuously adjusted to reach a certain temperature (T_{mix}), at which the water is delivered to the floor heating system. The set value of T_{mix} , varying between 25 °C and 38°C, is calculated as a function of the outdoor temperature, by means of a heating curve (Figure 3). The limit values of the outdoor temperature, defining the slope of the line are -15°C and +15°C, according to the Austrian regulations and to the recommendations of the manufacturing company.

The considered control unit includes an optional “compensation function” which aims at maintaining the room temperature as close as possible to the set value chosen by the users. The function adjusts the water set temperature at the mixing valve from T_{mix} to $T_{mix,comp}$ according to (Eq 1).

$$T_{mix,comp} = T_{mix} + P_{comp} \cdot (T_{room,set} - T_{room}) \quad (1)$$

where P_{comp} is a control parameter, T_{room} is the actual room temperature and $T_{room,SET}$ is the room temperature setpoint. If for instance the indoor temperature is above the set value, then $T_{mix,comp}$ is lower than T_{mix} , and the compensation function has the effect of moving downwards the heating curve. Consequently, water is delivered to the floor heating system at a lower temperature, thus lowering the heat transfer rate to the room and avoiding overheating.

In this study, a new TRNSYS Type (Type 251) was implemented to simulate the control unit, including the compensation function.

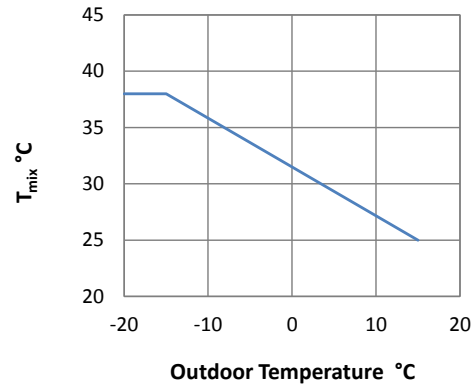


Fig. 3 – Heating curve defining the water inlet temperature to the floor heating system

2.2.2 DHW supply system control unit

In the considered system configuration, the hot water tank is used only for the storage of domestic hot water, and does not serve as a buffer for the floor heating system. The solar collectors heat the lower part of the stratified tank: when the difference between the water temperature at the outlet of the collectors and the water temperature at the bottom of the storage tank exceeds 7 K, the circulation pump of the solar circuit is activated.

If the heat production of the collectors is not sufficient to maintain a minimum temperature of 48°C inside the storage tank, then the pellet boiler starts to heat the upper part of the tank. The boiler operation continues, with priority on the heating system, until the water temperature at the top of the tank increases to 60°C.

The maximum allowable water temperature inside the storage tank is 85°C, due to safety reasons. If this value is reached, the circulation pump leading to the solar collectors is immediately stopped. The control of the hot water supply system was simulated using the TRNSYS Type 2.

2.3 Simulation parameters

The simulation developed in this study was complex and required several input parameters.

The thermal properties the building envelope were found in the Energy Performance Certificate (EPC) of the house, which was provided by the house manufacturer including all the thermal properties of the construction materials. Interviews with the house owners allowed us to define occupation schedules, internal heat gains, DHW demand profiles as well as the settings of heating system

control unit. Technical documentations of the solar collector and of the DHW storage tank provided the necessary parameters to calibrate these components. In a previous study, the boiler model Type 869 was calibrated and validated by means of laboratory tests performed on the same 6 kW pellet boiler as the one installed in the monitored house (Carlón et al., 2015).

3. Results and discussion

3.1 Annual efficiency and operational behavior of the pellet boiler

The main focus of the simulation presented in this study is heating and DHW supply system, and in particular the pellet boiler, which had two different operational regimes (“Summer mode” and “Winter mode”) depending on the season. Between May and September 2013, the boiler was only used to support the solar collectors for DHW supply. Hence, the boiler operation was completely independent of the building envelope (“Summer mode”). During the remaining months (from January to April and from October to December), the boiler, set to “Winter mode”, heated the house and supplied DHW, together with the solar collectors. In this case, the boiler operated to fulfill both the heating and the DHW demands. The dates when the operating mode was changed from “Winter” to “Summer” (April 2013) and then again from “Summer” to “Winter” (October 2013) were specified by the house owners and used as input data for the simulation.

In Figure 4, simulation results concerning the boiler operation during 2013 are compared with the monitoring data. The deviation between the simulated and the measured annual efficiency is below 1%. For the hours of operation and for the number of ignitions, the deviations are 7.3% and 4% respectively.

Table 2 – Comparison of monitoring data and simulation results concerning the boiler operation

	Simulation	Monitoring
Hot water production [kWh]	9401	9278
Annual efficiency [%]	74.6	75.3
Annual pellet consumption [kg]	2570	2582
Number of ignitions [-]	494	516
Hours of operation [h]	1926	2077

3.2 Boiler operation in different months

The monthly pellet consumption and hot water production calculated by the simulation are compared with the monitoring data in Figure 4, on a monthly basis. Simulation results are in good agreement with the monitoring data, except for June 2013, when the simulation underestimated both the boiler heat production and pellet consumption. A deeper analysis of the monitoring data showed that the first half of June was rather cold, therefore the heating system was manually activated for some days. In the simulation, where the boiler was set to supply only DHW during the summer months, this manual start of the heating system could not be foreseen.

In June, July and September 2013, the house did not have any heat demand, and the hot water demand was almost completely covered by the solar collectors. Monitoring data show that, during these months, the boiler operated for 23 hours in total. Also the simulation results show short operation times during the summer season, resulting in a total operation time of 30 hours. The pellet consumption in the period June-September 2013 was 63 kg, representing only 2.4% of the annual pellet consumption.

4. Conclusions and future work

In this study, a coupled simulation of a low energy house and its heating and DHW supply system was set-up. The boiler operation was simulated with a good accuracy throughout the whole year of 2013. Results also showed that the simulation could not take into account all the user behaviours. Therefore, during some specific time intervals when particular conditions occurred, simulation results were less accurate. The next step of this study will be a detailed calibration of the coupled simulation, with a focus on the parameters influenced by the users' behaviour. The calibrated

simulation will be used to explore new control strategies, with the aim of improving the thermal comfort in the house. Optimal control strategy shall be defined by maximising the thermal comfort and minimising the pellet consumption of the boiler.

Finally, the simulation will be used to find different system configurations to heat low energy houses by means of biomass-based system. Different system components, such as radiators, and buffer storage tanks will be tested to find optimal system solutions for pre-fabricated houses.

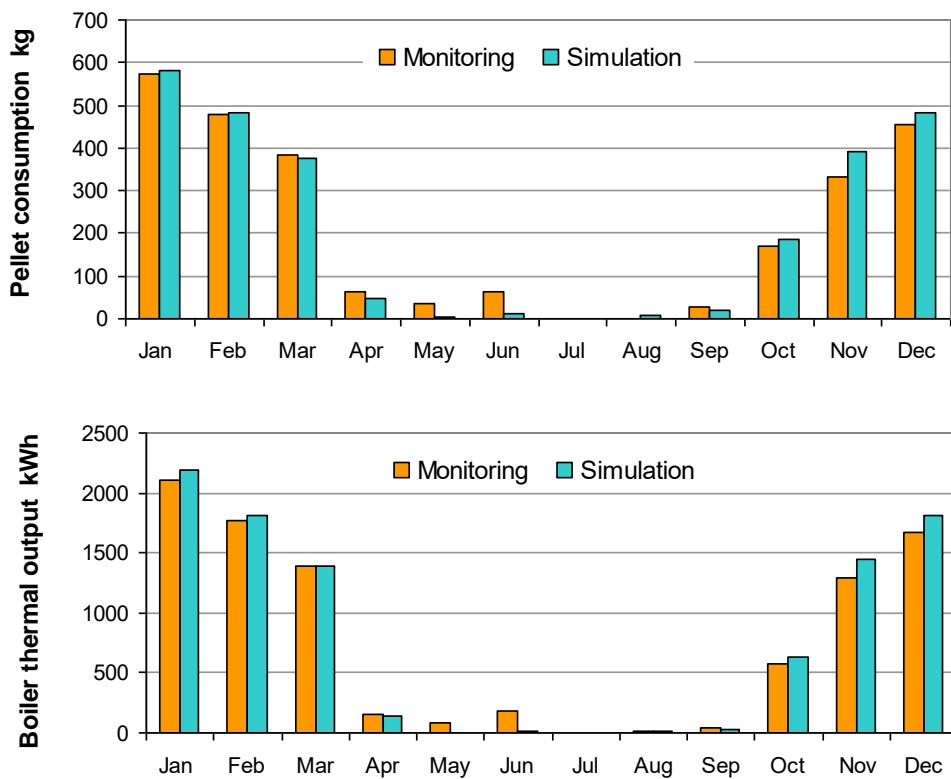


Fig. 4 Comparison of simulation results and monitoring data

5. Acknowledgement

The research leading to these results has received funding from the European Union Seventh Framework Programme (FP7/2007-2013) under Grant Agreement n° 268217. The cooperation with the Austrian company Windhager Zentralheizung Technik GmbH is also gratefully acknowledged.

6. Nomenclature

Symbols

DHW	Domestic Hot Water
EPC	Energy Performance Certificate
P_{comp}	Compensation parameter (-)
T_{mix}	Water temperature at the three-way valve (°C)
$T_{\text{mix,comp}}$	Water temperature at the three-way valve, corrected by the compensation function
T_{room}	Room temperature (°C)
$T_{\text{room,SET}}$	Room temperature set value (°C)
SHGC	Solar Heat Gain Coefficient (-)
U_{value}	Overall heat transfer coefficient ($\text{W}\cdot\text{m}^{-2}\cdot\text{K}^{-2}$)

References

BioMaxEff project website, Accessed October 27, 2014 <http://www.biomaxeff.eu>

Carlton, Elisa, Markus Schwarz, Christoph Schmidl, Marco Baratieri, Andrea Gasparella, Walter Haslinger. 2014. "Low energy houses heated by biomass boilers: optimization of the heating system control strategy by means of dynamic simulation." in *Proceedings of the 3rd International High Performance Building Conference at Purdue*, 14th -17th July 2014, West Lafayette, USA, accessed November 20, 2014.

Carlton, Elisa, Vijay Kumar Verma, Markus Schwarz, Laszlo Golicza, Alessandro Prada, Marco Baratieri, Walter Haslinger, Christoph Schmidl. 2015. "Experimental validation of a thermodynamic boiler model under steady state and dynamic conditions" *Applied Energy*,

138C: 505-516. doi: 10.1016/j.apenergy.2014.10.031

Haller M.Y., J. Paavilainen, L. Konersmann, R. Haberl, A. Dröscher, E. Frank, C. Bales and W. Streicher. 2011. "A unified model for the simulation of oil, gas and biomass space heating boilers for energy estimating purposes. Part I: Model development" *Journal of Building Performance Simulation*, 4 (1): 1–18.
doi: 10.1080/19401491003671944

Oberösterreich Energiesparverband, Accessed November 20, 2014. <http://www.esv.or.at/?id=2125>.

TESS component libraries - General Descriptions, Accessed November 20, 2014. http://www.trnsys.com/tesslibraries/TESSLibs17_General_Descriptions.pdf

TRNSYS 16, a TRaNsient System Simulation program - Volume 6, Multizone Building modeling with Type56 and TRNBuild, Accessed November 20, 2014.
<http://web.mit.edu/parmstr/Public/Documentation/06-MultizoneBuilding.pdf>

Windhager Zentralheizung Technik GmbH, "Operating Manual of Windhager VarioWIN Pellet central heating boiler pneumatic + direct", accessed November 20, 2014. http://www.windhager.com/fileadmin/user_upload/VarioWIN_OP_Manual0810.pdf

Windhager Zentralheizung Technik GmbH, "MESplus, Systemregelung für bis zu zehn Heizkreise, accessed November 20, 2014." <http://www.windhager.com/at/produkte/regelu/mesplus-47>

A parametric design-based methodology to visualize building performance at the neighborhood scale

Giuseppe Peronato – Ecole Polytechnique Fédérale de Lausanne (EPFL) – giuseppe.peronato@epfl.ch

Emilie Nault – Ecole Polytechnique Fédérale de Lausanne (EPFL) – emilie.nault@epfl.ch

Francesca Cappelletti – Università Iuav di Venezia – francesca.cappelletti@iuav.it

Fabio Peron – Università Iuav di Venezia – fabio.peron@iuav.it

Marilyne Andersen – Ecole Polytechnique Fédérale de Lausanne (EPFL) – marilyne.andersen@epfl.ch

Abstract

This paper focuses on parametric design-based visualization methods to represent building performance at the neighborhood scale in the perspective of an integrated design-support system. The goal of the developed methodology is to convey the relative effectiveness of different design alternatives according to a wide range of building performance indicators, including the potential for active solar applications, the energy need for space heating/cooling and (spatial) daylight autonomy.

The proposed methodology is applied to a case study of a typical urban renewal project in Switzerland for which several design variants were analyzed using validated climate-based simulation engines. For each design variant, simulation results are represented qualitatively using multiple false-color maps and quantitatively through comprehensive plots.

We conclude by showing the applicability of this methodology to a large number of neighborhood-scale design variants as well as the complementarity of the proposed visualization methods. On the basis of the case study application, a possible implementation as a design-support tool is finally discussed.

1. Introduction

The early-design stage often corresponds to the definition of a project at the neighborhood scale, when some of the most important design choices, such as building typology and dimensions, are made. Attia et al. (2009) stress the importance of graphical representation of building simulation results and comparative evaluation of design alternatives at the early-design stage, when

architects are usually involved. Haeb et al. (2014) list the typical visualization requirements, including visual feedback on the impact of design decisions, the integration of spatio-temporal analysis and suggestions on design improvements. Some building performance simulation (BPS) tools for the early-design phase, like DIVA (Jakubiec and Reinhart 2011), provide spatio-temporal representation of performance metrics in the popular Rhino/Grasshopper parametric modeling environment (McNeel 2013a; McNeel 2013b). The visual evaluation of multiple design variants can be hence obtained through the animation of daylight maps in the 3D scene (Lagios, Niemasz, and Reinhart 2010) or the comparative visualization of energy and daylight results (Doelling 2014). However, such techniques have not been fully applied to urban design yet, as existing scale-specific BPS tools are limited to daylight analysis (Dogan, Reinhart, and Michalatos 2012) or not oriented to parametric design (Robinson et al. 2009; Reinhart et al. 2013).

This paper therefore focuses on techniques to visualize building performance in a neighborhood-scale parametric-design workflow. The case-study application on a typical urban renewal project in Switzerland involved the evaluation of several design alternatives, generated by the variation of building dimensions, using different metrics calculated on the basis of climate-based simulations run in Radiance/Daysim (Ward-Larson and Shakespeare 1998; Reinhart and Walkenhorst 2001) and EnergyPlus (EERE 2013) through the DIVA-for-Grasshopper interface (Jakubiec and Reinhart 2011).

2. Proposed methodology

This section presents a set of six metrics, either directly based on or derived from existing ones, and proposes a unified framework to visualize them at the neighborhood-scale. After a short description of each of them, the approach chosen for their visual representation is provided, and the applicability of these proposals is discussed in the subsequent section. A summary of all metrics and corresponding visualizations is given in Table 8.

Table 8 – The proposed metrics and corresponding visualizations

Metrics	Visualizations
Cumulative	Comprehensive plots
Active Solar energy production	
Energy Need for space heating/cooling	
spatial Daylight Autonomy	
Space- and time- varied	False-color maps
Solar Irradiation	
Active Solar suitability	
Daylight Autonomy	
temporal Daylight Autonomy	

2.1 Cumulative metrics

Cumulative metrics allow for a quantitative evaluation of design variants by providing a value expressing the overall performance of the analyzed buildings over time and space. The ones we present here are particularly suitable for a neighborhood-scale application, as they require only a few parameters to be set.

2.1.1 Active Solar energy production

As an extension of the solar potential concept developed by Compagnon (2004), solar irradiation data is used to estimate the energy production by solar thermal (ST) and photovoltaic (PV) systems. The irradiation of each simulated surface unit is considered in the metric calculation only if it achieves the thresholds of Table 9. Moreover, a 15% constant efficiency is assumed as a standard value for commercial polycrystalline PV panels, while 70% is considered appropriate for low-temperatures heating purposes using standard flat-plate ST collectors. In order to estimate the surface unavailable for active solar systems (e.g. windows), a surface coverage ratio was set for each system (PV/ST) and each type of surface (roof or façade). Moreover, only surfaces with at least half of the available area achieving the thresholds of Table 9 are considered. These parameters are all included in the metric calculation, as detailed in Peronato (2014).

It should be noted that PV and ST are presumed mutually excluding alternatives, as the appropriate ratio of their usage is usually defined at a later design phase, when energy needs have already been estimated. Therefore, this metric should be considered as a general indicator of the maximum performance of active solar systems, rather than an effective energy production value.

Table 9 – Irradiation lower thresholds for solar active systems (Compagnon 2004)

	PV	ST
Roof	1000 kWh/m ²	600 kWh/m ²
Facade	800 kWh/m ²	400 kWh/m ²

2.1.2 Energy Need for space heating/cooling

The annual heating (or cooling) load is calculated as «the sum of the hourly heating [or cooling] loads for the one-year simulation period» (ASHRAE 2014) converted from J to kWh and then normalized per conditioned floor area (kWh/m²). This metric corresponds to the Energy Need for space heating and cooling, defined as «heat to be delivered to, or extracted from, a conditioned space

to maintain the intended temperature conditions during a given period of time» (EN ISO 13790: 2008).

Here it is considered as the most appropriate indicator to assess the building thermal energy performance at the early-design phase, when most details about the HVAC system have not been fixed yet.

2.1.3 Spatial Daylight Autonomy

Spatial Daylight Autonomy (sDA) is an indicator of the annual sufficiency of ambient daylight levels in interior environments (IESNA 2012). $sDA_{300/50\%}$ (where the subscript indicates the illuminance goal in lx and the minimum time threshold in %) is defined as the percentage of working plane surface achieving the 300 lx requirement for at least 50% of the occupied times.

It is the preferred metric for the analysis of daylight sufficiency recommended by the Daylight Metrics Committee, allowing comparisons to be made to a consistent standard. Only surfaces achieving $sDA_{300/50\%} \geq 55\%$ are considered adequately daylight (*ibid.*).

2.2 Space- and time-varied metrics

Space and time-varied metrics convey information about the performance of a surface over time. They provide useful information for further design exploration, such as the placement of windows and active solar systems or the allocation of the interior space.

2.2.1 Daylight Autonomy

Daylight Autonomy (DA) is defined as the percentage of the occupied times of the year when the minimum illuminance requirement is met by daylight alone (Reinhart and Walkenhorst 2001).

Even if at the early design phase the building occupancy schedules are usually not fixed yet, as they depend on the specific building functions, the standard occupied hours (8 am to 6 pm) and the illuminance goal (300 lx) suggested by IESNA (2012) were chosen for consistency with the spatial Daylight Autonomy definition as well as to compare the results from different case studies.

2.2.2 Active Solar suitability

In this work, the Active Solar suitability is a binary metric defining whether a surface is suitable for a given active solar system. It is calculated on the basis of the thresholds of Table 9 and of the annual cumulative solar irradiation. The non-null values can be substituted by the actual irradiation, to provide information about the variable degree of suitability.

2.2.3 Temporal Daylight Autonomy

Dynamic daylight performance metrics as the Daylight Autonomy do not include time-based variability, but only retain information about the number of hours when a threshold is achieved. Kleindienst and Andersen (2012) proposed to reverse this approach by using a temporal metric condensing the spatial variation into a single number while displaying variation over time, named Acceptable Illuminance Extent (AIE).

Based on the Daylight Autonomy illuminance target value and the AIE definition, the temporal Daylight Autonomy (tDA_{300}) is defined in this work as the percentage of space achieving the illuminance goal (300 lx) for a given time period.

2.3 Visualization

The analysis of comprehensive plots allows a quantitative comparison of the performance of the design variants and the influence of the different design parameters, while false-color maps give a qualitative assessment of the building performance for further design exploration. Both methods can be combined into an integrated visualization method through the animation of maps and plots. Finally, by imposing the required design constraints and objectives, the analysis of decision plots is aimed at the selection of the optimal solutions among the simulated design variants.

2.3.1 Variant-performance plots

Variant-performance plots are scatter plots presenting the indicator values (y-axis) for each design variant (x-axis). Multiple plots with the same x-axis scale can be presented in a vertical layout, so as to simultaneously compare the performance of the design variants for different indicators.

The presentation of the parameter variation as an additional plot, with the design variants in the x-axis and the parameter values in the y-axis, allows a visual assessment of the influence of each design parameter on the building performance.

2.3.2 False-color maps

Spatial and temporal maps use the same color gradient to convey information about the achievement of the illuminance goal, respectively, for a particular sensor point over the occupied hours or for a particular number of hours over the surface. A spatial map has Euclidean dimensions for its x and y axes, whereas a temporal plot orders data by day of year (x-axis) and time of day (y-axis).

Spatial maps can be represented either through orthogonal plans or perspective views, in which the simulated surfaces are rendered with a color gradient according to their performance.

Temporal maps were first introduced by Glaser and Ubbelohde (2001) as a complementary visualization to standard spatial plots in a “brushing and linking” method. The temporal-map visualization for illuminance values is limited to one sensor point per plot, unless average values are used. Differently, time-varied metrics allows the visualization of the performance of an entire space in form of one or more percent values while, unlike averaging methods, preserving the understanding of surface variability. The use of temporal maps was aimed at creating a user-friendly method to communicate information generated by daylight simulation to the designer (Kleindienst and Andersen 2012). This is particularly useful for early-stage design decisions, where the specifics of the space are not already defined (*ibid.*).

2.3.3 Parameter-sensitivity plots

Parameter-sensitivity plots represent the performance for a given indicator over the variation of a design parameter. A one-way sensitivity analysis is conducted by visual comparison of such plots.

Provided that the extremes of the axes are fixed according to the range of the design parameters and of the simulation results, the relevance of the

parameters in the given range can be evaluated by examining the slope of the curves in the plots: the steeper is the curve, the more influential is that parameter on the indicator’s performance. Although this visualization cannot take into consideration the mutual influence of each design choice but only of the selected parameters combinations, it can give an overview of the sensitivity of the indicator based on the variation of each design parameter.

2.3.4 Decision plots

Decision plots are scatter plots in which each axis represents an indicator to be optimized. For minimization objectives (e.g. the Energy Need for space heating/cooling), values are ordered from the maximum to the minimum so as to be compared in the same plot with maximization objectives (e.g. Active Solar energy production).

Decision plots are used to find the optimal solutions as well as to select solutions respecting the given constraints. As long as the indicators used as optimization goals are no more than three, for visualization convenience, the results can be plotted in a 2D or 3D graph in which, for a maximization problem, the most external solutions with respect to the origin of the axes correspond to the non-dominated solutions. These solutions, also called Pareto-efficient solutions, are characterized by the fact that their values «cannot be improved in one dimension without being worsened in another» (Legriél et al. 2010). Restricting the considered variants to the non-dominated solutions allows the trade-off between the objectives to be explored within a smaller solution space, rather than considering the full range of parameters combinations.

3. Application

The *Plan Directeur Localisé Gare-Lac* (Bauart 2010) is an urban renewal master plan in a brown field area of Yverdon-les-Bains (CH). The intent of this case-study application was the evaluation of a large number of parametrically generated design variants in order to optimize solar potential and

built density, while respecting the master plan constraints.

Geometric modifications were equally applied on all buildings through the parametric variation of design parameters within the range of values prescribed by the master plan (i.e. building height), or those considered representative of possible design choices (width and setback). 768 design variants (#1 to #768) were obtained by combination of the parameters defining the height and the horizontal layout of the building blocks (Fig. 1).

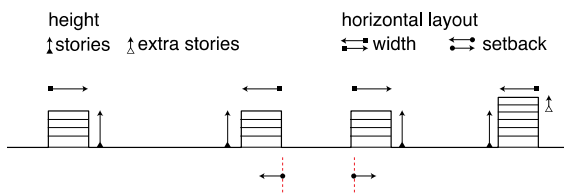


Fig. 1 – Schematic of the parametric model

Due to the computational cost, the simulations were conducted only on three buildings (hereinafter referred to as S, NE and NW blocks because of their relative position in the neighborhood), while taking into account their surrounding context in terms of shading and reflection. For similar reasons, only 32 design variants (#'1 to #'32), defined by a combination of the maximum and minimum values of each design parameter (Fig. 3), were simulated for hourly illuminances.

The metrics were calculated by post-processing the simulation results in custom MATLAB scripts. The generation of plots and temporal maps was also done in MATLAB, while spatial maps were created through the Rhinoceros/Grasshopper interface.

Only results concerning daylighting are presented in performance and sensitivity analyses, as they provide the widest range of visualizations. All results, as well as details on the modeling and simulation phases, can be found in Peronato (2014).

3.1 Performance Analysis

This analysis aims at comparing the trend of performance indicators in relation with the variation of design parameters.

By analyzing Fig. 2 and Fig. 3, it can be noted that block width is by far the most relevant design

parameter affecting spatial Daylight Autonomy. Moreover, design variants with the minimum number of stories (i.e. 3) show a better performance, while the extra stories do not seem to be so influential. The influence of setbacks is limited and differentiated. In fact, the north-south setback slightly increases the sDA as it augments the daylight potential on the south-exposed external facades, while east-west setback seems not to affect sDA.

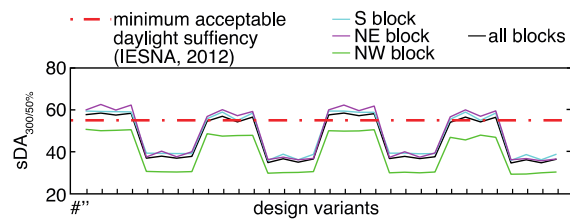


Fig. 2 – Variant-performance plot: spatial Daylight Autonomy

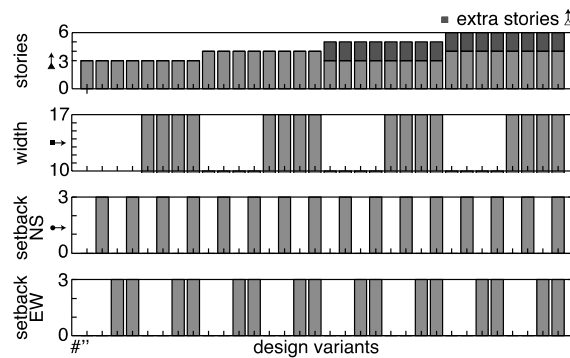


Fig. 3 – Parameter-variation plot: set of 32 design variants

Both spatial and temporal false-color maps are arranged in a parametric matrix (Fig. 4 and Fig. 5) confirming that block width is definitely the most relevant design parameter for daylighting.

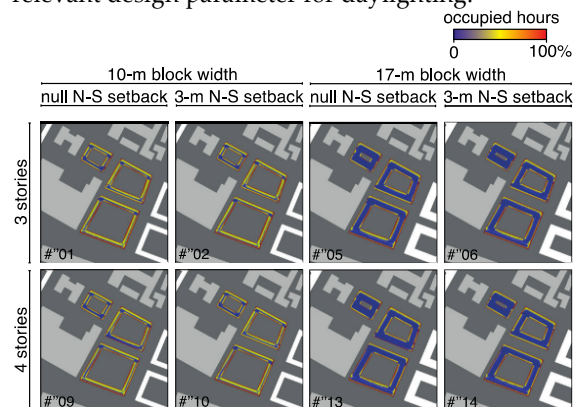


Fig. 4 – False-color spatial maps: DA₃₀₀

In the spatial maps, it can be noted that the number of stories is particularly crucial for the daylighting of the south side of the north-east block, but a 3-m setback partially compensates the negative effect of the building height, as it can be seen in map #''10.

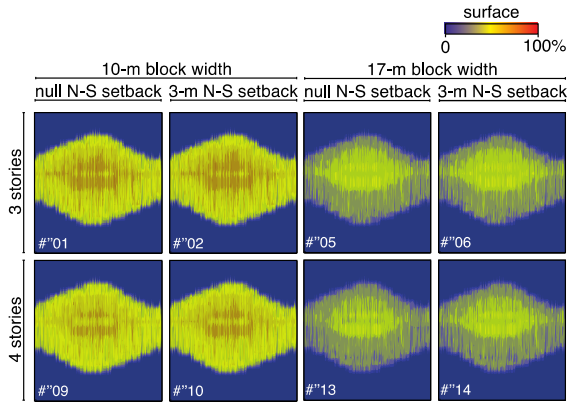


Fig. 5 – False-color temporal maps: tDA_{300}

In the temporal maps, the effect of design parameters is more evident in the time period 12-16 p.m. from April to September for design variants with a 10-m block width (left half side of the matrix), when design variants with 4 stories (second row of the matrix) have a smaller orange area, corresponding to a smaller floor area achieving the 300 lx threshold. However, setbacks contribute to re-increasing the dimension of this area, counterbalancing the negative effect of the building height.

3.2 Sensitivity Analysis

Because of the large number of design parameters, only a few combinations representing the extreme values of each parameter were considered in this analysis.

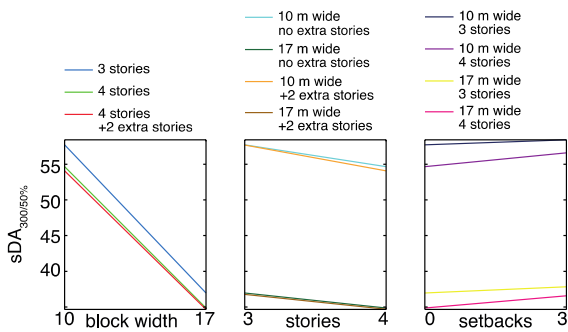


Fig. 6 – Parameter-sensitivity plot: sDA_{300}

In addition to what has already been observed (e.g. the relevance of the block width for daylighting), Fig. 6 shows that augmenting the building height from 3 to 4 storeys has a comparable effect as adding a 3-m setback on 4-storey high buildings, as the curves have similar slopes but opposite angles. Conversely, in 3-storey high buildings, the effect of setbacks is much less relevant.

3.3 Optimization

The selection of the optimal design solutions was done through the analysis of two decision plots. The decision plot of Fig. 7, in which the space of acceptable solutions is defined by the constraints $sDA_{300/50\%} \geq 50\%$ and Floor Area Ratio (FAR) ≥ 1.7 , allows the selection of a set of six acceptable design variants. The density lower limit is a master plan requirement, while the minimum $sDA_{300/50\%}$ was fixed to 50%, as using the minimum daylight sufficiency value (55%) suggested by IESNA (2012) produced an empty solution space.

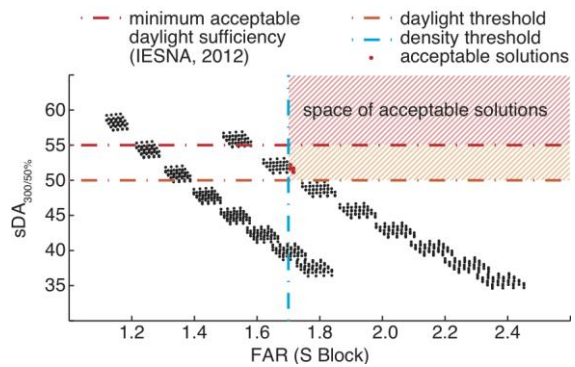


Fig. 7 – Decision plot: selection of the acceptable solutions

The decision plot of Fig. 8 uses the HVAC primary energy (assuming for the heating system a 5% heat losses and, for both heating and cooling systems, an efficiency of 3.1 and a primary energy conversion factor for electricity of 2.0) and Active Solar energy production as the two objectives to be respectively minimized and maximized. It should be noted that all acceptable solutions, previously selected in Fig. 7, show here a low performance for the optimization objectives, while the best solutions, located at the extremes of the axes, do not achieve the density and/or daylight thresholds. However, by restricting the search for non-dominated solutions (as explained in paragraph

2.3.4) to only the acceptable solutions, three design variants (#145, #401 and #657) were selected.

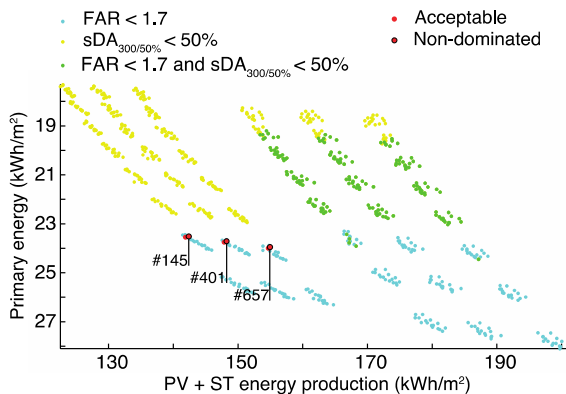


Fig. 8 – Decision plot: selection of the optimal solutions

Table 10 – Parameter values of the acceptable solutions

Variant	Setback NS	Setback EW	Block width	Stories	Extra stories
#145*	0	0	11	4	0
#146	1	0	11	4	0
#401*	0	0	11	4	1
#402	1	0	11	4	1
#657*	0	0	11	4	2
#658	1	0	11	4	2

*non-dominated

Table 10 shows the geometry characteristics of all acceptable solutions, including the non-dominated ones. All design variants present 4 stories (the maximum), an 11-m block width, which almost corresponds to the minimum value (10 m), as well as a null east-west setback. Moreover, the range of north-south setbacks is limited to a 0-to-1-m depth, while all optimal solutions have a null setback. The designer should hence consider these parameters as particularly important for the performance of the buildings, whereas he/she can have a greater degree of freedom in choosing the extra storeys according to other design criteria.

4. Conclusion

This paper has shown a flexible methodology to provide dynamic visualization of the results of building performance simulation for a large number of neighborhood-scale design variants.

The proposed visualizations convey complementary information on the influence of each parameter on the different performance indicators. The false-color maps, for example, help visualize the suitability of each surface and space for different uses, while, at a larger scale, sensitivity analysis highlights the relationship between each design parameter and building performance indicator, so that the designer is more conscious of his/her choices. Finally, the decision plots allow the designer to visualize the optimal solutions for some given objectives and constraints among the whole set of simulated design variants. However, in the case-study application, only a few variants were acceptable for the chosen constraints, while presenting among the poorest results for the optimization objectives. This proves that optimization is first of all a question of priorities and that the choice to be made by the designer (or the decision maker) about which objective(s) to give priority to is fundamental.

The main limitations of the methodology are linked to the computational cost of simulations, in particular those of interior illuminances, as well as to the assumptions made for the metrics calculation. Further work should be done to implement the proposed workflow in an interactive design-support system and to verify its effectiveness in a usability testing study. The support in the choice of parameters and their range of values through a first evaluation of simpler metrics would limit the use of time-expensive simulations. Such a platform should be finally released as a standalone software or plugin to be used in real design practice.

References

- ASHRAE. 2014. "Annual Heating Load." *ASHRAE Terminology*. Accessed November 28, 2014. <https://www.ashrae.org/resources--publications/free-resources/ashrae-terminology>
- Attia, Shady, Liliana Beltrán, André de Herde, and Jan Hensen. 2009. "'Architect Friendly': A

- Comparison of Ten Different Building Performance Simulation Tools." In *Proceedings of BS2009*, 204–11. Glasgow: IBPSA.
- Bauart. 2010. *Rapport Plan Directeur Localisé Gare-Lac*. Yverdon-les-Bains (CH)
- Compagnon, R. 2004. "Solar and Daylight Availability in the Urban Fabric." *Energy and Buildings* 36 (4): 321–28. doi:10.1016/j.enbuild.2004.01.009.
- Doelling, Max C. 2014. "Space-Based Thermal Metrics Mapping for Conceptual Low-Energy Architectural Design." In *Proceedings of BSO2014*. London: IBPSA-England.
- Dogan, Timur, Christoph F. Reinhart, and Panagiotis Michalatos. 2012. "Urban Daylight Simulation: Calculating the Daylit Area of Urban Designs." In *Proceedings of SimBuild 2012*, 613–20. Madison: IBPSA-USA.
- EERE. 2013. "EnergyPlus Engineering Reference: The Reference to EnergyPlus Calculations." U.S. Department of Energy - Energy Efficiency & Renewable Energy (EERE).
- EN ISO 13790. 2008. "Energy Performance of Buildings - Calculation of Energy Use for Space Heating and Cooling (ISO 13790:2008)." CEN.
- Glaser, Daniel C., and M. Susan Ubbelohde. 2001. "Visualization for Time Dependent Building Simulation." In *Proceedings of BS2001*, 423–30. Rio de Janeiro: IBPSA.
- Haeb, Kathrin, Stephanie Schweitzer, Diana Fernandez Prieto, Eva Hagen, Daniel Engel, Michael Bottinger, and Inga Scheler. 2014. "Visualization of Building Performance Simulation Results: State-of-the-Art and Future Directions." In *Proceedings of PacificVis 2014*, 311–15. IEEE. doi:10.1109/PacificVis.2014.34.
- IESNA. 2012. *IES LM-83-12 IES Spatial Daylight Autonomy (sDA) and Annual Sunlight Exposure (ASE)*. IES LM-83-12. IESNA Lighting Measurement. New York.
- Jakubiec, Alstan, and Christoph F. Reinhart. 2011. "DIVA 2.0: Integrating Daylight and Thermal Simulations Using Rhinoceros 3D, DAYSIM and EnergyPlus." In *Proceedings of BS2011*, 2202–9. Sidney: IBPSA.
- Kleindienst, Siân, and Marilyne Andersen. 2012. "Comprehensive Annual Daylight Design through a Goal-Based Approach." *Building Research & Information* 40 (2): 154–73. doi:10.1080/09613218.2012.641301.
- Lagios, Kera, Jeff Niemasz, and Christoph F. Reinhart. 2010. "Animated Building Performance Simulation (ABPS) - Linking Rhinoceros/Grasshopper with Radiance/Daysim." In *Proceedings of SimBuild 2010*, 321–27. New York: IBPSA-USA.
- Legriel, Julien, Colas Le Guernic, Scotto Cotton, and Oded Maler. 2010. "Approximating the Pareto Front of Multi-Criteria Optimization Problems." In *Tools and Algorithms for the Construction and Analysis of Systems*. Berlin-Heidelberg: Springer-Verlag
- McNeel. 2013a. *Rhinoceros v. 5.0* Windows. Seattle: Robert McNeel & Associates.
- McNeel. 2013b. *Grasshopper v. 0.9* Windows. Seattle: Robert McNeel & Associates.
- Peronato, Giuseppe. 2014. "Built Density, Solar Potential and Daylighting: Application of Parametric Studies and Performance Simulation Tools in Urban Design." Master's thesis, Venice: Università Iuav di Venezia.
- Reinhart, Christoph F., Timur Dogan, J. Alstan Jakubiec, Tarek Rakha, and Andrew Sang. 2013. "UMI - An Urban Simulation Environment for Building Energy Use, Daylighting and Walkability." In *Proceedings of BS2013*. Chambéry: IBPSA.
- Reinhart, C.F., and O. Walkenhorst. 2001. "Validation of Dynamic RADIANCE-Based Daylight Simulations for a Test Office with External Blinds." *Energy and Buildings* 33 (7): 683–97. doi:10.1016/S0378-7788(01)00058-5.
- Robinson, Darren, Frédéric Haldi, Philippe Leroux, Diane Perez, Adil Rasheed, and Urs Wilke. 2009. "CitySim: Comprehensive Micro-Simulation of Resource Flows for Sustainable Urban Planning." In *Proceedings of BS2009*, 1083–90. Glasgow: IBPSA.
- Ward-Larson, Greg, and Rob Shakespeare. 1998. *Rendering with Radiance: The Art and Science of Lighting Visualization*. San Francisco: Morgan Kaufmann Publishers

Exploring the occupancy behaviour and perception in an office building

Livia Seres – livia.seres@yahoo.com

Ulrich J. Pont – BPI, Vienna University of Technology – ulrich.pont@tuwien.ac.at

Matthias Schuss – BPI, Vienna University of Technology – Matthias.schuss@tuwien.ac.at

Ardeshir Mahdavi – BPI, Vienna University of Technology – amahdavi@tuwien.ac.at

Abstract

The representation of people's presence and control-oriented behaviour in building performance representation requires a large empirical database for model development and evaluation. Toward this end, empirical case studies in different buildings and different locations are necessary. In this context, this contribution presents the results of a study of user behaviour regarding building systems operation in an office building located in the south of Vienna, Austria, ventilated by mechanical means only. Moreover, users' perception of the indoor climate conditions at their workspaces was assessed. Empirical data concerning indoor climate conditions were collected by measuring the inside temperature, relative humidity, and illuminance levels over a period of ten months. Data regarding external weather conditions were obtained from the Central Institute for Meteorology and Geodynamics, Vienna. Occupancy data and the status of the user-controlled building's systems (thermostat, electrical lighting and shades) were additionally collected via hourly observations over a period of six months.

The main objective of the study was to explore the general patterns of occupant's control-orientated behaviour at their workplaces in relation to the indoor/outdoor conditions. The results contribute to a better understanding of user behaviour in office buildings and the evaluation of the influence of occupancy on building energy use. The results also support the efforts toward integrating behavioural models in building performance simulation applications and improving building management and automation

1. Introduction & Background

The interaction between building systems and building occupants is generally considered to be

one major influence on both the thermal comfort inside the building and the energy consumption of the building. Knowledge in this field can help in many fields of planning and operation of buildings. For instance, building control and automations systems can be adapted to the needs of the building occupants to optimize both comfort and energy consumption. Furthermore, the detailed knowledge about occupant behavioural patterns can help to better educate people in sustainable operation of the building systems in the future.

Multiple studies were carried out internationally to collect data on building user behaviour towards the building systems and devices. The following list of prior research efforts, for instance, states publications in the field of artificial lighting, and shade operation. Studies addressing the operation of artificial lighting systems include the following findings:

- Boyce (1980) found that generally the absolute number of operated luminaries is less in summer than in winter (following the seasonal change in daylight availability). Carter et al. (1999) further established this seasonal dependency of the lighting loads within buildings.
- Concerning the time of operation, Hunt (1979) identified the beginning and end of working days as the most frequent operation of lighting systems in offices with constant daytime occupancy. Reinhart and Voss (2003) observed that 86% of switching-on-operations are conducted upon arrival in the office.
- The correlation between illuminance levels on workplanes and switching on probability were examined by Hunt (1979), Love (1998), Reinhart and Voss (2003), and Mahdavi et al. (2007).

- Pigg (1996), Boyce (1980), Reinhart (2001) and Mahdavi et al. (2007) illustrate a strong connection between the probability of switching off the lights and the time elapsing until the user returns to the office: people are more likely to switch off the light if they leave their workplaces for a long period of time.

Studies addressing the manual operation of shades include the following findings:

- Rubin et al. (1978), Inoue et al. (1988) and Mahdavi et al. (2007) all document a strong dependency between shade operation and façade orientation.

- The main motivation for the blind operation is overheating and avoidance of direct insolation of the working spaces, according to Rubin et al. (1978), Rea (1984), Inoue (1988), Bülow-Hube (2000), and Reinhart (2001).

- Blinds are rarely changed, once they are set up following Rea (1984), Rubin et al. (1978), and Inoue (1988). Short-term changes in irradiance values are regularly not considered by building users.

The majority of the mentioned studies only considered the operation of the systems, and not the occupancy in the buildings. Therefore, there is a need for further research of user behaviour including both operation of systems and user occupancy behaviour. This could help to eliminate uncertainties if certain system operations take place or do not take place due to tolerable inside/outside conditions or due to the absence of users from the monitored spaces.

This contribution describes the efforts and results of observations of control-oriented occupant behaviour in a mechanically ventilated office building in Austria over a monitoring period of 10 months.

2. Methodology

2.1 Object description

The offices spaces monitored in this study are situated on the fifth floor of an office building that is situated in Lower Austria close to Vienna and was erected in 1963. The building will be referred to as SV in this contribution. The object serves as

the headquarters of a big international company. The building features 7 floors plus a setback roof floor, and a reinforced concrete frame structure enveloped by curtain façade elements consisting of alloy metal and insulated glazing. The overall dimensions of the building measure 138 m length, 14 m width and 31.5 m height. The building's longitudinal axis is aligned to north, leading to offices with east and west oriented windows. The building is fully air-conditioned and its windows are not operable for ventilation purposes. Figure 1 illustrates the west façade of the building and highlights the floor housing the monitored offices.



Fig. 1 – View of west façade of SV. The floor housing the monitored offices is highlighted.

Two types of offices can be found in SV: single workplace offices (1 workstation, “closed”, area from 13.41 to 27.22 m²), and multiple workplace offices (2 – 5 workstations, “open”-space, area from 27.22 and 41.03 m²). Separation walls follow the 2.50 m distance between structural axes and are made of glass or fabric-covered wood elements. The space between two axes is occupied by one or two workspaces and features a window that is inoperable including internal horizontal blind, one heating/cooling and air-conditioning unit and 2 rows of fluorescent luminaries. Figures 2 and 3 illustrate typical open and closed offices.

The heating/cooling and air-conditioning system of the building is controlled centrally. However, users can adjust the function of the units within each axis module. The system is capable of exchanging air (that can be pre-heated or pre-cooled) up to a maximum air change rate of 4 h⁻¹ (180 m³.h⁻¹). The HVAC-system is operated during working days between 05:00 am and 20:00 pm.

The luminaries are set in 2 rows (one close to the window, one close to the central hallway). Each

luminaire is equipped with 2 x 38 W fluorescent tubes. Luminaires rows can independently switched on / off by the users via switches next to the corresponding office door.

Each window features an adjustable internal horizontal blind, which can be manually operated by the users.



Fig. 2 (left) – closed office; Fig. 3 (right) – open-space office.

2.2 Data collection & processing

Monitoring was realized in 22 offices for a time period between May 2013 and March 2014. The data collection included both objective (measurements) and subjective (via interviews) methods. An overview about the monitored offices is provided in table 1.

Objective data collection included recording of temperature, relative humidity and illuminance in the offices via data loggers in five minute intervals, as well as hourly observations of occupancy and building systems status (shades, electrical lighting and thermostat) on random days during the observation period.

The status of the building systems was assessed according to the following scheme:

- The status of the heating/cooling & air-conditioning units was derived in steps of 0.1 from the state of the control unit, as depicted in Figure 4. During the winter period the “Max” setting represents a maximum of space heating, while “Min” represents the heating turned to minimum. During the summer period “Max” represents a maximum of cooling, while “Min” denotes that the system is barely cooling.
- The luminaries were assessed as rows. A value of 1 was logged if both rows inside of an office were turned on, a value of 0.5 was logged if just one row was switched on. A value of zero was noted in the record log if no artificial light was turned on at all at the moment of observation.

Table 1 – Monitored offices in the SV building. Data logger abbreviations: θ ... temperature [$^{\circ}$ C], RH... relative humidity [%], I... Illuminance [lx]

Orientation	Office No	Type	Installed Data logger	Users	Area [m ²]
E	1	Closed	θ	1	13.41
E	2	Open	Θ , RH, I	4	41.03
E	3	Open	θ	3	41.03
E	4	Closed	θ	1	13.41
E	5	Closed		1	13.41
E	6	Closed		1	27.22
E	7	Closed	θ	1	13.41
E	8	Closed	θ	1	13.41
E	9	Open		3	27.22
E	10	Open	Θ , RH, I	3	41.03
E	11	Closed	θ	1	13.41
E	12	Open	θ	3	27.22
W	13	Closed	Θ , RH, I	1	13.41
W	14	Closed	θ	1	13.41
W	15	Open	Θ , RH, I	3	41.03
W	16	Open		2	27.22
W	17	Closed	θ	1	27.22
W	18	Open	Θ , RH, I	5	41.03
W	19	Open	θ	2	27.22
W	20	Closed	θ	1	13.41
W	21	Open	θ	3	27.22
W	22	Closed	Θ , RH, I	1	13.41
Total				43	530

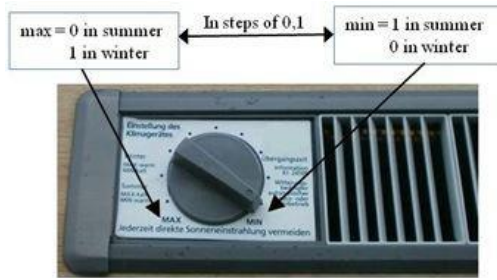


Fig. 4 – Heating/Cooling & Air Conditioning control settings.

- The position of the shades was recorded according to the percentage of shade deployment from completely open (0%) to completely closed shade (100%) in a step width of 20%, as illustrated in Figure 5. Additionally the angle of the shade elements was assessed following its daylight transmission: A value of 0 was recorded for completely closed angle on both sides, 0.8 for an angle 45° upwards, 0.6 for a 90° angle, and 0 for an angle of 45° downwards.

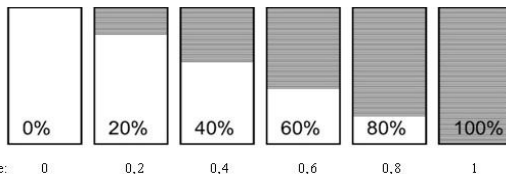


Fig. 5 – Shades positions and derived values.

External weather data were acquired from the ZAMG (Central Institute for Geometry and Geodynamics, Vienna) from a nearby weather station. This data included temperature, relative humidity, and solar irradiance for six months of the observation period.

The subjective evaluations of the offices were assessed via interviews. In sum, 35 building users were asked a structured query, containing personal information, perception of the indoor climate and control systems, operation and accessibility of the control systems, energy conscious behaviour and personal preferences. The results of the subjective queries were added to the fitting sections in the result section of this contribution.

Data processing was performed with standard spreadsheet applications and Matlab (2014). Data processing included generation of psychrometric charts out of the 5-minute interval data, and hourly aggregation of the values to couple them with the hourly observation data.

3. Results & Discussion

3.1 Occupancy

Occupancy patterns inside the offices can vary considerably. Figure 6 illustrates the mean occupancy load of the examined offices for a reference day. A heating load per person inside the office was defined via division of the standard load of 100 W (by a person) through the office’s total area of 530 m². This value of roughly 0.2 W.m⁻² was then used as multiplier for the average percentage of occupancy. The reference day shows peaks of occupancy loads around 10 am (11 W.m⁻²) and on early afternoon (10 W.m⁻²). Such estimations can be used as input data for detailed numeric building simulation.

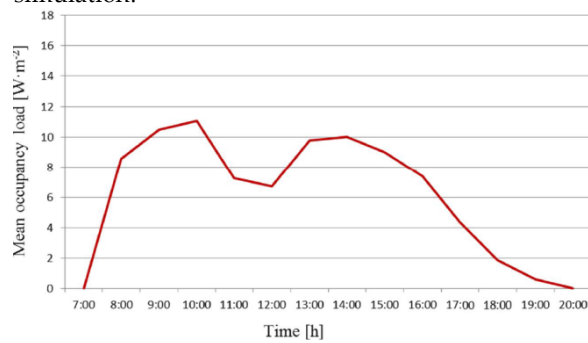


Fig. 6 – Occupancy load on a reference day.

The mean occupancy is 31% during working hours. This reveals that offices are not fully used during the day. An explanation could be that the structure of the people’s work often includes external meetings and to be away on construction jobs. Furthermore, the time considered as working hours was assumed from 08:00 am to 07:00 pm, exceeding the average employee’s 8-hour day. Moreover, many employees do not work full time but part time, limiting their time in the offices.

3.2 Heating/Cooling Units

A total of 39 heating/cooling units were observed in the 22 monitored offices. The different units vary in the frequency of control actions. Figure 7 shows the number of control actions in relation to the adjusted units. The majority of units were adjusted twice or less during the observation period. It can be said that the status of the heating/cooling units

was very seldom changed in the observation period.

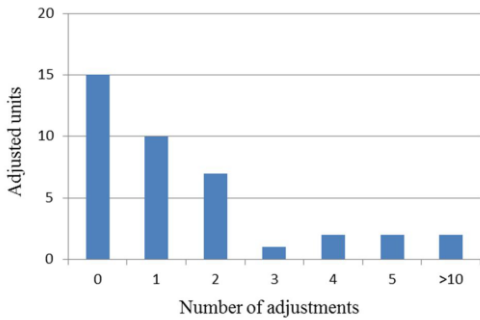


Fig. 7 – Adjusted thermostat units in relation to the number of adjustments over the observation period.

Figures 8 and 9 illustrate the monthly frequencies of attempts to increase and decrease the temperature. In both cases, October showed the highest tendency for control actions to change the internal conditions.

Fig. 8 – Monthly frequency of attempts to increase the temperature

To determine possible correlations between the performed control actions and indoor and outdoor temperatures, the frequencies of control actions were expressed as functions of indoor and outdoor temperatures. Figure 10 illustrates these frequencies.

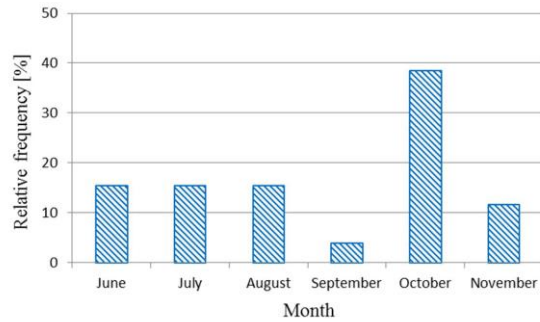


Fig. 9 – Monthly frequency of attempts to decrease the temperature

While attempts to increase temperature occurred for indoor temperatures between 20 and 24 °C and attempts to cool the indoor environment occurred for indoor temperatures between 23 and 28 °C, no clear pattern can be identified. The same is true for the relation between control actions and outdoor temperatures.

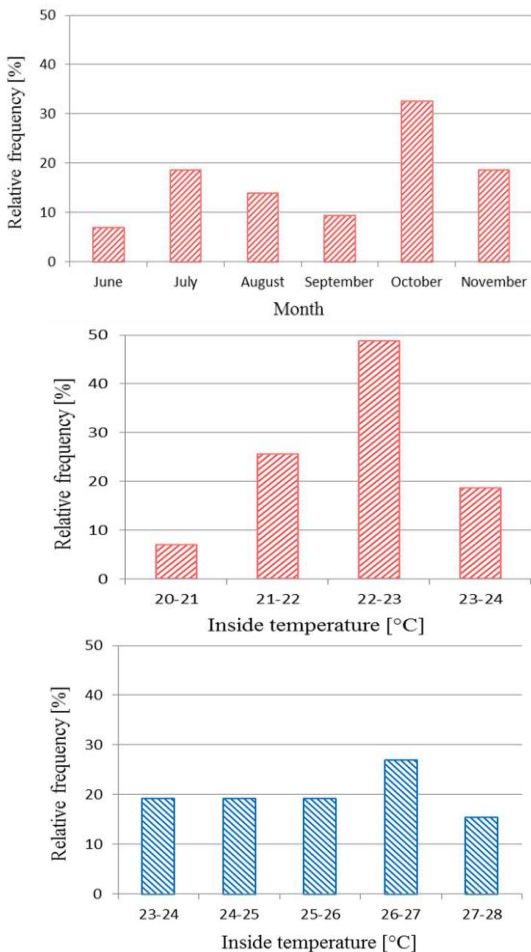


Fig. 10 – Frequency of attempts to increase the temperature as a function of the indoor (up left) and outdoor (up right) temperature. Frequency of attempts to decrease the temperature as a function of the indoor (low left) and outdoor (low right) temperature.

The high number of control actions in October could be explained by the fact that the general system changed from cooling to heating mode in that month. Interviews with the employees (as described in the data collection section) reveal that users mostly think that the adjustment of the control units barely changes the indoor temperatures, and is considered not able to be adapted to personal requirements. Although the building’s system was quite well designed for the time of the building’s erection, and since then constantly checked and updated, 54% of the building’s users consider the improvement of the heating/cooling system in the building as an urgent improvement necessity. Moreover, 80% of the building users felt dissatisfied with the fact that the windows of the buildings cannot be opened and that they are dependent on the fresh air from the heating/cooling and air conditioning units.

3.3 Electrical Lighting

Both the status of the luminaries and the operation of turning on and off the luminaries were examined. The overall mean lighting operation probability of luminaries turned on in SV ranges between 30 and 40% between 8:00 am and 4:00 pm, and drops to 10% at 7:00 pm (Figure 11). To examine the impact of season and orientation on the lighting operation, corresponding data splits were analysed. Figures 12 and 13 illustrate these impacts. Summertime shows significantly lower lighting operation probability. The same is true for east-oriented offices. During the observation period, the different offices showed a probability of between 5 and 100% that the light is turned on when offices are occupied, and a probability of between 0 and 40% that the light is turned on when offices are unoccupied. On average, the luminaries were switched on 56% of the occupied time and 15% of the unoccupied time.

Similar to the mentioned studies before, a high probability of switching the luminaries on could be found at the beginning of the workday: over 70% of all switching on actions were performed between 8:00 and 9:00 am. This seems to be widely independent from the mean global irradiance (Figure 14).

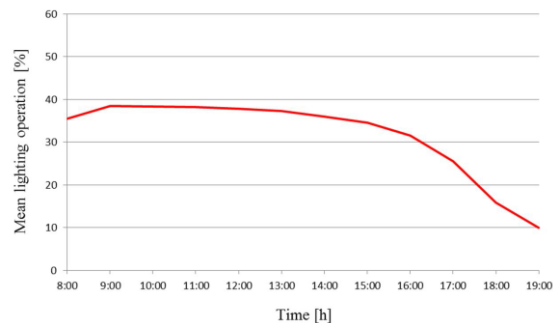


Fig. 11 – Mean lighting operation in the offices of SV

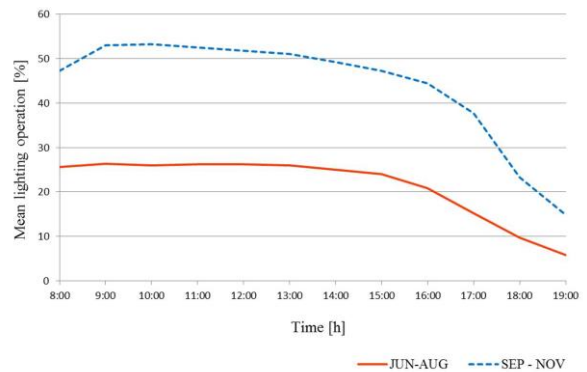


Fig. 12 – Seasonal differences in lighting operation probability

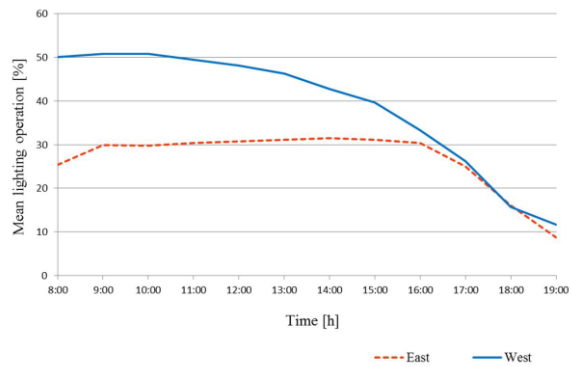


Fig. 13 – Operational differences in lighting operation probability.

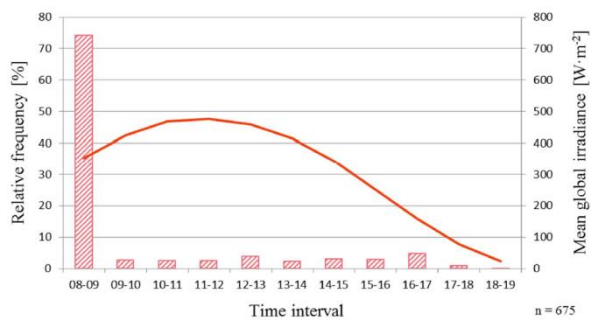


Fig. 14 – Light switching on operations over the course of the day. Line: course of global irradiance.

Furthermore, a correlation between the prevailing illuminance levels inside the offices and the frequency of switching on operations can be seen: the lower the prevailing illuminance is, the higher the probability for switching operation is (for an illuminance between 0 and 100 lux a switching on probability of 73% could be assessed). Switching off operations are high likely to be performed if the occupancy absence is long (71% for absences of over 180 minutes), while medium absence times only show low probabilities of switching the light off.

3.4 Internal Shades

Shading deployment is dependent on season and orientation of the offices. In summer (Jun – Aug) the mean shade deployment ranges on the east façade between 73 and 82% and on the west façade between 61 and 73%. In autumn (Sep – Nov) these values range between 60 and 65% (east) and 60 and 70% (west). A correlation between both global irradiance and outdoor temperature and the deployment of shades could be recognized. Figure 15 illustrates the monthly shade deployment degree in the SV offices and the mean global irradiance.

Concerning the opening and closing of shades, similar to the luminaries, a strong operation could be identified between 8:00 and 9:00 am. Later, the deployment and opening probabilities barely surmount 10%, depending on orientation and corresponding sun penetration.

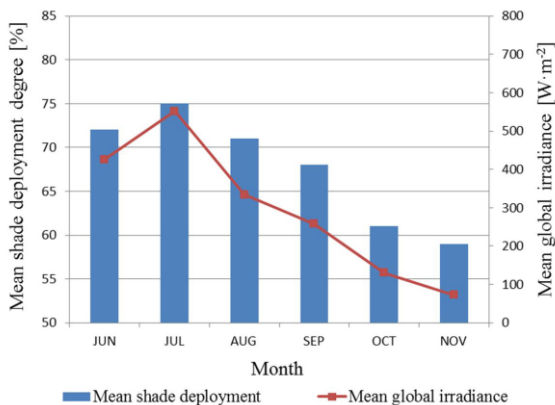


Fig. 15 – Mean monthly shade deployment degree and mean global irradiance.

3.5 Thermal Comfort

Concerning thermal comfort, the majority of observation data points were found to be within the limits of comfort zones. Figure 16 illustrates the psychrometric charts for office no. 2 in all four seasons.

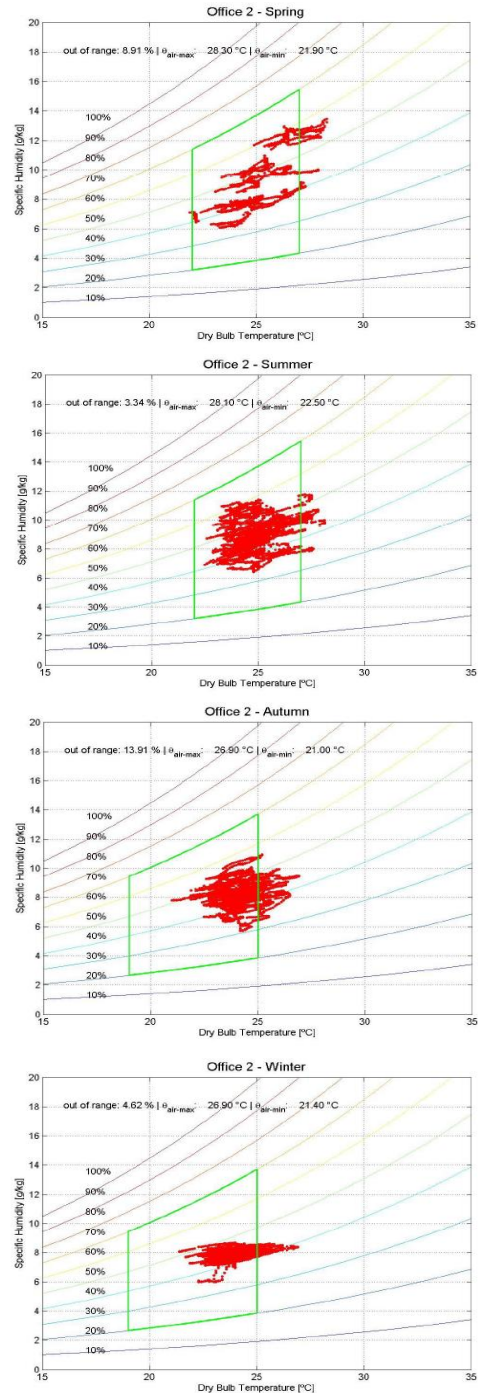


Fig. 16 – Psychrometric charts for office no 2 for spring, summer, autumn and winter

Averaged over all offices, spring months (May – Jun 2013) showed around 8.13% data tuples outside the comfort limits. In summer (Jun–Sep 2013) 3.13%, in autumn (Sep–Dec. 2013) 9.7% and in winter (Dec 2013–Mar 2014) 4.44% of the data tuples were in average found outside of the comfort limits. Detailed graphs can be found in Seres (2014).

4. Conclusion

This contribution analysed system operation and user behaviour patterns in the offices of a mechanically ventilated building. Results show distinctive patterns: for instance, the lighting load profile and the mean occupancy profile are not similar to each other, portraying that users do not show a very energy conscious behaviour. Even if the indoor climate conditions in the building stay within the comfort limits, users show a big dissatisfaction with the HVAC system.

The findings of this study are expected to increase the knowledge of user behaviour in office buildings. This potentially will help to model user behaviour in numeric thermal building simulation.

Future research in the field of user behaviour should focus on a larger sample of buildings with different geographical and cultural backgrounds. This could improve the understanding of control-oriented behaviour and the human factor of buildings.

Furthermore, the results of the multitudes of studies conducted on human behaviour in buildings could be unified and compared based on the research methodology. As a long-term goal, research efforts could adopt the best approaches of the different research techniques to develop a unique and ubiquitous method for developing occupancy models through building observation. Such a standardized assessment method would ease further investigation in the field of occupancy monitoring and occupancy modelling.

References

Boyce, P. 1980 Observations of the manual switching of lighting. *Lighting Research & Technology* 12(4): 195-205

- Bülou-Hube, H. 2000. *Office worker preferences of exterior shading devices: a pilot study*. EuroSun2000. June 19-22, Copenhagen, Denmark
- Carter, D., Slater, A. & Moore, T. 1999. *A study of lighting in offices equipped with occupant controlled systems*. Proceedings of the 24th Session of CIE, Warsaw, Poland; CIE, Vienna, Austria: 1999; 108-110, 1(2).
- Hunt, D. 1979. The use of artificial lighting in relation to daylight levels and occupancy. *Building Environment* 14, 21-33
- Inoue, T., Kawase, T., Ibamoto, T., Takakusa, S. & Matsuo, Y. 1988. The development of an optimal control system for window shading devices based on investigations in office buildings. *ASHRAE Transaction* 94, 1034-1049
- Mahdavi, A., Suter, G., Pröglhöf, C., Mohammadi, A., Lambeva, L., & Kabir, E. 2007. *People as power plant – Final Report*. Energiesysteme der Zukunft, Bundesministerium für Verkehr, Innovation und Technologie, Projektnummer 80808563-8846
- Matlab 2014. <http://de.mathworks.com/> (last accessed Nov 2014)
- Pigg, S., Eilers, M., Reed, J. 1996. Behavioral aspects of lighting and occupancy sensors in private offices: a case study of a university office building. Proceedings of the 1996 ACEEE Summer Study on Energy Efficiency in Buildings, 8.161-8.171
- Rea, M.S. 1984. Window blind occlusion: a pilot study. *Building & Environment* 19(2), 1984, 133-137
- Reinhart, C. 2001. *Daylight availability and manual lighting control in office buildings – simulation studies and analysis of measurements*. PhD.-Dissertation, University of Karlsruhe, Germany
- Reinhart, C. & Voss, K. 2003. Monitoring manual control of electric lighting and blinds. *Lighting Research & Technology* 35(3), 243-260
- Rubin, A.I., Collins, B.L., & Tibbott, R.L. 1978. *Window blinds as potential energy saver – a case study*. NBS Building Science Series, Vol. 112, National Institute for Standards and Technology, Gaithersburg, MA, USA.
- Seres, L. 2014. User's Behaviour and Perception of the Indoor Climate in a mechanically ventilated office Building. Diploma Thesis, Vienna University of Technology, 2014.

Window shades: selecting optical properties for visual comfort

Ying-Chieh Chan – School of Civil Engineering, Purdue University – ychan@purdue.edu

Athanasios Tzempelikos – School of Civil Engineering, Purdue University – tzempel@purdue.edu

Abstract

Currently, there is no methodical procedure for selecting solar-optical properties of roller shades, which affect the energy and indoor environmental performance of perimeter building zones. This paper presents a new systematic methodology for identifying the range of shading properties (openness factor and visible transmittance) that can significantly reduce the risk of glare. A model that calculates angular beam-beam and beam-diffuse shading optical properties using minimum inputs is used within a hybrid ray-tracing and radiosity daylighting model, validated with full-scale experiments. The temporal variation of beam and total vertical illuminance is used to define the annual visual discomfort frequency and establish a process for selecting the range of acceptable shading properties for each set of external parameters (location, orientation, glazing visible transmittance, and buffer zone). Recommendations for openness factors and visible transmittance values are made for different scenarios. Selecting the upper limits of suggested ranges can provide more daylight into the space and reduce the probability of high contrast. These guidelines may be used for selection of shading products, followed by considerations about energy savings and provision of outside view.

1. Introduction

Interior roller shades, commonly used in North America, allow occupants to control daylight, solar heat gain, visual connection to the outdoors, as well as visual comfort. Several studies have shown the lighting energy saving potential of shading control (Hviid et al., 2008; Shen and Tzempelikos, 2012). However, there is no systematic procedure for selecting solar-optical properties of roller shades, to assist engineers, building scientists and designers in their decisions that affect the energy and indoor environmental performance of

perimeter building zones (Tzempelikos, 2008).

In the fenestration and shading selection and decision-making process, visual comfort should be a priority for any manual or automated shading system. Nevertheless, roller shade selection lacks widely adopted guidelines addressing visual comfort concerns. In this paper, a new systematic methodology is proposed for identifying the range of shading optical properties (openness factor and visible transmittance) that can significantly reduce daylight glare issues. A hybrid ray-tracing and radiosity daylighting model, using adjusted solar-optical properties is used to analyze the temporal frequency of two vertical illuminance criteria violations (annual visual discomfort frequency) and determine a range of acceptable openness factors and visible transmittance values. Finally, guidelines for selecting properties of shading fabrics are provided for different scenarios. Using these recommendations as a basis, designers and engineers can consider other factors such as energy savings, outside view and daylight availability for selecting shading products.

2. Solar optical properties of roller shades

Roller shades come in a wide variety of colors and patterns with varying degrees of shading and weave construction that result in different degrees of openness and transmission/reflection characteristics. Visible transmittance, openness and color have a direct impact on indoor daylight conditions and discomfort glare. Other factors, such as reflectance and absorptance, are more important for controlling solar heat gain. When direct radiation strikes the shade surface, it is split into two portions: the unobstructed portion,

directly transmitted through the openings (beam-beam portion), and the interrupted portion –part of which will be scattered in the forward direction (transmitted), another part scattered in the reverse direction (reflected), and the rest is absorbed by the fabric material. As a result, except for the angular dependence, the beam-diffuse split of solar radiation (or illuminance) through roller shades needs to be considered.

However, detailed property measurements are rarely conducted for most available products since they are expensive and time-consuming. Usually, shading fabric manufacturers provide a single value of (average) visible and solar total transmittance and reflectance at normal incidence when demonstrating or specifying their products, together with openness factor and color. Even these properties are often not properly measured (Chan et al., 2014). Therefore, a reliable approach to estimate the detailed (off-normal and beam-to-diffuse) properties from such limited information, such as the method proposed by Kotey et al. (2009), is desired for more accurate thermal and daylighting modeling. Other methods (EnergyPlus, 2013) are either inaccurate (using constant values or ignoring angular characteristics) or too complex, such as the geometrical radiosity method to estimate BSDFs of woven shades (Carli Inc., 2014).

2.1 Visible transmittance (VT), openness factor (OF) and color

The term “openness factor” refers to the “open” or “see-through” percentage of the shading fabric. Openness allows a visual connection to the outside, as well as direct light transmission. Different solar shading fabrics have different degrees of weave density and therefore different openness factors. Beam-diffuse transmission was often ignored in simplified daylighting calculations (i.e., in EnergyPlus shading module); consequently, the error in daylight autonomy and annual glare risk predictions could reach 60% (Chan et al., 2014). VT describes the percentage of visible light transmitted through the fabric and is related to the color and openness factor of the fabric. However, the relationship between openness factor, color,

and visible transmittance cannot be simply formulized.

2.2 Semi-empirical model by Kotey et al. (2009)

Kotey et al. (2009) developed a semi-empirical model for direct-direct, direct-diffuse and angular shade properties. The model was extracted from detailed integrated sphere measurements (Collins et al., 2012) of the spectral beam-beam transmittance, beam-diffuse transmittance, and beam-diffuse reflectance of different shading fabrics at incident angles ranging from 0° to 60°. The spectral data was converted to solar optical properties according to ASTM standards, and a cosine power function was fitted to the measured properties at different incident angles. This method seems to be reliable and useful, since it is based on physical quantities and allows to extract the necessary shade properties (for straightforward use in detailed models) using only beam-total transmittance at normal incidence, usually provided by manufacturers. Therefore, for all typical cases when limited fabric properties information is available, this model is preferred and is used in the methodology described later.

3. Daylighting model

To understand the impact of fabric properties on visual comfort and daylight availability, the semi-empirical properties model was embedded in a hybrid ray-tracing and radiosity model that maintains satisfactory levels of efficiency and accuracy. The model was then used to run a series of simulations to study the role of different properties and establish a methodology for selecting appropriate values for glare protection.

The daylighting model (Chan and Tzempelikos, 2012) uses TMY3 weather data (or sub-hourly computed or measured data) and first calculates direct and diffuse daylight incident on a window using solar geometry and the Perez et al. model (1987). If field measured data is available, then these are used as inputs (e.g., for validation purposes or for real-time, model-based control).

Daylight transmission through any (simple or complex) fenestration system is next, and in this case, detailed beam-beam, beam-diffuse and off-normal properties of roller shades were calculated using the semi-empirical model (Kotey et al., 2009) described above. The glazing optical properties are determined using the WINDOW 7 software (LBNL, 2013). Direct sunlight transmitted and/or specular reflections in the room are tracked with the ray-tracing module, while the radiosity module computes interior diffuse reflections and final illuminance distributions. The daylight transmitted through the window is not uniformly distributed; the model corrects the sky and ground luminance according to sky and ground illuminance, occupant (or sensor) view direction, and then uses these values to further estimate work plane and vertical illuminances. Given the space geometry and interior reflectivities, the model finally calculates interior illuminance and luminance distributions, glare indices, as well as respective annual metrics. The model has been validated with full-scale experimental measurements, and comparison with Radiance and Daysim for various shading scenarios (Chan and Tzempelikos, 2012).

4. Methodology for selecting shade properties and visual comfort restrictions

4.1 Criteria for visual comfort

Several different criteria and metrics have been introduced to identify daylight discomfort glare. Illuminance-based criteria, such as work plane illuminance, are used in design guidelines. For example, IES Standard LM-83-12 (2012) recommends that no more than 10% of the work plane area should receive more than 1000 lux of direct sunlight for more than 250 hours per year (ASE metric). Useful daylight illuminances (*UDI*) were defined with an upper work plane illuminance limit of 2000 lux (Nabil and Mardaljevic, 2006) to identify conditions that might result in visual or thermal discomfort. However, field studies have showed significant differences in preferred illuminance levels (Van Den

Wymelenberg and Inanici, 2014). Luminance-based criteria (luminance ratios or constant thresholds) are also widely used for glare (Konis, 2014) and are reported in IES lighting handbooks (Rea, 2000). Glare indices that combine the illuminance- and luminance-based criteria, also using the position index and glare source size, are forward-looking approaches. However, due to their complexity, they have not been extensively used in design guidelines. Daylight Glare Probability (Wienold and Christoffersen, 2006) considers both the vertical (eye) illuminance and glare source luminance, while DGI focuses on the impact of luminance contrast. Several studies have shown that DGP performs better (Vincent, 2012; Van Den Wymelenberg and Inanici, 2014) while others reported the opposite (Hirning, 2014). Researchers hardly reproduce the same results when applying the same metrics to different spaces and different fenestration systems. The different methods have their advantages and limitations. The authors of this paper agree with the statement by Jakubiec and Reinhart (2013) that multiple criteria are required for an integrated visual discomfort evaluation, especially if direct sunlight is somehow transmitted into the space. The exact metrics and criteria need to be further studied.

The situation is more complex for the case of roller shades, which transmit direct and diffuse light into the space and allow a view of the sun through the fabrics. Discomfort glare studies in spaces with roller shades are scarce. A recent study (Konstantzos and Tzempelikos, 2014) pointed out the issue of seeing the sun through a shading fabric has not been studied. Even for fabrics with very low openness (1%), when the sun is within the field of view, its contributed luminance could be greater than 10^6 cd/m², but at the same time the direct-direct illuminance received by occupants' eyes can be very low –less than 300 lux. Although this usual scenario will fail all luminance-based glare criteria (absolute luminance, luminance ratio, DGI, DGP), most 1% open fabrics are not expected to result in significant glare problems (Fernandes and Lee, 2014). More occupant-based studies are needed in spaces with roller shades to reach solid conclusions.

Based on the above, illuminance-based criteria are used in this study. Vertical illuminance on the eye (E_v) is selected as a more appropriate parameter (compared to work plane light levels) since recent findings support that it outperforms all commonly used visual comfort metrics (Van Den Wymelenberg and Inanici, 2014). In addition, the original DGP study also demonstrates a good correlation between E_v and glare probability.

The proposed method utilizes two vertical illuminance criteria to evaluate the risk of visual discomfort:

- $E_{v, beam} < 1000$ lux
- $E_{v, total} < 2670$ lux

The first criterion is used to check if the occupant (virtual sensor in the simulation model) receives more than 1000 lux of beam illuminance (sunlight) on the eye –a modification of IES LM-83-12. The second criterion checks for total vertical illuminance on the eye and is derived from the simplified version of daylight glare probability, DGPs:

$$DGPs = 6.22 \times 10^{-5} E_v + 0.184 \quad (1)$$

When E_v exceeds 2670 lux, glare probability reaches 0.35, which is considered the (lower) limit of acceptable values. This criterion addresses the overall impact of vertical illuminance, including transmitted direct, direct-diffuse and diffuse light and contribution from interior reflections. The only limitation of this method is that it cannot adequately capture all contrast effects (Wienold, 2009) as discussed later. The two criteria *and the temporal frequency of violations* are used in the annual simulation as described below to determine acceptable openness factors and visible transmittance values respectively.

4.2 Selection of shade properties based on annual visual discomfort frequency

Fig. 2 presents the process of identifying an acceptable range of roller shade properties. For any scenario (location, orientation, window properties, room configuration), the developed model runs a series of annual parametric simulations containing fabrics with variable openness factors and visible transmittance values (from 1% to 20%). Vertical

illuminance on the eye level is calculated at different distances from the window (buffer zone limit), but always for the case facing the window, to determine maximum property values for the worst case scenario (highest risk of glare). The logic consists of three steps:

- The annual simulation results are first used to calculate the percentage of working hours in the year (8am – 6pm) during which the first criterion (direct vertical illuminance >1000 lux) is not satisfied. These results are used to determine the acceptable range of fabric openness factors based on a strict and a more flexible constraint (0% and 5% frequency).
- The next step is to calculate the percentage of working time in the year during which none of the two criteria are satisfied. This value is defined as the **annual visual discomfort frequency** and is used to determine the range of maximum visible transmittance in a similar way.
- In most cases, the selected openness factor is smaller than the selected visible transmittance values ($OF < VT$). However, for some scenarios with few sunlight hours, diffuse illuminance dominates in annual-based considerations, resulting in more restricted visible transmittance values, sometimes smaller than the openness factors determined in the first step. In such cases, the acceptable range of openness factors is adjusted to match (equal) the selected VT values.

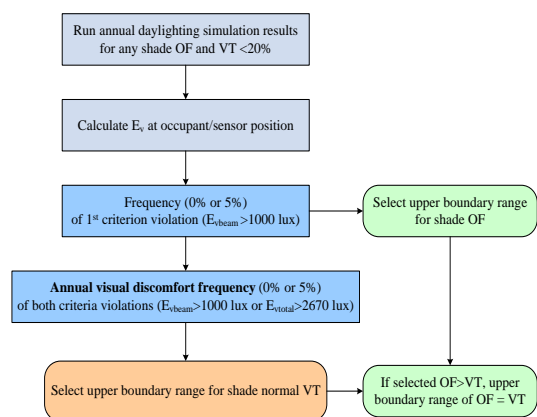


Fig. 2 – Process for selecting acceptable ranges of shade openness factor and visible transmittance based on annual temporal frequency of vertical illuminance restriction violations

5. Results

Following the above methodology, simulation results and shade selection guidelines are presented for different locations, orientations, window properties and occupant positions (buffer zones) as shown in Table 1. The analysis was done for a medium-size perimeter office space (12 m × 12 m × 3 m high) having one exterior façade with 70% window-to-wall ratio. The reflectances of ceiling, vertical walls and floor are 80%, 50% and 20% respectively. Continuous daylight autonomy is also presented as a design reference (work plane illuminance set point is 500 lux). Tables 2 and 3 in section 5.2 show the overall results and recommendations for selecting shading properties for every studied scenario.

Table 11 – Variable simulation parameters

Parameter	Range
Shade Visible Transmittance	1% - 20%
Openness Factor	1% - 20%
Location	Phoenix, New York
Orientation	South, Southwest, West, Northwest, North
Glazing Visible Transmittance	65%, 50%, 35%
Buffer Zone (occupant distance from window)	0.91m, 1.83m, 2.74m

5.1 Impact of shade Openness Factor and Visible Transmittance

While one would expect higher OF and VT to result in higher risk of glare, the combined impact of visible transmittance and openness factor on annual discomfort frequency is non-linear and complex, since it involves the implications of simultaneous beam-to-beam and beam-to-diffuse daylight transmission. Higher differences between VT and OF values indicate light-colored fabrics with more diffuse characteristics. Fig. 3 presents annual visual discomfort frequency results for Phoenix, with 0.91m buffer zone and 65% glazing visible transmittance, for a south and a northwest façade. For the south facade, there is no significant discomfort for shades with $OF < 3\%$ and $VT < 6-7\%$, thus these would be the upper boundary ranges for this case. Higher OF or VT values will result in

unacceptable discomfort values; for higher openness factors, the two criteria overlap and the VT lines converge. For the northwest façade, smaller variations are observed (due to less hours of sunlight) and shades with $VT < 10\%$ satisfy the 5% discomfort frequency limit for almost any OF value. The 0% restriction is never satisfied because the sun is low for several hours in the year for this orientation.

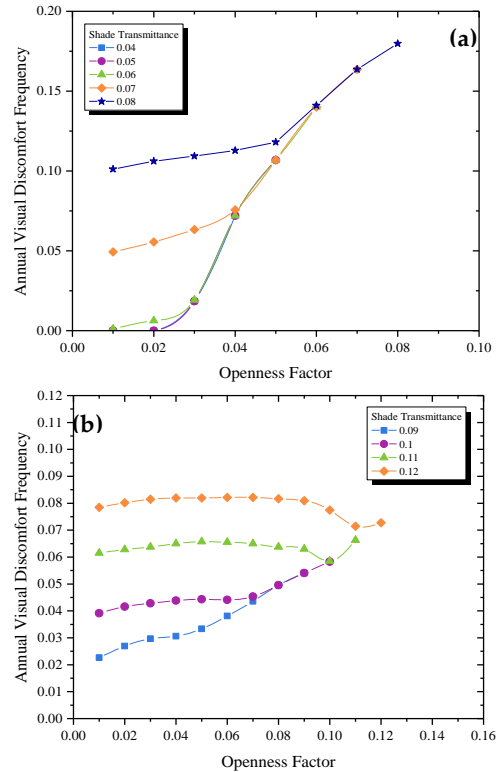


Fig. 3 – Combined impact of openness factor and visible transmittance on annual visual discomfort frequency for (a) south and (b) northwest orientation in Phoenix (0.91m buffer zone, 65% glazing normal VT)

The significance of the two vertical illuminance criteria and their overlap with respect to selection of shade properties are presented in Fig. 4, showing temporal graphs with violation frequency of each criterion and their combination for the same space facing south (Fig. 3a), using three fabrics with different properties. The first criterion restricts OF and direct sunlight transmission; using the first fabric (3% OF, 6% VT) that has a minimum discomfort frequency as a baseline, increasing OF to 4% (2nd set of graphs), causes $E_{v,beam}$ to exceed 1000 lux for more hours. The second criterion restricts VT and total light transmission; when VT increases to

7% (3rd set of graphs), $E_{v,total}$ exceeds 2670 lux for more hours. Their combined effect on annual visual discomfort frequency (last graph in every set) is used to restrict both OF and VT as shown in Fig. 2.

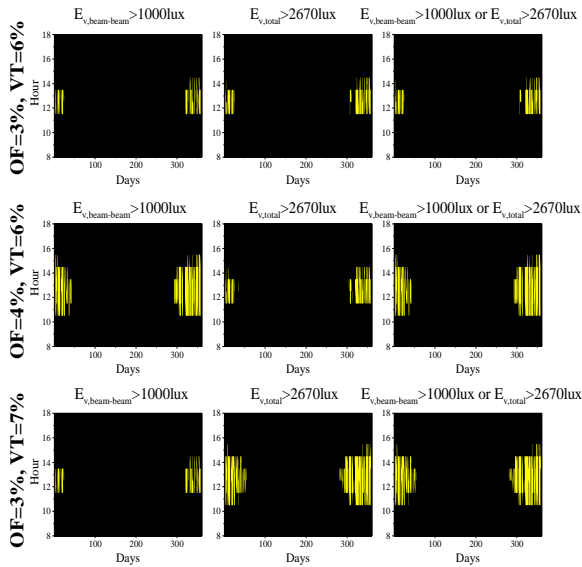


Fig. 4 – Temporal graphs of violation frequency of each vertical illuminance criterion and their combination (annual visual discomfort frequency) for three shading properties

5.2 “Glare-safe” boundaries of shade properties

A graphical representation of utilizing simulation results to select shading properties is presented in Fig. 5. Annual discomfort frequency values are shown in contour plots for every set of external parameters, with shade OF on the y-axis and shade VT on the x-axis. The curved shape of contours indicates the non-linear effects of both properties

(for higher, non-recommended values, VT becomes the dominant factor). For the case presented here, values within the 0% or within the 5% area in Fig. 12(a) are considered acceptable for visual comfort. This allows for the selection of different combinations of shade OF and VT values within these boundaries, resulting in the same effect on visual discomfort. However, the impact of these acceptable combinations on daylight autonomy are quite different, as shown in Fig. 5(b), with dashed lines showing the upper boundary limits. Products with higher VT and smaller OF within these “glare-safe” boundaries provide more daylighting benefits. The results for all studied scenarios with recommended shading OF and VT (maximum acceptable values) are summarized in Tables 2 and 3, for annual visual discomfort frequency of 0% and 5% respectively. These results are consistent with the previous sections findings and contain the impact of orientation, location, glazing properties and buffer zone limit on the selection process. The 5% frequency results of Table 3 are presented because visual discomfort is always subjective and occupants might tolerate slightly higher values of vertical illuminance for 5% of the working time (and higher shading property values allowing more daylight and outside view). Note that, in that case, Phoenix has stricter limitations than New York, because of more sunlight hours. North-facing facades are not bounded by any OF limit for most cases.

Table 12 – Recommended maximum values of shade OF (and VT in parenthesis) for 0% annual visual discomfort frequency

Buffer Zone	Orientation	New York			Phoenix		
		Glazing Visible Transmittance			Glazing Visible Transmittance		
		0.65	0.5	0.35	0.65	0.5	0.35
0.91m	S	2% (5%)	3% (7%)	4% (9%)	2% (5%)	3% (6%)	4% (6%)
	SW	2% (5%)	2% (6%)	4% (8%)	2% (4%)	2% (6%)	3% (8%)
	W	2% (5%)	3% (7%)	4% (9%)	2% (5%)	2% (6%)	4% (7%)
	NW	3% (7%)	5% (9%)	7% (11%)	3% (6%)	4% (8%)	6% (10%)
	N	-	-	-	-	-	-
2.74m	S	2% (9%)	3% (10%)	4% (13%)	3% (9%)	4% (12%)	6% (15%)
	SW	2% (7%)	2% (10%)	4% (12%)	2% (7%)	2% (9%)	3% (12%)
	W	2% (9%)	3% (10%)	4% (13%)	2% (8%)	2% (10%)	4% (12%)
	NW	3% (12%)	5% (14%)	7% (17%)	3% (10%)	4% (12%)	6% (15%)
	N	-	-	-	-	-	-

Table 3 – Recommended maximum values of shade OF (and VT in parenthesis) for 5% annual visual discomfort frequency

Buffer Zone	Orientation	New York			Phoenix		
		Glazing Visible Transmittance			Glazing Visible Transmittance		
		0.65	0.5	0.35	0.65	0.5	0.35
0.91m	S	4% (7%)	6% (8%)	8% (10%)	3% (6%)	4% (8%)	6% (9%)
	SW	4% (7%)	5% (8%)	7% (10%)	3% (6%)	4% (7%)	5% (9%)
	W	4% (7%)	5% (8%)	8% (10%)	3% (6%)	4% (7%)	5% (9%)
	NW	13% (13%)	15% (15%)	16% (16%)	8% (10%)	10% (11%)	13% (13%)
	N	-	-	-	-	-	-
2.74m	S	7% (14%)	10% (16%)	14% (19%)	12% (12%)	15% (15%)	18% (18%)
	SW	4% (12%)	6% (14%)	9% (16%)	3% (10%)	4% (12%)	6% (14%)
	W	5% (12%)	6% (15%)	9% (17%)	3% (9%)	4% (11%)	5% (15%)
	NW	-	-	-	17% (17%)	-	-
	N	-	-	-	-	-	-

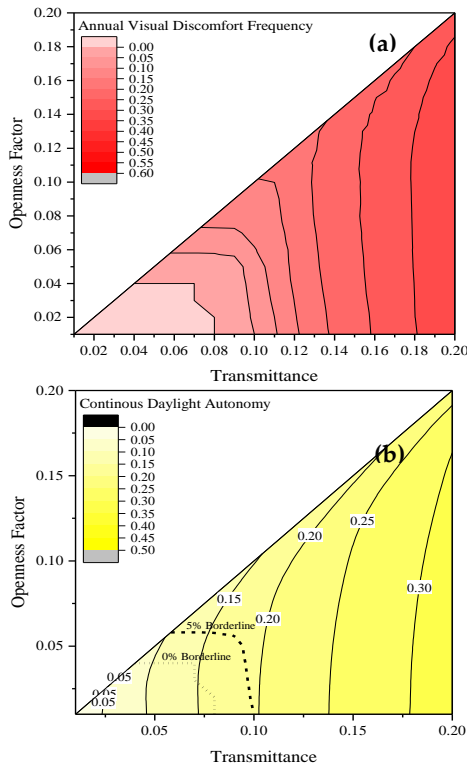


Fig. 5 – Selection of “glare-safe” boundaries of shade OF and VT based on annual visual discomfort frequency (a) and impact on continuous daylight autonomy (b), for the case of a west facing office in Phoenix, 0.91m buffer zone, 35% glazing normal VT)

6. Conclusion

This paper presents a new systematic methodology for identifying the range of shading optical properties (openness factor and visible transmittance) that can significantly reduce the risk of daylight glare. A semi-empirical model that calculates angular beam-beam and beam-diffuse shading optical properties using minimum inputs provided by shading manufacturers is used in a hybrid ray-tracing and radiosity daylighting model. Two vertical illuminance criteria, for beam and total illuminance on the eye, are used to establish visual comfort restrictions. The temporal variation of the two criteria is used to calculate the annual visual discomfort frequency, which is used to define a process for selecting the range of acceptable shading properties for each set of external parameters (location, orientation, glazing visible transmittance, and buffer zone).

The combined impact of visible transmittance and openness factor on annual discomfort frequency is complex. Following the proposed methodology, recommendations for roller shade properties are provided for different scenarios. Different openness factors and visible transmittance values are recommended for different locations, orientations and glazing properties. Smaller values are required for orientations between south and west, while north facing facades have essentially negligible restrictions. The upper limits of suggested ranges of these properties are recommended to provide more daylight into the

space and reduce the possibility of higher contrast. Using these recommendations as a basis, designers and engineers can consider other factors such as energy savings, outside view and daylight availability for selecting shading products. Further research is needed towards a glare index applicable to cases with direct sunlight transmitted into the building, and towards overall fenestration system optimization including related system controls.

7. Acknowledgment

The authors would like to thank the Purdue Research Foundation and Lutron Electronics Co Inc for partially funding this research, and Professor Michael Collins from the University of Waterloo for conducting the integrated sphere measurements and providing accurate shading properties.

References

- Carli Inc., Implementation of wovenshade method in layeroptics.dll, retrieved 8/2014, from: <http://windows.lbl.gov/software/window/Docs/Woven%20Shade%20Technical%20Documentat%20ion.pdf>
- Chan, Y.C., Tzempelikos A., A hybrid ray-tracing and radiosity method for calculating radiation transport and illuminance distribution in spaces with venetian blinds, *Solar Energy* 86 (11) (2012) 3109-3124.
- Chan, Y.C., Tzempelikos A., Protzman B., Solar optical properties of roller shades: modeling approaches, measured results and impact on energy use and visual comfort, Proc. of 3rd International High Performance Buildings conference at Purdue, West Lafayette, Indiana, July 2014.
- Collins, M., Wright J.L., Kotey N.A., Off-normal solar optical property measurements using an integrating sphere, *Measurement* 45(1) (2012) 79-93.
- EnergyPlus. EnergyPlus Engineering Reference – The Reference for EnergyPlus Calculations, Lawrence Berkeley National Laboratory (LBNL), 2013.
- Fernandes, L.L., Lee E.S., DiBartolomeo D.L., McNeil A., Monitored lighting energy savings from dimmable lighting controls in The New York Times Headquarters Building, *Energy and Buildings* 68 (2014) 498-514.
- Hirning, M.B., Isoardi G.L., Cowling I., Discomfort glare in open plan green buildings, *Energy and Buildings* 70 (2014) 427-440.
- Hviid, C.A., Nielsen T.R., Svendsen S., Simple tool to evaluate the impact of daylight on building energy consumption, *Solar Energy* 82(9) (2008) 787-798.
- IESNA. IES Standard LM-83-12. Approved method: IES spatial daylight autonomy (sDA) and annual sunlight exposure (ASE). Illuminating Engineering Society of North America, New York, 2012.
- Jakubiec, J.A., Reinhart C.F., Predicting visual comfort conditions in a large daylit space based on long-term occupant evaluations: a field study, Proceedings of IBPSA13 conference, Chambéry, France, 2013.
- Konis, K., Predicting visual comfort in side-lit open-plan core zones: results of a field study pairing high dynamic range images with subjective responses, *Energy and Buildings* 77(0) (2014) 67-79.
- Konstantzos I., Tzempelikos A., Chan Y-C., Experimental and simulation analysis of daylight glare probability in offices with dynamic shading, *Building and Environment*, under review, 2014.
- Kotey, N.A., Wright J.L., Collins M.R., Determining off-normal solar optical properties of roller blinds, *ASHRAE Transactions* 115(1) (2009) 145-154.
- LBNL, 2013. WINDOW 7 simulation manual. Lawrence Berkeley National Laboratory. <http://windows.lbl.gov/software/window/7>
- Nabil A, Mardaljevic J., Useful daylight illuminances: a replacement for daylight factors, *Energy and Buildings* 38 (2006) 905-913.
- Perez, R., Seals R., Ineichen P., Stewart R., Menicucci D., A new simplified version of the perez diffuse irradiance model for tilted surfaces, *Solar Energy* 39(3) (1987) 221-231.

- Rea, M.S., *The IESNA lighting handbook: reference & application*, Illuminating Engineering Society of North America, New York, 2000.
- Shen, H. and Tzempelikos A., Daylighting and energy analysis of private offices with automated interior roller shades, *Solar Energy* 86(2) (2012) 681-704.
- Tzempelikos, A., A review of optical properties of shading devices, *Advances in Building Energy Research* 2(1) (2008) 211-239.
- Van Den Wymelenberg, K., Inanici M., A critical investigation of common lighting design metrics for predicting human visual comfort in offices with daylight. *Leukos* 10(3) (2014) 145-164.
- Vicent, W, Comparing visual comfort metrics for fourteen spaces using simulation-based luminance mapping, MS Dissertation, University of Southern California, 2012.
- Wienold J., 2009. Dynamic daylight glare evaluation. Proceedings of IBPSA 2009 conference, Glasgow, Scotland, pp. 944-951.
- Wienold, J., Christoffersen J., Evaluation methods and development of a new glare prediction model for daylight environments with the use of CCD cameras, *Energy and Buildings* 38(7) (2006) 743-757.

ProCasaClima 2013: CasaClima building simulation software

Matteo Rondoni – Energy Agency South Tyrol – CasaClima, Bolzano-Bozen, Italy

matteo.rondoni@agenziacasaclima.it

Ulrich Santa – Energy Agency South Tyrol – CasaClima, Bolzano-Bozen, Italy

ulrich.santa@agenziacasaclima.it

Ulrich Klammsteiner – Energy Agency South Tyrol – CasaClima, Bolzano-Bozen, Italy

ulrich.klammsteiner@agenziacasaclima.it

Martina Demattio – Energy Agency South Tyrol – CasaClima, Bolzano-Bozen, Italy

martina.demattio@agenziacasaclima.it

Mariadonata Bancher – Energy Agency South Tyrol – CasaClima, Bolzano-Bozen, Italy

mariadonata.bancher@agenziacasaclima.it

Alexander Told – Energy Agency South Tyrol – CasaClima, Bolzano-Bozen, Italy

alexander.told@agenziacasaclima.it

Thomas Zelger – Austrian Institute for Healthy and Ecological Building, Vienna, Austria

Thomas.zelger@ibo.at

Abstract

Since 2002 the CasaClima building quality certification system has been a widely recognized method. Certification of buildings is carried out with standard parameters of calculation. For this reason the results obtained do not show the real consumption, but they are indexes that allow us to compare different buildings from each other. However, the CasaClima Program has been developed in order to guarantee a high level of quality of the construction process for low-energy buildings. Looking not only at the certification, but also at a proper building design, CasaClima has integrated into its software a dynamic simulation of the building, whose characteristics and results will be presented in this paper. Having to deal with technicians, whose work is focused on the rapidity of the design, the goal, from the beginning of the development, was to allow these professionals to make the calculation for energy certification and at the same time, without further additional working, offer them the results of a dynamic simulation. For this reason some input of the calculation is fixed and unchangeable. In the CasaClima philosophy, the energy efficiency starts from the building envelope, which is associated with a system that is simple, but efficient, and able to cover the small energy needs required. For this reason, the building envelope plays a leading role and CasaClima dynamic simulation serves mainly to its design. Thus, the results show the air and

operating temperature within the environment, without any air conditioning system, from which it is also possible to obtain an evaluation of the indoor comfort.

1. Introduction

Many designers still make the mistake of thinking that the results of an energy certification represent the real consumption of the building, not considering that many inputs in that calculation are standardized (e.g. internal loads, hours of operation of the systems, etc.) and then, that the results are simply indexes used to make comparisons between buildings. CasaClima has integrated a dynamic simulation within its software certification to enable designers to perform a correct design of the building envelope. Modern buildings cannot be designed and built only with the idea of reducing consumption, but also the results of comfort must be evaluated along with the energy ones. The living comfort cannot be ignored inside a modern building. In this paper the interesting approach of CasaClima is analyzed, which allows the designer to make a dynamic simulation with the input of steady-state calculation, which means no further work

compared to the certification of the building. This paper analyzes the input needed, the characteristics of the calculation algorithm and the results that are obtained. In the final section strengths and weaknesses of the calculation tool are also highlighted, with a reflection on future developments.

2. Methodology

With the CasaClima calculation tool it is possible to:

- Calculate heating, cooling, domestic hot water and lighting demand (UNI TS 11300: 2008 and UNI EN 15193: 2008)
- Calculate the internal temperature of a room during the summer without air conditioning systems (UNI EN ISO 13791: 2012)
- Classify the internal environment based on thermal comfort and humidity according to UNI EN 15251: 2008 and according to the adaptive comfort method of Nicol and Humphreys.

To obtain the numerical and graphical output, it is necessary to enter the characteristics of the site, of the building envelope and of the systems.

3. Simulation parameters

3.1 Weather data

The weather data used in the heating and cooling steady-state calculation are referred to the UNI 10349: 2008. Whereas the data of all Italian municipalities are not available, the software allows us to carry out an interpolation of the climatic conditions of the two neighboring provinces to the municipality, taking into account the relative distances and height differences. For the dynamic simulation hourly weather data provided by the Italian Heat Technology Committee (CTI) on its website are used.

3.2 Building elements

All the external elements, both vertical and horizontal, opaque and glazed, must be included in the calculation. The inclusion of the interior walls and floors is also recommended to take into account the real heat capacity of the building and then to make a better assessment of the use of solar and internal gains.

To characterize the opaque elements it is necessary to specify the characteristics of the materials that compose them, defining the following parameters for each material.

Table 1 – Material parameters

Parameters	Units
Conductivity (λ)	W/mK
Density	Kg/m ³
Thermal capacity	kJ/kgK
Water vapor permeability (μ)	-
Water content of material (k)	Kg/kg

It is possible to evaluate up to four non homogeneous sections within a single stratigraphy.



Fig. 1 – Building envelope

For each stratigraphy the following are obtained:

- thermal transmittance
- periodic thermal transmittance
- internal heat capacity
- external heat capacity
- time shift
- decrement factor
- internal thermal admittance

To characterize the glazed elements the characteristics of their glass, frame and spacer must be included.

3.3 Ventilation

In the software there is a sheet dedicated to the evaluation of the building ventilation, both natural and mechanical, during summer and winter. For the natural ventilation it is possible to enter the air change rate (vol / h) directly as well as to assess more in detail the benefits that a night ventilation has on the cooling demand, selecting among six different configurations of the openings, according to the UNI EN ISO 13791: 2012. For the mechanical ventilation, it is possible to insert up to ten ventilation devices with recuperative or regenerative heat exchanger and even up to three ventilation devices with heat pump inside.

3.4 Internal gains

The calculation tool provides standard values [W/m²] for the internal gains, according to the use of the building. The values are normally identical for both winter and summer. However, it is possible to assign different values between the two periods

3.5 Solar gains

The software takes into account the solar gains both on the opaque and glazed building elements. It is possible to evaluate the effect of solar shading devices, mobile or fixed, placed in correspondence of windows.

The mobile shading devices are characterized by the shading factor Fc, which can be entered directly (certified value of the product), or calculated according to:

- The position of the shading device (internal or external);
- type of shading device;
- optical parameters of absorption and transmission of the shading device.

The overhangs can be assessed through both a simplified or detailed method.

While the simplified method uses a fixed factor for the reduction of the solar radiation, the detailed one takes into account the actual geometry of the overhangs. Thanks to this method, it is also possible to consider not only the overhangs of the building, but also those due to external obstacles, modeled through azimuthal coordinates.

3.6 Schedule

The hourly schedule of the internal loads (people, equipment and lighting) and ventilation cannot be changed by the user. In order to simplify and speed up the work of the technicians, some standard profiles have been defined according to the intended use of the building.

4. Discussion and results

The results are expressed both in final (thermal or electric) and primary energy.

Final energy	Montepulciano		Siena			
	Thermal	Electric	Thermal	Electric		
Heating	1.080	1.002	822	689	kWh/a	
Cooling		1.179		1.700	kWh/a	
Hot water	316	2.411	282	2.533	kWh/a	
Lighting		1.977		1.977	kWh/a	
electrical auxiliaries		1.384		1.247	kWh/a	
	Q _{EP}		1.396	7.952	1.104	8.145 kWh/a

Primary Energy	Montepulciano		Siena			
	kWh/a	kWh/m ² a	kWh/a	kWh/m ² a		
Heating	3.257	24.5	2.319	17.5	EP _{th}	
Cooling	2.562	19.3	3.095	27.8	EP _{cl}	
Hot water	5.558	41.8	5.789	43.6	EP _{hw}	
Lighting	4.298	32.4	4.298	32.4	EP _{li}	
electrical auxiliaries	3.009	22.7	2.710	20.4	EP _{aux}	
	Q _{EP}		18.684	140.7	18.812	141.7 kWh/a

Fig. 2 – Energy results

The CasaClima rating takes into account the demand for the heating of the building envelope and the CO₂ emissions for the use of heating, cooling, domestic hot water and lighting.

	heating building envelope [kWh/m ² a]		overall efficiency [kg CO ₂ /m ² a]		
Gold	10	25	15		
A	30		30		
B	60		61	41	B
C	70		71		
D	90		92		
E	120		123		
F	160		164		
G	> 160		> 164		

Fig. 3 – CasaClima rating

The graph of the dynamic simulation shows the annual trend of the air temperature as well as the absolute humidity inside and outside the building, the operative temperature and the perceived temperature. The perceived temperature also takes into account the internal humidity; in this way the comfort is more accurately evaluated.

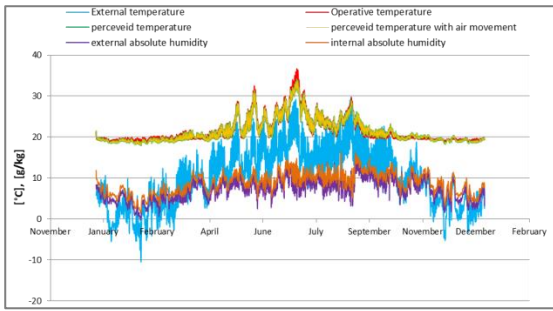


Fig. 4 – Dynamic simulation diagram

The results of the dynamic simulation, besides on the graph, are also summarized as numbers. It is possible to know the maximum and minimum values of the quantities listed in the graph above along with the time in which they occur. It is also very useful to know the percentage of the hours of the year in which the internal air temperature and the internal absolute humidity exceed certain fixed values.

Internal temperature	Air temperature	Operative temperature	Perceived temperature	day of the year	hour
max	35.9 °C	36.7 °C	34.2 °C	188	14
min	20.0 °C	18.4 °C	17.9 °C	42	5
hour above 26°C	9%	11%	10%		
hour above 28°C	4%	5%	4%		
Hour below 20°C	0%	50%	46%		
Internal absolute humidity	RH		Day of the year	Hour	
max	79%		256	15	
min	8%		41	16	
hour above 70%	3%				
Hour below 30%	9%				
External temperature	T _{ext}		Day of the year	Hour	
max	29.8 °C		239	15	
min	-10.5 °C		42	3	
External absolute humidity	AH		Day of the year	Hour	
max	16 g/kg		243	18	
min	0 g/kg		41	15	

Fig. 5 – Dynamic simulation results

The results of the dynamic simulation allow us to classify the comfort of the indoor environment according to the UNI EN 15251: 2008. The first class was further divided to provide a more detailed assessment of the highest levels of comfort. The results are shown as the percentage of hours of the year outside of each class.

Free running (without thermal systems)					
comfort					
I+++	I++	I+	I	II	III
10,2%	9,8%	8,8%	6,9%	4,9%	3,4%

Fig. 6 – comfort results

The results of comfort can be viewed even in graphical form. The red points represent the internal temperature and internal relative humidity of each day of the year. The internal grey trapeze

represents the area of optimum comfort, while the external trapeze the zone of minimum comfort. Figure 7 shows there are some summer days outside the comfort zone, as highlighted by the peak of the internal temperature between June and July in figure 4.

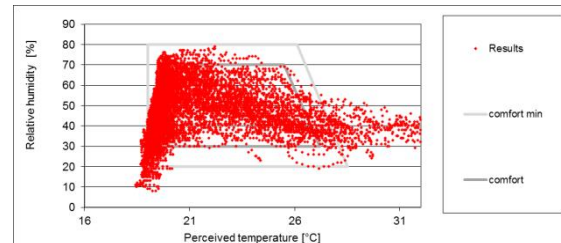


Fig. 7 – comfort diagram

5. Conclusions

The limits of the instrument are represented mainly by the fact that the analysis is carried out for a single zone. Therefore there is the risk of making a slightly inaccurate calculation in the analysis of an entire building. For this reason, the instrument should be used to assess single portions of interest of the building. Another limit is represented by not considering the thermal plants in the hourly calculation and, thus, the energy demand is obtained by the steady-state calculation. However, a tool that integrates a steady-state calculation with a dynamic one that uses its same input is certainly a very powerful tool for a technician who works daily in the design of high-energy efficient buildings. The data entry is in fact simple and results can be obtained both in terms of energy requirements and indoor comfort. Furthermore, thanks to the hourly calculation, the results are much more reliable and realistic than a simple steady-state calculation. The inclusion of the set point of heating and cooling in the dynamic calculation is probably the main future development of the software.

References

- ASHRAE Standard 55, 2004 – Thermal Environment Conditions for Human Occupancy.
- Corgnati, Stefano Paolo, Roberta Ansaldi, Marco Filippi, 2009. Thermal comfort in Italian classrooms under free running conditions during mid seasons: Assessment through objective and subjective approaches. *Building and Environment*, Vol. 44, 785–792.
- de Dear, Richard J., Gail S. Brager, 2002. Thermal comfort in naturally ventilated buildings: revisions to ASHRAE Standard 55. *Energy and Buildings*, 34 (6): 549–561.
- Fanger, P.O., 1972. *Thermal Comfort, Analysis and Applications in Environmental Engineering*. McGraw-Hill, New York.
- Gagge, A.P., A.P. Fobelets, L.G. Berglund, 1986. A Standard Predictive Index of Human Response to the Thermal Environment. *ASHRAE Trans.*, Vol. 92, 709-731
- Haldi, Frédéric, Darren Robinson, 2009. A comprehensive stochastic model of blind usage: Theory and validation. *Building Simulation 2009: 11th International IBPSA Conference*, Glasgow, United Kingdom, 529–536
- Humphreys, Michael A., J. Fergus Nicol, 2002. The validity of ISO-PMV for predicting comfort votes in every-day thermal environments. *Energy and Buildings*, Vol. 34 (6): 667–684.
- Humphreys, Michael A., J. Fergus Nicol, 2004. Do people like to feel neutral? Response to the ASHRAE scale of subjective warmth in relation to thermal preference, indoor and outdoor temperature. *ASHRAE Transactions*, 110(2): 569-577.
- Humphreys, Michael A., J. Fergus Nicol, Iftikhar A. Raja, 2007. Field Studies of Indoor Thermal Comfort and the Progress of the Adaptive Approach. *Advances in Building Energy Research*, Vol. 1, 55 – 88.
- Jendritzky, G., G. Menz, H. Schirmer, W. Schmidt-Kessen, 1990. Methodik zur raumbezogenen Bewertung der thermischen Komponente im Bioklima des Menschen (Fortgeschriebenes Klima-Michel-Modell). *Beitr.Akad. Raumforsch. Landespl.* 114.
- McCartney, Kathryn J., J. Fergus Nicol, 2002. Developing an adaptive control algorithm for Europe. *Energy and Buildings*, 34 (6): 623–635.
- Moujalled, Bassam, Richard Cantin, Gérard Guarracino, 2008. Comparison of thermal comfort algorithms in naturally ventilated office buildings. *Energy and Buildings*, 40, 2215–2223.
- Nicol, Fergus, 2004. Adaptive thermal comfort standards in the hot-humid tropics. *Energy and Buildings*, 36, 628–637.
- Nicol, J. Fergus, Michael A. Humphreys, 2010. Derivation of the adaptive equations for thermal comfort in free-running buildings in European standard EN15251. *Building and Environment* 45, 11–17.
- Nicol, J. Fergus, Michael A. Humphreys, 2004. A stochastic approach to thermal comfort – Occupant behaviour and energy use in buildings. *ASHRAE Transactions*, 110 (2): 554–568.
- CEN, 2005, Standard EN 7730:2005 Ergonomics of the thermal environment – Analytical determination and interpretation of thermal comfort using calculation of the PMV and PPD indices and local thermal comfort criteria.
- CEN, 2007, Standard EN 15251:2007 Indoor environmental input parameters for design and assessment of energy performance of buildings addressing indoor air quality, thermal environment, lighting and acoustics.
- ISO, 2007, Standard EN ISO 13790:2007 Energy performance of buildings - Calculation of energy use for space heating and cooling.
- UNI/TS 11300-1:2008 Prestazioni energetiche degli edifici - Parte 1: Determinazione del fabbisogno di energia termica dell'edificio per la climatizzazione estiva ed invernale.
- UNI/TS 11300-2:2008 Prestazioni energetiche degli edifici - Parte 2: Determinazione del fabbisogno di energia primaria e dei rendimenti per la climatizzazione invernale, per la produzione di acqua calda sanitaria, per la ventilazione e per l'illuminazione in edifici non residenziali.
- CEN, 2007, Standard EN 15193:2007 Energy performance of buildings - Energy requirements for lighting.
- ISO, 2012, Standard EN ISO 13791:2012 Thermal performance of buildings - Calculation of internal temperatures of a room in summer

without mechanical cooling - General criteria and validation procedures.

ISO, 2012, Standard EN ISO 13792:2012 Thermal performance of buildings - Calculation of internal temperatures of a room in summer without mechanical cooling - Simplified methods.

UNI 10349:1994 Riscaldamento e raffrescamento degli edifici. Dati climatici.

Graphic and parametric tools for preliminary design stage of natural ventilation systems

Margherita Ferrucci – Université Paris-Est, IUAV University of Venice – marferit@gmail.com

Maurizio Brocato – ENSA Paris-Malaquais – maurizio.brocato@mac.com

Fabio Peron – IUAV University of Venice – fperon@iuav.it

Francesca Cappelletti – IUAV University of Venice – francesca.cappelletti@iuav.it

Abstract

In this paper we developed a simplified graphical visualization to provide a preliminary understanding of aerodynamic pressure distributions around tall buildings and to estimate the best positions for ventilation openings. This graphical model is based on a database of pressure coefficients hold by parametrical two-dimensional CFD (Computational Fluid Dynamics) simulations over several rectangular shape profiles. The pressure values are obtained by CFD simulations of a stationary flow (High Reynolds), with a K-epsilon turbulence model coupled with Navier-Stokes equations, by using Finite Elements Methods. Whilst turbulence model is well-known, the innovative application is the parameterization of the CFD simulations. The parameters considered here are the ratio between length and width of a rectangular shape and the wind direction (degrees azimuth). Our model adapts automatically to different shapes and various wind directions. Though not able to capture the same level of detail as the three-dimensional CFD simulations or experimental tests, it provides a rapid and intuitive guidance for architects at the preliminary design stage of a natural ventilation system. The final graphical visualizations, together with some simple recommendations, can be exploited by designers having no knowledge in aerodynamics.

1. Introduction

1.1 Airflow around buildings

The use of natural ventilation as a passive strategy for cooling needs reduction has been largely discussed by many authors, since free and mechanical ventilation can reduce the plant capacity and the energy consumption in air-

conditioned buildings. Moreover, the use of airflow to remove indoor pollutants and to guarantee a good indoor thermal environment is quality is probably the most recognized advantage of natural ventilation. Mochida (Mochida et al. 2005) demonstrated that wind-driven natural ventilation is an effective way to maintain a comfortable and healthy indoor environment, as well as offering an energy-saving alternative to mechanical ventilation, even though its effectiveness, for a given climatic condition, is strongly affected by the position of the openings on the facades. In fact, natural ventilation, infiltration and exfiltration are affected by wind, causing variable surface pressures on envelope buildings.

The major efficacy of natural ventilation in removing pollutant is achieved when the air flows through an indoor space, determining the so-called cross-ventilation. Cross-ventilation depends on the impact of the wind over the building envelope, which produces a variable pressure field (positive and negative). This pressure difference is the driving force for the airflow through the building. So the effectiveness of wind-driven ventilation depends on the external wind conditions and on the building design (Etheridge et al., 1996).

In a tropical humid climate, for example, the speed of the airflow is used to improve the thermal comfort. Consequently, to obtain cross-ventilation, buildings are designed by choosing their location, orientation, shape, window positions and the internal partitions (Gandemer J.,1992, Olgyay V.,1973).

On the other hand, stack ventilation is driven by the difference between outdoor and indoor air density, caused by temperature difference. Also in

this case, the direction and velocity of the wind and the shape of the building affect the system. (Katarzyna Gładyszewska-Fiedoruk et al. 2012). Consequently, it is impossible to dissociate the design of the shape of a building from the ventilation systems (either natural or mechanical). The pressure distributions expressed by the pressure coefficients, caused by the flow around the building, plays an important role at the beginning stages of design.

1.2 The pressure coefficients

Wind pressure distributions are described by pressure coefficients

$$C_p = \frac{P_s - P_o}{P_d} \text{ with } P_d = \frac{\rho U_h^2}{2}$$

where P_s is the static pressure at a given point on the building facade, P_o is the static reference pressure, P_d is the dynamic pressure (the pressure is expressed in Pascal units), ρ is the air density (kg/m^3) and U_h is the wind speed of undisturbed flow (m/s).

Pressure coefficients can be obtained by full-scale tests, wind tunnel tests, fluid dynamic simulations, parametric equations and databases derived from measurements. The first three methods are more accurate than the parametric equations, even though, being based on non-parametric methods, it is not possible to transpose the obtained results to other different cases.

These studies are focalized on a geometry with only few wind directions. Moreover, they are expensive, time consuming, and they require consequential time and expertise. In addition, these methods are out of reach for architects and designers who, in the early stages of their project, need to visualize the pressure distributions to choose the opening positions and the best orientation of the building.

The most popular parametric equation for low-rise buildings is that of Swami and Chandra (Swami et al. 1987), used also in the ASHRAE guidelines (ASHRAE 2001). Other authors, Grosso (Grosso M.,1992.) and Eldin (Eldin AS. 2007) expand this work to include the effects of shielded environment. Recently, Patrizi and Muehleisen (Muehleisen R. T. et al. 2013) developed a

parametric equation derived on the Tokyo database. An interesting review of several equations and methodologies was provided by Cóstola (Cóstola et al. 2009). This research proves that the pressure coefficients on building facades are influenced by a wide range of parameters, so that it is practically impossible to take into account the full complexity of the C_p variation. Every method gives the surface-averaged wind pressure coefficients on the facade for each side of a low-rise parallelepiped (or cubic) building, with variable depth-to-breadth short-side and depth-to-height ratios, and for variable wind angle direction. For a non-expert user, to collect the pressure coefficients is not as immediate as knowing their spatial variation, because there does not exist a quick and simple approach to estimate the C_p positions.

1.3 Aim of the study

In this paper a simplified graphical visualization has been developed to provide a preliminary understanding of aerodynamic pressure distributions around rectangular shapes. The same computation methodology and post-data processing can be easily applied to different 2D geometries. The 2D fluid dynamic simulations over the profiles corresponds to the cross-section 3D fluid dynamic simulations over an infinitely long body. Due to the fact that this tool is addressed to architects and designers for the preliminary conception of a ventilation opening system integrated in a building, we make the assumption that the results around a 2D shape can be transposed to a cross section of a tall building in an area not influenced by the ground and the roof. Our results, though not reliable if applied to the whole building, give the tendencies of pressure distributions on a cross section. It is important to note that our study concerns only one aspect of the design process, namely, the best location of openings.

2. Method

The geometry considered here is a rectangular shape of width W and height H , located in a canal

(height: 14 m; length: 20,5 m). The ratio r between H and W is variable and the perimeter P is taken constantly equal to 4 m. So the edge lengths change on the basis of their aspect ratio r . The values of the ratio chosen for the analysis are

$$r = \{1/n, n\} \text{ with } n=1, \dots, 8$$

which are the most commonly used for the cross section of buildings. In this way it is possible to cover a wide range of building typologies. The geometry is therefore identified only with one parameter, i.e. the aspect ratio r (Fig. 6).

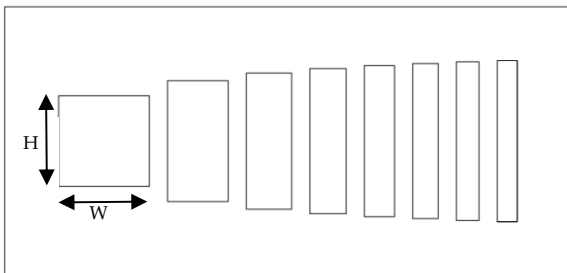


Fig. 6 – Shapes with variable ratios $r=\{1,2,3,4,5,6,7,8\}$ in this order

The model was studied as it was located towards different wind directions determining different incidence angles of the wind stream over the building facades. The wind directions considered for the study have the following azimuth:

$$\alpha = \{0^\circ, 10^\circ, 20^\circ, 30^\circ, 40^\circ, 45^\circ\}.$$

The wind direction has been simulated pivoting the rectangle around its centroid (Fig. 7). A counterclockwise pivoting corresponds to a positive wind azimuth. The reduced azimuth range (from 0° to 45°), coupled with the double symmetry of the rectangular shape (along the middle x -axis and the middle y -axis), gives the possibility to investigate the pressure field for all degrees from 0° to 350° . Combining the azimuth angles with the different aspect ratios, a total of 90 cases has been computed.

2.1 Simulations

A database of pressure coefficients has been computed by means of parametrical two-dimensional CFD simulations over all the 90 cases. The geometry, the meshing generation and the computational simulations have been performed in Cast3M environment, a computer code used

mainly in the analysis of structures by Finite Elements Methods and also for CFD simulations. Thanks to this software we can launch a series of simulations adapting the mesh to the geometry. The flow domain is split into a structured grid with quadrilateral meshes. The domain contains around 5000 elements (the number of elements is variable with the aspect ratio). The mesh is fined progressively near the rectangle (Fig.2).

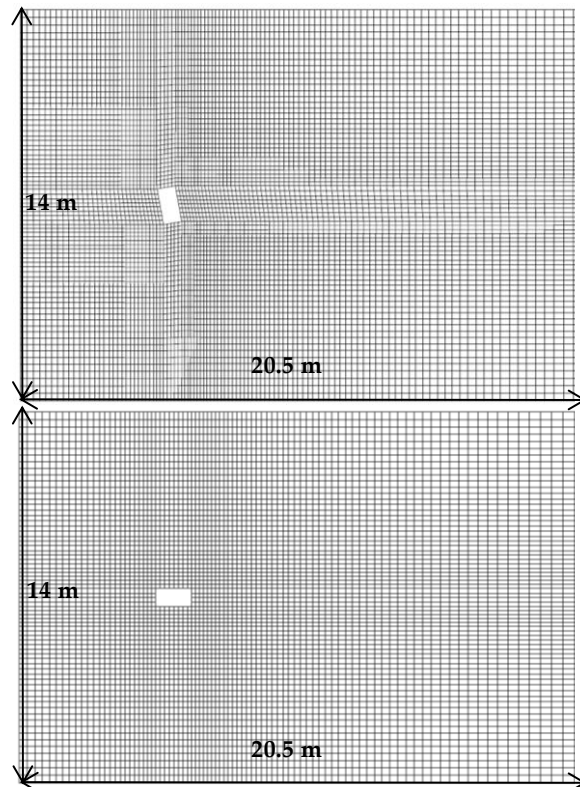


Fig. 7 – Mesh grid of the rectangle in the canal; up: $r = 2, \alpha = 10^\circ$; down: $r = 0.5, \alpha = 0^\circ$

The pressure values have been obtained by CFD simulations of a stationary airflow (High Reynolds, $Re = 5.5 \cdot 10^5$, with kinematic viscosity equal to $15.6 \cdot 10^{-6} \text{ m}^2/\text{s}$) with the standard K-epsilon turbulence model coupled with Navier-Stokes equations by using Finite Elements Methods. The wall-law is applied on each side of the rectangle. The flow has a uniform velocity on the inlet (right of the canal), with only the horizontal component. Whilst the turbulence model is well-known, the innovative application is the parameterization of a CFD simulation. The parameters considered are the aspect ratio of the rectangular shape and the wind

direction. The model is able to adapt automatically to different shapes and various wind directions.

2.2 Data processing

The data processing of the pressure coefficients and the resulting graphical visualizations have been developed within Wolfram Mathematica®.

The pressure coefficients are plotted along the development line of the rectangle, whose length corresponds to the perimeter $P = 4$ m. However, to compare all sides of every shape in the same graphic, we scaled the dimension of each edge to its maximum length. In this way, rectangles with edges of different length can be plotted in the same graph. With these assumptions, it is possible to compare the pressure coefficients and their positions for rectangles with edges of different length and different aspect ratio. This operation was applied to each case study. The rectangle sides have been enumerated in the following way: 1 for the windward side, 3 for the leeward side, 2 for the underside and 4 for the upper side.

We present here three types of visualizations (for a reduced number of study cases): Fig.3 and Fig.5 show the evolution of pressure coefficients over the shape for the different aspect ratios when the latter varies, whereas Fig.6 shows the evolution of pressure coefficient for different azimuth angles and a fixed aspect ratio. The pressure distribution around the scaled rectangles is shown in Fig. 8, and the pressure distribution along the contour in Fig. 5 and Fig. 6.

In Fig. 5 and Fig. 6 the pressure coefficients (C_p) are in the y -axis and their position in the x -axis (contour perimeter). The rectangular side 1 is represented between the abscissa 0 and 1, side 2 between 1 and 2, side 3 between 2 and 3, and side 4 between 3 and 4. The total length of the contour is the same for every rectangle. To simplify the comprehension in Fig. 5, the lines representing the rectangles with $r = \{ 1, 2, 4, 8, 1/2, 1/4, 1/8 \}$ are thicker than the others. The line corresponding to $r=1$ is always a red line.

In the second representation (Fig. 3) the C_p 's are plotted around a square. The square represents simultaneously the scaled rectangles in order to compare the C_p 's and their positions for rectangles

with edges of different length and different ratio. The positive values are inside the shape, the negative ones outside. The shape orientation is the same for the CFD simulation: the windward side (side 1) on the left, the leeward side (side 3) on the right. For a better visualization, we represented the computations for a small choice of the ratios: $r = \{ 1, 2, 4, 8, 1/2, 1/4, 1/8 \}$.

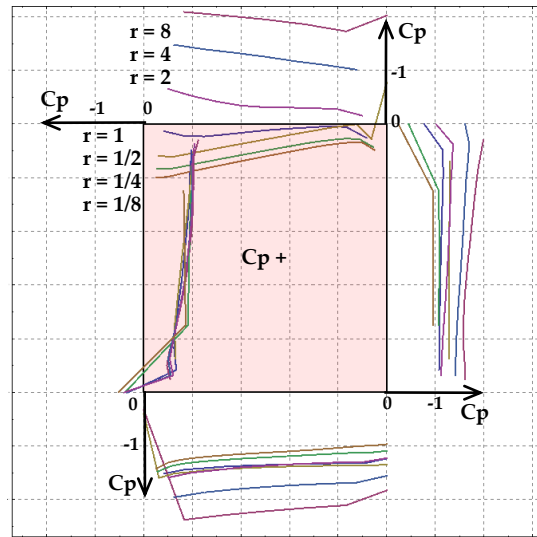


Fig. 8 – Pressure coefficient (C_p) distribution for azimuth $\alpha = 30^\circ$.

At a later stage, a fourth data processing is performed to extrapolate more information about the pressure difference potential. For an upwind point A and a downwind point B, the pressure difference can be taken as an indicator of the force driving the internal flow, with unique openings in A and B.

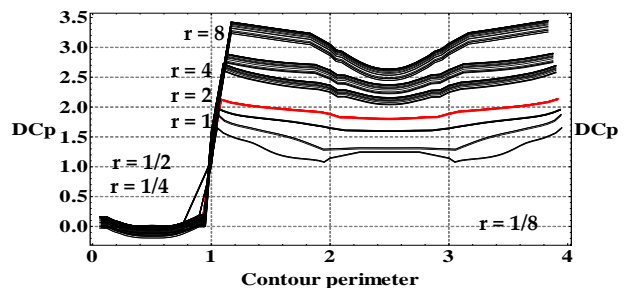


Fig. 9 – Pressure coefficient difference (DC_p) for azimuth $\alpha = 0^\circ$

The obtained results are displayed in Fig. 9: the difference between pressure coefficients (DC_p) at two different points of the contour perimeter is represented in the y -axis and its position in the x -axis (the DC_p 's computed with respect to upwind

points of side 1 is plotted against the downwind points of side 2, 3 and 4). For each aspect ratio r , coupled with a particular wind azimuth α , we get a line passing through each point of side 1. Therefore, the number of lines increases with the value of r .

3. Discussion

Thanks to this graphic giving the pressure coefficient distribution, architects may optimize the ventilation system of a project by choosing the opening positions that maximize the pressure difference. Similarly, they are able to understand which side, or part of it, is in a low/high pressure area. We note here that in this work we focus on the external flow without considering the internal flow paths and their losses.

The graphics of pressure coefficient distribution (Fig. 9, Fig. 5 and Fig. 6) are helpful for the preliminary design. For instance, they show when sides 1 and 4 have positive or negative pressure and the corresponding value. For example, the pressure on side 4 (rectangles with $r = 1$) becomes positive for azimuths $> 30^\circ$. Therefore, for a tall building with $r = 1$ situated in an open environment, the openings on sides 1 and 4 will be inlet openings when the azimuth wind is around 30° .

With the graphic typology of Fig. 5, architects can apply the pressure coefficients on the perimeter of a cross section of a tall building which is already oriented. In this way, they can evaluate the best aspect ratio to have a specific pressure distribution; they may also choose the position of the openings for a cross ventilation by reading the opening positions on the x -axis. Similarly, using the Fig. 6, they can estimate the best building position to develop a good cross ventilation with a fixed aspect ratio.

With some more data processing, it is possible to visualize the pressure difference between a point on side 1 (windward) and all the other points.

As the long edge is on the windward side, the ventilation potential increases, since this maximizes the pressure differences between the opposite sides. Therefore, for a high ventilation

potential, the solutions are those with the aspect ratio $r > 1$. Fig. 9 shows that the pressure difference increases with the aspect ratio. This happens for every azimuth until 45° , then the trend reverses. The smallest possible variation between minimum and maximum DC_p 's is the rectangle with $r = 1$ (the square). The maximum DC_p is 3.4 and it occurs with $r = 8$, the minimum is 1.1 with $r = 1/8$. As an example, with a dynamic pressure of 15 Pa (wind velocity 5 m/s and air volumetric mass density equal to 1,2 Kg/m³), we obtain a maximum pressure difference of 51 Pa and a minimum pressure difference of 16.5 Pa.

There are pressure discontinuities on the edges caused by vortex detaching: in Fig. 9, Fig. 10 and Fig. 6 the jumps of the plotted functions corresponds to these edges. For a wind azimuth $\alpha = 0^\circ$, the maximum values of DC_p are near the edges.

4. Conclusions

Our graphic tools provide a rapid and intuitive guidance for architects at the preliminary design stage of a natural ventilation system.

An original application is the parameterization of CFD airflow building simulation. In fact, though the use of parametric design in architecture is well known, the CFD parametric studies are developed mostly in aerodynamics (aerospace and aeronautic engineering).

This method can be efficiently applied to simple two-dimensional objects, in particular for rectangular shapes (defined by their aspect ratio, r), which can be identified to cross sections of a standard building. Since the pressure coefficients for rectangles are well known in scientific literature, we can easily verify our results.

By a specific data processing we compare the pressure coefficients and the pressure coefficient difference for every rectangle with different aspect ratio. Therefore, we provided three different types of graphic giving the pressure coefficient distribution around the rectangles (Fig. 8, Fig. 5 and Fig. 6) and the pressure difference potential (Fig. 4). The latter can be taken as an indicator of the force driving the internal flow.

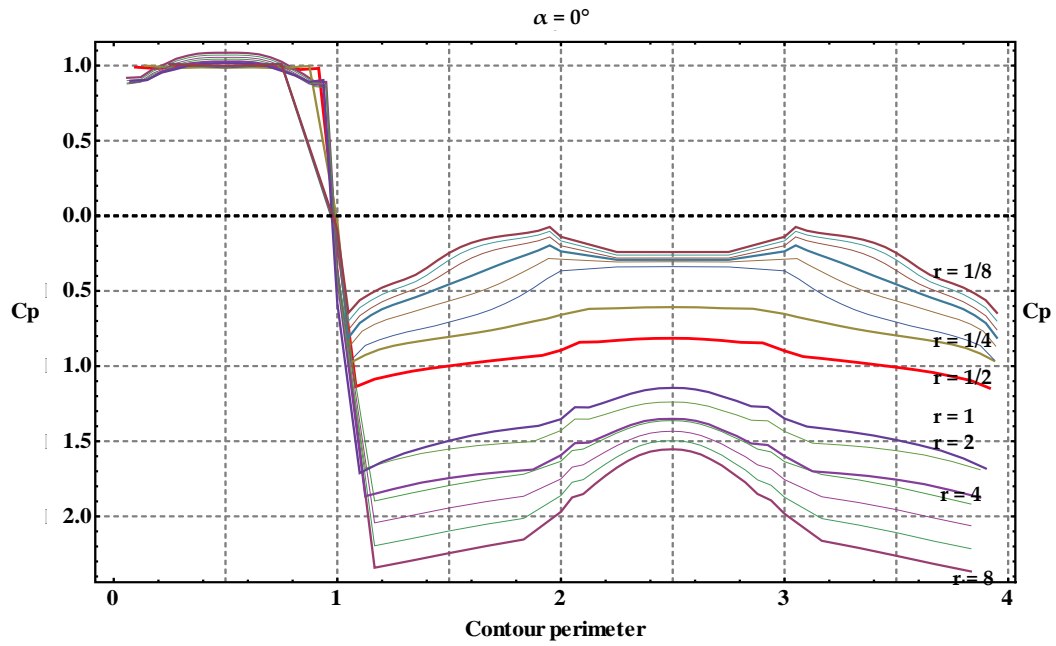


Fig. 10 – Pressure coefficient (C_p) along the contour for $\alpha = 0^\circ$

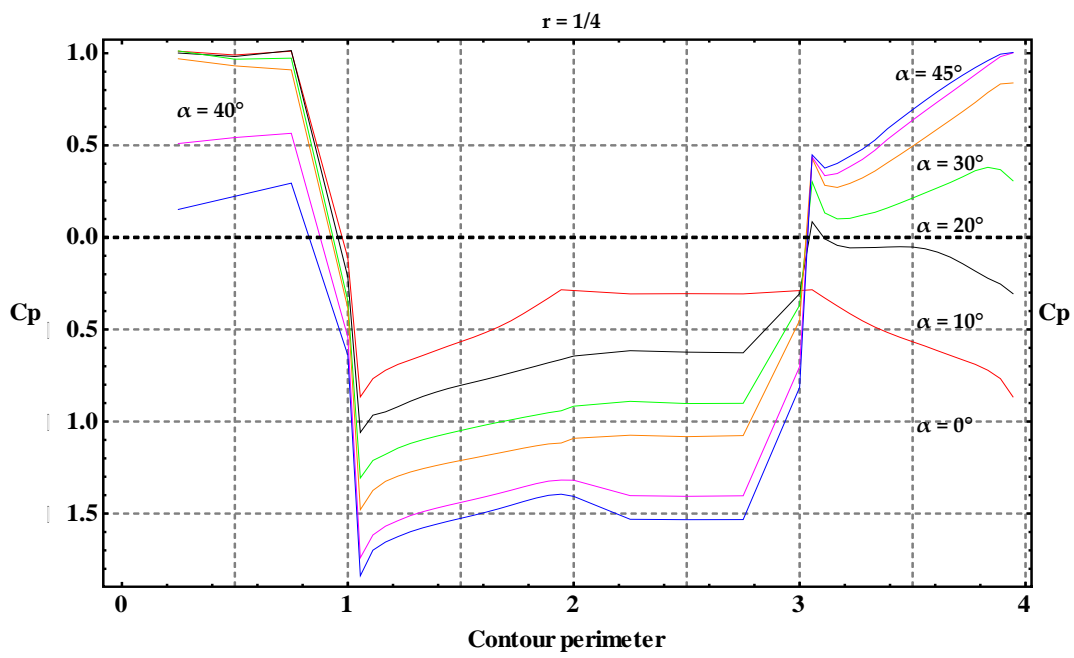


Fig. 11 – Pressure coefficient (C_p) along the contour for $r = 1/4$

5. Acknowledgement

The first author is partially supported by *Université Franco Italienne* and *Paris-Est University*. The authors wish to thank the «*Commissariat français à l'Énergie Atomique et aux énergies alternatives (CEA)*» for making Cast3M freely available.

6. Nomenclature

Symbols

H	height (m)
W	width (m)
P	perimeter (m)
r	length/width (aspect ratio)
α	azimuth angle (°)
C_p	pressure coefficient
DC_p	pressure coefficient difference

References

Journal papers

- Cóstola D., Blocken B., Hensen J.L.M.. 2009. "Overview of pressure coefficient data in building energy simulation and airflow network programs." *Building and Environment* 44: 2027–2036.
- Eldin AS. 2007. "A parametric model for predicting wind-induced pressures on low-rise vertical surfaces in shielded environments." *Solar Energy* 2007: 81:52–61.
- Grosso M. 1992. "Wind pressure distribution around buildings: a parametrical mode." *Energy and Buildings* 18:101–31.
- Katarzyna Gładyszewska-Fiedoruk, Andrzej Gajewski. 2012. "Effect of wind on stack ventilation performance." *Energy and Buildings* 51: 242–247.
- Mochida A., Yoshino H., Takeda T., Kakegawa T., Miyauchi S. 2005. "Methods for controlling airflow in and around a building under cross ventilation to improve indoor thermal comfort." *Journal of Wind Engineering and Industrial Aerodynamics* 93 (2005) 437–449.
- Muehleisen R. T., Patrizi S. 2013. "A new parametric equation for the wind pressure

coefficient for low-rise buildings." *Energy and Buildings* 57: 245–249.

- Swami MV, Chandra S.1988. "Correlations for pressure distribution on buildings and calculation of natural-ventilation airflow." *ASHRAE Transactions* 94: 243–66.
- Swami MV, Chandra S. 1987."Procedures for calculating natural ventilation airflow rates in buildings-Final report FSEC-CR-163-86." *Cape Canaveral: Florida Solar Energy Center*.

Books

- ASHRAE. ASHRAE handbook – fundamentals. Atlanta: ASHRAE; 2001.
- Etheridge D., Sandberg M. 1996. *Building Ventilation: Theory and Measurement*. John Wiley and Sons.
- Gandemer. 1992. *Guide sur la climatisation naturelle de l'habitat en climat tropical humide, Tome 1: Méthodologie de prise en compte des paramètres climatiques dans l'habitat et conseils pratiques*. CSTB, Nantes, pp. 64–68.
- Olgyay V. 1973. *Design with Climate: Bio –climatic Approach to Architecture Regionalism*, Princeton University Press, Princeton, NJ, USA pp.94–112.

Online resource

- Tokyo Polytechnic University, Aerodynamic, Database of Low-Rise Buildings, <http://www.wind.arch.t-Kougei.ac.jp/system/eng/contents/code/tpu>

Advancement in the development of an Open Source Object Oriented BPSt: development methodology

Livio Mazzarella – Politecnico di Milano – livio.mazzarella@polimi.it

Martina Pasini – Politecnico di Milano – martina.pasini@polimi.it

Abstract

In order to promote its readability, modularity and maintainability, a new Object Oriented (OO) tool for the simulation of buildings performance, has been developed in the last years. The first results of a comparative validation done on our tool, following the BESTEST standard, have been published in the 2013 IBPSA International Conference. The chosen development methodology aims to achieve efficient and high quality software development in the field of Building Performance Simulation tools (BPSts) and is based on an Open Source (OS) development approach. Given the selected approach, the contribution of volunteer developers should be encouraged and supported. To effectively support the work of an OS community, key aspects are tasks automation, traceability and communication in the developing phase. The implemented development methodology is then based on: 1) the use of a Software Forge (SF) to promote communication between community members and to help in the management of the software development life-cycle, 2) the use of UML diagrams to describe community-agreed architectural decisions and enforce their implementation into the project, in a way that their implementation can be automatically checked, 3) the ability to group single tests of different modules in one automatic test session of validation, which also simplifies final reporting, 4) the use of inheritance, offered by Object Oriented Programming (OOP), to specialize existing classes which, avoiding rewriting, partially automate code writing. Regarding the quality of the tool, the definition of specific standards for programming, documenting and validating is also important. In particular, the validation phase has to be carried out in a well-documented pool of verifiers, and provided as an integral part of the documentation available to the user.

1. Introduction

Some of the most important available BPSts, such as ESP-r and EnergyPlus, have followed, even if in different ways, the Open Source approach since the beginning. Today, both of them have enlarged the public availability of their source code, by exposing their source code repository on a public web site for developers (GitHub for ESP-r and SourceForge for EnergyPlus). The first fundamental advantage gained by following such an approach is related to the possibility to find errors in a shorter time, as Raymond's thesis states: "given enough eyeballs, all bugs are shallow" (Raymond, 1999).

Another tremendous advantage is the union between users and developers, since "treating your users as co-developers is your least-hassle route to rapid code improvement and effective debugging" (Raymond, 1999).

Meanwhile, in the IT field, different tools and methodologies have been created to increase programming efficiency, promote communication among involved actors and improve code readability & browsability. Some of these utilities are even more vital when following an OS approach, given the un-schedulable and disperse nature of its community's members. In fact, OS communities need, more than others, tools to:

- provide an organic structure for all process phases (development, validation, testing, etc.);
- aid organizing communication between different community's members;
- help old and new members to understand the project
- promote developers' efficiency, also through automation.

In order to promote the readability, modularity and maintainability of a BPSt, some years ago we started the development of a new OO tool for the simulation of buildings performance, following the best practice of an OS approach. For practical reasons, until the project reaches a critical minimum size, it will not be really open to the world. Anyhow, the design of the project structure is following the OS approach, in order to be ready when such a minimum size is reached.

In this paper, we describe what tools and methodologies have been applied to the development of our OO BPSt.

2. The software forge

In an OS project, the most important points are source code management, software development support and project promotion. This is usually done through a web application, called "Software Forge" (SF). Among other possibilities, for instance the SourceForge web site, we have decided to directly host on our servers an OS SF, at least for this development phase, to avoid being linked with any provider that might not be available in the future. The chosen SF is Allura, hosted on an Ubuntu server, which provides, among others, the following important features:

- source code management systems (SVN, Git);
- issue tracking;
- threaded discussion forums/ mailing list; wikis;
- documentation facilities.

The main goals of our forge are therefore to:

- host the source code revision's control, the software's home page, installer and documentation;
- promote communication among community members;
- provide tools for development, planning and managing.

2.1 Hosting the source code

Commonly, in a SF, different places, such as branches, tags, and trunk, are devoted to host

different versions of the current project. In our SF the "branches" are used to test critical changes before incorporating them into the main development branch, located in the "trunk", while the "tags" are used to host stable releases of the project. Every time the repository is changed, through a commit, a message is associated with it to briefly explain the reason for the new commit. Effective Graphical User Interfaces (GUIs) that show differences in the source code between chosen revisions are provided by Allura.

2.2 Promoting communication among actors

An efficient communication between involved actors is essential, not only to avoid misunderstandings in what should be done, but also to improve planning and strengthen the involvement of each member. Consequently, in our project we have tried to identify appropriate places and tools to improve communication:

- with the user (Documentation, Download and Install web pages);
- with the developer (development procedure, support tools identification and description, etc);
- between developers (dashboards to understand who is working on what, what is he/she doing and with which plan, which are the unassigned activities, etc);
- between users (mailing lists and forum to share experiences);
- between users and developers (issue tracking for discovering bugs & performance bottlenecks, dashboards for suggesting innovation opportunities, or localizing shortfalls, links with feedbacks on addressed/solved issues, etc.);
- between building and systems component manufactures and users (promotion of real products in the DB or DLL of the software).

In fact the SF should put as many stakeholders as possible in contact with each other, starting from the users (both at design and operation time), to manufacturers. Linking users, developers, industries, software models and building

performance monitored data is a vital key to improve design from the smaller scale to policy making at the larger scale.

Consequently, when users need something to be changed, they can start a discussion in the SF to understand if the required change is agreed by the community, and, after that, they can submit their request through tickets.

Another important ingredient for the good evolution of the project is user feedback on addressed issues and requests. Every time a request is made, feedback is welcomed to strengthen the motivation and sense of belonging to the community of each member.

On the other hand, manufacturers willing to promote the performances of their products can find in such an environment a third party legitimation. In fact, manufacturers can ask their products to be added to the project in two ways. If they ask to add a new model, representing their system, to the project (in case such a model has not yet been implemented), this new model should pass the validation procedure. Otherwise, they can ask to add a “prefilled class” to the appropriate DB of the project (i.e. the DB used to collect that kind of products). In this case, the user will find in the DB an object with “pre filled” and unable to be modified, which identifies that particular product. In this second case, the manufacturer will be required to perform experimental tests and provide their documentation to the user together with the prefilled class. Maybe, at the beginning, more effort will be required from the manufacturer, but “free publicity” will be gained as a counterpart. In the meantime, ease of use will be gained by the user, who will be allowed to choose from a list of “correctly” precompiled objects, existing in the real market.

2.3 Communicating current and future project's state

Concerning developers, one of the most important parts in the management of the development is effective communication of what has already been done, what should be done, who is doing what and what are their plans when doing it.

The communication concerning the current and

future state of the project takes place, for our project, inside the Integrated Development Environment (IDE). This is due to the possibility, provided by the used IDE, which is Visual Studio Ultimate 2013, to use an UML diagram linked with the source code. This opportunity improves readability and browsability of existing code and the communication of software decisions. This part will be discussed in section 3.1: Modelling tools.

Inside the SF milestones and tickets are created and managed. This second kind of objects is meant to list current, past and future activities involved in the development process and contains process information such as Author/Creator, Assignees/Owners, Priority, estimated work-effort or time-to-complete, Dependency/Predecessor, Tested by, Labels, related Milestone, Status, etc.

This variety of information, contained in the SF, should be “captured” and synthesized to community's members to provide all the stakeholders, in an easy-to-consume form, statistics on the life and features of the project.

Thus, not only work progress, but also statistics about user feedbacks, model validation results, etc., should be reported in such “dashboards”. Unfortunately, such an enriched dashboard still does not exist. However, it could be easily implemented in the future if the validation procedure and the software structure allows it.

3. Promoting Programming Efficiency

Programming efficiency is promoted by:

- communication;
- an appropriate software structure (which allow code reuse);
- the implementation of automatic routines/activities.

3.1 Modelling tools

As previously said, the communication of what has been done, which models are waiting to be implemented and which architectural choices have been taken, is of great importance to promote development efficiency.

This kind of communication is implemented

through UML diagrams and has been grouped in a Modelling Project (linked with the rest of the source code) inside our software solution. As a matter of fact, the selected IDE allows a full coupling of UML diagrams and source code, automatically writing code while visually creating a diagram or automatically generating or modifying diagrams when the code is changed.

The generated UML diagrams help in:

- exploring existing architectures;
- understanding activities' dependency and sequence;
- specifying and enforcing (with layer diagrams) the structure or behavior of a system;
- providing a template that guides in constructing a system;
- documenting decisions, etc.

3.2 Software structure & features

The structure of our software has been conceived to simplify modifications of the source code. The OO paradigm perfectly responds to this aim by encapsulation and inheritance.

Everything is a class with properties that exposes a behavior and hides its implementation. In this way, developers can easily modify and extend the system limiting the effects on other parts and reducing the line of written code (when inheriting by a father class).

Besides, through reflection, the addition of a new class inheriting by a father class, allow the automatic list on this new item in the GUI to the user.

The chosen programming language is C#, which fulfills such requirements and also combines the .NET framework portability with enough high efficiency and a powerful Integrated Developing Environment (Visual Studio).

The .NET Framework is a software framework developed by Microsoft that runs primarily on Microsoft Windows. It is open source and Microsoft with .NET 2015 is extending it to run on Mac OS platforms and Linux. (Microsoft, 2014a and Microsoft, 2014b).

Before .NET 2015, the Xamarin MONO project, an open source implementation of Microsoft's .NET

Framework, based on the ECMA standards for C# and the Common Language Runtime, assured code portability to Linux and Mac OS platforms, even if with some compatibility issues.

3.3 Tasks' Automation

The used IDE also provides tools that help to check that architectural and programming guidelines have been correctly implemented.

This family of tools, addressed with "profiling tools", measures a system's class structure, coupling, complexity, cohesion, memory allocation, CPU use, resource contention, etc.

Applying such automatic testing helps find bottlenecks or low-performing code and can be useful for a first check of codes developed by others.

Together with the automatic check of the "programming quality" of the source code, other useful tools, provided by the IDE, for task automation are snippets and unit tests.

Snippets are code template that can be easily called while programming to be pasted in a context. They have been used, for example, to provide a similar structure to different classes (such as different code's regions for "Constructors", "Private Fields", "Public Methods", "Virtual Methods", "Overridden Methods", etc.).

Unit tests, however, have been used to explicitly declare, given some input, the expected output of a specific part of a program. After their implementation, it is possible to automatically check all the unit tests created inside the project with only one click. This event will trigger the execution of all the tests and the generation of a report showing which tests are met and which are not.

The used IDE also provides tools to scan the percentage of coverage of the code with tests, encouraging a development methodology where code and tests grow in parallel to assure the quality of the software produced in each iteration.

4. Development and Validation (D&V) procedures

The focus of D&V procedures is on simplifying/automating these activities as much as possible.

As procedures should be repeatable, apart from possible bifurcations, they should be translated as much as possible into automatic tasks or templates, as we have seen in the previous paragraph, with snippets, unit test checking, etc.

Even if automation is not strictly possible, having a document that explains the commonly agreed best way to test a module, or a spreadsheet for comparing results, will allow for their search and implementation to be skipped.

4.1 Development procedures

Regarding the development procedures provided in our SF, they consist basically in programming guidelines and explanation about which contribution should be submitted in which context inside the SF or IDE, as previously explained.

The programming guidelines, meant to “assure” that each developer’s approach is consistent with that of the others, cover a range of subjects, starting from naming and usage conventions, arriving to performance and security considerations. However, having written guidelines does not guarantee that developers will read and follow those practices.

The desire to automate the process of evaluating code for compliance with these guidelines led to the creation of Code Analysis tools implemented inside the IDEs. These tools are based on rules, also grouped by subjects, ad-hoc defined for the project or already implemented as a result of the numerous years of experience of a specific community of developers. Once enabled and configured, code analysis will be performed at each build and a report will be automatically generated. Besides the standard for code writing, some standards for the documentation of the code are provided too.

Documentation and code writing should go hand in hand. The documentation provided is located inside the code, through comment and indentation, and is created in three kinds of documents, i.e:

- the User Manual,
- the Engineering Manual
- and the Validation Reports.

In the User Manual there are also sections to explain to users how to interact with developers and become a vital part of the community. In this way unforeseen problems collected by users can be directly forwarded to developers for fast analysis and correction.

Technical information about each implemented model is contained in the Engineering Manual.

The detailed description of Validation Reports will be addressed in the next section.

4.2 Validation procedures

Once a new module has been developed, before it can be included in the “main” project, it should pass the validation process.

To complete this process:

- the developers have to redact the Validation Report for their module and produce all the associated results;
- a figure belonging to the community, like the Editor does for a scientific journal, has to select, according to criteria of impartiality and competence, a shortlist of eligible validators, among community members;
- those community members belonging to the shortlist that will accept that specific task will have to control and legitimize the success of this phase.

The selected validators, as happens in peer review processes, should be unconnected with the developers, should have enough knowledge of the problem addressed by the module to be validated and preferably should be in the number of two per each validation procedure.

Each Validation Report, related to a specific component or part of code, contains a short summary and a detailed description of the module and its validation results. A template for this report is available on the SF, partially based on the template developed for by Nordtest Company (Torp, 2003).

The short summary is meant to “present” the new module. It will contain information to locate the

new module in the project, a synthetic description of the objectives and scope of the module and its developers' and validators' identification.

To locate the module, the namespace in which the module is created (ExtendedMath, Utilities, etc.) should be declared and pictures of class diagram and sequence diagrams, with the new module highlighted, should be provided. As a matter of fact, locating the new component among the others in "space and time/activities" is important because it states what the "nature" of the module is.

Depending on the nature and complexity of the physical problem implemented by a computational model and on our knowledge of its behavior, we can have different terminology and validation procedures.

Following a flow chart, developer are able to identify the types of test they have to perform to assess the "accuracy" of the model.

A physical process modelling requires the incremental identification of a Physical/real Model (PM), described by a more or less simplified Mathematical Model (MM), which can have an analytical or numerical solution, implemented on a Computational Model (CM).

First, the MM should be well posed or stable, i.e. it should admit a unique solution that depends on the continuity on the data (Quarteroni et al., 2007). Otherwise, without doing anything else (MM regularization) we cannot pretend that a numerical method applied to it will solve its pathologies (Quarteroni et al., 2007).

Secondly, the simplifications made to create the MM should be "quantified" as much as possible. One or more parameters should be identified to define a range of applicability of the MM to reach an accuracy that is adequate for the intended use. Thus, we should define the Application Domain (AD) for that model. This phase is sometimes referred to as: MM Qualification and might be seen as a quantitative evaluation of the Consistency of the MM to the PM.

After that, when possible, the mathematical model should be characterized by an "error", due to the uncertainties involved with the experimental observations (measurements) of its input parameters. Technologies with similar performances might have different solution errors,

thus, such information may drive choices made during the design of the system. If also a sensitivity analysis is possible on the MM, it might be useful to identify unexpected/wrong high sensitivity to certain physical parameters of the CM.

The MM can have an analytical solution or might need a numerical method (consistent and stable, thus convergent) to be solved. This second case is the most problematic, since going from a continuum to a discrete space, some information is lost and consequently, great care should be devoted to the characterization of discretization's errors.

On the CM a validation campaign should be performed to cover, as much as needed, the AD identified for that model with the Validation Domain (VD) for that CM. Vice versa, we will need to provide supported inferences to allow this possibility.

When trying to validate the solution of a numerical method with "exact" or "pseudo-exact" solutions, before continuing with the comparison, discretization errors should be carefully removed, for example, through Grid Convergence Index analysis.

To evaluate the solution of the CM, we can use:

- "exact" analytical solution -generally available only for very specific Boundary Conditions (BCs)-;
- "pseudo-exact" experimental measures;
- the results of other tools already validated.

Depending on the availability of analytical solutions, or experimental measurements, or other validated software, different precautions should be taken during the validation.

Indeed, an analytical solution for that MM might exist for a limited number of BCs. In this case we will have to take care to collect BCs with "enough" significance. For example validating a model in steady state is a necessary but not sufficient step, since it is not validating its dynamics (the VD will still not span all the AD).

In case exact analytical solutions are not available, pseudo-exact experimental "solutions" can be recorded through monitoring. In this case we can follow, among other methods, three steps described in (Obercampf et al., 2002):

- characterization of the uncertainty of input parameter;
- selection of an ensemble of computations (through statistical methods like Monte Carlo, Latin Hypercube, etc.);
- quantification of the uncertainty of the output.

The validation-metric success criteria chosen in this phase is also extremely important. Mean value and uncertainty range should be compared among computational and experimental data, to gain a good knowledge of the CM's behavior.

More in general, applying these three steps will be a way to obtain the mean value for each simulation's result, instead of a value whose probability is unknown. This information might, again, drive the choice among different technologies during the building's design.

To incrementally increase our certainty about the coverage of the AD by the VD, a good possibility is offered by a continuous interaction with monitoring activities performed at operation time. This ongoing dialogue between prediction and measurement may enhance the credibility of the results of the simulation in the design phase and improve the knowledge of the methods implemented within the instrument, as well as of their range of applicability.

After having validated the CM, performing a sensitivity analysis on it can have the further advantages to:

- control that the same behavior of the MM is shown by the CM, if error propagation and/or sensitivity analysis was possible on the MM, or if experience showed a particular behavior;
- check the sensitivity of the numerical method to the choice of the discretization parameters values and inform the user about that;
- warn the user about which input he/she should choose with more care (e.g. finding a manufacturer that has conducted good tests to characterize the performance of his/her products);
- guide the user on which model should be chosen to calculate specific input of the current model (e.g. systems highly

sensible to the Mean Radiant Temperature will require the coupling with the more accurate available model for the calculation of View Factors).

5. Conclusions

In this paper we have tried to summarize the lessons learned during the development of our OO BPSt, aimed at implementing an enriched modularity (Mazzarella et al, 2009) for improving readability, maintainability and easy of validation. The current developing stage of our BPSt is summarised as follows:

- SF: implemented on an Ubuntu server thanks to the Allura Project, ready and currently used by the internal developing team only;
- code kernel: first parallelized (Mazzarella et al., 2014) beta release -building envelope only- currently under tests (previous tests have been performed on its sequential version and their results have been published in: Mazzarella et al., 2013);
- Engineering Manual: currently under development;
- Programming Standards & Developer Manual: first release;
- Validation Reports: currently under development/revision.

During the development of our BPSt, we have seen the continuous evolution of exciting and promising possibilities offered by today's technologies.

However, homogeneity of achieved results is still needed in order to be able to confront different models with each other and with real systems.

In our opinion, the creation of an environment that tries to help promote communication and cooperation between extremely different words (research, profession, manufacture) and that tries to unite design and operation is the first step to achieve a final goal.

This final goal consists in being able to assert and show with numerous case studies that the whole simulation, together with each implemented model, produces results which are correct enough for the intended use.

6. Acknowledgments

Work done under the “TRIBOULET” project, funded by Regione Lombardia.

Thanks also to Narges Shahmandi Hoonejani, who as contributed to the implementation of our SF.

Nomenclature

Acronyms

AD	Application Domain
BCs	Boundary Conditions
BPSts	Building Performance Simulation tools
CM	Computational Model
DB	Data Base
DLL	Dynamic Link Library
D&V	Development and Validation
GUIs	Graphical User Interfaces
IDE	Integrated Development Environment
MM	Mathematical Model
OO	Object Oriented
OOP	Object Oriented Programming
OS	Open Source
PM	Physical/real Model
SF	Software Forge
UML	Unified Modeling Language
VD	Validation Domain

References

- Mazzarella L., Pasini M., 2019. Building energy simulation and object-oriented modelling: review and reflections upon achieved results and further developments. *Conference Proceedings of “IBPSA Building Simulation 2009”*, University of Strathclyde, Glasgow, Scotland, 27th - 30th July, (pp. 638-645).
- Mazzarella L., Pasini M., 2013. Development of a new tool for the co-simulation of multiple autonomous object. In “Building Simulation 2013”, *Proceedings of BS2013: 13th Conference of International Building Performance Simulation Association*, Etienne Wurtz Ed., Chambéry, France, August 26-28 2013 , (pp. 3794- 3801), ISBN 978-2-7466-6294-0
- Mazzarella L., Pasini M. and Shahmandi Hoonejani N, 2014. Challenges, limitations, and success of cloud computing for parallel simulation of multiple scenario and co-simulation. *ASHRAE/IBPSA-USA, Building Simulation Conference*, Atlanta, GA, September 10-12, 2014
- Microsoft, 2014a, “.NET Core is Open Source”. .NET Framework Blog. Microsoft. Retrieved 12 November 2014. Accessed November 28th 2014. <http://blogs.msdn.com/b/dotnet/archive/2014/11/12/net-core-is-open-source.aspx>
- Microsoft, 2014b, Microsoft takes .NET open source and cross-platform, adds new development capabilities with Visual Studio 2015, .NET 2015 and Visual Studio Online. Accessed November 30th 2014. <http://news.microsoft.com/2014/11/12/microsoft-takes-net-open-source-and-cross-platform-adds-new-development-capabilities-with-visual-studio-2015-net-2015-and-visual-studio-online/>
- Oberkampf, W. L., Trucano, T. G., & Hirsch, C., 2004. Verification, validation, and predictive capability in computational engineering and physics. *Applied Mechanics Reviews*, 57(5), pp 345-384. doi:10.1115/1.1767847.
- Quarteroni, A., Sacco, R., Saleri, F. (2nd Edition), 2007. *Numerical mathematics* (Vol. 37). Springer.
- Raymond, E. S., 1999. *The Cathedral and the Bazaar: Musings on Linux and Open Source by an Accidental Revolutionary*. O'Reilly Media. ISBN 1-56592-724-9. Accessed November 28th 2014. <http://www.catb.org/~esr/writings/cathedral-bazaar/cathedral-bazaar/index.html>
- Torp, C.E., 2003. “Method of Software Validation (NT TR 535 - Validation scheme)”. Accessed November 28th 2014. <http://www.nordtest.info/index.php/technical-reports/item/method-of-software-validation-nt-tr-535-validation-scheme.html>

A methodology to integrate advanced lighting and thermal analyses for building energy simulation

Silvia Cammarano – Politecnico di Torino, Department of Energy – silvia.cammarano@polito.it

Anna Pellegrino – Politecnico di Torino, Department of Energy – anna.pellegrino@polito.it

Valerio R. M. Lo Verso – Politecnico di Torino, Department of Energy – valerio.loverso@polito.it

Chiara Aghemo – Politecnico di Torino, Department of Energy – chiara.aghemo@polito.it

Abstract

It is well known that an appropriate daylighting design can influence the global energy performance of a building as well as the visual and thermal comfort for the occupants. Furthermore the increasing awareness of the potential benefits of daylight has resulted in an increased need for objective information and data on the impact that different design solutions can have on the daylighting condition within a space, in relation with the architectural features. This kind of analysis is becoming more and more requested, during all stages of the design process.

The purpose of this paper is to describe a reliable simulation approach to consider daylight when assessing the energy performance of a building. The methodology is based on the use of both Daysim and EnergyPlus which were employed in synergy for a parametric study to assess lighting and energy performances of rooms with different architectural features: orientation, window size and glazing visible transmittance, room depth, external obstruction angle and site. Daysim was chosen to perform daylighting analyses since it allows us to accurately estimate the annual amount of daylight in a space and calculating climate-based daylight metrics as well as the annual electric lighting use for different lighting controls. The Daysim output file that describes the status of all lighting and shading groups in the space during the year was then used as input in EnergyPlus to estimate the influence of the daylighting and artificial lighting design on the global energy performance of a space.

The paper presents some considerations on the simulation approach adopted in the study and the most important results that were obtained in terms of daylighting conditions and energy demand for lighting, heating and cooling, to demonstrate the substantial

influence of daylight harvesting on the reduction of the global energy performance.

1. Introduction

Recent directives and legislation aimed at reducing energy consumption in private and public buildings (EN 15603, 2008; COM 772, 2008; Directive 2010/31/CE, 2010) have noticeably changed the focus on the building design approach over the last decade. In the lighting sector, a substantial reduction in electricity consumption for electric lighting could be obtained through a greater use of daylight, together with the use of the most energy efficient lighting technologies, such as LEDs or lighting controls. At the same time daylight harvesting in indoor spaces can influence the global energy performance of a building also in terms of heating and cooling loads. In fact the internal gains from lighting can be affected by the solar radiation that enters through the openings and by the electric lighting systems' load. For this reason it is always necessary to consider a balance between daylighting benefits and energy requirements, as shown in some recent studies (Chan et al., 2013; Didonè et al., 2011; Shen et al., 2011; Tzempelikos et al., 2007). Daylight has to be studied according to its dynamic behaviour over a period of time to accurately predict illuminance levels within a space. In this context, the 'Climate-Based Daylight Modelling (CBDM)' approach was recently proposed (Reinhart et al., 2006). CBDM allows daylighting to be studied taking into account the contribution of both direct and diffuse solar radiation and the variation due to local climate conditions over a period of time. This

approach involves the calculation of the indoor illuminances at predefined time-steps, usually for a full year period. In order to summarize the huge number of illuminance data that can be obtained, new metrics have been proposed, the so-called climate-based daylight metrics (Daylight Autonomy, Continuous Daylight Autonomy, Maximum Daylight Autonomy, Useful Daylight Illuminance and Annual Light Exposure) (Nabil et al., 2005; Reinhart et al., 2001; Reinhart et al., 2006; Rogers, 2006). Recently, two new daylight metrics have been defined and adopted by the Illuminating Engineering Society of North America, IESNA (IES, 2012). The spatial Daylight Autonomy (sDA), which assesses the sufficiency of annual illuminance in an interior work environment, and the Annual Sunlight Exposure (ASE), which expresses the annual glare potential risk. In more detail, sDA_{300/50%} is defined as the percent of an analyzed area that meets a minimum daylight illuminance level of 300 lx for 50% of the operating hours per year, while ASE_{1000,250h} is defined as the percent of an analysed area that exceeds a direct sunlight illuminance level of 1000 lx for more than 250 hours per year. It is important to note that the above metrics have been adopted in the rating system of the 'LEED Reference Guide for Building Design and Construction' (USGBC, 2014) as possible options to obtain the credit concerned with the quantity of daylight.

This kind of dynamic analysis implies the need for climate-based simulation tools. Software such as Radiance, Daysim and EnergyPlus are available for daylighting and energy simulations. Radiance and Daysim are validated dynamic daylight programs specifically developed for the analysis and visualization of lighting in a space (Ward et al., 1998; Reinhart, 2006) while EnergyPlus is a whole building energy simulation program that models heating, cooling, lighting, ventilation and other energy flows, taking the daylight contribution into account (US-DOE). These tools are based on different simulation approaches and algorithms. EnergyPlus calculates daylight through the split-flux method. Radiance is a simulation program that employs a backward ray-tracing algorithm based on the physical behaviour of light in a three-dimensional model. Daysim allows illuminance

values to be accurately calculated, through the integration of the Radiance algorithm with the Daylight Coefficient method (Reinhart, 2006).

Some studies demonstrated that EnergyPlus tends to overestimate the contribution of daylight. Ramos and Ghisi (Ramos et al., 2010) analysed the difference in the calculation of internal illuminance and external horizontal illuminance between EnergyPlus, Daysim and TropLux simulation programs using three different models. The most relevant difference between EnergyPlus and Daysim was found with regard to the calculation of internal reflections: the greater the importance of reflected light, the greater the difference in illuminances calculated by the two programs.

In 2010, Versage (Versage et al., 2010) examined the difference of modelling daylight using EnergyPlus and Daysim and the consequent influence on the simulation of the global energy consumption. They found that the availability of daylight during a year has similar values only within the first three meters from the window, presenting huge divergences at the points further away from the window. The higher lighting levels simulated by EnergyPlus reduced the energy demand for electric lighting and consequently the cooling loads due to the use of electric lighting.

In this context, it is evident that there is a need to couple different software for daylighting and global energy simulation to reach more accurate building energy analyses.

The purpose of this paper is to describe a reliable, integrated simulation approach to consider daylight when assessing the energy performance of a building, highlighting potentials and drawbacks of the entire simulation process.

Results related to the daylight available in a space (in terms of spatial Daylight Autonomy) and annual energy demand for lighting, heating and cooling are presented to highlight the substantial influence of a proper daylighting design approach on the global energy performance.

2. Methodology

The method is based on a parametric study to assess through simulations how the daylight

availability and the consequent energy demand for lighting, heating and cooling vary as the building/room architectural characteristics vary. Simulations were performed using a 2-step process. In step 1, Daysim 3.1 was used to calculate the annual illuminance profile of each space configuration. Starting from these profiles, Daysim calculates the spatial distribution within a room of climate-based daylight metrics (DA , DA_{con} , DA_{max} , UDIs), as well as the corresponding annual electric lighting demand for different lighting controls based on available daylight. Besides, a program in Matlab was specifically written to elaborate the annual illuminance data and to calculate the $sDA_{300/50\%}$. This paper focuses on $sDA_{300/50\%}$ since this is the most recent dynamic daylight metric that has been proposed by the scientific community and is the only one for which target values were defined to assess the lighting performance of a space.

Among the simulation results, Daysim also provides a Comma Separated Value (CSV) file which contains hourly schedules of the status of all lighting and shading groups within the model.

In step 2, this output was directly used as input in EnergyPlus. The parametric analysis in EnergyPlus was conducted using jEPlus, a graphical interface that allows us to set alternative values for all the parameters and simultaneously run multiple simulations calling EnergyPlus.

As a final output of the 2-step process, annual energy demands for lighting, heating and cooling were calculated and converted into primary energy data for every room configuration.

Some considerations were then drawn comparing $sDA_{300/50\%}$ and primary energy demand results.

2.1 Definition of the model

A single office room was used as a 'case study' and the analysis was carried out changing its characteristics in terms of orientation, Room Depth (RD), window area (expressed in terms of Window-to-Wall ratio, WWR), external obstructions (γ) and visible glazing transmittance of the window system (τ_{vis}). The room was assumed to be located in three different sites. All the design variables are summarized in Table 1.

The results presented in the paper refer to a sub-dataset highlighted with a grey background.

The room width and height were kept constant at 12 m and 3 m respectively. The effect of an automated shading system, consisting of a venetian blind, was considered in the simulations to dynamically control glare and overheating. The control strategy used for the venetian blind is explained in the following section.

The room was considered to be continuously occupied Monday through Friday from 8:30 a.m. to 6:30 p.m. over a whole year.

Table 1 – Design variables used in the overall parametric study

Site	Orientation	RD [m]	WWR [-]	γ [°]	τ_{vis} [%]
Turin (45.1°N)	South	4.5	0.2	0	35
	North	6	0.3	15	50
Catania (37.5°N)	West	7.5	0.4	30	70
		9	0.5	45	90
Berlin (52.5°N)		10.5	0.6	60	
		12		75	

2.2 Lighting input parameters

In this section the input data used in Daysim simulations are introduced.

The room was modeled with all walls and window frames with a diffuse reflectance of 50%, while the diffuse reflectance values of the floor and the ceiling were set to 30% and 70%, respectively.

The daylight illuminances were calculated according to a 50 cm * 50 cm calculation grid over the whole working plane (minus a 50 cm deep peripheral stripe all along the walls, which typically is a space for furniture). The work plane was set at a distance of 80 cm from the floor.

The daylighting system included in the model to control glare is a venetian blind with a diffuse transmittance of 25% (when in closed position). The blind is a movable shading system and the control is based on the algorithm implemented in Daysim, which assumes the presence of active and/or passive users. Active users open the blinds in the morning and partly close them to avoid visual discomfort when direct sunlight above 50

W/m² is incident on the work plane calculation greed points. Passive users keep the blinds lowered throughout the year (Reinhart, 2006). The strategy adopted in this study refers to mixed behaviour, i.e. both types of users were assumed to equally influence the blind control.

The target task illuminance was initially set to 500 lx, a typical value required for office activities according to the European standard CEN 12464-1:2011 (CEN, 2011). Climate based daylight metrics have been calculated based on this value. For further development of the study and for the calculation of the sDA_{300/50%} metric the target task illuminance was then set equal to 300lx.

Two different electric lighting control systems were simulated in Daysim, namely a manual on-off switch and a daylight responsive dimming system. The first one is based on the Lightswitch algorithm (Reinhart, 2006) taking into account a user that does not turn electric lights on if there's sufficient daylight on the workplane. The daylight responsive dimming system takes advantage of the daylight availability over the working plane and reduces, proportionally, the electric light use by dimming the luminaire light output.

The analysis was carried out considering a lighting power density of 12 W/m².

The Radiance simulation parameters were set as: ab = 6; ad = 1000; as = 20; ar = 300; aa = 0.05; the simulations were run using the climate files of the considered locations with a time-step of 5 minutes.

2.3 Thermal input parameters

In this section all the input data that were used in the EnergyPlus simulation program are introduced. It was assumed that the space has only one wall exposed to the outdoor environment. As a consequence interior walls, floor and ceiling were modeled as adiabatic elements.

The wall and the window facing the outdoor environment were modeled with a thermal transmittance of 0.25 W/m²K and 1.6 W/m²K, respectively. The Solar Heat Gain Coefficient of the glazing was set equal to 0.67.

The occupancy index and air change rate were fixed according to the Italian Standard UNI EN 10339:1995 (CTI, 1995) while internal loads (people

and equipment) were set according to the Italian Technical Standard UNI TS 11300-1:2008 (CTI, 2008). Winter and summer setpoint temperatures are based on the Italian Standard UNI EN 15251:2008 (CTI, 2008). The latter input parameters are all summarized in Table 2.

Table 2 – Thermal input parameters

Parameter	Definition	Source
Occupancy hours	8:30 a.m. - 6:30 p.m.	
People definition	0.12 people/m ²	UNI 10339
Air change rate	11 l/s-person	UNI 10339
People loads	70 W/person	UNI TS 11300-1
Equipment loads	3 W/m ²	UNI TS 11300-1
Lighting loads	12 W/m ²	
Winter setpoint temperature	21 °C 7:00 a.m. - 9:00 p.m. 18 °C 9:00 p.m. - 7:00 a.m.	UNI EN 15251
Summer setpoint temperature	26 °C 7:00 a.m. - 9:00 p.m. 28 °C 9:00 p.m. - 7:00 a.m.	

HVAC systems were modeled in EnergyPlus considering an ideal air load simplification. This object permits us to assess the theoretical thermal loads needed to achieve the thermal balance at any time step of the simulation.

2.4 Integrated approach

In order to evaluate the global energy demand of each space configuration and the influence of the daylighting design project on internal loads, the assumptions made for the lighting analysis needed to be coupled with the thermal analysis. In particular the control strategy used for the venetian blind and the control system adopted to automatically dim electric lighting in Daysim generate a schedule of the status of all shading and lights that has to be used for the thermal simulation.

For the present study, this connection was realized using the jEPlus tool (www.jeplus.org). jEPlus allows us to perform a parametric analysis that can be applied to all the design variables present in a

model simultaneously. It can create and manage multiple simulation jobs and collect results afterwards.

The parametric analysis starts with the use of jEPlus graphical interface, which allows us to specify a search string with all alternative values for each parameter that has to be varied: site, orientation, Room Depth, Window-to-Wall Ratio, external obstruction angle and visible glazing transmittance. Then jEPlus allows us to open one single EnergyPlus IDF model and put search strings in the places of each parameter. Then the software picks the set of values that were specified, and it puts them in every search string in the IDF model and then calls EnergyPlus.

Two specific search strings were elaborated to pick up for each room configuration the output provided by Daysim related to the use of electric lighting and blinds as a function of daylight availability.

This kind of approach can represent a reliable method to evaluate a building's whole energy performance exploring multiple design options, starting from a detailed climate-based daylighting analysis.

3. Results

A synthesis of the results that could be obtained after this integrated approach is presented in this section, with reference to the sub-dataset of configurations highlighted in Table 1.

Results are divided in two different subsections. The first subsection refers to the simulations conducted in Daysim and presents a comparison between $sDA_{300/50\%}$ values and energy demand for electric lighting (Q_{EL}) results.

The second subsection refers to the simulations conducted in EnergyPlus using the jEPlus interface analyzing the overall energy performance of each room configuration compared with the amount of daylight available in the space.

In order to correctly sum lighting (Q_{EL}), heating (Q_H) and cooling (Q_C) energy, the primary energy equivalent demand has been considered and calculated as follows:

$$E_p = Q_H/\eta_H + (Q_C/EER) \cdot \eta_{el} + Q_{EL} \cdot \eta_{el} \quad (1)$$

where η_H is the mean thermal energy generation

efficiency, EER is the Energy Efficiency Ratio of a "reference" air-to-air chiller and η_{el} is the mean National electricity generation efficiency. For the present study the following values were assumed: $\eta_H = 0.85$; $EER = 3$; $\eta_{el} = 2.17$.

3.1 Daylight availability and energy demand for electric lighting

The parametric analysis conducted in Daysim generated results about the influence that different architectural features have on daylight availability and, consequently, on the energy demand for electric lighting. In this section, results obtained for a daylight responsive dimming system are shown in comparison with a "base-case" in which lights are always turned on.

Figure 1 shows the results for room configurations without external obstructions ($\gamma=0^\circ$). It could be noted that $sDA_{300/50\%}$ values are on average lower for South-facing than North-facing rooms ($sDA_m=60.8\%$ and 78% respectively). This is mainly due to the presence of the movable shading device which avoids direct sunlight on the workplane and admits 25% of diffuse light only into the space.

As a consequence the mean annual energy demand for electric lighting is higher for south-facing than north-facing rooms ($Q_{EL,m}= 21.7 \text{ kWh/m}^2\text{-a}$ and $18.8 \text{ kWh/m}^2\text{-a}$ respectively).

Room Depth and Window-to-Wall Ratio also have a massive influence on daylight availability and energy demand for electric lighting: a progressive increase in the RD and a decrease of WWR result in a decrease of $sDA_{300/50\%}$ values and an increase in the energy demand.

In order to compare with a more effective approach the daylight amount in a space and the consequent energy demand for electric lighting, the sDA performance criteria suggested by IESNA were used as a reference (IES, 2012). Two levels of criteria were identified to assess the luminous performance of a space: spaces with $sDA_{300/50\%}$ that meets or exceeds 55% of the analysis area and spaces with $sDA_{300/50\%}$ that meets or exceeds 75% of the analysis area. According to these criteria a space can be rated respectively as "neutral" and "favourable" with regard to the sufficiency of the available ambient daylight. A space with $sDA_{300/50\%}$ below 55% is

considered as an insufficiently daylit space.

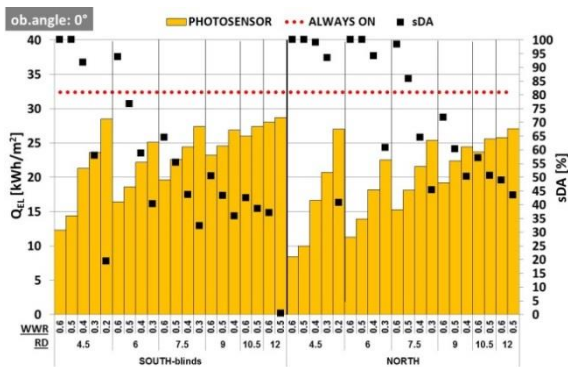


Fig. 1 – Annual energy demand for electric lighting (Q_{EL}) and $sDA_{300/50\%}$ values for all room configurations with $\gamma=0^\circ$.

The entire database of results was then divided according to these criteria. For each performance class the mean annual energy demand for electric lighting ($Q_{EL,m}$) value was calculated and compared to the base-case. Figures 2-3 show the results for south and north-facing rooms.

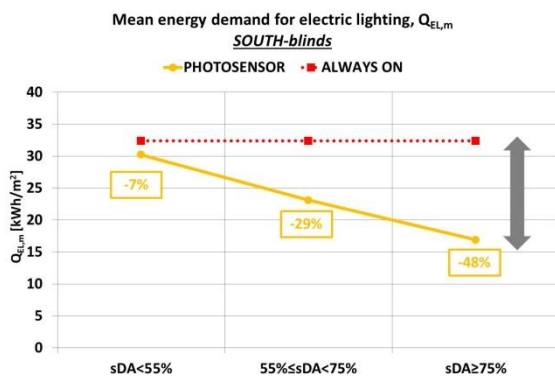


Fig. 2 – Mean annual energy demand for electric lighting ($Q_{EL,m}$) for each $sDA_{300/50\%}$ performance class (South-facing spaces)

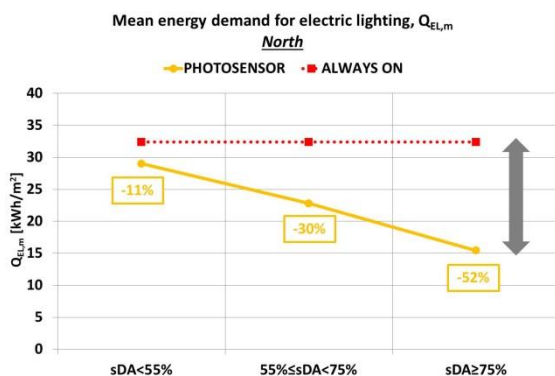


Fig. 3 – Mean annual energy demand for electric lighting ($Q_{EL,m}$) for each $sDA_{300/50\%}$ performance class (North-facing spaces)

As might be expected, the higher the daylight availability ($sDA_{300/50\%} \geq 75\%$), the lower the energy

demand for electric lighting, especially in presence of a daylight responsive dimming system. This was observed for both orientations: the mean percentage difference with respect to the case with lights always on can reach -48% for south orientation and -52% for north orientation.

Values of $sDA_{300/50\%}$ below 55% (showing that the amount of daylight is not sufficient) result in a lower reduction in the energy demand for electric lighting, even in the presence of a daylight responsive dimming system (-7% for south orientation, -11% for north orientation).

Furthermore it was observed that the glare potential risk, assessed by the Maximum Daylight Autonomy metric, is very low for all simulated case studies. DA_{max} values are always below 5%, even for cases with $sDA \geq 75\%$. This is mainly due to the lack of direct solar radiation for north-facing rooms and to the presence of movable shading devices for south-facing rooms.

3.2 Overall energy performance

The parametric analysis conducted in EnergyPlus using the jEPlus interface allows the global energy performance of a room with multiple design options to be analyzed. This section focuses on the effect on cooling and heating loads concerned with an advanced daylighting analysis.

Figure 4 shows the results for south and north-facing rooms without external obstructions ($\gamma=0^\circ$) considering a daylight responsive dimming system. In the graph, the Room Depth was shown on the x-axis in terms of S/V ratio (surface which is exposed to the outdoor environment to the space volume ratio).

For each room configuration the corresponding $sDA_{300/50\%}$ values are also shown. The data shown in the figure demonstrated that spaces with $sDA_{300/50\%} \geq 75\%$ are not only well daylit environments but they can achieve a better energy performance.

Figures 5 and 6 show that, for both south and north-facing rooms, the mean global primary energy demand ($EP_{glob,m}$) is lower for spaces rated “favorably” daylit ($sDA_{300/50\%} \geq 75\%$) than for spaces not enough daylit ($sDA_{300/50\%} \leq 55\%$).

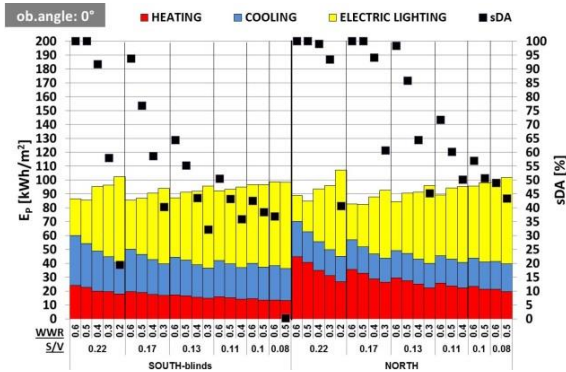


Fig. 4 – Global primary energy demand and sDA_{300/50%} values for all room configurations with $\gamma=0^\circ$.

For south-facing rooms the mean annual global primary energy demand is 112.4 kWh/m²·a when sDA_{300/50%} is below 55% and 89.7 kWh/m²·a when sDA_{300/50%} is above 75%. The mean global reduction that can be obtained is 20% (Fig. 5).

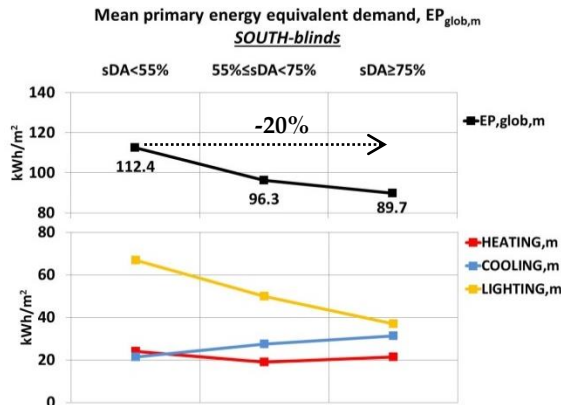


Fig. 5 – Mean annual global primary energy demand for each sDA_{300/50%} performance class (South-facing spaces).

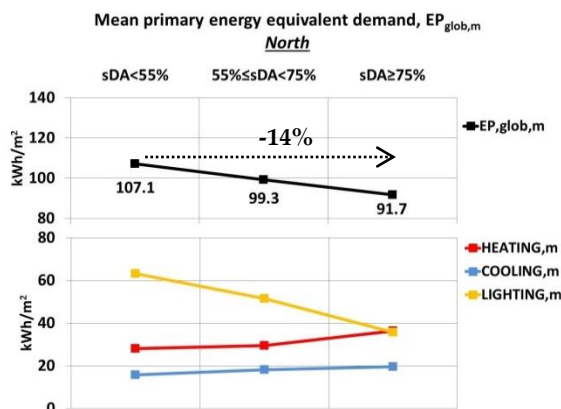


Fig. 6 – Mean annual global primary energy demand for each sDA_{300/50%} performance class (North-facing spaces).

For north-facing rooms the mean annual global primary energy demand is 107.1 kWh/m²·a when

sDA_{300/50%} is below 55% and 91.7 kWh/m²·a when sDA_{300/50%} is above 75%. The mean global reduction that can be obtained is 14% (Fig. 6).

4. Discussion and conclusion

The purpose of this paper was to describe a reliable simulation approach to consider daylight when assessing energy performance in buildings, in order to demonstrate the substantial influence of daylight harvesting on the global energy performance.

The methodology was based on the use of both Daysim and EnergyPlus which were employed in synergy for a parametric study to assess the lighting and energy performance of rooms with different architectural features.

The results presented proved that a building design based on the optimization of daylight (i.e. sDA_{300/50%} over 75%) could achieve a reduction in the global energy demand of a space. However, it has to be highlighted that results refer to a sub-dataset that includes data on north and south-facing rooms located in Turin with a visible glazing transmittance of 70%. Furthermore these results were obtained using specific software and input data. If different software and input data were used to run the dynamic simulations, the results might be different.

One important consideration about the simulation approach which was presented is that this 2-step process could be a big effort for a design team, especially during the first stages of the design process when a parametric analysis could be useful to base the first decisions about the building shape and orientation, window sizes and characteristics of glazing and shading systems. In general, it could be said that there is a lack of sufficiently accurate prediction tools for a design team to optimize a project integrating advanced daylighting analysis into energy analysis.

One further problem could be the right choice of all the input data needed for an advanced simulation. There is increasingly the need for extensive libraries which can fill in all required inputs automatically when a model has to be handled.

References

- Chan, Y.C., and A. Tzempelikos. 2013. "Efficient venetian blind control strategies considering daylight utilization and glare protection". *Solar Energy*, 98: 241-254.
- COM 772. 2008. Communication from the Commission - Energy efficiency: delivering the 20% target. Commission of the European Communities, Brussels.
- Didoné, E. I., and F.O.R. Pereira. 2011. "Integrated computer simulation for considering daylight when assessing energy efficiency in buildings". In 12th Conference of International Building Performance Simulation Association, Sydney, Australia.
- Directive 2010/31/CE. 2010. Directive 2010/31/EU of the European Parliament and of the Council of 19 May 2010 on the energy performance of buildings (recast). Official Journal of the European Union.
- European Standard EN 15603. 2008. Energy Performance of buildings – Overall energy use and definition of energy ratings. Distributed through the CEN (European Committee for Standardization), Brussels.
- European Standard EN 12464-1. 2011. Light and lighting – Lighting of work places – Part 1: Indoor work places. Distributed through the CEN (European Committee for Standardization), Brussels.
- IES Daylight Metrics Committee. 2012. IES Spatial Daylight Autonomy (sDA) and Annual Sunlight Exposure (ASE). Report LM-83-12. Accessed December 3. <http://www.ies.org>.
- Italian Standard UNI EN 10339. 1995. Impianti aeraulici a fini di benessere. Generalità, classificazione e requisiti. Regole per la richiesta d'offerta, l'offerta, l'ordine e la fornitura. Distributed through the Ente Italiano di normazione, Milan.
- Italian Technical Standard UNI TS 11300-1. 2008. Evaluation of energy need for space heating and cooling. Distributed through the Ente Italiano di normazione, Milan.
- Italian Standard UNI EN 15251. 2008. Criteri per la progettazione dell'ambiente interno e per la valutazione della prestazione energetica degli edifici, in relazione alla qualità dell'aria interna, all'ambiente termico, all'illuminazione e all'acustica. Distributed through the Ente Italiano di normazione, Milan.
- Nabil, A., and J. Mardaljevic. 2005. "Useful Daylight Illuminance: A New Paradigm to Access Daylight in Buildings". *Lighting Research and Technology*, 37: 41-59.
- Ramos, G., and E. Ghisi. 2010. "Analysis of daylight calculated using the EnergyPlus programme". *Renewable and Sustainable Energy Reviews*, 14: 1948-1958.
- Reinhart, C.F., and O. Walkenhorst. 2001. "Dynamic RADIANCE-based daylight simulations for a full-scale test office with external blinds." *Energy and Buildings*, 33: 683-697.
- Reinhart, C.F. 2006. "Tutorial on the use of DAYSIM simulations for sustainable design". <http://www.daysim.ning.com>.
- Reinhart, C.F., J. Mardaljevic, and Z. Rogers .2006. "Dynamic daylight performance metrics for sustainable building design". *Leukos*, 3: 1-25.
- Rogers, Z. 2006. "Daylighting Metric Development Using Daylight Autonomy Calculations In the Sensor Placement Optimization Tool."
- Shen H., and A. Tzempelikos (2011). "Daylighting and energy analysis of private offices with automated interior roller shades." *Solar Energy*, 86: 681-704.
- Tzempelikos A., and A.K. Athienitis (2007). "The impact of shading design and control on building cooling and lighting demand." *Solar Energy*, 81: 369-382.
- US-DOE. EnergyPlus v7.2 from US Department of Energy, Building. <http://www.energy.gov>.
- USGBC. 2014. LEED Reference Guide for Building Design and Construction (v4).
- Versage, R., A.P. Melo, and R. Lamberts. 2010. "Impact of different daylighting simulation results on the prediction of total energy consumption." Proc. of the Fourth National Conference of IBPSA-USA, New York City, New York, August, 11-13.
- Ward, L.G., and R. Shakespeare. 1998. "Rendering with RADIANCE. The Art and Science of Lighting Visualization." Edited by Morgan Kaufmann. San Francisco, California, U.S.A.

BIM-generated data models for EnergyPlus: A comparison of gbXML and IFC Formats

Ira Ivanova – Department of building science and building ecology, TU Wien, Vienna, Austria

Kristina Kiesel – Department of building science and building ecology, TU Wien, Vienna, Austria

Ardeshir Mahdavi – Department of building science and building ecology, TU Wien, Vienna, Austria

Abstract

Building Information Modelling (BIM) aims to promote collaboration between project partners by providing a single model with the required relevant information. BIM data is meant to be provided to multiple domain-specific applications in an effective manner. We consider two data formats used to facilitate this interoperability: (i) gbXML format, developed by Green Building Studio and (ii) IFC format, developed by buildingSMART. Both of these formats can be used to provide geometry information and other data to Building Performance Simulation (BPS) applications. However, gbXML and IFC have unique data structures, which has consequences for how the original geometrical and spatial data from the BIM model is translated. In this context, the present contribution aims to assess and compare the usage of IFC and gbXML data formats in separate workflows, thereby observing consistency of building data and efficiency of the process. First, the main differences and specifics of the two formats are investigated and several case models are developed. Using a BIM authoring tool both formats are then tested in a typical workflow including the use of a BPS tool. To explore the implications of the quality of the BIM model, a second workflow (with the same case models) was set up in a different BIM authoring tool. These workflows and their outcome with regard to BPS were analyzed and the capabilities and differences of the two formats were studied in detail. The results of this study show that both data formats are capable of extracting and transferring geometrical information from BIM models. However, the successful transfer of this information is strongly related to the quality of the BIM representation. Demonstrative simulation runs show that incorrect BIM-based building geometry data can produce misleading results. Moreover, the overall approach to using gbXML and IFC to perform BPS is currently rather cumbersome and difficult to validate.

1. Introduction

In recent years more attention has been paid to improving the quality of exchanged data and to managing information integrity between professions involved in building projects. Building Information Modelling (BIM) promotes collaboration between disciplines by providing a single 3D CAD model, containing relevant data about a building throughout its life cycle, which can be exported to various function-specific software (Eastman, 2008). BIM can help to increase the efficiency of BPS by facilitating the data input for simulation and therefore allowing more scenarios to be investigated. (Maile et al., 2007). A BIM model provides detailed information on a building, which can serve as input for BPS and therefore reduce the amount of time needed to set up a simulation model manually (Laine et al., 2007). The Architecture Engineering Construction (AEC) industry has developed two data formats to facilitate interoperability between software and to exchange building information between disciplines. One is gbXML format, developed by Green Building Studio (gbXML, 2014). The other one is IFC, which is an object-based, open file format, developed by buildingSMART (former AIA) and has been used to transfer data between various participants in a building project (buildingSMART, 2014).

For the purpose of Building Performance Simulations (BPS) both formats have the ability to extract building data necessary for energy simulation from the BIM model and transfer it to the respective software. In most cases, simulation

processes require information on building geometry (Maile et al., 2013). Simulation engines typically require complex 3D geometry to be broken down to space boundary surfaces (Jones et al., 2013). There are numerous software tools, which convert rich geometry and prepare it for simulation (Bazjanac, 2008; Bazjanac et al., 2011; Hitchcock and Wong, 2011).

This paper aims to assess and compare the transfer of building geometry data via IFC and via gbXML format into BPS. For this purpose, two different workflows are developed and tested with regard to consistency of data, efficiency of the workflow and the validity of the results.

2. gbXML and IFC

The gbXML data format was initially developed in 1999 by Green Building Studio Inc. strictly for the purpose of energy analysis (gbXML, 2014). It retrieves geometry and non-geometrical information from the model and saves it in a text format under pre-defined notations. The information is divided into three different categories: *ShellGeometry*, *SpaceBoundary* and *Surface*. Software tools employing gbXML do not always use all three in order to retrieve geometry. Most of them implement *ShellGeometry* and *SpaceBoundary* since in combination they represent geometry more accurately. Some use solely the *Surface* element to obtain the geometrical information (gbXML, 2013).

Industry Foundation Classes, or IFC, is the official international standard for open BIM and is registered with the International Standardization Organization (ISO). EXPRESS data definition language is used to describe entities and relationships, including data verification rules in the data scheme. In addition, EXPRESS-G (graphical data notations) is used to display large information models (buildingSMART, 2014; Dong et al., 2007). The IFC adopts the "top-down" approach, which creates a complex, hierarchical schema in a large data file (Dong et al., 2007). Additionally buildingSMART developed a standard for the information flow in an integrated project called Information Delivery Manual (IDM).

The main goal of the IDM is to ensure that all relevant data for a specific task is described in the 3D BIM model in such a way that it is accurately imported and processed by the respective software

3. Methodology

In order to analyse and compare the effects of building geometry data transfer for the purpose of BPS, two different workflows were defined (Fig.1).

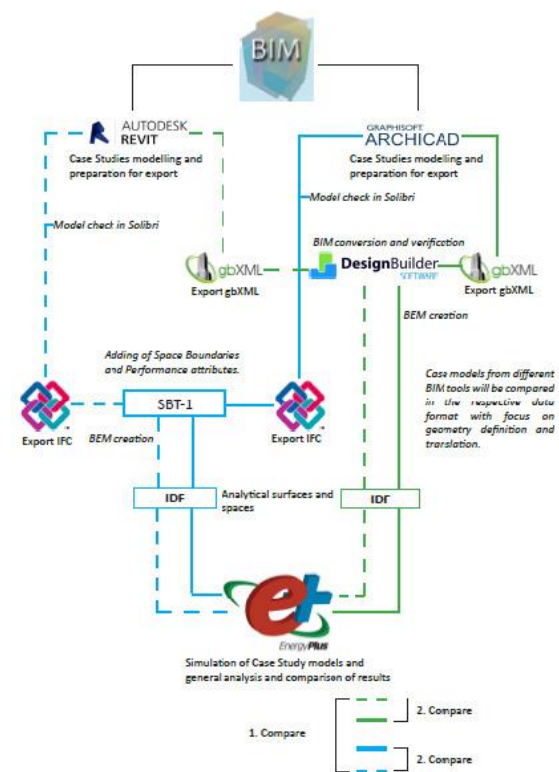


Fig. 1 – Two different workflows to transfer BIM data to BPS

Furthermore, several models were developed and created using two different BIM authoring tools (Fig. 2).

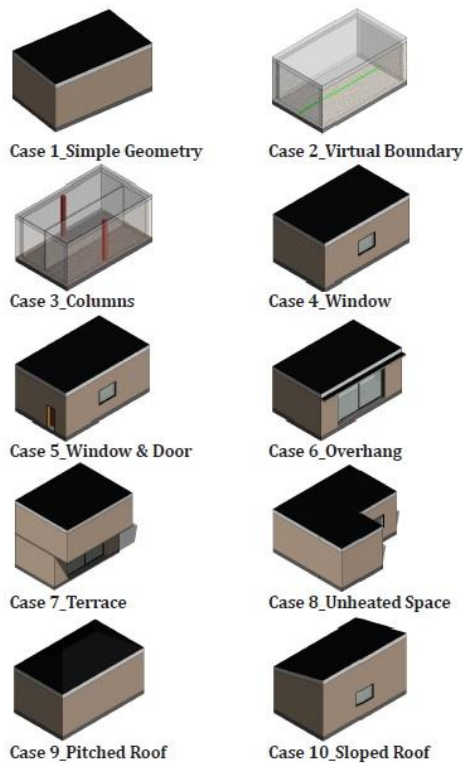


Fig. 2 – Case Study Models

3.1 Selection of Software

Autodesk Revit (Autodesk, 2014) and Graphisoft ArchiCAD (Graphisoft, 2014) are among the leading BIM software platforms (AEC, 2013). Therefore, they are chosen as the BIM authoring tool. An important precondition for the seamless export of both data formats is the creation of a "clean" 3D BIM model that has a comprehensive and consistent geometry structure.

DesignBuilder is the selected pre-processing tool for gbXML. It supports importing BIM through gbXML and allows for IDF export, which is the format needed to be imported into EnergyPlus (EnergyPlus, 2014). Lawrence Berkeley National Laboratory (LBNL, 2014) has developed a semi-automated tool, called Space Boundary Tool (SBT-1) that retrieves building and spatial geometry data from the IFC schema and breaks it down to heat transferring surfaces. SBT-1 has been made commercially available and is used for the present case. In its current and only version it imports IFC2x3 Coordination View 2.0, an earlier variant of

the IFC schema, and exports v. 7.2 IDF format for EnergyPlus.

For the comparison of data quality throughout the process the Solibri Model Viewer was used to visualize the information (Solibri, 2014).

3.2 Case Study Models

The main objective for the design of the Case Study models is to incorporate building elements, which have been frequently reported to have problems with geometry during export of either gbXML or IFC (Hitchcock and Wong, 2011; Moon et al., 2011). The basic design is kept as simple as possible. All Case Studies contain basic geometry information regarding walls, floor, and roof. Thermal specifications are defined and at least one zone is assigned. The models are shown in Fig.2.

3.3 Performance Study

The process of generating, extracting, transforming and simulating building geometry for the purpose of BPS is defined by an array of actions, necessary for a successful workflow. These operations are done in consecutive steps to outline a workflow, which facilitates data format comparison at different stages. Figure 3 gives a detailed outline of the steps taken.

First a case study model is created either in Revit or ArchiCAD. The definitions for the building elements and the spaces are identical. Next, the data is exported using the IFC or the gbXML format. The files are then imported into the respective pre-processing tool – DesignBuilder or SBT-1. Using these software, IDF-files are created and finally imported to EnergyPlus and simulated. Additionally all the cases were simulated in EnergyPlus via manual data input, in order to create reference models for the comparison of the results.

After each step, the data is analysed and compared with the original files to establish if and how the conversion process has affected the quality of the information.

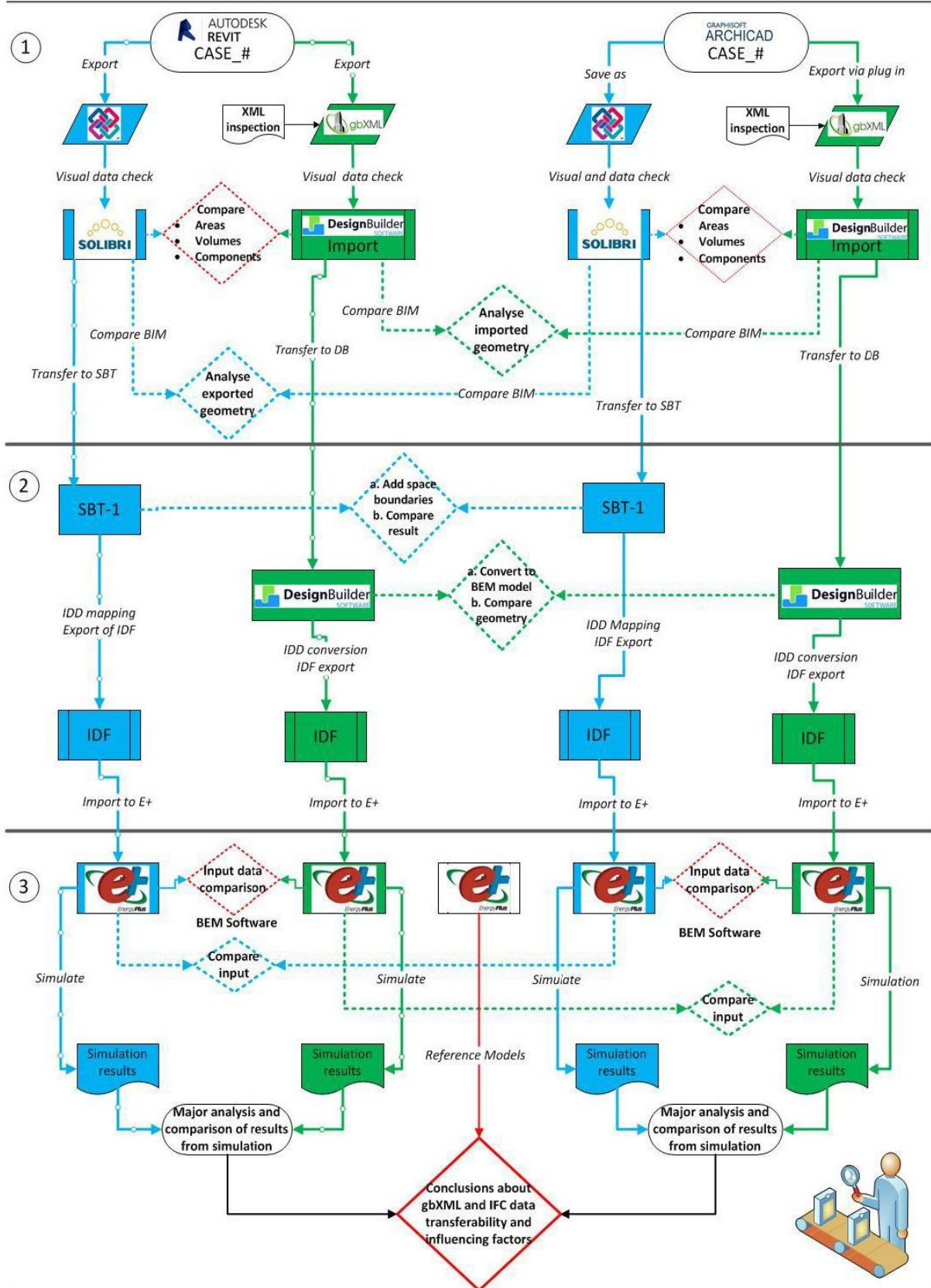


Fig. 3 – Detailed diagram of the workflow

4. Results and Discussion

Both gbXML and IFC have shown reasonable performance in extracting and storing building geometry data and its non-geometric specifications. Four in all twenty exported gbXML formats appeared to be incorrect and only one of the IFCs (see Table 1). The parameters analysed for this comparison are the volume, the area, and the geometry. The measured accuracy is the percentage of the correct data obtained.

The gbXML recognizes and defines the required information for energy analysis from the BIM model and locates information under predefined elements in its schema. This stresses the fact that the created model and its geometry have to be sufficiently accurate at the time of export.

IFC has a fairly complicated data structure and strict hierarchy, which defines relationships between

building elements and space in a contingent manner. This is why it is important that the information in the BIM model is structured in accordance to IDM. This provides a more coherent data structure for further processing.

Table 2 shows the results after the original data was processed and transformed to IDF. Some of the errors were caused by the definition of the native model in the BIM authoring tool and some are due to the technical performance of the intermediate tools. By comparing tables 1 and 2 it can be seen that the original BIM data has been altered during the conversion to IDF via SBT-1, leading to several errors. There are also some inconsistencies in the gbXML workflow.

Fig. 4 and Fig. 5 show the absolute difference in Total Site Energy [$kWhm^{-2}$] for all the cases

Table 1 – Comparison of extracted IFC and gbXML data (extraction failures are denoted via cross marks)

Extracted building data	gbXML		IFC	
	Revit	ArchiCAD	Revit	ArchiCAD
Case1_Simple Geometry	✓	✓	✓	✓
Case2_Virtual Boundary	✓	✓	✓	✓
Case3_Column	✓	✓	✓	✓
Case4_Window	✓	✓	✓	✓
Case5_Window and Door	✓	✗	✓	✓
Case6_Overhang	✗	✓	✓	✓
Case7_Terrace	✓	✓	✓	✓
Case8_Unheated Space	✓	✗	✓	✓
Case9_Pitched Roof	✓	✓	✓	✗
Case10_Sloped Roof	✓	✗	✓	✓
Measured accuracy	90%	70%	100%	90%

Table 2 – Comparison of processed IFC and gbXML data (transfer failures are denoted via cross marks)

BEM generated building data	gbXML-DB		IFC- SBT-1	
	Revit	ArchiCAD	Revit	ArchiCAD
Case1_Simple Geometry	✓	✓	✓	✓
Case2_Virtual Boundary	✗	✗	✓	✓
Case3_Column	✓	✓	✗	✓
Case4_Window	✓	✓	✓	✗
Case5_Window and Door	✓	✗	✓	✗
Case6_Overhang	✗	✓	✓	✗
Case7_Terrace	✓	✓	✓	✗
Case8_Unheated Space	✓	✗	✓	✗
Case9_Pitched Roof	✗	✗	✓	✗
Case10_Sloped Roof	✗	✗	✓	✗
Measured accuracy	60%	50%	90%	30%

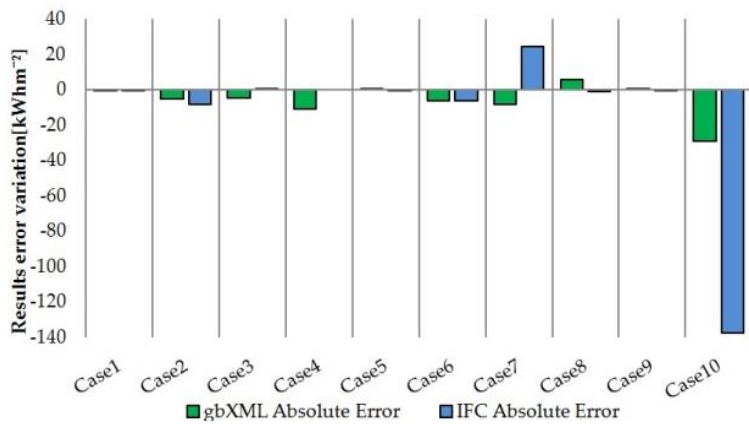


Fig. 4 – Error variation in results- Revit

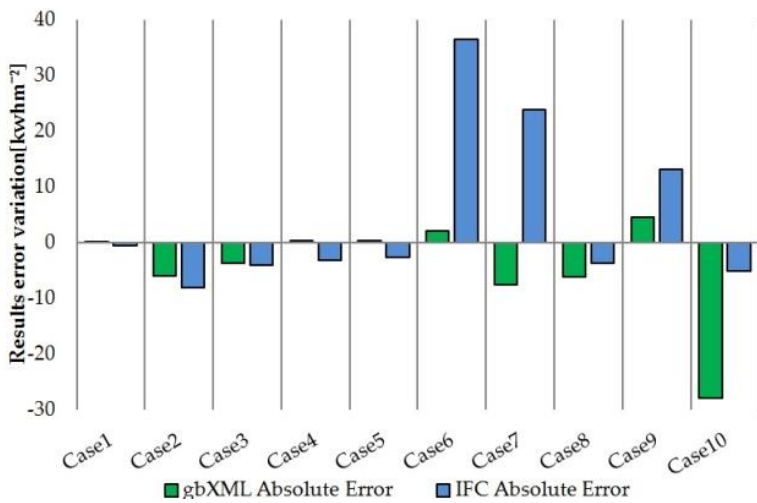


Fig. 5 – Error variation in results- ArchiCAD

5. Conclusion

In the course of evaluating and comparing the use of IFC and gbXML for the purpose of BPS, it becomes clear that both data formats are capable of extracting and transferring spatial and geometrical information from BIM models. Successful data export is strongly related to the quality of the building model, generated in a BIM-authoring tool. In order to preserve the quality of the data, one is highly dependent on the receiving software, which converts and prepares the information for input to EnergyPlus.

In its default schema, populated with building semantics, gbXML stores building geometry in a pre-defined structure, which does not preserve the integrity of the geometric model. Its primary function is to facilitate work between BIM and building performance analysis. It has been the preferred format for that purpose. Future improvements should be focused on making it a more reliable and robust data format.

IFC has been developed in view of the needs of the AEC industry to assist integrated BIM work and exchange of building data between disciplines. In its role as an open data format, it provides a contingent and hierarchical informational structure, which captures the needed building geometry for conducting building performance analysis. More efforts could be invested by energy software vendors to use this format, given its promising way of storing and translating data.

For the particular workflow studies, both gbXML and IFC require pre-processing BEM tools. DesignBuilder, used for gbXML data conversion and IDF export, provides an integrated platform for energy analysis with BIM and EnergyPlus. But using the software to appropriately prepare the data for simulation in EnergyPlus requires expertise. On the other hand, SBT-1 for IFC is a basic tool for simplification of geometry, but its potential to convert complex geometry into Space Boundaries has not been further developed. Currently the development is disrupted. Both workflows have been proven to be tedious and rather time consuming. Furthermore, a certain level of knowledge is required regarding the whole process, tools applied, and technical specifications.

In addition, the process does not result in a direct feedback to the original model, reducing its potential toward effective iterative design improvement.

References

- AEC. 2013. AECbytes Newsletter #62 (February 28, 2013); Aconex Survey; Accessed 15 August 2014 http://www.aecbytes.com/newsletter/2013/issue_62.html
- Autodesk. 2014. "Green Building Studio 2014." Accessed September 12 2014. <http://www.autodesk.com>
- Bazjanac, V.. 2008. "IFC BIM- based Methodology for Semi- Automated Building Energy Performance." *Proceedings of the 25th International Conference on Information Technology in Construction.*
- Bazjanac, V., Maile, T., O'Donnell, J. and Rose, C., Mrazovic, N., 2011. "An Assessment of the Use of Building Energy Performance Simulation in Early Design" *Proc. of BS2011*, 14-16 November, Sydney, Australia
- buildingSMART. 2014. "IFC Open BIM." Accessed 27 September 2014. <http://www.buildingsmart-tech.org>;
- Dong, B., Lam, K. P., Huang, Y.C., Dobbs, G. M.. 2007. "A Comparative Study of the IFC and gbXML Informational Infrastructures for Data Exchange in Computational Design Support Environments." *Proceedings BS 2007*. 3-6 Sept 2007. Beijing, China
- Eastman, C., Teicholz, P., Sacks, R., Liston, K.. 2008. "BIM Handbook: A Guide to Building Information Modeling." New Jersey, Canada
- EnergyPlus. 2014. Accessed November 2 2014. <http://apps1.eere.energy.gov/buildings/energyplus/>
- gbXML 2013; "Implementation Agreement Draft, Phase I gbXML Test Case Documentation 2013." Accessed on February 27 2014 <http://www.gbxml.org/testcasedocs.php>
- gbXML, 2014; Accessed October 1 2014. <http://www.gbxml.org>
- Hitchcock, R. J., Wong, J.. 2011. "Transforming IFC Architectural View BIMs For Energy

- Simulation." *Proceedings BS2011*. 14-16 Nov. Sidney, Australia
- Graphisoft. 2014. Accessed 18 July 2014 <http://www.graphisoft.com/archicad/>
- Hitchcock, R. J., Wong, J., 2011. "Transforming IFC Architectural View BIMs For Energy Simulation: 2011" *Proc. of BS2011*. 14-16 November. Sydney, Australia
- LBNL. 2014. Space Boundary Tool (SBT-1)-. Accessed 15 September 2014 <https://simulationresearch.lbl.gov/projects/space-boundary-tool>
- Jones, N. L., McCrone, C. J., Walter, B. J., Pratt, K. B., Greenberg, D. B.. 2013. „Automated translation and thermal zoning of digital building models for energy analysis." *Proc. of BS2013*. 26-28 August. Chambéry, France
- Laine, T., Hänninen, R., Karola, A.. 2007. „Benefits of BIM in Thermal Performance Management." *Proceedings: BS 2007*. 3-6 Sept 2007. Beijing, China
- Maile, T., O'Donnell, J., Bazjanac, V. and Rose, C.. 2007. "Building Performance Simulation Tools- A Life Cycle and Interoperable Perspective" *Stanford University*
- Maile, T., O'Donnell, J., Bazjanac, V. and Rose, C., Mrazovic, N.. 2011. "An Assessment of the Use of Building Energy Performance Simulation in Early Design." *Proceedings BS2011*. 14-16 November. Sidney, Australia
- Maile, T., O'Donnell, J., Bazjanac, V. and Rose, C.. 2013. "BIM- Geometry Modelling Guidelines for Building Energy Performance Simulation." *Proceedings: BS 2013*. 26-28 August. Chambéry, France
- Moon, H. J., Choi, M.S., Kim, S.K., Ryu, S.H., 2011. "Case Studies for the evaluation of interoperability between a BIM based Architectural Model and Building Performance Analysis Programs" *Proc. of BS2011*. 14-16 November. Sydney, Australia
- Solibri. 2014. Accessed November 20 2014. www.solibri.com

Passive solutions for the optimization of the indoor environmental quality: a case study

Fabio Sicurella – Planair SA – fabio.sicurella@planair.ch

Perla Colamesta – Freelance engineer – perlacolamesta@libero.it

Abstract

An integrated energy concept of a building should include not only its energy consumption but also the quality of the indoor environment in terms of thermal, visual comfort and indoor air quality.

Shadings, window construction materials and ventilation strategies have a significant impact on the “health” of the building and of its occupants; they should be studied carefully during the pre-design phase of the building.

Evaluating thermal, visual comfort or IAQ individually is quite easy thanks to reference standards and simulation tools but it can imply non-optimised solutions or even design errors.

Conversely, an integrated approach should include a simultaneous analysis of all these aspects of the indoor environmental comfort in order to propose optimised technical solutions or design strategies.

Previous studies have proposed statistical indicators to manage thermal and visual comfort simultaneously. In the present study further indicators of IAQ (here CO₂ was considered) were included in order to achieve a global environmental quality. This integrated approach was used for the optimisation of a new large office building in Switzerland. A parametric multi-objective analysis was carried out by means of EnergyPlus. This approach allowed for the optimization of design strategies (shadings, window materials, ventilation) for both energy savings and indoor environmental quality of the building.

1. Introduction

During the concept and the design of a new building, one of the hardest tasks for a building physics engineer is probably to fulfil the occupant wellness. A “healthy building” means a building

where the majority of the occupants feel comfortable from a thermal, visual and IAQ point of view. Following a bioclimatic approach without the use of HVAC systems, the number of the main physical parameters that govern this “feeling of comfort” may be reduced to a few: the operative temperature, the illuminance and the concentration of pollutants. The ranges of their optimal values are defined in the literature and in technical standards (EN 15251, 2007; Nabil et al., 2005).

Actually, in order to understand if the indoor comfort of a building will be achieved or not, one should be able to quantify the intensity of discomfort inside the building and its duration during occupancy.

This kind of analysis can be carried out by using statistical indicators as already described in the literature (Sicurella et al., 2011).

On the basis of such analysis, a building physics engineer should be able to propose optimised technical solutions in order to fulfil thermal, visual and IAQ comfort simultaneously.

In the present work a case study of a real building design will be presented as well as a method to find out optimised technical solutions. This optimisation analysis concerned the choice of glazing, shadings and ventilation strategies.

2. The methodology

The main goal of this study was to propose technical solutions in order to fulfil thermal, visual and IAQ comfort simultaneously.

It is important to state that the shape and orientation of the building as well as the WWR were already defined by the architect. Other

constraints were given by the client who did not want to have mechanical ventilation for the building but he wanted a “bioclimatic building” exploiting natural ventilation and daylighting.

As a consequence, our analysis was focused on the optimisation of glazing, shading devices and natural ventilation strategies.

Due to the fact that ventilation does not have an impact on daylighting, the authors decided to optimise first the windows and the shadings devices and then the natural ventilation strategies.

For this reason, the present work is divided in two main phases (Figure 1): the first one, in which the characteristic of glazing and shading devices were optimized for thermal (TC) and visual comfort (VC) purposes; the second one in which the ventilation strategies were analysed for thermal and IAQ comfort purposes.

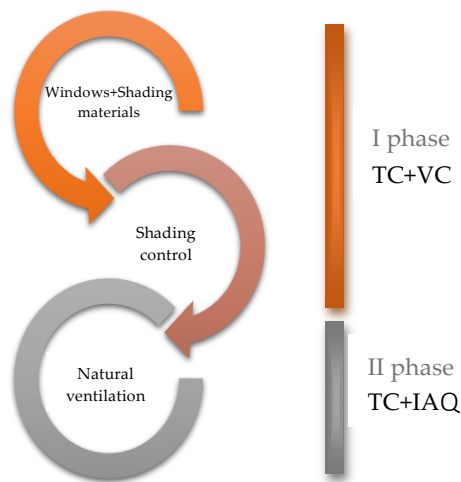


Fig. 1 – Work phases of the optimization process

The analyses were evaluated from June to September during occupation hours (from 8.00am to 7.00 pm). All the performances of the office were simulated on EnergyPlus v.8.1 (EnergyPlus, 2013), able to analyse simultaneously different conditions.

Simulations were run in free running mode; the parametric optimization was made by using the simulation manager jEPlus.

2.1 Thermal Comfort evaluation

Thermal Comfort was evaluated considering the adaptive comfort, according to the standard EN15251, category II: “Normal level of expectation and should be used for new buildings and renovations” (EN 15251, 2007).

The objective function was the minimization of the number of occupation hours in the office room during which the operative temperature were out of the range limits defined by the above-mentioned standards.

2.2 Visual Comfort evaluation

Concerning daylighting, the range of visual comfort should take into account the actual working context, the visual task, the luminance all around, etc. Many studies provide full credit only to values between 100 lux and 2000 lux by suggesting that horizontal illumination values outside of this range are not useful (Nabil A et al., 2005). Due to the fact that the landscape is often **snowy** the authors decided to prudently reduce the optimal daylight illuminance range from 300 to 1500 lux.

The objective function was the minimization of the number of occupation hours during which the workplane illuminance is out of this range. This value was obtained as an average calculated upon two points inside the office room at a height of 0.8m (Figure 2).

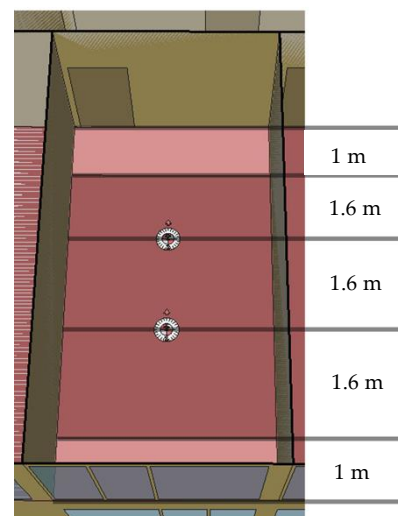


Fig. 2 – Sensors position inside the office room

The two illuminance sensors were considered to be at 2.6m and 4.2m from the façade respectively in order to limit the impact of the boundaries. (Fig. 2)

2.3 Indoor Air Quality evaluation

The calculation model used for simulating the ventilation airflow rate is a function of wind speed and thermal stack affect, combined with the infiltration effect.

The equation used to calculate the ventilation rate driven by wind is:

$$Q_w = C_w A_{\text{opening}} F_{\text{schedule}} V$$

where:

Q_w =Volumetric air flow rate driven by wind [m^3s^{-1}]

C_w = Opening effectiveness [dimensionless]

A_{opening} = Opening area [m^2]

F_{schedule} = Open are fraction [dimensionless]

V = Local wind speed [ms^{-1}]

The equation used to calculate the ventilation rate due to stack effect is:

$$Q_s = C_d A_{\text{opening}} F_{\text{schedule}} \sqrt{2g \Delta H_{\text{NPL}} (|T_{\text{zone}} - T_{\text{odb}}| / T_{\text{zone}})}$$

where:

Q_s = Volumetric air flow rate driven by wind [m^3s^{-1}]

C_d =Discharge coefficient for opening [dimensionless]

A_{opening} = Opening area [m^2]

F_{schedule} = Open are fraction [dimensionless]

ΔH_{NPL} = Height from midpoint of lower opening to the neutral pressure level [m]

T_{zone} = Zone air dry-bulb temperature [K]

T_{odb} =Local outdoor air dry-bulb temperature [K]

The total ventilation rate is given by:

$$\text{Ventilation}_{\text{Wind and Stack}} = \sqrt{Q_w^2 + Q_s^2}$$

Concerning IAQ, in literature and technical standards it is possible to find different values of suitable ventilation rate (AiCARR, 2009; UNI EN 15251, 2007; ASHRAE 62.1, 2007).

A way to evaluate IAQ is to refer to the actual CO_2

concentration inside the building.

Following the ASHRAE Standard 62, 1989, this limit can be set at 1000 ppm even though the standard revision (ASHRAE Standard 62, 1999), suggests 700 ppm above the outdoor concentration as an upper limit. According to studies of Bern University, published by the Swiss Federal Office for the Environment (OFEV,2008) the outdoor CO_2 concentration is 400 ppm.

As a consequence the authors decided to choose the more restrictive of these rate values for CO_2 concentration, which in this case study was set at 1000 ppm.

The objective function was to minimize the number of working hours during which the CO_2 concentration is higher than 1000 ppm.

3. The case study

The analysed building is a multifunctional three-story building of around 14.500 m^3 designed by the Atelier of architecture Manini Pietrini based in Neuchâtel for the Chocolate Manufacture enterprise Camille Bloch. It is located in Northern Switzerland (Courtelary, near Basel) at 800m asl and includes offices, conference rooms, a restaurant and exposition halls.

It is a north/south oriented building with large glazing on the main façades (on average WWR of 43%), (Figure 3).

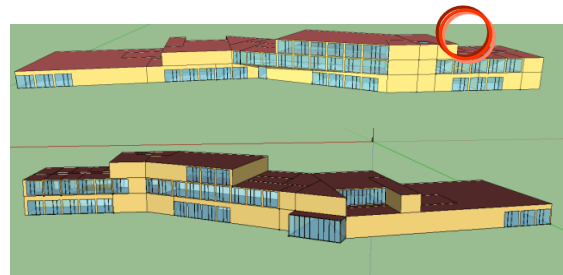


Fig. 3 – Southern and Northern view of the building with in evidence the analysed office (red circle)

For brevity, the results presented in this work will refer to a south-oriented office room only. It is 3.65 m wide, 6.80 m long and 2.8 m high (Figure 2 and 3), and it is occupied by two people from 8.00 am to 7.00 pm. Each office is characterized by 8.8 m^2 of window, only 2.2 m^2 is an openable area.

On the eastern side of the building there are two openable bottom hung windows of 2.2 m² (Fig. 4) (opening area: 25%).

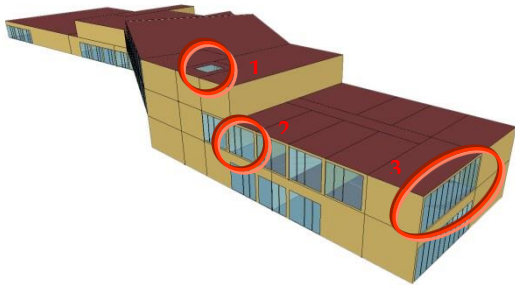


Fig. 4 – Building model: 1: skylight on the stairs; 2: opening window in office room; 3 opening window at the Eastern facade

The doors between the offices and corridor were considered open all the time; the corridor is connected to a stairwell which has a 4m² openable skylight (Figure 4).

4. Thermal and Visual Comfort

4.1 TC+VC Windows + Shading materials Parameters

The windows are low emissivity triple glazing (U_g -value of 0.6 Wm⁻²K⁻¹ filled with Ar) with PVC frames (U_f -value of 1.1 Wm⁻²K⁻¹).

Exterior perforated protections placed in front of the windows are automatically lowered when the total solar irradiance on the façade exceeds 200 Wm⁻².

Infiltrations were taken into account following the Sherman and Grimsrud model (Sherman et al., 1980), and by using the coefficient recommended in ASHRAE HoF 2009, while, only during this first phase (windows and shadings optimisation), the hygienic ventilation was set equal to 0.5 ACH.

The reflectivity of interior walls, ceiling and floor was set at 0.5, 0.7 and 0.3 respectively.

The Solar Transmittance (G_v) and the Visible Transmittance (T_v) for both glazing and shadings were varied so obtaining 3⁴ combinations (Table 1). Similar combinations can be achieved by real glasses.

Table 1 – Properties of glazing and shadings considered for the parametric analysis

Window glazing	W_ Gv	{0.35,0.45,0.55}
	W_ Tv	{0.55,0.65,0.75}
Shadings	S_ Gv	{0.10,0.15,0.20}
	S_ Tv	{0.15,0.20,0.25}

4.2 TC+VC Windows + Shadings materials Optimization Results

The results of this first parametric analysis are shown in Figure 5 and 6.

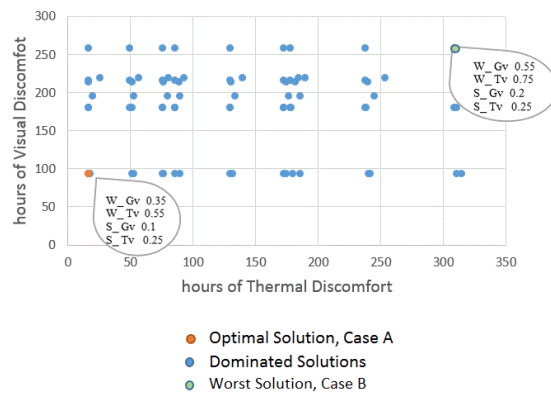


Fig. 5 – Results of windows and shading materials optimization

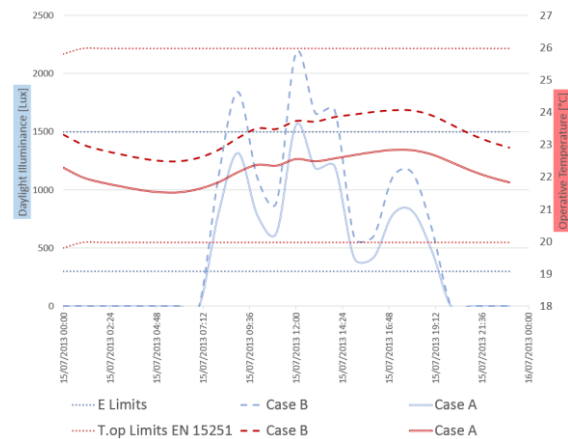


Fig. 6 – Comparison between the best and worst case in a typical day

As can be observed in Figure 5, the best results are obtained by the combination W_G_v : 0.35; W_T_v : 0.55 for the windows glazing, and S_G_v : 0.1 S_T_v : 0.25 for the shadings materials.

As can be seen in Figure 6, during a typical

summer day, with a high value of visible transmittance (Case B: W_{Tv} : 0.75; S_{Tv} : 0.25) visual discomfort can occur while the lowest solar transmittance value (Case A) is always preferable for thermal comfort.

4.3 TC+VC Shading control Parameters

Once the window and shading characteristics were set, a further optimization was focused on the set point of solar irradiance for shadings control.

The simulations were run with three different set point values for the incident total solar radiation upon the façade (100, 150 and 200Wm^{-2}), and with a so called “shading control based on the daylight glare”. This method consists in activating shadings when the daylight glare index at the first reference point, calculated with the eq. of Hopkinson, (Hopkinson, 1970,1972) exceed the value of 22.

4.4 TC+VC Shading control Optimization Results

The results are shown in Table 2 from 01/06 to 30/09 and in Figure 7 for a typical sunny day.

As can be seen in Table 2 and in Figure 7, the daylight glare control is not optimized for thermal purposes. On the other hand, the 800-1600 lux range seems to be the optimal range for visual comfort following this control strategy.

Table 2 – Results of shading control evaluation

Type of shading control	Hours of thermal discomfort	Hours of visual discomfort
“Daylight glare”	73	194
Total solar irradiance $\geq 100\text{Wm}^{-2}$	12	254
Total solar irradiance $\geq 150\text{Wm}^{-2}$	12	75
Total solar irradiance $\geq 200\text{Wm}^{-2}$	17	93

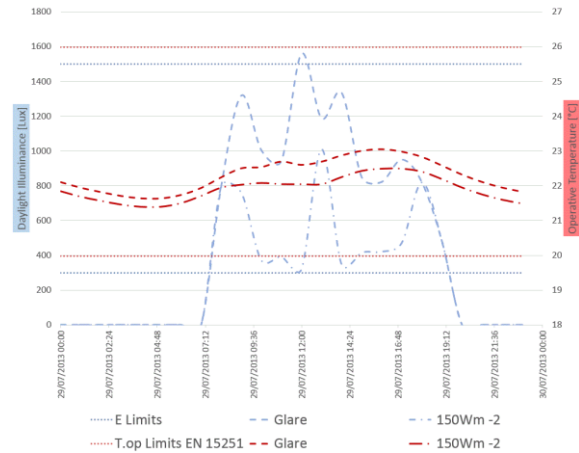


Fig. 7 – Comparison between “daylight glare” and 150Wm^{-2} irradiance control for shadings in a typical day

In the authors’ opinion this type of shading control might empathise daylighting for a long part of the occupation hours while penalising thermal comfort.

Due to the fact that the site is often snowy and in a seasonal optimisation perspective the authors decided a shading control based on solar irradiance upon the façade set at 150Wm^{-2} .

In fact this value reduces both thermal and visual discomfort (Table 2).

5. Thermal Comfort and Indoor Air Quality

5.1 TC+IAQ Parameters

For the following part of the study the hygienic mechanical ventilation was removed, while the shading control previously optimised was maintained.

This analysis considered a carbon dioxide generation rate in the office room of $3.82 \cdot 10^{-8}\text{m}^3\text{s}^{-1}\text{W}^{-1}$, obtained from ASHRAE Standard 62.1 by assuming a constant activity level of 1 met.

A constant outdoor CO_2 concentration of 400 ppm was considered according to studies of Bern University, published by the Swiss Federal Office for the Environment (OFEV, 2008).

As already introduced in paragraph 3, only 25% of the glazing is an openable window. This part of the window can be opened in two different modes: automatically (by assuming an ideal occupant’s behaviour) in bottom hung mode and manually in

side hung mode.

Concerning the automatic mode, it is based on outdoor/indoor temperature gradient and on the internal temperature. The window is open when the gradient temperature is higher than 1°C and when the indoor air temperature is over 22 °C; the occupants may open the window partially (in bottom hung mode) or totally (side hung mode).

The simulations were run considering different opening type mode combined with different time ranges of possible opening, and with the opportunity or not to exploit the cross ventilation by the skylight over the stairs and by the opening windows at the Eastern facade (Figure 4).

5.2 TC+IAQ Optimization Results

The results are shown in Figure 8 and 10 from 01/06 to 30/09 and in Figure 9 for a typical sunny day.

In Figure 8, the number of occupation hours from 8.00am to 7.00pm during which the operative temperature and CO₂ concentration surpass the comfort range are plotted simultaneously.

Figure 9 shows the operative temperature and CO₂ concentration profiles for four different cases in a typical day.

A number of simulations for different ventilation strategies were run; here, for brevity, only the following cases are reported:

- Case 0: without natural ventilation, only infiltration;
- Case A: natural ventilation through the skylight (100%) all day long;
- Case B: natural ventilation through the skylight (100%) and through the eastern windows (in bottom hung mode) all day long;
- Case C: Case B + office windows in bottom hung mode (during occupation hours);
- Case D: office windows in side hung mode from 6.00am to 7.00pm only;
- Case E: office windows in side hung mode from 8.00am to 7.00pm only;
- Case F: natural ventilation through office windows in bottom hung mode from 7.00pm to 8.00 am only (night ventilation).

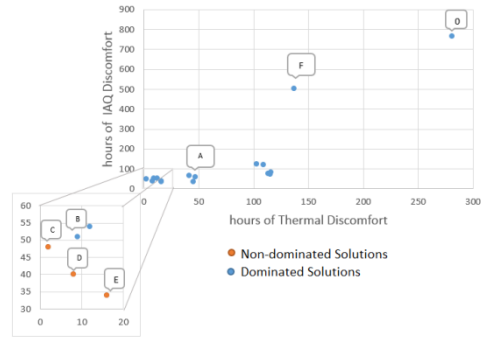


Fig. 8 – Thermal and IAQ discomfort for different ventilation strategies

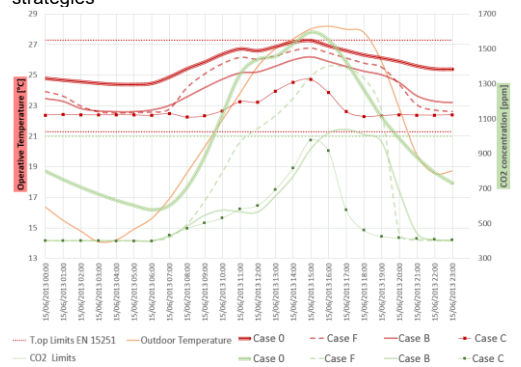


Fig. 9 – Comparison between operative temperature and CO₂ concentration for four different cases in a typical day

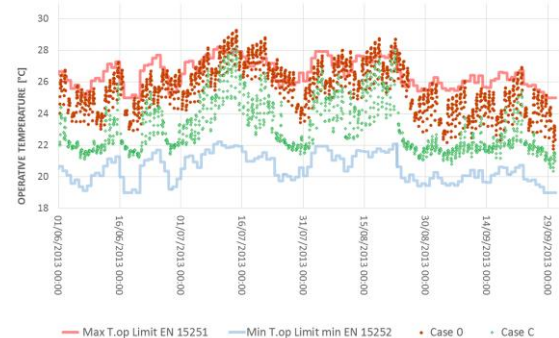


Fig. 10 – Adaptive thermal comfort: comparison between Case 0 and Case C

As can be expected, the worst case for IAQ occurs without natural ventilation (Case 0).

Night ventilation reduces thermal discomfort but the IAQ is not good enough (Case F); this strategy may result in discomfort for excessive CO₂ since people might hesitate to open windows in the early morning (Figure 9).

Only by exploiting natural cross ventilation (Case A and B) does the IAQ increase significantly even without opening the window in the office room. These strategies can be considered very effective for those sites where the window is open infrequently (for example in noisy sites).

The solutions C, D and E represent the non-dominated solutions and they are very similar and excellent solutions for IAQ.

In Figure 10, the operative temperature for Case 0 and Case C is shown from June to September; as can be seen a good IAQ strategy has a positive effect on thermal comfort too. This last strategy was retained for the project since it is relatively easy to apply and does not significantly depend on occupant behaviour.

6. Conclusion

In the present study the results of a parametric analysis for comfort and IAQ design optimisation were presented.

Simulations run on EnergyPlus for a real case study allowed us to define the characteristics of glazings and shading devices as well as natural ventilation strategies in a “healthy building” design perspective.

The results show the importance of simulation in order to find the best compromise for thermal, and visual comfort and for IAQ by choosing optical characteristics of materials, shading control and ventilation strategies.

Solar and visual transmittance of glazings and shading devices as well as shading control have a significant impact on thermal and visual comfort and have to be chosen carefully to fulfil both perspectives simultaneously.

Cross natural ventilation through skylights when the openings are correctly sized, can be enough and is not very influenced by occupant behaviour.

On the basis of the methodology and the statistical indicators presented in this study, thermal and visual comfort, as well as IAQ can be managed and optimised simultaneously. By following this approach it is also possible to evaluate the discomfort given by other pollutants (TVOC, Formaldehyde, noise, etc) if they occur.

These results will be presented in a future work.

References

Standards

ASHRAE. 1989. Standard 62. Ventilation for acceptable Indoor Air Quality

ASHRAE. 1999. Standard 62. Ventilation for acceptable Indoor Air Quality

ASHRAE. 2007. Standard 62.1 Ventilation for acceptable Indoor Air Quality

ASHRAE. 2007. Standard 62.1-2007 User's manual

ASHRAE. 2009. Handbook of Fundamentals

EN Standard 15251. 2007. Indoor environmental input parameters for design and assessment of energy performance of building addressing indoor air quality, thermal environment, lighting and acoustics.

Books

AiCARR. 2009. Manuale d'ausilio alla progettazione termotecnica. Milano

Apte, M.G., W.J.Fisk, and J.M. Daisey. 2000. Associations between indoor CO₂ concentrations and sick building syndrome symptoms in US office buildings: An analysis of the 1994-1996 BASE study data.

Energy plus. 2013. Engineering Reference; Input Output Reference.

Mendell, M.J: 1993. Non-specific symptoms in office workers: A review and summary of the epidemiologic literature.

Sherman, M.H. and D.T Grimsrud. 1980. Infiltration-pressurization correlation: Simplified physical modelling.

Journal articles

Hopkinson, R.G. 1970. Glare from Windows. Construction Research and Development Journal 2, 98

Hopkinson, R.G. 1972. Glare from Daylighting in Buildings. Applied Ergonomics 3, 206

Nabil A, & Mardaljevic J. 2005. Useful Daylight Illuminance: A New Paradigm to Access Daylight in Buildings. Lighting Research & Technology, 37.

Nabil A, & Mardaljevic J. (2005b). Useful Daylight Factors. Energy and Buildings, 38.

OFEV. 2008. “Ne pas agir maintenant, c’est faire un preuve d’un négligence grave.” *Environnement. Le défi climatique*

Sicurella, F., Evola, G. and Wurtz, E. 2011. A statistical approach for the evaluation of thermal and visual comfort in free-running buildings. Energy and buildings

Modelling of domestic fine particles indoor exposure, its main sources and potential mitigation measures: the case of Beijing

Sandra Stefanović – University of Belgrade, Vinča Institute of Nuclear Sciences, Laboratory of Thermal Engineering and Energy – sandras@vinca.rs

Žarko Stevanović – University of Belgrade, Vinča Institute of Nuclear Sciences, Laboratory of Thermal Engineering and Energy – zare@vinca.rs

Abstract

This paper presents a case study with an aim to examine the indoor impact of fine particles with a maximum aerodynamic diameter of 2.5 microns (PM_{2.5}) and evaluate its main sources of generation within one typical residential dwelling of Beijing's housing stock in order to define optimal mitigation measures. Based upon available data, through the validated multi-zone indoor air quality (IAQ) model the relationship between impact of indoor/outdoor factors and indoor mass concentration of PM_{2.5} was examined. As a referent dwelling, one of Beijing's housing stock representatives was selected. Its key parameters were combined and modelled in order to create the universal framework consisted of five baseline typical housing stock cases. The main modelling drive parameters were physical and mechanical dwelling performances: five envelope's permeability (p) values (10, 20, 30, 40 and 50 m³/m²/h @50Pa) and different types of ventilating, throughout the year (heating and non-heating period). The simulation results suggest that under present day conditions, average indoor concentrations of PM_{2.5} are appreciably higher than the outdoor annual average value of 102µgm⁻³ because of indoor sources. In the case of naturally ventilated dwellings during heating period, cooking represents the largest contributor, generating particulate matter at concentrations four times greater than annual average outdoor mass concentration of PM_{2.5}. Modelling demonstrated that removal of PM_{2.5} generated by cooking activity depends on the type of ventilation and most important on its use pattern. Furthermore, modelling provided fundamental data for evaluating indoor pollutant reduction measures. Based on previous analysis, following mitigation measures are analysed: increased EF capacity and its period of use, kitchen isolation (by closing the door) from the rest of dwellings and change of occupant behaviour regarding smoking

activity. Compared to the naturally ventilated dwelling in winter period, analysed measures could decrease average indoor PM_{2.5} mass concentrations by almost 50%. This kind of method was found to be suitable for questioning different measures of improvement and the way for this framework to be easily broadened to the bigger scale, at the urban level.

1. Introduction

Concentrations of ambient air pollution in China have changed considerably during the last decade reaching an extremely critical state. The World Health Organization (WHO) is concerned about the situation in China, where cities such as Beijing regularly experience dangerously high levels of outdoor air pollution. In 2012, a total of 2.8 million deaths were estimated to be caused by air pollution in the Western Pacific Region (WHO China). The size of pollutant particles is directly linked to their potential for causing health problems. Fine particles less than 2.5 micrometres in diameter (PM_{2.5}) pose the greatest problems, because they can lodge deep in the lungs, and some may even enter the bloodstream. They are capable of penetrating deeply into human lungs and represent serious offenders as indoor pollution (Listorti, et al., 2001).

Considering indoor air quality (IAQ), concentrations of PM_{2.5} in houses are affected by the infiltration of outdoor particles, emissions from indoor sources and the removal from the internal air by deposition, filtration and exfiltration, though some re-suspension also occurs largely related to domestic activities (Gehin et al., 2008).

The primary sources of ambient or outdoor air pollution include natural dust particles blown by the wind, large combustion plants, industrial and motor vehicle emissions and household heating. The main sources of household or indoor pollution are cooking emissions, as well as second-hand smoke from tobacco products (WHO China).

Respiratory infections are transmitted by airborne particles, droplets or physical contact, which are extremely difficult to control, mostly due to implementation problems of necessary behavioural change in highly populated areas especially cities (Listorti, et al., 2001). Outdoor climate and weather conditions combined with occupant behaviour affect IAQ. Weather conditions influence whether building occupants keep windows open or closed and whether they operate air conditioners (AC) or heaters, all of which can impact IAQ.

The study was based on the application of CONTAM (Emmerich, 2001), a validated multi-zone IAQ model, to predict concentrations of $PM_{2.5}$ from both indoor and outdoor sources, in specific zones/rooms of one typical dwelling in Beijing. The objective was to examine indoor $PM_{2.5}$ mass concentration values and evaluate impact of its sources throughout the year. In order to create and examine potential mitigation scenarios, this paper examines how occupant behaviour affects the reduction of indoor pollutants.

2. Modelling of $PM_{2.5}$ indoor exposure-baseline scenario

With respect to the whole housing stock of Beijing and available data, one typical dwelling on the 2nd floor of one typical multi-apartment building (MAB), of a total of 75m² in area, was selected in order to model indoor fine particle mass concentration and investigate potential changes through given scenario (Fig. 1). Regarding the apartment's physical, mechanical properties and the outdoor pollution impact, five typical case models were suggested (Fig. 2). Later, each of these five models varied by five levels of permeability creating the baseline framework of 25 cases.

The modelling was performed using CONTAMW software (version 3.1.), a multi-zone indoor air

quality and ventilation analysis computer program, in order to determine airflows, contaminant concentrations and personal exposure.

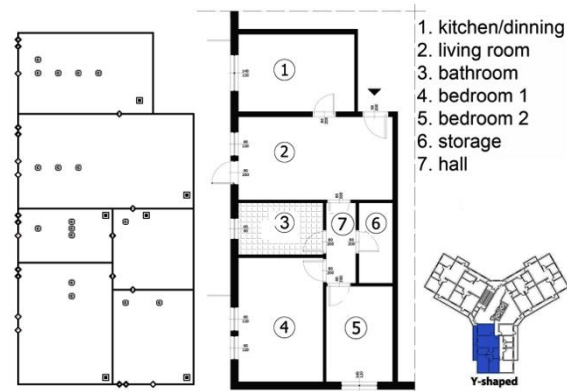


Fig. 1 – Typical multi-apartment building (MAB) dwelling unit

2.1 Modelling dwelling parameters

2.1.1. Physical parameters of dwelling

Air pollutants enter/exit buildings through open doors, open windows, cracks in structures and ventilation systems. Regarding that, cracks in structure (wall permeability) were the physical key input parameter, considered to potentially have a significant impact on the building performance and IAQ. Permeability represents the airflow through the fabric of a building, made at a steady high pressure difference, normally 50Pa, when the effects of wind and buoyancy forces are effectively eliminated (Etheridge, 2012). Since there is no reliable data detailing building permeability in Beijing, wall permeability was varied by increments of 10 from 10 to 50m³/(h.m²)@50Pa in order to capture a range of building air-tightness. Internal walls were considered impermeable.

2.1.2. Mechanical parameters of dwelling

Over the key inputs selection in terms of the mechanical parameters of the dwelling, the time of year played the most important role, regarding district heating use. Since the majority of residents in Beijing use a natural gas district heating system at present, modelling included only this type of heating. However, the dwelling was modelled with two scenarios during the heating period (district heating) and three scenarios during non-heating period. The heating period implied two cases: 1)

only natural ventilated dwellings (NV) and 2) natural ventilated dwellings with extract fans use (NV+EF). The non-heating period involved the same cases as the heating period and one more case which involves AC use (EF+AC) (Fig. 2). This approach was selected to determine the key building features that affect dwelling indoor environment.

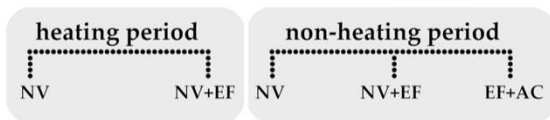


Fig. 2 – Modelling of indoor $PM_{2.5}$ exposure – baseline scenario scheme

2.2. Modelling input data

2.2.1. Ambient $PM_{2.5}$ mass concentration, weather and wind data

Since the ambient $PM_{2.5}$ value in Beijing is stochastic variable with high value oscillations during the day and whole year (Fig. 3), as a modelling input the average annual value was used (U.S. Department of State, the Mission China air quality monitoring program, Beijing).

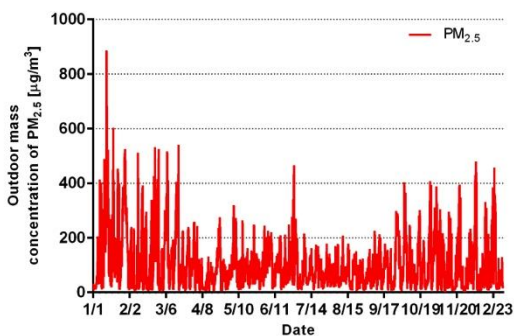


Fig. 3 – Ambient mass concentration data of $PM_{2.5}$ during the year of 2013. in Beijing.

Thus, as an input ambient mass concentration of $PM_{2.5}$, the annual average constant value of $102\mu\text{g}/\text{m}^3$ was used. This mean value is nearly three times higher than the value ($35\mu\text{g}/\text{m}^3$) of the interim target-1 standard for annual mean $PM_{2.5}$ recommended by the WHO (Zhang R. Et al., 2013). However, in the short periods the level of $PM_{2.5}$ in Beijing reaches the value even 8 times greater than the average (fig. 3).

Modelling was performed using transient weather and wind data for Beijing, taken from the EnergyPlus energy simulation software data (U.S. Department of Energy).

2.2.2. Cooking $PM_{2.5}$ emission rate

Previous studies in the United States have indicated that the cooking of food is one of the largest sources of fine organic aerosols in urban areas, especially in major cities where millions of people must be fed several times per day. It was established that the composition of particles emitted from the cooking of food is strongly dependent on cooking procedure, including the materials used, cooking temperature, and cooking time (Wang, et al., 2009). However, only a few studies have examined the impact of cooking on ambient air quality (Huang et al., 2006; Zhao et al., 2007). A recent study carried out by Berkeley National Laboratory, USA provided a database of pollutant emission rates associated with cooking. The study collected cooking emission rate data for 541 cooking events from 13 studies and, by analyzing and comparing them, found that the $PM_{2.5}$ cooking emission rates resulted in distinctly different distributions depending on several cooking parameters: food type, type of oil, type of cooking and type of appliance used (Hu, 2014). Considering that the goal of modelling was a general assessment of $PM_{2.5}$ emissions during cooking episodes, for the generation rate the average value of 2.2 mg min^{-1} was taken from the Berkeley National Laboratory study, as the average value of four high impact cooking conditions (Hu, 2014). Of all the above mentioned parameters which condition the amount of emitted particles, in order to model the mitigation scenario, only the duration of cooking activities was taken into consideration. As a reference, frequency of cooking and cooking time study (Hokoi, 2013) were used. Approximately 100 - 200 residential units in two cities in China were surveyed. According to this study, the cooking time for breakfast was established to be 0–10 min during weekdays and 10–20 min during weekends. The cooking time for lunch or dinner formed two peaks at 20–30 min or 50–60 min. Based on this study, the cooking schedule applied in modelling is shown in table 1.

Table 1 – Applied cooking schedule

day	breakfast	lunch	dinner
weekday	07:20-07:30	12:00-12:40	18:00-18:30
weekend	09:00-09:20	12:00-13:00	18:00-18:40

2.2.3. Smoking PM_{2.5} emission rate and schedules

Internally dominant sources of PM_{2.5} included environmental tobacco smoke (ETS). Tobacco smoke consists of solid particles and gases. More than 4,000 different chemicals have been identified in tobacco smoke. The number of these chemicals that are known to cause cancer in animals, humans, or both is reported to be in the range from 30 to 60 (Canadian Centre for Occupational Health and Safety). Based on the absence of suitable data, all models are assumed to be smoking dwellings. Modelling of smoking emissions assumed the presence of one smoker per unit. Smoking was practiced only in the kitchen and living room. The number of smoked cigarettes in each of the smoking permitted rooms ranged from 0 to 10. Modelling assumed 7 cigarettes on weekdays and 10 at weekends in the living room, 3 cigarettes on weekdays and smoke-free weekend in the kitchen, giving 0.99 mg min⁻¹ emissions of PM_{2.5} at 5 min per cigarette (Shrubsole, 2012).

2.2.4. PM_{2.5} deposition rate and air exchange rate

In indoor environments, particle deposition rate and air exchange rate are the two main components of the overall particle removal rate from the air (He, et al., 2005). For the mean PM_{2.5} deposition rate value of 0.39 1 h⁻¹ was used, guided by the Particle Total Exposure Assessment Methodology (PTEAM) study carried out by United States Environmental Protection Agency (US EPA) and National Exposure Research Laboratory (NERL) (Clayton, 1992).

Since it is noted that windows are usually closed in the winter when central heating is used and in the summer when air conditioning is on, the air exchange rate maintained at 1.0 1 h⁻¹ during both summer and winter, in accordance with JCJ134-2001: design standards for energy efficiency of

residential buildings in hot summer and cold winter zones (Wang, et al., 2004).

2.2.5. Occupant behavior - airflow path and equipment schedules

CONTAM software entails an airflow path as a building component through which air can move between two adjacent zones. These components can be cracks in the building envelope (wall permeability), windows, open doorways, exhaust fans, etc. Weather conditions are a key factor influencing window opening behaviour and also subject to high uncertainty (Rune, A. et al. 2009). For the Beijing dwelling, we assumed a seasonal window opening schedule as presented in table 2.

Table 2 – Window opening schedule

room type	summer	winter
kitchen	100% open during cooking activities, otherwise 10%	only 10% open during cooking activities
living room	from 9 to 21h 10% open	3 times a day for 15 min 100% open
bathroom	50% open during shower/bath activities, otherwise 10%	50% open for 15 min after shower/bath activities
bedrooms	always open 10%	100% open for 15 min 2 times a day

In the absence of suitable data, the assumed schedule for the doorway airflow paths was: kitchen door was closed during cooking activities; in the living room the door was open during day activities, from 8 to 23h; the bathroom door was closed during shower/bath activities and bedroom doors were closed during sleeping activities only.

Regarding equipment that influences IAQ, in some modelling cases intermittent extract fans (EF) and constant air conditioners (AC) were applied. Application of EF implied installation of one with a capacity value of 300 m³h⁻¹ in the kitchen and 80 m³h⁻¹ in the bathroom in accordance with GB50096-1999: Residence design standard (Wang, et al.,

2004). Cases with EF use practiced ventilation only during cooking activities.

AC was modelled only in one case of the non-heating period where the optimal indoor temperature was maintained at 26-28°C in summer and 16-18°C in winter, according to JCJ134-2001: design standards for energy efficiency of residential buildings in hot summer and cold winter zones (Wang, et al., 2004).

3. Modelling results

The simulation results suggest that under present day conditions, average indoor concentrations of PM_{2.5} are appreciably higher than the outdoor annual average value of 102µgm⁻³ because of indoor sources. Figure 4 presents calculated average indoor PM_{2.5} mass concentration dependence on wall permeability for the analysed 5 baseline cases. The highest concentration (up to 400 µgm⁻³) is obtained for case a (for naturally ventilated dwelling in winter heating period). For case b (same dwelling but with extra fan ventilation in winter heating period) a much lower indoor concentration (up to 250 µgm⁻³) is obtained. In summer (non-heating) period (case c, d and e) average indoor PM_{2.5} mass concentration is much lower compared with analogue cases in winter, due to much longer periods of natural ventilation of the dwelling by opened windows. In all five cases average indoor PM_{2.5} mass concentration decreases when the façade permeability value is increased. However, a higher façade permeability value will result in lower energy efficiency of the building due to increased heat loss through the envelope.

The main contribution to the increased indoor PM_{2.5} mass concentration is from cooking-related sources as indicated in Fig. 5 where daily kitchen indoor mass concentration of PM_{2.5} for naturally a ventilated apartment during heating period is presented. There are high peaks in kitchen mass concentration of PM_{2.5} after cooking activities.

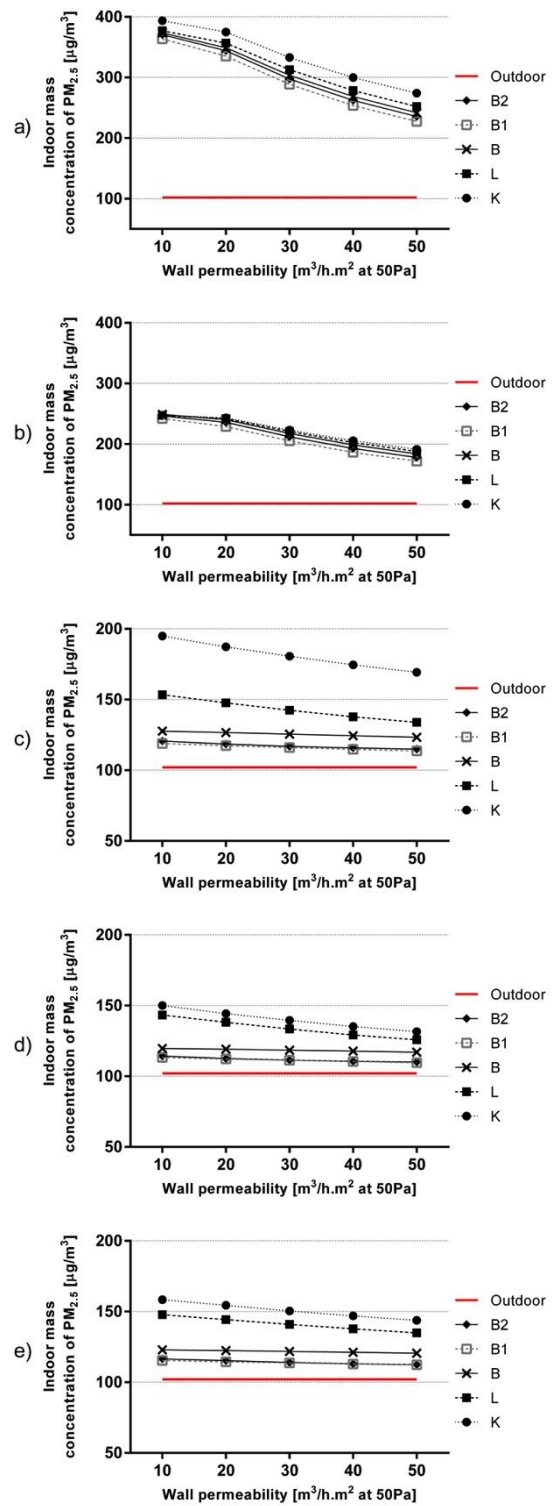


Fig. 4 – Typical dwelling unit average indoor mass concentration of PM_{2.5} for the range of wall permeability values for: a) naturally ventilated during heating period; b) naturally ventilated during heating period, with EF use; c) naturally ventilated during non-heating period; d) naturally ventilated during non-heating period, with EF use; e) during non-heating period with EF and AC use.

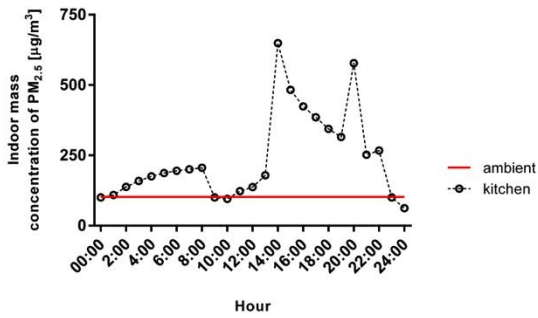


Fig. 5 - Daily kitchen indoor mass concentration of PM_{2.5} for naturally ventilated apartment during heating period

Particles are able to spread quickly, thus the kitchen and living room are most endangered, with the average PM_{2.5} mass concentration several times bigger than the ambient average value. During the heating period, the naturally ventilated dwelling in comparison with the same one with EF use during cooking activities has up to 44% higher indoor emissions (Fig. 4 a compared to 4 b).

The contribution from EF use can be noticed in the cases during the non-heating period as well, but more frequent and longer natural ventilation effects indoor emissions to be reduced up to 33% (Fig. 4 c compared to 4 d).

The non-heated dwelling with EF and AC use has 5.3% higher emissions due to the absence of natural ventilation (Fig. 4 e compare to 4 d).

4. Mitigation scenario

PM_{2.5} exposures in homes can be mitigated through various approaches including kitchen exhaust ventilation, filtration, pollution source reduction and designing ventilation systems to reduce the entry of PM_{2.5} from outdoors (Hu, 2014).

Based on previous analysis, the following mitigation measures are analysed: increased EF capacity and its period of use, kitchen isolation (by closing the door) from the rest of dwellings and change of occupant behaviour (smoking habit).

4.1 Discussion

In the previous discussion, the importance of EF use during cooking-related activities was emphasized. Results of the simulation of the extract fan with higher capacity value (500 m³h⁻¹)

installed in the kitchen, (in accordance with GB50096-1999: Residence design standard) instead of EF with a capacity value of 300 m³h⁻¹ are presented on Fig. 6. Figure presents kitchen average indoor mass concentration for the cases b, d and e from Fig. 4 (with the wall permeability value of 10 m³/(h.m²)@50Pa only) for two EF capacity values. The results suggest that this mitigation measure is most effective in winter while in summer it has lower benefits.

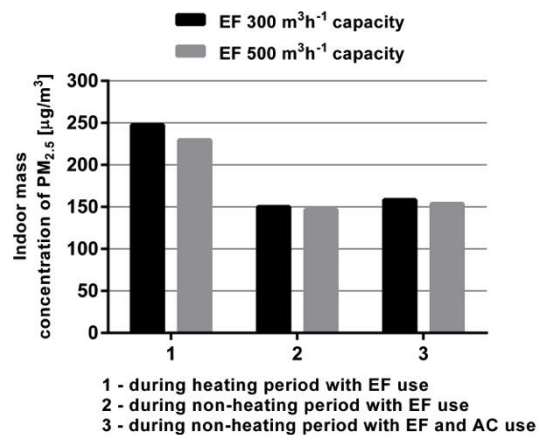


Fig. 6 – The kitchen average indoor mass concentration of PM_{2.5} with the use of EF with different capacity for three typical cases.

Figure 7 presents simulation results for the proposed mitigation measures in the winter period when indoor PM_{2.5} concentrations are expected to be the highest (Fig 7a = Fig 4b). Change of occupant behaviour regarding smoking activity (no smoking indoors) could decrease average indoor PM_{2.5} concentrations by ~9% (Fig. 7b compared to 7a). Keeping the kitchen door closed as much as possible (Fig. 7c) compared to the case when it is closed only during cooking (Fig. 7a) will increase average PM_{2.5} concentrations in the kitchen but decrease in all other rooms. Installation of EF in the kitchen with increased capacity, 500m³h⁻¹ (Fig. 7d) compared with lower EF capacity, 300m³h⁻¹ (Fig. 7c) would further decrease average PM_{2.5} concentrations in the kitchen and in all other rooms. In case of implementation all analysed mitigation measures, average indoor PM_{2.5} concentrations in the winter period (Fig. 7e) would be ~20% lower than in the baseline case (Fig. 7a). Compared to the naturally ventilated dwelling in winter period, without EF use (Fig. 4a), analysed

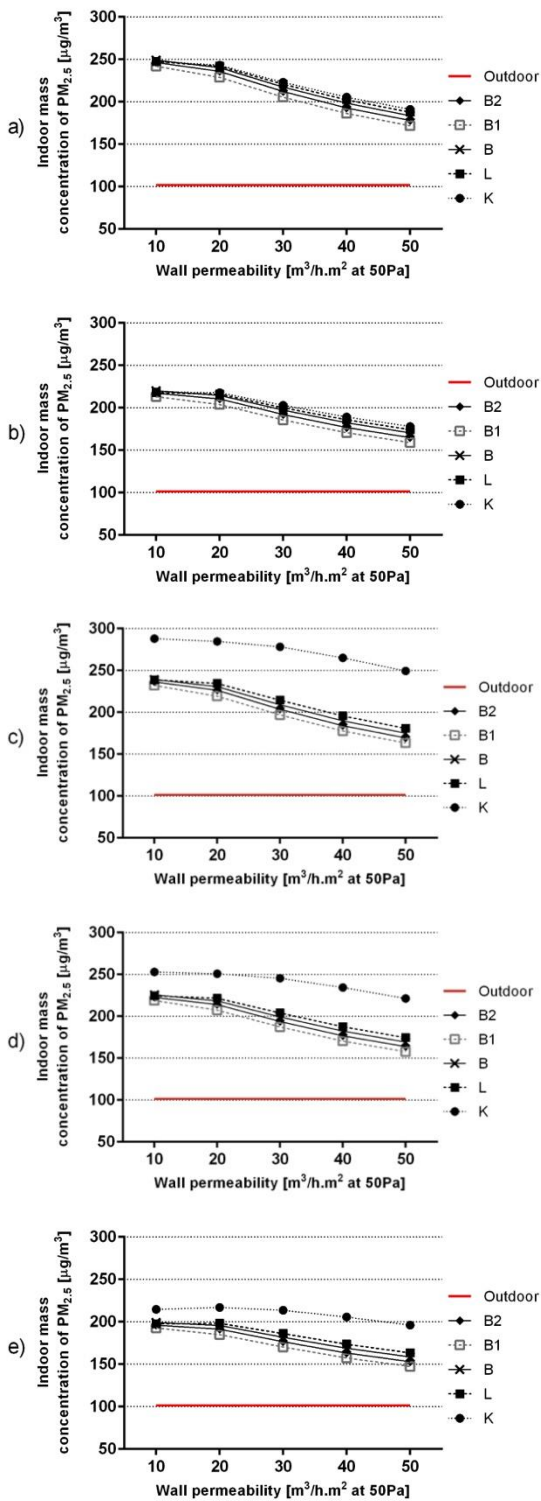


Fig. 7 – Impact of mitigation measures on average indoor PM_{2.5} mass concentration of naturally ventilated dwelling during heating period for the range of wall permeability values: a) with EF (300m³h⁻¹) use; b) with EF (300m³h⁻¹) use and without tobacco emission sources; c) with EF (300m³h⁻¹) use and closed kitchen door; d) with EF (500m³h⁻¹) use; e) with EF (500m³h⁻¹) use, without tobacco emission sources and with closed kitchen door.

measures (Fig. 7e) could decrease average indoor PM_{2.5} concentrations in almost 50%. Further decreases in indoor PM_{2.5} concentrations could be obtained only by implementing more expensive measures like installation of special cooking filters.

4. Conclusion

Considering the mechanical and physical properties, the IAQ modelling of the referent dwelling units in Beijing was performed. High indoor exposure to PM_{2.5} has been found, especially the one generated by cooking activity. Dwellings with the highest peak results are those with no mechanical ventilation, with the average indoor level of PM_{2.5} up to four times greater than the already very high annual average outdoor concentrations. Mitigation scenario simulation demonstrated that generation of PM_{2.5} greatly depends on EF use during cooking-related activities, its capacity, kitchen isolation (by closing the door) from the rest of dwellings and change of occupant behaviour (smoking habit). This resulted in a PM_{2.5} reduction of up to 50%. Implementation of more expensive measures like improved capture of cooking emissions above the stove by fume extraction and filtration would contribute substantially to improvements in both indoor and outdoor air quality, and hence a reduction in human exposure.

5. Acknowledgement

This work was carried out within the framework of research project FP7-ENV-2010, PURGE: Public health impacts in urban environments of greenhouse gas emissions reduction strategies, Project number: 265325, financed by the European Commission.

5. Nomenclature

Symbols

PM _{2.5}	fine particles less than 2.5 micrometres in diameter (µg/m ³)
p	wall permeability (m ³ /m ² /h @ 50Pa)

Subscripts/Superscripts

AC	air conditioners
EF	extract fan
ETS	environmental tobacco smoke
IAQ	Indoor air quality
MAB	multi apartment building
NV	natural ventilation

References

- Clayton, C. A. et al. 1992. "Particle Total Exposure Assessment Methodology (PTEAM) study: distributions of aerosol and elemental concentrations in personal, indoor, and outdoor air samples in a southern California community." *Journal of exposure analysis and environmental epidemiology* 3 (2): 227-250.
- Etheridge, D.W. (2012). *Natural Ventilation of Buildings: Theory, Measurement and Design*, John Wiley and Sons.
- Gehin, E. et al. 2008. "Size distribution and emission rate measurement of fine and ultrafine particle from indoor human activities." *Atmospheric Environment* 42: 8341-8352. doi:10.1016/j.atmosenv.2008.07.021.
- Hokoi, Sh. Et al. 2013. "Field survey on energy consumption due to hot water supply and cooking in Nanjing and Hefei, China." *Frontiers of Architectural Research* 2 (2) (2013): 134-146. doi:10.1016/j.foar.2013.03.001.
- He, C. et al. 2005. "Particle deposition rates in residential houses." *Atmospheric Environment* 39 (21): 3891-3899. doi:10.1016/j.atmosenv.2005.03.016.
- Hu, T. et al. 2014 "Compilation of Published PM_{2.5} Emission Rates for Cooking, Candles and Incense for Use in Modeling of Exposures in Residences." Berkeley, USA.
- Huang, X. et al. 2006. "Annual variation of particulate organic compounds in PM_{2.5} in the urban atmosphere of Beijing." *Atmospheric Environment* 40:2449-2458. doi:10.1016/j.atmosenv.2005.12.039.
- Jones, B. M. et al. 2012. "The relationship between permeability and infiltration in conjoined dwellings." The 33rd AIVC Conference and 2nd TightVent Conference: Optimising Ventilative Cooling and Airtightness for [Nearly] Zero-Energy Buildings, IAQ and Comfort, Copenhagen, Denmark.
- James A. Listorti and Fadi M. Doumani. 2001. Environmental Health Background Analyses. *Environmental Health: Bridging the Gaps* vol. 422, Washington: The World Bank.
- Rune, A. et al. 2009. "Survey of occupant behavior and control of indoor environment in Danish dwellings." *Energy and Buildings* 41 (1): 11-16. doi:10.1016/j.enbuild.2008.07.004.
- Shrubsole, C. et al. 2012. "Indoor PM_{2.5} exposure in London's domestic stock: Modelling current and future exposures following energy efficient refurbishment." *Atmospheric Environment* 62: 336-343. doi:10.1016/j.atmosenv.2012.08.047.
- U.S. Department of State, the Mission China air quality monitoring program, Beijing - Historical Data, Accessed September 12. <http://www.stateair.net/web/historical/1/1.html>
- Canadian Centre for Occupational Health and Safety, Environmental Tobacco Smoke (ETS): General Information and Health Effects, Accessed October 30. http://www.ccohs.ca/oshanswers/psychosocial/ets_health.html
- Wang, Z. et al. (2004), "Regulatory standards related to building energy conservation and indoor-air-quality during rapid urbanization in China." *Energy and Buildings* 36 (12): 1299-1308. doi:10.1016/j.enbuild.2003.09.013.
- Wang, Q. et al. 2009. "Source apportionment of fine organic aerosols in Beijing." *Atmospheric Chemistry and Physics* 9 (21): 8573-8585. doi:10.5194/acp-9-8573-2009.
- Zhang, Y. et al. 2007. "Source profiles of particulate organic matters emitted from cereal straw burnings." *Journal of Environmental Sciences* 19: 167-175. doi:10.1016/S1001-0742(07)60027-8.
- U.S. Department of Energy, EnergyPlus Energy Simulation Software, Add-Ons, Weather data. Accessed September 10. http://apps1.eere.energy.gov/buildings/energyplus/cfm/weather_data3.cfm/region=2_asia_wmo_region_2/country=CHN/cname=China?utm_source=EnergyPlus&utm_medium=redirect&utm_campaign=EnergyPlus%2Bredirect%2B1

Application of aerogel-based plaster towards thermal retrofit of historical facades: A computational assessment

Olga Proskurnina –olga.proskurnina@gmail.com

Ulrich J. Pont – BPI, Vienna University of Technology – ulrich.pont@tuwien.ac.at

Mirosława Kornicki – Kornicki GmbH

Ardeshir Mahdavi – BPI, Vienna University of Technology – amahdavi@tuwien.ac.at

Abstract

The retrofit of historical facades of the building stock has grown in importance due to energy efficiency considerations in the building sector. Among other recent new construction technologies, aerogel-based plaster systems with high thermal insulation have been developed in the past few years by the AEC-industry. Although still rather expensive, these systems offer opportunities to insulate highly-articulated historical facades in compliance with the principles of heritage protection.

This contribution analyses the effect of the application of such aerogel-based plasters on historical building facades in terms of thermal bridges. Thermal bridges are considered to be of high importance for both the building's overall energy performance and the quality assurance in terms of healthy indoor environment. The latter includes aspects of interior surface temperatures, condensation risk, and mould growth. Typical construction details of historical building facades were selected based on relevant literature. These details were analysed and evaluated with the help of a numeric thermal bridge simulation tool. A set of scenarios including original state and different retrofit measures were applied to these details and their effect was evaluated in view of thermal bridge calculation. This contribution includes – along with basic information about the aerogel-plaster systems and related background – description of the methodology and a discussion of the results.

1. Introduction & Background

An incontrovertible fact in the ongoing discussion about climate change and global energy consumption is that buildings have a major share

of both energy consumption and emission of climate-harming substances (DENA, 2013). There are multiple strategies to reduce the energy demand of buildings: one of the most common and obvious tactics is the insulation of the building envelope. While this can be generally realized for new buildings, older buildings with strongly-articulated and historical meaningful facades require sophisticated approaches. Typical insulation panels would lead to a loss of the architectural value of such buildings, and is thus forbidden by relevant authorities (BDA, 2011).

One option for thermal retrofitting of buildings with rich articulated facades are highly-insulating plasters. Typical insulation plasters are based on perlite. These plasters have been available on the market for many years, but possess only limited thermal insulation potential in comparison to insulation panels. A new development in the field of insulating plasters is plaster systems based on Silica aerogel. This material, explored already many decades ago (Kistler, 1931), is a synthetic porous ultralight material derived from a gel, in which the liquid component of the gel has been replaced with air. Such structures offer, due to their high porosity, very low thermal conductivity. The present contribution analyses the effect of application of an aerogel-based plaster product to historical facades. The impact of the application to planar elements can be simply evaluated via the change in U-Value. In contrast, the impact of such systems on non-planar elements or component joints is not trivial. Thermal retrofit of non-planar elements is difficult both regarding building construction detailing as well as in view of assessing the impact of thermal bridges. Moreover,

ill-conceived retrofitting concepts could even increase (as compared to pre-retrofit state) the effect of thermal bridges. Therefore, a numeric simulation tool is utilized to assess the impact of such highly-insulated plaster systems on thermal bridges in building envelopes.

The performance of five typical details from central-European historical buildings was evaluated without any improvement and under different improvement scenarios (application of perlite and aerogel plaster systems). To additionally be able to assess the impact of such options at the whole building level, a typical building from the "Gründerzeit" Vienna (historical building of around 1900) was used as a case study. For this building, the heating demand and transmission losses attributable to (2-D) thermal bridges were calculated via a simple normative procedure for its original state and different retrofit scenarios. The calculation method allows for different levels of inclusion of thermal bridges: Calculations were performed with "default" and with "detailed" consideration of thermal bridges.

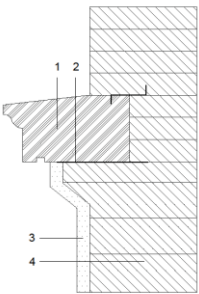
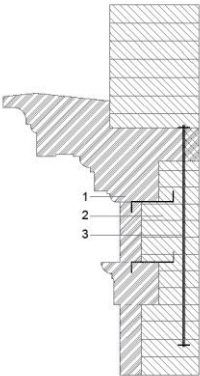
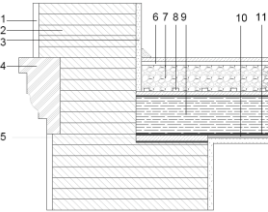
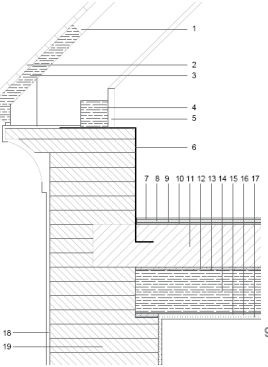
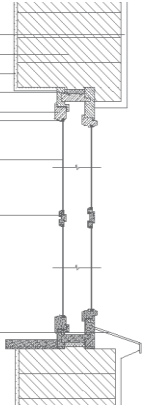
2. Methodology

2.1 Evaluated details

Five typical architectural details (Riccabona and Mezera, 2003; Eicke-Hennig et al., 1997) of historical buildings were used for the 2-dimensional thermal bridge evaluation (see Table 1):

Details 1-3 represent different cornice variants, including natural stone cornices with and without a steel anchor and a junction of a wooden slab next to a masonry cornice. **Detail 4** is the attic parapet junction with a ventilated roof. **Detail 5** represents a casement window and wall junction. The latter detail was examined both in terms of vertical and horizontal sections. The respective assumed material properties (Kornicki 2014) are summarized in Table 2.

Table 1 – Overview about evaluated details. The numbers in the illustrations refer to the assumed building material properties.

Detail 1	Details 2	Detail 3	Detail 4	Detail 5
Brick wall with natural stone cornice	Natural stone cornice with steel anchoring	Wooden slab with a gravel filling (with cornice articulation)	Ventilated attic with retrofitted ceiling slab	Casement window
				

2.2 Scenarios

For all five details retrofit scenarios were developed (Table 3). Scenario A for all details represents the pre-retrofit state. For Details 1-3 five different scenarios were generated and examined, while for Details 4 and 5 a further scenario was considered. For all scenarios the same boundary conditions within the applied linear thermal bridge evaluation were applied ($\theta_i = 20^\circ\text{C}$, $\theta_e = -10^\circ\text{C}$). Moreover, all details were assessed based on the same calculation settings concerning the level of detail and iterative calculation steps in the numeric thermal bridge simulation tool.

Table 2 – Material properties of the assumed building components (numbers refer to illustrations in Table 1).

No. and Name of Material	λ [W.m ⁻¹ .K ⁻¹]	μ [-]	
Detail 1	1. Natural Stone	2.30	35
	2. Reinforced Steel	60	100000
	3. Lime cement plaster	0.90	15
	4. Old brick masonry	0.71	8
Detail 2	1. Natural Stone	2.30	35
	2. Old brickwork	0.71	8
	3. Reinforced Steel	60	100000
Detail 3	1. Lime cement plaster	0.90	10
	2. Old brick masonry	0.71	8
	3. Gypsum plaster	0.80	10
	4. Natural stone	2.30	35
	5. Plank flooring	0.13	40
	6. False Floor	0.13	40
	7. Gravel filling	0.70	1
	8. Wood	0.15	125
	9. Hard Wood	0.185	100
Detail 4	10. Fire clay	0.75	1
	11. Cardboard	0.17	50000
	1. Air cavity	0.025	1
	2. Roofing tile	0.7	10
	3. Wood	0.15	50
	4. Hard wood	0.182	125
	5. Gypsum cardboard	0.21	10
	6. Reinforced steel	60	100000
	7. Coating	0.26	1
	8. Concrete screed	1.4	50
	9. Mineral wool	0.041	50
	10. Lime Cement plaster	0.90	15
	11. Reinforced concrete	2.3	100
	12. Plank flooring	0.13	40
	13. Cardboard	0.17	50000
	14. Hard wood	0.182	125
	15. Rough spruce formwork	0.14	50
	16. Fire clay	0.75	1
	17. Gypsum plaster	0.8	10
18. Lime cement plaster	0.90	15	
19. Old brickwork	0.71	8	
Detail 5	1. Lime cement plaster	0.90	15
	2. Old brick masonry	0.71	8
	3. Gypsum Plaster	0.80	10
	4. PU-foam (R=55)	0.031	50
	5. Wood (R=800)	0.8	50
	6. Gluing material	0.001	50000
	7. Air cavity	0.025	1
	8. Glass (d=4mm)	31	10000
	9. Air Layer	0.2	1

Table 3–Evaluation scenarios for the Details 1 – 5. (PW: planar wall, DE: decorative element, IR: Improved Roof, PP: Perlite Plaster, AP: Aerogel Plaster; SI: Styrofoam Insulation above cornice, IW: Improved Windows)

Scenario	Detail 1	Details 2	Detail 3	Detail 4	Detail 5
A	Original state of detail (prior to retrofit)				
B		PW: 50 mm PP		IR	IW
C		PW: 50 mm PP, DE 20mm PP & SI		IR, PW 50 mm PP	IW, PW 20 mm PP
D		PW: 50 mm AE		IR, PW: 50 mm PP DE: 20mm PP & SI	IW, PW 50 mm PP
E		PW: 50 mm AP DE: 20mm AP & SI		IR PW: 50 mm AP	IW PW 20 mm AP
F				IR, PW: 50mm AP DE: 20mm AP &SI	IW, PW 50 mm AP

2.3 Case study building

To assess the overall impact of the described retrofit strategies, they were applied virtually to a case study building (Figure 1). This building is a typical Viennese residential building from around 1900 .



Fig. 1 – Case study building (left: front view, right: SketchUp-Model).

2.4 Cases

For the whole building evaluation, a set of different cases were calculated. These were based on the scenarios A (original state, referred to as case 1), C (case 2) and E (case 3). All these cases were calculated with two different approaches concerning thermal bridges

- (i) Using the rough default estimation via the Austrian Standard B8110 (ASI, 2014)
- (ii) Using detailed values for thermal coupling coefficients.

Results of the thermal bridge evaluation of details

1 – 5 were used for this calculation. For thermal bridges of the building envelope that were not evaluated in detail within this study, typical thermal coupling coefficients were used (Hauser & Stiegler, 2001; DIN, 2008). The evaluations were based on a climate data file for Vienna, Austria.

2.5 Applied evaluation tools & data exchange

The thermal bridge evaluations were performed with AnTherm 7.125 (Kornicki, 2014). The whole building evaluation including transmission loss and heating demand calculations was based on the Austrian Energy Certificate method (OIB, 2011) as implemented in the software Archiphysik 11 (A-Null, 2014). For geometry modelling, SketchUp Make was used (SketchUp, 2014). The geometry model was then transferred to Archiphysik. For consideration of the thermal bridges the ψ -values results from AnTherm were added to the default thermal bridges library of Archiphysik.

3. Results & Discussion

3.1 Results of Thermal Bridges Evaluation

The application of insulation to the outer surfaces of the details results in the following:

- Improvement of U-Values of the undistorted “planar” building components.
- Changes in the values of indicators related to thermal bridges, i.e., thermal coupling coefficient (L2D according to ISO, 2008), ψ -values, and f_{Rsi} -values (ASI, 2014)

While the impact of insulation on the U-Value of the planar components is rather easy to capture, the effects related to thermal bridges require more detailed analysis. Table 4 illustrates all mentioned indicators for all details. Note that some indicators show two instead of one value: this is due to two adjacent building components to outside and two indoor spaces adjacent to the detail (Detail 3 & 4, upper component/upper room), or to results of different sections through the detail (Detail 5, horizontal section mentioned first). Figure 2 illustrates the graphical output of the numeric simulation for Detail 1. Scenarios D and E involve a significant increase in indoor surface temperatures. Both Figure 2 and Table 4 show the improvement of the detail in terms of U-Value of planar components and thermal bridge indicators. Details 2, 3, 4, and 5 show f_{Rsi} -values below the standard thresholds (ASI, 2003) of 0.71 (mould grow) or even 0.69 (surface condensation) in some scenarios. The application of insulation in general seems to improve the thermal performance of the analysed junctions. The scenarios with applied Aerogel plaster significantly decrease the thermal coupling coefficients of the details (28 to 71% improvement). The application of Perlite plaster in case of detail B does not raise the f_{Rsi}

above the threshold value. The application of Aerogel plaster raises the f_{Rsi} above the threshold of 0.71. This might be due to the fairly large natural stone cornice part. In case of Detail 4, retrofitting only one adjacent building component (roof) might leave the thermal bridge critical. This suggests that treating single components of an existing building's envelope may lead to subpar performance. Rather, a detailed thermal bridge analysis should accompany all projected changes to existing building envelope construction details. Furthermore, Table 4 illustrates that retrofit strategies that exclude articulated elements of the facades might offer reduce U-values of the planar components, but not necessarily reduce the impact of thermal bridges (this is, for instance, illustrated via the quite large ψ -values in the scenarios without insulation of decorative elements).

3.2 Results of building-related Heating demand and thermal transmittance

The case study building's heating demand and transmission losses were evaluated for case 1 – 3 with both approximated (using default values) and detailed thermal bridges. Building components adjacent to the thermal bridges evaluated within this contribution were considered with the U-values described in the sections before, while other components were assumed with default values (OIB, 2011). Table 5 offers an overview of the applied U- and g-values.

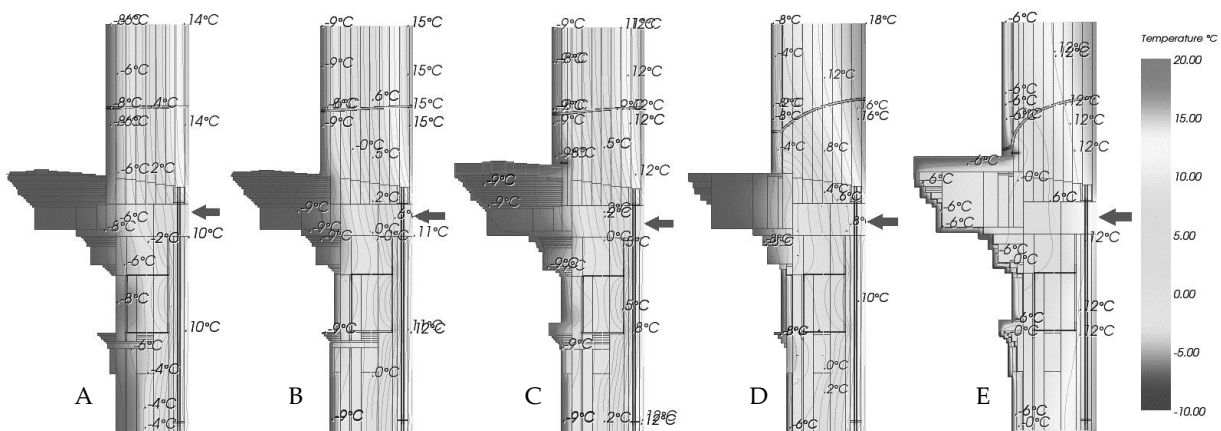


Fig. 2 – Simulation Output of Scenario A (left) to E (right) for Detail 1.

Table 4 – Results for details 1-3. Bold values in the f_{Rsi} -column imply condensation and/or mould growth risk. Data cells with two instead of one value represent two adjacent building components (Detail 3 and 4), two adjacent indoor spaces (Details 3 and 4), or details with more than one two-dimensional thermal bridge evaluation (Detail 5, horizontal and vertical sections). Values printed in bold letters indicate that they are below the f_{Rsi} -threshold values of 0.69 / 0.71.

Detail & Scenario	U-Value [W.m ⁻² .K ⁻¹]	U-Value-Improvement	L2D [W.m ⁻¹ .K ⁻¹]	L2D-Improvement	Ψ [W.m ⁻¹ .K ⁻¹]	f_{Rsi} [-]	
Detail 1	A	1.26	-	3.39	-	0.19	0.73
	B	0.93	26%	2.67	21%	0.31	0.77
	C	0.93	26%	2.55	25%	0.19	0.81
	D	0.37	71%	1.63	52%	0.71	0.81
	E	0.37	71%	1.13	67%	0.21	0.90
Detail 2	A	0.86	-	3.03	-	0.69	0.62
	B	0.70	19%	2.63	13%	0.82	0.65
	C	0.70	19%	2.62	14%	0.80	0.65
	D	0.33	62%	2.18	28%	1.18	0.72
	E	0.33	62%	1.58	48%	1.58	0.77
Detail 3	A	1.67 / 1.23	- / -	3.22	-	-0.09	0.65 / 0.79
	B	1.19 / 1.13	29% / 8%	2.71	16%	0.07	0.73 / 0.85
	C	1.19 / 1.00	29% / 19%	2.54	21%	0.04	0.75 / 0.87
	D	0.43 / 0.37	74% / 70%	1.25	61%	0.38	0.79 / 0.90
	E	0.40 / 0.42	76% / 66%	1.07	67%	0.13	0.86 / 0.92
Detail 4	A	1.35 / 1.24	- / -	5.14	-	1.26	0.70 / 0.79
	B	0.11 / 1.24	92% / 0%	2.63	49%	0.62	0.71 / 0.79
	C	0.11 / 0.92	92% / 25%	2.05	60%	0.50	0.78 / 0.85
	D	0.11 / 0.92	92% / 25%	2.01	61%	0.40	0.79 / 0.85
	E	0.11 / 0.37	92% / 70%	2.02	61%	1.31	0.85 / 0.94
	F	0.11 / 0.37	92% / 70%	1.07	79%	0.40	0.86 / 0.67
Detail 5	A	1.20	-	3.64 / 8.62	-	1.29 / 3.84	0.44 / 0.43
	B	1.20	-	1.94 / 3.99	46% / 54 %	-0.27 / -0.86	0.73 / 0.74
	C	1.06	12%	1.79 / 3.67	49% / 57%	-0.30 / -0.52	0.76 / 0.76
	D	0.90	25%	1.62 / 3.52	55% / 59%	-0.32 / -0.35	0.78 / 0.76
	E	0.60	50%	1.29 / 2.89	65% / 67%	-0.36 / 0.46	0.78 / 0.76
	F	0.36	70%	1.06 / 2.47	71% / 71%	-0.39 / 1.01	0.78 / 0.76

Table 5 – U-Value [$\text{W}\cdot\text{m}^{-2}\cdot\text{K}^{-1}$] and g-value [-] assumptions for case 1-3.

Element		Case 1	Case 2	Case 3
$U_{\text{ground slab}}$		1.20	0.35	0.35
$U_{\text{exterior wall}}$		1.20	0.93	0.37
U_{window}	$[\text{W}\cdot\text{m}^{-2}\cdot\text{K}^{-1}]$	2.15	0.98	0.98
U_{roof}		1.35	0.11	0.11
U_{door}		2.50	1.70	1.70
g_{glass}		[-]	0.67	0.67

For the detailed calculation of the thermal bridges, the ψ -values illustrated in table 6 were used. Note that negative ψ -value results of the thermal bridge evaluation were set to zero to avoid inconsistency in heating demand calculation.

Table 6 – ψ -Values [$\text{W}\cdot\text{m}^{-1}\cdot\text{K}^{-1}$] assumed for case 1-3. Values written in italics indicate that these values were derived from thermal-bridge-calculations

Thermal Bridge		Case 1	Case 2	Case 3
ψ_{cornice}	$[\text{W}\cdot\text{m}^{-1}\cdot\text{K}^{-1}]$	<i>0.19</i>	<i>0.19</i>	<i>0.21</i>
$\psi_{\text{window (vert)}}$		<i>3.84</i>	<i>0.00</i>	<i>0.00</i>
$\psi_{\text{window (hor)}}$		<i>1.29</i>	<i>0.00</i>	<i>0.00</i>
ψ_{roof}		<i>5.04</i>	<i>0.40</i>	<i>0.40</i>
$\psi_{\text{ground slab}}$		0.65	0.65	0.65
ψ_{door}		0.10	0.10	0.10
ψ_{corner}		0.00	0.00	0.00
$\psi_{\text{floor slab}}$		0.60	0.60	0.60

The other, approximate approach uses an equation from an Austrian Standard (ASI, 2014) to derive a cumulative value for all thermal bridges within the building's envelope. This equation uses the conductance values and areas of the building envelope elements as input data.

Table 7 illustrates the results of the case study building evaluation for heating demand (HWB) and Linear transmittance of the thermal bridges.

While the absolute values of the approximation and the detailed calculation show differences, the percentages of improvement, especially for the heating demand, tend to be similar.

The approximation seems to offer sufficient accuracy for benchmarking purposes. However, for detailed thermal bridge evaluation and planning purposes, the detailed values from simulation or catalogues are indispensable.

Table 7 – Results for Cases 1-3 of overall heating demand and linear transmittance of thermal bridges.

	HWB [$\text{kWh}\cdot\text{m}^{-2}\cdot\text{a}$]		Linear transmittance [$\text{W}\cdot\text{K}^{-1}$]	
	approx.	detailed	approx.	detailed
Case 1	316	387	329	541
Impr.	-	-	-	-
Case 2	207	229	241	357
Impr.	-35 %	-41 %	-27 %	-34%
Case 3	96	102	108	192
Impr.	-70 %	-74 %	-67 %	-64 %

4. Conclusion and Future Research

This contribution explored the application of Aerogel plasters to historical building envelopes. The application of such systems has a high impact on the thermal performance of both planar components and articulated architectural details. If properly planned, it is possible to significantly reduce both the building's heating demand and the impact of thermal bridges, without compromising the building's architectural appearance. Concerning the U-values of the planar surfaces of the examined details, a reduction of 26 – 71% could be realized with application of Aerogel plasters (Perlite plaster: 19 – 26% reduction). The thermal coupling coefficients reduction by application of Aerogel-plasters ranges between 28 – 79% for the details (Perlite plaster: 13 – 61%).

However, an application of Aerogel plaster systems on heritage protected architectural buildings still requires specific approval by relevant authorities and might be hampered by the comparatively high price of aerogel plasters and the complexity of application.

Future research efforts in this field should address the following aspects:

- Broadening the scope of examined details based on typical construction details from different architectural époques that would allow a usage of Aerogel-plaster systems.
- 3D simulations of thermal bridges
- Conducting transient thermal performance simulations of the thermal bridges and comparison with measurements of corresponding details.

- The details illustrated in this contribution were retrofitted following straightforward approaches. There is, for sure, potential for more sophisticated solutions such as a partial material replacement, and detailing based on traditional techniques. For instance, the application of the plaster without edge profiles and stabilizing net should be explored via long-term-durability tests, as this seems to be important for retrofitting highly-articulated façade profiles.
- Currently, the behaviour of the Aerogel-plaster can be modelled in view of parameters such as conductivity, water vapour resistance, and specific heat. However, long-term monitoring of the thermal and hygric behaviour of the aerogel plaster in different scenarios, such as drought stress, high sun exposure, and wind-driven rain should be considered.
- To popularise aerogel plasters in the market, comprehensive efforts in communication, involvement, and coordination of all potential stakeholders of a retrofit processes (clients, craftsmen, and historical preservation officials) is required.

5. Acknowledgements

This study was conducted in the framework of the project AGelFa, funded by the FFG (Austrian Research Agency), grant-No: 840605).

This research was kindly supported by the A-Null Bauphysik GmbH via software licences. Furthermore, the authors want to thank A.Gertschnigg and T.Dürnegger for provision of detailed data about their Aerogel-plaster products.

References

- A-Null. 2014. "Archiphysik 11". www.archiphysik.com (accessed November 2014)
- ASI 2003. Austrian Standard B 8110-2, 2003. „Wärmeschutz im Hochbau, Teil 2: Wasserdampfdiffusion und Kondensationschutz“ Available via <http://www.austrian-standards.at> (accessed November 2014)
- ASI 2014. Standard Series B 8110. 2014. Available via <http://www.austrian-standards.at> (accessed November 2014)
- BDA 2011, „Richtlinie Energieeffizienz am Baudenkmal“. Bundesdenkmalamt (Editor). <http://www.bda.at/documents/944221227.pdf> (accessed November 2014)
- DENA. 2013 Christina Rocker: „Transparenz in Datenbanken: Beispiel Energieeffizienz-Expertenliste für Förderprogramme des Bundes“. Berlin, 14. November 2013 Zukunft Haus – Energie sparen – Wert gewinnen. available via: <http://www.energieeffizienz-online.info> (last accessed July 2014)
- DIN. 2008 "DIN EN ISO 14683 – Wärmebrücken im Hochbau – Lagenbezogener Wärmedurchgangskoeffizient – Vereinfachte Verfahren und Anhaltswerte (ISO 14683:2007)". Normenausschuss Bauwesen (NABau) im DIN, Deutsches Institut für Normung e.V.
- Eicke-Hennig, W., Siepe, B., & Zink, J. 1997. Konstruktionshandbuch – Verbesserung des Wärmeschutzes im Wohngebäudebestand. Darmstadt 1997. Available via <http://www.iwu.de/dateien/Konstruktionshandbuch.pdf> (accessed November 2014)
- Hauser, G. & Stiegler H. 2001. "Wärmebrücken-Atlas für den Mauerwerksbau" Bauverlag BV GmbH; 3. Auflage, August 2001 (ISBN: 978-3762533245)
- Kistler, S. 1932. Coherent expanded aerogel. In: Journal of Physical Chemistry 36(1), pp. 52-64. DOI: 10.1021/j50331a003
- Kornicki, M. 2014 "AnTherm 7.125" www.kornicki.eu (accessed November 2014)
- OIB. 2011. Leitfaden zur OIB-Richtlinie 6. OIB 2011. Available via www.oib.or.at (accessed November 2014)
- Riccabona, C. & Mezera, K. 2003. Baukonstruktionslehre 5, Sanierungen-Industriebau-Fassaden. Manz, 2003.
- SketchUp. 2014. "Trimble SketchUp Make 2014", www.sketchup.com (accessed November 2014)

Long-term and spatial evaluation of the integrated performance of a window-shade system in an open space office located in Rome

Anna Maria Atzeri – Free University of Bolzano/Bozen, Faculty of Science and Technology, Italy - annamaria.atzeri@natec.unibz.it

Francesca Cappelletti – University IUAV of Venezia, Dpt. of Design and Planning in Complex Environments, Venezia, Italy - francesca.cappelletti@iuav.it

Athanasios Tzempelikos – Purdue University, School of Civil Engineering and Ray W. Herrick Labs, West Lafayette, Indiana, USA – ttempel@purdue.edu

Andrea Gasparella - Free University of Bolzano/Bozen, Faculty of Science and Technology, Italy – andrea.gasparella@unibz.it

Abstract

The building façades, as a boundary between external and internal environments, play a central role in energy reduction and suitable comfort conditions maintenance. Their evaluation requires an integrated assessment approach, focused on occupants' thermal and visual comfort, in time and space, as well as on maximizing daylight and achieving energy saving goals. In this paper, dynamic simulation is used to evaluate the integrated performance of different fenestration systems in an open space office located in Rome. The illuminating analysis has been performed using DIVA, and the results, processed by means of a Matlab code, have been used as an input for Energy Plus thermal and energy analysis. Then, the Energy Plus outputs have been post processed to calculate the solar radiation influence on occupants thermal comfort. Some new metrics have been introduced in such a way that it is possible to assess the comfort performance with comprehensive indicators.

1. Introduction

The quantity of energy used to operate a building often depends on the comfort level perceived by the occupants (Nielsen et al., 2011). There are different physical elements which can influence the occupants' comfort perception. Some of those have been analysed and their effects can be easily represented. Others, like the transient solar radiation effects, have had less exposition due to the complexity of solar radiation behaviour. At the same time, the modern buildings are characterized,

especially the offices, by a more and more intensive use of glazing surfaces. The transparent components of the envelope can have both positive and negative effects, often contrasting, on the comfort conditions and on the energy needs. At the moment there are few examples of comprehensive studies which analyse both the overall energy demand (heating, cooling and lighting), and comfort conditions (thermal and visual). In most of the cases the metrics used to assess the thermal comfort do not consider the effect of solar radiation on the occupants' perception and often the space distribution of comfort is neglected. Moreover, the building's comfort performance assessed by means of comprehensive metrics, able to consider both long-term and spatial distribution, is rarely discussed.

This paper puts together all these aspects, considering the effects of different windows' glazing systems and shading devices, both on thermal and visual comfort and on overall building energy demand for an open space office located in Rome. The shades are managed in order to avoid or to reduce the visual discomfort and overheating conditions. The lighting system and shading devices work together to ensure a suitable illuminance level on the work-plane. The influence of the control setting on the energy performance has been evaluated calculating the overall primary energy demand, while the capacity in maximizing the natural light use has been assessed through the illuminance values. The analysis of the long-term comfort conditions has been conducted on a seasonal basis, taking

into account both the thermal and visual comfort. The visual comfort has been assessed calculating the Daylight Glare Probability (DGP) in 9 different positions in the office, while the thermal comfort has been evaluated considering the Predicted Percent of Dissatisfied, including also the effect of the diffuse and beam solar radiation directly reaching the occupants (Cappelletti et al., 2014). Using Daylight Glare Probability (DGP) and People Percentage of Dissatisfied (PPD) two comprehensive metrics have been calculated to assess the long-term and spatial comfort performance.

2. Modelling Methodology

Previous studies (Ramos & Ghisi, 2010) pointed out that Energy Plus is not able to simulate precisely the real indoor lighting conditions, since its algorithm cannot solve the internal reflectance properly as well as calculate exactly the external horizontal illuminance. This causes an overestimation of the interior daylight and an underestimation of the lighting needs. To overcome this problem it is possible to couple Energy Plus with DIVA, which performs a daylight analysis via integration with Radiance and DAYSIM, whose algorithms are well developed and widely validated. DIVA’s lighting and shading schedules can be used as input for Energy Plus analysis. This approach works well if we consider a side-lit room. If we analyse a room with windows located on facades and we want to manage the shades according to the illuminance related with their specific orientation, the DAYSIM simulation assumption and simplification makes it impossible. As specified in the user guide, DAYSIM calculates the daylight coefficient and the annual illuminance profiles for the bare case plus each additional shading device state. In our study we supposed one shade state in addition to the bare case, with the shades totally closed. Considering a room with windows on opposite facades, this means that the software should simulate all these combinations:

1. Both shades fully opened;
2. One shade opened and the other closed and vice versa;
3. Both shades fully closed.

Actually, DAYSIM does not calculate all the possible shading combinations; it only makes an estimation

of what the illuminance should be with only one shading state closed. This approach removes too much light from one of the two control sensors and keeps the relative shades from triggering due to the assumption the software makes. For this reason, we used DIVA only to obtain the illuminance and DGP profiles for each one of the shading states and we used a MATLAB code to combine them in order to obtain the lighting and shading schedules for Energy Plus and the daylighting metrics. Through the Energy Plus simulation we obtained the overall primary energy needs and a list of outputs which have been post processed through MATLAB to calculate the influence of solar radiation on occupants’ thermal sensation and the thermal comfort indicators.

3. Simulation Settings

3.1 Geometrical Model and Parametrical Analysis

The model is an open space office of 100 m² of floor area and 3 m of interior height located in Rome - Italy (Lat. N 42° 54' 39''; HDD18: 1420 K d - CDD18: 827 K d). The windowed façade has been simulated east oriented. A parametrical analysis has been performed by varying some building envelope characteristics, as summarized in Table 1.

Table 1 – Variables used in the analysis

Building Parameter	Values
Glazing	DH Double Glazing high SHGC Ugl = 1.14 W m ⁻² K ⁻¹ ; SHGC = 0.60; τ _{vis} = 0.81
	DL Double Glazing low SHGC Ugl = 1.08 W m ⁻² K ⁻¹ ; SHGC = 0.35; τ _{vis} = 0.58
	TH Triple Glazing high SHGC Ugl = 0.60 W m ⁻² K ⁻¹ ; SHGC = 0.59; τ _{vis} = 0.73
	TL Triple Glazing low SHGC Ugl = 0.61 W m ⁻² K ⁻¹ ; SHGC = 0.35; τ _{vis} = 0.63
WWR	S1: 45%; S2: 75%
Shading devices (located internally and externally)	W/O: Without shades SH1: High solar transmittance: q _s =0.58; τ _s =0.16; q _v =0.51; τ _v =0.15 SH2: Medium solar transmittance: q _s =0.37; τ _s =0.10; q _v =0.35; τ _v =0.10 SH3: Low solar transmittance q _s =0.13; τ _s =0.05; q _v =0.06; τ _v =0.05

3.2 Characteristics of Components - Energy Plus and DIVA

Regarding Energy Plus, the walls and roof have been modelled as external while the floor as an adiabatic surface. The composition of the opaque elements is identical, with a thermal transmittance of $0.45 \text{ W m}^{-2} \text{ K}^{-1}$. The solar absorptance is 0.6 for the floor (internal side) and 0.3 for the walls and the roof (both sides). The wall emissivity is 0.9, internally and externally.

The Radiance simulation parameters have been fixed with the aim of analyzing the effect of the fabric throughout the depth of the office.

Table 2 – Radiance parameters' values

Radiance parameters	Values
ambient bounce (ab)	5
ambient division (ad)	1000
ambient sampling	20
ambient resolution	300
ambient accuracy	0.1

All the opaque components have been simulated through the RADIANCE material PLASTIC. Wall and ceiling's reflectance are equal to 0.7, and the floor ones is equal to 0.4, which corresponds to plaster and tiles very light colored. The specularity and the roughness have been set equal to 0. For the glazing systems the material GLASS has been used, converting the glass transmittance in transmissivity at normal incidence. The roller shades have been simulated through the material TRANS, which allows defining beam/diffuse ratio but still does not consider angular differences (Chan et al. 2014). Apian-Bennewitz (2013) pointed out that this function is the most suitable one for modeling roller shades in RADIANCE when BSDF information, or other angular solar optical properties, are not available. A TRANS material is defined through its RGB reflectance, transmissivity and transmitted specular component. Two of the shades simulated, SH1 and SH3, are commercial, produced by Helioscreen. For these it has been possible to obtain the direct and diffused part of the light transmission. The properties of shade SH2 has been calculated by means of analytical

regression in order to obtain intermediate characteristics between SH1 and SH3.

3.3 Internal gains

The office is occupied from Monday to Friday from 8:00 a.m. to 6:00 p.m. The occupancy index has been fixed as 0.12 people m^{-2} . The occupants' metabolic heat flux is equal to 70 W m^{-2} (75 W sensible portion, 55 W latent). The clothing unit thermal resistance is 1 clo during the heating season (1st October-31st March), and 0.5 clo during the cooling season (1st April-30th September). The electrical equipment internal loads are equal to 1.31 W m^{-2} , while the Light Power Density is 12 W m^{-2} .

3.4 Controls Setting

The artificial lights have been managed, through a photo-sensor-controlled dimming system, to maintain 500 lux on the work plane area. In order to maximize the contribution of the incoming daylight, a control point for each row of lights parallel to the windows has been chosen. The roller shading control operates in order to avoid excessive daylighting levels inside the confined space considering two possible shade positions, fully opened or fully closed. The shade's position depends on the illuminance values measured by an internal sensor, located on the work plane closest to the transparent surface, which uses 500 and 2000 lux like limit values; 500 lux represents the desired work plane illuminance and 2000 lux is considered as limit value to avoid visual discomfort (Nabil & Mardaljevic, 2006). The shades are also closed during the unoccupied hours for all the year.

The heating and cooling systems functioning depends on two bands for the operative temperature, 20°C to 24°C during the heating season and 23°C to 26°C during the cooling season, to comply with the comfort Category B (normal level of expectation about the conditions of comfort for users). The temperature bands operate on weekdays from Monday to Friday and from 8 a.m. to 6 p.m. A heating setpoint of 15°C and a cooling setpoint of 38°C have been considered for the nighttime and weekends. This way, while the heating setpoint is fixed in order to prevent the air temperature becoming too low, the cooling set-

point is fixed in order to guarantee that the system is switched off. To assess the thermal comfort conditions inside the office, a grid consisting of 9 points at 0.8 m from the floor level was considered, while for visual comfort the same points have been considered at 1.1 m from the floor level.

4. Performance metrics

The performance of the simulated environment has been evaluated by means of two different types of indicators. The first type, which has been called “*Extensive - Long-term quantitative performance metrics*”, describes the percentage of annual working hours during which each point belonging to a specified grid is above a specified level. Through this indicator we can obtain a spatial description of the simulated environment.

The second type, called “*Synthetic - Spatial long-term quantitative performance*”, describes the percentage of floor area in which the respect of a specified limit value, for a certain percentage of working hours, is maintained.

4.1 Comfort performance metrics

Both the thermal and visual comfort conditions have been evaluated only during the occupancy period. Regarding the comfort performances, the extensive metrics used express a condition of discomfort, while the synthetics express a positive performance. For the thermal comfort, the metrics used have been created calculating the PPD but, besides the standard index, a corrected PPD (PPD_{irr}) has been evaluated considering the effect of solar radiation that directly reaches the occupant (La Gennusa et al., 2007). In this case the extensive metric has been called *Thermal Discomfort Time* (TDT_{PPD}), and it represents the percentage of annual working hours during which the PPD at a given point in the space overcomes the limit value, 10%, threshold values for B category, according to EN ISO 1251:2008. Otherwise, since the objective of the study is also the evaluation of the office’s performance in its entirety, a comprehensive indicator, *Spatial Thermal Comfort* ($sTC_{10,90\%}$), has been calculated. It represents the percentage of floor area in which the PPD is less

than 10% for the 90% of annual working hours considering both the standard and the irradiated index.

The visual comfort has been analyzed by means of the Daylight Glare Probability (Wienold & Christoffersen, 2006), calculated in 9 positions over the space, considering a specified view’s direction. The extensive performance has been evaluated by means of the metric called *Visual Discomfort Time* (VDT_{DGP}), which expresses the percentage of annual working hours during which the DGP at a given point in the space overcomes 0.35, which is considered the lower limit of acceptable glare values (Wienold & Christoffersen, 2006). Finally, a comprehensive metric has been calculated to account for the glare’s spatial variability, called *spatial Visual Comfort* ($sVC_{0.35,100\%}$), and it has been defined as the percentage of floor area in which there is never glare discomfort.

4.2 Daylighting and energy performance metrics

As an extensive metric, the percentage of working hours when the daylight illuminance is above 500 lux has been used (*Daylight Autonomy - DA*).

As a synthetic metric to summarize annual daylighting performance throughout the space the *spatial Daylight Autonomy* (sDA) has been calculated. sDA (IES, 2012) provides a measure of daylight illuminance sufficiency for a given area, reporting the percentage of floor area that exceeds a specified illuminance level, 500 lux, for a specified amount of working hours, 50%.

Concerning the energy performance the heating, cooling and lighting energy demands have been evaluated in terms of *Primary Energy* use (PE). As described in Cappelletti et al. (2014), controlling the heating and cooling systems by means of the operative temperature, allows us to interpret the energy demand as a double indicator of the envelope’s passive energy and comfort performance. In this way, the energy performance of different cases can be compared under equivalent comfort conditions. Moreover, the control of the operative temperature allows us to ascribe the discomfort only to the inlet solar radiation striking the occupant, thus helping in the assessment of the

shading device efficacy. To convert the energy needs in primary energy, we used 0.8 as seasonal energy production efficiency for heating and a seasonal Energy Efficiency Ratio of 3 for cooling. A value of 2.174 of primary energy content per unit of electrical energy has been assumed according to the Italian electrical system. Finally, the synthetic metric related to the energy performance has been built considering the ratio between the energy performance of a specific case with shade and the reference case without shade ($EP_{sh/wo}$).

5. Results

5.1 Indoor thermal comfort

The $sTC_{10,90\%}$ metric calculated with the standard index (Fig. 2) highlights a thermal environment able to stay within the chosen limit, except for the internal shades. When we consider the contribution of the solar radiation (Fig. 1), with the small windows coupled with the external shades, we are always able to ensure the right thermal comfort conditions, but the unshaded configurations and the internal shades can respect the threshold only using the low SHGC glazing. With the biggest windows, the comfort conditions requested can be reached only through the TL glazing coupled with the external shades. The TDT_{PPD} index (Fig. 5) highlights the distribution of the thermal discomfort sensation through the space. In this case, if we analyze the results correlated with the standard index, the thermal environment keeps homogenous, regardless of the shade's presence. The irradiated TDT_{PPD} , instead, shows how and how much the thermal discomfort arises as we consider the positions closest to the transparent surfaces. Moreover, whereas the shade SH3, located externally, can reduce the thermal discomfort time up to 60% compared to unshaded configuration, the same shade located internally is not able to reduce the TDT_{PPD} more than 35%.

5.2 Indoor visual comfort and daylighting performance

For visual comfort and daylighting performance, we obtain very similar results regardless of the

shade's position. The use of the roller shading system leads, globally, to a decrease of the $sDA_{500,50\%}$ (Fig. 3) for both the window's size and the DA_{500} (Fig. 6) decreases faster distancing from the transparent surfaces. The view's direction used for the simulation makes sure that even the unshaded combinations remain close to the limit chosen for the $sVC_{0.35,100\%}$ (Fig. 4), but only thanks to the shades can we ensure the visual comfort for all the positions analyzed. If we analyze the visual discomfort locally (Fig. 7), with the bare windows the points closest to the biggest windows can stay under discomfort conditions up to 29% of the annual working hours.

5.3 Primary energy use

With the smallest windows, the use of the roller solar shading systems leads to an increase in the primary energy needs except for the configurations with the glazing DH, TH or TL coupled with the shade SH1 located externally. With the biggest windows and the shades located externally we obtain for all the configurations analyzed a reduction of the overall primary energy consumption except for the glazing DH coupled with the shade SH3. Essentially, considering that the use of the roller shading systems cause, in all the cases analyzed, an increase in the primary energy consumptions related with the lighting and heating systems, we can obtain a reduction of the overall primary energy needs only when the cut of the cooling needs is important enough to overcome the other two increases.

6. Conclusions

As we underlined before, one of the aims of this study is the representation of the fenestration system's influence on the overall performance of the confined environment. To reach this goal, we tried to build a methodology able to take into account at the same time the requirements of indoor thermal and visual comfort, the maximization of daylight availability and the reduction of the energy consumption due to heating, cooling and lighting systems. From a graphical point of view, we

Configuration	sTC _{10,90%} - IRRADIATED																															
	WO				SH1 _{ext}				SH2 _{ext}				SH3 _{ext}				SH1 _{int}				SH2 _{int}				SH3 _{int}							
	DH	DL	TH	TL	DH	DL	TH	TL	DH	DL	TH	TL	DH	DL	TH	TL	DH	DL	TH	TL	DH	DL	TH	TL	DH	DL	TH	TL				
E_S1	56%	100%	67%	100%	100%	100%	100%	100%	100%	100%	100%	100%	100%	100%	100%	100%	89%	100%	89%	100%	89%	100%	89%	100%	67%	100%	67%	100%	67%	100%	67%	100%
E_S2	67%	89%	78%	100%	78%	89%	67%	100%	89%	89%	89%	100%	89%	89%	89%	100%	33%	78%	22%	78%	22%	67%	22%	78%	33%	67%	22%	78%	33%	67%	44%	67%

Fig. 1 – Spatial Thermal Comfort Irradiated

Configuration	sTC _{10,90%} - STANDARD																															
	WO				SH1 _{ext}				SH2 _{ext}				SH3 _{ext}				SH1 _{int}				SH2 _{int}				SH3 _{int}							
	DH	DL	TH	TL	DH	DL	TH	TL	DH	DL	TH	TL	DH	DL	TH	TL	DH	DL	TH	TL	DH	DL	TH	TL	DH	DL	TH	TL				
E_S1	100%	100%	100%	100%	100%	100%	100%	100%	100%	100%	100%	100%	100%	100%	100%	100%	100%	100%	100%	100%	100%	100%	100%	100%	100%	100%	100%	100%	100%	100%	100%	100%
E_S2	100%	100%	100%	100%	100%	100%	100%	100%	100%	100%	100%	100%	100%	100%	100%	100%	67%	100%	33%	100%	44%	100%	33%	89%	44%	67%	44%	67%	44%	67%	44%	67%

Fig. 2 – Spatial Thermal Comfort Standard

Configuration	sDA _{500,50%}																											
	WO				SH1 _{ext}				SH2 _{ext}				SH3 _{ext}				SH1 _{int}				SH2 _{int}				SH3 _{int}			
	DH	DL	TH	TL	DH	DL	TH	TL	DH	DL	TH	TL	DH	DL	TH	TL	DH	DL	TH	TL	DH	DL	TH	TL	DH	DL	TH	TL
E_S1	56%	44%	56%	44%	37%	33%	38%	33%	33%	31%	32%	32%	11%	22%	20%	22%	37%	33%	36%	33%	32%	31%	32%	32%	11%	22%	17%	22%
E_S2	73%	56%	67%	56%	44%	40%	42%	38%	33%	33%	33%	33%	11%	22%	11%	21%	41%	38%	41%	38%	33%	33%	32%	33%	10%	22%	11%	19%

Fig. 3 – Spatial Daylight Autonomy

Configuration	sVC _{0.35,100%}																											
	WO				SH1 _{ext}				SH2 _{ext}				SH3 _{ext}				SH1 _{int}				SH2 _{int}				SH3 _{int}			
	DH	DL	TH	TL	DH	DL	TH	TL	DH	DL	TH	TL	DH	DL	TH	TL	DH	DL	TH	TL	DH	DL	TH	TL	DH	DL	TH	TL
E_S1	93%	96%	93%	96%	100%	100%	100%	100%	100%	100%	100%	100%	100%	100%	100%	100%	100%	100%	100%	100%	100%	100%	100%	100%	100%	100%	100%	100%
E_S2	89%	94%	91%	93%	100%	100%	100%	100%	100%	100%	100%	100%	100%	100%	100%	100%	100%	100%	100%	100%	100%	100%	100%	100%	100%	100%	100%	100%

Fig. 4 – Spatial Visual Comfort

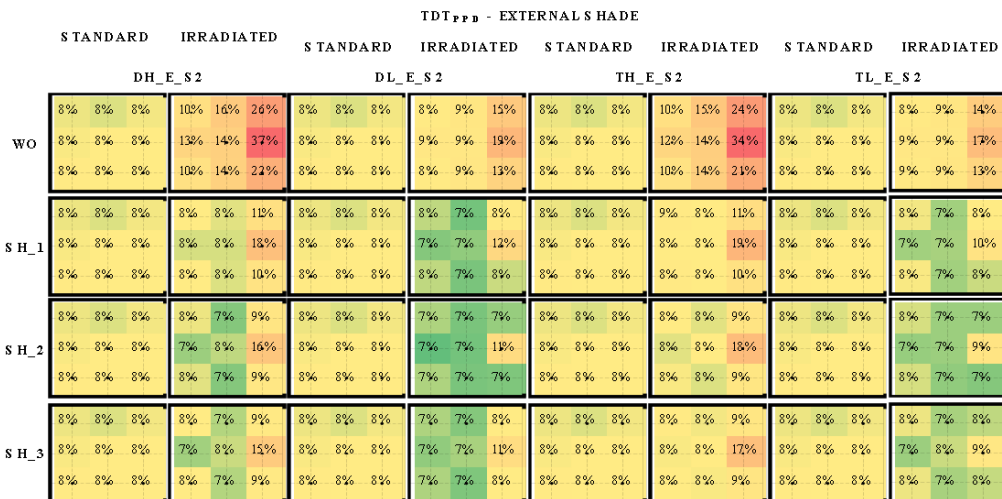


Fig.5 – Thermal Discomfort Time

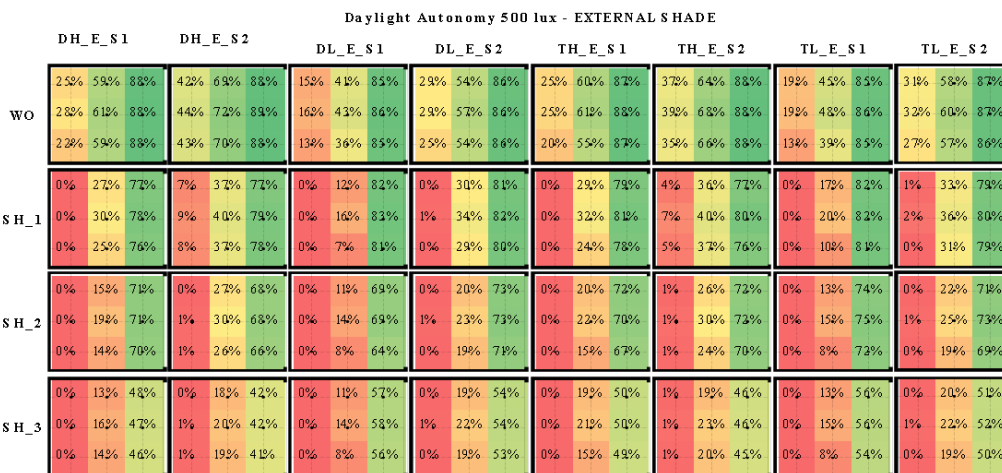


Fig. 6 – Daylight Autonomy

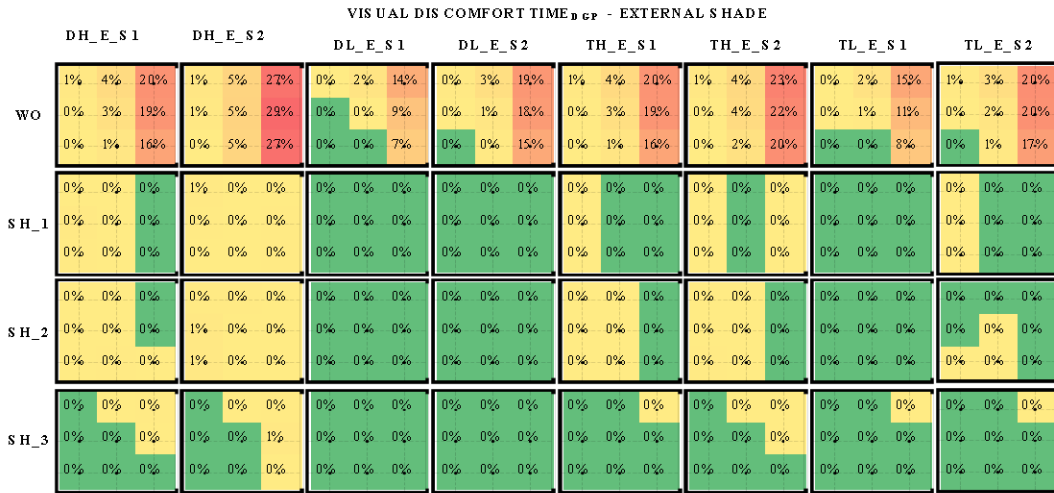


Fig. 7 – Visual Discomfort Time

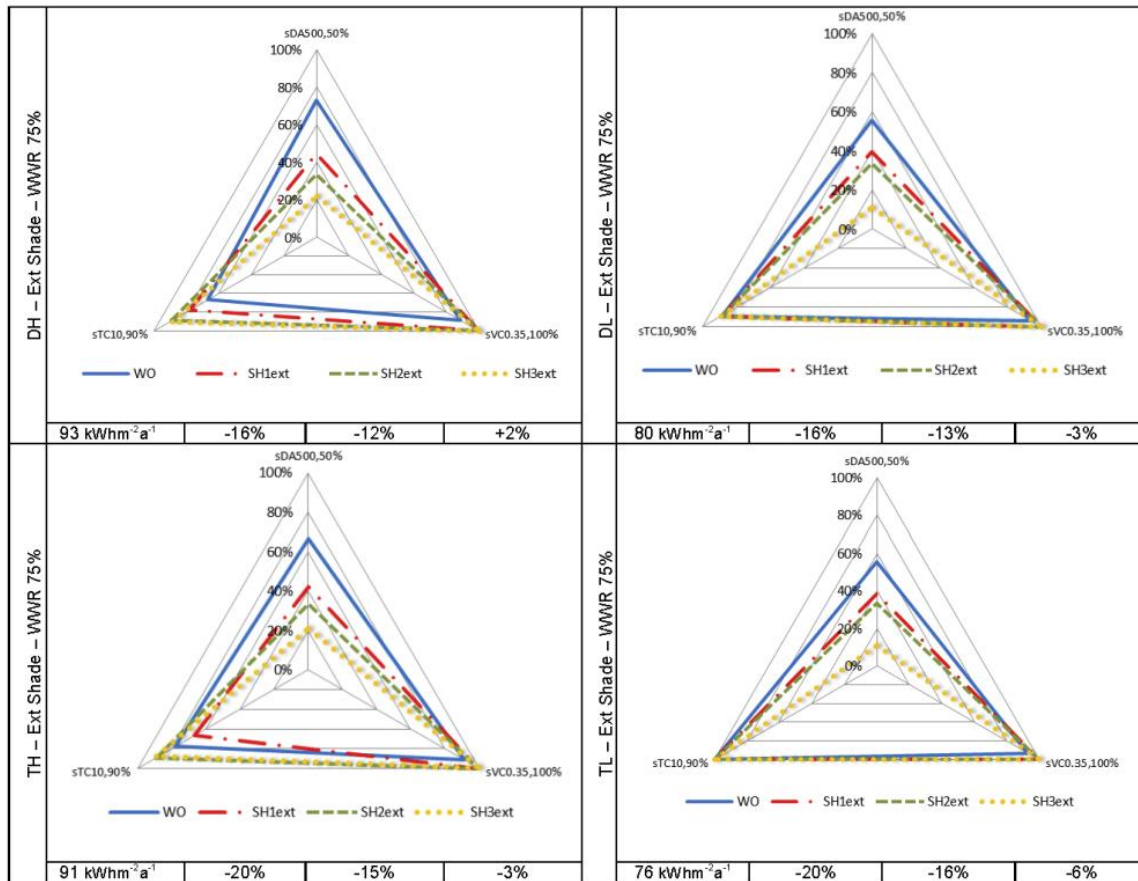


Fig. 8 – Integrated Performance

summarized through a single graph (Fig. 8) all the configurations analyzed by means of the variation of the synthetic metrics. We can notice that the settings used to ensure suitable internal visual and thermal comfort conditions for the occupants, with the specific orientation chosen, lead to a general increase of the total primary energy consumptions calculated. It is known that the building's energy consumption is related to the balance between gains and losses (climate, envelope and equipment) and this balance depends also on his operation. Whereas it is possible to predict the energy consumption related to envelope and equipment, the energy used to operate a building is strictly connected with the occupants' behavior, which is more difficult to predict. To maintain the building's energy use as close as possible to what we calculated, ensuring a satisfying internal environmental quality plays a very important role. The methodology proposed underlines:

- i. the importance of analyzing together the overall performance of a building façade
- ii. the contribution of simulation in the analysis of the integrated performance of façades and the necessity of using different simulation codes;
- iii. the great importance of considering the effect of the direct and diffuse solar radiation on occupants well-being.

References

- Apian-Bennwitz P., 2013. Review of Simulating Four Classes of Window Materials for Daylighting with Non-Standard BsdF Using the Simulation Program Radiance. Retrieved 04/08, 2014, from <http://arxivweb3>.
- Cappelletti F, Prada A., Romagnoni P., Gasparella A., 2014, Passive performance of glazed components in heating and cooling of an open-space office under controlled indoor thermal comfort, *Building and Environment*, vol. 72, p. 131-144.
- Chan Y., Tzempelikos A., Protzman B., 2014, Solar optical properties of roller shades: modeling approaches, measured results and impact on daylighting and visual comfort, *Proc. of High Performance Buildings Conference*, West-Lafayette, USA.
- La Gennusa M., Nucara A., Pietrafesa M., Rizzo G., 2007. A model for managing and evaluating solar radiation for indoor thermal comfort, *Solar Energy* vol. 81, p. 594–606.
- Illuminating Engineering Society, 2012, Standard IES LM-83-12. Approved Method: IES Spatial Daylight Autonomy (sDA) and Annual Sunlight Exposure (ASE), New York, U.S.A.
- Nabil A., Mardaljevic J., 2006. Useful daylight illuminances: a replacement for daylight factors. *Energy and Buildings*, vol. 38, p. 905–913.
- Nielsen M.V., Svendsen S. et Jensen B. L. 2011. Quantifying the potential of automated dynamic solar shading in office buildings through integrated simulations of energy and daylight, *Solar Energy*, vol. 85, p. 757-768
- Ramos G., Ghisi E., 2010. Analysis of daylight calculated using the EnergyPlus programme. *Renewable and Sustainable Energy Reviews*, 14(7): p. 1948-1958.
- Reinhart C.F., Jakubiec J.A., Ibarra D., 2013. Definition of a reference office for standardized evaluations of dynamic façade and lighting technologies, *Proc. of Building Simulation*, Chambéry, France
- Wienold J., Christoffersen J., 2006. Evaluation methods and development of a new glare prediction model for daylight environments with the use of CCD cameras, *Energy and Buildings*, vol. 38, p. 743–75

Energy cost and discount rate influence on the optimal packages of energy efficiency measures

Vincenzo Corrado – Department of Energy, Politecnico di Torino (Italy) – vincenzo.corrado@polito.it

Ilaria Ballarini – Department of Energy, Politecnico di Torino (Italy) – ilaria.ballarini@polito.it

Ilenia Ottati – Department of Energy, Politecnico di Torino (Italy) – ilenia.ottati@polito.it

Simona Paduos – Department of Energy, Politecnico di Torino (Italy) – simona.paduos@polito.it

Abstract

The Commission Delegated Regulation No. 244/2012 supplementing Directive 2010/31/EU on the comparative methodology framework for calculating cost-optimal levels of minimum energy performance requirements enforces Member States to perform an analysis to determine the sensitivity of the calculation outcomes to changes in the energy price developments and the discount rates, as well as other parameters which are expected to have a significant impact on the outcome of the calculations.

In Italy the cost optimal methodology has been performed by using a simulation tool enforced on a quasi-steady state numerical model (UNI/TS 11300) while the cost optimisation procedure is based on a sequential search-optimisation technique considering discrete options, as introduced in a previous work (Corrado et al., 2014). Packages of energy efficiency measures giving optimal EP levels have been found for different buildings and climatic conditions (Italian Ministry of Economic Development, 2013; Corrado et al., 2013). Results show that the optimal solutions are strongly influenced by energy costs of the different energy wares, and this can affect the suitable technical solutions for refurbishment.

The present work is focused on the definition of different economic scenarios. The aim is to assess a wide economic framework as to determine the influence of the energy cost and discount rate on the costs/benefits analysis and how cost optimal solutions can change according to these trends. Different energy cost variations are considered for electricity and natural gas, which are the most used energy carriers in Italy. The economic framework is applied to four Italian reference buildings to emphasize its influence when different building uses and climatic boundary conditions are considered. Discrepancies in results are then discussed.

1. Introduction

1.1 The comparative methodology framework

European Directive 2010/31/EU (European Union, 2010) on the energy performance of buildings requires Member States to take the necessary measures to ensure that minimum energy performance requirements for buildings or building units are set with a view to achieving cost-optimal levels. Member States shall calculate cost-optimal levels of minimum energy performance requirements using a comparative methodology framework.

The comparative methodology framework has been established by the Commission Delegated Regulation No. 244/2012 (European Union, 2012a) supplementing the Directive 2010/31/EU, in order to calculate cost-optimal levels of minimum requirements for the energy performance of buildings and building elements. The Guidelines that accompany the Regulation (European Union, 2012b) include information to help Member States to apply the comparative methodology at the national level.

A cost-optimal level is the energy performance (EP) level which leads to the lowest global cost during the estimated economic lifecycle, taking into account energy-related investment costs, maintenance and operating costs (including energy costs and savings, the category of building concerned, earnings from energy produced), and disposal costs, where applicable.

The comparative methodology includes the following steps:

- definition of reference buildings (RBs), representative of the building stock in terms of function and climatic conditions,
- identification of energy efficiency measures (EEMs), in terms of different packages/variants for each RB,
- calculation of the primary energy demand resulting from the application of the EEMs to a RB,
- calculation of the global cost in terms of net present value for each RB in the expected economic lifecycle,
- derivation of a cost-optimal level of energy performance for each RB and, consequently, the optimal EEM package/variant.

Several studies have been carried out on this topic, concerning, for instance, the methodology for cost-optimal analysis (Ascione et al., 2105; Hamdy et al., 2013) and the definition of reference buildings (Brandão de Vasconcelos et al., 2015).

1.2 Sensitivity analysis on some key parameters

For the purpose of adapting the comparative methodology framework to national circumstances, the Commission Delegated Regulation No. 244/2012 (European Union, 2012a) requires Member States to determine the estimated economic lifecycle of a building and/or building element, the appropriate cost for energy carriers, products, systems, maintenance, operational and labour costs, primary energy conversion factors, and the energy price developments. Member States should also establish the discount rate to be used in both macroeconomic and financial calculations.

In addition, the Regulation requires the Member States to undertake some sensitivity analyses, when outcomes depend on assumptions on key parameters of which the future development can have a significant impact on the final result. A sensitivity analysis is required on different price scenarios for all energy carriers of relevance in a national context, plus at least two scenarios each for the discount rates to be used for the macroeconomic and financial cost optimum calculations.

Starting from the outcomes of a previous study

(Italian Ministry of Economic Development, 2013; Corrado et al., 2013) in which energy efficiency measures and related costs were identified for several reference buildings and climatic conditions, the present article investigates different economic scenarios in order to determine the influence of the energy cost and of the discount rate on the costs/benefits analysis and to verify how the cost optimal solutions might change in case of different variations of the energy price development. The most used energy carriers in Italy, i.e. electricity and natural gas, are taken into account in the analysis.

2. Economic scenarios in the cost-optimal analysis

2.1 Description of the reference buildings

In order to analyse different economic scenarios, two reference buildings are selected among those introduced in previous works (Italian Ministry of Economic Development, 2013; Corrado et al., 2013), each one considered in two different Italian climatic zones, Milano (zone E – 2404 HDD) and Palermo (zone B – 751 HDD).

The first reference building is a multi-family house taken from the Italian “National Building Typology”, as developed in the *Intelligent Energy Europe* TABULA project (Corrado et al., 2011). The second reference building is an office building-type as defined by ENEA (Margiotta, 2010).

Table 1 – Main geometric data of the reference buildings

Reference Building	Main geometric data				no. units
	V_g [m ³]	$A_{t,n}$ [m ²]	A_{env}/V_g [m ⁻¹]	A_w [m ²]	
 Residential	3076	827	0.51	150	12
 Office	1339	363	0.60	115	12

Both the case studies belong to the construction period ranging from 1946 to 1976. The main geometric data do not differ across the climatic zones (see Table 1).

2.2 Identification of the cost-optimal level of energy performance through a cost-optimisation procedure

The energy efficiency measures (EEMs) applied to each reference building have been defined by the Italian Ministry of Economic Development (2013) and by Corrado et al. (2013). An appropriate parameter is associated to each measure; e.g. the U -value for the thermal insulation of the building envelope, the heat generator efficiency (either η or COP or EER) for the technical systems replacement, the collectors area (A_{coll}) for the thermal solar system installation, the peak power (W_{FV}) for the photovoltaic system installation. For each measure, up to five energy efficiency options or levels (EEOs) are defined. The first level usually represents an inefficient solution used as a test value; the second level represents the requirement fixed by current legislation (Italian Government, 2005); the levels from the third to the fifth (if applicable) are more efficient solutions.

The initial investment cost associated to each EEO comes either from extensive market surveys or from official databases. The costs of the energy carriers are derived from the National Authority for Electricity and Natural Gas (AEEG), considering the rates applied for the enhanced protection service. The estimated energy carriers price development trends are those provided by the European Commission on a biannually updated basis (PRIMES model), according to Annex 2 of the Commission Delegated Regulation No. 244/2012 (European Union, 2012a). These trends have been extrapolated beyond 2030, which is the last year taken into account in the available projections.

Other input data and assumptions are detailed in the report of the Italian Ministry of Economic Development (2013) and in Corrado et al. (2013).

The energy performance is calculated according to the Italian technical specification UNI/TS 11300 (Italian Organisation for Standardisation, 2010-

2014) and the global cost analysis is performed according to EN 15459 (European Committee for Standardization, 2007), considering an estimated economic lifetime of 30 years for the residential buildings and 20 years for the offices, a discount rate of 4%, and applying a financial cost optimum calculation.

The cost optimisation is carried out by means of a procedure based on a sequential search-optimisation technique considering discrete options, as described in Corrado et al. (2014). The optimal level of annual primary energy use for heating, cooling and domestic hot water, and the corresponding actualized global cost are shown in Table 2 for the selected reference buildings. The related optimal values of the design parameters are listed in Table 3.

Table 2 – Cost optimal level of the reference buildings

Reference Building	Climatic Zone	EP [kWh m ⁻²]	Global cost [€ m ⁻²]
 Residential	Milano (2404 HDD)	61.0	495
	Palermo (751 HDD)	36.6	384
 Office	Milano (2404 HDD)	86.9	781
	Palermo (751 HDD)	65.3	695

2.3 Description of the economic scenarios

Cost calculations and projections with many assumptions and uncertainties, including for example energy price developments over time, are generally accompanied by a sensitivity analysis to evaluate the robustness of the key input parameters. For the purpose of the cost-optimal calculations, the Regulation No. 244/2012 (European Union, 2012a) requires that the sensitivity analysis should at least address the discount rate and the energy price developments.

2.3.1 Discount rate scenario

The discount rate means a definite value for comparison of the value of money at different times

Table 3 – Optimal values of the energy efficiency measures for the analysed reference buildings

EEM		Optimal EEO			
		Residential / Milano	Residential / Palermo	Office / Milano	Office / Palermo
Wall insulation (on external surface) or Wall insulation (on cavity)	U_{wl} [W m ² K ⁻¹]	- 0.34	- 0.48	- 0.20	- 0.44
Upper floor insulation	$U_{fl,up}$ [W m ² K ⁻¹]	0.40	0.50	0.27	0.38
Lower floor insulation	$U_{fl,lw}$ [W m ² K ⁻¹]	0.45	0.65	-	-
Windows	U_w [W m ² K ⁻¹]	1.60	3.00	1.60	3.00
Solar shading devices	τ_{sh} [-] / M or F (*)	0.4 / F	0.2 / F	0.4/F	0.2 / F
Heat generator for space heating	$\eta_{H,gn}$ [-] or COP [-]	-	-	-	-
+ Heat generator for domestic hot water	$\eta_{W,gn}$ [-]	-	-	-	-
+ Chiller	EER [-]	-	-	-	-
or Combined heat generator for space heating and domestic hot water	$\eta_{H,W,gn}$ [-]	-	-	0.93	0.93
+ Chiller	EER [-]	-	-	3.50	3.50
or Combined generator for heating, cooling and domestic hot water	COP [-]	4.20	4.20	-	-
	EER [-]	3.10	3.10	-	-
Thermal solar system	A_{coll} [m ²]	14	14	2	2
Photovoltaic system	W_{pv} [kW _p]	2	2	5	5
Ventilation heat recovery	NO or YES (η_{ru} [-])	NO	NO	YES (0.6)	YES (0.6)
Efficiency of the heat control system	η_{rg} [-]	0.995	0.995	0.97	0.97
Lighting power density(**)	W_{lgt} [W m ⁻²]	N/A	N/A	4.60	4.60
Lighting control system parameters(**)	F_O [-]	N/A	N/A	0.8	0.8
	F_C (F_D) [-]	N/A	N/A	0.9	0.9

(*) M = mobile louvres; F = fixed louvres.

(**) Not applicable (N/A) for the residential buildings.

expressed in real terms, hence excluding inflation. The global cost is directly linked to the duration of the calculation period t , as shown in Eq. (1). The calculation of the global cost $C_g(t)$ referred to the starting year t_0 may be performed by a component or system approach, considering the initial investment C_I , and, for every component or system j , the annual costs C_a and the discount factor $R_{disc}(i)$ for every year i (referred to the starting year), and the final value Val_F .

$$C_g(t) = C_I + \sum_j \left[\sum_{i=1}^t (C_{a,i}(j) \cdot R_{disc}(i)) - Val_{F,j}(j) \right] \quad (1)$$

The discount factor $R_{disc}(i)$, for every year i , is a multiplicative number used to convert a cash flow occurring at a given point in time to its equivalent

value at the starting point. The discount factor is derived from the discount rate r and is calculated as:

$$R_{disc}(i) = \left(\frac{1}{1 + \frac{r}{100}} \right)^i \quad (2)$$

where, i is the number of years from the starting period.

According to the Guidelines accompanying the Regulation (European Union, 2012b), a higher discount rate – typically higher than 4% excluding inflation – would reflect a purely commercial, short-term approach to the valuation of investments. A lower rate – typically ranging from 2% to 4% excluding inflation – would more closely reflect the benefits that energy efficiency invest

ments bring to building occupants over the entire investment's lifetime.

The first economic scenario on the reference buildings consists in the variation of the discount rate, from 4% of the base scenario to 5%.

2.3.2 Energy price development scenario

The information provided in Annex 2 of the Regulation (European Union, 2012a) is taken from energy trend scenarios developed with the PRIMES model, i.e. a modelling system that simulates a market equilibrium solution for energy supply and demand in the EU27 and its Member States.

The baseline price assumptions for the EU27 are the result of world energy modelling (using the PROMETHEUS stochastic world energy model) that derives price trajectories for oil, gas and coal under a conventional wisdom view of the development of the world energy system.

The latest update (2009) implies a 2.8% annual increase in gas prices, a 2.8% annual increase in oil prices and a 2% annual increase in coal prices. As regards electricity, estimated long-term after-tax electricity price developments in €/MWh are shown in Table 4.

Table 4 – Estimated long-term after-tax electricity price developments (€/MWh; source: European Commission)

Sector	2000	2005	2010	2015	2020	2025	2030
Residential	127	133	144	164	180	191	192
Services	123	124	124	139	152	159	159

According to the Guidelines (European Union, 2012b), the trends of the energy prices may be extrapolated beyond 2030 until more long-term projections become available. In order to consider the whole estimated economic lifetime of the residential buildings and of the offices, the extrapolation is done up to 2050 (considering 2013 as the starting year).

Table 5 – Identification of price development scenarios of electricity (E) and/or natural gas (NG)

Scenario	E	NG	E and NG
50% lower annual estimated increment of price	I	III	V
50% higher annual estimated increment of price	II	IV	VI

Starting from the base scenario for each reference building, the second economic analysis consists in applying the scenarios listed in Table 5 to the energy trend of the Annex 2 of the Regulation.

For each of the scenarios listed in Table 5, a discount rate of 4% is applied. The energy price trends of the base scenario are shown in Fig. 1.

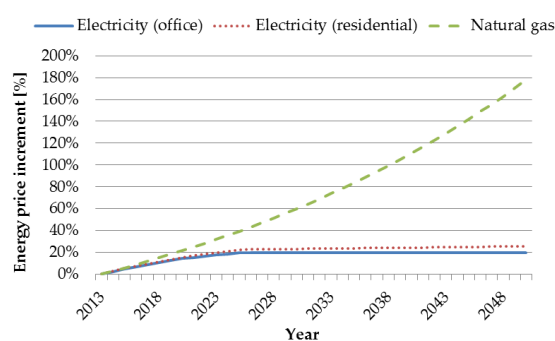


Fig. 1 – Base scenario energy price trends

3. Result analysis and discussion

The results of the economic scenarios on the reference buildings are shown in Figs. 2-3 for residential buildings and offices respectively, where “DR” stands for the variation of the discount rate, the roman numerals correspond to the cases in Table 5 and the lines represent the base scenario Cost Optimality trend for the two climatic zones considered. The results show the robustness of the residential buildings optimal EEM package, as the energy performance approximately keeps the value of 36.6 kWh m⁻² in Palermo and of 61.0 kWh m⁻² in Milano when different economic scenarios are applied. Concerning the economic aspects, as an effect of the financial calculation principle, the amount of global costs is lower when

a higher discount rate is applied, but the deviation from the base scenario is only of 25 € m⁻² in Palermo and of 31 € m⁻² in Milano. By applying the different energy costs scenarios in Table 5 the global cost deviation in respect with the base scenario is not significant.

Concerning the offices in Palermo, the energy performance still approximately remains at the base scenario same value of 65.3 kWh m⁻² when different economic scenarios are applied; the only relevant difference is shown for Milano, where the highest deviation between the DR and the base scenario is of 5.0 kWh m⁻², as the increasing discount rate involves a reduction of the EEMs optimal performance levels of the roof thermal insulation and of the photovoltaic system peak power installed. Other changes in the optimal level of the energy efficiency measures are shown for the offices in Milano, as follow: when the electricity cost increase is lower (scenario I) the optimal solution consists of the installation of a lower surface of PV panels; when the natural gas cost increase is lower (scenarios III and V) the optimal solution consists of lower roof thermal insulation as well as of PV system performance levels. Conversely, in Palermo when the natural gas cost increase is higher (scenarios IV and VI), the roof thermal insulation optimal level is higher.

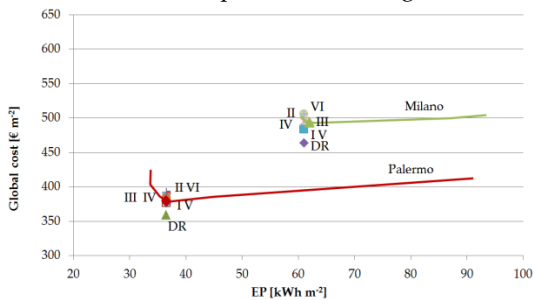


Fig. 2 – Residential Cost Optimal values for different economic scenarios

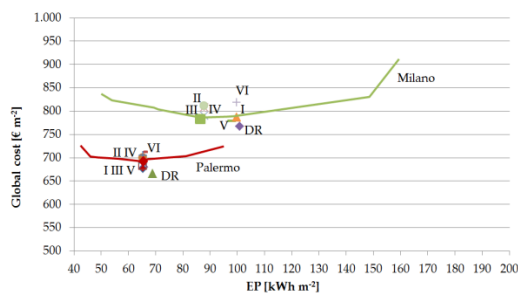


Fig. 3 – Office Cost Optimal values for different economic scenarios

Figs. 4-5 show the optimal global costs for the different economic scenarios mentioned above, for residential and office respectively, where “MI” stands for Milano and “PA” for Palermo. The energy costs are subdivided in investment, energy and operating & maintenance. With regard to the residential buildings, the investment costs are generally twice the amount of the energy costs and of the operating & maintenance costs; as the energy efficiency measures and levels do not change with the different economic scenarios, the investment costs remain fixed, while the operating & maintenance costs only change when the discount rate varies. In addition, the energy costs vary with the energy scenarios, but the highest deviation is lower than 25 € m⁻² in Milano and 15 € m⁻² in Palermo.

Concerning the offices, the energy costs are comparable with respect to the investment costs: in terms of energy costs the highest deviation corresponds to 50 € m⁻² either for Milano (between III and VI scenarios) and Palermo (between DR and II scenarios), while deviations in investment costs never exceed the 15 € m⁻².

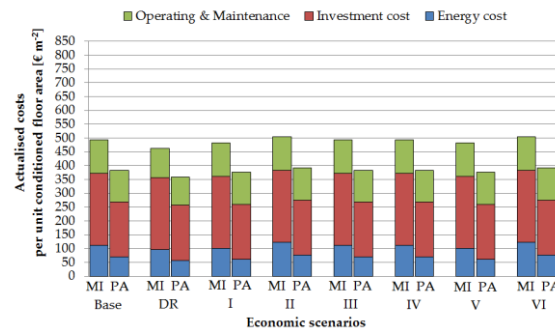


Fig. 4 – Residential Cost Optimal actualized costs for different economic scenarios

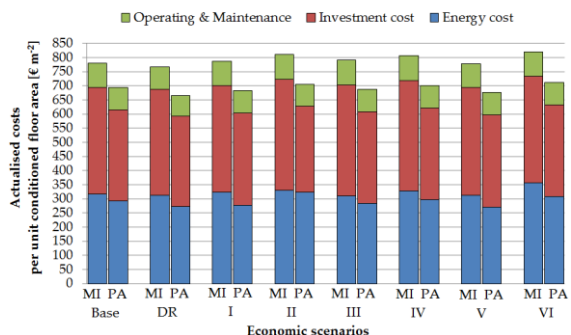


Fig. 5 – Office Cost Optimal actualized costs for different economic scenarios

4. Conclusion

In the present article different economic scenarios have been investigated in order to determine the influence of the discount rate and of the energy price trend on the cost optimal packages of EEMs and on the corresponding levels of building EP.

For some reference buildings different in use and location, it has been verified that the optimal level of energy efficiency usually corresponds to a set of design parameters consistent with the requirements fixed by the current legislation (Italian Government, 2005), which mainly concern the insulation-value of the vertical building enclosures.

Through the application of a sensitivity analysis in the cost optimisation procedure, the robustness of the optimal solutions of EEMs packages has been demonstrated, as both the discount rate and the energy price development variations have a weak influence on the cost optimal level of building energy performance and on the choice of the optimal energy efficiency measures (EEMs) package. This result is especially true in the case of residential buildings, as the weight of the investment costs is twice the amount of the energy costs and of the operating & maintenance costs.

A future analysis will consist in conducting additional sensitivity analyses for other cost drivers as identified in the calculation, for instance the initial investment cost of the building components. In this regard, a range of variation should be defined for each investment cost and the costs differentiated by climatic zone.

5. Acknowledgement

This work has been carried out within a cooperation agreement with ENEA (*Italian National agency for new technologies, Energy and sustainable economic development*) concerning the “*Development and updating of the cost optimal methodology for assessing the compliance of national energy standards according to Directive 2010/31/EU*”.

6. Nomenclature

Symbols

A	area (m ²)
C	cost (€)
COP	coefficient of performance (-)
EEM	energy efficiency measure
EEO	energy efficiency option
EER	energy efficiency ratio (-)
EP	energy performance (kWh m ⁻²)
F, R	factor (-)
r	rate (-)
U	thermal transmittance (Wm ⁻² K ⁻¹)
V	volume (m ³)
Val	value (€)
W	power (W)
η	efficiency (-)
τ	transmission coefficient (-)

Subscripts/Superscripts

a	annual
C	constant (illuminance)
coll	solar collectors
D	daylight
disc	discount
env	envelope
F	final
f	floor
fl,lw	lower floor
fl,up	upper floor
g	global, gross
gn	generation (system)
H	heating
I	investment
lgt	lighting
n	net
O	occupancy
PV	photovoltaic (system)
rg	control (system)
ru	heat recovery unit
sh	shading
W	domestic hot water
w	window
wl	wall (opaque)

References

- Ascione, F., N. Bianco, C. De Stasio, G. M. Mauro, and G. P. Vanoli. 2015. "A new methodology for cost-optimal analysis by means of the multi-objective optimisation of building energy performance". *Energy and Buildings* 88: 78-90. doi: 10.1016/j.enbuild.2014.11.058.
- Brandão de Vasconcelos, A., M. Duarte Pinheiro, A. Manso, and A. Cabaço. 2015. "A Portuguese approach to define reference buildings for cost-optimal methodologies". *Applied Energy* 140: 316-328. doi: 10.1016/j.apenergy.2014.11.035.
- Corrado, Vincenzo, Ilaria Ballarini, Stefano Corgnati, and Novella Talà. 2011. *Building Typology Brochure – Italy. Fascicolo sulla Tipologia Edilizia Italiana*. Torino: Politecnico di Torino.
- Corrado, Vincenzo, Ilaria Ballarini, and Simona Paduos. 2013. *Sviluppo della metodologia comparativa cost-optimal secondo Direttiva 2010/31/UE*. ENEA RdS/2013/144.
- Corrado, V., I. Ballarini, and S. Paduos. 2014. "Assessment of cost-optimal energy performance requirements for the Italian residential building stock" *Energy Procedia* 45: 443-452. doi: 10.1016/j.egypro.2014.01.048.
- European Committee for Standardization. 2007. EN 15459. Energy performance of buildings - Economic evaluation procedure for energy systems in buildings.
- European Union. 2010. Directive 2010/31/EU of the European Parliament and of the Council of 19 May 2010 on the energy performance of buildings (recast). Official Journal of the European Union, 18 June 2010.
- European Union. 2012a. Commission Delegated Regulation (EU) No 244/2012 of 16 January 2012 supplementing Directive 2010/31/EU of the European Parliament and of the Council. Official Journal of the European Union, 21 March 2012.
- European Union. 2012b. Guidelines accompanying Commission Delegated Regulation (EU) No 244/2012 of 16 January 2012 supplementing Directive 2010/31/EU of the European Parliament and of the Council. Official Journal of the European Union, 19 April 2012.
- Hamdy, M., A. Hasan, and K. Siren. 2013. "A multi-stage optimization method for cost-optimal and nearly-zero-energy building solutions in line with the EPBD-recast 2010". *Energy and Buildings* 56:189-203. doi: 10.1016/j.enbuild.2012.08.023.
- Italian Government. 2005. Legislative Decree 19 August 2005, no. 192 (and subsequent modifications and additions), complying the European Directive 2002/91/EC on the energy performance of buildings.
- Italian Ministry of Economic Development. 2013. "Applicazione della metodologia di calcolo dei livelli ottimali in funzione dei costi per i requisiti minimi di prestazione energetica (Direttiva 2010/31/UE Art. 5)". Accessed December 2014. http://ec.europa.eu/energy/efficiency/buildings/doc/2013_it_cost-optimal_en.zip
- Italian Organisation for Standardisation (UNI). 2010-2014. UNI/TS 11300 (series). Energy performance of buildings.
- Margiotta, Francesca. 2010. *Metodologia per la determinazione delle caratteristiche strutturali ed impiantistiche di "Edifici Tipo" del Parco Edilizio Nazionale ad uso ufficio e Valutazione del Potenziale di Risparmio energetico sulla base della fattibilità degli interventi di riqualificazione Energetica*. ENEA RdS/2010/197.

Energy building retrofitting of a multifamily house: a case study

Chiara Dipasquale – Eurac research Institute of Renewable Energy – chiara.dipasquale@eurac.edu

Roberto Fedrizzi – Eurac research Institute of Renewable Energy – roberto.fedrizzi@eurac.edu

Diego Bertesina – Manens-Tifs s.p.a. - verona@manens-tifs.it

Alessandro Bellini – Eurac research Institute of Renewable Energy –alessandro.bellini@eurac.edu

Abstract

The residential sector contributes largely to energy consumption in Europe: around 40% of the EU energy use (RHC-ETP, 2011).

For a massive reduction of the energy consumption in the European residential sector, a common practice is the retrofitting of existing buildings. In this context, multifamily houses (MFHs) are considered to be easier to retrofit, partly because their exteriors are more uniform than single-family houses' - which makes external insulation and glazing replacement easier to install - and partly because each building contains multiple dwellings - therefore a single action can affect more living area.

The purpose of this paper is to report on the design phase of a multifamily house located in Madrid, Spain. The refurbishment concerns the installation of both passive and active solutions. In particular, transmissions through the envelope are reduced by the addition of an insulation layer and new windows. DHW production, space heating and cooling are guaranteed by an air-to-water heat pump. Heating demand and Domestic Hot Water (DHW) production are also partially covered by solar thermal panels installed on the parapet of the building.

The impact of the retrofitting measures on the energy consumption have been assessed starting from energy audit data, going through modelling and simulating the building's envelope before and after the retrofit, and finally analysing the building and energy plant together.

The simulation work shows a set of integrated measures suitable to achieve a primary energy consumption for heating, cooling and domestic hot water, lower than 50 kWh/m²y.

1. Introduction

The total residential floor area in the 27 European countries is approximately 17.6 billion m². Of this

15.1 billion m² is estimated to be heated. For the sake of simplicity, the residential building stock can be divided in two main typologies: single-family house (SFH), with a single dwelling unit within its own building and multi-family house (MFH) where a dwelling is in a multi-occupancy building. SFHs and MFHs distribution is different across the Europe. Denmark, Ireland, the Netherlands and the United Kingdom have the highest proportions of SFHs (all above 70%) whereas Estonia, Italy, Latvia and Spain have the lowest proportions of SFHs (all below 40%). The age distribution of the residential building stock varies from country to country, but the age of both single and multi-family houses is broadly similar across Europe with a growth rate peak between the 1950s and 1970s. The rate of new builds has been slowing since the 1970s, with a strong reduction occurring after 2000. Spain had higher than average construction during 1971-1980 and after 2000.

For a massive reduction of the energy consumption in the European residential sector, a great retrofitting of existing buildings is needed. In this context, MFHs are often thought to be more cost effective targets for retrofit, because of the consistent architecture and economies of scale on a large block of apartments. Moreover, they are considered to be easier to retrofit because their exteriors are more uniform than single-family houses - which makes external insulation or replacement glazing easier to install (Birchall S. et al, 2014).

In this sense, the purpose of this work is to present the renovation process applied to a demo case, which uses non-invasive techniques and aims to reduce the total amount of energy consumption.

The methodology foresees the use of numerical models to assess the actual building demands and the assessed energy savings.

The building presented in the following is a MFH of the 1960s located in Madrid. In line with the above observations, this kind of building can be considered as representative of a big portion of the Spanish residential building stock.

The building is located in the suburbs of Madrid and it is composed of two linear blocks for a total of twenty dwellings (50 m² living area each) on five floors. In this study, only one of the two has been analysed (in the red circle in Fig.1).



Fig. 1 – North façade of the demo case—in the red circle the analysed building

The refurbishment concerns the installation of both passive and active solutions. In particular, transmissions through the envelope are reduced by the addition of an insulation layer and new low transmittance windows. DHW production, space heating and cooling are guaranteed by an air-to-water heat pump. Heating demand and Domestic Hot Water (DHW) production are also partially covered by solar thermal panels installed on the parapet of the building.

2. Methodology

The impact of the retrofitting measures on the energy consumption have been assessed through the following steps:

- 1) building energy audit for the definition of the building characteristics and consumptions;
- 2) modelling of the existing building's envelope and calculation of the building demands;

3) modelling of the renovated building's envelope and assessment of the building demands;

4) modelling of the thermal plant and simulation of the whole system (building + energy system + control strategies);

5) planning of the renovated case by using non-invasive techniques, allowing the owners to live in the building while the renovation takes place.

Simulations have been run in the dynamic environment of TRNSYS Simulation Studio (Klein S.A., 2009), while the geometry of the building has been developed in Google SketchUp and set up in TRNBuild.

2.1 Building energy audit

The energy audit concerns building characteristics, uses and energy consumption. Information comes from technicians and surveys distributed through the tenants. Daily and yearly profiles have been defined for the occupation and electric use, distinguishing between workdays and weekends. Some examples of these schedules are showed in Fig. 2 and Fig. 3.

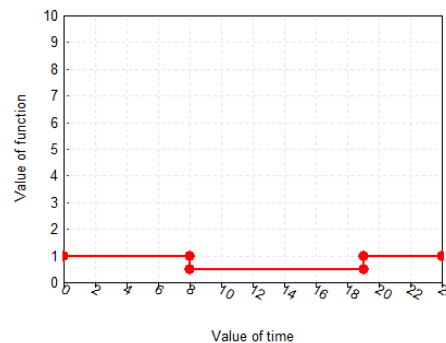


Fig. 2 – Schedule of occupancy during the weekdays

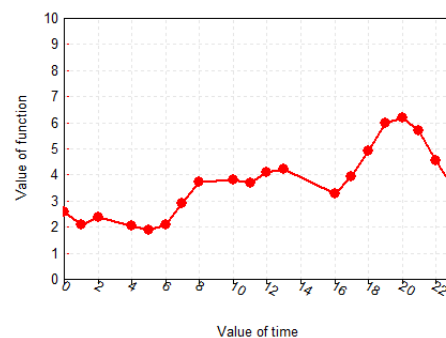


Fig. 3 – Use of electric devices during the weekdays

Thermal characteristics have been calculated for the envelope elements: external walls, roof, ground

floor, windows, internal partitions, adjacent walls (towards the second part of the building block). Thickness and heat transfer coefficient (U_{value}) of opaque and glazed surfaces are reported in Table 1 and 2.

Table 1 – Thermal characteristics of the envelope

Wall	Thickness [m]	Heat transfer coefficient (U_{value}) [W/m ² K]
External wall 1	0.35	1.51
External wall 2	0.32	1.57
Roof	0.68	1.51
Ground floor	0.27	2.19
Adjacent wall	0.25	1.54

Table 2 – Window characteristics

Window	$U_{value_glazing}$ [W/m ² K]	U_{value_frame} [W/m ² K]	$g_{value_glazing}$ [-]
Window single glazed	6.11	5.88	0.81

The following figures (Fig.4 and Fig. 5) show the wall construction for the external wall and ground floor. The latter has an aerated cavity below the concrete layer. In the numerical model, the air cavity has been not modelled; however, the outer surface bounds with a temperature that takes into account the presence of it (UNI EN 13370, 2008).



Fig. 4 – Drawing of the external wall construction



Fig. 5 – Drawing of the ground floor construction

The existing case does not have any insulation for the external surfaces. For more detail, please refer to D7.1b P15 Energy Audit Madrid (García J. et al., 2014).

2.2 Building - existing case

The model of the existing envelope has been defined following characteristics and boundary conditions defined in the Energy Audit. For some physical and geometrical features, a parametric analysis has been carried out in order to investigate the effect they have on the building loads assessment and simulation run time. For the sake of relevance, only the results of the study above mentioned are reported. The whole work can be found in (García J. et al., 2014 p. 40-53).

First of all, as this model is used afterwards in an integrated environment, where energy and distribution systems and control strategy are implemented together, it has been designed to limit the computational effort.

Starting from a first model elaborated using a common best practice approach (IBPSA-USA, 2012), variations on the definition of the number of floors or zones, thermal capacitance, internal walls, internal or external surface measures and thermal bridges have been applied one per time.

The first investigation has involved the definition of the optimal number of zones for truthful results and limited computational effort. A good trade-off between developing one thermal zone per room rather than one per floor is to create one zone per apartment or per orientation. This last case, in fact, takes into account also the distribution of temperature inside the apartment due to a different exposition (see Fig.6).

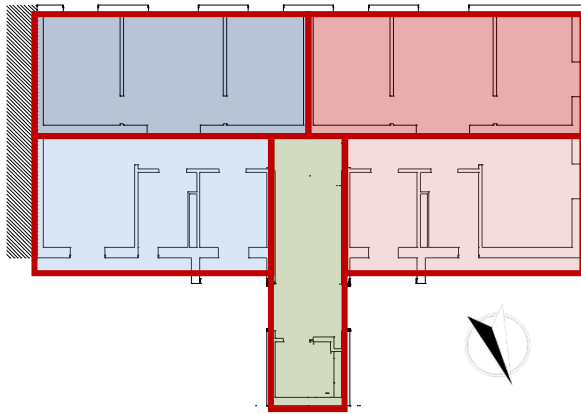


Fig. 6 – Thermal zoning of a typical floor

In case of buildings with more than 3 floors, a reasonable simplification consists of relating in-between floor behaviour to a unique intermediate floor. Loads and demands of this storey are then accounted also for the others.

Considerations have been carried out also on the thermal air capacitance value: it plays a role mainly in the distribution of internal temperature through the day; in fact it does not influence loads neither demands assessment. As a consequence, the thermal air capacitance has an effect on the comfort levels: models with higher thermal mass have smoother temperature profiles with respect to models with low thermal capacitance up to reduce the peak temperature of around 1°C, and to shift the loads from 1 to 5 hours.

The definition of the building geometry has been delineated in the SketchUp tool. For the sake of simplicity, the plant of the renovated case has been developed and used for the existing case too, in order to compare results referred to the same volume. The definition of the geometry with this tool entails a-dimensional surfaces. Consequently, these can be delineated by means of internal edge, external edge or centreline measures.

The surface area influences transmission losses, therefore to assess the approximation due to the use of one of the above measurements, comparisons on the heating and cooling demands have been carried out. When internal edges or external edges are used, geometrical thermal bridges have been modelled, too. The linear transmission coefficient Ψ can be calculated by default values from norms or by software based on Finite Elements Method. In the first case, a high

uncertainty can occur; in the second case, expertise and time consuming in the definition phase can be needed. In this sense, a simplification, which however maintains a real behaviour, consists of using the centreline measures.

In those cases where more than one thermal zone is modelled for each dwelling, an air coupling of adjacent rooms shall be accounted for. Simulations had shown that the convective air coupling between zones has not a relevant influence on building loads and energy demands, whereas it affects internal temperature distribution. The most evident effect is that a more homogeneous temperature distribution occurs within the same flat, but simulation runtime can triple. Air coupling is therefore useful when a thermal comfort study is carried out, but for maintaining limited computational effort, it can be neglected when only demands are to be assessed.

In light of the above considerations, the geometrical model of the actual building has been defined with centreline measures; one zone per orientation per dwelling; first, last and an intermediate floor accounting for the all in-between floors. In this first phase, no coupling has been used and thermal capacitance of air plus internal walls has been fixed for each zone.

Other boundary conditions implemented in the model and used for both existing and renovated case are shown in the Table 3.

Table 3 – Boundary conditions used in the building model

Parameter	Units	Value
Electrical gains	[W/m ²]	1.44
Heating set temperature	[°C]	20
Cooling set temperature	[°C]	25
Infiltration rate	[vol/hr]	0.15
Ventilation rate	[vol/hr]	0.30

Using the above explained building model and boundary conditions, simulation showed the results seen in the following Table 4.

Table 4– Heating and cooling demands and peak loads for the ground floor, second floor and last floor, referred to the actual case

Zone	Heat demand	Cool demand	Heat peak power	Cool peak power
	[kWh/m ² y]	[kWh/m ² y]	[W/m ²]	[W/m ²]
GF	151	18	72	38
2F	93	30	55	44
4F	151	35	85	51
BUI	116	29	85	51

To date, each dwelling has its own and peculiar thermal system installed. DHW and heating are provided to all the dwellings, while just three of them are provided with cooling. The energy resource varies for each dwelling: the most common for DHW is natural gas; for heating, it varies between natural gas and electricity; electricity is also used for to run mono-split units. Some dwellings have butane gas bottles for DHW and heating. Those dwellings with gas boiler for heating have hot water radiators for the distribution system, while the rest of them are provided with independent electric radiators or butane heaters.

Due to the complexity of the heating systems, generation and distribution systems have not modelled for the existing case. For the sake of simplicity, energy consumption has been calculated from demands.

2.3 Building - renovated case

In general, renovation measures on existing buildings can involve both passive and active solutions. On the one hand, the attempt is to reduce demands and loads, on the other the improvement of heating and cooling systems efficiency is focused. In the demo case, both solutions are foreseen.

The high transmission losses due to high transmittance values through external walls, roof and ground floor are reduced thanks to the installation of an insulation layer of 8 (on the

external walls) and 6 cm (on the roof and ground floor). The existing roof consists of an air cavity of 40 cm above the last ceiling, closed by a system of small vaults and covered by ceramics and a waterproof layer. During the renovation work, the air cavity is substituted with the insulation layer, and is covered by ceramics.

In this way, the building air-tightness has also been improved. Moreover, new windows with low emissivity are installed externally, in addition to the existent ones, in order to reduce the impact of the installation work on the tenants.

The envelope model of the renovated case is based on the existing case, with the addition of the retrofit measures (insulation and windows).

The implementation of these passive solutions has the effect of a strong reduction in the heating demand, of around 83%, and a slighter decrease in cooling demands of around 16%. Due to the higher thermal capacity of the building after the renovation, the decrease in cooling demand is lower than the one for the heating, despite the use of external shadings.

Looking at the peak loads, the maximum heating load decreases by 66% and the cooling load by 47% (see Table 5). Despite the small reduction of cooling demand in the renovated case, the reduction to almost 50% of the peak load implies a smaller installed chiller capacity.

Table 5 – Heating and cooling demands and peak loads for the ground floor (GF), second floor (2F) and last floor (4F), referred to the renovated case

	Heat Demand	Cool Demand	Heat peak power	Cool peak power
	[kWh/m ² y]	[kWh/m ² y]	[W/m ²]	[W/m ²]
GF	29	20	25	25
2F	14	25	20	24
4F	31	24	29	27
BUI	20	24	29	27

After the renovation, a centralized system covers the heating and domestic hot water preparation. Moreover, the new A/W heat pump of 15 kW

provides cooling to all dwellings. Solar collectors installed on the parapet, for a total of 28m², contribute to the heating and domestic hot water preparation.

A new low-temperature heating distribution system is installed and, for this purpose, radiant ceilings allow for a temperature under 30-35°C.

In addition, shading elements are foreseen to be installed onto the windows at the south and west oriented façade, in order to avoid overheating in summer.

In the renovation, piping is distributed outside the north façade, embedded in the insulation, in order to reduce the heat losses.

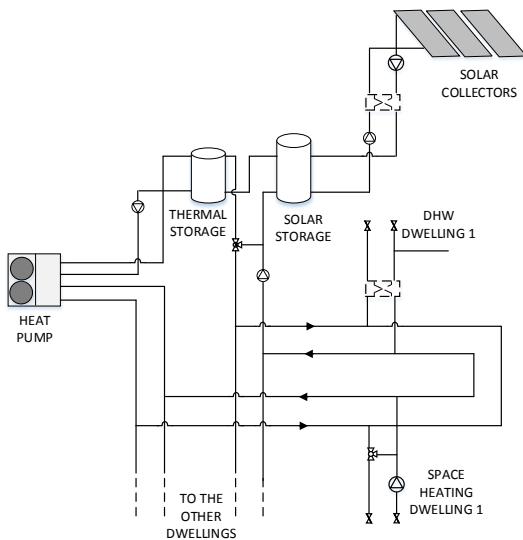


Fig. 7 – Sketch of the TRNSYS deck: building + generation and distribution system + control system

2.4 Simulation of building and energy system

As already mentioned, the building and system numerical models have been developed and simulated in the TRNSYS environment. The envelope model of the renovated case has been integrated with the heating and cooling system and relative control. Each element of the new heating and cooling system has been modelled and thermal and electric consumption calculated.

The TRNSYS deck includes all the hydronic and electronic components of the generation and distribution systems. In particular, type 832 (Haller M., 2013) is used for the 28 m² of flat plate solar collectors oriented to the south façade and with a

slope of 90°. The 15 kW heat pump is modelled with type 927; it reads a performance map, which gives thermal and electrical powers depending on the inlet temperatures and mass flows on the source and load sides. Solar collectors feed a 1000 l of stratified thermal storage; the latter charges another thermal storage of 500 l. The DHW preparation is therefore covered by solar energy and heat pump in case of too low temperature inside the smaller storage. Space heating can be provided directly by the heat pump or by solar energy through the second storage. The heat pump provides cooling during the summer season.

The profiles for the DHW demand have been generated for a number of inhabitants of the building using a stochastic model developed by researchers at Uppsala University (Widén et al., 2010). These profiles have a day-to-day variation over the whole year; they are also smoother and more realistic than an aggregate of only one repeated for all the apartments.

The distribution system consists of radiant ceilings. They are characterized by an aluminium structure with embedded copper pipes. The standard module is 1.2 x 2.4 x 0.02 m and they have been installed in order to partially cover the ceiling of each room.

The TRNSYS deck has been built gathering several “subdecks” which represent a technology or device. The subdecks used in this system are:

- WEATHER FILE with external conditions for Madrid (Meteonorm, 2013)
- FLAT PLATE COLLECTORS composed by the solar collectors type and pipes for the distribution system losses;
- STORAGE TANK for the three thermal storages;
- AIR-TO-WATER HEAT PUMP connected to a performance map and with an internal control to regulate the winter or summer working modes;
- RADIANT CEILINGS linked to each thermal zone of the building as wall gain;
- HYDRAULIC MODULE which contains pumps, valves and heat exchangers;
- MAIN CONTROL, which regulates the whole functioning of the system;
- BUILDING MODEL.

The main control regulates all the parts of the system in order to guarantee the thermal comfort inside the building and the DHW preparation. It receives information from all the subdecks and gives control signals to all the active components.

Table 6 – Heating and cooling demands calculated ideally and with the whole system (building + energy plant)

	Heating demand [kWh/m ² y]	Cooling demand [kWh/m ² y]
Ideally	20	24
Whole	21	31

Table 7 – Performance figures of the renovated building + energy plant system

	SF DHW [%]	SF heat [%]	SPF [kWh _{UE} /m ² y/ kWh _{FE} /m ² y]	PE [kWh/m ² y]
YEARLY	38%	15%	4,3	47

Simulations have been run following the requirements foreseen in the design and sizing phase. Further optimization of components size and control strategies are foreseen, but not included in this paper.

Table 6 compares the building demands for heating and cooling calculated ideally and with the modelled system. The temperature set points for heating and cooling in the ideally case have been fixed at 20 and 25°C respectively; while for the whole system, hysteresis between 19.5-20°C for winter and 24.5-25°C for summer have been defined. Due to the difference of the set points, differences on the Table 6 results comes up, especially for the summer case.

In line with the aim of the study to reach a total Primary Energy consumption of 50 kWh/m²y, it is interesting to have a look at Table 7. In particular, the renovated case shows a Solar Fraction (SF) (Malencovic I., 2012) of 15% for the heating and 38% for the yearly DHW production. With respect to the installed system, the low values of SF for the DHW preparation is due to the higher DHW consumption. An average of 2.4 people is usually

considered to live in a dwelling of 50 m². Besides in our case, there are some apartments where up to 5 people live, consequently there is a higher DHW demand.

The Seasonal Performance Factor (SPF) (defined in Malencovic I., 2012), that represents the useful energy compared to the final energy, amounts to 3.6 and 5.1 respectively in the winter and summer season. The high values of SPF are related to the decrease of the building demands and, above all, the efficient use of renewable sources (air and solar sources).

Finally, the total Primary Energy (PE) consumption for space heating, cooling and DHW production amounts to 47 kWh/m²y. For this calculation, a Primary Energy Factor (PEF) for the electricity of 2.461 has been used (IDEA, 2014).

2.5 Non-invasive techniques

In the demo case, the retrofit takes place together with some structural works for the whole building. This strategy allows reducing the costs for the renovation because coupled with other needed maintenance activities.

Passive solutions are mainly installed externally on the façade in order not to affect the daily-users' life. Piping has been, in fact, developed along the façade as well as the insulation. Existing windows are not replaced and new ones are installed externally.

With regard to the active solutions, heat pump, storages and solar collectors are installed on the roof and parapet. The only work within the dwelling consists in installing piping and radiant ceilings.

3. Conclusions

The significant energy consumption related to the residential sector suggests a massive refurbishment of the existing buildings all over the Europe needs to be undertaken. In this sense, a structured approach for the entire process may help to identify the best retrofitting solutions, assess the new building consumption and foresee those

interventions with low impact on the owners' daily life.

In this paper, a methodology for building refurbishment is applied on a multifamily house. An energy audit on the existing building gave all needed information on wall construction and internal gains.

The modelling of the existing building identifies the base case for further improvements on the building envelope and system performances.

A parametric analysis has been carried out in this work in order to create a building model which is reliable, but at the same time, manageable within the simulation of the whole system. The final building model therefore contains 3 out of 5 floors, where the in-between represents all the intermediate storeys. One zone per orientation (north-south) per dwelling has been modeled in order to take into account the different internal loads.

Renovation measures on the existing building consist of the addition of an insulation layer on the external walls, roof and ground floor and of new windows externally to the existing ones. These actions help to reduce the building heating demand by up to 83% and the cooling demand by 16%. The energy system described allows us to reach a total PE consumption of 47 kWh/m²y.

The implementation of these renovation measures shows building consumption can be drastically reduced with non-invasive techniques.

4. Acknowledgement

The research leading to these results has received funding from the European Union's Seventh Programme for research, technological development and demonstration under grant agreement No. 314461.

References

Birchall S., Wallis I., Churcher D., Pezzutto S., Fedrizzi R., Causse E., D2.1a Survey on the energy needs and architectural features of the EU building stock, iNSPiRe EU FP7 project 2014, www.inspirefp7.eu 2014.

García J., Romera D., Dipasquale C., Fedrizzi R., D'Antoni M., D7.1b Energy audit – Case study Madrid, iNSPiRe EU FP7 project 2014, www.inspirefp7.eu

Haller M., TRNSYS Type 832 v5.01 "Dynamic Collector Model by Bengt Perers" Updated Input-Output Reference. SPF Institut für Solartechnik and HSR University of Applied Research Rapperswil 2013

IBPSA-USA. Modeling Best Practice. Building Energy Modelling. IBPSA-USA, Rocky Mountain Institute, ASHRAE 2012. <http://bembook.ibpsa.us/>,

IDAE, Factores de Emisión de CO₂ y Coeficientes de Paso a Energía Primaria de Diferentes Fuentes de Energía Final Consumidas en el Sector Edificios en España, Ministerio de Industria, energía y turismo 2014

Klein S.A. et al. Trnsys 17. A transient simulation program. Solar Energy Laboratory, University of Wisconsin, Madison 2009

Malenkovic I., Definition of performance figures for solar and heat pump systems. Technical report 5.1.3, QAISt, Austrian Institute of Technology 2012

Meteonorm database, Version 5 and 7, 2013. <http://meteonorm.com/>.

RHC-ETP, "Common vision for the Renewable Heating and Cooling Sector in Europe", public report, 2011

UNI EN 13370: Thermal performance of buildings – Heat transfer via the ground – Calculation method, 2008

Widén, J., Wäckelgård, E. A high-resolution stochastic model of domestic activity patterns and electricity demand. Applied Energy 87 (2010) 1880-1892.

The use of biomass in the building renovation: a cost-optimal perspective analysis

Enrico De Angelis – Politecnico di Milano – enrico.deangelis@polimi.it

Giorgio Pansa – Politecnico di Milano – giorgio.pansa@polimi.it

Martina Cereda – Politecnico di Milano – martina.cereda@mail.polimi.it

Abstract

Reduction of energy consumption and the use of energy from renewable sources constitute important measures needed to reduce energy needs for existing buildings. Among all different options, the use of biomass could be an efficient strategy worthy of being explored during the refurbishment design. Although their use has been limited in the Italian legislation for environmental issues (particulate and fine dust emissions), the promising low primary energy conversion factor and their low cost (in comparison with other fossil fuels) allow us to investigate this option. A technical and economic analysis of different system refurbishment, framed in the cost-optimal context, has been addressed, in order to evaluate the feasibility of such interventions. Several case studies (single family house, apartment block, a school and a district made of several single and multi-family houses, served by a district heating system based on biomass) and different strategies have been analyzed:

- No interventions on building envelope (installation of a biomass heating system);
- Deep renovation of building envelope, with a “traditional” heating system (condensing boiler or heat pump);
- A standard renovation of the building envelope and the installation of a biomass heating system.

An analysis of the cost of intervention and operation (in terms of euro per kilowatt and euro per kilowatt-hour) is presented, so that it is possible to estimate what the cost-optimal levels are for the different case studies analyzed.

1. Introduction

The work presented is about the technical and economic analysis of biomass plants for the production of thermal energy, in the range of the

energetic refurbishment design of buildings with residential and scholastic uses. The starting point (De Angelis et. al., 2014) is the requalification of the building envelope, taken as the reference for the reduction of buildings’ energy consumption. The choice about the use of biomass represents a valid alternative to fossil fuels, especially if we consider the increasing need for the reduction of primary energy consumption and the use of energy from renewable sources. The aim of the work is to evaluate the technological feasibility and economic benefits of the intervention on heating plants, by the substitution of the original heat generator with a biomass one, in integration or in alternative with the requalification of the building envelope. We considered different interventions on the building envelope, the so-called ‘Deep Retrofit’ (Shnapp et. Al., 2013), which implies replacing existing systems in a building with similar ones that are of higher quality and performance, which leads to a better energy performance of an existing building. After the deep retrofit the buildings energy reduction is 50% or more compared to the existing building energy need.

1.1 Biomass

Biomass can be used as fuels in substitution of fossil fuels, for the production of thermal and electric energy. In this work solid biofuels have been considered, and in particular we focused on “pellets”, which are a product with a cylindrical form of 6 – 8 mm of diameter and 5 – 50 mm of length. This product is a result of a process of densification of the primary element, wood.

At the national level, the use of biofuels is rewarded with a low value of the primary energy conversion factor, which is equal to 0.3 (according

to Raccomandazione CTI R14/2013). At a local level there are some variations, for instance in Lombardy, where the primary energy conversion factor for biomass is equal to 0.5 (according to ddg. n. 5796/2009)

1.2 Diffusion of biomass plants

The diffusion of biomass plants in Italy has had the following trend, represented in Fig. 1 and Fig. 2. In the graph of Fig. 1 the Mm³ of solid wood equivalent (swe) consumed is presented. The bars of the graph, from left to right, represent the situation in 2010 and the forecasts for 2020, 2030.

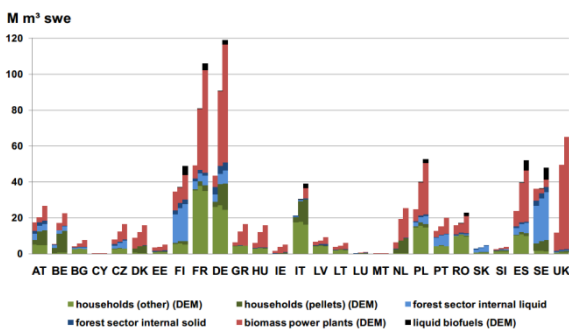


Fig. 1 – Current and future amounts of wood energy (by country and consumer sector) (Source: Mantau et. Al., 2010)

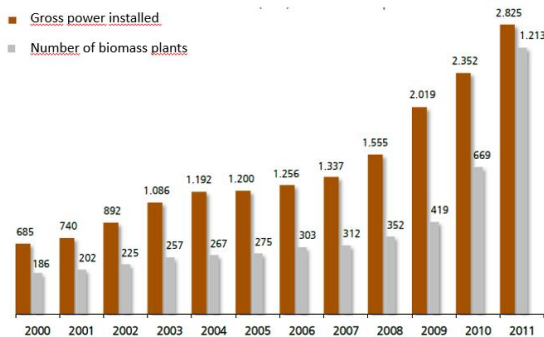


Fig. 2 – Evolution of the number of biomass plants and of the gross power installed in Italy (Source: GSE, 2012)

Data for Italy (Fig. 2) show that from 2000 to 2011 the number of plants increased every year by 19% on average, while for the power an average increase of 14% has been recorded. The last three years are particularly interesting: 2009 for the increase in power (around 500 MW); 2010 for the increase of 260 plants (mainly due to the inclusion, in the survey, of small-scale plants); 2011, for the significant increase both of the number (+544 plants) and of the power (+474 MW).

1.3 Environmental and primary energy issues

The use of wood biomass as fuel involves the emission of several pollutant elements, which can be potentially dangerous for people who come into contact with them (for example fine dust and ultra-fine dust, nitrogen oxide, dioxin). The quantity of emission depends on the fuel used. In Italy, there are some limits for the emissions from biomass plants in civil applications for the production of thermal energy (DLgs 152/2006). The limits presented in Table 1 are referred to a power included from 0.15 MW to 1 MW, for a one-hour operation of the plant and in the hardest conditions of operations, excluding the period of start, stops and breakdown.

At a local level, there could be different limits about the installation of biomass plants. In Lombardy there are some limitations (Dgr 735/2008) for the use of plants fueled with wood biomass in territories at more than 300 m of altitude, and in some other specific areas of the region. In these territories, if a building has other plants with different fuels, it cannot use biomass plants for the heating of the building in:

- a) Open chimneys;
- b) Closed chimneys, stoves and other devices fueled with wood biomass if they have been bought before 1990, and that has an efficiency lower than 63%. They also have to guarantee low emissions of carbon monoxide, that is $\leq 0.5\%$, with an oxygen standard of 13%.

It is not strictly precise to consider next to zero the balance of the carbon emissions in the atmosphere, because of the time it takes for cut woods to regrow, if compared with the demand for wood as biofuels. As a consequence, there is not the complete absorption of the carbon emissions due to the wood combustion. If we consider the increase in the demand for wood, this implies that more and more wood is taken from forests, and the consequent increase of time for the absorption of carbon. A valid way to avoid this phenomenon is the re-forestation or fertilization of other areas.

Table 1 – Upper limits for the emissions in biomass-based systems (Source Dlgs 152/2006)

Emission	Dlgs 152/2006	Proposal of recast
Total dust [mg/Nm ³]	100 (*)	30 (**)
Total organic carbon	-	-
Carbon monoxide [mg/Nm ³]	350	250
Ammoniac [mg/Nm ³]	-	5
Nitrogen oxide [mg/Nm ³]	500	300
Sulphur oxide [mg/Nm ³]	200	150

(*) For systems with nominal thermal power ranging from 35 kW to 150 kW, the emission value for the total dust is equal to 200 mg/Nm³ (*) or 100 mg/Nm³ (**)

1.4 Economic incentives for the use of biomass plants

For the installation of biomass plants there are some incentives for the production both of thermal and of electrical energy. In this work, we consider the ones about the production of thermal energy, with reference to the regulation in force at the end of 2014. Building renovation interventions can obtain the same incentives, with different rules (which are not stated in this paper).

CONTO TERMICO. The access to the Conto Termico is both for private and for public subjects, in a direct or indirect way by means of an ESCO. The facilitations consist of a subsidy, given over a period of 2 or 5 years (for interventions respectively with less than 35 kW of power and with a power included from 35 kW to 500 kW). The calculation of the amount of the subsidy is the following:

$$I_{a \text{ tot}} = P_n \cdot h_r \cdot C_i \cdot C_e \quad (1)$$

where:

$I_{a \text{ tot}}$ is the annual amount of the subsidy in €;

C_i is the coefficient linked to the promotion of the thermal energy produced, according to the installed technology;

P_n is the nominal thermal power of the plant;

h_r are the hour of operation, linked to the climatic zone considered;

C_e is the coefficient linked to the quantity of dust emissions, according to the installed technology.

For example, in climatic zone E and considering dust emissions (PPBT) lower than 10 mg/Nm³, the subsidy I_{tot} is equal to 8'032.5 € (for a 35 kW plant power) and 127'500 € (for a 500 kW plant power).

The subsidy (which cannot be higher than 65% of the entire amount of the cost of intervention, according to Dlgs 4/07/2014 n. 102) is given for the substitution of the heating generator with a biomass one, excluding the case where the original fuel is natural gas.

The requirements for obtaining the subsidy are:

- Installation of thermostatic valves (or analogue systems);
- Heating generator compliant with the class 5 of the UNI EN 303-5;
- Thermal efficiency (%) not lower than $87 + \log(P_n)$, where P_n is the nominal power of the heating generator;
- Respect of emission limits;
- Installation of a water tank;
- Use of pellet of class A1 or A2 (according to UNI EN 14961-2);
- Biennial maintenance of the thermal generator;
- Energy diagnosis and energy certification (mandatory only if the power is higher than 100 kW), for which is expected a subsidy.

65 % DEDUCTIONS. This incentive consists of a tax deduction of 65%, given over a period of 10 years, for interventions related to the increase in the energy efficiency of the building. To obtain this incentive, it is necessary to fulfill the following requirements:

- Respect the limit value of the energy performance indicator, for heating (DM 11/3/2008);
- Heating generator efficiency greater than 85 %;
- Thermal transmittance of windows lower than 1.8 W/(m²K), for the climatic zone E.

The maximum deduction is equal to € 100,000.

From 2015 it is possible to obtain an incentive (with a maximum deduction equal to €30,000) even for

the case of substitution of the existing heat generator with a biomass one.

50% DEDUCTIONS. This facilitation consists in a tax deduction of 50%, given over a period of 10 years, without the requirements existing for the 65% deduction. The maximum deduction is €48,000.

2. The economic model

The economic analysis has been made evaluating the global cost. The global cost is defined (according to EU Regulation 244/2012) in the following way:

$$C_g(\tau) = C_I + \sum_j \left[\sum_{i=1}^{\tau} (C_{a,i}(j) \times R_d(i)) - V_{f,\tau}(j) \right]$$

Where:

- τ is the period of the calculation;
- $C_g(\tau)$ is the global cost (referred to the starting year τ_0) in the period of calculation;
- C_I is the initial cost of the investment, for the measure or for the set of measures j ;
- $C_{a,i}(f)$ is the annual cost during the year i , for the measure or for the set of measures j ;
- $R_d(i)$ is the discount factor for the year i , based on the discount rate r ;
- $V_{f,\tau}(j)$ is the remaining value of the measure or of a set of measures j , at the end of the period of calculation (actualized at the starting year τ_0). In this work the remaining value hasn't been considered.

The global costs have been estimated on the base of the following hypothesis:

- Cost of gas: 0.85 €/m³;
- Lower Heating Value of gas: 9.56 kWh/m³;
- Annual increase of the cost of gas: 5% (nominal value);
- Annual increase of the cost of pellet: 2% (nominal value);
- Actualization rate: 5% without inflation (nominal value) and 2.94% with inflation del 2% (real value);
- Efficiency of the original heating generator: 85% (90% in the school);

- Efficiency of the biomass heating generator: 93%;
- VAT: 10% for biomass plants, 22% in other cases.

COST OF PELLETS

For pellets in sacks, €4.30 for a 15 kg sack (287 €/t). For the unpackaged pellet delivered by a tanker, costs are represented in the following graph.

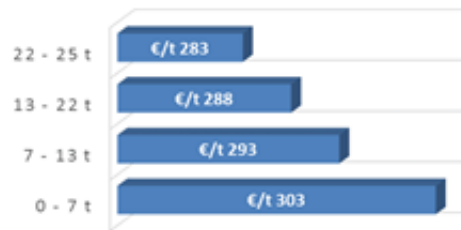


Fig. 3 – Cost of unpackaged pellet delivered by a tanker, transport distance 20 – 30 km. Source: average values from different quotations.

COST OF MAINTENANCE

As regards the maintenance, the cost of ordinary maintenance (emission test, annual controls) has been considered, but not for extraordinary maintenance, such as the necessity of substitution, in future, of the components of plants.

Also for the building envelope, the cost of maintenance, such as the painting of the façade, has not been considered. For the maintenance of the plants, costs (for each year) are represented in Fig. 4. The graph considers the interventions of ordinary and extraordinary maintenance of the plants. In this work we only considered the ordinary ones, represented in the table 2.



Fig. 4 – Yearly cost of the maintenance for plants with different fuels (Source: Francescato et al., 2009).

Table 2 – Costs of ordinary interventions, assumed in the calculation.

Power	Interventions	Cost
8 kW – 36 kW	Annual cleaning by a specialist	€300
50 kW – 160 kW	Annual cleaning and 1 – 2 periodical cleans	€450

ELECTRIC ENERGY CONSUMPTION

Regarding the consumption of electrical energy, we considered the following costs: 107 €/year for plants of 35 kW of power or less and 179 €/year for plants with more than 35 kW of power.



Fig. 5 – Cost of the consumption on electrical energy for plants with different fuels (Source: Francescato et al., 2009).

SET-UP COSTS

For the put-in-service of the intervention, costs are the following ones.

Table 3 – Set-up costs for different plants, assumed in the calculation (Source: Hoval, 2014)

Intervention	Set-up costs
Plants with a power included between 8 kW and 36 kW	€320
Plants with a power included between 50 kW and 160 kW	€420
Heat exchangers of the district heating system	€90 each

Following costs (installation and other costs) have been derived from an analysis of different quotations.

INSTALLATION COSTS

For plants with less than 35 kW of power, the cost of installation has been considered 7% of the plant components' costs, while for plants with more than 35 kW of power 12% has been considered.

OTHER COSTS

- Certificate for the Prevention of Fire, plants with power > 116 kW: €2,000; plants with power < 116 kW: €1,000;
- Procedure of control and test made by ISPESL, for plants with power > 35 kW: €500;
- Energy certification: €300 for mono-familiar residences, €600 for the block of flats and €700 for the school;
- Energy diagnosis: €1,500 (considered only for power > 100 kW).
- Design calculation: €450 for plants with power < 116 kW and €950 for plants with power > 116 kW.

For the substitution of the original heat generator with a condensing one, the costs considered are:

- €1,500 for the generator;
- Maintenance: 50 €/year for the annual control and other 50 €/year for the biennial emission test;
- Costs for the consumption of electrical energy and other costs (certification, procedures) equal to the case of biomass plants.

2.1 Plant layouts

In the following graphs are presented the layout of the solutions designed for the heating station and the one of the heat exchangers for the district heating system case.

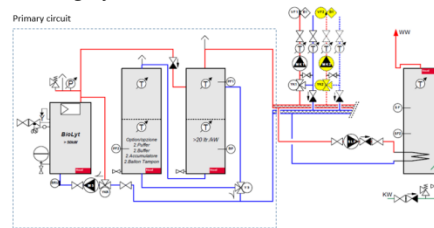


Fig. 6 – Layout of a biomass plant with a single generator and a single tank

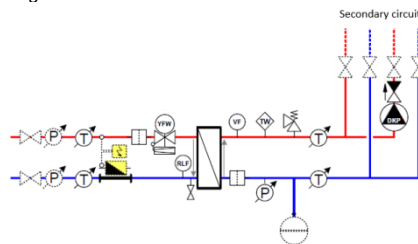


Fig. 7 – Layout of the heat exchangers for the district heating system

The strategy is to intervene on the original heating plants by the substitution of the components of the primary circuit: one or more heating generator fueled by biomass, one or more tanks and the other additional components and valves. These elements constitute the primary circuit, connected to the secondary one, made by the heating circuit and the one for the production of domestic hot water. The substitution of the boiler of the DHW and of the flue is also envisaged.

It is possible to consider also different solutions for the pellet loading:

- Manual loading, for low energy consumption (i.e. a single residence);
- Automatic loading from a textile silo,
- Automatic loading from a dedicated local, for high energy consumption.

2.2 DHW and tank

The need of domestic hot water DHW has been evaluated with a statistic approach, based on a normal level of comfort of the residences, considering a contemporaneity of use of DHW depending on the number of residences served. For the district, the sum of the single needs of DHW has been considered, considering that each building is provided with its own boiler.

Table 4 – DHW needs, as designed.

Case study	N° of residences	l/10min	l/h	l/day
Single residence	1	143	286	343
Block of flats	24	765	1886	5957
District	35	5'005	10'010	12'005

The calculation of the capacity of the tank depends on the power offered by the heat generator: 20 l/kW if the power offered is near to the requested one (until 95%), and 25 l/kW or 30 l/kW if the offered one is less than 90% and 85% of the requested one respectively.

2.3 Cost curves

Following can be seen the curves of costs for the principal and secondary components of the plant.

Those curves are obtained from the analysis of quotation and price list of Hoval (Hoval, 2014).

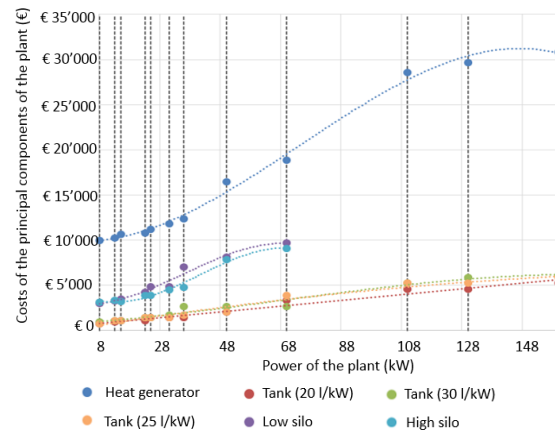


Fig. 8 – Costs of the principal elements of the biomass plants

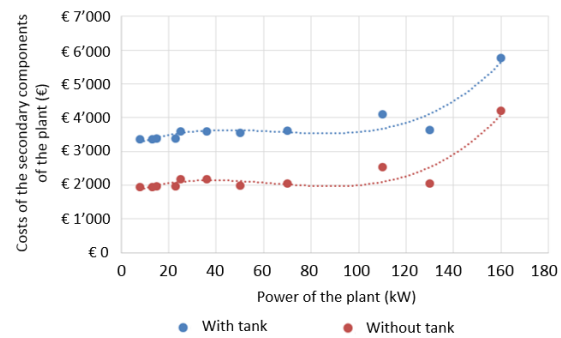


Fig. 9 – Costs of the secondary elements of the biomass plants

3. The case studies

Four different case studies have been analyzed in this work: a portion of a detached house, a block of flats, a school building and a neighborhood (consisting of 40 single and detached houses). For the calculation of energy savings (during the winter season) the quasi-steady state calculation method (ISO 13790) has been used. The values of real energy consumption have been acquired from bills, if available. For every case study a parameter (called *scale factor*) has been derived which represents the ratio between the real consumption of energy and the calculated one at the actual status, so it has been possible to predict the energy consumption for the different scenarios of intervention, scaling the energy savings obtained from the calculation model with the scale factor obtained in the reference case.

The analysis of convenience has been made evaluating the global cost, considering three different duration of time: 10, 20 and 30 years. The different scenarios of interventions considered are the following:

- CASE 0: no intervention, reference case;
- CASE 1: biomass plant in substitution of the existing one;
- CASE 2: deep retrofit of the envelope; CASE 2A: (in substitution to the CASE 2) condensing heat generator in substitution of the existing one (for the single residence and for the district case);
- CASE 3: deep retrofit of the building envelope and biomass plant in substitution of the existing one;
- CASE 4: retrofit of the envelope; CASE 4A: (in alternative to the CASE 4) retrofit of the building envelope and condensing heat generator in substitution of the existing one (for the single residence and for the district case).
- CASE 5: retrofit of the building envelope and biomass plant in substitution of the existing one.

For the case of the district there we considered:

- CASE 6: district heating system and deep retrofit of the building envelope.



Fig. 11 – (above) NW view of the building (single unit of a detached house) and (below) SE view of the building (block of flats building)

A graph has been built where the global cost is compared to the EP_H of the scenarios, in order to

evaluate the convenience (represented by the slope of the lines) of the interventions and the potential of renovation (represented by the difference, in terms of global costs, between the actual status and the corresponding scenario).

Table 5 – Main data of analyzed buildings (A: single family house, B: block of flats building, C: school building)

	A	B	C
Net floor surface [m ²]	107	2'046	3'071
Net volume [m ³]	318	5'871	10'450
Gross floor surface [m ²]	129	2'444	3'695
Gross volume [m ³]	424	7'984	14'060
Envelope surface [m ²]	375	3686	5'428
S/V [m ⁻¹]	0.88	0.46	0.39
EP_H [kWh/(m ² year)]	197.8	246.4	219.0
Scale factor	0.46	0.70	0.75
EPH lim. [kWh/(m ² year)]	96.28	60.57	-
EP _H , lim for 65 % incentives [kWh/(m ² year)]	78.01	49.05	-

4. Results and Conclusions

From the analysis of the case studies it emerges that the installation of a biomass plant in the building renovation is convenient when the power demand and the consumption of energy are high, such as in the case of the block of flats and school buildings.

In the case of the **single house**, it is evident that the most convenient intervention is represented by the substitution of the original heat generator with a condensing one (in each duration period), thanks to the low economic investment and to the higher efficiency of the new heat generator. In this case, the achieved reduction of energy consumption (and primary energy for heating) is equal to 23 %. If we compare the existing scenario to the '*deep retrofit + biomass*' scenario the global cost at 10 year redoubles. The intervention on the building envelope is more convenient than the biomass scenario (this is particularly true if a silo for the storage of pellets is installed, dashed points in the

figure 12.a). The scenario ‘*deep retrofit*’ involves a higher global cost but allows the reduction of primary energy consumptions by 77 %.

The scenario ‘*biomass*’ allows for a reduction of (real) energy consumptions of 9 %.

Considering the case of the block of flats, the “*biomass*” scenario allows for a reduction of (real) energy consumptions of 9% and a reduction of the global cost of 32% over 10 years. In the scenario “*deep retrofit*” the primary energy consumption reduction is equal to 74% and the global cost reduction in 30 years is equal to 61%. In the case of “*deep retrofit and biomass*” the global cost reduction in 30 years is equal to 74%.

Further, attention focused on a neighborhood, made of 40 buildings, which are served by a district heating system, fueled by biomass, after the deep retrofit of the envelope. The buildings are the ones analyzed in the first case study. Five buildings have already been renovated and therefore are not considered in the calculation. As a simplification, average data have been represented and used. It has to be pointed out that usually the users have to pay the duty for the connection (this aspect is not considered in this work); in addition, usually the realization of the plant is in charge of an ESCO. The hypothesis of this work is that the cost for the realization of the plant is divided among the users. It emerges that the cost is nearly the same of the global cost for the realization of a single biomass plant for each residence. As a consequence, the global cost for the district heating system scenario (after the deep retrofit of buildings) is almost the same of the global cost for the “*deep retrofit and biomass*” scenario (where a biomass plant has been considered for each residential unit).

Finally, costs of system intervention (with biomass heating generator) have been represented in the following graph, considering the nominal power of the system. There is an elevated cost for the 13 kW plant, equal to 1,700 €/kW. This cost decreases to 370 €/kW for the 290 kW plant. There is an increase in cost moving from 110 kW to 140 kW, since there is the need to use two heating generators in the second case. It is evident (see Fig. 8) that the cost of the heat generator weights on the final cost in a higher way compared to the other plant

components. This fact can be observed also for the 160 kW and 200 kW plants. We can finally observe that the cost of intervention for the deep retrofit of the envelope ranges from 270 €/m² to 210 €/m² (with reference to the heated floor area), respectively for a small building (single residence) and biggest buildings (block of flats and school). The addition of the biomass plant requires an increasing of costs ranging from 185 €/m² (small building) to 27 €/m² (biggest buildings).

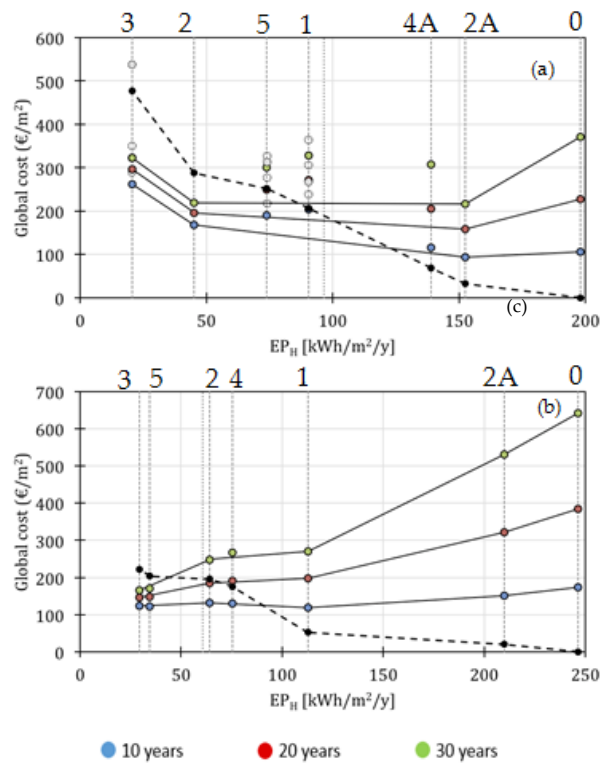


Fig. 12 – Results for the single unit of the detached house (a), and block of flats building (b). Values of the global cost (y-axis) vs EP_H (on x-axis). Dashed lines represent the cost of intervention at $\tau = 0$. Letters above the pictures represent the case studies, as listed in §.3.

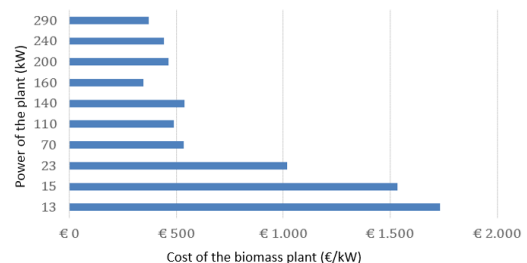


Fig. 13 – Cost of realization of a biomass plant (y-axis) vs the installed nominal power (x-axis).

Acknowledgement

The technical and economic data about the biomass plants have been collected through collaboration with Hoval srl. The authors would like to thank Eng. Barbieri and Eng. Perra for the useful discussions and valuable insights while carrying out the present work.

References

- Valter Francescato, Eliseo Antonini, Luca Zuccoli Bergomi; *“Manuale pratico di impianti termici a legna e cippato”*, 2009, AIEL – Associazione Italiana Energie Agroforestali
- Enrico De Angelis, Giorgio Pansa, Ermanno Serra, *“Research of economic sustainability of different energy refurbishment strategies for an apartment block building.”*, in Energy Procedia, Volume 48, 2014, Pages 1449–1458
- Mantau, U. et al. 2010, *“EUwood - Real potential for changes in growth and use of EU forests. Final report.”* Hamburg/Germany, June 2010. 160 p.
http://ec.europa.eu/energy/renewables/studies/doc/bioenergy/euwood_final_report.pdf
- Sophie Shnapp, Rosa Sitjà, Jens Laustsen; *“What is a deep renovation definition? – Technical report”*; 2013, Global Buildings Performance Network (GBPN)
http://www.gbpn.org/sites/default/files/08.DR_TechRep.low_.pdf
- COMMISSION DELEGATED REGULATION (EU) No 244/2012 of 16 January 2012 supplementing Directive 2010/31/EU of the European Parliament and of the Council on the energy performance of buildings by establishing a comparative methodology framework for calculating cost-optimal levels of minimum energy performance requirements for buildings and building elements
- Hoval, *“Manuale Tecnico Hoval”*, 2014.
- GSE, 2013, *“Incentivazione della produzione di energia termica da impianti a fonti rinnovabili ed interventi di efficienza energetica di piccole dimensioni. Regole applicative del D.M. 28.12.2012.”*
- GSE, 2012, *“Rapporto statistico 2011 Impianti a fonti rinnovabili”*

Passive cooling strategies in the refurbishment of Mediterranean buildings: simulation analysis of thermal mass and natural ventilation combination

Filippo Calcerano – PDTA Dept. Sapienza University, Rome, Italy – filippo.calcerano@gmail.com

Carlotta Cecchini – PDTA Dept. Sapienza University, Rome, Italy – carlotta.cecchini@gmail.com

Abstract

This paper aims to analyse in existing building refurbishments the complex relation between natural ventilation systems (single sided and cross ventilation, thermal chimney, evaporative cooling tower and earth pipes) and thermal inertia (medium-light and heavy) in the Mediterranean climate represented by three locations, Rome, Naples and Messina. Results show that, assuming equal comfort, the energy reduction potential is 67.7% with single-sided ventilation, 76.5% with cross ventilation, 30.2% with a thermal chimney, 20.1% with a cooling tower and 95.5% with earth pipes (where the consumption is due to the fan). In combination with the above-mentioned cooling strategies, the 30 cm thick wall maintains its role of thermal flywheel, while the 18 cm thick wall shows an excessive reactivity to climatic stresses, resulting in an average of 2.8% greater energy consumption. The scenario in Rome reaches the highest average energy consumption reduction for all the analysed systems (88.0%). Naples follows (83.1%) because of poor performance of the cool tower system (-23.4%), while the scenario in Messina is last (71.4%) because of the low thermal range that limits the efficiency of all the systems without the pre-treatment of the outside air (-37.4%).

1. Introduction

The existing building stock in Europe accounts for over 40% of the global demand of primary energy: buildings in Europe consume approximately 40% of the economy's incoming materials and are responsible for over 45% of the total amount of greenhouse gases produced (Ardente et al., 2011). With the increased air tightness of buildings,

Mechanical Ventilation (MV) has been responsible for the largest increase in energy consumption of the building sector in recent years (Kwon et al., 2013; Heiselberg, 2002). Considering that in Europe new constructions account for 1.5% of the building stock, there is great potential for reducing global energy consumption and mitigating the environmental impact through interventions on existing buildings (Economidou et al., 2011; Baek et al., 2012). Energy refurbishment consists of applying the most appropriate technology to achieve improved energy performance while maintaining satisfactory levels of service and indoor thermal comfort, under a operational constraints (Ma et al., 2012). For retrofits that exploit thermal inertia and natural ventilation, it is essential to analyse the complex relationship between the two bioclimatic control strategies and environmental, technological and design-specific factors (Braun, 2003).

2. Research framework

2.1 The Mediterranean Area and building regulations issue

The Mediterranean area defined in this study follows Köppen-Pinna climatic classification (Fig. 1). The definition refers to those territories directly facing the Mediterranean basin, because of their climatic specificity. The following subtypes are defined: subtropical (Csa prone to Bs), a humid tropical climate with very hot summers prone to arid climate with average temperature above 18°C, low and irregular rainfall; mild temperate (Csa), a

humid tropical climate with very hot and dry summers with average temperature of the hottest month above 22°C; sub-coastal (Csb prone to Cfb), a humid temperate climate with hot summers and average temperature of the hottest month below 22°C.



Fig. 1 - Reference areas of the Mediterranean basin

The Köppen-Pinna Mediterranean classification for Italy is compared with the national legal classification (only valid for winter conditions) that is largely employed as a reference in architectural practice and energy certification (Fig. 2).

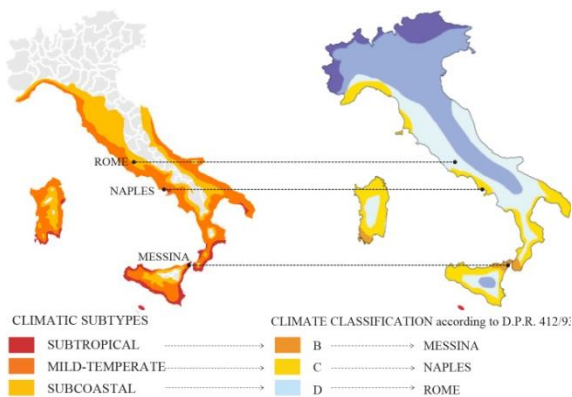


Fig. 2 - Reference location matching to the climatic subtype compared with climatic classification according to D.P.R. 412/93

The regulatory asymmetry between winter and summer conditions, with the emphasis on envelope insulation is already inside Directive 2002/91/EC and has produced with its implementation in southern Europe a number of side effects such as the reduction of the thermal mass of the buildings, a standardization of materials and technologies in stark contrast to the Mediterranean building tradition, with an overall reduction of the effectiveness of traditional passive cooling systems, based on thermal mass, air permeability and natural ventilation (D’Orazio et al., 2010; Tronchin et al., 2008). The analysis of microclimatic thermal

stresses influencing thermal mass and natural ventilation represents an important step for the passive building refurbishment, as the thermal mass is most effective when interacting with intermittent heat sources (both internal and external), operating in swinging temperature conditions. Several studies show that in certain climatic circumstances, such as the Mediterranean area, an acceptable Thermal Range (TR), of about 15°C is able to maintain the temperature of a confined environment within the limits of comfort (Givoni, 1998). The thermal range amplitude (a key element for the future legislation for the summer conditions) represents a prerequisite to the optimal operation of both thermal inertia and natural ventilation strategies, especially under summer conditions when it is necessary to facilitate the dispersion of the high heat load gained during the day (Szokolay, 1985; Balaras, 1996). To choose the test cities to be used in this study, a map of thermal range is used (Cecchini 2014). Three climatic subtypes, according to Köppen-Pinna classification of the Mediterranean climate in Italy, are selected: the subtropical subtype represented by Messina with a TR of 6°C, below the threshold of efficient application of the strategies examined (Givoni, 1998; Szokolay, 1985), the mild-temperate subtype represented by Naples and the sub-coastal subtype, represented by Rome (both with TR above 14°C).

2.2 Thermal Inertia

The thermal mass of the building acts as one of the most important ways to achieve occupant comfort by controlling the internal environment through passive strategies (unlike a low thermal transmittance value that limits heat losses and therefore the optimization of the building dynamic behaviour): it allows the building to maintain the internal temperature within a certain range, theoretically close to the range of comfort, giving the building thermal stability (Kossecka et al., 2002). The choice of two representative measures of thermal mass is useful to show the effect on reducing the cooling load of the building and to analyse how the thermal mass cooperates with the natural ventilation in convective heat dissipation.

The two thermal mass measurements chosen are: a medium-light one, and a heavy one, representative of a massive wall with high heat absorption and capable of modulating the external thermal oscillations.

2.3 Existing building stock

In Europe, residential buildings cover approximately 75% of the total building stock and are the main energy consumer, because they were mainly built before laws on energy saving (Economidou et al., 2011). In Italy the most common and most energy-consuming buildings were built between 1961 and 1981 (Corrado et al. 2012; Decanini et al. 2010; Sorrentino et al. 2011) as shown in Fig. 3. Typically, these buildings have massive concrete structures with medium-light or heavy massive envelope (Pasca, 2012).

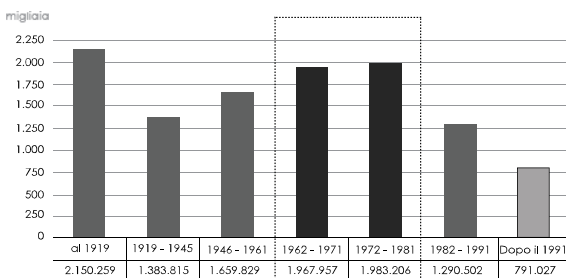


Fig. 3 - Data relating to the 2001 ISTAT census of Italian building (Corrado et al. 2012)

2.4 Natural Ventilation Systems

In the process of ventilation inside a building, air exchange occurs within the confined environment. Ventilation performs two main functions: it regulates the concentration of air pollutants and affects the igrothermal condition of the environment (Tucci, 2012). Ventilation that uses simple physical principles such as driving force is called natural (NV). Natural Ventilation principles, techniques, heat exchange type and element classification are described in Grosso (1997), Siew (2011), Calcerano et al. (2014). In this paper five different natural room ventilation systems (characterised by igrothermal comfort limits for the occupants) with automatic control (with the exception of the thermal chimney) are simulated: single sided (SSV) and cross ventilation (CV) that occur through envelope openings, thermal

chimney (TC), evaporative cool tower (CT) and earth pipes (EP) that occur through spaces specifically designed.

2.5 The Simulation Contribution

The impact of strategic decisions on energy and environmental characteristics of bioclimatic design is higher when these decisions are close to the early stages of the process (Lechner, 1991). In order to maximize comfort and reduce energy consumption the design of a naturally ventilated massive building has to adapt to site-specific microclimatic conditions on a daily basis. A simulation analysis can be a useful starting point for solving the problem (Stephan et al., 2007). A numerical simulation allows to analyse the "behavioural" model of a building (reduced to a certain level of abstraction) and is therefore a key tool to improving the energetic retrofit of the building stock, because it treats the building as a system of interrelated elements that can be optimised, rather than a sum of a number of elements designed and optimised separately for subsystems (Augenbroe, 2002; Hensen, 2004). The simulations in this paper address two specific questions: in the Mediterranean climate thermal mass and natural ventilation together interact with each other to play a dominant role in the energy behaviour of a building. What is the impact in terms of comfort and energy savings of their interaction and which are the sensitive variables (Attia et al., 2013) for maximizing the benefit of this effect? Among various simulation sub-categories (Calcerano et al. 2014) multi-zonal software was chosen to tackle our questions. This approach represents a good compromise between computation time and the degree of knowledge acquired on the simulated building, thus allowing immediate results on the igrothermal state of the simulated environments, air flow, comfort, and energy consumption. (Morbiter, 2003; Clarke, 2001; Chen, 2009; Hensen, 2003; Fouquier et al., 2013; Ramponi et al., 2012).

2.6 Performance Indicators

During the last two decades, the time spent by people in confined environments has increased (it is currently around 90% of a person's life).

European and national legislation have gradually tightened quality standards on living spaces (Lopardo, 2011), placing indoor environmental comfort (including igrothermal comfort and indoor air quality, IAQ) as the ultimate goal, and as the main condition for the success of adopted refurbishment strategies. According to an approach that places the comfort as an "objective" and the energy consumption as a "cost" aimed at achieving comfort, the passive behaviour of the building is assessed through a comparison of the energy performance index and the environmental comfort achieved (both in the hot season). Since this study focuses on the passive thermal mass and natural ventilation simulated control in Mediterranean area, it will be possible to proceed according to the adaptive comfort model defined by EN 15251:2008 which identifies three categories in relation to the ideal operating temperature trend T_o , among which the paper chooses the second with $T_o = 0.33 T_e$ (external temperature) $+18.8 \pm 3$ (with an 80% of acceptability). The above-mentioned indicator is associated with the ideal energy consumption value for cooling (shown in kWh/m²y), in order to relate the modelling to professional practice. The considered range for the ideal building plant's setting refers to the adaptive comfort temperature range, larger than that of Fanger - in order to better evaluate the contribution of a passive strategy to the reduction in energy consumption without the overestimation of the impact of technology (Corgnati, et al., 2008). A third synthetic indicator, air changes per hour (ach), is used to monitor and control that natural ventilation systems ensure the minimum air changes per hour required for IAQ (0.7 ach according to EN 15251:2008) inside a building with low infiltration (average 0.23 ach with Class 3 EN 12207/1999 windows); that simulation results show the difference between systems that use a larger crack (such as the openings on the building envelope of 3.45 m²) and can generate many air changes per hour with relatively low internal air speed, and systems that use smaller ducts (0.09 or 0.07 m²) and linear paths to avoid air flow losses and therefore have lower air changes per hour to prevent internal air speed becoming annoying for the occupants, with the

advantage of eliminating problems of safety related to intrusion (Allard, 1998).

3. Simulation

The simplified model, representative of the most diffuse and energy-consuming building typology in both European and national area (Corrado et al. 2012), is a south and north-facing apartment (7 m width x 8 m depth and a height of 3 m with two opposite low-emissivity air tight glass windows of 3.45 m² according to the hygiene regulations in force in Italy), located inside a multi-storey building and characterized by two thicknesses of the external concrete massive envelope: heavy (A, 30 cm) and medium-light (B, 18 cm). All the remaining surfaces are considered adiabatic. Internal gains (lights, people and electric equipment) are set according to a hypothetical residential occupancy pattern. A set of numerical multi-zonal simulations is then run using single sided and cross ventilation that occur through envelope openings, thermal chimney, evaporative cool tower and earth pipes that, with automatic control in their interactions with two different thermal masses, referring to the hot season (from the 1st June to the 30th September) for three different cities (Rome, Naples and Messina).

Table 1 - Model envelope thermo physical properties (*adiabatic)

Constr. Type	U [W/(m ² K)]	Y _{ie} [W/(m ² K)]	Φ [h]	F _d -
Upper floor*	1.34	0.46	8.37	0.34
Lower floor*	1.49	0.64	7.82	0.43
30 CLS wall	2.01	0.48	9.14	0.24
18 CLS wall	2.41	1.13	6.00	0.47
Window	1.00	SHGC = 0.3		

The software adopted for the simulations is EnergyPlus (Henninger and Witte 2011). For each combination between natural ventilation system (NV Syst.), locations and envelope type (e.g.

SSV_R_A), two Benchmark Simulations (BS), set with a minimum of 0.23 ach from infiltration, paired with two natural ventilation simulation, are run to carry out a correlational analysis. The first simulation, called Discomfort Benchmark Simulation (DBS) that serves as a reference case for subsequent analysis, calculates the model as it is and shows the total hours of discomfort during the simulation running period (expressed in hours/yearly in reference to the heat excess discomfort in the summer period). The DBS relative simulation with Natural Ventilation systems (DNVS) allows obtaining an estimate of the Discomfort hours Reduction Potential (DRP) expressed as a percentage, of the passive systems in examination. The other benchmark simulation, called Energy Benchmark simulation (EBS), has a thermostat that activates (on adaptive comfort range) a theoretical plant whenever the igrothermal condition of the building goes beyond a normalized temperature threshold for comfort (EN 15251), taking into account the subsequent primary energy consumption (expressed in kWh/m²y for cooling purpose). The EBS relative simulation with Natural Ventilation (ENVS) along with thermostat and theoretical plants shows the Energy Consumption Reduction Potential (ERP). The relationship between these two reductions and the effectiveness of natural ventilation and thermal mass are then investigated. In order to simulate single sided and cross ventilation, the Airflow Network model of EnergyPlus that allows for calculation of multi-zone airflows due to wind and surface leakage, is adopted (NREL, 2013) implementing a ventilation control mode based on the temperature differential between inside and outside temperature (if the room temperature $T_{room} > \text{outdoor temperature } T_{out}$, $T_{room} > \text{summer threshold temperature (21 °C)}$), windows are opened with an opening factor set to 0.5, with a T_{room} and T_{out} difference lower and upper limit set to 2 °C and 10 °C. The Thermal chimney (designed in the model with a 18 m high tower with low emissivity glass on the south facade and a cross section of 0.09 m²), evaporative cool tower (18 m height with a cross section of 0.09 m² and a water pump of 0.016 l/m) and earth pipes (25 m concrete duct 0.004 thick with a cross section of 0.07 m²) are

simulated through in built Zone Airflow model of EnergyPlus (NREL, 2013).

4. Analysis and discussion of the results

Results are shown in table 2. The absolute values of discomfort hours and energy consumption of the simulations confirm the results of previous research (Cesaratto et al., 2010; Sibilio et al. 2009) around 18.3 kWh/m²y and 2300 discomfort hours per year in Rome and Naples with a sharp rise in Messina (on average 1.2 times the hours of discomfort, 2 times the energy consumption).

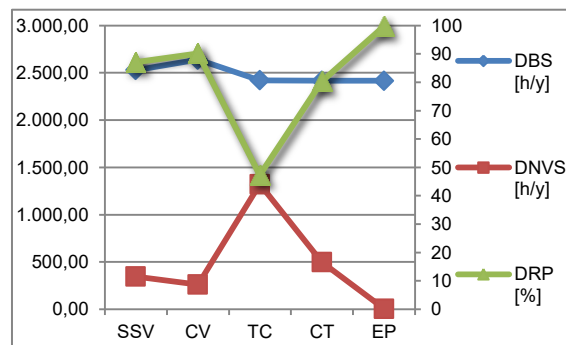


Fig. 4 - Discomfort hour analysis

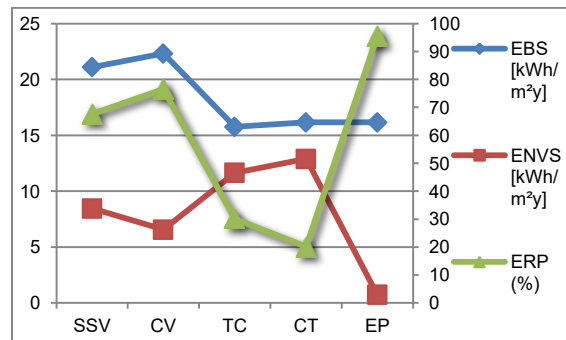


Fig. 5 - Energy consumption analysis

DRP of natural ventilation simulations is 88.0% in Rome, 83.2% in Naples because of poor performance of the cool tower system: -25% compared to Rome although not dependent on the average temperature and relative humidity (RH), but probably by the dynamic behaviour of Naples during the season. The RH standard deviation is 18% compared to 14% of Rome, which results in greater fluctuations of the value, the days of

extreme heat are double in comparison to Rome, precipitation one and a half, heavily reducing the effectiveness of the system in the most critical hours). DRP is 71.4% in Messina because of the low thermal range that limits the efficiency of all the systems without pre-treatment of the outside air (-19.6% compared to Rome and Naples). In absolute terms the energy saved and the largest decrease of discomfort hours take place in Messina (average reduction of 9.9 kWh/m²y against 7.8). Concerning ventilation systems earth pipes reach highest average discomfort hours reduction in every location with a DRP of 99.7 % (optimized design flow are assumed constant with a small fan), single sided and cross ventilation follows

(88.6 %) while the thermal chimney is last due to small air changes per hour without air pre-treatment (47.3%). Assuming equal comfort, the energy reduction potential is 67.7% with single-sided ventilation, 76.5% with cross ventilation, 30.2% with thermal chimney, 20.1% with cool tower and 95.5% with earth pipes (where the energy consumption is due to the fan). In combination with the above-mentioned cooling strategies, the 30 cm thick wall maintains its role of thermal flywheel (with the exception of the CV), while the 18 cm thick one shows an excessive reactivity to climatic stresses, resulting an average of 2.8 % greater energy consumption.

Table 2 – Simulation results (NV Syst: Natural Ventilation System: SSV, CV, TC, CT, EP, TM: Thermal Mass - DBS: Discomfort Benchmark Simulation - DNVS: Discomfort Naturally Ventilated Simulation - DNVS syst: infiltration due to natural ventilation system in DNVS - DRP: Discomfort hours Reduction Potential - EBS: Energy Benchmark simulation - ENVS: Energy Naturally Ventilated Simulation - ENVS Syst.: infiltration due to natural ventilation system in ENVS - ERP: Energy Consumption Reduction Potential – *average)

NV syst._ City_TM	DBS [h/y]	DBS [ach]*	DNVS [h/y]	DNVS inf. [ach]*	DNVS syst. [ach]*	DRP [%]	[EBS] [kWh/m ² y]	EBS [ach]*	ENVS [kWh/m ² y]	ENVS [ach]	ENVS syst. [ach]*	ERP [%]
SSV_R_A	2359	0.23	144	/	2.14	93.90	14.59	0.22	1.69	/	2.07	88.41
SSV_R_B	2212	0.23	150	/	2.17	93.22	15.09	0.22	2.70	/	2.07	82.10
SSV_N_A	2540	0.17	46	/	2.05	98.19	17.11	0.15	2.42	/	1.98	85.85
SSV_N_B	2449	0.17	88	/	2.09	96.43	17.73	0.15	3.56	/	1.98	79.91
SSV_M_A	2816	0.21	775	/	2.54	72.48	29.83	0.18	18.95	/	1.69	36.48
SSV_M_B	2797	0.21	879	/	2.57	68.56	32.20	0.18	21.43	/	1.70	33.44
CV_R_A	2444	0.23	210	/	3.95	91.40	15.83	0.20	1.74	/	3.65	89.02
CV_R_B	2355	0.23	279	/	2.62	88.15	16.30	0.20	0.68	/	2.97	95.80
CV_N_A	2638	0.19	59	/	3.06	97.76	18.21	0.15	3.13	/	2.80	82.82
CV_N_B	2575	0.19	313	/	2.42	87.85	18.79	0.15	1.65	/	2.33	91.25
CV_M_A	2926	0.21	564	/	4.44	80.74	31.29	0.16	16.54	/	3.55	47.12
CV_M_B	2899	0.21	146	/	4.34	94.97	33.52	0.16	15.65	/	3.52	53.32
TC_R_A	2241	0.23	935	0.92	0.69	58.28	11.15	0.23	6.60	0.99	0.76	40.84
TC_R_B	2012	0.23	775	0.93	0.70	61.50	11.25	0.23	6.97	0.99	0.76	37.98
TC_N_A	2420	0.23	1078	0.90	0.67	55.46	11.97	0.23	7.39	0.98	0.75	38.28
TC_N_B	2127	0.23	957	0.91	0.68	55.03	12.05	0.23	7.80	0.99	0.76	35.25
TC_M_A	2885	0.23	2129	0.99	0.76	26.20	23.52	0.23	19.95	1.21	0.98	15.17
TC_M_B	2836	0.23	2060	0.99	0.77	27.37	24.60	0.23	21.19	1.21	0.98	13.86
CT_R_A	2246	0.23	32	0.23	1.81	98.56	11.39	0.23	7.59	0.23	1.81	33.38
CT_R_B	2020	0.23	87	0.23	1.81	95.69	11.56	0.23	8.15	0.23	1.81	29.48
CT_N_A	2423	0.23	628	0.23	1.81	74.07	12.22	0.23	11.07	0.23	1.81	9.42
CT_N_B	2132	0.23	642	0.23	1.81	69.89	12.40	0.23	11.59	0.23	1.81	6.54
CT_M_A	2859	0.23	758	0.23	1.81	73.48	24.09	0.23	18.83	0.23	1.81	21.85
CT_M_B	2816	0.23	840	0.23	1.81	70.18	25.31	0.23	20.16	0.23	1.81	20.34
EP_R_A	2246	0.23	0	0.23	0.77	100.00	11.39	0.23	0.45	0.23	0.77	96.07
EP_R_B	2020	0.23	1	0.23	0.97	99.96	11.56	0.23	0.56	0.23	0.97	95.12
EP_N_A	2423	0.23	0	0.23	0.82	100.00	12.22	0.23	0.48	0.23	0.82	96.10
EP_N_B	2132	0.23	27	0.23	1.01	98.76	12.40	0.23	0.59	0.23	1.00	95.26
EP_M_A	2859	0.23	5	0.23	1.66	99.82	24.09	0.23	0.97	0.23	1.67	95.99
EP_M_B	2816	0.23	6	0.23	2.26	99.80	25.31	0.23	1.31	0.23	2.26	94.81

5. Conclusions

Reported results highlight:

1. the effectiveness of minimally invasive refurbishment actions for energy retrofits of existing buildings, such as implementing automatic control on already existing openings on the building envelope because single sided and cross ventilation produce the greatest benefits in relation to their cost;
2. an effectiveness reduction of systems without air pre-treatment due to a lower daily thermal range, and an effectiveness reduction of the evaporative cool tower due to a higher average humidity ratio;
3. the variation of some parameters for the optimization of automatic control systems in different climates: in Rome to avoid discomfort hours from cold in the simulated period, the activation threshold of the systems is 22°C with the difference between outside and inside air temperature between 2 and 5°C, in Naples and Messina the activation threshold drops to 21°C and the difference increases from 2 to 7°C in Naples, from 2 to 12°C in Messina;
4. the increased efficacy demonstrated by the earth pipes should be related to the higher invasiveness and difficulty of implementation that make this type of intervention only recommended when working on large refurbishments;
5. when retrofitting a single apartment of a multi-storey building, the small solar gains make it less significant the effect of the thermal mass compared to an intervention on a building where all surfaces are exposed (cf. Calcerano et al. 2014).

6. Acknowledgement

Research carried out as part of the PhD in Environmental Design of the PDTA Department of Sapienza University of Rome, Coordinator Prof. E. Cangelli and Tutor Prof. F. Tucci.

References

- Allard, F. 1998. *Natural Ventilation in Buildings: A Design Handbook*. London: James & James Ltd.
- Ardente, F., M. Beccali, M. Cellura, M. Mistretta. 2011. "Energy and Environmental Benefits in Public Buildings as a Result of Retrofit Actions." *Ren. and Sust. En. Rev.* 15 (1): 460–70.
- Attia, S., M. Hamdy, W. O'Brien, S. Carlucci. 2013. "Assessing Gaps and Needs for Integrating Bldg. Perf. Optimization Tools in NZEB Design." *En. and Bldg.* 60: 110–24.
- Augenbroe, G. 2002. "Trends in Bldg. Simulation." *Building and Environment* 37 (8–9): 891–902.
- Baek, C., S. Park. 2012. "Changes in Renovation Policies in the Era of Sustainability." *Energy and Buildings* 47 (April): 485–96.
- Balaras, C.A. 1996. "The Role of Thermal Mass on the Cooling Load of Bldg. An Overview of Compt. Methods." *En. and Bldg.* 24 (1): 1–10.
- Braun, J. E. 2003. "Load Control Using Building Thermal Mass." *J. Sol. Energy Eng. Journal of Solar Energy Engineering* 125 (3): 292.
- Calcerano, F., C. Cecchini. 2014. "Mediterranean Building Refurbishment: Thermal Mass and Natural Ventilation Simulated Control." *Proceedings of 5th German-Austrian IBPSA Conference BAUSIM 2014 "Human Centered Buildings" 22-24 September 2014*, 8.
- Cecchini, C. 2014. "Incremento, Gestione Ed Ottimizzazione Dei Sistemi Ad Elevata Massa Termica Nella Riquilificazione Energetico-Ambientale Del Costruito in Ambito Mediterraneo." Roma: La Sapienza.
- Cesaratto, P., M. De Carli. 2010. *Studio comp. tra fabb. en. netti, lato edificio, sia per la clim. estiva che per quella inv. di ed. res. e del settore terziario situati in climi diff.* Roma: ENEA.
- Chen, Q. 2009. "Ventilation Performance Prediction for Buildings: A Method Overview and Recent Applications." *Building and Env.* 44 (4): 848–58.
- Clarke, J. A. 2001. *Energy Simulation in Building Design*. Oxford: Butterworth-Heinemann.
- Corgnati, S. P., E. Fabrizio, M. Filippi. 2008. "The Impact of Indoor Thermal Conditions, System Controls and Building Types on the Bldg. Energy Demand." *En. and Bldg.* 40 (4): 627–36.
- Corrado, V., I. Ballarini, S. P. Corgnati, N. Talà.

2012. "Building Typology Brochure - Italy. Fascicolo Sulla Tipologia Edilizia Italiana." Politecnico di Torino - Dipartimento di Energetica, Gruppo di Ricerca Tebe.
- Decanini, L.D., L. Liberatore, F. Mollaioli. 2010. "Damage Suffered by RC Buildings during the 2009 L'Aquila Earthquake, a General Overview and a Case Study." Proc. of 14th European Conference on Earthquake Engineering.
- D'Orazio, M., C. Di Perna, and E. Di Giuseppe. 2010. "The Effects of Roof Covering on the Thermal Performance of Highly Insulated Roofs in Mediterranean Climates." *Energy and Buildings* 42 (10): 1619–27.
- Economidou, M., B. Atanasiu, C. Despret, J. Maio, I. Nolte, and O. Rapf. 2011. "Europe's Buildings under the Microscope. A Country-by-Country Review of the Energy Performance of Buildings." (BPIE).
- Foucquier A., S. Robert, F. Suard, L. Stephan, A. Jay 2013. "State of the Art in Building Modelling and Energy Performances Prediction: A Review." *Renewable Sustainable Energy Rev Renewable and Sustainable Energy Reviews* 23: 272–88.
- Givoni, B. 1998. "Effectiveness of Mass and Night Ventilation in Lowering the Indoor Daytime Temperatures. Part I: 1993 Experimental Periods." *Energy and Buildings* 28 (1): 25–32.
- Grosso, M. 1997. *Il raffrescamento passivo degli edifici: concetti, precedenti architettonici, criteri progettuali, metodi di calcolo e casi di studio.* Rimini: Maggioli.
- Heiselberg, P. 2002. *Principles of Hybrid Ventilation. Vol. Annex 35 Hybrid ventilation in new and retrofitted office building, IEA energy conservation in buildings and community systems programme.* Aalborg University, Aalborg, Denmark.
- Henninger, H. R., and M. J. Witte. 2011. "EnergyPlus Testing with ASHRAE 1052-RP Toolkit–Building Fabric Analytical Tests." Lawrence Berkeley National Laboratory, USA.
- Hensen, J. 2003. "Integrated Building Airflow Simulation." In *Advanced Building Simulation*, Spon Press. New York and London.
- Hensen, J. 2004. "Towards More Effective Use of Building Performance Simulation in Design." In Leeuwen, J.P. van & Timmermans, H.J.P. (Eds.). *Proceedings of the 7th International Conference on Design & Decision Support Systems in Architecture and Urban Planning*, 2-5 July. Eindhoven University of Technology.
- Kossecka, E., and J. Kosny. 2002. "Influence of Insulation Configuration on Heating and Cooling Loads in a Continuously Used Building." *Energy and Buildings* 34 (4): 321–31.
- Kwon, O., M. Kim, A. Choi, J. Jeong. 2013. "Energy Saving Potential of a Hybrid Ventilation System Integrated with Heat Storage Material." *Energy and Buildings* 57 (February): 346–53.
- Lechner, N. 1991. *Heating, Cooling, Lighting: Sustainable Design Methods for Architects.* Hoboken, N.J.: John Wiley & Sons.
- Lopardo, G. 2011. "Un Modello Matematico Di Termoregolazione Del Corpo Umano." Salerno: Università degli studi di Salerno - Dipartimento di Ingegneria Meccanica.
- Ma, Z., P. Cooper, D. Daly, L. Ledo. 2012. "Existing Building Retrofits: Methodology and State-of-the-Art." *Energy and Buildings* 55: 889–902.
- Morbiter, C. 2003. "Towards the Integration of Simulation in the Building Design Process." Strathclyde: PHD thesis, Energy System Research Unit, University of Strathclyde.
- NREL. 2013. "EnergyPlus Input Output Reference."
- Pasca, M. 2012. "Il Costruito Italiano: Tipologie, Problematiche, Interventi Pre E Post Sisma." *Tafer Journal Esperienze E Strumenti per Cultura E Territorio.*
- Ramponi, R., B. Blocken. 2012. "CFD Simulation of Cross-Ventilation for a Generic Isolated Building: Impact of Computational Parameters." *Building and Environment* 53: 34–48.
- Sibilio, P., M. D'Agostino, M. Fatigati, M. Citterio. 2009. "Valutazione Dei Consumi Nell'edilizia Esistente E Benchmark Mediante Codici Semplificati: Analisi Di Edifici Residenziali."
- Siew, C.C., A.I. Che-Ani, N.M. Tawil, N.A.G. Abdullah, and M. Mohd-Tahir. 2011. "Classification of Natural Ventilation Strategies in Optimizing Energy Consumption in Malaysian Office Buildings." *Procedia Engineering* 20: 363–71.
- Sorrentino, L., E. Raglione, D. Liberatore, L. D.

- Decanini. 2011. Chiesa Di San Biagio D'Amiternum a L'Aquila. Catalogo Sismico Locale E Meccanismi Di Collasso. L'università e la ricerca per l'Abbruzzo. Il come ed il perchè dei danni ai monumenti. L'Aquila: Textus.
- Stephan, L, A Bastide, E. Wurtz, and B. Souyri. 2007. "Ensuring Desired Natural Ventilation Rate by Means of Optimized Openings." Proceedings of 11th International IBPSA Conference - Building Simulation 2009, BS 2009; Glasgow; United Kingdom; July 2007.
- Szokolay, S. 1985. "Passive and Low Energy Design for Thermal and Visual Comfort." Passive and Low Energy Ecotechniques: Proceedings of the Third International PLEA Conference, Mexico City, Mexico, 6-11 August 1984.
- Tronchin, L., K. Fabbri. 2008. "Energy Performance Building Evaluation in Mediterranean Countries: Comparison between Software Simulations and Operating Rating Simulation." Energy and Buildings 40 (7): 1176-87.
- Tucci, F. 2012. Atlas of Technological Systems for Bioclimatic Architecture. Natural ventilation. Firenze: Alinea Editrice.

Daylighting optimization for informal settlements in Cairo, Egypt

Ayman Wagdy –The American University in Cairo – aymanwagdy@aucegypt.edu

Ahmed Abdelghany – Fine Arts Hellwan University – masterlinegroup@yahoo.com

Mohamed Amer Hegazy – Transsolar Energietechnik GmbH – hegazy@transsolar.com

Abstract

In developing countries, the phenomenon of informal settlements has increased significantly. For instance, Cairo is considered to have four out of the thirty biggest “mega-slums” in the world, with a total of 11.8 million inhabitants. These settlements occupy 62% of the Greater Cairo area. Sustainable development is urgently needed to ensure better quality of life for now and the following generations. One of the characteristics of informal settlements is having narrow streets and dense urban fabric. Thus, only a small amount of natural lighting enters indoor spaces, which has adverse effects on the physical and psychological health of the inhabitants.

This paper aims to identify the most reasonable window ratios in relatively narrow street widths (4, 6 and 8 meters) based on the amount of light reaching the ground floor levels. This paper utilizes brute force procedure based on daylighting performance criterion. The parametric daylighting simulations were conducted using the Diva-for-Rhino, a plug-in for Rhinoceros 3D modeling software, which is used to interface Radiance and Daysim daylighting simulation engines. For the parametric tool, Grasshopper was used to generate the parametric urban model based on a generic case study taken in Cairo, Egypt.

This paper presents quantitative results and measurements aiming to help decision makers address development strategies for informal settlements and to provide essential data for setting regulations for newly built urban spaces.

1. Introduction

Informal settlements are characterized by being illegal residential settlements that are not committed to any urban regulations and codes (Von Rabenau, 1995). Informal housing is an unauthorized development that occurs around and

in city master plan causing undesired adverse impacts. Land and natural green area around cities are been chewed up by new roads, residential and commercial buildings. On one hand, informal areas have been a standardized lifestyle for large populations in developing countries (Srinivas, 1991), and eventually they provide affordable living standards and a steady job market.

On the other hand, informal settlements have many opposing effects on both local inhabitants and the whole society. They cause a significant threat to the housing market and urban development in the country, in addition to other problems concerning sanitation, health, environmental facilities and services.

Informal areas in Cairo have taken an epidemic toll in the last three years, especially after the revolution of 25 January. That was simply a direct result of the official neglect of the fast spatial expansion of the city as shown in Fig. 1.

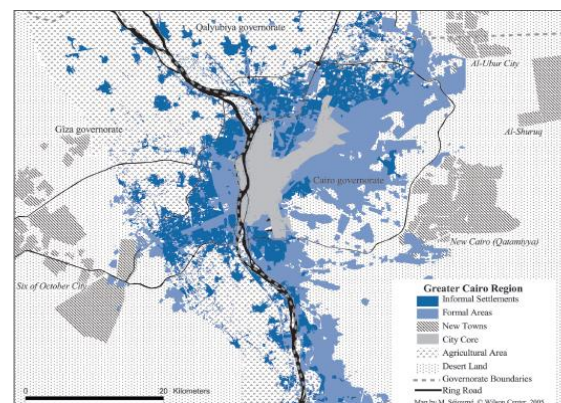


Fig. 1 – Distribution of the formal and Informal Settlements in Cairo

The unorganized expansion has extended over serial agricultural areas around the city. Immigration from villages and other governorates has exponentially risen which has led to an

enormous increase in population in the big cities forming unorganized vertical expansion with very dense urban fabric. These densities in some areas have reached 350,000 inhabitants per square kilometer which is beyond the standard limits (Sejourne, 2002).

2. Informal settlements features

Three key features are common to all informal areas around the world: social, physical and legal features (Sirinivas, 1991). First, physical features are represented by a lack of services, inadequate housing, degrading environmental conditions, insufficient lighting, ventilation and air quality. In addition, there is a scarcity of infrastructure and services such as a clean water supply, public sewer network, public transportation, efficient streets, schools, policing and fire fighting.

Regarding social features, informal settlement inhabitants usually have the lowest income, they work in temporary and informal jobs, and they are also the poor and acquire no or little education. Lastly, legal features are evident through illegally occupying land plots that belong to the government or even individuals.

It is possible to see buildings on agricultural lands, which are built without the permission of the local authorities and are not committed to urban planning codes or regulations as shown in Fig. 2 and 3.



Fig. 2 – A typology of Informal Settlements in Cairo

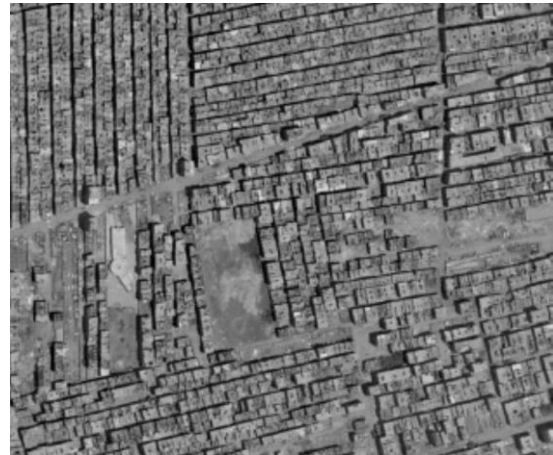


Fig. 3 – Another typology of Informal Settlements in Cairo on agricultural lands

3. Urban Daylighting

Many researchers have investigated the influence of urban morphology on daylighting and daylighting planning tools. Previous work identified an empirical relationship between street widths and daylighting for interior zones, aiming to identify city forms that consider daylighting requirements (DeKay, 2010). Lately, urban daylighting has been granted an extensive interest from the research community. A new tool for assessing daylighting on the urban scale has been developed by MIT sustainable lab (Dogan et al., 2012). Moreover, this tool is capable of calculating other aspects, such as walkability and energy consumption (Reinhart et al., 2013).

Some contributions from Egypt tried to provide some solutions to enhance daylighting in the informal settlements. Changing window ratios and external façade reflections can provide daylighting with more than 50% than the original cases (Hegazy and Attia, 2014). Others have developed a device that is attached to the top of the buildings that provides diffuse daylighting on the opposite buildings' facades (Nassar et al., 2014).

It is hard to unify settings for informal settlements; thus there is a need to generate a set of solutions based on the random variations that are given in any informal area. The aim is to identify most reasonable window sizes according to narrow street widths (4, 6 and 8 meters) based on the amount of daylight that reaches indoor spaces on

the ground floor levels. However, due to time and efforts constraints, only the south façade was examined. In the end, this research provides decision makers with informative data, which helps in determining the recommended building heights and window ratios based on the road width.

4. Methodology

A broad investigation has been conducted on the conditions and conventional ways of dealing with informal settlements. In addition, a review of previous literature helped to find solutions for narrow street designs. A hypothetical model for an extreme urban context was modeled and parametrically simulated with a set of multiple variables. Optimum solutions were sorted based on the predefined urban dimensions limits. The Grasshopper for Rhinoceros 3D modeling tool was used in this research work (Wagdy, A. 2013). A typical living room is modeled on the ground floor in the defined context. The daylighting was assessed based on the approved method IES Spatial Daylight Autonomy (sDA_{300/50%}) and Annual Sunlight Exposure (ASE_{1000/250hr}) (IES, 2012). The results show possible solutions under different configurations for increasing the Daylit area in residential zones.

4.1 Experimentation approach

It is barely possible to extract a fixed building regulation; the case study does not represent a particular informal area in Cairo. The context was modeled considering extreme urban conditions for building heights and street widths in a very dense urban fabric. In this context, a dwelling living room was modeled oriented to the south; it is located on the ground level in order to represent the zone with the least amount of daylight.

Table 1 – Living room configuration

Living Room Configurations			
Floor Level		Ground Level	
Dimensions		6m x 4m x 3m	
Area		24 m ²	
Reflectivity Ratios	Ceiling	80%	White
	Walls	50%	Off- White
	Floor	20%	Wooden
Window orientation		South	
Occupancy Schedules		08:00 – 18:00	

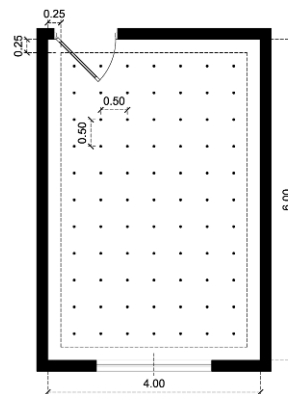


Fig. 4 – Room dimensions

Radiance parameters of the simulation model are set to meet the minimum requirements for LEED v4 for a valid simulation results. Namely, Spatial Daylight Autonomy (sDA_{300/50%}) Metric followed Annual Sunlight Exposure (ASE_{1000/250hr}) is shown in Table 2. (IES, 2012 & Elghazi et al., 2014).

Table 2 – shows radiance simulation parameters for [sDA and ASE Metrics respectively].

Ambient bounces	Ambient divisions	Ambient sampling	Ambient accuracy	Ambient resolution
6	1000	20	0.1	300
0	1000	20	0.1	300

The analysis runs through three primary variables. The first variable is window ratio, which ranges from 20% to 90% as shown in (Fig. 5). Consequently, window ratios represent the possible solution that can be done by any inhabitant individually.

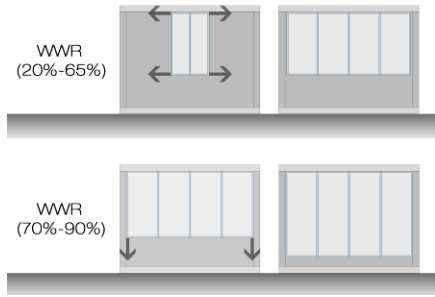


Fig. 5 – Window sizes and positions.

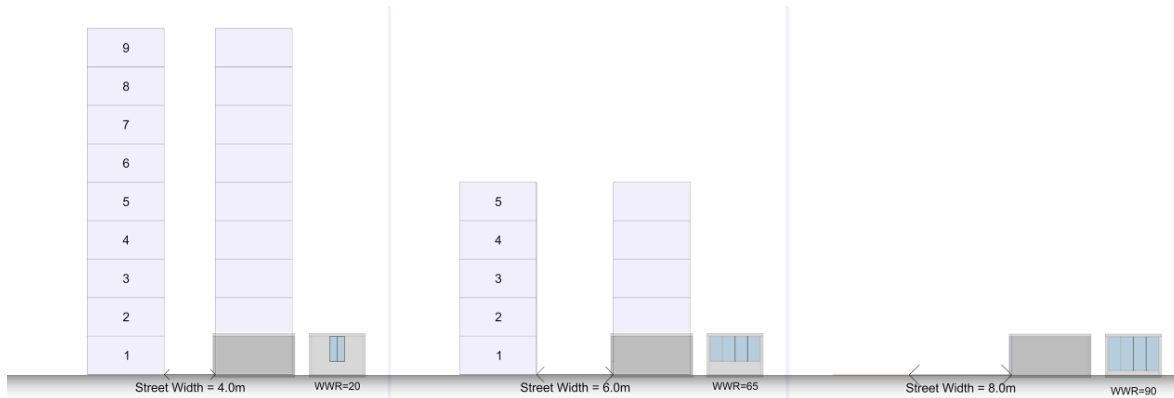


Fig. 6 – Street widths range from 4 to 8 meters and the building heights range from zero to 9 floors.

The second variable is the height of the opposing building, which varies from no neighboring buildings till nine storeys for extremely densely populated areas. The third and last variable is street width; the street width is set to start from 4, 6 and 8 meters for a relatively wide street in an informal area as shown in Fig. 6. The tested room is simulated attached to multi adjacent buildings representing the dense urban fabric of informal areas, and to increase the accuracy of the assessment that should be based on the opposite buildings’ heights only. In Table 3, the three variables are summarized so that parametric iterations took place representing all possible combinations of the different variables resulting 450 different situations.

Table 3 – Variables and parameters of the simulation model.

Parametric Parameters	
WWR	20% - 90% (5% Increment)
Street Width	4 - 6 - 8 (2 meter Increment)
Number of floors	0 - 9 (1-floor Increment)

5. Results

The results are generated parametrically based on brute force technique to create 450 different cases. This research explores the influence of urban configurations on the daylighting performance in the interior zones of the opposite buildings. This evaluation is necessary to understand the daylight performance according to building height, street width, and window size, considering constant values for the weather condition, schedules for occupancy and no shading devices. The results of this exhaustive search are divided into three sections, according to street widths, with 150 results each explaining the effect of each variable on daylight performance, by which optimum solutions are identified.

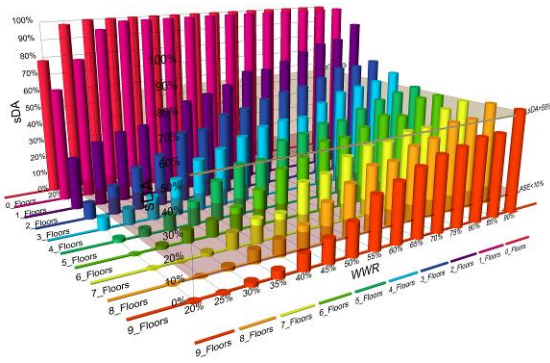


Fig. 7 – sDA results of different window ratios according to the various heights of the opposite building for a 4 meters street width.

The narrowest street width of 4 meters in Fig. 7, and the results of daylighting performance for 150 cases are shown. The cutting edge for the successful cases lies on the 55% sDA. All the cases with a 90% WWR reached or exceeded the threshold. With 85% WWR the results reached the threshold only when the opposite building height was reduced to six and five floors. Then, more results were accepted when facing a building with three floors above the ground level. The accepted range of WWR percentages increases with lower height of the surrounding buildings, which allow more sunlight into the indoor spaces. However, the values of Annual Sunlight Exposure (ASE) increases as well. The ASE analysis illustrated in Fig. 8 shows a constant value of 0% when the space faces a building with a height of 3 storeys or more. Thus, high buildings in narrow streets entirely block sunbeams from entering indoor spaces. However, only the case changes when building heights are reduced to two floors allowing more sunlight, which may overheat the space in that case.

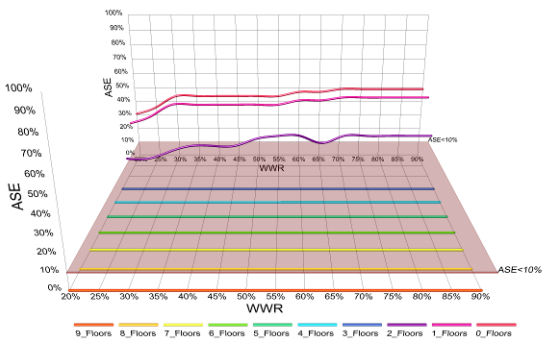


Fig. 8 – ASE performance of each WWR based number of floors for 4 meters street width.

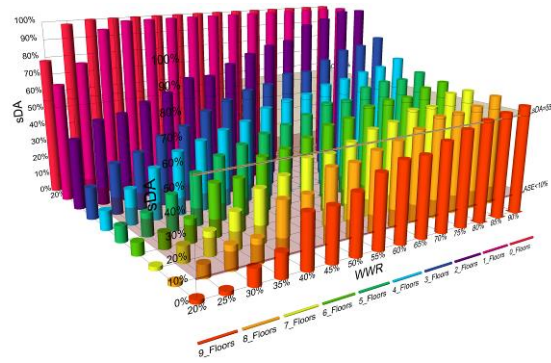


Fig. 9 – sDA performance of each WWR based number of floors for 6 meters street width.

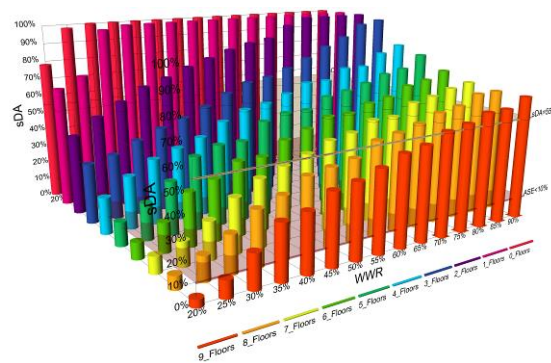


Fig. 10 – sDA performance of each WWR based number of floors for 8 meters street width.

The cases with wider streets have correspondingly better performance. The analysis shows larger range of accepted window ratios especially when the analyzed zone faces mid-height to high building 3 to 9 floors as shown in shown in Fig. 9 & 10.

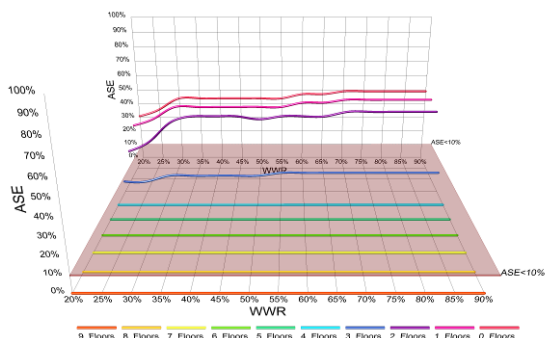


Fig. 11 – ASE performance of each WWR based number of floors for 6 meters street width.

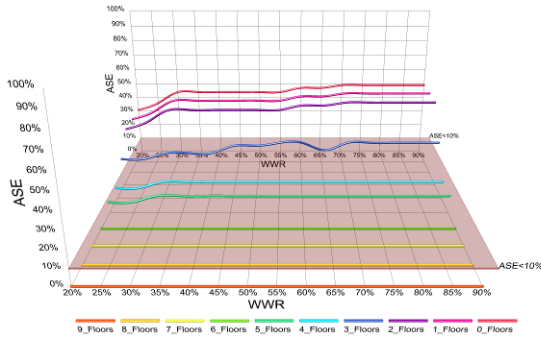


Fig. 12 – ASE performance of each WWR based number of floors for 8 meters street width.

Nevertheless, according to the IES and LEED v4, the quality of daylighting is not assessed with only the amount of daylighting inside the zone. Direct sunlight counts as well as a discomfort factor when it reaches more than 10% of the room area, due to the excess heat that is accompanied by direct sunlight or potential for discomfort glare. The ASE values increase with the rise of street widths or the decrease of the heights of the opposite buildings as shown in Fig. 11 & 12.

Drawing conclusions from the results above would help decision makers set strategies and regulations that consider daylighting qualities in the informal settlements. As shown in Figs 13, 14 and 15 only accepted window ratios are presented according to the number of floors in the opposite building for each street width.

In a street of 4 meters in width, only larger WWRs reach the threshold when building heights reach up to 9 storeys. In a street of 6 meters in width, WWRs starts from 80% and achieve a proper amount of daylighting with a maximum building height of nine storeys. The results are limited to a lower number of storeys due to the increasing annual sunlight exposure. Lastly in a street of 9 meters in width, accepted window ratios are more limited with lower building heights. It starts to achieve adequate amount of daylighting from 70% WWR with 8 or 9 storeys, while it drops to 65% and 60% with 7 and 8 storeys.

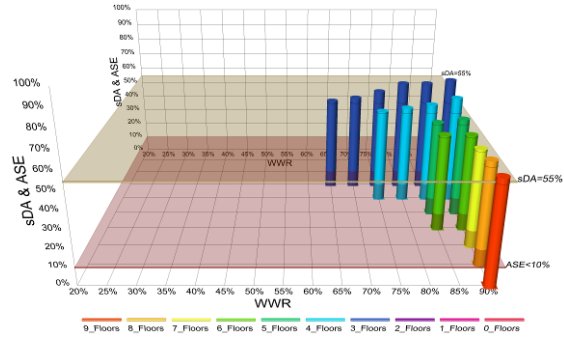


Fig. 13 – sDA and ASE performance of the accepted WWR based on the number of floors for 4 meters street width.

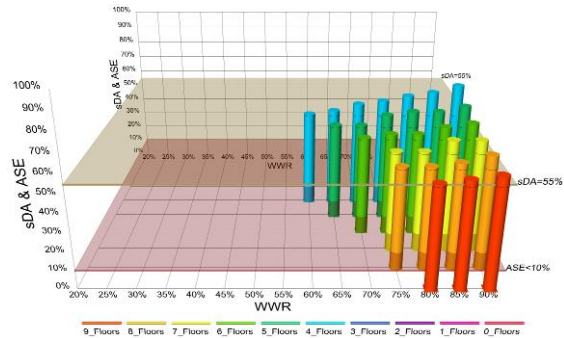


Fig. 14 – sDA and ASE performance of the accepted WWR based on the number of floors for 6 meters street width.

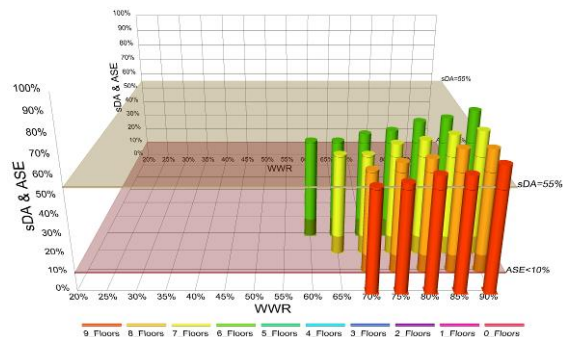
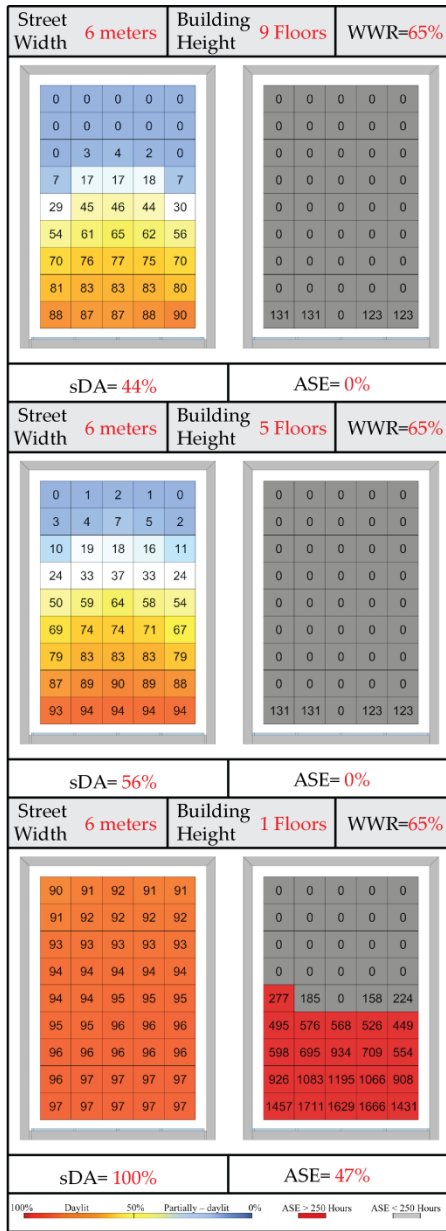


Fig. 15 – sDA and ASE performance of the accepted WWR based on the number of floors for 8 meters street width.

Table 4 – sDA and ASE performance based on the number of floors for 6 meters street width at 65% WWR.



In Table 4, a comparison is illustrated showing the difference between the daylight performance of one window ratio on the same street width but with different heights of opposite buildings; nine, five and one storey buildings. It explains the phenomenon of increasing the amount of sunlight exposure when decreasing the number of the opposite storeys, while the decline of sDA with higher storeys. The same also happens with bigger and smaller window ratios.

6. Conclusion

The results of this study are compiled in the above table to make it easier to read and for decision makers to choose the right strategy for development shown in table 5. The blue rectangle colors represent the results with low daylight performance, while the red represents the performance with high sunlight exposure. The right-ticked rectangles represent the recommended configuration for window ratio or building height for a constant street width. One observation was extracted from the simulation process; it was found that ground reflectivity has a minor effect on the overall indoor daylighting performance. This finding gives the table another way to be read, by which the recommended height of the opposite building can be given starting from the level of the storey where the daylighting performance will be assessed.

Table 5 – Shows the accepted window size based on the opposing building height and street width.

Height of the opposing building	Street Width	20% - 55 %			60%			65%			70%			75%			80%			85%			90%			
		4 meters	6 meters	8 meters	4 meters	6 meters	8 meters	4 meters	6 meters	8 meters	4 meters	6 meters	8 meters	4 meters	6 meters	8 meters	4 meters	6 meters	8 meters	4 meters	6 meters	8 meters	4 meters	6 meters	8 meters	
9																										
8																										
7																										
6																										
5																										
4																										
3																										
2																										
1																										
0																										

7. Discussion

In this research, it is important to mention that the results have been extracted without considering any shading device, curtains or occupancy behavior. These aspects are important to ensure privacy, which will affect the overall performance of the daylighting. However, the primary aim is to provide minimum bare configurations of an urban context and window ratios. It provides the primarily accepted amount of daylighting indoor spaces. Moreover, it presents a fast track measuring tool for decision makers, knowing that the simulation process for each case requires experts, which is not an applicable process in real life. On the governmental side, one of the greatest challenges is to deal with informal areas and to limit the physically deteriorated conditions of buildings and provide better building configurations and dimensions.

Many policies were initially considered by the government such as land clearance, rehabilitation, and the upgrading of informal settlements. However, the key element in choosing a suitable strategy is the financial conditions and the value of the selected informal area. This concerns both the buildings and land since most of the new informal urban extensions have occurred in high land value on a large scale, which makes the land clearance policy not applicable most of the time. Therefore, a way to find retrofitting measures turns out to be more applicable and affordable at the moment. Thus, solutions including either changing window sizes or demolishing a couple of floors at the top of the building can be applicable.

References

- DeKay, M. 2010. "Daylighting and Urban Form: An Urban Fabric of Light" *Architecture and Urban Planning* 27:1 (35)
- Dogan, T., Reinhart, C., Michalatos, P. 2012. "Urban Daylight Simulation Calculating The Daylit Area Of Urban Designs" *Fifth National Conference of IBPSA-USA, USA*.
- Elghazi, Y., Wagdy, A., Mohamed, S., & Hassan, A. 2014. "Daylighting driven design: optimizing Kaleidocycle facade for hot arid climate". *BauSIM 2014, Aachen, Germany*.
- Hegazy, MA., Attia, S. 2014. "Investigating the Influence of External Facades Reflectivity on the Indoor Daylight Autonomy in Hot Arid Climates" *Second IBPSA, England Conference*
- IES. 2012. Spatial daylight autonomy (sDA) and annual sunlight exposure (ASE). New York (NY): IES. LM-83-12. Lighting Measurement #83.
- Nassar, K., Safwat, A. M., Darwish, A., El-Henawy, S. I., Mashaly, I. A., Mohamed, O. N., & Mohamed, M. W. 2014. "Designing a Light Redirecting System for Southern Skies" *Second IBPSA, England Conference*
- Reinhart, C., Dogan, T., Jacubiec, A., Rakha, T., Sang, A. 2013 "UMI-An Urban Simulation Environment for Building Energy Use, Daylighting and Walkability" *13th Conference of International Building Performance Simulation Association, Chambéry, France*
- Srinivas, hari. 1991. "Viability of informal credit to finance low income housing, case study of three squatter settlements in Bangalore, India" *unpublished master's thesis report Bangkok: division of human settlements development Asian institute of technology*
- The Egyptian Cabinet. 2008. Information and the decision support center "Informal areas in Egypt, analytical study" p 20
- USAID, Woodrow Wilson, International Center for Scholars "Urban Studies in Cairo, Egypt" April 2006, no.8
- Von Rabenau B. 1995. "CRP741: urban sector planning for developing countries " class notes, Columbus, Ohio: the Ohio state university (unpublished)
- Wagdy, A. 2013. "New parametric workflow based on validated day-lighting simulation". *1st IBPSA-Egypt Conference. Cairo, Egypt*.

CFD vs. lumped models applied to HAM: a comparison between HAM-Tools and Comsol

Amos Ronzino – Politecnico di Torino, Department of Energy, TEBE Research Group – amos.ronzino@polito.it

Vincenzo Corrado – Politecnico di Torino, Department of Energy, TEBE Research Group – vincenzo.corrado@polito.it

Maximilian Neusser – Vienna University of Technology, Department of Building Physics – maximilian.neusser@tuwien.ac.at

Thomas Bednar – Vienna University of Technology, Department of Building Physics – thomas.bednar@tuwien.ac.at

Abstract

CFD models have several advantages in comparison with zonal-models, due to the more accurate calculation of the airflow distribution within the built environment. Nevertheless, in currently available CFD software the simulation of mass transfer cannot be directly extended from the fluid region to the solid region. In the whole-building moisture transport studies, the mass coupling between the indoor environment and the wall system is usually achieved by third party programming. The Annex 41 research project of the International Energy Agency (IEA) was carried out to explore the complex physics governing the whole building heat, air and moisture (HAM) transfer, by developing several models to couple 3-D CFD simulations with hygrothermal models of walls.

The objective of this study is to develop a coupled CFD model able to simulate the HAM transport in a single environment (i.e. a simple test room), influenced by the room factors. A numerical method was utilized to model the indoor environment and the moisture transport process in the simple room and inside the wall system as influenced by the moisture loads and ventilation conditions.

The comparison between the CFD and a lumped model allows us to demonstrate how a simplified model can be reliable in predicting the RH variation inside a room, also taking into account the indoor material buffering effect.

1. Introduction

HAM-Tools is a building simulation software implemented on the Simulink-Matlab platform by the Chalmers University of Technology (Gotheborg, Sweden) and the Technical University of Denmark (Lygby, Denmark) within the Annex 41 project. The main objective of this tool is to run simulations of transfer processes related to building physics, i.e. heat and mass transport in buildings and building components in operating conditions. Nevertheless, results from literature demonstrate how simulations made with the HAM-Tools lumped model over-estimate about twice the moisture dampening effect than what was actually measured experimentally (Ramos et al., 2012). The authors then focused on the air-flow pattern, comparing experimental measurement results to theoretical ones. An appreciable difference between the measured hygroscopic inertia and the calculated one was found due to the air velocity field that caused the development of several dead zones inside the test chamber. This meant that the perfect mixing of the room air, a simplification commonly assumed in HAM simulations, had a clear impact on the results of this kind of problem. If perfect mixing is assumed, all the hygroscopic surfaces would be fully active; but since this is not true, the flux chamber simulations overestimated the moisture buffering effect.

The CFD model has the advantage to overcome the limitations of the zonal-model applied to HAM-Tools, but it encounters another limitation due to the calculation in different environments. The moisture flux on the wall surface calculated by CFD is used as the input for the wall model to determine the distribution of the moisture inside the wall material at each time step (i.e. using MatLab), and the mass fraction on the wall surface is calculated and sent back to the CFD model as the boundary condition for the next time step.

In the Annex 41 research project (2004-2008) of the International Energy Agency (IEA), several models were developed to couple CFD simulations with hygrothermal models of walls. For instance, Neale (2007) solved the heat and moisture transport in air and porous materials by developing a simplified hygrothermal model in MATLAB coupled to FLUENT software; Steeman et al. (2009) used the effective penetration depth (EPD) approach to couple CFD and moisture transport inside the wall which allows the simplified quantification, while it has been argued that the reliance on the moisture penetration depth concept necessitates comprehensive material properties (Janssen et al., 2007). Amissah (2005) coupled a 1D HAM model to a low-Reynolds number κ - ϵ turbulence model and Erriguible et al. (2006) coupled indirectly a 2-D CFD model with a 2-D hygrothermal material model. In these models, similar limitations can be found, and the main reason is that all these models are not simulated in one single simulation environment.

This paper presents the fitting between the time variation of the vapour concentration according to the CFD model and to the lumped model. The CFD output – in this case the relative humidity variation φ – is an average value over the room air volume, depending on the air velocity field.

The aim of the study is the coupling, within the COMSOL simulation environment, of the CFD and of the moisture transfer models and the comparison of the results with those obtained by the HAM-Tools lumped model.

2. Validation of the diffusion equations in COMSOL

Due to the simplified modelling of the air volume, HAM-Tools considers that each part of the wall absorbs the same amount of moisture, overestimating the material buffer. In real conditions, the influence of the ventilation system and of the air velocity pattern causes the presence of dead zones, where the moisture buffer decreased due to a higher surface vapour resistance. The calibration of the HAM-Tools simplified air ventilation lumped model will be carried out using the computational fluid dynamics from COMSOL.

This section is based on the validation, through HAM-Tools, of the equations of coupled heat and moisture transfer in building components implemented in Nusser and Teibinger (2012) using the physical approach modelled in WUFI, a well-known and worldwide used commercial software for calculating the HAM-transfer developed at the Fraunhofer Institute for Building Physics. Regarding the transport process, the coupled heat and moisture transfer is calculated from WUFI according to the following equations:

$$\frac{dH}{dT} \frac{\partial T}{\partial t} = \nabla(\lambda \nabla T) + h_v \nabla[\delta_p \nabla(\varphi \cdot p_{v,s})] \quad (1)$$

$$\frac{dw}{d\varphi} \frac{\partial \varphi}{\partial t} = \nabla(D_\varphi \nabla \varphi) + \delta_p \nabla(\varphi \cdot p_{v,s}) \quad (2)$$

where $dw/d\varphi$, or ξ , [kg/m³] is the moisture storage capacity, D_φ [kg/(m s)] the liquid conduction coefficient, h_v [J/kg] the latent heat of evaporation and dH/dT [J/(m³ K)] is the volumetric heat capacity, calculated as:

$$\frac{dH}{dT} = \left(c_p + \frac{1}{\rho_0} c_{p,w} \cdot w \right) \rho_0 \quad (3)$$

where c_p and $c_{p,w}$ [J/(kg K)] are the specific heat capacities of the dry material and of water respectively. In this approach, the temperature and the relative humidity are the driving potentials. Both potentials affect both transport processes, so

they have to be deviated with respect to space in both equations.

$$\delta_p \nabla(\varphi \cdot p_{v,s}) = \delta_p \varphi \frac{\partial p_{v,s}}{\partial T} \nabla T + \delta_p p_{v,s} \nabla \varphi \quad (4)$$

With Equation (4) the heat and moisture transport equation can be described in the following way:

$$\frac{dH}{dT} \frac{\partial T}{\partial t} = \nabla \left[\left(\lambda + h_v \delta_p \varphi \cdot \frac{dp_{v,s}}{dT} \right) \nabla T + h_v \delta_p p_{v,s} \nabla \varphi \right] \quad (5)$$

$$\frac{dw}{d\varphi} \frac{\partial \varphi}{\partial t} = \nabla \left[\left(\delta_p \varphi \cdot \frac{dp_{v,s}}{dT} \right) \nabla T + (D_\varphi + \delta_p p_{v,s}) \nabla \varphi \right] \quad (6)$$

and can be compared to Fick's second law equation model used in HAM-Tools, here described together with the heat transfer equation in order to have a direct comparison between the two models:

$$\rho_0 c_p \frac{\partial T}{\partial t} = - \frac{\partial}{\partial x} \left(\lambda \frac{\partial T}{\partial x} + \dot{g}_a c_{p,a} T + \dot{g}_v h_v \right) \quad (7)$$

$$\frac{\partial w}{\partial t} = - \frac{\partial}{\partial x} \left(\lambda_l \frac{\partial p_c}{\partial x} - \delta_p \frac{\partial p_v}{\partial x} + \dot{g}_a u \right) \quad (8)$$

Rearranging the transport equations (5) and (6) into matrix notation in order to input them in COMSOL, we finally obtain:

$$\begin{bmatrix} \lambda + h_v \delta_p \varphi \cdot \frac{dp_{v,s}}{dT} & h_v \delta_p p_{v,s} \\ \delta_p \varphi \cdot \frac{dp_{v,s}}{dT} & D_\varphi + \delta_p p_{v,s} \end{bmatrix} \begin{bmatrix} \nabla^2 T \\ \nabla^2 \varphi \end{bmatrix} = \begin{bmatrix} \left(c_p + \frac{1}{\rho_0} c_{p,w} \cdot w \right) \rho_0 & 0 \\ 0 & \xi \end{bmatrix} \begin{bmatrix} \frac{\partial T}{\partial t} \\ \frac{\partial \varphi}{\partial t} \end{bmatrix} \quad (9)$$

After the implementation of the HAM transport equations in COMSOL, the validation with the HAM-Tool model was carried out. The study will match the two models by gradually increasing the level of complexity. As a first approach to the matching between the results, a simple 3-layers wall case study has been chosen: 10 cm foam insulation, 10 cm aerated concrete, 3 cm gypsum

plaster; apart from the measured plaster's properties, the other material data were taken from Annex 24 (Kumaran, 1996). Several simulations were carried out in order to evaluate the influence of the layer discretization on the hygrothermal performance results in HAM-Tools and COMSOL. As the increase of the mesh detail leads to a longer simulation time, this process aimed at defining the best detail level for an acceptable simulation time, especially with regard to COMSOL. After the detail of the wall discretization was set for the three layers at 4, 10 and 6 nodes respectively (fine mesh settings), a 1-D HAM transfer simulation was carried out focusing on the temperature and on the relative humidity trends within the wall. Both the variables were monitored at nodes no. 3, 9 and 17 (central nodes of the layers) by using the two simulation tools. In this phase, any CFD was used to solve the indoor air in COMSOL, since only the indoor boundary conditions were set because the target was the moisture diffusion process within the building component first.

The simulations were carried out using the climate data of Turin as outdoor boundary conditions, for the first two weeks of January. The indoor temperature and relative humidity were set respectively at 20 °C and 50% and maintained constant throughout the simulation period; the same values were set for the materials' starting conditions, then left floating. According to Rode et al. (2005) the moisture transfer coefficients for outdoor and indoor respectively are $\beta_{ext} = 2 \cdot 10^{-7}$ kg/(m² s Pa) and $\beta_{int} = 2 \cdot 10^{-8}$ kg/(m² s Pa).

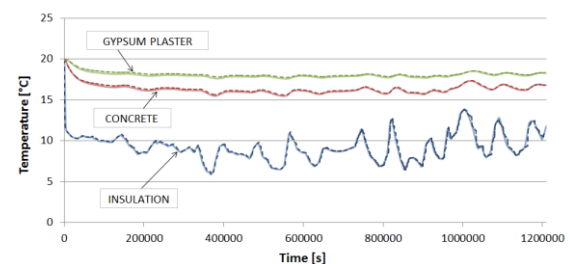


Figure 1 – Temperature trend for nodes n. 3-9-17 in the first 2 weeks of January (Turin weather data). The dotted and the continuous curves are related respectively to the HAM-Tools and to the COMSOL simulations.

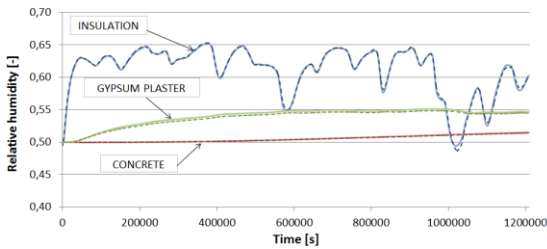


Figure 2 – Relative humidity trend for nodes n. 3-9-17 in the first 2 weeks of January (Turin weather data). The dotted and the continuous curves are related respectively to the HAM-Tools and to the COMSOL simulations.

No solar radiation nor ventilation was taken into account for the airtight structure. The simulation results show the perfect matching between the two models both for the temperature and for the RH trends (Fig. 1 and 2), validating the implemented equations from Nusser and Teibinger (2012).

3. Influence of the ventilation configuration on the room hygroscopic performance

At the room level, the two air models were compared after ensuring that the HAM-transfer model for building components was implemented in the same way for both the simulation tools.

As the solution time for CFD calculation is still a big issue, a 2-D model was set in a specific way to solve both the air balance and the moisture transfer in porous media on the same platform. Several attempts were performed on COMSOL to test the simulation time according to the calculation regime and the meshing size. Even with high CPU capabilities, solving both the domains in a time dependent regime means a simulation time closer to real time, so it would take too long without obtaining effective advantages. Since the influence of different flow patterns and velocity fields in the air volume on the moisture buffering was investigated, transient fluctuations of the velocity field on the component response to humidity variations can be neglected in favour of a simplified model that considers local equilibrium between the fluid region turbulence and the material surface.

The air movement inside the simulated room is turbulent with mixed convection conditions. In

COMSOL, two turbulence models are available: the $\kappa\text{-}\epsilon$ model and the $\kappa\text{-}\omega$ model. Theoretically, the $\kappa\text{-}\epsilon$ model is based on the assumption that the Re number is moderate or high and the turbulence in boundary layers is in equilibrium. The $\kappa\text{-}\omega$ model provides a better prediction in the free flows close to the wall, but it is less accurate in the free-stream flow simulation. In addition, the $\kappa\text{-}\omega$ model is harder to reach convergence. Meanwhile, the accuracy of CFD simulation results is related not only to the turbulent model selection, but it also depends on the wall surface conditions. In this 2-D simulation of the momentum, heat and mass coupling in different regions, using $\kappa\text{-}\epsilon$ model is a fair trade-off of saved computational resources compared to the more complicated turbulence models. The balance equations for the coupled heat and moisture transfer in air and within the building components were set to be solved in sequence in the COMSOL environment according to the following order:

- Air velocity field with CFD: steady state regime. For solution time and computing memory capacity reason – the use a coarse mesh (less detailed) is possible – the $\kappa\text{-}\epsilon$ turbulence model has been adopted (Figure 3);
- HAM-transfer: transient regime. After the air velocity field had been calculated for each point of the considered volume, the coupled heat and moisture transfer was solved for the zone and for the building components considering the boundary conditions reported below. The moisture source was placed in the middle of the room and the average RH level over the air volume was monitored.

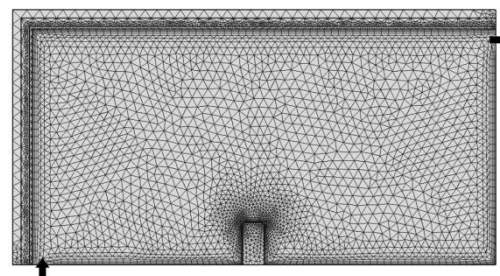


Figure 3 – Mesh definition for the air velocity field calculation. The inlet and outlet positions are indicated

The study has been applied to a simple room as defined by EN ISO 13791. The room volume in HAM-Tools was adapted to fit the 2-D model in COMSOL, which provides a 1 m deep third dimension for the building components for a total of 14.85 m³. For the air velocity field calculation a ventilation rate of 0.5 h⁻¹ was considered. Since the inlet and outlet vents comply with the described room dimensions a 0.1x1.0 m vent area was set, considering a 1 m long development along the wall. In this way, the volumetric air flow to the zone in HAM-Tools was normalized on the vent section. Thus, the corresponding air velocity at the inlet is 0.02 m/s.

The cyclic gain in the adapted test room (200 g/h) was set considering half of the moisture load in the full-sized simple room defined by EN ISO 13791, for which an 80 g/h (medium activity in offices in accordance with UNI TS 11300-1:2014) per person was considered for a 5 people occupancy.

The room is ventilated and the outdoor air conditions (temperature and relative humidity) were set according to the weather data for Turin (EnergyPlus weather data). The start RH level in the room and within the material was set at 30% and a gypsum plaster layer was applied as interior finishing together with an aerated concrete and foam insulation envelope. The study aims at demonstrating:

- the deviation between results obtained from HAM-Tools (lumped model) and COMSOL (CFD model) with regard to the indoor relative humidity trend for both cases when the environment is subjected to a cyclic moisture gain, constant for each scenario, and when there is no moisture load. According to recent studies from literature, a higher relative humidity level is expected within the room, due to the development of “dead zones” on the finishing material surface which do not fully interact in the moisture buffer process;
- the deviation on results between simulations carried out with different inlet and outlet vent positions, in order to evaluate how the configuration can affect the RH trend and the moisture buffer.

4. Results

In Figure 4 the relative humidity trend for scenarios with and without moisture gain are shown (4 curves). The simulation is related to a 0.5 h⁻¹ ventilation rate calculated with COMSOL and HAM-Tools.

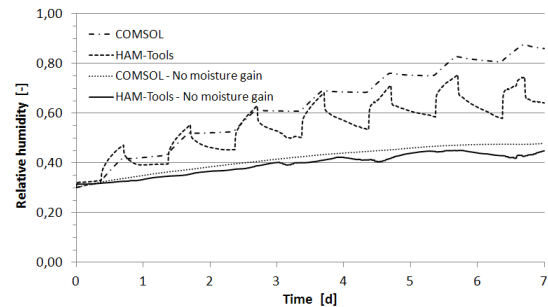


Figure 4 – Relative humidity trend for a 0.5 h⁻¹ ventilation rate. COMSOL and HAM-Tool results for scenarios with and without moisture gain

While a good fitting is reached between the curves without any vapour generation, the moisture gains determines a deviation of the RH trend denotes between COMSOL and HAM-Tools.

The cyclic load has a lower impact on RH peaks in the COMSOL environment, as the RH curve looks flattened. This behaviour is probably due to the RH averaging above the room volume, which involves the diversification between those zones directly affected by the moisture generation and those more distant not subjected to a sudden increase in the vapour concentration. This leads to a slower rise of the RH level during the loading period (8 hours) and to a likewise unloading phase that appears more like a “stabilisation” phase, where a real discharge of the RH level due to the ventilation mechanism does not occur. The average value of relative humidity for the 4 cases is reported in Table 1. The average relative humidity μ_{φ} [-] calculated in COMSOL denotes a $\Delta RH = +7\%$ for the case without moisture gain and a $\Delta RH = +10\%$ for the case with moisture gain, with respect to HAM-Tools results.

Table 1 – RH average value for the 4 simulated cases. 0.5 h⁻¹ ventilation rate, 200 g/h moisture gain.

Moisture load \dot{G}_{gen} [g/h]	μ_{φ} [-] (HAM-Tools)	μ_{φ} [-] (COMSOL)
0	0.39	0.42
200	0.57	0.63

In order to match the RH trends obtained from the two models, the following correction were applied to HAM-Tools:

- correction factor $C_{\beta} = 0.4$ applied to the indoor surface moisture transfer coefficient β_{int} . This aims at reducing the buffer capacity of the finishing layer by increasing its surface vapour resistance of 60 %;
- reduction of the building components area (-50 %). This allows us to consider that not all the surfaces are involved in the moisture buffer.

The above correction is in accord with a recent experimental study (Ramos, 2012), which demonstrates that the final buffer effect is half of the expected one.

Figure 5 shows the two approaches. In both the cases the calibration leads to an increase of the fluctuation amplitude of relative humidity – with an average RH value $\mu_{\varphi} = 58\%$ in either case – and not to a trend similar to the one obtained with COMSOL.

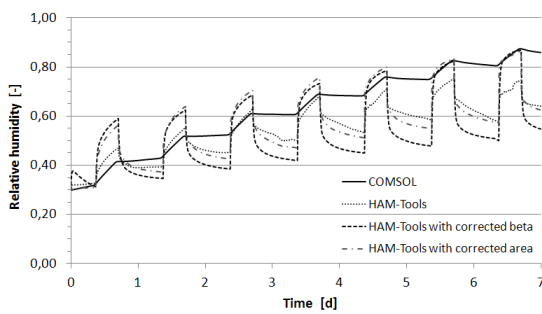


Figure 5 - HAM-Tools calibration on the results previously obtained for the scenario with moisture gain. The graph shows both cases: 1) application of a correction factor $C_{\beta} = 0.4$ to the indoor surface moisture transfer coefficient β_{int} ; 2) and reduction of the building components area (-40 %)

The next step was the evaluation of the influence of the vents configuration on the RH trend inside the room. Five different vent positions for the inlet and

outlet were considered, in order to make a sensitivity analysis. A deviation between results is expected, due to the affection of the air velocity field on the indoor surface vapour resistance of building components that leads to different amounts of buffered moisture. The scenario adopted for the sensitivity analysis is the 0.5 h⁻¹ ventilation rate, considering a 200 g/h moisture gain for the whole week (Turin weather data). In Figure 6, the air velocity field calculated in steady-state conditions and a snapshot of the respective relative humidity distribution over the air volume (transient conditions, 1-week simulation) according to vent configuration no. 1 is reported.

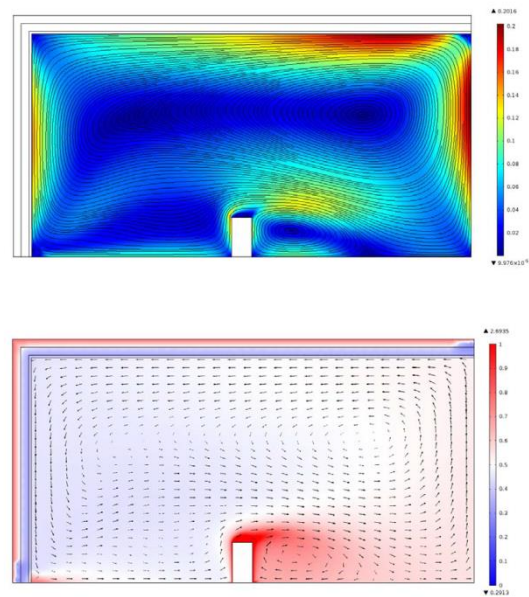


Figure 6 – The air velocity field calculated in steady-state conditions (above) and a snapshot of the relative humidity distribution in the air volume and within the envelope for vents configuration n.1

According to the different configurations and to the resulting air flow patterns, the zones with a reduced air velocity (i.e. $v < 0.02$ m/s) are clearly visible and not only localized in the corners of the room, but also in the central areas of the walls. This leads to localized surface moisture transfer coefficients that are characterized by several vapour resistances; in this way the interior finishing do not interacts in the same way with the moisture flux they come in contact with, defining a more detailed response to humidity variations by the building components.

The results highlight a deviation between the RH trends for the different vents configuration as expected. Figure 7 shows the humidity trend for each case, while the average value of RH is reported in Table 2. It is so possible to identify which configuration is most inconvenient for the moisture dampening inside the environment.

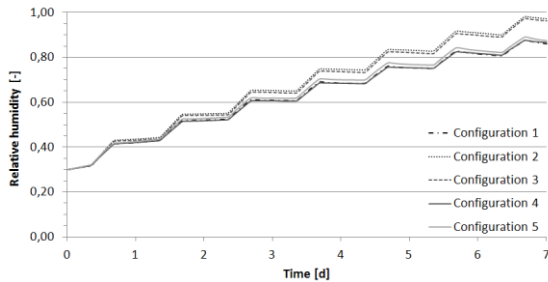


Figure 7 – Relative humidity trend for a 0.5 h^{-1} ventilation rate. COMSOL results for scenarios with different vents configurations

From the sensitivity analysis it is clear that configurations no. 2 and no. 3 lead to a higher RH level inside the room. This is probably due to the inlet vent position, located at the height of 2.70 m. Since the density of water vapour is lower than that of dry air, the generated moisture tends to go upwards, stratifying in the air volume in contact with the ceiling; the presence of the exhaust air vent in the upper part helps the moisture removal. A maximum ΔRH equal to 5 % is achieved between the lowest and the highest average RH value. However, configuration no. 5 does not account for any vent in the upper part of the wall but still shows an average RH level close to the first solutions.

Table 2 – RH average value for the 5 simulated vent configurations cases. 0.5 h^{-1} ventilation rate, 200 g/h moisture gain.

$\mu_{\varphi,1}$ [-]	$\mu_{\varphi,2}$ [-]	$\mu_{\varphi,3}$ [-]	$\mu_{\varphi,4}$ [-]	$\mu_{\varphi,5}$ [-]
0,63	0,68	0,67	0,63	0,64

The air velocity field is also responsible for the removed amount of moist air through the mechanical ventilation system, but how much this depends on one variable or another is still to be investigated.

5. Conclusion

COMSOL Multi-physics provides a simulation environment by coupling HAM equations and heat and moisture transfer between indoor air and enclosure without a third party programming. In the present work, the fully coupled model was established in this single simulation environment. This model has several advantages: 1) it overcomes the main limitations of the currently available CFD coupling models in simulating the whole building HAM transport, and 2) it has great application potential for the aspects related to ventilation design, HAM-transport through wall system and prediction of the room hygric inertia. The influence of the position of ventilation vents on the indoor RH trend, especially under low ventilation rates has been evaluated. The comparison between the lumped model (HAM-Tools) and the CFD model (COMSOL), when the HAM-transfer is applied, generated uncertainties. The first part of the investigation resulted in a good matching with regard to the diffusion equation implementation in COMSOL, validated by means of numerical simulation with HAM-Tools. The component behaviour with regard to the moisture transfer has been evaluated and both the simulation tools produce the same results.

The second phase, where the air zone has been solved with the CFD in COMSOL instead of using lumped conditions, was found critical with respect to the matching between the two software. The original intention to “rectify” the lumped model with another closer to reality generated difficulties to find a correction coefficient able to match the results. The CFD-HAM model on COMSOL should be validated by experimental data and needs to be improved and implemented. For this reason, we cannot assume it as the reference model and calibrate the lumped model with non-validated results.

6. Acknowledgement

This work was carried out within a research activity supported by Saint-Gobain PPC Italia S.p.A. about the *Influence of hygroscopic interior finishing on indoor comfort conditions*.

7. Nomenclature

Symbols

D_{φ}	liquid conduction coefficient (kg/ms)
c_p	specific heat capacity (J/kgK)
\dot{g}_a	density of air flux (kg/m ² s)
\dot{g}_v	density of moisture flux (kg/m ² s)
H	volumetric heat capacity (J/m ³ K)
h_v	evaporation enthalpy of water (J/kg)
T	absolute temperature (K)
t	time (s)
p_c	suction pressure (Pa)
p_v	vapour pressure (Pa)
$p_{v,s}$	vapour pressure at saturation (Pa)
u	moisture content by mass (kg/kg)
w	moisture content by volume (kg/m ³)
x	thickness (m)
δ_p	vapour permeability (kg/m s Pa)
λ	thermal conductivity (W/m K)
λ_l	liquid conductivity (s)
ρ_0	density of dry material (kg/m ³)
φ	relative humidity (-)
ξ	moisture storage capacity (kg/m ³)

References

P. Amisshah. 2005. "Indoor air quality - Combining air humidity with construction moisture." PhD thesis. Glasgow, U.K.: University of Strathclyde.

EN ISO 13791:2012. Thermal performance of buildings. Calculation of internal temperatures of a room in summer without mechanical cooling. General criteria and validation procedures.

A. Erriguible, P. Bernada, F. Couture, and M. Roques. 2006. "Simulation of convective drying of a porous medium with boundary conditions

provided by CFD." *Chemical Engineering Research and Design* 84 (A2): 113-123.

H. Janssen, B. Blocken, and J. Carmeliet. 2007. "Conservative modeling of the moisture and heat transfer in building components under atmospheric excitation." *International Journal of Heat and Mass Transfer* 50 (5-6): 1128-1140.

M. K. Kumaran. 1996. "Heat, Air and Moisture Transfer in Insulated Envelope Parts. Final Report, Volume 3, Task 3: Material Properties." In *International Energy Agency Annex 24*. Belgium: K. U. Leuven.

A. Neale. 2007. "A study in computational fluid dynamics for the determination of convective heat and vapour transfer coefficients". Master's thesis. Montreal: Concordia University.

B Nusser and M. Teibinger. 2012. "Coupled heat and moisture transfer in building components - implementing WUFI approaches in COMSOL Multiphysics." In *Proceedings of the COMSOL Conference, Milan*.

N.M.M. Ramos, Kalagasidis A.S., de Freitas V.P., and Delgado J.M.P.Q. 2012. "Numerical simulation of transient moisture transport for hygroscopic inertia assessment." *Journal of Porous Media* 15 (8): 793-804.

C. Rode, R. Peuhkuri, L.H. Mortensen, K. Hansens, B. Time, A. Gustavsen, T. Ojanen, J. Ahonen, K. Svennberg, L.E. Harderup, and J. Arfvidsson. 2005. "Moisture buffering of building materials." *Technical Report ISSN 1601-2917, ISBN 87-7877-195-1*, Technical University of Denmark.

H.J. Steeman, A. Janssens, J. Carmeliet, and M. De Paepe. 2009. "Modeling indoor air and hygrothermal wall interaction in building simulation: Comparison between CFD and well-mixed zonal model." *Building and Environment* 44 (3): 572-583.

UNI TS 11300-1:2014. Energy performance of buildings. Part 1: Evaluation of energy need for space heating and cooling.

Optimizing Window size of South Facades in Tehran City and the Environmental Impacts

Fazel Khayatian – Politecnico di Milano – fazel.khayatian@polimi.it

Seyed Amin Tabatabaei Fard – Shiraz University – amintaba@shirazu.ac.ir

Maryam Meshkin Kiya – Islamic Azad University – m.meshkinkiya@gmail.com

Abstract

This paper investigates the effects of altering the glazing size of lounge spaces in Tehran city houses. The magnitude of effects is demonstrated through comparing the energy consumption of various models. A great portion of the global energy consumption and resource depletion is dedicated to the construction sector. Considering the low thermal resistance of windows and their role in a building's aesthetic, optimizing window to wall ratio is a key factor in the design process. This research attempts to find the optimum glazing area of lounge spaces while monitoring energy consumption and daylight factor simultaneously. A total of 16 samples with different width to length ratios are studied by exploring the minimum satisfactory daylight factor according to BREEAM regulations. Considering the importance of south facades in Tehran city's urban texture, this paper is concentrated on south façade glazing proportions. Final results indicate that increasing the glazing area of a south façade after meeting the minimum required daylight factor may double the annual energy consumption of a living space. Results also show that altering the window to wall ratio of the south façade has a liner impact on the annual energy consumption of lounge spaces.

1. Introduction

Since the Industrial revolution, the amount of carbon dioxide and nitroxide emitted into the atmosphere has increased by 30% and 15% respectively, and the methane ratio has doubled. It is predicted that by continuing air pollution with current rate, the amount of carbon dioxide in the atmosphere will have increased by about 50% by 2050 (NRC 2008). Studies indicate that the construction sector is responsible for consuming

one-third of the earth's resources, i.e. energy, water and materials (Long et al. 2007). It is noteworthy that more than half of the total energy consumed by the construction sector is associated with residential buildings (DoE 2011). Recent studies have noted that about 40% of the global energy consumption and 36% of the total carbon dioxide emissions in the world is linked to the residential sector (IEA 2012). Unfortunately, Iran, with a carbon dioxide emission of 8 tons per capital, is considered the 7th most polluting country per capita in the world. Moreover, an energy consumption rate of 314 kWh per capita, places Iran as the 11th most energy-consuming country globally (EIA 2011). Regarding the fact that windows consist of high thermal conductivity, and are also responsible for a major share of the thermal waste, optimal design of building glazing areas seems inevitable.

2. Research Background

Due to the aesthetic importance of windows in building facades, also considering their role in indoor solar absorption and thermal waste, these components have been carefully studied in energy optimization fields (Bodart and Herde 2002; Stegou-Sagia et al. 2007; Hassouneh, Alshboul and A. Al-Salaymeh. 2010; Ebrahimpour and Maerefat 2011). Among the most significant literature in the field of building glazing optimization is the research conducted by Jonson and his colleagues (Johnson et al. 1982; Johnson et al. 1984). They concluded that it is possible to reduce the electric energy consumption of a building by 31 percent, only via optimizing the Window to Wall Ratio

(WWR). Yet, the recommendations made in these studies are limited to office buildings. Another study conducted by Inanici & Demirbilek suggests that for hot arid climates, the optimum WWR is 25 percent (Inanici and Demirbilek 2000). Generally, optimizing the window area has a great effect on heating and cooling loads. However, a study reveals that in cold climates, reducing the WWR by 20-50 percent might not affect the heating loads greatly (Presson, Roos and Wall 2006). Therefore, the recommended window area of south façades, while taking into account the Daylight Factor (DF) and visual comfort varies greatly. For the Netherlands, the suggested optimum WWR is 21 percent, whereas for Slovenia the ideal WWR is recommended between 36 and 46 percent (Ochoa et al. 2012; Leskovar and Premrov 2012). By monitoring the relation of glazing size and energy consumption in various Asian cities, Lee and colleagues proposed some recommendations in this field. They suggested that for cities that are categorized under ASHRAE type 3 climates (such as Tehran), a 25% WWR for triple layer windows is optimal. However, they did not discuss the daylight availability (Lee et al. 2013). Khatami and colleagues introduced a method for optimizing the window area in Iran by using EnergyPlus™ software. Yet, the research is solely focused on the relation between solar insolation and energy consumption, while not taking into account the daylight factor (Khatami et al. 2012). Other studies suggested that the optimum window area for low-rise buildings in Tehran city is about 15 percent of the room floor area (Fayyaz 2012). Nevertheless, regulations instructed by authorities have always been the basis for building design. Regarding section 19 of Iran’s National Building Regulations, it is suggested that the glazing area in residential buildings should not exceed more than 25% of the façade area (Iran National Building Regulations 2010).

3. Methodology

Considering the regular dimensions used in residential building design, the minimum and maximum width and depth of a living room is

considered to be between 3 and 6 meters. Also the living room net height is presumed to be 2.7 meters, as this proportion is very popular and commonly used. Between the smallest possible sample (with a width and depth value of 3 meters) and the largest model (with 6 meters of width and depth), a total of 16 samples (Table 1) are studied. In order to make the comparison conclusive, only the south façade is equipped with a window in this paper. Studies have concluded that for similar climates, the south façade is most energy efficient for installing windows (Lee et al. 2013).

Table 1 - Dimensional properties of samples

Sample	width (m)	depth (m)	height (m)	w/d	d/h
S1	3	3	2.7	1	1.11
S2	3	4	2.7	0.75	1.48
S3	3	5	2.7	0.6	1.85
S4	3	6	2.7	0.5	2.22
S5	4	3	2.7	1.33	1.11
S6	4	4	2.7	1	1.48
S7	4	5	2.7	0.8	1.85
S8	4	6	2.7	0.66	2.22
S9	5	3	2.7	1.66	1.11
S10	5	4	2.7	1.25	1.48
S11	5	5	2.7	1	1.85
S12	5	6	2.7	0.83	2.22
S13	6	3	2.7	2	1.11
S14	6	4	2.7	1.5	1.48
S15	6	5	2.7	1.2	1.85
S16	6	6	2.7	1	2.22

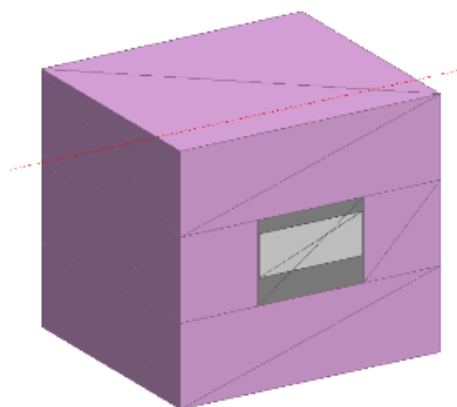


Fig. 1 - Graphical illustration of a modeled sample

3.1 Modelling

Samples are modelled with DesignBuilder software Version 4.2, which runs simulations using an Energyplus™ engine Version 8.1. Except for the south façade, all the vertical surfaces of the lounge zone are modeled as interior walls with no glazing. This approach is utilized in order to minimize the effects of thermal conductivity and solar radiation on non-dominant walls. A similar approach was utilized in some research for studying a room in a cellular office (Gratia and Herde 2003). The composition and layers of the south façade is illustrated in Table 2, where the mean thermal conductivity of the wall is set to 0.249 W/m²K. Also, the average thermal conductivity of the window with a UPVC frame and the floors are 2.665 W/m²K and 0.15 W/m²K respectively. The studied façade has a uniform window which is placed at the center of the wall with no shades. As we attempt to minimize the effects of roof and ceiling, also neutralizing their thermal conductivity and reflections received from the ground, samples are placed one story above the ground level (Fig. 1).

Table 2 - Materials and properties in the south facade

Wall		Window	
Materials	Thickness (mm)	Materials	Thickness (mm)
Composite Cladding	6	Clear Glass	6
Polystyrene XPS	128.6	Air	13
Stucco	13	Clear Glass	6

3.2 Climate conditions

Samples are studied in Tehran city weather conditions, which are categorized as 3B in ASHRAE classifications. The city features a semi-arid climate according to Koppen-Geiger classifications with a latitude and longitude of 35.68N and 51.32E respectively at 1190 meters above sea level. Regarding thermal comfort, the climate consists of approximately 2850 Heating Degree Days (HDD) and 2770 Cooling Degree Days (CDD) (ASHRAE 2001; Heidarinejad, Heidarinejad and Delfani 2008; Peel, Finlayson and McMahon

2007). The weather data file used for simulation is supported by the DesignBuilder database. In software settings, the site wind exposure is set to “standard” option, while the orientation is due south and no shading obstacles are defined.

3.3 Variables

The variables studied are width to depth ratio of spaces and the glazing area of the south façade. Samples are simulated for 8760 hours, which is equivalent to one year. Afterwards, the energy and daylight performance are monitored. In this study, the quantity of natural daylight is presented as Daylight Factor (DF). Different environmental assessment methods such as LEED, BREEAM and GreenStar, have diverse requirements for an acceptable daylight. The Building Research Establishment (BRE) in the UK issues one of the strictest standards for acceptable daylight. Two main factors are measured in the BREEAM method. First, at least 80% of the occupied area must have uniform daylight, where the minimum average DF is 2.0%. Second, it is mandatory to have a uniform ratio of 0.4, or a minimum point DF of at least 0.8% (DCLG 2009).

It is notable that in the BREEAM assessment method, both mentioned standards have to be met simultaneously. DesignBuilder software has made it possible to check whether the samples meet with BREEAM daylight regulations. The precision setting for daylight assessment is adjusted to option number five, “Accurate”.

Towards finding optimum WWRs, DesignBuilder software is coupled with a trial and error optimizing process. In this method, the WWR of the south façade is increased from zero percent, until BREEAM daylight requirements are met. Meanwhile, the annual energy consumption is measured for the optimum glazing size of each sample (Fig. 2). Afterwards, the WWR is increased until the window covers the whole façade (WWR of 100%). At this time, the annual energy consumption of samples is measured in 10 percent intervals. This approach is adopted to demonstrate the effects of excess glazing area from an energy performance point of view.

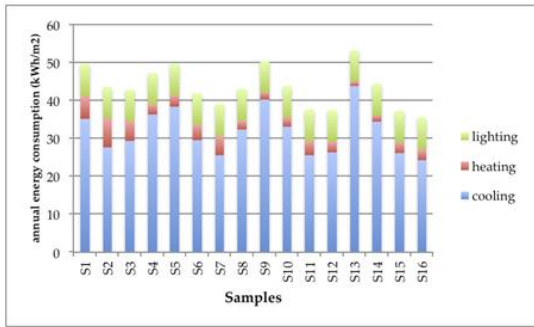


Fig. 2 - HVAC and lighting performance of optimum samples

4. Results and Discussion

Final results indicate that rooms with different width or depth meet their optimum glazing area in various proportions. Sample S1 required a 27% glazing area of the studied façade in order to meet the daylight regulations, while sample S4 required 62% WWR for an acceptable daylight. It is notable that both samples have the same width values which means they consist of similar façade areas. Therefore, it is clear that dictating a certain WWR value for a fixed façade area is not reasonable. The annual energy consumption and WWR of optimum samples is displayed in Table 3. Samples that consist of a small width (S1, S2, S3, and S4) show great variation in their optimum WWR. Meanwhile, the models that have a have greater width (S13, S14, S15, S16) express a smaller difference in their optimum WWR. Similar assumptions could be drawn concerning the depth of samples. Models that have a 3 meters depth (S1, S5, S9, and S13) show little variation between their optimum WWR, while the ideal glazing size in models with greater depth (S4, S8, S12, S16) vary significantly. Therefore, it is obvious that sample S4 consisting of a small width and a great depth, requires the most glazing size.

It may be suggested that optimizing daylight factor is strongly related to a room’s width to depth proportion. However, samples with the same w/d factor display various WWRs. Therefore, it can be concluded that another factor that affects the optimal WWR is the relation between a sample’s depth and height. When the depth to height ratio (d/h) increases, more glazing area is required in order to obtain a satisfactory daylight level. This is

why sample S4 needs more WWR than samples S8, S12 and S16 considering that they all have the same w/d. Sample S4 consists of the least w/d ratio and the greatest d/h ratio simultaneously (as seen in Table 1). Also, this fact explains why sample S1 requires the smallest WWR compared to others. Sample S1 has the greatest w/d and the smallest d/h at the same time.

Table - 3 Energy consumption and WWR of optimum samples

Sample	Floor Area (m)	Energy Consumption (kWh/m².a)	Window size (WWR)
S1	9	64,59	27
S2	12	55,6	30
S3	15	54,93	42
S4	18	61,28	62
S5	12	64,7	31
S6	16	53,7	34
S7	20	49,55	37
S8	24	55,52	56
S9	15	65,32	33
S10	20	56,69	37
S11	25	47,73	38
S12	30	47,49	49
S13	18	68,71	37
S14	24	57,21	39
S15	30	47,15	40
S16	36	44,75	45

Studying the net energy consumption of samples with optimum WWR reveals that most of the energy utilization is dedicated to cooling loads (Fig. 2). However, the relation between window size and energy consumption is not entirely clear. Sample S13 has the most energy consumption while its WWR is not the greatest. There is a possibility that the energy consumption of optimum samples is related to the window size per floor area. Yet, there are definitely other factors affecting this relation. Figure 3 demonstrates a possible relativity between energy consumption and window to floor ratio of the samples. It seems that this relation is driven from the massive cooling loads which is also related to excessive solar abortion through windows.

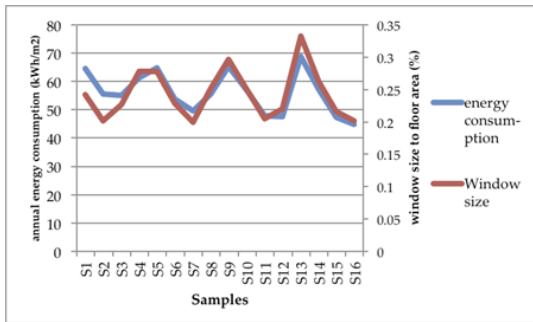


Fig. 3 - Possible relation between energy consumption and window size of optimum samples

Figure 4 shows the effects of increasing window size after reaching a satisfactory daylight level. Samples with a small width seem to be more affected than samples with a greater width. For example, the energy consumption of sample S1 will increase about 16% for each 10 percent extra glazing. This increase rate is much smaller (about 9%) for sample S4. However, models with the same depth, display similar performances regarding excessive glazing size. This fact can be confirmed by analysing the samples presented in figure 5.

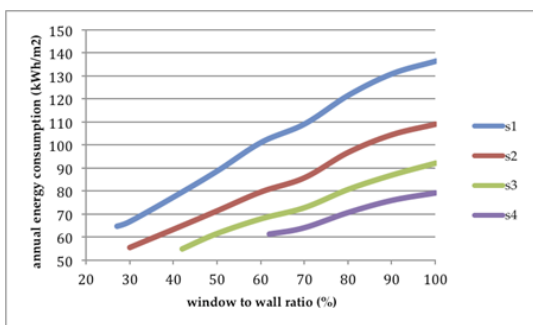


Fig. 4 - The relation between annual energy consumption and WWR of samples with similar width

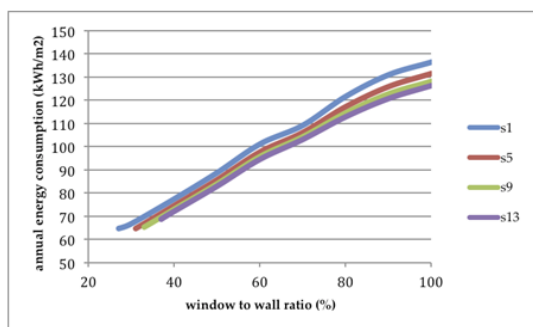


Fig. 5 - The relation between annual energy consumption and WWR of samples with similar depth

Regarding the energy consumption of samples, it can be inferred that increasing the WWR of south façades has a linear impact on a room’s environmental performance. This conclusion may be a great aid to architects and designers working at the early stages of design. Therefore, performing numerous simulations will be unnecessary and architects can anticipate the environmental performance of their building by performing only a few simulations. It also reduces the possibility of compromising the design aesthetic, as the glazing area can be modified at early stages of design.

5. Conclusion

Utilizing vast amounts of glass in building façades has gained great popularity between contemporary Iranian architects who practice residential buildings. Applying such façades in some countries, especially those with a cold climate, has been a great benefit from a sustainable point of view. However, due to high solar radiation in most of the major cities in Iran, applying total glazed and frameless glass facades requires a good knowledge of building physics and their environmental performance. Therefore, this paper intends to study the effects of increasing glazing area of south façades in Tehran houses, from an environmental point of view. The results of this study indicate that the optimum glazing area is related to width to depth ratio and depth to height ratio. As the width to depth ratio increases, less glazing area is required for adequate daylight. On the other hand, increasing depth to height ratio has an inverse effect on daylight performance. Also, it is suggested that the relation between the glazing area and energy consumption is mostly related to cooling loads in Tehran’s climate. Results show that the relation between window to wall ratio and energy consumption is linear. Yet, the steep of the linear increase is relative to a room’s depth and varies between 9% to 16% for each 10% added to the WWR. Finally, it was found that expanding the window size after reaching a satisfactory daylight could increase the annual energy consumption up to twice the minimum necessary amount.

References

- Bodart, Magali, and André De Herde. "Global energy savings in offices buildings by the use of daylighting." *Energy and Buildings* 34, no. 5 (2002): 421-429. doi:10.1016/S0378-7788(01)00117-7
- DCLG, UK. "Code for Sustainable Homes Technical Guide." London: Communities and Local Government Publications (2009).
- DoE, U. S. "Buildings energy databook." Energy Efficiency & Renewable Energy Department (2011).
- Ebrahimpour, Abdulsalam, and Mehdi Maerefat. "Application of advanced glazing and overhangs in residential buildings." *Energy Conversion and Management* 52, no. 1 (2011): 212-219. doi:10.1016/j.enconman.2010.06.061
- EIA, US. "International energy statistics." US Energy and Information Administration, Washington, DC [available at <http://www.eia.gov/countries/data.cfm>] (2011).
- Fayyaz, Rima, "Optimum Window Area of Buildings in Tehran and Ardebil." *Letter of Architecture and Urbanism* 10, (2012): 105-119. (in Persian)
- Gratia, Elisabeth, and André De Herde. "Design of low energy office buildings." *Energy and Buildings* 35, no. 5 (2003): 473-491. doi:10.1016/S0378-7788(02)00160-3
- Handbook, A. S. H. R. A. E. "Fundamentals." American Society of Heating, Refrigerating and Air Conditioning Engineers, Atlanta 111 (2001).
- Hassounah, K., A. Alshboul, and A. Al-Salaymeh. "Influence of windows on the energy balance of apartment buildings in Amman." *Energy Conversion and Management* 51, no. 8 (2010): 1583-1591. doi:10.1016/j.enconman.2009.08.037
- Heidarinejad, Ghassem, Mohammad Heidarinejad, and Shahram Delfani. "Outdoor design conditions data for the cities of Iran." In *Proceedings of AIAA 6th International Energy Conversion Engineering Conference (IECEC)*, Cleveland, Ohio. 2008. doi:10.2514/6.2008-5702
- Inanici, Mehlika N., and F. Nur Demirbilek. "Thermal performance optimization of building aspect ratio and south window size in five cities having different climatic characteristics of Turkey." *Building and Environment* 35, no. 1 (2000): 41-52. doi:10.1016/S0360-1323(99)00002-5
- National Office of Building Regulations, Iran. Chapter 19 of the National Building Regulations: Energy Efficiency in Buildings, (2010). (in Persian)
- Johnson, Richard, Stephen Selkowitz, Frederick Winkelmann, and Michael Zentner. "Glazing optimization study for energy efficiency in commercial office buildings." In *Third International Symposium on Energy Conservation in the Built Environment*, Dublin, Ireland. 1982.
- Johnson, R., R. Sullivan, S. Selkowitz, S. Nozaki, C. Conner, and D. Arasteh. "Glazing energy performance and design optimization with daylighting." *Energy and Buildings* 6, no. 4 (1984): 305-317. doi:10.1016/0378-7788(84)90014-8
- Khatami, M., M. Kordjamshidi, B. Mohammad Kari, and S.A.R. Zolfaghari, "Analyzing the Effects of Windows Thermal Resistance and the Orientation of the Transparent Area on Optimizing Glazing Areas in Tehran." In *1st National Conference on Insulation*, Iran Institute of Polymers and Petrochemicals, Iran, 2012. (in Persian)
- Lee, J. W., H. J. Jung, J. Y. Park, J. B. Lee, and Y. Yoon. "Optimization of building window system in Asian regions by analyzing solar heat gain and daylighting elements." *Renewable Energy* 50 (2013): 522-531. doi:10.1016/j.renene.2012.07.029
- Leskovar, Vesna Žegarac, and Miroslav Premrov. "Influence of glazing size on energy efficiency of timber-frame buildings." *Construction and Building Materials* 30 (2012): 92-99. doi:10.1016/j.conbuildmat.2011.11.020
- Long, Nicholas, Paul Torcellini, Ron Judkoff, Drury Crawley, and John Ryan. *Assessment of the technical potential for achieving net zero-energy buildings in the commercial sector*. Golden, CO: National Renewable Energy Laboratory, 2007.
- Ochoa, Carlos E., Myriam BC Aries, Evert J. van Loenen, and Jan LM Hensen. "Considerations on design optimization criteria for windows

providing low energy consumption and high visual comfort." *Applied Energy* 95 (2012): 238-245. doi:10.1016/j.apenergy.2012.02.042

Peel, Murray C., Brian L. Finlayson, and Thomas A. McMahon. "Updated world map of the Köppen-Geiger climate classification." *Hydrology and earth system sciences discussions* 4, no. 2 (2007): 439-473 doi:10.5194/hessd-4-439-2007

Persson, Mari-Louise, Arne Roos, and Maria Wall. "Influence of window size on the energy balance of low energy houses." *Energy and Buildings* 38, no. 3 (2006): 181-188. doi:10.1016/j.enbuild.2005.05.006

Statistics, I. E. A. "CO2 emissions from fuel combustion-highlights." IEA, Paris <http://www.iea.org/co2highlights/co2highlights.pdf>. (2011).

Stegou-Sagia, A., K. Antonopoulos, C. Angelopoulou, and G. Kotsiovelos. "The impact of glazing on energy consumption and comfort." *Energy Conversion and Management* 48, no. 11 (2007): 2844-2852. doi:10.1016/j.enconman.2007.07.005

Analysis of energy efficiency measures on envelope and control systems: case study for an existing building

Giovanni Semprini, DIN, School of Engineering and Architecture, Alma Mater Studiorum – University of Bologna, Bologna, Italy, giovanni.semprini@unibo.it

Alessandro Gober, CIRI, School of Engineering and Architecture, Alma Mater Studiorum – University of Bologna, Bologna, Italy, alessandro.gober@unibo.it

Francesca Zandi, Building engineer, School of Engineering and Architecture, Alma Mater Studiorum – University of Bologna, Bologna, Italy, francesca.zandi@gmail.com

Abstract

The buildings dating back to the Italian economic boom of the 60s and 70s are the biggest part of the national building heritage. In general they have an envelope with very poor thermal insulation and a central heating system with high energy consumption, sometimes due to the lack of a proper control system, obsolete components and a not balance pipe network. This group of buildings is one of the first targets to be addressed through building renovation and improving plant.

Energy retrofiting actions is the main direction not only to provide a reduction in CO₂ emissions and money saving but also to achieve thermal comfort for a large number of families.

In order to reach both these objectives, a pipe balancing and proper control systems must accompany every kind of envelope upgrading.

This paper deals with the interaction between the envelope refurbishment and the optimization of the plant control system in a typical 60s-70s Italian residential multi-floor building served by a central heating system, focusing on a single flat.

After a proper calibration of the model, based on experimental measurements of the internal temperature and operating conditions of the heating plant, the dynamic simulation assessed through EnergyPlus was used to analyze the efficiency of different control systems to improve the energy performances: use of climatic curve control, zone control with ambient thermostat or thermostatic valves, and different proportional bands.

Simulation results indicate high energy savings.

1. Introduction

The use of building automation control systems to improve energy efficiency of heating systems and thermal comfort inside buildings has become an increasingly important over the years. In many buildings from the 60s and 70s, the water in the pipe network is usually set to 75-80 °C; consequently, the radiators were "sized" with these temperature values. Renovation works made in single apartments over the years, and different thermal loads for rooms with different solar exposition, resulted in discomfort conditions and high energy consumption. To optimize the control systems of these extremely energy-intensive, different systems of thermoregulation were compared. In the process of choice of systems related to energy conservation, it is essential to support energy-efficient design decisions with the help of dynamic analysis. This type of analysis can justify the choice of such interventions.

The dynamic energy simulation is a time-dependent simulation, which allows us to estimate the actual thermodynamic behavior of the apartment. The effect of the outdoor climate conditions and of the occupants' behavior, both measured hour by hour, add complexity to the problem and make it possible to predict building performance.

2. Description of the case study

2.1 The building envelope

The apartment under study is part of a linear building located in the extreme northern suburbs of Bologna, part of the pole settlement P.E.E.P. of Corticella, dated 60/70, served by a central thermal plant and a district heating network.

The opaque walls are of three different types: bearing structure of reinforce concrete, internal and external masonry walls, and precast concrete panels on the façades characterized by ribbon windows. These are single glazed, with non-thermal break aluminum frame.



Fig. 1 – External view of the building (north façade)

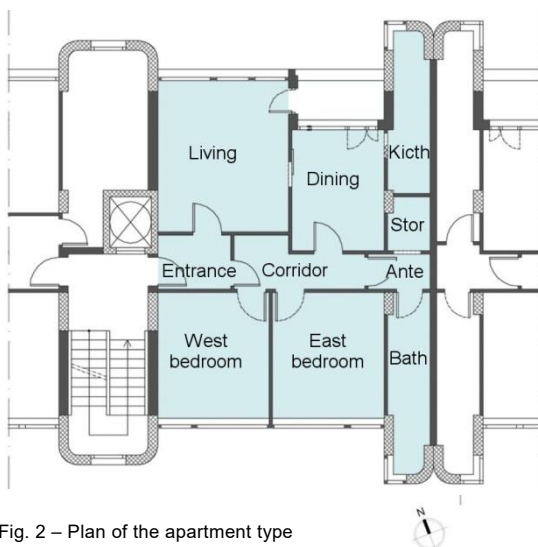


Fig. 2 – Plan of the apartment type

All data, such as the geometry and the components of building envelope, were known; otherwise, thermal properties of different building structures, in the absence of original data, were calculated according to actual technical standards: UNI/TS 11300-1, UNI 10351 and UNI 10355.

2.2 The heating plant

The terminal units of the heating plant are convective heaters (Fig. 3). Due to the impossibility to know the effective thermal power output, each terminal was sized according to the calculation procedure required by UNI EN ISO 12831.



Fig. 3 – View of an installed heater

The heaters are units with low thermal inertia, which can quickly satisfy changes in thermal needs of the room, working predominantly by natural convective heat transfer.

Terminal units were considered to be fed with a rated average water temperature of 70°C and sized according to a thermal gradient of 50°C.

3. Actual situation: modelling and calibration

3.1 Energy Modeling

The dynamic simulations were performed through 'EnergyPlus' (version 8.1) software (energy calculation) and the corresponding 'Legacy OpenStudio' SketchUp plug-in (geometrical input data, see Fig. 4).

After the construction of the model, the comparison between simulation data and experimental measurements allowed us to calibrate the building-plant system.

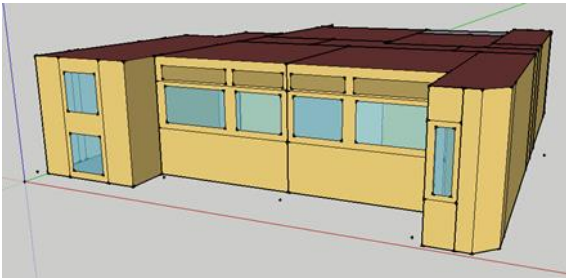


Fig. 4 – 3D model of the apartment

Afterward, simulations were performed to evaluate the energy consumption of the plant in the actual configuration, and compare it with the technical solutions proposed to improve the efficiency of control systems.

3.2 Calibration of the model

The calibration of the model was not easy to achieve due to the uncertainty of some features of the building envelope and the heating system. Due to the inability to carry out direct measurements of energy consumption, calibration was performed based only on temperatures, moving by successive approximations.

A campaign of measurements was conducted, monitoring the following parameters for each room:

- indoor air temperature at the center of the room, at an height of 1,20 m;
- temperature of the air coming out from the terminal unit.

Furthermore, we asked people living in the flat to record their time staying in the various rooms and the aeration duration intervals.

Data analysis suggested reducing the rated terminal units power outputs compared to those calculated according UNI EN ISO 12831 of more than 40%, bringing to values reported in Tab. 1.

A qualitative trend matching of measured and calculated internal temperatures, and their punctual deviations within 1°C when plant is on, were deemed satisfactory for the purpose of the present study (see Fig. 5).

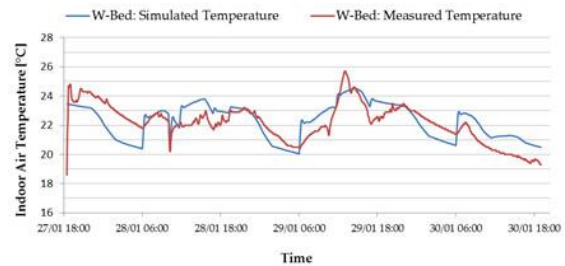


Fig. 5 – Comparison between measured and simulated indoor air temperature in west bedroom

Table 1 – Size of terminal units

Room	P _{unit}	M'	M',ratio
	[W]	[kg/s]	[%]
Dining	655	0,011565	11,2
Kitchen	983	0,023480	22,8
Living	1056	0,025430	24,6
West bedroom	655	0,011565	11,2
East bedroom	655	0,011565	11,2
Bathroom	819	0,019570	19,0
Ante-bathroom	0	0,00000	0,0
Storage room	0	0,00000	0,0
Corridor	0	0,00000	0,0
Entrance	0	0,00000	0,0

4. Control system

In order to understand how to model a more properly controlled system for radiators with thermostatic valves, it is worth analysing these two basic components, for which EnergyPlus does not have explicit objects for modelling.

4.1 Plant terminal units performances

4.1.1 Product standard

In plant design, radiator and convector performance is regulated by a specific product standard (UNI EN 442). They are rated in terms of heat output to room air $P_{w/a}$ at standard condition ($\Delta t_{w/a, std} = 50^\circ\text{C}$) with an exponent 'n' to correct

their thermal performances, if different to standard conditions:

$$P_{w/a} = P_{w/a, std} (\Delta t_{w/a} / \Delta t_{w/a, std})^n \quad (1)$$

From the point of view of the terminal unit, the energy balance reduces to well-known equation:

$$P_w = M'_{w} c_{p,w} \Delta t_w \quad (2)$$

with the two powers $P_{w/a}$ and P_w obviously equal in a steady state condition.

After setting their design values and keeping the supply temperature $t_{w, in}$ constant it is possible to solve the system equations (1) and (2) and express the percentage of terminal heat output in terms of percentage of water mass flow rate (both referred to their design values, as graphed in Fig. 6.

4.1.2 EnergyPlus object method

The most suited EnergyPlus inbuilt plant components to represent radiators or convectors are the “baseboard” objects “ZoneHVAC: Baseboard: Convective: Water” (*conv-bb*) and “ZoneHVAC :Baseboard: RadiantConvective: Water” (*radconv-bb*) (EnergyPlus Engineering Reference). These two objects are simulated by the same algorithm with two small differences: first, in *radconv-bb* a quote of radiant heat exchange can be added to the convective one; second, the way the thermal performance at standard conditions of the unit is described. *Conv-bb* requires directly the UA value, rather than *radconv-bb* where input fields are the rated water mass flow rate $M'_{w, std}$, the rated average water temperature $t_{w, avg, std}$ and the rated thermal output $P_{w, std}$ (EnergyPlus Input/Output Reference). Starting from these values, before performing the energetic simulation, assuming a rated inlet air temperature of 18°C ($t_{a, in, std} = 18^\circ\text{C}$) and a rated air mass flow twice of the rated water mass flow rate ($M'_{a, std} = 2 M'_{w, std}$), the code runs a basic calculation based on LMTD method to achieve the UA value even for *radconv-bb* component. Running the simulation, the code evaluates at each timestep the component performance through the NTU-e method, with the efficiency expressed by the characteristic equation of the counter-flow heat exchanger (EnergyPlus Engineering Reference), (ASHRAE HOF, 2009).

The resulting mass flow / heat output relationships are graphed in Fig. 6.

Two different approaches are shown, which lead to

different performance assessments: product standard deals with radiators and convectors as plant terminal units, rather than EnergyPlus algorithm that models them as a generic counter-flow heat exchangers.

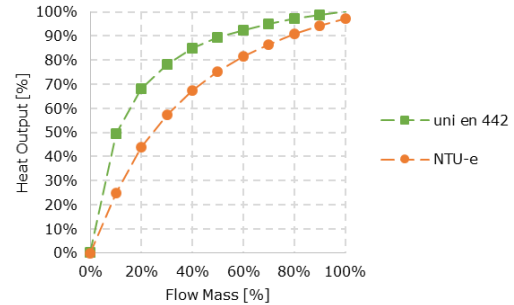


Fig. 6 – Terminal unit characteristic curves for radiator according to UNI EN 442 and NTU-e method

4.2 Valves performances

Thermostatic radiator valves (TRVs) are a control system consisting of a sequence of sensor -> regulator -> actuator.

4.2.1 Sensor and regulator

Sensor and regulator are both embodied in the valve head that performs as self-operated temperature proportional regulator. The sensing head moves the stem and the shutter proportionally (kp) to the air room temperature detected (t_{room}) due to expansion or contraction of the sensing element itself, according to:

$$U = b + kp e \quad (3)$$

where the output ‘U’ is the stem travel (ST) or valve opening, ‘b’ is the bias, the proportional gain ‘kp’ can be expressed as the reverse of the proportional band PB ($kp=1/PB$), and the error ‘e’ is $\Delta t = t_{room} - t_{setpoint}$ (see Fig. 7) (AICARR, 2009), (Socal 2013).

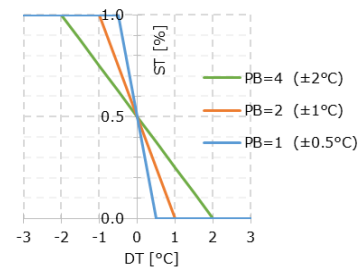


Fig. 7 – Signal control (stem travel ST for TRVs) for different working proportional bands PB

4.2.2 Actuator

The shutter is the actuator in the control chain: it acts on the water flow rate to be passed to the radiator, based on the signal control output and following its characteristic curve. There are four main types of valve characteristic curves (Miccio, 2012) (Scali, 2006): 1-Quick Opening (QO), 2-Linear (LIN), 3-Parabolic or Quadratic (PAR), and 4-Equal Percentage or Exponential (EQP), all suitable to perform control operations, except the quick opening (see Fig. 8 and Tab. 2).

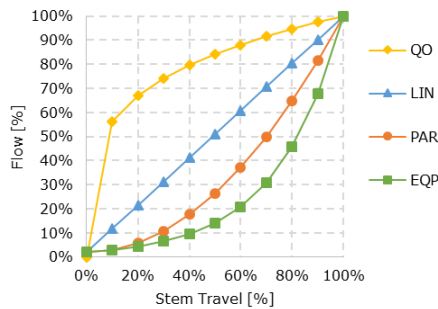


Fig. 8 – Valve characteristic curves, built with $R=50$ and $\delta = 4$

Table 2 –Four main types valve characteristic curves and their equations

Valve Type	Curve equation
Quick Opening (QO)	$\text{Flow} = \text{ST}^{(1/\delta)}$
Linear (LIN)	$\text{Flow} = \text{ST} + (1-\text{ST})/R$
Parabolic or Quadratic (PAR)	$\text{Flow} = \text{ST}^2 + (1-\text{ST}^2)/R$
Equal Percentage or Exponential (EQP)	$\text{Flow} = R^{(\text{ST}-1)}$

$R = \text{Valve rangeability} = Kvs/Kvr$ (30-100 typical for TMVs)

4.3 Terminal-Valve matching

With the hypothesis of a linear behavior of the thermal problem (i.e. fixed room air temperature value by means of a variation of the thermal power delivered by a terminal unit), we looked for a linear relationship between the process variable (room air temperature) and the parent variable (heat output from terminal unit) (Belimo, 2014). As shown in Fig. 9, an equal percentage valve characteristic better matches the standard product terminal unit characteristic, while a parabolic valve better matches the output terminal unit as

implemented into EnergyPlus with baseboard objects.

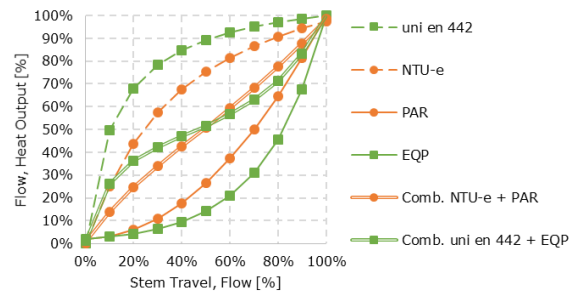


Fig. 9 – Terminal and valve characteristic curves combinations to obtain linear output

Some extra considerations are necessary. The proportional gain k_p of the regulator (or similarly its proportional band PB) depends, in real cases, on the pressure drop Δp between upstream and downstream of the valve and can be evaluated with appropriate choice of the valve body and its pre-setting. Similarly, the effectiveness of flow control by the valve is subject to the condition that the pressure drop generated by the same valve never becomes marginal with respect to those realized on its branch, that is, its authority ($a = \Delta p_{\text{valve}} / \Delta p_{\text{branch}}$) maintains high enough in every flow rate conditions (Russo, 2013), (Socal 2013). EnergyPlus code ignores the pressure drop for the evaluation of flow rates in various branches (pressure drop simulations are allowed to only correct pump consumption) (EnergyPlus Engineering Reference), therefore it is quite simple to introduce a TRV with unitary authority and any proportional band via EMS as explained below. Beyond considerations about characteristics of real thermal plants and effective performances of commercially available thermostatic valves, in this paper we consider a TRV with constant intrinsic characteristic (small distortion at every flow rates) and operating with the desired proportional band (appropriate thermal inertia of the bulb sensor – wax, liquid or gas - and stem travel pre-setting).

4.4 Valves implementation

In EnergyPlus many control types are pre-defined, but nothing with the TRVs properties previously described. However, by using the *Energy*

Management System (EMS), almost any control system can be introduced combining into algorithms sensors, actuators, and other specifically defined parameters through a basic and simplified programming language (*EnergyPlus Runtime Language – Erl*) for which the same calculation engine serves also as a parser (*EnergyPlus Application Guide for EMS*).

In the control algorithm written for modeling the TRV's behavior (see Fig. 10) the 'T_Room_Air' is the sensor (*EMS:Sensor object*) detecting the 'Zone Mean Air Temperature' variable for the thermal zone, while the 'MFR' is the actuator (*EMS:Actuator object*) acting on the 'Mass Flow Rate Maximum Available Setpoint' control type on the inlet node for the baseboard. The program is then called by the manager (*EMS:ProgramCallingManager object*) at the 'InsideHVACSystemIterationLoop' calling point.

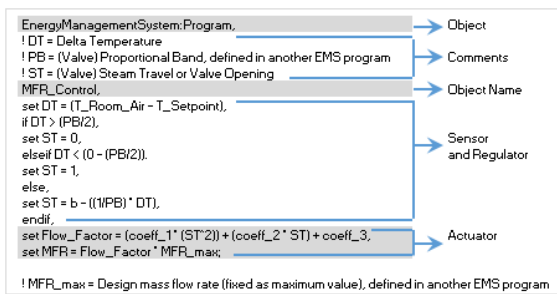


Fig. 10 – EMS Program modelling TRVs behavior, actuator parabolic characteristic curve written in standard form

4.5 Assessment of effectiveness of valve implementation algorithm

Simulations including specific EMS programs for TRVs, reveal the consistency of theoretical assumptions.

As expected, when a perturbing event happens, the smaller the proportional band, the closer to the setpoint the process variable is, but with higher fluctuations and a longer tail. Moreover, because of the only proportional nature of control, the process variable shows off a standing offset to the value required (Fig. 11).

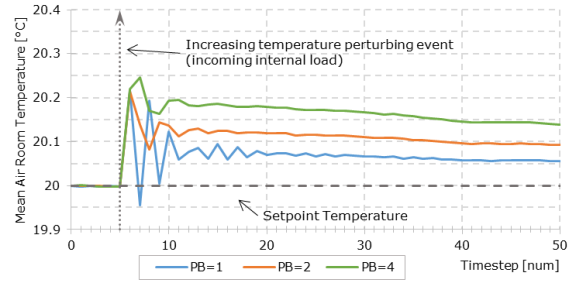


Fig. 11 – Room air temperature trend following a perturbing event with different values of proportional band for the regulator (parabolic characteristic curve applied for the actuator)

A parabolic characteristic applied to the actuator shows a more accurate process variable control, and this behavior is between the linear (higher) and equal percentage (lower) characteristic curves (Fig. 12).

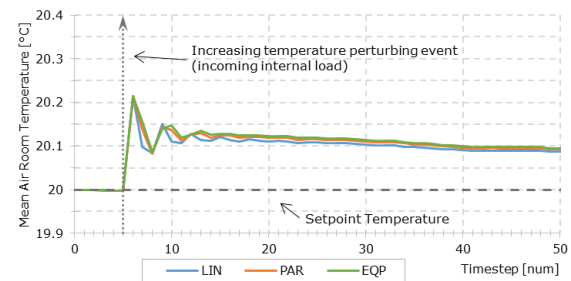


Fig. 12 – Room air temperature trend following a perturbing event with different curve types for the actuator (PB=2 for the regulator, characteristic curves built with R=50)

5. Simulations with different control systems

The final objective concerns the evaluation of energy efficiency and improved comfort conditions resulting from the installation of different kinds of thermoregulation systems, and from the reduction of energy dissipations through the windows.

Therefore, the project of upgrading the energy efficiency of the apartment was assessed by comparing six types of improvements.

All proposed actions are applicable to a single unit in a context of a building's central heating, where other boundary conditions (the opaque building envelope and the central heating plant) are kept fixed.

The following 6 cases were analyzed:

1-1_Current Condition: external climatic regulation only with temperature curve;

1-2_External climatic regulation and zone control (all TRVs act in the same way as the one in the living room, where the thermostat is placed);

1-3_External climatic regulation and thermostatic valves (every TRV acts independently from the other);

2-1_Replacement windows and external climatic regulation only with temperature curve;

2-2_Replacing windows, external climatic regulation and zone control;

2-3_Replacing windows, external climatic regulation and thermostatic valves (PB = 2).

Each simulation holds the following basic setting parameters:

- Winter heating period: 15 Oct-15 April
- Continues (not stepped) climatic regulation
- Internal loads as in Table 9 UNI/TS 11300-1
- Infiltration value, only for the exposed rooms (0,3 vol/h)
- Communicating zone air mixing (1 lt/s)
- Shading devices active 22:00 - 06:00
- PB = 2°C (only for x-2 and x-3)
- Setpoint temperature = 20°C (only for x-2 and x-3)

6. Analysis results

In Fig. 13, energy consumption is compared to the percentage of hours falling within the air temperature range during plant operation time for the whole heating season. The graphed data, related to the whole apartment, are calculated as averages of respective values of thermal zones. The hours outside the throttling range are distinguished between excess (red) and lesser (blue).

Fract time when plant on included within $\pm 1^\circ\text{C}$ (PB=2)	Case x-y	Energy consumption [kWh/m ²]
28% (0%)	1-1	81.8 (0%)
31% (+2%)	1-2	61.4 (-25%)
49% (+21%)	1-3	68.2 (-17%)
26% (-2%)	2-1	78.6 (-4%)
34% (+5%)	2-2	47.9 (-41%)
67% (+39%)	2-3	59.8 (-27%)

Fig. 13 – Comparison for the whole apartment of different control systems (y) applied to different envelope configurations (x), in terms of energy consumption and air temperature control

The distribution of the temperature values, reported in Tab. 3, shows that the thermostat for the whole apartment realizes an effective control only in the room in which it is placed (Living). TRV installation brings better comfort conditions in all the rooms because they take advantage of both endogenous and exogenous thermal gains, varying in time and space through the apartment. Despite these comfort conditions, throughout the whole apartment there are lower energy savings. Furthermore, if an energy saving measure is performed on the building envelope (replacing external windows), a more advanced control system has to be coupled with the original climatic regulation in order to a better thermal comfort and energy saving.

Figs 14 and 15 show, for all six cases, the mean air temperature trend of two rooms with different exposure and different use:

- east bedroom: south exposure and internal thermal loads mainly in night hours (23:00-07:00);
- living: north exposure, and internal thermal loads (higher than bedroom) mainly in the late afternoon and in the evening (17:00-23:00).

The TRVs always perform better than other control systems. The zone control system shows good behavior for the living room because of its position in that room. Notice how the variation of the mean air temperature levels with respect to the setpoint (20°C) presents little dependence on thermal gains while it mainly depends on the heating power of the terminal unit in the room.

7. Conclusion

This paper has investigated different heating control systems for a single unit, part of a building heated by means of a central plant water heating system. A deep investigation on terminal units and control systems allowed us to model them properly in a dynamic simulation tool (EnergyPlus), even by means of lines of code written for the purpose. A control system acting actively on each room (TRVs) proved to be the only one able to effectively combine an increase in comfort conditions with a reduction of heating energy consumptions.

Table 3 – Room air temperature distribution

Room	A (m ²)	Fract time when plant on								
		1-1			1-2			1-3		
		in PB=2 (±1°C)	over htg	under htg	in PB=2 (±1°C)	over htg	under htg	in PB=2 (±1°C)	over htg	under htg
Dining	12	36%	52%	12%	47%	9%	44%	69%	11%	20%
Kitchen	8.2	30%	35%	35%	6%	0%	94%	54%	1%	45%
Living	22	38%	56%	6%	69%	15%	16%	71%	15%	14%
West bedroom	15.4	24%	38%	38%	20%	14%	66%	42%	13%	45%
East bedroom	15.4	23%	35%	41%	15%	11%	74%	39%	13%	49%
Bathroom	8.2	22%	30%	48%	7%	2%	91%	43%	3%	54%
Ante-bathroom	2.5	19%	29%	52%	15%	4%	81%	26%	5%	70%
Storage room	1.7	17%	30%	53%	14%	2%	84%	23%	3%	73%
Corridor	6.2	21%	32%	47%	14%	11%	75%	22%	11%	66%
Entrance	4.5	20%	30%	50%	15%	13%	72%	20%	11%	69%
Flat	96.1	28%	41%	30%	31%	10%	59%	49%	11%	40%

Room	A (m ²)	Fract time when plant on								
		2-1			2-2			2-3		
		in PB=2 (±1°C)	over htg	under htg	in PB=2 (±1°C)	over htg	under htg	in PB=2 (±1°C)	over htg	under htg
Dining	12	1%	93%	0%	57%	10%	33%	85%	14%	1%
Kitchen	8.2	44%	48%	8%	7%	0%	93%	70%	1%	29%
Living	22	1%	93%	0%	82%	17%	1%	80%	20%	1%
West bedroom	15.4	45%	53%	2%	15%	6%	79%	76%	6%	18%
East bedroom	15.4	40%	51%	9%	14%	4%	82%	66%	6%	28%
Bathroom	8.2	33%	33%	33%	5%	0%	95%	53%	0%	47%
Ante-bathroom	2.5	31%	34%	35%	14%	1%	86%	29%	3%	68%
Storage room	1.7	32%	36%	32%	12%	1%	88%	28%	3%	69%
Corridor	6.2	42%	50%	8%	13%	8%	79%	37%	6%	58%
Entrance	4.5	37%	43%	19%	15%	10%	75%	29%	5%	66%
Flat	96.1	26%	66%	8%	34%	8%	59%	67%	9%	24%

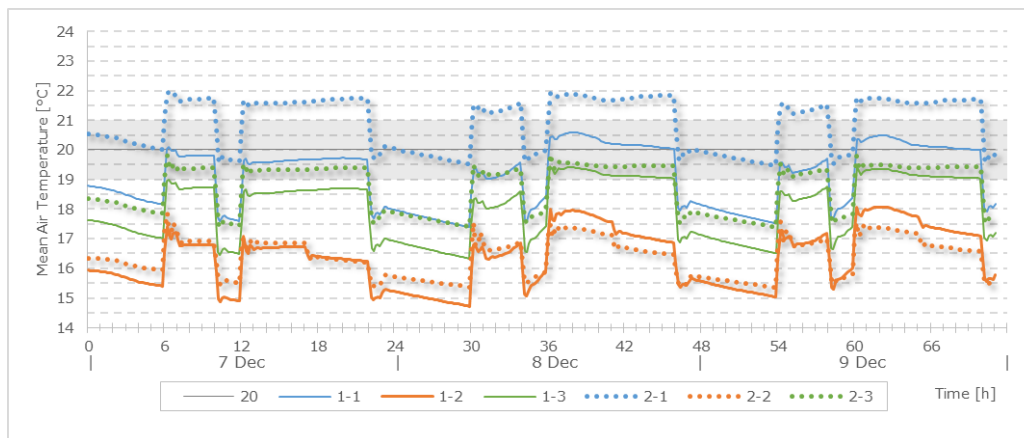


Fig. 14 – East bedroom: mean air temperature in three December days for various control systems and envelope configurations

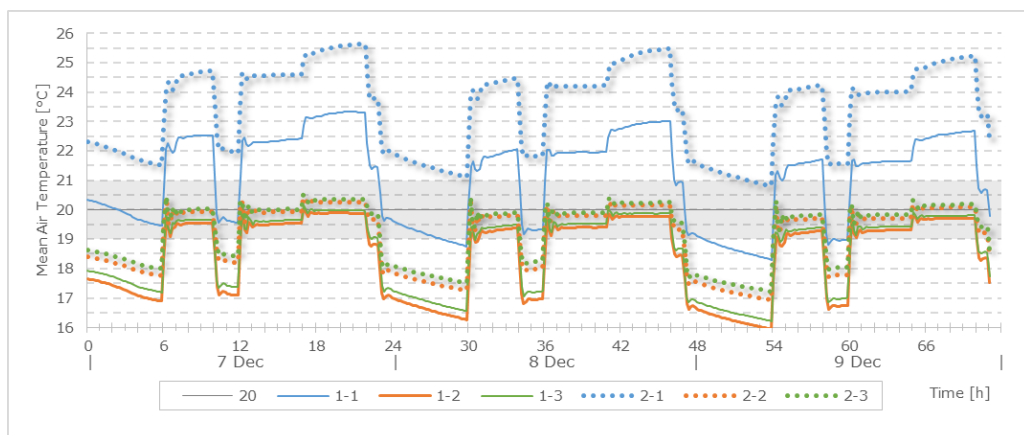


Fig. 15 – Living: mean air temperature in three December days for various control systems and envelope configurations

8. Nomenclature

Symbols

P	heat output power [W]
ΔT	temperature difference [$^{\circ}\text{C}$]
M'	mass flow rate [kg/s]
cp	specific heat [J/kg-K]
LMTD	logarithmic mean temp. difference [$^{\circ}\text{C}$]
NTU	number of transfer units [-]
e	effectiveness [-]
U	regulator output [-] or [%]
b	bias [-] or [%]
kp	proportional gain [1/ $^{\circ}\text{C}$]
e	error [$^{\circ}\text{C}$]
PB	proportional band [$^{\circ}\text{C}$]
t	temperature [$^{\circ}\text{C}$]
ST	stem travel or valve opening [-] or [%]
R	valve rangeability = K_{vs}/K_{vr} (30-100 typical for TMVs) [-]
K_{vs}	mass flow rate through the valve fully open at standard conditions ($\Delta P=10$ kPa) [m^3/s]
K_{vr}	minimum mass flow rate the valve can regulate at standard conditions ($\Delta P=10$ kPa) [m^3/s]
ΔP	pressure difference [Pa]
a	valve authority

Subscripts/Superscripts

w	water
a	air
w/a	water to air
std	at standard conditions
in	inlet terminal unit section
out	outlet terminal unit section
avg	average in thermal unit
room	relative to the thermal zone
setpoint	required value
valve	relative to the valve
branch	relative to the branch whose flow rate is controlled by the valve

References

- AICARR, Manuale d'ausilio alla progettazione termotecnica (Miniguia AICARR), III Edition, Press. 2009.
- ASHRAE Handbook Fundamentals 2009, Chapter 4 Heat Transfer.
- Belimo, Water Book, Documentazione tecnica, July 2014 Edition, Version 2.0, Accessed October 2014, http://www.belimo.it/pdf/i/WB_2014.pdf
- EnergyPlus documentation (v.8.1): Input/Output Reference, Engineering Reference, Application Guide for EMS, http://apps1.eere.energy.gov/buildings/energyplus/energyplus_documentation.cfm
- M. Miccio, 2012, Calcolo e rappresentazione grafica della Caratteristica Intrinseca per una valvola a globo, Accessed October 2014, http://asp.diin.unisa.it/MCS/miccio/WEBtracciamento_car_int_rangeab.xmcd
- G. F. Russo, 2013, Valvole termostatiche valutazione prestazioni (parte 1 e 2), Accessed October 2014, <http://independent.academia.edu/RussoGaetanoFabio>
- C. Scali, 2006, SCPC – Cap. IV: Valvole di Regolazione, Accessed October 2104, http://www1.diccism.unipi.it/Scali_Claudio/SCPC/SCPC4-Valvole.pdf
- L. R. Socal, 2013. Herzbook: Le Valvole Termostatiche. Digital version, Accessed October 2014, <http://www.klimit.it>
- UNI/TS 11300-1:2008 Determinazione del fabbisogno di energia termica dell'edificio per la climatizzazione estiva ed invernale.
- UNI EN ISO 12831:2006 Impianto di riscaldamento negli edifici, Metodo di calcolo del carico termico di progetto.
- UNI EN 442-1:2004 Radiatori e convettori, Specifiche tecniche e requisiti.
- UNI EN 442-2:2004 Radiatori e convettori, Metodi di prova e valutazione.
- UNI EN 215:2007 Valvole termostatiche per radiatori, Requisiti e metodi di prova.

Robustness of multi-objective optimization of building refurbishment to solar radiation model

Alessandro Prada – Free University of Bozen-Bolzano – alessandro.prada@unibz.it

Giovanni Pernigotto – University of Padova – pernigotto@gest.unipd.it

Francesca Cappelletti – IUAV of Venezia francesca.cappelletti@iuav.it

Andrea Gasparella – Free University of Bozen-Bolzano – andrea.gasparella@unibz.it

Abstract

The energy saving potential of existing buildings in highly urbanized world areas stimulates interest in the introduction of renovation measures. Due to the high economic impact of those interventions, special attention has to be paid to balance energy and economic performance, leading to the definition of the best combination through multi-objective approach. The recourse to building simulation, to improve the resolution and discrimination capability between different renovation configurations, forces us to consider the quality of the input data and leads to robustness issues for the optimal solution. In this regard, a reliable estimation of the global irradiation incident on various tilted surfaces is essential in order to account for the solar heat gains. Nonetheless, many meteorological stations monitor only global solar radiation on a horizontal plane. As a consequence, a variety of mathematical and empirical models have been proposed in the literature for both the subdivision of horizontal solar irradiation into direct and diffuse components and for the calculation of irradiation on tilted surfaces. Besides introducing inter-model uncertainty, no pair of diffuse and tilt irradiation models can provide results with the same reliability for worldwide localities different from those considered for the definition of each model.

This research work investigates the extent to which the choice of solar irradiation models affects the confidence levels of the optimal solutions provided by multi-objective optimizations. With this purpose, several multi-objective optimizations are carried out with different solar irradiation models. Semi-detached houses, penthouses and intermediate flat in multi-storey buildings are analyzed with the purpose of broadening the representativeness of the conclusions.

1. Introduction

A careful design of new buildings and building renovation can provide high energy savings. However, since new buildings represent a small amount of the whole construction activities, the interest in optimizing building renovation has greatly increased in the last few years.

Moreover, the coming into force of the Directive 31/2010 (European Commission, 2010), and the Commission Delegated Regulation EU 244/2012 (European Commission, 2012) highlights the necessity to consider the cost-optimal levels in the framework of the building energy refurbishments.

For this reason, the minimization of net present value (*NPV*) and of the achievable energy performance index (*EP*) are often used among many possible goals for the selection of the optimal mix of energy saving measures (*ESMs*). However, the extensive evaluation of all possible combinations of *ESMs* through a full factorial plan can be extremely time consuming and difficult to handle. The application of multi-objective optimization techniques (*MOO*), such as those based on the genetic algorithm (*GA*), can overcome this problem, ensuring a greater reduction of the computational time.

However, the suitability of *MOO* in finding optimal solutions has to deal with their robustness to imprecise input data. In fact, the higher capabilities of hourly simulation codes imply more complex and detailed inputs. In this regard, while *GA* robustness to algorithm parameters have been widely investigated (Wright and Alajmi, 2005; Ihm and Krarti, 2012), little attention has been paid to imprecise input (Prada *et al.* 2014a).

In this framework, the representativeness of solar irradiation data assumes relevance in building simulation results, especially in nearly-zero energy buildings (*nZEB*), which rely on solar irradiation for reducing the heating demand (Prada *et al.*, 2014b). The reliability of numerical models used in the pre-processing of solar data is a key aspect, since most of the meteorological stations monitor only global solar irradiation on a horizontal plane. Hence, a variety of mathematical and empirical models has been proposed in the literature (Prada *et al.*, 2015) for both the subdivision of horizontal solar irradiation into direct and diffuse components (*horizontal diffuse irradiance models*) and for the calculation of irradiation on tilted surfaces (*irradiance models for tilted surfaces*). Moreover, models can hardly provide results with the same reliability for localities different from those in which they have been derived. Therefore, the choice of the couple of solar irradiation models can greatly affect the reliability of the building energy simulation (Prada *et al.*, 2014b).

The aim of this work is to investigate the robustness of the NSGA II procedure (Deb *et al.*, 2002) in finding optimal *ESMs* in building energy renovation when different solar irradiation models are used. *MOO* has been repeated with three relevant couples of models, chosen from the entire population of 264 combinations studied in (Prada *et al.*, 2015) for three kind of buildings, in the climate of Rome.

2. Methods

2.1 Case of study

Three building typologies are investigated (Fig. 1) with the purpose of generalizing the main findings. In particular, semi-detached houses ($S/V = 0.97 \text{ m}^{-1}$), penthouses ($S/V = 0.63 \text{ m}^{-1}$) and intermediate flats in multi-story buildings ($S/V = 0.3 \text{ m}^{-1}$) have been considered. These buildings were developed starting from a reference building module, which is a typical flat having 100 m^2 floor surface, 3 m internal height and façades oriented towards the main cardinal directions. The floor area is consistent with the weighted average surface of the

European residential buildings (UNECE, 2006) and the other characteristics derived from the screening analysis (Pernigotto *et al.*, 2014). Windows are all in the same façade and the window to floor ratio is equal to 0.144. Either a south or an east windows orientation is considered. As a whole, 12 alternative configurations are considered for *MOO*. An adiabatic boundary condition is imposed when the envelope structures are adjacent to other buildings. In all the other cases, the surfaces are directly exposed to the external environment.

Two alternatives of opaque envelope are modelled: *REF 1*, representative of constructions built prior to the first Italian energy law in 1976 (Italian Parliament 1976), has a thermal resistance of $0.97 \text{ m}^2 \text{ K W}^{-1}$ while *REF 2*, representative of constructions built before the second energy legislations (Italian Parliament 1991), has a thermal resistance of $2.04 \text{ m}^2 \text{ K W}^{-1}$. Windows have a single pane glass with thermal transmittance of $5.7 \text{ W m}^{-2} \text{ K}^{-1}$ and SHGC of 0.81 and standard timber frame with thermal transmittance of $3.2 \text{ W m}^{-2} \text{ K}^{-1}$ and a projected area equal to 19.9 % of the whole window area.

The infiltration rate is estimated according to EN 12207 (CEN, 1999) and EN 15242 (CEN, 2007a). The reference air tightness n_{50} is 7 ACH and the associated infiltration rates are 0.20 ACH, 0.13 ACH and 0.062 ACH, respectively for semi-detached houses, penthouses and intermediate flats. Similarly, the heating system is a standard gas boiler coupled with radiators and on-off system control are used.

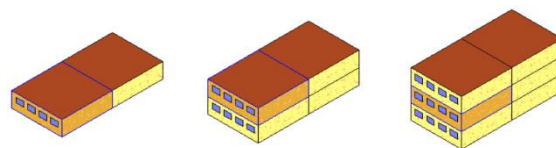


Fig. 1 – Test cases used in GA optimization.

2.2 Energy Saving Measures

The optimal mix of *ESMs* comes from the trade-off between energy performance for heating EP_h and NPV , according to the EN ISO 15459:2007 (CEN, 2007b). For this scope, an Elitist Non-dominated sorting GA algorithm, NSGA-II, (Deb 2002) was implemented in Matlab. The fitness function used in the analysis is a Matlab code that launches the

building energy simulation (i.e., TRNSYS model) and reads TRNSYS output file. Following on from this point, the code computes the *NPV* by means of the method proposed by the technical standard EN ISO 15459:2007 and it returns the two objectives to the NSGA-II algorithm. In particular, *NPV* and EP_h are chosen as goals for the multi-objective optimization.

We evaluated conventional *ESMs*, applied both to the envelope components and to the heating and ventilation system (Penna *et al.*, 2015):

1. external insulation of the opaque envelope with an EPS layer (thermal conductivity of $0.04 \text{ W m}^{-1} \text{ K}^{-1}$, specific heat of $1470 \text{ J kg}^{-1} \text{ K}^{-1}$ and density of 40 kg m^{-3}) in a range of thicknesses between 0 and 20 cm. The insulation thickness is changed differently for vertical walls, roof and floor and different installation costs are considered;
2. replacement of existing windows with four higher performance glazing systems (i.e. double or triple pane with either high or low SHGC) with improved aluminum frames with thermal break, whose thermal transmittance is $1.2 \text{ W m}^{-2} \text{ K}^{-1}$;
3. substitution of the heating boiler with either modulating or condensing boiler both with a climatic control adjustment;
4. installation of a mechanical ventilation system *MVS* with a cross flow heat recovery system.

Furthermore, some secondary energy performance improvements induced by the primary *ESMs* are considered:

1. the effects of thermal bridges are reduced depending on the insulation thickness and on window typology. The linear thermal transmittances have been computed using the polynomial regressions derived in (Penna *et al.*, 2015);
2. the infiltration rate is reduced with the installation of new windows. Hence, the infiltration rate is considered as a half of the starting values;
3. since the radiators are not changed, the decreasing heating needs allows reducing the emission power. Thus, when the boiler is replaced, the use of the climatic control allows the variation of the hot water supply temperatures and, consequently, the reduction of the distribution losses.

2.3 Solar radiation models

The hourly distributions of 264 couples of models presented in Prada *et al.* (2015) have been investigated for the city of Rome in order to select three representative couples of models. The predicted solar irradiations on vertical surfaces oriented towards the four cardinal points are computed and, for each hour, the results obtained by means of different models are sorted in ascending order. Then, the three pairs of models that more often fall in the first 66 positions (i.e., within the first quartile), in the last 66 positions (i.e., beyond the third quartile), and between first and third quartiles are chosen.

These models (Tab. 1) are considered representative of the average and extreme behaviors of the entire population, as highlights in Fig. 2.

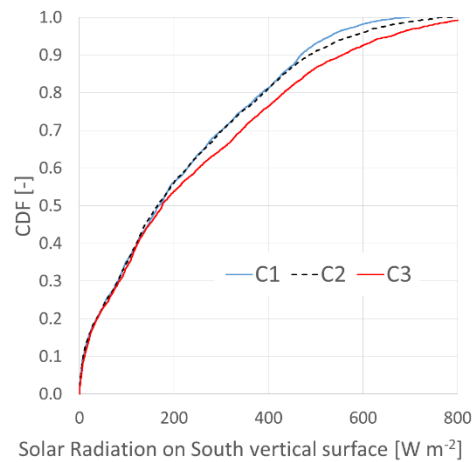


Fig. 2 – Cumulative distribution functions of the hourly solar irradiation with the three model combinations.

Table 1 – Solar irradiation models.

Combination	Horizontal Diffuse Irradiance models	Irradiance models for tilted surface
C1	Perez <i>et al.</i> 1992	Liu and Jordan 1960
C2	Boland <i>et al.</i> 2008	Burgler 1977
C3	Erbs <i>et al.</i> 1982	Perez <i>et al.</i> 1990

2.3.2 Horizontal diffuse irradiance models

The selected diffuse irradiance models have different characteristics. The older works, i.e., Erbs *et al.* (1982), correlate the diffuse fraction of solar irradiation with the clearness index that represents the portion of horizontal extraterrestrial radiation reaching the surface. Erbs *et al.* (1982) developed a regression model using a dataset of 65 months covering five locations over the U.S. On the contrary, Perez *et al.* (1992) proposed a modification to the DISC model proposed by Maxwell (1987). In particular, the modification dealt with the dynamics effect in time series. Besides, the authors introduced a new parameterization by using the weather data collected for several locations. The last model, proposed by Boland *et al.* (2008), involved a logistic function instead of piecewise linear or simple nonlinear functions.

2.3.3 Irradiance models for tilted surface

The model for the evaluation of solar irradiation on tilted surface in the first couple was developed by Liu and Jordan (1960). They assumed an isotropic behavior of the sky and, consequently, the diffuse irradiation can be evaluated using trigonometric relations. On the contrary, Bugler (1977) observed both an increased intensity of diffuse irradiation near the horizon and in the circumsolar region of the sky. Therefore, he introduced two corrective coefficients. The last selected model is the one proposed by Perez *et al.* (1990). In this work, the authors defined a model based on a subdivision of the sky diffuse irradiance in three components, i.e., the horizon brightness, the isotropic and the circumsolar irradiation. All the models cited in the previous paragraphs were implemented and combined in a Matlab code.

3. Results and discussions

The first result that we want to focus on is the effect of irradiation models on the annual energy performance (EP) of the not-renovated buildings. In particular, Table 2 presents the percentage

variation with respect to the C2 couple of models and its EP values. In most of the cases, the variations are in the range of $\pm 3\%$ but higher values larger than 10% are noted for compact buildings (i.e. $S/V=0.30\text{ m}^{-1}$ or $S/V=0.63\text{ m}^{-1}$) with south-faced windows. For those buildings, the energy balance is more related to solar heat gains, thus the variability of incident solar irradiation has a greater weight on the needs. This result is an indication of the level of robustness of dynamic simulation to the epistemic uncertainty introduced by the choice of solar irradiation models.

Starting from these results, the effect of the solar irradiation models on the Pareto's front is investigated. Figure 3 presents the different Pareto's fronts obtained with the three couples of irradiation models according to the S/V ratios and windows orientation for the REF 2 case. Similar results have been obtained also for the REF 1 buildings. In the trade-off between NPV and EP, there are two groups: the solutions with mechanical ventilation system (MVS) in the higher left-hand side and those with natural ventilation (NAT) in the lower right-hand side. In buildings with low heating needs, such as the intermediate flat in multi-storey buildings, the choice of solar irradiation models seems to affect scarcely the Pareto's front.

Due to the low EP in renovated compact buildings, the incident solar irradiation is much greater than the solar gains exploitable to reduce the limited heat losses. For this reason, the choice of the solar models have a weak impact on predicted heating needs. Larger differences are evident in the less compact buildings. A shift of Pareto's fronts is the primary effect of the different solar irradiation models. Although there are a few intersections in Pareto's curves obtained with the three couples of models, the choice of models alters the number of optimal solutions in the Pareto's front.

This is more evident in the less compact buildings with East oriented windows. For these buildings, the graphs show a different number of non-dominated solutions in the three fronts obtained with C1, C2 and C3.

Table 2 – Variation ΔEP [%] in the initial EP [kWh m^{-2}] of the reference cases. The subscripts referred to the model combinations

S/V	REF 1			REF 2			
	EP_2	ΔEP_{1-2}	ΔEP_{3-2}	EP_2	ΔEP_{1-2}	ΔEP_{3-2}	
0.3	East	76.1	-2.2	-0.9	57.1	-2.6	-1.3
	South	61.8	3.3	-9.5	44.1	4.7	-11.8
0.63	East	122.1	-2.1	0.0	105.3	-2.3	0.0
	South	107.9	0.9	-4.9	92.7	0.9	-5.0
0.97	East	169.2	-1.6	0.0	151.9	-1.5	0.1
	South	155.4	0.6	-3.4	139.8	0.8	-3.2

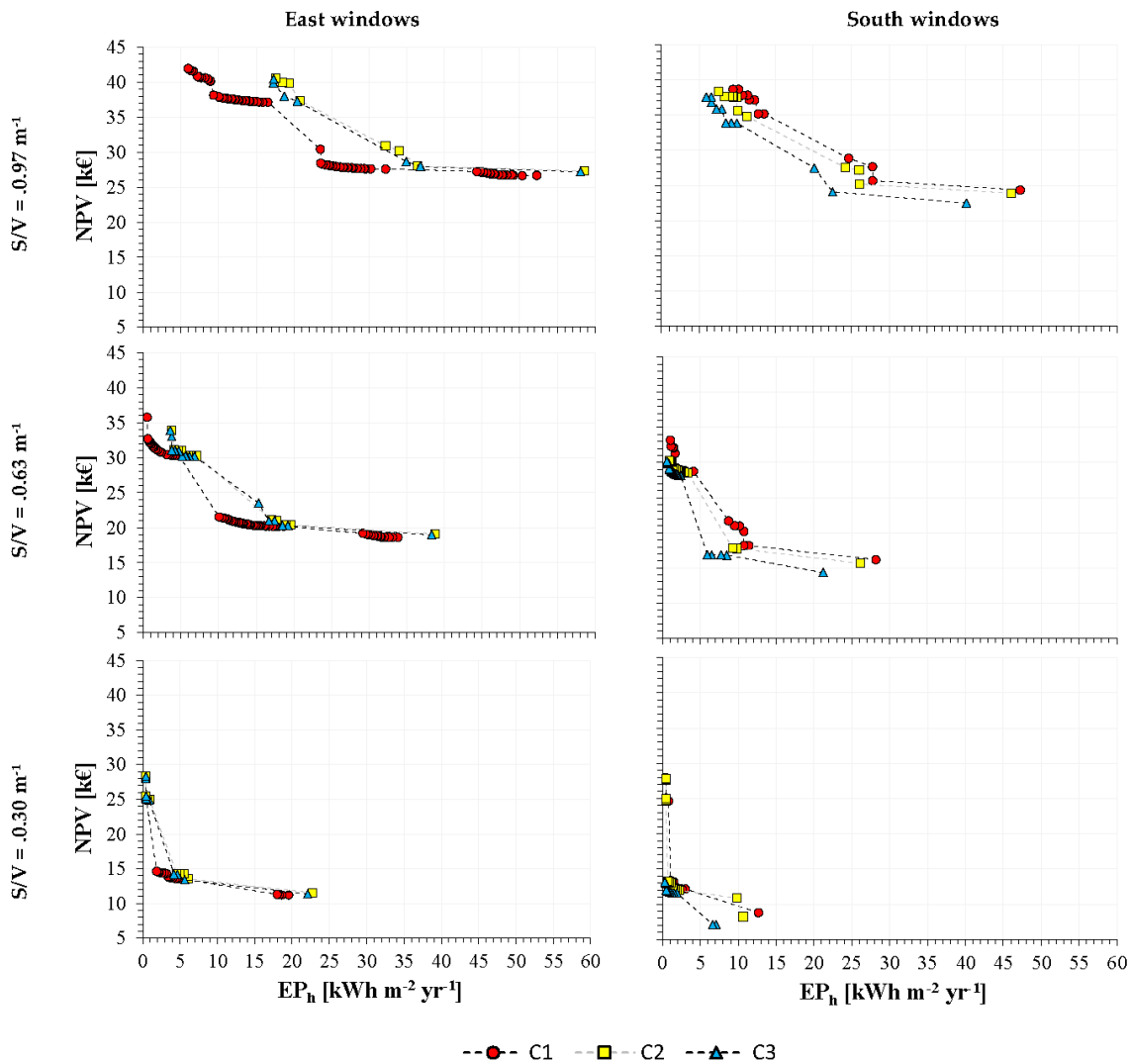


Fig. 3 – Pareto Fronts of the REF 2 cases

In particular, there are more optimal solutions in the front obtained with the combination C1. The additional solutions in C1 fronts are characterized by a greater insulation thickness for both walls and roof, and often by the replacement of windows with triple glazing with high SHGC. (TH) In fact, the

effectiveness of ESMs related to lower heat losses through the envelope increases since the C1 combination is characterized by lower solar irradiation on vertical surfaces. In the other combinations, however, these solutions are dominated by other retrofit solutions.

3.1 ESMs of Energy and Cost Optima

The mix of ESMs ensuring the minimum of a single objective are investigated in order to evaluate the effects of the different solar irradiation models.

Table 3 shows how the use of C1 induces an underestimation of solar gains, especially on east façades, thus making higher insulation thickness more economically advantageous. This is less

emphasized for buildings with windows facing south, since higher solar gains tend to reduce the effect. Table 4 also shows that only ESMs dealing with the opaque envelope are present in the retrofit solution ensuring the cost optimal retrofit due to the mild climate investigated. Similar behaviors are shown also for ESMs able to minimize the energy requirements of the buildings analyzed (Tab 4).

Table 3 – Combination of ESMs ensuring the minimum NPV for the REF 2 buildings.

	EST windows orientation						South windows orientation					
	Insulation thickness [cm]			Win code	Boiler code	Ventil. code	Insulation thickness [cm]			Win code	Boiler code	Ventil. code
	Wall	Roof	Floor				Wall	Roof	Floor			
Intermediate flat in multi-story buildings S/V=0.30 m⁻¹												
C1	15	-	-	SG	STD	NAT	11	-	-	SG	STD	NAT
C2	11	-	-	SG	STD	NAT	11	-	-	SG	STD	NAT
C3	11	-	-	SG	STD	NAT	10	-	-	SG	STD	NAT
Penthouse S/V=0.63 m⁻¹												
C1	16	12	-	SG	STD	NAT	11	11	-	SG	STD	NAT
C2	11	11	-	SG	STD	NAT	11	11	-	SG	STD	NAT
C3	11	11	-	SG	STD	NAT	11	11	-	SG	STD	NAT
Semi-detached houses S/V=0.97 m⁻¹												
C1	15	11	12	SG	STD	NAT	11	10	11	SG	STD	NAT
C2	10	10	11	SG	STD	NAT	10	10	11	SG	STD	NAT
C3	10	10	11	SG	STD	NAT	10	11	11	SG	STD	NAT

Table 4 – Combination of ESMs ensuring the minimum EP for the REF 2 buildings

	EST windows orientation						South windows orientation					
	Insulation thickness [cm]			Win code	Boiler code	Ventil. code	Insulation thickness [cm]			Win code	Boiler code	Ventil. code
	Wall	Roof	Floor				Wall	Roof	Floor			
Intermediate flat in multi-story buildings S/V=0.30 m⁻¹												
C1	11	-	-	DH	COND	MVS	8	-	-	DH	COND	VMC
C2	11	-	-	DH	COND	MVS	7	-	-	DH	COND	VMC
C3	11	-	-	DH	COND	MVS	12	-	-	TH	STD	NAT
Penthouse S/V=0.63 m⁻¹												
C1	20	20	-	TH	COND	MVS	12	12	-	TH	COND	VMC
C2	12	12	-	TH	COND	MVS	12	12	-	TH	STD	VMC
C3	12	12	-	TH	COND	MVS	12	12	-	TH	STD	VMC
Semi-detached houses S/V=0.97 m⁻¹												
C1	19	19	20	TH	COND	MVS	12	11	12	TH	COND	VMC
C2	11	11	11	TH	COND	MVS	12	12	12	TH	COND	VMC
C3	11	11	11	TH	COND	MVS	11	11	12	TH	COND	VMC

The measures minimizing the consumed primary energy involve the windows' replacement and the use of advanced and more efficient energy systems.

However, the choice of the solar models has a greater effect almost exclusively on the insulation thicknesses, especially in buildings with east oriented windows when C1 is used.

3.2 Comfort variations in Pareto's solutions

The previous paragraphs show a good robustness of the MOO method to the epistemic uncertainty introduced by the choice of solar models. However, substantial differences can be highlighted when assessing the comfort performance. The thermal comfort indicators used for the investigation is the discomfort weighted time (WDT) index, as proposed by the EN 15251 (CEN, 2007c) through the degree hours criteria. The graph in Fig. 4 clearly shows the WDT variations of REF1 semi-detached house caused by the choice of the models when NPV and EP are chosen as objectives. This greater sensitivity of WDT to solar models has repercussions on the robustness of MOO procedure when three different goals such as NPV, EP and WDT are considered. The Pareto's fronts in Fig. 5 show a greater dispersion of the results obtained with the three different combinations of solar models. In this case, therefore, the choice of a combination of models leads to the selection of different optimal mix of ESMs.

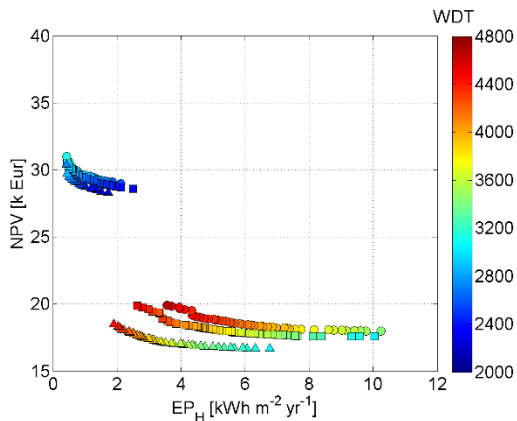


Fig. 4 – Pareto's fronts of the semi-detached house REF 1 with south oriented windows. The data points are colored according to WDT while circle referred to C1, square to C2 and triangle to C3.

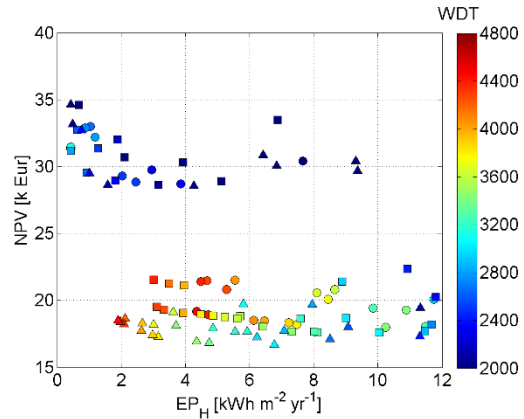


Fig. 5 – Pareto's fronts of the semi-detached house REF 1 with south oriented windows obtained with a 3 objective optimization. The data points are colored according to WDT while circle referred to C1, square to C2 and triangle to C3.

4. Conclusion

This work assessed the robustness of NSGA II in finding optimal building energy refurbishment when three different couples of solar irradiation models are adopted. The results show the variability of the EP index in the range of $\pm 3\%$ for most of the test cases for the simulation performed on the initial state.

As regards Pareto's fronts, the utilization of the C1 models makes some solutions not-dominated instead of dominated as they are for in cases C2 and C3. In particular, these new optimal solutions have higher insulation thickness and triple glazings due to the lower incident solar irradiation provided by C1 models.

Notice that slight differences are present in the mix of ESMs able to guarantee either the minimum NPV or the minimum EP. Again, the greatest differences occur with C1, which tends to increase the thickness of the insulating layers for both the optima.

The NSGA-II then shows a good robustness when the solutions are optimized in terms of NPV and EP. In fact, substantial changes are noted on the thermal discomfort of optima solutions. This greater sensitivity of the WDT index to solar irradiation implies a decrease of MOO robustness when the minimization of WDT becomes an objective.

5. Nomenclature

Symbols

A	area (m ²)
COND	Condensing boiler
DH	Double glazing with high SHGC
S	Surface of dispersing envelope (m ²)
SG	Single Glazing
SHGC	Solar heat gain coefficient (-)
STD	Standard boiler
TH	Triple glazing with high SHGC
V	Conditioned volume (m ³)

References

- Boland, J., Ridley B., Brown, B., 2008, *Models of diffuse solar radiation*. *Renewable Energy*, 33:584–116.
- Bugler, J.W., 1977, *The determination of hourly insolation on an inclined plane using a diffuse irradiance model based on hourly measured global horizontal insolation*. *Solar Energy*, 19(5):477 – 491.
- CEN European Committee of Standardization, 1999. *EN 12207:1999, Windows and doors. Air permeability – Classification*.
- CEN, European Committee of Standardization, 2007a. *EN 15242:2007, Ventilation for buildings – Calculation method for the determination of air flow rates in buildings including infiltration*.
- CEN European Committee of Standardization, 2007b. *EN 15459:2007, Energy performance of buildings - Economic evaluation procedure for energy systems in buildings*.
- CEN European Committee of Standardization 2007c. *EN 15251, Indoor environmental input parameters for design and assessment of energy performance of buildings*.
- Deb, K., Pratap, A., Agarwal, S., 2002. A Fast and Elitist Multi-objectives Genetic Algorithm: NSGA-III, *IEE Transactions on Evolutionary Computation*, 6 (2):182-197
- Erbs, D. G., Klein, S. A., Duffie, J. A., 1982, *Estimation of the diffuse radiation fraction for hourly, daily and monthly-average global radiation*. *Solar Energy*, 28(4): 293–302.
- European Commission, 2010. *Directive 2010/31/EU of the European Parliament and of the council of 19 may 2010 on the energy performance of buildings (recast)*, Official Journal of European Union 153 (2010) 13 – 35.
- European Commission. 2012. *Commission delegated regulation (EU) No 244/2012 of 16 January 2012*. Official Journal of European Union L81/18 (2012).
- Ihm P., Krarti M., 2012. *Design optimization of energy efficient residential buildings in Tunisia*, *Building and Environment*, vol.58, p.81-90
- Italian Parliament. 1976. *Law 373 Norme per il contenimento del consume energetico per usi termici negli edifici*.
- Italian Parliament. 1991. *Law 10, Norme per l'attuazione del piano energetico nazionale in materia di uso nazionale dell'energia, di risparmio energetico e di sviluppo delle fonti rinnovabili di energia*
- Liu, B.Y.H., Jordan, R.C., 1960, *The interrelationship and characteristic distribution of direct, diffuse and total solar radiation*. *Solar Energy*, 4(3):1 – 19.
- Maxwell, E.L. 1987. *A quasi-physical model for converting hourly global horizontal to direct normal insolation*. Technical Report of Solar Energy Research Institute, SERI/TR-215-3087.
- Penna, P., Prada, A., Cappelletti, F., Gasparella, A., 2015, *Multi-objectives optimization of Energy Efficiency Measures in existing buildings*. *Energy and Buildings*. In Press
- Perez, R.R., Ineichen, P., Seals, R., 1990, *Modeling daylight availability and irradiance components from direct and global irradiance*. *Solar Energy*, 44(5):271–289
- Perez, R.R., Ineichen, P., Maxwell, E.L., 1992, *Dynamic global-to-direct irradiance conversion models*. *ASHRAE Transactions*, 98(1): 354-369.
- Pernigotto, G., Prada, A., Gasparella, A., Hensen, and J.L.M., 2014, *Development of a set of simplified building models for building simulation*. In 3rd Int. High Performance Building Conference, Purdue (U.S.).
- Prada, A., Pernigotto, G., Cappelletti, F., Gasparella, A., Hensen, J.L.M., 2014a, *Robustness of multi-*

objective optimization of building refurbishment to suboptimal weather data. In 3rd Int. High Performance Building Conference, Purdue (U.S.).

Prada, A., Pernigotto, G., Baggio, P., Gasparella, A., Mahdavi, A., 2014b, *Effect of solar radiation model on the predicted energy performance of buildings.* In 3rd Int. High Performance Building Conference, Purdue (U.S.).

Prada, A., Pernigotto, G., Gasparella, A., Mahdavi, A., 2015, *Combined effects of diffuse fraction and tilted surface radiation models.* In ECPPM 2014 eWork and eBusiness in Architecture, Engineering and Construction, p. 251-257, Vienna (Austria).

UNECE, 2006. *Bulletin of Housing Statistics for Europe and North America*, Technical Report, United Nations Economic Commission for Europe.

Wright, J., Alajmi, A., 2005, *The robustness of genetic algorithms in solving unconstrained building optimization problems.* Proc. of 9th Building Simulation, p. 1361-1368.

The impact of thermal comfort in multi-objective optimization of buildings refurbishment

Paola Penna – Free University of Bozen-Bolzano – paola.penna@natec.unibz.it

Alessandro Prada – Free University of Bozen-Bolzano – alessandro.prada@unibz.it

Francesca Cappelletti – University IUAV of Venice – francesca.cappelletti@iuav.it

Andrea Gasparella – Free University of Bozen-Bolzano – andrea.gasparella@unibz.it

Abstract

The European Committee is encouraging the Member States to adopt the so-called “cost optimal approach” to define new energy performance requirements for new and existing buildings. However, the cost-optimal should not neglect the indoor thermal comfort. The improvement of the building energy performance, especially if related to the addition of high insulation thickness, can increase the risk of overheating. A small energy input raises the internal temperature considerably. Therefore, in order to move beyond the mere economic optimization of retrofit interventions, it is important to understand what the solutions able to enhance the performance of the buildings are, also in terms of thermal comfort. In this paper, this problem has been investigated. The analysis has been carried out on a set of different residential building modules, representative of different building typologies and construction periods, located in two different climatic contexts. By means of a multi-objective optimization approach, the best combination of EEMs has been defined first optimizing only the energy and economic aspects, then the indoor thermal comfort has been added and the optimization re-run. A Genetic Algorithm (NSGA-II) coupled with a simulation tool has been used to optimize the different objectives.

1. Introduction

Designing the energy refurbishment of existing buildings is not an easy task. Firstly, the wide selection of Energy Efficiency Measures (EEMs) currently available on the market has to be evaluated. Then, the choice among EEMs has to be made considering the objectives to be reached. The European Commission promotes the improvement

of the energy performance of the existing building stock, through the so-called “cost optimal approach” in the definition of new energy performance requirements. Even though the Delegated Regulation 244/2012 suggests that the selected EEMs shall be compatible with air quality and indoor comfort levels, according to EN 15251 (CEN, 2007a), the cost-optimal approach does not include this important aspect in the optimization process. As highlighted by the EPBD recast (EU, 2010), retrofit strategies should enhance the thermal comfort of the buildings, limiting the employment of air conditioning system. The overheating issue, connected to high performance buildings, has been already pointed out in the literature (Mlakar J. et al., 2011; McLeord R.S. et al., 2013; Penna P. et al., 2014). For this reason, it is important to understand what solutions are able to enhance the performance of the buildings, also in terms of comfort, to move beyond the mere economic optimization of retrofit interventions.

In this paper, the effect of thermal comfort in defining the optimal EEMs has been investigated. The analysis has been conducted on a set of different residential building modules, representative of different building typologies and construction periods, located in two different climatic contexts. Conventional retrofit measures, such as the insulation of the external envelope, substitution of glazing system, replacement of the boiler and addition of a mechanical ventilation system have been analysed. A multi-objective optimization approach has been repeated, firstly to define the combination of EEMs able to minimize energy consumptions and costs, then also the indoor thermal discomfort. A genetic algorithm

(NSGA-II) coupled with the simulation code TRNSYS (Solar Energy Laboratory, 2012) has been used.

2. Building modules description

A single storey residential unit with a floor area of 100 m² and an internal height of 3 m has been considered as the reference building module. The vertical walls are oriented towards the main cardinal points, with window surface equal to 14.4 m² on a single side. The window system is a single pane glass ($U_{gl}=5.7 \text{ W m}^{-2} \text{ K}^{-1}$) with a standard timber frame ($U_{fr}=3.2 \text{ W m}^{-2} \text{ K}^{-1}$). The thermal bridges have a linear transmittance of $0.098 \text{ W m}^{-1} \text{ K}^{-1}$ for corners, $0.182 \text{ W m}^{-1} \text{ K}^{-1}$ for the intermediate floor and walls and $0.060 \text{ W m}^{-1} \text{ K}^{-1}$ for the windows' perimeter, calculated according to EN 10211 (CEN, 2007b). The heating system is a standard gas boiler coupled with radiators.

Some characteristics of this shoebox-like module have been changed to create a set of residential buildings and generalize the results for different configurations, architectural typologies and construction period:

- *compactness ratio* changes to consider a detached-house-like typology ($S/V=0.97 \text{ m}^{-1}$), a penthouse-like ($S/V=0.63 \text{ m}^{-1}$) and an intermediate flat in a multi-storey buildings ($S/V=0.3 \text{ m}^{-1}$);
- *envelope thermal resistance* varies to consider two construction periods, before the first Italian energy legislation, (Italian Parliament, 1976), REF 1 ($R_1 = 0.97 \text{ m}^2 \text{ K W}^{-1}$), and between the first and the second energy legislations (1976÷1991) (Italian Parliament, 1991), REF 2 ($R_2 = 2.04 \text{ m}^2 \text{ K W}^{-1}$);
- *window orientation*: South and East.

A set of 8 shoebox-like buildings were obtained by combining the above variations. Those buildings are evaluated in two different climatic contexts: Milano and Messina, representative for northern and southern Italy.

The infiltration rate and the nominal power of the heating system change according to the reference building module. The reference air tightness n_{50} is 7

ACH and the associated infiltration rates, calculated according to the EN 12207 (CEN, 1999) and EN 15242 (CEN, 2007c), change depending on the compactness ratio (Table 1). The nominal heating power has been calculated for each reference case according to the EN 12831 (CEN, 2003) and the boiler nominal capacity has been selected from market available products.

Table 1 – Infiltration rate values (ACH) according to different compactness ratios

S/V=0.3	S/V=0.63	S/V=0.97
0.062	0.130	0.200

3. Retrofit Strategies

The following Energy Efficiency Measures have been considered to improve the performance of the building modules:

- external insulation of walls, roof and/or floor with EPS (conductivity $\lambda=0.04 \text{ W m}^{-1} \text{ K}^{-1}$, specific heat $c=1470 \text{ J kg}^{-1} \text{ K}^{-1}$, density $\rho=40 \text{ kg m}^{-3}$) in a range between 1 to 20 cm, incremented by 1 cm;
- replacement of existing window systems with four higher performance glazing systems (Table 2) and improved aluminum frames with thermal break ($U_{fr}=1.2 \text{ W m}^{-2} \text{ K}^{-1}$);
- substitution of heating generator with modulating or condensing boiler both with a climatic control system;
- installation of mechanical ventilation system with heat recovery (Ventilation rate $q_v=150 \text{ m}^3 \text{ h}^{-1}$, Power $P=60 \text{ W}$).

The following listed EEMs bring energy performance improvements without extra-costs:

- the linear thermal transmittance of thermal bridges is reduced depending on the insulation thickness and on window type. By means of a finite element tool (LBNL, 2013), a polynomial regression was calculated, considering a progressive increase of 5 cm of insulation, to consider the variation of the thermal bridge effect;

- the infiltration rates are considered as half of the original value (Table 1) if the windows are replaced, because of the improvement of air tightness;
- if the boiler is substituted, the radiators' supply temperatures can be lower than the design one, because the capacity of radiators does not change and the climatic control system allows the supply temperature regulation depending on the external one.

Table 2 – Characteristics of the different glazing system

Glazing system	U (W m ⁻² K ⁻¹)	SHGC
DH – Double, high SHGC (4/9/4, krypton, low-e)	1.140	0.608
DL – Double, low SHGC (6/16/6, krypton, low-e)	1.099	0.352
TH – Triple, high SHGC (6/12/6/12/6, krypton, low-e)	0.613	0.575
TL – Triple, low SHGC (6/14/4/14/6, argon, low-e)	0.602	0.343

4. Multi-Objective approaches

4.1 Genetic Algorithm (NSGA II)

The optimization process has been implemented through the Non-dominated Sorting Genetic Algorithm, NSGA II (Deb K. et al. 2002), coupled with the dynamic simulation tool, Trnsys. This approach is particularly useful in the problem characterized by the competing nature of the objectives. By means of the NSGA II, it is possible to find a set of optimal solutions, the so-called non dominated solutions, for which no alternatives exist that increase the fulfilment of an objective without hampering the attainment of another. The parameters set for the genetic algorithm are 0.5 as for the fraction of tournament selection without replacement (TSWOR), 0.8 as for the arithmetic crossover and a mutation rate of 0.1. Sobol's sequences sampling is used to define the 128

individuals of the initial population. This pseudo-random number generator avoids the oversampling of same region that can occur with random sampling (Saltelli A., 2004), giving a good individuals' collection as first population. A Matlab (Matlab 7.7.0 R 2008) code executes automatically the TRNSYS model of the building, evaluates the attainment of the objectives and selects the best individuals that are used as parents of the following generation. The iterative process is repeated until the maximum number of iterations or the convergence level is reached. The final population contains the optimal solutions.

4.2 Optimization 1: Energy and Costs

This NSGA II algorithm has been used to define the best combination of EEMs for the analysed reference residential modules, in a bi-optimization process. The minimization of energy consumption and costs has been pursued setting as objective functions the Energy Performance for Heating (EPH) and the Net Present Value (NPV), described in the following sections.

4.2.1 Energy performance for Heating

The Energy Performance for Heating (EP_H) is calculated through the simulation code TRNSYS v.17 (Solar Energy Laboratory, 2012). National Test Reference Years of Milano and Messina (Comitato Termotecnico Italiano, 2012) are used to consider the weather conditions. The thermo-physical properties of the building are simulated with the Type 56, multi-zone building subroutine. The heating system is modelled by means of the Type 869 (Haller M.Y. et al., 2011a; Haller M.Y. et al., 2011b), able to simulate the behavior of modulating and condensing boilers (Carlon et al., 2015). In combination with the replacement of the boiler, a climatic adjustment of the water supply temperature, controlled by an external air temperature probe, is considered. A heating thermostatic control keeps the air temperature in the range between 20 and 22°C. The occupancy schedule and the internal gains, considered half radiative and half convective, are modelled according to the Italian technical specification UNI/TS 11300 (UNI, 2008). The internal gains (Table 4) are defined on the base of the room type.

The floor area is considered half as living rooms and half as bedrooms. The air change rate, during the occupancy time, is set to 0.5 ACH. The same air change rate is set when the occupants are present in case that mechanical ventilation system is considered. In this last configuration, the outdoor inlet air is pre-heated in the heat recovery. In the summer season, the mechanical ventilation system is also operated to avoid the indoor overheating. In this case, during the occupied and not-occupied periods, whenever the operative temperature overcomes the upper limit of the comfort range (see paragraph 4.3.1) and the outside conditions can improve the internal comfort (the outside temperature is lower than the indoor one) the mechanical ventilation system turns on, bypassing the heat recovery. If the outdoor conditions are worse than those inside (too cold or too hot), the mechanical ventilation is operated with a fixed airflow rate of 0.5 ACH and with heat recovery just during the occupied periods.

4.2.2 Net Present Value

The Net Present Value (NPV) is calculated according to the comparative framework methodology of the cost-optimal level (European Committee, 2012). The NPV, considering different time series of cash flows, allows to evaluate the economic benefits associated with the possible retrofit solutions. The NPV is evaluated for a lifespan of 30 years and takes into account:

- the *initial Investment Costs (IC)*, reported in Table 5 and defined from the comparison of different regional databases (Regional Price List, RPL, of Lombardy, Lazio and Sicily);
- the annual running costs, composed of the *Annual Energy Cost (EC)* and the *Maintenance Cost (MC)*. The EC has been calculated considering the fuel and electricity price rising (Table 4);
- the *replacement cost (RC)*, for the periodic substitution of building/system elements;
- the *residual value (RV)* for the equipment with longer lifespan (CEN, 2007d).

Table 3 – Investment costs without VAT of the considered retrofit strategies

Retrofit strategies	IC
Vertical walls insulation	$IC_W = 160 x^* + 38.53$ [EUR m ⁻²] *insulation thickness [m]
Horizontal walls insulation	$IC_H = 188 x^* + 8.19$ [EUR m ⁻²] *insulation thickness [m]
DH – Double, high SHGC	$IC_{DH} = 404.33$ [EUR m ⁻²]
DL – Double, low SHGC	$IC_{DL} = 439.06$ [EUR m ⁻²]
TH – Triple, high SHGC	$IC_{TH} = 477.65$ [EUR m ⁻²]
TL – Triple, low SHGC	$IC_{TL} = 454.49$ [EUR m ⁻²]
Standard Boiler (STD)	$IC_{STD} = 1000$ [EUR]
Modulating Boiler (MD)	$IC_{MDL} = 1500$ [EUR]
Condensing Boiler (CD)	$IC_{CND} = 2000$ [EUR]
Mechanical ventilation system (MVS)	$IC_{MVS} = 6000$ [EUR]

Table 4 – Parameters for the definition of the Energy Costs

Fuel Cost (natural gas) ⁽¹⁾	0.85 [EUR Sm ⁻³]
Lower Heating Value	32.724 [MJ Sm ⁻³]
Annual rate of increase fuel price ⁽²⁾	2.8%
Electricity Costs ⁽¹⁾	0.25 [EUR kWhel ⁻¹]
Annual rate of increase electricity price ⁽²⁾	1.71%
Real Interest Rate ⁽³⁾	3%
VAT ⁽⁴⁾	10%

⁽¹⁾ Domestic customer (AEEG 2013); ⁽²⁾ (European Commission 2009); ⁽³⁾ (European Commission 2012); ⁽⁴⁾ Italian Parliament (1972)

4.3 Optimization 2: Energy, Costs and Comfort

A second Optimization has been run, considering the thermal comfort as the third objective. In this case the best combination of EEMs are defined to minimize the Energy Performance for Heating (EPH), the Net Present Value (NPV) and the Weighted Discomfort Time (WDT).

4.3.1 Weighted Discomfort Time (WDT)

The WDT is calculated according to the Annex F of the EN 15251 (CEN, 2007a), through the Degree Hours Criteria. This index weights the occupied hours, during which the actual operative temperature lies outside the comfort range, by a weighting factor that depends on the entity of the deviation (Equation 1 and 2).

$$\text{WDT} = \sum wf \cdot \text{time} \quad (1)$$

$$wf = \Theta_0 - \Theta_{0,\text{limit}}$$

$$\text{when } \Theta_0 < \Theta_{0,\text{limit,lower}} \text{ or } \Theta_0 > \Theta_{0,\text{limit,upper}} \quad (2)$$

The comfort range is defined on the basis of a normal level of expectation (Category II) for an activity level of 1.2 met and a clothing index of 1 clo. The lower and upper limits vary according to the heating and non-heating season. During the heating season, defined pursuant to the Italian legislation (Italian Parliament, 2013), the lower and upper values for the operative temperature are fixed, i.e. 20°C and 25°C. During the rest of the year, the comfort range is set according to the adaptive comfort approach (passive operational mode), defined by the annex A of the EN 15251:2007, as follow (Equation 3a and 3b):

$$\Theta_{o,\text{limit,upper}} = 0.33 \Theta_{\text{rm}} + 18.8 + 3 \quad (3a)$$

$$\Theta_{o,\text{limit,lower}} = 0.33 \Theta_{\text{rm}} + 18.8 - 3 \quad (3b)$$

Those limits consider the individual's thermal experience described by the exponentially weighted running mean of the daily outdoor mean air temperature, Θ_{ed} , calculated on the seven days immediately before the analysed one:

$$\Theta_{\text{rm}} = (1-\alpha) \cdot (\Theta_{\text{ed-1}} + \alpha \Theta_{\text{ed-2}} + \alpha^2 \Theta_{\text{ed-3}} + \dots + \alpha^6 \Theta_{\text{ed-7}}) \quad (4)$$

5. Results and discussion

5.1 Comparison between Optimization 1 and 2

Figures 1 and 2 show the Pareto Front solutions obtained with the Optimization 1 and 2. The cases reported are those of REF 2 buildings, east oriented, located in Milan and in Messina. Different colors have been used to describe the comfort performance of the non-dominated solutions, identifying five different comfort ranges. Blue dots pinpoint the solutions with the best

performance in terms of comfort, while, red dots the ones with the worse performance. The highest WDTs characterize the configurations with smaller compactness ratios, because of the overheating issue. In fact, for those cases, the small area of the external envelope reduces the thermal losses in winter increasing the EP_H performance, but, in summer and in intermediate seasons, it is difficult to get rid of the excess heat. Looking to the Pareto Front of Optimization 1, the most comfortable solutions generally lie in the upper side of the front: this is probably due to the adoption of mechanical ventilation that raises the NPV. Looking at the Optimization 2 the more comfortable solutions lie in the right-upper side of the graph: this means that higher comfort performance solutions have a higher NPV and a lower EP_H . Moreover, the graphs show that the Pareto fronts obtained from the Optimization 1 are located in the left-down area of the Pareto surfaces of the Optimization 2 and they are characterized by high values of WDT. This means that optimizing only the energy and cost objectives leads to reject the most comfortable solutions. Considering the thermal comfort in the optimization process does not affect the definition of the global energy and cost optima, but it allows to select a larger number of optimal configurations that are discarded if only the energy and cost perspectives are taken into account. This aspect is also highlighted by the percentage distributions of single EEMs in the Pareto front reported in Table 5.

5.2 Thermal comfort and EEMs

The non-dominated solutions of the Optimization 1 present in almost all the cases the highest insulation levels, especially in the REF 1 cases, while in the solutions of the Optimization 2 all the insulation levels appear. This is due to the competing nature of the energy, cost and comfort objectives. In the Optimization 1, reducing the thermal losses plays a crucial role in improving the EP_H performance and to reduce the energy cost item. On the other hand, considering the comfort perspective highlights the overheating issue of high insulated buildings. In those buildings, a small energy input can significantly raise the

indoor temperature and, if the excess of heat is not discharged, the indoor comfort could be compromised. Another important difference between the Pareto fronts of the Optimization 1 and 2 is the presence of the windows with low SHGC: in fact, the cost-optimization does not include this retrofit action in the optimal solutions, while it is considered in Optimization 2, because of their advantage in maintaining a better indoor thermal comfort. Concerning the replacement of the boiler, this action rarely appears in the Pareto solutions of the bi-optimization for the building with 0.3 of compactness ratio, is considered in 6 to 25% of the solutions for the compactness ratio 0.63 and in the 26 to 73% of the solutions for the highest compactness ratio. The higher the heating energy need, the better the boiler performance should be.

5.3 Global optima and best comfort performance optima

Table 6 shows the comparison between the global costs and energy optima (Global Optima, GO) and the optima of the solutions belonging to the best comfort level, WDT<1000 (Comfort Optima, CO), obtained with Optimization 2. This comparison allows us to understand what the main features of the solutions able to guarantee the best comfort performance are. As previously highlighted, some of the cases are characterized by the problem of overheating and for those it is not possible to assure comfort performance with a WDT less than 1000 K h. Hence, for the cases with windows East oriented, REF 1, 0.3 and 0.63 and REF 2, 0.3 located in Milan, the optima solutions of the best comfort performance refers to cases with a WDT less than 2000 K h even though bigger than 1000 K h.

Concerning the cost optimality, it is possible to see that for some cases (REF 1, East, 0.3 and REF 2, South, 0.3 located in Messina and REF 2, East, 0.3 located in Milan) the cost-optimal solutions of the best comfort level coincide with the reference cases. This means that for those configurations it is not possible to improve the comfort performance in a cost effective way. The configurations of cost and energy optima of the first comfort level are mainly characterized by a smaller insulation thickness and a lower windows' SHGC. Especially

for the cases with smaller compactness ratio, the insulation on the external walls is often not considered.

Mechanical Ventilation should enhance the energy performance preserving the indoor comfort.

Table 5 – Percentage distribution of the EEMs for cases REF1.

		REF 1							
		0.3				0.63			
		EAST		SOUTH		EAST		SOUTH	
		MI		ME		MI		ME	
		OPTI 1	OPTI 2						
WALLS	0-5 cm	0%	43%	0%	43%	0%	39%	2%	45%
	5-10 cm	0%	28%	18%	28%	8%	28%	25%	30%
	10-15 cm	20%	16%	39%	16%	27%	21%	42%	19%
	15-20 cm	80%	14%	44%	14%	65%	13%	31%	6%
	S	0%	0%	0%	36%	0%	23%	34%	44%
WINDOWS	DH	58%	17%	73%	13%	69%	24%	66%	18%
	SL	0%	24%	0%	17%	0%	16%	0%	18%
	TH	38%	16%	25%	21%	31%	16%	0%	14%
	TL	4%	44%	2%	14%	0%	22%	0%	7%
	STND	96%	56%	91%	49%	95%	57%	96%	61%
VENTI BOILER	MD	4%	31%	9%	34%	5%	35%	4%	33%
	CD	0%	13%	0%	17%	0%	7%	0%	5%
	NAT	68%	66%	98%	73%	68%	68%	100%	75%
MVS	32%	34%	2%	25%	32%	32%	0%	25%	
		0.97							
		EAST		SOUTH		EAST		SOUTH	
		MI		ME		MI		ME	
		OPTI 1	OPTI 2						
WALLS	0-5 cm	0%	36%	0%	33%	0%	34%	0%	33%
	5-10 cm	0%	25%	0%	22%	0%	26%	0%	22%
	10-15 cm	4%	22%	31%	25%	0%	24%	43%	26%
	15-20 cm	96%	17%	69%	20%	100%	16%	57%	19%
	S	0%	0%	0%	18%	0%	8%	16%	18%
WINDOWS	DH	94%	25%	78%	26%	86%	25%	73%	35%
	SL	0%	50%	0%	31%	0%	20%	0%	20%
	TH	6%	15%	22%	22%	14%	19%	11%	14%
	TL	0%	10%	0%	3%	0%	28%	0%	14%
	STND	27%	6%	59%	43%	41%	20%	74%	45%
VENTI BOILER	MD	17%	10%	33%	43%	33%	36%	20%	38%
	CD	56%	83%	7%	15%	26%	44%	6%	18%
	NAT	55%	64%	64%	66%	67%	59%	70%	69%
MVS	45%	36%	36%	34%	33%	41%	30%	31%	

Nevertheless, this solution does not appear in the CO cost-optimal solutions (except for the cases REF 1 and 2, 0.3, South and REF 2, 0.63, East located in Milan) because of the high initial investment costs. In table 6 the energy performance of the GO and CO solutions have been compared to the reference case without retrofits: the percentage difference between the EP_H , the NPV and WDT of energy and comfort optima are reported. The red negative values mean a worse indicator than the reference case. In almost all the cases, the building energy consumptions are reduced. However, the GO solutions present higher performance in terms of energy savings, with a greater economic effectiveness. Setting the best comfort level leads to solutions less effective in terms of energy and costs, but the difference between the comfort of the GO solutions is very relevant. This could compromise the effectiveness of the refurbishment, deteriorating the indoor comfort.

6. Conclusion

Comparing the results found with the cost-optimal approach and the ones in which also the thermal comfort performance is optimized, it was possible to highlight the effect of the comfort performance on the definition of the optimal retrofit solutions. The results of the cost-optimal approach show that optimizing only the energy and costs leads to rejecting the most comfortable measures, such as windows, with low SHGC or smaller insulation level. On the other hand, adding the thermal comfort as an objective function allows us to select a larger number of optimal configurations that are discarded because of the higher NPV. The most energy and cost effective measures alone generally lead to uncomfortable conditions if no other strategies are considered. Considering that the above results depended only on the envelope and systems performance, renovated buildings are likely to require a more careful operation management to avoid the overheating issue. Whether this role is played by the manual intervention of somehow trained occupants, or by some building automation technologies, the control strategies are of crucial importance in building

renovation. Further developments should investigate the potential of building management strategies also based on automated systems to maintain adequate comfort condition while reducing the energy demand.

Table 6 - Global Optima (GO) and Comfort Optima (CO) for cases REF 1-2, 0.3-0.97, South oriented, located in Milan and Messina.

	REF 1							
	0.3				0.97			
	MI		ME		MI		ME	
	GO	CO	GO	CO	GO	CO	GO	CO
	COST OPTIMAL							
Wall	12	0	11	5	15	10	12	12
Roof	-	-	-	-	14	15	11	11
Floor	-	-	-	-	15	8	10	10
Wind	DH	DL	0	0	DH	0	0	0
Boiler	STD	STD	STD	STD	STD	MD	STD	STD
Vent	STD	MVS	STD	STD	STD	STD	STD	STD
EPH	8	41	13	19	43	87	35	35
NPV	14	32	9	10	32	37	21	21
WDT	6337	855	1270.3	951	2466	977	542	542
% EPH	92	59	68	51	76	51	71	71
% NPV	49	-16	22	12	35	24	36	36
% WDT	-519	16	-136	-77	-161	-3	38	38
	ENERGY OPTIMAL							
Wall	17	0	18	3	19	9	18	17
Roof	-	-	-	-	18	15	20	20
Floor	-	-	-	-	19	9	18	12
Wind	TH	DL	DH	DL	TH	TL	TH	TL
Boiler	STD	STD	STD	MD	CD	CD	CD	CD
Vent	MVS	MVS	STD	MVS	MVS	MVS	MVS	MVS
EPH	0.493	41	0.3	1	12.84	39	0.6	3
NPV	27.45	32	13	27	43.41	46	40	39
WDT	5261	855	8054.3	950	2352	946	1667	720
% EPH	100	59	99	97	93	78	99	97
% NPV	0	-16	-12	-138	11	6	-21	-18
% WDT	-414	16	-1395	-76	-149	0	-91	18
	REF 2							
	COST OPTIMAL							
Wall	11	0	8	0	10	8	9	9
Roof	-	-	-	-	11	10	10	10
Floor	-	-	-	-	11	7	10	10
Wind	0	DL	0	0	DH	TL	0	0
Boiler	STD	STD	STD	STD	STD	MD	STD	STD
Vent	STD	MVS	STD	STD	STD	STD	STD	STD
EPH	25	38	4	25	48	60	27	27
NPV	12	32	6	7	31	36	18	18
WDT	3333	875	2348.8	687	1951	998	684	684
% EPH	65	46	83	0	79	74	74	74
% NPV	39	-61	18	0	51	43	37	37
% WDT	-153	34	-242	0	-144	-25	18	18
	ENERGY OPTIMAL							
Wall	12	0	6	3	11	8	12	10
Roof	-	-	-	-	12	11	11	11
Floor	-	-	-	-	11	8	12	10
Wind	TH	TL	TL	TL	TH	TL	TH	DH
Boiler	CD	MD	STD	CD	CD	MD	CD	MD
Vent	MVS	MVS	MVS	MVS	MVS	MVS	MVS	MVS
EPH	0.735	35	0.3	0.7	26.5	44	2.9	5
NPV	29.72	33	26	28	43.16	45	37	35
WDT	4641	839	1508.7	968	1654	875	1102	975
% EPH	99	50	99	97	88	81	97	95
% NPV	-50	-66	-243	-300	32	29	-25	-18
% WDT	-253	36	-120	-41	-107	-10	-32	-17

REF 2 – EAST – MILAN

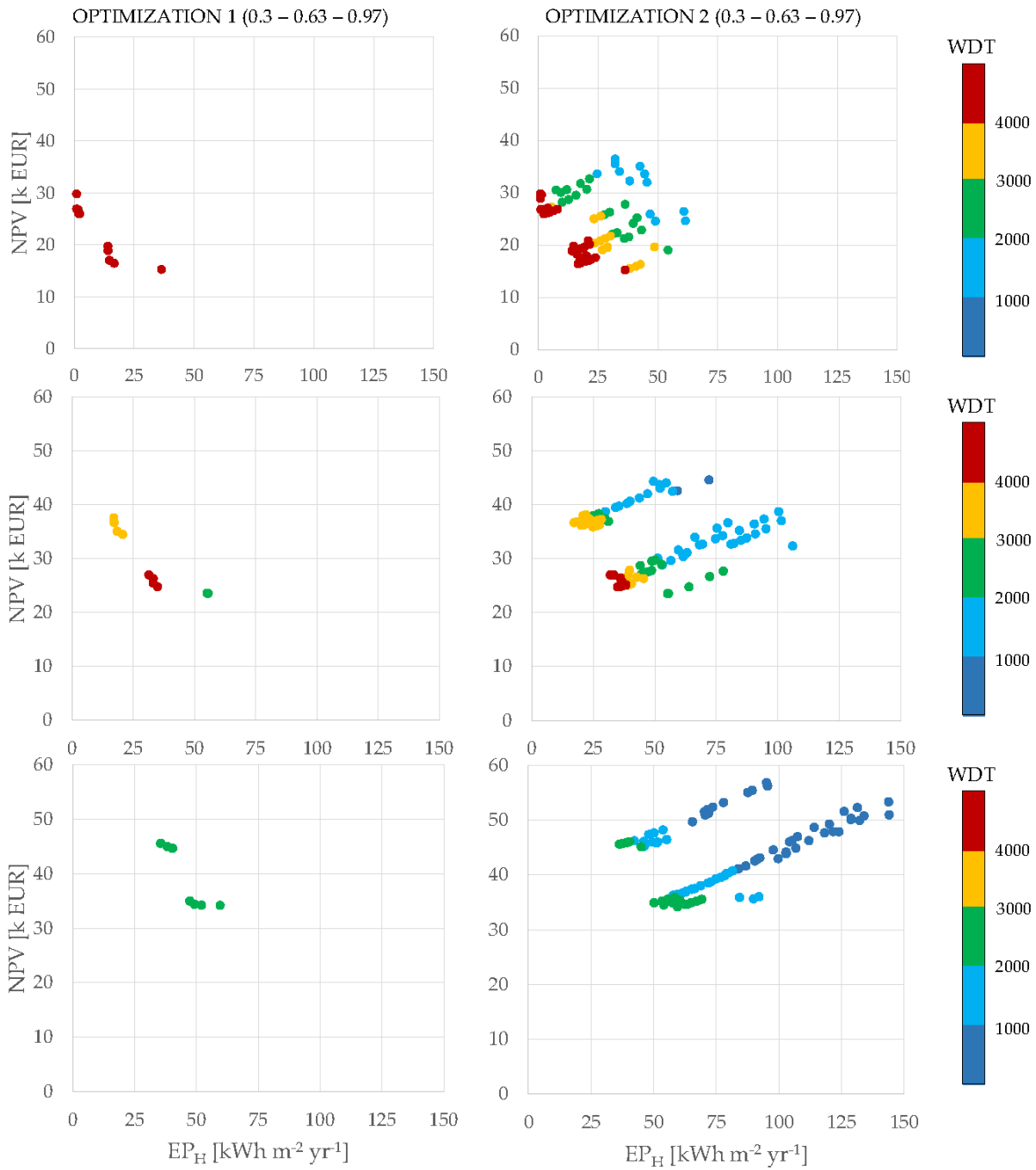


Fig. 1 – Pareto fronts of the Optimization 1 and 2 for the cases REF 2, windows east oriented, located in Milan according to the compactness ratios. The Weighted Discomfort Time represents the comfort performance, grouped according to the comfort level

REF 2 – EAST – MESSINA

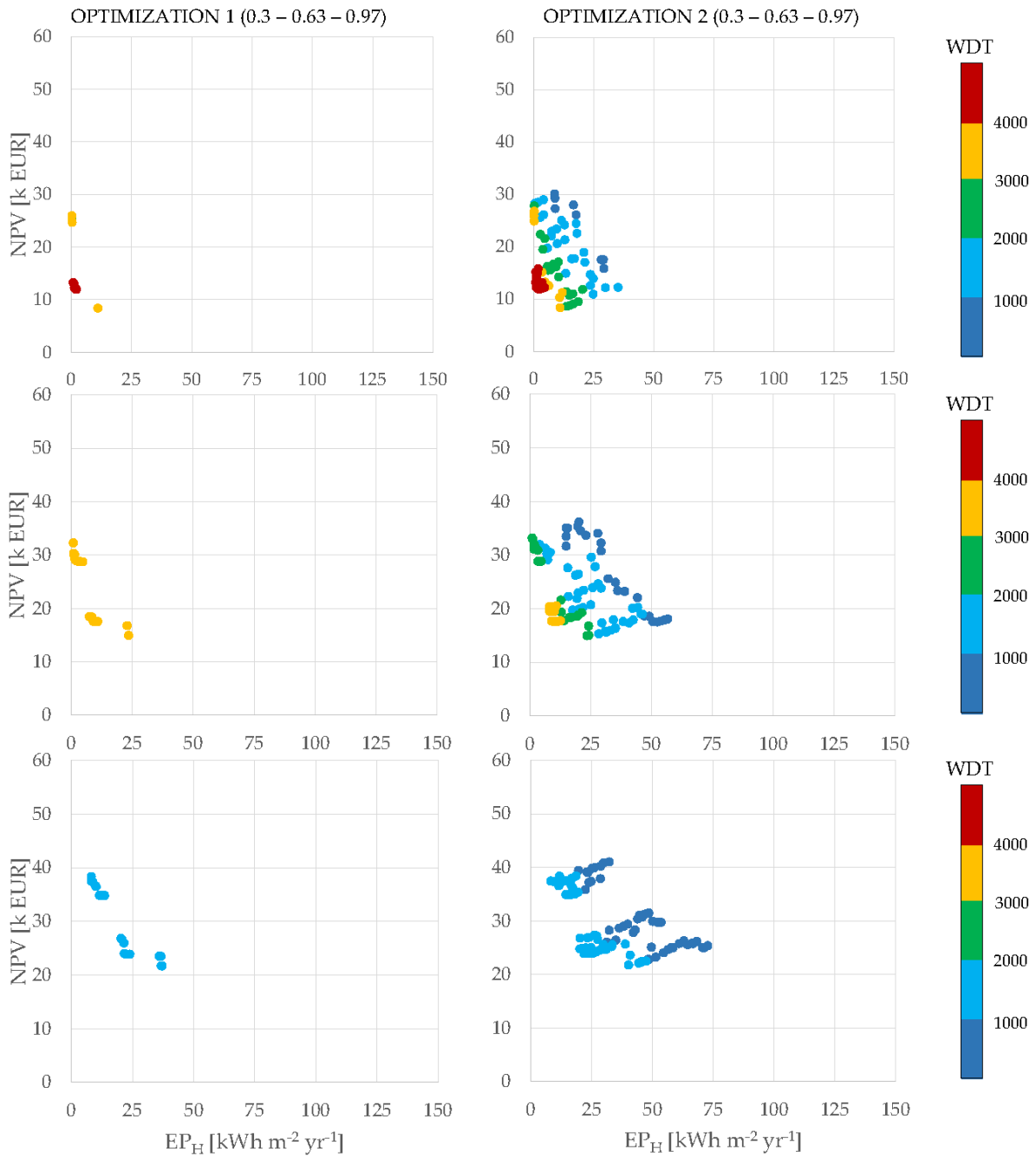


Fig. 2 – Pareto fronts of the Optimization 1 and 2 for the cases REF 2, windows east oriented, located in Messina according to the compactness ratios. The Weighted Discomfort Time represents the comfort performance, grouped according to the comfort level.

References

- Carlson C., Verma V. K., Schwarz M., Golicza L., Prada A., Baratieri M., Haslinger W., Schmidl C., 2015. Experimental validation of a thermodynamic boiler model under steady state and dynamic conditions, *Applied Energy*, 138:505-516.
- CEN European Committee of Standardization, 1999. EN 12207:1999, Windows and doors. Air permeability – Classification.
- CEN, European Committee of Standardization, 2003. EN 12831:2003, Heating systems in buildings – Method for calculation of the design heat load.
- CEN, European Committee of Standardization, 2007a. EN 15251, Indoor environmental input parameters for design and assessment of energy performance of buildings addressing indoor air quality, thermal environment, lighting and acoustics.
- CEN European Committee of Standardization, 2007b. EN ISO 10211:2007, Thermal bridges in building construction - Heat flows and surface temperatures - Detailed calculations.
- CEN, European Committee of Standardization, 2007c. EN 15242:2007, Ventilation for buildings – Calculation method for the determination of air flow rates in buildings including infiltration.
- CEN European Committee of Standardization, 2007d. EN 15459:2007, Energy performance of buildings - Economic evaluation procedure for energy systems in buildings.
- Comitato Termotecnico Italiano. 2012. Anno tipo climatico per le provincie italiane. <http://www.cti2000.it/>
- Deb, K., Pratap, A., Agarwal, S., 2002. A Fast and Elitist Multi-objectives Genetic Algorithm: NSGA-III, *IEE Transactions on Evolutionary Computation*, 6 (2):182-197.
- European Commission. 2009. EU energy trends to 2030.
- European Commission, 2010. Directive 2010/31/EU of the European Parliament and of the Council, Official Journal of European Union, L 153/13, 18/06/2010.
- European Commission. 2012. Commission delegated regulation (EU) No 244/2012 of 16 January 2012.
- Haller M.Y., Paavilainen J., Konersmann L., Haberl R., Dröscher A., Frank E., 2011a. A unified model for the simulation of oil, gas and biomass space heating boilers for energy estimating purposes. Part I: Model development. *Journal of Building Performance Simulation* 4(1):1-18.
- Haller M.Y., Paavilainen J., Konersmann L., Haberl R., Dröscher A., Frank E. 2011b. A unified model for the simulation of oil, gas and biomass space heating boilers for energy estimating purposes. Part II: Parameterization and comparison with measurements. *Journal of Building Performance Simulation* 4(1):19-36.
- LBNL, 2013. Lawrence Berkeley National Laboratory, THERM 6.3 / WINDOW 6.3 NFRC. Simulation Manual, July 2013 <http://windows.lbl.gov/software/window/6/>
- Matlab 7.7.0 R 2008, Settembre 2008.
- McLeod RS, Hopfe CJ, Kwan A..2013. An investigation into future performance and overheating risks in Passivhaus dwellings. *Building and Environment*. 70:189-209
- Mlakar J, Štrancar J., 2011. Overheating in residential passive house: Solution strategies revealed and confirmed through data analysis and simulations. *Building and Environment*; 43:1443-51
- Penna P, Prada A, Cappelletti F, Gasparella A, 2014. Multi-objectives optimization of Energy Efficiency Measures in existing buildings, *Energy Buildings*, <http://dx.doi.org/10.1016/j.enbuild.2014.11.003>
- Saltelli A., Tarantola S., Campolongo F., Ratto M., 2004. Sample generation, in Sensitivity analysis in practice. A guide to assessing scientific models, Chichester (UK): *John Wiley & Sons*, 193 - 204.
- Solar Energy Laboratory, TRNSYS 17, 2012. A transient system simulation program, <http://sel.me.wisc.edu/trnsys>
- UNI 2008. UNI/TS 11300-1:2008, Energy performance of buildings - Part 1: Evaluation of energy need for space heating and cooling.

A multi-objective optimization analysis on high-performance buildings connected to district heating-CHP system

Dario Prando – Free University of Bolzano – dario.prando@unibz.it

Alessandro Prada – Free University of Bolzano – alessandro.prada@unibz.it

Fabian Ochs – University of Innsbruck – fabian.ochs@uibk.ac.at

Andrea Gasparella – Free University of Bolzano – andrea.gasparella@unibz.it

Marco Baratieri – Free University of Bolzano – marco.baratieri@unibz.it

Abstract

The European energy policy is strongly promoting the refurbishment of buildings and this affects the energy and economic performance of the district heating (DH) systems. The refurbishment of buildings connected to a DH system leads to the under-utilization of the DH capacity. This paper aims to define the energy and economic performance of a district heating (DH) considering the impact of cost-optimal refurbishment solutions of the connected buildings. For this purpose, an integrated model for both buildings and network has been developed. Several refurbishment measures for the existing buildings have been investigated and a multi-objective (energy and economic) optimization has been conducted, by means of a genetic algorithm. The possibility to shift to a low-temperature DH and the implementation of a CHP system have been investigated as feasible solutions to compensate for the loss of performance of the network.

The results highlight that the building refurbishment strongly influence both the energy and economic performance of the DH system. The DH performance is considerably low when a high number of refurbished buildings is considered in the district. The implementation of the minimum network temperature allows for a partial compensation for both the energy and the economic losses deriving from the refurbishment. However, this measure is not sufficient for a profitable DH. The installation of a CHP system in the network, thanks to the revenue from the electricity trade, allows for a profitable operation of DH network with a heat density of $0.15 \text{ MWh (m year)}^{-1}$. Although the installation of a CHP system is economically convenient, its primary energy saving (PES) index is negative for such a micro DH networks.

1. Introduction

The recast of Energy Performance of Buildings Directive (EPBD) (European Commission, 2010) states that by the end of 2020, all new buildings should be nearly zero-energy buildings, and in the meanwhile, the performance of the buildings that undergo major renovation should be upgraded in order to meet new minimum energy performance requirements, defined in accordance with the cost-optimal approach (European Commission 2012).

On one hand, the reduction of buildings' heating demand leads to the reduction of fuel consumption in the DH area (Nielsen and Möller, 2013). On the other hand, it causes a reduced utilization of the DH capacity with a consequent reduction of both the distribution efficiency (because constant network losses will be a higher fraction if the total heat is reduced) and the revenues.

The building refurbishment could reduce the difference of thermal power between the heating season and the period with only DHW demand (Lund et al., 2014). A more constant heat load during the year would enable a higher equivalent utilization time of a new CHP system installed with a proper size. However, also in the case of DH networks, the minimum heat demand could be very low and would not justify the installation of a CHP plant (Sartor et al., 2014).

The reduction of the grid temperatures (i.e., supply and return) is another measure, mentioned in the literature, to upgrade the DH systems. Both heat exchangers and radiators are usually oversized because they are usually designed for the most critical weather conditions. Actually, this condition

rarely occurs and, therefore, a reduced network temperature could be sufficient to satisfy the building heat need. A lower temperature means lower network losses and thus higher distribution efficiency of the DH network.

A pilot project carried out in Denmark, showed that the low temperature district heating (LTDH), i.e., 55/25 °C (supply/return), is a suitable solution for DH systems in low heat density area with low energy buildings (Li and Svendsen, 2012). In accordance with Dalla Rosa and Christensen (2011), LTDH systems in areas with linear heat density of 0.20 MWh m⁻¹ year⁻¹ are supposed to be feasible from an energy and economic point of view. A study carried out on a DH plant based on a CHP system highlighted that a decrease of the DH network temperature of 10°C can improve the electric efficiency of the ORC generator of one percentage point (Prando et al., 2015).

This work aims to define the energy and economic performance of the DH system, considering cost-optimal solutions for the refurbishment of buildings connected to the DH system. Several measures have been considered for the refurbishment of buildings and a genetic algorithm is used to reduce the number of configurations to investigate among all the possible combinations to get the optimal ones. Different scenarios, with a different number of refurbished buildings in the network, have been analyzed comparing two strategies as for the supply temperature: the current fixed network temperature (i.e., 90 °C) and the lowest network temperature required by the most critical building. Moreover, the installation of a CHP system has been considered as a potential measure to improve the DH profitability.

2. Materials and methods

2.1 Buildings retrofitting

2.1.1 Reference buildings

The retrofitting of buildings is investigated by means of several energy simulations in order to find the cost optimal solutions. The multi-objective optimization analysis focuses on different residential buildings representative of the South

Tyrol context. The floor area has been sized on the weighted average surface for residential buildings computed from the data provided by the National Statistical Institute (i.e., Istituto Nazionale di Statistica – ISTAT). Each building has been simplified as a base module with a square floor and an internal height of 3.0 m.

Besides, 14 representative buildings have been defined in order to represent a typical set of building connected to the micro-grid in South Tyrol. Each building has been assigned to one of the three construction periods according to the statistics provided by National Statistical Institute (i.e., Istituto Nazionale di Statistica – ISTAT). In South Tyrol, 37% of the residential buildings were built before 1960, 49% between 1960 and 1991, and 14% after 1991 (ISTAT, 2001). The construction period is important since it is associated with a specific type of building envelope, as reported in the Italian technical report UNI/TR 11552 (UNI, 2014).

All the characteristics of the reference buildings and the networks are reported by Ref. (Prando et al., 2014b). The heating need of the buildings has been computed by means of a dynamic simulation model – developed in TRNSYS environment – with a time step of 1 hour. The analysis has been carried out using the weather conditions of Bolzano, HDD₂₀ = 2791 K d, which is the most populated city of the province.

2.1.2 Refurbished buildings performance and economic analysis

The research aims to analyze the extent to which the refurbishment of a building connected to district heating can become an issue for the district heating utility. For this reason, the main standard energy saving measures that contribute to the reduction of the building's energy needs have been investigated:

- external insulation of the vertical walls with a possible thickness increment from 1 cm to 20 cm using a 1 cm step;
- external insulation of the roof with a possible thickness increment from 1 cm to 20 cm using a 1cm step;

- external insulation of the floor with a possible thickness increment from 1 cm to 20 cm using a 1cm step and screed replacement;
- replacement of existing glazing systems with higher thermal performance windows such as double or triple-pane with either high or low solar heat gain coefficients. Besides, also the frames are replaced with an improved aluminum frames with thermal break;
- installation of a mechanical ventilation system with heat recovery to control the air exchange;
- replacement of the high temperature hydronic system with a underfloor heating, that ensure a reduction of the supply water temperature of the house. Also this intervention requires the screed replacement.

The reference prices of the different refurbishment measures are obtained from a survey comparing the prices in different zones of the national territory (Penna et al., 2014). The adopted prices are reported by Ref. (Prando et al., 2014b).

The NPV for each retrofit solution is based on the methodology proposed by the regulation EU 244/2012 (European Commission, 2012) and computed according to the EN 15459:2009 (UNI, 2007) procedure.

The full parametric analysis of the energy conservation measures would take a considerable computational time. To overcome this problem, a Genetic Algorithm code has been implemented in Matlab environment (Holland, 1975; Haupt and Haupt, 2004). The details of the algorithm implementation are reported by Penna et al. (2014).

2.2 District heating system

2.2.1 Numerical model of the DH system

A numerical model has been developed to simulate the thermal behavior of a DH network and calculate its performance. The network has been configured based on the arithmetic mean – in terms of the number of buildings and length of each pipe segment – from a survey of 13 micro DH networks located in South Tyrol. The study focused on micro DH networks because they are particularly affected by refurbishment of the connected buildings due to the limited number of users. However, the results of this study can be extended to larger systems.

The detailed characteristics of the modeled network are reported by Prando et al. (2014b).

The network has been sized based on the design heat load of the connected buildings, which has been calculated in accordance with the European normative EN 12831:2003 (CEN, 2003). This approach can be used to calculate the size of the network piping, the heat exchanger of each substation and the boiler. In accordance with the normative, the design heat load is calculated considering the transmission and ventilation heat losses without taking into account the solar and internal heat gains. For residential buildings, the minimum ventilation thermal loss is calculated with an air change rate per hour of 0.5 ACH. According to the national specification (UNI, 2006), the external design temperature for Bolzano, county town of South Tyrol, is -15°C.

The network temperature is defined per each hour in accordance with the temperature requirement of the most critical building in terms of temperature. The radiators of each building have been sized to provide the nominal power at the design heat load condition with an average temperature around 70°C, i.e. typical value if not regulated according to the outside air temperature. During the heating season, in particular for the refurbished buildings, the heating load of each building is lower than the design heat load. For this reason, the radiator temperature, and therefore the network temperature, can be lower. On this basis, the minimum temperature required on the network has been hourly calculated and it represents the minimum theoretical temperature for the network.

The minimum limit temperature of the network has been fixed at 65°C in order to ensure the domestic hot water (DHW) production (Brand et al., 2013). Although a lower temperature in the supply line (i.e., 50-55°C) could be sufficient for DHW production, it strongly depends on the heat exchanger characteristics (Brand et al., 2010; Dalla Rosa and Christensen, 2011).

The size of the pellet boiler has been determined in accordance with the design load calculated through the EN 12831:2003 (CEN, 2003), as mentioned at the beginning the section. The generation efficiency has been considered to be 0.9 at nominal load and 0.88 at 30% of the nominal

load, considering a linear trend in between (KWB 2014). These values have been used for the calculation consumption of the pellet boiler. The circulation pump operates at fixed speed. Its electricity consumption has been hourly calculated depending on the water mass flow rate and pressure drop in each segment of the network.

2.2.2 Energy and economic analysis of the DH plant

Among the cost-optimal configurations, obtained through the multi-objective optimization, those with the lower NPV are more likely to be implemented. The DH scenario changes every time that an additional building connected to the network is refurbished. For each scenario (15 in total considering the reference case with no refurbished buildings), the Energy Performance index (EP) and the net present values (NPV) of the district heating have been calculated.

The EP (kWh year⁻¹) of the DH system is:

$$EP = m_{\text{pellet}} \cdot LHV_{\text{pellet}} + E_{\text{el}} \cdot f_{PE}$$

where m_{pellet} (kg) is the pellet consumption of the boiler, LHV_{pellet} (kWh kg⁻¹) is the lower heating value of pellet, E_{el} (kWh) is the electricity self-consumption of the auxiliaries and f_{PE} is the conversion coefficient from electrical to primary energy. In Italy, f_{PE} is currently 2.174 (AEEGSI, 2008) but it is periodically updated according to the average electrical efficiency of the national grid. The lower heating value of pellet has been considered 4.7 kWh kg⁻¹ (UNI, 2011).

The NPV of the DH system has been calculated as the sum of the discounted cash flow over a period of 30 years (Dalla Rosa and Christensen, 2011, Reidhav and Werner 2008). The present work investigates the refurbishment of the existing DH systems and, therefore, does not consider the investment costs of both plant and network. However, the biomass boiler is considered to have a lifespan of 15 years and therefore one substitution has been considered in the economic analysis (Viessmann, 2014). The formula for NPV is the following:

$$NPV = \sum_{n=0}^{n=30} \frac{(E_n + E_{\text{DHW}}) \cdot p_{\text{heat}} - m_{\text{pellet}} \cdot p_{\text{pellet}} - E_{\text{el}} \cdot p_{\text{electricity}} - m_{\text{ash}} \cdot p_{\text{ash disposal}} - C_{\text{maint.}}}{(1+i)^n}$$

where E_h (kWh) is the space heating need, E_{DHW} (kWh) is the DHW need, p_{heat} is the price of the heat delivered to the users, p_{pellet} is the price of the input pellet and $p_{\text{electricity}}$ is the price of electricity used by the auxiliary equipment, m_{ash} is the ash production, $p_{\text{ash, disposal}}$ is the price for ash disposal, $C_{\text{maint.}}$ is the maintenance cost, n is the time of the cash flow and i is the real discount rate (i.e., $i = 3\%$). The inflation rates of electricity and heat have been considered to be 1.71% and 2.8%, respectively (see Table 1). The inflation of pellet price, as well as the remaining prices, has been considered the same of heat (i.e., 2.8%). The ash production has been calculated as 1.5% the pellet consumption (UNI 2011). Table 1 shows the investment costs (IC), the operational costs, the feed-in tariff and the revenues (VAT and other taxes excluded) required for economic analysis.

Table 1 - Prices for the economic analysis.

Item	Price
Heat ⁽¹⁾	0.1 EUR kWh ⁻¹
Pellet ⁽²⁾	263.5 EUR t ⁻¹
Electricity ^(3,4)	0.1358 EUR kWh ⁻¹
Ash ⁽¹⁾	150 EUR t ⁻¹
Maintenance ⁽⁵⁾	3.2 EUR kW ⁻¹
Boiler substitution ⁽⁵⁾	70 EUR kW ⁻¹

⁽¹⁾Network survey; ⁽²⁾(IRE 2014); ⁽³⁾(AEEGSI 2013); ⁽⁴⁾Industrial customer; ⁽⁵⁾(Viessmann 2014).

Moreover, both EP and NPV have been calculated considering two additional scenarios with different floor areas in order to assess the influence of the size of the buildings on both energy and economic analysis. The building stock has been divided in two categories; the buildings that are smaller than the median and the ones that are larger. A scenario with smaller buildings has been defined considering twice the buildings below the median and a scenario with larger buildings has been defined considering twice the buildings above the median.

Finally, the installation of a CHP system has been considered as a potential measure to improve the DH profitability. A gasification system has been considered as a possible solution to produce electricity – to be delivered to the national grid – and heat that can be delivered to the buildings through the DH network – the excess heat is considered to be discharged to the atmosphere. The smallest CHP system available in the market

has been considered to be operated continuously for entire year. In this case, the biomass boiler is used as a back-up boiler and to supply heat when the DH demand is higher than the CHP heat production. The economic analysis for the DH system with a CHP generator has been conducted considering the costs in Table 1 and in Table 2, namely the investment costs (IC), the operational costs, the feed-in tariff and the revenues (VAT and other taxes excluded) related to the CHP system. The details of the energy and economic performance of the gasification system are reported in Prando et al. (2014a).

Table 2 – Costs for the economic analysis (Prando et al., 2014a).

Item	Price
IC, gasifier	4000 EUR kW _{el} ⁻¹
IC, engine	500 EUR kW _{el} ⁻¹
Maintenance cost	0.050 EUR kWh _{el} ⁻¹
Biomass cost	165 EUR t ⁻¹
Feed-in-tariff	0.220 EUR kWh _{el} ⁻¹
Cogeneration bonus	0.040 EUR kWh _{el} ⁻¹
Char disposal	150 EUR t ⁻¹

3. Results

3.1 Building retrofitting

The multi-objective optimization has been carried out in accordance with the cost-optimal approach for each building connected to the network. The figure in Annex I shows the Pareto front for all the buildings connected to the DH network. The blue dots in the graph are the optimal ones. The red dots correspond to the reference case. Among the different cost-optimal configurations (Pareto front) of each building, the one with the lowest NPV is selected as the refurbishment measure that would be adopted by the building owner.

Once the cost-optimal configurations have been defined, the buildings have been ranked from the lowest to the highest NPV, since a smaller NPV values correspond to buildings that are more likely to be refurbished among the whole building stock, assuming a rational approach of the decision makers.

3.2 DH system

Fig. 1 shows the heat share delivered to the network for the scenario with high supply temperature “T=90°C” (column with texture in Fig. 1) and the scenario with low supply temperature “T min”. For the latter, the graph reports a column for each additional refurbished building. Heat for DHW is constant for both refurbished and not refurbished buildings and it is 45 MWh year⁻¹. Network heat loss is constant for almost all the degrees of refurbishment (i.e., 114 MWh year⁻¹) while it is slightly lower when all the buildings are refurbished (i.e., 106 MWh year⁻¹).

The reduction of the network losses is strictly related to the buildings to be refurbished because one single building can prevent the reduction of the network temperature. In the event the network temperature is constant at 90°C during the year, the network loss is 168 MWh year⁻¹. The simple implementation of the minimum network temperature required by the buildings (not yet refurbished), enables a considerable reduction of the network loss (i.e., 32%). Only the refurbishment of all the buildings enables a further small reduction of the network loss (i.e., 5%).

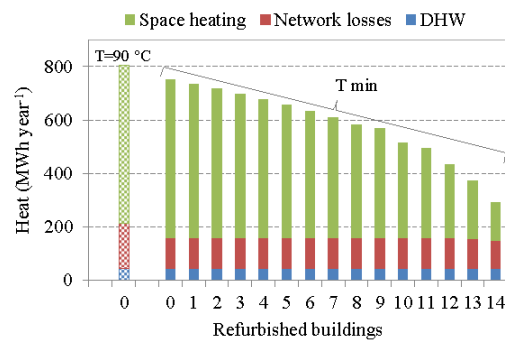


Fig. 1 – Heat shares delivered to the network for the scenario with constant network temperature (column with texture) and minimum network temperature (solid columns).

NPV and EP of the DH system have been calculated (Fig. 2). From the DH utility’s point of view, a positive NPV is expected from the operation of the DH system. The blue dots (i.e., T=90°C) correspond to the case in which a constant network temperature of 90°C is kept along the network. The red dots (i.e., T min) correspond to the cases in which the minimum network temperature, the one required by the most critical

building, is adopted. The dots with a black border correspond to the reference cases (i.e., no refurbished building). Each point refers to an additional refurbished building and therefore to a new DH state. For all the DH scenarios, a complete refurbishment of the buildings would lead to a negative NPV that means the DH system would be no longer profitable. The operation of the DH system with the minimum network temperature (red dots) allows a constant benefit in terms of NPV and EP, and partially compensate for the loss economic profitability deriving from the refurbishment.

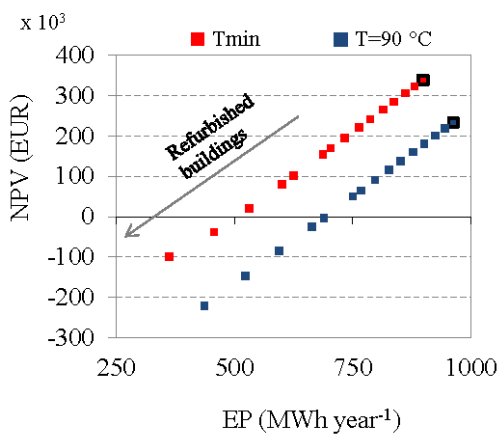


Fig. 2 – NPV and EP of the DH system for the two scenarios: T=90 °C, T_{min}.

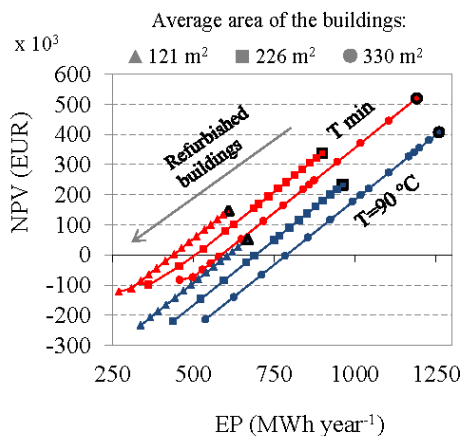


Fig. 3 – NPV and EP of the DH system for larger and smaller buildings.

Fig. 3 shows EP and NPV considering different size of the connected buildings. According to the survey, the reference buildings have a floor area that corresponds to an average area of the

buildings stock of 225 m². A scenario with smaller buildings involves buildings with a floor area between 75 m² and 178 m² (average area of 121 m²) while a scenario with larger buildings corresponds to a floor area between 182 m² and 421 m² (average area of 330 m²). The EP, and therefore NPV, is much higher for larger buildings. Nevertheless, for a high number of refurbished buildings, the NPV for smaller and larger buildings is not considerably different because the income from heat sale is a minor share of the cash flow, which is dominated by the costs to manage the network. This result is similar for both the scenarios with “T=90°C” and “T min”.

Finally, the installation of a CHP system (30 kW_{el} and 80 kW_{th}) has been investigated. The minimum size currently available in the market has been selected in order to limit the heat discharge. The plant has been considered to be constantly operated for the whole year, which is the most profitable strategy with the Italian incentive on the electricity production (Prando et al., 2014a). Fig. 4 shows EP and NPV considering the scenario with and without CHP system. The dots with a black border correspond to the reference cases (i.e., no refurbished building). The scenarios with the CHP system enable a higher NPV due to the revenues from the electricity sale. However, also EP is higher due to the CHP input energy to produce electricity. The benefit coming from the implementation of the minimum temperature is weakened – the two curves are closer – because the dominant revenue is due to the electricity sale (in particular when the buildings are refurbished). The slope of the curves (orange and green) is higher - increasing the refurbished building - because the EP of the CHP system is constant even if the heat required by the DH is lower.

The NPV of the abovementioned scenarios is reported depending on the linear heat density (MWh m⁻¹ year⁻¹) in Fig. 5. The linear heat density is defined as the ratio between the heating annually sold to the customers and the trench length of the DH network. Studies in the literature state that areas with a linear heat density of 0.2-0.3 MWh (m year⁻¹) can be supplied by DH in a cost-efficient way (Dalla Rosa and Christensen, 2011; Zinko et al., 2008), which is confirmed by the

present study. Moreover, the graph in Fig. 5 highlights that the implementation of a CHP system could shift this threshold to 0.15 MWh (m year)⁻¹.

NPV and PES of the DH system can be seen in Fig. 6. Each point refers to an additional refurbished building and the dots with black border correspond to the reference cases (i.e., no refurbished building). PES is lower when the minimum network temperature is implemented because the heat demand is reduced and therefore a larger amount of heat has to be discharged – since the CHP system is not operated at partial load. Although the Italian incentive regime enables the profitability for all the scenarios considered in this work, none of them have positive primary energy saving (PES) index, as reported in Fig. 6.

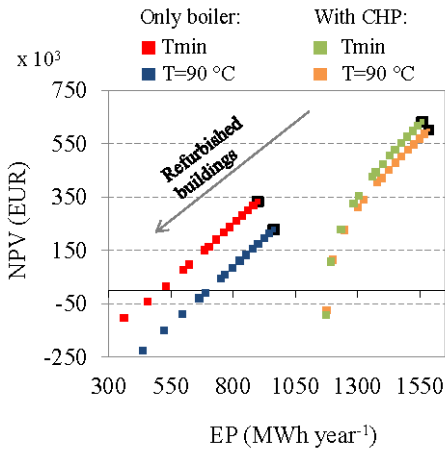


Fig. 4 – NPV and EP of the DH system for T=90 °C, T_{min} with (red and blue dots) and without CHP system (green and yellow dots).

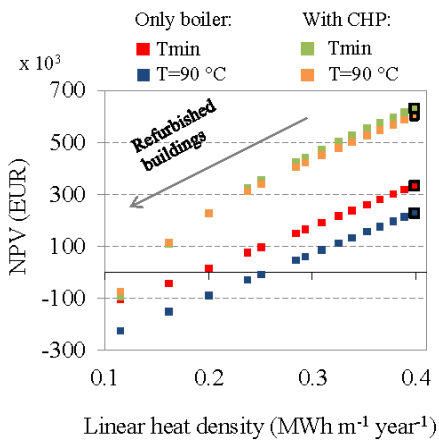


Fig. 5 – NPV and EP of the DH system for T=90 °C, T_{min} with (red and blue dots) and without CHP system (green and yellow dots).

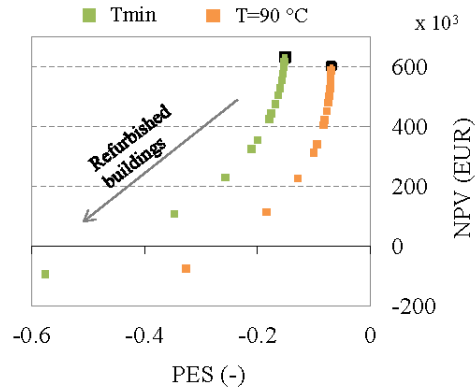


Fig. 6 – NPV and PES of the DH system for T=90 °C, T_{min}.

4. Conclusion

This work aims to define the energy and economic performance of the DH system considering cost-optimal solutions for the refurbishment of buildings connected to the DH system.

The implementation of the minimum network temperature required by the buildings (no refurbished building), enables a reduction of 32% of the network loss. This is possible because both heat exchangers and radiators are usually oversized, since they are usually designed for the most critical weather conditions. The complete refurbishment of the buildings leads to a negative NPV that means the DH system would be no longer profitable. The operation of the DH system with the minimum network temperature leads to a constant benefit in terms of NPV and EP, and partially compensate for the loss economic profitability deriving from the refurbishment.

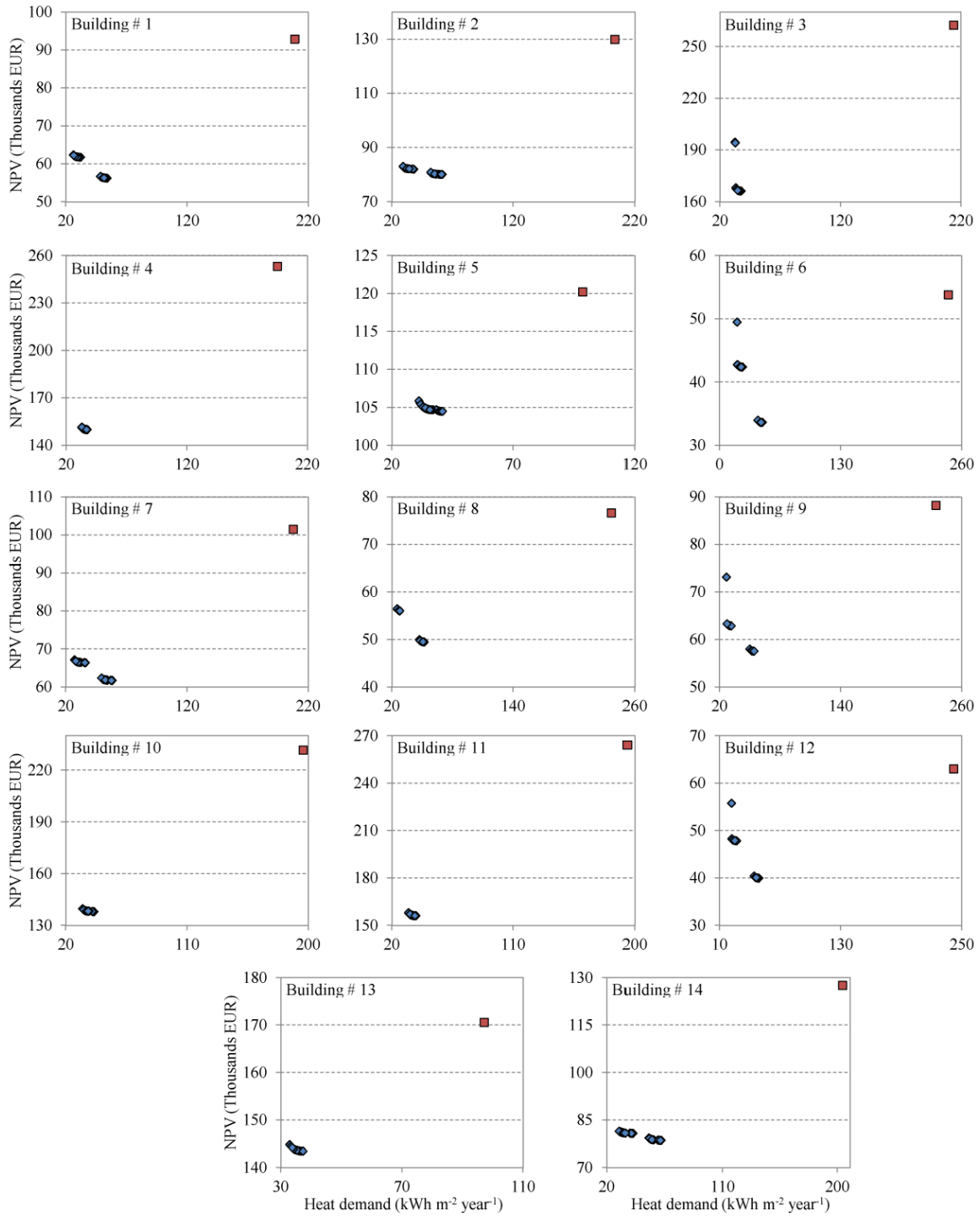
Furthermore, it has been shown that EP - and therefore NPV - are much higher for larger buildings. Nevertheless, for a high number of refurbished buildings in the district, the NPV for smaller and larger buildings is not considerably different because the revenues from heat sale are a minor share of the cash flow, which is dominated by costs of the network management.

The implementation of a CHP system allows for higher NPV mainly due to the revenue from the electricity trade. Areas with a linear heat density of 0.15 MWh (m year)⁻¹ can be supplied by DH-CHP in a cost-efficient way.

References

- AEEGSI (Italian Regulatory Authority for Electricity, Gas and Water). 2008. Approval EEN 3/08 Update of the conversion coefficient from kWh to tons of oil equivalent related to the mechanism of the energy efficiency.
- AEEGSI (Italian Regulatory Authority for Electricity, Gas and Water). 2013. Annual report on the state of services and regulatory activities. Milan (Italy).
- Autonomous Province of Bolzano. 2014. Energy service of the Autonomous Province of Bolzano (In Italian: Ufficio Risparmio Energetico Provincia di Bolzano).
- Brand, M., A. Dalla Rosa, P.S. Svendsen. 2010. *Performance of Low-Temperature District Heating Systems for Low-Energy Houses*. In: The Future for Sustainable Built Environments with High-Performance Energy Systems Conference. Munich - Germany.
- Brand, M., S., Svendsen. 2013. Renewable-based low-temperature district heating for existing buildings in various stages of refurbishment. *Energy* 62:311–319.
- CEN 2003. EN 12831: Heating system in buildings - Method for calculation of the design heat load.
- Dalla Rosa, A., J.E. Christensen. 2011. Low-energy district heating in energy-efficient building areas. *Energy* 36:6890–6899.
- European Commission. 2009. EU energy trends to 2030.
- European Commission. 2010. Directive 2010/31/EU of the European Parliament and of the Council of 19 May 2010 on the energy performance of buildings (recast).
- European Commission. 2012. Commission delegated regulation (EU) No 244/2012 of 16 January 2012.
- Haupt, R.L., S.E. Haupt. 2004. *Practical Genetic Algorithm*, II. ed. John Wiley & Sons, Hoboken - New Jersey.
- Holland, J.H. 1975. *Adaptation in natural and artificial systems*. University of Michigan Press, Ann Arbor.
- IRE (Institute for the Economic Research). 2014. Price list of the Chamber of Commerce of Bolzano Available at: www.camcom.bz.it/19338.pdf [Accessed: 04 May 2014].
- ISTAT (The National Institute of Statistics). 2001. 14° Building and population census. Available at: <http://dawinci.istat.it/MD/> [Accessed: 04 May 2014].
- KWB (Kraft und Wärme aus Biomasse). 2014. Available at: www.kwb-heating.co.uk/fileadmin/media/%C3%96sterreich/Downloads/Technik_Planung/TP_Powerfire_2014_EN_Low.pdf [Accessed: 02 December 2014].
- Li, H., S. Svendsen. 2012. “Energy and exergy analysis of low temperature district heating network”. *Energy* 45: 237–246.
- Nielsen, S., B. Möller. 2013. GIS based analysis of future district heating potential in Denmark. *Energy* 57:458–468.
- Penna P., A. Prada, F. Cappelletti, A. Gasparella. 2014. Multi-Objectives optimization of Energy Saving Measures in existing buildings. *Energy and Buildings*, Article in press DOI: 10.1016/j.enbuild.2014.11.003.
- Prando, D., F. Patuzzi, G. Pernigotto, A. Gasparella, M. Baratieri. 2014a. “Biomass gasification systems for residential application: An integrated simulation approach”. *Applied Thermal Engineering* 71(1): 152–160.
- Prando, D., A. Prada, F. Ochs, A. Gasparella, M. Baratieri. 2014b. “Enhanced performance buildings connected to district heating systems: multi-objective optimization analysis”. In *3rd International High Performance Buildings Conference*. Purdue (US), pp. 3525(1–10).
- Prando, D., M. Renzi, A. Gasparella, M. Baratieri. 2015. “Monitoring of the energy performance of a district heating CHP plant based on biomass boiler and ORC generator”. *Applied Thermal Engineering* 79: 98–107.
- Reidh, C., S. Werner. 2008. “Profitability of sparse district heating”. *Applied Energy* 85: 867–877.
- Viessmann. 2014. *Boiler fed by lignocellulosic biomass*. Bressanone: Viessmann Engineering.
- Zinko H., B. Bøhm, H. Kristjansson, U. Ottosson, M. Rama, K. Sipilä. *District heating distribution in areas with low heat demand density*. International Energy Agency 2008.

Annex I – NPV and EP for the reference case (red dots) and the cost-optimal configurations (blue dots) of the buildings for the scenario with constant heat price.



Experimental characterization of the dynamic thermal properties of opaque elements under dynamic periodic solicitation

Giovanni Pernigotto – University of Padova, Vicenza, Italy – pernigotto@gest.unipd.it

Alessandro Prada – Free University of Bozen-Bolzano, Bolzano, Italy – alessandro.prada@unibz.it

Francesco Patuzzi – Free University of Bozen-Bolzano, Bolzano, Italy – francesco.patuzzi@unibz.it

Marco Baratieri – Free University of Bozen-Bolzano, Bolzano, Italy – marco.baratieri@unibz.it

Andrea Gasparella – Free University of Bozen-Bolzano, Bolzano, Italy – andrea.gasparella@unibz.it

Abstract

A modified hotbox facility has been used at the Free University of Bozen-Bolzano to measure heat fluxes under a periodic pulse solicitation for some timber structures with different number and kind of layers. The simplest one – a single layer timber structure, has also been modelled with ANSYS Fluent® and the results compared to the experimental data for validation. Then, the numerical model has been used to study different forcing signals and boundary conditions. In order to characterize the response to a periodic dynamic solicitation with simple indexes, the EN ISO 13786:2007 (CEN, 2007) dynamic parameters have also been calculated.

1. Introduction

The increasing use of building energy simulations, *BES*, is bringing new solutions, aimed at exploiting the dynamic behaviour of the building envelope in order to improve its energy efficiency and the occupants' comfort. However, some hypotheses adopted in *BES* for the modelling of the elements of the opaque components (e.g., homogeneous layer with constant and isotropic thermal conductivity) can be very inaccurate for some kind of walls, such as those with air gaps or innovative materials. In this perspective, experimental methods can be the most effective approach to characterize dynamic thermal behaviour and to quantify it by means of simple parameters, such as periodic thermal transmittance, decrement factor and time shift defined by EN ISO 13786:2007.

While technical standards, such as EN 1934:1998 (CEN, 1998) and the literature (Asdrubali and Baldinelli, 2011) can provide instructions and examples about the measurement of the steady state heat transfer properties, there are no established references for the evaluation of wall dynamic behaviour by means of experimental laboratory tests.

In order to measure time shift and decrement factor, Ulgen (2002) built a simulation unit consisting of two volumes separated by the wall specimen: in the first one, adiabatic boundaries and no heat generation were realized while in the other one a sinusoidal temperature signal was generated. Sala *et al.* (2008) modified a calibrated guarded hotbox unit to measure the dynamic thermal properties of insulated brick walls. They used a triangular solicitation of 10°C amplitude and a 2 h period as forcing temperature. Moreover, they compared the results also with finite volume simulation. From the experimental output of the same apparatus, Martín *et al.* (2010) calculated also wall response factors without any measurement of the material properties. By means of an adiabatic hotbox apparatus, Yesilata and Turgut (2007) compared effective thermal transmittances of both isotropic (e.g., ordinary concrete) and anisotropic building materials (e.g., rubberized concrete). More recently, Sun *et al.* (2013) and Ferrari and Zanotto (2013) measured the time shift and the decrement factor in laboratory by artificially reconstructing the profiles of external air temperature.

Despite the number of examples, no standard procedure is given. Moreover, a detailed evaluation of error propagation in modified hotbox apparatus is

still missing, especially regarding the boundary conditions to which the wall specimen is exposed during a dynamic test. If the aim of the test rig is to measure EN ISO 13786:2007 dynamic parameters, then the standard also provides the boundary conditions to apply – constant temperature on one side and sinusoidal forcing temperature on the other one. However, it could be challenging to keep the air temperature constant and to realize a sinusoidal forcing signal in practice. As explained by Prada *et al.* (2013), the encountered difficulties in designing a modified hotbox for dynamic tests brought to choose a different kind of forcing signal and to use numerical techniques to extract the first harmonic (i.e., the part of the output signal originated by a sinusoidal input signal) from the whole measured heat flux. In this research, with the support of finite volume simulation models calibrated with experimental results, we discussed the effectiveness of the implemented experimental procedure and we analysed the main sources of errors due the imposed boundary conditions.

2. Experimental and numerical methods

2.1 Hotbox apparatus description

The hotbox apparatus at the Free University of Bozen-Bolzano was designed according to EN 1934:1998 to perform steady state tests and consists of two insulated boxes (170 cm of height/width and 110 cm of length) made by aluminium plates filled with 10 cm of polyurethane insulation. The square specimen (with a side of 150 cm) is positioned to complete the open side of the two boxes.

In each box, a black screen (thickness 1.5 cm) separates the inner zone from the air gap zone of 3.9 cm adjacent to the test wall. In this way, heat exchange by radiation between the hotbox internal surfaces and the specimen is prevented. Moreover, a cylindrical horizontal fan generates a regular-shaped airflow stream in the air gap, flowing from the bottom to the top of the sample surface and reducing issues of vertical air temperature stratification. Each box is equipped with a cooling unit (an evaporator) and a heating unit (an electrical resistance), which are controlled by a PID regulation unit, tuned up to

keep an internal constant temperature in a range of $\pm 0.1^\circ\text{C}$ with respect to the setpoint temperature in steady state test. For the measurement of the wall thermal conductance in steady state tests, both chambers are kept at constant temperatures (generally 20°C and -10°C , respectively). The thermal flux is measured on a central square section (50 cm by 50 cm).

For dynamic tests, the configuration is modified and only one chamber is used, to maintain steady state conditions on one side of the specimen (i.e., the internal side). In order to impose the forcing temperature signal on the other side (i.e., the external side), a copper coil electrical heater of around 120×120 cm is positioned very close to the wall surface. This allows us to minimize air buoyancy effects, which could cause temperature gradients between the bottom and the top parts. The electrical heater can generate a nominal thermal power of 1500 W.

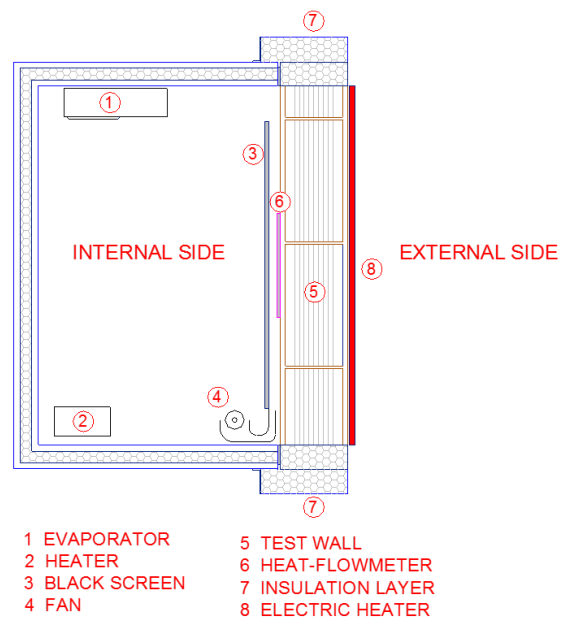


Fig. 1 – Modified hotbox apparatus.

As in the steady state tests, the heat flow variations on the internal side of the component are measured with a heat flow meter, *HFM*, namely a thermopile made of 250 type T thermocouples on an area of 50×50 cm. It consists of a layer of rubber of 1.05 cm between two layers of aluminum (thickness 0.1 cm), for a total mass of 2.3 kg. According to the calibration certificate, *HFM* thermal conductivity is

0.1905 W m⁻¹ K⁻¹. A guard ring with similar thermal resistance surrounds the *HFM*. 8 and 4 type T thermocouples measure, respectively, the temperature of the wall surface in touch with the guard ring and that in touch with the *HFM*. On the external side, 12 thermocouples are placed in the same positions, 1 mm under the external surface of the specimen, in order to avoid the influence of direct irradiation due to the electrical heater.

2.2 Experimental procedure for the evaluation of dynamic parameters

During the dynamic tests, the internal side temperature is held at a constant value: specifically, for this work, a setpoint of 23°C was considered in order to minimize the heat exchanges with the environment. The airflow rate was set to 1.5 m s⁻¹ and the relative humidity was not controlled. A dynamic test starts once steady state conditions are realized and this requires, typically, 24 h. Then, the external side is exposed to cycles of thermal irradiation of 1500 W for 2 h followed by 22 h of rest. A test can require repeating the cycles of forcing irradiation for two weeks (e.g., 14 times), depending on the kind of examined walls. This is necessary both for the minimization of the influence of the initial conditions and for the achievement of steady periodic conditions. For the specimen analysed in the present research, 10 days were sufficient. In particular, the transient effects were negligible after a couple of days but usually 3 or 4 days are required. Once the steady periodic state is reached – i.e., when the amplitude of the thermal flux is constant between two periods – the heat flux on the internal side and the external surface temperatures is recorded.

The Fast Fourier Transform (*FFT*) algorithm (Press *et al.*, 2007) is applied, computing the first 720 harmonics of experimental temperature and heat flux per each day of recorded series. The first term of the Fourier approximation is then used to compute the periodic thermal transmittance and the time shift according to EN ISO 13786:2007. Actually, since surface heat fluxes and temperatures are directly measured and used in calculations, the surface resistances are neglected and, thus, the estimated quantity is a periodic thermal transmittance without

the effects of surface resistances.

The periodic thermal transmittance Y_{ie} is computed as the ratio between the amplitude of the first harmonic of the internal heat flux $\phi_{i,1}$ and the amplitude of the first harmonic of the external surface temperature $\theta_{e,1}$.

$$Y_{ie} = \frac{\phi_{i,1}}{\theta_{e,1}} \quad (1)$$

The time shift Δt_{ie} is calculated using the phase displacements (respectively, φ and ψ) of the first harmonics.

$$\theta_e \approx \bar{\theta}_e + \theta_{e,1} \cos(\omega t + \varphi) \quad (2)$$

$$\phi_i \approx \bar{\phi}_i + \phi_{i,1} \cos(\omega t + \psi) \quad (3)$$

$$\Delta t_{ie} = \frac{\psi - \varphi}{\omega} = \frac{\psi - \varphi}{2\pi} \times 24 [h] \quad (4)$$

Y_{ie} and Δt_{ie} are determined for each day of the series of recorded data after the periodic steady state condition is reached. From the sample of daily dynamic parameters, mean values and standard deviations are calculated and presented.

2.3 Experimental specimens

Some timber walls have been tested according to the described procedure. For example, in a previous work (Prada *et al.*, 2013) the dynamic performance of two platform frame timber walls were presented. The two specimens were first tested according to EN 1934:1998 in order to determine their thermal conductance C_s and then according to the proposed procedure to estimate periodic thermal transmittance and time shift (specimens 1 and 2 in Tab. 1). However, the considered walls were too complex to analyze the inaccuracy introduced by the boundary conditions, because of the uncertainty of the material properties of many different layers. For this reason, we selected a new specimen (3 in Tab. 1): a single-layer wall of massive timber with a thickness of 24 cm. Also in this case the thermal properties were unknown. Nonetheless, being the specimen composed by a single material, it was possible to perform more efficiently a numerical model calibration from experimental measures.

Table 1 – Experimental analysis of the previous (1 and 2) and current (3) specimens.

Wall	C_s [W m ⁻² K ⁻¹]	Y_{ie} [W m ⁻² K ⁻¹]	Δt_{ie} [h]
1	0.172	0.031	9.18
2	0.240	0.101	6.73
3	0.475	0.130	11.64

As it can be seen, both thermal conductance and periodic thermal transmittance of specimen 3 are larger than those of 1 and 2. It means that this wall can be more susceptible to the choice of the forcing signal and to the generated external surface periodic temperature, making it more suitable for the purpose of our analysis.

2.4 Numerical simulation models

2.4.1 Definition and calibration of the numerical model

A numerical model has been defined and calibrated, considering both a proper abstraction level and the characterization of the unknown material properties. The outcome of this first part was a numerical model able to simulate the specimen behavior in the modified hotbox apparatus and under the test conditions. Since the final aim of the dynamic test rig is to measure EN ISO 13786:2007 dynamic parameters, the values shown in Tab. 1 were considered as calibration targets, with an acceptable tolerance of approx. 5 %. Moreover, since the measurement approach relies on *FFT* calculations on the monitored heat flux, the first harmonic signals from numerical results were calculated as well and compared to the experimental ones.

As regards the numerical aspects, ANSYS Fluent® finite volume approach with conjugated heat transfer modelling between solid and fluid regions was chosen. For the flow model, since the fan operates at constant velocity and there is low turbulence in the air gap adjacent to the specimen, Fluent DNS was used. The radiative heat exchange was calculated by means of the surface-to-surface model. Some preliminary tests were performed in order to balance numerical errors and computational costs, optimizing meshing, time-discretization and convergence criteria. In the final model, the mesh has more than 21000 quadrilateral cells and the

transient problem is solved considering a time-discretization of 60 s, which is the same time between two consecutive measurements in the experiments. A convergence criterion of $\mathcal{E} = 10^{-8}$ was adopted and the simulations were run with double precision solver.

2.4.2 Geometric modelling and boundary conditions

As far as the simplification level is concerned, we adopted a 2D approach: indeed, the hotbox facility is well insulated and the heat flows through the lateral walls of the specimen, including its surrounding 20 cm of EPS and the additional 10 cm of sheep wool, are negligible. Similarly, the same is true for the heat flows through the bottom and the top wall surfaces and this allowed us to impose adiabatic boundary conditions.

In order to delimit the thermo-dynamic system, we focused on the specimen and on its adjacent zones. We defined the external wall surface exposed to the electrical heater as a solid domain boundary and used the measured surface average temperature as boundary condition. Considering the vertical length of the domain, we chose to have the same length of the heater (i.e., 120 cm). On the top and the bottom of the heater, as well as on the lateral sides, the surface temperature is slightly different from the average value because of border effects. Nonetheless, since our aim is to compare the heat flux where the *HFM* is installed (i.e., centered with respect to the electrical heater), the introduced inaccuracy is expected to be negligible. On the internal side, the air gap between the black screen and the specimen was included in the numerical model as a fluid domain and the measured temperature of the incoming air used as input. The inlet boundary was modelled as a velocity inlet while the outlet boundary as an outflow condition. The border effects were not included in the model but they are supposed to have low impact on the measurement area, whose lower and upper sides are 36 cm far from air inlet and outlet, respectively. The black screen was included as solid domain in order to account for the radiative exchanges on the internal side of the specimen. A boundary conditions of 23.7°C (i.e., the average measured temperature of the chamber internal air for the current experimental

campaign) was imposed on the side faced towards the rest of the chamber and adiabatic conditions were set on top and bottom surfaces.

In the experimental setup, the internal side of the specimen is not directly exposed to the air gap because of the *HFM* and its guard ring. We performed some preliminary tests without modelling *HFM* and guard ring but the numerical heat flow resulted influenced by the instability of air gap temperature more than it was actually in the experimental data. This suggested that *HFM* disturbs the measurement in such a way to require its modelling, together with the guard ring. Perfect contact (i.e., no contact resistance) was assumed between guard ring and *HFM* and between the two of them and the internal side of the specimen. Adiabaticity was imposed to top and bottom surfaces of the guard ring, coherently with the assumptions for both specimen and black screen.

2.4.3 Material properties

Some material properties were unknown but only those that have a significant impact on the dynamic parameters of the specimen were considered for calibration.

The black screen is in plywood and the same first-run properties of the specimen were assumed, together with a unitary surface emissivity. However, since the difference between the boundary temperature and the average air gap temperature is around 0.4°C and the black screen temperature is very stable during the simulation, no further in-depth analysis was performed. Indeed, the introduced error affects the mean value of the heat flux and not its shape and, thus, not the dynamic parameters, which are the actual calibration target. For the *HFM*, the data from its calibration certificate were used to estimate the material properties: thermal conductivities of 202 W m⁻¹ K⁻¹ and 0.16 W m⁻¹ K⁻¹, specific heat capacities of 871 J kg⁻¹ K⁻¹ and 840 J kg⁻¹ K⁻¹ and densities of 2719 kg m⁻³ and 360 kg m⁻³ were used, respectively, for aluminum and rubber layers. For the guard ring, the same thermal conductivity of the *HFM* was used. Density and specific heat capacity were unknown and values of 1000 kg m⁻³ and 840 J kg⁻¹ K⁻¹ were considered for the first-runs. We observed that the penetration depths of the harmonics of the forcing solicitation were

clearly influenced but this affected marginally the measurement area. Consequently, we decided to concentrate our calibration efforts on the specimen and to consider a more accurate characterization of the guard ring in the future developments. For all surfaces exposed to the air gap an emissivity of 0.9 was assumed.

As far as the specimen is concerned, we used constant properties, as done for the other solid domains. This assumption can introduce some discrepancies because the temperature in some regions of the domain ranges from 20°C to 50°C. From the experimental thermal conductance (Tab. 1), a thermal conductivity of 0.114 W m⁻¹ K⁻¹ was determined. Further developments are likely to include thermo-physical properties function of the temperature, using the measurements from other experimental devices (e.g., laser flash, LFA, tests for thermal diffusivity). Once defined the thermal conductivity, the specific heat capacity and the density were varied in ranges admissible for timber structures, i.e., respectively, from 1000 to 2000 J kg⁻¹ K⁻¹ and from 300 to 400 kg m⁻³, starting from the lower values. Specimen material properties compatible with our targets were found to be a thermal conductivity of 0.114 W m⁻¹ K⁻¹, a specific heat capacity of 2000 J kg⁻¹ K⁻¹ and a density of 300 kg m⁻³.

2.4.4 Simulated cases

First, we focused on the actual shape and on the errors in the repetition of the forcing signal (i.e., in realizing each day the same forcing condition). For this reason, we performed two simulations: in case (a) the series of daily first harmonic of the external surface temperature as forcing signal are considered; in case (b) a single average sinusoidal temperature perfectly repeated for ten days is imposed. In order to investigate the effect of actual instable internal air temperature, the same cases were run again considering constant internal conditions: specifically, case (c) has the same external surface temperature of case (a) and case (d) the same single average sinusoidal of case (b).

The second part of our analysis was dedicated to the numerical assessment of the role of the shape of the forcing signal, validating the findings of the first part. Two new forcing surface temperatures were

considered: a square (1) and a triangle wave (2) built from the same average sinusoidal applied in cases (b) and (d) (Fig. 2). As a whole, considering both actual and constant internal air temperature conditions - respectively, groups (b) and (d), four new cases were simulated and discussed.

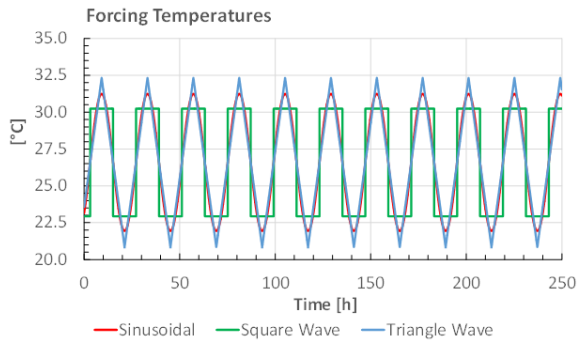


Fig. 2 – Sinusoidal, square and triangle external surface forcing temperatures.

3. Results and discussion

3.1 Calibrated numerical model

Measured and numerical heat fluxes have different average values ($\Delta\phi \approx 1 \text{ W m}^{-2}$) but similar shapes (i.e., very close amplitudes and small differences between phases). For example, this can be seen for the days IV and V of the data series in Fig. 3, where the measured heat flux, both the original signal and the one processed with a second order Butterworth low-pass filter, is represented on the left vertical axis and the numerical heat flux on a right vertical axis that is shifted of 1 W m^{-2} with respect to the left one. The first harmonics from *FFT* analysis confirm the findings from the comparison of the whole heat fluxes: regarding the amplitude, the average deviation from the 3rd to the 10th day (i.e., in periodic steady conditions) is 0.01 W m^{-2} (i.e., 2 %) while for the phase the average deviation is 0.19 rad (i.e., 2.8 %). The numerical average Y_{ie} and Δt_{ie} , are $0.133 \pm 0.10 \text{ W m}^{-2} \text{ K}^{-1}$ and $10.97 \pm 0.54 \text{ h}$ – very close to the experimental ones (respectively, $0.130 \pm 0.07 \text{ W m}^{-2} \text{ K}^{-1}$ and $11.64 \pm 0.29 \text{ h}$).

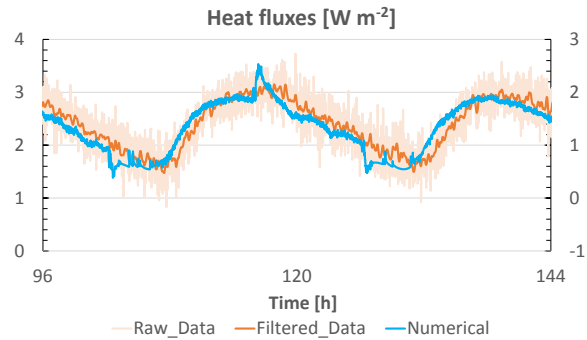


Fig. 3 – Overlapped experimental and numerical heat fluxes for day IV and V. Experimental raw and filtered data are represented on the left axis and the numerical data on the shifted right axis.

With the considered material properties, the analytical values of Y_{ie} and Δt_{ie} are $0.153 \text{ W m}^{-2} \text{ K}^{-1}$ and 9.89 h . This means that experimental and numerical periodic thermal transmittance are -15% and -13% lower and time shifts are +18% and +11% higher than the corresponding analytical values. Since both experimental and numerical approaches lead to similar results, some other elements and errors besides material uncertainty influence the accuracy of the experimental procedure adopted for the evaluation of EN ISO 13786:2007 wall dynamic parameters.

3.2 Analysis of the boundary conditions

According to the theoretical conditions prescribed by EN ISO 13786:2007, we should keep a constant temperature on the internal side and a sinusoidal forcing signal on the external side of the specimen. Regarding the internal side, we observed that when the experimental apparatus is modified to perform dynamic tests, its control system is still not optimized to keep a constant internal temperature. For the current test, the average air gap temperature is $23.3 \pm 0.1^\circ\text{C}$ but, as shown in the graph on the top of Fig. 4, there are peaks and minimums as an effect of the hotbox heating and cooling units turning on and off. On the other hand, the operating cycles of the electrical heater realize an external surface temperature far from being sinusoidal. Moreover, no pair of consecutive days has exactly the same forcing signal because of the variations of the lab air temperature. This means that boundary conditions do not perfectly comply with those of a periodic steady state regime. However, as it can be seen in the bottom graph of Fig. 4, the series of the daily first harmonics of the external surface temperature are very close to the sinusoidal function developed from

their average phase and amplitude. Analysing the daily first harmonics of the heat flux from day III to X, we can see differences from one day to another both in experimental and calibrated models (Fig. 5).

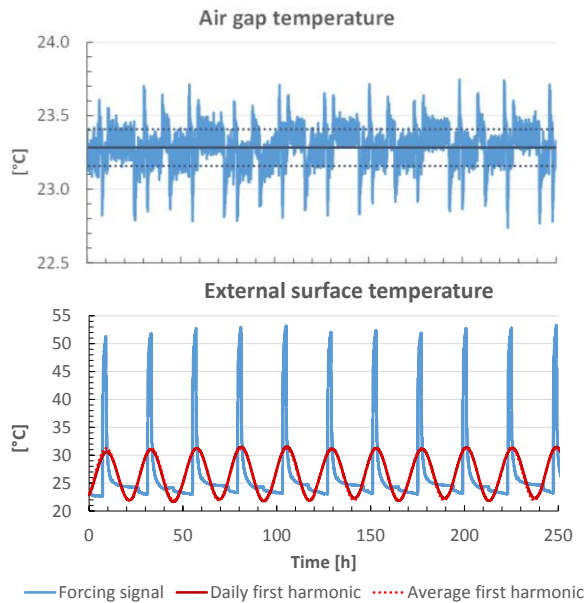


Fig. 4 – Air gap temperature and external surface temperatures from day I to X.

In numerical case (a), applying the series of first harmonics instead of the external surface temperature, the differences between the days decrease but, even using the same sinusoidal signal repeated 10 times in case (b), they do not disappear (Fig. 5). In case (c), differently from case (a), a constant internal air temperature is set and some improvements can be found. Finally, in case (d), which respects the conditions prescribed by the theoretical method, each period has exactly the same first harmonic signal of the monitored heat flux. That suggests that not only the shape and the errors in the replication of the external surface temperature affect the monitored heat flux and the outcome of *FFT* analysis but also the non-constant internal conditions.

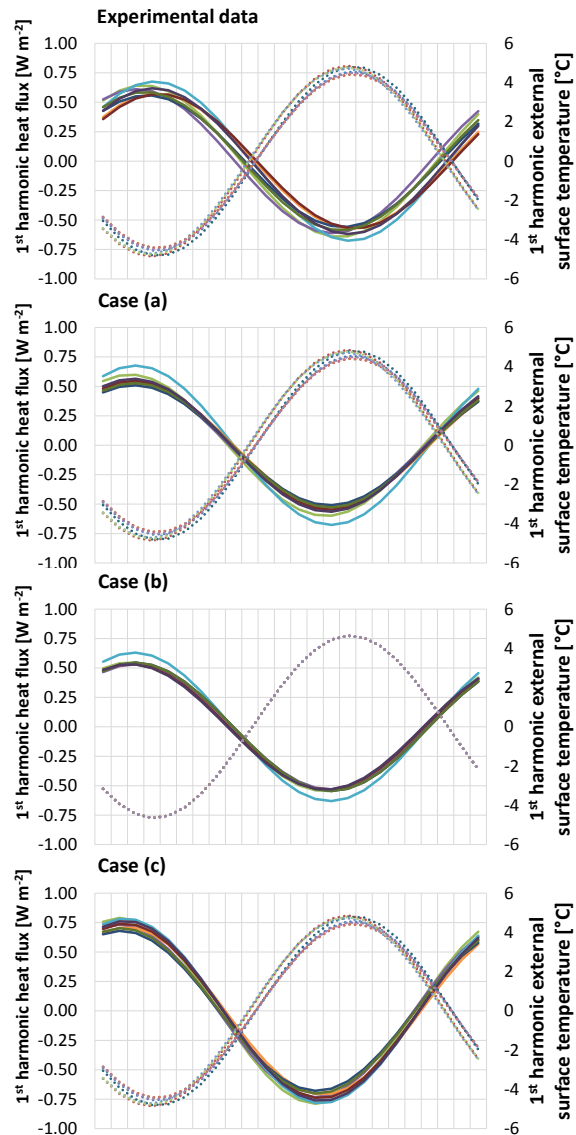


Fig. 5 – First harmonics from day III to X of the heat flux (solid lines, left axis) and of the external surface temperature (dotted lines, right axis) for experimental data, cases (a), (b) and (c).

Calculating the dynamic parameters for cases (a) and (b), we got very close values, with slightly larger standard deviations for case (a) (Tab. 2). For both configurations, Y_{ie} and Δt_{ie} decrease of about 10 % and 3 %, respectively, compared to the calibrated model. Also cases (c) and (d) are close to each other but both are also very close to the EN ISO 13786:2007 analytical solution: indeed, for Y_{ie} the deviation is, respectively, +4 % and +2 % while for Δt_{ie} it is around -1.5 %. Comparing cases (c) and (d) to (a) and (b), the presence of non-stable internal conditions is confirmed to affect the calculated dynamic parameters dramatically, much more than applying non-sinusoidal forcing temperatures to the external

side. Furthermore, the good agreement between the case (d) and EN ISO 13786:2007 analytical solution underlines the numerical model robustness and its adequacy for further in-depth analyses with different forcing signals.

Table 2 – Dynamic parameters for numerical cases (a), (b), (c) and (d).

Case	Y_e [W m ⁻² K ⁻¹]	$\Delta(Y_{ie})$ [W m ⁻² K ⁻¹]	Δt_{ie} [h]	$\Delta(\Delta t_{ie})$ [h]
(a)	0.121	0.011	10.67	0.23
(b)	0.118	0.007	10.66	0.14
(c)	0.159	0.001	10.05	0.14
(d)	0.156	0.000	10.03	0.02

3.3 Assessment of different forcing temperatures

As showed in Fig. 6, sinusoidal, square and triangle external surface temperatures originate very similar heat fluxes. In particular, for the cases of group (d) all heat fluxes are almost sinusoidal with small differences in phase and amplitude. The wall filters the transmission of almost all harmonics with frequencies higher than that of the first one and this makes small differences between the heat fluxes by different forcing signals built starting from the same first harmonic.

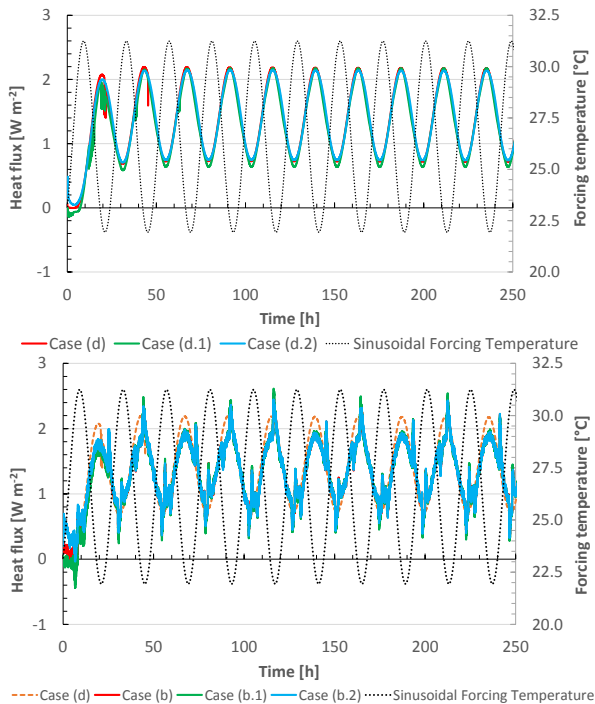


Fig. 6 – Heat fluxes for cases (b), (b.1), (b.2), (d), (d.1) and (d.2).

Comparing group (b) to (d), it can be observed that the internal conditions significantly altered the shape of the heat flux: in particular, neglecting the perturbation due to the air-conditioning units, the amplitude results lower. Mapping amplitude and phase of the first harmonic of the heat flux from days III to X (Fig. 7), we can see different behaviors. Concerning the experimental data and calibrated model, we have variability of around 0.1 W m⁻² and 0.15 W m⁻² for the amplitude and 0.35 rad and 0.25 rad for the phase. In cases (b), a periodic forcing signal is adopted and the variability is lowered to 0.1 rad for the phase and small changes are detected for the amplitude. In cases (d), every day the first harmonic of the flux has almost the same amplitude and phase: residual errors are indeed due to numerical model and FFT errors. The three different forcing solicitations realized fluxes with differences very small if compared to previous cases. For example, the triangle wave temperature induced a heat flux whose first harmonic has slightly lower phase and amplitude with respect to the other cases.

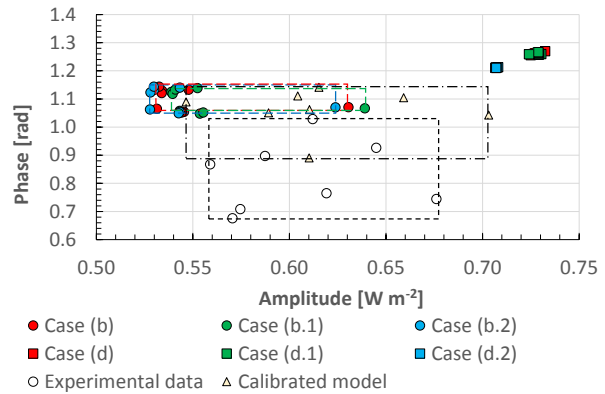


Fig. 7 – Phase and amplitude of the heat fluxes for cases (b), (b.1), (b.2), (d), (d.1) and (d.2) for days from III to X.

Table 3 – Dynamic parameters for numerical cases (b.1), (b.2), (d.1) and (d.2).

Case	Y_e [W m ⁻² K ⁻¹]	$\Delta(Y_{ie})$ [W m ⁻² K ⁻¹]	Δt_{ie} [h]	$\Delta(\Delta t_{ie})$ [h]
(b.1)	0.120	0.007	10.67	0.14
(b.2)	0.117	0.006	10.66	0.15
(d.1)	0.157	0.000	10.02	0.01
(d.2)	0.152	0.000	10.22	0.00

Considering EN ISO 13786:2007 dynamic parameters, changing the forcing signal has not

remarkable effects: indeed, cases (b.1) and (b.2) have periodic thermal transmittances and time shifts within ± 2 % with respect to case (b) results and cases (d.1) and (d.2) have dynamic parameters within ± 3 % with respect to case (d) ones.

4. Conclusion

In this work, we exploited a numerical ANSYS Fluent® model to simulate the dynamic behavior of a single layer timber wall during a dynamic test with the modified hotbox apparatus at the Free University of Bozen-Bolzano for the experimental evaluation of EN ISO 13786:2007 dynamic parameters. Once the numerical model was calibrated with experimental results, we focused on the boundary conditions applied to the specimen, considering both actual and constant internal air temperatures and different external surface forcing solicitations. We found that different forcing temperature profiles have little and acceptable effects on the estimation of the dynamic parameter according to the proposed experimental procedure (i.e., we can use non-sinusoidal periodic forcing signals). On the contrary, large sensitivity was registered to the internal conditions, which can affect the final output more than expected. These findings will be used as drivers for the next upgrade of the modified hotbox apparatus in order to improve the accuracy of the experimental results. Further steps of this work will focus on the heat flow meter *HFM* in order to characterize not only the noises that *HFM* introduces but also its response in transient conditions.

5. Acknowledgement

The research leading to these results has received funding from the European Union (FESR 2007-2013) in the framework of the programme “Competitività regionale ed occupazionale” of the Autonomous Province of South Tyrol.

References

- Asdrubali, F., Baldinelli, G., 2011, Thermal Transmittance measurements with the hot box method: Calibration, experimental procedures, and uncertainty analyses of three different approaches. *Energy & Buildings*, 43: 1618-1626
- CEN, 1998, EN 1934:1998 - Thermal performance of buildings - Determination of thermal resistance by hot box method using heat flow meter
- CEN, 2007, EN ISO 13786:2007 - Thermal performance of building components - Dynamic thermal characteristics - Calculation methods.
- Ferrari, S., Zanotto, V., 2013, The thermal performance of walls under actual service conditions: Evaluating the results of climatic chamber tests. *Construction and Building Materials*, 43: 309-316
- Martín, K., Flores, I., Escudero, C., Apaolaza, A., Sala, J.M., 2010, Methodology for the calculation of response factors through experimental tests and validation with simulation. *Energy & Buildings*, 42: 461-467
- Prada, A., Gigli, D.S., Gasparella, A., Baratieri, M., 2013, Energy simulation and design of a hot box suitable for dynamic tests of building envelope components. *Proc. Of BSA 2013 - 1st IBPSA-Italy conference*, Bolzano, Italy, 2013
- Press, W.H., Teukolsky, S.A., Vetterling, W.T., Flannery, B.P., 2007, Numerical Recipes 3rd Edition: The Art of Scientific Computing, Cambridge University Press, Cambridge (U.K.)
- Sala, J.M., Urresti, A., Martín, K, Flores, I., Apaolaza, A., 2008, Static and dynamic thermal characterisation of a hollow brick wall: Tests and numerical analysis. *Energy & Buildings*, 40
- Sun, C., Shu, D., Ding, G., Zhang, X., Hun, X., 2013, Investigation of time lags and decrement factors for different building outside temperatures. *Energy & Buildings*, 61: 1-7
- Ulgen, K., 2002, Experimental and theoretical investigation of effects of wall's thermophysical properties on time lag and decrement factor. *Energy & Buildings*, 34: 273-278
- Yesilata, B., Turgut, P., 2007, A simple dynamic measurement technique for comparing thermal insulation performances of anisotropic building materials. *Energy & Buildings*, 39: 1027-1034

Re-thinking of energy consumption classification by the patterns of occupant behaviour in dwellings: a conceptual framework

Gülsu Ulukavak Harputlugil – Çankaya University Architecture – gharputlugil@cankaya.edu.tr

Timuçin Harputlugil – Çankaya University Architecture – tharputlugil@cankaya.edu.tr

Abstract

The aim of this paper is to present the conceptual framework of a TÜBİTAK funded project titled “*Developing a New Methodology to Improve Housing Quality in Turkey Based on Effects of Occupant Behavior on Energy and Comfort of the Dwellings*”. Although the objective of the project is the development of new methodologies and tools to be used for the definition of effects of behavior profiles of housing occupants on the energy consumption and usage of this knowledge for building new houses and renovation of existing buildings, here the first step of research has been executed. By defining sensitivity of occupant behavior on energy consumption, it is planned to classify different models of occupant behavior. With data provided, the aim is to develop an “occupant behavior labeling” which rates occupants instead of buildings. To provide the mentioned data, sensitivity analysis of existing occupant behavior will be analysed based on the Monte Carlo Methodology. This methodology is one of the most used methodologies to analyse accurate distribution of possible outputs relied on inputs based on probability. Inputs for this research are (1) number of occupants for each space (for weekdays and weekend) (2) behaviour for ventilation (Window open/closed and mechanical ventilation on/off) (3) control of heating systems (radiator on/off and/or thermostat degree). These data will be provided with survey and data logging of chosen a house occupant group.

As a consequence of the research, the aim is not only to rate the behavior of housing occupants but also determine occupancy groups/labels. With this approach, based on occupant’s behavior labeling, the aim is to realize fast and affective applications for renovation of existing buildings. Moreover, by evaluation/assessment of houses which will be designed in the future based on determined occupant profiles allow to produce high performance dwellings.

1. Introduction

Basically, there are two main issues associated with the world’s energy consumption and related political decisions. Firstly, there is a significant decrease in energy sources due to common consumption manners. The second issue is the interaction of fossil-based energy sources with the natural environment. The greenhouse gas emissions caused by the consumption of fossil-based energy sources have a high rate of negative effect on human and nature. Nowadays, it is accepted that economic development would not be possible without accomplishing environmental measures. Regarding the various sectors that consume energy in the developed countries, the building sector is the third highest one following industry and transportation. The indicators showed and the related research revealed that it is essential to make all the stakeholders of the building sector aware of the situation. Reducing environmental impact at the maximum level shall only be possible by fulfilment of their responsibilities within the whole building process beginning from planning and design to construction, usage and renovation. This is not only a requirement for the new constructions but also more essential for renovation of current building stock. As common sense, the sustainable measures are the subject of the design process of new buildings; however, it is obvious that the total environmental impact of the current building stock is huge enough to be considered primarily.

Within the continuous global effort to make the built environment more energy efficient, there is an increasing interest in the role of occupants on building energy use. For instance, the International Energy Agency has recently (late 2013) launched Annex 66 on Definition and Simulation of Occupant

Behavior in Buildings (www.annex66.org). Occupants make a passive contribution to the building energy balance by their very presence; they also can have an active role through activities like opening windows, changing thermostat set points etc. Furthermore, in existing buildings, occupants also play a role in decisions regarding any interventions in the fabric and systems, especially where occupants own the building.

TÜBİTAK funded research started in August 2014, and it will take about 2 years. The main focus of this research is proposing a new perspective to current understanding of occupant effectiveness on energy consumption of the dwellings.

In this paper, only the conceptual frame of the research is introduced, the methodology is discussed and expected outcomes are listed.

2. Literature Review

The literature review on sustainable renovation process has been done based on two main issues. One is the clear understanding of the renovation process of the dwellings. It is not possible to suggest new approaches without a deep understanding of the current situation. Second is the effect of occupant behaviour on renovation process. The main difference between the design process and renovation process of a dwelling is the “real” occupants. During design process, designers usually make assumptions about the behaviours of the occupant. This is acceptable since most of the designs are finalised without any information about the exact users. Nevertheless the renovation process is realised having the whole information about the occupants. By understanding occupant behaviour, it is possible to generate a methodology considering occupants’ perspective.

2.1 Renovation process of the dwellings

In the report of IEA (2008), there are six priorities for the renovation of housing; listed as: i) increasing the comfort of life, ii) limiting energy consumption, iii) limiting drinking water consumption, iv) increasing the water resources, v) limiting the production of waste, vi) limiting consumption territory and

resources.

Renovation is usually a way of redesigning the building, even though structural characteristics are the same and most of the components are only renewed instead of redesigned. However the process shall be defined as a redesigning process. From this point of view it is necessarily to be aware of the energy and sustainable objectives.

Hazucha (2009) stated in the report of the IEE project “PASSNET” that the building renovation should include; a) the design of appropriate insulation with the thermal characteristics of construction according to passive house recommendations, b) the thermal bridge free solution of construction details (e.g. windows, attics, roof, etc.), c) the airtight layer design with the used sealing materials, d) windows optimised (type of glazing, frame, summer shading, etc.), e) the mechanical ventilation design (appropriate ventilation system, noise and fire, protection, regulation and controlling), f) the heating system regulation and appropriate piping insulation (eventually the heat source replacing), g) energy demand calculation according to national standards and economical calculation of cost-benefits.

Thomsen and Flier (2009) searched for the answer to the question “What is better; replacement or renovation of dwellings?” from the sustainability perspective. The motivation to demolish is related to (a) physical quality of the dwellings (technical, functional) and (b) micro economic quality (market potency, return potency). They stated that the main part of the demolition in the Netherlands occurs in social housing. The literature survey done by Thomsen and van der Flier reveals that the environmental impact of life cycle extension in most cases is less than demolition and new construction, although in practice the better energy performance of new construction reduces the differences.

Kara (2010) worked on three case studies from the Dutch housing stock to reveal the life cycle assessment perspective of selection: renovate or rebuild? He emphasised in his study that in the results of two of the three cases, the new building alternative has a better environmental performance among all alternatives 50 years after the intervention. The life span of the building and related technological developments is highly

relevant to the results. Besides he stated that among the environmental categories he considered, operational energy use revealed higher contribution, compared to the contribution due to materials.

2.2 Occupant Behaviour

Energy consumption rate of any space is directly related to the presence of the occupant in that area. Assumptions that are made without the presence of an occupant would give weak results. Being present within the space is a necessary condition for being able to interact with it.

Page (2007) emphasised in his thesis that impacts of occupants' presence and behaviour on a building are; i) control of HVAC set-points, ii) production of internal metabolic heat gains and pollutants, iii) position of blinds (solar gains), iv) use of artificial lighting (associated electricity consumption and internal heat gains), v) use of windows and doors (ventilation rate and associated heat gains and losses), vi) use of appliances (associated with electricity and hot and cold water consumption, internal heat gains and production of grey and waste water).

One of the latest works on the relationship between occupant behaviour and energy consumption was done by Santin (2010). The results of the statistical analysis that she executed showed that the determinants of occupant behaviour that have an effect on energy consumption are i) type of temperature control, ii) type of mechanical ventilation, iii) household characteristics (presence of elderly, children, etc.). Based on the analysis, she figured out five behavioural factors in occupant behaviour: i) 'appliances and space' that related to more use of space and heavy appliances; ii) 'energy intensive' that related to behaviour leading to more use of energy; iii) 'ventilation' that referred to more hours of ventilation; iv) 'media' that related to behaviour seen as more use of computers and electronics, less use of space and more ventilation, v) 'temperature comfort' that related to preferences for a warmer indoor environment and less ventilation.

Occupant behaviour that affects the renovation process is also a subject of the discussion within the

literature. In the guidebook of the IEE project PASS-NET (2010), the main problems of occupant behaviours which decrease the expected energy efficiency after the first year of renovation are listed as; i) use of the natural ventilation via windows especially during the winter instead of mechanical ventilation with heat recovery, ii) too high air change rate (ventilation intensity) can cause too dry indoor air, iii) too high indoor temperature – after renovation interior surfaces of walls, windows, etc. are warmer so the room temperature can be lowered while the same thermal comfort is kept, iv) not using the radiator's valves to control the temperature – thermostatic valves can keep the set-up room temperature, v) during the summer time the shading elements are not used properly and the windows are opened during the daytime – this can lead to interior overheating and users discomfort.

In the report of ERABUILD, Itard (et al. 2008) listed key barriers of existing residential buildings. The highlighted barriers of the owner-occupied dwellings are seen as i) lack of professional advice and support, limited offers, complicated procedures; ii) lack of specific knowledge/knowledge of alternatives; iii) lack of complex decision making process.

Mlecnik (2010) stated in the report of LEHR project that i) increased space, ii) structural improvement and iii) improved comfort are more important drivers than energy saving for owner-occupants during renovation.

In the literature there are various models discussed on occupant behaviour. The most common approach is to develop stochastic models while considering occupant behaviour aspects. Page (2007) summarised the various approaches of occupant behaviour models based on presence and different usages of the components. For instance, i) occupant presence models as Lightswitch model (Newsham et al, 1995; Reinhart 2004) and statistical properties of occupancy by Wang (et al 2005); ii) occupant behaviour model of appliance use by Mc Queen (2004); iii) occupant behaviour model of window opening as either a model to simulate the changes of state during winter by Fritsch (et al., 1990) or the variable modelled the state of the window at each time step rather than the change of the state of the window by Nicol (2001).

Besides, most of these models were attempts to integrate simulation programs to gather more realistic results regarding possible calculations simultaneously the behaviour within a reasonable short time.

3. Proposed Methodology

The aim of the research is to determine occupant behaviour patterns quantitatively and to reveal robustness of occupant behaviour against energy consumption of dwellings. The results will guide the renovation process of the dwellings that considers occupants' 'real' behaviour and related effective intervention level on the building. Based on this perspective the proposed methodology includes the following steps.

3.1 Collecting information of occupants (survey)

The first step of the work includes collecting relevant information about the occupants. A survey is going to be held at the locations that TOKI (Toplu Konut İdaresi Başkanlığı – Housing Development Administration of Turkey) pointed at four different climatic regions in Turkey. The survey questions involved the basic issues listed below:

- *General information of the occupants:* the number of the people living in the dwelling, the ages and gender of each, educational levels, the hours that each of them stays at home during both weekdays and weekends.
- *Exploring physical comfort conditions (feelings) of occupants:* They are queried to rate comfort conditions at the dwelling. Based on thermal, visual and aural comfort, they are expecting to define the levels of comfort in each room at the dwelling.
- *Exploring occupant behaviour based on comfort:* Besides comfort feelings of the occupants, it is necessary to find out how they behave to change the conditions in support of improving the comfort like opening/closing the window, increasing/decreasing thermostat degree, on/off radiator tunes, etc. This information will help to classify user behaviour patterns.

3.2 Collecting physical properties of dwellings (monitoring)

Physical properties of the dwellings are necessary for modelling and simulation.

- *Materials, plans and typologies of the dwellings:* The site plans, floor plans and construction details are collected from TOKİ. This information is required for simulation of base dwelling models.
- *Actual energy consumption of each dwelling:* Based on the bills that the occupants paid for both electricity and fuel (usually natural gas) the energy consumption levels of each dwelling will be revealed. This information will be used both for statistical analysis outcomes gathered from survey results and for calibration of simulation models.
- *Monitoring of each dwelling by means of data loggers:* The information gathered from occupants by the means of survey questions usually assessed subjectively. Thus monitoring is necessary to support these subjective feelings of the occupants with actual conditions in numerically. Thermal comfort conditions (by means of dry-bulb temperature, mean radiant temperature, humidity and air flow measurements); visual comfort conditions (by means of luminance level measurements of both natural and artificial lighting); and aural comfort conditions (by means of noise level measurements of both among rooms inside the dwelling and caused by outside of the dwelling) are monitored.

3.3 Determining energy performance levels of dwellings in current state (energy simulation)

All information gathered from both the survey and measurements are going to be used in simulation models. Firstly a base model is defined with the help of physical properties and actual energy bills of the dwellings. Determining the current state of the dwellings by simulation is important since this is going to be a base model for further evaluations of derived sample models. Moreover, the revealed energy performances of each dwelling type will help to develop renovation levels and a

classification based on renovation necessities. This information is also useful for improvement models based on occupant behaviour of the dwellings.

3.4 Determining sensitivity of occupant behaviour on energy consumption

Since the objective of the research considers robustness of the behaviour, the research methodology is based on sensitivity analysis. As a general definition, sensitivity analysis is the study of how the variation in the output of a model can be apportioned, qualitatively or quantitatively, to different sources of variation. In sensitivity analysis, a mathematical model is defined by a series of equations, input factors, parameters, and variables aimed to characterize the process being investigated. Input is subject to many sources of uncertainty including errors of measurement, absence of information and poor or partial understanding of the driving forces and mechanisms. This uncertainty imposes a limit on the confidence in the response or output of the model (Hamby, 1994; Helton et al. 2006; Saltelli et al. 2006). There are several examples of the application of sensitivity analysis in building thermal modelling (Spitler et al. 1989; Corson, 1992; Lam and Hui, 1996; Fülbringer and Roulet, 1999; McDonald, 2004; Westphal and Lamberts, 2005; Harputlugil et al. 2009). For sensitivity of energy simulation models, a set of input parameters and their values are defined and applied to a building model. The simulated energy consumption of the model is used as a base for comparison to determine how much the output (here measured in terms of energy use per year) changes due to particular increments of input values (Corson, 1992). Consequently the results show which parameters can be classified as "sensitive" or "robust". Sensitive parameters are the parameters that by a change in their value cause effective changes on outputs (in this case energy consumption). Contrarily, change of robust parameters causes negligible changes on outputs. The sensitivity of occupant behaviour; which is considered here as factors influencing energy use by behaviour; will be analysed by the Monte Carlo method. The Monte Carlo method is one of the most commonly used methods to analyse the

approximate distribution of possible results on the basis of probabilistic inputs (Lomas and Eppel, 1992; Hopfe et al. 2007). Here the inputs (parameters) are several usages that affect energy consumption of the dwelling; listed as, i) presence of occupant (hours that they stay at home during weekdays and weekends); ii) use of heating system (by means of changing thermostat settings and/or radiator tunes), iii) use of ventilation system (by means of operating windows and/or mechanical ventilation system); iv) use of lighting system (by means of operating lightings). The data used for analysis is gathered from both the survey among households and monitoring dwellings in Ankara/Turkey. The steps of the analysis are as follows (Figure-1):

- i) Reprocessing survey data within statistical analysis program (the mean and standard deviations (SD) of the input parameters are determined)
- ii) Gathering Latin-Hypercube samples from Sim-Lab (2007) pre-processor
- iii) Simulating each sample by a dynamic simulation program to collect output data,
- iv) Combination of inputs and outputs in post-processor of Sim-Lab to get Monte-Carlo Analysis results
- v) Interpretation of the results by classifying the behaviours as "sensitive" and "robust".

The sensitive and robust behavioural patterns will be used on the background of a decision tool that aims to help owner-occupants on their decisions for renovating their dwellings.

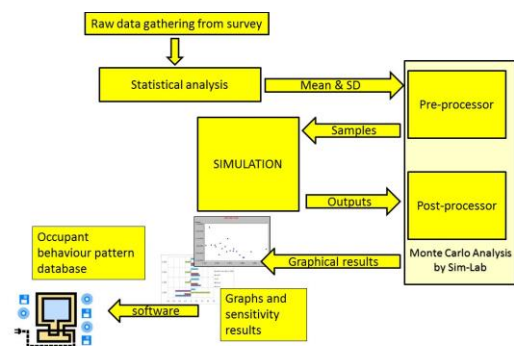


Fig. 1 – Flow chart of sensitivity analysis

3.5 Developing a decision tool based on behavioural patterns of occupants

Revealing the sensitive (or robust) behaviour that is effective on energy consumption of the dwellings leads to the generation of a database. The database consists of occupant behaviour, actual energy consumptions and necessary renovation levels are aimed to use developing a new approach to labelling system of EPC (Energy Performance Certificate). This new classification will group occupants as A, B, C class. The sensitive and robust behaviours will guide the development of behavioural patterns which will be a base for occupant group classes. Although it may not be possible to assign a specific metric for occupants, the numeric response of occupant behaviour will be gathered from the correlation between energy consumptions and behavioural patterns. The more sensitive behaviour will be an indicator of a high level of class. In other words, occupants controlling any of their sensitive behaviour, which means that energy consumption is under control as well, will achieve a high class label. This labelling will assist current occupants during renovation of the dwellings. Besides, designers of future dwellings will use this database while defining occupant related design parameters during design process. Matching the energy class of the dwellings with the energy class of the occupants is expected to be another challenge during design. The web-based decision tool aims to propose a media for all the stakeholders of the design process in order to provide insights into occupant behaviour from an energy consciousness perspective.

4. Discussion and Future Work

Here in this research, the main frame of the hypothesis is: "The patterns of occupant behaviour which directly or indirectly affects energy consumption and indoor air quality can be determined by quantitative methods. Revealing the robustness of the occupant behaviour will be utilized particularly during renovation of the dwellings. Re-thinking of energy consumption classification will bring about a new approach while

defining influence rate of occupant behaviour quantitatively".

In this paper, only the conceptual framework of the research is introduced. The work was started in August 2014 and the first results of the survey will be obtained at the end of December 2014.

The expected outcomes of the research can be group into three;

i) The proposed methodology of the research includes sensitivity analysis. The results of sensitivity analysis will assist to suggest a way to define occupant profiles in simulation. If occupant behaviour patterns are clearly defined at the end of the sensitivity analysis, this information will be used for ready-to-use occupant packages to simulation tools.

ii) The data gathered at the end of the research will lead to develop a web-based decision tool which will provide feedback for not only the designers of the future dwellings but also decision-makers of renovation process.

iii) Recently a big revision has been achieved in Turkish energy politics. Considering local and global perspectives on energy efficiency, developing and newly established Turkish laws and regulations are essential. Particularly improvement strategies in current building stock will give an opportunity to save more energy than expected. The aim of this research is to create a base for new and developing energy efficiency regulations and provide a different frame from occupant potential perspective.

5. Acknowledgement

The authors would like to thank Scientific and Technical Research Council of Turkey (TÜBİTAK) where the project titled "*Developing a New Methodology to Improve Housing Quality in Turkey Based on Effects of Occupant Behavior on Energy and Comfort of the Dwellings*" is funded under SOBAG No: 113K799 (2014-2016).

References

Hazucha, J., 2009, *Renovation of social buildings, Guidelines for complex renovations*, IEE Project

- PASS-NET, Czech Republic.
- Thomsen, A., Flier, K., 2009, Replacement or renovation of dwellings: the relevance of a more sustainable approach, *Building Research and Information*, 37 (5-6), 649-659.
- Kara, E., 2010, *Renovate or rebuild? A life cycle assessment based case study: 3 examples from the Dutch housing stock*, Master of Science Thesis, Delft University of Technology.
- Page, J., 2007, *Simulating occupant presence and behaviour in buildings*, PhD thesis dissertation, École Polytechnique Fédérale De Lausanne, Switzerland.
- Santin, O. G., 2010, *Actual Energy Consumption in Dwellings, The effect of Energy Performance Regulations and Occupant Behaviour*, PhD Thesis, OTB Research Institute, Delft University of Technology, The Netherlands.
- Itard, L., Meijer, F., Vrins, E., Hoiting, H., 2008, Building Renovation and modernisation in Europe: State of the art review, *Final report of ERABUILD*, OTB Research Institute, Delft, NL.
- Mlecnik, E. 2010, Adoption of Highly energy efficient renovation, open house international, Vol. 35, No:2, pp.39-49.
- G. Newsham, A. Mahdavi, and I. Beausoleil-Morrison, 1995, Lightswitch: a stochastic model for predicting office lighting energy consumption. In *Right Light Three, the Third European Conference on Energy Efficient Lighting*, Newcastle-upon-Tyne, UK, pp 60-66.
- C. Reinhart, 2004, Lightswitch-2002: a model for manual and automated control of electric lighting and blinds. *Solar Energy* 77, 15-28.
- D. Wang, C. Federspiel, and F. Rubinstein, 2005, Modeling occupancy in single person offices. *Energy and Buildings* 37, 121-126.
- D. McQueen, P. Hyland, and S. Watson, 2004, Monte Carlo simulation of residential electricity demand for forecasting maximum demand on distribution networks, *IEEE Transactions on Power Systems* 19, pp 1685-1689.
- R. Fritsch, A. Kohler, M. Nygard-Ferguson, and J.-L. Scartezzini, 1990, A stochastic model of user behaviour regarding ventilation, *Building and Environment* 25, pp 173-181.
- J. F. Nicol, 2001, Characterising occupant behaviour in buildings: towards a stochastic model of occupant use of windows, lights, blinds, heater and fans. In *Seventh International IBPSA Conference*, Rio de Janeiro, Brazil.
- Hamby, D. M., 1994, "A Review of Techniques for Parameter Sensitivity Analysis of Environmental Models", *Environmental Monitoring and Assessment*, v.32, pp.135-154.
- Helton, J. C., Johnson, J. D., Sallaberry, C. J., Storlie, C. B., 2006, Survey of Sampling Based Methods for Uncertainty and Sensitivity Analysis, *Reliability Engineering and System Safety*, Volume 91, pp. 1175-1209.
- Saltelli, A., Ratto, M., Tarantola, S., Campolongo, F., 2006, Sensitivity Analysis Practices: Strategies for Model Based Inference, *Reliability Engineering and System Safety*, Volume 91, pp. 1109-1125.
- Spitler, J. D., Fisher, D. E., Zietlow, D. C., A Primer on the Use of Influence Coefficients in Building Simulation, *Proceedings of Building Simulation '89 Conference*, IBPSA, Vancouver, Belgium, (1989) 299-304.
- Corson G. C., Input-Output Sensitivity of Building Energy Simulations, *ASHRAE transactions*, 98 (Part I), (1992), 618-626.
- Lam J. C. and Hui S. C., Sensitivity Analysis of Energy Performance of Office Buildings, *Building and Environment*, Vol.31 No.1, (1996) 27-39.
- Fülbringer and Roulet, Confidence of Simulation Results: Put a Sensitivity Analysis Module in Your Model, *Energy and Buildings*, Volume 30, (1999), 61-71.
- Mc Donald, 2004, Assessing the Significance of Design Changes when Simulating Building Performance Including the Effects of Uncertain Input Data, *Proceedings of e-Sim'04*, Vancouver.
- Westphal and Lamberts, 2005, Building Simulation Calibration Using Sensitivity Analysis, *Proceedings of Building Simulation '05 Conference*, IBPSA, Montreal, Canada, 1331-1338.
- Harputlugil, G.U., de Wilde, P.J.C.J, Hensen, J.L.M., Çelebi, G., 2009, Development of a thermally robust school outline design for the different climate regions of Turkiye, *Proceedings of Building Simulation '09, 11th International IBPSA Conference*, Glasgow, United Kingdom, July 27-30, 1292-1298.

Lomas K.J., Eppel H., 1992, Sensitivity analysis techniques for building thermal simulation programs, *Energy and Buildings*. Vol. 19, no. 1, 21-44.

Hopfe, C., Hensen, J., Plokker, W., 2007, Uncertainty and Sensitivity Analysis for Detailed Design Support", *Proceedings of the 10th IBPSA Building Simulation Conference*, 3-5 September, Tsinghua University, Beijing, 1799-1804.

SIMLAB, 2007, Simlab version 2.2 manual, <http://simlab.jrc.ec.europa.eu/>

Building Simulation applications (BSA) 2015 was the second IBPSA-Italy conference on building performance simulation to take place at the Free University of Bolzano, from February 4th to 6th 2015. The main topics dealt with were: detailed modelling of phenomena and components, integrated and non-energy performance analysis, optimization techniques for high performance buildings and retrofit, and development and validation of new tools.

The principal mission of the International Building Performance Simulation Association (IBPSA) is to promote and advance the practice of building performance simulation in order to improve the design, construction, operation and maintenance of new and existing buildings.

IBPSA-Italy is the Italian regional affiliate, a non-profit-making association, which includes researchers, developers and practitioners acting on the topic of building performance simulation. IBPSA-Italy was founded in January 2011 and has now more than 140 members including university professors, researchers, professionals, software developers and students.

bu,p

